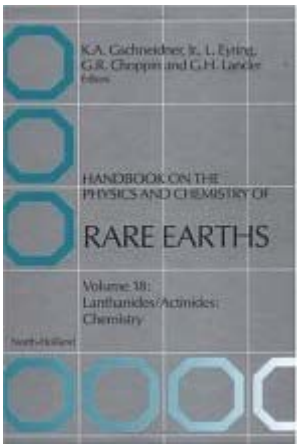

Handbook on the Physics and Chemistry of Rare Earths, volume 18

Lanthanides/Actinides: Chemistry

Elsevier, 1994

Edited by: Karl A. Gschneidner, Jr., LeRoy Eyring, G.H. Lander and G.R. Choppin
ISBN: 978-0-444-81724-2

Handbook on the Physics and Chemistry of Rare Earths
Vol. 18 – Lanthanides/Actinides: Chemistry
edited by K.A. Gschneidner, Jr., L. Eyring, G.R. Choppin and G.H. Lander

PREFACE

Karl A. GSCHNEIDNER, Jr., LeRoy EYRING, Gregory R. CHOPPIN, and Gerry H. LANDER

These elements perplex us in our rearches [sic], *baffle us in our speculations, and haunt us in our very dreams. They stretch like an unknown sea before us – mocking, mystifying, and murmuring strange revelations and possibilities.*

Sir William Crookes (February 16, 1887)

This volume of the Handbook is the second of a three-volume set of reviews devoted to the interrelationships, similarities, differences, and contrasts of the lanthanide and actinide series of elements. The idea of these volumes grew out of a conversation between one of the editors, KAG, and a member of the editorial board, Stefan Hüfner, in early June 1986. This idea was enthusiastically received by the other editor (LE) and editorial board members, and also the publishers. Numerous topics and authors were suggested and soon it was apparent that this special subject was too large to be covered in one or possibly two volumes, and that the editors (KAG and LE) of this series would need help from two leading scientists who had considerable experience and knowledge of both series of elements. Thus, Gerry H. Lander and Gregory R. Choppin were invited to be guest editors for this special set of volumes on the lanthanides/actinides. After they accepted, the four editors carefully and critically chose the various topics, and top experts in the various areas were invited to write reviews, keeping in mind that the emphasis was to be on the interrelationships of the lanthanides and actinides. More than seven years after Stefan Hüfner's initial suggestion, the first volume, which is devoted to the physical aspects, has been published. In the present volume comparisons of the chemistry of the lanthanide and actinide elements are considered.

The observations and comments of Sir William Crookes (as noted above) over 107 years ago about the lanthanides is even more appropriate to these lanthanide/actinide tomes. This is especially noteworthy because only two members of the actinide series of elements were then known (Th and U) and the concept of such a series was not to develop for about 50 years. But we hope that the material presented in these three lanthanide/actinide volumes will shed light on some of the mysteries of yesterday, but as surely as we begin to understand them, new ones will arise to continue to haunt us as we move forward and ever onward.

These volumes on the lanthanide and actinide elements are dedicated to Professor Glenn T. Seaborg. Professor Seaborg is a central figure in the development of ideas linking the lanthanides and actinides as is made clear by the dedicatory statement of Dr. J.J. Katz and the review by Professor Seaborg himself in chapter 118. Seaborg was the co-discoverer of plutonium and nine other trans-neptunium elements. Element 106 was recently and appropriately named seaborgium and given the symbol Sg in his honor.

In chapter 118 Seaborg reviews the background for placing the heaviest elements in the periodic table, the discovery of the transuranium elemetns and the publication specifically proposing an actinide series of 5f elements in 1945. The chemistry of the lanthanides played an important role in the establishment of the actinide hypothesis. The value of this 1945 hypothesis in predicting the chemical properties of the soon-to-be synthesized remainder of the actinide series and beyond is apparent. Professor Seaborg concludes by placing the heavier elements, discovered and yet-to-be-found, up to element number 153 in the periodic table.

The lanthanide and actinide elements present a plethora of challenging physical and chemical problems resulting from the involvements of open f-shell electronic configurations. This is made clear in the chapters of these volumes. Much less discussed are the relativistic effects that arise in both the lanthanide and actinide elements and their compounds. K. Balasubramanian introduces us to the basic theory and discusses these effects in chapter 119.

James V. Beitz explores, in chapter 120, the experimental and theoretical aspects of solution absorption and luminescence spectra to reveal similarities and differences in the two f-series. The rich detail of the visible and near-infrared absorption spectra serve to identify the ions in solution. The review reveals the limits of spectral assignments.

Basic to any studies of the lanthanides and actinides is the ability to separate the members of these difficultly separable series. Kenneth L. Nash reviews the methods and effectiveness of separation by solvent extraction, ion exchange and necessary accompanying reactions in chapter 121.

A background against which to place the comparative studies of our concern is thermodynamics. Any physical or chemical property of a substance is at some level reflected in its thermodynamic properties. Lester Morss has reviewed, in chapter 122, the comparative thermochemical and oxidation–reduction properties of lanthanide and actinide materials.

Generic descriptions of the phase behaviors in the lanthanide and actinide hydrides, as well as a thorough examination and explanation of the thermodynamic relationships of these metal–hydrogen systems, are given by John W. Ward and John M. Haschke in chapter 123.

Interrelationships and comparisons of the halides are reviewed in chapter 124, by Harry A. Eick. Synthesis and characterization, especially structure, are emphasized but the new literature on other properties is also considered.

The actinide elements express a wider range of oxidation states, in their compounds, than do the lanthanides. Chapter 125 by R.G. Haire and L. Eyring on the oxides mentions oxides over the whole range of compositions but emphasizes those that

exist in common. Synthesis, characterization and properties are considered. Structure characterization is emphasized.

In chapter 126, by Scott A. Kinkead, Kent D. Abney, and Thomas A. O'Donnell, comparisons between the behavior of lanthanides and the early actinides in superacids are considered. The reasons involve the fact that more reduced species are observed in superacid media.

Since so much chemistry is done in aqueous media a study of the stability and structure of the species that exist is of primary importance. In chapter 127, Emil N. Rizkalla and Gregory R. Choppin examine the relative hydration and hydrolysis behaviors of the lanthanides and actinides.

Chapter 127 serves as an introduction to chapter 128 by Gregory R. Choppin and Emil N. Rizkalla where the broad field of aqueous solution chemistry is compared and contrasted. Thermodynamics, structure and kinetics are all considered.

The final chapter (129) of this volume introduces the important topic of the role of the f-families of elements in biochemistry. The chapter is written by John R. Duffield, David R. Taylor and David R. Williams. This chapter introduces us to the many important ways the lanthanides and actinides impinge on biosystems in the nuclear age.

Dedicated to

GLENN T. SEABORG

Among the many noteworthy scientific achievements of the 20th century, there are only a very few that can match the discovery of the actinide elements in its impact on science and society. The addition of an entire new family of largely man-made elements to the Periodic Table, and the formulation of the actinide concept have had a profound influence on the way physicists and chemists think about the electronic structures of the elements. The new insights arising from studies on the chemistry and physics of the heaviest elements has had an especially important influence on the way we think about the more familiar elements of the Periodic Table, in particular, the rare earths. In the saga of the actinide elements, Glenn Seaborg has been the pivotal figure. The dedication to Glenn Seaborg of these volumes of *the Handbook on the Physics and Chemistry of Rare Earths*, which deal with the relationships of the lanthanide and actinide elements, is thus a fitting recognition of the exceptionally important contribution that his actinide element studies have made to many branches of science.

Glenn Seaborg's scientific career began in the 1930's as a research associate of G.N. Lewis at the University of California. He early became convinced that the science of nuclear chemistry, then in its infancy, provided challenging opportunities for scientific discovery. In the Lawrence Radiation Laboratory, in the course of a few years, he validated his intuition by the discovery of a host of isotopes, many of which have become important in research and medicine. Among these are cobalt-60, iodine-131, technetium-99m, cesium-137, and, of course, the plutonium isotopes. In 1944, he formulated the actinide concept of heavy-element electronic structure that accurately predicted the existence of a family of rare earth-like elements at the end of the Periodic Table as it was generally presented at that time. The actinide concept was the guide to the discovery of the remaining members of the actinide elements. In addition to the fissile plutonium isotopes, he and his co-workers over the years discovered no less than nine additional members of the new rare earth-like family of elements. These discoveries have been of great relevance not only to purely scientific matters but also to such global problems as nuclear energy and the control of nuclear weapons.

In addition to his life as an active scientist, Glenn Seaborg has had a distinguished career in academic and public life. He served at various times as Chancellor of the University of California at Berkeley, Chairman of the Atomic Energy Commission for a period of ten years, and Chairman of the Lawrence Hall of Science, to name only a few of his extra-scientific activities. He was the recipient of a Nobel Prize (1951) for his discoveries in the chemistry of the transuranium elements, and has received encomiums from most of the scientific societies of the world.

In spite of worldly distractions, Glenn Seaborg has never wavered in his life-long commitment to science. He continues his research into the chemistry and nuclear systematics of the actinide elements. Recently, he has focused his attention on the possible existence of still another family of superheavy elements at the end of the Periodic Table, and the development of new methods for the synthesis of superheavy elements. The dedication of these volumes to Glenn Seaborg is not only a testimonial to his scientific achievements, it is also an appreciation of the example that he continues to set.

J.J. Katz
December 5, 1991

CONTENTS

Preface v

Dedication ix

Contents xi

Contents of Volumes 1 – 17 xiii

118. G.T. Seaborg
Origin of the actinide concept 1

119. K. Balasubramanian
Relativistic effects and electronic structure of lanthanide and actinide molecules 29

120. J.V. Beitz
Similarities and differences in trivalent lanthanide- and actinide-ion solution absorption spectra and luminescence studies 159

121. K.L. Nash
Separation chemistry for lanthanides and trivalent actinides 197

122. L.R. Morss
Comparative thermochemical and oxidation–reduction properties of lanthanides and actinides 239

123. J.W. Ward and J.M. Haschke
Comparison of 4f and 5f element hydride properties 293

124. H.A. Eick
Lanthanide and actinide halides 365

125. R.G. Haire and L. Eyring
Comparisons of the binary oxides 413

126. S.A. Kinkead, K.D. Abney and T.A. O'Donnell
f-element speciation in strongly acidic media: lanthanide and mid-actinide metals, oxides, fluorides and oxide fluorides in superacids 507

127. E.N. Rizkalla and G.R. Choppin
Lanthanides and actinides hydration and hydrolysis 529

128. G.R. Choppin and E.N. Rizkalla
Solution chemistry of actinides and lanthanides 559

129. J.R. Duffield, D.M. Taylor and D.R. Williams
The biochemistry of the f-elements 591

Author index 623

Subject index 659

CONTENTS OF VOLUMES 1–17

VOLUME 1: Metals
1978, 1st repr. 1982, 2nd repr. 1991; ISBN 0-444-85020-1

1. Z.B. Goldschmidt, *Atomic properties (free atom)* 1
2. B.J. Beaudry and K.A. Gschneidner Jr, *Preparation and basic properties of the rare earth metals* 173
3. S.H. Liu, *Electronic structure of rare earth metals* 233
4. D.C. Koskenmaki and K.A. Gschneidner Jr, *Cerium* 337
5. L.J. Sundström, *Low temperature heat capacity of the rare earth metals* 379
6. K.A. McEwen, *Magnetic and transport properties of the rare earths* 411
7. S.K. Sinha, *Magnetic structures and inelastic neutron scattering: metals, alloys and compounds* 489
8. T.E. Scott, *Elastic and mechanical properties* 591
9. A. Jayaraman, *High pressure studies: metals, alloys and compounds* 707
10. C. Probst and J. Wittig, *Superconductivity: metals, alloys and compounds* 749
11. M.B. Maple, L.E. DeLong and B.C. Sales, *Kondo effect: alloys and compounds* 797
12. M.P. Dariel, *Diffusion in rare earth metals* 847
    Subject index 877

VOLUME 2: Alloys and intermetallics
1979, 1st repr. 1982, 2nd repr. 1991; ISBN 0-444-85021-X

13. A. Iandelli and A. Palenzona, *Crystal chemistry of intermetallic compounds* 1
14. H.R. Kirchmayr and C.A. Poldy, *Magnetic properties of intermetallic compounds of rare earth metals* 55
15. A.E. Clark, *Magnetostrictive RFe_2 intermetallic compounds* 231
16. J.J. Rhyne, *Amorphous magnetic rare earth alloys* 259
17. P. Fulde, *Crystal fields* 295
18. R.G. Barnes, *NMR, EPR and Mössbauer effect: metals, alloys and compounds* 387
19. P. Wachter, *Europium chalcogenides: EuO, EuS, EuSe and EuTe* 507
20. A. Jayaraman, *Valence changes in compounds* 575
    Subject Index 613

VOLUME 3: Non-metallic compounds – I
1979, 1st repr. 1984; ISBN 0-444-85215-8

21. L.A. Haskin and T.P. Paster, *Geochemistry and mineralogy of the rare earths* 1
22. J.E. Powell, *Separation chemistry* 81
23. C.K. Jørgensen, *Theoretical chemistry of rare earths* 111
24. W.T. Carnall, *The absorption and fluorescence spectra of rare earth ions in solution* 171
25. L.C. Thompson, *Complexes* 209
26. G.G. Libowitz and A.J. Maeland, *Hydrides* 299
27. L. Eyring, *The binary rare earth oxides* 337
28. D.J.M. Bevan and E. Summerville, *Mixed rare earth oxides* 401
29. C.P. Khattak and F.F.Y. Wang, *Perovskites and garnets* 525
30. L.H. Brixner, J.R. Barkley and W. Jeitschko, *Rare earth molybdates (VI)* 609
    Subject index 655

VOLUME 4: Non-metallic compounds – II

1979, 1st repr. 1984; ISBN 0-444-85216-6

31. J. Flahaut, *Sulfides, selenides and tellurides* 1
32. J.M. Haschke, *Halides* 89
33. F. Hulliger, *Rare earth pnictides* 153
34. G. Blasse, *Chemistry and physics of R-activated phosphors* 237
35. M.J. Weber, *Rare earth lasers* 275
36. F.K. Fong, *Nonradiative processes of rare-earth ions in crystals* 317
37A. J.W. O'Laughlin, *Chemical spectrophotometric and polarographic methods* 341
37B. S.R. Taylor, *Trace element analysis of rare earth elements by spark source mass spectroscopy* 359
37C. R.J. Conzemius, *Analysis of rare earth matrices by spark source mass spectrometry* 377
37D. E.L. DeKalb and V.A. Fassel, *Optical atomic emission and absorption methods* 405
37E. A.P. D'Silva and V.A. Fassel, *X-ray excited optical luminescence of the rare earths* 441
37F. F.W.V. Boynton, *Neutron activation analysis* 457
37G. S. Schuhmann and J.A. Philpotts, *Mass-spectrometric stable-isotope dilution analysis for lanthanides in geochemical materials* 471
38. J. Reuben and G.A. Elgavish, *Shift reagents and NMR of paramagnetic lanthanide complexes* 483
39. J. Reuben, *Bioinorganic chemistry: lanthanides as probes in systems of biological interest* 515
40. T.J. Haley, *Toxicity* 553
Subject index 587

VOLUME 5

1982, 1st repr. 1984; ISBN 0-444-86375-3

41. M. Gasgnier, *Rare earth alloys and compounds as thin films* 1
42. E. Gratz and M.J. Zuckermann, *Transport properties (electrical resitivity, thermoelectric power and thermal conductivity) of rare earth intermetallic compounds* 117
43. F.P. Netzer and E. Bertel, *Adsorption and catalysis on rare earth surfaces* 217
44. C. Boulesteix, *Defects and phase transformation near room temperature in rare earth sesquioxides* 321
45. O. Greis and J.M. Haschke, *Rare earth fluorides* 387
46. C.A. Morrison and R.P. Leavitt, *Spectroscopic properties of triply ionized lanthanides in transparent host crystals* 461
Subject index 693

VOLUME 6

1984; ISBN 0-444-86592-6

47. K.H.J. Buschow, *Hydrogen absorption in intermetallic compounds* 1
48. E. Parthé and B. Chabot, *Crystal structures and crystal chemistry of ternary rare earth–transition metal borides, silicides and homologues* 113
49. P. Rogl, *Phase equilibria in ternary and higher order systems with rare earth elements and boron* 335
50. H.B. Kagan and J.L. Namy, *Preparation of divalent ytterbium and samarium derivatives and their use in organic chemistry* 525
Subject index 567

VOLUME 7

1984; ISBN 0-444-86851-8

51. P. Rogl, *Phase equilibria in ternary and higher order systems with rare earth elements and silicon* 1
52. K.H.J. Buschow, *Amorphous alloys* 265
53. H. Schumann and W. Genthe, *Organometallic compounds of the rare earths* 446
Subject index 573

VOLUME 8

1986; ISBN 0-444-86971-9

54. K.A. Gschneidner Jr and F.W. Calderwood, *Intra rare earth binary alloys: phase relationships, lattice parameters and systematics* 1
55. X. Gao, *Polarographic analysis of the rare earths* 163
56. M. Leskelä and L. Niinistö, *Inorganic complex compounds I* 203
57. J.R. Long, *Implications in organic synthesis* 335
Errata 375
Subject index 379

VOLUME 9

1987; ISBN 0-444-87045-8

58. R. Reisfeld and C.K. Jørgensen, *Excited state phenomena in vitreous materials* 1
59. L. Niinistö and M. Leskelä, *Inorganic complex compounds II* 91
60. J.-C.G. Bünzli, *Complexes with synthetic ionophores* 321
61. Zhiquan Shen and Jun Ouyang, *Rare earth coordination catalysis in stereospecific polymerization* 395
Errata 429
Subject index 431

VOLUME 10: High energy spectroscopy

1988; ISBN 0-444-87063-6

62. Y. Baer and W.-D. Schneider, *High-energy spectroscopy of lanthanide materials – An overview* 1
63. M. Campagna and F.U. Hillebrecht, *f-electron hybridization and dynamical screening of core holes in intermetallic compounds* 75
64. O. Gunnarsson and K. Schönhammer, *Many-body formulation of spectra of mixed valence systems* 103
65. A.J. Freeman, B.I. Min and M.R. Norman, *Local density supercell theory of photoemission and inverse photoemission spectra* 165
66. D.W. Lynch and J.H. Weaver, *Photoemission of Ce and its compounds* 231
67. S. Hüfner, *Photoemission in chalcogenides* 301
68. J.F. Herbst and J.W. Wilkins, *Calculation of 4f excitation energies in the metals and relevance to mixed valence systems* 321
69. B. Johansson and N. Mårtensson, *Thermodynamic aspects of 4f levels in metals and compounds* 361
70. F.U. Hillebrecht and M. Campagna, *Bremsstrahlung isochromat spectroscopy of alloys and mixed valent compounds* 425
71. J. Röhler, *X-ray absorption and emission spectra* 453
72. F.P. Netzer and J.A.D. Matthew, *Inelastic electron scattering measurements* 547
Subject index 601

VOLUME 11: Two-hundred-year impact of rare earths on science

1988; ISBN 0-444-87080-6

H.J. Svec, *Prologue* 1
73. F. Szabadváry, *The history of the discovery and separation of the rare earths* 33
74. B.R. Judd, *Atomic theory and optical spectroscopy* 81
75. C.K. Jørgensen, *Influence of rare earths on chemical understanding and classification* 197
76. J.J. Rhyne, *Highlights from the exotic phenomena of lanthanide magnetism* 293
77. B. Bleaney, *Magnetic resonance spectroscopy and hyperfine interactions* 323
78. K.A. Gschneidner Jr and A.H. Daane, *Physical metallurgy* 409
79. S.R. Taylor and S.M. McLennan, *The significance of the rare earths in geochemistry and cosmochemistry* 485
Errata 579
Subject index 581

VOLUME 12

1989; ISBN 0-444-87105-5

80. J.S. Abell, *Preparation and crystal growth of rare earth elements and intermetallic compounds* 1
81. Z. Fisk and J.P. Remeika, *Growth of single crystals from molten metal fluxes* 53
82. E. Burzo and H.R. Kirchmayr, *Physical properties of $R_2Fe_{14}B$-based alloys* 71
83. A. Szytuła and J. Leciejewicz, *Magnetic properties of ternary intermetallic compounds of the RT_2X_2 type* 133
84. H. Maletta and W. Zinn, *Spin glasses* 213
85. J. van Zytveld, *Liquid metals and alloys* 357
86. M.S. Chandrasekharaiah and K.A. Gingerich, *Thermodynamic properties of gaseous species* 409
87. W.M. Yen, *Laser spectroscopy* 433
Subject index 479

VOLUME 13

1990; ISBN 0-444-88547-1

88. E.I. Gladyshevsky, O.I. Bodak and V.K. Pecharsky, *Phase equilibria and crystal chemistry in ternary rare earth systems with metallic elements* 1
89. A.A. Eliseev and G.M. Kuzmichyeva, *Phase equilibrium and crystal chemistry in ternary rare earth systems with chalcogenide elements* 191
90. N. Kimizuka, E. Takayama-Muromachi and K. Siratori, *The systems R_2O_3–M_2O_3–$M'O$* 283
91. R.S. Houk, *Elemental analysis by atomic emission and mass spectrometry with inductively coupled plasmas* 385
92. P.H. Brown, A.H. Rathjen, R.D. Graham and D.E. Tribe, *Rare earth elements in biological systems* 423
Errata 453
Subject index 455

VOLUME 14

1991; ISBN 0-444-88743-1

93. R. Osborn, S.W. Lovesey, A.D. Taylor and E. Balcar, *Intermultiplet transitions using neutron spectroscopy* 1
94. E. Dormann, *NMR in intermetallic compounds* 63
95. E. Zirngiebl and G. Güntherodt, *Light scattering in intermetallic compounds* 163
96. P. Thalmeier and B. Lüthi, *The electron–phonon interaction in intermetallic compounds* 225
97. N. Grewe and F. Steglich, *Heavy fermions* 343
Subject index 475

VOLUME 15

1991; ISBN 0-444-88966-3

98. J.G. Sereni, *Low-temperature behaviour of cerium compounds* 1
99. G.-y. Adachi, N. Imanaka and Zhang Fuzhong, *Rare earth carbides* 61
100. A. Simon, Hj. Mattausch, G.J. Miller, W. Bauhofer and R.K. Kremer, *Metal-rich halides* 191
101. R.M. Almeida, *Fluoride glasses* 287
102. K.L. Nash and J.C. Sullivan, *Kinetics of complexation and redox reactions of the lanthanides in aqueous solutions* 347
103. E.N. Rizkalla and G.R. Choppin, *Hydration and hydrolysis of lanthanides* 393
104. L.M. Vallarino, *Macrocycle complexes of the lanthanide(III) yttrium(III) and dioxouranium(VI) ions from metal-templated syntheses* 443
Errata 513
Subject index 515

MASTER INDEX, Vols. 1–15
1993; ISBN 0-444-89965-0

VOLUME 16
1993; ISBN 0-444-89782-8

105. M. Loewenhaupt and K.H. Fischer, *Valence-fluctuation and heavy-fermion 4f systems* 1
106. I.A. Smirnov and V.S. Oskotski, *Thermal conductivity of rare earth compounds* 107
107. M.A. Subramanian and A.W. Sleight, *Rare earths pyrochlores* 225
108. R. Miyawaki and I. Nakai, *Crystal structures of rare earth minerals* 249
109. D.R. Chopra, *Appearance potential spectroscopy of lanthanides and their intermetallics* 519
Author index 547
Subject index 579

VOLUME 17: Lanthanides/actinides: Physics – I
1993; ISBN 0-444-81502-3

110. M.R. Norman and D.D. Koelling, *Electronic structure, Fermi surfaces, and superconductivity in f electron metals* 1
111. S.H. Liu, *Phenomenological approach to heavy-fermion systems* 87
112. B. Johansson and M.S.S. Brooks, *Theory of cohesion in rare earths and actinides* 149
113. U. Benedict and W.B. Holzapfel, *High-pressure studies – Structural aspects* 245
114. O. Vogt and K. Mattenberger, *Magnetic measurements on rare earth and actinide monopnictides and monochalcogenides* 301
115. J.M. Fournier and E. Gratz, *Transport properties of rare earth and actinide intermetallics* 409
116. W. Potzel, G.M. Kalvius and J. Gal, *Mössbauer studies on electronic structure of intermetallic compounds* 539
117. G.H. Lander, *Neutron elastic scattering from actinides and anomalous lanthanides* 635
Author index 711
Subject index 753

Handbook on the Physics and Chemistry of Rare Earths
Vol. 18 – Lanthanides/Actinides: Chemistry
edited by K.A. Gschneidner, Jr., L. Eyring, G.R. Choppin and G.H. Lander

Chapter 118

ORIGIN OF THE ACTINIDE CONCEPT

Glenn T. SEABORG
Lawrence Berkeley Laboratory, University of California, Berkeley, CA 94720, USA

Contents

1. Background 1
2. Suggestion of actinide concept 4
3. Further development of actinide concept 9
   3.1. Electronic configurations 9
   3.2. Possible deductions without data on transuranium elements 11
   3.3. Position in periodic table and nomenclature 12
   3.4. Predicted properties of transcurium elements 15
   3.5. Summary 15
4. Completion of actinide series 16
5. Superactinide elements 18
6. Status of actinide elements 19
7. Transactinide elements 21
8. Modern periodic table 25
References 25

1. Background

A typical periodic table of the time just prior to World War II, with predicted positions for elements beyond uranium, is shown in fig. 1. The heaviest natural elements, thorium, protactinium and uranium, of atomic numbers 90, 91 and 92, respectively, were placed in corresponding positions just below the sixth period "transition" elements – hafnium, tantalum and tungsten – in which the 5d electron shell is being filled. Hafnium, tantalum and tungsten are similar in their chemical properties to the corresponding transition elements in the fifth period – zirconium, columbium (nowadays better known as niobium) and molybdenum – in which the 4d shell is being filled.

It had long been known that the chemical properties of thorium, protactinium and uranium resemble those of the 4d and 5d elements. For this reason most of the textbooks and standard works on chemistry and physics in which the electronic structure was discussed accepted the view that it was the 6d shell that was being filled.

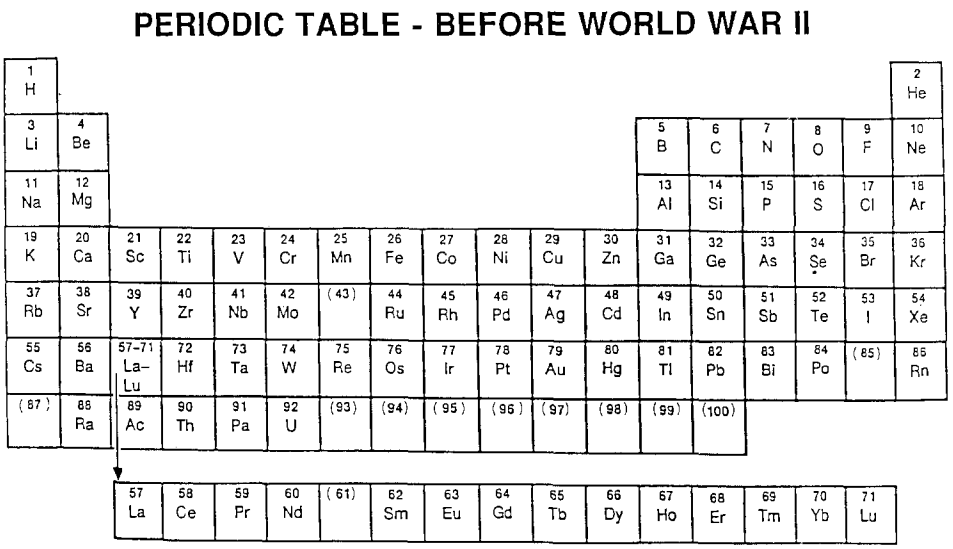

Fig. 1. Periodic table before World War II (atomic numbers of undiscovered elements are shown in parentheses).

Thus, the structures of the elements above radon (element 86) through uranium were written to show the addition of the next two electrons in the 7s shell for element 87 (francium) and element 88 (radium) and addition in the 6d shell for actinium, thorium, protactinium and uranium (Latimer and Hildebrand 1940; Richtmeyer and Kennard 1942; Taylor and Glasstone 1942).

Many of the early papers that appeared after Bohr's (1913) classical work on the quantized nuclear atom discussed the electronic structure of the heaviest elements. It was recognized by many that the next hypothetical rare gas should have the atomic number 118 in a place 32 elements beyond radon ($Z = 86$), thus implying transition groups similar to those between xenon ($Z = 54$) and radon ($Z = 86$). Rydberg (1913) as early as 1913 implied that this was to be expected. There was general agreement that some type of transition group should begin in the neighborhood of uranium, although there were differences of opinion as to where it begins and as to which electron shell is involved. A number of the earliest publications suggested that this transition series involves the filling of the 5f shell, thus possibly giving rise to a "rare-earth" group in a manner analogous to that resulting from the filling of the 4f shell. The filling of the 4f shell results in the well-known group of fourteen rare-earth elements of atomic numbers 58 to 71, inclusive; these elements follow lanthanum. It is of interest here to note a few of the early and also the later suggestions in order to review the general previous status of this question. Most of these early investigators thought that the filling of the 5f shell should begin at some point beyond uranium, i.e., beyond the elements that were known to them.

In early papers Bohr (1923) suggested that the addition of the 5f electrons might begin in this region, and in a Bohr–Thomsen type of periodic table he pictured the first

entry at the element with atomic number 94. Goldschmidt (1924) thought the transuranium elements up to atomic number 96 should be homologs of the platinum group, and Hahn (1929) thought this view was worthy of serious consideration. Suguira and Urey (1926), using the old quantum theory, published the results of their calculations, which indicated that the first entry of an electron into the 5f shell should occur at element 95, whereas Wu and Goudsmit (1933), on the basis of a more refined calculation, showed that their solution of the Schrödinger equation indicated such entry at uranium or element 93. McLennan et al. (1926) suggested, as an alternative to the filling of the 6d shell, the possibility that the 5f shell begins to be occupied in thorium. In a review article Dushman (1926) stated that it is doubtful that the added electrons enter the 6d level (thus implying an analogy with cerium, etc.). Swinne (1926) pointed out that the available evidence on thorium and uranium was consistent with the first entry of 5f electrons at protactinium or uranium, but he also thought that it might occur beyond uranium. Saha and Saha (1934) suggested as an alternate possibility to the filling of the 6d shell, the entry of the first 5f electron at thorium. Karapetoff (1930) suggested that the element with atomic number 93 might be the first in which the 5f shell begins to be filled, and Von Grosse (1928, 1930, 1935) suggested as a possible alternative to filling of the 6d shell, the entry of the first electron in the 5f shell at uranium. Quill (1938), largely for the purpose of illustration, presented periodic table arrangements in which the first 5f electron appears in element number 95 in one case and in element number 99 in another. Perrin (1935), Rudy (1927) and Carranza (1935), on general considerations, proposed as a possibility the theory that the first 5f electron appears in thorium, and Villar (1942, 1940) suggested that some of the chemical evidence supports this viewpoint. Somewhat earlier, on the basis of his crystallographic work, Goldschmidt (1937) had changed his original point of view and had come to the view that the first 5f electron enters at protactinium, although he pointed out the possibility that this might occur earlier, in thorium, or later, in uranium, or in the (at the time unknown) transuranium elements. By analogy with the name "lanthanide" series, which Goldschmidt et al. (1925) had already proposed for the rare-earth elements because these fourteen elements following lanthanum have lanthanum as their prototype, he proposed the name "thoride" series for the fourteen elements following thorium. At the same time he was the first to suggest that terms such as "actinide", "protactinide" and "uranide" might describe the group if it should eventually be found to begin earlier or later than this.

It can be seen that although many interesting and perspicacious proposals had been made up to this time, the electronic structure and place in the periodic table of these elements could not be regarded as established.

The discovery of the transuranium elements and the study of their properties, especially the chemical properties, furnished a tremendous amount of additional evidence of just the type needed to clarify this problem. It is in the transuranium elements that the really definitive chemical properties, from the standpoint of placing the heaviest elements in the periodic table, first appear. The first conclusive evidence that the 5f shell undergoes filling in this heavy region came from the tracer chemical observations of McMillan and Abelson (1940) on element 93, neptunium. Upon their discovery of neptunium, the first transuranium element, McMillan and Abelson were

able to show definitely that it resembles uranium in its chemical properties and bears no resemblance to rhenium, which is the element immediately above it in the periodic table of that time. This excellent experimental evidence was interpreted by them to indicate that this new "rare-earth" group of similar elements starts at the next element beyond uranium. The later calculations of Mayer (1941) indicated that the energy and spatial extension of the 5f eigenfunctions drop sharply at about element 91 and therefore that the filling of the 5f shell might begin at the first element beyond protactinium or uranium. Daudel (1943), in commenting on Mayer's paper, made some remarks concerning the special nature of the f electrons at the beginning of the rare-earth and the heavy-transition groups. Starke (1943) and Bedreag (1943) also interpreted the tracer experiments with element 93 as indicating that the first 5f electron comes at element 93, but Strassmann and Hahn (1942) thought, on the basis of their tracer experiments with this element, that it was difficult to make any deduction. As a result of our first tracer experiments with element 94, together with our consideration of the tracer investigations with element 93, Wahl and I (Seaborg and Wahl 1942, 1948, 1949) made the suggestion that this transition group might begin earlier and that thorium or actinium might be the zero element in the series. On the basis of his complete crystallographic evidence, including especially observations on the transuranium elements, Zachariasen (1944a,b) agreed with Goldschmidt that a thoride series is involved. Some spatial classifications of the elements appeared in which the heaviest elements, starting with thorium as the homolog of cerium, are listed as the chemical homologs of the rare-earth elements, but the reason in these cases appears to be mainly connected with the symmetry of and the ease of making such an arrangement (Djounkovsky and Kavos 1944, Talpain 1945).

2. Suggestion of actinide concept

I considered all of the evidence, especially the chemical properties of the elements with the atomic numbers 93 and 94, and made the suggestion that a rare-earth-like series begins with actinium in the same sense that the rare-earth or "lanthanide" series begins with lanthanum. On this basis it might be termed the "actinide" series and the first 5f electron might – although would not necessarily – appear in thorium. The salient point is that the characteristic oxidation state would be the III state.

This suggestion was advanced in a secret report (Seaborg 1944) I prepared in July 1944 at the wartime Metallurgical Laboratory of the University of Chicago, which is quoted in its entirety as follows.

> "Plutonium is the eighth element in the seventh period of the periodic table. The correlation of its chemical properties with its atomic structure can best be accomplished by considering it together with a number of the other elements in the seventh period (elements 89 to 94) in a discussion involving the chemical and physical properties of these elements.
>
> It seems very probable that some kind of a transition group should begin in the neighborhood of these elements. The elements 90 to 94 lie in corresponding positions just below the sixth-period transition elements hafnium to osmium (atomic numbers 72 to 76), in which the 5d shell is being filled. The transition elements hafnium to osmium are very

similar in their chemical properties to the corresponding 4d transition elements of the fifth period (zirconium to ruthenium, atomic numbers 40 to 44). Although the first members ($_{90}$Th, $_{91}$Pa) of the group 90 to 94 show a great deal of resemblance in chemical properties to the first members ($_{72}$Hf, $_{73}$Ta) in the 5d transition series and to the first members ($_{40}$Zr, $_{41}$Cb) in the 4d transition series, the later members ($_{93}$Np, $_{94}$Pu) show practically no resemblance to $_{75}$Re and $_{76}$Os or to element 43 and $_{44}$Ru. Neptunium and plutonium are much more electropositive in character than the noble elements rhenium, element 43, osmium and ruthenium. There is no evidence for a volatile plutonium tetroxide in contrast with the volatile osmium and ruthenium tetroxides, and there is no evidence for an oxidation number of VIII in plutonium. Thus it seems certain that the transition in the elements 89 to 94 does not involve the simple filling in of the 6d shell.

On the other hand, the chemical properties of neptunium and plutonium are very similar to those of uranium and thorium and are such as to suggest that the 5f shell is being filled and that we are dealing with another rare-earth series similar to the well-known lanthanide series, $_{58}$Ce–$_{71}$Lu, in which the 4f shell becomes filled. Many people had suggested, on the basis of considerations of electronic structure, that a rare-earth-like series should begin in this region. There has been a large degree of uncertainty in these predictions with regard to the starting point of this series. The two principal choices have been between a thoride and a uranide series. From the standpoint of the chemical properties of $_{90}$Th, $_{91}$Pa and $_{92}$U considered alone, the evidence for such a series was not strong. However, with the discovery of neptunium and plutonium and the observation of the marked similarity of these elements to uranium and thorium in chemical properties, the chemical evidence for a rare-earth-like series has become very strong.

The persistence of the IV oxidation state through the elements thorium, uranium, neptunium and plutonium is certainly good evidence that electrons are going into the 5f shell. The observation by Zachariasen of the isomorphism of the compounds ThO_2, UO_2, NpO_2 and PuO_2 and his observation of the regular decrease in radius of the metallic ion in these oxides in the anticipated manner are also very good evidence that the electrons are going into the 5f shell. A number of other crystallographic observations by Zachariasen lend support to this view. There are other points of evidence, e.g., (1) magnetic susceptibility measurements on uranium and plutonium, (2) the sharpness of the optical absorption in aqueous solutions of uranium and plutonium and (3) evidence for organic complexes of U^{+4} and Pu^{+4} in which these elements have a coordination number of 8 (indicating that the 6d, 7s and 7p orbitals are available), which facts also give strong support to this conclusion. It seems very probable from these lines of evidence that uranium and plutonium (and neptunium) have electrons in the 5f shell; however, it is not possible to deduce whether or not uranium is the first element in the series for which this is the case. It would be consistent with this evidence for thorium and protactinium to have no electrons in the 5f shell and for uranium to have two electrons in this shell.

An attractive hypothesis is that this rare-earth-like series begins with actinium in the same sense that the lanthanide series begins with lanthanum. On this basis it may be termed the "actinide series", and the first 5f electron may appear in thorium. Thus, the ground state of thorium may have the structure $5f^1\ 6d\ 7s^2$ beyond the radon core. With an actinide series, uranium may have the electron configuration $5f^3\ 6d\ 7s^2$, neptunium the configuration $5f^4\ 6d\ 7s^2$ and plutonium the configuration $5f^5\ 6d\ 7s^2$. It is very interesting to note that Kiess et al. (1944) give a preliminary description of the analysis of the spectrum of neutral uranium atoms and come to the conclusion that the electron configuration of the lowest state of uranium is $5f^3\ 6d\ 7s^2$ (with the term symbol $^5L_6$), which supports the above view.

It may be that, as in the lanthanide series, electrons do not tend to occupy the 6d orbital; rather, an additional electron goes into a 5f orbital and gives, e.g., the configuration $5f^2\,7s^2$ for thorium and the configuration $5f^4\,7s^2$ for uranium. There is evidence that thorium emits a complex spectrum corresponding to a rare earth with an electron structure like that of $_{58}$Ce, whose ground state is known to have the configuration $4f^2\,6s^2$, and that uranium has a spectrum similar to that of the rare-earth element $_{60}$Nd, whose ground state is known to have the configuration $4f^4\,6s^2$.

It may be, of course, that there are no 5f electrons in thorium and protactinium and that the entry into a rare-earth-like series begins at uranium, with three electrons in the 5f shell. It would still seem logical to refer to this as an actinide series.

In an actinide series it may seem rather peculiar at first sight that the persistent oxidation number of IV should be in this region. The IV oxidation state seems to be most prevalent and generally most stable among these elements. However, as referred to above, in the lanthanide series there are usually only two electrons present in the 5d and 6s shells, whereas the persistent oxidation state is certainly III. This generally involves the removal of a 4f electron. There are also a number of cases in the lanthanide series where the oxidation number IV is found. In the "actinide" series, although the oxidation number IV is perhaps prevalent, the oxidation number III seems also to be found in most of the members of the series. Zachariasen has recently reported crystallographic evidence for tripositive thorium compounds (ThF_3 and ThOF), although magnetochemical experiments by Selwood have failed to confirm this report.

There is one way in which the actinide series definitely differs from the lanthanide series. This is in the existence of oxidation states higher than IV [protactinium (V), uranium (VI), neptunium (VI), plutonium (VI)] in this series. It must be concluded that the 5f electrons are not so tightly bound as the 4f electrons. This is certainly reasonable. However, the evidence so far is in favor of a maximum oxidation number of VI in this series, so that the removal of three electrons, or four if there are no electrons in the 6d orbitals, from the 5f orbitals is the maximum that occurs in ordinary chemical reactions.

It is interesting to speculate a little about the chemical properties of the series members which we have not yet had an opportunity to study. The element $_{91}$Pa is obviously interesting to study from a chemical and crystallographic point of view in order to throw further light on the situation. It seems very likely that this element will have oxidation states of IV and III in addition to the V state, and probably at least the IV state will have a reasonable amount of stability. It seems almost certain, also, that neptunium will have an oxidation state of III, intermediate in stability between U^{+3} and Pu^{+3}. If the picture of the actinide series is correct, the configuration $5f^7\,6d^1\,7s^2$ may be reached with element 96 (similar to the configuration of $_{64}$Gd); this configuration should be especially stable. The prediction may be made that with element 96 it will be very difficult, if not impossible, to reach any oxidation states above III or IV. In the case of element 95 the configuration of $5f^7\,7s^2$, similar to $_{63}$Eu, may be possible, and it may be expected that the oxidation state II will exist. Oxidation states higher than IV may also be difficult or impossible to reach in the case of element 95. There already seems to be some evidence for a trend toward greater stability for the lower oxidation states in the members of the series that have been studied so far. Thus, in going from uranium to plutonium, there seems to be a trend toward greater stability of the III oxidation state and greater difficulty in reaching the VI state. If the series is truly a thoride or a uranide series, the most stable lower oxidation states will occur at elements beyond 95 and 96; however, even in this event some tendency may be expected in this direction at elements 95 and 96. It would obviously be of great interest and value in elucidating the nature of this series to study the chemical properties of elements such as 95 and 96."

The recognition that the elements with the atomic numbers 95 and 96 should have relatively stable lower (i.e., III) oxidation states made it possible, during the ensuing months, to chemically identify (i.e., discover) these elements at the wartime Metallurgical Laboratory following their production by nuclear synthesis reactions. I made the announcement of this discovery at a symposium at Northwestern University on Friday, November 16, 1945 (following my premature disclosure of this discovery to a national radio audience when I appeared as a guest on the "Quiz Kids" program the preceding Sunday). This talk was published by me in *Chemical and Engineering News* the following month (Seaborg 1945). This was my first open publication of a description of the actinide concept. Following is a quote from the article.

"The elements 90 to 94 lie in corresponding positions just below the sixth period transition elements Hf to Os (atomic numbers 72 to 76) in which the 5d electron shell is being filled. The transition elements Hf to Os are similar in their chemical properties to the corresponding 4d transition elements in the fifth period (Zr to Ru, atomic numbers 40 to 44). Although the first members ($_{90}$Th, $_{91}$Pa) of the group 90 to 94 show a great resemblance in chemical properties to the first members ($_{72}$Hf, $_{73}$Ta) in the 5d transition series and to the first members ($_{40}$Zr, $_{41}$Cb) in the 4d transition series, the later members ($_{93}$Np, $_{94}$Pu) show practically no resemblance to $_{75}$Re and $_{76}$Os and to element 43 and $_{44}$Ru. This suggests that it is the 5f electron shell which is being filled, although it is not possible to deduce from this chemical evidence alone whether uranium is the first element in the series for which this is the case. While it is beyond the scope of this discussion to give all the supporting evidence, we would like to advance the attractive hypothesis that this rare-earth-like series begins with actinium in the same sense that the "lanthanide" series begins with lanthanum. On this basis it might be termed the "actinide" series and the first 5f electron might appear in thorium. Thus, the characteristic oxidation state – i.e., the oxidation state exhibited by those members containing seven 5f and fourteen 5f electrons – for this transition series is III.

The oxidation state of IV demonstrated by thorium is then analogous to the IV oxidation state of cerium. From the behavior of uranium, neptunium and plutonium it must be deduced that as many as three of the assumed 5f electrons are readily given up, so that the failure of thorium to demonstrate an oxidation state of III is accounted for. On the basis of this hypothesis, elements 95 and 96 should exhibit very stable III states; in fact, element 96 should exhibit the III state almost exclusively because, with its seven 5f electrons, it should have an electron structure analogous to that of gadolinium, with its seven 4f electrons.

The experiments of G.T. Seaborg, R.A. James, L.O. Morgan and A. Ghiorso in the Metallurgical Laboratory have recently led to the identification of isotopes of elements 95 and 96, making it possible to study the chemical properties of these isotopes by the tracer technique. These investigators have studied the products produced as a result of the bombardment of ^{238}U and ^{239}Pu with very high energy (40 MeV) helium ions in the Berkeley cyclotron. This work was made possible by the vital participation and cooperation of J.G. Hamilton and his group at the University of California, who have recently rebuilt the 60-inch cyclotron to produce the high-energy particles needed and who performed the bombardments.

Of course, in the case of some of the elements in the series it may be something of an academic matter to assign electrons to the 5f or 6d shells, as the energy necessary for the shift from one shell to the other may be within the range of chemical binding energies. The electron configuration may differ from compound to compound of an element or even with

PERIODIC TABLE SHOWING HEAVY ELEMENTS AS MEMBERS OF AN ACTINIDE SERIES

Arrangement by Glenn T. Seaborg, 1945

1 H 1.008																1 H 1.008	2 He 4.003
3 Li 6.940	4 Be 9.02											5 B 10.82	6 C 12.010	7 N 14.008	8 O 16.000	9 F 19.00	10 Ne 20.183
11 Na 22.997	12 Mg 24.32	13 Al 26.97										13 Al 26.97	14 Si 28.06	15 P 30.98	16 S 32.06	17 Cl 35.457	18 A 39.944
19 K 39.096	20 Ca 40.08	21 Sc 45.10	22 Ti 47.90	23 V 50.95	24 Cr 52.01	25 Mn 54.93	26 Fe 55.85	27 Co 58.94	28 Ni 5869	29 Cu 63.57	30 Zn 65.38	31 Ga 69.72	32 Ge 72.60	33 As 74.91	34 Se 78.96	35 Br 79.916	36 Kr 83.7
37 Rb 85.48	38 Sr 87.63	39 Y 88.92	40 Zr 91.22	41 Cb 92.91	42 Mo 95.95	43	44 Ru 101.7	45 Rh 102.91	46 Pd 106.7	47 Ag 107.880	48 Cd 112.41	49 In 114.76	50 Sn 118.70	51 Sb 121.76	52 Te 127.61	53 I 126.92	54 Xe 131.3
55 Cs 132.91	56 Ba 137.36	57 LA 138.92	58-71 SEE La SERIES	72 Hf 178.6	73 Ta 180.88	74 W 183.92	75 Re 186.31	76 Os 190.2	77 Ir 193.1	78 Pt 195.23	79 Au 197.2	80 Hg 200.61	81 Tl 204.39	82 Pb 207.21	83 Bi 209.00	84 Po	85	86 Rn 222
87	88 Ra	89 AC	SEE Ac SERIES	90 Th	91 Pa	92 U	93 Np	94 Pu	95	96							

LANTHANIDE SERIES	57 La 138.92	58 Ce 140.13	59 Pr 140.92	60 Nd 144.27	61	62 Sm 150.43	63 Eu 152.0	64 Gd 156.9	65 Tb 159.2	66 Dy 162.46	67 Ho 163.5	68 Er 167.2	69 Tm 169.4	70 Yb 173.04	71 Lu 174.99
ACTINIDE SERIES	89 Ac	90 Th 232.12	91 Pa 231	92 U 238.07	93 Np 237	94 Pu	95	96							

Fig. 2. Periodic table showing heavy elements as members of an actinide series. Arrangement by Seaborg (1945).

the physical state of a given compound. This shifting of electron configuration would probably be most pronounced with the middle members of the first half of the series – i.e., uranium, neptunium and plutonium. Since the energy difference between the 5f and 6d shells is rather small and since the resonance effects should be rather large, the latter may predominate in determining which energy level lies lowest.

It is probably worthwhile to make a brief summary at this point with the following statements. As of today, the periodic system consists of 96 known, identified elements – i.e., there is now positively known at least one isotope, stable or radioactive, for each of the elements from atomic number 1 to atomic number 96, inclusive. The evidence points to an atomic structure for the heaviest elements – i.e., those elements with atomic number greater than 88 – corresponding to a transition series in which the 5f shell of electrons is being filled. This series differs in chemical properties from the rare-earth series (the 14 elements of atomic number 58 to 71, inclusive, following lanthanum) in which the 4f shell of electrons is being filled, in that the first members of this heavy series are much more readily oxidized to oxidation states greater than III. As the atomic numbers of the elements in this series increase, the lower oxidation states, and particularly the III state, increase in stability. The first 5f electron probably appears in thorium and the stable configuration consisting of seven 5f electrons probably comes with element 96."

Included in that article was the version of the periodic table shown in fig. 2.

The clearance process (i.e., removal of secrecy classification) did not allow me to state explicitly in the article that elements 95 and 96 exhibited very stable lower (i.e., III) oxidation states. This was stated explicitly in a later article (Seaborg 1946). I announced names for these elements – americium (Am) for element 95 and curium (Cm) for element 96, by analogy with the naming of the homologous lanthanide elements, europium and gadolinium – on April 10, 1946 at a meeting of the American Chemical Society in Atlantic City the following spring.

3. Further development of actinide concept

About three years later (in 1949), I published the following account of the status of the actinide concept (Seaborg 1949).

"CORRELATIONS AND DEDUCTIONS"

3.1. *Electronic configurations*

Table 5 gives what appears to be the configuration or the best prediction for the configuration, beyond the radon structure, of the ground state of the neutral gaseous atom for each of the elements actinium to curium, inclusive. The trend in the chemical properties with its implication that the 5f becomes progressively of lower energy, compared to the 6d level, as the atomic number increases, has been used as an aid in making the predictions.

The configurations beyond xenon, of the corresponding neutral rare-earth elements are given (Yost et al. 1947, Meggers 1947, Klinkenberg 1947) for comparison. The ground states given for cerium and praseodymium are those predicted (Yost et al. 1947, Klinkenberg 1947) on the basis of the recently determined ground states of the singly ionized atoms

TABLE 5
Suggested electron configurations (beyond radon and xenon) for gaseous atoms of actinide and lanthanide elements.

Atomic No.	Element	Configuration	Atomic No.	Element	Configuration
89	Ac	$6d\,7s^2$	57	La	$5d\,6s^2$
90	Th	$6d^2\,7s^2$ (or $5f\,6d\,7s^2$)	58	Ce	$4f^2\,6s^2$
91	Pa	$5f^2\,6d\,7s^2$ (or $5f\,6d^2\,7s^2$)	59	Pr	$4f^3\,6s^2$
92	U	$5f^3\,6d\,7s^2$	60	Nd	$4f^4\,6s^2$
93	Np	$5f^5\,7s^2$ (or $5f^4\,6d\,7s^2$)	61	Pm	$4f^5\,6s^2$
94	Pu	$5f^6\,7s^2$ (or $5f^5\,6d\,7s^2$)	62	Sm	$4f^6\,6s^2$
95	Am	$5f^7\,7s^2$	63	Eu	$4f^7\,6s^2$
96	Cm	$5f^7\,6d\,7s^2$	64	Gd	$4f^7\,5d\,6s^2$

(Meggers 1942) and that of element 61 is obtained by interpolation; consequently, these are subject to some doubt. The ground states given for neodymium (Schuurmans 1946), samarium, europium and gadolinium are those spectroscopically determined (Meggers 1942) for the neutral atoms and should be considered as well established.

It should be emphasized that it would be entirely consistent from the point of view that we are dealing here with a series of actinide elements if it should eventually be found that there are no 5f electrons present in thorium (or protactinium). It is quite possible, on the basis of present evidence, that protactinium, or even uranium, may be the first to have 5f electrons. It seems very likely, however, that electrons will be placed in the 5f shell earlier in the series than uranium and that protactinium will have at least one such electron. An essential point is that curium definitely seems to have seven 5f electrons, and element 103 probably would have fourteen 5f electrons.

In the case of some of the elements in the series it may be difficult to assign electrons to the 5f or 6d shells, because the energy necessary for the shift from one shell to the other may be within the range of chemical binding energies. Many of the experimental facts already described, such as the ease of oxidation to higher states and the more complicated situation for the magnetic susceptibilities as compared to the rare-earth elements, point to lower binding and less electrostatic shielding by outer electrons of 5f than of 4f electrons. This was to be expected, and the magnitude of these effects seems reasonable. The electronic configuration may differ from compound to compound or even with the physical state of a given compound. Moreover, one certainly cannot be sure that the configuration of the gaseous atom, e.g., will correspond to that of the compounds or of the hydrated ions in solution. In the case of the lanthanides, in fact, the configuration of the gaseous atom has in general only two electrons (beyond the xenon structure) outside the 4f shell, although the predominant oxidation state is certainly the III state. Since the energy difference between such far-outlying levels as the 5f and 6d shells is rather small, and since resonance effects should be rather large, these may predominate in determining that a composite energy level lies lowest. Thus, some of these elements may possibly constitute what might more properly be called a 5f–6d range in this series rather than being considered as part of a totally 5f transition group.

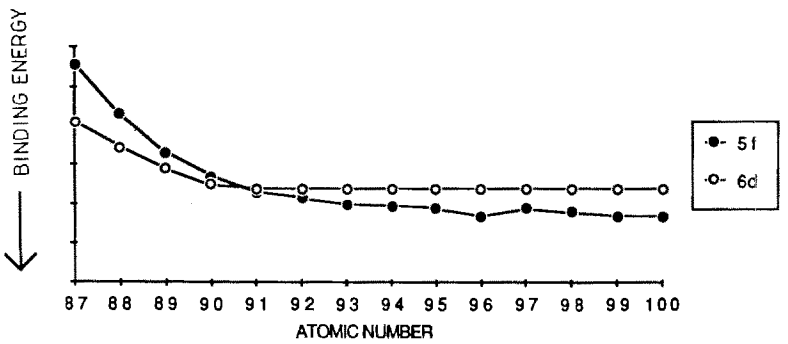

Fig. 3. Qualitative representation of electronic binding energies in the heaviest elements.

The evidence that has accumulated so far seems, nevertheless, to point to lower energies for the 5f levels, as compared to the 6d levels, for the compounds of the element, as early as uranium in this series. It is in the case of the elements thorium and protactinium that the relative energy positions of these levels are as yet most uncertain. As in the other transition series, the relative energy level of the shell that is undergoing the filling process becomes lower as the successive electrons are added, and by the time americium and curium, and presumably the subsequent members of the series, are reached, the 5f shell seems clearly to be of lower energy than the 6d shell. Also, it is not yet possible to place the electrons in neptunium and plutonium with confidence, and hence in table 5 alternative structures for gaseous neptunium and plutonium are suggested. It seems quite possible, for those elements in which the energies are so nearly equal, that the 5f as well as the 6d and outer orbits may be involved in the chemical binding in some compounds and complex ions, an interesting possibility for a new type of bonding.

Figure 3 is an extremely rough and qualitative pictorial representation of the binding energy of the most easily removable 5f and 6d electron (of those present) for each of the heaviest elements. A rough representation such as this can be justified only if it helps somewhat in the understanding of the situation. It is hoped that such is the case.

3.2. *Possible deductions without data on transuranium elements*

Although it is the information on the transuranium elements that has been decisive in enabling us to come to the present view concerning the electronic structure of, or, more properly speaking, the best position in the periodic table for, the heaviest elements, it is interesting to conjecture, in retrospect, whether it would have been possible to arrive at a similar conclusion without this information. Actually, there has been much information about actinium, thorium, protactinium and uranium, especially about the latter, which pointed in this direction... there is the similarity among the metals of these elements with respect to electropositive character. In addition, the melting point of uranium metal seems to relate it more closely to the immediately preceding elements than to tungsten and molybdenum...

Uranium differs considerably from tungsten and molybdenum in the chemistry of the lower oxidation states. Uranium (III) has great similarity to the tripositive rare-earth elements and actinium, and uranium (IV) resembles thorium and cerium (IV). Thus uranium (III) and uranium (IV) are not acidic in character; they do not tend, like tungsten

and molybdenum, to form such exceedingly strong complex ions in solution; they have fluorides that are insoluble and isomorphous with the fluorides of the rare-earth elements; and they have other halides with crystal structures that are in general isomorphous with the corresponding rare-earth halides. On the other hand, tungsten (III) and tungsten (IV) exist in aqueous solution predominantly as strong complex ions; e.g., tungsten (III) has a strong chloride complex ion, and tungsten (IV) forms strong fluoride and cyanide complex ions. In this connection Thompson (1947) has pointed out that tungsten (IV) forms the very stable complex ion $W(CN)_8^{-4}$ with the stable configuration of eighteen outer electrons, but uranium (IV) possesses no significant tendency to form an analogous complex cyanide ion, as would probably be expected if uranium possessed the same outer electronic structure as tungsten.

Although molybdenum dioxide and tungsten dioxide have isomorphous crystal structures, tungsten dioxide and uranium dioxide do not, but uranium dioxide, thorium dioxide, and cerium dioxide do have isomorphous structures. It is interesting to note that although uranium is not associated with tungsten in minerals, uranium and thorium minerals practically always have the rare-earth elements associated with them, and the rare-earth minerals practically always contain uranium or thorium.

Arguments on the basis of the scanty evidence from the chemical properties of thorium and uranium alone have been given by others, including Villar (1940) and, more recently, Stedman (1947), for a 5f-type transition series in the heaviest elements, beginning with thorium.

3.3. *Position in periodic table and nomenclature*

Soon after the establishment of the concept of atomic number, the rare-earth elements could be properly fitted into the classification of the elements, and the periodic table took its present form. There is general agreement as to the various groups and subgroups, with differences only in regard to the best geometrical arrangements for presenting the information. Thus, even the undiscovered elements with atomic numbers within the confines of this classification had their places fixed, and, when they were discovered, no reasons were found to change their positions. However, this is not the situation with respect to the transuranium elements, whose positions could only be fixed after experimental determination of their properties. Their positions, in turn, apparently influence the positions of elements that had been given places previously.

Since this seems to present a new problem, it is necessary to consider carefully the facts that have given rise to the present classification in order to try to find the traditional criteria for placement in the periodic table to apply to the elements now under consideration. The chemical properties, especially in aqueous solution, have been important criteria. Thus, the rare-earth elements assumed a position by virtue of their predominant trivalency in aqueous solution, a property that is not deducible from the electronic structure of their atomic ground states. However, the spectroscopic data have determined the general regions of the transition series, where the 3d, 4d, 5d and 4f shells undergo filling, and seem to have influenced the practice of uninterrupted placing of the transition elements in subgroups. (That is, all ten 3d transitioin elements from $_{21}$Sc to $_{30}$Zn are usually in uninterrupted subgroups, and the same holds true for the 4d, 5d and 4f transition series.)

With such criteria the best method of presenting the actinide elements in the periodic table seems to be that shown in fig. 4. Here are shown the fourteen elements of atomic

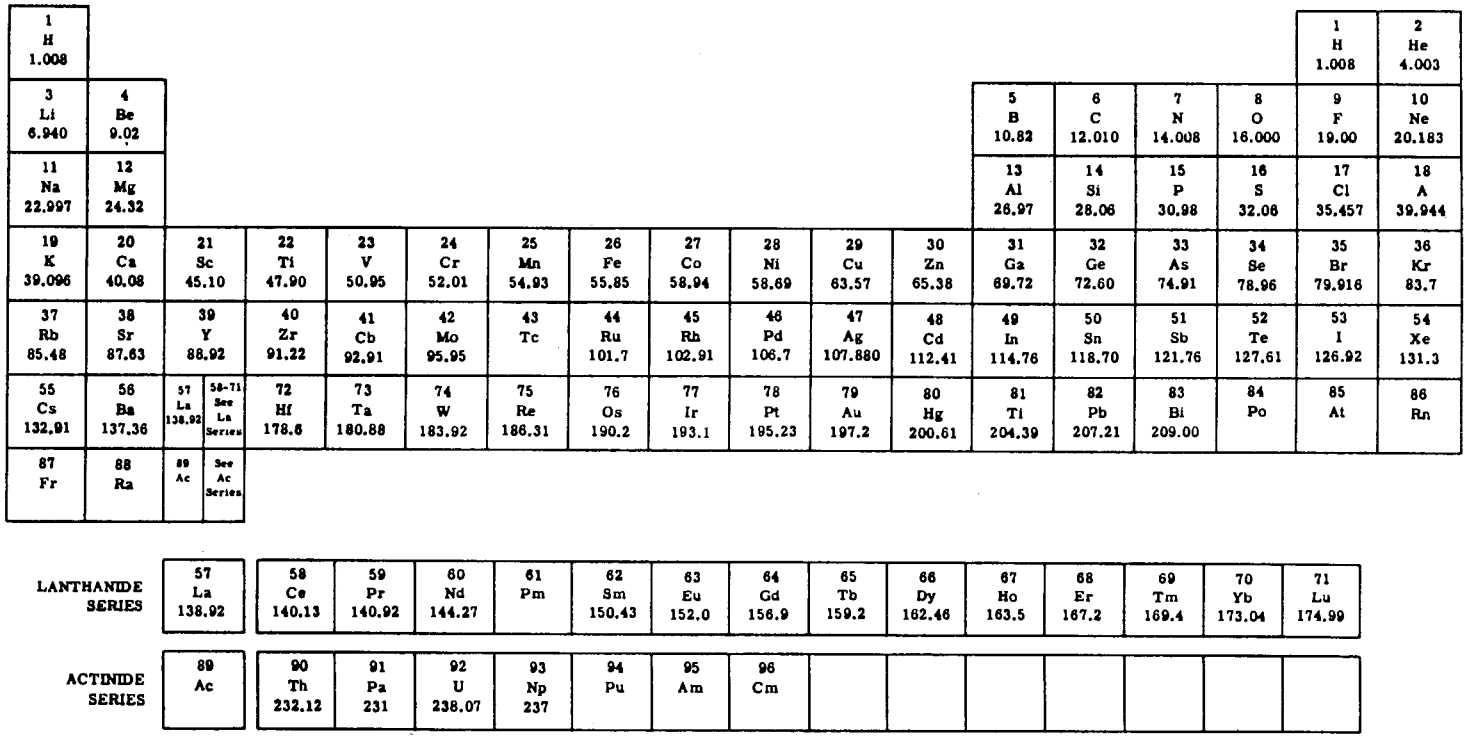

Fig. 4. Periodic table showing heavy elements as members of an actinide series in 1949.

numbers 90 to 103, inclusive, with actinium, element 89, as the prototype. These fourteen elements are listed as a series below, and in a manner similar to the common listing of the fourteen rare-earth elements of atomic numbers 58 to 71, inclusive, for which lanthanum, element 57, is the prototype. It is not suggested that this particular form of the periodic table has any more merit than any of a number of others that place these elements in positions homologous to the rare-earth elements, because it is obvious that they can be analogously placed in a number of other types of tables or charts. The elements 90 to 96, inclusive, or the first few of them, could in addition be listed separately below the 5d elements in recognition of the resemblance of the first few of these to 5d elements. This appears to be undesirable, however, because the last members of this group bear no such resemblance, and it is probably impossible to draw a line as to just where the resemblance ends.

Since my suggestion (Seaborg 1945, 1946) that the information on the transuranium elements appeared to have reached such a state as to make it possible to place the heaviest elements in definite positions in the periodic table (as an actinide transition series), a number of publications (Zimen 1948, Harvey 1948, Meggers 1947, Spence 1949, Maddock 1948, Purkayastka 1948, Hardwick 1947) commenting on this proposal have appeared. These in general agree with the suggestion, although in some cases the reasons therefore differ and in others there is an understandable expression of desire to see more of the evidence in detail. A number of different periodic tables in which these elements have been placed as actinides homologous to the lanthanides have been published recently (Wheeler 1947, Summons 1947, Villar 1947, Oppegaard 1948, Akhumov 1947).

As mentioned above, a very important point is the presence of seven 5f electrons in stable tripositive curium (element 96), making this element very actinium-like. A series of thoride elements, e.g., would imply stable IV oxidation states in elements 95 and 96 and the presence of seven 5f electrons and the IV state almost exclusively in element 97. A series of this type seems to be ruled out by the now-known instability of americium in solution in the IV state and by the apparent non-existence in aqueous solution of any oxidation state other than III in curium. Moreover, the III state of uranium would be surprising on this basis, because this element would be the second member of a thoride, or "IV oxidation state", series. The fact that nearly a year was spent in an unsuccessful effort to separate tracer amounts of americium and curium from the rare earths, immediately following the discovery of these two elements, illustrates how unnatural it would be to regard them as members of a thoride, or IV oxidation state, group.

The group probably could have been described just as well by some other term, such as "curide series", rather than "actinide", which is derived by analogy with the term "lanthanide". Another possibility would be to use a term such as "type 5f rare earths" or another name analogous to rare earths. A possibility here might be "synthetic earths" in view of the synthetic source of all except the first three members. [The best source of actinium is synthetic; actinium comes from pile neutrons by the reactions Ra^{226} (n, γ) $Ra^{227\beta^-} \rightarrow Ac^{227}$.] Irrespective of the name that usage will finally assign to this group of elements, however, it seems that the outstanding characteristics of the group, namely, the ekagadolinium character of curium (and the presumed ekalutecium character of element 103), together with the regularly increasing trend toward actinium-like character in going from thorium to curium, are best represented by listing these elements in corresponding positions under the rare-earth elements if it is desirable to give each element only one place in the periodic table.

3.4. *Predicted properties of transcurium elements*

There has been a great deal of speculation concerning the upper limit of atomic number for the existence of elements, consideration being given to the fact that such a limit might arise from either atomic or nuclear (radioactivity or spontaneous fission) instability. If the former is not the limiting factor, it appears likely, on the basis of extrapolation from the nuclear properties of the heaviest elements, that the first few elements above element 96 will have isotopes of sufficiently long life to make possible their investigation at least on the tracer scale, if the problem of their production in detectable amount should be solved.

It is interesting to speculate about the chemical properties of these undiscovered elements beyond curium. The seven elements immediately following i.e., elements 97 to 103, inclusive, should constitute the second half of this rare-earth-like transition group. It appears likely that the electrons added in proceeding up this series will be placed in a 5f shell of definitely lower energy than the 6d shell. Element 97 will probably have a IV as well as a III oxidation state, and in view of the lower binding energy of the 5f as compared to the 4f electrons it might be easier to oxidize element 97 (ekaterbium) to this IV state than is the case for terbium since the hydration and lattice energies do not appear to reverse the simple prediction for oxidation potentials from ionization potentials in these elements. Correspondingly, it should be easier to oxidize element 98 (ekadysprosium) to the IV and V oxidation states than is the case for dysprosium, for which oxidation above the III state is practically impossible. Toward the end of the series, elements 102 and 101 should be capable of being reduced to the II oxidation state, which would be analogous to the reduction of ytterbium and thulium, and element 103 should be similar to lutetium with respect to the complete stability of the III state.

Element 104 should continue with the filling of the 6d shell and be a true ekahafnium. After the filling of the 6d shell in the following elements there would be addition to the 7p shell, with the attainment of the rare-gas structure at hypothetical element 118 (on the logical assumption that the 5g shell does not start to fill before this point).

3.5. *Summary*

All available evidence leads to the view that the 5f electron shell is being filled in the heaviest elements, giving rise to a transition series. This transition series begins formally with actinium in the same sense that the rare-earth or "lanthanide" series begins with lanthanum. Such an "actinide" series is suggested on the basis of the following evidence: (1) chemical properties, (2) absorption spectra in aqueous solution and crystals, (3) crystallographic structure data, (4) magnetic susceptibility data and (5) spectroscopic data. This series differs from the rare-earth series in having more oxidation states above the III state, and it differs in other ways that are connected with the lower binding of 5f compared to 4f electrons. The salient point is that the characteristic oxidation state is the III state, and the group is placed in the periodic table on this basis. (The characteristic oxidation state is exhibited by the member containing seven 5f electrons and presumably also by the member containing fourteen 5f electrons, curium and element 103.) The data also make it possible to give a suggested table of electronic configurations of the ground state of the gaseous atom for each of the elements from actinium to curium, inclusive."

4. Completion of actinide series

The following seven elements, completing the actinide series as predicted at element 103, were synthesized and identified (i.e., discovered) during the following twelve years (i.e., by the year 1961). Their chemical properties conformed very well with those predicted on the basis of the actinide concept. Elements 104 and 105, the first elements beyond the actinide series, were later also shown to have the predicted chemical properties. I summarized the situation in my book, *Man-Made Transuranium Elements* (Seaborg 1963), as follows.

"Table 6 presents the electronic configuration, or the best prediction for the electronic configuration, of the gaseous atoms of the actinide elements. Similar information for the lanthanide elements is given for purposes of comparison. The configurations enclosed in parentheses are predicted ones.

As shown in table 6, fourteen 4f electrons are added in the lanthanide series, beginning with cerium (atomic number 58) and ending with lutetium (atomic number 71); and in the actinide elements fourteen 5f electrons are added, beginning formally (although not actually) with thorium (atomic number 90) and ending with lawrencium (atomic number 103). In the cases of actinium, thorium, uranium and americium, the configurations were determined from an analysis of spectroscopic data obtained by the measurement of the emission lines from neutral and charged gaseous atoms. The knowledge of the electronic structures for protactinium, neptunium, plutonium and curium results from atomic-beam experiments.

TABLE 6
Electronic configurations for gaseous atoms of actinide and lanthanide elements (predicted configurations are given in parentheses).

Atomic number	Element	Electronic configuration[a]	Atomic number	Element	Electronic configuration[b]
89	actinium	$6d\,7s^2$	57	lanthanum	$5d\,6s^2$
90	thorium	$6d^2\,7s^2$	58	cerium	$4f\,5d\,6s^2$
91	protactinium	$5f^2\,6d\,7s^2$	59	praseodymium	$4f^3\,6s^2$
92	uranium	$5f^3\,6d\,7s^2$	60	neodymium	$4f^4\,6s^2$
93	neptunium	$5f^4\,6d\,7s^2$	61	promethium	$4f^5\,6s^2$
94	plutonium	$5f^6\,7s^2$	62	samarium	$4f^6\,6s^2$
95	americium	$5f^7\,7s^2$	63	europium	$4f^7\,6s^2$
96	curium	$5f^7\,6d\,7s^2$	64	gadolinium	$4f^7\,5d\,6s^2$
97	berkelium	$(5f^8\,6d\,7s^2$ or $5f^9\,7s^2)$	65	terbium	$4f^9\,6s^2$
98	californium	$(5f^{10}\,7s^2)$	66	dysprosium	$4f^{10}\,6s^2$
99	einsteinium	$(5f^{11}\,7s^2)$	67	holmium	$4f^{11}\,6s^2$
100	fermium	$(5f^{12}\,7s^2)$	68	erbium	$4f^{12}\,6s^2$
101	mendelevium	$(5f^{13}\,7s^2)$	69	thulium	$4f^{13}\,6s^2$
102		$(5f^{14}\,7s^2)$	70	ytterbium	$4f^{14}\,6s^2$
103	lawrencium	$(5f^{14}\,6d\,7s^2)$	71	lutetium	$4f^{14}\,5d\,6s^2$

[a] In addition to the electronic structure of radon (element number 86), whose electronic configuration is : $1s^2\,2s^2\,2p^6\,3s^2\,3p^6\,3d^{10}\,4s^2\,4p^6\,4d^{10}\,4f^{14}\,5s^2\,5p^6\,5d^{10}\,6s^2\,6p^6$.

[b] In addition to the electronic structure of xenon (element number 54), whose electronic configuration is: $1s^2\,2s^2\,2p^6\,3s^2\,3p^6\,3d^{10}\,4s^2\,4p^6\,4d^{10}\,5s^2\,5p^6$.

It is important to realize that the electronic structures listed in table 6 are those of the neutral (un-ionized) gaseous atoms, whereas it is the electronic structure of the ions and compounds that we are chiefly concerned with in chemistry. The relationship of the electronic structure of the gaseous atom of an element to that of its compounds can be rather complicated. For example, in the case of the actinide and lanthanide elements, one would not necessarily predict the predominance of the III oxidation state from the electronic structures of the gaseous atoms; there are usually only two so-called "valence electrons", the 7s or 6s electrons, which might indicate a preference for the II oxidation state.

Apparently, specific factors in the crystal structure of, and the aquation (hydration) energies of, the compounds and ions are important in determining the stability of the III oxidation state. Thus, the characteristic tripositive oxidation state of the lanthanide elements is not related directly to the number of "valence electrons" outside the 4f subshell, but is the somewhat accidental result of a nearly constant small difference between large-energy terms (ionization potentials on the one hand, and hydration and crystal energies on the other) which persists over an interval of fourteen atomic numbers. Therefore, if we could somehow have a very extended periodic table of elements containing numerous "f" transition series, we might expect that the 5f, rather than the 4f, elements would be regarded as more nearly representative of such f series.

Nevertheless, the electronic structures given in table 6 will have some relevance to the electronic structures of the ions and compounds of these elements. Fortunately, it is possible to determine the electronic structure of the ions and compounds by a number of methods, such as the measurement of such properties as paramagnetic resonance, paramagnetic susceptibility, light absorption, etc. These measurements, together with consideration of the chemical and other properties of these elements, have provided a great deal of information about the electronic configurations of the aqueous actinide ions and of the actinide compounds. It is interesting to note that these data do show that, in general, all of the electrons – in addition to the radon core – in the actinide compounds and in aqueous actinide ions are indeed in 5f orbitals. There are very few exceptions (such as U_2S_3) and subnormal compounds (such as Th_2S_3) where 6d electrons are present.

Except for the early actinide elements, the III oxidation state is the characteristic oxidation state for each series of elements ... ease of oxidation of the early members of the actinide series is due to the looser binding of the 5f electrons early in the series and the nearness in energy of several electronic levels in this region (7s, 6d and 5f).

The electronic configurations $5f^7$ or $4f^7$, representing the half-filled f shells of curium and gadolinium, have special stability. Thus, tripositive curium and gadolinium, are especially stable. A consequence of this is that the next element in each case readily loses an extra electron through oxidation, so as to obtain the f^7 structure, with the result that terbium and especially berkelium can be readily oxidized from the III to the IV oxidation state. Another manifestation of this is that europium (and to a lesser extent samarium) – just before gadolinium – tends to favor the $4f^7$ structure with a more stable than usual II oxidation state. Similarly, the stable f^{14} electronic configuration leads to a more stable than usual II oxidation state in ytterbium (and to a lesser extent in thulium) just before lutetium (whose tripositive ion has the $4f^{14}$ structure). This leads to the prediction that element 102, the next to the last actinide element, will have an observable II oxidation state.

After the completion of the 5f shell at lawrencium (element 103, the last actinide element, it is predicted that electrons will be added to the 6d shell in the succeeding transactinide elements. It might be added, mainly for the sake of completeness, that the filling of the 6d

TABLE 7
Predicted electronic structures of some transactinide elements.

Element	Electronic structure[a]	Element	Electronic structure[a]
104	$5f^{14}\ 6d^2\ 7s^2$	112	$5f^{14}\ 6d^{10}\ 7s^2$
105	$5f^{14}\ 6d^3\ 7s^2$	113	$5f^{14}\ 6d^{10}\ 7s^2\ 7p^1$
106	$5f^{14}\ 6d^4\ 7s^2$	118	$5f^{14}\ 6d^{10}\ 7s^2\ 7p^6$
107	$5f^{14}\ 6d^5\ 7s^2$	120	$5f^{14}\ 6d^{10}\ 7s^2\ 7p^6\ 8s^2$
108	$5f^{14}\ 6d^6\ 7s^2$	125	$5f^{14}\ 5g^5\ 6d^{10}\ 7s^2\ 7p^6\ 8s^2$

[a] In addition to the electronic structure of radon (element number 86).

shell should be followed by the addition of electrons to the 7p shell, with the attainment of the rare-gas structure at hypothetical element 118. The filling of the 5g shell, corresponding to a wholly new kind of inner transition series of eighteen elements, is predicted to begin at about this region of atomic numbers. It is unfortunate that nuclear instability precludes the possibility of synthesizing and studying such very interesting elements. The predicted electronic structures of some transactinide elements are given in table 7".

5. Superactinide elements

In table 7 note is taken of the existence of the next "rare-earth" series containing 5g electrons. The predicted nature of this inner transition series, corresponding to the filling of the 5g and 6f electron shells, and which I characterized as a "superactinide" group, is described in an article I published in 1968 (Seaborg 1968).

" Predicted electronic configuration and chemical properties of superactinide elements. Although it is uncertain as to the exact point where the 5g or 6f subshells begin to be filled (because the energy levels of the two subshells may be very close together), it seems likely that in a formal sense this would begin at element 122. It is interesting to speculate on the electronic structure and chemical properties of such a "superactinide" group of elements in which the 18 places in the 5g electron shell and the 14 places in the 6f electron shell might be filled in a comingling fashion, leading to a mixed transition series of 32 elements terminating at $Z = 153$. I believe that the best way of fitting them into the periodic table of the elements – although this is admittedly an approximation and a matter of finding the best compromise – is as a third rare-earth type of transition series below the lanthanide and actinide series. Thus in this oversimplification of a complicated situation the elements beyond element 121 would be considered as homologs of the elements beyond lanthanum (atomic number 57) and actinium (atomic number 89) on an element-by-element basis ... If the analogy is valid, the III oxidation state of the "superactinide" group should be typical. However, there are reasons to expect deviations. At the beginning of the series, as is the case for the actinides and for similar reasons, we might expect higher oxidation states to be readily reached. Somewhat later in the series we might expect to find a prominent II oxidation state, analogous to the effect observed in the heavier actinides ".

6. Status of actinide elements

As the result of increasing sophistication of the experiments, a large range of oxidation states of the actinide elements is known, which are summarized in table 14.4 of Katz et al. (1986) which is reproduced here. These are well understood on the basis of the actinide concept, fitting in well with the expected stability of the III oxidation state of the middle element (element 96 with the half-filled $5f^7$ structure) and the last element (element 103 with the filled $5f^{14}$ structure).

The actinides show an unusually broad range of oxidation states, ranging from +2 to +7 in solution, as summarized by Loveland and I (Seaborg and Loveland 1990). The most common oxidation state is +3 for the transplutonium actinide elements, similar to the lanthanides, with +2 oxidation states being observed for the heaviest species. A stable +4 state is observed for the elements thorium through plutonium and berkelium. The +5 state is well established for protactinium through americium and the +6 state for uranium through americium. Following the normal trend for polyvalent cations, lower oxidation states are stabilized by acid conditions while the higher oxidation states are more stable in basic solutions. Complexing can, of course, change this general trend.

In compounds of the +2, +3, +4 oxidation states, the elements are present as simple M^{+2}, M^{+3} or M^{4+} cations but for higher oxidation states, the most common forms in compounds and in solution are the oxygenated actinyl ions MO_2^+ and MO_2^{2+}. Disproportionation reactions are an important part of the chemistry of the actinide elements, especially for the +4 and +5 oxidation states.

A few comments on the various oxidation states found in solution follow:

M (I) The existence of Md^+ has been reported by Mikheev et al. (1973) but studies by other groups have failed to confirm these observations (Hulet et al. 1980).

M (II) Both No^{2+} and Md^{2+} form readily in solution. No^{2+} is the most stable oxidation state of nobelium, a result of the stability of the completely filled $5f^{14}$ shell. Pulse radiolysis of acid solutions has been used to make unstable Am^{2+}, Cm^{2+}, Bk^{2+}, Cf^{2+} and Es^{2+}. Fm^{2+} is more stable than these ions but less stable than Fm^{3+}.

M (III) The +3 oxidation state is the most stable oxidation state for americium through mendelevium and for lawrencium. It is easy to produce Pu^{3+} and Np^{3+}, but U^{3+} is such a strong reducing agent that it is difficult to keep in solution.

M (IV) The most stable oxidation state of thorium is +4. Pa^{4+}, U^{4+} and Np^{4+} are stable but are oxidized by O_2. Pu^{4+} is stable in acid solutions with low plutonium concentration. Americium, curium and californium can be oxidized to the +4 state with strong oxidizing agents like persulfate, pulse radiolysis or other strong oxidation and complexation techniques. Bk^{4+} is relatively stable as a result of the half-filled shell, $5f^7$.

M (V) The actinides protactinium through americium form MO_2^+ ions in solution. PuO_2^+ may be the dominant species in solution in low concentrations in natural waters that are relatively free of organic materials.

TABLE 14.4

The oxidation states of the actinide elements. The most common oxidation states are underlined, unstable oxidation states are shown in parentheses. Question marks indicate species that have been claimed but not substantiated.

Atomic number	89	90	91	92	93	94	95	96	97	98	99	100	101	102	103
Element	Ac	Th	Pa	U	Np	Pu	Am	Gm	Bk	Cf	Es	Fm	Md	No	Lr
Oxidation States															
													1?		
							(2)	(2)		(2)	(2)	2	2	2	
	3	(3)	(3)	3	3	3	3	3	3	3	3	3	3	3	3
		4	4	4	4	4	4	4	4	4	(4)	4?			
			5	5	5	5	5	5?		5?					
				6	6	6	6	6?							
					7	(7)	7?								

M(VI) UO_2^{2+} is the most stable oxidation state of uranium. Neptunium, plutonium and americium form MO_2^{2+} ions in solution with the stability ordering being U > Pu > Np > Am.

M(VII) M(VII) species, in oxygenated form such as MO_5^{3-}, have been reported for neptunium, plutonium and americium but are unstable.

7. Transactinide elements

The transactinide elements with atomic numbers 104–109, inclusive, have been synthesized and identified (i.e., discovered) (Seaborg and Loveland 1990). The known elements beyond 103 (rutherfordium, hahnium, seaborgium, nielsbohrium, hassium and meitnerium) should be members of a new fourth d-electron transition series extending from rutherfordium to element 112, in which the 6d electronic shell is being filled. The chemical properties of the members of this group should generally resemble those of their homologs hafnium to mercury in the third d-electron transition series. The chemical properties of these elements, as predicted by Keller and I in 1977, are shown in table 3 of our paper (Keller and Seaborg 1977), which is reproduced here. The predicted chemical properties are generally the result of a judicious extrapolation of periodic-table trends for each group together with consideration of relativistic effects predicted for these elements. Of especial interest are the properties of element 112, ekamercury. Pitzer (1979) has suggested that relativistic effects will make 112 more noble than mercury and that element 112 will be a volatile liquid or a gas.

Of the transactinide elements, only the chemistry of rutherfordium and hahnium has been studied. These elements all have short half-lives and study of their chemical properties must occur at the accelerators where they are produced. Since typical production rates are such that the elements are produced one-atom-at-a-time, the experiments to deduce the chemistry of these elements must be carried out many times

TABLE 3
Predicted chemical properties of elements 104–112.

	Rf	Ha	106	107	108	109	110	111	112
Stable oxidation states	III, IV	IV, V	IV, VI	III–VII	II–VIII	I–VI	I–VI	III, (−1)	I, II
First ionization energy (eV)	5.1	6.6	7.6	6.9	7.8	8.7	9.6	10.5	11.4
Standard electrode potential (V)	4→0 −1.8	5→0 −0.8	4→0 −0.6	5→0 +0.1	4→0 +0.4	3→0 +0.8	2→0 +1.7	3→0 +1.9	2→0 +2.1
Ionic radius (Å)	(+4) 0.71	(+5) 0.68	(+4) 0.86	(+5) 0.83	(+4) 0.80	(+3) 0.83	(+2) 0.80	(+3) 0.76	(+2) 0.75
Atomic radius (Å)	1.50	1.39	1.32	1.28	1.26				
Density (g cm^{-3})	23	29	35	37	41				
Heat of sublimation (kJ mol^{-1})	694	795	858	753	628	594	481	335	29
Boiling point (K)	5800								
Melting point (K)	2400								

with the results of the individiual experiments being added together to produce a statistically significant result. The experiments must be very reproducible and involve sensitive detection techniques such as high-resolution α-particle spectroscopy and fission counting.

The chemistry of rutherfordium has been shown to be similar to the chemistry of hafnium rather than the chemistry of the heavier actinides, a clear demonstration of the expected end of the actinide series at lawrencium. This demonstration involved both aqueous and gas-phase chemistry. In the gas-phase experiments by Zvara et al. (1972a,b) the 3-s isotope ^{259}Rf, produced in the ^{242}Pu (^{22}Ne, 5n) reaction was used. Zvara and co-workers attempted to use thermochromatography to show a difference in volatility of $RfCl_4$ which seemed to condense at $\sim$220°C as compared to the chlorides of the heavier actinides which have much higher condensation temperatures.

In aqueous solution experiments, the 1-min isotope ^{261}Rf produced in the ^{248}Cm (^{18}O, 5n) reaction, was used by Silva et al. (1970). Atoms of rutherfordium recoiling from the target were caught in an NH_4Cl layer sublimed onto platinum discs, dissolved with ammonium α-hydroxyisobutyrate solution and added to a heated Dowex-50 cation-exchange resin column, The neutral and anionic complexes of hafnium, zirconium and rutherfordium were not adsorbed on the cation-exchange column while actinides were strongly absorbed. Thus, the hafnium, zirconium (tracers) and the rutherfordium atoms eluted within a few column volumes while the actinides eluted after several hundred column volumes. The time from end of bombardment to start of sample counting was less than one half-life of ^{261}Rf and after several hundred experiments Silva and co-workers were able to detect the decay of 17 atoms of ^{261}Rf in the eluant.

This work was extended by Hulet et al. (1980) to the chloride complexes of rutherfordium. Computer automation was used to help perform the chemical operations rapidly and reproducibly. An HCl solution containing ^{261}Rf was passed through an extraction chromatography column loaded with trioctylmethylammonium chloride which strongly extracts anionic chloride complexes. Such complexes are formed by the group IV elements such as rutherfordium while the actinides, and members of groups I and II, form weaker complexes and are not extracted. Thus, the actinide recoil products elute first and zirconium, hafnium and rutherfordium were shown to elute in a second fraction as expected for group IV elements.

However, more recent work shows that the chemical properties of rutherfordium differ in subtle ways from those of its homologs zirconium and hafnium, due to the complexities introduced by the presence of relativistic valence electrons in its larger electronic structure. For example, Czerwinski (1992), using the 6.5-s ^{261}Rf isotope, has shown for the tributylphosphate-chloride system, at high chloride concentrations, that rutherfordium unlike zirconium and hafnium, forms anionic chloride species, similar to plutonium (IV). Furthermore, rutherfordium extraction increases with increasing hydrogen-ion concentration, while zirconium and hafnium do not, suggesting the formation of a neutral salt. These differences in chemistry show that chemical properties exhibited by the lighter homologs cannot be extrapolated in a simple manner to predict the properties of the transactinide elements.

Similarly, Türler et al. (1992) showed that Rf Br_4 is unexpectedly more volatile than $HfBr_4$, and $RfCl_4$ has a surprisingly high volatility. This may be due to relativistic effects leading to more covalent bonding in the rutherfordium halides.

Hahnium (Ha) is expected to have the valence-electron configuration $7s^2\,6d^3$ and thus to be a homolog of tantalum (with the valence electron configuration $6s^2\,5d^3$). Zvara et al. (1976) have carried out a set of thermochromatography experiments similar to those done with rutherfordium. The isotope used for the study was the 1.8-s ^{261}Ha produced in the ^{243}Am(^{22}Ne, 4n) reaction, with detection by observation of its decay by spontaneous fission. The results of the experiments show the volatility of the chlorides and bromides of hahnium to be less than that of niobium (a $4d^3$ element which has the same deposition temperature in the chromatographic apparatus as tantalum) but relatively similar to that of hafnium. Gäggeler et al. (1992) and Türler et al. (1992), using the isotopes $^{262,\,263}$Ha (half-lives 34 s and 27 s), similarly find that the bromide(s) of hahnium are less volatile than the bromides ($NbBr_5$ and $TaBr_5$) of its lighter homologs niobium and tantalum. This is at variance with the theoretical, relativistic considerations of Pershina et al. (1992) for $HaBr_5$, but the formation of an oxybromide or tribromide of hahnium, expected to have a lower volatility than the pentabromide, cannot be ruled out. In any case, the experiments show that hahnium behaves in a generally similar manner to niobium and tantalum in the volatility of their bromides.

Gregorich et al. (1988) have investigated some aqueous solution chemistry of hahnium, using the 35-seconds ^{262}Ha, produced in the ^{249}Bk (^{18}O, 5n) reaction. With nearly a thousand batch experiments, hahnium was found to hydrolyze in strong HNO_3 solution and adhere to glass surfaces. Such hydrolysis is characteristic of group V elements and different from group IV elements as verified in experiments with tantalum and niobium, and zirconium and hafnium, tracers under the same conditions. In other experiments, hahnium did not form extractable anionic fluoride complexes in HNO_3/HF solutions under conditions in which tantalum was extracted nearly quantitatively. This observation may be explained by an extrapolation of the properties of group V elements, in that the tendency to hydrolyze or to form polynegative fluoride-complexes may be stronger for hahnium than for tantalum, leading to a failure to observe extraction. In the pioneering work of Gregorich et al. (1988), the total study involved the identification of 47 atoms of ^{262}Ha on the basis of observation of decay by spontaneous fission and α-particle emission, including the time correlation of α-particle decays from ^{262}Ha and its 4-s daughter ^{258}Lr.

To confirm the formation of such polynegative hahnium species, anion-exchange chromatographic separations using triisooctyl amine (TIOA) were performed by Kratz et al. (1989). They compared the halide complexation of hahnium (using ^{262,263}Ha) with the lighter group V elements niobium and tantalum, and the pseudo-group V element protactinium, and found that the halide complexes of hahnium are different from those of tantalum, and more like those of niobium and protactinium, indicating a reversal in the trend in going from niobium to tantalum to hahnium. It was suggested that the non-tantalum-like halide complexation of hahnium is indicative of the formation of oxyhalide or hydroxyhalide complexes, in contrast to the pure halide complexes of tantalum.

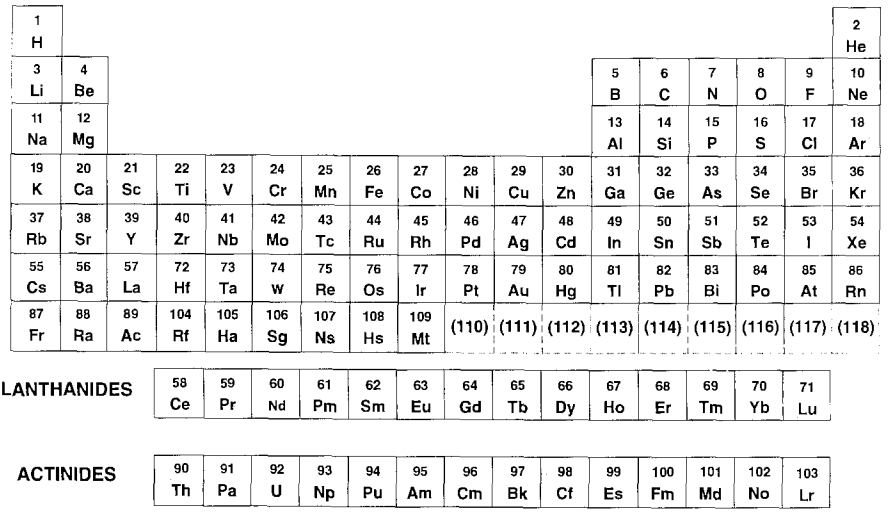

Fig. 5. Modern periodic table of the elements (atomic numbers of undiscovered elements are shown in parentheses).

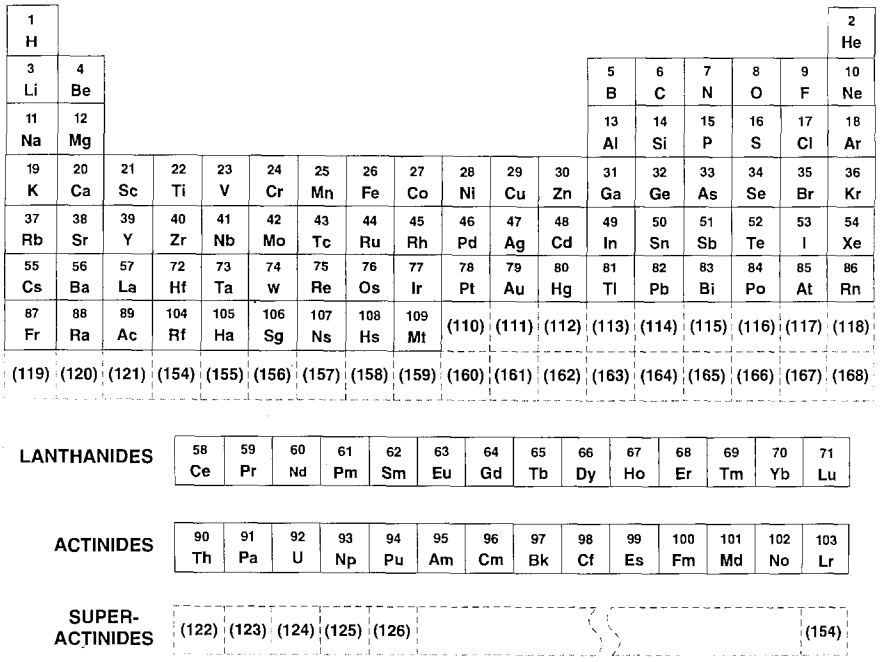

Fig. 6. Futuristic periodic table (atomic numbers of undiscovered elements are shown in parentheses).

The close similarity of the chemical behavior of hahnium to that of protactinium and niobium motivated Gober et al. (1992) to investigate this further using diisobutylcarbinol (DIBC) as an extractant. The extraction yield was greatest for protactinium, less for niobium, and least for hahnium. Since the extraction into DIBC is restricted to neutral or singly charged metal complexes, while polynegative species cannot be extracted, the results indicated that the tendency of hahnium to form polynegative complexes at high halide concentrations is stronger than for niobium and much stronger than for protactinium.

Thus, although rutherfordium and hahnium behave in the main in a manner highly consistent with that expected for members of group IV and group V, their chemical properties cannot be determined reliably in detail from trends exhibited by their lighter homologs because of the important, and probably understandable, role played by relativistic effects in these heavier elements.

8. Modern periodic table

A periodic table that places the actinide elements and the transactinide elements in positions that best represent our present understanding is shown in fig. 5. A more futuristic periodic table that includes the unattainable "superactinide" group of elements with 5g and 6f electrons is shown in fig. 6.

Acknowledgment

This work was supported in part by the Director, Office of Energy Research, Division of Nuclear Physics of the Office of High Energy and Nuclear Physics of the US Department of Energy under Contract No. DE-AC03-76SF00098.

References

Akhumov, A.I., 1947, J. Gen. Chem. USSR **17**, 1241.

Bedreag, C.G., 1943, Naturwissenschaften **31**, 490.

Bohr, N., 1913, Philos. Mag. **26**, 476.

Bohr, N., 1923, Nature **112**, 30.

Carranza, M., 1935, Bol. Soc. Quim. Peru (I) **6**, 41.

Czerwinski, K.R., 1992, Ph.D. Thesis, Lawrence Berkeley Laboratory Report LBL-32233, April.

Daudel, R., 1943, C.R. Acad. Sci. (Paris) **217**, 396.

Djounkovsky, G.E., and S. Kavos, 1944, J. Phys. Radium (8) **5**, 53.

Dushman, S., 1926, Chem. Rev. **5**, 137.

Gäggeler, H.W., D.T. Jost, J. Kovacs, U.W. Scherer, A. Weber, D. Vermeulen, A. Türler, K.E. Gregorich, R.A. Henderson, K.R. Czerwinski, B. Kadkhodayan, D.M. Lee, M.J. Nurmia, D.C. Hoffman, J.V. Kratz, M.K. Gober, H.P. Zimmerman, M. Schädel, W. Brüchle, E. Schimpf and I. Zvara, 1992, Radiochim. Acta **57**, 93.

Gober, M.K., J.V. Kratz, H.P. Zimmerman, M. Schädel, W. Brüchle, E. Schimpf, K.E. Gregorich, A. Türler, N.J. Hannink, K.R. Czerwinski, B. Kadkhodayan, D.M. Lee, M.J. Nurmia, D.C. Hoffman, H.W. Gäggeler, D.T. Jost and J. Kovacs, 1992, Radiochim. Acta **57**, 77.

Goeppert-Mayer, M., 1941, Phys. Rev. **60**, 184.

Goldschmidt, V.M., 1924, Geochemische Verteilungsgesetze der Elemente, Nor. Vidensk.-Akad. Skrifter **2**, 23.

Goldschmidt, V.M., 1937, Travaux du Congres Jubilaire Mendeleev II, 387.

Goldschmidt, V.M., T. Barth and G. Lunde, 1925,

Geochemische Verteilungsgesetze der Elemente V, Nor. Vidensk.-Akad. Skrifter **1**, 10.
Gregorich, K.E., R.A. Henderson, D.M. Lee, M.J. Nurmia, R.M. Chasteler, H.L. Hall, D.A. Bennett, C.M. Gannett, R.B. Chadwick, J.D. Leyba, D.C. Hoffman and G. Herrmann, 1988, Radiochim. Acta **43**, 223.
Hahn, O., 1929, Angew. Chem. **42**, 924.
Hardwick, T.J., 1947, in: Proc. Conf. in Nuclear Chemistry, Part I (McMaster University, Canada) p. 44.
Harvey, B.G., 1948, Nucleonics **2**, 30.
Hulet, E.K., R.W. Lougheed, J.F. Wild, J.H. Landrum, J.M. Nitschke and A. Ghiorso, 1980, J. Inorg. & Nucl. Chem. **42**, 79.
Karapetoff, V., 1930, J. Franklin Inst. **210**, 609.
Katz, J.J., G.T. Seaborg and L.R. Morss, 1986, Chemistry of the Actinide Elements, 2nd Ed. (Chapman and Hall, London) p. 1139.
Keller Jr, O.L., and G.T. Seaborg, 1977, Annu. Rev. Nucl. Sci. **27**, 139.
Kiess, C.C., C.J. Humphreys and D.D. Laun, 1944, Report A-1747 (US National Bureau of Standards, Feb. 7).
Klinkenberg, P.F.A., 1947, Physica **13**, 1.
Kratz, J.V., H.P. Zimmerman, U.W. Scherer, M. Schädel, W. Brüchle, K.E. Gregorich, C.M. Gannett, H.L. Hall, R.A. Henderson, D.M. Lee, J.D. Leyba, M.J. Nurmia, D.C. Hoffman, H.W. Gäggeler, D. Jost, U. Baltensperger, Ya Nai-Qi, A. Türler and Ch. Lienert, 1989, Radiochim. Acta **48**, 121.
Latimer, W.M., and J.H. Hildebrand, 1940, Reference Book of Inorganic Chemistry (The MacMillan Company, New York) p. 519.
Maddock, A.G., 1948, Research **1**, 690.
McLennan, J.C., A.B. McLay and H.G. Smith, 1926, Proc. R. Soc. London A **112**, 76.
McMillan, E.M., and P.H. Abelson, 1940, Phys. Rev. **57**, 1185.
Meggers, W.F., 1942, Rev. Mod. Phys. **14**, 96.
Meggers, W.F., 1947, Science **105**, 514.
Mikheev, N.B., V.I. Spitsyn, A.N. Kamenskaya, I.A. Rumer, B.A. Grozdez, N.A. Rosenkevich and L.N. Auérman, 1973, Dokl. Akad. Nauk **208**, 1146.
Oppegaard, A.G., 1948, J. Chem. Soc., pp. 318–321.
Perrin, J., 1935, Grains de Matière et de Lumière, Vol. II (Hermann & Cie, Paris) p. 30.
Pershina, V., W.-D. Sepp, B. Fricke and A. Rosen, 1992, J. Chem. Phys. **96**, 8367.
Pitzer, K.S., 1979, Acc. Chem. Res. **12**, 271.
Purkayastka, B.C., 1948, Nucleonics **3**, 2.
Quill, L.L., 1938, Chem. Rev. **23**, 87.
Richtmeyer, F.K., and E.H. Kennard, 1942, Introduction to Modern Physics (McGraw-Hill, New York) p. 707.
Rudy, R., 1927, Gen. Sci. **38**, 671.
Rydberg, J.R., 1913, Lunds Univ. Arsskr. **2**, 9.
Saha, M.N., and N.K. Saha, 1934, Treatise on Modern Physics (Indian Press, Allahabad) pp. 583, 588.
Schuurmans, P., 1946, Physica **11**, 419.
Seaborg, G.T., 1944, Metallurgical Project Report CK-1968 (A-2845) (July 17) p. 55; Metallurgical Laboratory Memorandum, MUC-GTS-858 (July 17).
Seaborg, G.T., 1945, Chem. Eng. News **23**, 2190.
Seaborg, G.T., 1946, Science **104**, 379.
Seaborg, G.T., 1949, Electronic Structure of the Heaviest Elements, Paper 21.1, in: The Transuranium Elements – Research Papers, National Nuclear Energy Series IV, Vol. 14B, Part II, eds G.T. Seaborg, J.J. Katz and W.M. Manning (McGraw Hill, New York) p. 1492.
Seaborg, G.T., 1963, Man-Made Transuranium Elements (Prentice Hall, Englewood Cliffs, NJ) pp. 80–82.
Seaborg, G.T., 1968, Elements Beyond 100, Present Status and Future Prospects, Annu. Rev. Nucl. Sci. **18**, 53.
Seaborg, G.T., and W.D. Loveland, 1990, The Elements Beyond Uranium (Wiley, New York) pp. 84–86, 113–116.
Seaborg, G.T., and A.C. Wahl, 1942, Report A-135 to Uranium Committee (Washington, DC, March 19).
Seaborg, G.T., and A.C. Wahl, 1948, J. Am. Chem. Soc. **70**, 1128.
Seaborg, G.T., and A.C. Wahl, 1949, The Chemical Properties of Elements 94 and 93, Paper 1.6, in: The Transuranium Elements: Research Papers, National Nuclear Energy Series IV, Vol. 14B, Part II, eds G.T. Seaborg, J.J. Katz and W.M. Manning (McGraw Hill, New York) p. 25.
Silva, R.J., J. Harris, M.J. Nurmia, K. Eskola and A. Ghiorso, 1970, Inorg. & Nucl. Chem. Lett. **6**, 871.
Spence, R., 1949, Research **2**, 115.
Starke, K., 1943, Z. Anorg. Allg. Chem. **251**, 251.
Stedman, D.F., 1947, Can. J. Res. B **25**, 199.
Strassmann, F., and O. Hahn, 1942, Naturwissenschaften **30**, 256.
Suguira, Y., and H.C. Urey, 1926, Kgl. Danske Videnskab. Selskab, Math. Fys. Medd. **7**, 3.
Summons, B.M., 1947, J. Chem. Educ. **24**, 588.

Swinne, Z., 1926, Tech. & Physik **7**, 205.
Talpain, L., 1945, J. Phys. Radium **6**(8), 176.
Taylor, H.S., and S. Glasstone, 1942, Treatise on Physical Chemistry, Vol. I (Van Nostrand, New York) p. 298.
Thompson, S.G., 1947, private communication, October.
Türler, A., H.W. Gäggeler, K.E. Gregorich, H. Barth, W. Brüchle, K.R. Czerwinski, M.K. Gober, N.J. Hannink, R.A. Henderson, D.C. Hoffman, D.T. Jost, C.D. Kacher, B. Kadkhodayan, J. Kovacs, J.V. Kratz, S.A. Kreek, D.M. Lee, J.D. Leyba, M.J. Nurmia, M. Schädel, U.W. Scherer, E. Schimpf, D. Vermeulen, A. Weber, H.P. Zimmerman and I. Zvara, 1992, J. Radioanal. Nucl. Chem. **160**(2), 327.
Villar, G.E., 1940, Anais Acad. Brasil. Cienc. **12**, 51.
Villar, G.E., 1942, J. Chem. Educ. **19**, 329.
Villar, G.E., 1947, Bol. Soc. Quim. Peru **13**, 73.
Von Grosse, A., 1928, Chem. Ber. **61**, 233.
Von Grosse, A., 1930, J. Am. Chem. Soc. **52**, 1742.
Von Grosse, A., 1935, J. Am. Chem. Soc. **57**, 440.
Wheeler, T.S., 1947, Chem. Ind. (London), pp. 639–642.
Wu, T.Y., 1933, Phys. Rev. **44**, 727.
Wu, T.Y., and S. Goudsmit, 1933, Phys. Rev. **43**, 496.
Yost, D.M., H. Russell Jr and C.S. Garner, 1947, The Rare-Earth Elements and Their Compounds (Wiley, New York) pp. 3, 4.
Zachariasen, W.H., 1944a, Metallurgical Project Report CK-1518 (March) p. 3.
Zachariasen, W.H., 1944b, Metallurgical Project Report CN-1807 (June).
Zimen, K.E., 1948, in: Festskrift Tillagnad J. Arvid. Hedvall, p. 635.
Zvara, I., V.Z. Belov, V.P. Domanov, Yu.S. Korotkin, L.P. Chelnokov, M.R. Shalavskii, V.A. Shchegolev and M. Hussonnois, 1972a, Radiokhim., p. 119.
Zvara, I., V.Z. Belov, V.P. Domanov, Yu.S. Korotkin, L.P. Chelnokov, M.R. Shalavskii, V.A. Shchegolev and M. Hussonnois, 1972b, Sov. Radiochem. **14**, 115.
Zvara, I., V.Z. Belov, V.P. Domanov and M.R. Shalzevskii, 1976, Sov. Radiochem. **18**, 328.

Handbook on the Physics and Chemistry of Rare Earths
Vol. 18 – Lanthanides/Actinides: Chemistry
edited by K.A. Gschneidner, Jr., L. Eyring, G.R. Choppin and G.H. Lander

Chapter 119

RELATIVISTIC EFFECTS AND ELECTRONIC STRUCTURE OF LANTHANIDE AND ACTINIDE MOLECULES

K. BALASUBRAMANIAN*
Department of Chemistry, Arizona State University, Tempe, AZ 85287-1604, USA

Contents

1. Introduction 30
2. Relativistic effects and methods 32
2.1. The nature of relativistic effects 33
2.2. Relativity and lanthanide contraction 35
2.3. Basic relativistic quantum techniques 40
3. Theoretical methods for lanthanide and actinide molecules 43
3.1 *Ab initio* techniques 43
3.1.1. ECP method 43
3.1.2. SCF, CASSCF, CI, RCI methods for the electronic structure of molecules containing lanthanides and actinides 47
3.2. Approximate methods 50
3.2.1. Ligand-field theory 50
3.2.2. Local-density functional (LDF) method 50
3.2.3. Intermediate neglect of differential overlap/spin–orbit CI method (INDO/S-CI) 52
4. Electronic structure of lanthanide hydrides 52
4.1. YH and ScH 52
4.2. YH_2 and ScH_2 59
4.3. LaH 63
4.4. LaH^+ 67
4.5. LaH_2^+ 71
4.6. LaH_2 75
4.7. HfH, ZrH and TiH 80
4.7.1. HfH 80
4.7.2. ZrH 84
4.7.3. TiH 85
4.7.4. Effect of lanthanide contraction on the TiH, ZrH and HfH triad 88
4.8. HfH_2 and ZrH_2 89
4.8.1. HfH_2 89
4.8.2. ZrH_2 93
4.8.3. The effect of lanthanide contraction on the difference in properties of HfH_2 and ZrH_2 95
4.9. UH, UH^+ and UH^- 96

* Camille and Henry Dreyfus Teacher-Scholar.

4.10. AcH, TmH, LuH and LrH 97
4.11. Ground-state properties of lanthanide hydrides 99
5. Electronic states of diatomic lanthanide and actinide halides 101
5.1. LaF 101
5.2 YF and YCl 103
5.3. UF and UF^- 105
5.4. Ground states of LaF–LuF 106
6. Electronic states of lanthanide oxides 110
6.1. LaO 111
6.2. CeO 111
6.3. PrO 114
6.4. SmO 118
6.5. EuO 121
6.6. GdO 124
6.7. DyO 127
6.8. HoO 128
6.9. TmO 130
6.10. YbO 131
7. Electronic structure of selected lanthanide and actinide polyatomics 135
7.1. Polyatomic oxides and complexes 136
7.2. Uranocene and actinocenes 139
7.3. Lanthanides and actinides inside carbon cages ($M@C_n$, $M@C_n^+$) 146
8. Conclusion 152
References 154

1. Introduction

The electronic structures of molecules containing lanthanide and actinide atoms are extremely interesting due to the complex array of electronic states resulting from open f-shell electronic configurations. There are seven possible real projections for the 4f orbitals which could accommodate up to 14 electrons. As a result, numerous possible electronic states of varied spin multiplicities and spatial symmetries result even for a simple diatomic molecule consisting of a lanthanide or actinide element. A wealth of spectroscopic data has been accumulated up to now on several diatomics containing f-block elements. The spectra are considerably complex and definitive assignments are not always feasible.

The 4f-shell electrons are challenging to deal with since they exhibit all kinds of chemical behavior – i.e., they behave sometimes like non-bonding electrons while at other times are involved in the chemical bonds. The book by Salahub and Zerner (1989) as well as the recent introductory remarks by Atkins (1991) entitled "f for facts, factors and fallacies" beautifully summarize the rather intriguing behavior of 4f electrons.

The next important fact of lanthanide and actinide chemistry is going to be one of the central themes of this chapter, namely, relativistic effects. Relativistic effects arise from the differences in the assumed infinite speed of light in non-relativistic mechanics (whether classical or quantum mechanical) and the true speed of light. Although the special theory of relativity was proposed by Einstein in the very early part of the century, its impact in chemistry came about much later. In fact, it is not an exaggeration

if one states that the discovery of several super-heavy actinide elements at Berkeley by Seaborg and co-workers provided considerable impetus to the growth of relativistic quantum chemistry pioneered in particular by Pitzer and co-workers at Berkeley. The recent article by Hoffman (1990) outlines the connection between relativity and super-heavy elements.

Just prior to the 1970s, quantum mechanics made a significant impact in the chemistry of molecules containing light elements in the periodic table due to the advent of computers. Although the Schrödinger equation and the underlying quantum principles were considerably old by then, the practical difficulties in applying those equations to chemistry were immense, due to the numerical complexities of equations pertaining to polyatomic molecules. However, thanks to the advent of computers and now supercomputers and the pioneering work of Boys which showed that the underlying integrals can be evaluated very easily if one used Gaussians to represent atomic orbitals, today *ab initio* quantum chemists are bolstered to carry out calculations approaching a billion electronic configurations (Olsen et al. 1990).

In recent years, there has been significant growth in our understanding of the nature of bonding and electronic states of molecules containing very heavy atoms with the advent of relativistic quantum mechanical tools combined with the power of supercomputers. The relativistic effective core potential (RECP) method which is a chemist's view of a very heavy atom, made it possible to study molecules containing almost any element in the periodic table. The underlying philosophy of the RECP method is that the chemical properties of molecules are governed primarily by the valence electrons and the other core electrons are deeply buried and do not take an active part in chemical bonding. Hence the ECP approximation simply replaces these core electrons by an effective potential which therefore effectively leads to the treatment of gold atom, eg., as a eleven-electron system ($5d^{10}\,6s^{1}$). Balasubramanian and Pitzer (1987) as well as several others (Christiansen et al. 1985, Krauss and Stevens 1984, Ermler et al. 1988, Balasubramanian 1989a, b) have written reviews on the subject of the ECP method and hence we will not dwell on the details and advantages of the ECP method.

Relativistic effects play an important and interesting role in the electronic structure of lanthanides, actinides and post-lanthanide molecules. As a matter of fact, in 1975 Pitzer and co-workers (Bagus et al. 1975) showed that not all of the "lanthanide contraction" is due to incomplete screening of the 4f-shell electrons. In fact, the magnitude of the 4f-shell effect and relativistic effects were found to be comparable and hence indeed nearly half of "lanthanide contraction" itself is due to relativistic effects. In this chapter, we will illustrate this point further by considering the electronic states of HfH, HfH_2, Pt- and Au-containing molecules and comparing them with their light analogs (ZrH and ZrH_2). The lanthanide contraction plays a very important role in the third-row transition-metal compounds containing Hf–At as well as the chemistry of molecules containing Hf–At. The third-row transition-metal elements (Hf–Au) form stronger chemical bonds compared to the second-row elements because of the 4f-shell incomplete screening and the relativistic mass–velocity effect both of which lead to the contraction of the 6s orbital of Hf–Au. For the same reason, the $6s^2$ shell of Hg, Tl, Pb and Bi, etc. is considerably lower in energy and hence this shell is relatively inert leading to the "inert-pair effect" phenomenon.

The electronic spectra of rare-earth diatomics such as LaO, CeO, PrO, etc. are notoriously complex as noted by Field and co-workers (see, e.g., Field 1982). Since an array of molecular electronic states result from incomplete 4f shells, several electronic states have nearly the same properties. Furthermore, spectroscopic bands arising from one set of states can be highly perturbed by another set of states in the near proximity. Moreover, there are several isotopes for lanthanides with large nuclear spins which lead to complex hyperfine structures.

In spite of the above-mentioned complexities, progress on electronic structure computations of lanthanide and actinide molecules as well as spectroscopy of lanthanide molecules in general and oxides in particular, has been impressive. The fact that molecules such as $C_{60}La$ (Chang et al. 1991), $U(C_8H_8)_2$ (Chang and Pitzer 1989), etc. can be computed is a testimonial to the progress in this area and the impact that large-scale *ab initio* computations has made in the chemistry of molecules containing lanthanides and actinides.

The objective of this chapter is to review these developments in both theoretical computations and experimental spectra of molecules containing lanthanides and actinides. It is not our intent to provide a comprehensive set of available data on these molecules. That would be an overwhelming and rather ambitious task. Instead, my objective will be to identify a few molecules of both experimental and theoretical interest and emphasize the interplay between theory and experiment. I propose to summarize the insight gained from theoretical computations especially in regard to the importance of relativistic effects in lanthanide and actinide chemistry as well as post-lanthanide chemistry.

We have enumerated a list of such species. As seen from the contents, even such a focused list is rather long. We hope to discuss as many of these species in as much detail as possible, but due to the bias of the chapter, all molecules and all references pertaining to all lanthanide and actinide molecules will not be included. That is merely to make this difficult task of reviewing a subject of such a large scope possible. We lay special emphasis on species which elucidate some interesting theoretical concept or relativistic effects. We have organized this chapter into seven sections, each section containing subsections. Section 2 discusses rather briefly relativistic effects and theoretical techniques to compute them. Section 3 focuses on *ab initio* and semi-empirical techniques for lanthanides and actinides. Sections 4–7 offer a list of molecules containing lanthanides and actinides for which both experimental and theoretical (although these may not be complete) data exist.

2. Relativistic effects and methods

There are several review articles (Pitzer 1979, Pyykkö and Desclaux 1979, Krauss and Stevens 1984, Balasubramanian and Pitzer 1987, Malli 1982a, b, Christiansen et al. 1985, Pyykkö 1986, 1988, Balasubramanian 1989a, b, 1990a, b) which deal with the importance of relativistic effects on the chemical and spectroscopic properties of molecules containing very heavy atoms. For a detailed description of these effects and a survey of the literature, the reader is referred to these reviews. However, in this chapter

we will elucidate the basic nature of relativistic effects and in particular their role in lanthanide and actinide chemistry. We will also describe the basic relativistic quantum chemical methods briefly. For more details on these methods, the reader is referred to the above-mentioned reviews.

2.1. *The nature of relativistic effects*

Relativistic effects can be defined as differences in chemical and spectroscopic properties arising from the true velocity of light as opposed to the assumed infinite velocity of light in non-relativistic models. Relativistic effects are far more important for molecules containing very heavy atoms since the inner electrons in such atoms are subjected to the electric field generated by a large number of protons. Consequently, to maintain balance with the large electrostatic force the inner electrons of very heavy atoms move with speeds that are comparable to the speed of light. For example, it is estimated that the 1s electrons of post-lanthanide atoms such as gold attain 60% of the speed of light.

There are several effects of relativity on chemical bonding and spectroscopic properties. We first focus on a relativistic effect called the "mass–velocity" effect. As the electron approaches the speed of light, its mass increases with velocity since in special theory of relativity mass is no longer a constant and varies as

$$M = \frac{M_0}{\sqrt{1 - v^2/c^2}},$$

where M_0 is the rest mass (mass when $v = 0$) and M is the actual mass. It is clear that when v approaches 60% of c, M becomes

$$M = 1.25\, M_0.$$

That is, even at 60% of the speed of light the mass of an inner 1s electron of the gold atom increases by 25%. The 25% increased mass means an increase in its kinetic energy. Since the total energy is conserved, the electrostatic energy has to become more negative. The electrostatic energy of an electron is inversely proportional to its averaged orbital radius and this evidently leads to the contraction of the inner 1s orbitals of atoms such as Au, Pt, Tl, etc. To keep balance with the core orbitals, which by far experience most of the relativistic effects, the valence orbitals also contract. For example, the 6s orbital of the gold atom contracts. Bagus et al. (1975) showed that nearly half of the lanthanide contraction is actually attributed to relativity. We discuss this in detail in the next section.

Another relativistic effect of considerable importance in the chemical properties of molecules containing very heavy atoms is the spin–orbit interaction. The spin–orbit interaction is a relativistic effect in the sense that it goes to zero in the limit $c \to \infty$ due to the presence of α^2 ($\alpha = 1/c$) term in the numerator of the spin–orbit operator. Physically it arises from the coupling of the orbital angular momentum (l) of the electron with its spin (s). As Z (the atomic number) increases, the coupling of l and s increases significantly. Thus a new quantum number for the atoms, $j = l + s$, becomes a good

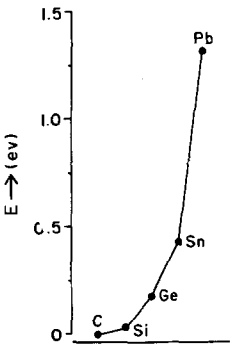

Fig. 1. The spin–orbit coupling in the fourth group atoms C–Pb. The $^3P_0$–$^3P_2$ atomic energy separations are shown. Reproduced from Balasubramanian (1989a, b).

quantum number and l and s are no longer good quantum numbers. This, in turn, introduces significant mixing of electronic states of different spin multiplicities and different l values for an atom.

Figure 1 shows the periodic trend in the $^3P_0$–$^3P_2$ splitting of the group IV elements where the suffixes are the J quantum numbers. Note the dramatic increase in the $^3P_0$–$^3P_2$ splitting of Pb (1.3 eV) compared to Sn (0.4 eV). The ground state of the Pb atom is thus 88% $^3P_0$ and 12% $^1S_0$ compared to Sn which is 97% $^3P_0$ and only 3% $^1S_0$. Non-relativistically, electronic states of different spin multiplicities do not mix and thus the mixing of ^3P with ^1S is purely a relativistic effect. Likewise, the $J = 2$ state of Pb is 70% $^3P_2$ and 30% $^1D_2$.

The spin–orbit coupling makes significant impact on the electronic structure and spectroscopy of lanthanide and actinide molecules. First electronic states of different spin multiplicities and spatial symmetries are mixed by spin–orbit coupling. Consequently, the conventional $\Delta S = 0$, $\Delta\Lambda = \pm 1$ selection rules, where S and Λ are total spin and angular momentum along the molecular axis, do not hold for diatomics containing lanthanides and especially actinides. This is because the intensity of such electronic transitions depend on the magnitude of an integral called the transition moment. The spin–orbit coupling increases the transition moments and therefore the transition probabilities of electronic transitions which are rigorously zero non-relativistically. This is brought about primarily through mixing of different electronic states which do not mix non-relativistically.

The spin–orbit effect can destabilize chemical bonds and enhance chemical reactivity through coupling of different electronic states. For example, the D_e of Pb_2 (Balasubramanian and Pitzer 1983) is reduced to half of its value primarily through the spin–orbit effect. For example, the D_e of Pb_2 is ~ 1.8 eV in the absence of spin–orbit coupling, but becomes 0.88 eV when spin–orbit effects are included. This is primarily because the spin–orbit stabilizations of atomic states and molecular states are not always the same. In the case of Pb, the ground state of the lead atom is considerably more stabilized than the Pb_2 dimer and thus the D_e is decreased significantly compared to the D_e of Sn_2 which is 1.94 eV. The ground state of Pb_2 is a mixture of $^3\Sigma_g^-(0_g^+)$, $^1\Sigma_g^+(0_g^+)(\pi_u^2)$ as well as $^1\Sigma_g^+(0_g^+)(\pi_u^2)$.

The enhancement of reactivity through spin–orbit coupling occurs when potential energy surfaces of electronic states of different spin multiplicity cross. For molecules containing very heavy atoms, if this happens, the spin–orbit coupling at the points of intersection could be large leading to a significant number of non-adiabatic surface hoppings from one surface to the other. Typically high spin electronic states of heavy atoms do not insert into H_2 but the low spin states do. Hence if the high spin surfaces cross the low spin surfaces there could be considerable interaction between the two surfaces primarily brought about by spin–orbit coupling in the heavy species. In this event, there could be hopping of electrons from high spin to low spin states non-adiabatically and thus the high spin atoms, which are intrinsically non-reactive, become more reactive. This is exemplified by several studies from our laboratory on the reactivity of third-row transition-metal atoms. For example, spin–orbit coupling enhances the reactivity of high spin state Ir with H_2 (Balasubramanian and Dai 1990). In this chapter, we show how the reactivity of Hf with H_2 is contrasted compared to Zr and H_2 due to lanthanides and relativistic effects.

2.2. *Relativity and lanthanide contraction*

Bagus et al. (1975) have studied the effects of relativity and the lanthanide contraction (gradual decrease of atomic radii from La to Lu) on Hf to Bi atoms which follow the lanthanides. It is important to know how much of the contraction on the 6s valence orbital is caused by relativity as opposed to incomplete screening of the 4f shells. To accomplish this goal, Bagus et al. made Hartree–Fock calculations on "pseudo-atoms" corresponding to Hf, Re, Au, Hg, Tl, Pb and Bi without 4f electrons, but with the atomic number reduced by 14. The orbital energies of the pseudo-atoms were compared with Dirac–Fock orbital energies of the real atoms by Bagus et al. Of course, this technique would thus separate the contraction effect due to 4f shells and relativity.

Typically the seven projections of the 4f shells occupy a small volume and thus fail to screen the nucleus. This results in an incomplete screening of the 4f-shell electrons. Consequently, e.g., the 6s orbital of the Hf atom is not fully shielded by the 4f shell of electrons. This, in turn, leads to a contraction of the outer 6s orbital. The contraction of the radii of the outer electrons is more commonly referred to as the "lanthanide contraction". However, not all of the orbital-radii contraction arises from the incomplete screening of the 4f shells. As a matter of fact, nearly half of the contraction is due to relativity.

Table 1a reproduces the results of Bagus et al. (1975) which shows a critical comparison of the orbital energies in Hartree atomic units for both the HF pseudo-atom (without 4f shells) and the actual atom for which relativistic Dirac–Fock energies are listed. Note that the actual orbital energies are negative and for convenience the magnitudes of these energies are shown in table 1a. The difference in the orbital energies of the pseudo-atom and HF atom measures the effect of the 4f shell. The difference in the DHF orbital energy and HF orbital energy measures the effect of relativity.

As seen from table 1a, the difference in the 6s orbital energy of the pseudo-Hf and Hf (HF) is 0.0299 Hartrees while the difference between Hf (HF) and Hf (DHF) energy is

TABLE 1a

Orbital binding energies in a.u. of atoms Hf–Bi. Both pseudo, relativistic and non-relativistic atoms are compared. Reproduced from Bagus et al. (1975).

	5d		6s		6p	
	$(5d_{3/2})$	$(5d_{5/2})$	$(6s_{1/2})$	$(6p_{1/2})$		$(6p_{3/2})$
pseudo-Hf		0.3192	0.1805			
Hf(HF)[a]		0.2992	0.2104			
Hf(DHF)[b]	0.2473	0.2355	0.2397			
pseudo-Re		0.4660	0.2031			
Re(HF)		0.4538	0.2347			
Re(DHF)	0.3972	0.3661	0.2783			
pseudo-Au		0.5372	0.1905			
Au(HF)		0.5210	0.2208			
Au(DHF)	0.4935	0.4287	0.2917			
pseudo-Hg		0.7191	0.2288			
Hg(HF)		0.7142	0.2610			
Hg(DHF)	0.6501	0.5746	0.3280			
pseudo-Tl		0.9472	0.3162		0.1836	
Tl(HF)		0.9683	0.3611		0.1924	
Tl(DHF)	0.8945	0.8062	0.4492	0.2114		0.1765
pseudo-Pb		1.1772	0.4025		0.2268	
Pb(HF)		1.2245	0.4589		0.2398	
Pb(DHF)	1.1388	1.0360	0.5665	0.2751		0.2199
pseudo-Bi		1.4131	0.4906		0.2693	
Bi(HF)		1.4874	0.5582		0.2862	
Bi(DHF)	1.1389	1.2710	0.6862	0.3385		0.2612

[a] Reference [1] of Bagus et al. (1975).

[b] Reference [3] of Bagus et al. (1975).

TABLE 1b

Comparison of radial expectation values (R) for Hf, Re, Au, Hg, Tl, Pb and Bi. Reproduced from Bagus et al. (1975).

	5d		6s		6p	
	$d_{3/2}$	$d_{5/2}$		$p_{1/2}$		$p_{3/2}$
pseudo-Hf		2.5048	4.6934			
Hf(HF)		2.2277	4.0684			
Hf(DHF)	2.3376	2.4198	3.6939			
pseudo-Re		2.0326	4.2162			
Re(HF)		1.7999	3.6942			
Re(DHF)	1.8301	1.9047	3.2770			
pseudo-Au		1.7228	4.2230			
Au(HF)		1.5433	3.7006			
Au(DHF)	1.5359	1.6185	3.0609			
pseudo-Hg		1.6040	3.7500			
Hg(HF)		1.4327	3.3284			
Hg(DHF)	1.4312	1.4987	2.8434			
pseudo-Tl		1.5042	3.3294		4.2434	
Tl(HF)		1.3412	2.9669		3.9262	
Tl(DHF)	1.3387	1.3940	2.5792	3.5166		4.0123
pseudo-Pb		1.4214	3.0475		3.7532	
Pb(HF)		1.2671	2.7242		3.4569	
Pb(DHF)	1.2641	1.3119	2.3916	3.0739		3.5162
pseudo-Bi		1.3506	2.8336		3.4116	
Bi(HF)		1.2046	2.5939		3.1366	
Bi(DHF)	1.2012	1.2439	2.2429	2.7802		3.1862

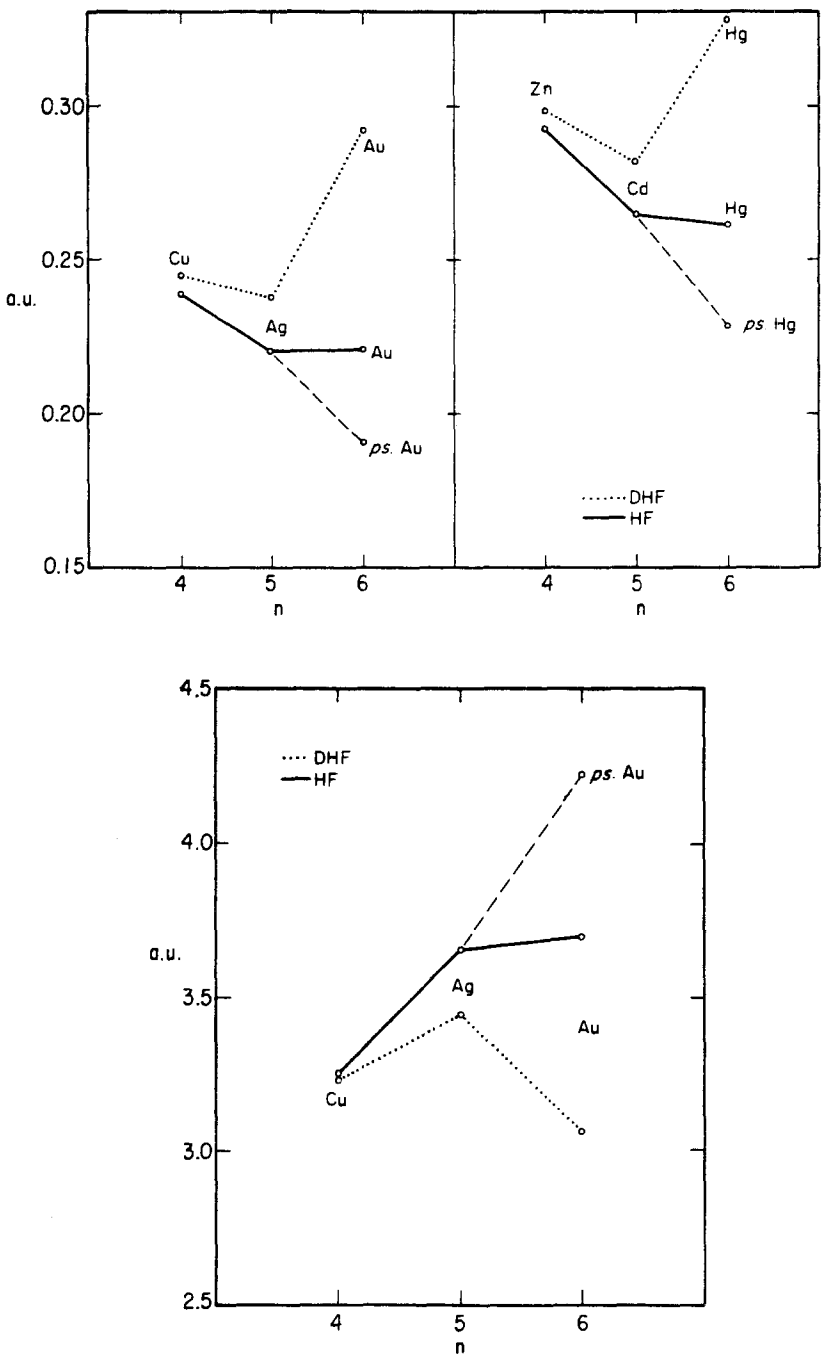

Fig. 2. Illustration of lanthanide contraction. Magnitude of orbital energies of valence s electrons of radii Cu, Ag, Au as well as Zn, Cd and Hg. Also shown are the expected values. The label ps is the pseudo-atom without $4f^{14}$ shells. Reproduced from Bagus et al. (1975).

0.0293. The former energy of stabilization is due to the incomplete screening of the $4f^{14}$ shell while the latter energy of stabilization is due to relativity. This means that the effect of the lanthanide contraction is comparable to the effect of relativity.

Figure 2 shows systematically the magnitude of orbital energies of Cu, Ag and Au as well as the Zn, Cd and Hg triad. The plot joining the pseudo-atom (without $4f^{14}$ shells and without relativity) is almost collinear (expected trend). The dotted curve is the actual Dirac–Fock trend including relativistic effects and $4f^{14}$ shells while the full curve is the HF line without relativistic effects. It is clear that the dramatic change in trend for Au and Hg is due to both incomplete screening of the $4f^{14}$ shell and the effect of relativity.

Table 1b shows the orbital radii expectation values for the pseudo-, HF and DHF atoms. Figure 2 shows the orbital radii expectation values obtained by Bagus et al. As seen from both table 1b and fig. 2, the $6s_{1/2}$ orbitals of Hf–Bi are contracted both due to lanthanide contraction and relativity. For the gold atom (fig. 2), the contraction due to lanthanide contraction is 0.523 a.u. The relativistic contraction is 0.64 a.u. Consequently, the relativistic contraction effect is larger than the lanthanide contraction effect for the gold atom. For the Hf atom, the contraction is 0.625 a.u. while the relativistic contraction is only 0.3745 a.u. Hence, for Hf, the lanthanide contraction is larger than the relativistic contraction.

The above effect of relativistic and lanthanide contraction has dramatic impact in the chemical and spectroscopic compounds of molecules containing Hf to Bi. For example, the color of gold is due to this effect. Figure 3 compares the ionization potentials of Cu, Ag and Au atoms. As seen from fig. 3, the IP of gold is substantially larger than Cu and Ag, which is an anomaly since generally the IP decreases as one goes down the group. The trend in fig. 3 is akin to the DHF orbital energies of Cu, Ag and Au computed by Bagus et al. (fig. 2). Hence, it is clear that nearly half of the anomalous behavior of the gold atom is due to relativity while the other half is due to the lanthanide contraction.

The lanthanide and relativistic contractions have other important consequences on molecular and chemical properties. Figure 4 compares the equilibrium bond distances of NiH, PdH and PtH. Note that the PtH diatomic has a significantly shorter bond distance compared to PdH which is attributed to the contractions of the outer 6s orbital of the Pt atom arising from both lanthanide contraction and relativity.

Figure 5 compares the D_es of Cu_2, Ag_2 and Au_2 triad. Once again, the trend from Cu_2 to Ag_2 is reversed in going from Ag_2 to Au_2. That is, instead of the expected decrease in the binding energy of Au_2 it actually increases. This is also due to the contraction of the 6s valence orbital of the gold atom which leads to a stronger and shorter bond for Au_2 compared to Ag_2.

Atoms such as Hg, Tl, Pb and Bi form considerably weaker bonds compared to the lighter members in the same group. This too is a consequence of the contraction of the 6s orbital of these elements. Note that for Hg–Bi the $6s^2$ shell is complete. The unusual stability of the 6s shell leaves the filled $6s^2$ shell inert in that it does not actively participate in bonding. Hence, two Hg atoms form only a van der Waals dimer Hg_2, while Cd_2 and Zn_2 are strongly bound. For the same reason Hg_2^{2+} is unusually stable (Nessler and Pitzer 1987).

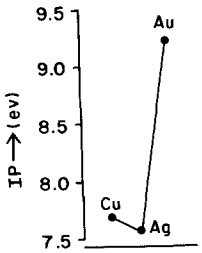

Fig. 3. The IPs of Cu, Ag and Au. Reproduced from Balasubramanian (1989a, b).

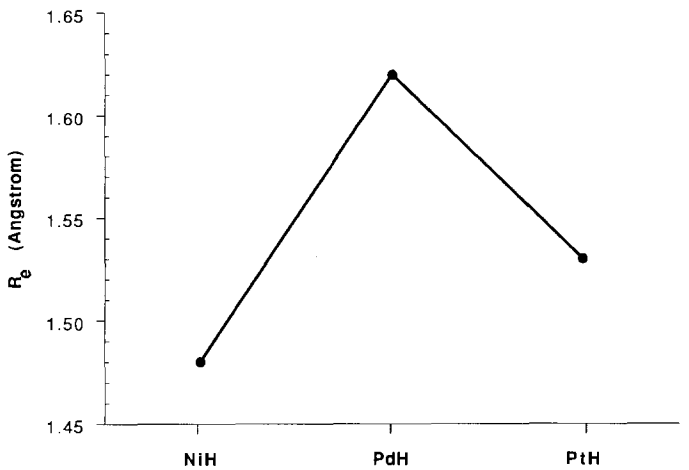

Fig. 4. The R_e values of the $^2\Delta_{3/2}$ states of NiH, PdH and PtH diatomics.

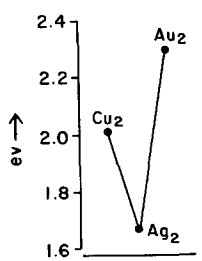

Fig. 5. The D_es of schematic Cu_2, Ag_2 and Au_2. Reproduced from Balasubramanian (1989a, b).

The formation of Hg–Hg bonds would require promotion of an electron from the 6s orbital to the 6p orbital. Figure 6 compares the *n*s–*n*p promotion energy by comparing the $(ns^2)^1$S-$(nsnp)^1$P energy separations of Zn, Cd and Hg. As evidenced from fig. 6, mercury has got an usually larger promotion energy resulting from stabilization of the 6s orbital due to the lanthanide and relativistic contractions. Consequently, these effects are extremely significant and often dramatically alter the spectroscopic proper-

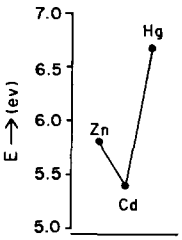

Fig. 6. The ns^2 (^{1}S)-$nsnp$(^{1}P) energy separations for Zn, Cd and Hg. Reproduced from Balasubramanian (1989a, b).

ties and the reactivities of the third-row transition-metal compounds as well as compounds of Hg–Bi.

2.3. *Basic relativistic quantum techniques*

Since the difference between non-relativistic and relativistic mechanics is in the treatment of the speed of light, the natural origin for all relativistic methods of treating energy levels is the Einstein energy expression,

$$E^2 = m_0^2 c^4 + p^2 c^2.$$

If one uses the quantum postulates to introduce operators for E and p as it is done to derive the Schrödinger equation from energy conservation laws, one obtains an equation called the Klein–Gordon equation which involves second derivatives both in spatial coordinates and time. This leads to the possibility that the probability density $\rho = \psi\psi^*$ could be negative which makes it difficult to interpret ρ.

In an attempt to overcome the above-mentioned difficulty, Dirac discovered an equation now well known as the Dirac equation which is essentially a relativistic analog of the Schrödinger equation. The resulting equation for a single electron in a central Coulombic field is

$$H_D \psi' = E\psi,$$

where

$$H_D = (\boldsymbol{\alpha}\cdot\boldsymbol{p} + c^2\beta - Z/r), \quad \alpha = \begin{pmatrix} 0 & \sigma_P \\ \sigma_P & 0 \end{pmatrix}, \quad \beta = \begin{pmatrix} I & 0 \\ 0 & -I \end{pmatrix},$$

where the σ_P are the 2×2 Pauli matrices and I is the 2×2 identity matrix.

The Dirac Hamiltonian for a many-electron atom can also be written as

$$H_D = \sum_i h_D(i) + \sum_{i<j} \frac{1}{r_{ij}},$$

where $h_D(i)$ is the one-electron Dirac Hamiltonian,

$$h_D(i) = (\boldsymbol{\alpha}_i\cdot\boldsymbol{p}_i + \beta_i c^2 - Z/r_i).$$

Note that the above Hamiltonian ignores the two-electron relativistic Breit interaction. Introduction of the Breit interaction as a perturbation shows that it is very small in the

valence region and more important for the properties of core electrons, for which this makes a significant contribution.

Since the one-particle Dirac Hamiltonian involves 4×4 matrices instead of scalar functions and differential operators, the solution of the Dirac equation is a vector of four components. This is referred to as a four-component spinor which takes the form

$$\psi_{nkm} = \frac{1}{r}\begin{bmatrix} P_{nk}(r) & \chi_{km}(\theta,\phi) \\ iQ_{nk}(r) & \chi_{-km}(\theta,\phi) \end{bmatrix},$$

where

$$\chi_{km}(\theta,\phi) = \sum_{\sigma=\pm 1/2} C(l\tfrac{1}{2}j; m-\sigma,\sigma) Y_{\lambda}^{m-\sigma}(\theta,\phi)\,\phi_{1/2}^{\sigma},$$

$Y_{\lambda}^{m-\sigma}$ is a spherical harmonic,

$$\phi_{1/2}^{1/2} = \alpha = \begin{pmatrix} 1 \\ 0 \end{pmatrix}, \qquad \phi_{1/2}^{-1/2} = \beta = \begin{pmatrix} 0 \\ 1 \end{pmatrix},$$

are the Pauli spinors, $C(l\frac{1}{2}j; m-\sigma,\sigma)$ are the Clebsch–Gordon coefficients, k is the relativistic quantum number, defined as

$$\begin{aligned} k &= j + \tfrac{1}{2}, && \text{if } j = l - \tfrac{1}{2}, \\ &= -(j - \tfrac{1}{2}), && \text{if } j = l + \tfrac{1}{2}, \end{aligned}$$

and λ is defined as

$$\begin{aligned} \lambda &= k, && \text{if } j = l - \tfrac{1}{2}, \\ &= -(k+1), && \text{if } j = l + \tfrac{1}{2}. \end{aligned}$$

The Q_{nk} are known as the small components and P_{nk} are the large components. They satisfy the following coupled differential equations for a central force field,

$$\frac{dP_{nk}}{dr} + \frac{kP_{nk}}{r}\left(\frac{2}{\alpha} + \alpha[v(r) - \varepsilon_{nk}]\right)Q_{nk} = 0,$$

$$\frac{dQ_{nk}}{dr} - \frac{kQ_{nk}}{r} + \alpha[v(r) - \varepsilon_{nk}]P_{nk} = 0.$$

Desclaux's (1975) numerical Dirac–Fock implementation in a computer is widely used to generate relativistic numerical all-electron wavefunctions for almost any atom in the periodic table. This appears to be one starting point for *ab initio* relativistic quantum computations of molecules containing very heavy atoms.

The small components Q_{nk}s in relativistic four-component spinor solutions make small contributions especially for valence properties. Their contributions are far more important for core electrons. This can be best illustrated by a comparison of the large and small components of the 6s valence orbital of the lead atom. Figure 7 reproduces this comparison made by Lee et al. (1977). As seen from fig. 7, the $Q_{6s_{1/2}}$ spinor makes an

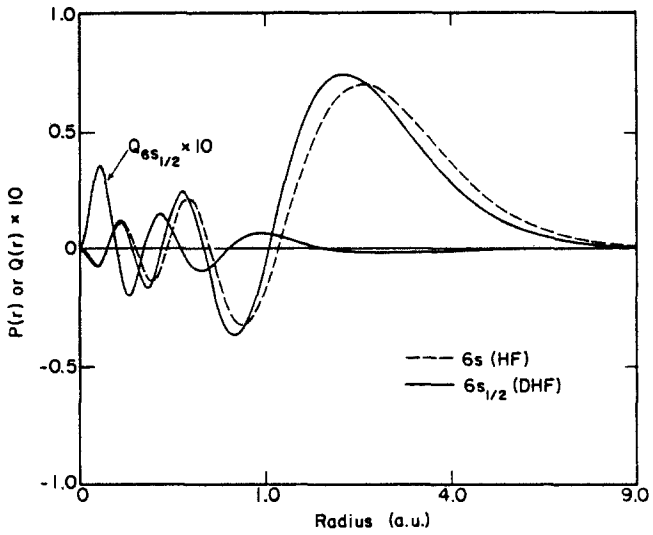

Fig. 7. A comparison of small and large components of the $6s_{1/2}$ spinor of the Pb atom. Note that the $Q_{6s_{1/2}}$ components make negligible contribution in the valence region. Reproduced from Lee et al. (1977).

appreciable contribution only near the nucleus and is far less important in the valence region.

The above discussion leads to a natural approximation called the Pauli approximation to the Dirac equation which is tantamount to ignoring the small Q components. This is the method used in practice for most of the chemical problems.

Another starting point for relativistic effects is the perturbational Breit–Pauli Hamiltonian,

$$H_{BP} = H_O + H_D + H_{MV} + H_{SO},$$

where

H_O = non-relativistic Hamiltonian,

$$H_D = +\frac{\alpha^2}{8}(\nabla^2 V) \quad \text{(Darwin)},$$

$$H_{MV} = -\frac{\alpha^2}{8}\sum_i p_i^4 \quad \text{(mass–velocity)},$$

$$H_{SO} = \frac{\alpha^2}{2}\left(\sum_i \frac{Z}{r_i^3}(\boldsymbol{L}_i \cdot \boldsymbol{S}_i) \sum_{i \neq j} \frac{1}{r_{ij}^3}(\boldsymbol{r}_{ij} \times \boldsymbol{P}_i) \cdot (\boldsymbol{S}_i + 2\boldsymbol{S}_j)\right) \quad \text{(spin–orbit)},$$

where α is the fine-structure constant, and

$$V = -Z\sum_i \frac{1}{r_i} + \sum_{i<j} \frac{1}{r_{ij}}.$$

The Pauli Hamiltonian is ideally suited for carrying out relativistic corrections as a first-order perturbation to a non-relativistic Hamiltonian. However, the Pauli terms have been used with considerable success in variational self-consistent field (SCF) calculations. Wadt and Hay (1985) used the above Hamiltonian within the Cowan–Griffin approximation to include relativistic effects for heavy atoms except that they typically do not include the spin–orbit effect variationally in the molecular calculations.

There are several other semi-empirical methods such as the relativistic extended Hückel method formulated by Pyykkö and co-workers. The Dirac–Slater multiple $X\alpha$ method (Case 1982) has also been employed to include relativistic effects approximately. Zerner and co-workers use the INDO/CI method to study lathanide compounds. We will discuss these in section 3.2.

3. Theoretical methods for lanthanide and actinide molecules

3.1. *Ab initio techniques*

3.1.1. *ECP method*

Ab initio methods for lanthanide and actinide molecules are mostly based on the effective core potential (ECP) method, especially if the molecules in question have several heavy atoms. The philosophy of the ECP method is to replace the chemically unimportant core electrons by an effective core potential and treat the remaining valence electrons explicitly. There are several techniques to derive RECPs which we now briefly describe and refer to the reviews by Christiansen et al. (1985), Krauss and Stevens (1984), Balasubramanian and Pitzer (1987) for further details.

An *ab initio* effective core potential method derived from the relativistic all-electron Dirac–Fock solution of the atom, which we call the relativistic effective core potential (RECP) method, has been widely used by several investigators to study the electronic structure of polyatomics including the lanthanide- and actinide-containing molecules. This RECP method was formulated by Christiansen et al. (1979). It differs from the conventional Phillips–Kleinman method in the representation of the nodeless pseudo-orbital in the inner region. The one-electron valence equation in an effective potential V_c of the core electron can be written as

$$(h + V_c)\,\phi_v = E_v \phi_v,$$

where $\langle \phi | \phi_c \rangle = 0$, $H\,\phi_c = E_c \phi_c$. In the Phillips and Kleinman approximation ϕ_v is written as

$$\phi_v = \chi_v - \sum_c \langle \chi_v | \phi_c \rangle \phi_c.$$

Substitution of the above expression in the one-electron equation yields

$$(h + V_c + V_{EP})\chi_v = E_v \chi_v,$$

$$V_{EP} = \sum_c (E - E_c) | \phi_c \rangle \langle \phi_c |,$$

where the V_{EP}s are known as Phillips–Kleinman effective core potentials. The problem

with these ECPs, as pointed out in the literature, is that they underestimate the repulsive region of the potential energy surfaces. This method can be adapted to relativistic Dirac–Fock equations as follows.

In the relativistic method, the Dirac–Fock four-component spinors are partitioned into core and valence spinors. The many-electron relativistic wavefunction for a single configuration can be thus expressed as

$$\psi = A\left[\left(\psi_1^c \psi_2^c \cdots \psi_m^c\right)\left(\psi_1^v \psi_2^v \cdots \psi_n^v\right)\right],$$

where A is the antisymmetrizer, $\psi_1^c, \ldots, \psi_m^c$ are core orbitals, m being the number of core electrons, and $\psi_1^v, \ldots, \psi_n^v$ are the valence orbitals, n being the number of valence electrons. The total energy E_T can be partitioned into core, valence and core–valence iterative energies. In symbols,

$$E_T = E_c + E_v + E_{cv}.$$

This leads to the following expressions

$$E_v + E_{cv} = \langle \psi_v^R | H_v^{rel} | \psi_v^R \rangle,$$

$$H_v^{rel} = \sum_i \left\{ h_D(i) + \sum_c \left[J_c(i) - K_c(i) \right] \right\} + \sum_{i<j} \frac{1}{r_{ij}},$$

where the indices i and j run over valence electrons. For an orthonormal set of valence orbitals, it can be shown that the Dirac–Hartree–Fock (DHF) equation for a single electron is given by

$$\left[h_D + \sum_c (J_c - K_c) \right] \psi_v = \varepsilon_v \psi_v + \sum_c \psi_c \varepsilon_{cv},$$

where the ε_{cv} are the off-diagonal Lagrange multipliers given by

$$\varepsilon_{cv} = \left\langle \psi_v | h_D + \sum_c (J_c - K_c) | \psi_c \right\rangle.$$

The adaptation of the Phillips–Kleinman method to relativistic spinors yields relativistic pseudo-orbitals and relativistic ECPs given by

$$\chi_v^R = \psi_v^R + \sum_c a_c \psi_c^R, \qquad \psi_v^R = (1 - P)\chi_v^R, \quad P = \sum_c |\psi_c\rangle\langle\psi_c|,$$

$$V^{RPK} = -PH_v^{rel} - H_v^{rel} P + PH_v^{rel} P + \varepsilon_v P,$$

where

$$(H_v^{rel} + V^{RPK})\chi_v^R = \varepsilon_v \chi_v^R,$$

$$(h_D + U^{core})\chi_v^R = \varepsilon_v \chi_v, \quad \text{if } U^{core} = \sum_c (J_c - K_c) + V^{RPK}.$$

In the above method, one could introduce the Pauli approximation by neglecting the small Q component spinors of the Dirac equation. This leads to RECPs expressed as two-component spinors. The use of non-relativistic kinetic energy operator for the

valence region together with two-component spinors leads to Hartree–Fock-like expressions involving the pseudo-orbitals. The V^{EP}s (effective potentials) in this expression are not the same for pseudo-orbitals of different symmetry. The RECPs are thus expressed as products of angular projectors and radial functions. In the Dirac–Fock approximation, the orbitals with different total j but which have the same l value are not degenerate, and thus the potentials derived from the Dirac–Fock calculations would be j dependent. The RECPs can thus be expressed by introducing the lj-dependent radial potentials U_{lj}^{REP}, as

$$U^{REP} = \sum_{l=0}^{\infty} \sum_{j=|l-1/2|}^{l+1/2} U_{lj}^{REP}(r)|ljm\rangle\langle ljm|,$$

where the $|ljm\rangle$ are Pauli two-component spinors.

The above expression for the RECPs involves an infinite sum over l which in turn requires calculations of the radial potentials for all the excited states of the atom. The radial functions U_{lj}^{REP} do not change significantly with l and j after these numbers exceed the maximum values of l and j of electrons in the core.

Hence, a practical approximation which stops the summation at maximum l and j values denoted by L and J, respectively, is introduced. This leads to RECPs expressed as

$$U^{REP} = U_{LJ}^{REP}(r) + \sum_{l=0}^{L-1} \sum_{j=|l-1/2|}^{l+1/2} \sum_{m=-j}^{j} (U_{lj}^{REP} - U_{LJ}^{REP})|ljm\rangle\langle ljm|.$$

Christiansen, Lee and Pitzer (1979) have proposed that the pseudo-orbital can be expressed as

$$P_l^{PS} = r\sum_{i}^{N} C_i r^i, \quad \text{for } r \le r_m,$$
$$= \phi_l(r), \qquad \text{for } r > r_m,$$

where r_m is a match radius, and ϕ_l is the all-electron Dirac–Fock orbital. In this method the coefficients C_i are determined by matching the value and the first three derivatives of the P_l and ϕ_l at r_m with the condition that P_l is normalized. The r_m value is minimized stipulating that P_l can have only one maximum and two inflection points. This method is one of the most widely used *ab initio* RECP methods to include both spin–orbit and electron correlation effects.

In recent years, Ross et al. (1990), Hurley et al. (1986), La John et al. (1987) and Pacios and Christiansen (1985) have provided convenient analytical Gaussian forms for the RECPs derived using the above procedure. This is based on the Kahn–Baybutt–Truhlar form for Gaussian ECPs,

$$U_{LJ}^{REP}(r) - U_{lj}^{REP}(r) = \frac{1}{r^2}\sum_{i=0}^{N} C_i r^{ni} \exp(-\alpha_i r^2),$$

where the C_i, n_i and α_i are parameters chosen to obtain the best fit for the numerical potentials. The RECPs, when averaged with respect to spin, take the following form,

$$U^{AREP}(r) - U_L^{AREP}(r) \times \sum_{l=0}^{L} \sum_{m=-l}^{l} [U_l^{AREP}(r) - U_L^{AREP}(r)]|lm\rangle\langle lm|,$$

where

$$U_L^{AREP} = \frac{1}{2l+1}[lU^{REP}_{l,\,l-1/2}(r) + (l+1)\,U^{REP}_{l,l+1/2}(r)].$$

The advantage of the above form is that it can be fit into conventional non-relativistic codes since the two-component spinor projections have been eliminated and we obtain simple $|lm\rangle$ projections involving ordinary spherical harmonics. However, the averaging method eliminates the spin–orbit operator. Fortunately, the spin–orbit operator itself can be expressed in terms of RECPs as shown by Hafner and Schwarz (1978, 1979) and Ermler et al. (1981). This form is shown below,

$$H^{SO} = \sum_{l=1}^{L-1} \Delta U_l^{REP}(r)\left(\frac{l}{2l+1}\sum_{-l-1/2}^{l+1/2} |l,l+\tfrac{1}{2},m\rangle \times \langle l,l+\tfrac{1}{2},m| - \frac{l+1}{2l+1}\sum_{-l-1/2}^{l-1/2} |l,l-\tfrac{1}{2},m\rangle\langle l,l-\tfrac{1}{2},m|\right),$$

where

$$\Delta U_l^{REP}(r) = U^{REP}_{l,\,l+1/2}(r) - U^{REP}_{l,\,l-1/2}(r).$$

At present, Ermler, Christiansen and co-workers have systematically generated averaged ECPs and spin–orbit operators expressed in the above forms for all elements in the periodic table except Ce–Lu and the actinides. Progress is being made to generate RECPs of these elements as well. However, we note that Pitzer and Winter have generated RECPs for U, NP and Pu which have been successfully employed in molecular computations.

Hay and Wadt (1985a, b) have published ECPs which are in form identical to the averaged RECPs of Christiansen, Ermler and co-workers. However, there are differences. First, the Hay–Wadt potentials are derived from the Cowan–Griffin adaptation of the Breit–Pauli Hamiltonian into a variational computation of the atomic wavefunction. From these solutions the ECPs are generated. It should be noted that the spin–orbit coupling is *not* included in the Hay–Wadt ECPs. Consequently, molecular calculations done using these ECPs would not include spin–orbit coupling.

Hafner and Schwarz (1979) proposed quasi-relativistic model potentials expressed as

$$V_{rel}^{eff} = V_{rel} + \sum_{l,j,m_j}^{core} |ljm_j\rangle V_{lj}(r)\langle ljm_j|$$

where $V_{rel}(r)$ and $V_{lj}(r)$ are parametrized as

$$V_{rel}(r) = \frac{-Z_{eff} + A\exp(\alpha r)}{r},$$

$$V_{lj}(r) = B_{lj}\exp(-\beta_{lj} r),$$

where Z_{eff} is the effective charge of the atomic core. The parameters α, β_{ij}, A and B_{lj} are obtained so that the effective Hamiltonian reproduces the valence-electron spectrum of

the alkali-like systems. The resulting effective potentials include spin–orbit interaction.

Preuss, Stoll and co-workers at Stuttgart have adapted several other ECP methods which include core polarization effects with considerable success in molecular calculations (see Igelmann et al. 1988, Dolg et al. 1989a, b, Müller et al. 1984, Szentpaly et al. 1982). They have generated complete sets of ECPs for all elements in the periodic table including lanthanides and actinides (Dolg et al. 1989). Preuss, Stoll and co-workers have in particular applied these ECPs for computing the spectroscopic constants and potential energy curves of lanthanide oxides such as GdO, EuO, YbO, etc. We will describe the results of the specific calculation on these species in a subsequent section.

Pyykkö and Desclaux (1978) (see also Desclaux and Pyykkö 1974, 1976) have used the one-center Dirac–Fock method to study diatomic hydrides containing very heavy atoms. In particular, the work of Pyykkö (1987) on several lanthanide hydrides is worth citing. We will describe the results of these calculations subsequently. It should be stated that the one-center DF method is applicable only to diatomic hydrides. A critical comparison of the properties computed by this method with the state-of-the-art *ab initio* method suggests that the properties obtained by the one-center method are not always in good agreement with more accurate procedures. Also, the properties of the excited states have not been computed using this method.

There have been several all-electron relativistic calculations on very heavy diatomic hydrides such as AgH and AuH. The calculations of Lee and McLean (1982a, b) employed four-component STO spinors as basis sets for all-electron calculations of AuH, AgH, Ag_2, etc. More recently, Ramos et al. (1988) have used this method to study the sixth-row hydrides. We have critically compared the results of Ramos et al. (1988) with those of Balasubramanian et al. (1991). The main problem with all these techniques is that they do not include electron-correlation effects and suffer greatly in this regard. Therefore, computed properties are often not in good agreement.

Sadlej and co-workers (Sadlej and Urban 1991, Kellö and Sadlej 1991a, b) have had considerable success in using the Breit–Pauli Hamiltonian in all-electron relativistic calculations which included electron-correlation effects. Techniques which include electron-correlation effects such as the coupled cluster method or Moller–Plesset (MP) perturbation method have been adapted to include relativistic effects. The authors have carried out such computations on molecules such as AgH, AuH, etc.

3.1.2. *SCF, CASSCF, CI, RCI methods for the electronic structure of molecules containing lanthanides and actinides*

The simplest of the *ab initio* methods which ignores electron-correlation effects completely is the self-consistent field (SCF) method and is described in sufficient details in the textbooks. In principle, it treats the many-electron problem as a one-electron equation in the effective field created by the rest of the electrons. The resulting equation, known as the Hartree–Fock equation, is solved iteratively to self-consistency.

A more accurate method which serves as the basis to generate orbitals for higher-order electron-correlation effects is the complete active space multi-configuration self-consistent field (CAS-MCSCF or CASSCF) method. In this method, a set of the most active electrons, usually the valence electrons, are distributed in all possible ways

among a chosen set of most important orbitals called the active orbitals. This leads to an electronic configuration space called the full configuration interaction (CI) space. There are several methods of solving self-consistent field equations in a multi-configuration space. Typically eigenfunctions of the density matrix, called the natural orbitals, are used in the CASSCF methods to achieve self-consistency. The augmented Hessian method, the linear-equation method, etc., which are widely used in solving CASSCF equations, are described well in the literature and thus we do not repeat these details here. See, e.g., the review by McLean et al. (1990) or Roos (1987).

The CASSCF method is an excellent zeroth-order starting point, which generates orbitals optimized in the full CI space of active orbitals. The disadvantage of this method is that the number of configurations grows astronomically for a given number of electrons as more and more orbitals are included in the active space. For this reason, only for a few compounds, such as MH, MO, MF, M_2, M_3, etc. (M denotes a heavy atom), a full CASSCF is possible. One method that can be used to bring down the number of configurational spin functions (CSF)in the CASSCF is to reduce the active space. This calls for judgement and alternative choices and is never a size-consistent method in comparing different regions of the potential energy surfaces (valley versus dissociated regions). More recently, Malmquist et al. (1990) and Merchan et al. (1991) have developed and applied a restricted active space method (RASSCF) in which only selected excitations are included for the active space of orbitals. That is, instead of the full CI in the CASSCF one can choose, e.g., important excitations in the RASSCF. In general, the truncation procedure of electronic excitations leads to slower convergence in the RASSCF and thus the possible quadratic convergence in the CASSCF may not always be accomplished in the RASSCF.

Typically, since the CASSCF/MCSCF procedures only provide zeroth-order description of orbitals, higher-order correlation effects are included using a configuration interaction (CI) method. In the CI method, electrons are excited in the external space of orbitals. A linear-variational approximation is used for these configurations. This requires diagonalizing matrices of the order of $n \times n$, where n is the number of configurations. Fortunately, only a few lowest roots are required in practice. Hence, iterative procedures such as the Davidson method could be used for the diagonalization method. The advances in graphical-unitary group approach (GUGA) (see Paldus 1976, Shavitt 1978, Brooks and Schaefer 1979) as well as the symbolic CI method (Liu and Yoshimine 1981) have made it possible to do direct CI which can include several million configurations. The recent advances in full CI technology have provided avenues for the CI calculations approaching a billion configurations (Olsen et al. 1990).

Following CASSCF typically a multi-reference singles + doubles CI (MRSDCI) method is used to introduce higher-order electron correlation effects. In this method, all possible single + double excitations are allowed for all configurations with coefficients larger than a threshold T. Usually T is chosen as 0.07 although a choice of 0.05 or 0.03 is more accurate. However, for other complex molecules even the choice of $T=$ 0.07 may lead to too large a number of CSFs. Hence, the choice of T varies with molecules. A special case of the MRSDCI is the SDCI method which includes only single + double excitations from the leading configuration. The SDCI procedure is used normally with the SCF method.

Higher-order correlation effects not included in the MRSDCI or SDCI could be estimated using the empirical formula of Langhoff and Davidson (1974) commonly called the Davidson correction. The approximation which includes this correction is denoted by SDCI + Q or MRSDCI + Q. The Davidson correction is more important in the SDCIor MRSDCI method rather than the SOCI method, since the SOCI expansion is more complete and the Davidson correction usually over-shoots that for the SOCI.

There are other techniques for introducing electron-correlation effects such as the coupled-cluster method (Bartlett 1989, Paldus and Cizek 1989). The coupled-electron pair formalism (CPF) (Arhlichs 1985), modified coupled-pair formalism (MCPF) and more recently averaged coupled pair formalism (ACPF) have been used (see, e.g., the papers of Bauschlicher and Langhoff 1989, 1991). The coupled-cluster methods have been mostly used for lighter molecules and have not yet been used for molecules containing lanthanides or actinides. However, the MCPF method has been used for La-containing species by Bauschlicher and co-workers.

All the methods described above take into account electron-correlation effects but completely ignore spin–orbit coupling which is known to be very significant for molecules containing actinides and lanthanides. A method to introduce electron correlation and spin–orbit coupling for diatomics based on a SCF procedure was developed in 1982 by Christiansen et al. and was called the spin–orbit CI (SOCI) method. This should be contrasted with the second-order CI method which is also abbreviated as SOCI. In the spin–orbit CI method which we prefer to call the relativistic CI method, all electronic configurations which can mix in the presence of the spin–orbit operators are included variationally. However, this method was restricted to diatomics and only up to 5000 configurations could be included.

The author (Balasubramanian 1988) and independently Pitzer and Winter (1988) developed the relativistic CI procedures for polyatomics to include the electron-correlation effect and spin–orbit coupling simultaneously. The author's procedure used the CASSCF/MRSDCI natural orbitals as the basis set for the relativistic configuration interaction (RCI) and is done using real natural orbitals and hence the RCI matrices are in general real or imaginary. Pitzer and Winter showed that for molecules with C_{2v} or bigger point groups the spin functions can be symmetry adapted in the double group of the molecular point group which leads to real CI matrices. Both techniques include configurations (in the former case primitive Slater determinants) that have the same symmetry in the double group of the molecular point group.

Lastly, we mention the basis sets. All *ab initio* ECP computations after 1984 described in this chapter were done using valence Gaussian basis sets in conjugation with effective core potentials. Typically, valence Gaussian basis sets for the heavy metal are of (3s 3p 3d) quality where the numbers in front of s, p and d specify the numbers of contracted Gaussian functions. For lanthanides and actinides, obviously 4f-type Gaussian functions are included in the basis set. We will describe in individual sections the basis sets used prior to describing the calculational results. We will also describe the valence space of electrons when ECPs are included.

Throughout this chapter, we will use acronyms such as SCF, MCSCF, CASSCF, MRSDCI, RCI, etc. The readers are referred to this section for their meaning.

3.2. *Approximate methods*

3.2.1. *Ligand-field theory*

Field (1982) has combined the well-known molecular-orbital pictures of s and p orbitals with the ligand-field theoretical treatment of the d and f orbitals. This approach has provided very simple and yet promising interpretation for lanthanide oxides. Lanthanide oxides such as CeO, PrO, etc. are highly ionic. The conventional MO theory for the AB diatomic molecule by itself ignores the A^+B^- or $A^{+2}B^{-2}$ ionic character of such compounds. Although indirectly from MO theory, this can be rationalized as well but the amount of effort is usually more significant using the LCAO-MO approach.

The ligand-field theory combines the electrostatic model of the AB molecule with the MO picture. It tends to rationalize how the energy levels of the metal ion are affected by the surrounding field generated by the ligand. The simplest form of the ligand-field theory is the crystal-field theory and is described in textbooks (Cotton and Wilkinson 1976). The more accurate forms of ligand-field theory take into consideration the electronic structures from a MO standpoint. This theory considers the overlap of the metal orbitals with the ligand orbitals. There are many variations of this theme.

The $(n-1)$d and $(n-2)$f orbitals occupy a small volume, as discussed before, and thus especially the overlap of the $(n-2)$f orbital with ligand orbitals would be rather small. Consequently, the potential energy curves of states belonging to a specific electronic configuration with metal df orbitals and σ and π MOs derived from s and p with ligand orbitals are similar. This is the underlying philosophy of the implementation of ligand-field theory to interpret complex spectra of lanthanide oxides. We will illustrate this procedure further in section 6.

3.2.2. *Local-density functional (LDF) method*

As illustrated in section 2.2.2, accurate determination of many electron wavefunctions which include electron-correlation effects to a high order is an extremely difficult many-body problem requiring a multi-million CI expansion. The philosophy behind the density functional method is that the properties of the ground state of a molecule can be determined if its charge density is known, even though the electronic wavefunction may not be known. Thus, if the density can be computed directly without the knowledge of wavefunctions, then one can circumvent the tedious problem of having to determine the wavefunction. The density functional method seeks to replace the Hartree–Fock non-local exchange potential with other forms of potentials. The first form of the density functional theory is the Slater local-exchange approximation. The Hobenberg–Kohn theorem (Hobenberg and Kohn 1964) is the basis of subsequent LDF methods which basically state that knowledge of the charge density suffices to determine the ground-state properties. The multiple-scattering $X\alpha$ method or muffin-tin method and its relativistic analog is one way of implementing the LDF method. There are, of course, several basis-set expansion techniques. The major advantage of the LDF method is that the replacement of the conventional HF non-local potential with some forms of local potential, which includes both correlation effects and exchange effects, lead to simple Hartee–Fock-like equations. There are no CI diagonal-

izations involving matrices of the order of a million × million. Instead, computationally inexpensive HF-like equations are solved. Recently, the LDF method has been extended to include relativistic effects through complex exchange potentials (see, e.g., Becke 1986). The reader is also referred to the excellent book by Parr and Yang (1989) on density functional theory.

Kohn and Sham (1965) showed that the exact ground-state energy E_0 is given by

$$E_0 = -\frac{1}{2}\sum_i \langle \psi_i(1)|\nabla_i^2|\psi_i(1)\rangle - \int \sum_\mu \frac{Z_\mu \rho(1)}{r_{1\mu}} d\tau_1 + \frac{1}{2}\iint \frac{\rho(1)\rho(2)}{r_{12}} d\tau_1 d\tau_2 + E_{xc}(\rho),$$

where ρ is the density and $\psi_i(1)$s are called the Kohn–Sham orbitals and E_{xc} (exchange-correlation energy) is a function of the density ρ, which can be expressed as the sum of the probability associated with $\psi_i s$. The Kohn–Sham orbitals are obained variationally solving Hartree–Fock-like equations,

$$\hat{F}(1)\psi_i(1) = \varepsilon_i \psi_i(1),$$

where

$$\hat{F}(1) = -\frac{1}{2}\nabla_1^2 - \sum_\mu \frac{Z_\mu}{r_{1\mu}} + \sum_j J_j(1) + V_{xc}(1),$$

where $V_{xc}(1)$ is the exchange-correlation functional given by

$$V_{xc} = \frac{\delta E_{xc}(\rho)}{\delta \rho}.$$

The Fock-like equation above can thus be solved iteratively leading to self-consistency if the functional $E_{xc}(\rho)$ is known. Several approximations have been used in the literature for E_{xc} (see Parr and Yang 1989). In the local-density functional method, E_{xc} is approximated as

$$E_{xc} = \int \rho_{(x,y,z)}\, \varepsilon_{xc}(\rho)\, d\tau,$$

where ε_{xc} is the exchange-correlation energy per atom in a homogeneous electron gas. The practical implementation of the LDF method uses an initial guess for ρ to find E_{xc}, V_{xc} and then the Fock-like equation is iterated. The Kohn–Sham orbitals can be expressed as a linear combination of Gaussians or localized muffin-tin orbitals in the muffin-tin approximation. The main problem with the DF method is in the choice of E_{xc} for which several approximations are made including the $X\alpha$ approximation.

The LDF method is generally applied for the ground state although in recent years Salahub (1987) has used it to obtain excited-state properties. There is also a question as to whether the density functional method can treat electronic states of different spin multiplicities size-consistently and if it produces correct dissociation behavior. Often the dissociated atoms are above their true energies which leads to dissociation energies higher than the experimental values. It should also be stated that the assignment of electronic states arising from a complex set of open-shell d and f electric configurations from Kohn–Sham orbital occupancies is not always unambiguous. There appears to

be difficulty in differentiating electronic states which have similar occupancies in the Kohn–Sham orbitals. Hence, at present, it appears that all electronic states derived from complex open-shell d and f electronic configurations are not always well differentiated by the LDF method. Finally, in the LDF method, one seeks to replace the complex many-body nature of the electron-correlation problem by one set of local potential. It is not evident that this could always be accomplished in practice, although in principle such a function should exist.

3.2.3. *Intermediate neglect of differential overlap/spin–orbit CI method (INDO/S-CI)*

In recent years, Zerner and co-workers (Kotzian et al. 1991a, b, 1989a, b) have extended the previous intermediate neglect of differential overlap for spectroscopy INDO/S method (Ridley and Zerner 1973a, b) to include spin–orbit interaction through a spin–orbit interaction enhanced INDO/S-CI method. In the INDO/S method, one-center core integrals are taken from experimental IPs. The two-center electron integrals are parametrized using the Weiss–Matya–Nishimoto formula (a variation of the integral parametrization used in the Paraisen–Parr–Pople method). All one-center integrals are fully accounted for explicitly for d and f electrons. The one-center spin–orbit operator $H_{so} = \zeta(r)\boldsymbol{l}\cdot\boldsymbol{s}$ is used to evaluate spin–orbit integrals. The radial ζ integrals are taken from atomic spectroscopy.

The spin–orbit CI part of the INDO/S-CI is an adaptation of the Pitzer double-group CI approach which we have already described. This method has been applied by Zerner, Rösch and co-workers for several lanthanide compounds such as LaO, CeO, GdO, LuO, PrO, etc. We will describe the results of these calculations is section 6.

4. Electronic structure of lanthanide hydrides

In this section, we review the results of calculations and comparison with experiments for lanthanide hydrides. Although YH and ScH are strictly not lanthanide or rare-earth compounds, it is important to investigate these compounds as well to compare and contrast these compounds with their periodic analog, namely, LaH. For this reason we include some discussions on Sc and Y compounds. With the intent of demonstrating the effect of the lanthanide contraction, we also include the results of HfH and HfH_2 and compare them with ZrH and ZrH_2. In each section, we briefly describe with acronyms the method of computations. The reader is referred to section 2.1.2 for their meanings. We also include the periodic trends within a group and emphasize any anomalies.

4.1. *YH and ScH*

Balasubramanian and Wang (1989a, b) carried out CASSCF followed by full second-order CI (SOCI) calculations which included excitations from all CASSCF configurations. They used a (3s3p3d1f) valence Gaussian basis set together with RECPs which retained $4d^1\,5s^2$ shells of the Y atom in the valence space. For the hydrogen

TABLE 2
Spectroscopic properties of low-lying electronic states of YH. Reproduced from Balasubramanian and Wang (1989a, b).

State	R_e(Å)	T_e(cm^{-1})	ω_e(cm^{-1})
$^1\Sigma^+(0^+)$	1.865	0	1510
$^1\Sigma^+$	1.865	11	1510
$^3\Pi(0^-)$	1.907	7884	1488
$^3\Pi(0^+)$	1.907	7905	1488
$^3\Pi(1)$	1.907	8187	1489
$^3\Pi(2)$	1.907	8458	1489
$^3\Pi$	1.907	8179	1489
$^3\Delta(3)$	1.944	9062	1432
$^3\Delta(2)$	1.944	9000	1431
$^3\Delta$	1.944	9002	1432
$^3\Delta(1)$	1.944	9047	1433
$^3\Sigma^+(1)$	1.944	10164	1337
$^3\Sigma^+(0^-)$	1.944	10171	1342
$^3\Sigma^+$	1.944	10175	1334
$^1\Delta(2)$	1.950	10991	1366
$^1\Delta$	1.950	10992	1366
$^1\Pi(1)$	1.944	12687	1380
$^1\Pi$	1.944	12685	1380
$^1\Sigma^+(II)(0^+)$	2.034	15049	
$^1\Sigma^+(II)$	2.034	15050	
$^3\Pi(II)(2)$	1.965	20226	1418
$^3\Pi(II)(1)$	1.965	20478	1418
$^3\Pi(II)(0^-)$	1.965	20789	1417
$^3\Pi(II)(0^+)$	1.965	20789	1417
$^3\Pi(II)$	1.965	20510	1418
$^1\Pi(II)(1)$	1.955	21990	1386
$^1\Pi(II)$	1.955	21991	1386
$^1\Gamma(4)$	1.988	30051	1298
$^1\Gamma$	1.988	30051	1298

atom, van de Duijneveldt's (5s1p/3s1p) basis set was used. Balasubramanian and Wang studied 29 electronic states of YH. In addition, spin–orbit coupling was included through the RCI method. Langhoff et al. (1987) studied four electronic states of YH using the SCF/MCPF method and the Hay–Wadt ECPs (Hay and Wadt 1985a, b) which included $4s^2\,4p^6\,4d^1\,5s^8$ shells of Y. The spin-orbit coupling was neglected in this work.

Table 2 shows the spectroscopic constants obtained by Balasubramanian and Wang (1989a, b) for the electronic states of YH while fig. 8 shows the computed potential-energy curves.

Both Langhoff et al. and Balasubramanian and Wang predicted the ground state of YH to be $^1\Sigma^+$, in noticeable disagreement with Bernard and Bacis (1977) who had carried out the rotational analysis of a system which they designated as a $^3\Phi$-$^3\Delta$ system. It now appears that this assignment is incorrect. The most consistent assignment for this system appears to be a $^3\Delta$-$^3\Pi$ system.

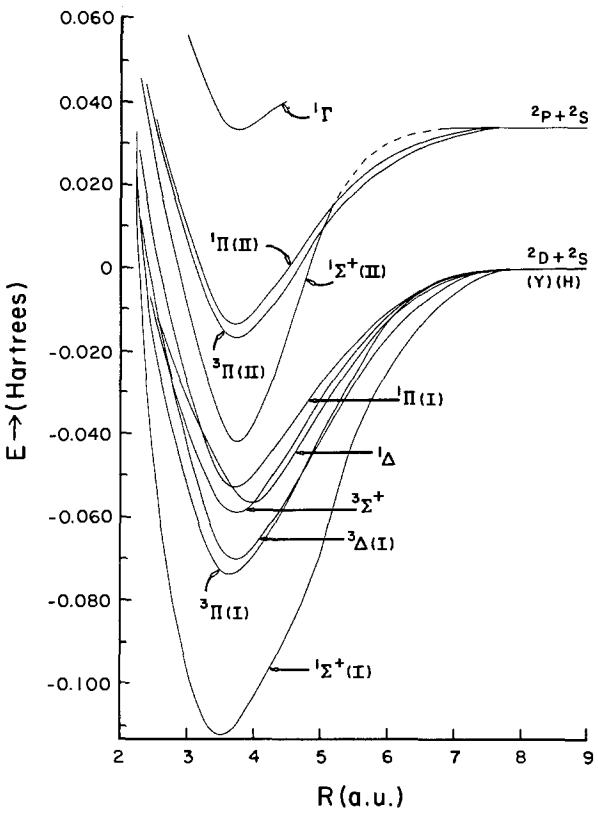

Fig. 8. Potential-energy curves of the selected states of YH. Reproduced from Balasubramanian and Wang (1989a).

Bernard and Bacis (1977) observed six electronic systems ascribed to YH. They also carried out the rotational analysis of these systems and identified the transitions as $^3\Phi \rightarrow {}^3\Delta$, ($^1\Pi$,$^1\Sigma$)-$^1\Sigma$ and ($^1\Sigma$,$^1\Delta$) $\rightarrow {}^1\Pi$. These assignments appear to be incorrect and in any case are not consistent with the theoretically predicted $^1\Sigma^+$ ground state for YH. Their $B'^1\Sigma^+$-$A'^1\Sigma^+$, when reassigned as $B^1\Sigma^+$-$^1\Sigma^+$ system, agrees with the computed T_e of the $^1\Sigma^+$(II) state of Balasubramanian and Wang (1989a, b).

The v_{00} value of the experimental system is $\sim 14\,300\,\text{cm}^{-1}$ while the computed SOCI value for the $^1\Sigma^+$(II) state is $15\,049\,\text{cm}^{-1}$ including spin–orbit coupling. The $B^1\Delta$-$A^1\Pi$ system of Bernard and Bacis has a v_{00} value of $11\,378\,\text{cm}^{-1}$. This system corresponds to the $^1\Pi$-$X^1\Sigma^+$ system whose computed transition energy is $12\,687\,\text{cm}^{-1}$ (Balasubramanian and Wang). Likewise, the $^3\Phi$-$^3\Delta$ system of Bernard and Bacis should also be reassigned.

The Balasubramanian–Wang computed dissociation energy of YH (3.05 eV) agreed with a value of 2.95 eV obtained by Langhoff et al. (1986). However, the dipole moment computed recently by Balasubramanian (1990) using ($4s^2\,4p^6\,4d^1\,5s^2$) RECPs with a large basis set was found to be 0.3 D lower than the value of Langhoff et al.

Following the theoretical calculations, Simard and co-workers (Simard et al. 1991) have obtained $C^1\Sigma^+$-$X^1\Sigma^+$ spectroscopic system of YH as well as a system in the

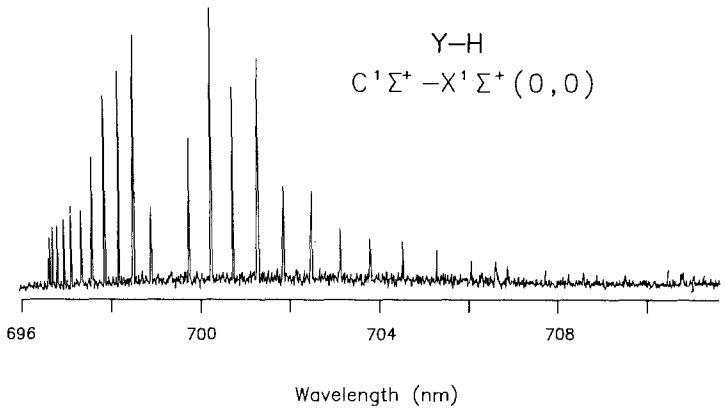

Fig. 9. The C-X system of YH. Reproduced from Simard et al. (1991).

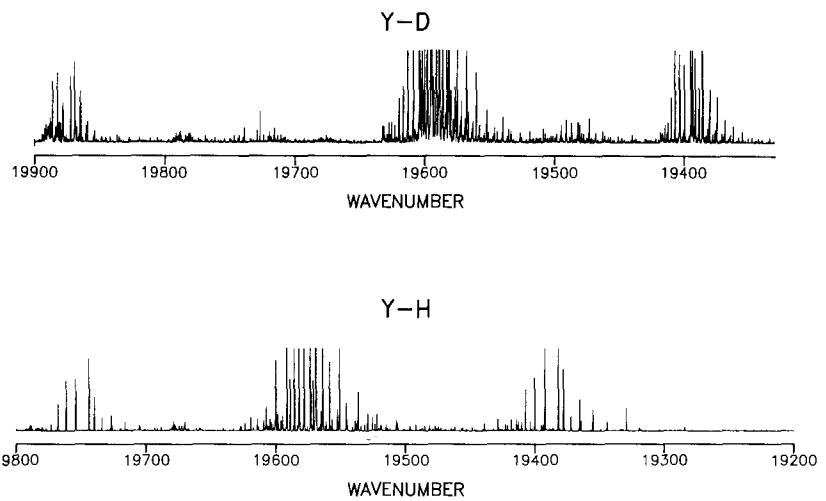

Fig. 10. The spectra of YD and YH in the 19 600 cm^{-1} region. Reproduced from Simard et al. (1991).

19 600 cm^{-1} region. These spectra are shown in figs. 9 and 10. As seen from the assignment of the observed spectra, Simard and co-workers confirm the theoretically predicted $X^1\Sigma^+$ ground state of YH.

Figure 11 shows the calculated energy levels of YH and the experimentally observed levels. As seen from fig. 11, the computed values are in excellent agreement with experiment considering the approximations introduced in the theoretical procedures.

Table 3 shows the contributions of important configurations in the SOCI of the electronic states of YH. In table 3, the π and δ orbitals are non-bonding yttrium orbitals. The contribution from the 5*p* orbital of Y is very noticeable. Most of the other

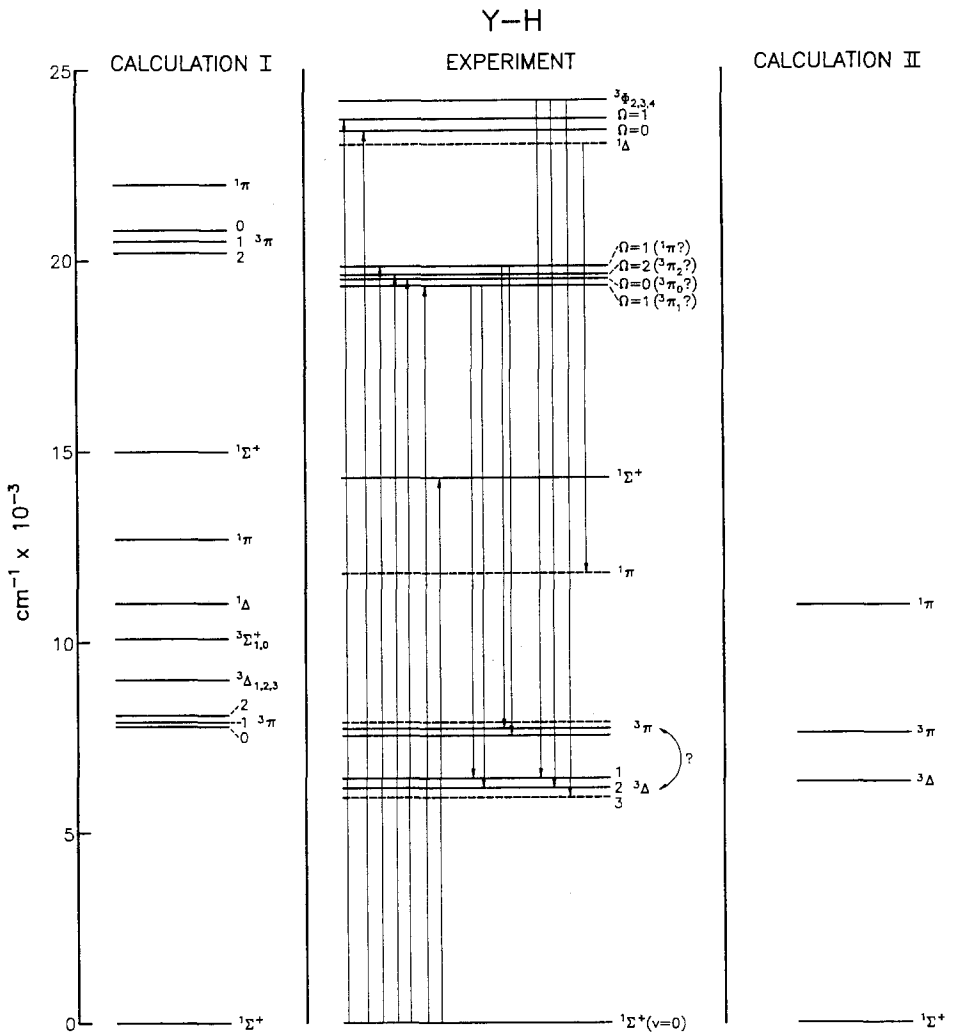

Fig. 11. Predicted and observed energy levels of YH. Calculation I is due to Balasubramanian and Wang (1989a), while calculation II is due to Langhoff et al. (1987). Reproduced from Simard et al. (1991).

electronic states are dominated by a single configuration except the $^1\Sigma^+$(II) state which is a mixture of several configurations.

Table 4 shows the Mulliken populations of various electronic states of YH. As one can see from that table, the gross yttrium populations of all the electronic states are considerably smaller than 3.0 indicating the ionic character of the YH bond with the Y^+H^- polarity. Note that the 5*p* population is between 0.2 and 0.986 in various states. This indicates considerable *dsp* hybridization. This hybridization is the smallest for the $^1\Gamma$ state (0.126) and the largest for the $^1\Pi$(II) (0.986), $^3\Pi$(II) (0.61), $^3\Sigma^+$ (0.751), $^3\Pi$

TABLE 3
The contributions of important configurations in the SOCI wavefunctions of YH. Reproduced from Balasubramanian and Wang (1989a, b).

State	Percentage of contributions
$^1\Sigma^+$	$1\sigma^2 2\sigma^2$ (86), $1\sigma^2 1\pi^2$ (8),
$^3\Pi$	$1\sigma^2 2\sigma^1 1\pi^1$ (94)
$^3\Delta$	$1\sigma^2 2\sigma^1 1\delta^1$ (96)
$^3\Sigma^+$	$1\sigma^2 2\sigma^1 3\sigma^1$ (81)
$^1\Delta$	$1\sigma^2 2\sigma^1 1\delta^1$ (81)
$^1\Pi$	$1\sigma^2 2\sigma^1 1\pi^1$ (80)
$^1\Sigma^+$(II)	$1\sigma^2 2\sigma^1 3\sigma^1$ (58), $1\sigma^2 1\pi\, 2\pi$ (7), $1\sigma^2 1\delta^2$ (6), $1\sigma^2 2\sigma\, 4\sigma$ (5), $1\sigma^2 3\sigma^2$ (5)
$^3\Pi$(II)	$1\sigma^2 1\pi^1 1\delta^1$ (89)
$^1\Pi$(II)	$1\sigma^2 2\sigma^1 2\pi^1$ (85)
$^1\Gamma$	$1\sigma^2 1\delta^2$ (89)

TABLE 4
Mulliken-population analyses of electronic states of YH. Reproduced from Balasubramanian and Wang (1989 a, b).

	Gross							Overlap
State	Y	Y(s)	Y(p)	Y(d)	H	H(s)	H(p)	Y–H
$^1\Sigma^+$	2.694	1.550	0.454	0.690	1.306	1.296	0.010	0.639
$^3\Pi$	2.696	0.947	0.663	1.086	1.304	1.295	0.009	0.690
$^3\Delta$	2.709	0.962	0.368	1.380	1.291	1.283	0.008	0.672
$^3\Sigma^+$	0.735	1.025	0.751	0.959	1.265	1.258	0.007	0.700
$^1\Delta$	2.700	0.791	0.610	1.300	1.300	1.292	0.008	0.680
$^1\Pi$	2.769	0.918	0.350	1.500	1.231	1.224	0.007	0.653
$^1\Sigma^+$(II)	2.782	0.900	0.522	1.361	1.218	1.211	0.006	0.670
$^3\Pi$(II)	2.730	0.293	0.681	1.757	1.270	1.262	0.007	0.680
$^1\Pi$(II)	2.827	0.632	0.986	1.209	1.173	1.168	0.005	0.652
$^1\Gamma$	2.758	0.345	0.126	2.287	1.242	1.235	0.007	0.664

(0.603), and $^1\Delta$ (0.610) states. The *d* population of the ground state is 0.690, and the *d* populations of many other states are between 0.96 and 1.5 with the exception of the $^1\Gamma$ and $^3\Pi$(II) states.

Bauschlicher and Walch (1982) have considered full valence MCSCF/CI calculations on the lowest six electronic states of ScH. Subsequently, Chong et al. (1986) have studied the dipole moments of the first-row hydrides using the MCPF and CASSCF/MRCI techniques.

Table 5 shows the CASSCF and FOCI results for ScH obtained by Bauschlicher and Walch. We note that they too obtain a $^1\Sigma^+$ ground state for ScH analogous to YH. An initial comparison of table 5 with table 2 reveals that the energy separations of the excited states of ScH are below the corresponding values of YH.

The ground state of ScH was found to be mainly composed of Sc(d) and H(s) σ bond while the excited states of ScH exhibited sp hybrid bonds. The dipole moment of ScH in

TABLE 5
Summary of FV-MCSCF and first-order CI for ScH (R_e is in bohr and T_e in cm^{-1}). Reproduced from Bauschlicher and Walch (1982).

	MCSCF		FOCI	
State	R_e	T_e	R_e	T_e
$^1\Sigma^+$	3.39	0	3.37	0
$^3\Delta$	3.67	1412	3.65	2328
$^3\Delta^a$	3.67	2098	3.65	3023
$^3\Pi^a$	3.68	4502	3.61	4995
$^3\Sigma^{+a}$	3.91	5875	3.90	6317

[a] Core taken from $^1\Sigma^+$ SCF.

its $^1\Sigma^+$ state was computed as 1.374 D using the MCPF method if four electrons are correlated and 1.641 D if twelve electrons are correlated.

Figure 12 shows the contour plots of the highest-occupied σ and π orbitals of the $^1\Sigma^+$ ground state of ScH obtained by Bauschlicher and Walch (1982). As for fig. 12, the 7σ orbital is mainly Sc(4s) but is polarized outward perpendicular to the bond axis. The 3π orbital is a non-bonding Sc(4p) orbital. The 6σ bonding orbital is mainly Sc(3dσ) + H(1s) orbital.

Following the Bauschlicher–Walch calculation, Balasubramanian (1987) studied ScH using RECPs and a CASSCF/FOCI method. Table 6 compares the all-electrons result with the ECP result. As seen from table 6, the agreement between the ECP and all-electron result is good.

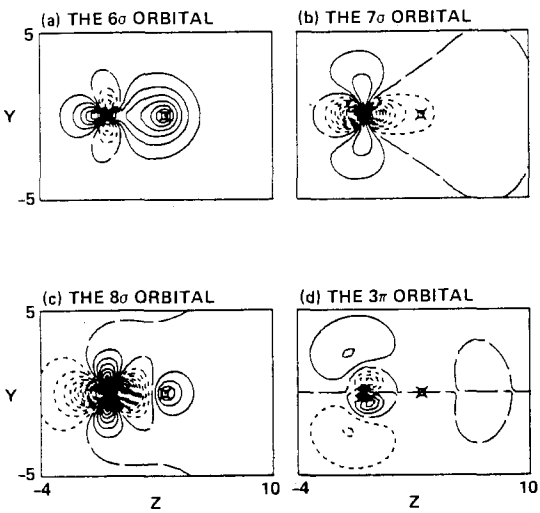

Fig. 12. The highest-occupied natural orbitals of the ground state of ScH. Reproduced from Bauschlicher and Walch (1982).

TABLE 6
Comparison of ECP and all-electron results for ScH. Reproduced from Balasubramanian (1987).

	R_e(Å)		T_e(cm^{-1})	
State	ECP	All-electron[a]	ECP	All-electron
$^1\Sigma^+$	1.744	1.78	0	0
$^3\Delta$	1.884	1.93	2050	2328

[a] Bauschlicher and Walch (1982).

TABLE 7
Energies and equilibrium structures for the low-lying states of YH_2. Reproduced from Balasubramanian and Ravimohan (1988).

	CASSCF			MRSDCI		
State	R (Å)	θ (deg)	E (eV)	R (Å)	θ (deg)	E (eV)
$^2A_1$	1.95	123	0.0[a]	1.94	123	0.0[a]
$^2\Sigma_g^+$	2.02	180	0.37	2.01	180	0.36
$^2B_1$	2.04	133	1.11	2.02	132	1.04
$^2\Pi_g$	2.10	180	1.18	2.08	180	1.16
$^2A_2$	2.04	130	1.66	2.02	126	1.56
$^2\Delta_g$	2.10	180	1.74	2.08	180	1.71

[a] The absolute CASSCF valence energy of $^2A_1$ is -2.550578 Hartree and the MRSDCI valence energy of $^2A_1$ is -2.573984 Hartree.

4.2. *YH_2 and ScH_2*

Balasubramanian and Ravimohan (1988) have computed the potential energy surfaces of three electronic states of YH_2 of $^2A_1$, $^2B_1$ and $^2A_2$ symmetries. They employed a (3s2p4d/3s2p3d) valence Gaussian basis set in conjunction with RECPs which retained the outer $4d^1\,5s^2$ shells of the Y atom in the valence space. A full CASSCF followed by MRSDCI calculations which retained all configurations in the CASSCF with coefficients ≥ 0.05 as reference configurations were made.

Table 7 shows the computed equilibrium geometries and energy separations of the electronic states of YH_2, while fig. 13 shows the potential energy surfaces of three electronic states of YH_2 obtained by Balasubramanian and Ravimohan (1988).

It is evident from table 7 and fig. 13 that $^2A_1$ is the ground state of YH_2 with a bent equilibrium geometry ($R_e = 1.94$ Å, $\theta_e = 123°$). This state is more stable than $^2\Sigma_g^+$ by 0.36 eV. Balasubramanian and Ravimohan (1988) found that the equilibrium structures in all the cases are bent rather than linear. However, unlike in the $^2A_1$ state, $^2A_2$ and $^2B_1$ are very close to the linear states in energy. The stability of the $^2A_1$ ground state with respect to $Y + H_2$ dissociation was found to be 31 kcal/mol at the CASSCF level of theory. It should be mentioned that Balasubramanian and Ravimohan inadvertently compared their computed dissociation energy with the enthalpy of the solid $Y + H_2$ reaction.

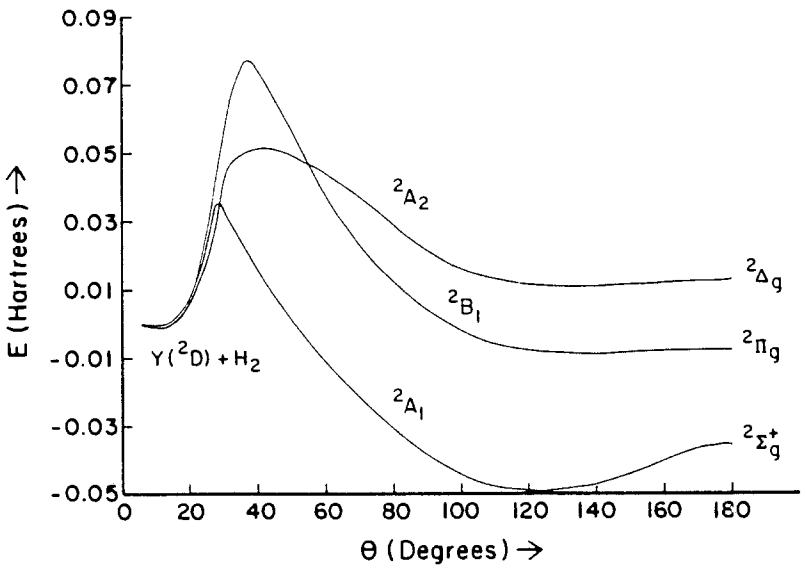

Fig. 13. Potential-energy surfaces of YH_2. Reproduced from Balasubramanian and Ravimohan (1988).

In fig. 13 for each $\theta = H\overset{Y}{\diagup\diagdown}H$ bond angle, Y–H bond lengths were optimized. All the three states have barriers for the insertion of the yttrium atom into H_2 to form YH_2. The saddle points occur near 28, 37 and 40° for $^2A_1$, $^2B_1$ and $^2A_2$ states, respectively. The saddle points were obtained as the superposition of the surfaces obtained by starting from the CASSCF wavefunction of the linear structure and the CASSCF wavefunction of the dissociated structure ($Y + H_2$). The barrier height of the $^2A_1$ surface (0.98 eV) is lower than the corresponding values of $^2B_1$ (2.09 eV) and $^2A_2$ (1.41 eV) states.

Table 8 shows the dipole moments of the $^2A_1$, $^2B_1$ and $^2A_2$ states at their bent equilibrium geometries obtained from the MRSDCI density matrices. All three states have Y^+H^- polarities. The dipole moment of the $^2A_1$ state is the smallest, while that of $^2A_2$ state is the largest. The large dipole moments of these states reveal the ionic character of Y–H bonds.

TABLE 8
Dipole moments for the low-lying states of YH_2. Reproduced from Balasubramanian and Ravimohan (1988).

State	μ(D)[a]
$^2A_1$	1.41
$^2B_1$	3.81
$^2A_2$	6.01

[a] Polarity Y^+H^-.

TABLE 9
Mulliken-population analysis for the low-lying states of YH_2. Reproduced from Balasubramanian and Ravimohan (1988). Populations of the two H atoms are combined together.

State	Gross populations					Y–H overlaps
	Y (total)	H (total)	Y (s)	Y (d)	Y (p)	
$^2A_1$	2.36	2.64	0.83	1.01	0.52	1.35
$^2\Sigma_g^+$	2.40	2.60	0.98	0.92	0.50	1.36
$^2B_1$	2.34	2.66	0.41	1.47	0.45	1.34
$^2\Pi_g$	2.38	2.62	0.44	1.46	0.48	1.34
$^2A_2$	2.47	2.53	0.54	1.55	0.38	1.33
$^2\Delta_g$	2.51	2.49	0.53	1.42	0.56	1.34

The analyses of the leading configurations near equilibrium geometries of the three states of YH_2 revealed that they are dominated by their leading configuration with coefficients ≥ 0.98. The $^2A_1$ ground state is composed of the $1a_1^2 2a_1 1b_2^2$ configuration, wherein the $1a_1$ and $2a_1$ orbitals are mixtures of Y(5s) + H(1s) + H_2(1s) and Y(4d) + H_1(1s) + H_2(1s), respectively. The $1b_2$ orbital is composed of Y($5p_y$) + H_1(1s) − H_2(1s).

Table 9 shows the Mulliken-population analyses of the electronic states of YH_2. The Y population strongly deviates from its neutral 3.0 population suggesting transfer of up to 0.6 electrons to the hydrogen atoms. We also note significant deviation from the neutral $4d^1 5s^2$ electronic configuration near the equilibrium geometries. TheY–H overlaps are also quite significant.

Balasubramanian (1987) studied the insertion of Sc(^{2}D) into H_2 in the $^2A_1$ state. In addition, the linear $^2\Sigma_g^+$, $^2\Pi_g$ and $^2\Delta_g$ states of the ScH_2 molecule were studied. He used a complete active space MCSCF method followed by full second-order CI (SOCI). For the Sc atom, RECPs which retained the outer $3d^1 4s^2$ shells were retained in the valence space. The (4s5d/3s3d) valence Gaussian basis set augmented by two sets of p functions suggested by Wachters was used for the Sc atom.

Figure 14 shows the bending potential energy surface of ScH_2. Again θ is the H$\overset{\text{Sc}}{\diagdown\diagup}$H bond angle, as in fig. 13. For each θ, Sc–H bond lengths were optimized. Table 10 shows the geometries and energy separations of three linear electronic states of ScH_2 at the CASSCF and SOCI levels of theory.

As seen from both fig. 14 and table 10, the Sc atom has to surpass a large barrier of 1.57 eV (SOCI) to insert into H_2 to form the $^2\Sigma_g^+$ state. The $^2\Sigma_g^+$ state thus formed is only 0.22 eV more stable than the dissociated Sc + H_2 species. As seen from fig. 14, there exists a shallow obtuse angle bent minimum for ScH_2. At the CASSCF level, this minimum has $R_e = 1.81$ Å and $\theta_e = 133.4°$. At this level, this minimum was found to be 0.04 eV below $^2\Sigma_g^+$. The author thus suggested that the possibility of an obtuse angle $^2A_1$ ground state for ScH_2 cannot be ruled out, but such a minimum formed only a shallow potential well.

Table 11 shows the Mulliken populations of the SOCI natural orbitals of ScH_2 obtained by Balasubramanian (1987). The leading configuration of the $^2\Sigma_g^+$ state of

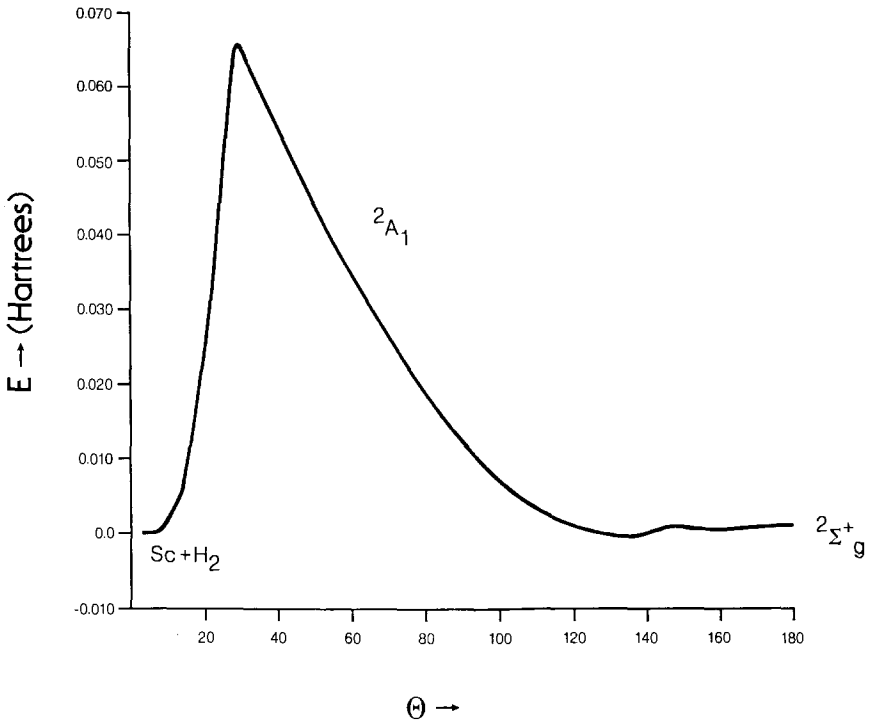

Fig. 14. Potential-energy surface of the $^2A_1$ state of ScH_2. Reproduced from Balasubramanian (1987).

TABLE 10
Geometries and energies of low-lying states of ScH_2. Reproduced from Balasubramanian (1987).

Method	State	R_e (Å)	θ_e (degrees)	E (eV)
SOCI	$^2\Sigma^+_g$	1.84	180.0	0.0[a]
SOCI	$^2\Pi_g$	1.91	180.0	0.16
SOCI	$^2\Delta_g$	1.91	180.0	0.62
SOCI	Sc + H_2			0.22
SOCI	$^2A_1$ (barrier)			1.57[b]
CASSCF	$^2\Sigma^+_g$	1.86	180.0	0.0[c]
CASSCF	$^2\Pi_g$	1.94	180.0	0.19
CASSCF	$^2\Delta_g$	1.94	180.0	0.68
CASSCF	$^2A_1$	1.83	29.0	1.81[d]

[a] SOCI energies reported with respect to the energy of the $^2\Sigma^+_g$ state at its equilibrium geometry.
[b] The energy splitting between the linear geometry and the barrier evaluated at the CAS geometries.
[c] Energies reported with respect to the $^2\Sigma^+_g$ CASSCF energy.
[d] The energy of the barrier at the estimated CASSCF geometry with respect to the $^2\Sigma^+_g$ minimum.

TABLE 11
Mulliken-population analysis (net and overlap) of the low-lying states of ScH_2 at their equilibrium geometries. Populations of both the hydrogen atoms are grouped together. Reproduced from Balasubramanian (1987).

	Net population							
State	Sc	H	Sc (s)	Sc (d)	Sc(p)	H(s)	H(p)	Overlap
$^2\Sigma_g^+$	1.77	1.90	0.75	0.81	0.22	1.89	0.01	1.33
$^2\Pi_g$	1.67	1.99	0.41	1.16	0.21	1.98	0.01	1.35
$^2\Delta_g$	1.74	1.92	0.47	1.14	0.25	1.91	0.01	1.35

ScH_2 is $1\sigma_g^2\, 1\sigma_u^2\, 1\sigma_g^1\,(-0.967)$. The $1\sigma_g$ orbital is primarily a bonding orbital of Sc 4s and H 1s (Sc 3d makes non-negligible contributions). The $2\sigma_g$ orbital is dominantly Sc 3d and 1s but is slightly anti-bonding with respect to hydrogen 1s orbitals. The $1\sigma_u$ is primarily Sc(4p) + H_1(1s) − H_2(1s). As seen from table 11, the Sc(4s) net population is smaller but the 4p population is not zero suggesting considerable 4p mixing in the $1\sigma_u$ orbital.

Now we compare YH_2 with ScH_2 while the bending potential-energy surface of the $^2A_1$ state of ScH_2 has a shallow bent minimum ($\theta_e = 133.4°$, $R_e = 1.81$ Å), the $^2A_1$ surface YH_2 has a well-bound minimum ($\theta_e = 123°$, $R_e = 1.95$ Å). The $^2A_1$–$^2\Sigma_g^+$ splitting is very small for ScH_2 while it is somewhat large for YH_2. The barrier to insert the Sc atom into H_2 is about 36 kcal/mol in the $^2A_1$ surface, while for the Y atom the corresponding barrier is about 23 kcal/mol, which is much smaller. Thus, the Y atom is found to be more reactive with H_2 than Sc. The $^2A_1$ bent YH_2 state is more stable with respect to Y + H_2 by about 31 kcal/mol while the $^2\Sigma_g^+$ state of ScH_2 is only 5 kcal/mol more stable than Sc + H_2. Thus, bonding in YH_2 is much stronger than in ScH_2.

The total gross population of Sc in the $^2\Sigma_g^+$ state of ScH_2 is 2.44 while the corresponding population is 2.40 in YH_2. This suggests greater charge transfer from Y to H in YH_2 compared to ScH_2. The Y(5p) population of all electronic states of YH_2 (cf., table 9) are considerably larger than the corresponding Sc(4p) populations. This suggests greater involvement of the Y ($5p_y$) orbital in the $1b_2$ orbital of YH_2.

4.3. *LaH*

Das and Balasubramanian (1990) computed the spectroscopic constants and potential energy curves of 20 electronic states of LaH. They used RECPs with $5s^2\, 5p^6\, 5d^1\, 6s^2$ valence shells for the La atom together with a (5s5p3d1f) valence Gaussian basis set. CASSCF followed by the FOCI method of calculation was used to compute the potential-energy curves while the spectroscopic constants were obtained using the SOCI method. In addition, the spin–orbit effects were introduced using the RCI method.

Table 12 shows the computed energy separation for the atomic states of La compared with experimental values together with the possible molecular states of LaH. As evidenced from table 12, there are several possible low-lying electronic states for LaH.

TABLE 12
Dissociation relationships for some low-lying electronic states of LaH. Reproduced from Das and Balasubramanian (1990).

Molecular state	Atomic state (La + H)	Energy (cm^{-1}) SOCI	Energy (cm^{-1}) Exp.[a]
$^1\Sigma^+, ^1\Pi, ^1\Delta, ^3\Sigma^+, ^3\Pi, ^3\Delta$	$a\,^2D(d^1s^2) + {}^2S$	0	0
$^1\Sigma^-, ^1\Pi, ^1\Delta, ^1\Phi, ^3\Sigma^-, ^3\Pi, ^3\Delta, ^3\Phi$	$a\,^2F(d^2s^1) + {}^2S$	5706	6961
$^1\Sigma^+, ^1\Pi, ^1\Delta, ^3\Sigma^+, ^3\Pi, ^3\Delta$	$b\,^2D(d^2s^1) + {}^2S$	9437	8249
$^1\Sigma^+, ^1\Pi, ^1\Delta, ^1\Phi, ^1\Gamma, ^3\Sigma^+, ^3\Pi, ^3\Delta, ^3\Phi, ^3\Gamma$	$a\,^2G(d^2s^1) + {}^2S$	11193	9280

[a] Averaged over J.

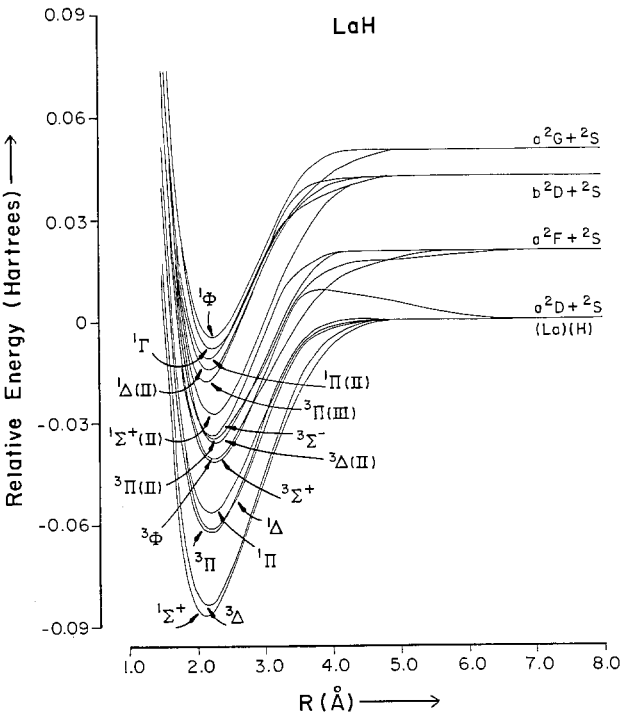

Fig. 15. Potential-energy curves for LaH. Reproduced from Das and Balasubramanian (1990).

Figure 15 shows the potential-energy curves for LaH obtained using the CASSCF/FOCI method while table 13 shows the SOCI spectroscopic constants of LaH. As seen from table 13, the ground state of LaH is a $X\,^1\Sigma^+$ state with $R_e = 2.08$ Å and $\omega_e = 1433\,cm^{-1}$.

Bernard and Bacis (1976) have observed B↔A, C→A and b→a systems of LaH. They have made rotational analysis of the observed systems and assign these three systems to $^1\Delta$–$^1\Pi$, $^1\Sigma$–$^1\Pi$ and $^3\Phi$–$^3\Pi$ systems, respectively.

TABLE 13
Spectroscopic properties of LaH. Reproduced from Das and Balasubramanian (1990).

State	R_e (Å)	ω_e (cm^{-1})	T_e (cm^{-1})	D_e (eV)	μ_e (D)
$X^1\Sigma^+$	2.08	1433	0	2.60	2.42
$^3\Delta$	2.13	1352	2805	2.24	3.63
$a\,^3\Pi$	2.12	1341	5147	1.92	2.32
$^1\Pi$	2.13	1309	6226	1.80	3.95
$^1\Delta$	2.16	1299	6510	1.77	0.25
$^3\Phi$	2.19	1240	10612	2.00	4.89
$^3\Sigma^+$	2.20	1203	11794	1.20	−0.49
$^3\Pi$ (II)	2.19	1228	11956	1.83	4.24
$^3\Sigma^-$	2.18	1247	12035	1.86	5.40
$A\,^1\Sigma^+$ (II)	2.20	1230	13025	2.17	2.17
$^3\Delta$ (II)	2.24	1166	14020	1.61	1.63
$B^1\,\Pi$ (II)	2.16	1293	15729	1.77	3.24
$^3\Pi$ (III)	2.09	1377	15880	1.81	3.14
$^3\Sigma^-$ (II)	2.17	1251	16107	1.35	4.17
$^1\Gamma$	2.18	1260	16838	1.88	6.51
$^1\Phi$	2.18	1259	17333	1.79	4.46
$^1\Delta$ (II)	2.18	1234	17427	1.60	5.49
$^1\Delta$ (III)	2.20	1226	20109	–	2.21
$C\,^1\Pi$ (III)	2.19	1342	20170	–	6.15
$b\,^3\Delta$ (III)	2.10	1364	23256	–	4.48

It is evident from table 13 that the $^1\Pi$ state is not the ground state of LaH. Hence, Das and Balasubramanian (DB) argued that the A state of Bernard and Bacis should be reassigned to the $X\,^1\Sigma^+$ ground state of LaH. Das and Balasubramanian suggested reassignment of the Bernard–Bacis assignment in accordance with table 13. These suggested assignments are also consistent with LaF (Barrow et al. 1967, Schall et al. 1987). The ground state of LaF is now well known to be a $X\,^1\Sigma^+$ state. For LaF excited $A\,^1\Sigma^+$, $B\,^1\Pi$, $C\,^1\Pi$, $D\,^1\Sigma^+$ and $E\,^1\Sigma^+$ states have been observed and assigned through the analysis of $A \leftarrow X$, $B \leftarrow X$, $C \leftarrow X$, $D \leftarrow X$, and $E \leftarrow X$ systems. The v_{00} values for these transitions are 11 662, 16 184, 20 960, 22 485 and 22 574 cm^{-1}, respectively. The well-characterized spectra of LaF supported the assignment in table 12.

The $A\,^1\Sigma^+ \leftrightarrow X\,^1\Sigma^+$ system predicted at 13 000 cm^{-1} has not yet been observed. The corresponding transition for LaF has been observed at 11 662 cm^{-1}. The $B \leftrightarrow X$ system, with a theoretically predicted T_e value of 15 730 cm^{-1}, is consistent with the v_{00} band head of the experimentally observed $B \leftrightarrow A$ system (15 619 cm^{-1}). It is also consistent with the rotational analysis of Bernard and Bacis which suggested that $\Delta\lambda = +1$ for this transition. For LaF, this system appears with $v_{00} = 16\,184\,cm^{-1}$.

The $C \rightarrow A$ system of Bernard and Bacis with a $v_{00} = 18\,595\,cm^{-1}$ was found to be most consistent with the $C\,^1\Pi \rightarrow X\,^1\Sigma^+$ system by DB, with a theoretical $T_e = 20\,170\,cm^{-1}$. Likewise, the triplet–triplet transition observed with $v_{00} = 16\,000\,cm^{-1}$ was assigned to $b\,^3\Delta \leftrightarrow a\,^3\Pi$ by DB with a theoretical $v_{00} = 18\,100\,cm^{-1}$. The differences between theoretical and experimental values were found to be within the error bars of calculations for excited states.

TABLE 14
Contribution of various leading configurations to the SOCI wavefunctions at the equilibrium geometries of the electronic states of LaH. Reproduced from Das and Balasubramanian (1990).

State	Electronic configurations (percentage)
$^1\Sigma^+$	$1\sigma^2 2\sigma^2$ (86), $1\sigma^2 1\delta^2$ (6), $1\sigma^2 1\pi^2$ (4)
$^3\Delta$; $^1\Delta$	$1\sigma^2 2\sigma 1\delta$ (97); $1\sigma^2 2\sigma 1\delta$ (87), $1\sigma^2 1\pi^2$ (10)
$^3\Pi$; $^1\Pi$	$1\sigma^2 2\sigma 1\pi$ (95); $1\sigma^2 2\sigma 1\pi$ (74), $1\sigma^2 1\delta 1\pi$ (20)
$^3\Phi$; $^1\Phi$	$1\sigma^2 1\delta 1\pi$ (95; 90)
$^3\Sigma^+$	$1\sigma^2 2\sigma 3\sigma$ (52), $1\sigma^2 2\sigma 4\sigma$ (24), $1\sigma^2 2\sigma 5\sigma$ (12)
$^3\Sigma^-$	$1\sigma^2 1\delta^2$ (60), $1\sigma^2 1\pi 2\pi$ (4), $1\sigma^2 2\pi 3\pi$ (4), $1\sigma^2 1\pi^2$ (3), $1\sigma^2 1\delta 2\delta$ (3)
$^3\Pi$(II); $^1\Pi$(II)	$1\sigma^2 1\delta 1\pi$ (86; 56), $1\sigma^2 2\sigma 1\pi$ (3; 16)
$^1\Sigma^+$(II)	$1\sigma^2 2\sigma 3\sigma$ (23), $1\sigma^2 1\delta^2$ (32), $1\sigma^2 2\sigma 4\sigma$ (11), $1\sigma^2 2\sigma 5\sigma$ (10)
$^3\Delta$(II)	$1\sigma^2 2\sigma 1\delta$ (42), $1\sigma^2 3\sigma 1\delta$ (17), $1\sigma^2 4\sigma 1\delta$ (14), $1\sigma^2 5\sigma 1\delta$ (10), $1\sigma^2 6\sigma 1\delta$ (7)
$^3\Sigma^-$(II)	$1\sigma^2 1\delta^2$ (30), $1\sigma^2 1\pi 2\pi$ (12), $1\sigma^2 1\pi 3\pi$ (12), $1\sigma^2 1\pi^2$ (5), $1\sigma^2 2\pi 3\pi$ (5)
$^3\Pi$(III); $^1\Pi$(III)	$1\sigma^2 2\sigma 1\pi$ (55), $1\sigma^2 2\sigma 2\pi$ (22); $1\sigma^2 1\delta 1\pi$ (39), $1\sigma^2 2\sigma 1\pi$ (17), $1\sigma^2 1\delta 2\pi$ (16)
$^1\Gamma$	$1\sigma^2 1\delta^2$ (95)
$^1\Delta$(II)	$1\sigma^2 2\sigma 1\delta$ (40), $1\sigma^2 1\pi^2$ (11), $1\sigma^2 3\sigma 1\delta$ (8), $1\sigma^2 1\pi 2\pi$ (8), $1\sigma^2 4\sigma 1\delta$ (7)
$^1\Delta$(III)	$1\sigma^2 1\pi^2$ (36), $1\sigma^2 2\sigma 1\delta$ (22), $1\sigma^2 1\pi 2\pi$ (13), $1\sigma^2 1\pi 3\pi$ (9)
$^3\Delta$(III)	$1\sigma^2 1\pi 2\pi$ (41), $1\sigma^2 1\pi 3\pi$ (17), $1\sigma^2 1\pi 4\pi$ (12), $1\sigma^2 2\pi 5\pi$ (9)

The dipole moments in table 13 are large and positive suggesting La^+H^- polarities. Some of the excited states have very large dipole moments showing significant La^+H^- charge separations.

Table 14 shows the weights of the leading configurations for the electronic states of LaH. Even the ground state of LaH is a mixture of $1\sigma^2 2\sigma^2$, $1\sigma^2\delta^2$ and $1\sigma^2\pi^2$ configurations. The excited electronic states are considerably more complex as evidenced from table 14.

We now compare the properties of ScH, YH, and LaH. In comparing the R_e values of the three molecules in their $^1\Sigma^+$ ground states, we note that there is a sharp rise in comparing the bond lengths of ScH with YH. However, the bond lengths of YH (1.95 Å) and LaH (2.08 Å) are quite similar. This is primarily because of the sharp rise in the $5p_y$ orbital participation in YH compared to ScH. Although the 6p population decreases for LaH, the 6s population rises slightly. The La(5d) population is enhanced in the $^1\Sigma^+$ state.

Figure 16 compared the D_es of ScH, YH and LaH. We note that the M–H bond strength is significantly enhanced in going from ScH to YH, but the D_e decreases in going from YH and LaH.

Another quantity of interest is the μ_e/R_e ratio. This quantity compares the extent of charge transfer in the three species. As seen from fig. 17, the μ_e/R_e values are similar for ScH and YH, but dramatically increases for LaH. This suggests significant ionic character of the La–H bond.

The 1σ valence orbital of LaH is composed of La(6s) + H(1s) while the 2σ orbital is composed of La(5d), La($6p_z$) and H(1s). Of course, the π and δ orbitals are non-bonding. The Mulliken-population analysis of the $^1\Sigma^+$ ground state of LaH revealed that the La population is $6s^{1.52}\,6p^{0.22}\,5d^{0.97}$.

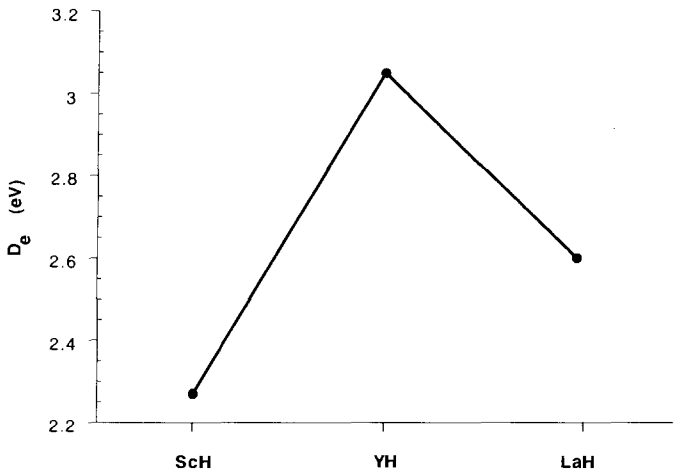

Fig. 16. Dissociation energies of ScH, YH and LaH.

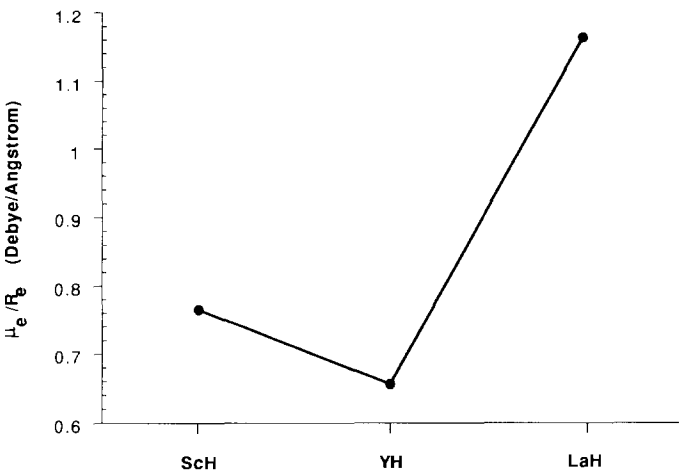

Fig. 17. Dipole moment per unit M–H distance for ScH, YH and LaH.

4.4. LaH^+

Das and Balasubramanian (1991c) have computed the spectroscopic constants and potential-energy curves of LaH^+. They used a CASSCF method followed by full second-order CI calculations in conjugation with $5s^2\,5p^6\,5d\,6s^2$ RECPs of Ross et al. (1990). The basis set used was (5s5p3d) valence Gaussian basis set. At both CASSCF and SOCI levels, excitations from the $5s^2\,5p^6$ shells were not allowed. The CASSCF calculations

TABLE 15
Dissociation relationships of the low-lying states of LaH^+. Reproduced from Das and Balasubramanian (1991c).

Atomic states	Molecular states	Energy (cm^{-1})	
		Theory	Exp.[a]
$a\,^3F\,(5d^2) + {}^2S$	$^2\Sigma^-$, $^2\Pi$, $^2\Delta$, $^2\Phi$, $^4\Sigma^-$, $^4\Pi$, $^4\Delta$, $^4\Phi$	0	0
$a\,^1D\,(5d^1\,6s^1) + {}^2S$	$^2\Sigma^+$, $^2\Pi$, $^2\Delta$	288	179
$a\,^3D\,(5d^1\,6s^1) + {}^2S$	$^2\Sigma^+$, $^2\Pi$, $^2\Delta$, $^4\Sigma^+$, $^4\Pi$, $^4\Delta$	1604	1590

[a] Experimental values are J averaged from Moore (1971).

included four a_1, one b_2, one b_1 and one a_2 orbitals in the active space. The spin–orbit effects were included using the RCI method.

Elkind and Armentrout (1986a, b) have studied the periodic trends in the reactivity of Sc^+, Y^+, La^+ and Lu^+ with H_2 using ion–molecular collision of the type

$$La^+ + H_2 \longrightarrow LaH^+ + H$$

They measure the D_0^0 value of LaH^+ as 2.48 ± 0.09 eV. Elkind and Armentrout (1986a, b) proposed several mechanisms for the formation of LaH^+. The theoretical calculations of Das and the author not only provided an unambiguous mechanism for the formation of LaH^+, but also explained the observed branching ratios of LaD^+ and LaH^+ in the $La^+ + HD$ reaction. There are similar studies by Elkind and Armentrout (1986a, b) on the reactivities of other transition metal ions with H_2, see also Armentrout and Beauchamp (1989), as well as Martinho and Beauchamp (1990).

Table 15 compares the computed dissociation limits of the electronic states of LaH^+ by Das and Balasubramanian together with experimental atomic data from Moore's book (Moore 1971). The experimental values are averaged with respect to J, so that comparison of energies can be made in the absence of spin–orbit coupling. As seen from table 15, although the ground state of La^+ is a ^3F state arising from the $5d^2$ configuration, the excited electronic state of ^1D and ^3D symmetries arising from the $5d^1\,6s^1$ configuration are quite closer. Although the ground state of the La atom is ^2D arising from $5d^1\,6s^2$, it is quite interesting that La^+ has a $5d^2$ ground state rather than $5d^1\,6s^1$ or $6s^2$ ground states. Since the lanthanide contraction is experienced only by Hf onwards, the 6s orbital of La has no contraction from this effect since the 4f shells have not yet started filling up. The effect of relativity is also rather small. Consequently, the removal of a 6s electron is favored for La^+. Subsequent to the removal of a 6s electron the electronic configuration rearranged to form a ^3F state for La^+. We note that Hf^+ has a $5d\,6s^2$ (^2D) ground state rather than $5d^2\,6s$ since removal of a 6s electron becomes considerably more difficult for Hf primarily due to lanthanide contraction and to a less extent because of relativity.

As evidenced from table 15, there are several doublet and quartet low-lying electronic states of LaH^+. Figure 18 shows the potential-energy curves for several electronic states of LaH^+ computed by Das and Balasubramanian (1991c). Table 16 shows

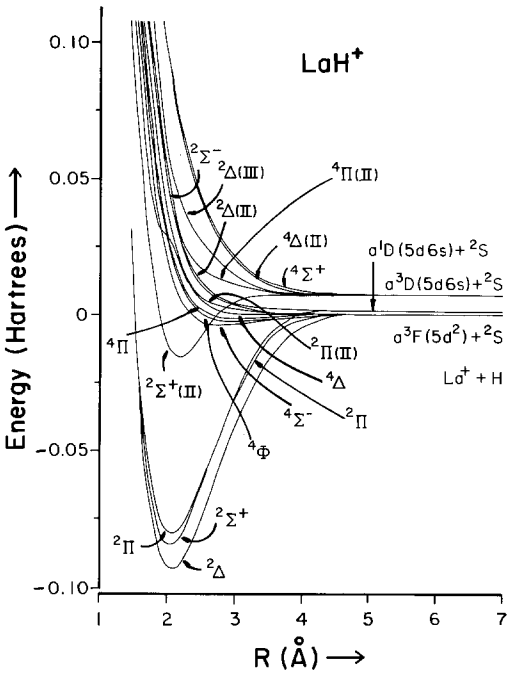

Fig. 18. Potential-energy curves for LaH^+. Reproduced from Das and Balasubramanian (1991c).

TABLE 16
Spectroscopic constants of the low-lying states of LaH^+. Reproduced from Das and Balasubramanian (1991c).

State	R_e (Å)	ω_e (cm^{-1})	T_e (cm^{-1})	μ_e (D)	D_e (eV)	
					Theory	Exp.[a]
$^2\Delta$	2.074	1480	0	4.41	2.54	2.57 ± 0.09
$^2\Sigma^+$	2.040	1517	1948	3.60	2.33	
$^2\Pi$	2.064	1462	2855	4.08	2.19	
$^2\Sigma^+$ (II)	2.184	1287	17082	–	–	
$^4\Sigma^-$	2.774	407	19597	–	–	
$^4\Phi$	2.972	346	19874	–	–	
$^4\Pi$	3.087	229	20127	–	–	

[a] The experimental D^0 from Elkind et al. (1989) was corrected for zero-point correction using our calculated ω_e to obtain experimental D_e.

the spectroscopic constants of bound electronic states of LaH^+. As evidenced from fig. 18, doublet states dissociating into $La^+(^3F) + H$ are bound. The $^4\Sigma^-$, $^4\Phi$ and $^4\Pi$ states have only long-range minima.

The quartet states of LaH^+ do not form very deep potential wells since La^+ in these states does not hybridize much and remain in a configuration closer to the La^+ $5d^2$ configuration. The low spin states of La^+, to the contrary, undergo significant 5d–6s as well as 5d6s6p hybridization so that pronounced minima are formed.

As seen from table 16, the ground state of LaH^+ is $^2\Delta$. Several authors (Schilling et al. 1987, Alvarado-Swaisgood and Harrison 1985, Aglada et al. 1981) have studied ScH^+. They find that ScH^+ too has a $^2\Delta$ ground state. The first excited $^2\Sigma^+$ state of LaH^+ in only $\sim 1950\,cm^{-1}$ above the ground state. The R_e values of all doublet states are uniformly between 2.04 and 2.18 Å. The quartet states to the contrary from longer R_es consistent with the high spin characters of these states.

The $^4\Pi$–$^2\Delta$, $^4\Phi$–$^2\Delta$ weak spin-change transitions are predicted in the $20\,000\,cm^{-1}$ region. The $^2\Sigma^+(II)$–$^2\Sigma^+$ transition occurs in the $15\,000\,cm^{-1}$ region. Since the dipole moments of charged species are gauge-dependent, all μ_es listed in table 16 were obtained by placing the dipole operator on the La atom. The positive polarity of the dipole moment of the doublet states indicates that there is electronic charge transfer from La^+ to H. Since the IP of La is much smaller than H, most of the ionization takes place on La.

As we stated before, Elkind et al. (1989) have measured the $D^0(LaH^+)$ as 2.48 eV using guided ion-mass spectrometry. The experimental D_e value including zero-point correction is 2.57 eV. The CASSCF/SOCI value of 2.54 eV computed by Das and Balasubramanian (1991c) was in excellent agreement with the experiment.

The ground state of LaH is a $^1\Sigma^+$ state with $R_e = 2.08$ Å and $\omega_e = 1433\,cm^{-1}$ (see section 4.3). The adiabatic ionization energy for the process

$$LaH(^1\Sigma^+) \longrightarrow LaH^+(^2\Delta) + e^-$$

was computed as 5.33 eV by Das and the author. They also computed the SOCI IP of the La atom as 5.3 eV in reasonable agreement with the experimental value of 5.61 eV (Moore 1971). Therefore, Das and the author predicted theoretical adiabatic IP of LaH to be roughly 0.3 eV below its true value and thus 5.65 ± 0.1 eV.

Das and the author computed the spin–orbit effects for low-lying states of LaH^+. They found that the spin–orbit splittings of the low-lying doublet electronic states of LaH^+ to be between 590 and $694\,cm^{-1}$. The $^2\Pi_{1/2}$–$^2\Pi_{3/2}$ spin–orbit splitting was found to be $694\,cm^{-1}$ while the ground state splitting was calculated as $590\,cm^{-1}$. The spin–orbit mixing of different states was found to be rather small for all states except the $\frac{3}{2}$ states for which $^2\Delta_{3/2}$ and $^2\Pi_{3/2}$ mixing was roughly 2%. Since the ground state of LaH^+ is formed through promotion of some of the 5d electronic density to the 6s orbital, the spin–orbit separation reduces near the potential well of LaH^+.

Table 17 shows the leading configuration in the SOCI wavefunctions of LaH^+ computed by Das and Balasubramanian (1991c). The $^2\Delta$ ground state of LaH^+ is predominantly $1\sigma^2\,1\delta$. The 1σ orbital was found to be a mixture of $La^+(d\sigma)$ and $La^+(6s)$ + H(1s) orbital while the 1δ is a non-bonding $La^+(d\delta)$ orbital. The $^2\Sigma^+$ state is somewhat more complex in that it is a mixture of $1\sigma^2\,2\sigma$, $1\sigma^2\,3\sigma$ and $1\sigma^2\,4\sigma$ configurations. The La(6s) orbital makes significant contribution to the 2σ orbital. The $^2\Pi$ state is analogous to the $^2\Delta$ state. Two quartet states of LaH^+, the $^4\Sigma^-$ and $^4\Pi$ states, are especially complex while the $^4\Phi$ state is relatively simple. Since 2σ participates in the second leading configuration of $^4\Pi$ (36%), the La(6s) orbital makes non-negligible contribution to the $^4\Pi$ state. The $^4\Sigma^-$ state is a mixture of $1\sigma\,1\pi^2$ and $1\sigma\,1\delta^2$.

Table 18 shows Mulliken-population analyses of electronic states of LaH^+ obtained by Das and Balasubramanian (1991c). There is a transfer of 0.24 eV from La^+ to H in

TABLE 17
Contributions of important configurations in the SOCI wavefunctions of LaH^+. Reproduced from Das and Balasubramanian (1991c).

State	Configuration (percentage)
$^2\Delta$	$1\sigma^2 1\delta(97)$
$^2\Sigma^+$	$1\sigma^2 2\sigma$ (73), $1\sigma^2 3\sigma$ (10), $1\sigma^2 4\sigma$ (5)
$^2\Pi$	$1\sigma^2 1\pi$ (97)
$^2\Sigma^+$(II)	$1\sigma^2 2\sigma$ (34), $1\sigma^2 3\sigma$ (27), $1\sigma^2 4\sigma$ (10), $1\sigma^2 5\sigma$ (9), $1\sigma^2 6\sigma$ (6)
$^2\Sigma^-$	$1\sigma\, 1\pi^2$ (85), $1\sigma\, 1\delta^2$ (15)
$^4\Phi$	$1\sigma\, 1\pi\, 1\delta$ (99)
$^4\Pi$	$1\sigma\, 1\pi\, 1\delta$ (58), $1\sigma\, 2\sigma\, 1\pi$ (36)

TABLE 18
Mulliken-population analyses of the low-lying states of LaH^+. Reproduced from Das and Balasubramanian (1991c). The $5s^2\, 5p^6$ core populations are subtracted from the Mulliken populations in this table.

	Gross population						Overlap
State	La	H	La(s)	La(p)	La(d)	H(s)	population
$^2\Delta$	1.76	1.24	0.15	0.04	1.56	1.24	0.53
$^2\Sigma^+$	1.79	1.21	0.87	0.04	0.88	1.20	0.53
$^2\Pi$	1.79	1.21	0.18	0.06	1.55	1.20	0.53
$^2\Sigma^+$ (II)	1.70	1.30	0.32	0.57	0.82	1.29	0.47
$^4\Sigma^-$	2.07	0.93	0.03	0.03	2.01	0.93	0.09
$^4\Phi$	2.06	0.94	0.02	0.02	2.02	0.94	0.09
$^4\Pi$	2.06	0.94	0.12	0.02	1.92	0.94	0.08

the $^2\Delta$ ground state. Note that the $^2\Sigma^+$ state has a $5d^{0.88}\, 6s^{0.87}$ population since 2σ orbital is singly occupied in the leading configuration of the $^2\Sigma^+$ state. The $^2\Sigma^+$(II) state has larger $La^+(6s)$ population compared to other states. The La(6p) population is relatively small in all but the $^2\Sigma^+$(II) state. In the ground state, the La population is $5d^{1.56}\, 6s^{0.15}$, and hence 6s population is rather small. Note that La experiences the effects of neither lanthanide contraction nor relativity as much as Hf and ensuing elements.

4.5. LaH_2^+

Das and Balasubramanian (1991c) computed the bending potential-energy surfaces of eight electronic states of LaH_2^+ arising from the insertion of $La^+(^3F; 5d^2)$ and $La^+(^1D; 5d^1\, 6s^1)$ into H_2. They used the CASSCF/SOCI methods together with the same RECPs and basis sets described in section 4.4. Rosi and Bauschlicher (1990) have studied binding of La^+ and La^{2+} to C_2H_2, C_2H_4 and C_3H_6.

Figure 19 shows the computed potential energy surfaces of eight electronic states of LaH_2^+. In fig. 19, θ is the $H\overset{La}{\diagdown\diagup}H$ bond angle. For each θ, the La – H bond lengths were optimized and the optimized energies are plotted in fig. 19. Separate CASSCF calculations were made for each state. The CASSCF active space included four a_1, two b_2, one

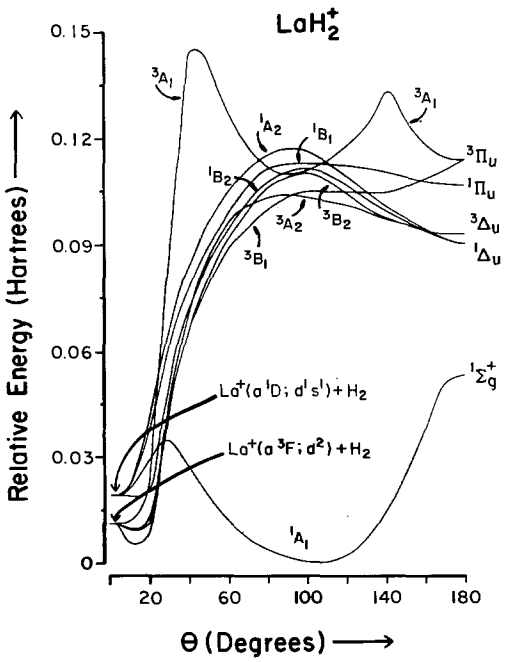

Fig. 19. Potential-energy curves for LaH_2^+. Reproduced from Das and Balasubramanian (1991c).

b_1 and one a_2 orbitals in the C_{2v} symmetry. For very small bond angles ($\theta \sim 5°$), the optimized La–H bond lengths become very long, hence leading to $La^+ + H_2$ dissociation. Consequently, the bending potential-energy surfaces model insertion La^+ into H_2.

As evidenced in fig. 19, La^+ in its ^1D excited state ($5d^1\,6s^1$) inserts into H_2 with a small barrier of < 8 kcal/mol. This is not the case for the ^3F ground state of H_2. It forms only small angle complexes in three channels. Subsequent, for the formation of these complexes La^+ has to surmount a high barrier to insert into H_2 in all channels for the triplet state. The intersection of the $^1A_1$ surface with the triplet surfaces could facilitate non-adiabatic channels for the reactivity of ^3F state of La^+. However, spin–orbit coupling which is one possible source of interaction was found to be rather small. Also, the La–H bond lengths at the θ intersection of the two states are quite different. However, since $La^+(^1D)$ is only a few hundred cm^{-1} above $La^+(^3F)$, initial beam could consist of $La^+(^1D)$ in large percentage and then could undergo insertion into H_2.

The insertion of ^1D state of La^+ into H_2 leads to several states among which $^1A_1$ is decisively the only favorable state. The ground state of LaH_2^+ is $^1A_1$ and has a bent equilibrium geometry. Table 19 shows the equilibrium geometries of the low-lying electronic states of LaH_2^+, from which it can be seen that the ground state of LaH_2^+ is a $^1A_1$ state with $R_e = 2.057$ Å and $\theta_e = 106°$. We note that $^3A_1$ is the only other state exhibiting a bent molecular geometry.

The $^3B_1$, $^3B_2$ and $^3A_2$ states contain small angle minima corresponding to loose complexes of La^+ with H_2. These weak complexes are 2–3 kcal/mol more stable than

TABLE 19
Geometries and energies of the low-lying states of LaH_2^+. Reproduced from Das and Balasubramanian (1991c).

State	CASSCF			SOCI		
	R_e (Å)	θ_e (deg)	E (eV)	R_e (Å)	θ_e(deg)	E (eV)
$^1A_1$	2.070	105.0	0.0	2.057	106.0	0.0
$^1\Sigma_g^+$	2.205	180.0	1.44	2.193	180.0	1.42
$^1\Delta_u$	2.277	180.0	2.49	2.263	180.0	1.42
$^3\Delta_u$	2.274	180.0	2.53	2.263	180.0	2.68
$^3\Pi_u$	2.258	180.0	3.10	2.219	180.0	2.87
$^1\Pi_u$	2.289	180.0	2.90	2.265	180.0	3.00
$^3A_1$	2.280	92.3	3.00	2.260	92.6	3.11

$La^+(^3F) + H_2$. Hence, they are not likely to have long-enough lifetimes to be observed in hot molecular beams.

Alvarado-Swaisgood and Harrison (1985) found that ScH_2^+ has a $^1A_1$ ground state with $R_e = 1.745$ Å and $\theta_e = 106.7°$ compared to LaH_2^+ which also has a θ_e of 106°. The longer La–H bond lengths are excepted since La is neither subjected to lanthanide contraction nor relativistic effects as much as Hf–Au.

Table 20 shows the geometries of the saddle points in the LaH_2^+ bending potential-energy surfaces. As seen from this table, the $^1A_1$ state exhibits a relatively weaker saddle point at $\theta = 29°$ (a barrier height of 8 kcal/mol). The $^3A_1$ surface contains a very acute θ saddle point (barrier height = 77 kcal/mol). The barrier in the $^3A_1$ surface arises from an avoided crossing. Three other triplet states contain saddle points with obtuse bond angles ($\theta \geq 90°$) with larger barrier heights (> 56 kcal/mol). The La–H bond lengths at the saddle point are longer than the bond lengths at minima. Hence, for the complete insertion of La^+ into H_2, to form the LaH_2^+ molecule, the $La^+(^3F)$ ion has to surmount a barrier of at least 56 kcal/mol.

TABLE 20
Saddle points in the potential energy surfaces of LaH_2^+. Reproduced from Das and Balasubramanian (1991c). Bond lengths were optimized at the SOCI level while bond angles were obtained from CASSCF results.

State	R (Å)	θ (deg)	Barrier height (kcal/mol)[a]
$^1A_1$	2.10	29.4	8
$^1B_1$	2.32	118.5	61
$^3A_1$	2.33	140.3	67
$^3A_1$	2.43	45.5	77
$^3B_1$	2.27	122.0	57
$^1B_2$	2.35	99.0	60
$^1A_2$	2.34	92.4	61
$^3B_2$	2.33	98.6	61
$^3A_2$	2.28	90.0	56

[a] Barrier heights were calculated with respect to the corresponding dissociated limits at the SOCI level.

The dissociation energy for the process,

$$LaH_2^+(^1A_1) \longrightarrow La^+(^3F; d^2) + H_2$$

was computed by Das and Balasubramanian (1991c) as 11.3 kcal/mol at the SOCI level of theory. The D_e relative to La^+ (^1D; 5d6s) was found to be 12.5 kcal/mol. The D_e ($HLa-H^+$) was computed by these authors as 58.6 kcal/mol at the SOCI level. The D_e (HLa^+-H) is almost identical to the D_e (La^+-H). Alvarado-Swaisgood and Harrison (1985) found the first and second bond energies of ScH_2^+ to be 54.7 and 51.7 kcal/mol.

Elkind et al.'s (1989) experiment on the reactivities of La^+, Sc^+, Y^+ and Lu^+ with H_2 using guided ion beam mass spectrometry revealed that La^+ reacted with H_2 primarily through an insertion mechanism. Their surface ionization (SI) beam of La^+ was found to be 69% ^3F (d^2), 12% ^1D (ds) and 15% ^3D (ds). Since the La^+ (^3F; d^2) forms only loose complexes with H_2 [2–3 kcal/mol more stable than La^+ (^3F) + H_2], at experimental translational energies > 4 eV it is not expected that these loose complexes will be long-lived. Neither do their collisions result in $LaH^+ + H$ unless substantial barriers are surpassed.

As seen from fig. 19, the La^+ [^1D(ds)] is an attractive candidate for insertion into H_2 as it forms a stable LsH_2^+. Hence, the primary mechanism for the reactivity of La^+ with H_2 to produce LaH^+ is the insertion of La^+ [^1D(ds)] into H_2 to produce LaH_2^+ ($^1A_1$). The possibility suggested by Elkind et al. (1989), viz., through the insertion of La^+ (^3F; d^2) was not supported by the calculations of Das and Balasubramanian (1991c), since the triplet surfaces have to surpass a substantial barrier. The experimentally observed statistical behavior of the branching ratio in the $La^+ + HD$ reaction was also explainable from theory.

Table 21 shows the important configurations in the SOCI wavefunctions for the minima of LaH_2^+. All states of LaH_2^+ with the exception of $^3A_1$ were found to be dominated by a single configuration. The la_1 orbital of $^1A_1$ near its θ_e was composed of La(5d), and smaller amounts of La(6s) and H_1(ls) + H_2(ls) orbitals. The lb_2 orbital was found to be a mixture of La(dπ) and $H_2(\sigma_u)$, H_1(1s)–H_2(1s) orbital. The contribution of La^+ (6p) was found to be rather small. However, in the $^1\Sigma_g^+$ state the La(6p) orbital makes enhanced contribution to the $1\sigma_u$ orbital.

TABLE 21
Leading configurations of the low-lying states of LaH_2^+. Reproduced from Das and Balasubramanian (1991c).

State	Configuration (percentage)
$^1A_1$	$1a_1^2 1b_2^2$ (95)
$^1\Sigma_g^+$	$1\sigma_g^2 1\sigma_u^2$ (96)
$^1\Delta_u$	$1\sigma_g^2 1\sigma_u 1\delta_g$ (93) $1\sigma_g 2\sigma_g 1\sigma_u 1\delta_g$ (4)
$^3\Delta_u$	$1\sigma_g^2 1\sigma_u 1\delta_g$ (93) $1\sigma_g 2\sigma_g 1\sigma_u 1\delta_g$ (4)
$^3\Pi_u$	$1\sigma_g^2 1\sigma_u 1\pi_g$ (92) $1\sigma_g 2\sigma_g 1\sigma_u 1\pi_g$ (4)
$^1\Pi_u$	$1\sigma_g^2 1\sigma_u 1\pi_g$ (92) $1\sigma_g 2\sigma_g 1\sigma_u 1\pi_g$ (5)
$^3A_1$	$1a_1 2a_1 1b_2^2$ (88), $1a_1^2 2a_1 3a_1$ (3), $1a_1 2a_1 1b_2 2b_2$ (3)

TABLE 22
Mulliken-population analyses for the low-lying states of LaH_2^+. Reproduced from Das and Balasubramanian (1991c).

State	Gross population						Overlap population
	La	H	La(s)	La(p)	La(d)	H(s)	
$^1A_1$	1.52	2.48	0.27	0.09	1.16	2.46	1.05
$^1\Sigma_g^+$	1.42	2.58	0.28	0.43	0.71	2.57	1.07
$^1\Delta_u$	1.88	2.12	0.20	0.07	1.61	2.11	0.63
$^3\Delta_u$	1.88	2.12	0.21	0.07	1.60	2.11	0.64
$^3\Pi_u$	1.93	2.07	0.23	0.09	1.61	2.06	0.65
$^1\Pi_u$	1.92	2.08	0.26	0.07	1.59	2.07	0.59
$^3A_1$	1.88	2.12	0.43	0.07	1.38	2.11	0.62

The $^3A_1$ double hump in the surface arises from two avoided crossings. For $\theta \ll 60°$, this state was found to be predominantly $la_1^2 2a_1 3a_1$ (90%). For larger θs [$60 < \theta < 140$], this state was found to be dominated by the $la_1 2a_1 lb_2^2$. The overlap of La(dπ) and La(6π) with H_2 ($1\sigma_u^*$) orbital becomes larger as θ increases, leading to larger occupancy of the lb_2 orbital. The minimum at $\theta = 92°$ therefore arises from this avoided crossing. As $\theta > 140°$, the $la_1^2 lb_2 2b_2$ configuration (90%) dominates. The second barrier near $\theta = 140°$ in the $^3A_1$ surface is due to the avoided crossing of $la_1 2a_1 lb_2^2$ with $la_1^2 lb_2 2b_2$. The saddle point in the $^1B_1$ surface ($\theta = 119°$) was found to arise from the avoided crossing of $la_1^2 lb_2 la_2$ and $la_1 lb_2^2 lb_1$. At $\theta = 120°$, the $^1B_1$ state was found to be 56% $la_1^2 lb_2 la_2$ and 32% $la_1 lb_2^2 lb_1$ while at $\theta = 100°$ it was found to be 59% $la_1^2 lb_2^2 lb_1$ and 29% $la_1^2 lb_2 la_2$.

The saddle point in the $^3B_1$ surface ($\theta = 122°$) was found to arise from the avoided crossing of $la_1^2 lb_2 la_2$ and $la_1 lb_2^2 lb_1$. At $\theta = 110°$, the $^3B_1$ state was found to be 56% $la_1^2 lb_2 la_2$ and 34% $la_1 lb_2^2 lb_1$. The $^3A_2$ surface near its saddle point ($\theta = 90°$) was found to be 52% $la_1^2 lb_2 lb_1$ and 38% $la_1 lb_2^2 la_2$. For all larger angles the $la_1^2 lb_2 lb_1$ configuration was found to dominate.

Table 22 contains the Mulliken populations of the electronic states of LaH_2^+. The equilibrium bond angle (106°) for the $^1A_1$ state was found to be determined by the La $5d^{1.16} 6s^{0.27}$ hybridization. The 5d population is attributed to both (5dπ) orbital mixing in the lb_2 orbital and 5d(σ/δ) mixing in the la_1 orbital. The 6p population of the linear $^1\Sigma_g^+$ state was found to be larger (0.43). All triplet and excited singlet electronic states except $^3A_1$ were found to have similar populations [La(6s) = 0.20–0.26, La(5d) = 1.59–1.61]. The $^3A_1$ state differed from this trend (see table 22). The La^+–H overlap populations for each bond was found to be 0.525 for the $^1A_1$ ground state. This is identical to the La–H^+ overlap population of 0.53 (see table 18).

4.6. *LaH_2*

Das and Balasubramanian (1991a) studied the bending potential-energy surfaces of four doublet and four quartet electronic states of the LaH_2 molecule. They used a CASSCF method followed by full second-order CI calculations. They used (5s5p3d1f)

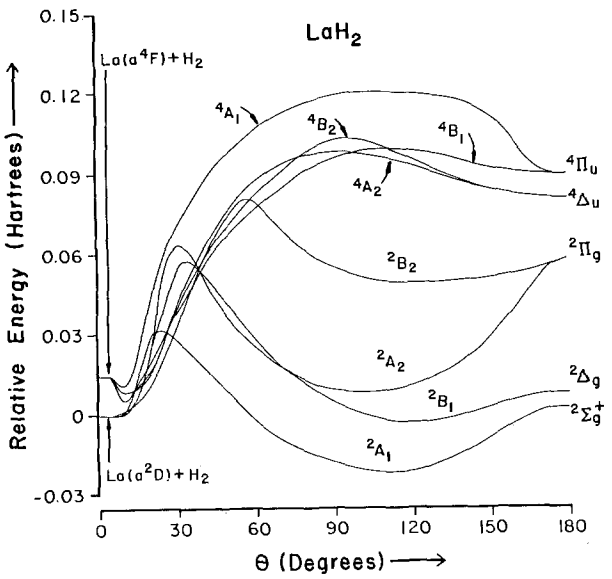

Fig. 20. Potential-energy surfaces for LaH_2. Reproduced from Das and Balasubramanian (1991a).

as well as (5s5p3d) valence Gaussian basis sets in conjugation with an active space comprising four a_1, two b_2, one b_1 and one a_2 orbitals.

Figure 20 shows the bending potential energy surfaces for LaH_2 arising from ^2D and ^4F electronic states of LaH_2. The ground state of La is ^2D ($5d^1\,6s^2$) while there are several excited states arising from $5d^2\,6s^1$. We considered the ^4F state with the objective of comparing and contrasting high spin and low spin reactivities of the La atom.

As evidenced from fig. 20, the ^2D ground state of La atom inserts into H_2 relatively easier compared to the excited high spin ^4F. This is reminiscent of LaH_2^+ discussed in section 4.5. The ^2D state of La also forms other bent doublet electronic states but these are somewhat higher in energy and also need to surmount larger barriers for insertion into H_2 (see fig. 20). All quartet states have to surpass substantial barriers for insertion into H_2.

Table 23 shows the geometries of the bent and linear states of LaH_2 computed by Das and Balasubramanian (1991a) at both CASSCF and SOCI level of theories. In that table also listed are the results with and without 4f functions. It is easily seen that 4f functions do not play an important role for LaH_2.

The ground state of LaH_2 is of $^2A_1$ symmetry with $R_e = 2.14$ Å and $\theta_e = 111.9°$. The higher-order correlation effects in the SOCI do not change the geometries much compared to the CASSCF. The ground-state geometry of LaH_2 is similar to YH_2 computed by Balasubramanian and Ravimohan (1988). YH_2 also has a $^2A_1$ ground state (see section 4.2) with $R_e = 1.94$ Å and $\theta_e = 123°$. The dissociation energy for $LaH_2(^2A_1)$ to yield $La(^2D) + H_2$ was computed as 11 kcal/mol at the SOCI level.

Table 24 reports the geometries of the saddle points and barrier heights relative to the dissociation limits. All saddle points have longer La–H bond lengths compared to

TABLE 23
Geometries and energies of the low-lying states of LaH_2. Reproduced from Das and Balasubramanian (1991a).

	CASSCF			SOCI			
			E, eV			E, eV	
State	R_e, Å	θ_e, deg	(5s5p3d)	R_e, Å	θ_e, deg	(5s5p3d)	(5s5p3d1f)
$^2A_1$	2.158	111.4	0.0	2.140	111.9	0.0	0.0
$^2B_1$	2.225	120.5	0.52	2.190	119.7	0.48	0.48
$^2\Sigma_g^+$	2.277	180.0	0.66	2.260	180.0	0.69	0.68
$^2A_2$	2.200	102.2	0.83	2.174	102.8	0.76	0.75
$^2\Delta_g$	2.339	180.0	0.81	2.312	180.0	0.84	0.88
$^2B_2$	2.207	122.4	1.94	2.195	119.8	1.32	1.30
$^2\Pi_g$	2.322	180.0	2.17	2.310	180.0	1.50	1.49
$^4\Delta_u$	2.314	180.0	2.80	2.298	180.0	2.94	3.01
$^4\Pi_u$	2.279	180.0	3.03	2.259	180.0	3.11	3.12

TABLE 24
Saddle points in various potential energy curves of LaH_2. Reproduced from Das and Balasubramanian (1991a). Barrier heights were calculated with respect to the corresponding dissociation limits.

State	R, Å	θ, deg	Barrier height, kcal/mol
$^2A_1$	2.21	24	21
$^2B_1$	2.16	33	36
$^2A_2$	2.17	31	40
$^2B_2$	2.11	57	51
$^4A_2$	2.42	93	52
$^4B_1$	2.40	110	53
$^4B_2$	2.44	97	55
$^4A_1$	2.45	108	66

minima. The saddle point θs are also similar to YH_2. For YH_2 the $^2A_1$, $^2B_1$ and $^2A_2$ states contain saddle points near $\theta = 20, 37$ and 40°, respectively.

The $^2A_1$ surface of LaH_2 intersects the $^4B_1$, $^4B_2$, and $^4A_2$ surfaces at $\theta \approx 25°$, while the $^2A_2$ and $^2B_1$ surfaces cross these quartet surfaces near 40°. These intersections may provide non-adiabatic channels for the quartet-state atom to hop to the doublet-state surfaces. The spin–orbit couplings among electronic states of different spin multiplicities near intersections are negligible. The RCI calculations suggested small SO coupling.

Table 25 shows the important configurations for the low-lying states of LaH_2. The $^2A_1$ ground state was found to be predominantly $1a_1^2 2a_1 1b_2^2$ (95%). The $^2B_1$ and $^2A_2$ excited states were composed of $1a_1^2 1b_2^2 1b_1$ and $1a_1^2 1b_2^2 1a_2$ configurations, respectively. The low-lying $^2\Sigma_g^+$ is composed of $1\sigma_g^2 2\sigma_g 1\sigma_u^2$ (95%). The highly excited quartet linear states were found to be considerably pure. The $^4\Delta_u$ and $^4\Pi_u$ states could be

TABLE 25
Leading configurations for the electronic states of LaH_2. Reproduced from Das and Balasubramanian (1991a). Numbers in parentheses are in percentages.

State	Configuration
$^2A_1$	$1a_1^2 2a_1 1b_2^2$ (95)
$^2B_1$	$1a_1^2 1b_2^2 1b_1$ (95)
$^2\Sigma_g^+$	$1\sigma_g^2 2\sigma_g 1\sigma_u^2$ (95)
$^2A_2$	$1a_1^2 1b_2^2 1a_2$ (94)
$^2\Delta_g$	$1\sigma_g^2 1\sigma_u^2 1\delta_g$ (96)
$^2B_2$	$1a_1^2 1b_2^2 2b_2$ (94)
$^2\Pi_g$	$1\sigma_g^2 1\sigma_u^2 1\pi_g$ (95)
$^4\Delta_u$	$1\sigma_g^2 2\sigma_g 1\sigma_u 1\delta_g$ (92), $1\sigma_g 2\sigma_g 3\sigma_g 1\sigma_u 1\delta_g$ (3)
$^4\Pi_u$	$1\sigma_g^2 2\sigma_g 1\sigma_u 1\pi_g$ (88), $1\sigma_g 2\sigma_g 3\sigma_g 1\sigma_u 1\pi_g$ (3)

represented mainly by $1\sigma_g^2 2\sigma_g 1\sigma_u 1\delta_g$(92%) and $1\sigma_g^2 2\sigma_g 1\sigma_u 1\pi_g$ (88%) configurations, respectively. The saddle points in the doublet potential-energy surfaces arise from avoided curve crossings. The saddle point at $\theta = 24°$ of the $^2A_1$ state arises due to the avoided crossing of the $1a_1^2 2a_1 1b_2^2$ configuration with the $1a_1^2 2a_1^2 3a_1$ configuration. For $\theta < 30°$, the $^2A_1$ state is dominated by $1a_1^2 2a_1^2 3a_1$, while for $\theta > 30°$, the state is predominantly described by the $1a_1^2 2a_1 1b_2^2$ configuration. At the saddle point, these two configurations mix strongly. Similar avoided crossings occur for the $^2B_1$, $^2B_2$, and $^2A_2$ states. Near $\theta = 30°$, the potential energy curve of the $^2B_1$ state arising from the $1a_1^2 1b_2^2 1b_1$ configuration undergoes an avoided crossing with the $^2B_1$ $(1a_1^2 1a_1^2 1b_1)$ surfaces. The saddle point in the $^2A_2$ state surface is due to the avoided crossing of $^2A_2$ $(1a_1^2 1b_2^2 1a_2)$ and $^2A_2$ $(1a_1^2 2a_1^2 1a_2)$ configurations. For the $^2B_2$ state, the dominant configuration for $\theta > 60°$ is $1a_1^2 1b_2^2 2b_2$ (90%), while for $\theta < 60°$, the state is predominantly $1a_1^2 2a_1^2 1b_2$ (90%).

Table 26 shows the Mulliken-population analyses of LaH_2. The total gross population of the lanthanum atom is less than 3.0 for all electronic states of LaH_2, indicating La^+H^- polarity of La–H bonds. Except the excited $^4\Delta_u$ and $^4\Pi_u$ states, 0.6 electronic population is transferred from the lanthanum atom to the two hydrogen atoms of LaH_2. There is a significant loss of the electronic density from the 6s orbital of the lanthanum atom. The La(6p) populations are large for most of the low-lying states. The 5d orbitals of the lanthanum atom also gain significant amounts of electron density. In the $^2A_1$ ground state, there is significant electronic charge transfer from the 6s orbital to the 6p and 5d orbitals. The La–H bond is composed of 31% La(6s), 11% La(6p), and 58% La(5d) at the equilibrium geometry.

The first excited $^2B_1$ state has a rather low La(6s) population. The La(5d) population of this state is nearly 2.0 while the La(6p) population is comparable to that of the ground state. Thus, the mixing of different configurations of La is very large. For the low-lying linear state ($^2\Sigma_g^+$) the La(6p) population is 1.01. Thus, the participation of the 6p orbital in the La–H bonding is significant. The La–H bonds for this state have 37%

TABLE 26
Mulliken-population analyses for the electronic states of LaH_2. Reproduced from Das and Balasubramanian (1991a).

State	Gross populations						Overlap population
	La(total)	H(total)	La(s)	La(p)	La(d)	H(s)	
$^2A_1$	2.38	2.62	0.74	0.27	1.37	2.16	1.09
$^2B_1$	2.37	2.63	0.14	0.28	1.95	2.62	1.13
$^2\Sigma_g^+$	2.39	2.61	0.89	0.49	1.01	2.60	1.14
$^2A_2$	2.46	2.54	0.21	0.20	2.05	2.53	1.13
$^2\Delta_g$	2.36	2.64	0.22	0.48	1.66	2.62	1.15
$^2B_2$	2.45	2.55	0.18	0.70	1.58	2.53	1.15
$^2\Pi_g$	2.49	2.51	0.27	0.56	1.66	2.50	1.17
$^4\Delta_u$	2.82	2.18	0.87	0.10	1.85	2.17	0.62
$^4\Pi_u$	2.88	2.13	0.85	0.16	1.86	2.11	0.64

La(6s), 21% La(6p), and 42% La(5d) characters. The La(6p) population of the $^2\Pi_g$ state is also large. For these two doublet linear states, the overlap of the La ($6p_y$) orbital with $H_2(1\sigma_u)$ along the internuclear axis is stronger. The excited $4\Delta_u$ and $^4\Pi_u$ states have relatively low La(6p) populations. The La–H bonds for these two states have about 30% La(6s), 4% La(6p), and 66% La(5d) characters. Consequently, the La atom almost retains the $5d^2\,6s^1$ configuration in these two quartet states. The overlap populations of all the doublet states are above 1.0 while the two quartet linear states have overlaps of 0.63.

The high spin states of LaH_2 form linear structures but the low spin states form bent minima. This is primarily because the low spin state of the La atom can form bond pairs with the H(1s) electrons while the high spin state is primarily non-bonding. Hence, the bent minima are formed through the La(d), La($d_{x^2-z^2}$), La($d_{x^2-2y^2+z^2}$), La(6p) and La(6s) hybridization in the low spin states, while effective orbital overlap in the high spin states is achieved primarily through the La(dσ), La(6s), and H(1s) orbitals. The most effective overlap of La(dσ), La(6s) and H(1s) is achieved for the linear geometry; consequently, high spin states are linear while many low spin states are bent. The La–H bond lengths of the linear high spin states are longer than the La–H bond lengths in the bent states. For example, the $^4\Delta_u$ linear state has $R_e \sim 2.298$ Å while the $^2A_1$ ground state has $R_e \sim 2.14$ Å. There are several factors which contrast the bond lengths. The primary factor is that La(dσ) + La(6s) overlap with H(1s) is considerably smaller in the linear geometry compared to the La(dδ) + La(dσ) + La(6s) overlap with H(1s) in the bent geometry. This is consistent with the La–H overlap Mulliken populations in table 26. For example, the La–H overlap is 1.09 in the $^2A_1$ state compared to 0.62 for the linear $^4\Delta_u$ state. The La–H overlaps are also much smaller for the $^4\Pi_u$ state.

Table 27 shows the computed dipole moments of doublet states of LaH_2 at their equilibrium geometries. All four states exhibit strong La^+H^- polarities. The strong La^+H^- polarities of the La–H bonds are quite consistent with the Mulliken populations shown in table 26.

TABLE 27
Dipole moments for the bent minima of LaH_2. Reproduced from Das and Balasubramanian (1991a).

State	μ, D
$^2A_1$	3.79
$^2B_1$	5.42
$^2B_2$	4.72
$^2A_2$	7.42

4.7. *HfH, ZrH and TiH*

Balasubramanian and Das (1991) compared the potential-energy curves of 14 electronic states of HfH using the CASMCSCF followed by the SOCI method. They also included spin–orbit effects using the RCI method. Balasubramanian and Wang (1989a, b) computed the potential-energy curves and spectroscopic constants of 30 electronic states of ZrH using comparable CASSCF/SOCI methods. Chong et al. (1986) computed the properties of two electronic states of TiH. Chen et al. (1991) have recently considered the gas-phase thermochemistry of TiH. The experimental D_0^0 (Ti–H) was determined using guided ion beam mass spectrometry as 2.12 eV in agreement with Chong et al.'s computed CASSCF/CI D_e of 2.12 eV. Of course, zero-point correction to the experimental value yields a D_e of 2.21 ± 0.09 eV. We discuss the results of all these computations and compare them primarily to show the effect of lanthanide contraction on HfH.

4.7.1. *HfH*

We discuss HfH, ZrH and TiH in the order of title. The potential-energy curves of 14 electronic states of HfH computed by Balasubramanian and Das (1991) are shown in fig. 21. Table 28 shows the computed spectroscopic constants of HfH in the absence of spin–orbit coupling. Balasubramanian and Das (1991) predicted $^2\Pi(II)$–$X\,^2\Delta$, $^2\Delta(II)$–$X\,^2\Delta$ and $^2\Pi(III)$–$X\,^2\Delta$ transitions of HfH to occur in the 15 000, 17 000 and 19 000 cm^{-1} region, respectively, in the absence of spin–orbit effect.

Table 29 contains the spectroscopic constants of HfH including spin–orbit effects. It is evident from table 29 that spin–orbit coupling strongly mixes several electronic states of HfH leading to an intermediate coupling description of electronic states. The T_e values also change up to 1500 cm^{-1}.

Balasubramanian and Das (1991) computed the D_e of HfH without spin–orbit coupling as 2.87 eV. The correction to D_e due to spin–orbit coupling was, however, found to be only 0.01 eV which yielded spin–orbit corrected D_e of 2.88 eV.

Tables 29 and 30 show the composition of electronic states of HfH with and without spin–orbit coupling, respectively. Although $^2\Delta$, $^2\Pi$, $^4\Pi$, $^4\Delta$ and $^2\Phi$ states are relatively simple in that weights of the leading configurations are larger than 71%, this is not the case with other states of HfH such as $^4\Sigma^-$, $^2\Sigma^+$, $^2\Pi(II)$, etc. (see table 29).

The spin–orbit coupling has noticeable effects on some of the electronic states of HfH (see table 30). For example, the $\frac{1}{2}$ state is a strong mixture of $^2\Pi$, $^2\Sigma^+$ and $^4\Sigma^-$.

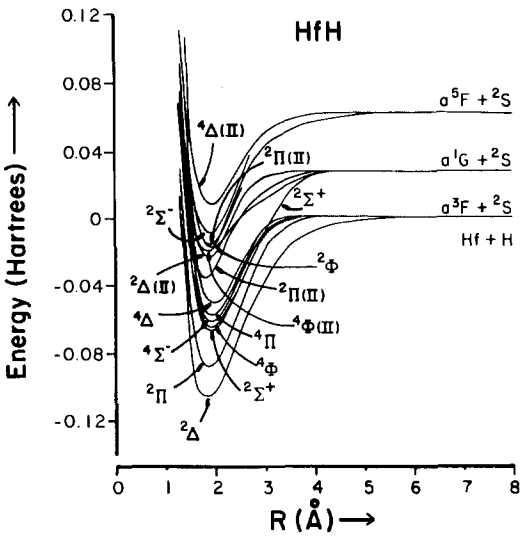

Fig. 21. Potential-energy surfaces for HfH. Reproduced from Balasubramanian and Das (1991).

TABLE 28
Spectroscopic constants of low-lying electronic states of HfH. Reproduced from Balasubramanian and Das (1991).

State	R_e (Å)	T_e (cm^{-1})	ω_e (cm^{-1})	μ_e (D)	D_e (eV)
$^2\Delta$	1.852	0	1702	0.71	2.87
$^2\Pi$	1.841	1964	1682	0.86	2.65
$^4\Phi$	1.882	8078	1617	1.41	1.86
$^4\Sigma^-$	1.882	8807	1609	1.71	1.76
$^2\Sigma^+$	1.900	9071	1540	−0.29	2.47
$^4\Pi$	1.887	9995	1596	1.25	1.64
$^2\Pi$(II)	1.838	15133	1612	1.85	–
$^4\Delta$	1.942	15857	1451	0.06	–
$^2\Phi$	1.907	16973	1449	2.41	–
$^2\Delta$(II)	1.875	17093	1593	1.80	–
$^2\Sigma^-$	1.870	18414	1506	1.70	–
$^2\Pi$(III)	1.837	18803	1672	3.14	–
$^4\Phi$(II)	1.832	21411	1682	3.32	–
$^4\Pi$(II)	1.924	22524	1441	−0.08	–

Likewise, the $\frac{3}{2}$(II) state is a mixture of $^2\Pi$, $^4\Phi$ and $^4\Sigma^-$. Even the ground state of HfH is contaminated by $^2\Pi$ (8%).

Table 31 shows the Mulliken populations of the electronic states of HfH. The Hf(6s) population is larger in $^2\Delta$ and $^2\Pi$ states compared to quartet states. The Hf(6p) populations are uniformly larger. The Hf–H overlap populations are larger than 0.5.

TABLE 29
Spectroscopic constants of the low-lying ω–ω states of HfH. Reproduced from Balasubramanian and Das (1991).

State	$\lambda-s$ description	R_e (Å)	ω_e (cm^{-1})	T_e (cm^{-1})	μ_e (D)
$\frac{3}{2}$	$^2\Delta + {}^2\Pi$	1.854	1704	0	0.66
$\frac{1}{2}$	$^2\Pi + {}^2\Sigma^+ + {}^4\Sigma^-$	1.853	1651	3807	0.81
$\frac{3}{2}$(II)	$^2\Pi + {}^4\Phi + {}^4\Sigma^-$	1.855	1654	3921	0.89
$\frac{5}{2}$	$^2\Delta + {}^4\Phi$	1.853	1701	4742	0.67
$\frac{3}{2}$(III)	$^4\Phi + {}^2\Pi$	1.884	1611	8989	1.38
$\frac{5}{2}$(II)	$^4\Phi + {}^2\Delta$	1.884	1616	10252	1.39
$\frac{1}{2}$(II)	$^4\Sigma^- + {}^2\Pi + {}^2\Sigma^+$	1.881	1625	11261	1.59
$\frac{7}{2}$	$^4\Phi$	1.881	1618	11788	1.42
$\frac{3}{2}$(IV)	$^4\Sigma^- + {}^2\Pi$	1.882	1607	12581	–
$\frac{9}{2}$	$^4\Phi$	1.888	1608	12929	1.40

TABLE 30
Contributions of various λ-s states to the low-lying ω–ω states of HfH. Reproduced from Balasubramanian and Das (1991).

ω–ω state	Contribution
$\frac{3}{2}$	82% $^2\Delta$, 8% $^2\Pi$
$\frac{1}{2}$	72% $^2\Pi$, 9% $^2\Sigma^+$, 4% $^4\Sigma^-$
$\frac{3}{2}$(II)	68% $^2\Pi$, 20% $^4\Phi$, 4% $^4\Sigma^-$
$\frac{5}{2}$	90% $^2\Delta$, 2% $^4\Phi$
$\frac{3}{2}$(III)	95% $^4\Phi$, 1% $^2\Pi$
$\frac{5}{2}$(II)	97% $^4\Phi$, 0.2% $^2\Delta$
$\frac{1}{2}$(II)	85% $^4\Sigma^-$, 6% $^2\Pi$, 5% $^2\Sigma^+$
$\frac{7}{2}$	98% $^4\Phi$
$\frac{3}{2}$(IV)	92% $^4\Sigma^-$, 5% $^2\Pi$
$\frac{9}{2}$	96% $^4\Phi$

TABLE 31
Mulliken-populations of the low-lying states of HfH. Reproduced from Balasubramanian and Das (1991). The $5s^2\,5p^6$ core electrons are omitted for convenience in accounting for Mulliken populations.

State	Hf	Gross H	Hf(s)	Hf(p)	Hf(d)	Overlap Hf–H
$^2\Delta$	3.72	1.28	1.68	0.44	1.59	0.50
$^2\Pi$	3.74	1.26	1.60	0.41	1.73	0.54
$^4\Phi$	3.74	1.26	1.08	0.42	2.24	0.59
$^4\Sigma^-$	3.75	1.25	1.09	0.37	2.29	0.59
$^2\Sigma^+$	3.72	1.28	1.56	0.69	1.47	0.55
$^4\Pi$	3.75	1.25	1.08	0.44	2.23	0.59

TABLE 32
Spectroscopic properties of thirty-six electronic states of ZrH. Reproduced from Balasubramanian and Wang (1989b).

State	R_e (Å)	T_e (cm^{-1})	ω_e (cm^{-1})
$^2\Delta_{3/2}$	1.77	0	1777
$^2\Delta_{5/2}$	1.77	546	1779
$^2\Delta$	1.77	292	1743
$^4\Phi_{3/2}$	1.82	1279	1604
$^4\Phi_{5/2}$	1.82	1571	1605
$^4\Phi_{7/2}$	1.82	1857	1606
$^4\Phi_{9/2}$	1.82	2148	1606
$^4\Phi$	1.82	1720	1605
$^4\Pi_{1/2}$	1.78	2337	1740
$^2\Pi_{3/2}$	1.78	2637	1740
$^2\Pi$	1.78	2526	1742
$^4\Sigma^-_{1/2}$	1.82	2533	1613
$^4\Sigma^-_{3/2}$	1.82	2533	1613
$^4\Sigma^-$	1.82	2533	1613
$^4\Pi_{1/2}$	1.82	3521	1585
$^4\Pi_{3/2}$	1.82	3678	1585
$^4\Pi_{5/2}$	1.82	3841	1585
$^4\Pi$	1.82	3683	1585
$^2\Sigma^+_{1/2}$	1.85	5227	1598
$^2\Sigma^+$	1.85	5221	1597
$^4\Delta_{1/2}$	1.92	9731	1413
$^4\Delta_{3/2}$	1.92	9928	1413
$^4\Delta_{5/2}$	1.92	10 136	1413
$^4\Delta_{7/2}$	1.92	10 353	1414
$^4\Delta$	1.92	10 045	1413
$^2\Pi(II)_{1/2}$	1.85	10 615	1565
$^2\Pi(II)_{3/2}$	1.85	10 758	1567
$^2\Pi(II)$	1.85	10 687	1564
$^2\Delta(II)_{3/2}$	1.88	10 764	1534
$^2\Delta(II)_{5/2}$	1.86	11 149	1551
$^2\Delta(II)$	1.87	10 960	1548
$^4\Delta(II)_{1/2}$	1.88	12 940	1512
$^4\Delta(II)_{3/2}$	1.88	13 104	1511
$^4\Delta(II)_{5/2}$	1.88	13 278	1512
$^4\Delta(II)_{7/2}$	1.88	13 467	1513
$^4\Delta(II)$	1.88	13 205	1512

4.7.2. *ZrH*

Balasubramanian and Wang (1989a, b) have computed the spectroscopic constants of 36 electronic states of ZrH using the CASSCF/SOCI method together with RECPs which retained the $4d^2\,5s^2$ outershells in the valence space and (3s2p4d1f/3s2p3d1f) basis sets. A subsequent study by Balasubramanian (1990b) also compared the properties obtained using 4e and 12e RECPs for ZrH. Langhoff et al. (1987) have studied two electronic states of ZrH using the SCF/SDCI/MCPF methods.

Table 32 shows the spectroscopic constants of ZrH obtained by Balasubramanian and Wang (1989a, b). Figure 22 shows the actual potential-energy curves of some of these electronic states of ZrH. Note that the potential energy curves in fig. 22 were obtained using the inferior FOCI method whereas the results in table 32 were obtained using the superior SOCI method.

The spin–orbit splitting of the ground state of ZrH is $546\,cm^{-1}$ while the $^4\Phi_{3/2}$–$^4\Phi_{4/2}$ excited state spin–orbit separation is $870\,cm^{-1}$. Since the spin–orbit contamination of different of different electronic states is rather small, Balasubramanian and Wang did not find significant changes in the R_e and ω_e values due to the spin–orbit coupling effect.

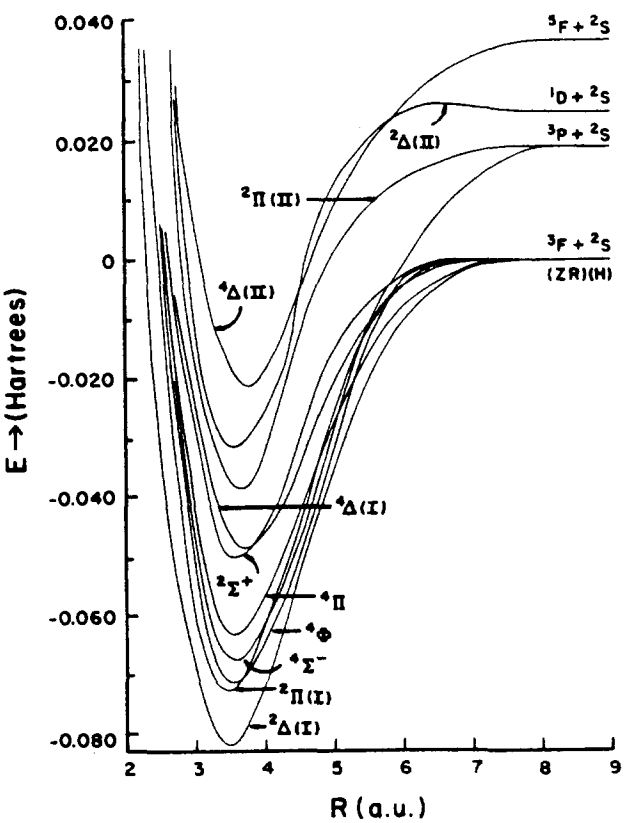

Fig. 22. Potential-energy surfaces for ZrH. Reproduced from Balasubramanian and Wang (1989b).

TABLE 33
The contributions of important configurations in the SOCI wavefunctions of ZrH. Reproduced from Balasubramanian and Wang (1989b).

States	Percentage of contributions
$^2\Delta$	$1\sigma^2 2\sigma^2 1\delta^1$ (75), $1\sigma^2 2\sigma^1 3\sigma^1 1\delta^1$ (6)
$^4\Phi$	$1\sigma^2 2\sigma^1 1\delta^1 1\pi^1$ (96)
$^2\Pi$	$1\sigma^2 2\sigma^2 1\pi^1$ (33), $1\sigma^2 2\sigma^2 2\pi^1$ (28), $1\sigma^2 2\sigma^1 1\pi^1 1\delta^1$ (7)
$^4\Sigma^-$	$1\sigma^2 2\sigma^1 1\pi^2$ (48), $1\sigma^2 2\sigma^1 1\delta^2$ (46)
$^4\Pi$	$1\sigma^2 2\sigma^1 1\delta^1 1\pi^1$ (87)
$^2\Sigma^+$	$1\sigma^2 2\sigma^2 3\sigma^1$ (59), $1\sigma^2 2\sigma^1 1\pi^2$ (20)
$^4\Delta$	$1\sigma^2 2\sigma^1 3\sigma^1 1\delta^1$ (90)
$^2\Pi$(II)	$1\sigma^2 2\sigma^1 1\pi^1 1\delta^1$ (51), $1\sigma^2 2\sigma^1 2\pi^1 1\delta^1$ (23)
$^2\Delta$(II)	$1\sigma^2 2\sigma^1 3\sigma^1 1\delta^1$ (67), $1\sigma^2 2\sigma^1 1\pi^2$ (10), $1\sigma^2 1\pi^2 1\delta^1$ (9)
$^4\Delta$(II)	$1\sigma^2 1\pi^1 1\delta^2$ (83)

The ground state predicted by Balasubramanian and Wang agreed with Langhoff et al.'s (1987) SCF/SDCI/MCPF computation. In a subsequent study, Balasubramanian (1990b) computed the properties of eight electronic states of ZrH using a superior basis set and ($4s^2 4p^6 5d^2 5s^2$) RECPs. The spectroscopic constants obtained using either procedures were comparable ($\Delta R_e = 0.04$ Å, $\Delta\omega_e = 40\,cm^{-1}$, $\Delta D_e = 0.17$ eV).

Table 33 shows the contribution of the important configurations to the electronic states of ZrH. In table 33, the $^2\Delta$, $^4\Phi$, $^4\Pi$ and $^4\Delta$(II) states have leading configurations with weights $> 76\%$. All other states are heavily mixed. Table 34 shows the Mulliken-population analyses of the electronic states of ZrH. The 5p contribution is quite significant for all states of ZrH. The 4d population of the $^2\Delta$ state is smaller in comparison to other states. The total gross populations of the Zr atom are less than 4.0 in all the states indicating that these states are ionic with the polarity Zr^+H^-.

Balasubramanian (1990b) computed the dipole moment of ZrH (μ_e) as 1.24 D in the $^2\Delta$ state with Zr^+H^- polarity. The $^4\Phi$ excited state has significantly larger dipole moment of 2.13 D. Langhoff et al. (1987) obtain μ_es of 1.23 and 2.42 D, respectively, using the SCF/MCPF method. Both calculations suggest that ZrH is ionic with Zr^+H^- polarity.

4.7.3. *TiH*

There are several studies on TiH but the ones by Chong et al. (1986) as well as an earlier study of Bauschlicher and Walch (1983) provide accurate data for comparison with ZrH and HfH. In the former study, Chong et al. used all electron SCF/SOCI/CPF/MCPF methods in conjugation with a (8s6p4d3f) Gaussian basis set for Ti and the (4s3p) basis set for the hydrogen atom. Their computed spectroscopic constants of the $^4\Phi$ and $^2\Delta$ states of TiH are shown in table 35.

At all levels of theory (SOCI, CPF, MCPF), the high spin $^4\Phi$ state is the ground state of TiH in contrast with both ZrH and HfH. The 3d population is ~ 0.3 electron larger in the $^4\Phi$ state of TiH compared to $^2\Delta$.

TABLE 34
Mulliken-population analyses of ZrH. Reproduced from Balasubramanian and Wang (1989b).

	Net							Gross							Overlap
State	Zr	Zr(s)	Zr(p)	Zr(d)	H	H(s)	H(p)	Zr	Zr(s)	Zr(s)	Zr(p)	H	H(s)	H(p)	Zr–H
$^2\Delta$	3.441	1.323	0.346	1.551	0.972	0.966	0.006	3.734	1.481	0.419	1.834	1.266	1.255	0.011	0.587
$^2\Pi$	3.428	1.121	0.350	1.720	0.939	0.936	0.003	3.745	1.334	0.412	1.999	1.255	1.247	0.008	0.632
$^4\Phi$	3.399	0.849	0.285	2.177	0.955	0.950	0.005	3.722	1.001	0.363	2.358	1.278	1.268	0.010	0.646
$^4\Sigma^-$	3.398	0.831	0.249	2.219	0.957	0.952	0.005	3.721	0.989	0.321	2.411	1.279	1.270	0.010	0.645
$^4\Pi$	3.388	0.833	0.270	2.189	0.965	0.959	0.005	3.712	0.990	0.342	2.379	1.288	1.278	0.010	0.647
$^2\Sigma^+$	3.394	1.048	0.439	1.704	0.983	0.978	0.005	3.705	1.203	0.593	1.910	1.295	1.285	0.009	0.623
$^4\Delta$	3.342	0.838	0.474	1.953	0.993	0.992	0.001	3.674	0.974	0.639	2.061	1.326	1.322	0.003	0.665
$^2\Pi$(II)	3.430	1.081	0.348	1.717	0.947	0.946	0.001	3.741	1.321	0.419	2.001	1.259	1.252	0.006	0.622
$^2\Delta$(II)	3.402	0.710	0.489	2.211	0.983	0.982	0.002	3.709	0.761	0.610	2.339	1.291	1.286	0.005	0.615
$^4\Delta$(II)	3.435	0.282	0.282	2.862	0.935	0.930	0.004	3.750	0.447	0.346	2.957	1.250	1.242	0.008	0.631

TABLE 35
Spectroscopic constants and other properties for the $^4\Phi$ and $^2\Delta$ state of TiH. Reproduced from Chong et al. (1986).

	SDCI	CPF	MCPF	CASSCF/CI
	$^4\Phi$ ground state – 5 electrons correlated			
E (Hartree) + 840	−8.99683	−9.00155	−9.00126	−9.01689
R_e (bohr)	3.439	3.440	3.440	3.443
ω_e (cm^{-1})	1506	1592	1548	1444
D_e (eV)	1.99	2.07	2.06	2.12
μ (D)	1.899	2.308	2.185	
dμ/dR (D/bohr)	1.373	1.246	1.283	
3d population	2.27	2.33	2.30	2.26
	$^4\Phi$ ground state – 13 electrons correlated			
E (Hartree) + 840	−9.27128	−9.29987	−9.29979	
R_e (bohr)	3.397	3.347	3.365	
ω_e (cm^{-1})	1515	1327	1407	
D_e (eV)	2.06	2.07	2.05	
μ (D)	1.777	2.307	2.122	
dμ/dR (D/bohr)	1.523	0.589	1.064	
3d population	2.29	2.45	2.41	
	$^2\Delta$ excited state – 5 electrons correlated			
E (Hartree) + 840	−8.98095	−8.99095	−8.99102	
T_e (eV)	0.432	0.289	0.279	
R_e (bohr)	3.264	3.369	3.352	
ω_e (cm^{-1})	1323	1025	1705	
D_e (eV)	1.55	1.78	1.78	
μ (D)	1.916	1.585	1.557	
dμ/dR (D/bohr)	1.288	0.821	0.928	
3d population	2.04	2.04	2.05	
	$^2\Delta$ excited state – 13 electrons correlated			
E (Hartree) + 840	−9.24561	−9.28862	−9.28957	
T_e (eV)	0.698	0.306	0.278	
R_e (bohr)	3.198	3.270	3.271	
ω_e (cm^{-1})	1694	1561	1594	
D_e (eV)	1.36	1.76	1.77	
μ (D)	2.057	1.828	1.709	
dμ/dR (D/bohr)	1.687	0.706	0.752	
3d population	2.09	2.17	2.16	

The dipole moment of the $^4\Phi$ state is 2.12 D at the highest level of theory while the corresponding value is 1.71 D for the $^2\Delta$ state. The R_es of the $^4\Phi$ and $^2\Delta$ states are 1.781 and 1.73 Å, respectively.

The $3d^2\,4s^2$–$3d^3\,4s^1$ energy separation of the Ti atom is 0.81 eV and thus the $^4\Phi$ state is favored via spin-exchange stabilization energy. Note that the 3d population of the $^4\Phi$ state is between 2.0 and 3.0 indicating considerable mixing of the two configurations. The dipole moment of TiH is increased compared to ScH and VH (Chong et al. 1986).

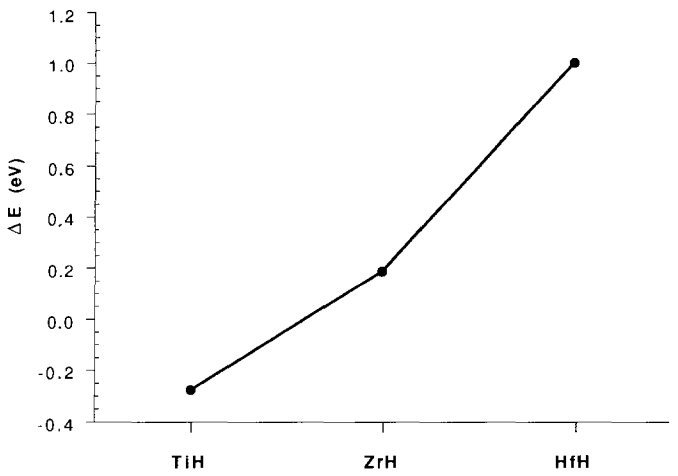

Fig. 23. Relative trend in the $^2\Delta$–$^4\Phi$ energy separations of TiH, ZrH and HfH.

4.7.4. *Effect of lanthanide contraction on the TiH, ZrH and HfH triad*

The $^2\Delta$ electronic states of the three species have R_es of 1.78, 1.811 and 1.85 Å, respectively, while the D_es of the three molecules in the $^2\Delta$ state are 1.77, 2.47 and 2.87 eVs. The effect of lanthanide contraction is not fully manifested in the R_es of the three species compared to the D_es. The stronger Hf–H bond compared to the Zr–H bond is partly attributed to the lanthanide contraction. The μ_e value of TiH, ZrH and HfH in the $^2\Delta$ state are 1.92, 1.24 and 0.71 D, respectively. We note a steep decrease in the HfH's μ_e.

The most dramatic manifestation of the lanthanide contraction is in the $^2\Delta$–$^4\Phi$ energy separation. This is plotted in fig. 23 for the three species. For Ti, we noted before that the $3d^2\,4s^2$–$3d^3\,4s^1$ energy separation is small and hence the $^4\Phi$ state exhibits a mixed character. The spin-exchange energy overcomes in the $^4\Phi$ state, resulting in a $^4\Phi$ ground state for TiH. The $^2\Delta$–$^4\Phi$ energy separation therefore increases from TiH to ZrH. However the $^2\Delta$–$^4\Phi$ energy separation is substantially larger for HfH as seen from fig. 23. That is, ΔE values of the $^4\Phi - {}^2\Delta$ separation are -0.28, 0.19 and 1.0 eV. The steep rise in the energy of the $^4\Phi$ state is due to the lanthanide contraction. The $^4\Phi$ state involves enhanced ns character. The 6s–5d promotion energy is considerably larger for Hf since the 6s orbital is stabilized and contracted primarily due to lanthanide contraction and secondarily due to relativity.

The above trend can be explained by comparing the $(nd^2\,ns^2)^3$F–$(nd^3\,ns^1)^5$F energy separation of Ti, Zr and Hf (fig. 24). As is clear from fig. 24, this separation is dramatically larger for Hf. As noted before, lanthanide contraction is somewhat more important for Hf compared to relativity while the opposite trend is true for the latter third-row transition elements such as Pt, Au, etc.

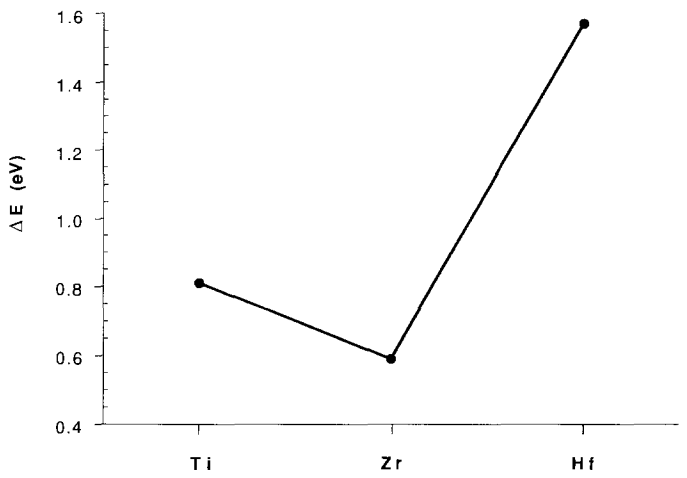

Fig. 24. $(nd^2\,ns^2)\ ^3F$–$(nd^3\,ns^1)\ ^5F$ energy separations of Ti, Zr and Hf.

4.8. *HfH_2 and ZrH_2*

4.8.1. *HfH_2*

Das and Balasubramanian (1991d) have obtained the potential-energy surfaces of 12 electronic states of HfH_2. Related YH_3^+ and ZrH_2^+ have been studied by Das and Balasubramanian (1989). They employed CASSCF followed by full second-order CI (SOCI) using RECPs which retained the outer $(5s^2\,5p^6\,5d^2 6s^2)$ shells of Hf in the valence space. The computed potential-energy surfaces are shown in fig. 25. As seen from fig. 25, the excited $^1\Delta$ state of Hf atom $(5d^2\,6s^2)$ inserts into H_2 spontaneously to yield the $^1A_1$ ground state of the HfH_2 molecule. The ^3F ground state of Hf has to surmount barriers for insertion into H_2. The smallest barrier is for the $^3A_2$ state and it was computed as 17 kcal/mol.

The crossing of $^1A_1$ with triplet surfaces could result in surface hoppings from triplet to singlet surfaces. The primary mechanism for this would be spin–orbit coupling. Das and Balasubramanian (1991d) used the RCI method to study spin–orbit coupling at θ intersections and found this effect to be small but non-negligible. The Hf atom in the ^5F $(5d^3\,6s^1)$ state exhibits a different behavior. It forms small angle complexes with H_2 and subsequently forms linear minima.

Tables 36 and 37 show the geometries and energy separations of bent and linear electronic states of HfH_2, respectively. The ground state of HfH_2 is a $^1A_1$ state with $R_e = 1.842$ Å and $\theta_e = 126.7°$ (table 36). The linear electronic states in table 37 have longer bond lengths compared to the bent states primarily due to enhanced 6p participation in the $1\sigma_u$ orbital of the linear state.

Table 38 shows the saddle points in the potential energy surfaces of HfH_2. Only the $^5A_2$ state exhibits an obtuse-angle saddle point. All other very acute angle saddle points of HfH_2 are due to avoided crossings.

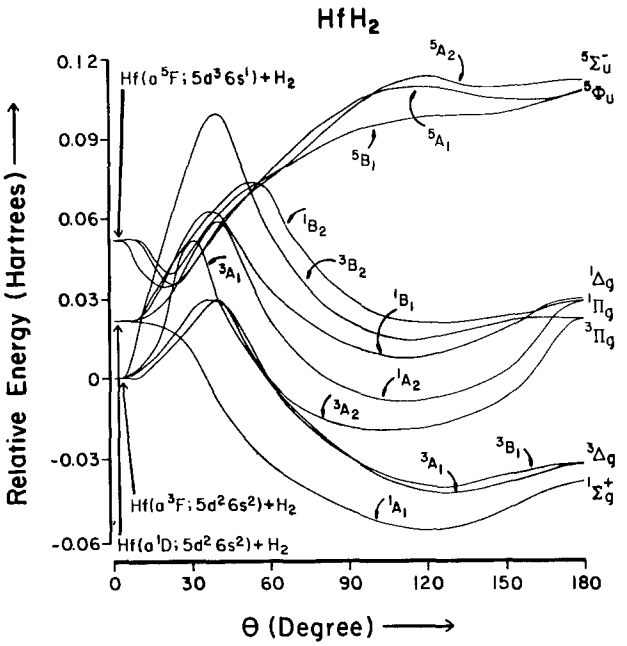

Fig. 25. Potential-energy surfaces of HfH_2. Reproduced from Das and Balasubramanian (1991d).

TABLE 36
Geometries and energy separations of the bent low-lying states of HfH_2. Reproduced from Das and Balasubramanian (1991d).

	CASSCF			SOCI			
State	R_e, Å	θ_e, deg	E, eV	R_e, Å	θ_e, deg	E, eV without f	E, eV with f
$^1A_1$	1.862	120.0	0.0	1.842	126.7	0.0	0.0
$^3B_1$	1.900	125.5	0.44	1.875	125.7	0.52	0.51
$^3A_1$	1.896	127.1	0.38	1.877	127.8	0.54	0.53
$^3A_2$	1.878	105.6	1.01	1.855	109.3	1.05	1.03
$^1A_1$	1.891	111.6	1.31	1.867	112.6	1.19	1.18
$^1B_2$	1.888	123.6	2.11	1.880	121.5	1.56	1.59
$^1B_1$	1.885	113.1	1.76	1.859	113.2	1.66	1.60
$^3B_2$	1.924	114.5	1.94	1.894	116.8	1.94	1.91
$^5A_2$	2.073	23.3	2.48	2.020	24.4	2.77	2.73
$^5A_1$	2.088	22.7	2.45	2.022	24.3	2.79	2.75
$^5B_1$	2.153	21.7	2.61	2.074	23.4	2.06	2.96

Das and Balasubramanian (1991d) computed the D_e for $HfH_2(^1A_1) \rightarrow Hf(^1\Delta) + H_2$ as 46 and 30 kcal/mol relative to $Hf(^3F)$ ground state. Hence, HfH_2 is considerably more stable than $Hf + H_2$.

Table 39 shows the effect of spin–orbit coupling on the electronic states of HfH_2, while table 40 shows the composition of the RCI wavefunctions obtained including spin–orbit coupling. It is evident from tables 39 and 40 that while the spin–orbit effect

TABLE 37

Geometries and energies of linear states of HfH_2. Reproduced from Das and Balasubramanian (1991a). Energies were calculated from the $^1A_1$ ground-state energy.

	CASSCF		SOCI		
State	R_e, Å	E, eV	R_e, Å	E, eV without f	E, eV with f
$^1\Sigma_g^+$	1.934	0.49	1.902	0.34	0.41
$^3\Delta_g$	1.958	0.62	1.937	0.81	0.84
$^3\Pi_g$	1.947	2.14	1.936	1.64	1.67
$^1\Pi_g$	1.953	2.28	1.942	1.76	1.81
$^1\Delta_g$	1.957	2.35	1.934	2.19	2.10
$^5\Sigma_u^-$	2.024	4.56	1.956	4.31	4.22
$^5\Phi_u$	2.011	4.48	1.981	4.27	4.25

TABLE 38

Saddle points in potential energy surfaces of HfH_2. Reproduced from Das and Balasubramanian (1991d). Geometries of the saddle points were estimated at the CASSCF level of calculation.

State	R, Å	θ, deg	Barrier ht,[a] kcal/mol	State	R, Å	θ, deg	Barrier ht,[a] kcal/mol
$^1B_1$	1.85	38	27	$^3B_1$	1.86	37	25
$^1A_2$	1.88	40	23	$^3A_2$	1.86	40	17
$^1B_2$	1.84	55	34	$^3B_2$	1.89	40	62
$^3A_1$	1.91	31	32	$^5A_2$	2.06	120	38

[a] Barrier heights were calculated with respect to the corresponding dissociation limits at the CASSCF level.

TABLE 39

Effect of spin–orbit contamination on geometries and energies of low-lying states of HfH_2. Reproduced from Das and Balasubramanian (1991d).

State	R_e, Å	θ_e, deg	E, eV	State	R_e, Å	θ_e, deg	E, eV
$^1A_1(A_1)$	1.842	126.3	0	$^3A_1$	1.877	127.8	0.55
$^1A_1$	1.842	126.7	0.01	$^3B_1(A_1)$	1.875	125.8	0.51
$^3A_1(A_2)$	1.875	127.3	0.40	$^3B_1(B_2)$	1.878	126.6	0.59
$^3A_1(B_2)$	1.875	127.3	0.44	$^3B_1(A_2)$	1.877	126.5	0.64
$^3A_1(B_1)$	1.878	127.9	0.55	$^3B_1$	1.875	125.7	0.52

TABLE 40

Weights of different low-lying states of HfH_2 in the relativistic CI wavefunctions. Reproduced from Das and Balasubramanian (1991d).

State	Contribution (%)	State	Contribution (%)
$^1A_1(A_1)$	$^1A_1$ (97), $^3A_2$ (0.3)	$^3B_1(A_1)$	$^3B_1$ (98), $^1A_1$ (0.8), $^3A_2$ (0.1)
$^3A_1(A_2)$	$^3A_1$ (65), $^3B_1$ (32)	$^3B_1(B_2)$	$^3B_1$ (64), $^3A_1$ (33)
$^3A_1(B_2)$	$^3A_1$ (64), $^3B_1$ (33)	$^3B_1(A_2)$	$^3B_1$ (66), $^3A_1$ (33)
$^3A_1(B_1)$	$^3A_1$ (98), $^3A_2$ (0.1)		

TABLE 41
Dipole moments of low-lying states of HfH_2. Reproduced from Das and Balasubramanian (1991d). Positive values of μ indicate Hf^+H^- polarity of the bonds.

State	μ, D	State	μ, D
$^1A_1$	0.31	$^1B_1$	1.60
$^3B_1$	1.28	$^3B_2$	3.67
$^3A_1$	1.02	$^5A_2$	0.26
$^3A_2$	1.91	$^5A_1$	0.48
$^1A_2$	0.90	$^5B_1$	−1.48
$^1B_2$	1.96		

is rather small for the $^1A_1$ state of HfH_2, this is not the case for the triplet states. The $^3A_1$ and $^3B_2$ states are heavily mixed due to the near-degeneracy of the two states leading to substantial spin–orbit mixing of the two states. Consequently, the spin–orbit effects are important for nearly degenerate states.

Table 41 shows the computed dipole moments of the electronic states of HfH_2 which means that although the $^1A_1$ ground state HfH_2 has only a small dipole moment (0.31 D) this is not the case for the excited states. The negative dipole moment of the $^5B_1$ state is consistent with electronic charge transfer from the hydrogens to Hf in the $^5B_1$ weak complex.

Table 42 shows the Mulliken-population analyses of the electronic states of HfH_2. The bent $^1A_1$ ground state of HfH_2 has a Hf population of $5d^{1.47}\,6s^{1.46}\,6p^{0.52}$. The

TABLE 42
Mulliken-population analyses of low-lying states of HfH_2. Reproduced from Das and Balasubramanian (1991d).

	Gross populations					Tot. overlap
State	Hf	H	Hf(s)	Hf(p)	(Hf(d)	pop.
$^1A_1$	3.46	2.54	1.46	0.52	1.47	1.11
$^3B_1$	3.44	2.56	1.03	0.49	1.93	1.19
$^3A_1$	3.44	2.56	1.05	0.51	1.88	1.20
$^3A_2$	3.51	2.49	1.04	0.54	1.93	1.17
$^1A_2$	3.50	2.50	0.97	0.63	1.90	1.17
$^1B_2$	3.53	2.47	1.00	0.67	1.86	1.23
$^1B_1$	3.51	2.49	1.06	0.62	1.84	1.12
$^3B_2$	3.53	2.47	0.69	0.45	2.39	1.23
$^5A_2$	3.94	2.06	0.97	0.37	2.59	0.34
$^5A_1$	3.94	2.06	0.97	0.32	2.65	0.33
$^5B_1$	3.94	2.06	1.00	0.59	2.34	0.25
$^1\Sigma_g^+$	3.49	2.51	1.48	0.56	1.45	1.25
$^3\Delta_g$	3.48	2.52	1.06	0.54	1.89	1.26
$^3\Pi_g$	3.56	2.44	1.08	0.58	1.90	1.28
$^1\Pi_g$	3.56	2.44	1.06	0.58	1.92	1.27
$^1\Delta_g$	3.50	2.50	1.08	0.58	1.84	1.22

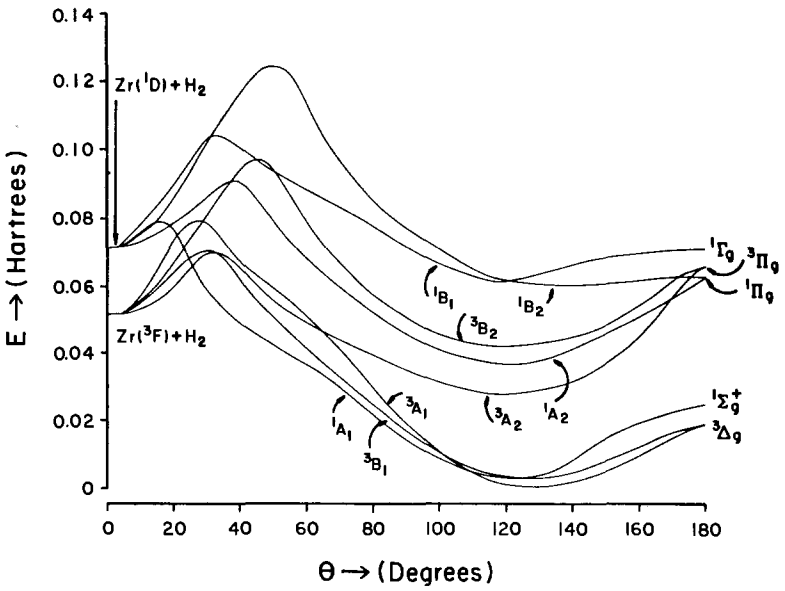

Fig. 26. Potential-energy surfaces of triplet and singlet states of ZrH_2. Reproduced from Wang et al. (1990).

participation of the 6p orbital is thus noticeable in this state. Note that the Hf atom has populations smaller than 4.0 in all low spin states suggesting transfer of electronic charge to the hydrogen atom. The substantial difference in the behavior of the $^3B_2$ state compared to other states is explained by the differences in the Mulliken population.

4.8.2. *ZrH_2*

Wang et al. (1990) have computed the potential energy surfaces of ZrH_2. They used the CASSCF/MRSDCI methods together with RECPs which retained the outer $4d^2\,5s^2$ shells of Zr. They used an extended (4s4p4d1f) valence Gaussian basis set for the Zr atom. It should be noted that the state-averaging procedure was used by Wang et al. to ensure proper dissociation. The MRSDCI included all configurations in the CASSCF with coefficients ≥ 0.07.

Figures 26 and 27 show the computed potential energy surfaces of low and high spin states of ZrH_2, respectively. The ^1D excited state of the Zr atom inserts spontaneously into H_2 to form the bent $^1A_1$ state of the ZrH_2 molecule. The high spin ^3F state, to the contrary, needs to surpass barriers for insertion into H_2.

Figure 27 shows small-angle complexes of $Zr(^5F)$ with H_2. The formation of these complexes is facilitated by exchange of electronic density from hydrogens to the half-filled 5s orbital of Zr in the $^5F(4d^3\,5s^1)$ state.

Table 43 shows the computed geometries and energy separations of electronic states of ZrH_2 (bent). It is noted that several electronic states of ZrH_2 are nearly degenerate ($^1A_1$, $^3B_1$, $^3A_1$). As a matter of fact, the CASSCF method predicts $^3A_1$ ground state

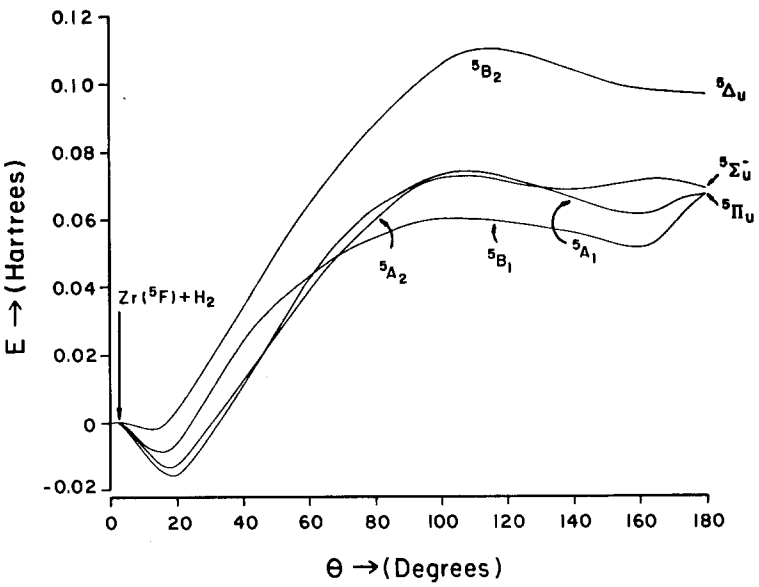

Fig. 27. Potential-energy surfaces of the quintet states of ZrH_2. Reproduced from Wang et al. (1990).

TABLE 43
Geometries and energy separations of bent electronic states of ZrH_2. Reproduced from Wang et al. (1990).

	CASSCF				MRSDCI			
State	R_e(Å)	θ_e(°)	E(eV)	State	R_e(Å)	θ_e(°)	E(eV)	D_e(eV)
$^3A_1$	1.865	127	0	$^1A_1$	1.806	123	0	1.11
$^3B_1$	1.866	125	0.061	$^3B_1$	1.837	125	0.086	1.02
$^1A_1$	1.839	121	0.072	$^3A_1$	1.837	127	0.145	0.965
$^3A_2$	1.864	121	0.747	$^3A_2$	1.832	121	0.725	0.39
$^1A_2$	1.865	120	0.981	$^1A_2$	1.836	120	0.794	0.32
$^3B_2$	1.924	120	1.144	$^1B_2$	1.887	135	1.074	0.04
$^1B_2$	1.908	136	1.641	$^3B_2$	1.885	119	1.104	
$^1B_1$	1.828	116	1.648	$^1B_1$	1.787	124	1.484	

while MRSDCI predicts $^1A_1$ ground state. Wang et al. computed the D_e of ZrH_2 ($^1A_1$) to yield $Zr(^3F) + H_2$ as 1.11 eV or 26 kcal/mol.

Table 44 shows the dipole moments of electronic states of ZrH_2 while table 45 shows the Mulliken populations. The ground state and $^1B_1$ are the least ionic while all other states of ZrH_2 are very ionic with Zr^+H^- polarities of bond.

The $^1A_1$ ground state of ZrH_2 was found to be 69% $1a_1^2\,2a_1^2\,1b_2^2$, 13% $1a_1^2\,1b_2^2\,1b_1^2$ and 12% $1a_1^2\,3a_1^2\,1b_2^2$ near its R_e and θ_e. As seen from table 45, the $^1A_1$ state has $4d^{1.907}\,5s^{1.108}\,5p^{0.422}$ Mulliken population. The 4d populations of the excited states are larger. The Zr–H overlaps are between 1.29 and 1.35.

TABLE 44
The dipole moments of bent electronic states of ZrH_2. Reproduced from Wang et al. (1990). Positive polarity means Zr^+H^- polarity of bonds.

State	μ_e/Debye
$^1A_1$	0.738
$^3B_1$	1.499
$^3A_1$	1.335
$^3A_2$	1.271
$^1A_2$	0.940
$^3B_2$	4.635
$^1B_1$	0.681
$^1B_2$	2.419

TABLE 45
Mulliken-population analyses of bent states of ZrH_2. Reproduced from Wang et al. (1990).

			Gross			Overlaps
State	Zr	H	Zr(s)	Zr(p)	Zr(d)	Zr–H
$^1A_1$	3.437	2.562	1.108	0.422	1.907	1.294
$^3B_1$	3.402	2.598	0.870	0.387	2.144	1.304
$^3A_1$	3.400	2.600	0.887	0.402	2.110	1.316
$^3A_2$	3.473	2.528	0.798	0.467	2.208	1.320
$^1A_2$	3.465	2.534	0.765	0.526	2.175	1.328
$^3B_2$	3.460	2.540	0.544	0.341	2.575	1.296
$^1B_1$	3.452	2.548	0.861	0.461	2.131	1.258
$^1B_2$	3.461	2.540	0.480	0.546	2.147	1.350

4.8.3. *The effect of lanthanide contraction on the difference in properties of HfH_2 and ZrH_2*

The most noticeable difference between HfH_2 and ZrH_2 attributed mostly to lanthanide contraction and less to relativity is the enhanced stability of HfH_2. We note that the D_e of HfH_2 is 30 kcal/mol while the D_e of ZrH_2 is 24 kcal/mol.

The 6s population of Hf in the $^1A_1$ state of HfH_2 is 0.35e larger than the 5s population of the corresponding state of ZrH_2. The 5d population of Hf is correspondingly smaller than Zr (1.47 vs. 1.91). The 6p population of Hf is also increased (0.1) compared to Zr. This leads to a larger bond angle for HfH_2.

The larger 6s populations and enhanced stability of HfH_2 is evidently due to the lanthanide contraction and to a lesser extent to relativity. We note that the atomic 5d–6p promotion energy is smaller for Hf compared to Zr. This leads to enhanced 6p character in all states of HfH_2 (compare tables 42 and 45).

TABLE 46
Relativistic and non-relativistic bond lengths of LaH, AcH, TmH, LuH and LrH. Reproduced with modification from Pyykkö (1979).

	R_e(Å)		
Molecule	Non-relativistic	Relativistic	Exp.
LaH	2.210	2.2222	2.101[a]
AcH	–	2.371	
TmH	–	2.056	
LuH	2.019	2.013	1.422[b]
LrH	–	2.041	

[a] Bernard and Bacis (1977).
[b] Effantin and d'Incan (1974).

4.9. *UH, UH^+ and UH^-*

Krauss and Stevens (1983a, b) have used the RECP method and a single configuration SCF treatment to study the high spin high Λ states of UH and UH^+. They found that bonding in UH is amazingly similar to SrH. This is not surprising since the radial maximum of the 7s orbital of U occurs at 3.66 bohr (Desclaux 1973) while the radial maxima of the 6p, 6d and 5f orbitals of the U atom occur at substantially shorter distances. This means that in the valence configuration of U ($6s^2\,6p^6\,5f^3\,6d\,7s^2$, ^{5}L), the 6p, 6d and 5f orbitals will behave atom-like and bonding will be primarily between 7s and H. However, it was noted by Krauss and Stevens (1983a, b) that the 6p, 6d and 5f do extend to the bonding region and were distorted by overlap repulsion and electrostatic effects. Consequently, bonding in UH was found to be similar to SrH.

The $UH^{\pm}$ ions were found to exhibit a more complicated structure due to the presence of $6s^2\,6p^6\,5f^3\,6d\,7s$, ^{6}L configuration only a few hundred cm^{-1} above the $6s^2\,6p^6\,5f^3\,7s^2$, ^{4}I state. The role of 6p, 5f and 6d orbitals in all actinide compounds needs to be understood. As mentioned in the introduction for the majority of ionic compounds of lanthanides, the ligand-field model works so well because of the atomic nature of the 4f shells in these compounds.

Krauss and Stevens considered the $^6\Lambda$ state correlating into U(^{5}L) + H(^{2}S) at the SCF level with the configuration $1\sigma^2$(U6s) $2\sigma^2$(U6p) $3\sigma^2$(H1s) 4σ(U7s) $1\pi^4$(U6p) 2π(U5f) 1δ(U5f) 2δ(U6d) 1ϕ (U5f). At long distances, the SCF configuration used involved transfer of an electron from hydrogen to U(7s) so that it dissociates into U(^{5}L) + H(^{2}S). The Morse curve fit for the energies in table 46 yielded $R_e = 2.16$ Å, $\omega_e = 1357\,cm^{-1}$ and $\omega_e x_e = 18\,cm^{-1}$ for UH. The D_e was computed as 1.93 eV.

Figure 28 shows the amplitude contour plot of the 3σ, 4σ and 2σ orbitals of UH. The 2σ orbital is almost entirely U($6p_\sigma$) while the 4σ orbital is polarized 7s orbital on U. The 3σ orbital has predominant change in s distribution centered on H. The H^- charge distribution appears to envelop non-bonding U valence orbitals.

The similarity between UH and SrH is rather striking. The SrH has an $R_e = 2.146$ Å compared to UH which has an $R_e = 2.16$ Å. The ω_e values of UH and SrH are 1357 and

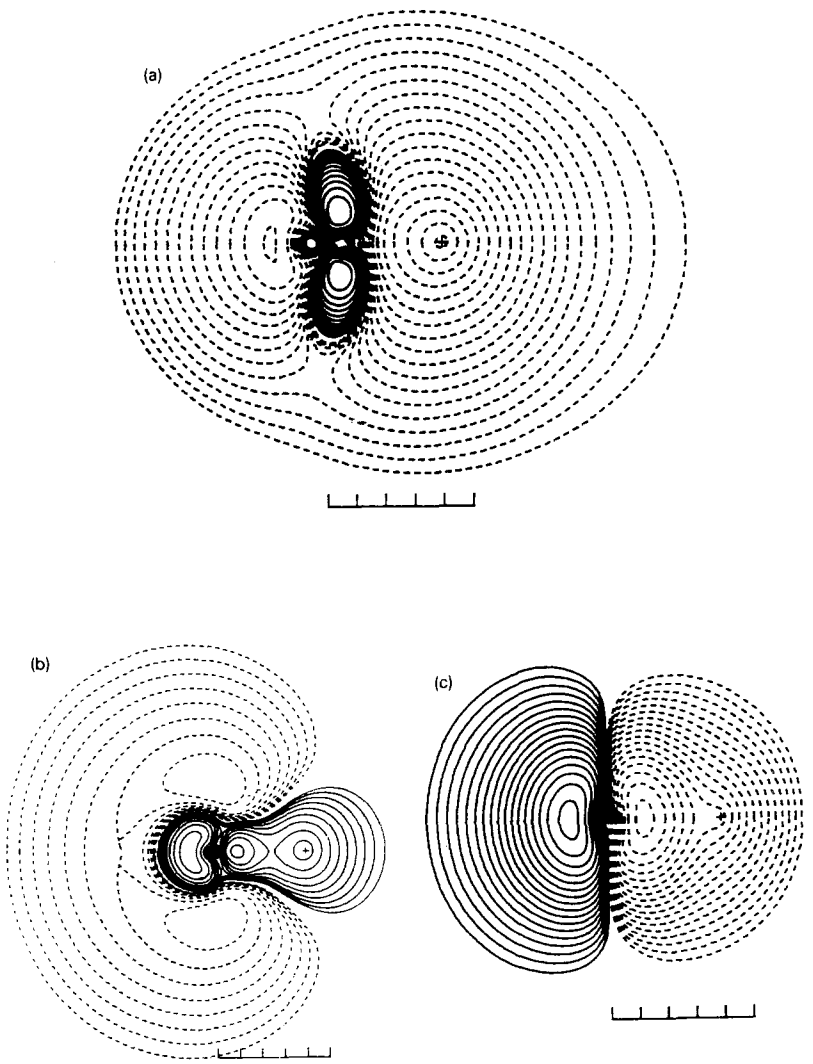

Fig. 28. UH amplitude contour plots. Plots (a), (b) and (c) are for 3σ, 4σ and 2σ orbitals, respectively, for the $^6\Lambda$ state at 4.0 bohr. Each scale division is 1 bohr and the nuclei are marked by a (+). Reproduced from Krauss and Stevens (1983a).

1206 cm^{-1}, respectively. These constants support the atomic-like behavior of 6p, 6d and 5f orbitals of U in UH.

4.10. *AcH, TmH, LuH and LrH*

Pyykkö (1979) has made Dirac–Fock one-center (DFOC) calculations on AcH, TmH, LuH, LrH as well as ScH, YH and LaH. He considered only the $^1\Sigma^+$ states of

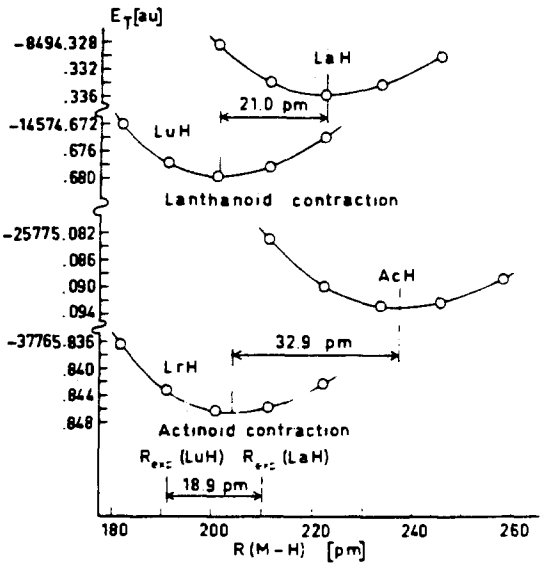

Fig. 29. Plot of relativistic energies and Morse potentials for LaH, LuH, AcH and LaH. Reproduced from Pyykkö (1979).

these species to gain insight into the nature of bonding in these species. For YH, LaH and LuH, the DFOC bond lengths are 5% longer than experiment. Pyykkö has provided very insightful comparisons of the orbital energies and hybridizations across the periodic table which are quite interesting. Since we have already considered ScH, YH and LaH, we will not discuss these results again.

Table 46 shows the computed relativistic and non-relativistic bond lengths of AcH, TmH, LuH and LrH computed by Pyykkö. Pyykkö (1979) defined lanthanide and actinide contraction as

$$\Delta_{lan} = R_e(LaH) - R_e(LuH),$$

$$\Delta_{act} = R_e(AcH) - R_e(LrH).$$

The values computed this way are 0.210 and 0.329 Å, respectively. Non-relativistically the lanthanide contraction is only 0.191 Å. One could also compare the experimental Δ_{lan} as 0.189 Å in good agreement with the value of Pyykkö. Figure 29, obtained by Pyykkö, nicely demonstrates the lanthanide and actinide contraction.

Pyykkö (1979) noted that non-relativistic *n*s orbital energies increase monotonically from Sc(4s) to Ac(7s). To the contrary, the relativistic 7s orbital energy of Ac is lower than La(6s) for the free atoms as well as for AcH and LaH.

Since LaH and LuH differ by the $4f^{14}$ shells, a comparison of the two molecules is in order. Pyykkö shows the plot of the spherically averaged radial electron densities (fig. 30). As seen from fig. 30, the LuH 6s electron distribution is shifted to the left with a maximum occurring to the left of the corresponding maximum of LaH. This means that the 6s orbital of Lu is contracted since the $4f^{14}$ shells incompletely shield the nucleus but the nuclear charge is increased by 14 for Lu compared to La. This is the effect of the lanthanide contraction. However, the LuH 5d electron distribution is more extended

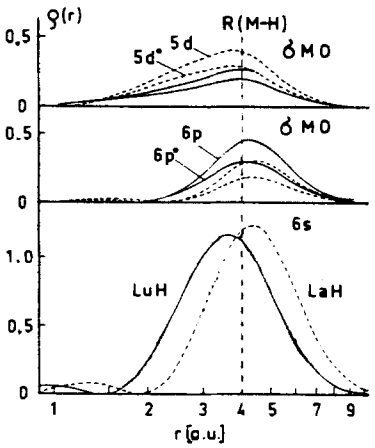

Fig. 30. Spherically averaged electron densities for the valence orbitals of LaH (broken curve) and LuH (full curve) at $R = 3.988$ a.u. Reproduced from Pyykkö (1979).

both inwards and outwards compared to LaH. The inward extension is attributed to the lanthanide contraction of the 4d core shell. Pyykkö attributed the outward extension to the attraction of the proton.

4.11. *Ground-state properties of lanthanide hydrides*

Dolg and Stoll (1989) have generated non-relativistic and quasi-relativistic energy-adjusted pseudo-potentials for the rare-earth elements La–Lu. They have tested their ECPs by studying energetically low-lying superconfigurations of all lanthanide hydrides, fluorides and oxides. It certainly would be of interest to summarize their findings.

Table 47 shows the spectroscopic constants [R_e(Å), D_e(eV)] of the lanthanide hydrides computed by Dolg and Stoll at various levels of theory. The column which corresponds to $Q = 11$ represents the results of calculations with 11-e pseudo-potential with the superconfiguration $(4f^{n+1})\sigma^1$ while $Q = 10$ corresponds to the $(4f^n)\sigma^2$ superconfiguration. Thus, the Q values are the core charges in the two ECPs. There is very little experimental information on the lanthanide hydrides. The experimental R_es for YbH and LuH listed in Huber and Herzberg (1979) are 2.053 and 1.912 Å, respectively. We also note that Dolg and Stoll's R_e for the LaH ground state at SDCI + Q level (2.075 Å) is in excellent agreement with the value computed by Das and Balasubramanian (1990) (2.08 Å) at the CASSCF/SOCI level of theory. The D_e computed by Dolg and Stoll for LaH is 2.42 eV at the SDCI + Q level compared to a value of 2.60 eV obtained by Das and the author at the SOCI level.

Dolg and Stoll (1989) also report the vibrational frequencies and the dipole moments of various lanthanide hydrides. The reader is referred to their original paper for these data. For LaH, their best ω_e of 1450 cm^{-1} agrees well with the value of 1433 cm^{-1} obtained by Das and Balasubramanian (1990). The dipole moment they report for LaH are 2.86, 2.30 and 2.20 D at three levels of theory. The last two values are in agreement with a value of 2.42 D obtained by Das and Balasubramanian.

TABLE 47
Spectroscopic constants [R_e(Å), D_e(eV)] of lanthanide hydrides at various levels of theory. Reproduced from Dolg and Stoll (1989).

		R_e (Å)				D_e (eV)				
		$Q=11$		$Q=10$		$Q=11$			$Q=10$	
LnH		CI	+Q	CI	+Q	CI	+Q	+AC	CI	+Q
LaH	a,d	2.066	2.075			2.35	2.42	2.42		
	b,d	2.082	2.089			2.50	2.57	2.57		
	c,d	2.077	2.084			2.51	2.58	2.58		
	b,e	2.079	2.085			2.61	2.71	2.71		
	c,e	2.057	2.062			3.02	3.18	3.18		
CeH	a,d	2.047	2.056			2.35	2.43	2.43		
PrH	a,d	2.032	2.042			2.36	2.43	1.88		
NdH	a,d	2.020	2.028	2.253	2.257	2.37	2.45	1.61	1.71	1.63
PmH	a,d	2.011	2.020	2.242	2.247	2.39	2.46	–	1.67	1.59
SmH	a,d	2.001	2.010	2.236	2.241	2.40	2.48	0.24	1.64	1.57
EuH	a,d	1.990	1.999	2.230	2.235	2.42	2.50	−0.83	1.62	1.55
	b,d	2.010	2.017	2.225	2.232	2.66	2.74	−0.59	1.28	1.23
	b,e	1.997	2.002	2.199	2.203	2.72	2.82	−0.51	1.60	1.59
GdH	a,d	1.981	1.989			2.44	2.52	2.52		
TbH	a,d	1.978	1.986			2.47	2.55	2.52		
DyH	a,d	1.972	1.980			2.50	2.59	1.65		
HoH	a,d	1.967	1.975			2.54	2.62	1.58		
ErH	a,d	1.962	1.969			2.58	2.66	1.77		
TmH	a,d	1.958	1.965	2.164	2.169	2.62	2.70	1.07	1.43	1.37
YbH	a,d	1.955	1.962	2.173	2.179	2.67	2.74	−0.13	1.42	1.35
	b,d	1.976	1.981	2.148	2.156	3.12	3.18	0.30	1.04	1.01
	b,e	1.958	1.963	2.126	2.132	3.09	3.19	0.31	1.35	1.35
LuH	a,d	1.951	1.958			2.71	2.79	2.79		
	b,d	1.968	1.973			3.18	3.24	3.24		
	b,e	1.949	1.954			3.14	3.24	3.24		

(a) MEFIT, HF pseudo-potential
(b) MEFIT, WB pseudo-potential
(c) As (b) but the f-pseudo-potential is adjusted to $La^{10+}4f^1$ and $5f^1\ ^2F$
(d) Ln (7s6p5d)/[5s4p3d], H (5s1p)/[3s1p]
(e) Ln (7s6p5d2f)/[5s4p3d2f], H (10s5p1d)/[5s3p1d]

An interesting outcome of the Dolg–Stoll computation is the manifestation of lanthanide contraction in the computed R_es of LaH–LuH. As seen from table 47, the bond lengths for a given level of theory and Q gradually decrease in going from LaH to LuH. For example, at the best level of theory the R_es of LaH and LuH are 2.079 and 1.949 Å, respectively. Likewise, the D_es of the two species are 2.61 and 3.18 eV, respectively.

Dolg et al. (1991b) have recently used the CASSCF/CPF/MRCI/CIPSI methods in conjunction with quasi-relativistic effective core potentials to study YbH. They found that the ground state of YbH is a $\Omega=\frac{1}{2}$ state arising from the $4f^{14}\sigma^2\sigma(^2\Sigma^+)$ configuration with theoretical $R_e = 2.074$ Å, $D_0 = 1.43$ eV, $\omega_e = 1276\,cm^{-1}$, in excellent

agreement with experimental values of $R_e = 2.053$ Å, $D_0 \leq 1.93$ or ≤ 1.55 eV and $\omega_e = 1249\,\text{cm}^{-1}$. They found an $A\,^2\Sigma^+$ excited state with an energy separation of 1.0–2.0 eV, depending on the level of theory.

5. Electronic states of diatomic lanthanide and actinide halides

In this section, we summarize the results of recent experimental and theoretical studies on diatomic lanthanide and actinide halides. It is pointed out that there exists a large set of spectroscopic data on these species. These are already summarized in Huber and Herzberg (1979). The present section is focused primarily on those diatomic molecules for which extensive studies have been made recently. The reader is referred to the excellent book of Huber and Herzberg for previous studies. A recent paper by Gotkis (1991) provides theoretical insight and systematic comparison of bonding in lanthanide halides.

5.1. *LaF*

The electronic states of LaF are qualitatively similar to LaH, although LaF is significantly more ionic compared to LaH. The ground state of LaF is also of $^1\Sigma^+$ symmetry and is very ionic. Among others, Barrow et al. (1967) have studied the diatomic LaF molecule. They have analyzed the $A \leftarrow X$, $B \leftarrow X$, $C \leftarrow X$, $D \leftarrow X$, and $E \leftarrow X$ systems with v_{00} values of 11 662, 16 184, 20 960, 22 485 and 22 574 cm^{-1}, respectively. The A, B, C, D and E states of LaF are assigned to $A\,^1\Sigma^+$, $B\,^1\Pi$, $C\,^1\Pi$, $D\,^1\Sigma^+$, and $E\,^1\Sigma^+$ states, of course, the X ground state is of $^1\Sigma^+$ symmetry.

Schall et al. (1983) have studied LaF using resolved fluorescence laser spectroscopy. Tunable dye lasers were used to excite known systems of LaF. However, the resolved fluorescence spectra subsequent to excitation of $B\,^1\Pi$–$X\,^1\Sigma^+$ and $C\,^1\Pi$–$X\,^1\Sigma^+$ bands also showed transitions to $X\,^1\Sigma^+$ and a $^3\Delta$ states. They found yet another $\Omega = 2$ state which was tentatively assigned to $^1\Delta_2$. These high-resolution spectral bands facilitated accurate determination of the spectroscopic constants of these states. Schall et al. (1983) also used the ligand-field theory to rationalize their assignments.

Table 48 shows the spectroscopic constants of LaF. The values for the X, a_1, a_2, $^1\Delta_2$, 0^+, $B\,^1\Pi$ state are improved and from Schall et al.'s work (1983). Other constants are from Huber and Herzberg (1979). Figure 31 summarizes the electronic states of LaF observed up to now.

There are several similarities between the electronic states of LaH studied by Das and Balasubramanian (1990) theoretically and LaF (compare tables 13 and 48). The ground state of LaH is also $X\,^1\Sigma^+$ with $R_e = 2.08$ Å and $\omega_e = 1433\,\text{cm}^{-1}$. The shorter LaF bond length is primarily due to large ionicity of the La–F bond. The $^3\Delta_1$, $^3\Delta_3$ and $^3\Delta_2$ states of LaH are computed at 2580, 2588, 2789 cm^{-1}, respectively, while the $^3\Delta_1$ and $^3\Delta_2$ states of LaF are at 1432 and 1808 cm^{-1}, respectively. The $^1\Delta_2$ states of LaH has a T_e of 6567 cm^{-1} while the corresponding state of LaF has a T_v of 5478 cm^{-1}.

The $A\,^1\Sigma^+(\text{II})$ state of LaH has a T_e of 13 025 cm^{-1} while the corresponding state of LaF has a T_e of 16 638 cm^{-1}. The $B\,^1\Pi$ state of LaH is also close to the A state. The

TABLE 48
Spectroscopic constants of LaF. Prepared from Schall et al. (1987) and Huber and Herzberg (1979).

State	R_e (Å)	ω_e (cm^{-1})	T_2 (cm^{-1})
$X\,^1\Sigma^+$	2.0265	570	0
$a_1\,^3\Delta_1$	2.05994	537.14	1432(3)
$a_2\,^3\Delta_2$	2.0543	537.65	1808
$^1\Delta_2$	–	528	5478
$AO^+(^1\Sigma^+)$	2.0929	[489]	16637.96
$B\,^1\Pi$	2.0971	475.91	16184
$C\,^1\Pi$	[2.0671]	[549]	20959
$D\,^1\Sigma^+$	[2.04]		22485
$E\,^1\Sigma^+$	[2.10]	[421]	22574
$c_1\,^3\Delta_3$			
$c_2\,^3\Delta_2$	2.0548		
$c_3\,^3\Delta_1$			
$d\,^3\Phi$			
$e^3\Phi$			

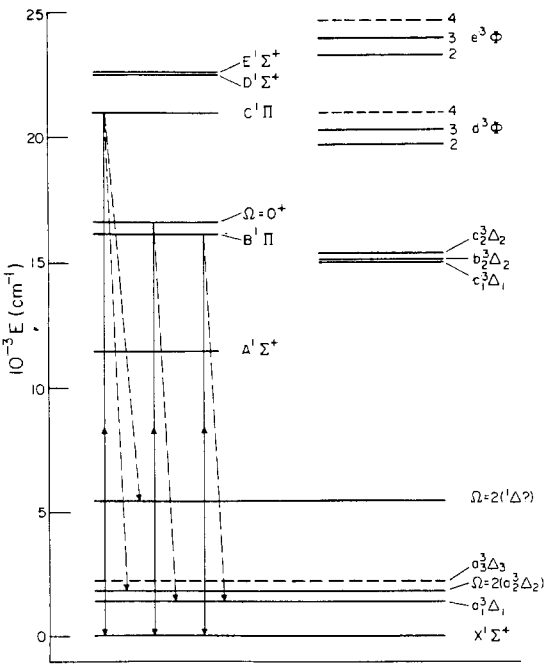

Fig. 31. Energy levels of LaF known up to now. The broken lines are uncertain in an absolute sense but are placed correctly relative to other states. The solid vertical lines stand for laser-induced transitions studied by Schall et al. (1983) while the broken vertical lines are observed fluorescence transitions. Reproduced from Schall et al. (1983).

C $^1\Pi$ state of LaH has a T_e of 20 170 cm^{-1} while the corresponding state of LaF has a T_e of 20 959 cm^{-1}. Consequently, there are many similarities between LaH and LaF. This similarity appears to reveal that these excited states arise primarily from the excitations of the La electrons to upper orbitals composed predominantly of La.

5.2. *YF and YCl*

The diatomic yttrium halides have been the topic of both *ab initio* and experimental studies. Fischell et al. (1980) have studied the excitation spectra of the YCl diatomic molecule using the laser-induced fluorescence (LIF) method. More recently, Xin et al. (1991) have studied the B $^1\Pi$–X $^1\Sigma^+$ system of YCl in high resolution. The rotational analysis of the observed bands has yielded very accurate molecular constants for the X and B states of YCl. Shirley et al. (1990) have studied the molecular-beam optical Stark spectrum of the B $^1\Pi(v=0)$–X $^1\Sigma^+(v=0)$ band system of YF. The permanent dipole moment μ and the magnetic hyperfine parameter a for the B $^1\Pi$ state have been determined as 2.96(4) D and 146.8(3) MHz, respectively. The dipole moment of the X $^1\Sigma^+$ state was determined as 1.82(8) D. More recently, Shirley et al. (1991) have employed the molecular-beam millimeter-wave optical pump-probe spectroscopy to study pure rotational transitions of the YF $^1\Sigma^+$ ground state. This study has yielded improved ground-state rotational constants as $B = 8683.65(1)$ MHz and $D = 0.0079(2)$ MHz, respectively.

TABLE 49
Spectroscopic constants for the excited states of YCl. Reproduced from Langhoff et al. (1988). R_e is reported in a_0 and T_e and ω_e are given in cm^{-1}.

	MRCI			MRCI + Q			Exp.[a]		
State	R_e	ω_e	T_e	R_e	ω_e	T_e	R_e	ω_e	T_e
X $^1\Sigma^+$	4.592	365	0	4.590	364	0	4.547	381	0
A $^1\Delta$	4.733	335	9594	4.729	335	9557			
B $^1\Pi$	4.775	315	12 417	4.770	315	12 284	4.667	330.6	12 128
C $^1\Sigma^+$	4.744	314	15 260	4.741	316	15 161	4.694	325	14 908
D $^1\Pi$	4.723	391	23 147	4.704	337	22 765	4.654	345	22 787
E $^1\Delta$	4.723	326	23 916	4.715	327	23 792			
F $^1\Gamma$	4.760	312	25 841	4.743	308	25 460			
G $^1\Sigma^+$	4.729	325	25 985	4.723	341	25 425			
H $^1\Phi$	4.749	342	26 624	4.729	322	26 023			
I $^1\Delta$	4.801	313	28 599	4.775	314	27 722			
J $^1\Pi$	4.758	315	28 770	4.727	318	27 747	4.668	335	27 116
a $^3\Delta$	4.712	339	6524	4.707	339	6673			
b $^3\Pi$	4.722	331	8753	4.716	332	8788			
c $^3\Sigma^+$	4.732	316	10 154	4.724	323	10 255			
d $^3\Phi$	4.771	309	19 165	4.765	310	19 305			
e $^3\Pi$	4.718	325	20 076	4.701	339	20 001			
g $^3\Delta$ [b]	4.786	306	20 332	4.779	307	20 459			
h $^3\Pi$	4.756	347	21 027	4.763	340	21 018			

[a] Huber and Herzberg (1979), except the B $^1\Pi$ state whose constants are from Xin et al. (1991).
[b] The letter *f* is reserved for the lowest $^3\Sigma^-$ state, which is expected to lie in this region – see text.

Langhoff et al. (1988) have computed the spectroscopic constants of scandium and yttrium halides using *ab initio* method. In particular, the YCl diatomic molecule has been studied using CASSCF followed by MRCI and MRCI + Q methods. These authors have computed the spectroscopic constants of 18 electronic states of YCl and reassigned the observed spectra of Fischell et al. (1980). We discuss this in this section.

Table 49 shows the MRCI and MRCI + Q results of Langhoff et al. (1988) for YCl together with the experimental data from Huber and Herzberg (1979). Fischell et al. have observed the excitation spectra of YCl using LIF but the two observed bands were not assigned. Figures 32 and 33 show the energy-level diagrams for the singlet and triplet states of YCl, together with all dipole transitions.

Langhoff et al. (1988) assigned to the excitation spectra of YCl at 27 116 cm^{-1} to the $J\,^1\Pi$–$X\,^1\Sigma^+$ transition. They noted that their computed lifetime (13 ns) is lower than the experimental value of 21 ns. They found that this system contained significant component of Y^+ 5s → 5p atomic excitation.

The spectra observed by Fischell et al. with $T_e \sim 22\,787\,cm^{-1}$ were assigned by Langhoff et al. (1988) to the $D\,^1\Pi$–$X\,^1\Sigma^+$ system. The computed lifetime of 23 ns was found to be in excellent agreement with the experimental value of 28 ns supporting further the $D\,^1\Pi$–$X\,^1\Sigma^+$ agreement.

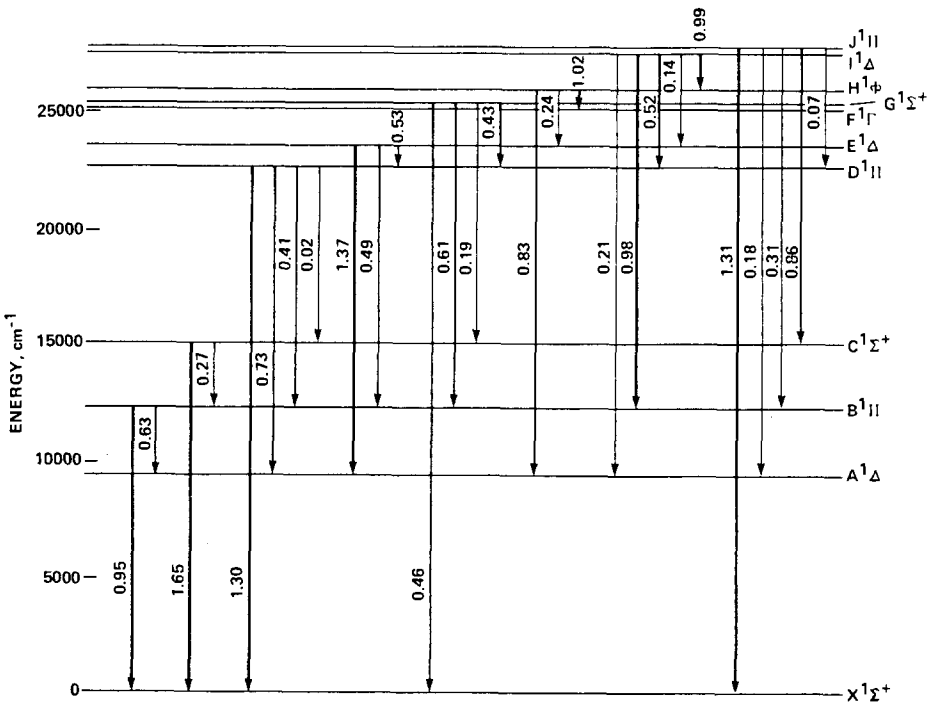

Fig. 32. Energy-level diagrams and the dipole-allowed transition for the singlet states of YCl. Reproduced from Langhoff et al. (1988).

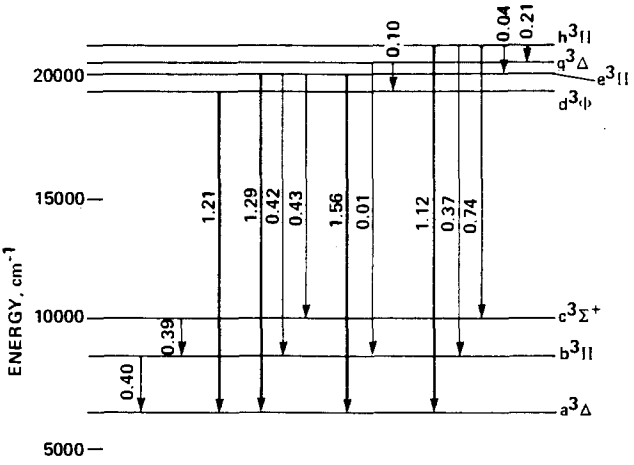

Fig. 33. Energy-level diagrams and the dipole-allowed transitions for the triplet states of YCl. Reproduced from Langhoff et al. (1988).

As seen from table 49, A and B states were assigned to $^1\Delta$ and $^1\Pi$, respectively, by Langhoff et al. The B–X system was also recently analyzed by Xin et al. (1991). The lifetime of the B $^1\Pi$ state was computed as $\sim$ 291 ns by Langhoff et al. (1988). Xin et al. (1991) confirmed Langhoff et al.'s computed properties of the B $^1\Pi$ state. The experimental T_e for the B state obtained by Xin et al. (12 128 cm^{-1}) is in excellent agreement with the computed value of Langhoff et al. (12 284 cm^{-1}).

As seen from table 49 and figs. 32 and 33, there are numerous allowed dipole transitions predicted for YCl many of which are yet to be observed. Hence, there is further scope for experimental studies on YCl.

5.3. *UF and UF^-*

Krauss and Stevens (1983a) have studied the diatomic UF and its ions. The bonding in UF was found to be similar to alkaline-earth fluorides. These authors studied the $^6\Lambda$ state of UF. The SCF configuration used near R_e by these authors, is

$$1\sigma^2(\text{F1s})\,2\sigma^2(\text{U6s})\,3\sigma^2(\text{F2s})\,4\sigma^2(\text{U6p})\,5\sigma^2(\text{F2p})\,6\sigma(\text{U7s})\,1\pi^4(\text{U6p})\,2\pi^4(\text{F2p})$$
$$3\pi(\text{U5f})\,1\delta(\text{U5f})\,2\delta(\text{U6d})\,1\phi(\text{U5f}).$$

The UF molecule was found to be ionic with a U 7s electron transferring to the F 2p at long distance. The spectroscopic constants of the $^6\Lambda$ ground state of UF were computed as $R_e = 4.12$ bohr, $\omega_e = 511\ cm^{-1}$, $\omega_e x_e = 2.0\ cm^{-1}$ and $D_e = 4.92$ eV relative to the neutral separated atoms.

Figure 34 shows the amplitude contour plots of the 5σ and 6σ orbitals of UF for the $^6\Lambda$ state at 4.5 bohr. Figure 35 shows the amplitude contour plots of the atomic valence orbitals (4σ, 3π, 1δ, 1ϕ) of $^6\Lambda$ state of UF at the same distance. The 5σ orbital is predominantly F2p_σ although the lobe towards U is compressed by overlap with uranium orbitals. On the other hand, 6σ orbital is mainly composed of U 7s.

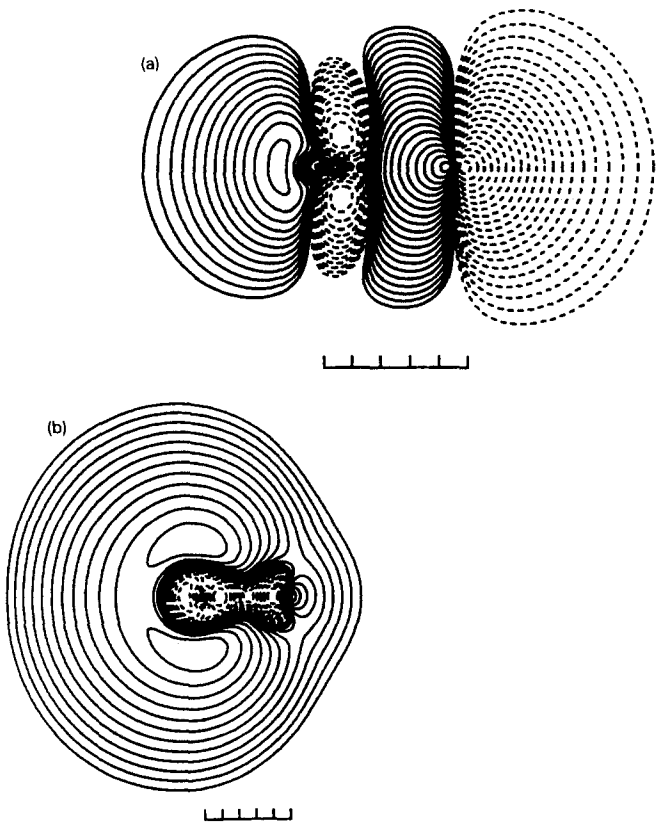

Fig. 34. The amplitude contour plots of the 5σ and 6σ orbitals of UF $^6\Lambda$ state at $R = 4$–5 bohr (see fig. 28 for definition). Reproduced from Krauss and Stevens (1983a).

Krauss and Stevens (1983a) considered the $^5\Lambda$ state of UF^-. The spectroscopic constants of this state at the SCF level were $R_e = 4.30$ bohr, $\omega_e = 429\,cm^{-1}$, $\omega_e x_e = 1.7\,cm^{-1}$ and $D_e = 3.1$ eV. The larger D_e and smaller R_e for UF^- compared to UH^- was rationalized by Krauss and Stevens based on the smaller size of F^- compared to H^-.

5.4. *Ground states of LaF–LuF*

Dolg and Stoll (1989) have computed the ground-state properties of LaF–LuF using different ECPs and SCF/SDCI + Q levels of theory. We focus mainly on their computed R_es and D_es. The reader is referred to their original paper for the vibrational frequencies and dipole moments.

Tables 50 and 51 show the R_es and D_es computed by Dolg and Stoll for LaF–LuF. We omitted the SCF result from their original tables since the SCF results are inferior as they do not include electron-correlation effects at all. The computed R_es of

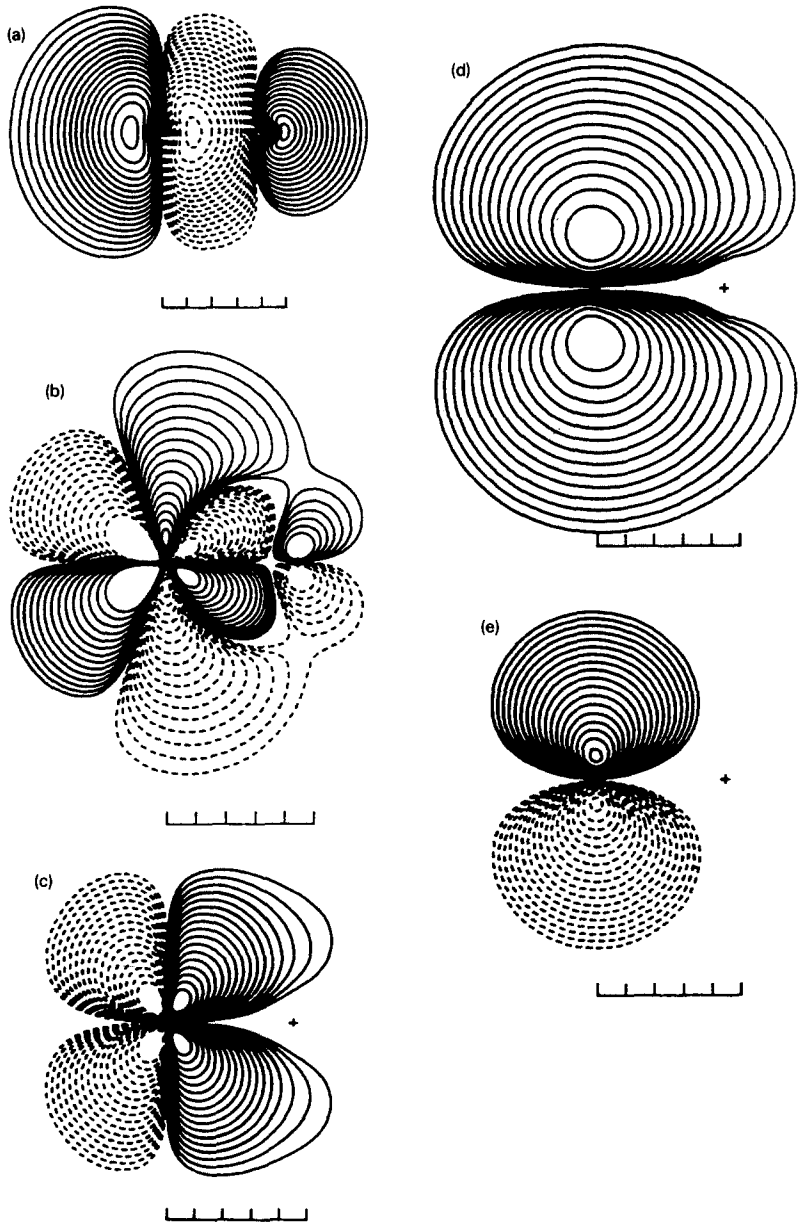

Fig. 35. The amplitude contour plots of the atomic valence (a) 4σ, (b) 3π, (c) 1δ, and (e) 1ϕ orbitals of UF,$^6\Lambda$ at 4–5 bohr (see caption for fig. 28). Reproduced from Krauss and Stevens (1983a).

TABLE 50
Bond lengths of the rare-earth monofluorides (Å) from SCF and CI (SD) calculations [including Davidson's correction (+ Q)] and experiment. The core charges $Q = 11$ and $Q = 10$ denote the pseudopotentials for a $(4f^n)\,\sigma^2$ and a $(4f^{n+1})\,\sigma^1$ superconfiguration, respectively. Reproduced from Dolg and Stoll (1989).

		$Q = 11$		$Q = 10$	
LnF		CI	+Q	CI	+Q
LaF	a, d	2.178	2.181		
	b, d	2.179	2.183		
	c, d	2.169	2.172		
	b, e	2.115	2.116		
	c, e	2.070	2.072		
	b, f	2.116	2.118		
	c, f	2.068	2.070		
CeF	a, d	2.156	2.159		
PrF	a, d	2.142	2.145	2.249	2.252
NdF	a, d	2.127	2.130	2.240	2.242
PmF	a, d	2.112	2.115	2.226	2.229
SmF	a, d	2.099	2.103	2.214	2.216
EuF	a, d	2.087	2.090	2.203	2.206
	b, d	2.084	2.088	2.204	2.208
	b, e	2.020	2.022	2.144	2.145
	b, f	2.017	2.018	2.138	2.138
GdF	a, d	2.076	2.079		
TbF	a, d	2.065	2.067		
DyF	a, d	2.055	2.059		
HoF	a, d	2.045	2.049		
ErF	a, d	2.037	2.041		
TmF	a, d	2.029	2.033	2.146	2.148
YbF	a, d	2.021	2.025	2.143	2.146
	b, d	2.013	2.017	2.136	2.140
	b, e	1.953	1.955	2.079	2.080
	b, f	1.944	1.946	2.066	2.067
LuF	a, d	2.014	2.018		
	b, d	2.002	2.007		
	b, e	1.944	1.946		
	b, f	1.934	1.936		

(a) MEFIT, HF pseudo-potential
(b) MEFIT, WB pseudo-potential
(c) As (b) but the f-pseudo-potential is adjusted to La^{10+} $4f^1$ and $5f^1$ ^2F
(d) Ln (7s6p5d)/[5s4p3d], F (9s6p)/[4s3p]
(e) Ln (7s6p5d1f)/[5s4p3d1f], F (9s6p1d)/[4s3p1d]
(f) Ln (7s6p5d2f)/[5s4p3d2f], F(9s6p2d)/[4s3p2d]

LaF–LuF also show the lanthanide contraction trend. The experimental R_es for LaF, TbF, HoF, YbF and LuF are 2.027, 1.96, 1.94, 2.016 and 1.917 Å respectively. The ground-state results of Dolg and Stoll are thus in good agreement with experiment. At present, there is not much known on the excited electronic states of lanthanide halides.

The SDCI + Q method based on a single-reference configuration underestimates the dissociation energies uniformly as seen from table 51. This is expected in view of a

TABLE 51

Dissociation energies of the rare-earth monofluorides (eV) [AC denotes the CI (SD) + Q results after the energy correction to the experimentally observed atomic ground state of the rare-earth atom was applied]. Reproduced from Dolg and Stoll (1989). See table 47 for a–f footnotes. Most of the experimental constants from Huber and Herzberg (1979). Readers are referred to Dolg and Stoll (1989) for further details.

		$Q = 11$			$Q = 10$		
LnF		CI	+Q	+AC	CI	+Q	Exp.
LaF	a,d	5.14	5.45	5.45			6.20
	b,d	5.46	5.77	5.77			
	c,d	5.50	5.81	5.81			
	b,e	5.55	5.98	5.98			
	c,e	5.68	6.11	6.11			
	b,f	5.56	6.02	6.02			
	c,f	5.68	6.15	6.15			
CeF	a,d	5.17	5.48	5.48			
PrF	a,d	5.19	5.50	4.95	4.84	4.99	
NdF	a,d	5.22	5.54	4.70	4.83	4.98	5.87
PmF	a,d	5.26	5.58		4.79	4.94	
SmF	a,d	5.31	5.63	3.39	4.77	4.91	5.46
							5.81
EuF	a,d	5.36	5.68	2.35	4.75	4.89	5.42
	b,d	5.77	6.09	2.76	4.38	4.51	5.60
	b,e	5.88	6.32	2.98	4.58	4.87	
	b,f	5.90	6.37	3.04	4.68	5.02	
GdF	a,d	5.41	5.73	5.73			6.08
TbF	a,d	5.46	5.78	5.75			
DyF	a,d	5.53	5.85	4.91			5.46
HoF	a,d	5.60	5.92	4.87			5.57
ErF	a,d	5.66	5.98	5.09			5.83
TmF	a,d	5.72	6.04	4.41	4.57	4.72	5.25
YbF	a,d	5.80	6.12	3.24	4.52	4.67	4.80
	b,d	6.38	6.69	3.81	4.03	4.20	5.00
	b,e	6.47	6.91	4.03	4.25	4.54	
	b,f	6.50	6.97	4.09	4.36	4.70	
LuF	a,d	5.87	6.18	6.18			
	b,d	6.45	6.76	6.76			
	b,e	6.56	6.99	6.99			
	b,f	6.57	7.04	7.04			

single-reference and SCF treatment for the MOs. Yet, one could obtain a meaningful relative trend as seen from table 51.

Gotkis (1991) has recently developed a simple electron-structure model to investigate bonding in lanthanide halides. He has investigated the ionization energies for various lanthanides and has obtained systematic trends. Gotkis (1991) has shown that deviations from monotonic trend are due to a field-stimulated restructuring of the lanthanide cation core, which involves promotion of an electron from 4f to an out-of-core extended σ_{6s} orbital. He has grouped lanthanide fluorides into two groups; one which has f^n core (PrF, NdF, SmF, EuF and YbF) and the other with an f^{n-1} core (LaF, GaF, TbF, HoF, ErF, LuF). The former group was found to be similar to

alkaline-earth monohalides while the latter group consisted of Ln^{+3} ($4f^{n-1}$) and F^- and a lone pair $(\sigma_{6s})^2$ localized on the lanthanide atom. Gotkis (1991) found that the energies of the two configurations are close for DyF and TmH. He has predicted the R_e and ω_e values for the ground state and excited states of these halides. He has discussed the Johnson rule for the variation of properties of lanthanide halides. For the actual tables of molecular constants that Gotkis predicts, the reader is referred to his paper.

Dolg et al. (1991b) has recently used the CASSCF/MRCI/CPF method in conjunction with quasi-relativistic pseudo-potentials to study both YbF and YbH including spin–orbit coupling. For YbF, they computed the molecular constants as $R_e = 2.045$ Å, $D_0 = 4.87$ eV and $\omega_e = 492\ cm^{-1}$, in excellent agreement with the experimental values of $R_e = 2.016$ Å, $D_0 = 4.80$ eV, or > 5.36 eV, $\omega_e = 502\ cm^{-1}$. The ground state of YbF was found to be a $\Omega = \frac{1}{2}$ state arising from the $4f^{14}\sigma^2\sigma^2\pi^4\sigma^2$ ($^2\Sigma^+$) configuration. An excited A $^2\Sigma^+$ state of YbF was also found by Dolg et al. (1991b) with $T_e = 0.44$–1.51 eV depending on the level of treatment. The predicted ground state of YbF was in accord with the ESR studies of Van Zee et al. (1977).

6. Electronic states of lanthanide oxides

Among diatomic lanthanide molecules, lanthanide oxides have been the most studied experimentally since there is a large wealth of experimental information on the lanthanide oxides. The reader is referred to the book of Huber and Herzberg (1979) for this information. We focus here mainly on more recent experimental studies. The electronic spectra of lanthanide oxides are very complex due to numerous possible electronic states of varied spin multiplicities. Analysis of the spectra and unambiguous assignment are difficult since many of these states have similar spectroscopic constants and since the 4f orbitals do not take part in bonding. The ligand-field theory and, more recently, *ab initio* and INDO/S-CI techniques have aided the assignment of the observed spectra.

We start with the recent theoretical SDCI + Q computation of Dolg and Stoll (1989) on the ground states of lanthanide oxides. These authors have computed the R_e, D_e, μ_e and ω_e values for the ground states of LaO–LuO using various levels of theories. At present, experimental bond lengths and dissociation energies of several lanthanide oxides are known. The reader is referred to the book by Huber and Herzberg (1979) for these details. The experimental R_es of LaO, CeO, PrO, SmO, EuO, GdO, TbO, DyO, HoO, YbO and LuO are 1.826, 1.820, 1.801, 1.803, 1.812, 1.809, 1.814, 1.796, 1.799, 1.807 and 1.790 Å, respectively. The computed SDCI + Q bond lengths are too long for many of these oxides compared to the experimental values despite the fact that large basis sets have been employed. It should be noted that the SDCI method even after inclusion of quadruple correction for a single reference underestimates the dissociation energies of all these oxides uniformly. Although we do not discuss actinide oxides, we mention that Krauss and Stevens (1983b) have computed the properties of UO. More recently, Krauss (unpublished) has considered NdO.

Carette and Hocquet (1988) have recently applied the ligand-field theory to study the lower-energy lines of the lanthanide monoxides. The spin–orbit parameters were also

included in the ligand-field model. We will discuss their results on CeO, PrO and SmO in the individual sections.

In the ensuing sections, we discuss experimental spectra and theoretical studies on individual oxides. We restrict ourselves to those species which were studied extensively in the recent years either experimentally or theoretically.

6.1. *LaO*

Earlier experimental studies and known electronic states of LaO are summarized in Huber and Herzberg (1979). A recent spectroscopic study is due to Carette (1990). The ground state of LaO is well established as the $X\,^2\Sigma^+$ state with $R_e = 1.825$ Å, $\omega_e = 813\,cm^{-1}$. There are several excited states of $A\,^2\Delta$, $A\,^2\Pi$, $B\,^2\Sigma^+$, $C\,^2\Pi$, $D\,^2\Sigma$ and $F\,^2\Sigma$ symmetries. Recent experimental studies on LaO and other oxides include the pulsed Fourier-transform microwave spectroscopy of YO, LaO, ZrO and HfO by Suneram et al. (1991). The related YO has also been studied extensively. In particular Steimle and Al-Ramadin (1989) have studied the microwave-optical double-resonance (MODR) spectra of YO. Childs et al. (1988) have obtained the fine and magnetic hyperfine structure in the $X\,^2\Sigma^+$ and $A\,^2\Pi$ states of YO.

There are several theoretical studies on LaO and related lanthanide oxides. We have already mentioned the ligand-field theory model calculations of Field (1982) as well as Carette and Hocquet (1988). More recently, Kotzian et al. (1991a,b) have applied the INDO technique (Pople et al. (1967) extended to include spin–orbit coupling [see also Kotzian et al. (1989a, b)] to lanthanide oxides (LaO, CeO, GdO and LuO). The authors call it INDO/S-CI method. The INDO parameters were derived from atomic spectra, model Dirac–Fock calculations on lanthanide atoms and ions to derive ionization potentials, Slater–Condon factors and basis sets. The spin–orbit parameter (ξ) is derived from atomic spectra in this method.

The INDO/S-CI computations were made on LaO by Kotzian et al. (1991a, b) at an experimental bond distance of 1.826 Å. For LaO, the ground-state configuration is $(1\sigma/O2s)^2\,(1\pi/O2p)^4\,(2\sigma/O2p)^2\,(3\sigma/La6s)^1\,(1\delta/La5d)^0\,(2\pi/La6p)^0\,(4\sigma/La6p)^0\,(3\pi/LaUf)^0\,(1\phi/La4f)^0\,(5\sigma/La4f)^0\,(2\delta/La4f)^0\,(4\pi/La5d)^0\,(6\sigma/La5d)^0$.

Table 52, reproduced from Kotzian et al.'s work, compares the INDO/SCI energy separations with experiment for several electronic states of LaO. It is evident from table 52 that the INDO/S-CI method predicts the energy separations for these compounds reasonably well. Kotzian et al. also computed the transition moments for the observed $A \leftrightarrow C$, $B \leftrightarrow X$, $C \leftrightarrow X$, $D \leftrightarrow X$ and $F \leftrightarrow X$ systems.

6.2. *CeO*

There are several recent experimental studies on the CeO diatomic molecule. Schall et al. (1986) have studied CeO using the sub-doppler Zeeman spectroscopy. Again, the ligand-field model is so successful in explaining the observed spectra due to the ionic nature of the diatomic lanthanide oxide. Linton et al. (1979, 1981, 1983a, b) as well as Linton and Dulick (1981) have studied the electronic spectrum of CeO using absorption, emission as well as laser spectroscopic method. There are many 0–0 bands for

TABLE 52

Calculated and experimental states of LaO. State energies T_e are given in cm^{-1}. The molecular spin–orbit constant A is defined by the relation $\langle J\Omega\Lambda S\Sigma|H_{SO}|J\Omega\Lambda S\Sigma\rangle = A\Lambda\Sigma$. Reproduced from Kotzian et al. (1991a).

INDO/S-CI				Experiment		
State	Config.	T_e	A	State	T_e	A
$1\,^2\Sigma^+_{1/2}$	3σ 100%	0		$X\,^2\Sigma^+$	0	
$1\,^2\Delta_{3/2}$	1δ 100%	8488	353	$A'\,^2\Delta_r$	7468.9	350.5
$1\,^2\Delta_{5/2}$	1δ 100%	9195			8168.4	
$1\,^2\Pi_{1/2}$	2π 99%	13 856	869	$A^2\Pi_r$	12 635.7	862.7
$1\,^2\Pi_{3/2}$	2π 100%	14 724			13 497.6	
$2\,^2\Sigma^+_{1/2}$	4σ 93%	19 715		$B\,^2\Sigma^+$	17 837.8	
$2\,^2\Pi_{1/2}$	3π 94%	22 986			22 618.9	
$2\,^2\Pi_{3/2}$	3π 79%	23 241	255	$C\,^2\Pi_r$	22 839.6	221.4
	2δ 20%					
$1\,^2\Phi_{5/2}$	1φ 93%	23 310	560			
$1\,^2\Phi_{7/2}$	1φ 100%	24 990				
$2\,^2\Delta_{3/2}$	2δ 79%	24 788				
	3π 21%		451			
$2\,^2\Delta_{5/2}$	2δ 93%	25 691				
$3\,^2\Sigma^+_{1/2}$	5σ 90%	26 007		$D\,^2\Sigma$	26 959.0	
$3\,^2\Pi_{1/2}$	4π 99%	30 180	408	$F\,^2\Sigma$	28 049.0	
$3\,^2\Pi_{3/2}$	4π 99%	30 588				
$4\,^2\Sigma^+_{1/2}$	6σ 100%	41 616				

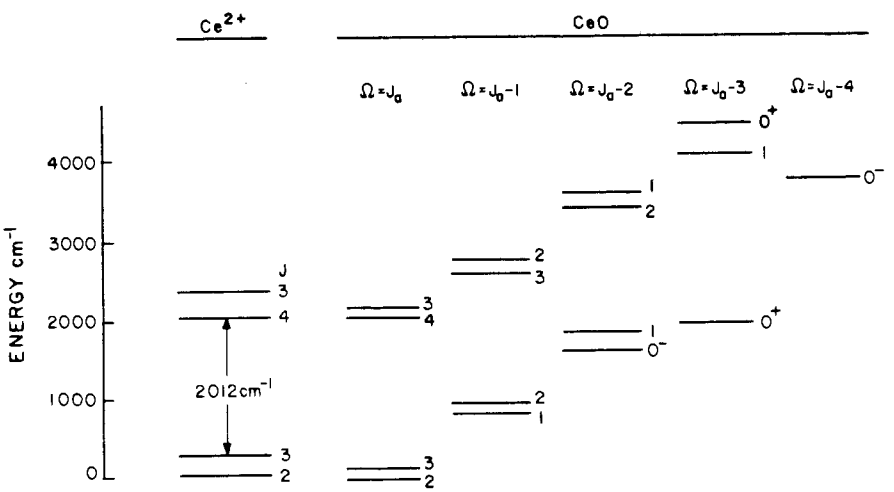

Fig. 36. Energy-level diagram of Ce^{+2} arising from the 4f6s configuration and the corresponding states of the diatomic CeO. All states of CeO are arranged by their Ω values. Reproduced from Schall et al. (1986).

CeO arising from electronic transitions between various Ω components of excited states and the Ω states arising from ... (4f)(6s) electronic configurations. The CeO molecule is also the simplest lanthanide oxide containing a single 4f electron.

The electronic states of CeO are best rationalized in terms of the electronic states of Ce^{+2} ion since the bonding in CeO is best described as $Ce^{+2}O^{-2}$ ionic bond. Figure 36 shows the energy level diagram of Ce^{+2} 4f6s configuration and the corresponding state of CeO [reproduced from Schall et al. (1986)]. It is evident from fig. 36 that there are 16 Ω states arising from the Ce^{+2} 4f6s configuration itself.

Table 53 shows the spectroscopic constants of CeO derived by Linton et al. (1983a, b) from their spectra. As seen from table 53, the X_1 ground state with $\Omega = 2$ and X_2 state with $\Omega = 3$ are very close to each other. Note that X_3 and X_4 states arise from the same principal λ-s state but the splitting between (X_1, X_2) duo with $(X_3 - X_4)$ duo is roughly the atomic Ce^{+2} splitting between $J = 2, 3$ and $J = 3, 4$ pairs (see fig. 36). The energy levels in table 53 approximately correspond to the levels in fig. 36.

TABLE 53
Constants for the low-lying states of CeO (cm^{-1}). Reproduced from Linton et al. (1983a, b).

State	J_a	J_c	T_0	B_0	$10^7 D_0$	$\Delta G_{1/2}$	Note
$U_3\ 0^+$	3	$\frac{7}{2}$	*4457.7 (30)	0.367	–	–	
$U_2\ 1$	4	$\frac{7}{2}$	*4133 (5)	–	–	–	c
$T_1\ 0^-$	4	$\frac{7}{2}$	3821.5 (30)	0.375	–	–	
$V_4\ 1$	3	$\frac{7}{2}$	*3642 (5)	–	–	–	c
$V_3\ 2$	4	$\frac{7}{2}$	3462.6 (25)	0.355	–	820.7	
$W_4\ 2$	3	$\frac{7}{2}$	2771.7 (15)	0.35999 (1)	2.21 (1)	823.4	d
$W_3\ 3$	4	$\frac{7}{2}$	2617.3 (21)	~0.356	–	824.7	e
$X_4\ 3$	3	$\frac{7}{2}$	2140.6 (15)	0.35658 (2)	2.72 (2)	824.1	f
$X_3\ 4$	4	$\frac{7}{2}$	2039.8 (21)	0.35327 (1)	2.24 (1)	822.1	g
$U_1\ 0^+$	3	$\frac{5}{2}$	*1931.8 (30)	0.377	–	–	
$V_2\ 1$	3	$\frac{5}{2}$	*1869.7(30)	0.343	–	–	
$V_1\ 0^-$	2	$\frac{5}{2}$	1679.4 (25)	0.35788 (1)	2.52	–	
$W_2\ 2$	3	$\frac{5}{2}$	912.2 (15)	0.36139 (6)	7.3 (4)	823.0	h
$W_1\ 1$	2	$\frac{5}{2}$	811.6 (25)	~0.361	–	–	i
$X_2\ 3$	3	$\frac{5}{2}$	80.3 (15)	0.35692 (1)	2.71 (1)	822.8	j
$X_1\ 2$	2	$\frac{5}{2}$	0	0.35454 (1)	2.46 (1)	824.3	

* Levels of the correct Ω, closest to the predicted positions.
[a] Numbers in parentheses represent estimates of the standard deviation in the last two digits.
[b] With the exceptions of the X_1 and X_2 states, uncertainties in $\Delta G_{1/2}$ are ~2 cm^{-1}.
[c] These states have each been observed only once, in fluorescence, at $J \sim 25$: their B values are not known.
[d] Originally labelled v (2).
[e] Originally labelled w (3).
[f] $10^3 \alpha = 1.4$
[g] $10^3 \alpha = 1.27$
[h] Originally labelled u (2).
[i] Originally labelled y (1).
[j] $10^3 \alpha = 1.9$

A combination of laser-induced fluorescence with classical absorption and emission spectroscopy has yielded a wealth of data on the excited electronic states of CeO. However, as noted by Linton et al., the spectroscopic data of upper states is less complete and are shown in table 54. Linton et al. (1983a, b) used empirical notation taken from atomic spectroscopy to designate these states.

The vibrational frequencies ($G_{1/2}$, ω_e) are of the order of 800 cm^{-1} for the low-lying states of CeO. Linton et al. (1983a, b) observed several laser-induced fluorescence transitions of CeO. They are shown in fig. 1 of their paper. They have provided a rather detailed and extensive analysis of their fluorescence excitation spectra. The reader is referred to their original paper for further discussion of their spectra.

Linton et al. (1983a, b) noted that the 4f6s configuration of Ce^{+2} exhibits a j–j rather than l–s coupling. This is expected in view of the fact that the 4f orbital spin–orbit coupling is larger than the $^1F_3$–$^3F_3$ energy separation. Hence, they conclude that lanthanide oxide configurations including 4f electrons would tend towards Case (c) coupling.

It should be noted that although Ce^{+2} ion has a $4f^2$ configuration, the ligand-field calculations of Linton et al. (1983a, b) predict reordering of free ion configurations for the oxides:

$$4f6s \ll 4\delta^2 < 4f5d < 4f6p.$$

Hence, Linton et al. conclude that for all lanthanide oxides, except EuO and YbO, the lowest states should arise from $(4f)^n6s$ configuration rather than $(4f)^{n+1}$.

Schall et al. (1986) have deduced the electronic G value for four lower states of CeO and compared them with the values derived from the ligand-field theory. The agreement was found to be very good.

Kotzian et al. (1991a, b) as well as Kotzian and Rösch (1991a, b) have applied the INDO/S-CI method extended to include spin–orbit coupling on the diatomic CeO. They have studied 16 electronic states of CeO arising from the 4f6s configuration of Ce^{+2} at the experimental R_e of 1.820 Å. The results of their computations are shown in table 55. Note that Kotzian et al. have also compared the INDO/S-CI results with ligand-field theories LFT1 and LFT2. As seen from table 55, the agreement between the experimental values and the INDO/S-CI as well as ligand-field models is quite good.

Kotzian et al. (1991a, b) also find that low-lying states of CeO arise from the 4f6s configuration. The charge-transfer excitations $O \rightarrow Ce$ were omitted in the Kotzian et al.'s INDO/S-CI since the energy for this excitation is $> 55\,000\ cm^{-1}$. Overall, the experimental trend is reproduced by the INDO/S-CI except that two pairs of states (U_1O^+, and V_21; U_21 and U^3O^+) have reverse order in the INDO/S-CI calculation compared to the experiment. Mulliken-population analyses of Kotzian et al. (1991a, b) revealed that the oxygen atom has $O(2s^{1.923}\,2p_\sigma^{1.731}\,2p_\pi^{3.046})$ population in the ground state. The corresponding Ce population is Ce $4f_\sigma^{1.81}\,4f_\pi^{0.329}\,4f_\sigma^{0.284}\,4f_\phi^{0.286}\,6s^{0.920}\,5d_\sigma^{0.308}\,5d_\pi^{0.882}$.

6.3. *PrO*

PrO was first studied at complete low resolution by Shenyavskaya et al. (1973). These authors reported vibrational analyses of 22 electronic transitions of PrO in the

TABLE 54

Constants for the excited states of CeO (cm^{-1}). Reproduced from Linton et al. (1983a, b).

State[a]		T_0	B_0	$10^7 D_0$	$\Delta G_{1/2}$	Transitions[b]
[28.6] 1		28 596.1	(e) 0.36122 (f) 0.36079	3.04	–	[28.6] $1-V_1\,0^-$
[26.7] 4	E_3	26 715.2	0.35294	4.9	795.5	[26.7] $4-X_3\,4$
[26.2] 3	H_2	26 200.0	0.3514	2.2	732.54	[26.2] $3-X_2\,3$
[26.1] 2	F_1	26 067.5	0.3522	3.75	–	[26.1] $2-X_1\,2$
[25.3] 3	G_2	25 292.3	0.3502	3.03	733.90	[25.3] $3\leftarrow X_2\,3$
[25.0] 2	E_1	25 011.5	0.34863	2.81	744.3	[25.0] $2-X_1\,2$
[23.7] 0^-		23 674.3	0.35348	0.48	–	[23.7] $0^--V_1\,0^-$
[22.7] 0^-		22 722.8	0.35407	2.63	–	[22.7] $0^--V_1\,0^-$
[22.6] 5	D_3	22 556.0	0.35069	2.61	786.0	[22.6] $5-X_3\,4$
[22.5] 1		22 505.8	(f) 0.3576	6.2	–	[22.5] $1\rightarrow V_1\,0^-$
[22.5] 3	h_2	22 498.4	0.3568	5.0	792.3	[22.5] $3\rightarrow W_2\,2$ F.-X_2 3, -X_4 3, -W_2 2, -W_4 2
[22.0] 4	A_4	22 012.3	0.35443	2.81	768.0	[22.0] $4-X_4\,3$
[21.7] 4		21 713.2	0.35353	2.14	–	[21.7] $4-X_2\,3$
[21.4] 1	D_1	21 379.2	0.35241 0.35203	2.75 2.59	–	[21.4] $1-X_1\,2$
[21.1] 2	g_2	21 061.9	0.35662	3.98	–	[21.1] $2-X_2\,3$; [21.1]$2-W_2\,2$ F.-X_2 3, -X_4 3, -W_2 2, -W_4 2
[20.9] 4	F_2	20 914.5	0.35294	2.97	–	[20.9] $4-X_2\,3$
[20.3] 3	C_1	20 273.8	0.34988	2.99	783.6	[20.3] $3-X_1\,2$
[19.9] 1		19 926	–	–	–	[19.9] $1-X_1\,2$ F.-X_1 2, -W_4 2, -$V_1\,0^-$, -V_2 1, -V_3 2, -$U_1\,0^+$, -$U_3\,0^+$, -$T_1\,0^{-1}$
[19.3]3		19 287.5	0.3485	0.4	–	[19.3] $3\rightarrow X_4\,3$
[18.4] 4	C_3	18 386.2	0.34176	2.3	750.7	[18.4] $4\leftarrow X_3\,4$ F.-X_3 4, -X_2 3, -X_4 3, -W_3 3
[17.2] 3	e_2	17 169.5	0.35037	2.44	765.0	[17.2] $3\leftarrow X_2\,3$ F. -X_1 2, -X_2 3, -X_3 4, -X_4 3, -W_2 2, -W_4 2
[16.7] 1		16 714.8	(e) 0.35616 (f) 0.35643	4.28 3.45	–	[16.7] $1\leftarrow V_1\,0^-$ F. -X_1 2, -W_1 1, -W_2 2, -W_4 2, $V_1\,0^-$, -V_2 1, -V_3 2, -$U_1\,0^+$, -$U_3\,0^+$, -$T_1\,0^-$
[16.5] 2	B_1	16 524.2	0.3436	–	720.7	[16.5] $2\leftarrow X_1\,2$ F. -X_1 2, -X_2 3, -X_4 3, -W_1 1, -W_2 2, -W_3 3, -W_4 2
[16.5] 4	E_2	16 495.4	0.35363	5.1	753.9	[16.5] $4\leftarrow X_2\,3$ F. -X_2 3, -X_3 4, -X_4 3, -W_2 2, -W_3 3
[16.0] 3	D_2	16 039.2	0.35953	5.3	–	[16.0] $3\leftarrow X_2\,3$
[15.8] 4	C_2	15 813.8	0.35216	3.03	–	[15.8] $4\leftarrow X_2\,3$
[15.5] 5	B_3	15 489.4	0.34534	2.45	–	[15.5] $5\leftarrow X_3\,4$
[14.7] 3		14 701.6	0.35255	2.51	–	[14.7] $3\leftarrow W_2\,2$, [14.7] $3\leftarrow W_4\,2$
[14.2] 3	A_3	14 201.8	0.36024	4.48	–	[14.2] $3\leftarrow X_3\,4$
[14.2] 0^-		14 197.0	0.35216	7.8	–	[14.2] $0^-\leftarrow V_1\,0^-$
[13.9] 4	B_2	13 884.3	0.34711 0.35974	2.86 4.97	747.39	[13.9] $4\leftarrow X_2\,3$, [13.9] $4\leftarrow X_4\,3$
[13.2] 1	a_1	13 201.6	0.35921	5.51	–	[13.2] $1\leftrightarrow X_1\,2$
[12.8] 2	A_2	12 768.0	0.3535	4.5	–	[12.8] $2\leftrightarrow X_2\,3$
[12.6] 3	A_1	12 595.8	0.34672	2.90	–	[12.6] $3\leftrightarrow X_1\,2$

[a] Designations of states prior to Linton et al. (1983a, b) are given in the second column.

[b] F. indicates a transition observed in fluorescence.

TABLE 55

Calculated and experimental states of CeO of the configuration 4f6s [reproduced from Kotzian et al. (1991a)]. Energies are given in cm^{-1}. In the first column the experimental labeling is given. Λ is the projection of the total orbital angular momentum, Ω the projection of the total angular momentum in the molecular system, and J_a the value of the atomic total angular momentum from which the molecular state originates. The values of Λ and J_a, are taken from the leading determinant. Ligand-field (LFT1, LFT2) and experimental values are taken from Dulick et al. (1986), Carette and Hocquet (1988), and Linton et al. (1983a, b), respectively. Reproduced from Kotzian et al. (1991a).

							INDO/S-CI		
State	Λ	Ω	J_a	Exp.	LFT1	LFT2	Energy	Configuration	
X_1	3	2	2	0.0	0.0	0	0	$1\phi 4\sigma$ 91%	
X_2	3	3	3	80.3	121.6	197	71	$1\phi 4\sigma$ 90%	
W_1	2	1	2	811.6	805.6	1026	857	$1\delta 4\sigma$ 84%	
W_2	2	2	3	912.2	910.8	1160	918	$1\delta 4\sigma$ 82%	$2\pi 4\sigma$ 17%
V_1	1	0^-	2	1679.4	1777.7	1756	1812	$2\pi 4\sigma$ 73%	$3\sigma 4\sigma$ 25%
V_2	1	1	3	1869.7	1878.4	1919	1937	$2\pi 4\sigma$ 70%	$3\sigma 4\sigma$ 27%
U_1	1	0^+	3	1931.8	1866.3	1978	1850	$2\pi 4\sigma$ 75%	$3\sigma 4\sigma$ 22%
X_3	3	4	4	2039.8	2021.8	2495	2084	$1\phi 4\sigma$ 99%	
X_4	3	3	3	2140.6	2185.4	2146	2154	$1\phi 4\sigma$ 98%	
W_3	2	3	4	2617.3	2632.2	3268	2726	$1\delta 4\sigma$ 84%	
W_4	2	2	3	2771.7	2762.7	2994	2791	$1\delta 4\sigma$ 84%	
V_3	1	2	4	3462.6	3501.5	3944	3453	$2\pi 4\sigma$ 80%	$1\delta 4\sigma$ 17%
V_4	1	1	3	3642.	3600.9	3724	3562	$2\pi 4\sigma$ 81%	$1\delta 4\sigma$ 14%
T_1	0	0^-	4	3821.5	4035.2	4109	4176	$3\sigma 4\sigma$ 72%	$2\pi 4\sigma$ 25%
U_2	0	1	4	4133.	4101.9	4391	4234	$3\sigma 4\sigma$ 68%	$2\pi 4\sigma$ 29%
U_3	0	0^+	3	4457.7	4262.8	4476	4217	$3\sigma 4\sigma$ 70%	$2\pi 4\sigma$ 23%

500–1120 nm region. Shenyavskaya et al. (1973) designated the observed systems I through XXII. Delaval et al. (1977) studied the systems VII and X, but no definitive assignment of the observed electronic transitions came forth. Beaufils et al. (1979) observed the first lines in $\Delta\Omega = +1$ XVII and XX transitions. This led to the assignment for XVII $\Omega'' = 3.5$ and $\Omega' = 4.5$, and $\Omega'' = 4.5$ and $\Omega' = 5.5$ for system XX. As pointed out by Dulick and Field (1985), some of the earlier assignments of the observed spectra of PrO were either incorrect or speculative.

Dulick and Field (1985) provided extensive analyses of the observed systems. They studied the (0, 0) bands of nine prominent systems in the 500–800 nm region. For the first time definitive Ω assignments for the upper and lower electronic states participating in these transitions were provided by Dulick and Field.

Dulick et al. (1986), as well as Carette and Hocquet (1988), have used the ligand-field theory to compute the energy levels of PrO. More recently, Kotzian and Rösch (1991a, b) used the INDO/S-CI method to investigate the electronic states of PrO and TmO. They computed the properties of 33 electronic states of PrO and compared their computed energies with experiment and ligand-field theory. All of these studies have provided significant insight into the low-lying electronic states of PrO.

Table 56 shows the Dulick–Field assignment of the observed systems of PrO designated by their Ω quantum numbers. Note that Dulick and Field suggest that the

TABLE 56
Twelve observed electronic transitions of PrO and their suggested assignments by Dulick and Field (1985). Reproduced from Dulick and Field (1985).

System	Ω'	T'_0 (cm^{-1})	Ω''	T''_0 (cm^{-1})
VI	5.5	11 102	4.5	2157
IX	4.5	16 597	3.5	3887
X	5.5	13 259	4.5	220
XI	5.5	13 865	4.5	220
XIV	5.5	16 595	4.5	2157
XVI	5.5	19 169	4.5	3720
XVII	4.5	16 597	3.5	0
XVIII	7.5	21 321	6.5	3965
XIX	6.5	19 687	5.5	2111
XX	5.5	18 069	4.5	220
XXI	4.5	18 885	4.5	220
XXII	5.5	19 169	4.5	220

lowest state has a Ω quantum number of 3.5. A diagrammatic interpretation of the observed systems and the energy levels of PrO was provided by these authors. We reproduce this in fig. 37. Figure 37 nicely summarizes the electronic states of PrO and the observed transitions. Table 57 shows the comprehensive assignment of systems I–XXII for PrO observed by Shenyavskaya et al. (1973). Tables 56 and 57 together yield the experimentally known states of PrO. We now proceed to theoretical calculations and insight into the nature of electronic states of PrO.

As mentioned before, there are INDO/S-CI as well as ligand-field theoretical studies on PrO. The recent work of Kotzian and Rösch (1991b) provides a beautiful summary of all known information on PrO up to now. We will use this work and the paper of Dulick and Field as basis for discussion of the electronic states of PrO. Table 58 shows the Ω values of several electronic states of PrO, their energy separations obtained using the INDO/S-CI method by Kotzian and Rösch (1991b) as well as the ligand-field theoretical values of Dulick et al. (1986) and Carette and Hocquet (1988). Figure 38 shows schematically the computed energy levels of PrO using various methods together with known experimental data up to now.

The electronic states of PrO are best rationalized using the energy levels of the Pr^{+2} ion which has the configuration $4f^2\,6s$. Figure 39 shows the energy levels arising from $4f^2(^3H)6s$ and $4f^2(^3H)6p_{1/2}$ configurations of the Pr^+. As seen from fig. 39, the coupling is j–j. The spin–orbit coupling of the $4f^2$ shell (^3H) is roughly 2000 cm^{-1}. The PrO diatomic states are rationalized as arising from $Pr^{+2}O^{-2}$. The INDO/SCI yields a ground state electronic configuration of $(1\sigma/O2s)^2(1\pi/O2p)^4(2\sigma/O2p)^2$-$(1\phi/Pr4f)^{4/7}(1\delta/Pr4f)^{4/7}(2\pi/Pr4f)^{4/7}(3\sigma/Pr4f)^{2/7}(4\sigma/Pr6s)^1$. This configuration is, of course, consistent with $Pr^{+2}O^{-2}$ picture. The INDO calculations revealed that the $4f^2\,4\sigma$ configuration is the lowest while $4f^2\,2\delta$ and $4f^3$ configurations are 8200 and 18 300 cm^{-1} above the $4f^2\,4\sigma$ configuration. Other configurations are much higher (energy > 41 850 cm^{-1}). Hence, the INDO-SCI studies were focused on the electronic

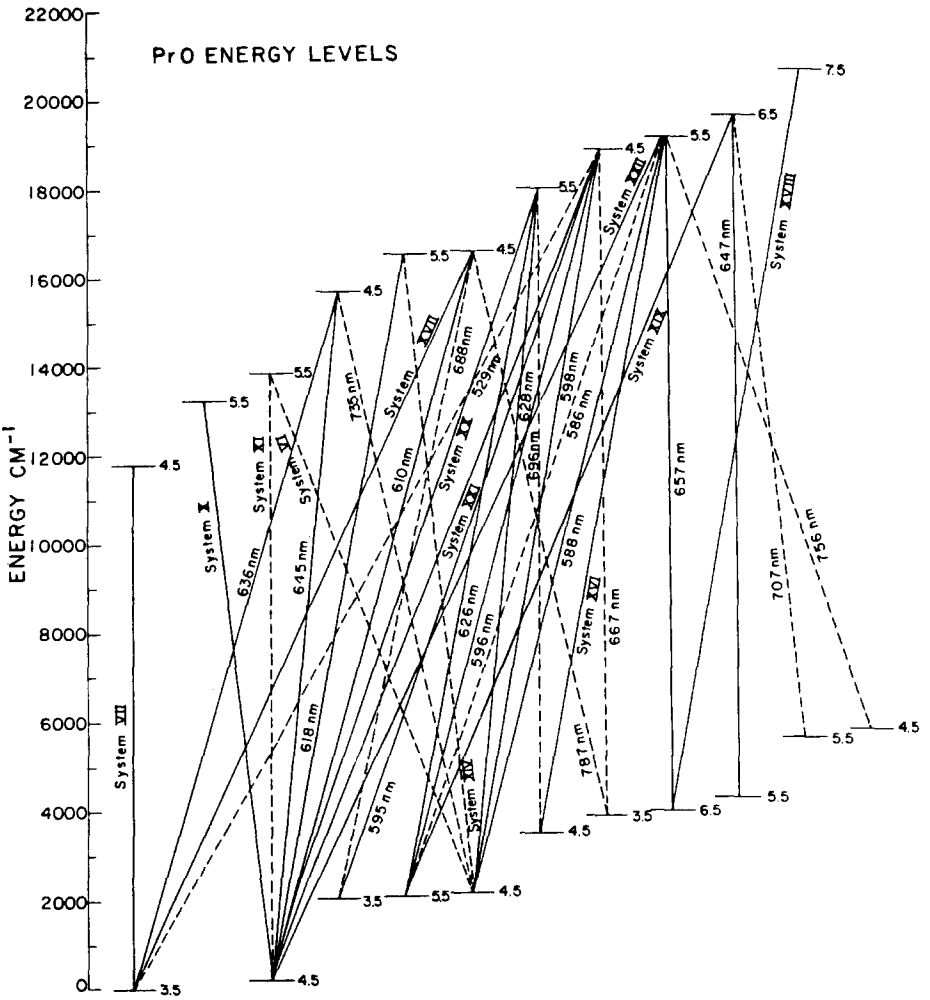

Fig. 37. Energy-level diagram and the electronic transitions of PrO. The full line designates electronic transition examined under high resolution. Reproduced from Dulick and Field (1985).

states arising from $4f^2 4\sigma$. As seen from table 58, the INDO-SCI model as well as ligand-field models reproduce the energies of the experimentally known states ($\Omega \geq 3.5$).

6.4. *SmO*

The spectra of samarium monoxide (SmO) have been studied by Dekock and Weltner (1971), Hannigan (1983), Dickson and Zare (1975), Linton et al. (1987), Bujin and Linton (1989) and recently by Bujin and Linton (1991). The recent work of

TABLE 57
Electronic assignments of Pro for systems I–XXII of Shenyavskaya et al. (1973) suggested by Dulick and Field (1985).

System	Bandhead[a] v (cm^{-1})	Ω'[b]	Ω''
I	9233	?	?
II	9996	?	?
III	10205	?	?
IV	10438	5.5	4.5 (XX)[c]
V	10976	?	?
VI	11109	5.5 (X)	4.5[d]
VII	11777	4.5	3.5 (XVII)[c,e]
VIII	11922	2.5	3.5 (XVII)[c]
IX	12711	4.5 (XVII)	3.5[d]
X	13047	5.5	4.5 (XX)[c,e]
XI	13657	5.5	4.5 (XX)
XII	14006	?	?
XIII	14090	?	?
XIV	14384	5.5 (XX)	4.5[d]
XV	14439	3.5	4.5 (XX)[c]
XVI	15442	5.5 (XXII)	4.5
XVII	16610	4.5	3.5
XVIII	17346	7.5	6.5
XIX	17567	6.5	5.5
XX	17863	5.5	4.5
XXI	18680	5.5	4.5 (XX)
XXII	18961	5.5	4.5 (XX)

[a] Shenyavskaya et al. (1973).
[b] System designations enclosed in parentheses share the indicated upper or lower electronic state.
[c] $\Delta\Omega$ assignments taken from Shenyavskaya and Kaledin (1982).
[d] Assignments suggested by Dulick and Field (1985).
[e] Assignments taken from Beaufils et al. (1979).

Bujin and Linton (1991) summarizes the known electronic states of SmO up to now. Carette and Hocquet (1988) have used the ligand-field theory to calculate the lower electronic energy levels of SmO. These authors found 11 electronic states of SmO below 2280 cm^{-1}. The ground state of SmO was calculated as the XO^- electronic state.

Table 59 shows the most recent spectroscopic data on the energy separations of the electronic states of SmO. Both experiment and theory seem to agree on the XO^- ground state of SmO. The two ligand-field calculations are in reasonable agreement with the experimental energy separations. Figure 40 shows the energy-level diagram of the electronic states of SmO. The calculation of Dulick et al. (1986) yields more energy levels than known experimentally. As seen from fig. 40, the Carette–Hocquet ligand-field calculation is slightly in better agreement with experiment. Linton et al. (1987) attributes this to differences in the choice of Sm^{2+} atomic-orbital basis sets; the Carette–Hocquet eigenfunctions are considered probably more realistic.

TABLE 58

Energies of molecular states of PrO (in cm^{-1}) arising mainly from the atomic states of Pr. III. Reproduced from Kotzian and Rösch (1991a, b).

	INDO/S-CI			LFT[b]	LST[c]
Ω	Energy	Composition[a]		Energy	Energy
3.5	0	|H 4 3.5⟩53%	|H 5 4.5⟩25%	0	0
		|H 4 4.5⟩11%			
4.5	235	|H 4 4.5⟩57%	|H 5 5.5⟩35%	233	225
2.5	1678	|H 4 3.5⟩71%	|H 4 4.5⟩14%	1867	
3.5	1985	|H 4 4.5⟩66%	|H 4 3.5⟩18%	2074	1696
5.5	2136	|H 5 5.5⟩59%	|H 6 6.5⟩39%	2094	1995
0.5	2155	|H 6 6.5⟩30%	|P 2 2.5⟩23%	2866	
4.5	2197	|H 5 4.5⟩60%	|H 6 5.5⟩30%	2144	2059
1.5	2395	|H 4 3.5⟩21%	|H 5 5.5⟩18%	2924	
		|P 2 2.5⟩14%	|F 4 4.5⟩11%		
0.5	2519	|P 2 1.5⟩17%	|H5 4.5⟩15%	3107	
		|H 6 5.5⟩14%			
1.5	2774	|H 4 3.5⟩40%	|H 4 4.5⟩27%	3125	
2.5	2835	|H 4 4.5⟩62%	|G 4 4.5⟩15%	3099	
		|H 4 3.5⟩14%			
4.5	3618	|H 5 5.5⟩47%	|H 4 4.5⟩41%	3767	3285
3.5	3753	|H 5 4.5⟩48%	|H 4 3.5⟩26%	3824	3357
		|H 5 5.5⟩11%			
6.5	4033	|H 6 6.5⟩100%		3960	3998
0.5	4326	|F 3 2.5⟩ 19%	|H 5 5.5⟩17%	4941	
		|F 3 3.5⟩17%	|P 0 0.5 ⟩17%		
		|P 1 0.5⟩12%			
5.5	4329	|H 6 5.5⟩97%		4246	4313
1.5	4439	|H 4 4.5⟩28%	|H6 6.5⟩21%	4946	
		|P 1 1.5⟩10%			
0.5	4456	|H 6 5.5⟩21%	|H 4 3.5⟩19%	5022	
		|H 4 4.5⟩15%	|H 6 6.5⟩14%		
		|P 2 1.5⟩10%			
2.5	4508	|H 5 5.5⟩59%	|P 2 2.5⟩14%	4853	
3.5	4568	|H 5 5.5⟩72%	|H 5 4.5⟩21%	4786	4195
1.5	4652	|H 5 4.5⟩32%	|F 4 3.5⟩13%	5070	
		|H 5 5.5⟩11%			
2.5	4811	|H 5 4.5⟩81%		4992	
5.5	5363	|H 6 6.5⟩57%	|H 5 5.5⟩41%	5548	5210
4.5	5779	|H 6 5.5⟩46%	|H 5 4.5⟩28%	5812	5490
		|H 6 6.5⟩18%			
0.5	6050	|P 0 0.5⟩31%	|H4 4.5⟩15%	6560	
		|F 2 1.5⟩13%			
1.5	6213	|H 5 5.5⟩29%	|P 1 1.5⟩23%	6679	
		|H 6 6.5⟩12%			
2.5	6422	|H 6 6.5⟩54%	|F 2 2.5⟩12%	6849	
0.5	6427	|P 1 0.5⟩24%	|H 5 4.5⟩17%	6866	
		|F 2 2.5⟩12%	|H 5 5.5⟩10%		
4.5	6540	|H 6 6.5⟩68%	|H 6 5.5⟩23%	6702	6170
3.5	6576	|H 6 6.5⟩88%		6848	6377
1.5	6737	|H 6 5.5⟩29%	|H 5 4.5⟩12%	7069	
		|P 2 1.5⟩10%			
3.5	7044	|H 6 5.5⟩90%		7085	6781
2.5	7069	|H 6 5.5⟩73%		7233	

[a] The atomic states are labeled according to $|L_f J_f J_a\rangle$. Only states contributing more than 10% are listed.

[b] Dulick et al. (1986).

[c] Carette and Hocquet (1988).

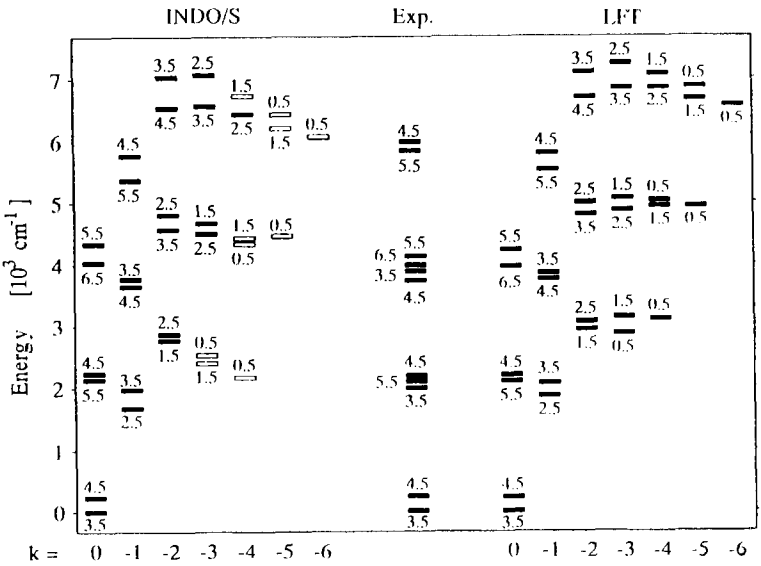

Fig. 38. Energy levels of PrO as computed by INDO/S and LFT methods together with known experimental energies. Reproduced from Kotzian and Rösch (1991a, b).

The spectra of SmO exhibited significant Ω doubling for the lowest states. This was anticipated by calculations although calculations were not found to be in accord with the observed values. Bujin and Linton (1991) attribute this to incorrect ordering of the e and f levels in calculations.

The electronic states of SmO can be rationalized from the $Sm^{+2}\,4f^2\,6s(^6H)$ supermultiplet. The overall ordering of the electronic states of SmO closely resembles the low-lying states of Sm^{+2} derived from the $(4f^2\,6s)^6H$ electronic supermultiplet. This is further supported by the remarkable agreement of the observed energy levels with the values obtained from ligand-field models.

6.5. *EuO*

Experimental data on EuO are rather limited at the present time. Dulick et al. (1986) have derived the dissociation energy of EuO as 4.92 ± 0.1 eV from a thermodyamic study. They have also discussed the electronic structure of EuO using the ligand-field model. The $4f^7$–$4f^6\,\sigma$ (excited) superconfiguration energy separation was found to be 0.60 ± 0.1 eV from thermodynamical studies and 0.41 eV from ligand-field theory, although Carette and Hocquet (1988) found a different value of 0.98 eV for this energy separation.

Gabelnick et al. (1984) have obtained the vibrational frequency (ω_e) of Ar-isolated EuO as $672\,cm^{-1}$. McDonald (1985) obtained a ω_e of $688\,cm^{-1}$ confirming that the ground state arises from a $4f^7$ superconfiguration. An R_e of 1.891 Å was estimated from the rotational constant of ^{151}EuO.

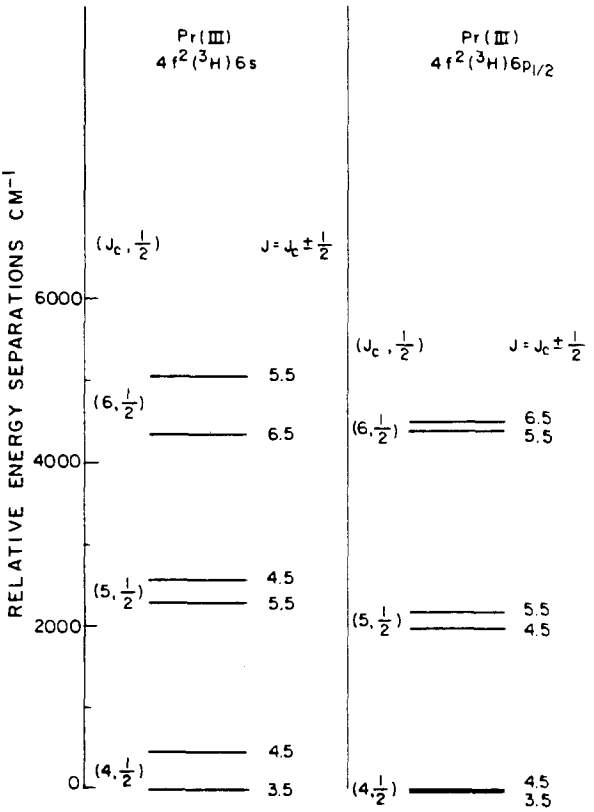

Fig. 39. Energy levels of Pr^{+2} from $4f^2(^3H)6s$ and $4f^2(^3H)6p$. Reproduced from Dulick and Field (1985).

TABLE 59
The energies (in cm^{-1}) of the observed low-lying states of SmO. Reproduced from Bujin and Linton (1991).

State	Experimental	Calculated (1)[a]	Calculated (2)[b]
$X0^-$	0.0	0.0	0.0
(1)1	146.98	115.0	130.1
(1)2	566.77	498.0	549.0
(2)0^+	582.25	640.0	982.0
(2)1	879.30	873.0	1167.3
(1)3	1280.49	1189.0	1299.7
(3)0^-	1546.36	1359.0	2018.4
(2)2	1604.25	1517.0	1741.6
(4)0^+	1661.0	1603.0	2030.0
(3)1	1661.39	1472.0	2182.9
(3)2	2239.91	1998.0	2839.5
(4)1	2013.5	1963.0	2317.4
(1)4	2286.57	2226.0	2417.1
(5)0^+	2520.0	2603.0	2990.0
(5)1	2867.3	2718.0	3272.9

[a] From Carette and Hocquet (1988).
[b] From Dulick et al. (1986).

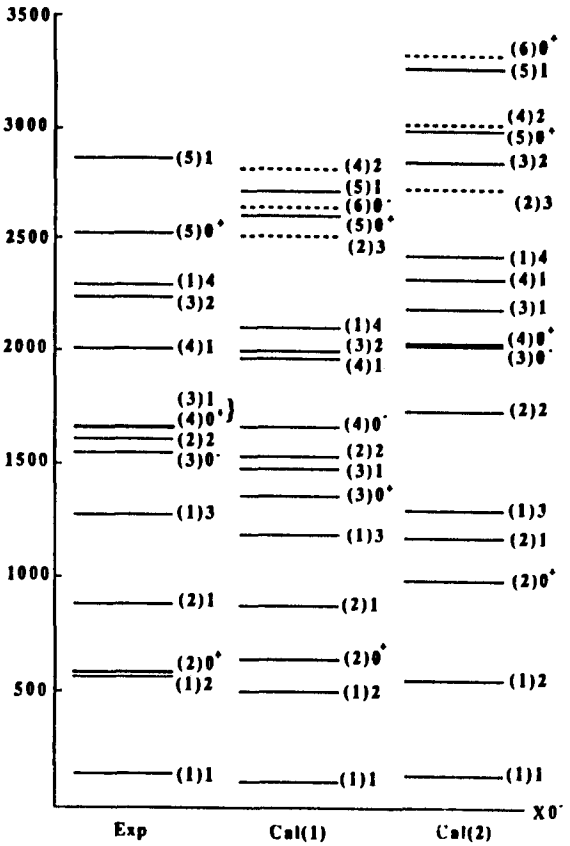

Fig. 40. Energy-level diagram for the electronic states of SmO. The experimental energies are compared with Cal (1) by Carette and Hocquet (1988) as well as Cal (2) by Dulick et al. (1986). Both calculations are ligand-field calculations. Reproduced from Bujin and Linton (1991).

Dolg et al. (1990a, b) have studied the $^8\Sigma^-$ ground state and the first excited $^8\Sigma^-$ state of EuO using *ab initio* SCF and SDCI methods in conjunction with non-relativistic and quasi-relativistic effective core potentials. They obtained the spectroscopic constants of these two states and their potential energy curves. They employed the Wood–Boring (WB) quasi-relativistic ECPs as well as ECPs derived from non-relativistic Hartree–Fock (HF) calculations. They used an energy optimized GTO basis sets of (7s6p5d2f)/[5s4p3d2f] and (12s11p9df)/[9s8p6d5f] types for Eu. For the oxygen atom, (9s5p)/(4s2p) basis set of Dunning was used together with one set of d-functions. They also include the effect of unlinked quadruple clusters using the Davidson method. The spin–orbit effects were estimated using ECPs which included spin–orbit operators. The spin–orbit effects were obtained using the double group CI method of Pitzer and Winter (1988).

Table 60 shows the spectroscopic constants of two electronic states of EuO ($X\ ^8\Sigma^-$ and $A\ ^8\Sigma^-$). The theoretical constants were obtained by Dolg et al. (1990a, b) using CISD, CISD + Q levels of theories. The experimental values are from Dulick et al. (1986), McDonald (1985) and Gabelnick et al. (1984). As seen from table 60, experi-

TABLE 60
Spectroscopic constants of two electronic states of EuO. CISD and CISD + Q values from Dolg et al. (1990a, b). We show only the quasi-relativistic values computed by Dolg et al. (1990a, b)

State	R_e (Å)			D_e/T_e (eV)			ω_e (cm^{-1})			μ_e (D)
	CISD	+ Q	Exp.	CISD	+ Q	Exp.	CISD	+ Q	Exp.	CISD
$X\,^8\Sigma^-$ [a]	1.912	1.919	~ 1.89	3.573	3.916	4.88	716	702	672	9.175
$X\,^8\Sigma^-$ [b]	1.940	1.953	–	3.56	4.13	–	699	676	–	9.67
$A\,^8\Sigma^-$ [a]	1.807	1.814	–	0.002	0.041	0.60	806	834	–	3.987

[a] 4f orbitals in the valence space.
[b] 4f orbitals in the core.

mental data on EuO are restricted to the X ground state which arises from the $4f^7$ superconfiguration. The $A\,^8\Sigma^-$ state arises from the $4f^6\sigma^1$ superconfigurations and it appears that no experimental spectroscopic data exist on this state with the exception of an estimate of T_e. Evidently, this estimate differs significantly from the CISD + Q value of only 0.04 eV and hence further studies are warranted on the $A\,^8\Sigma^-$ state.

The spin–orbit contribution estimated from quasi-relativistic CI is – 0.77 eV for the ground state of EuO. Dolg et al. found that the $A\,^8\Sigma^-$ excited state of EuO, which is split into $\Omega = 0.5$, 1.5, 2.5 and 3.5 states, is significantly contaminated by the $^8\Pi$ state. All Ω components of the $^8\Sigma^-$ state were found to be within 1400 cm^{-1}.

The Mulliken-population analysis of the SCI wavefunction yields that Eu has a positive charge of 1.04 with a population of $4f^{7.04}\,5d^{0.84}\,6s^{0.04}\,6p^{0.04}$ while the oxygen atom has a $O\,2s^{1.9}\,2p^{5.14}$ population. Dolg et al. rationalize that the $X\,^8\Sigma^-$ ground state arises from a $4f^7$ supermultiplet while the $A\,^8\Sigma^-$ state arises from the $4f^6\,\sigma$ supermultiplet. Dolg et al. found that 99.3% of the unpaired electronic population is in the 4f orbital in the $X\,^8\Sigma^-$ ground state. The doubly occupied σ orbital of EuO is composed of 21% Eu and 79% O orbitals. However, in the $A\,^8\Sigma^-$ state 99.7% of the six unpaired electrons are on Eu 4f orbitals while the seventh unpaired electron is 98% on Eu (6s 80.6%, 6p 16.6%, 5d 3.0%).

6.6. *GdO*

Carette et al. (1987) have studied the spectra of GdO. From their spectra, energy separations of six electronic states of GdO could be derived. These authors have also used the ligand-field model to derive the energy levels of eight electronic states of GdO. Dolg et al. (1990a, b) have studied the $^9\Sigma^-$ and $^7\Sigma^-$ states of GdO using *ab initio* SCF/CISD methods in conjuction with quasi-relativistic ECPs. More recently, Kotzian et al. (1991a, b) have used the INDO/S-CI method to compute the energy separations of 45 Ω electronic states of GdO. We use the Kotzian et al. (1991a, b) and the Dolg et al. (1990a, b) works as the basis for discussion on the electronic states of GdO.

Table 61 shows the Dolg et al. (1990a, b) CISD and CISD + Q results on GdO for two electronic states. As seen from table 61, the agreement between the computed SDCI, SDCI + Q properties with experiment is quite good with the exception of the D_e.

TABLE 61
Spectroscopic constants of two electronic states of GdO. Quasi-relativistic CISD, + Q results are by Dolg et al. (1990b).

State	R_e (Å)			D_e/T_e (eV)			ω_e (cm^{-1})			μ_e (D)
	CISD	+ Q	Exp.	CISD	+ Q	Exp.	CISD	+ Q	Exp.	CISD
$^9\Sigma^-$	1.814	1.822	1.812	863	845	824	6.07	6.37	7.39	4.585
$^7\Sigma^-$	1.812	1.820	–	866	849		0.23	0.23	0.22	4.364

It is, however, well-known that the dissociation energies cannot be computed very accurately using the SDCI + Q level of theory as this method ignores electron-correlation effects from other reference configurations. This method is also not a size-consistent method. Dolg et al. found that relativistic effects lead to a bond expansion of 0.016 Å and lowering of D_e by 0.44 eV. Relativistic effects also increase the dipole moment significantly as a consequence of bond expansion. The Mulliken-population analysis of the SCF orbitals by Dolg et al. revealed that seven of the eight unpaired electrons in GdO occupy the 4f orbitals of Gd (99%). Van Zee et al. (1981) have studied the ESR spectra of GdO which revealed that the singly occupied σ orbital is mainly the Gd 5d, in conflict with the ligand-field calculations of Carette et al. which revealed that the singly occupied σ orbital is 77% 6s, 21% 6p and only 2% 5d. Dolg et al. (1990a, b) from the Mulliken population analysis found that 81% of the singly occupied σ orbital is composed of Gd 6s. The charge distribution derived from Mulliken population generally supported the Gd^+O^- form rather than $Gd^{+2}O^{-2}$ used in the ligand-field model.

Table 62 shows the results of INDO/S-CI computation of Kotzian et al. (1991a, b) together with known experimental data from Carette et al. (1987). All INDO/S-CI energy separations were computed at single experimental bond length of 1.812 Å. Table 62 also shows the overall composition of the Ω states of GdO. As seen from table 62, the agreement of the energy levels predicted by the INDO/S-CI method with known experimental T_es for the first three excited electronic states is good and for the $B\,^9\Sigma^-$ and $B_1\,^7\Sigma^-$ states somewhat less accurate. The ligand-field model predicts reverse ordering for the $B\,^9\Sigma^-$ and $B_1\,^7\Sigma^-$ states compared to the INDO/S-CI model and experiment.

The composition of the Ω states of GdO in table 62 evidently suggests that for the excited states, especially low Ω states arising from $^9\Pi$, $^7\Pi$ and $^9\Sigma^-$, the spin–orbit contaminations are quite significant. For example, the excited $\Omega = 1$ state is 69% $^9\Pi$ and 26% $^7\Pi$. Likewise, the excited $\Omega = 3$ state is 45% $^9\Pi$ and 48% $^7\Pi$, suggesting that these two states undergo an avoided crossing due to spin–orbit coupling.

According to Kotzian et al. (1991a, b), the ground-state electronic configuration of GdO is $(1\sigma/O2s)^2\,(1\pi/O2p)^4\,(2\sigma/O2p)^2\,(1\phi/Gd4f)^2\,(1\delta/Gd4f)^2\,(2\pi/Gd4f)^2\,(3\sigma/Gd4f)^1\,(4\sigma/Gd6s)^1$. Hence, Kotzian et al.'s calculation also support that most of the singly occupied 4σ orbital is made of Gd 6s. The low-energy state of GdO arises from $4f^7\,4\sigma\,(1\,^9\Sigma^-, 1\,^7\Sigma^-)$, $4f^7\,2\delta\,(1\,^9\Delta, 1\,^7\Delta)$, $4f^7\,3\pi\,(1\,^9\Pi, 1\,^7\Pi)$ and $4f^7\,5\sigma\,(2\,^9\Sigma^-, 2\,^7\Sigma^-)$ configurations.

TABLE 62

INDO-SCI energy separation of Kotzian et al. (1991a) and experimental separations of Carette et al. (1987) for GdO. State energies T_e are given in cm^{-1}. The composition of states is given in reference to the non-relativistic states that most resemble the pure configurations. The ligand-field energies are multiplet-averaged values for Carette et al. (1987). This table is reproduced from Kotzian et al. (1991[a]).

INDO/S-CI			Experiment		LFT
Ω	T_e	Composition	State	T_e	T_e
	0	$1\,^9\Sigma^-$ 100%	$X\,^9\Sigma^-$	0	0
	1166	$1\,^7\Sigma^-$ 100%	$Y\,^7\Sigma^-$	1840	1999
2	8505	$1\,^9\Delta$ 100%			
1	8612	$1\,^9\Delta$ 99.7%			
0	8723	$1\,^9\Delta$ 99.5%			
1	8839	$1\,^9\Delta$ 99.3%			
2	8959	$1\,^9\Delta$ 99.2%			11 594
3	9084	$1\,^9\Delta$ 99.2%			
4	9216	$1\,^9\Delta$ 99.3%			
5	9355	$1\,^9\Delta$ 99.5%			
6	9503	$1\,^9\Delta$ 100%			
5	14 177	$1\,^7\Delta$ 99.4%			
4	14 317	$1\,^7\Delta$ 99.2%			
3	14 449	$1\,^7\Delta$ 99.1%			
2	14 575	$1\,^7\Delta$ 99.1%			18 188
1	14 695	$1\,^7\Delta$ 99.3%			
0	14 810	$1\,^7\Delta$ 99.5%			
1	14 922	$1\,^7\Delta$ 99.7%			
3	17 194	$1\,^9\Pi$ 96.1%			
2	17 283	$1\,^9\Pi$ 89.5% $1\,^7\Pi$ 6.1%			
1	17 372	$1\,^9\Pi$ 81.8% $1\,^7\Pi$ 12.8%			
0^-	17 430	$1\,^9\Pi$ 74.5% $1\,^7\Pi$ 18.8%			
0^+	17 562	$1\,^9\Pi$ 77.9% $1\,^7\Pi$ 18.9%			17 647
1	17 630	$1\,^9\Pi$ 69.4% $1\,^7\Pi$ 25.9%	$^9\Pi_1$	18 181	
2	17 750	$1\,^9\Pi$ 58.2% $1\,^7\Pi$ 35.8%			
3	17 892	$1\,^9\Pi$ 45.0% $1\,^7\Pi$ 47.9%			
4	18 060	$1\,^9\Pi$ 27.5% $1\,^7\Pi$ 64.2%	$A\,^9\Pi_4$	18 472	
5	19 846	$1\,^9\Pi$ 99.9%			
4	20 092	$1\,^7\Pi$ 27.1% $1\,^9\Pi$ 71.9%			
3	20 294	$1\,^7\Pi$ 44.5% $1\,^9\Pi$ 54.2%			
2	20 471	$1\,^7\Pi$ 57.7% $1\,^9\Pi$ 41.0%			
1	20 630	$1\,^7\Pi$ 68.5% $1\,^9\Pi$ 30.4%			19 956
0^-	20 767	$1\,^7\Pi$ 76.5% $1\,^9\Pi$ 22.3%			
0^+	20 784	$1\,^7\Pi$ 79.3% $1\,^9\Pi$ 20.3%			
1	20 910	$1\,^7\Pi$ 86.2% $1\,^9\Pi$ 13.3%			
2	21 035	$1\,^7\Pi$ 93.5% $1\,^9\Pi$ 6.3%			
0^-	23 507	$2\,^9\Sigma^-$ 92.1%			
1	23 510	$2\,^9\Sigma^-$ 92.0%			
2	23 510	$2\,^9\Sigma^-$ 91.8% $1\,^7\Pi$ 5.7%	$B\,^9\Sigma^-$	21 647	26 317
3	23 533	$2\,^9\Sigma^-$ 91.3% $1\,^7\Pi$ 6.9%			
4	23 554	$2\,^9\Sigma^-$ 90.8% $1\,^7\Pi$ 8.7%			
3	26 039	$2\,^7\Sigma^-$ 96.8%			
2	26 047	$2\,^7\Sigma^-$ 96.6%			
1	26 051	$2\,^7\Sigma^-$ 96.4%	$B_1\,^7\Sigma^-$	22 261	25 394
0^+	26 053	$2\,^7\Sigma^-$ 96.4%			

Kotzian et al. (1991a, b) found evidence from strong transitions with $\Delta\Omega = 0$ between the states of the same multiplicities of $1\Sigma^-$ and $2\Sigma^-$ symmetry since the computed oscillator strengths were about 0.35 (nonent) and 0.39 (septet). The strongest transitions ($\Delta\Omega = \pm 1$) were calculated between $1\,^9\Sigma^-$ and $1\,^{(9,7)}\Pi$ as well as $1\,^7\Sigma^- \rightarrow 1^{(9,7)}\Pi$. The band system between 16004 and 17669 cm^{-1} observed by Yadav et al. (1981) could not be assigned by Kotzian et al. (1991a, b), since at the present time there exists no experimental information on the electronic quantum numbers.

6.7. *DyO*

Linton et al. (1986) have studied DyO using the laser spectroscopic method. They used high-resolution wavelength selected excitation and resolved fluorescence spectroscopy to study the electronic, vibrational and rotational structures. These studies have provided information on five low-lying electronic states and three high-lying states of DyO. The Ω quantum numbers of these states were assigned. The ligand-field model was used to gain insight into the electronic structure of DyO which shows that the observed states can be described as arising from $Dy^{+2}O^{-2}$ in which Dy^{+2} has $4f^9(^6H)$ 6s electronic configuration. The ground state of DyO was found to be a $\Omega = 8$ electronic state arising from this configuration.

Table 63 shows the spectroscopic constants of states observed by Linton et al. (1986). Linton et al. (1986) have also compared their B_0 constants with those of Kaledin and Shenyavskaya (1981). Table 63 also includes ligand-field theoretical values (numbers under column theory). As evidenced from table 63, the ground state of DyO is a X8 Ω state. The A7 state is only 770 cm^{-1} above the X state. The B6, C7 and D6 states are also very close in energies. The ligand-field model seems to fit the observed spectra

TABLE 63
Energies and constants (cm^{-1}) of observed states of DyO. Some of the upper states without alphabet designates that these states were not observed by Linton et al. (1986). Reproduced from Linton et al. (1986).

	T_0		B_0		
State	Exp.	Theory	Note[a]	Note[b]	$\Delta G_{1/2}$
[19.0]9	18994			0.3570	
[18.5]9	18502			0.3562	
[18.3]8	18300				
[18.2]6	18203				
[18.0]9	18017			0.3505	780
[17.1]7	17070				
D6	2420	2382			
C7	1683	1428			
B6	1630	1641	0.35967		830
A7	770	845	0.35862		828.5
X8	0	0	0.35867	0.3588	842

[a] From Linton et al. (1986).
[b] Kaledin and Shenyavskaya (1981).

quite well (table 63). Figure 41 shows the energy-level diagram of DyO. The observed states are compared with the states predicted by the ligand-field model. As evidenced from fig. 41, the agreement is quite good. The Ω assignments in fig. 41 and table 63 were deduced by Linton et al. (1986) from the first lines in each branch and thus these authors consider this assignment reliable.

The assignment of the observed states is also consistent with the ligand-field model which predicts $\Omega = 8$ ground state and two $\Omega = 7$, $\Omega = 6$ states close to the ground state all arising from the $4f^9(^6H_{7/5})$ 6s configuration of Dy^{+2}. There are, of course, several other electronic states arising from the $4f^9$ 6s configuration which are yet to be observed. It appears that such experiments are in progress.

6.8. *HoO*

There are three experimental studies on HoO by Kaledin and Shenyavskaya (1981), Liu et al. (1984) and Linton and Liu (1988). The paper by Liu et al. (1984) provides a comprehensive table of known electronic states of HoO. The paper of Linton and Liu (1988) deals primarily with the rotational and hyperfine structure in holmium oxide. They have compared the observed and computed hyperfine constants of X_1 8.5, X_2 7.5 and W_2 6.5 Ω states of HoO.

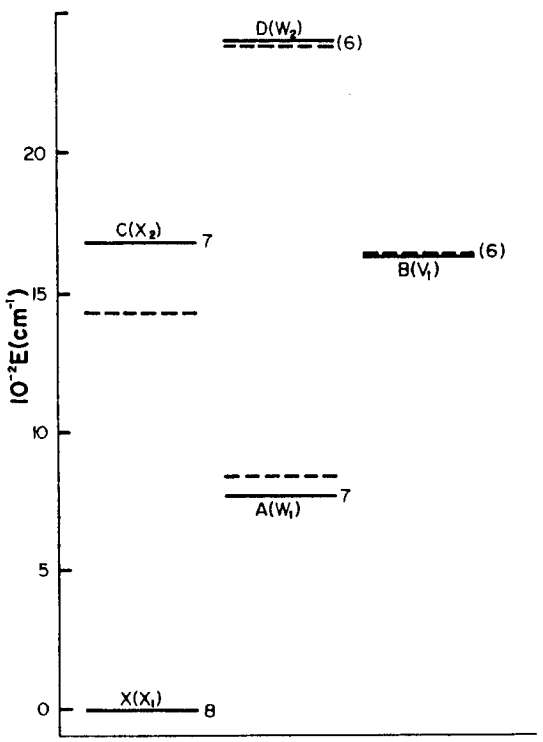

Fig. 41. Energy-level diagrams for DyO. The broken lines are the levels predicted by the ligand-field model while the full lines are the states observed by Linton et al. (1986). Reproduced from Linton et al. (1986).

Liu et al. (1984) employed laser spectroscopic techniques to study the electronic vibrational, rotational and hyperfine structure of HoO. The high-resolution excitation spectra of HoO were obtained which revealed the existence of four low-lying states and four higher electronic states of HoO. These authors have also assigned the Ω values of these electronic states. The ground state of HoO was found to be a X_1 8.5 state. The ligand-field model suggests an ionic $Ho^{+2}O^{-2}$ description of these states arising from Ho^{+2} configuration of $4f^{10}(^5I)6s$. The ligand-field model fits very well the observed spectra and the assignment of the observed electronic states. Liu et al. (1984) also estimated the relative contribution of the 4f and 6s electrons to the hyperfine structure.

Table 64 shows the spectroscopic constants of HoO deduced by Liu et al. (1984) together with the constants obtained by Kaledin and Shenyavskaya (1981). Figure 42 shows the energy-level diagram and the electronic transitions for HoO. As seen from table 64, the ground state of HoO is assigned to the X_1 8.5 state. The X_2 state is only 609 cm^{-1} above the ground state. The W_1 and W_2 states are relatively low lying while all other upper states have $T_0 > 17\,500\,cm^{-1}$. The observed electronic states fit an ionic $Ho^{+2}O^{-2}$ description of HoO wherein the Ho^{+2} ion arises from the $4f^{10}(^5I)6s$ electronic configuration. The ground-state configuration of HoO can therefore be best described as $4f^{10}\,\sigma$, where the σ orbital is composed of Ho 6s and O 2p orbitals. The

TABLE 64
Spectroscopic constants (cm^{-1}) for the observed states of HoO. Reproduced from Liu et al. (1984).

State	T_0	B_0 Note[a]	B_0 Note[b]	$\Delta G_{1/2}$	Hyperfine width (low J)	d[c]
[22.4] 8.5[d]	22 371.56		0.3448			
[20.2] 8.5[d]	20 168.63		0.3508			
[19.4] 9.5[d]	19 386.01		0.3565			
[19.0] 7.5	19 010				1.0	0.15
[18.4] 6.5	18 361.53	0.3485	0.3485		1.1	0.19
[18.3] 8.5	18 300					
[17.6] 7.5	17 552.72	0.3559		787	1.2	0.18
W_2 6.5	1 861.1	0.3502			0.8	0.14
W_1 7.5	1 130			841	2.0	0.28
X_2 7.5	608.78	0.3560	0.3561		1.4	0.19
X_1 8.5	0	0.3575	0.3573	841.4	2.4	0.35

Band origins: [17.6] 7.5–X_1 8.5 (0,0): 17 552.72
(0,1): 16 711.34
[17.6] 7.5–X_2 7.5 (0,0): 16 943.94
[18.4] 6.5–W_2 6.5 (0,0): 16 500.51

[a] Values of Liu et al. (1984).
[b] Values of Kaledin and Shenyavskaya (1981).
[c] For [17.6] 7.5 and X_1 8.5, d was calculated from combination differences. For all other states, d was estimated from hyperfine width. Both hyperfine width and d are very rough approximation.
[d] Not observed in the experiments of Liu et al. (1984).

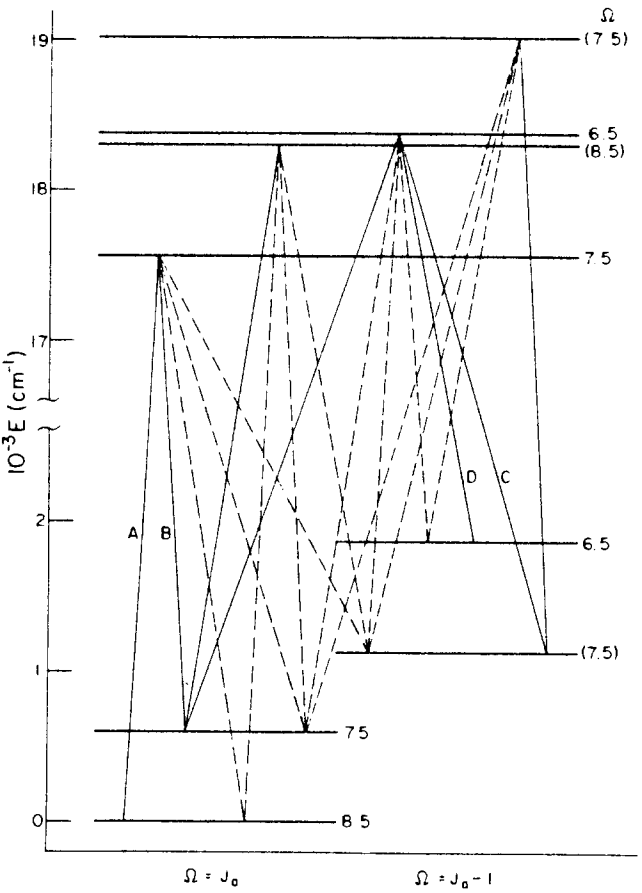

Fig. 42. Energy-level diagram and electronic transitions for HoO. The full lines represent transitions excited by the laser while the broken lines are transitions observed in the resolved fluorescence spectra by Liu et al. (1984). Reproduced from Liu et al. (1984).

analysis of the hyperfine pattern indicated that the 4f electrons contribute to a greater extent to the hyperfine pattern compared to the 6s by a factor of between two and four. This is in contrast with PrO for which the f and s contributions were found to be similar. Consequently, Liu et al. (1984) concluded that the 4f-electron contribution to hyperfine structure increases as the number of 4f electrons (or holes if 4f is less than half full) increases.

6.9. *TmO*

Kotzian and Rösch (1991a, b) have studied the low-lying electronic states of TmO with energy separations less than 13 528 cm^{-1} relative to the ground state. They have also compared the results of their INDO/S-CI technique with the ligand-field theoretical study of Dulick et al. (1986) as well as Carette and Hocquet (1988). Since the Kotzian and Rösch (1991a, b) work is the most recent on the topic, we use their table and figure as a basis for the discussion on the electronic states of TmO. At present, it appears that there exists no experimental data on TmO.

Table 65 shows the energies of the molecular states of TmO obtained by Kotzian and Rösch together with two ligand-field model energy separations. We note that the INDO/S-CI method yields a different ground state of $\Omega = 3.5$ while the LFT models predict a $\Omega = 0.5$ ground state. Kotzian and Rösch (1991a, b) argued that their INDO/S-CI treatment is consistent with the non-relativistic $^4\Delta$ ground state for TmO which would yield a Ω state of 3.5 when projected. Overall, as seen from table 65, the ligand-field and INDO/S-CI methods agree reasonably well, when one considers the fact that the $\Omega = 1.5$ state is only $\sim 100\,\text{cm}^{-1}$ above the 0.5 state in the LFT methods.

Figure 43 shows a diagramatic comparison of the energy levels obtained from the INDO/SCI method with the LFT methods. As seen from fig. 43, overall both the methods yield quantitatively similar ordering of states although there are quantitative differences. The state manifold arising from the low-lying multiplet components exhibits a montonic energy dependence in k ($k = \Omega - J_a$) as noted by Kotzian and Rösch (1991a, b).

Kotzian and Rösch (1991a, b) did other model calculations by changing the INDO bonding parameter β_f and elongating the bond distance. Both changes were found to yield a linear dependence of k of the corresponding energies. Kotzian and Rösch (1991a, b) concluded that the rather small discrepancy in energies and different ground states in the two methods should probably be due to the crude point-charge approximation used in the LFT model on the Tm 6s orbital. However, since at present there exists no experimental data on TmO it is hard to conclude which model predicts the correct ground state and energies for TmO. It would certainly be interesting to obtain the spectra of TmO.

6.10. *YbO*

McDonald et al. (1990) have recently studied YbO using a laser spectroscopic method. Linton et al. (1983a, b) have studied YbO before and analyzed the $O^+ - {}^1\Sigma^+$ transitions of YbO. The study of McDonald et al. (1990) seems to provide evidence of linkage of the $Yb^{+2}f^{13}$ s and f^{14} configurations. McDonald et al. (1990) find that the $X\,{}^1\Sigma^+$ ground state of YbO arises for the $Yb^{+2}\,4f^{14}$ configuration while five excited states with $\Omega = 0, 1, 2$; 1 and 3 arise from the $4f^{13}\,6s$ configuration of Yb^{+2}. This is not quite consistent with the ground-state calculations by Dolg et al. (1988) and Dolg and Stoll (1989).

Dolg et al. (1992) have recently studied YbO together with YbH and YbF using SCF, CASSCF, large-scale CPF, MRCI as well as CIPSI calculations employing quasi-relativistic effective core potentials (ECP). Dolg et al. (1991b) use both non-relativistic and quasi-relativistic energy-adjusted *ab initio* pseudo-potentials for Yb with extended Gaussian basis sets. They computed the spectroscopic constants of 13 low-lying electronic states of YbO. Spin–orbit effects were incorporated using energy-adjusted *ab initio* spin–orbit operators. They find 25 Ω states for YbO. In particular their computed spectroscopic constants ($R_e = 1.895$ Å, $D_0 = 2.47$ eV, $\omega_e = 653\,\text{cm}^{-1}$) are not in entire agreement with the constants deduced by McDonald et al. (1990) for the $4f^{14}\sigma^2\sigma^2\pi^4\ {}^1\Sigma^+(0^+)$ state ($R_e = 1.807$ Å, $D_0 = 4.29$ eV, $\omega_e = 499\,\text{cm}^{-1}$).

TABLE 65
Energies of molecular states of TmO (in cm^{-1}) arising mainly from the atomic states of H and F of Tm III.

	INDO/S-CI			LFT	LST
Ω	Energy[a]	Composition		Energy[b]	Energy[c]
3.5	0	|H 6 6.5⟩90%	|H 6 5.5⟩9%	905	731
2.5	24	|H 6 6.5⟩95%		413	323
1.5	187	|H 6 6.5⟩73%	|H 6 5.5⟩25%	128	97
2.5	320	|H 6 5.5⟩95%		1375	951
4.5	416	|H 6 5.5⟩87%	|H 6 6.5⟩11%	1649	1381
0.5	512	|H 6 6.5⟩85%	|H 6 6.5⟩11%	0	0
1.5	629	|H 6 5.5⟩72%	|H 6 6.5⟩24%	881	536
3.5	668	|H 6 5.5⟩89%	|H 6 6.5⟩9%	2150	1625
0.5	859	|H 6 5.5⟩85%	|H 6 6.5⟩10%	643	336
5.5	1671	|H 6 6.5⟩95%		2653	2331
4.5	1914	|H 6 5.5⟩88%	|H 6 6.5⟩11%	3194	2602
6.5	2461	|H 6 6.5⟩100%		3899	3583
5.5	2655	|H 6 5.5⟩95%		4485	3881
3.5	5201	|F 4 4.5⟩83%		6982	
2.5	5261	|F 4 3.5⟩68%	|F 4 4.5⟩23%	7115	
2.5	6289	|F 4 4.5⟩68%	|F 4 3.5⟩22%	7396	
1.5	6355	|F 4 3.5⟩47%	|F 4 4.5⟩45%	7246	
0.5	6387	|F 4 4.5⟩44%	|F 4 3.5⟩12%	7313	
			|P 2 2.5⟩9%		
4.5	6457	|F 4 4.5⟩97%		6870	
3.5	6630	|F 4 3.5⟩89%		7325	
0.5	6637	|F 4 3.5⟩54%	|F 4 4.5⟩19%	7588	
1.5	6644	|F 4 3.5⟩38%	|F4 4.5⟩36%	7514	
1.5	7911	|H 5 4.5⟩46%	|F 5 5.5⟩44%	8682	7771
2.5	7928	|H 5 5.5⟩74%	|H 5 4.5⟩16%	9147	8093
1.5	8039	|H 5 5.5⟩49%	|H 5 4.5⟩46%	9161	8119
0.5	8040	|H 5 5.5⟩90%		8502	7669
0.5	8065	|H 5 4.5⟩90%		8682	7790
3.5	8318	|H 5 5.5⟩78%	|H 5 4.5⟩12%	9858	8691
2.5	8382	|H 5 4.5⟩74%	|H 5 5.5⟩16%	9894	8722
4.5	8892	|H 5 5.5⟩86%	|H 5 4.5⟩10%		9648
3.5	8930	|H 5 4.5⟩83%	|H 5 5.5⟩13%		9678
5.5	10038	|H 5 5.5⟩100%			11010
4.5	10070	|H 5 4.5⟩89%	|H 5 5.5⟩11%		11034
1.5	11636	|H 4 3.5⟩67%	|H 4 4.5⟩23%		14048
2.5	11728	|H 4 4.5⟩72%	|H 4 3.5⟩18%		14649
0.5	12076	|H 4 3.5⟩48%	|H 4 4.5⟩29%		13798
1.5	12100	|H 4 4.5⟩59%	|H 4 3.5⟩17%		14546
0.5	12688	|H 4 4.5⟩47%	|H 4 3.5⟩28%		14094
3.5	12849	|H 4 4.5⟩84%	|H 4 3.5⟩12%		15752
2.5	12859	|H 4 3.5⟩78%	|H 4 4.5⟩19%		15553
3.5	13469	|H 4 3.5⟩83%	|H 4 4.5⟩13%		17122
4.5	13528	|H 4 4.5⟩97%			17385

[a] From Kotzian and Rösch (1991a, b). The atomic states are labeled according to $|L_f J_f J_a\rangle$. Only states contributing more than 9% are listed.
[b] Dulick et al. (1988).
[c] Carette and Hocquet (1988).

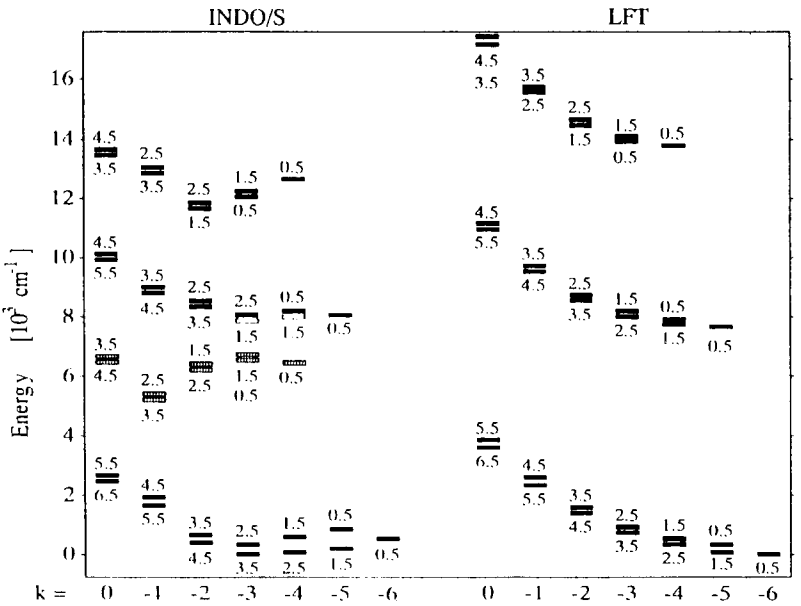

Fig. 43. Energy-level diagram for TmO as obtained from INDO/S-CI and LFT methods. All states are derived from the low-lying Tm^{+2} H and F atomic terms. Formally assigned states are indicated by empty boxes while the F derived states are indicated by hatched boxes. Reproduced from Kotzian and Rösch (1991a, b).

It should also be mentioned that at the best level of theory, Dolg et al. (1991b) obtain the $\Omega = 0^-$ state arising from the $4f^{13}\,\sigma^2\,\sigma^2\,\pi^4\,\sigma$ configuration 0.93 eV lower than the experimentally assigned $\Omega = 0^+$ ground state arising from the $4f^{14}\,\sigma^2\,\sigma^2\,\pi^4$ configuration. Dolg et al. (1991b) noted that differential correlation effects and relativistic effects are quite significant for YbO. When this chapter was being prepared, Dolg communicated to the author that work on YbO was still in progress.

Dolg et al. (1991b) note that their computed $R_e = 1.895$ Å for the $^1\Sigma^+$ is too long compared to a value of 1.807 Å derived by Linton et al. (1983a, b), while the computed R_e for the $^3\Sigma^+$ state (1.768 Å) is closer to the experimentally deduced value. The major disagreement between the work of Dolg et al. (1991b) and McDonald et al. (1990) is probably in the energy separation of $4f^{14}$ and $4f^{13}\,\sigma$ configurations. Whereas McDonald et al. (1990) deduce this energy separation as 910 cm^{-1} ($4f^{14}$ being lower), Dolg et al. (1991a, b, 1992) computed an energy separation of 6200 cm^{-1}, $4f^{13}\,\sigma$ being lower in the absence of spin–orbit coupling.

Dolg communicated to the author that the spin–orbit coupling between the 0^+ states causes further complication. When spin–orbit coupling is included, the ground state appears to change from $4f^{13}\,\sigma$ to $4f^{14}$ in the bonding region. This demonstrates strong coupling of the 0^+ states arising from these two electronic configurations. This could, in turn, lead to different spectroscopic constants in the presence of the spin–orbit operator. YbO is certainly thus an interesting candidate from the standpoint of

relativistic effects and electronic correlation effects. The reader is referred to the Dolg et al. (1991b) paper for further details.

Table 66 shows the spectroscopic constants of YbO as derived from experimental spectra as well as three ligand-field models. Figure 44 depicts the energy-level diagram for YbO showing all observed and computed states of YbO. The $X\,^1\Sigma^+$ state arising from Yb^{+2} ($4f^{14}$) is assigned as the ground state of YbO in table 66. The $4f^{13}6s$ configuration of Yb^{+2} yields several Ω states among which the $\Omega = 0^-$ and $\Omega = 1$ states are very close to each other. The $\Omega = 0^+$ state from the $4f^{13}6s$ configuration of Yb^{+2} has not yet been observed. The $\Omega = 2$, 1, and 3 states are higher than the $\Omega = 0^+$ state of YbO. The state at 4637 cm^{-1} is tentatively assigned to the $4f^{13}5d$ (0^+) state by McDonald et al. (1990).

The assignment of McDonald et al. (1990) of the observed states is based on the fact that the vibrational frequencies associated with states arising from $4f^{14}$ and $4f^{13}6s$ configurations are expected to be very different near the $Yb^{+2}O^{-2}$ atomic-ion-in-molecule limit. They argued that the $4f^{14}\,^1\Sigma^+$ will have a ω_e close to that of BaO whose ground state ω_e is 605.7 cm^{-1}. Since the ground state ω_e of YbO was deduced as 683 cm^{-1} by McDonald et al. (1991), they suggest the assignment of the ground state as

TABLE 66
Spectroscopic constants of the low-lying YbO states (in cm^{-1}).

State	Exp.[a]	LFT fit[b]	LFT calc.[c]	LFT calc.[d]
(J_a, Ω)				
$f^{14}(0, 0^+)$	0	−11	276	−11
$f^{13}s(4, 0^-)$	910	910[e]	910[e]	910[e]
$f^{13}s(4, 1)$	1015	1125	997	1013
$f^{13}s(3, 0^+)$	–	1628	1262	1289
$f^{13}s(4, 2)$	2408	2330	1697	1646
$f^{13}s(3, 1)$	2702	2688	1895	1807
$f^{13}s(4, 3)$	4287	4319	2950	2840
$f^{13}d?(?, 0^+)$	4637	–	–	–
$f^{13}s(3, 2)$	–	4818	3197	3021
$f^{13}s(4,4)$	–	6868	4597	4676
$f^{13}s(3, 3)$	–	7559	4894	4467
$f^{13}s(2, 0^-)$	–	11 341	–	11 208
$f^{13}s(3,1)$	–	11 675	–	11 415
$f^{13}s(3, 0^+)$	–	11 981	–	11 562
$f^{13}s(2, 1)$	–	13 807	–	12 559
$f^{13}s(3, 2)$	–	13 973	–	12 665
$f^{13}s(2, 2)$	–	16 882	–	14 508
$f^{13}s(3, 3)$	–	17 305	–	14 697

[a] McDonald et al. (1990).
[b] Fit of five experimental $f^{13}s$ energies, varying only G_3 and B_0^2 in the ligand-field effective Hamiltonian by McDonald et al. (1990).
[c] Ligand-field calculation with no adjustable parameters. Dulick et al. (1986).
[d] From Carette and Hocquet (1988).
[e] Calculated energies shifted to coincide with lowest energy observed $f^{13}s$ state by McDonald et al. (1990).

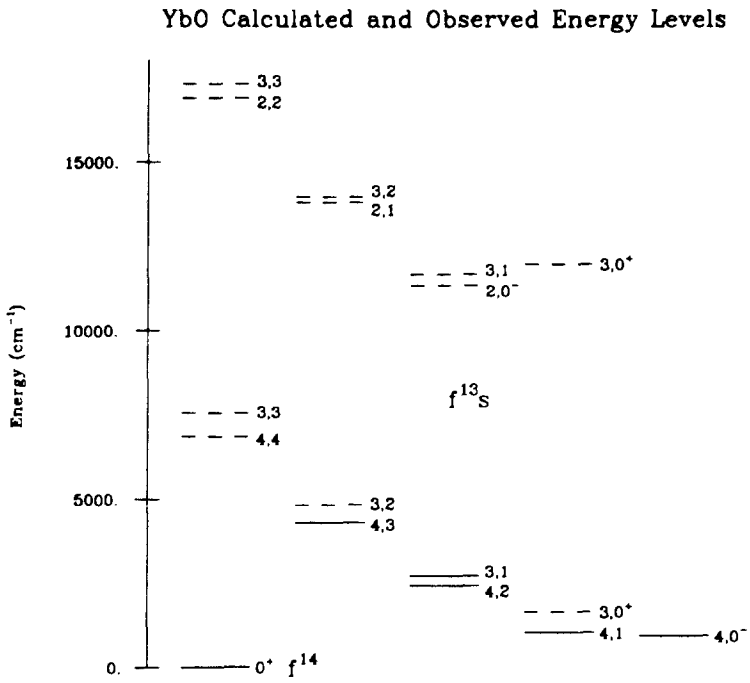

Fig. 44. Energy-level diagram for YbO showing all observed and calculated states arising from $4f^{14}$ and $4f^{13}6s$ configurations. Reproduced from McDonald et al. (1990).

$X\,^1\Sigma^+(4f^{14})$. The $4f^{13}\,6s$ states have larger ω_es. It should be noted [as done by McDonald et al. (1990)] that the vibrational frequencies were deduced by Yb isotope shift and thus may not be reliable for multiply perturbed upper states arising from Yb^+O^- states. McDonald et al. (1990) noted that the electronic states arising from $f^N s$ configurations of other species such as CeO, PrO, SnO, DyO, HoO have larger ω_es compared to f^{N+1} configuration. The LFT calculations also yield results in reasonable agreement with the experimentally deduced energies. The reader is referred to the paper by Dolg et al. (1992) for the most recent information concerning the ground state of YbO and the effect of spin–orbit coupling. The spin–orbit coupling of $4f^{14}$, $4f^{13}\,6s$ states can certainly lead to different spectroscopic constants in the bonding region.

7. Electronic structure of selected lanthanide and actinide polyatomics

There are numerous polyatomics containing lanthanides and actinides that have been studied in the literature. Comprehensive review of such species is evidently beyond the scope of this chapter. Nevertheless, a review of recent theoretical and related experimental studies on polyatomics containing lanthanides and actinides can shed significant light on the nature of chemical bonds in such systems. In this connection, we

point out two reviews on the topic which provide a comprehensive summary of the literature on the topic. A review by Pyykkö (1987) on developments in the theory of f-element molecules, especially polyatomics, should be consulted. This review of Pyykkö contains references and a table of relativistic calculations on molecules containing f elements. To summarize in addition to the molecules already reviewed, Pyykkö lists polyatomic hydrides such as CeH_4, ThH_4, UH_6, MH^+, MH_2 (M = Yb, No), UO_2^{+2}, AnX_n (An = U–Pu, X = F–I for several n), AnO_n^{-m} (for several n, m, An = actinide), An $(Cn)_n$ ($Cn = C_nH_n$), $An(BH_4)_4$ and other inorganic multicenter complexes. The level of theory included extended Hückel theory, Dirac–Slater discrete variational method, Dirac–Slater multiple-scattering method, quasi-relativistic multiple-scattering, pseudo-potential, perturbative Hartree–Fock method, relativistic extended Hückel theory, CNDO, INDO, etc. Hay et al. (1979) have studied UF_6 and UF_6^+ theoretically. The reader is referred to the literature cited by Pyykkö (1987) for the actual details on these computations. Pyykkö et al. (1989) have used the REX method [Pyykkö and Lohr (1981), Larsson and Pyykkö (1986)] to study ThO_2 and UO_2^{+2}.

The second review is due to Pepper and Bursten (1991). This review focussed on the electronic structure of actinide-containing molecules. Note that the present chapter complements this in that our chapter is mostly on lanthanide-containing species. Consequently, the reader is referred to the excellent review by Pepper and Bursten (1991) for a comprehensive summary of the electronic structure of actinide-containing species. The review by Pepper and Bursten (1991) contains the details of calculations on actinide hydrides, actinide halides, actinide oxides, cyclopentadienyl-actinide complexes, actinocenes, metal–metal bonding in actinide systems and miscellaneous other actinide systems. This review also consists of descriptions of theoretical techniques employed to study the actinide-containing molecules. The reader is directed to this review for further details on such calculations on actinide-containing molecules.

In the present section we identify a few lanthanide- and actinide-containing polyatomics, which provide a basis to gain insight into bonding in some of these systems. We select only those lanthanide- or actinide-containing polyatomics which are topical and interesting or which provide a basis to gain significant insight into the nature of bonding in such systems. Therefore, the choice of such molecules is certainly biased and by no means this choice is meant to constitute a comprehensive review on the recent developments in the electronic structure of polyatomics.

7.1. *Polyatomic oxides and complexes*

Pyykkö and Zhao (1991) have investigated the uranium-oxygen clusters such as UO_2^{m+}, UO_2^{-2}, UO_6^{-2}, UO_6^{-6} and $(UOU^+)_2$ using quasi-relativistic pseudo-potential studies at Hartree–Fock or MP2 level of theories. They found that the U–O distances for OUO^{+2}, UO_4^{-2} and cubic UO_6^{-6} are comparable to the crystal data. They found that the theoretical calculations of the large variation in $U–O_{ax}$ distance as a function of $U–O_{eq}$ distance for UO_6^{-6} (D_{4h}) followed the experimental curve. These variations were interpreted by Pyykkö and Zhao as a frozen soft e_g mode. Apparently, the large uranyl bond length is a classical problem as illustrated in the handbook of Dennig (1983).

TABLE 67
Calculated relativistic U–O bond lengths, R (in pm), and breathing frequencies $\nu_1(a_1)$ (in cm^{-1}). Reproduced from Pyykkö and Zhao (1991).

Species	Method	R	ν_1	Note
UO_2^{2+}	HF	162.5	1216	
	MP_2	173.2	922	
	HF	163		a
	HFS	170.0		b
	Exp.		ca.830	c
UO_2^{+}	HF	171.2	1031	
	MP2	177.0	1074	
	Exp.		808	d
UO_2	HF	181.8		d
	MP2	179.7		
	HFS	187.3		e
	HFS	183.4		f
	Exp.		765	g
UO_4^{2-}	HF	187.3	872	
	Exp.	199		h
UO_6^{6-}	HF	214.8	592	
	Exp.	208–209		
	Exp.		797	i
UN_2	HF	181.8	783	
	MP2	191.1	816	

[a] Wadt (1981).
[b] Van Wezenbeek et al. (1991).
[c] A typical value for U–O_{ax} around 170 pm (Glebov 1983).
[d] Green et al. (1976) (av.).
[e] Purposely omitted for this single-configuration open-shell $\phi^1\,\delta^1$ triplet state.
[f] Allen et al. (1988).
[g] Gabelnick et al. (1973).
[h] In Na_4UO_5 and Li_4UO_5, Hoekstra and Siegel (1964).
[i] Jorgensen and Reisfeld (1982).

Pyykkö and Zhao (1991) used the quasi-relativistic effective core potential of Hay and Wadt (1985a, b) and the Gaussian 90 codes to study these uranium-oxygen clusters. Table 67 shows the results of the Pyykkö–Zhao calculations for various UO_n^{m+} and UN_2 clusters. As seen from table 67, the agreement between the Pyykkö and Zhao calculation and the experiment is quite reasonable for the vibrational frequencies.

Coussan et al. (1984) found $(ONpO^+)_2$ to have the structure shown in fig. 45a. Pyykkö and Zhao (1991) also find a similar structure for $(OUO^+)_2$ dimer shown in fig. 45b, which is a stable geometry.

Pyykkö and Jové (1991) have made relativistic extended Hückel calculations to interpret ^{237}Np nuclear quadrupole coupling and isomer shifts in neptunyl compounds. They also reviewed actinide compounds containing multiple bonds. Pyykkö and Jové (1991) noted that the diffuse weakly bound 7s and 7p orbitals are relatively

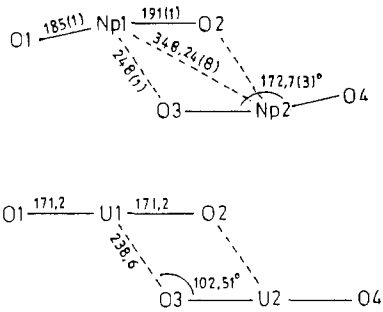

Fig. 45 (a) The structures of $(ONPO^+)_2$ from Cousson et al. (1984). (b) The structure of $(OUO^+)_2$ computed by Pyykkö and Zhao (1991).

unimportant in the actinide bonding. The 6d and 5f orbitals appear to be more important for the covalent bonding of the early actinides (Th–Am) and the 6p semi-core orbital. The possibility of the unusual O=An=O^{n+} and An = Pa–Am bonding over a large domain by varying the equilateral ligands was discussed by Pyykkö and Jové.

Multiple bonding in actinides is indeed quite interesting. Katz et al. (1986) as well as Gmelin (Handbook) (1983) list examples of such compounds. For example, the O=U=O^{+2} molecule with a U–O bond length of 1.50–2.08 Å is known. Likewise, Wadt (1981) has found O=Th=O multiple bonding in thorium dioxide, while Marian et al. (1988) and Heaven et al. (1985) have found multiple bonding in Th≡O and U≡O, respectively.

The other interesting species, although not polyatomic, is the uranium dimer, U_2, which exhibits interesting metal–metal bonding. Pepper and Bursten (1990) have studied the U_2 molecule. Although actinide–actinide bonding has been a topic of several synthetic and computational studies, as noted by Pepper and Bursten (1991) no discrete molecules containing a direct bond between two actinide atoms has been isolated, although U_2 appears to have been observed in the gas phase by Gingerich (1980). Pepper and Bursten (1990) in their most recent U_2 relativistic ECP-CASSCF computation have reviewed the previous literature. They have identified two distinct sets of states with potential energy minima. The first set of states (^1A_g) have approximately 3.0 Å R_es; these states essentially comprise atomic 5f and bonding 6d and 7s orbitals. The second set of states (^5A_g) has relatively shorter R_e (2.2 Å); the bonds in these states are composed of 5f, 6d and 7s orbitals of the two atoms. There are other studies on An–An bonding. Ortiz (1986) and Makhyon et al. (1987) have investigated Th(η^5-Cp)$_2$-(μ-PH_2)$_2$Ni(Co)$_2$ complex using EHT and QR-MS levels of theories, respectively. Ortiz (1986) reported the Th–Ni overlap populations as a function of bond distance. The overlaps were negative in all cases, however, the short bond distance structure exhibited the least negative overlap. Hay et al. (1986) have reported ECP calculations on similar heterobimetallic systems.

Hay (1991) has studied the high-coordinate metal complexes containing lanthanide (III) ions using molecular mechanics calculations. He has applied the molecular mechanics technique to 58 known structures of eight- to twelve-coordinate aqua- and nitratolanthanide (III) complexes. He has also presented various required parameters for the computation of these species. He has studied complexes such as $M(OH_2)_9X_3$,

$M(OH_2)_9$ $(BrO_3)_3$, etc. (where X = OTf, $EtSO_4^-$) for M = La, Nd, Gd, Ho, Lu in the former case and M = Pr, Nd, Sm and Yb in the latter case.

Meyer and Hoffmann (1991) have studied the layered halides Pr_2X_5 (X = Br, I). These authors achieved the unusual composition of M_2X_5 for lanthanide halides (M = La, Ce, Pr; X = Br, I). The Pr_2X_5 layered halide was found to be weakly semi-conducting (Pr_2Br_5: 3800 Ω cm; Pr_2I_5: 1600 Ω cm). Magnetic studies revealed transitions to antiferromagnetic ordering for the paramagnetic phases of Pr_2Br_5 and Pr_2I_5 below T_N (T_N = 50 and 37 K). Meyer and Hoffmann made extended Hückel calculations of the bond structure of these compounds which revealed two narrow low-lying half-occupied d bonds with two electrons per Pr_4X_{10} unit cell. Pr_2Br_5 crystallizes monoclinic forming a layered structure. The metal atoms form zig-zag layers derived from a hexagonal layer.

Kotzian et al. (1991b) have applied the INDO/S-CI method including spin–orbit coupling based on Rumer spin functions to the hydrated cerium ion. They have described an efficient technique to obtain excitation energies, transition moments and Mulliken populations based on the Rumer-adapted functions method. They have obtained the energies of the ground and excited states of $[Ce(CH_2O)_9]^{+3}$. The 4f → 5d transitions were found to be split by 10 000 cm^{-1} due to spin–orbit coupling and ligand-field interaction. Kotzian and Rösch are also considering application of this method to other lanthanide hydride ions $[Ln(H_2O)_n]^{3+}$ ($n = 8, 9$).

Kotzian et al. (1991b) have considered several structures of D_{3h}, D_3, C_{3h} and C_3 symmetries. They noted that the agreement with the experimental spectrum could be obtained for a geometry with low symmetry, (i.e., with the three-fold axis removed) although for simplicity, Kotzian et al. (1991a, b) considered $[Ce(H_2O)_9]^{+3}$ complex as if it had D_{3h} point-group symmetry. The INDO/S-CI method confirmed the previous Okada et al. (1984) assignment of the bands in the 37 000–51 000 cm^{-1} region to 4f → 5d transition. The spin–orbit splitting was computed as 2200 cm^{-1} for the 4f state. The Mulliken-population analysis revealed a 4f occupation of 1.01 electron. It was noted by Kotzian et al. (1991a, b) that due to the compactness of the 4f shell, the 4f valence electron of Ce^{+3} does not contribute to metal–ligand bonding. This is reminiscent of the $M^{+2}O^{-2}$ bonding discussed before for the diatomic lanthanide oxide. The bonding of $[Ce(H_2O)_9]^{+3}$ is facilitated by donation of lone-pair electrons from H_2O to Ce^{+3}. The σ-type loan pair has the largest overlap with Ce (6s, 6p and $5d_{z^2}$) and the π-type bonding is composed of H_2O $1b_2$ overlap with Ce($5d_{yz}$) orbital.

7.2. *Uranocene and actinocenes*

Streitwieser and Müller-Westerhoff (1968) prepared the uranocene, $U(C_8H_8)_2$, sandwich complex. They speculated that the U(5f) orbitals might play an important role in the metal–ligand bonds in uranocene. The reactivity properties of uranocene have been studied quite extensively by Streitwieser et al. (1973) and Streitwieser and Kinsley (1985). Other actinocenes and substituted uranocenes have been experimentally synthesized as well (Karraker et al. (1970), Karraker 1972).

Many actinocenes exhibit beautiful color with strong absorption in the visible region of the spectrum. Uranocene is green, $N_p(C_8H_8)_2$ is yellow to blood red depending on concentration, and $Pu(C_8H_8)_2$ is cherry red (Karraker et al. 1970).

Uranocene, like other actinocenes, is readily prepared by the following reactions:

$$2K + C_8H_8 \xrightarrow{THF} 2K^+ + C_8H_8^{-2},$$

$$M^{+6} + 2C_8H_8^{-2} \xrightarrow{THF} M(C_8H_8)_2,$$

where M is the actinide. For example, $Np(C_8H_8)_2$ is made by reacting $NpCl_4$ with $C_8H_8^{-2}$ generated by potassium in tetrahydro furan (THF) solution. The resulting sandwich complex is crystallized. Uranocene is green and sublimes at 180°C and is very stable in oxygen-free surroundings (Streitwieser and Müller-Westerhoff 1968). Several spectroscopic studies (Raman, ^{13}C NMR, H NMR, visible spectra, and photoelectron spectra) of these compounds have been made.

Chang and Pitzer (1989) have computed the electronic states of uranocene using *ab initio* relativistic effective core potential (RECP) including spin–orbit coupling. Chang and Pitzer employed Gaussian functions which resulted in a basis set of 208 generally contracted functions. Ninety-four valence electrons of uranocene were explicitly treated. The molecular orbitals were obtained using the SCF method while virtual orbitals were improved by the improved virtual orbital computation for a better description of excited electronic states. The spin–orbit coupling was included using the double-group CI method.

The overall ground state of uranocene is a E_{3g} state in the D_{8h}^2 double group arising from the $5f^2$ electronic configuration of U. For example, the $f^2\ ^3H_4$ states in the D_{8h}^2 double group correlate into A_{1g}, E_{1g}, E_{2g}, E_{3g}, B_{1g} and B_{2g} ($|M_g| = 4$) representations. Overall, the 6d orbitals play an important role in bonding in $U(C_8H_8)_2$ but the open-shell $5f^2$ configuration determines the possible electronic states as concluded by Chang and Pitzer (1989).

The Mulliken-population analysis of the SCF orbitals obtained by Chang and Pitzer (1989) reveals that the charge on U is + 0.98 (rather than the formal + 4 charge). This means U has donated a significant portion of its positive charge to the ligands. The U population in the ground state is $U(7s^{0.43}\ 7p^{0.11}\ 6d^{1.98}\ 5f^{2.5})$. This is consistent with the primary role of the 6d orbitals in the bonding of $U(C_8H_8)_2$.

Figure 46 shows the energy level diagrams for the experimental and the theoretically computed states by Chang and Pitzer of $U(C_8H_8)_2$. As seen from fig. 46, the Chang–Pitzer calculation predicts the E_{3g} state as the ground state with a low-lying E_{2g} state only ~ 0.1 eV above the E_{3g} state. The B_{1g} and B_{2g} states corresponding to $|M_J| = 4$ are virtually degenerate. Next, there exists an E_{1g} state and degenerate E_{3g} and A_{1g} states. Figure 47 shows the lowest possible electronic states arising from exciting a 5f electron into 6d.

Table 68 shows the computed energy separations of the first 38 electronic states of uranocene obtained by Chang and Pitzer (1989). Table 69 shows the excitation energies for the electronic states arising from the promotion of a 5f electron into 6d, together with whether an electronic transition into that state is dipole allowed or not.

Figure 48 shows three possible electronic transitions that correspond to the visible spectrum as proposed by Chang and Pitzer (1989). As evidenced from fig. 48, the

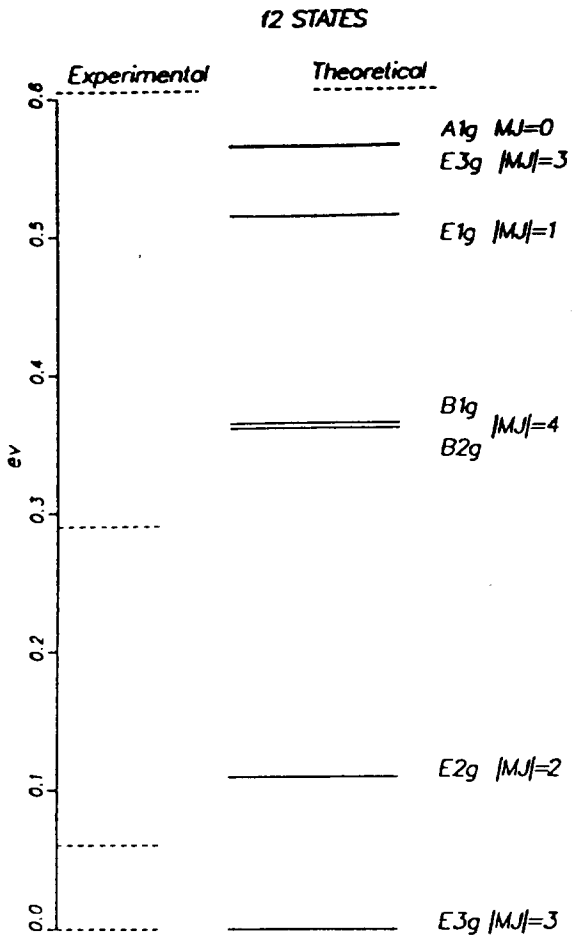

Fig. 46. The lowest $5f^2$ electronic states of uranocene. Reproduced from Chang and Pitzer (1989).

first-allowed transition from the ground state is an f→d ($E_{3g} \rightarrow E_{2u}$) transition at 2.84 eV while the second-allowed transition is an f→d E_{3u} transition at 2.905 eV (z-polarized). This corresponds to band I (fig. 48) whose experimental transition energy is 2.017 eV and is z-polarized. Band II ($E_{3g} \rightarrow E_{2u}$) has an experimental transition energy of 1.939 eV compared to the calculated value of 2.837 eV and is (x, y)-polarized. Chang and Pitzer suggest that the (x, y) polarized $E_{2g} \rightarrow E_{3u}$ transition (theory 2.796 eV) with an expected experimental energy of 1.959 eV may be buried under band II. Overall, theoretically computed energies of Chang and Pitzer (1989) are 0.9 eV too high compared to experimental values. Nevertheless, they reproduced the relative trend of experimental energies. Consequently, Chang and Pitzer (1989) reassigned the observed bands as follows.

The visible bands previously assigned to the ligand to metal π→f charge-transfer transitions were reassigned to the 5f→6d transition. Table 70 gives a summary of a few dipole-allowed electronic transitions of $U(C_8H_8)_2$. The characteristic green color of

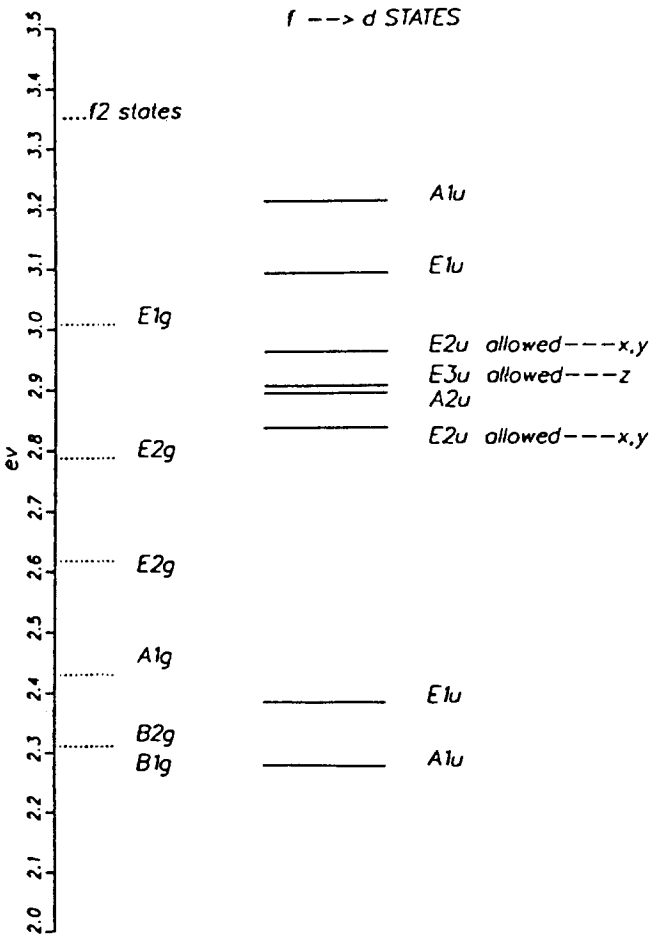

Fig. 47. The lowest 5f → 6d states of uranocene. Reproduced from Chang and Pitzer (1989).

uranocene was thus attributed by Chang and Pitzer (1989) to the 5f → 6d transition ($E_{3g} \rightarrow E_{2u}$, E_{3u}), but this transition also has some admixture of $\pi \rightarrow 6d$ charge-transfer character as inferred from the CI coefficients.

Chang and Pitzer (1991) have more recently investigated $Np(C_8H_8)_2$ as well as $Pu(C_8H_8)_2$. There are other crystal-field and ligand-field calculations as well on these species. The paper of Chang and Pitzer (1989) contains a comprehensive review of the literature. Neptunocene can be best described analogous to uranocene as arising from the $(^4I_{9/2}, 5f^3)$ configuration. The $(^4I_{9/2}, 5f^3)$ yields $E_{7/2u}$ ($|M_J| = \frac{7}{2}, \frac{9}{2}$), $E_{5/2u}$ ($|M_J| = \frac{5}{2}, \frac{11}{2}$) $E_{3/2u}$ ($|M_J| = \frac{3}{2}$) and $E_{1/2u}$ ($|M_J| = \frac{1}{2}$) electronic states. Table 71 shows the first 11 electronic states of $Np(C_8H_8)_2$ arising from the $5f^3$ electronic configuration. The electronic states shown in table 71 were computed by Chang and Pitzer (1991) using the SCF/IVNO/double-group CI procedures analogous to the uranocene. As seen from table 71, the ground state of neptunocene is an $E_{5/2u}$ state, although the $E_{3/2u}$ and $E_{7/2u}$ states are only 0.138 and 0.181 eV, respectively, above the ground state. Hayes and

TABLE 68
First 38 f^2 electronic states of uranocene. Reproduced from Chang and Pitzer (1989).

	State	Energy, eV		State	Energy, eV
38	E_{1g}	2.189	19	E_{1g}	1.234
37	A_{1g}	2.187	18	A_{1g}	1.153
36	E_{3g}	2.122	17	B_{1g}	1.121
35	E_{2g}	1.999	16	B_{2g}	1.118
34	A_{1g}	1.873	15	E_{2g}	1.111
33	E_{2g}	1.869	14	A_{2g}	1.090
32	E_{2g}	1.856	13	E_{3g}	0.999
31	E_{1g}	1.811	12	E_{3g}	0.844
30	E_{3g}	1.741	11	B_{2g}	0.816
29	B_{2g}	1.688	10	B_{1g}	0.811
28	A_{2g}	1.680	9	E_{2g}	0.773
27	B_{1g}	1.679	8	E_{1g}	0.754
26	E_{2g}	1.538	7	A_{1g}	0.565
25	E_{3g}	1.533	6	E_{3g}	0.564
24	E_{1g}	1.504	5	E_{1g}	0.514
23	E_{1g}	1.474	4	B_{1g}	0.364
22	E_{3g}	1.425	3	B_{2g}	0.360
21	E_{2g}	1.388	2	E_{2g}	0.109
20	A_{1g}	1.351	1	E_{3g}	0.000

TABLE 69
The f→d excitation energies for the electronic states of uranocene. Reproduced from Chang and Pitzer (1989). Six f^2 states also exist in this energy range.

State	Excitation energy, eV	Electric dipole transition	State	Excitation energy, eV	Electric dipole transition
A_{1u}	3.211	forbidden	A_{2u}	2.893	forbidden
E_{1u}	3.091	forbidden	E_{2u}	2.837	allowed (x, y)
E_{2u}	2.961	allowed (x, y)	E_{1u}	2.385	forbidden
E_{3u}	2.905	allowed (z)	A_{1u}	2.280	forbidden

Edelstein (1972) have also computed the same ground state and first excited state but compare $|M_J| = \frac{9}{2}$ for the second excited state using ligand-field theory. There is a large energy gap between the fifth and sixth states (table 71) and thus Chang and Pitzer suggested that the first five states from $J = \frac{9}{2}$ complex while the next six states comprised the $J = \frac{11}{2}$ complex.

Table 72 shows the computed energies of 13 electronic states of $Pu(C_8H_8)_2$ arising from the $5f^{14}$ configuration. The ground state of $Pu(C_8H_8)_2$ is thus an A_{1g} ($M_J = 0$) state while $|M_J| = 1$ (E_{1g}), and $|M_J| = 4$ (B_{1g}, B_{2g}) are the first and second excited states of $Pu(C_8H_8)_2$. The A_{1g} ground state computed by Chang and Pitzer (1991) was fully consistent with the diamagnetic character of $Pu(C_8H_8)_2$ observed by Starks and

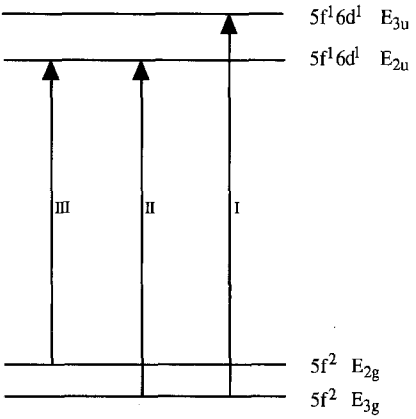

Fig. 48. Transitions of invisible spectrum of uranocene as assigned by Chang and Pitzer (1989).

TABLE 70
U $(C_8H_8)_2$ dipole-allowed states. Reproduced from Chang and Pitzer (1989).

State	ΔE, eV	Character	Polarization	State	ΔE, eV	Character	Polarization
B_{2u}	3.814	$\pi \rightarrow d$	x, y	E_{2u}	3.484	$\pi \rightarrow d$	x, y
B_{1u}	3.802	$\pi \rightarrow d$	x, y	E_{3u}	3.477	$f \rightarrow d$	z
E_{3u}	3.796	$\pi \rightarrow d$	z	E_{3u}	3.395	$\pi \rightarrow d$	z
E_{3u}	3.769	$\pi \rightarrow d$	z	B_{1u}	3.377	$f \rightarrow d$	x, y
B_{2u}	3.737	$\pi \rightarrow d$	x, y	B_{2u}	3.377	$f \rightarrow d$	x, y
B_{1u}	3.735	$\pi \rightarrow d$	x, y	E_{3u}	3.349	$\pi \rightarrow d$	z
E_{2u}	3.693	$\pi \rightarrow d$	x, y	B_{2u}	3.327	$\pi \rightarrow d$	x, y
E_{2u}	3.565	$\pi \rightarrow d$	z	B_{1u}	3.322	$\pi \rightarrow d$	x, y
E_{3u}	3.557	$\pi \rightarrow d$	z	E_{2u}	2.961	$f \rightarrow d$	x, y
E_{2u}	3.554	$\pi \rightarrow d$	x, y	E_{3u}	2.905	$f \rightarrow d$	z
E_{2u}	3.522	$\pi \rightarrow d$	x, y	E_{2u}	2.837	$f \rightarrow d$	x, y
B_{2u}	3.491	$\pi \rightarrow d$	x, y	E_{3g}	0.00	f^2	
B_{1u}	3.490	$\pi \rightarrow d$	x, y				

TABLE 71
The first 11 f^3 states of Np $(C_8H_8)_2$. Reproduced from Chang et al. (1991).

No.	State	Energy (eV)
11	$E_{5/2\,u}$	1.161
10	$E_{1/2\,u}$	1.002
9	$E_{3/2\,u}$	0.946
8	$E_{7/2\,u}$	0.943
7	$E_{7/2\,u}$	0.895
6	$E_{5/2\,u}$	0.848
5	$E_{7/2\,u}$	0.418
4	$E_{1/2\,u}$	0.351
3	$E_{7/2\,u}$	0.181
2	$E_{3/2\,u}$	0.138
1	$E_{5/2\,u}$	0.000

TABLE 72
The first 13 f^3 states of Pu $(C_8H_8)_2$. Reproduced from Chang et al. (1991).

No.	State	Energy (eV)
13	B_{2g}	1.122
12	B_{1g}	1.121
11	E_{3g}	1.050
10	E_{3g}	0.946
9	E_{2g}	0.898
8	A_{2g}	0.829
7	E_{1g}	0.766
6	E_{3g}	0.544
5	E_{2g}	0.445
4	B_{2g}	0.291
3	B_{1g}	0.291
2	E_{1g}	0.138
1	A_{1g}	0.000

Streitwieser (1973). The results of the Chang–Pitzer computation differed from the Hayes and Edelstein (1972) ligand-field computation only on the second excited state. Chang and Pitzer (1991) assigned the first six states to a $J = 4$ complex and the next seven states to a $J = 5$ complex.

Table 73 shows the possible excited u states of $Pu(C_8H_8)_2$ and their computed energy separations (Chang and Pitzer 1991). The first allowed $(x - y)$ polarized charge transfer

TABLE 73
The u symmetry excited states of Pu $(C_8H_8)_2$. Reproduced from Chang et al. (1991).

State	Excitation energy (eV)	Character	Electric dipole transition
E_{2u}	3.28	$\pi \rightarrow d$	forbidden
E_{3u}	3.21	$\pi \rightarrow d$	forbidden
A_{2u}	3.17	$\pi \rightarrow d$	allowed (z)
E_{3u}	3.16	$\pi \rightarrow d$	forbidden
A_{1u}	3.15	$\pi \rightarrow d$	forbidden
E_{2u}	3.14	$\pi \rightarrow d$	forbidden
E_{1u}	3.12	$\pi \rightarrow d$	allowed (x, y)
B_{1u}	3.11	$\pi \rightarrow d$	forbidden
B_{2u}	3.11	$\pi \rightarrow d$	forbidden
E_{1u}	3.09	$\pi \rightarrow d$	allowed (x, y)
A_{2u}	3.08	$\pi \rightarrow d$	allowed (z)
B_{2u}	2.99	$\pi \rightarrow d$	forbidden
E_{3u}	2.99	$\pi \rightarrow d$	forbidden
B_{1u}	2.98	$\pi \rightarrow d$	forbidden
E_{1u}	2.97	$f \rightarrow d$	allowed (x, y)
A_{1u}	2.93	$f \rightarrow d$	forbidden
E_{1u}	2.92	$\pi \rightarrow d$	allowed (x, y)
E_{2u}	2.91	$\pi \rightarrow d$	forbidden
E_{3u}	2.84	$f \rightarrow d$	forbidden
E_{2u}	2.77	$f \rightarrow d$	forbidden

π–d transition of $Pu(C_8H_8)_2$ from the A_{1g} ground state was computed by Chang and Pitzer to occur at 2.92 eV while the second transition ($f \rightarrow d$) is only 0.05 eV higher.

Bursten and Strittmatter (1991) have recently reviewed the cyclopentadienyl-acetinide complexes. They have presented the development of bonding models for CP-actinide complexes. They have considered the photoelectron spectra and bonding of several complexes such as $U(C_5H_5)_3Cl$, $An(C_5H_5)_4$, $U(C_5H_5)_2$, $An(C_5H_5)_3$, $An(C_5H_5)_3L$, $An(C_5H_5)_3X$, $An(C_5H_5)_2Cl_2$ and numerous other complexes of this kind. Since this is a recent review on the topic, we conclude this section by referring the reader to the excellent review by Bursten and Strittmatter on this topic for additional details. Bursten and Strittmatter (1987) have studied $(C_5H_5)_3$ UCO and related species.

Dolg et al. (1991a, b) have studied the ground states of di-π-cyclooctaheraene cerium (cerenocene). These calculations have revealed that the Ce ion is almost entirely in a $4f^1$ electronic configuration corresponding to $[Ce^{+3}(C_8H_8{}^{-1.5})_2]$. Dolg et al. also accounted for correlation energy using correlation-energy density functionals and by limited-coupled electron-pair approximations.

7.3. *Lanthanides and actinides inside carbon cages* ($M@C_n$, $M@C_n^+$)

Kroto et al. (1985) showed the existence of unusually stable C_{60} cluster obtained by the laser vaporization of graphite. The unusually stable C_{60} was called "buckminsterfullerene" or informally the buckyball. Since the appearance of the Kroto et al. (1985) paper, numerous theoretical and experimental studies have dealt with the buckyball and other carbon cages in the general class of compounds called the fullerene (see also Cox et al. (1988)). The biography of C_{60} has grown into such an astronomical size that one could write reviews on this topic itself. We refer the reader to contact Professor Rich Smalley at Rice University to receive up-to-date biography of never-ending buckyball literature.

Within a week after the discovery of C_{60}, Heath et al. (1985) and subsequently, Cox et al. (1986), Kaldor et al. (1986), Weiss et al. (1988) and O'Brien et al. (1986) have shown that metal complexes of the buckyball, especially the complex in which a lanthium atom at the center of the carbon cage ($La@C_{60}$), can be produced by laser vaporization of a graphite rod impregnated with $LaCl_3$ and subsequent irradiation with an ArF laser. Several metal complexes of the buckyball and other carbon cages such as $M@C_n$ (M = La, K, Cs, Ca, Ba and Sy) have been produced. Figure 49 shows the proposed structure of La^+ inside the C_{60} fullerene cage.

Chai et al. (1991) very recently (only a week before this chapter was prepared) have generated fullerenes with a single and a cluster of La atoms trapped inside of the carbon cages in macroscopic quantities. This was accomplished by Chai et al. (1991) by laser vaporization of a lanthanum oxide/graphite composite rod in a flow of Ar gas at 1200°C. Subsequently, when sublimed with C_{60} and C_{70}, they formed an air-stable film containing primarily LaC_{60}, LaC_{70}, LaC_{74} and LaC_{82}. A solution containing LaC_{82} was prepared by dissolving in toluene. The resulting solution was found to be uniquely stable. Chai et al. (1991) also obtained complexes containing up to three La atoms in large carbon cages such as La_3C_{88}. Chai et al. (1991) suggested the use of the @ symbol to represent an atom inside a cage which we follow in this section. For example, La inside C_{60} will be denoted by $La@C_{60}$.

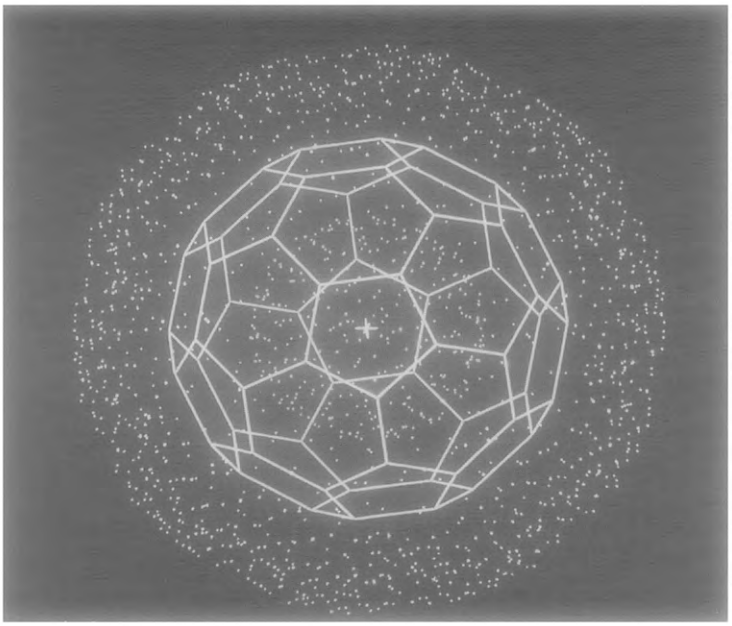

Fig. 49. The structure of La^+ inside C_{60}. Reproduced from Heath et al. (1985).

Chang et al. (1991) have studied the ground states of $M@C_{60}$ and $M^+@C_{60}$ for M = O, F, K, Ca, Mn, Cs, Ba, La, Eu and U. They employed relativistic ECPs for the metal atom and restricted Hartree–Fock (RHF) level of theory to study these complexes. There are other theoretical calculations based on the density functional method by Rosen and Wästberg (1988) as well as Ballster et al. (1990). The recent study of Chang et al. (1991) on $La@C_{60}$ showed that the lanthanum atom donates two electrons from the 6s orbital to the carbon cage. This, in fact, provided the basis to explain the unusual stability of $La@C_{82}$ observed by Chai et al. (1991). In this section we review recent theoretical and experimental developments so as to gain insight into these unusual carbon cages containing a lanthanide or actinide atom inside.

Chang et al. (1991) performed *ab initio* restricted Hartree–Fock (RHF) calculations on C_{60} cages with several metal atoms inside. They used a Gaussian basis set containing up to 556 basis functions and 257 valence electrons. All calculations of Chang et al. (1991) took full advantage of the icosahedral symmetry (I_h). In the I_h point group, the central atoms, s, p, d and f orbitals correlate into a_g, t_{1u}, h_g and $t_{2u} + g_u$ representations, respectively.

Table 74 shows the electronic states of $La@C_{60}$ and the energy separations computed by Chang et al. (1991). The ground state of $La@C_{60}$ is obtained by donating two 6s electrons to the t_{1u} orbital of the C_{60} cage. This results in a $t_{1u}^2 h_g^1$ configuration. Note that the single 5d electron of the La atom resides in a h_g orbital. The calculations by Chang et al. (1991) indicated a strong destabilizing interaction between the 6s orbital of La and the C orbitals. This results in a formal charge of +2 on La although the

TABLE 74
Electronic states of La@C_{60}. Reproduced from Chang et al. (1991).

Configurations		ΔE (eV)
$t_{1u}^2 h_g^1$	($S = 1.5$)	0.0000
$t_{1u}^1 h_g^2$	($S = 1.5$)	0.0018
h_g^3	($S = 1.5$)	0.28
$t_{1g}^1 h_g^1 t_{1u}^1$	($S = 1.5$)	1.39
$t_{1g}^1 h_g^2$	($S = 1.5$)	1.71
t_{1u}^3	^4A_u	2.22
	^2H_u	2.56
	(av. of config.)	2.56
$a_g^1 h_g^1 t_{1u}^1$	($S = 1.5$)	2.67
t_{1u}^3	$^2T_{1u}$	2.79
$a_g^1 h_g^2$	($S = 1.5$)	3.09
$h_g^2 t_{2u}^1$	($S = 1.5$)	3.30
$h_g^2 g_u^1$	($S = 1.5$)	4.95

Mulliken-population analysis of the RHF orbitals obtained by Chang et al. (1991) indicated a 0.8 charge as a result of mixing of cage orbitals. The energies computed in table 74 are for the average of $^4T_{1g}$, $^4T_{2g}$, ^4G_g and ^4H_g states. There is a nearly degenerate electronic state obtained from moving a 6s electron to t_{1u} and one to 5d ($t_{1u} h_g^2$). This corresponds to an average of ^4A_u, $^4T_{1u}$, $^4T_{2u}$, 2^4G_u and 3^4H_u states.

The ground state of $La^+@C_{60}$ was found to be h_g^2 yielding an IP of 4.4 eV compared to an upper limit of 6.42 eV obtained by Heath et al. (1985) and Cox et al. (1986). Other electronic states arising from $t_{1u} h_g$ and t_{1u}^2 configurations are 0.3 and 3 eV, respectively, higher in energy.

The density functional theory predicts different ground states for La@C_{60} and $La^+@C_{60}$. The calculations by Rosen and Wästberg (1988, 1989) yielded t_{1u}^3 and t_{1u}^2 as the ground states of La@C_{60} and $La^+@C_{60}$, respectively. The LDF method gave an IP of 6.9 eV. However, this is contrasted by Chang et al.'s calculations which place these states at 2.56 and 2.88 eV, respectively, above the ground state. Chang et al. (1991) attributed this to the difficulty in the LDF method of distinguishing the total energies of states for which closely spaced orbitals have different occupations.

Table 75 shows the electronic configurations, electronic states and energy separations for Eu@C_{60} computed by Chang et al. (1991). Again, the ground state of Eu@C_{60} is obtained by moving two 6s electrons from Eu to the C_{60} cage, leaving the $4f^7$ shell essentially an intact non-bonding shell. Since the 4f orbital correlates into $t_{2u} + g_u$, this leads to a $t_{1u}^2 t_{2u}^3 g_u^4$ configuration yielding a $^{10}T_{1u}$ ground state for Eu@C_{60}. Like La@C_{60}, although the formal charge on Eu is + 2, the Mulliken-population analysis yields a charge of + 0.5 on Eu.

Table 76 shows the electronic states of U@C_{60} obtained by Chang et al. (1991). In this case, the ground state is obtained by donating a 7s electron to the t_{1u} orbital of C_{60}

TABLE 75
Electronic states of Eu@ C_{60}. Reproduced from Chang et al. (1991).

Configurations		ΔE (eV)
$t_{1u}^2(t_{2u}^3 g_u^4)$	$^{10}T_{1u}$	0.00
$a_g^1 t_{1u}^1(t_{2u}^3 g_u^4)$	$^{10}T_{1g}$	0.62
$t_{1g}^1 t_{1u}^1(t_{2u}^3 g_u^4)$	($S = 4.5$)	1.39
$h_g^1 t_{1u}^2(t_{2u}^3 g_u^3)$	($S = 4.5$)	1.76
$a_g^1 h_g^1(t_{2u}^3 g_u^4)$	$^{10}H_u$	2.47
$a_g^2(t_{2u}^3 g_u^4)$	$^{8}A_u$	2.93
$h_g^1 t_{1u}^1(t_{2u}^3 g_u^4)$	($S = 4.5$)	3.28
$t_{1u}^3(t_{2u}^3 g_u^3)$	($S = 4.5$)	5.91
$t_{1u}^2(t_{2u}^4 g_u^4)$	($S = 3.5$)	14.42

TABLE 76
Electronic states of U@C_{60}. Reproduced from Chang et al. (1991).

Configurations		ΔE (eV)
$h_g^2 t_{1u}^1 t_{2u}^3$	($S = 3$)	0.00
$a_g^1 h_g^1 t_{1u}^1 t_{2u}^3$	($S = 3$)	0.07
$h_g^1 t_{1u}^2 t_{2u}^3$	($S = 3$)	0.19
$a_g^1 h_g^2 t_{2u}^3$	($S = 3$)	1.00
$a_g^1 h_g^1 t_{1u}^1 t_{2u}^2 g_u^1$	($S = 3$)	1.14
$a_g^1 h_g^2 t_{1u}^1 t_{2u}^2$	($S = 3$)	1.95
$a_g^2 h_g^1 t_{2u}^3$	$^{5}H_u$	2.06
$t_{1u}^3 t_{2u}^3$	$^{7}A_g$	2.40
$a_g^2 h_g^1 g_u^3$	($S = 2$)	2.60
$a_g^2 h_g^1 t_{2u}^2 g_u^1$	($S = 2$)	3.13
$t_{1u}^2 t_{2u}^4$	($S = 2$)	3.30
$a_g^2 h_g^1 t_{2u}^1 g_u^2$	($S = 2$)	3.31
$a_g^1 h_g^1 t_{1u}^2 t_{2u}^2$	($S = 3$)	3.88
$a_g^1 t_{1u}^1 t_{2u}^4$	($S = 2$)	4.12
$h_g^1 t_{1u}^1 t_{2u}^4$	($S = 2$)	4.36
$a_g^1 h_g^1 t_{2u}^4$	($S = 2$)	6.24
$a_g^2 t_{2u}^4$	$^{3}T_{2g}$	6.38
$h_g^1 t_{2u}^5$	($S = 1$)	12.57

and one to the 6d shell yielding a $t_{1u}^1 h_g^3 t_{2u}^3$ configuration with ^7A_g, $^7T_{1g}$, $^7T_{2g}$, $2\,^7G_g$ and $3\,^7H_g$ states. As seen from table 76, the $h_1^2 t_{1u}^1 t_{2u}^3$, $a_g^1 h_g t_{1u} t_{2u}^3$ and $h_g t_{1u}^2 t_{2u}^3$ configurations are very close to each other. Chang et al. (1991) predicted that the spin–orbit effects are likely to be larger for U@C_{60} especially in states which have increased 6d occupancy.

Table 77 shows the electronic states of $La^+@C_{60}$. The ground state of $La^+@C_{60}$ arises from a h_g^2 configuration which suggests that the ionization from the t_{1u} orbital of $t_{1u}h_g^2$ is more favorable leading to a h_g^2 configuration. The $t_{1u}h_g$ (triplet) state of $La^+@C_{60}$ is only 0.29 eV higher in energy. However, the $^3T_{1g}$ state arising from t_{1u}^2 is significantly higher.

Tables 78 and 79 show the electronic states of $Eu^+@C_{60}$ and $U^+@C_{60}$, respectively. Compared to the $t_{1u}^2(t_{2u}^2 g_u^4)$ ground state of $Eu@C_{60}$, $Eu^+@C_{60}$ has a $t_{1u}(t_{2u}^2 g_u^4)$

TABLE 77
Electronic states of $La^+@C_{60}$. Reproduced from Chang et al. (1991).

Configurations		IP (eV)*
h_g^2	($S = 1$)	4.43
$t_{1u}^1 h_g^1$	($S = 1$)	4.72
t_{1u}^2	$^3T_{1g}$	7.20
	(av. of config.)	7.31
	^1H_g	7.43
	^1A_g	7.77

* Relative to $La@C_{60}$ ground state.

TABLE 78
Electronic states of $Eu^+@C_{60}$. Reproduced from Chang et al. (1991).

Configurations		IP (eV)*
$t_{1u}^1(t_{2u}^3 g_u^4)$	$^9T_{1g}$	4.74
$h_{1g}^1(t_{2u}^3 g_u^4)$	^9H_u	4.90
$a_g^1(t_{2u}^3 g_u^4)$	^9A_u	5.06
$t_{1g}^1(t_{2u}^3 g_u^4)$	$^9T_{1u}$	6.46
$(t_{2u}^4 g_u^4)$	$^7T_{2g}$	18.86

*Relative to $Eu@C_{60}$ ground state.

TABLE 79
Electronic states of $U^+@C_{60}$. Reproduced from Chang et al. (1991).

Configurations		IP (eV)*
$h_g^2 t_{2u}^3$	($S = 2.5$)	4.42
$a_g^1 h_g^1 t_{2u}^3$	^6H_u	4.44
$h_g^1 t_{1u}^1 t_{2u}^3$	($S = 2.5$)	4.94
$a_g^1 t_{1u}^1 t_{2u}^3$	$^6T_{1g}$	5.75
$t_{1u}^2 t_{2u}^3$	$^6T_{1u}$	7.37

* Relative to $U@C_{60}$ ground state.

electronic configuration. The ionization thus takes place on a t_{1u} cage shell for Eu@C_{60} similar to La@C_{60}. The ground state of U^+@C_{60} arises for the $h_g^2 t_{2u}^3$ configuration compared to the $h_g^2 t_{1u} t_{2u}^3$ configuration of U@C_{60}. Hence, all lanthanide and actinide containing C_{60} cages lose an electron from the t_{1u} cage orbital upon ionization.

In the most recent experimental work, Chai et al. (1991) have extracted in solution the La@C_{82} complex. Figure 50 shows the FT-ICR mass spectrum of hot-toluene extract of fullerene material produced by laser evaporization of La_2O_3/graphite composite rod. As seen from fig. 50, the only La-containing fullerene which survived the exposure to moisture and air is the La@C_{82} cluster. This unusual stability of La@C_{82} and its extractability in toluene solution are rather intriguing. However, the calculation of Chang et al. (1991) on La@C_{60} sheds some light on the unusual stability of La@C_{82}. As noted before, the ground state of La@C_{60} is formed by promotion of two 6s electrons from La to the carbon cage. The magic numbers for large carbon cages are 60, 70, 84 and to some extent 76, in decreasing order of stability (Diederich et al. 1991). The closest magic number to 82, is 84 for C_n. Since La donates two 6s electrons, the carbon cage accepting this must have two electrons less for the unusual stability. This means C_{82} can accept two electrons from La leading to a closed-shell ground state with an unusual stability. This explains why La@C_{82} is unusually stable and is inert to air and moisture and can be extracted in toluene. It is also predicted that the La@C_{82} cluster would have a substantial HOMO–LUMO gap. This also explains La@C_{74} as being the next most stable fullerene containing La.

Coalescence of two carbon cages produces small clusters of up to three atoms present in larger carbon clusters. Strong signals for clusters of composition La_2C_n and even La_3C_n were found by Chai et al. (1991). Figure 51 shows a portion of FT-ICR spectrum obtained after laser-aging of the composite target disc. As seen from fig. 51, signals corresponding to La_3@C_{88}, La_3@C_{94}, La_2@C_{106}, La @C_{118} are quite prominent. The exact mechanism of the formation of these species is although not clearly established at present, Chai et al. (1991) speculated that they are generated by (La@C_n)–(La@C_n) coalescence reactions. Indeed, the recent transmission electron

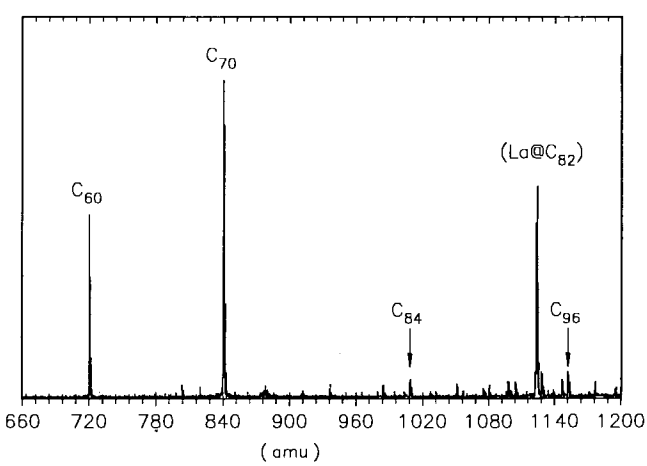

Fig. 50. FT-ICR mass spectra of hot-toluene extract of fullerene material produced by laser evaporization of a 10% La_2O_3/graphite composite rod. This was exposed to air and moisture. Reproduced from Chai et al. (1991).

microscopy of C_{60} films by Wang and Buseck (1991) show such evidence of C_{60}–C_{60} coalescence to form cylindrical bucky tubes in the solid film. The presence of small clusters up to three atoms of La in large fullerenes is certainly very interesting.

Several recent experimental studies have focused on the generation and properties of clusters containing lanthanides. For example, Guiodin et al. (1991) have generated La_mC_n metal–carbon clusters. Dayane et al. (1991) have produced clusters of lanthanide atoms through the inert-gas condensation technique. The mass spectral analysis of Yb_n^+ clusters revealed an overall Gaussian distribution, although Yb_n^+ clusters for $n = 13, 19, 23, 26, 29, 32, 34, 37, 39$ and 45 clearly emerge. Likewise, these authors have also generated Sm_n^+ clusters. The distribution of Sm_n^+ clusters exhibited magic numbers for $n = 13, 19, 26, 32$, and 45. Brechignac et al. (1991) have generated the clusters of Eu and Yb. They have also proposed possible structures for Yb_{14}^+ and Yb_{20}^+. It is evident that experimental studies of clusters containing lanthanide atoms are on the increase in recent years. There is a clear need for theoretical studies even on dimers of open-shell lanthanide atoms. However, such studies will be complicated by the fact that two 4f open shell atoms will yield numerous possible electronic states with different spin multiplicities. The role of 4f orbitals in the Ln–Ln bonding and the possibility of any multiple bonding between lanthanide atoms need to be explored.

8. Conclusion

In summary there has been considerable progress in our understanding of the spectroscopy of diatomic lanthanide oxides, fluorides and hydrides. Due to the ionic nature of these compounds, ligand-field models and more recently *ab initio* effective core potentials have made significant impact in the interpretation of the observed

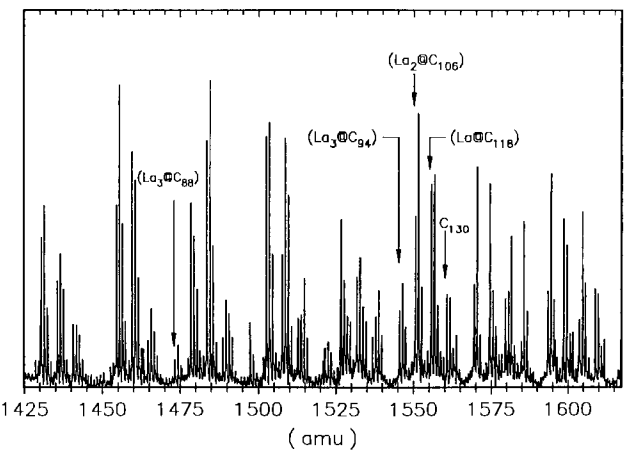

Fig. 51. FT-ICR mass spectrum showed the presence of fullerenes containing up to 3 La atoms. Reproduced from Chai et al. (1991).

spectra and in assisting the assignment of the observed spectra. Relativistic effects were shown to play a key role both in lanthanide and actinide compounds. The anomalous behavior exhibited by post-lanthanide transition-metal compounds was considered and explained. We also considered RECP CASSCF/SOCI computations on several La- and Hf-containing species. It was shown that lanthanide contraction is more important for Hf-containing molecules while relativistic contraction is more important for Pt- and Au-containing molecules. The bonding in LnO was primarily ionic ($Ln^{+2}O^{-2}$), whereas the Ln 4f orbital was essentially localized on the lanthanide.

Recent experimental and theoretical developments in the area of polyatomics containing lanthanides and actinides, especially sandwich and cage molecules consisting of these elements, were considered. The nature of bonding in simple diatomics and polyatomic oxide clusters containing U atoms was also discussed. The recent synthesis of macroscopic quantities of $La@C_{82}$ and other carbon cages containing small clusters of La containing up to three atoms by Chai et al. (1991) should certainly stimulate further theoretical calculations on carbon cages containing one or more lanthanides inside. The computations by Chang et al. (1991) on $La@C_{60}$, $U@C_{60}$, $Eu@C_{60}$, etc., have provided significant insight which, in fact, served as the basis for qualitative interpretation of the unusual stability of $La@C_{82}$. Chang et al.'s RECP/RHF calculation on $La@C_{60}$ showed that the La atom donates two 6s electrons to the carbon cage.

In spite of significant development in both spectroscopic studies and the ligand-field model interpretations of lanthanide oxides, there is less understanding of actinide chemistry. At present, relativistic *ab initio* studies on molecules containing actinides are restricted to very few species. While a ligand-field model has been applied to almost all diatomic oxides containing Ln atoms, this is not the case as far as *ab initio* methods are concerned. Even in cases to which such calculations have been applied (EuO, GdO, YbO, etc.), very few low-lying electronic states have been studied using such techniques. The INDO/S-CI method of Rösch, Zerner and co-workers, on the other hand, has enjoyed more success, although typically in this method all calculations are made at single experimental geometry and the integrals are parametrized. Consequently, there is a real need for further developments and application of *ab initio*-based techniques for molecules containing lanthanides and actinides. Of course, the recent computations of Chang and Pitzer (1989) and Chang et al. (1991) on both uranocene and carbon cages containing lanthanides have evidently demonstrated that indeed such calculations are doable and play a significant role in our comprehension of the nature of bonding in polyatomics containing lanthanides and actinides. Likewise, the CASSCF computation on U_2 by Pepper and Bursten (1990) has shown that relativistic *ab initio* computations are possible on species containing actinide–actinide bonds. Spectroscopic data and their interpretation of actinide compounds need to be addressed more rigorously in the future. It is evident from this chapter that relativistic effects cannot be ignored for such compounds even to gain a qualitative insight. Furthermore, the primarily non-bonding nature of the open 5f shells, at least in very ionic compounds containing actinides, is likely to result in a large array of electronic states due to the spin–orbit coupling. It is hoped that this chapter will stimulate more of such experimental studies, which in turn, will provide impetus for theoretical studies.

Acknowledgments

I thank the U.S. Department of Energy for supporting our work on Sc-, Y-, La-, Hf-, Pt- and Au-containing molecules, considered in this chapter, through the grant No. DEFG02-86ER13558. I thank my co-workers, Drs. Kalyan Das, Ch. Ravimohan and D. Dingguo, for their contributions to this topic. I am deeply indebted to Professors R.M. Pitzer, K.S. Pitzer, M. Zerner, N. Rösch, D. Bursten, H. Preuss, R.W. Field, P. Pyykkö, M. Krauss, B. Simard and R.E. Smalley who not only provided preprints of their works but also permission to reproduce some of their tables and figures. Finally, I express my indebtedness to Ms. Debra Wolf in typing this chapter.

References

Aglada, J., P.J. Bruna, S.D. Peyerimhoff and R.J. Buenker, 1981, J. Mol. Spectrosc. **93**, 299.

Allen, C.L., E.-J. Baerends, P. Vernooijs, J.M. Dyke, A.M. Ellis, M. Feher and A. Moris, 1988, J. Chem. Phys. **89**, 5363.

Alvarado-Swaisgood, A.E., and J.F. Harrison, 1985, J. Phys. Chem. **89**, 5198.

Arhlichs, R., 1985, J. Chem. Phys. **82**, 890.

Armentrout, P.B., and J.L. Beauchamp, 1989, Acc. Chem. Res. **22**, 315.

Atkins, P.W., 1991, Eur. J. Solid State & Inorg. Chem. **28**, 9.

Bagus, P.S., Y.S. Lee and K.S. Pitzer, 1975, Chem. Phys. Lett. **33**, 408.

Balasubramanian, K., 1987, Chem. Phys. Lett. **135**, 288.

Balasubramanian, K., 1988, Int. J. Quantum Chem., Symp. **22**, 465.

Balasubramanian, K., 1989a, J. Phys. Chem. **93**, 6585.

Balasubramanian, K., 1989b, Chem. Rev. **89**, 1801.

Balasubramanian, K., 1990a, Chem. Rev. **90**, 93.

Balasubramanian, K., 1990b, J. Chem. Phys. **93**, 8061.

Balasubramanian, K., and D.G. Dai, 1990, J. Chem. Phys. **93**, 7243.

Balasubramanian, K., and K.K. Das, 1991, J. Mol. Spectrosc. **145**, 142.

Balasubramanian, K., and K.S. Pitzer, 1983, J. Chem. Phys. **78**, 321.

Balasubramanian, K., and K.S. Pitzer, 1987, Adv. Chem. Phys. **67**, 287.

Balasubramanian, K., and Ch. Ravimohan, 1988, Chem. Phys. Lett. **145**, 39.

Balasubramanian, K., and J.Z. Wang, 1989a, J. Mol. Spectrosc. **133**, 82.

Balasubramanian, K., and J.Z. Wang, 1989b, Chem. Phys. Lett. **154**, 525.

Balasubramanian, K., P.A. Christiansen and K.S. Pitzer, 1991, Phys. Rev. A **43**, 2581.

Ballster, J.L., P.R. Antoniewicz and R. Smoluchowski, 1990, Astrophys. J. **356**, 507.

Barrow, R.F., B.W. Bastin, D.L.G. Moore and C.J. Pott, 1967, Nature **215**, 1072.

Barrow, R.F., R.M. Clements, S.M. Harris and P.P. Jenson, 1979, Astrophys. J. **229**, 439.

Bartlett, R.J., 1989, J. Phys. Chem. **93**, 1697.

Bauschlicher Jr, C.W., and S.R. Langhoff, 1989, Chem. Phys. Lett. **161**, 383.

Bauschlicher Jr, C.W., and S.R. Langhoff, 1991, J. Phys. Chem. **95**, 2278.

Bauschlicher Jr, C.W., and S.P. Walch, 1982, J. Chem. Phys. **76**, 4560.

Bauschlicher Jr, C.W., and S.P. Walch, 1983, J. Chem. Phys. **78**, 4597.

Beaufils, J.C.L., P. Carette and J.M. Blondeau, 1979, J. Mol. Spectrosc. **77**, 1.

Becke, A., 1986, Phys. Rev. A **33**, 2786.

Bernard, A., and R. Bacis, 1976, Can. J. Phys. **54**, 1509.

Bernard, A., and R. Bacis, 1977, Can. J. Phys. **55**, 1322.

Brechignac, C., Ph. Cahuzac, F. Carlier, M. de Fratos, A. Masson and J.Ph. Roux, 1991, Z. Phys. D **19**, 195.

Brooks, B.R., and H.F. Schaefer, 1979, J. Chem. Phys. **70**, 5092.

Bujin, G., and C. Linton, 1989, J. Mol. Spectrosc. **137**, 114.

Bujin, G., and C. Linton, 1991, J. Mol. Spectrosc. **147**, 120.

Bursten, B.E., and R.J. Strittmatter, 1987, J. Am. Chem. Soc. **109**, 6606.

Bursten, B.E., and R.J. Strittmatter, 1991, Angew. Chem. **30**, 1069.
Carette, P., 1990, J. Mol. Spectrosc. **140**, 269.
Carette, P., and A. Hocquet, 1988, J. Mol. Spectrosc. **16**, 301.
Carette, P., A. Hocquet, M. Douay and B. Pinchemel, 1987, J. Mol. Spectrosc. **124**, 243.
Case, D.A., 1982, Annu. Rev. Phys. Chem. **33**, 51.
Chai, Y., T. Guo, C. Jin, R.E. Haufler, L.P.F. Chibante, J. Fure, L. Wang, J.M. Alforld and R.E. Smalley, 1991, J. Phys. Chem. **95**, 7564.
Chang, A.H.H., and R.M. Pitzer, 1989, J. Am. Chem. Soc. **111**, 2500.
Chang, A.H.H., and R.M. Pitzer, 1991, unpublished results.
Chang, A.H.H., W.C. Ermler and R.M. Pitzer, 1991, J. Chem. Phys. **94**, 5004.
Chen, Y.M., D.E. Clemmer and P.B. Armentrout, 1991, J. Chem. Phys. **95**, 1228.
Childs, W.J., O. Poulsen and T.C. Steimle, 1988, J. Chem. Phys. **88**, 598.
Chong, D.P., S.R. Langhoff, C.W. Bauschlicher Jr, S.P. Walch and H. Partridge, 1986, J. Chem. Phys. **85**, 285.
Christiansen, P.A., Y.S. Lee and K.S. Pitzer, 1979, J. Chem. Phys. **71**, 4445.
Christiansen, P.A., K. Balasubramanian and K.S. Pitzer, 1982, J. Chem. Phys. **76**, 5087.
Christiansen, P.A., W.C. Ermler and K.S. Pitzer, 1985, Annu. Rev. Phys. Chem. **36**, 407.
Cotton, F.A., and G.W. Wilkinson, 1976, Basic Inorganic Chemistry (Wiley, New York).
Cousson, A., S. Dabos, H. Abazli, F. Nectoux, M. Pagés and G.R. Choppin, 1984, J. Less-Common Met. **99**, 233.
Cox, D.W., D.J. Trevor, K.C. Reichmann and A. Kaldor, 1986, J. Am. Chem. Soc. **108**, 2457.
Cox, D.W., K.C. Reichmann and A. Kaldor, 1988, J. Chem. Phys. **88**, 1588.
Das, K.K., and K. Balasubramanian, 1989, J. Chem. Phys. **91**, 2433.
Das, K.K., and K. Balasubramanian, 1990, Chem. Phys. Lett. **172**, 372.
Das, K.K., and K. Balasubramanian, 1991a, J. Phys. Chem. **95**, 42.
Das, K.K., and K. Balasubramanian, 1991c, J. Chem. Phys. **94**, 3722.
Das, K.K., and K. Balasubramanian, 1991d, J. Phys. Chem. **95**, 3979.
Dayane, D., A. Benamar, P. Melinon, B. Tribollet and M. Broyer, 1991, Z. Phys. D **19**, 191.
Dekock, R.L., and W. Weltner Jr, 1971, J. Phys. Chem. **75**, 514.
Delaval, J.M., J. Van Heems and J.C.L. Beaufils, 1977, Can. J. Spectrosc. **22**, 117.
Denning, R.G., 1983, Gmelin Handbook, Supplement A6 (Springer, Berlin) pp. 31–79.
Desclaux, J.P., 1973, Atomic and Nuclear Data **12**, 312.
Desclaux, J.P., 1975, Comput. Phys. Commun. **9**, 31.
Desclaux, J.P., and P. Pyykkö, 1974, Chem. Phys. Lett. **29**, 534.
Desclaux, J.P., and P. Pyykkö, 1976, Chem. Phys. Lett. **39**, 300.
Dickson, C.R., and R.N. Zare, 1975, Chem. Phys. **7**, 361.
Diederich, F., R. Ette, Y. Rubin, R.L. Whetten, R. Bell, M. Alvarez, S. Anz, D. Mesharma, F. Wudl, K.C. Khomani and A. Koch, 1991, Science **252**, 1548.
Dolg, M., and H. Stoll, 1989, Theor. Chim. Acta **75**, 369.
Dolg, M., H. Stoll, A. Savin and H. Preuss, 1988, Stud. Phys. & Theor. Chem. **62**, 265.
Dolg, M., H. Stoll, A. Savin and H. Preuss, 1989a, Theor. Chim. Acta. **75**, 173.
Dolg, M., H. Stoll and H. Preuss, 1989b, J. Chem. Phys. **90**, 1730.
Dolg, M., H. Stoll and H. Preuss, 1990a, Chem. Phys. Lett. **174**, 208.
Dolg, M., H. Stoll and H. Preuss, 1990b, Chem. Phys. **148**, 219.
Dolg, M., P. Fulde, W. Kuchle, C.-S. Neumann and H. Stoll, 1991a, J. Chem. Phys. **94**, 3011.
Dolg, M., H. Stoll, H.-J. Flad and H. Preuss, 1992, J. Chem. Phys. **97**, 1162.
Dulick, M., and R.W. Field, 1985, J. Mol. Spectrosc. **113**, 105.
Dulick, M.E., and R.F. Barrow, 1986, J. Chem. Phys. **85**, 385.
Effantin, C., and J. d'Incan, 1974, Can. J. Phys. **52**, 523.
Elkind, J.L., and P.B. Armentrout, 1986a, Inorg. Chem. **25**, 1078.
Elkind, J.L., and P.B. Armentrout, 1986b, J. Phys. Chem. **90**, 5736.
Elkind, J.L., L.S. Sunderlin and P.B. Armentrout, 1989, J. Phys. Chem. **93**, 3159.
Ermler, W.C., Y.S. Lee, P.A. Christiansen and K.S. Pitzer, 1981, Chem. Phys. Lett. **81**, 70.
Ermler, W.C., R.B. Ross and P.A. Christiansen, 1988, Adv. Quantum Chem. **19**, 139.

Field, R.W., 1982, Ber. Bunsenges. Phys. Chem. **86**, 771.

Field, R.W., D.P. Baldwin, E.J. Hill, M. Li and M.C. McCarthy, 1989, in: Future Trends in Spectroscopy, Spectrochim. Acta A, Special Supplement, pp. 75–90.

Fischell, D.R., H.C. Brayman and T.A. Cool, 1980, J. Chem. Phys. **73**, 4260.

Gabelnick, S.D., G.T. Reedy and M.G. Chasanov, 1973, J. Chem. Phys. **58**, 4468.

Gabelnick, S.D., G.T. Reedy and M.G. Chasanov, 1984, J. Chem. Phys. **60**, 1167.

Gingerich, K.A., 1980, Symp. Faraday Soc. **14**, 109.

Glebov, V.A., 1983, Electronic Structure and Properties of Uranyl Compounds (Energoatmoizdat, Moscow). In Russian.

Gmelin Handbook of Inorganic Chemistry, 1983, V. Supplement (Springer, Berlin) A6.

Gotkis, I., 1991, J. Phys. Chem. **95**, 6086.

Green, D.W., S.D. Gabelnick and G.T. Reedy, 1976, J. Chem. Phys. **64**, 1697.

Guiodin, A.G., A. Mele, G. Pizzella and R. Teghie, 1991, Z. Phys. D **20**, 89.

Hafner, P., and W.H.E. Schwarz, 1978, J. Phys. B **11**, 217.

Hafner, P., and W.H.E. Schwarz, 1979, Chem. Phys. Lett. **65**, 537.

Hannigan, M.C., 1983, J. Mol. Spectrosc. **99**, 235.

Hay, B.P., 1991, Inorg. Chem. **30**, 2876.

Hay, P.J., and W.R. Wadt, 1985a, J. Chem. Phys. **82**, 270.

Hay, P.J., and W.R. Wadt, 1985b, J. Chem. Phys. **82**, 299.

Hay, P.J., W.R. Wadt, L.R. Kahn, R.C. Rafenetti and D.H. Phillips, 1979, J. Chem. Phys. **71**, 1767.

Hay, P.J., R.R. Ryan, K.V. Salazar, D.A. Wrobloski and A.P. Sattelberger, 1986, J. Am. Chem. Soc. **108**, 313.

Hayes, R.G., and N.M. Edelstein, 1972, J. Am. Chem. Soc. **94**, 8688.

Heath, J.R., S.C. O'Brien, Q. Zhang, Y. Liu, R.F. Curl, H.W. Kroto, F.K. Tittel and R.E. Smalley, 1985, J. Am. Chem. Soc. **107**, 7779.

Heaven, M.C., J.-P. Nicolai, S.J. Riley and E.K. Parks, 1985, Chem. Phys. Lett. **119**, 229.

Hoekstra, H.R., and S. Siegel, 1964, J. Inorg. & Nucl. Chem. **26**, 693.

Hoffman, D.C., 1990, in: Fifty Years with Transuranium Elements, Robert A. Welch Foundation Conf. on Chemical Research XXXIV, Houston, TX, October 1990.

Hohenberg, P., and W. Kohn, 1964, Phys. Rev. B **136**, 864.

Huber, K.P., and G. Herzberg, 1979, Spectroscopic Constants of Diatomic Molecules (Van Nostrand Reinhold, Princeton, NJ).

Hurley, M.M., L.I. Pacios, P.A. Christiansen, R.B. Rossand and W.C. Ermler, 1986, J. Chem. Phys. **84**, 6840.

Igelmann, G., H. Stoll and H. Preuss, 1988, Mol. Phys. **65**, 1321.

Jørgensen, C.K., and R. Reisfeld, 1982, Struct. & Bonding **50**, 121.

Kaldor, A., D.M. Cox, D.J. Trevor and M.R. Zakin, 1986, Z. Phys. D **3**, 95.

Kaledin, L.A., and E.A. Shenyavskaya, 1981, J. Mol. Spectrosc. **90**, 590.

Karraker, D.G., 1972, Inorg. Chem. **12**, 1105.

Karraker, D.G., A.J. Stone, E.R. Jones and N.M. Edelstein, 1970, J. Am. Chem. Soc. **92**, 4841.

Katz, J.J., G.T. Seaborg and L.R. Morss, eds, 1986, The Chemistry of Actinide Elements, 2nd Ed. (Chapman and Hall, London) 2 volumes, 1677pp.

Kellö, V., and A.J. Sadlej, 1991a, J. Chem. Phys. **95**, 8248.

Kellö, V., and A.J. Sadlej, 1991b, Chem. Phys. Lett. **174**, 641.

Kohn, W., and L.J. Sham, 1965, Phys. Rev. A **140**, 1133.

Kotzian, M., and N. Rösch, 1991a, Eur. J. Solid State & Inorg. Chem. **28**, 127.

Kotzian, M., and N. Rösch, 1991b, J. Mol. Spectrosc. **147**, 346.

Kotzian, M., N. Rösch, N. Schröder and M.C. Zerner, 1989a, J. Am. Chem. Soc. **111**, 7687.

Kotzian, M., N. Rösch, R.M. Pitzer and M.C. Zerner, 1989b, Chem. Phys. Lett. **160**, 168.

Kotzian, M., N. Rösch and M.C. Zerner, 1991a, Theor. Chim. Acta **81**, 201.

Kotzian, M., N. Rösch and M.C. Zerner, 1991b, Int. J. Quantum Chem. **25**, 545.

Krauss, M., and W.J. Stevens, 1983a, J. Comput. Chem. **4**, 127.

Krauss, M., and W.J. Stevens, 1983b, Chem. Phys. Lett. **99**, 417.

Krauss, M., and W.J. Stevens, 1984, Annu. Rev. Phys. Chem. **35**, 357.

Kroto, H.W., J.R. Heath, S.C. O'Brien, R.F. Curl and R.E. Smalley, 1985, Nature (London) **318**, 162.

La John, L.A., P.A. Christiansen, R.B. Ross,

T. Atashroo and W.C. Ermler, 1987, J. Chem. Phys. **87**, 2812.
Langhoff, S.R., and E.R. Davidson, 1974, Int. J. Quantum Chem. **8**, 61.
Langhoff, S.R., L.G.M. Pettersson, C.W. Bauschlicher Jr and H. Partridge, 1987, J. Chem. Phys. **87**, 268.
Langhoff, S.R., C.W. Bauschlicher Jr and H. Partridge, 1988, J. Chem. Phys. **89**, 396.
Larsson, S., and P. Pyykkö, 1986, Chem. Phys. **101**, 355.
Lee, Y.S., and A.D. McLean, 1982a, J. Chem. Phys. **76**, 735.
Lee, Y.S., and A.D. McLean, 1982b, Stud. Phys. & Theor. Chem. **21**, 219.
Lee, Y.S., W.C. Ermler and K.S. Pitzer, 1977, J. Chem. Phys. **75**, 1861.
Linton, C., and M. Dulick, 1981, J. Mol. Spectrosc. **89**, 569.
Linton, C., and Y.C. Liu, 1988, J. Mol. Spectrosc. **131**, 367.
Linton, C., M. Dulick and R.W. Field, 1979, J. Mol. Spectrosc. **78**, 428.
Linton, C., M. Dulick, R.W. Field, P. Carette and R.F. Barrow, 1981, J. Chem. Phys. **74**, 189.
Linton, C., M. Dulick, R.W. Field, P. Carette, P.C. Leyland and R.F. Barrow, 1983a, J. Mol. Spectrosc. **102**, 441.
Linton, C., S.A. McDonald, S. Rice, M. Dulick, Y.C. Liu and R.W. Field, 1983b, J. Mol. Spectrosc. **101**, 322.
Linton, C., D.M. Gaudet and H. Schall, 1986, J. Mol. Spectrosc. **115**, 58.
Linton, C., G. Bujin, R.S. Rana and J.A. Gray, 1987, J. Mol. Spectrosc. **126**, 370.
Liu, B., and M. Yoshimine, 1981, J. Chem. Phys. **74**, 612.
Liu, Y.C., C. Linton, H. Schall and R.W. Field, 1984, J. Mol. Spectrosc. **104**, 72.
Makhyoun, M.A., B.D. El-Issa and A.B. Salsa, 1987, J. Mol. Structure (Theochem.) **153**, 241.
Malli, G.L., ed., 1982a, Relativistic Effects in Atoms, Molecules and Solids (Plenum, New York).
Malli, G.L., 1982b, Stud. Phys. & Theor. Chem. **21**, 199.
Malmquist, P.A., A. Rennel and B.O. Roos, 1990, J. Phys. Chem. **94**, 5477.
Marian, C.M., U. Wahlgren, O. Gropen and P. Pyykkö, 1988, J. Mol. Struct. (Theochem.) **169**, 339.
Martinho, J.A., and J.L. Beauchamp, 1990, Chem. Rev. **90**, 629.
McDonald, S.A., 1985, Ph.D. Thesis (MIT, Boston, MA).
McDonald, S.A., S.F. Rice, R.W. Field and C. Linton, 1990, J. Chem. Phys. **93**, 7676.
McLean, A.D., M. Yoshimine, B.H. Lengsfield, P.S. Bagus and B. Liu, 1990, in: Modern Techiques in Computational Chemistry, ed. E. Clementi (Escom, Leiden) pp. 593–637.
Merchàn, M., P.A. Malmquist and B.O. Roos, 1991, Theor. Chim. Acta **79**, 81.
Meyer, H.J., and R. Hoffmann, 1991, Inorg. Chem. **30**, 963.
Moore, C.E., 1971, Table of Atomic Energy Levels (National Institute of Standards and Technology, Washington, DC).
Müller, W., J. Flesch and W. Meyer, 1984, J. Chem. Phys. **80**, 3297.
Nessler, R., and K.S. Pitzer, 1987, J. Phys. Chem. **91**, 1084.
O'Brien, S.C., J.R. Heath, H.W. Kroto, R.F. Curl and R.E. Smalley, 1986, Chem. Phys. Lett. **132**, 99.
Okada, K., Y. Kaizu, H. Kobayashi, K. Tanara and F. Marumo, 1984, Mol. Phys. **54**, 1293.
Olsen, J., P. Jorgensen and J. Simons, 1990, Chem. Phys. Lett. **169**, 463.
Ortiz, J.V., 1986, J. Am. Chem. Soc. **108**, 550.
Pacios, L.F., and P.A. Christiansen, 1985, J. Chem. Phys. **82**, 2664.
Paldus, J., 1976, in: Theoretical Chemistry: Advances and Perspectives, eds H. Eyring and D.J. Henderson (Academic, New York).
Paldus, J., and J. Cizek, 1989, J. Chem. Phys. **90**, 4356.
Parr, R.G., and W. Yang, 1989, Density Functional Theories of Atoms and Molecules (Oxford University Press, New York).
Pepper, M., and D.E. Bursten, 1990, J. Am. Chem. Soc. **112**, 7803.
Pepper, M., and D.E. Bursten, 1991, Chem. Rev. **91**, 719.
Pitzer, K.S., 1979, Acc. Chem. Res. **12**, 271.
Pitzer, R.M., and N.W. Winter, 1988, J. Phys. Chem. **92**, 3061.
Pople, J.A., D.L. Beveridge and P.A. Dobush, 1967, J. Chem. Phys. **47**, 2026.
Pyykkö, P., 1979, Phys. Scripta **20**, 647.
Pyykkö, P., 1986, Relativistic Theory of Atoms and Molecules 1916-1985 (Springer, Berlin).
Pyykkö, P., 1987, Inorg. Chim. Acta **139**, 243.
Pyykkö, P., 1988, Chem. Rev. **88**, 563.
Pyykkö, P., 1993, Relativistic Theory of Atoms and Molecules 1986–1992 (Springer, Berlin).

Pyykkö, P., and J.P. Desclaux, 1978, Chem. Phys. **34**, 261.
Pyykkö, P., and J.P. Desclaux, 1979, Acc. Chem. Res. **79**, 276.
Pyykkö, P., and J. Jové, 1991, New J. Chem. **15**, 717.
Pyykkö, P., and L.L. Lohr Jr, 1981, Inorg. Chem. **20**, 1950.
Pyykkö, P., and Y. Zhao, 1991, Inorg. Chem. **30**, 3787.
Pyykkö, P., L.J. Laakonen and K. Tatsumi, 1989, Inorg. Chem. **28**, 1801.
Ramos, A.F., N.C. Pyper and G.L. Malli, 1988, Phys. Rev. A **38**, 2729.
Ridley, J., and M.C. Zerner, 1973a, Theor. Chim. Acta **32**, 111.
Ridley, J., and M.C. Zerner, 1973b, Theor. Chim. Acta **42**, 223.
Roos, B.O., 1987, Adv. Chem. Phys. **67**, 399.
Rosen, A., and B. Wästberg, 1988, J. Am. Chem. Soc. **110**, 8701.
Rosen, A., and B. Wästberg, 1989, Z. Phys. D **12**, 387.
Rosi, M., and C.W. Bauschlicher, 1990, Chem. Phys. Lett. **166**, 189.
Ross, R.B., J.M. Powers, T. Atashroo, W.C. Ermler, L.A. LaJohn and P.A. Christiansen, 1990, J. Chem. Phys. **93**, 6654.
Sadlej, A.J., and M. Urban, 1991, Chem. Phys. Lett. **176**, 293.
Salahub, D., 1987, Adv. Chem. Phys. **69**, 447.
Salahub, D., and M.C. Zerner, 1989, The Challenge of d and f Electrons, American Chemical Society Symp., No. 394.
Schall, H., C. Linton and R.W. Field, 1983, J. Mol. Spectrosc. **100**, 437.
Schall, H., J.A. Gray, M. Dulick and R.W. Field, 1986, J. Chem. Phys. **85**, 751.
Schall, H., M. Dulick and R.W. Field, 1987, J. Chem. Phys. **87**, 2898.
Schilling, J.B., W.A. Goddard III and J.L. Beauchamp, 1987, J. Phys. Chem. **87**, 481.
Shavitt, I., 1978, Int. J. Quantum Chem. Symp. **12**, 5.
Shenyavskaya, E.A., and L.A. Kaledin, 1982, J. Mol. Spectrosc. **91**, 22.
Shenyavskaya, E.A., I.V. Egorova and V.N. Lupanov, 1973, J. Mol. Spectrosc. **47**, 355.
Shirley, J., S.C. Scurlock, T.C. Steimle, B. Simard, M. Vasseur and P.A. Hackett, 1990, J. Chem. Phys. **93**, 8580.
Shirley, J., W.L. Barclay Jr, L.M. Ziurys and T.C. Steimle, 1991, Chem. Phys. Lett. **183**, 363.
Simard, B., H. Niki, W.J. Balfour, M. Vasseur and P.A. Hackett, 1991, unpublished results.
Starks, D.F., and A. Streitwieser Jr, 1973, J. Am. Chem. Soc. **95**, 3424.
Steimle, T.C., and Y. Al-Ramadin, 1989, Chem. Phys. Lett. **130**, 76.
Streitwieser Jr, A., and S. Kinsley, 1985, in: Fundamental and Technological Aspects of Organic f-Elemental Chemistry, eds T.J. Marks and I.L. Fragale (Reidel, Dordrecht) pp. 77–114.
Streitwieser Jr, A., and U. Müller-Westerhof, 1968, J. Am. Chem. Soc. **90**, 7364.
Streitwieser Jr, A., U. Müller-Westerhoff, U.G. Sonnichsen, F. Mares, D.G. Morrel, K.O. Hodgson and C.A. Harmon, 1973, J. Am. Chem. Soc. **95**, 8644.
Suneram, R.D., F.J. Lovas, G.T. Fraser and K. Matsumura, 1991, preprint.
Szentpaly, L.V., P. Fuentelaba, H. Preuss and H. Stoll, 1982, Chem. Phys. Lett. **93**, 555.
van Wezenbeek, E.M., E.J. Baerends and J.G. Snijders, 1991, Theor. Chim. Acta. **81**, 139.
Van Zee, R.J., M.L. Seely and W. Weltner Jr, 1977, J. Chem. Phys. **67**, 861.
Van Zee, R.J., R.F. Ferrante, K.J. Zeringue and W. Weltner Jr, 1981, J. Chem. Phys. **75**, 5297.
Wadt, W.R., 1981, J. Am. Chem. Soc. **103**, 6053.
Wadt, W.R., and P.J. Hay, 1985, J. Chem. Phys. **82**, 284.
Wang, J.Z., K.K. Das and K. Balasubramanian, 1990, Mol. Phys. **69**, 147.
Wang, S., and P.R. Buseck, 1991, Chem. Phys. Lett. **182**, 1.
Weiss, F.D., J.L. Elkind, S.C. O'Brien, R.F. Curl and R.E. Smalley, 1988, J. Am. Chem. Soc. **110**, 4464.
Xin, X., J.G. Edvinsson and L. Klynning, 1991, J. Mol. Spectrosc. **148**, 59.
Yadav, B.R., S.B. Rai and D.K. Rai, 1981, J. Mol. Spectrosc. **89**, 1.

Handbook on the Physics and Chemistry of Rare Earths
Vol. 18 – Lanthanides/Actinides: Chemistry
edited by K.A. Gschneidner, Jr., L. Eyring, G.R. Choppin and G.H. Lander

Chapter 120

SIMILARITIES AND DIFFERENCES IN TRIVALENT LANTHANIDE- AND ACTINIDE-ION SOLUTION ABSORPTION SPECTRA AND LUMINESCENCE STUDIES

James V. BEITZ
Chemistry Division, Argonne National Laboratory, Argonne, IL 60439, USA

Contents

Symbols and abbreviations 159
1. Introduction 160
   1.1. Scope 160
   1.2. Historical development 160
2. Observed spectra of aquated trivalent lanthanide and actinide ions 161
3. Theoretical treatment of f-state spectra 173
   3.1. Application of atomic theory 173
   3.2. Comparison of "free-ion" states and observed spectra 174
   3.3. Transition intensities 177
   3.4. Hypersensitive bands 180
   3.5. Vibronic bands 181
4. Luminescence of trivalent-ion f states 184
   4.1. Radiative and nonradiative decay rates 184
   4.2. Experimental observations 185
      4.2.1. Lanthanide ions 185
      4.2.2. Actinide ions 186
   4.3. Trends in luminescence dynamics 187
   4.4. Calculation of nonradiative decay rates 189
   4.5 Hydration and structure of aquated ions 189
   4.6. Photochemistry 191
   4.7. Selected applications 191
5. Concluding remarks 192
References 193

Symbols and abbreviations

A_T	total purely radiative decay rate of a state		angular momentum of all the electrons in an atom
C	energy-gap law parameter	L	quantum number associated with the total orbital angular momentum of all electrons in an atom
B_q^k	crystal-field parameters (k even)		
F^k	Slater parameters ($k = 0, 2, 4, 6$)		
J	quantum number associated with the total		

LIF	laser-induced fluorescence	$U^{(k)}$	squared unit tensor matrix element ($k = 2, 4, 6$)
M^h	Marvin-integral parameters ($h = 0, 2, 4$)	W_T	total nonradiative decay rate of a state
P^f	two-body pseudo-magnetic operator parameters ($f = 2, 4, 6$)	α	generalized Trees parameter, energy-gap law parameter
S	quantum number associated with total spin angular momentum for all the electrons in an atom	β, γ	generalized Trees parameters
		τ	luminescence lifetime
T^i	three-body operator parameters ($i = 2, 3, 4, 6, 7, 8$)	ζ_f	spin–orbit coupling constant for f electrons
		Ω_k	Judd–Ofelt model intensity parameters ($k = 2, 4, 6$)

1. Introduction

Comparison of experimental and theoretical studies of the solution absorption and luminescence spectra of lanthanide and actinide ions is the focus of this chapter. In aqueous solutions, the most stable oxidation state of lanthanide ions is 3+, but actinide-ion formal oxidation states ranging from 2+ to 7+ are known (Seaborg and Loveland 1990). Actinide elements heavier than plutonium exhibit more lanthanide-like behavior, however, in that 3+ is their most stable formal oxidation state in aqueous solution. The visible and near-infrared absorption spectra of trivalent lanthanide and actinide ions in solution provide such rich detail that the spectra may fairly be said to "fingerprint" the ion for identification. The abundance of sharp spectral features long confronted theoretical and experimental spectroscopists with difficult problems. The efforts of numerous workers have provided interpretation of many aspects of the spectra of these f-transition elements; significant challenges remain.

1.1. *Scope*

Absorption spectra spanning the broadest range of actinide elements are available for 3+ actinide ions in aqueous solution. Such experimental spectra start at U^{3+} and extend through Es^{3+}, the heaviest actinide available in sufficient quantity for conventional spectroscopic investigation. Many spectral studies of lanthanide ions in solution have been published, but systematic intepretation of the observed changes in energy-level structure, multiplet splitting, and transition intensities across the lanthanide series has not been reported. Spectral studies of complexed actinide ions are less numerous than those of lanthanides and have not been systematically interpreted. For these reasons, this chapter deals primarily with studies of trivalent lanthanide and actinide ions in dilute, noncomplexing acid solution where the inner coordination sphere of the metal ion consists of water molecules (i.e., aquated lanthanide and actinide ions).

1.2. *Historical development*

Freed (1942) reviewed early efforts to interpret the spectroscopic properties of lanthanides in condensed phases and noted that a polarized absorption spectra of

didymium sulfate octahydrate had been recorded by Bunsen in 1866. In reviewing solution spectra of lanthanide ions, Carnall (1979) noted that comparisons of lanthanide-ion fluorescence in solid compounds and solution were published in the early 1930s and that preparation of relatively pure lanthanide compounds enabled Prandtl and Scheiner (1934) to publish the first complete set (except for Pm^{3+}) of lanthanide solution absorption spectra in the range 220–700 nm. However, theoretical understanding of such spectra developed slowly. Bethe (1929) published a theory describing term splitting that results from the influence of an electric field of a given symmetry on an atom, but the gross term structure and nature of lanthanide absorption bands were not understood at the time. A comparison between theory and experiment for the spectrum of a thulium compound was given by Bethe and Spedding (1937), but complete treatment of more complex configurations became practical only with the development of the tensor-operator methods of Racah (1942). Much of the historical development of theoretical rare-earth spectroscopy has been reviewed by Judd (1988). Evidence of the close similarity of 4f-state energy-level structure of trivalent lanthanide ions in solids such as $LaCl_3$ and LaF_3 and aqueous ions in solution has been reviewed by Carnall (1979).

Carnall and Wybourne (1964) carried out the first systematic interpretation of the 5f-state energy-level structure of trivalent actinide ions in solution using observed absorption spectra for U^{3+} through Cm^{3+}. These workers varied two parameters in their theoretical model to obtain the best agreement between calculated 5f-state energies and observed absorption-band energies. The first comprehensive review of the absorption spectra of transuranic actinide ions (including U^{3+}) in dilute acid solution was published by Carnall (1973). He noted that considerable progress in theoretical modeling of 5f-state energy-level structure had been achieved by an interplay between calculation and experiment as well as between studies of solution and crystal spectra of a given actinide ion in a particular oxidation state. Good agreement between experiment and theory necessitated explicit inclusion of a number of electrostatic, magnetic, and configuration interaction parameters and diagonalization of the complete interaction matrices. A close similarity between 5f-state energy-level structure of actinide ions in solids such as $LaCl_3$ and as aquated ions in solution has been established (Carnall 1986). Absorption spectra of actinides, primarily as complexed ions in solution, have been reviewed by Ryan (1972). Spectra for many actinide oxidation states were systematically considered by Carnall (1986). Actinide-ion spectra, generally as complexed ions or in solid compounds, also are shown by, or referenced in, Katz et al. (1985).

2. Observed spectra of aquated trivalent lanthanide and actinide ions

Observed optical absorption spectra of trivalent lanthanide and actinide ions in aqueous solution at ambient temperature (nominally 295 K) are shown in figs. 1–21. The data are from the files of W.T. Carnall. The lanthanide-ion absorption data from Ce^{3+} through Yb^{3+} are essentially those reported by Carnall (1979) and the actinide data somewhat extend the spectra given by Carnall (1986) for U^{3+} through Es^{3+}. The spectra were recorded in dilute mineral acid solution (generally $HClO_4$) and solvent

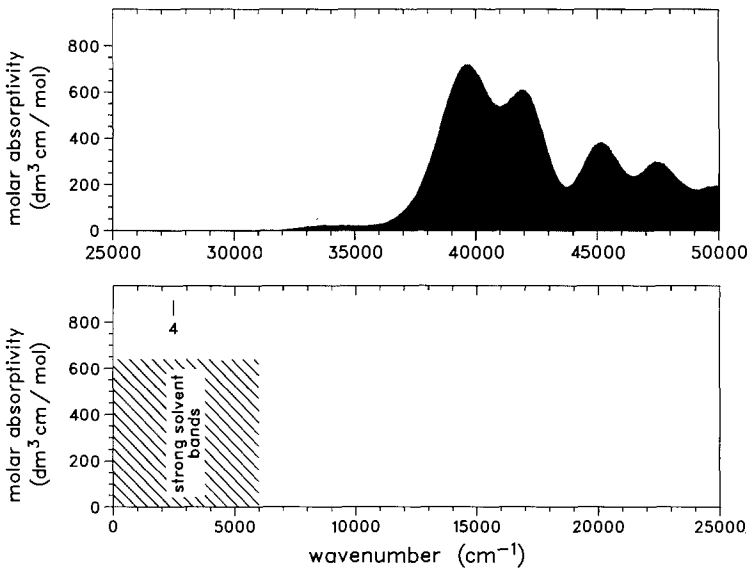

Fig. 1. Observed absorption spectrum (near-infrared to ultraviolet) and calculated 4f-state energies of aquated Ce^{3+}.

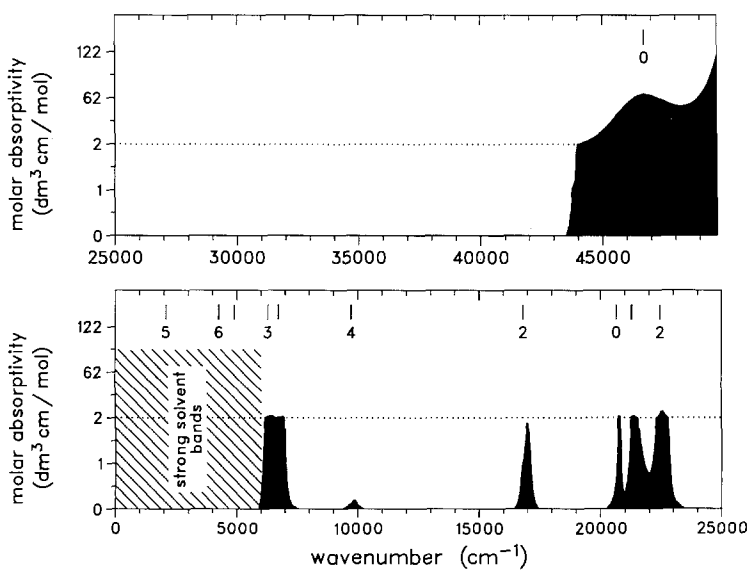

Fig. 2. Observed absorption spectrum (near-infrared to ultraviolet) and calculated 4f-state energies of aquated Pr^{3+}.

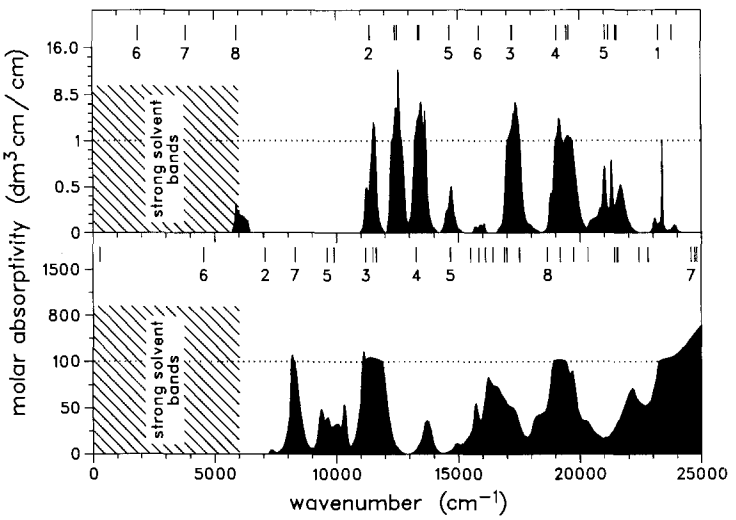

Fig. 3. Observed absorption spectrum (near-infrared to visible) and calculated f-state energies of aquated Nd^{3+} (upper panel) and aquated U^{3+} (lower panel).

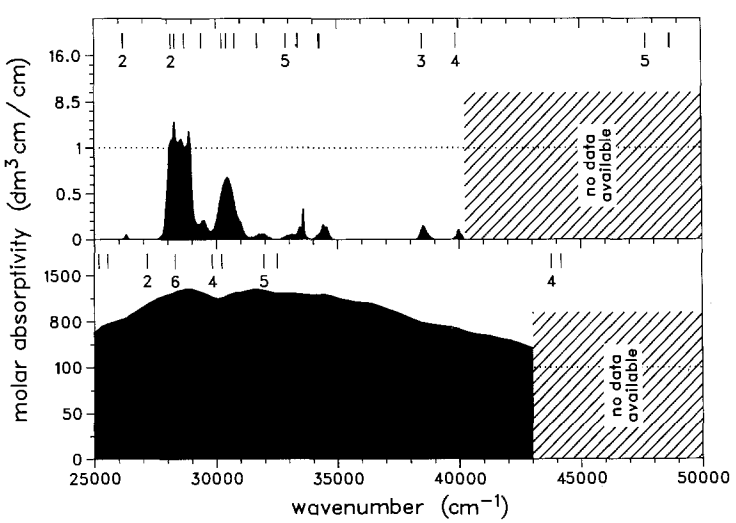

Fig. 4. Observed ultraviolet absorption spectrum and calculated f-state energies of aquated Nd^{3+} (upper panel) and aquated U^{3+} (lower panel).

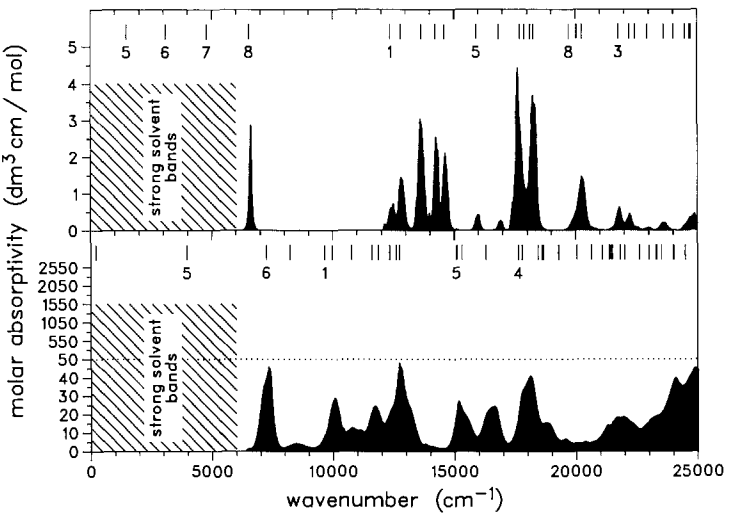

Fig. 5. Observed absorption spectrum (near-infrared to visible) and calculated f-state energies of aquated Pm^{3+} (upper panel) and aquated Np^{3+} (lower panel).

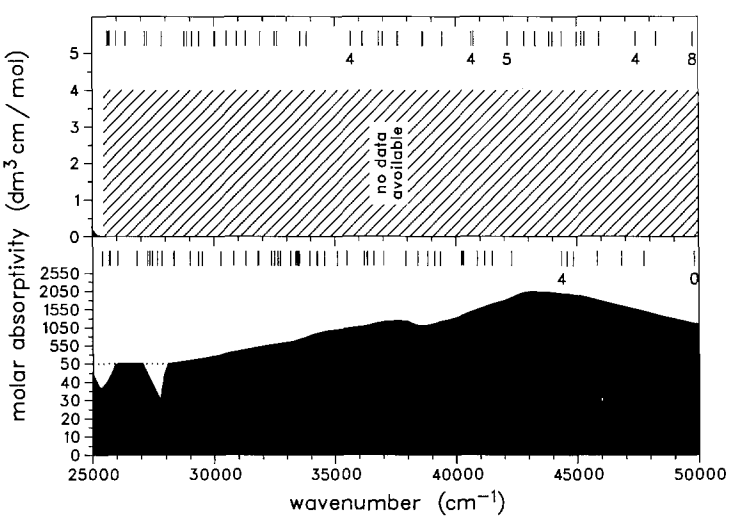

Fig. 6. Observed ultraviolet absorption spectrum and calculated f-state energies of aquated Pm^{3+} (upper panel) and aquated Np^{3+} (lower panel).

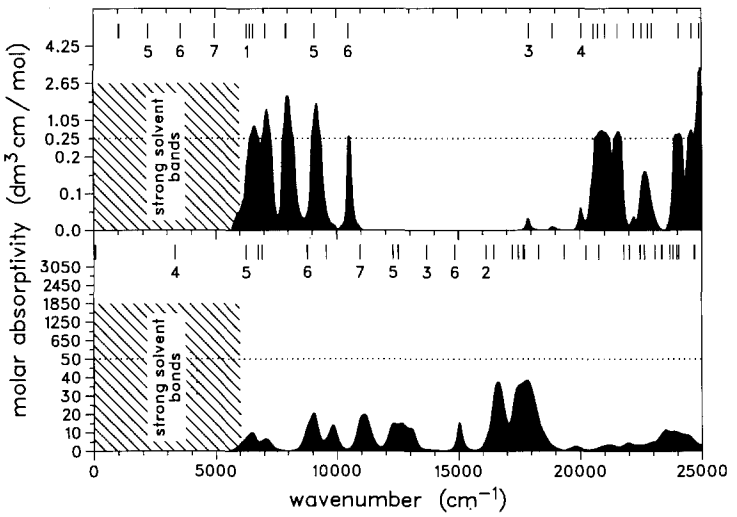

Fig. 7. Observed absorption spectrum (near-infrared to visible) and calculated f-state energies of aquated Sm^{3+} (upper panel) and aquated Pu^{3+} (lower panel)

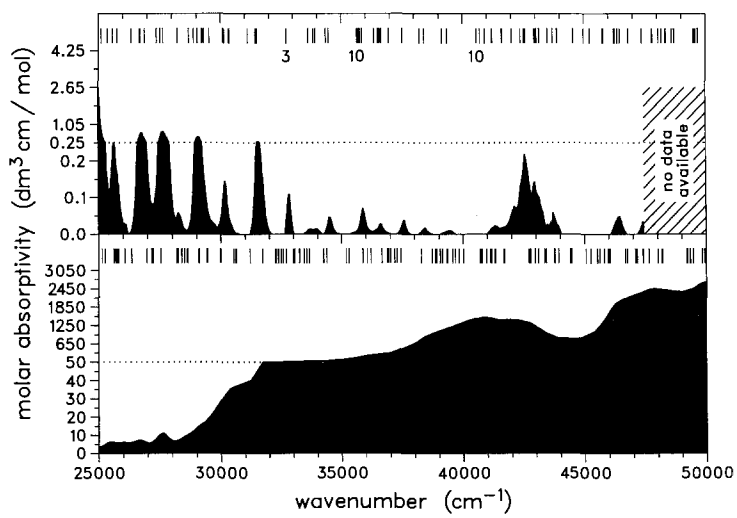

Fig. 8. Observed ultraviolet absorption spectrum and calculated f-state energies of acquated Sm^{3+} (upper panel) and aquated Pu^{3+} (lower panel).

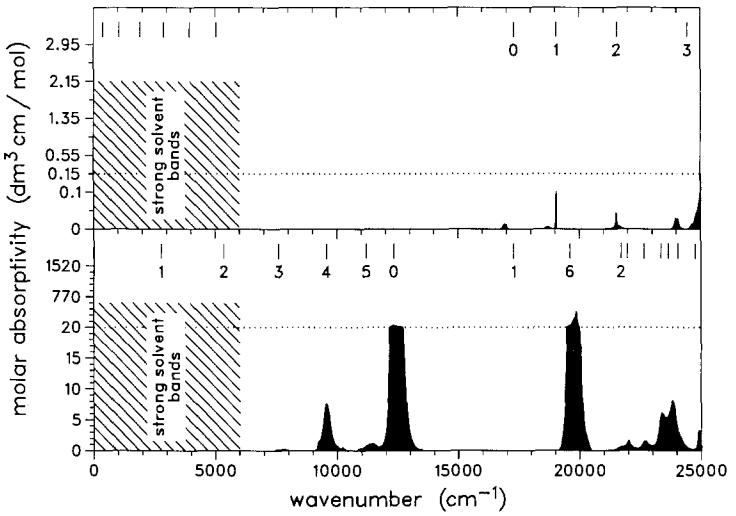

Fig. 9. Observed absorption spectrum (near-infrared to visible) and calculated f-state energies of aquated Eu^{3+} (upper panel) and aquated Am^{3+} (lower panel).

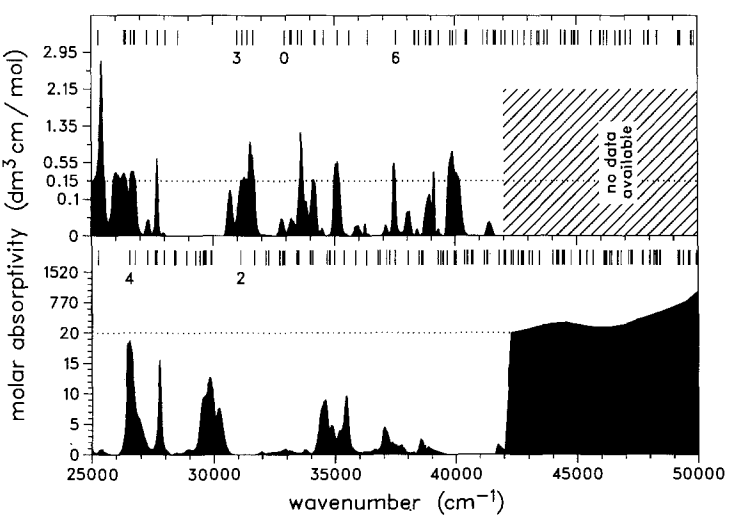

Fig. 10. Observed ultraviolet absorption spectrum and calculated f-state energies of aquated Eu^{3+} (upper panel) and aquated Am^{3+} (lower panel).

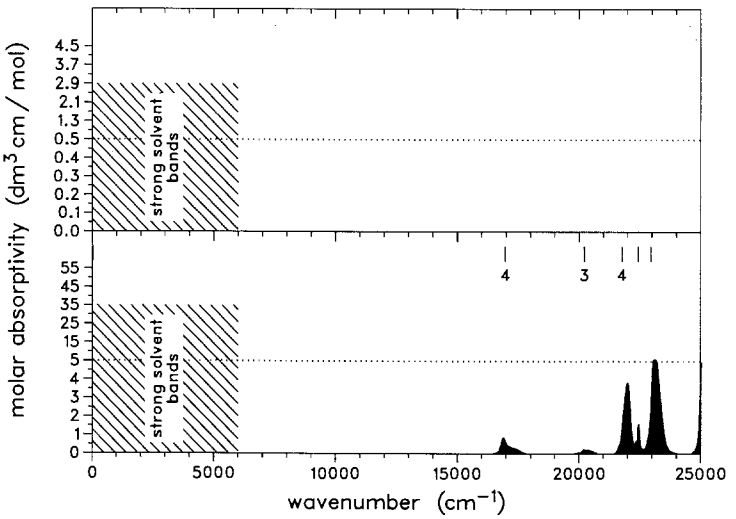

Fig. 11. Observed absorption spectrum (near-infrared to visible) and calculated f-state energies of aquated Gd^{3+} (upper panel) and aquated Cm^{3+} (lower panel).

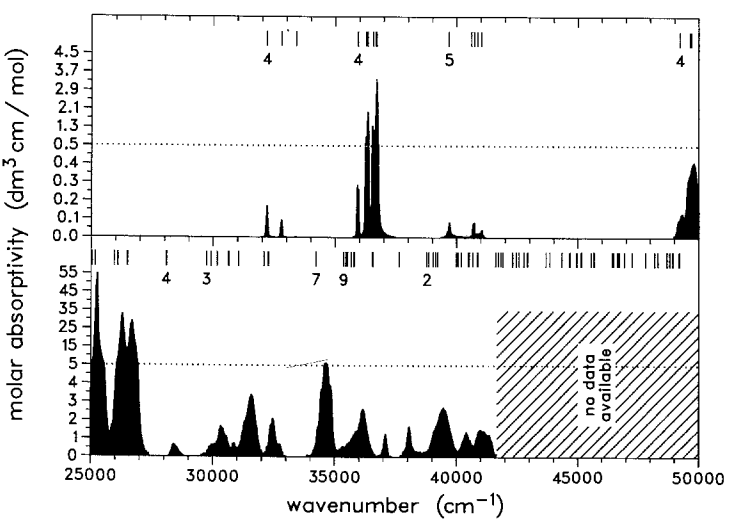

Fig. 12. Observed ultraviolet absorption spectrum and calculated f-state energies of aquated Gd^{3+} (upper panel) and aquated Cm^{3+} (lower panel).

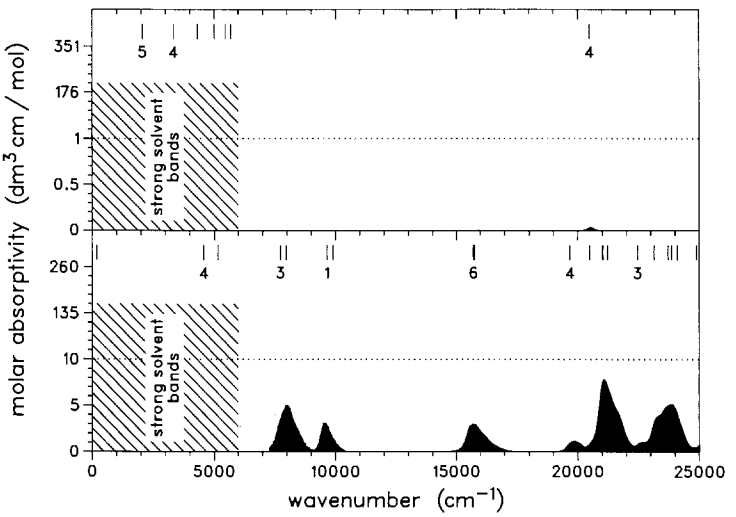

Fig. 13. Observed absorption spectrum (near-infrared to visible) and calculated f-state energies of aquated Tb^{3+} (upper panel) and aquated Bk^{3+} (lower panel).

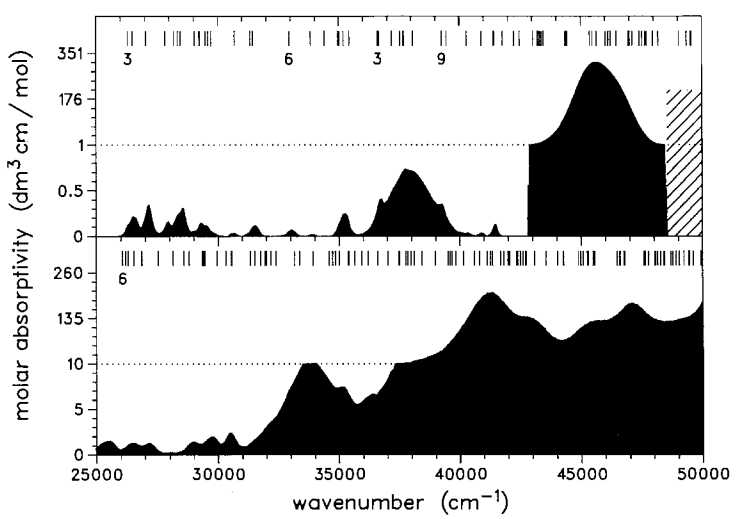

Fig. 14. Observed ultraviolet absorption spectrum and calculated f-state energies of aquated Tb^{3+} (upper panel) and aquated Bk^{3+} (lower panel).

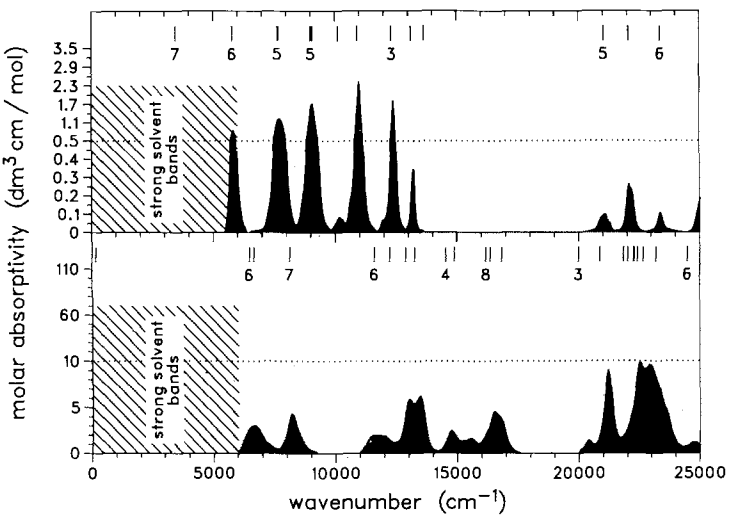

Fig. 15. Observed absorption spectrum (near-infrared to visible) and calculated f-state energies of aquated Dy^{3+} (upper panel) and aquated Cf^{3+} (lower panel).

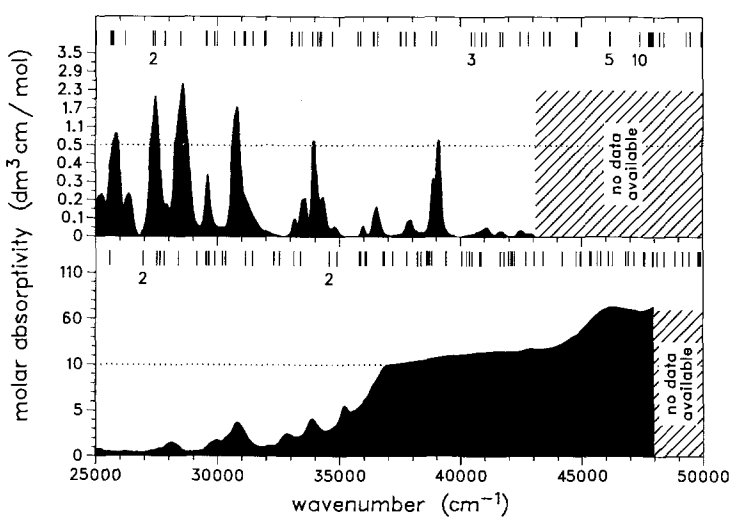

Fig. 16. Observed ultraviolet absorption spectrum and calculated f-state energies of aquated Dy^{3+} (upper panel) and aquated Cf^{3+} (lower panel).

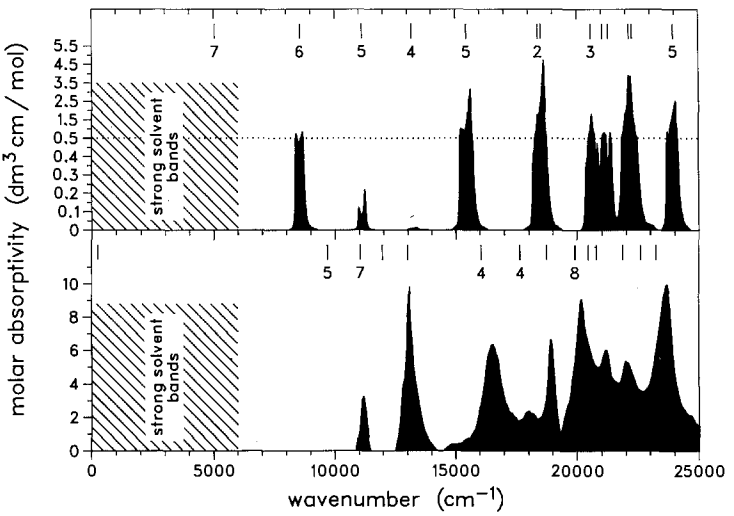

Fig. 17. Observed absorption spectrum (near-infrared to visible) and calculated f-state energies of aquated Ho^{3+} (upper panel) and aquated Es^{3+} (lower panel).

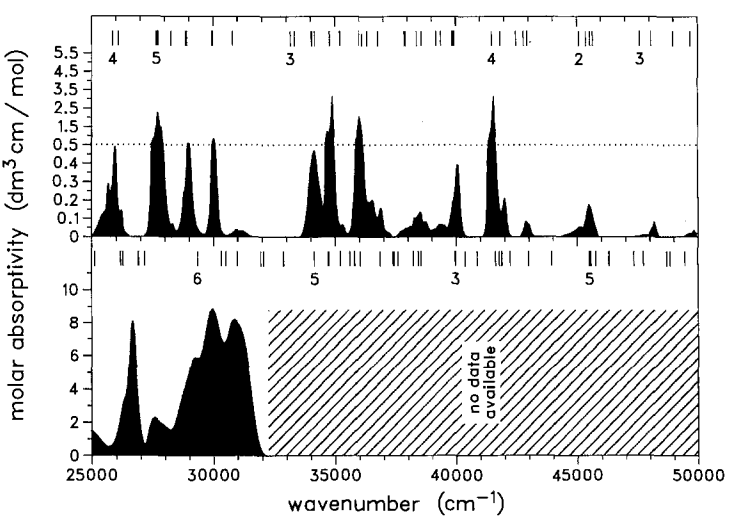

Fig. 18. Observed ultraviolet absorption spectrum and calculated f-state energies of aquated Ho^{3+} (upper panel) and aquated Es^{3+} (lower panel).

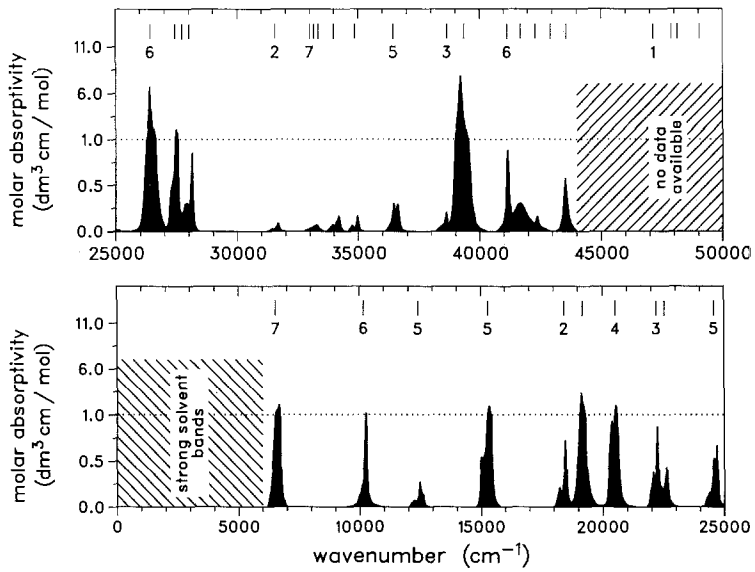

Fig. 19. Observed absorption spectrum (near-infrared to ultraviolet) and calculated 4f-state energies of aquated Er^{3+}.

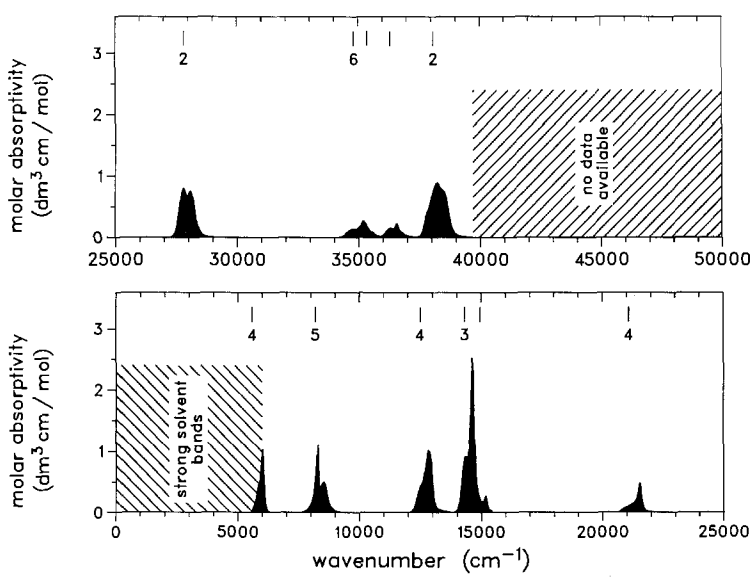

Fig. 20. Observed absorption spectrum (near-infrared to ultraviolet) and calculated 4f-state energies of aquated Tm^{3+}.

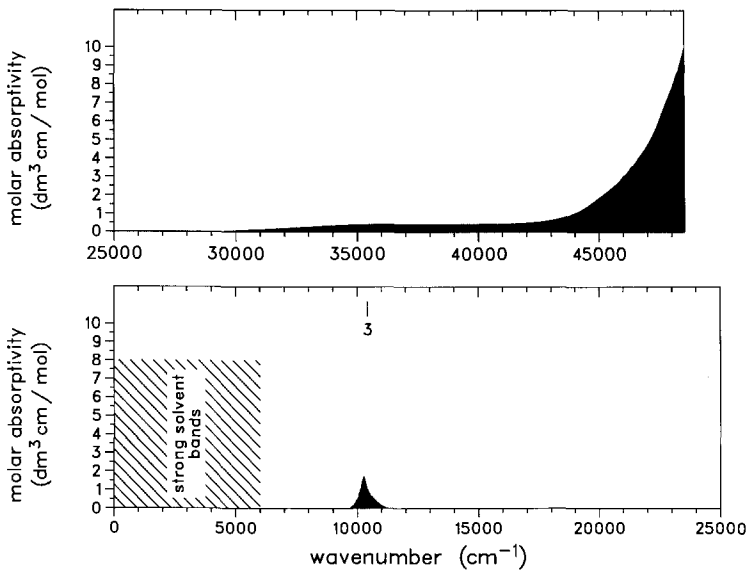

Fig. 21. Observed absorption spectrum (near-infrared to ultraviolet) and calculated 4f-state energies of aquated Yb^{3+}.

deuteration was used to improve optical transmission at long wavelenghts. Data for ions having the same number of f electrons are presented together for comparison purposes. In many cases, a split molar-absorptivity scale has been employed to improve the visibility of weak bands. The transition point for such split scales is shown as a horizontal dotted line. The absorption spectra are presented as a function of wavenumber (cm^{-1}), the traditional spectroscopic unit of energy (note that 8065.491 $cm^{-1} = 1eV$). At energies below about 6000 cm^{-1} (shown shaded by diagonal lines), strong interference from solvent absorption bands prevented recording f-state bands. To facilitate comparison, spectral data are plotted using the same energy ranges. Diagonal line shading is used to denote those high-energy regions where no spectral data are available. Broad underlying absorption in the ultraviolet has been subtracted from the reported absorption spectra of Cm^{3+} (Carnall and Rajnak 1975) and Es^{3+} (Carnall 1986) to improve the definition of f–f absorption bands. No absorption spectra have been reported for Pa^{3+} in solution, presumably due to the chemical instability of Pa^{3+}. No optical spectra are available for elements heavier than Es. Lanthanide-ion absorption bands are often said to provide a "fingerprint" for the element. It is evident from figs. 5–18 that the same can be said of the absorption spectra of trivalent actinide ions.

Comparing the absorption spectra of lanthanide and actinide ions having the same number of f electrons, the most striking differences occur in molar absorptivity at the light end of the actinide series. For example, in fig. 3, approximately 100-fold larger molar-absorptivity values are evident for U^{3+} bands whose widths are comparable to those of Nd^{3+}. Actinide-ion band molar absorptivities generally decrease across the

actinide series to Am^{3+}. For Cm^{3+} and heavier actinides, molar absorptivities become more or less constant but continue to remain larger, in general, than for heavy lanthanides.

3. Theoretical treatment of f-state spectra

For 3+ lanthanide and actinide ions, almost all transitions within the f shell are electric dipole in nature. These transitions are formally parity (Laporte) forbidden. That such transitions are observable is attributed to non-centro-symmetric terms in the crystal-field Hamiltonian. Such terms have the effect of mixing higher-lying, opposite-pairty d and g states into the f shell. As Judd (1988) noted in a review of atomic theory and optical spectroscopy of rare earths: "No doubt that we shall eventually be able to calculate much of what we want with a high degree of accuracy. That day has not yet arrived.".

3.1. *Application of atomic theory*

While accurate, direct calculation of f-state energy structure is not generally feasible for lanthanide and actinide ions, parametric models for f-state energy-level structure determination have been developed that take advantage of relationships established by relativistic Hartree–Fock calculations (Crosswhite and Crosswhite 1984). Works by Cowan (1981) and Szasz (1992) should be consulted for additional information on theoretical atomic spectroscopy and relativistic Hartree–Fock calculations.

Carnall et al. (1989) used such a parametric model to carry out systematic analysis of the 4f-state energy-level structure and crystal-field parameters of trivalent lanthanides (except Pm^{3+}) doped into LaF_3. Carnall (1992) extended such systematic modeling to the 5f-state energy-level structure and crystal-field parameters of trivalent actinide ions from U^{3+} through Es^{3+} doped into $LaCl_3$. These workers calculated f-state energy-level structure based on an effective-operator Hamiltonian using a single configuration model. The atomic part of the model is corrected for interaction of the f^N-configuration with all other configurations by treating such interactions as effective interactions within the f^N-configuration. The resulting Hamiltonian is

$$H = H_0 + \sum_{k=0}^{6} F^k(nf,nf)f_k + \zeta_f A_{SO} + \alpha L(L+1) + \beta G(G_2) + \gamma G(R_7)$$

$$+ \sum_{i=2,3,4,6,7,8} t_i T^i + \sum_{h=0,2,4} m_h M^h + \sum_{f=2,4,6} p_f P^f + \sum_{k,q,i} B_q^k (C_q^k)_i, \qquad (1)$$

where H_0 involves the kinetic energy of the electrons and their interaction with the nucleus and k is even. The F^k (Slater parameters) and ζ_f (spin–orbit coupling constant) represent the electrostatic and spin–orbit integrals, their coefficients, f_k and A_{SO}, being the angular parts of those respective interactions. Two- and three-body interactions are introduced to account for the effects of configuration interaction. Two-body operators are parameterized by α, β, and γ (often referred to as generalized

Trees parameters) with L being the total orbital angular momentum. $G(G_2)$ and $G(R_7)$ are Casimir's operators for groups G_2 and R_7, respectively. Three-body operators are denoted by t_i with corresponding parameters, T^i. Two-body pseudo-magnetic operators are denoted as p_j with corresponding parameters, P^j. The Marvin integrals, M^h, represent spin–spin and spin–other-orbit relativistic corrections. The last summation in the above equation represents the crystal-field interaction in which B_q^k are crystal-field parameters and C_q^k are spherical tensors of rank k that depend on the coordinates of the ith electron. The summation involving i is over all f electrons of the ion of interest. Equation (1) is used to calculate the expected energies of crystal-field split states. The values of parameters in eq. (1) are adjusted using a nonlinear least-squares method to obtain the best agreement with experimentally determined and assigned crystal-field levels.

The number of experimentally determined and assigned levels often exceeds the number of free-ion and crystal-field parameters by several fold. Even so, local minima are a significant problem in the least-squares adjustment procedure. The practice is to allow only a fraction of the parameters given in eq. (1) to vary freely. Note that fitting of model free-ion parameters to experimental data recorded in condensed phases results in parameter values that differ from the free-ion values found in atomic spectroscopy studies of lanthanide ions (Goldschmidt 1978) and actinide ions (Freed and Blasse 1986) in the vapor phase. For this reason, the term "free ion" is used to refer to parameters or energy levels determined from studies on ions in condensed phases.

3.2. *Comparison of "free-ion" states and observed spectra*

The energy level differences between 4f states of aquated trivalent lanthanide ions (i.e., the experimentally determined centers of gravity of observed 4f–4f bands), are quite similar to those deduced from studies of the same ions doped into $LaCl_3$ (Dieke 1968, Morrison and Leavitt 1982) or LaF_3 (Carnall et al. 1989) as Carnall (1979) stressed in his review of lanthanide-ion spectroscopy. Expressed in another way, there is little difference between the energy-level structure of "free-ion" 4f states of trivalent lanthanides doped into $LaCl_3$ or LaF_3 and the 4f-state energy-level structure deduced from spectral studies of aquated trivalent lanthanide ions (e.g., see Sinha 1983). A similar situation occurs for 5f bands of aquated trivalent actinide ions in that their centers of gravity occur at energies quite similar to the energy differences between the corresponding 5f-state multiplets of the same actinide ion doped into $LaCl_3$.

A graphic comparison of available aquated trivalent lanthanide- and actinide-ion spectra and "free-ion" f-state energies is made in figs. 1–21. These figures show the calculated f-state energies as short, vertical lines above the absorption bands. Where a significant energy gap exists between two f-states, the J value of the higher-lying of the two states is indicated (J is the quantum number associated with the total angular momentum of all the electrons in the ion). For ions having an odd number of f electrons, the value shown is $J + \frac{1}{2}$. The "free-ion" energies displayed in figs. 1–21 are those determined in systematic interpretations of the spectra of trivalent lanthanide ions doped into LaF_3 (Carnall et al. 1989) and actinide ions doped into $LaCl_3$ (Carnall 1992). Tables 1 and 2 list the values of the "free-ion" parameters used to calculate the f-state energies shown in figs. 1–23. Good agreement between the calculated "free-ion"

TABLE 1

Comparison of energy-level model parameters (in cm^{-1}) used in calculating 3+ lanthanide and actinide "free-ion" energy levels for f^1 through f^7 configurations. Lanthanide parameters are from Carnall et al. (1989) and actinide parameters are from Carnall (1992). *n* denotes the number of 4f or 5f electrons.

	n												
	1	2		3		4		5		6		7	
ion	Ce^{3+}	Pr^{3+}	Pa^{3+}	Nd^{3+}	U^{3+}	Pm^{3+}	Np^{3+}	Sm^{3+}	Pu^{3+}	Eu^{3+}	Am^{3+}	Gd^{3+}	Cm^{3+}
F^2		68 878	32 000	73 018	39 611	76 400	45 382	79 805	48 679	83 125	51 900	85 669	55 055
F^4		50 347	28 000	52 789	32 960	54 900	37 242	57 175	39 333	59 268	41 600	60 825	43 938
F^6		32 901	19 200	35 757	23 084	37 700	25 644	40 250	27 647	42 560	29 400	44 776	32 876
ζ_f	647.3	751.7	1 335	885.3	1 626	1 025	1 937	1 176	2 242	1 338	2 564	1 508	2 889
α		16.23	30	21.34	29.26	20.5	31.78	20.16	30	20.16	26.71	18.92	29.42
β		−566.6	−850	−593	−824.6	−560	−728	−566.9	−678.3	−566.9	−426.6	−600	−362.9
γ		1 371	1 100	1 445	1 093	1 475	840.2	1 500	1 022	1 500	977.9	1 575	500
T^2				298	306	300	200	300	190	300	150	300	275
T^3				35	42	35	45	36	54	40	45	42	45
T^4				59	188	58	50	56	45	60	45	62	60
T^6				−285	−242	−310	−361	−347	−368	−300	−487	−295	−289
T^7				332	447	350	427	373	363	370	489	350	546
T^8				305	300	320	340	348	322	320	228	310	528
M^0		2.08	0.67	2.11	0.672	2.4	0.773	2.6	0.877	2.1	0.985	3.22	1.097
M^2		1.16	0.38	1.18	0.372	1.3	0.428	1.46	0.486	1.18	0.546	1.8	0.608
M^4		.79	0.25	0.8	0.258	0.91	0.297	0.988	0.388	0.8	0.379	1.22	0.423
P^2		−88.6	1 000	192	1 216	275	1 009	357	949	360	613	676	1 054
P^4		−44.3	500	96	608	138	504.5	178	474.5	180	306.5	338	527
P^6		−8.66	100	19.2	121.6	27.5	100.9	35.7	94.9	36	61.3	67.6	105.4

TABLE 2

Comparison of energy level model parameters (in cm^{-1}) used in calculating 3+ lanthanide and actinide "free-ion" energy levels for f^8 through f^{13} configurations. Lanthanide parameters are from Carnall et al. (1989), and actinide parameters are from Carnall (1992). *n* denotes the number of 4f or 5f electrons.

	n											
	8		9		10		11		12		13	
ion	Tb^{3+}	Bk^{3+}	Dy^{3+}	Cf^{3+}	Ho^{3+}	Es^{3+}	Er^{3+}	Fm^{3+}	Tm^{3+}	Md^{3+}	Yb^{3+}	No^{3+}
F^2	88 995	57 697	91 903	60 464	94 564	63 174	97 483	65 850	100 134	68 454		
F^4	62 919	45 969	64 372	48 026	66 397	50 034	67 904	52 044	69 613	54 048		
F^6	47 252	32 876	49 386	34 592	52 022	36 199	54 010	37 756	55 975	39 283		
ζ_f	1 707	3 210	1 913	3 572	2 145	3 944	2 376	4 326	2 636	4 715	2 928	5 114
α	18.40	29.56	18.02	27.36	17.15	30.21	17.79	30.00	17.26	30.00		
β	−590.9	−564.9	−633.4	−587.5	−607.9	−761	−582.1	−600	−624.5	−600		
γ	1 650	839.8	1 790	753.5	1 800	488.2	1 800	450	1 820	450		
T^2	320	127	329	105	400	110	400	100	400	100		
T^3	40	24	36	48	37	45	43	45				
T^4	50	70	127	59	107	50	73	50				
T^6	−395	−388	−314	−529	−264	−256	−271	−300				
T^7	303	525	404	630	316	648	308	640				
T^8	317	378	315	270	336	408	299	400				
M^0	2.39	1.213	3.39	1.334	2.540	1.458	3.86	1.587	3.81	1.72		
M^2	1.34	0.672	1.9	0.738	1.420	0.807	2.16	0.878	2.13	0.951		
M^4	0.908	0.468	1.29	0.514	0.965	0.562	1.47	0.612	1.45	0.662		
P^2	373	667	719	820	605	506	594	600	695	600		
P^4	187	333.5	360	410	303	253	297	300	346	300		
P^6	37.3	66.7	71.9	82	60.5	50.6	59.4	60	69.5	60		

f-states of trivalent lanthanide ions and their observed aquated ion f–f absorption bands is visually evident when considering isolated "free-ion" states and their associated absorption bands. Strong absorption at ultraviolet wavelengths is often attributed to f→d transitions although in the case of easily oxidized ions, such as U^{3+}, metal-to-ligand charge-transfer states likely contribute as well. In many cases, particularly for the light actinides, it is clear that the f states occur in such close proximity that the observed absorption bands consist of contributions from several f states. In a few of the near-infrared absorbing bands of aquated U^{3+} (fig. 3), some systematic deviation evidently occurs between the calculated "free-ion" states and the centers of gravity of absorbing bands.

It may happen that a predicted band is too weak to be evident in recorded absorption spectra. This is the case in fig. 9 for the Am^{3+} $^7F_0 \rightarrow {}^5D_1$ band whose center of gravity is calculated to occur at 17271 cm^{-1}. This absorption band is expected to be very weak on theoretical grounds (Carnall and Wybourne 1964). However, confirmation of the energy of the $^5D_1$ state is available from fluorescence studies on aquated Am^{3+} (Beitz et al. 1986, Yusov 1990) and on Am^{3+} in a heavy-metal glass at 10 K (Valenzuela and Brundage 1990) that position the $^5D_1$ state within 100 cm^{-1} of its calculated energy. The absorption bands of Es^{3+} that are expected to be centered at 9701 and 11963 cm^{-1} (see fig. 17) are additional instances in which no absorption band is evident at the calculated "free-ion" state energy. Carnall et al. (1973) presented intensity calculations indicating that these bands should be very weak in absorption; experimental data on Es^{3+} doped into $LaCl_3$ at low temperature have identified all of the expected crystal-field components of both of these states (Carnall 1992). These Am^{3+} and Es^{3+} examples serve as reminders of the synergism that has occurred between energy-level structure and transition-intensity calculations for trivalent lanthanide and actinide ions. In addition, analysis of transition intensities can provide a basis for quantifying the relative contributions of individual "free-ion" states to an observed absorption band and so further aid in assigning aquated ion spectra.

The entire energy range of calculated "free-ion" f states is shown in fig. 22 for trivalent lanthanide ions and in fig. 23 for trivalent actinide ions. Several features are evident in comparing figs. 22 and 23. Actinide ions tend to have a somewhat more open energy-level structure near their ground states but a less open energy-level structure for higher-lying states. This arises from larger spin–orbit coupling parameters, but reduced Slater parameter values in the actinide series when parameter values for actinide and lanthanide ions having the same number of f electrons are compared (see tables 1 and 2). For mid-series lanthanide and actinide ions, it is evident that many or even most f states occur at energies corresponding to vacuum-ultraviolet or shorter wavelength light (i.e., at energies where little observed data on f-state energies exist). The present lack of relevant experimental data prevents assessment of the accuracy of the calculated energies for such very high lying f states.

3.3. *Transition intensities*

Using a theory independently developed by Judd (1962) and Ofelt (1962), observed strengths of absorption bands can be understood systematically in terms of a param-

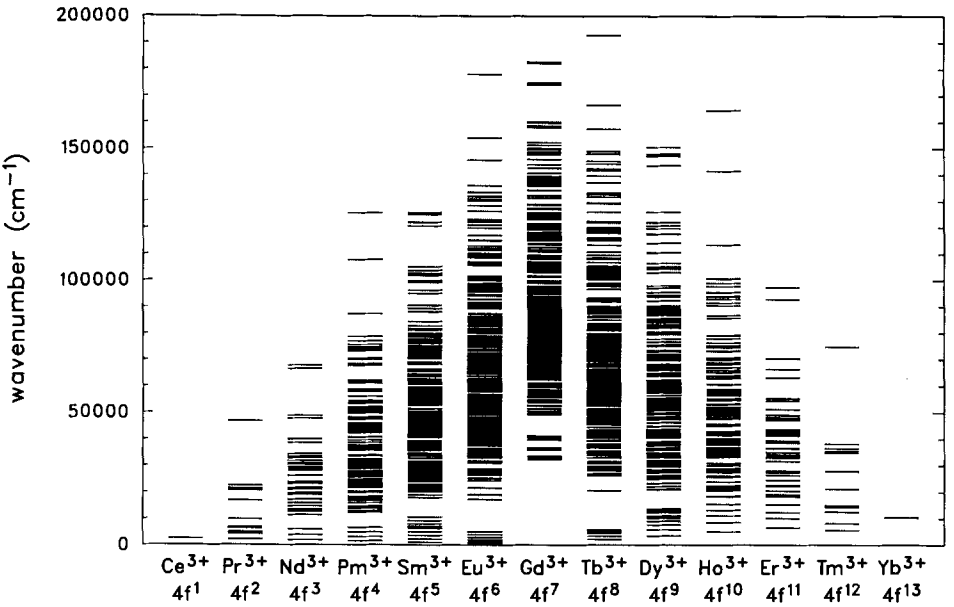

Fig. 22. Calculated "free-ion" energy-level structure of 4f states of trivalent lanthanide ions [energy-level data from Carnall et al. (1989)].

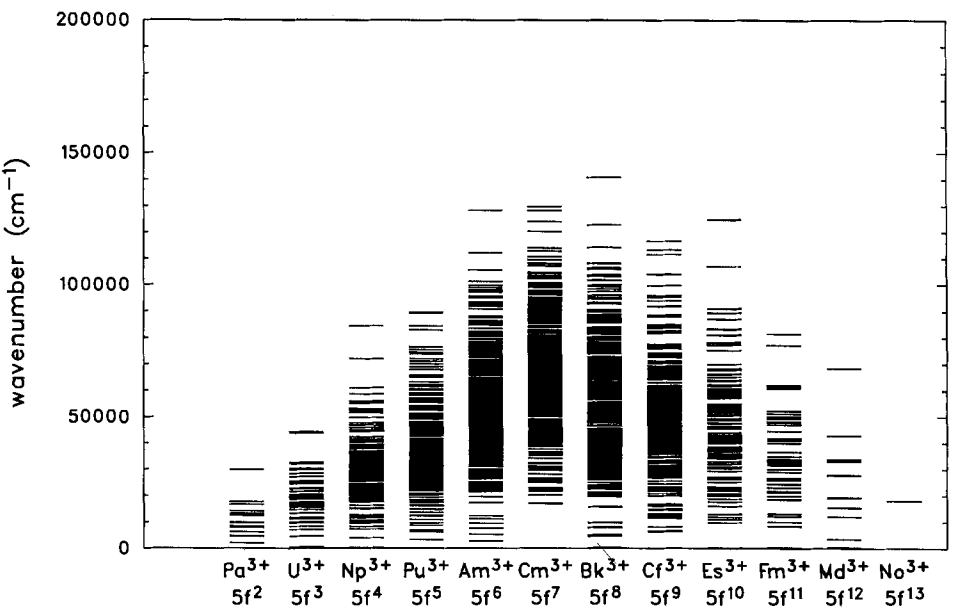

Fig. 23. Calculated "free-ion" energy-level structure of 5f states of trivalent actinide ions [energy-level data from Carnall (1989b)].

eterized model. This model has come to be termed the Judd–Ofelt model. The oscillator strength, P, of an absorption band is defined as the area under the band envelope as normalized to the concentration of the absorbing ion and the path length of the light through the absorbing medium. The experimentally determined oscillator strength can be related to electric- and magnetic-dipole contributions by the relationship (Condon and Shortley 1963)

$$P = \frac{8\pi^2 mc\sigma}{3he^2(2J+1)}\left[\frac{(n^2+2)^2}{9n}\bar{F}^2 + n\bar{M}^2\right], \tag{2}$$

where m is the mass of the electron, c is the speed of light, σ is the energy of the transition, h is the Planck constant, e is the charge of the electron, $\bar{F}$ and $\bar{M}$ are the electric-dipole and magnetic-dipole matrix elements, respectively, that connect the initial state, J, to the final state, J', and n is the index of refraction of the medium.

Only a few observed transitions of 3+ lanthanides and actinides have any significant magnetic-dipole character. For such transitions, the $\bar{M}^2$ values can be obtained from knowledge of the eigenvectors of the initial and final states. The magnetic-dipole contribution to the oscillator strength of f–f absorbing transitions has been calculated for 3 + lanthanide ions (Carnall et al. 1968a) and 3+ actinide ions (Carnall 1989b). Judd–Ofelt theory has been used to compute $\bar{F}^2$ via the relationship

$$\bar{F}^2 = e^2 \sum_{k=2,4,6} \Omega_k (\Psi J \| U^{(k)} \| \Psi' J')^2, \tag{3}$$

where $U^{(k)}$ is a unit tensor operator of rank k and Ω_k are three parameters that, in practice, are evaluated from measured band intensities. On theoretical grounds, these parameters involve the radial parts of the f-shell wave functions, the wave functions of interacting configurations such as those of higher-lying d and g states, and the interaction of the metal ion and the ligands surrounding it.

Interest in obtaining Judd–Ofelt model parameters often arises when intensities are required for transitions not ordinarily observable in absorption, such as from a fluorescing state to a lower lying state that is not the ground state. In fluorescence, the purely radiative rate of relaxation of an excited state, (ΨJ), to a particular lower state, $(\Psi' J')$, is the Einstein A coefficient, which, following Axe (1963), can be expressed as

$$A(\Psi J, \Psi' J') = \frac{64\pi^4\sigma^3}{3h(2J+1)}\left[\frac{n(n^2+2)^2}{9}\bar{F}^2 + n^3\bar{M}^2\right], \tag{4}$$

where the terms are as defined in eq. (2) above.

Transition-intensity analysis has proven to be a useful adjunct in assigning the states giving rise to spectrally overlapped absorption bands of lanthanide and actinide ions (see e.g., Carnall et al. 1984). Such bands are usually resolved into their constituent absorbing transitions by assuming that the underlying lines follow a modified Gaussian–Lorentzian form described by Carnall et al. (1968a). Analyses of this type have resulted in values of Ω_k for all aquated trivalent lanthanides (Carnall 1979) and many aquated trivalent actinides (Carnall and Crosswhite 1985a, b). These values are graphically compared in fig. 24. As Carnall (1979) observed, the Ω_k values for trivalent

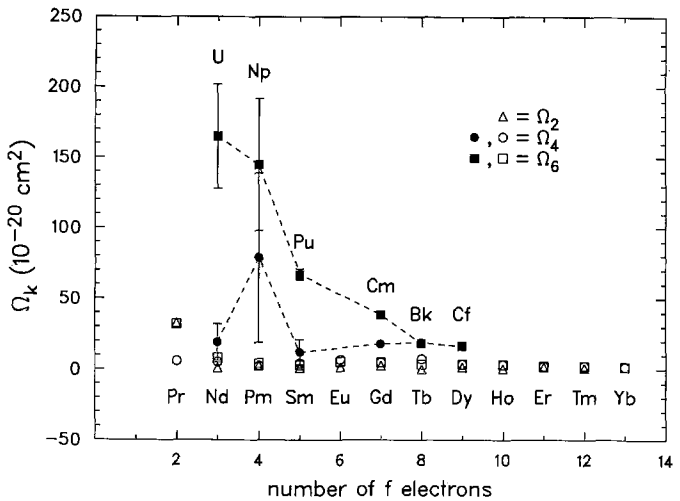

Fig. 24. Comparison of reported Judd–Ofelt theory parameters for aquated trivalent lanthanide ions (open symbols) and actinide ions (solid symbols, error limits shown, data points connected by broken line). Lanthanide data are taken from Carnall (1979), actinide data from Carnall and Crosswhite (1985b), based on fixing the value of Ω_2 at 1×10^{-20} cm^2.

lanthanides become essentially constant for elements heavier than Nd. A similar effect may be discerned in the actinide values beginning at Cf. Based on trends in Ω_k values, Carnall (1986) has argued that Am^{3+} and Cm^{3+} probably play roles similar to Pr^{3+} and Nd^{3+} among lanthanide ions. The comparatively large estimated errors for light actinide Ω_k values result from fitting to a small database (i.e., from the difficulty in determining oscillator strengths for more than a handful of 5f states for light actinides). In a qualitative sense, the large Ω_k values for light actinides can be attributed to the interaction of 5f electrons of these ions with d-electron states (Carnall 1986).

3.4. *Hypersensitive bands*

Although trivalent lanthanide- and actinide-ion f–f transitions usually are regarded as being insensitive to the nature of coordinated ligands, a few absorption bands of such ions do exhibit distinct sensitivity. These transitions satisfy the same selection rules as electric-quadruple radiation and have come to be termed hypersensitive transitions. Judd (1962) noted that large values of $(\Psi J || U^{(2)} || \Psi' J')^2$, generally symbolized as $U^{(2)}$, correlated with lanthanide-ion bands whose intensity differed significantly between chloride and nitrate solutions. Other early theories concerning this effect are presented by Peacock (1975). Henrie et al (1976) found a linear correlation of ligand basicity with oscillator strength for hypersensitive transitions of lanthanide ions and suggested a mechanism for hypersensitivity involving metal–ligand covalency via charge-transfer levels. Misra and Sommerer (1991) have reviewed

absorption spectra of lanthanide ions with an emphasis on hypersensitive transitions as well as transitions of Pr^{3+} and Nd^{3+} that arise from what these authors term "ligand-mediated pseudo-hypersensitivity". The literature is not in agreement as to which f–f bands should be considered hypersensitive [compare the entries in table 2 of Peacock (1975) to those in table 1 of Henrie et al. (1976)]. Carnall et al. (1968b–e) list $U^{(2)}$ values for Pr^{3+} through Yb^{3+}. Values of $U^{(2)}$ for 5f–5f transitions of the actinide ions from U^{3+} through Md^{3+} have been reported by Carnall (1992) in his analysis of the spectra of trivalent actinides in $LaCl_3$. Table 3 lists the term symbol, transition energy (based on "free-ion" energies), and $U^{(2)}$ values (if larger than 0.01 or hypersensitive) for trivalent lanthanide and actinide ions.

If one excludes states that give rise to absorption bands at 1.4 μm or longer wavelength (i.e., states obscured by solvent absorption in H_2O solutions) and states of Pm^{3+} (rarely studied because of the radioactivity of Pm isotopes), it is evident from table 3 that a $U^{(2)}$ value of 0.2 or larger for a lanthanide-ion absorption band correlates with that band being hypersensitive. No experimental absorption spectra are available for Fm^{3+} or Md^{3+}; U^{3+} is so easily reduced that studies on it in aqueous solution are very difficult and few have been reported. Assuming that one also can exclude the $^5G_2$ state of Np^{3+} and the $^6H_{13/2}$ state of Cf^{3+} (on the grounds of scarcity of reported solution absorption studies on these ions), then the same relationship holds for trivalent actinide ions: a $U^{(2)}$ value of 0.2 or larger correlates with that actinide-ion band being hypersensitive. As is evident from the data shown in table 3 for the bands of Pr, Nd, Sm, Eu, Dy, and Am that are considered to be hypersensitive by Henrie et al. (1976), a value of $U^{(2)} < 0.2$ does not preclude a band from being hypersensitive. For ions having the same number of f electrons, the data in table 3 show considerable correlation between a lanthanide $S\ L\ J$ state that has a larger $U^{(2)}$ value and the magnitude of the $U^{(2)}$ value of the corresponding actinide $S\ L\ J$ state. For example, the state of Dy^{3+} (a $4f^9$ ion) that has largest $U^{(2)}$ value is $^6F_{11/2}$; the state of the corresponding $5f^9$ ion, Cf^{3+}, that has the largest $U^{(2)}$ value is also $^6F_{11/2}$. Judd (1988) commented on the status of theoretical efforts to explain hypersensitivity. He suggests that the conclusion of Peacock (1975) that various mechanisms combine or interfere to different degrees under varying experimental conditions may still be valid.

3.5. *Vibronic bands*

Spectral bands of an aquated lanthanide ion arising from vibronic contributions were reported first by Haas and Stein (1971) in their study of the emission spectrum of aquated Gd^{3+}. These bands are termed vibronic because they arise from a simultaneous change in the electronic state of the metal ion and the vibrational state of a coordinated ligand. Stavola et al. (1981) noted additional examples of such bands and presented a theoretical model based on the importance of electronic factors for calculating the intensities of lanthanide-ion vibronic transitions. Their theoretical model also predicts selection rules for such transitions. The intensities of observed bands assigned by these workers as being vibronic typically were at least 50 times weaker than the parent purely electronic band. Faulkner and Richardson (1979) have

TABLE 3

Listing of absorption bands with calculated $U^{(2)} > 0.01$ for aquated trivalent lanthanide ions (Carnall et al. 1968a–e) to 50 000 cm^{-1} and trivalent actinides in $LaCl_3$ (Carnall 1989b)[a] to 31 000 cm^{-1} with data for experimentally observed hypersensitive bands (Henrie et al. 1976)[b] shown in bold type.

Lanthanide ion[c]	Excited state	Transition energy (cm^{-1})	Calculated $U^{(2)}$	Actinide ion[c]	Excited state	Transition energy (cm^{-1})	Calculated $U^{(2)}$
Pr^{3+}				Pa^{3+d}			
($^3H_4$)	$^3H_5$	2322	0.1095				
	$^3F_2$	5149	0.5089				
	$^3F_3$	6540	0.0654				
	$^3F_4$	6973	0.0187				
	$^1D_2$	**16 840**	**0.0026**				
	$^3P_2$	**22 535**	**~0**				
Nd^{3+}				U^{3+}			
($^4I_{9/2}$)	$^4I_{11/2}$	2007	0.0194	($^4I_{9/2}$)	$^4I_{11/2}$	4563	0.0214
	$^4G_{5/2}$	**17 167**	**0.8979**		$^2H_{9/2}$	9631	0.0544
	$^2G_{7/2}$	17 333	0.0757		$^4F_{5/2}$	9921	0.2016
	$^4G_{7/2}$	**19 103**	**0.0550**		$^4G_{5/2}$	11 220	0.7029
					$^4F_{7/2}$	11 518	0.0392
					$^4G_{7/2}$	13 297	0.0884
					$^2K_{13/2}$	16 133	0.0346
					$^2I_{11/2}$	21585	0.0134
Pm^{3+}				Np^{3+}			
($^5I_4$)	$^5I_5$	1577	0.0246	($^5I_4$)	$^5I_5$	3954	0.0192
	$^5G_2$	17 857	0.7215		$^5I_6$	7231	0.0134
	$^5G_3$	18 256	0.1444		$^5F_2$	8197	0.2275
	$^3G_3$	21 102	0.0228		$^3H_4$	10 752	0.0215
					$^5F_3$	11 588	0.0114
					$^5G_2$	11 853	0.4629
					$^5G_3$	12 732	0.1493
					$^3K_6$	15 087	0.0150
					$^3D_2$	18 424	0.0141
					$^3H_5$	21 809	0.0184
					$^3F_2$	22 595	0.0145
Sm^{3+}				Pu^{3+}			
($^6H_{5/2}$)	$^6H_{7/2}$	1080	0.2062	($^6H_{5/2}$)	$^6H_{7/2}$	3327	0.1312
	$^6H_{9/2}$	2290	0.0256		$^6H_{9/2}$	6254	0.0541
	$^6F_{1/2}$	6397	0.1939		$^6F_{3/2}$	6745	0.1481
	$^6F_{3/2}$	6641	0.1444		$^6F_{5/2}$	6751	0.0144
	$^6F_{5/2}$	7131	0.0332		$^6F_{1/2}$	6925	0.1513
	$^4D_{1/2}$	**26 573**	**0.0001**		$^4I_{9/2}$	17 471	0.0222
Eu^{3+}				Am^{3+}			
($^7F_0$)	$^7F_2$	1018	0.1375	($^7F_0$)	**$^7F_2$**	**5350**	**0.0961**
	$^5D_2$	**21 499**	**0.0008**		**$^5D_2$**	**21 709**	**0.0065[e]**
					$^5G_2$	**21 961**	**0.0112[e]**
Gd^{3+f}				Cm^{3+}			
($^8S_{7/2}$)				($^8S_{7/2}$)	$^6D_{5/2}$	20 208	0.0108
					$^6I_{9/2}$	22 949	0.0115
					$^6D_{7/2}$	28 078	0.0191
					$^6D_{5/2}$	30 644	0.0137

TABLE 3 (continued)

Lanthanide ion[c]	Excited state	Transition energy (cm^{-1})	Calculated $U^{(2)}$	Actinide ion[c]	Excited state	Transition energy (cm^{-1})	Calculated $U^{(2)}$
Tb^{3+}				Bk^{3+}			
($^7F_6$)	$^7F_5$	2112	0.5376	($^7F_6$)	$^7F_5$	4566	0.1373
	$^7F_4$	3370	0.0889		$^7F_4$	5156	0.4901
					$^5H_5$	21 020	0.0121
					$^5H_7$	21 036	0.0429
					$^5I_6$	26 071	0.0164
					$^5F_4$	26 529	0.0155
					$^5L_7$	26 858	0.0103
Dy^{3+}				Cf^{3+}			
($^6H_{15/2}$)	$^6H_{13/2}$	3506	0.2457	($^6H_{15/2}$)	$^6F_{11/2}$	6453	0.8901
	$^6H_{11/2}$	5833	0.0923		$^6H_{13/2}$	8103	0.2098
	$^6F_{11/2}$	**7730**	**0.9387**		$^2H_{11/2}$	11 585	0.1648
	$^4I_{15/2}$	**22 293**	**0.0073**		$^6H_{15/2}$	16 172	0.0258
	$^4G_{11/2}$	23 321	0.0004		$^4K_{17/2}$	20 869	0.0798
	$^4K_{17/2}$	26 365	0.0109		$^4I_{13/2}$	23 176	0.0616
					$^4K_{15/2}$	27 614	0.0143
					$^4I_{15/2}$	29 135	0.0176
					$^4H_{11/2}$	29 517	0.0398
					$^4H_{13/2}$	30 306	0.0178
Ho^{3+}				Es^{3+}			
($^5I_8$)	$^5I_7$	5116	0.0250	($^5I_8$)	$^5I_7$	11 039	0.0188
	$^3K_8$	21 308	0.0208		$^5I_6$	**13 009**	**0.5686**
	$^5G_6$	**22 094**	**1.5201**		$^3K_8$	19 904	0.0779
	$^3H_6$	**27 675**	**0.2155**		$^5G_6$	**19 933**	**1.0614**
	$^3L_9$	29 020	0.0185				
	$^3I_7$	38 470	0.0157				
Er^{3+}				Fm^{3+}			
($^4I_{15/2}$)	$^4I_{13/2}$	6610	0.0195	($^4I_{15/2}$)	$^2H_{11/2}$	10 037	0.7517
	$^4I_{11/2}$	**9256**	**0.7125**		$^4I_{11/2}$	21 365	0.7534
	$^4G_{11/2}$	**26 496**	**0.9183**				
	$^2K_{15/2}$	27 801	0.0219				
Tm^{3+}				Md^{3+}			
($^3H_6$)	$^3F_4$	5811	0.5375	($^3H_6$)	$^3F_4$	3500	0.5828
	$^3H_5$	8390	0.1074		$^3H_5$	15 487	0.1048
	$^3H_4$	**12 720**	**0.2373**		$^3H_4$	19 088	0.2177
	$^1G_4$	21 374	0.0483				
	$^1I_6$	34 886	0.0106				

[a] The principal SLJ component of the state is given as a label only. In many cases, the state has $< 50\%$ of the indicated character.

[b] Bands experimentally observed to be hypersensitive are included even if the calculated value of $U^{(2)}$ is < 0.01.

[c] Ground-state term symbol is shown in parantheses.

[d] No calculations reported (Carnall 1989b) for this ion.

[e] It is not known whether only one or both of these two states is hypersensitive.

[f] No bands have $U^{(2)} > 0.01$ and no observed bands are reported (Henrie et al. 1976) to be hypersensitive.

published a vibronic-coupling model for magnetic-dipole intensities of f–f transitions of octahedral complexes of lanthanides. Their model predicts that phonon-assisted (i.e., vibronic) magnetic-dipole lines will have intensities 100–1000 times weaker than pure (i.e., zero phonon) magnetic-dipole lines and phonon-assisted electric-dipole lines. It seems clear that these small intensities justify neglecting vibronic bands in carrying out Judd–Ofelt model analyses of the absorption spectra of aquated lanthanide ions. No vibronic bands built on 5f states of aquated actinide ions have been reported.

4. Luminescence of trivalent-ion f states

The sharp features in the emission spectra of lanthanide ions in solution and solid phases has long fascinated and challenged spectroscopists. The terms fluorescence and luminescence are used interchangeably in this chapter when referring to emission of light from f states of lanthanide and actinide ions. Fundamental concepts related to emission of light are defined before comparing experimental and theoretical studies of the luminescence of trivalent ions of these f-transition metals.

4.1. *Radiative and nonradiative decay rates*

The total purely radiative decay rate of state (ΨJ), symbolized as $A_T(\Psi J)$, is given by

$$A_T(\Psi J) = \sum_{\Psi' J'} A(\Psi J, \Psi' J'), \tag{5}$$

where the sum runs over all states lower in energy than the fluorescing state. The ratio of the integrated intensity of a particular fluorescing transition, $(\Psi J) \rightarrow (\Psi' J')$, to the integrated total fluorescence intensity of the emitting state is given by $A(\Psi J, \Psi' J')/A_T(\Psi J)$. This quantity, termed the branching ratio, can be calculated using Judd–Ofelt theory and is often comparatively simple to measure. The purely radiative lifetime, τ_r, of state (ΨJ) is inversely related to the total purely radiative rate by the expression

$$\tau_r(\Psi J) = \frac{1}{A_T(\Psi J)}. \tag{6}$$

The value of $\tau_r(\Psi J)$ is also referred to as the spontaneous emission rate. In dilute systems, at sufficiently low excited ion density and when the excited f state does not interact with a metastable ligand excited state, a simple relationship exists between the observed f-state luminescence lifetime and the radiative and nonradiative decay rates of that state. For a particular emitting state, (ΨJ), the inverse of its observed lifetime, $\tau_{obs}(\Psi J)$, is the sum of the purely radiative decay rate of that state and its total nonradiative decay rate, $W_T(\Psi J)$,

$$\frac{1}{\tau_{obs}(\Psi J)} = A_T(\Psi J) + W_T(\Psi J). \tag{7}$$

The fluorescence quantum yield of state (ΨJ) is given by the ratio $\tau_{obs}(\Psi J)/\tau_r(\Psi J)$. For simplicity in the following discussion, we delete the state label, (ΨJ), from these and other quantities related to emitting state dynamics.

For f states of many lanthanide ions doped into insulating solids, W_T can be related to the energy gap, ΔE, between the emitting state and the next lower lying state by the expression

$$W_T = Ce^{\alpha \Delta E}, \tag{8}$$

where C and α are constants characteristic of a particular medium (Riseberg and Moos 1968). The underlying relaxation mechanism is transfer of energy from an f-electron state to phonons in the medium surrounding the ion. The relationship shown in eq. (8) is often referred to as an "energy-gap law" expression. When this relationship holds, a plot of $\ln(W_T)$ versus ΔE gives the value of C and α as the slope and the y-axis intercept, respectively.

4.2. *Experimental observations*

As Carnall (1979) observed, early studies of the luminescence spectra of lanthanide ions in solution revealed similar patterns of emission wavelength and intensity in comparison with studies of the same ions in crystalline compounds. Mid-series lanthanide ions (Eu^{3+}, Gd^{3+} and Tb^{3+}) fluoresced strongly while much weaker fluorescence was found from Sm^{3+} and Dy^{3+}. Other lanthanide ions fluoresce poorly at best from excited f states. Such a ranking of lanthanide ions is to some degree arbitrary as many factors, including the degree to which excitation light is adsorbed by the ion of interest, influence fluorescence intensity. Among trivalent actinide ions, only Cm^{3+} has been observed to fluoresce strongly in aqueous solution. Despite weak fluorescence, studies of 5f-state fluorescence from some other trivalent actinide ions at sub-microgram levels are feasible when the excitation source is a high-brightness tunable laser. Current studies of luminescence from f states of lanthanide and actinide ions in solution commonly employ pulsed tunable lasers as excitation sources and exploit time-gated fluorescence detection to avoid interference from short-lifetime luminescing species.

4.2.1. *Lanthanide ions*

Early efforts to achieve an understanding of the factors influencing the luminescence decay of 4f states of trivalent lanthanides in solution include the pioneering work of Kropp and Windsor (1965). These workers examined changes in fluorescence intensity and lifetimes of Eu^{3+} and Tb^{3+} as a function of solvent composition, including use of D_2O, and studied the effect of dissolved oxygen and temperature. Kropp and Windsor (1965) concluded that radiationless deactivation of lanthanide ions occurs via loss of energy to hydrogen-stretching vibrations and that such loss is proportional to the number of hydrogen vibrations in the immediate environment of the ion. Heller (1965) reported that the quenching of 4f-state luminescence intensity of Sm^{3+}, Eu^{3+}, Tb^{3+} and Dy^{3+} in D_2O depended linearly on added H_2O. This effect, and related data, were interpreted as providing evidence that quenching of 4f states

was due to the O–H bond in coordinated water molecules rather than due to entire molecular species such as H_2O, HDO, $H_2O \cdot nD_2O$, etc.

Stein and Wurzberg (1975) correlated fluorescence yields of trivalent Pr, Sm, Eu, Gd, Tb, Dy, and Tm ions in H_2O and D_2O solutions in terms of a single variable, the energy gap between the fluorescing f state and the next lower lying f state. In addition, Haas et al. (1973) invoked a "junction" mechanism involving thermal population of the next state above the emitting level to explain the temperature dependence of Gd^{3+} and Eu^{3+} luminescence. These and many other early studies on the dynamics of 4f states of lanthanide ions have been reviewed (Carnall 1979, Sinha 1983). Buno-Core et al. (1990) have reviewed quenching processes that influence excited states of lanthanide ions and chelates in solution.

In the case of Eu^{3+} $^5D_1 \rightarrow {}^5D_0$ nonradiative decay, Marcantonatos et al. (1984) concluded that energy transfer occurs primarily to the bending mode of coordinated H_2O due to the smallness of the energy gap in comparison with the energy of the stretching vibrational modes of H_2O. As noted by Carnall (1979), the nonradiative decay of Gd^{3+} is unexpectedly large relative to the appreciable energy gap involved. The spectral and dynamics studies of Marcantonatos et al. (1986) provide an explanation for the behavior of Gd^{3+}. They interpret the nonradiative decay of the $^6P_{7/2}$ state of Gd^{3+} as arising from excited aquated Gd^{3+} losing two inner-sphere coordinated water molecules and subsequent conversion of the resulting hexa-coordinated species to a hydrolyzed species that forms an exciplex.

Dissolved oxygen gas is generally regarded as being unimportant in studies on dynamics of lanthanide-ion excited 4f states in solution (see, e.g., Kropp and Windsor 1965). However, two reports provide evidence that quenching of 4f states by dissolved oxygen does occur. Beitz and Sullivan (1989) reported that dissolved oxygen reduced the $^5D_0$ state lifetime of Eu^{3+} in an extractant complex in a chlorinated hydrocarbon solvent. Darmanyan et al. (1991) report that the rate parameter for oxygen quenching of the $^5D_0$ state of complexed Eu^{3+} in CCl_4 solution is 4.7×10^4 dm^3/(mol s). These workers directly identified the energy transfer product, excited singlet O_2, by its luminescence at 1.27 μm.

4.2.2. *Actinide ions*

In reviewing solution fluorescence data for aquated actinide ions in order of increasing atomic number, it should be noted that no solution luminescence has been reported from trivalent actinide ions lighter than Am^{3+}. Using a laser-induced fluorescence (LIF) method, Beitz et al. (1986) reported the first observation of fluorescence from aquated Am^{3+}. Yusov (1990) subsequently reported lifetime data for aquated Am^{3+} in H_2O and D_2O as well as Am^{3+} in organic solvents and complexed Am^{3+} in aqueous solutions. Yusov and Fedoseev (1991) investigated solution chemiluminescence of Am^{3+} following reduction of higher Am oxidation states.

Detailed investigation of 5f-state emission from trivalent curium ions in solution began with studies by Gutmacher et al. (1964). These workers observed autoradioluminescence (i.e., luminescence arising from energy released in radioactive decay, also termed self-luminescence) of Cm^{3+} in concentrated LiCl solution. Beitz and Hessler (1980) reported the first fluorescence spectra and lifetime data for aquated

Cm^{3+}. These workers employed LIF and found a single emission band peaking at 593 nm with estimated quantum yields of 0.03 in H_2O and 0.5 in D_2O. Based on these quantum yields and the known absorption spectrum of aquated Cm^{3+} (Carnall and Rajnak 1975), Beitz and Hessler concluded that aquated Cm^{3+} should be detectable at the level of 3×10^{-10} mol/dm^3 using a simple laser-induced fluorescence apparatus employing single-photon counting. Yusov et al. (1986a) determined that the luminescence of Cm^{3+} is linearly proportional to the D-atom fraction in mixtures of H_2O and D_2O. Subsequently, Yusov (1987) carried out autoradioluminescence studies on Cm^{3+} and selected lanthanides in solution. Yusov et al. (1986b) reported observation of chemiluminescence upon reduction of Cm^{4+}, Tb^{4+}, and Pr^{4+} in aqueous solution. Beitz et al. (1988) achieved a LIF detection limit of 8.5 parts per trillion for Cm^{3+} in dilute perchloric acid (1×10^8 Cm^{3+} ions in the laser beam) as well as for Cm^{3+} at near-neutral pH. Beitz (1991) reported LIF studies of complexed Cm^{3+} in H_2O and D_2O. Other recent LIF work on complexed Cm^{3+} includes determination of its interaction with humic and fulvic acids (Moulin et al. 1991), complexation with humic acid from Gorleben groundwater (Kim et al. 1991), and speciation in a variety of solution environments, including bicarbonate and groundwater (Klenze et al. 1991).

Only two studies of transcurium-ion fluorescence in solution have been published. Carnall et al. (1984) measured the absorption spectrum of Bk^{3+}, interpreted its energy-level structure in terms of a free-ion energy-level model, analyzed its absorption band intensities in terms of Judd–Ofelt theory, and reported luminescence lifetime data for aquated Bk^3 in D_2O. Beitz et al. (1983) carried out LIF studies on Es^{3+} in H_2O and D_2O solutions as well as complexed Es^{3+} in an organic phase. No luminescence studies have been reported for actinide elements heavier than Es.

4.3. *Trends in luminescence dynamics*

Energy gaps and observed lifetime data for trivalent aquated lanthanide and actinide ions are listed in table 4. Also shown are purely radiative lifetimes calculated using Judd–Ofelt theory and experimental values reported by Stein and Wurzberg (1975) based on their observed quantum yields and lifetimes. The agreement between calculated and experimental purely radiative lifetimes is not as good as might be desired, reflecting the approximations used in deriving Judd–Ofelt theory and the difficulties in measuring fluorescence quantum yields. Using the data in table 4, one can obtain fluorescence quantum-yield values for aquated ions by dividing the observed lifetime in H_2O (i.e., τ_{H_2O}) or D_2O (i.e., τ_{D_2O}) by the purely radiative lifetime for a given ion. For example, using calculated purely radiative lifetime data, the fluorescence quantum yield of Cm^{3+} in H_2O is 0.05 and that of aquated Tb^{3+} in H_2O is 0.044. Figure 25 compares the observed nonradiative decay rate, W_T, of trivalent hydrated lanthanide and actinide ions as a function of energy gap, ΔE, in D_2O solution at ambient temperature. For consistency, the W_T values were calculated from eq. (7) based on the observed lifetime and calculated purely radiative decay rate data shown in table 4. In fig. 25, it is evident that the lanthanide-ion data systematically deviate from, and the actinide data more closely follow, "energy-gap law" behavior [eq. (8)]. One use for such correlations is prediction of likely candidate ions for future

TABLE 4
Excited state luminescence properties of aqua lanthanide and actinide ions[a].

Ion	Emitting state	Energy gap, $\Delta E(cm^{-1})$[b]	Observed lifetime		Purely radiative lifetime, τ_r	
			τ_{H_2O} (ms)	τ_{D_2O} (ms)	Calculated[e] (ms)	Experimental[d] (ms)
Gd^{3+}	$^6P_{7/2}$	32 194	2.3[d]	(1.1)[d]	10.9	13
Cm^{3+}	$^6D_{7/2}$	16 943	0.065[e]	0.94[e]	1.3	
Tb^{3+}	$^5D_4$	14 804	0.40[d]	3.88[d]	9.02	4.75
Eu^{3+}	$^5D_0$	12 255	0.11[d]	4.00[d]	9.67	5.0
Es^{3+}	$^5F_5$	9456	0.00105[f]	0.0029[f]	2.4	
Sm^{3+}	$^4G_{5/2}$	7438	0.0023[d]	0.054[d]	6.26	1.4
Dy^{3+}	$^4F_{9/2}$	7374	0.0024[d]	0.038[d]	1.85	0.54
Bk^{3+}	$^7F_6$	5815		0.00010[g]	0.50	
Nd^{3+}	$^4F_{3/2}$	5473	0.00003[c]	0.00017[c]	0.42	
Am^{3+}	$^5D_1$	4942	< 0.00040[h]	0.00020[h]	(1.1)[i]	

[a] Estimated values shown in parentheses.
[b] Difference in energy between emitting "free-ion" state and next lower "free-ion" state.
[c] Carnall et al. (1983).
[d] Stein and Wurzberg (1975).
[e] Beitz and Hessler (1980).
[f] Beitz et al. (1983).
[g] Carnall et al. (1984).
[h] Yusov (1990).
[i] Observed lifetime of Am^{3+} in a heavy-metal fluoride glass at 10 K (Valenzuela and Brundage 1990).

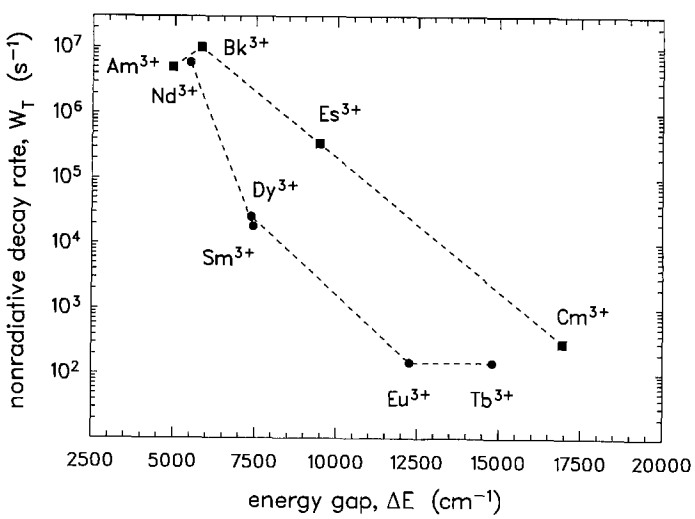

Fig. 25. Nonradiative decay rate of aquated lanthanide and actinide ions in D_2O solution as a function of energy gap (data points are connected by a broken line for clarity).

fluorescence studies. Considering the trends in fig. 4 and the energy gaps evident in fig. 28, it seems likely that luminescence should be observable from aquated Fm^{3+} and Md^{3+} using LIF methods, if these elements become available at the level of at least 10^9 atoms. In addition, it is surprising that studies on the 4f-state dynamics of aquated Yb^{3+} have not been reported.

4.4. *Calculation of nonradiative decay rates*

Accurate calculation of the nonradiative decay rate of trivalent lanthanide ions in aqueous solution has been challenging. An early effory by Terpilovskii (1968) invoked a vibronic coupling model involving all three vibrational modes of H_2O for calculating the lifetimes of Eu^{3+} and Tb^{3+} in H_2O and D_2O. Agreement with observed lifetimes was marginal for Eu^{3+} and poor for Tb^{3+}. Sveshnikova and Ermolaev(1971) and Ermolaev and Sveshnikova (1973) calculated nonradiative decay rates for trivalent Pr, Nd, Sm, Eu, Tb, Dy, and Yb ions in H_2O and methanol using a dipole–dipole energy-transfer model. Their calculated rates were too low in all cases but their calculated deuterium ratios are more in accord with experimental observations. The radiationless decay model of Hass and Stein (1972a, b) provides good agreement for the calculated ratio of OH to OD oscillator deexcitation rates, but only rough agreement for OH deexcitation rates for Sm^{3+}, Eu^{3+}, Tb^{3+} and Dy^{3+}.

Stavola et al. (1981) criticized the model of Haas and Stein on the grounds that deviation from the Born–Oppenheimer approximation is needed to explain the appearance of vibronic bands and an overly simplistic method was used to determine Frank–Condon factors. Unfortunately, Stavola and co-workers did not apply their theory to calculation of nonradiative decay rates of f-electron states. Difficulties in accurately calculating nonradiative decay rates of 4f states of lanthanides have also been encountered in solid-state luminescence studies of lanthanides. Stuck and Fonger (1990) summarize the challenges which they contend remain in achieving a predictive understanding of 4f-state nonradiative decay in solids. Among such challenges is the need to reflect the different levels of forbiddenness of the f-electron transitions involved as a larger energy gap might result in a slightly larger electronic integral. In contrast with lanthanide work, little theoretical work has been reported concerning the nonradiative decay of 5f states of actinide ions in solution. Given the many similarities between 5f states of actinides and 4f states of lanthanides, one might speculate that the underlying factors influencing nonradiative decay are similar between these two series of elements.

4.5. *Hydration and structure of aquated ions*

The use of Eu^{3+} and Tb^{3+} solution-fluorescence lifetime data, in H_2O and D_2O phases, to infer the number of coordinated inner-sphere water molecules has been reviewed by Horrocks and Albin (1984). The information obtained pertains directly to the luminescing state. For arguments concerning applicability to coordination of the metal ion in its ground-state electronic state as well as the rationale for the quoted

accuracy of the method (± 0.5 H_2O molecule) see Horrocks and Albin (1984). Determination of coordinated water molecules based only on lifetime data for complexed lanthanide ions in solution has been reported by Barthelemy and Choppin (1989). Presumably, this method is only applicable when nonradiative decay is almost entirely dominated by inner-sphere coordinated H_2O.

Rizkalla and Choppin (1991) have reviewed lanthanide-ion hydration and hydrolysis studies including those employing fluorescence-based methods. They state that the interpretation of fluorescence studies has not always agreed with that from other techniques such as thermodynamics, X-ray and neutron diffraction, and absorption spectroscopy. Considering information from all techniques, Rizkalla and Choppin concluded that light lanthanides (La^{3+}–Nd^{3+}) form aquated ions having a tricapped trigonal-prismatic structure with nine inner-sphere coordinated water molecules, whereas aquated ions based on heavy lanthanides (Tb^{3+}–Lu^{3+}) evidently have eight coordinated water molecules in a square anti-prismatic structure. Middle-series lanthanides (Nd^{3+}–Tb^{3+}) either assume intermediate structures or a rapid exchange equilibrium exists between both hydrate structures. The latter is likely favored by Marcantonatos et al. (1984) for Eu^{3+} as these workers concluded that the ratio of eight-coordinated aquated Eu^{3+} to nine-coordinated aquated Eu^{3+} is approximately 10 to 1.

In comparison with lanthanide ions, little experimental data concerning hydration of trivalent actinide ions is available. For example, ion mobility studies by Rosch and Khalkin (1990) tend to confirm the hypothesis of "S-shaped" changes in hydration parameters of carrier-free trivalent f-element ions in solution. These workers find that Eu^{3+} and Am^{3+} are the ions that mark the transition when ion mobilities of trivalent lanthanide and actinide ions are plotted versus crystallographic radii. It is clear that additional work is desirable on this point, however, as Rosch and Khalkin obtained actinide-ion mobility data only for Am^{3+} and Cf^{3+}. Beitz (1991) reported fluorescence lifetime data for complexed Cm^{3+} in H_2O and D_2O. He found agreement with the assumption that the correlation between observed fluorescence lifetime and number of coordinated water molecules for Eu^{3+} and Tb^{3+} [reviewed by Horrocks and Albin (1984)] also holds for Cm^{3+}, if one assumes that aquated Cm^{3+} has eight or nine inner-sphere coordinated water molecules. Hay (1991) has used molecular-mechanics methods to calculate the known structures of 58 eight- to twelve-coordinate aquo- and nitrato-complexes of trivalent lanthanide ions with generally good agreement between calculation and the known structure. His approach considers nonbonded interactions between ligand donor atoms and uses a harmonic metal–ligand stretching potential. This method seems likely to be applicable to actinide ions and their complexes.

Spectral evidence on the symmetry of coordinated ligands surrounding lanthanide and actinide ions is available for a few f-element aquated ions. Couture and Rajnak (1985) present evidence that similar 4f-state energy-level structures exist for Er^{3+} in $ErCl_3 \cdot 6H_2O$ and aquated Er^{3+} in fluid and frozen aqueous solution. These workers concluded that aquated Er^{3+} and aquated Gd^{3+} have approximately D_{4d} site symmetry with an inner coordination sphere consisting of eight water molecules. In a spectral study of Nd^{3+} in fluid and frozen aqueous solution, Rajnak and Couture (1981)

concluded that aquated Nd^{3+} has approximately D_{3h} symmetry and its inner coordination sphere consists of nine water molecules. Carnall (1989a) noted the similarity of the 5f-state spectra of Am^{3+} in $AmCl_3$, $Am^{3+}:LaCl_3$, and aquated Am^{3+} in fluid and frozen aqueous solutions. He concluded that the spectra of Am^{3+} in frozen solution is consistent with D_{3h} symmetry implying nine-fold coordination (nine inner-sphere water molecules).

4.6. *Photochemistry*

As might be expected from the formally nonbonding character of f electrons, relatively few photochemical studies have involved excited 4f- or 5f-electron states (Buno-Core et al. 1990). More typical photochemical work on f elements involves excited charge transfer or d-electron states. For example, Haas et al. (1970) investigated the photochemical consequences of exciting a charge-transfer state of Eu^{3+}; Okada et al. (1981) interpreted their study of aquated Ce^{3+} f–d transitions in terms of photoinduced metal–ligand dissociation. Bergamini et al. (1985) have reviewed f-element photochemistry and remarked that the photoreactivity of lanthanide complexes is mostly due to direct electronic excitation of ligand-to-metal charge-transfer states. Polymerization of vinyl compounds via ligand sensitization (i.e., transfer of energy from a metal-ion excited f state to a ligand) is cited as an example of photochemistry involving f-electron states. In a review of applied laser photochemistry, Donohue (1989) cites another example (a Sm^{3+} ligand photosubstitution reaction initiated by f-state excitation). Lanthanide and actinide element separations via photoreduction or photoxidation that are reviewed by Donohue evidently occur from photoactive states that are not f electron in character. No studies of solution photochemistry involving 5f states of trivalent actinide ions have been reported.

4.7. *Selected applications*

The "fingerprint" character of the f-state optical spectra of lanthanide ions has long been used for analytical purposes (see, e.g., Banks and Klingman 1956). The f states of trivalent lanthanide and actinide ions might best be termed "usefully insensitive" to coordinated ligands in that changes in f-state energies generally are large enough that the observed spectra permit determination of complexation but not so large as to make difficult the assignment of the complexed metal-ion bands. Much of the early Soviet work in this area has been reviewed by Panyushkin et al. (1977). A review with an emphasis on hypersensitivity and absorption spectra of complexed Pr^{3+} and Nd^{3+} has been published by Misra and Sommerer (1991).

Historically, fluorescence was viewed as complementing absorption work in determination of energy-level structure for those low-lying f states otherwise obscured by solvent optical absorption. The availability of tunable lasers and multichannel optical detectors permits full exploitation of the ability of laser-induced fluorescence methods to temporally and spectrally discriminate amongst luminescing solution species. Not unexpectedly, therefore, analytical determination of lanthanide and actinide ion species in solution via fluorescence has undergone a resurgence. High sensitivity is

achieved for metal ions with large energy gaps and which have emitting transitions that give rise to visible or near-infrared emission. When analytically acceptable, detection sensitivity often can be improved by tailoring the coordination environment to minimize nonradiative decay and enhance light absorption. For example, high carbonate concentration has been used to minimize nonradiative decay of f states of lanthanide ions (Berthoud et al. 1989) and actinide ions (Decambox et al. 1989) in aqueous solution. A solution detection of limit of 5×10^{-14} mol/dm^3 of Eu^{3+} has been reported using energy transfer from a coordinated ligand and isolation of the complexed lanthanide ion in the interior of a micelle (Hemmliä et al. (1984)). Applications of lanthanide-ion luminescence to studies of cation binding sites of interest in biochemistry have been reviewed by Petersheim (1991). The reviewed applications include studies of chirality via circularly polarized luminescence, investigation of cation binding site heterogeneity in proteins, and metal-ion–metal-ion distance determination by analysis of f-state energy-transfer dynamics.

5. Concluding remarks

The spectroscopy and excited f-state dynamics of trivalent aquated lanthanide and actinide ions are closely related. Changes in f-state energy-level structure are relatively small with variation of coordinated ligands for both of these series of ions. The f-state energy-level structure of these ions is believed to be well-understood, but many predicted f states occur at energies equivalent to vacuum-ultraviolet or shorter wavelengths and have not been observed experimentally. Larger spin–orbit coupling and smaller Slater integrals result in a generally more open energy-level structure near the ground state of trivalent actinides in comparison with trivalent lanthanides, and also reduce energy gaps between higher lying f states. These differences in energy-level structure, combined with larger nonradiative decay rate at a given energy gap, diminish the number of actinide elements whose trivalent ions fluoresce to an observable extent in aqueous solution in comparison with the lanthanide series. However, the solution-fluorescence quantum yield of aquated Cm^{3+} is comparable to that of aquated Tb^{3+}. The intensities of f–f transitions of many aquated trivalent lanthanide and actinide ions have been successfully interpreted via Judd–Ofelt theory. Some reported lanthanide-ion f-state fluorescence quantum yields differ significantly from those expected from transition intensities calculated on the basis of Judd–Ofelt theory and observed fluorescence lifetimes. No directly measured f-state quantum yields are available for trivalent actinide ions. Selected applications of trivalent lanthanide- and actinide-ion solution luminescence have been reviewed.

Acknowledgments

The author gratefully acknowledges many discussions with W.T. Carnall concerning f-electron spectroscopy and is indebted to him for providing most of the data shown in figs. 1–23 in digital form. E.N. Rizkalla and G.R. Choppin are thanked for

providing a preprint of their review of lanthanide hydration and hydrolysis prior to publication.

References

Axe, J.D., 1963, J. Chem. Phys. **39**, 1154.

Banks, C.V., and D.W. Klingman, 1956, Anal. Chim. Acta **15**, 356.

Barthelemy, P.P., and G.R. Choppin, 1989, Inorg. Chem. **28**, 3354.

Beitz, J.V., 1991, Radiochim. Acta **52/53**, 35.

Beitz, J.V., and J.P. Hessler, 1980, Nucl. Technol. **51**, 169.

Beitz, J.V., and J.C. Sullivan, 1989, J. Less-Common Met. **148**, 159.

Beitz, J.V., D.W. Wester and C.W. Williams, 1983, J. Less-Common Met. **93**, 331.

Beitz, J.V., G. Jursich and J.C. Sullivan, 1986, in: Rare Earths 1986, Vol. 1, eds H. Silber, L.R. Morss and L.E. DeLong (Elsevier Sequoia, Lausanne) p. 301.

Beitz, J.V., D.L. Bowers, M.M. Doxtader, V.A. Maroni and D.T. Reed, 1988, Radiochim. Acta **47/48**, 87.

Bergamini, P., S. Sostero and O. Traverso, 1985, f-element photochemistry, in: Fundamental and Technological Aspects of Organo–f-Element Chemistry, eds T.J. Marks and I.L. Fragala (Reidel, Dordrecht) pp. 361–385.

Berthoud, T., P. Decambox, B. Kitsch, P. Mauchien and C. Moulin, 1989, Anal. Chim. Acta **220**, 235.

Bethe, H., 1929, Ann. Phys. **3**, 133.

Bethe, H., and F.H. Spedding, 1937, Phys. Rev. **12**, 454.

Buno-Core, G.E., H. Li and B. Marciniak, 1990, Coord. Chem. Rev. **99**, 55.

Bunsen, R.W., 1866, Pogg. Ann. **128**, 100.

Carnall, W.T., 1973, Absorption and luminescence spectra, in: Gmelin Handbuch der Anorganischen Chemie, Vol. 8, Part A2, ed. G. Koch (Springer, Berlin) ch. 8.2.

Carnall, W.T., 1979, The absorption and fluorescence of rare earth ions in solution, in: Handbook on the Physics and Chemistry of Rare Earths, Vol. 3, eds K.A. Gschneidner Jr and L. Eyring (North-Holland, Amsterdam) ch. 24.

Carnall, W.T., 1986, J. Less-Common Met. **122**, 1.

Carnall, W.T., 1989a, J. Less-Common Met. **156**, 221.

Carnall, W.T., 1989b, A Systematic Analysis of Trivalent Actinide Chlorides in D_{3h} Site Symmetry, Report ANL-89/39 (Argonne National Laboratory, Argonne, IL).

Carnall, W.T., 1992, J. Chem. Phys. **96**, 8713.

Carnall, W.T., and H. Crosswhite, 1985a, Optical spectra and electronic structure of actinide ions in compounds, in: The Chemistry of the Actinide Elements, 2nd Ed., Vol. 2, eds J.J. Katz, G.T. Seaborg and L.R. Morss (Chapman and Hall, London) ch. 16.

Carnall, W.T., and H. Crosswhite, 1985b, Optical Spectra and Electronic Structure of Actinide Ions in Compounds and in Solution, Report ANL-84-90 (Argonne National Laboratory, Argonne, IL).

Carnall, W.T., and K. Rajnak, 1975, J. Chem. Phys. **63**, 3510.

Carnall, W.T., and B.G. Wybourne, 1964, J. Chem. Phys. **40**, 3428.

Carnall, W.T., P.R. Fields and K. Rajnak, 1968a, J. Chem. Phys. **49**, 4412.

Carnall, W.T., P.R. Fields and K. Rajnak, 1968b, J. Chem. Phys. **49**, 4424.

Carnall, W.T., P.R. Fields and K. Rajnak, 1968c, J. Chem. Phys. **49**, 4443.

Carnall, W.T., P.R. Fields and K. Rajnak, 1968d, J. Chem. Phys. **49**, 4447.

Carnall, W.T., P.R. Fields and K. Rajnak, 1968e, J. Chem. Phys. **49**, 4450.

Carnall, W.T., D. Cohen, P.R. Fields, R.K. Sjoblom and R.F. Barnes, 1973, J. Chem. Phys. **59**, 1785.

Carnall, W.T., J.V. Beitz, H. Crosswhite, K. Rajnak and J.B. Mann, 1983, Spectroscopic properties of the f-elements in compounds and solutions, in: Systematics and the Properties of the Lanthanides, ed. S.P. Sinha (Reidel, Dordrecht) ch. 9, pp. 389–450.

Carnall, W.T., J.V. Beitz and H. Crosswhite, 1984, J. Chem. Phys. **80**, 2301.

Carnall, W.T., G.L. Goodman, K. Rajnak and R.S. Rana, 1989, J. Chem. Phys. **90**, 3443.

Condon, E.U., and G.H. Shortley, 1963, The Theory of Atomic Spectra (Cambridge Univ. Press, London).

Couture, L., and K. Rajnak, 1985, Chem. Phys. **85**, 315.

Cowan, R.D., 1981, The Theory of Atomic Structure (University of California Press, Los Angeles, CA).
Crosswhite, H.M., and H. Crosswhite, 1984, J. Opt. Soc. Am. B **1**, 246.
Darmanyan, A.P., N. Lazorchak and P. Jardon, 1991, J. Photochem. & Photobiol. A **58**, 185.
Decambox, P., P. Mauchien and C. Moulin, 1989, Radiochim. Acta **48**, 23.
Dieke, G.H., 1968, Spectra and Energy Levels of Rare Earth Ions in Crystals (Interscience, New York).
Donohue, T., 1989, Applied laser photochemistry in the liquid phase, in: Laser Applications in Physical Chemistry, ed. D.K. Evans (M. Dekker, New York) ch. 4.
Ermolaev, V.L., and E.B. Sveshnikova, 1973, Chem. Phys. Lett. **23**, 349.
Faulkner, T.R., and F.S. Richardson, 1979, Mol. Phys. **38**, 1165.
Fred, M.S., and J. Blasse, 1986, Spectra and electronic structure of free actinide atoms and ions, in: The Chemistry of the Actinide Elements, 2nd Ed., Vol. 2, eds J.J. Katz, G.T. Seaborg and L.R. Morss (Chapman and Hall, London) ch. 15.
Freed, S., 1942, Rev. Mod. Phys. **14**, 105.
Goldschmidt, Z.B., 1978, Atomic properties (free atom), in: Handbook on the Physics and Chemistry of Rare Earths, Vol. 1, eds K.A. Gschneidner Jr and L. Eyring (North-Holland, Amsterdam) ch. 1.
Gutmacher, R.D., E.K. Hulet and J.G. Conway, 1964, J. Opt. Soc. Am. **54**, 1403.
Haas, Y., and G. Stein, 1971, Chem. Phys. Lett. **11**, 143.
Haas, Y., and G. Stein, 1972a, J. Phys. Chem. **76**, 1093.
Haas, Y., and G. Stein, 1972b, Chem. Phys. Lett. **15**, 12.
Haas, Y., G. Stein and M. Tomkiewicz, 1970, J. Phys. Chem. **74**, 2558.
Haas, Y., G. Stein and E. Wurzberg, 1973, J. Chem. Phys. **58**, 277.
Hay, B.P., 1991, Inorg. Chem. **30**, 2876.
Heller, A., 1965, J. Am. Chem. Soc. **88**, 2058.
Hemmliä, I., S. Dakubu, W.-M. Mukkala, H. Siitari and T. Lovgren, 1984, Anal. Biochem. **137**, 335.
Henrie, D.E., R.L. Fellows and G.R. Choppin, 1976, Chem. Rev. **18**, 199.
Horrocks Jr, W.DeW., and M. Albin, 1984, Lanthanide ion luminescence in coordination chemistry and biochemistry, in: Progress in Inorganic Chemistry, Vol. 31, ed. S.J. Lippard (Wiley, New York) ch. 1.
Judd, B.R., 1962, Phys. Rev. **127**, 750.
Judd, B.R., 1988, Atomic theory and optical spectroscopy, in: Handbook on the Physics and Chemistry of Rare Earths, Vol. 11, eds K.A. Gschneidner Jr and L. Eyring (North-Holland, Amsterdam) ch. 74.
Katz, J.J., G.T. Seaborg and L.R. Morss, eds, 1985, The Chemistry of the Actinide Elements, 2nd Ed., Vols. 1, 2 (Chapman and Hall, London).
Kim, J.I., H. Wimmer and R. Klenze, 1991, Radiochim. Acta **53**, 35.
Klenze, R., J.I. Kim and H. Wimmer, 1991, Radiochim. Acta **52/53**, 97.
Kropp, J.L., and M.W. Windsor, 1965, J. Chem. Phys. **42**, 1599.
Marcantonatos, M.D., M. Deschaux and J.-J. Vuilleumier, 1984, J. Chem. Soc. Faraday Trans. II **80**, 1569.
Marcantonatos, M.D., M. Deschaux, J.-J. Vuilleumier, J.-J. Combremont and J. Weber, 1986, J. Chem. Soc. Faraday Trans. II **82**, 609.
Misra, S.N., and S.O. Sommerer, 1991, Appl. Spec. Rev. **26**, 151.
Morrison, C.A., and R.P. Leavitt, 1982, Spectroscopic properties of triply ionized lanthanides in transparent host crystals, in: Handbook on the Physics and Chemistry of Rare Earths, Vol. 5, eds K. A. Gschneidner Jr and L. Eyring (North-Holland, Amsterdam) ch. 46.
Moulin, C., P. Decambox, P. Mauchien, V. Moulin and M. Theyssier, 1991, Radiochim. Acta **52/53**, 119.
Ofelt, G.S., 1962, J. Chem. Phys. **37**, 511.
Okada, K., Y. Kaizu and H. Kobayashi, 1981, J. Chem. Phys. **75**, 1577.
Panyushkin, V.T., Yu.A. Afanas'ev, A.D. Gamovskii and O.A. Osipov, 1977, Russ. Chem. Rev. **46**, 2105.
Peacock, R.D., 1975, Struct. & Bonding **22**, 83.
Petersheim, M., 1991, Luminescent trivalent lanthanides in studies of cation binding sites, in: Biophysical and Biochemical Aspects of Fluorescence Spectroscopy, ed. T.G. Dewey (Plenum, New York) ch. 2.
Prandtl, W., and K. Scheiner, 1934, Z. Anorg. Allgem. Chem. **220**, 107.
Racah, G., 1942, Phys. Rev. **62**, 438.
Rajnak, K., and L. Couture, 1981, Chem. Phys. **55**, 331.
Riseberg, L.A., and H.W. Moos, 1968, Phys. Rev. **174**, 429.
Rizkalla, E.N., and G.R. Choppin, 1991, Hydration and hydrolysis of lanthanides, in: Handbook on the Physics and Chemistry of Rare Earths,

Vol. 15, eds K.A. Gschneidner Jr and L. Eyring (North-Holland, Amsterdam) ch. 103.

Rosch, F., and V.A. Khalkin, 1990, Radiochim. Acta **51**, 101.

Ryan, J.L., 1972, Absorption spectra of actinide compounds, in: MTP International Review of Science, Vol. 7, ed. K.W. Bagnall (Butterworths, London) ch. 9.

Seaborg, G.T., and W.D. Loveland, 1990, The Elements Beyond Uranium (Wiley-Interscience, New York).

Sinha, S.P., 1983, Fluorescence spectra and lifetimes of the lanthanide aquo ions and their complexes, in: Systematics and the Properties of the Lanthanides, ed. S.P. Sinha (Reidel, Dordrecht) ch. 10.

Stavola, M., L. Isganitis and M. Sceats, 1981, J. Chem. Phys. **74**, 4228.

Stein, G., and E. Wurzberg, 1975, J. Chem. Phys. **62**, 209.

Stuck, C.W., and W.H. Fonger, 1990, Understanding Luminescence Spectra and Efficiency Using W_p and Related Functions (Springer, Berlin).

Sveshnikova, E.B., and V.L. Ermolaev, 1971, Opt. & Spektrosk. **30**, 379.

Szasz, L., 1992, The Electronic Structure of Atoms (Wiley-Interscience, New York).

Terpilovskii, D.N., 1968, Opt. & Spektrosk. **24**, 596.

Valenzuela, R.W., and R.T. Brundage, 1990, J. Chem. Phys. **93**, 8469.

Yusov, A.B., 1987, Sov. Radiochem. **29**, 114.

Yusov, A.B., 1990, J. Radioanal. Nucl. Chem. Articles **143**, 287.

Yusov, A.B., and A.M. Fedoseev, 1991, J. Radioanal. Nucl. Chem. **147**, 201.

Yusov, A.B., V.P. Perminov, N.N. Krot and V.P. Kazakov, 1986a, Sov. Radiochem. **28**, 365.

Yusov, A.B., A.M. Fedoseev, V.I. Spitsyn and N.N. Krot, 1986b, Dokl. Phys. Chem. (Engl. Trans.) **289**, 777.

Handbook on the Physics and Chemistry of Rare Earths
Vol. 18 – Lanthanides/Actinides: Chemistry
edited by K.A. Gschneidner, Jr., L. Eyring, G.R. Choppin and G.H. Lander

Chapter 121

SEPARATION CHEMISTRY FOR LANTHANIDES AND TRIVALENT ACTINIDES*

Kenneth L. NASH
Chemistry Division, Argonne National Laboratory, 9700 S. Cass Ave., Argonne, IL 60439–4831, USA

Contents

1. Introduction 198
   1.1. Previous reviews 199
2. Background 200
   2.1. The basics of separation chemistry 200
   2.2. General considerations for lanthanide/actinide separation 201
   2.3. Types of solvent-extraction reactions 201
   2.4. Ion exchange materials 202
   2.5. Reactions contributing to the separation reaction 203
   2.6. Lanthanide/actinide separation 204
   2.7. Characteristics of trivalent lanthanides/actinides which can be exploited in separation 205
3. Basic organization of the chapter 206
4. Relative efficiency of extraction 207
   4.1. Neutral organophosphorus extractants 207
   4.2. Amine extractants 210
   4.3. Acidic extractants 211
      4.3.1. Chelating ligands 211
      4.3.2. Acidic organophosphorus extractants 213
   4.4. Synergistic extraction systems 215
   4.5. Cyclic and linear polyethers in lanthanide/actinide separation 216
5. Medium effects 217
   5.1. Mixed aqueous media in ion exchange 217
   5.2. Salt effects in solvent extraction 218
   5.3. Extraction from alkaline and carbonate media 220
6. Diluent effects in solvent extraction 221
7. Role of aqueous complexation in lanthanide/actinide separation 224
8. The role of soft-donors in lanthanide/actinide separation 229
9. Summary and prospects 231
   9.1. Intra-group separation 231

*Work performed under the auspices of the Office of Basic Energy Sciences, Division of Chemical Sciences, US Department of Energy, under contract number W-31-109-ENG-38.

9.2. Trivalent lanthanide/actinide group separation 233
9.3. Future trends 235
References 236

1. Introduction

Most of the classical applications of the lanthanides require little or no separation of the metal ions. For example, Cotton and Wilkinson (1988a) state that 15% of commercial rare-earth production is as "Misch metal", an alloy of the light rare earths in the proportions in which they occur in the ore. Misch metal is used in steel making and as flints in cigarette lighters. Few large-scale applications require more than partial separation. An interesting summary of the commerce in the rare earths (in 1989) has recently been published in the Rare Earth Minerals and Metals Yearbook (1989).

More recent high-tech developments, e.g., the preparation of high-temperature superconducting oxides, rare-earth permanent magnets, magnetic-resonance contrast agents, and rare-earth phosphors, require fairly to very pure supplies of individual lanthanides. In addition to these very specific applications, essentially all of the scientific advances made in the understanding of the chemistry and material science of the lanthanides have been made because of the availability of pure samples of the individual lanthanides and their salts. Separation chemistry plays a central role to the availability of these pure samples.

Of the rare-earth ores, bastnasite and monazite are typically more concentrated sources for the light rare earths (which are more abundant), while xenotime generally contains relatively higher percentages of the heavy rare earths. The lanthanides are readily separated from matrix elements in the ore dissolution process, or in subsequent precipitation steps. Many approaches have been taken to the successful separation of individual lanthanides. A recent comprehensive review of lanthanide separations (Gmelin 1983) considers the separation of the lanthanides in detail.

The actinides uranium and thorium occur in nature as primordial matter. Actinium and protactinium occur in nature as daughters of thorium and uranium, while small amounts of neptunium and plutonium are present as a result of neutron-capture reactions of uranium. All other members of the series are man-made. Separation chemistry has been central to the isolation and purification of the actinides since their discovery. The formation of the transplutonium actinides was established only as a result of chemical-separation procedures developed specifically for that purpose. The continued application of separation science has resulted in the availability of weighable quantities of the actinides to fermium. Separation procedures are central to "one-atom-at-a-time" chemistry used to identify synthetic trans-actinide (superheavy) elements to element 107 and above (Report of a Workshop on Transactinium Science 1990).

A serious limiting factor in the continued development of nuclear power is the disposal of the high-level radioactive waste. One strategy for reducing the volume of

radioactive wastes requiring burial in a geologic repository is to transmute (or fission) the actinides into shorter-lived fission products in a nuclear reactor or by bombardment with accelerator produced neutrons. Typical fission yields include significant amounts of the lanthanides. Unfortunately, some of the lanthanides have very high neutron absorption cross sections, and thus act as neutron poisons, absorbing neutrons and reducing the efficiency of the transmutation process. Separation of the lanthanides from the actinides is therefore critical.

The separation of the lanthanides from thorium, uranium, plutonium, and neptunium can fairly readily be achieved by exploiting the greater extractability of the higher oxidation states of the light-actinide elements. However, the transplutonium actinides do not have stable higher oxidation states. In this case, separation of the lanthanide fission products from the transplutonium actinides must exploit the small differences in the solution chemistry of the lanthanides and actinides in the trivalent oxidation state. It is the separation of the lanthanides from the trivalent actinide cations that is the focus of this chapter.

1.1. *Previous reviews*

The topic of lanthanide/actinide separation has been reviewed previously, either in topical reviews, or as a part of a more general discussion of separation processes. The classic reference book for separation chemistry (both ion exchange and solvent extraction) has long been Marcus and Kertes (1969). In this book, the theory and practice of separation science is discussed in great detail. Solvent extraction separations chemistry was reviewed by Sekine and Hasegawa (1977). In addition to concentrating on solvent extraction, this work differs from Marcus and Kertes in that it references many more specific examples. Unfortunately, such encyclopedic coverage did not permit review of lanthanide/actinide separation (or any other individual topic) in detail. The unique theoretical aspects of ion exchange separation have been discussed by Helferrich (1962).

Recently, two "how-to" manuals have been published which describe in detail useful ion exchange separation procedures for the lanthanides and actinides (Handbook of Ion Exchange Resins, Volumes 1 and 2). As noted above, the separation chemistry of the lanthanides (ion exchange and solvent extraction) has been reviewed in a volume of Gmelin (1983). The latter review discusses very capably the more subtle aspects of lanthanide separation, performing the usual division of the work along the lines of solvent extraction–ion exchange.

On the topic of lanthanide/actinide separation, few reviews have dealt in detail with the most difficult aspect of this field, separation of the lanthanides from the trivalent transplutonium actinides. Jenkins (1979, 1984) reviewed ion exchange applications in the atomic-energy industry. Relatively short sections of these reviews dealt with the separation of the trivalent metal ions. Symposium volumes entitled "Actinide Separations" (Navratil and Schulz 1980) and "Lanthanide/Actinide Separations" (Choppin et al. 1985) are collections of papers from several authors covering all aspects of lanthanide/actinide separation, some of which deal with the purification of the trivalent metal ions.

The one review which treats lanthanide/trivalent actinide separation is that of Weaver (1974). Weaver's review is an excellent, if somewhat dated, source for a comprehensive discussion of solvent extraction separations of the lanthanides and trivalent actinides. Weaver discusses many of the historical aspects of lanthanide/actinide separation, and considers both the successes and failures in the separation of trivalent lanthanides and actinides.

In the present chapter, the recent literature is evaluated and the results discussed with greater emphasis on the reasons for success (or failure) of various separation strategies based on the solution chemistry involved in the inherently difficult separation of metal ions of such similar properties as the trivalent lanthanides and actinides.

2. Background

2.1. *The basics of separation chemistry*

Of typical separations methods, those based on volatility (like distillation) are of little importance in lanthanide/actinide separations. Precipitation methods and other biphasic separations processes are by far the most useful. For the separation of macroscopic amounts of the individual lanthanides, fractional crystallization was the principal technique in the early days of the investigation of the lanthanides. The small solubility differences required hundreds or even thousands of repetitions to achieve useful separation of the elements (Moeller 1963).

The inability of lanthanide production by fractional precipitation techniques to maintain pace with demand for lanthanide metals and compounds led to the development of first ion exchange and subsequently solvent extraction processes for the isolation of these metal ions. Although these methods also require elaborate recycle plans for efficient production of individual lanthanide compounds, they are much more effective than precipitation methods, and have largely replaced them.

In the processing of nuclear materials, precipitation/coprecipitation techniques are used for the separation of the actinides from most fission products. Both fluoride and oxalate complexes of these metal ions are sufficiently insoluble to accomplish this separation (Stary 1966). Coprecipitation with bismuth phosphate has also been used for this purpose (Stary 1966). Because of their insensitivity to subtle changes induced by minor cation-radius changes, such techniques are not useful for the separation of the lanthanides from the trivalent actinide metal ions.

Analytical methods based on coprecipitation techniques are used to determine the oxidation-state speciation of the light actinides, which can occur in solution in multiple oxidation states. An example of such a separation is the ability to selectively remove tri- and tetravalent actinide cations from penta- and hexavalent species by coprecipitation with lanthanide fluoride (Choppin 1985). Lanthanide fluoride coprecipitation has been used to perform oxidation-state identification in ground-water samples (e.g., Nash et al. 1988). There are numerous other examples of the application of the coprecipitation technique to environmental samples.

To accomplish the more difficult separation of trivalent lanthanides and actinides (individually and collectively), by far the most useful methods are ion exchange and

solvent extraction. Ion exchange and solvent extraction reactions offer the opportunity to exploit a variety of chemical effects resulting from the lanthanide/actinide radius contraction with increasing atomic number. These procedures are built around many different absorbing/extracting materials along with a wide range of solvation/complexation effects which can be exploited to enhance separation. It is important to note that energy differences of only 400–1800 joules/mole are required for a successful solvent extraction or ion exchange separations process[1]. These two methods provide the primary focus for the following discussion.

2.2. *General considerations for lanthanide/actinide separation*

The separation process in both ion exchange and solvent extraction consists, in its most elementary form, of the transfer of a (typically) charged metal ion (or complex), from a polar aqueous phase to an immiscible phase (with different solvating properties) with concomitant charged naturalization. The effectiveness of any separation process is a function of the ability of the reactions to accomplish phase transfer (because without phase transfer, there can be no separation), and the relative affinity of the counterphase for the species to be separated. In the case of the trivalent lanthanides and actinides, the latter aspect must exploit the slight differences in ionic radii and covalency of the metal ions. It is conceivable that differences in rate of reaction could be utilized, but such data are much more difficult to obtain, and few examples of kinetic-based separations are extant.

2.3. *Types of solvent-extraction reactions*

There are two basic types of solvent extraction reactions which are applied to metal-ion separations, those based on metal-complex solvation and those based on metal-ion complexation. A third extraction method, observed only with quaternary amine extractants, involves ion-pair formation between an anionic, aqueous complex and the positively charged, organic-soluble quaternary amine. Extraction by quaternary amines incorporates aspects of both basic processes. The development and use of extractants for actinide separations have been discussed by Shoun and McDowell (1980).

For extraction methods based on solvation processes, a neutral complex is formed, generally in the aqueous phase, and most often with the conjugate base of a strong acid (NO_3^-, Cl^-). The neutral complex generally exhibits some degree of hydrophobicity[2]. The absence of formal charge of the complex results naturally in a tendency to seek a less-polar medium (generally the organic phase). Solvating reagents in the organic solution interact with such complexes across an interfacial zone to

[1] If the distribution ratios for the species to be separated differ by a factor of 100 (e.g., $D_1 = 10$, $D_2 = 0.1$) the separation will be 99% efficient in one contact. Assuming that the extraction mechanism is the same for the two species, the free energy for the separation process is $\Delta G = -RT \ln (D_1/D_2)$. The net energy difference required is only 11.4 kJ/mol (or 2.7 kcal/mol), comparable to the bond energy for a single hydrogen bond. Even lower energy differences are required if multiple stages can be used.

[2] The term "hydrophobic" is used in this review to indicate metal complexes more soluble in less polar media (like organic solvents), hence it refers to extracted (or extractable) species.

complete transfer of the metal complex to the counter phase. Some examples of solvating ligands are amines (predominantly secondary or tertiary), neutral organophosphorus compounds (phosphates, phosphonates, phosphinates, and phosphine oxides), ethers and ketones. The extraction strength of the reagent is directly proportional to its Lewis-base strength.

The second type of solvent extraction reagent forms complexes with the water-soluble metal ion essentially by a cation exchange process. These complexants may be partially miscible in both phases (e.g., acetylacetone, and various crown ethers), but the most effective extractants of this type have minimal solubility in the aqueous phase. This characteristic necessitates that critical complex formation reactions must occur in or near the interfacial zone. Studies of the kinetics of such reactions typically indicate that the addition of the first ligand is often the rate-determining step in the reaction. Some examples of reagents of this type are the various β-diketones (e.g., thenoyltrifluoroacetone, isopropyltropolone), acidic organophosphorus compounds (phosphates, phosphonates, and phosphinates), carboxylic acids, sulfonic acids, and pyrazolones. The sulfonates and acidic organophosphorus extractants have much in common with cation exchange resins, and are often called liquid cation exchangers.

By combining an acidic extractant with a solvating extractant increased distribution ratios are often observed. A typical system would match a relatively weak chelating agent like TTA with a strong Lewis base solvating extractant like trioctylphosphine oxide (TOPO). Though no single mechanism describes this "synergistic" extraction system, expansion of the inner coordination sphere of the extracted metal complex or replacement of waters of hydration is the most common explanation for the effect. Ultimately the enhanced extraction must be ascribed to increased hydrophobicity of the final complex. The effectiveness of synergistic extraction systems in lanthanide/trivalent actinide separations is discussed in section 4.4.

2.4. *Ion exchange materials*

For cation exchange, both organic polymers and very insoluble inorganic materials can be utilized as the counter phase. The basic reactions involve "exchange" of (most often) hydrogen ions or alkali cations for polyvalent metal ions from the aqueous (or mixed aqueous/organic) solution. Electroneutrality must be maintained in the resin phase, as it is in the less polar organic phase in solvent extraction separations, so three equivalents of monovalent cations must be released when the trivalent lanthanide/actinide is bound by the resin.

Although the most common cation exchange material is based on benzene sulfonic acid functional groups, various other functional groups (phosphonate, carboxylate) have also been examined. Recent results by Choppin and Ohene-Aniapam (1983) indicate little difference in the sorption of Ce, Eu and Cm on Biorex 70 carboxylic acid resin. Mathur and Khopkar (1985) suggest that the chelating resin Dowex A-1 (functional group–iminodiacetic acid) may have some potential for Am/Cm or Am/Eu separation, but more extensive applications in lanthanide/actinide separation do not appear promising. A few examples exist for the use of inorganic ion exchangers for the separation of the trivalent lanthanide (Li and Yu 1987, Gmelin 1983), but no

examples of trivalent lanthanide/actinide separation based on inorganic ion exchangers were found.

Anion exchange materials are positively charged organic polymers containing methylpyridine or quaternary amine groups which represent the primary isolation pathway. For resin materials of this type to work, the metal ion must be in a medium having a sufficient concentration of a complexing ligand which forms anionic complexes with the subject metal ion. The formal negative charge of the metal complex is neutralized by the cationic amino group on the resin to form the basis of phase transfer. This sequence is exactly analogous to that of quaternary ammonium ion solvent extractants. A key characteristic of anion exchange separation in the presence of aqueous complexants is that both the phase-transfer reaction and aqueous complex formation reactions work in concert to enhance separation within the groups.

2.5. *Reactions contributing to separation reactions*

The sequence of reactions in the separation process is generally the same for both solvent extraction and ion exchange reactions. The principal difference between the two methods lies in the solvation of the hydrophobic complex in solvent extraction, which does not occur in ion exchange separation. In ion exchange separation, the resin effectively creates a second aqueous phase in which differences in aqueous-solvation processes are observed. An outline of these basic reactions follows.

Assuming that the metal cation enters the process in the aqueous phase with the immiscible phase as its target destination, it must first be made hydrophobic, at least in solvent extraction. This requires that the metal ion (or, in the case of the solvating extractants, the metal complex) must be at least partially dehydrated. This principle is violated only by the surfactant-type extractants which create hydrophilic zones (micelles) within the bulk hydrophobic environment. The basic process is outlined in equations (1) and (2).

$$\mathrm{R\,(H_2O)_9^{3+} \rightleftarrows R\,(H_2O)_{9-x}^{3+} + \mathit{x}\ H_2O,} \tag{1}$$

$$\mathrm{R\,(H_2O)_9^{3+} + \mathit{l}\ L\,(H_2O)_y^{-} \rightleftarrows RL_{\mathit{l}}\,(H_2O)_{9+ly-z}^{3-l} + \mathit{z}\ H_2O.} \tag{2}$$

[Typical first coordination sphere hydration numbers for the lanthanides and actinides are 8–10 (Nash and Sullivan 1991), 9 is selected here for illustrative purposes only]. For the extraction of the metal ion by solvating extractants (requiring neutral or anionic complexes), dehydration in reaction (2) must be near complete. This reaction sequence is also relevant for chelating extractants which exhibit significant miscibility in the aqueous phase (e.g., acac and various crown ethers). For ligands which form more hydrophilic complexes with the metal ions, complete dehydration is not observed, and the complex-formation reaction effectively opposes phase transfer. This characteristic is often exploited in lanthanide/actinide separation.

In the case of the acidic or chelating extractants with low aqueous solubility, dehydration can be considered to occur in the interfacial zone as a result of the complexation reaction to form the neutral, lipophilic complex

$$\mathrm{R\,(H_2O)_9^{3+} + 3HEx_i \ \rightleftarrows\ (R(Ex)_3\,(H_2O)_{\mathit{x}})_i + 3H^+ + (9-\mathit{x})\ H_2O.} \tag{3}$$

The subscript i indicates species existing in the interface. Complete dehydration of the metal ion is not required, but is often assumed.

The final step in the extraction process completes the transition to a hydrophobic species by transferring the neutral interfacial complex to the bulk organic phase with accampanying rearrangement of the solvent to stabilize the new complex in the counter-phase. How much rearrangement is necessary is a function of the structure of the hydrophobic complex, and the solvating ability of the counter-phase. If a solvating extractant is present simultaneously with a chelating extractant, the free energy for the synergistic enhancement usually is generated in the solvation step of the overall reaction. Solvation effects of this type are not relevant to ion exchange separation processes. Modification of the aqueous phase (e.g., by the addition of alcohol or high salt concentrations) can play a role in ion exchange processes, but that effect is more relevant to the dehydration reactions described above in equation (1).

For just the simplified series of processes outlined there are a variety of interactions which may be manipulated to take advantage of the slight differences in lanthanide/actinide reaction rates and equilibria to achieve the desired separation. The short list includes various types of solid sorbent materials (both inorganic and organic), several different classes of organic soluble complexants (extractants), the diluent (solvent) of the non-aqueous (and in some cases the aqueous) phase, various salting out reagents (like alkali-metal salts), and water-soluble complexing agents. The interplay of these chemical processes in accomplishing the desired separation are the focus of the discussion to follow.

2.6. *Lanthanide/actinide separation*

The multiplicity of oxidation states of the light actinides can be utilized to accomplish very efficient separation of these elements from the lanthanides. Except for actinium (only trivalent), the actinide ions to plutonium either exist predominantly in higher oxidation states [Th(IV), Pa(IV, V)] or can be interconverted with relative ease among any of four oxidation states (III, IV, V, VI). The upper two oxidation states exist in aqueous solutions as the dioxocations AnO_2^+ or AnO_2^{2+}. The relative strength of complexes formed by the actinide cations in these oxidation states is An(IV) > An(VI) $\geq$ An(III) > An(V), which order also applies to the separation reactions involving these cations. The dominant oxidation states for the light actinides are Ac(III), Th(IV), Pa(IV or V), U(IV or VI), Np(IV or V). For plutonium, the redox potentials indicate nearly equal stability for all four oxidation states in acidic solutions. The tri-, tetra-, and hexavalent oxidation states are most important in separations.

Thorium, neptunium and plutonium are usually (although not exclusively) extracted or adsorbed onto resins in the tetravalent oxidation state while uranium (VI) is the most common oxidation state in separations. In most separations of the actinides, there exists a great difference in the extractability of the (IV) and (VI) oxidation states relative to the trivalent oxidation state. It is reasonable to expect, therefore, that the removal of the lanthanides and transplutonium actinides from the light actinides is readily accomplished. In fact, the low extractability of the trivalent state, and the ease of reduction of plutonium forms the basis for the isolation of Pu from the other

actinides. The PUREX extraction process, central to actinide reprocessing and breeder fuel cycles, based on tributyl phosphate (TBP) extraction of the actinides from HNO_3, and successfully partitions Pu from U and from the transplutonium elements (which are not extracted).

2.7. *Characteristics of trivalent lanthanides/actinides which can be exploited in separation*

The slightly greater spatial extension of the 5f orbitals is believed to be responsible for the existence of some degree of covalency in the actinides. The greater spatial extent of the 5f orbitals has been shown experimentally (Cotton and Wilkinson 1988c). The ESR spectrum of UF_3 in a CaF_2 matrix shows structure which is attributable to the interaction of fluorine nuclei with the electron spin of the U(III) cation. The orbital overlap implied by this observation is not observed in the lanthanide electronic analogue neodymium, suggesting a 5f covalent contribution to the ionic bonding of the actinides.

For the heavier actinides covalent interactions involving s or p orbitals has been suggested, but covalency in actinide binding is still not firmly established.

The question of covalent bonding of the amine nitrogen of aminopolycarboxylate ligands to the actinides has been addressed in the work of Choppin et al. (1985, 1987), and Rizkalla et al. (1989). These authors determined the enthalpies of complex formation of aminopolycarboxylate complexes of americium(III) and curium(III), and compared them with available thermodynamic data for europium–polycarboxylate complexes. One should expect that increased covalency in the actinide–nitrogen bonding should be manifested as a more exothermic heat for the complexation reaction. Their analysis reveals no clear indication of a covalent contribution to actinide binding in this system.

But whether the result of metal–ligand covalent bonding or a more subtle polarizability effect, extractants and complexants containing "soft" donor atoms are central to most ion exchange and solvent extraction separations of lanthanides from actinides. To generalize, those materials with the greatest potential for increased covalent interactions provide the most significant opportunity for successful lanthanide/actinide separations. As discussed below, the sheer multiplicity of reactions involved in separations processes offer many opportunities to exploit this difference in soft donor interactions.

The other characteristic of the trivalent lanthanide and actinide series that can be exploited in separations is the decrease in ionic radius which occurs with increasing atomic number. This results in increased strength of cation–anion interactions and ion–dipole, ion-induced dipole type interactions. The expected increase in ion–dipole interactions across the series implies that the heavy members of both series should bind solute (and suitable solvent) molecules more tightly than the light members. For certain ion exchange separations, it is thus appropriate to expect elution trends to correlate with the hydrated cation radius rather than the simple cation radius.

Both the trivalent lanthanide and actinide series are characterized by a shrinking ionic radius with increasing atomic number. This results in increased strength of

TABLE 1
Trivalent lanthanide and actinide cation radii [from Shannon (1976) and Marcus (1983)].

Ln	Shannon			Marcus	An	Shannon	
	CN = 6	CN = 8	CN = 9			CN = 6	CN = 8
La	1.032	1.160	1.216	1.12(4)	Ac	1.12	
Ce	1.01	1.143	1.196	–	Th		
Pr	0.99	1.126	1.179	1.15(5)	Pa		
Nd	0.983	1.109	1.163	1.07(5)	U	1.025	
Pm	0.97	1.093	1.144	–	Np	1.01	
Sm	0.958	1.079	1.132	1.06(4)	Pu	1.00	
Eu	0.947	1.066	1.120	1.06(5)	Am	0.975	1.09
Gd	0.938	1.053	1.107	1.00(4)	Cm	0.96	
Tb	0.923	1.040	1.095	1.02(4)	Bk	0.96	
Dy	0.912	1.027	1.083	1.01(5)	Cf	0.95	
Ho	0.901	1.015	1.072	–	Es		
Er	0.890	1.004	1.062	0.98(5)	Fm		
Tm	0.880	0.994	1.052	0.97(5)	Md		
Yb	0.868	0.985	1.042	–	No		
Lu	0.861	0.977	1.032	0.95(5)	Lr		
Y	0.900	1.019	1.075	–			

cation–anion interactions and ion–dipole, ion-induced dipole type interactions. The increase in ion–dipole interactions across the series implies that the heavy members of either series will bind solute molecules more tightly than the light members. For certain ion exchange separations, it is thus appropriate to expect elution trends to correlate with the hydrated cation radius rather than the simple cation radius.

This constriction in the cation radii forms the basis for intra-group separations (i.e., Ln/Ln or An/An) but does not contribute significantly to efforts to separate lanthanides from actinides. As the data in table 1 indicate, the cation radii decrease by roughly 20 percent across the lanthanide series. However, unlike the main group and d-transition elements, the cation radii for the actinides are not significantly different from those of analogous lanthanide cations. The "lanthanide/actinide contraction", is discussed in the text by Cotton and Wilkinson (1988b). It results from the inability of the relatively small spatially extended 4f and 5f electrons to compensate for the steadily increasing nuclear charge. Except for the separation of certain, specific lanthanide/actinide pairs with well-separated radii, it should be fairly obvious that the effect of cation radii will not be useful for lanthanide/actinide separation.

3. Basic organization of the chapter

In the present chapter, the focus will be primarily on those techniques which have proven useful, or which have some potential to develop into useful methods. The coverage of the literature will therefore be somewhat selective, although developments of the last 10–15 years will be given particular attention. The use of the multiple actinide oxidation states in lanthanide/actinide and actinide/actinide separations are

discussed, but only in general terms emphasizing recent developments to improve the efficiency of such separations. The primary focus of this chapter will be on the more difficult separation of the trivalent actinides from the trivalent lanthanides, and trivalent actinides from each other. Interlanthanide separation by ion exchange and solvent extraction has been covered in a complete review (Gmelin 1983), and so will be given relatively little attention except where new results impact on the understanding of lanthanide/actinide separations.

In a "how-to" manual, it is reasonable and typical to discuss ion exchange and solvent extraction separations independently. In this chapter, those aspects of lanthanide/actinide solution chemistry most pertinent to separation are the focus, not necessarily the means of achieving the separation. Therefore, only an approximate division of ion exchange and solvent extraction processes will be utilized here. In any case, the division between ion exchange and solvent extraction is something of an artifice, as most solvent extraction processes can be run in a "chromatographic mode" (e.g., by sorbing the extractant/diluent on a neutral support and performing column chromatography using the sorbed extractant as the solid phase) to increase the number of theoretical plates and increase separation efficiency. Because there are so many experimental parameters which can be varied in a separation process, the focus is on some of the aspects which are common to all separation methods, and on how these various aspects effect the efficiency of lanthanide/actinide separations.

The material is divided into the following general topic areas:

(A) overall extraction efficiency of the various extraction/ion-exchange processes;

(B) medium effects in the aqueous phase, including the effect of non-aqueous additives, salting-out reagents and alkaline solutions;

(C) the effect of diluent on the mutual separability of the groups by solvent extraction;

(D) the role of aqueous complexation in Ln/An separation;

(E) the application of soft donor extractants or synergists.

4. Relative efficiency of extraction

Direct comparisons among the wide variety of extractant molecules is somewhat difficult because different mechanism are operant in solvating and chelating processes. However, considered from the point of view of the complexity of aqueous-phase composition, a general (if somewhat arbitrary) order of extracting strength can be established. Because they require high concentrations of either mineral acids or salt solutions, the neutral organophosphorus extractants (TBP in particular) are considered (for the purposes of this chapter) the weakest of the extractants discussed.

4.1. *Neutral organophosphorus extractants*

The most important early investigations of lanthanide separations by solvent extraction were studies of the extraction of the trivalent lanthanide cations by TBP. Work by Peppard and co-workers, and by McKay and co-workers [previously reviewed by Stary (1966)] showed an odd–even effect in the grouping of lanthanide extraction

constants. Best et al. (1959) reported the corresponding extraction data for the trivalent actinides to Es.

The extraction reaction from nitrate solutions is described by the following equat ion;

$$R^{3+} + 3\,NO_3^- + 3\,TBP_o \rightleftarrows R(NO_3)_3\,(TPB)_{3o}. \quad (4)$$

The trisolvate of the trisnitrato complex of the trivalent metal ion is extracted into the organic phase (yielding a formally nine-coordinate hydrophobic complex assuming nitrate is bidentate). Unlike the extraction of the tetravalent and hexavalent actinides, extremely high concentrations of nitric acid are required for even moderate extraction of the trivalent metal ions. Greater efficiency is observed for this system if alkali-metal salts are used as the aqueous medium as discussed below.

To overcome the relatively weak extraction of trivalent lanthanide/actinide cations by neutral phosphates, investigations have been made of more basic organophosphorus solvating extractants. The general order of extracting strength (ignoring diluent effects, etc.) for this class of ligands is phosphates [$(RO)_3PO$] < phosphonates [$(RO)_2RPO$] < phosphinates [$(RO)R_2PO$] < phosphine oxides (R_3PO), the order of the relative Lewis basicity of the extractants. The R groups represent a mix of aliphatic and aromatic substituents which control (to some degree) the solubility and basicity of the extractant. Results for the extraction and separation of the trivalent actinides and lanthanides by such compounds have been well-discussed in earlier reviews (Weaver 1974, Stary 1966).

As extractants of polyvalent metal ions from acidic solutions, these reagents have one additional limitation: they are also moderately efficient extractants for mineral acids. As the neutral organophosphorus compound extracts the free acid, the free-extractant concentration in the counter-phase is reduced, and metal-ion extraction efficiency suffers. To overcome this limitation, considerable effort has been expended in recent years to evaluate the ability of carbamoylphosphonates (CPs, $(RO)_2PO(CO)N(R')_2$), carbamoylmethyl phosphonates (CMPs $(RO)_2POCH_2(CO)N(R')_2$), and carbamoylmethylphosphine oxides (CMPOs, $R_2POCH_2(CO)N(R')_2$) to extract lanthanide and actinide metal ions. These extractants are referred to collectively as bifunctional extractants. The first report of these ligands were made by Siddall (1963, 1964).

In these extractants, HNO_3 interaction with the extractant occurs with the carbamoyl portion of the molecule (Horwitz et al. 1981), leaving the solvating phosphorus portion of the molecule to interact with the metal ion. These compounds are indeed more efficient extractants of the trivalent metal ions from acidic solutions, able to extract trivalent actinide and lanthanide ions from relatively dilute nitric-acid solutions. Horwitz et al. (1981) have studied the separation of the lanthanides and trivalent actinides from Am to Fm (table 2) using dihexyl-N, N-diethylcarbamoylmethylphosphonate (DHDECMP) and aqueous nitrate solutions. Steadily decreasing distribution ratios are observed for the lanthanides, but nearly constant D's are found for the trivalent actinides. Group separation does not appear feasible while interlanthanide (but probably not interactinide) separations are possible. However, substitu-

TABLE 2
Separation factors (relative to Am) for solvent extraction of trivalent lanthanides and actinides with 0.817 M DHDECMP/DIPB/1.0 M HNO_3 from Horwitz et al. (1981).

Actinides	S_R^{Am}	$S_R^{R'}$	Lanthanides	S_R^{Am}	$S_R^{R'}$
Fm	0.575		Lu	0.048	
		1.04			1.41
Es	0.595		Yb	0.067	
		1.15			1.34
Cf	0.685		Tm	0.090	
		1.05			1.15
Bk	0.719		Y	0.103	
		0.90			1.29
Cm	0.649		Er	0.133	
		1.54			1.40
Am	1.00		Ho	0.186	
					1.43
			Dy	0.266	
					1.32
			Tb	0.351	
					1.15
			Gd	0.403	
					1.49
			Eu	0.602	
					1.22
			Sm	0.735	
					1.16
			Pm	0.855	
					1.12
			Nd	0.962	
					1.26
			Pr	1.21	
					1.12
			Ce	1.36	
					1.04
			La	1.41	

tion of dilute NH_4SCN for HNO_3, americium/europium separation factors[3] as high as 10.8 are observed [0.244 M Dihexyl-N, N-diisobutylcarbamoylmethylphosphonate–0.06 M NH_4SCN, Muscatello et al. (1982)].

There have been two additional reports of the application of CMPs to intragroup separation schemes (Aly and Latimer 1970a, Yan and Ye 1989). Alkylene phosphine dioxides (Chmutova et al. 1975) have been shown to exhibit some ability to

[3] The term "separation factor" is a ratio of either distribution ratios (D's or K_d's) or extraction equilibrium constants (K_{ex}) used to indicate the mutual separability of the subject metal ions. The nomenclature adopted here is:

$$S_{R'}^{R} = \frac{D(R)}{D(R')} \quad \text{or} \quad \frac{K_{ex}(R)}{K_{ex}(R')}$$

enhance the separation of americium from californium ($S^{Cf}_{Am} \approx 25$), and curium from berkelium ($S^{Bk}_{Cm} \approx 10$).

4.2. *Amine extractants*

In general, extraction of trivalent lanthanides/actinides by amine extractants suffer from many of the same limitations as the neutral organophosphorus extractants. In fact, they are more severely limited as metal complexes are extracted as anions, analogously with anion exchange resins. Of primary and secondary amine extractants, only Primene JM-T and n-benzyl heptadecyl amine (BzHp-DA) (Weaver 1974) showed any utility in separating lanthanides.

Tertiary amines are poor extractants for lanthanides and actinides from dilute nitrate media, but extract these metal ions strongly from concentrated nitrate solutions of low acidity (as was true of TBP). Similar observations have been made for extraction from chloride media. Figure 1 indicates that for 30% Alamine 336/xylene/11 M LiCl group separations are good, some interactinide separations are possible, but lanthanide separation factors are small. Weaver briefly discusses the application of the TRAMEX (tertiary amine extraction) process for the purification of ^{242}Cm.

Quaternary ammonium compounds are analogous to tetramethylammonium-based anion-exchange resins. They offer additional possibilities over anion-exchange resins for trivalent lanthanide/actinide separation (over resins) in the ability to use solvation effects to enhance separation factors. The first application of quaternary amines to lanthanide/actinide group separation was made by Moore (1964), who examined the system Aliquat 336/xylene/H_2SO_4–NH_4SCN. A principal advantage of this method is the relatively low concentration of salts required to attain a usable separation (as compared with tertiary amine/nitrate systems). Several other applications of the method have been summarized by Weaver (1974).

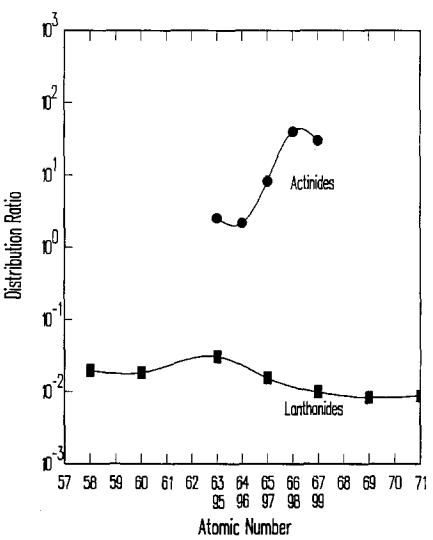

Fig. 1. Trivalent actinide and lanthanide extraction by 30% Alamine 336 in xylene from 11 M LiCl adapted from Stary (1966).

Besides the application of amine extractants as described above, there are numerous examples of the use of phenanthroline- and oxine-type ligands as extractants, both primary and secondary. Results relating to their application to lanthanide separations have been reviewed by Freiser (1988). Selected examples of their use in lanthanide/actinide separation are presented below in the discussion of soft-donor ligands (section 8).

4.3. *Acidic extractants*

Of the acidic extractants applied to lanthanide/actinide separations, the most common are chelating extractants like β-diketones, pyrazolones and (to a lesser extent) oxines, and the acidic organophosphorus extractants. Some work has been done evaluating the extraction of the subject metal ions by sulfonic acids, but this class of liquid cation exchangers exhibits little selectivity, and they have not proven particularly useful for lanthanide/actinide separation (Khopkar and Narayanankutty 1968).

Cation exchange resins in general resemble the sulfonic acid extractants most closely. Separation factors for cation exchange separations of the trivalent cations are extremely small. Successful lanthanide/actinide separation using cation exchange resins depend primarily on the use of aqueous complexants and/or alteration of the aqueous medium for the separation.

4.3.1. *Chelating ligands*

Studies of lanthanide/actinide separation by chelating extractants have focused principally on extraction by TTA, and, to a lesser degree, on related β-diketone ligands. For example, TTA is a favorite primary ligand for studies of synergistic (enhanced) extraction phenomena. Extraction by pyrazolones and oxines also is observed, usually in synergistic systems. The data of Alstad et al. (1974) indicate some potential for the system TTA/CCl_4/1 M $NaClO_4$ for individual lanthanide separations. Weaver (1974) cites early work by Werner and Perlman (1946) which indicate potential for lanthanide/actinide group separations. Other studies which have exploited the use of aqueous complexants in TTA extraction are discussed separately. In general, extraction of trivalent lanthanides and actinides requires dilute-acid conditions (pH 3–5) for efficient phase transfer. Separation factors for the trivalent actinides and lanthanides for extraction by TTA/benzene are presented in table 3.

A limitation of β-diketone extractants like TTA is the relatively low acidity of the extractant which requires that the aqueous pH be adjusted to above 4 for efficient extraction of the trivalent actinides and lanthanides. A class of extractants having a similar structure but greater acidity are the 1-phenyl-3-methyl-4-acyl-5-pyrazolones,

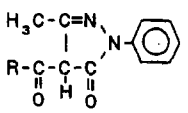

These extractants have received significant attention for their ability to extract and separate the subject metal ions.

TABLE 3
Separation factors for TTA extraction of trivalent lanthanides and actinides from Stary (1966) (TTA/toluene) and Alstad et al. (1974) (TTA/CCl_4).

Actinides	S^R_{Am}	$S^{R'}_R$	Lanthanides	S^R_{Am}	$S^{R'}_R$	$S^{R'}_R$ [a]
Fm	15		Lu	10.2		
		2			1.77	1.41
Es	7.4		Yb	5.75		
		1			1.74	1.82
Cf	7.4		Tm	3.31		
		2			–	2.29
Bk	3.7		Er	–		
		2.5				1.10
Cm	1.48		Y	–		
		1.48			–	1.17
Am	1.00		Ho	1.70		
					0.60	1.29
			Dy	2.82		
					3.03	1.74
			Tb	0.93		
					1.18	1.51
			Gd	0.79		
					1.20	1.41
			Eu	0.66		
					1.05	1.35
			Sm	0.63		
					2.33	1.86
			Pm	0.27		
					3.33	2.51
			Nd	0.081		
					0.81	1.51
			Pr	0.100		
					9.1	2.88
			Ce	0.011		
					12	3.24
			La	0.001		

[a] Data from Alstad et al. (1974). All other values from Stary (1966).

Extraction of metal ions by pyrazolones and a related extractant, N-benzoyl-N-phenylhydroxylamine, have been the topic of recent studies by Mathur and Khopkar (1983a, 1986, 1987a). The principal difference between the two extractants lies in the formation of six-membered rings in the pyrazolones versus five-membered rings for the complexes with the hydroxylamine extractant. The distribution data for the pyrazolones indicate some potential for intra-group separations, but successful lanthanide/actinide separation using pyrazolones alone appears unlikely. Thio-substituted pyrazolones have been shown to exploit the partial covalency in actinide binding (Smith et al. 1987, Ensor et al. 1988) in a synergistic extraction system. These results are discussed further in section 8.

Some selectivity for light/heavy (i.e. light lanthanides from heavy lanthanides or light actinides from heavy actinides) intra-group separations may be derived from the tendency of the metal ions to form self-adducts with the light members of the two series. This self-adduct results from coordination of a fourth ligand without ionization to form an extracted complex $R(Ex)_3(HEx)$ with 1:4 metal to extractant stoichiometry. Presumably, the light/heavy fractionation results from steric restriction caused by the shrinking radii of the heavier members of the respective series. An extraction chromatographic method for the separation of Bk from the trivalent actinides, lanthanides and inactive impurities using 1-phenyl-3-methyl-4-benzoyl-pyrazolone has been suggested (Mathur and Khopkar 1983a).

4.3.2. *Acidic organophosphorus extractants*

To avoid the requirement of dilute-acid aqueous solutions with acidic extractants (with attendant pH-control complications), acidic organophosphorus reagents were

TABLE 4
Separation factors for trivalent lanthanide/actinide extraction by HDEHP/toluene (Stary 1966) and HDEHP/kerosine (Sato 1989).

Actinides	S_{Am}^{R}	$S_{R}^{R'}$	Lanthanides	S_{Am}^{R}	$S_{R}^{R'}$	$S_{R}^{R'}$ [a]
Md	295		Lu	2.6×10^4		
		2			1.86	1.13
Em	144		Yb	1.4×10^4		
		–			3.1	1.12
Es	–		Tm	4.6×10^3		
		–			2.5	1.33
Cf	32.0		Er	1.8×10^3		
		1.7			2.24	1.25
Bk	18.8		Ho	810		
		10.8			1.95	2.58
Cm	1.74		Dy	420		
		1.74			2.09	1.62
Am	1.00		Tb	200		
					4.98	2.35
			Gd	41		
					1.45	1.46
			Eu	28		
					1.91	1.96
			Sm	15		
					3.02	–
			Pm	4.9		
					2.19	–
			Nd	2.24		
					1.38	1.17
			Pr	1.62		
					2.05	1.09
			Ce	0.79		
					2.96	1.30
			La	0.27		

[a] Data from Sato (1989), all other values from Stary (1966).

developed. Much of the early work on acidic organophosphorus extractants was done by Peppard and co-workers at Argonne National Laboratory and has been reviewed previously (Stary 1966, Weaver 1974). Principal among the acidic organophosphorus extractants are dialkyl (or aryl) phosphoric [$(RO)_2PO(OH)$] and phosphonic [(R) (OR) PO(OH)] acids. These extractants are generally much stronger acids than the β-diketones or carboxylic acids which they replaced. This characteristic implies that they can effectively complex and extract the trivalent metal ions from more acidic (pH < 2) solutions.

In general, this class of extractants give the greatest separation factors for the intra-group separation, but are not useful (alone) for group separation. This is most consistent with the discussion in section 2.7 of the relative importance of ionic radii and possible covalency effects. Mono-alkyl acid phosphorus extractants suffer from higher aqueous solubility and generally exhibit lower separation factors. Interactinide and interlanthanide separation factors from Stary (1966) and Sato (1989) are shown in table 4. Sato's report indicates slightly lower interlanthanide separation factors for extraction by 2-ethylhexyl(2-ethylhexyl)phosphonic acid.

There have been two reports (Kasting et al. 1979, Sekine and Dyrssen 1964) which suggest that enhanced lanthanide/trivalent actinide separation can be achieved by combining the features of multiple-extractant systems in a step-wise manner. Sekine and Dyrssen reported Eu/Am separation factors for 12 acidic extractants covering the spectrum of available materials (table 5 is adapted from their work). Based on their separation factors, one can envision a counter-current separation procedure involving first extraction by dibutyl phosphoric acid to preferentially remove Am, followed by contact of the aqueous phase with 5,7-dichloroxine to extract Eu. Substituting HDEHP for HDBP, Kasting et al. suggest just such a separation procedure could give actinide/lanthanide separation factors of several thousand.

TABLE 5
Europium/americium separation factors for a series of acidic extractants (Sekine and Dyrssen 1964).

Extractant	Diluent	S_{Am}^{Eu}
Dibutylphosphoric acid	$CHCl_3$	22.9
Dioctylphosphoric acid	$CHCl_3$	14.1
1-phenyl-3-methyl-4-acetylpyrazolone-5	$CHCl_3$	3.47
Thenoyltrifluoroacetone	$CHCl_3$	3.02
Neocupferron	$CHCl_3$	1.74
N-benzoylphenylhydroxylamine	$CHCl_3$	1.66
N-2, 4-dichlorobenzoyl-phenylhydroxylamine	$CHCl_3$	1.32
β-isopropyltropolone	$CHCl_3$	0.98
1-hydroxy-2-napthoic acid	hexone	1.07
2-hydroxy-1-napthoic acid	hexone	1.02
3-hydroxy-2-napthoic acid	hexone	0.95
5, 7-dichloroxine	$CHCl_3$	0.10

4.4. *Synergistic extraction systems*

With the goal of enhancing extraction strength of basic solvent extraction systems, much work has been done on solvent extraction systems involving (often) a chelating extractant and a secondary extractant, usually a solvating extractant. Successful combinations of this type exhibit a greater degree of extraction than either of the extractants would achieve alone. Such systems of ligands are called synergistic. Although successful systems do exhibit greater extraction strength, synergistic extraction systems rarely achieve much enhancement in group separations (except in the case of soft-donor synergists, discussed in section 8), or in the mutual separation of members of the groups.

The reactions which describe synergistic extraction begin with the equilibrium in eq. (4). In non-synergistic extraction systems, non-specific interaction between the hydrophobic metal complex and the organic diluent is presumed. In the presence of a synergistic reagent, the solvation process, described above as the final step in the extraction process, is enhanced by a specific interaction between the hydrophobic metal complex and synergist. Thermodynamically, this process can be described by introducing the further equilibrium (occurring in the organic phase),

$$R(Ex)_3(H_2O)_x + n\ Syn \rightleftarrows R(Ex)_3(Syn)_n + xH_2O. \tag{5}$$

Addition of the synergist may involve replacement of the remaining coordinated water molecules or expansion of the coordination sphere (e.g., if $x = 0$) to accommodate the solvating molecule (Kandil et al. 1975). The synergist may be the diluent (e.g., hexone), but more often it is a solute ligand.

Much of the work which has been done on lanthanide and actinide synergism has examined systems built around the chelating extractants, mainly β-diketones. This is primarily because these systems are well-behaved stoichiometrically, and often large synergistic enhancements are seen in metal-extraction efficiency. Synergistic enhancement is seldom important with organophosphorus acids as the primary ligand (although neutral organophosphorus species are effective synergists), and those studies of synergism with organophosphorus acids are often difficult to interpret because of interaction between primary and secondary extractants in the organic phase. The relevant literature on trivalent lanthanide/actinide separation by synergistic systems has been reviewed by Mathur (1983).

According to Mathur, the largest synergistic effects are observed with trialkyl (or aryl) phosphine oxides as synergists. However, Khopkar and Mathur (1977) report large synergistic enhancements for Aliquat 336·HCl for extraction of lanthanides and actinides into TTA, but no improvement in separation factors. An interesting report of synergism in lanthanide separations using LIX 51, LIX 54, and dibenzoyl methane as primary extractants, and TBP or TOPO as synergists indicates mean separation factors for adjacent lanthanides of 1.7 to 2.3 (Nakamura et al. 1987).

Extensive investigations by Chmutova and co-workers of 1-phenyl-3-methyl-4-benzoyl-5-pyrazolone (PMBP) indicate that the synergistic enhancement for TBP and TOPO adducts (in benzene) of the trivalent actinides (extracted from nitric acid) increases in the order Am < Cm < Bk < Cf (Chmutova et al. 1973). On the other hand,

Khopkar and Mathur (1982) do not observe any particular order in the extraction of these metal ions from hydrochloric acid solutions into the same extractant mixtures in xylene. Continued investigation by Mathur and Khopkar (1983b, 1987b) and by Dukov and Genov (1986, 1988) (lanthanides only) reported general increased extraction, but few useful separation systems.

4.5. *Cyclic and linear polyethers in lanthanide/actinide separation*

The concept of molecular recognition has its roots in coordination chemistry in the binding of metal ions by crown ethers. In this class of ligands, the size of the cavity is often the principle determinant of metal-ion selectivity. For the light lanthanides and trivalent actinides, the optimum cavity size is attained in the 1,4,7,10,13,16-hexaoxocyclooctadecane (18-crown-6) configuration,

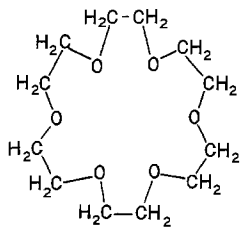

However, despite the nominal good match between the cation radii and the ligand cavity, recent data (Mathur and Choppin (1993)) indicate that only three of the six oxygens are strongly bound to lanthanum in aqueous solutions, implying a defect in the fit of the metal ion to the cavity.

Separations applications for the basic 18-crown-6 ligand are limited by the considerable aqueous solubility of the free ligand. Some alterations of the basic ligand structure have been made to improve the hydrophobicity of certain derivatives and their complexes.

There are a few reports of the use of crown ether extractants alone for lanthanide separations (Samy et al. 1988, Imura et al. 1987, Tang and Wai 1986), and others on the use of linear and crown ethers in cooperation with coextractant molecules (Chang et al. 1989, Manchanda and Chang 1986, Ensor and Shah 1983, 1984, Aly et al. 1985, Mathur and Khopkar 1988), some of which also discuss trivalent actinide extraction. Samy et al. (1988) investigated the extraction of lanthanides from 1 M lithium trichloroacetate (pH 3–4.5) with 0.01 M 18-crown-6 in 1,2-dichloroethane. They report that the separation factors for the lanthanides from La to Tb actually exceed those reported by Ceccaroli and Alstad (1981) for HDEHP extraction. Separation factors for the lanthanides after Tb are much smaller, probably indicating a defect in the lanthanide-crown fit. Tang and Wai (1986) report some intragroup separation of the lanthanides lighter than Tb using Sym-benzo-18-crown-5-oxyacetic acid/80% chloroform-20% heptanol.

Chang and co-workers (1986, 1989) have reported the equilibria and kinetics of the extraction of selected lanthanides by 1,7-diaza-4, 10, 13-trioxacyclopentadecane-N, N′-diacetic acid (DAPDA) and 1, 10-diaza-4, 7, 13, 16-tetraoxacyclooctadecane-N,

N′-diacetic acid (DACDA) in conjunction with TTA (chloroform). Ligands of this type offer interesting possibilities as they combine the characteristics of crown ethers with those of aminopolycarboxylic acid complexants. At pH 5, only $R(TTA)_3$ is extracted, while a 1:1:1 complex R(DAPDA, DACDA)TTA is extracted at pH 7.5–8.0. The extraction kinetics at pH 5 are slow, governed by the rate of dissociation of aqueous metal–crown complexes, but are relatively fast and independent of the aqueous macrocycle complex dissociation rate in the high-pH regime. These kinetic results suggest the possibility of interlanthanide separations based on differences in complexation rates.

The work of Mathur and Khopkar (1988) on the use of benzo-15-crown-5, (Bz 15-C-5), and di-cyclohexano-18-crown-6 (DCH 18-C-6) as synergists for lanthanide and actinide extraction with 1-phenyl-3-methyl-4-trifluoroacetyl-5-pyrazolone (PMPFT)/chloroform suggest some potential for such mixtures to accomplish certain specific group and inter-actinide separations. Aly et al. (1985) studied synergistic extraction using TTA and 15-crown-5 synergist for lanthanide and trivalent actinide extraction and found significant enhancement of the extraction, but little separation value. In both studies, 1 : 3 : 2 adducts are indicated for the 15-crown-5 synergists while Mathur and Khopkar report 1 : 3 : 1 adducts for the 18-crown-6 synergistic reaction.

There is also evidence that non-cyclic polyethers can function as synergists in lanthanide/actinide separation. Ensor and Shah (1983, 1984) report that 1, 13-bis(8-quinolyl)-1,4,7,10,13-pentaoxatridecane (Kryptofix-5, or K-5) enhances the extraction of Ce(III), Eu(III), Tm(III), Am(III), Cm(III), Bk(III) into chloroform solutions of TTA. The extracted complex has the stoichiometry $R(TTA)_3 \cdot K\text{-}5$, and the synergistic enhancement is comparable to that of TBP under the conditions studied. Intra-group separation factors for lanthanides and actinides are approximately two while the usual synergistic leveling effect is observed for Am/Eu separation (i.e., they are worse than those for TTA alone).

5. Medium effects

Both the (organic) diluent (in solvent extraction systems) and the composition of the aqueous solution can have a profound effect on extraction efficiency, group separation, and intra-group separation. An example of this effect has already been seen above in the reported enhancement of trivalent metal ion extraction by amines or neutral organophosphorus extractants from nitrate salts versus nitric acid (a "salting-out" effect).

Another example of an "aqueous" medium effect is the use of alcohol/water mixtures in several successful ion-exchange-based separation processes for the lanthanides and actinides. A third example, relevant to solvent extraction alone, is the effect of the diluent on the extraction process. The effect of these phenomena, and the reasons for their success (or failure) is the subject of the next section.

5.1. *Mixed aqueous media in ion exchange*

It is generally observed that partial substitution of water miscible organic solvents (like ethanol) into the aqueous phase results in increased extraction (or sorption), and,

in many cases, in improved group-separation behavior. It is likely that the improvements grow at least partly out of the changes induced in the solvation dynamics and metal coordination numbers observed when the medium is altered.

Lincoln (1986) discusses both the rates and solvation numbers of the aquo-lanthanide cations, and observes that there is great variety in both solvent-exchange rates and coordination numbers in non-aqueous media. The kinetic parameters for water exchange (Cossy et al. 1989) are consistent with a concerted associative mechanism, characterized by rapid exchange. Partial substitution of non-aqueous solvents for water must result in a net decrease in the exchange rate (as a result of the decreased concentration of water), thereby reducing the energetic requirements for desolvation and promoting phase transfer.

Stary (1966) cites the work of Street and Seaborg (1950) who found that group separation of the lanthanides and trivalent actinides can be done by cation exchange eluting with 20% ethanol saturated with HCl. The presence of the alcohol enhances the difference in chloride complex stability between the lanthanides and actinides as a result of partial dehydration of the cation in the 20% ethanol solution.

The work of Grigorescu-Sabau (1962) shows that water miscible organic solvents increase the sorption of Pr(III) to a cation resin which is interpreted as the result of a decrease in the free hydrogen ion concentration in solution, thus reducing competition between the metal cation and proton for resin-binding sites. More recent results from Sheveleva and Bogatyrev (1987) indicate enhanced separation of europium and gadolinium can be achieved in anion exchange separations (Dowex-1 X8) in mixed organic/aqueous solvents. Ethanol, acetone and acetonitrile solutions of HNO_3 modify both the internal structure of the resin, and solvation of the anionic nitrato complexes to alter the ionic mobility of the complexes to improve the separation.

The results of Guseva and Tikhomirova (1972) indicate a significant improvement in the group separation from 4% cross-linked Dowex 50 using 10.5 M HCl in 40% ethanol as the elutrient as compared with 12.5 M HCl in water. More recently, Guseva et al. (1987a, b) have demonstrated an efficient separation of trivalent actinides from all matrix elements (actinides and fission products) with both cation and anion exchange from aqueous-ethanol solutions of sulfuric acid. Usuda and co-workers (1987) and Usuda (1988) have presented a separation scheme for trivalent actinides using a three-step ion exchange partition of the trivalent actinides from light actinides and fission products.

5.2. *Salt effects in solvent extraction*

Some simple calculations reveal that the salting-out effect is simply a result of the reduction in water activity due to the presence of the salt. Taking the example of 10 M LiCl [density = 1.1812 g/cc, 8.24 molal solution, Chemical Rubber Company Handbook of Chemistry and Physics (1987)], we find that the nominal water concentration is reduced to 36.1 molal. However, if we also consider that the lithium ion is a tetrahydrate cation in aqueous solution (ignoring the hydration of the chloride ion), the "free" water concentration is reduced to only 3.2 molal. Although this model calculation is greatly oversimplified, it is clear that the reduced concentration of available water

molecules must have the effect of reducing the net rate of water exchange of the lanthanide cation (or perhaps even the degree of hydration) improving the energetic requirements of phase transfer reactions, much like the mixed aqueous solvents discussed above. In the separation of individual lanthanides from mixtures of the lanthanides, a "self-salting" effect is believed to be responsible for the enhanced separation factors observed in many extraction systems when operated at or near the saturation limit (Weaver 1974) due to the reduction of the effective water concentration by cation hydration.

A secondary effect of high salt concentrations on the chemistry of the aqueous medium is the enhancement which is observed in complex strength when the free water molecule concentration is reduced. Under these conditions, the weakly binding chloride and thiocyanate anions (soft-donor ligands) are better able to compete with water for the cation to form complexes which are extracted by amine extractants or bound to anion exchange resins. The minimization of the metal–water interaction permits the subtle covalent contribution to actinide binding to emerge, forming the basis for group separation from chloride and thiocyanate solutions.

An additional phenomenon related to the anion in the aqueous phase is a so-called "perchlorate effect" (Gmelin 1983). It has been often observed that extraction of metal ions from perchlorate media is greater than that from equivalent nitrate or chloride solutions. Marcus reports (Gmelin 1983) the effect in two different systems involving acidic extractant molecules. The enhanced extraction of metal ions is also observed in systems based on neutral molecules. In the latter case, formation of aqueous complexes of stoichiometry 1:3 (R:L) is required for neutrality in the extracted complex. As lanthanide perchlorate ion pairs normally do not exist in aqueous solution, it is something of a dichotomy that extraction from perchlorate medium should be more readily achieved than from more strongly complexing nitrate (or even chloride) solutions. An explanation for the phenomenon, and for the relative ease of extraction of metal ions from salt solutions (relative to that from equivalent acids), may lie in the effect of the solutes on water structure.

Choppin and co-workers (Choppin and Buijs 1963, Choppin and Violante 1972, Choppin 1978) have investigated the effect of various solutes on the hydrogen-bonded structure of water. Basically to consist of water can be considered of molecules having zero, one or two water molecules hydrogen bonded to the protons. A higher percentage of more highly hydrogen-bonded species implies greater three-dimensional structure in the solvent. The energetics of the fit of the metal ion into this structure constitutes an entropy contribution to the overall extraction reaction.

The solutes which make up aqueous solutions can either promote or disrupt the three-dimensional structure of water. Hydrogen ions (H^+) and hydroxide ions (OH^-) are the ultimate structure makers in aqueous solutions, as they fit perfectly into the water structure. Various water miscible solvents (e.g., methanol, ethanol, acetone) have more-or-less predictable effect on the structure of water. Small, hard-sphere metal cations tend to promote order in the solution while large cations tend to disrupt the structure. Among typical anions, fluoride is a strong structure maker, sulfate and nitrate less efficient structure makers, while the heavy halides and thiocyanate disrupt the water structure. Most effective among anions encountered in separations in

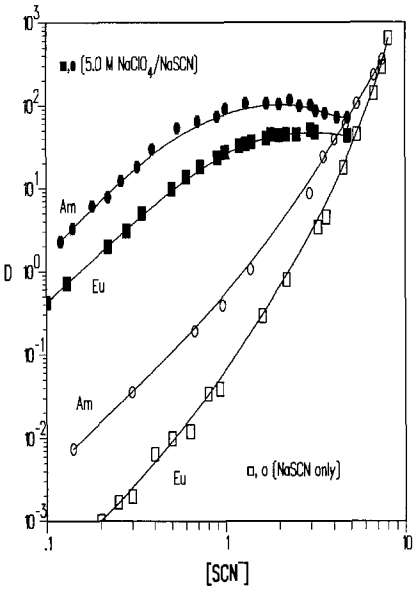

Fig. 2. Americium and europium distribution ratios for extraction by 5% tributyl phosphate (hexane) as a function of NaSCN concentration (pH 4–5) in the presence and absence of $NaClO_4$ as supporting electrolyte. Open symbols are for variable concentrations of NaSCN. Closed symbols represent $NaSCN/NaClO_4$ mixtures at 5.0 M total ionic strength. Data from Sekine (1965).

disrupting water structure is perchlorate. Although such effects are difficult to quantify, the observation of a perchlorate effect is almost certainly the result of a more favorable net entropy contribution growing out of the structure-breaking nature of the anion (recall that net energy changes of the order of only 400–1500 joules/mol are needed to accomplish extraction). Although this effect increases overall extraction efficiency, its effect on separation factors is more difficult to predict.

To illustrate, the results reported by Sekine (1965) show the combined effect of soft-donor ligands and perchlorate on Am/Eu separation using a solvating extractant. The extraction/separation of americium and europium with 5% TBP/hexane from 5.0 M $NaClO_4$/NaSCN, and from NaSCN solutions without supporting electrolyte (pH 4–5) exhibit strong dependence on the concentration of SCN^- (fig. 2). In the absence of perchlorate, the separation factors are higher at low [SCN^-], although distribution ratios are low. At constant ionic strength (5.0 M), the trend is reversed, that is, separation factors (S_{Eu}^{Am}) are higher at higher concentrations of SCN^-. Distribution ratios are also dramatically higher due to the "perchlorate effect". The free energies for extraction of either Am or Eu in the presence and absence of perchlorate (e.g., at 1 M NaSCN) is 12–17 kJ/mol more favorable. At the highest SCN^- concentrations, separation factors are near one because the water-structure disrupting effect of SCN^- and ClO_4^- essentially eliminate the effect of the soft-donor in actinide binding to the SCN^-.

5.3. *Extraction from alkaline and carbonate media*

An extreme example of an aqueous medium effect is the separation of lathanides and actinides from alkaline and carbonate solutions, reviewed by Karalova et al. (1988).

Because the lanthanide and actinide metal ions are readily hydrolyzed (and precipitated) in alkaline solutions, these studies require the presence of water-soluble complexants. Both solvating and chelating extractants have been used in these studies. Primary and quaternary amines, alkylpyrocatechols, β-diketones, pyrazolones, and N-alkyl derivatives of aminoalcohols are the extractants indicated as useful for alkaline extraction processes. A variety of diluents have been used, but their nature seems to have little effect on the extraction efficiency or separation factors.

The factors contributing to a successful separation procedure are not different from those relevant in more acidic solutions, i.e., the efficiency is dependent on the nature of the extractant and the aqueous complexant, the pH of the aqueous solution, and the strength of aqueous complexes. Two advantages provided by this approach are the relative ease of back extraction (contact with neutral salt solutions in usually sufficient), and the potential for kinetic-based separations. The disadvantage (from a practical standpoint) is the requirement of working with concentrated salt solutions, which create waste disposal problems.

Additionally, extraction from alkaline solutions and carbonate is characterized by the unusual preference (specificity) of the extraction processes for the trivalent oxidation state [in carbonate solutions the order of extraction is M(III) > M(IV) > M(V) > M(VI)]. A further benefit of operation in alkaline solutions is the greater tendency for air oxidation of trivalent metal ions to the tetravalent oxidation state (examples are Ce, Bk), thus prompting their removal.

Group separation factors for the trivalent actinides and lanthanides are ≈ 2 for extraction by Aliquat 336–EDTA in contact with an alkaline EDTA aqueous solution. Such a separation factor may be sufficient if the system is operated in the extraction chromatographic mode (Bukhina 1983).

Alkyl pyrocatechol extractants provide greater group separation factors. Eu/Am separation factors of 70 have been reported for a non-equilibrium extraction in the system 4-(α,α-dioctylethyl)-pyrocatechol/NaOH/DTPA (diethylenetriamine-N, N, N, N, N-pentaacetic acid) (or DTPP – diethylenetriamine-N, N, N′, N″, N″-pentamethylenephosphonic acid) (Karalova et al. 1982). The separation factors are based mainly on the difference in the rates of the metal–DTPA (or DTPP) complexation equilibria for Eu and Am. They are therefore highly dependent on the contact time. A principal limitation of the practical application of such a separation scheme is the relatively long contact times (> 10 min) required for extraction. However, the slow equilibration compares favorably with that for other lanthanide–actinide separation processes (e.g. TALSPEAK, section 7).

6. Diluent effects in solvent extraction

In the early days of solvent extraction, the organic diluent was often referred to as "inert". With further study it became obvious that the organic diluent was anything but inert. Many orders of magnitude variation was observed in the distribution coefficients of extracted metal ions as a function of the organic solvent. In some systems, the stoichiometry of the extracted species (or the extractant) was altered by

the properties of the diluent. In the case of lanthanide extraction by oxine-type extractants, the complexes formed are only soluble in a limited few diluents. Although the theory of the physical chemistry of organic solutions is not developed sufficiently to permit reasonable prediction of diluent effects in separations, it is clear that solvation phenomena in such solutions are important. In this section, the effect of this aspect of lanthanide/actinide separations is discussed.

The character of the diluent in a solvent extraction separation scheme generally can have a profound effect on the overall degree of extraction, but the effect of diluent on separation factors is usually much more subtle. Alteration of the diluent modifies metal-ion extraction equilibria primarily by its effect on the solvation of the hydrophobic metal complex. Although few recent studies have been made of diluent effects in lanthanide/actinide separation (with no truly systematic investigations), enough historical reports exist to make some general observations of the effect of diluent on lanthanide/actinide separation.

Stary (1966) discusses the results of Oak Ridge National Laboratory studies of americium/californium separation factors in HDEHP extraction as a function of the organic diluent. As presented in table 6, while the change in diluent from normal paraffin hydrocarbons to aromatic hydrocarbons to chlorinated solvents results in an order of magnitude variation in the overall extraction of Am and Cf, the Am/Cf separation factors remain constant at $110(\pm 8)$.

On the other hand, Dyrssen and Liem (1960) report (table 7) greater variation in both distribution ratios [for americium and europium extraction by dibutyl phosphoric acid (HDBP)] and in separation factors as a function of diluent. The separation factors and distribution coefficients are correlated (more or less consistently) inversely with the distribution ratio of the extractant between the phases. In this system, the largest separation factors are observed in n-hexane, chloroform, and carbon tetrachloride. Diluents capable of direct coordination (i.e., those possessing potential oxygen-donor atoms) are correlated with reduced distribution ratios and separation factors. The observations of greater separation factors in non-complexing diluents suggest that more effective separation is observed when the inner-coordination sphere of the hydrophobic complex is not disturbed.

For tertiary and quaternary amine extractants, Horwitz et al. (1966) report that the transition from benzene to xylene to diisopropylbenzene to cyclohexane enhances the

TABLE 6
Data from Stary (1966) on HDEHP extraction of Am, Cf as a function of diluent.

Diluent	$\log K_{Cf}$	$\log K_{Am}$	S_{Am}^{Cm}
n-Heptane	2.55	0.47	120
n-Decane	2.22	0.20	105
Cyclohexane	2.18	0.10	120
Diethylbenzene	1.85	−0.15	100
CCl_4	1.80	−0.20	100
Xylene	1.50	−0.54	110
Toluene	1.40	−0.65	112

TABLE 7
Data from Dyrssen and Liem (1960) on HDBP extraction of Am and Eu as a function of diluent, 0.1 M HDBP, 0.1 M acid.

Diluent	$\log D_{Eu}$	$\log D_{Am}$	S^{Eu}_{Am}	$\log D_{HDBP}$
n-Hexane	2.60	1.40	17	0.48
CCl_4	1.81	0.46	20	1.11
$CHCl_3$	0.09	−1.27	23	1.87
Diisopropylether	0.66	−0.44	13	1.02
Hexone[a]	−0.75	−1.81	11	1.42
TBP	−1.78	−2.08	2.9	1.73
Hexol[b]	−3.31	−3.64	2.1	1.91

[a] Methylisobutylketone (aka 4-methyl-2-pentanone).
[b] Methylisobutylcarbinol (aka 4-methyl-2-pentanol).

TABLE 8
The effect of diluent on the extraction of Am and Eu with 20% triisooctyl amine from 11.9 M LiCl/0.1 M HCl (Moore 1961).

Diluent	Percent extracted		Separation factor
	Am	Eu	
Xylene	91.7	15.7	59
Toluene	87.0	10.1	60
Benzene	80.8	7.0	56
Mesitylene	94.2	23.4	53
Hexone	87.3	12.7	47
β,β'-dichloroethyl ether	97.1	63.1	20
o-Dichlorobenzene	80.6	7.5	51
Nitrobenzene	87.2	11.8	51
n-Hexane	98.4	54.8	51
CH_2Cl_2	99.7	91.3	32
CCl_4	23.4	0.9	34
$CHCl_3$	0.6	< 0.3	–
Xylene–$CHCl_3$			
1:1	< 1.0	< 1.0	–
3:1	10.3	< 0.5	–
20:1	71.2	4.3	55
50:1	83.4	8.7	53

extraction of Am by Alamine-336 nitrate (range of 1.4 to 21), but retards the extraction of Am by the quaternary amine Aliquat-336 nitrate (from 149 to 87). The effect of diluent on separation factors was not explored.

Moore (1961) examined the effect of 12 diluents plus mixtures of xylene–chloroform on Am/Eu separation factors for the extraction of these metal ions by 20% triisooctylamine from 11.9 M LiCl/0.1 M HCl solutions (table 8). The highest Am/Eu separation factors are observed in those systems in which the diluent is most "inert". Hexone, which possesses an available oxygen-donor atom, slightly reduces the separation factor. The aliphatic chlorinated diluents reduce them by approximately a factor

of two. One might speculate that these diluents act to partially solvate the metal-chloride complex (formulated as MCl_5^{2-}) in the inner-coordination sphere of the extracted complex to reduce the net thermodynamic difference in complex stability of the Am and Eu complexes.

In his review of synergistic solvent extraction of the lanthanides and trivalent actinides, Mathur (1983) notes that, although some authors find a correlation between the dielectric constant of the diluent and distribution ratios (Kochetkova et al. 1972), this relationship is by no means universal. Factors relating to the nature of the diluent (dielectric constant, polarizability, etc.), the nature of the free ligand species, and the neutral metal complex must all contribute to relative extraction efficiency.

Recent small-angle neutron scattering (SANS) studies of the structure of praseodymium complexes in organic solutions containing neutral extractant molecules indicate that occasionally gross structural effects in the organic phase can have an effect on lanthanide extraction. Thiyagarajan et al. (1988) find that the extracted complex in the praseodymium-octyl (phenyl-N, N-diisobutylcarbamoylmethyl-phosphine) oxide system (PrX_3–CMPO) at moderate concentrations of the extracted metal ion (where X is either Cl^- or NO_3^-) forms large, ellipsoidal aggregates in both d-6 benzene and tetrachlorethylene (TCE). The aggregates are twice as large in TCE as in benzene (10 and 18 X 280 Å versus 13 X 140 Å), but the nature of the anions and presence of dissolved water have little effect on the size of the aggregate. A monofunctional analogue diamyl(amyl) phosphonate (DA(A)P) does not aggregate as the particle size corresponds to that expected of monomeric extracted complexes. The ability to probe such structures in the organic phase creates many exciting possibilities for explaining some observations in extraction processes.

7. Role of aqueous complexation in lanthanide/actinide separations

Weaver (1974) states "Much fruitless effort was expended in searching for extractants which separated the two groups of elements (i.e., rare-earth fission products and transplutonium actinides)···The separation was finally accomplished only by considerably modifying the aqueous medium." Notwithstanding the need for extraction efficiency for meaningful separation, success in lanthanide/trivalent-actinide separation is accomplished most efficiently through the agency of metal-complex formation in the aqueous phase. This is true for both ion exchange and solvent extraction separations.

The effect of aqueous complex formation on distribution ratios and separation factors can be readily understood in terms of equilibria already discussed. For the simplest case in which the aqueous metal complexes are not extracted into the counter-phase, the observed distribution ratio will represent a balance between the two phase extraction reaction, and the homogeneous complexation equilibria in the aqueous phase.

Taking an acidic chelating extractant as an example, the disotribution ratio for metal-ion extraction in the absence of aqueous complexation reactions is based on the equilibrium

$$R^{3+} + 3\,HEx_o \rightleftharpoons (R(Ex)_3)_o + 3\,H^+ . \qquad (6)$$

The equilibrium constant for this reaction is

$$K_{ex} = \frac{[R(Ex)_3]_o[H^+]^3}{[R^{3+}][HEx]_o^3} = D_o\frac{[H^+]^3}{[HEx]_o^3}. \tag{7}$$

Introduction of a water-soluble complexing agent requires that reactions like those described in eq. (2) must be accommodated in this expression. The metal-ion distribution ratio under these conditions becomes

$$D = \frac{[R(Ex)_3]_o^3}{[R^{3+}] + [RL] + [RL_2] + \cdots}. \tag{8}$$

The concentrations of the metal complexes in this expression can be written in terms of the aqueous equilibria as

$$D = \frac{[R(Ex)_3]_o^3}{[R^{3+}]\{1 + \Sigma(\beta_i[L]^i)\}} = \frac{D_o}{\{1 + \Sigma(\beta_i[L]^i)\}}, \tag{9}$$

where the β_i values are the equilibrium constant for the relevant aqueous complexation reactions.

The separation factor for two metal ions in a given system is the ratio of the respective distribution ratios (D's) or,

$$S^m_{m'} = \frac{D^m}{D^{m'}} = \frac{D_o^m\{1 + \Sigma(\beta_i^{m'}[L]^i)\}}{D_o^{m'}\{1 + \Sigma(\beta_i^m[L]^i)\}}. \tag{10}$$

The separation factor for the two metal ions is therefore directly proportional to the relative extraction efficiency of the metals ($D_o^m/D_o^{m'}$), but inversely proportional to the stability of the aqueous complexes. The most effective separations will be achieved in those systems with favorable differences in extraction efficiency and complementary differences in aqueous complex strength. A calculational model has been recently proposed for the prediction of separation efficiency based on stability parameters (Jedinbakova et al. 1988).

Because the relative distribution of the lanthanides and trivalent actinides onto ion exchange resins does not vary a great deal, separations based on ion exchange solids are quite dependent on complexation reactions in the aqueous solution. For anion exchange separations of cations, aqueous complexation to form anionic complexes is essential. The first separations of the transplutonium elements were accomplished by means of ion exchange (both cation and anion) using aqueous complexing media. The work of Street and Seaborg (1950) demonstrated that trivalent americium and curium could be separated from the lanthanides by hydrochloric acid solutions at concentrations above 12 M. Under these conditions, the actinide cations pass through the column of resin is accelerated by the enhanced complexation (relative to the lanthanides) by Cl^-. This work was extended to include the trivalent actinides to Es by Choppin and Chatham-Strode (1960). The latter authors were not completely enthusiastic about the earlier speculation connecting the actinide enhancement with covalent bonding.

To assess the role of covalence in the lanthanide/actinide separation observed in chloride solutions, Surls and Choppin (1957) investigated both cation and anion

exchange for the trivalent actinides from thiocyanate solutions. It was predicted that stronger covalent interaction would be observed in this system. While certain aspects of the chloride system were reproduced in the thiocyanate system, the bulk of the evidence suggests that the covalent interaction interpretation is an oversimplification. Polarizability of both metal ion and the ligand may also contribute to the observed lanthanide/actinide separation. These authors point out most significantly that free-energy changes of the order of only 400–1200 joules/mol are sufficient to cause a reversal of the elution positions of the metal ions. The results of Sekine (1965) on Am/Eu separation by TBP extraction from SCN^-/ClO_4^- media (as discussed in section 5.2) are consistent with this interpretation.

Based on earlier research on the separation of the lanthanides, ion exchange separations were also done using citric acid as a complexant. Because the citrate eluent is plagued by relatively slow kinetics, other hydroxy-carboxylic acids were tested as elutriants for the higher actinide elements. Lactic acid was among the first species tried, but better interactinide separations were observed using α-hydroxyisobutyric acid

TABLE 9
Separation factors (relative to Cm) for ammonium α-hydroxyisobutyrate cation exchange of trivalent lanthanides and actinides from Smith and Hoffman (1956), Choppin et al. (1956), and Choppin and Silva (1956).

Actinides	S^R_{Am}	$S^{R'}_R$	Lathanides	S^R_{Am}	$S^{R'}_R$
Md	0.035		Lu	0.011	
		1.41			1.33
Fm	0.049		Yb	0.014	
		1.88			1.30
Es	0.093		Tm	0.019	
		1.54			1.42
Cf	0.14		Er	0.026	
		2.25			1.49
Bk	0.31		Ho	0.039	
		2.22			1.09
Cm	0.71		Y	0.043	
		1.40			1.30
Am	1.00		Dy	0.056	
					1.79
			Tb	0.10	
					2.00
			Gd	0.20	
					1.39
			Eu	0.28	
					1.82
			Sm	0.51	
					1.69
			Pm	0.86	
					1.75
			Nd	1.5	
					1.67
			Ce	2.4	

(Choppin et al. 1954, 1956, Smith and Hoffman 1956). This system proved useful for intra-group separation of both the lanthanides and actinides (table 9). There are numerous examples of more recent applications of both the specific system and adaptations of it in lanthanide and actinide processing (Elesin et al. 1986, Vobecky 1989, Billion 1979, Aly and Latimer 1970b, 1967, Guseva and Tikhomirova 1979).

Similar ideas have been applied to improve actinide–actinide separation factors in solvent extraction processes. Aly and Latimer (1970b) studied the extraction of Cm, Bk, Cf, and Es by HDEHP/toluene from solutions of several hydroxycarboxylic acids. They established that the separation could be accomplished using this system if operated in the extraction-chromatographic mode, but observe that the separation using α-hydroxyisobutyric acid is less efficient than the same complexant used with cation exchange resin (Choppin et al. 1956). The reduced intra-group separation (relative to the cation exchange separation) should not be surprising, as both the distribution ratios and aqueous complexation strength increase across the series (with constricting cation radii). As eq. (10) indicates, these factors act in opposition, thus producing a leveling effect.

Though the above described systems are not useful for group separations, aqueous complexation can be applied to improve group separations. For example, Weaver and Kappelmann (1968) report that replacement of the mineral-acid solution used in the intra-group separation by various carboxylic acids, and mixtures of carboxylic and aminopolycarboxylic acids results in a very satisfactory group separation. The separation factors for interlanthanide and interactinide separations by HDEHP have been shown previously to average ≈ 2.5 (table 10). Group separations with this extractant system are not satisfactory. Weaver and Kappelmann observe that extraction from 1 M carboxylic acid (pH 1.8) solutions depresses the extraction of Am relative to the lanthanides. At higher pH (≈ 3), the separation factors are increased, with the most consistent enhancement observed for lactic acid. Addition of only 0.05 M diethylenetriaminepentaacetic acid (DTPA) to the solutions of carboxylic acids at pH 3

TABLE 10
Distribution coefficients for americium and Am/La separation factors for solvent extraction separation by HDEHP/carboxylic acid solutions in the presence and absence of DTPA (Weaver and Kappelmann 1968).

Carboxylic acid	No DTPA (pH 1.8)		0.05 M DTPA (pH 3.0)	
	D_{Am}	S_{Am}^{La}	D_{Am}	S_{Am}^{La}
Formic	150	0.14	0.0102	270
Acetic	33	0.24	0.0086	430
Propionic	180	0.41	0.0052	770
Glycolic	0.94	0.74	0.0124	145
Diglycolic	0.0025	4	–	–
Lactic	3.5	1.2	0.0085	380
Citric	0.36	0.90	0.0102	73
Malonic	20	0.31	0.0087	290
α-Hydroxyisobutyric	18	0.7	0.0132	370
Glycine–HNO_3	26	0.23	0.0111	270

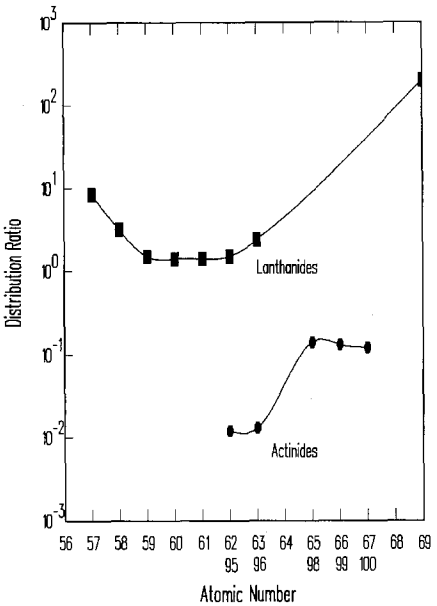

Fig. 3. Distribution ratios for trivalent lanthanides and actinides for the TALSPEAK separation system (0.3 M HDEHP/diisopropylbenzene/1.0 M lactic acid–0.05 M DTPA–pH 3.0), from Weaver and Kappelmann (1968).

resulted in dramatically improved separation factors. For extraction from 1 M lactic acid/0.05 M DTPA/pH 3 with 0.3 M HDEHP/ diisopropylbenzene (DIBP), the worst actinide/lanthanide separation factor is for $S_{Cf}^{Nd} \approx 10$. Lanthanide/actinide separation by this process is illustrated in fig. 3.

Investigation of the details of this system indicate that at low metal-ion loading the extractant dependence from (1 M lactic acid–0.05 M DTPA) is lowered to 2.7–2.9, dependent on the metal ion. Concentration isotherms for the extraction of lanthanum from lactic acid solutions, with and without DTPA present, indicate that saturation occurs at 1.5 equivalents of lanthanum per mol of extractant monomer, interpreted by the authors as indicative of the extraction of one mol of lactate per extracted metal ion. This observation is supported by actual measurement of extracted lactate concentration. Lactic acid is not extracted by HDEHP in the absence of lanthanum. This separation process has acquired the acronym TALSPEAK (trivalent-actinide/lanthanide separation by phosphorus reagent extraction from aqueous komplexes). The generic applicability of the concept is demonstrated by the work of Baybarz (1965), who finds only slightly reduced efficiency upon substitution of 2-ethyl(hexyl)phenylphosphonic-acid/diethyl benzene for HDEHP/DIPB.

A number of more recent reports have discussed applications, process experience, and modifications of TALSPEAK. Kosyakov and Yerin (1980) report that the Cm extraction from TALSPEAK-type aqueous solutions using HDEHP/decane solutions both extractant (HDEHP) and acid dependence are reduced to two, indicating the extraction of a 1 : 1 M-lactate complex for the aliphatic diluent. Similar extractant dependencies were reported for Bk, Eu, and Ce. The extraction reaction is established as independent of [DTPA] (i.e., DTPA complexes are not extracted).

Bourges et al. (1980) report a comparison of TALSPEAK with TBP-nitrate and trilauryl ammonium nitrate extraction for Am/Cm separation using DTPA as aqueous complexing agent (in extraction chromatographic mode). Although TALSPEAK gives higher lanthanide/actinide separation factors, these authors cite favorable chromatographic kinetics and improved Am/Cm separation as justification for the choice of TBP/DTPA over TALSPEAK. Ishimori (1980) find higher distribution ratios in a TALSPEAK-type system using di-isodecylphosphoric acid in place of HDEHP. Bond and Leuze (1980) describe a lanthanide/actinide removal and separation scheme using a 1 M lactic acid–0.05 M DTPA strip to separate trivalent actinides from the lanthanides.

In a recent application of HDEHP to actinide/actinide and actinide/lanthanide separations, Novikov and Myasoedov (1987) report the use of a "supported liquid membrane" impregnated with HDEHP for the separation of Am/Cm, Eu/Tb, and Am/Eu using DTPA, citric acid, and the potassium salt of a heteropolyacid ($K_{10}P_2W_{17}O_{61}$ – KPWO) as aqueous complexants. The optimum separation factors reported are $S_{Cm}^{Am} = 5.0$, $S_{Tb}^{Eu} = 10.8$, and $S_{Am}^{Eu} > 10^2$.

A chromatographic interlanthanide separation by cation exchange in the presence of 1, 4, 7, 10-tetraazacyclododecane-N, N′, N″, N‴-tetraacetic acid (DOTA), present as an aqueous complexant, has been reported by Merciny et al. (1986). In this system the lanthanides are separated into two groups based on the rate of decomposition of the R-DOTA complex. Separation factors are not large, but a chromatographic separation of Gd and Eu is suggested.

8. The role of soft-donors in lanthanide/actinide separation

Aside from the subtle effect of the An–amine binding in the An–DTPA complexes of TALSPEAK, and the chloride, thiosulfate interaction with the actinides in ion-exchange studies, we have not discussed the proposal that there is of slightly greater covalency in actinide complexation (both by hydrophobic and hydrophilic ligands). In this section, the effect of binding of actinides to nitrogen and sulfur donor molecules is discussed within this model.

The emphasis of work by French researchers has been the use of soft-donor extractants and complexants to enhance actinide/lanthanide group separation (Vitorge 1985, Musikas et al. 1980, Musikas 1985). The relative stability constants for lanthanide and actinide azide complexes reported by Musikas et al. (1980) suggest that hydrazoic acid could function as a useful reagent for this separation. This is confirmed in a later report for Am/Eu separation (Musikas 1985) in which americium extraction is suppressed by complex formation with azide. The separation factors are not very different from those reported by Sekine (1965) using SCN^- as the complexant in TBP extraction. However, Choppin and Barber (1989) find that, while the trivalent actinide-azide stability constants are somewhat larger than those of the trivalent lanthanides, the complexation enthalpies calculated from the temperature coefficient of the β's do not support the existence of a covalent bonding contribution.

A soft donor extractant system, mixtures of o-phenanthroline and nonanoic acid,

(Musikas 1985), extracts americium an order of magnitude more strongly than europium from 0.1 M $NaNO_3$ solutions at pH 4.5–5.1 [$S_{Eu}^{Am} = 17.4(\pm 0.9)$]. To accomplish the separation at higher acidity, research has been conducted on the complexant/extractant 2, 4, 6-tris(2-pyridyl)-1, 3, 5-triazine (TPTZ),

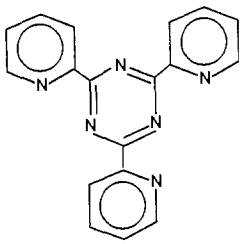

used in conjunction with carboxylate and sulfonate co-extractants. The latter are necessary because of the hydrophilicity of the $Am(NO_3)_3$ TPTZ complex. Replacement of nitrate by α-bromocaprate (decanol diluent) gives group separation factors ≈ 10 with little apparent variation in the distribution ratios for the members of the groups (Am, Cm, or Eu, Nd, Tb, Yb) (table 11) in the pH 2–3 range. Substitution of dinonylnaphthalenesulfonic acid (HDNNs) for α-bromocapric acid gives similar performance at 0.1 M acid.

The work of Musikas on the use of di-thio-substituted HDEHP as an extractant indicates possible significant Am/Eu separation factors when TBP is also present. However, Freiser (1988) disputes these results as being due to HDEHP contamination. Other researchers have considered thio-alkyl phosphate diesters for lanthanide extraction, but they offer only reduced extraction for the lanthanides (Inoue et al. 1989, Kondo et al. 1990).

The thio-derivative 4-benzoyl-2, 4-dihydro-5-methyl-2-phenyl-3H-pyrazol-3-thione (BMPPT), gives good americium/europium separation factors in synergistic extraction systems (Smith et al. 1987, Ensor et al. 1988).

TABLE 11
Extraction of selected trivalent actinides and lanthanides by 2,4,6-tris(2-pyridyl)-1,3,5-triazine (TPTZ)/decanol/1 M α-bromocapric acid (ABCA), and TPTZ,HDNNS/t-butylbenzene/nitric acid (Musikas 1985).

Metal	D(TPTZ/decanol/ABCA) pH 2.2	D(TPTZ,HDNNS/HNO_3) $[H^+] = 0.12$ M
Am	0.85	1.35
Cm	0.80	1.40
Ce	–	0.158
Nd	0.08	–
Eu	0.10	0.199
Gd	–	0.178
Tb	0.11	0.14
Yb	0.10	0.22

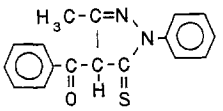

The mixture of 0.3 M BMPPT/0.01 M TOPO/benzene extracts (from 0.1 M $LiClO_4$, pH 3) americium preferentially over europium ($S_{Eu}^{Am} = 68$) (Smith et al. 1987). The analogous system based on the oxygen-donor analogue and TOPO (Chmutova and Kochetkova 1970) gave stronger extraction but no significant separation of curium from europium. Further substitution of the soft-donor synergist 4, 7-diphenyl-1, 10-phenanthroline (DPPHEN) for TOPO (Ensor et al. 1988) results in even greater selectivity for americium ($S_{Eu}^{Am} = 190$, pH 3.7, 0.03 M HBMPPT/0.0027 M DPPHEN). The extracted species is $M(BMPPT)_3(DPPHEN)$ (table 12).

9. Summary and prospects

The special insight of the earliest experimentation on trivalent lanthanide/actinide separations is well demonstrated by the continuing use and adaptation of solvent-extraction and ion exchange procedures developed 20–40 years ago. But the tendency to adopt (and adapt) historically proven technologies should not imply that there is no room for further improvements. Several recent developments indicate significant prospects for more efficient processes. The increasing need for supplies of pure lanthanides, and the possible requirement of actinide partitioning in radioactive-waste treatment imply that new science can have significant new technological impact in this field.

9.1. *Intra-group separation*

Of the separation methods discussed in this chapter, several are useful primarily for intra-group separations. Comparison of data from different authors is usually not

TABLE 12
Distribution ratios and separation factors for americium/europium extraction by 4-benzoyl-2,4-dihydro-5-methyl-2-phenyl-3H-pyrazol-3-thione/toluene (0.0297 M)/0.1 M $NaClO_4$ as a function of 4,7-diphenyl-1,10-phenanthroline (synergist) from Ensor et al. (1988).

[DPPHEN]	D_{Am}	D_{Eu}	S_{Eu}^{Am}
0.00269	25.3	0.138	183
0.00215	21.9	0.112	196
0.00144	14.8	0.077	192
0.00108	10.3	0.059	174
0.000718	6.1	0.039	156
0.000359	2.7	0.021	129

possible because slight differences in the experiments can cause completely different conclusions to be reached (e.g., the choice of diluent as in table 7). Therefore, only those studies which specifically considered intra-group separation factors can legitimately be compared.

A sampling of the methods which are (or could be) used for interlanthanide or interactinide separations are shown in figs. 4 and 5, respectively. These should not be

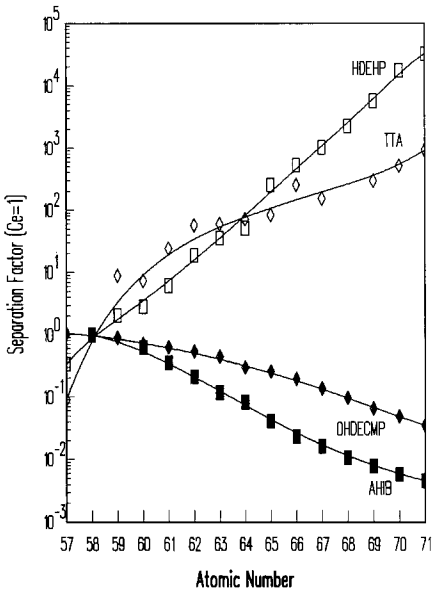

Fig. 4. Interlanthanide separation factors (relative to Ce) for selected methods; HDEHP and TTA data from Stary (1966), AHIB (α-hydroxyisobutyric acid/Dowex 50) data from Choppin and Silva (1956), and Smith and Hoffman (1956), DHDECMP (dihexyl -N, N-diethyl-carbamoylmethylphosphonate) data from Horwitz et al. (1981).

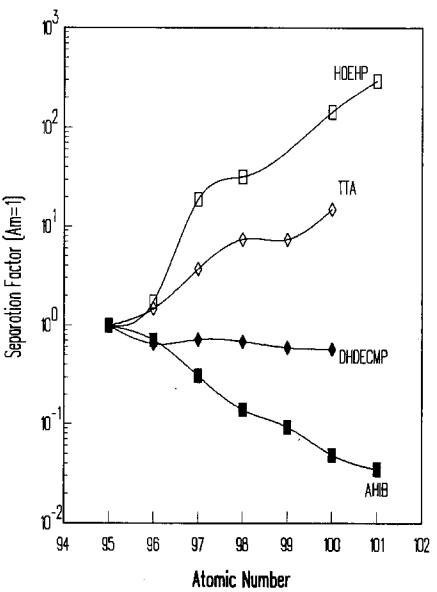

Fig. 5. Interactinide separation factors (relative to Am) for selected methods; HDEHP and TTA data from Stary (1966), AHIB (α-hydroxyisobutyric acid/Dowex 50) data from Choppin et al. (1956), and Smith and Hoffman (1956), DHDECMP (dihexyl -N, N-diethyl-carbamoylmethylphosphonate) data from Horwitz et al. (1981).

viewed as the only means of accomplishing the partitioning, but are systems which should be generally effective. The observed trends in the data are more-or-less systematically correlated with the decrease in cation radii with increasing atomic number. The most consistent trends are observed for solvent extraction using HDEHP and cation exchange using α-hydroxyisobutyric acid as elutriant. Extraction reactions based on DHDECMP exhibit small but consistent changes in D with changing atomic number. An extraction system of this type might be suitable for an extraction chromatographic application.

9.2. *Trivalent lanthanide/actinide group separation*

Unlike the intra-group separations, group separations are generally not directly dependent on the contraction of cation radii. As the prior discussion has attempted to demonstrate, group separations are based primarily on the difference in interaction strength of lanthanides and actinides with extractants or complexants which incorporate soft donor atoms like nitrogen and sulfur. In fig. 6, a broad spectrum of separation methods are presented to illustrate the central role of actinide–soft donor interactions in lanthanide/actinide separations. Because the contraction of ionic radii superimpose effects like those in figs. 4 and 5 on group separations, we compare the separation factor for the iso-electronic lanthanide/actinide pair americium/europium as representative of group separation in general. This is a reasonable representation of group-separation trends.

Included in fig. 6 are separation procedures covering the gamut of effects discussed in this chapter. On the left portion of the figure, americium is more strongly extracted, while on the right, europium is preferentially extracted. The overriding characteristic of this correlation is the effect of the actinide–soft donor interaction on group separations. In those systems furthest to the left, soft-donor interaction between americium and the extractant (or extractants) is observed. The highest separation factors based on preferential extraction of actinides is that reported by Ensor et al. (1988) (bar A). In this system both the primary extractant (HBMPPT) and the synergist (DPPHEN) are soft-donor ligands. Other members of this group include nitrogen-donor extractants like phenanthrolines and oxines (bars C and D). The second highest member of this group is an amine-based extraction from concentrated LiCl solution (bar B). We have noted above that this separation is based on actinide–soft donor interactions brought about by a shift in cation hydration equilibria. Bar F is the analogous anion exchange system. Bars E and J demonstrate the effect of thiocyanate on separation by neutral extractants.

The systems represented by bars L through R demonstrate little ability to successfully separate lanthanides from trivalent actinides. The common feature of this group of separation procedures is the absence of any soft-donor atoms in the extractants. The effect of changing the organic diluent on separation by TTA is shown by Bars M and S. Although neither of these two systems is exceptionally effective, the extraction order in reversed upon changing the diluent from benzene to chloroform. The lowest selectivity is demonstrated by HDNNS (bar O).

At the opposite extreme are the TALSPEAK (bar Y) and related 2-ethylhexyl

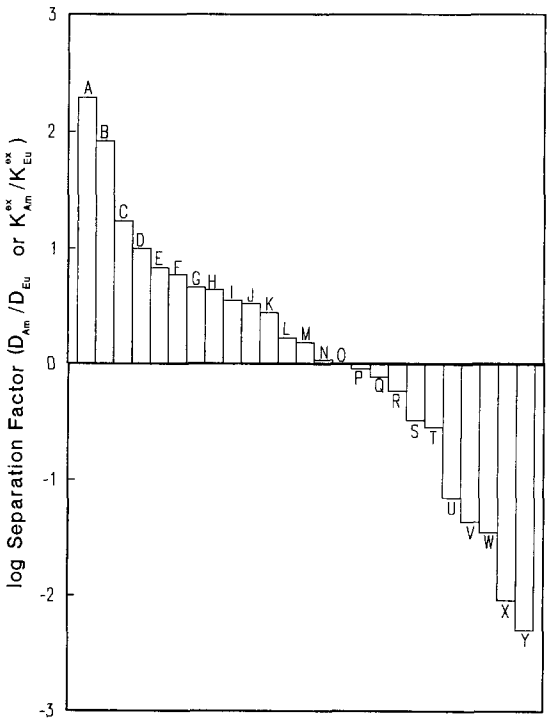

Fig. 6. Histogram representation of americium/europium separation factors (as representative of lanthanide/actinide group separation factors) for a representative collection of separation methods:
(A) HBMPPT/DPPHEN (thiopyrazolone/diphenylphenanthroline) (Ensor et al. 1988); (B) 30% Alamine 336/xylene/11 M LiCl (Stary 1966); (C) 1, 10-phenanthroline/nonanoic acid/decanol (Musikas 1985); (D) 5, 7-dichloroxine/$CHCl_3$ (Sekine and Dyrssen 1964); (E) DHDECMP/NaSCN (Muscatello et al. 1982); (F) Dowex 1/10 M LiCl/87° (Stary 1966); (G) 100% TBP/13 M HNO_3 (Stary 1966); (H) Dowex 50/10.5 M HCl/40% ethanol–water (Guseva and Tikhomirova 1972); (I) Dowex 50/ammonium-α-hydroxyisobutyric acid as elutriant (Choppin et al. 1956, Choppin and Silva 1956); (J) 5% TBP/hexane/1 M NaSCN-4 M $NaClO_4$ (pH 4–5) (Sekine 1965); (K) Dowex A1 (Mathur and Khopkar 1985); (L) DHDECMP/diisopropyl benzene/1.0 M HNO_3 (Horwitz et al. 1981); (M) TTA/benzene (Stary 1966); (N) Biorex 70 (Choppin and Ohene-Aniapam 1983); (O) Dinonylnapthalenesulfonic acid (Khopkar and Narayanankutty 1968); (P) 1-hydroxynapthoic acid (Sekine and Dyrssen 1964); (Q) N-benzoylhydroxylamine (Sekine and Dyrssen 1964); (R) neocupferron (Sekine and Dyrssen 1964); (S) TTA/$CHCl_3$ (Sekine and Dyrssen 1964); (T) 1-phenyl-3-methyl-4-acetyl-5-pyrazolone (Sekine and Dyrssen 1964); (U) Dioctylphosphoric acid (Sekine and Dyrssen 1964); (V) Dibutylphosphoric acid (Sekine and Dyrssen 1964); (W) Bis(2-ethylhexyl) phosphoric acid (Sekine and Dyrssen 1964); (X) 2-ethylhexyl (phenylphosphonic) acid/diethylbenzene/1.0 M Lactic acid–0.05 M DTPA–pH 3.0 (Baybarz 1965); (Y) TALSPEAK – 0.3 M HDEHP/diisopropylbenzene/1.0 M Lactic acid–0.05 M DTPA–pH 3.0 (Weaver and Kappelmann 1968).

(phenylphosphonic acid)/carboxylic acid/DTPA system (bar X) reported by Baybarz (1965). Central to these separations methods is the difference in the strength of interaction between the aminopolycarboxylate DTPA and the trivalent metal ions. Though there is no denying the effectiveness of soft-donor ligands in lanthanide/actinide separations, the discussion of actinide-aminopolycarboxylate complexation heats indicates that the source of this effect still is not clearly established.

There are two apparent artifacts in this correlation. First, one would not expect based on these arguments that the acidic phosphoric acid esters HDOP, HDBP, and HDEHP (bars U, V, and W) would demonstrate as great a selectivity for europium as is observed. Similarly, there is no apparent reason for the enhanced selectivity demonstrated by 100% TBP for americium for extraction from 13 M HNO_3 (bar G). In the case of the phosphoric-acid extractants, the apparent anomaly is a manifestation of the steep slope of the linear relationship between distribution ratios and atomic number (cation radii) as shown in figs. 4 and 5, and a mismatch of the ionic radii of americium and europium. It is generally believed that the cation radius of americium is more nearly comparable to that of promethium or neodymium than europium (see table 1). The log S_{Nd}^{Am} calculated from the the same data is -0.35.

9.3. *Future trends*

The two most potentially important developments in the design of new extractants for lanthanide/trivalent-actinide separation are the recent studies of both linear and cyclic polyethers as synergists in extraction reactions, and the design of soft-donor ligands. Crown-ether extractants incorporating both soft-donor (amine) binding and intrinsic chelation (e.g., the work of Chang et al. (1989) and Manchanda and Chang (1986)) have potential for providing significant improvements in lanthanide/actinide separation efficiencies if reaction kinetics can be improved.

The concept of accomplishing lanthanide/actinide separations by exploiting the differences in the reaction kinetics of the metal ions is another innovative concept with intriguing potential. Separations based on the use of alkaline solutions fall into this category, as does the use of crown-ether caboxylate extractants.

The potential of diluent modification in enhancing lanthanide/actinide separation factors has barely been tapped. The absence of a reliable predictive theory of solvation of both the extractant molecules and the extracted complexes hampers the development of this area. In view of the small energies required to reverse extraction order (a few hundred joules), subtle alteration of the organic diluent (or the aqueous medium in ion exchange procedures) also has the potential for significantly improving (at least) group separations.

The most successful group separations are achieved through the agency of aqueous complexing agents. The premier use of aqueous complexants in lanthanide/actinide separation is found in the TALSPEAK process, which relies on complexation of the metal ions by DTPA. Continued development and adaptation of this process indicate its general utility. Recent work in this laboratory (Nash and Horwitz 1990, Nash 1991) suggests that phosphonic acid ligands may have significant potential for improving intra-group separation factors. Based on the mathematical treatment described in eq. (10), sulfonic-acid extractants working in consort with aqueous complexing agents is an approach worthy of investigation.

References

Alstad, J., J.H. Augustson and L. Farbu, 1974, J. Inorg. & Nucl. Chem. **36**, 899.

Aly, H.F., and R.M. Latimer, 1967, J. Inorg. & Nucl. Chem. **29**, 2041.

Aly, H.F., and R.M. Latimer, 1970a, J. Inorg. & Nucl. Chem. **32**, 3081.

Aly, H.F., and R.M. Latimer, 1970b, Radiochim. Acta **14**, 27.

Aly, H.F., S.M. Khalifa, J.D. Navratil and M.T. Saba, 1985, Solvent Extr. & Ion Exch. **3**, 623.

Baybarz, R.D., 1965, J. Inorg. & Nucl. Chem. **27**, 1831.

Best, G.F., E. Hesford and H.A.C. McKay, 1959, J. Inorg. & Nucl. Chem. **12**, 136.

Billon, A., 1979, J. Radioanal. Chem. **51**, 297.

Bond, W.D., and R.E. Leuze, 1980, Removal of americium and curium from high-level wastes, in: Actinide Separations, ACS Symposium Series, Vol. 117, eds J.D. Navratil and W.W. Schulz (American Chemical Society, Washington, DC) p. 441.

Bourges, J., C. Madic and G. Koehly, 1980, Transplutonium element production program: extraction chromatographic process for plutonium irradiated targets, in: Actinide Separations, ACS Symposium Series, Vol. 117, eds J.D. Navratil and W.W. Schulz (American Chemical Society, Washington, DC) p. 33.

Bukhina, T.I., Z.K. Karalova and B.F. Myasoedov, 1983, Radiokhimiya **25**, 697.

Ceccaroli, B., and J. Alstad, 1981, J. Inorg. & Nucl. Chem. **43**, 1881.

Chang, C.A., V.K. Manchanda and J. Peng, 1989, Solvent Extr. & Ion Exch. **7**, 413.

Chemical Rubber Company Handbook of Chemistry and Physics, 1987, p. D-235.

Chmutova, M.K., and N.E. Kochetkova, 1970, Zh. Anal. Khim. **25**, 710.

Chmutova, M.K., G.A. Pribylova and B.F. Myasoedov, 1973, Zh. Anal. Khim. **28**, 2340.

Chmutova, M.K., N.P. Nesterova, O.E. Koiro and B.F. Myasoedov, 1975, Zh. Anal. Khim. **30**, 1110.

Choppin, G.R., 1978, J. Mol. Struct. **45**, 39.

Choppin, G.R., 1985, Separation of actinides in aqueous solution by oxidation state, in: Actinide/ Lanthanide Separations, Proc. Int. Symp., Honolulu, HI, 16–22 December 1984, eds G.R. Choppin, J.D. Navratil and W.W. Schulz (World Scientific, Singapore) p. 176.

Choppin, G.R., and D.W. Barber, 1989, J. Less-Common Met. **149**, 231.

Choppin, G.R., and K. Buijs, 1963, J. Chem. Phys. **39**, 2042.

Choppin, G.R., and A. Chatham-Strode, 1960, J. Inorg. & Nucl. Chem. **15**, 377.

Choppin, G.R., and F. Ohene-Aniapam, 1983, Solvent Extr. & Ion Exch. **1**, 585.

Choppin, G.R., and R.J. Silva, 1956, J. Inorg. & Nucl. Chem. **3**, 153.

Choppin, G.R., and M.R. Violante, 1972, J. Chem. Phys. **56**, 5890.

Choppin, G.R., S.G. Thompson, B.G. Harvey and G.T. Seaborg, 1954, J. Am. Chem. Soc. **76**, 6229.

Choppin, G.R., B.G. Harvey and S.G. Thompson, 1956, J. Inorg. & Nucl. Chem. **2**, 66.

Choppin, G.R., J.D. Navratil and W.W. Schulz, eds, 1985a, Actinide/Lanthanide Separations (World Scientific, Singapore).

Choppin, G.R., Q. Lin and J.C. Sullivan, 1985b, Inorg. Chem. **24**, 3968.

Choppin, G.R., E.N. Rizkalla and J.C. Sullivan, 1987, Inorg. Chem. **26**, 2318.

Cossy, C., L. Helm and A.E. Merbach, 1989, Inorg. Chem. **28**, 2699.

Cotton, F.A., and G. Wilkinson, 1988a, Advanced Inorganic Chemistry (Wiley Interscience, New York) p. 963.

Cotton, F.A., and G. Wilkinson, 1988b, Advanced Inorganic Chemistry (Wiley Interscience, New York) pp. 955, 956, 982, 983.

Cotton, F.A., and G. Wilkinson, 1988c, Advanced Inorganic Chemistry (Wiley Interscience, New York) p. 982.

Dukov, I., and L. Genov, 1986, Solvent Extr. & Ion Exch. **4**, 999.

Dukov, I., and L. Genov, 1988, Solvent Extr. & Ion Exch. **6**, 447.

Dyrssen, D., and D.H. Liem, 1960, Acta Chem. Scand. **14**, 1100.

Elesin, A.A., V.M. Nikolaev, V.V. Shalimov, Yu.S. Popov, V.N. Kovantsev, I.V. Tselischev, V.T. Filmonov, V.B. Mishenev, A.A. Yadovin, L.S. Golosovskii, A.P. Chetverikov and Yu.V. Efremov, 1986, Radiokhimiya **28**, 786.

Ensor, D.D., and A.H. Shah, 1983, Solvent Extr. & Ion Exch. **1**, 241.

Ensor, D.D., and A.H. Shah, 1984, Solvent Extr. & Ion Exch. **2**, 591.

Ensor, D.D., G.D. Jarvinen and B.F. Smith, 1988, Solvent Extr. & Ion Exch. **6**, 439.

Freiser, H., 1988, Solvent Extr. & Ion Exch. **6**, 1093.

Gmelin Handbook of Inorganic Chemistry (8th Ed.), 1983, Sc, Y, La–Lu Rare Earth Elements, Part D 6, Ion Exchange and Solvent Extraction Reactions, Organometallic Compounds (Springer, Berlin) pp. 1–136.

Grigorescu-Sabau, C., 1962, J. Inorg. & Nucl. Chem. **24**, 195.

Guseva, L.I., and G.S. Tikhomirova, 1972, Radiokhimiya **14**, 188.

Guseva, L.I., and G.S. Tikhomirova, 1979, J. Radioanal. Chem. **52**, 369.

Guseva, L.I., G.S. Tikhomirova and V.V. Stepushkina, 1987a, Radiokhimiya **29**, 629.

Guseva, L.I., G.S. Tikhomirova and V.V. Stepushkina, 1987b, Radiokhimiya **29**, 211.

Handbook of Ion Exchange Resins: Their Application to Inorganic Chemistry, Vol. 1, 1986, Principles, Rare Earth Elements (CRC Press, Boca Raton, FL) pp. 115–271.

Handbook of Ion Exchange Resins: Their Application to Inorganic Chemistry, Vol. 2, 1986, Actinides (CRC Press, Boca Raton, FL).

Hedrick, J.B., and D.A. Templeton, 1991, Rare Earth Minerals and Metals Yearbook 1989 (US Department of Interior, Bureau of Mines, May).

Helferrich, F., 1962, Ion Exchange (McGraw-Hill, New York).

Horwitz, E.P., C.A. Bloomquist, L.J. Sauro and D.J. Henderson, 1966, J. Inorg. & Nucl. Chem. **28**, 2313.

Horwitz, E.P., A.C. Muscatello, D.G. Kalina and L. Kaplan, 1981, Sep. Sci. Tech. **16**, 417.

Hulet, E.K., ed., 1990, Report of a Workshop on Transactinium Science, UCRL-LR-104538.

Imura, H., T.M. Samy and N. Suzuki, 1987, Proc. Symp. Solvent Extraction (Japan Assoc. Solvent Extraction, Hamamatsu, Japan).

Inoue, K., N. Kaneko, K. Yoshizuka and Y. Baba, 1989, Proc. Symp. Solvent Extraction (Japan Assoc. Solvent Extraction, Hamamatsu, Japan).

Ishimori, T., 1980, Studies on actinides separation in JEARI, in: Actinide Separations, ACS Symposium Series, Vol. 117, eds J.D. Navratil and W.W. Schulz (American Chemical Society, Washington, DC) p. 333.

Jedinakova, V., Z. Dvorak and P. Blasek, 1988, Radioisotopy **29**, 230.

Jenkins, I.L., 1979, Hydrometallurgy **5**, 1.

Jenkins, I.L., 1984, Solvent Extr. & Ion Exch. **2**, 1.

Kandil, A.T., H.F. Aly, M. Raieh and G.R. Choppin, 1975, J. Inorg. & Nucl. Chem. **37**, 229.

Karalova, Z.K., L.M. Rodinova and B.F. Myasoedov, 1982, Radiokhimiya **24**, 210.

Karalova, Z.K., B.F. Myasoedov, T.I. Bukina and E.A. Lavrinovich, 1988, Solvent Extr. & Ion Exch. **6**, 1109.

Kasting, G.B., E.K. Hulet, J.A. Heppert and J.F. Wild, 1979, J. Inorg. & Nucl. Chem. **41**, 745.

Khopkar, P.K., and J.N. Mathur, 1977, J. Inorg. & Nucl. Chem. **39**, 2063.

Khopkar, P.K., and J.N. Mathur, 1982, Sep. Sci. & Technol. **17**, 985.

Khopkar, P.K., and P. Narayanankutty, 1968, J. Inorg. & Nucl. Chem. **30**, 1957.

Kochetkova, N.E., M.K. Chmutova and B.F. Myasoedov, 1972, Zh. Anal. Khim. **27**, 678.

Kondo, K., K. Momota and F. Hakashio, 1990, J. Chem. Eng. Jpn. **23**, 30.

Kosyakov, V.N., and E.A. Yerin, 1980, J. Radioanal. Chem. **56**, 93.

Li, T., and J. Yu, 1987, Beijing Shifan Daxue Xuebao. Ziran Kexueban **1**, 60.

Lincoln, S.F., 1986, in: Advances in Inorganic and Bioinorganic Mechanisms, Vol. 4, ed. A.G. Sykes (Academic Press, London) pp. 217–287.

Manchanda, V.K., and C.A. Chang, 1986, Anal. Chem. **58**, 2269.

Marcus, Y., 1983, J. Solution Chem. **12**, 271.

Marcus, Y., and A.S. Kertes, 1969, Ion Exchange and Solvent Extraction of Metal Complexes (Wiley Interscience, London).

Mathur, J.N., 1983, Solv. Extr. & Ion Exch. **1**, 349.

Mathur, J.N., and G.R. Choppin, 1993, Solvent Extr. & Ion. Exch. **11**, 1.

Mathur, J.N., and P.K. Khopkar, 1983a, Solvent Extr. & Ion Exch. **1**, 597.

Mathur, J.N., and P.K. Khopkar, 1983b, Radiochem. & Radioanal. Lett. **57**, 259.

Mathur, J.N., and P.K. Khopkar, 1985, Solvent Extr. & Ion Exch. **3**, 753.

Mathur, J.N., and P.K. Khopkar, 1986, Radiochim. Acta **39**, 77.

Mathur, J.N., and P.K. Khopkar, 1987a, Polyhedron **6**, 2099.

Mathur, J.N., and P.K. Khopkar, 1987b, J. Radioanal. & Nucl. Chem. **109**, 329.

Mathur, J.N., and P.K. Khopkar, 1988, Solvent Extr. & Ion Exch. **6**, 111.

Merciny, E., J.F. Desreux and J. Fuger, 1986, Anal. Chim. Acta **189**, 301.

Moeller, T., 1963, The Chemistry of the Lanthanides (Reinhold, New York).
Moore, F.L., 1961, Anal. Chem. **33**, 748.
Moore, F.L., 1964, Anal. Chem. **36**, 2158.
Muscatello, A.C., E.P. Horwitz, D.G. Kalina and L. Kaplan, 1982, Sep. Sci. & Technol. **17**, 859.
Musikas, C., 1985, Actinide–lanthanide group separation using sulfur and nitrogen donor extractants, in: Actinide/Lanthanide Separations, Proc. Int. Symp., Honolulu, HI, 16–22 December 1984, eds G.R. Choppin, J.D. Navratil and W.W. Schulz (World Scientific, Singapore) p. 19.
Musikas, C., G. LeMarois, R. Fitoussi and C. Cuillerdier, 1980, Properties and uses of nitrogen and sulfur donor ligands in actinide separations, in: Actinide Separations, ACS Symposium Series, Vol. 117, eds J.D. Navratil and W.W. Schulz (American Chemical Society, Washington, DC) p. 131.
Nakamura, S., Y. Surakitbanbarn and K. Akiba, 1987, Proc. Symp. Solvent Extraction (Japan Assoc. Solvent Extraction, Hamamatsu, Japan).
Nash, K.L., 1991, Eur. J. Solid State & Inorg. Chem. **28**, 389.
Nash, K.L., and E.P. Horwitz, 1990, Inorg. Chim. Acta **169**, 245.
Nash, K.L., and J.C. Sullivan, 1991, Kinetics of complexation and redox reactions of the lanthanides in aqueous solutions, in: Handbook on the Physics and Chemistry of Rare Earths, Vol. 15, eds K.A. Gschneidner Jr and L. Eyring (Elsevier, Amsterdam). pp. 347-391.
Nash, K.L., J.M. Cleveland and T.F. Rees, 1988, J. Environ. Radioactivity **7**, 131.
Navratil, J.D., and W.W. Schulz, eds, 1980, Actinide Separations, ACS Symposium Series, Vol. 117 (American Chemical Society, Washington, DC).
Novikov, A.P., and B.F. Myasoedov, 1987, Solvent Extr. & Ion Exch. **5**, 111.
Rizkalla, E.N., J.C. Sullivan and G.R. Choppin, 1989, Inorg. Chem. **28**, 909.
Samy, T.M., H. Imura and N. Suzuki, 1988, J. Radioanal. & Nucl. Chem. **126**, 153.
Sato, T., 1989, Hydrometallurgy **22**, 121.
Sekine, T., 1965, Bull. Chem. Soc. Jpn. **38**, 1972.
Sekine, T., and D. Dyrssen, 1964, Talanta **11**, 867.
Sekine, T., and Y. Hasegawa, 1977, Solvent Extraction Chemistry (Marcel Dekker, New York).
Shannon, R.D., 1976, Acta Crystallogr. A **32**, 751.
Sheveleva, I.V., and I.O. Bogatyrev, 1987, Zh. Fiz. Khim. **61**, 1040.
Shoun, R.R., and W.J. McDowell, 1980, Actinide extractants: development, comparison, and future, in: Actinide Separations, ACS Symposium Series, Vol. 117, eds J.D. Navratil and W.W. Schulz (American Chemical Society, Washington, DC) p. 71.
Siddall III, T.H., 1963, J. Inorg. & Nucl. Chem. **25**, 883.
Siddall III, T.H., 1964, J. Inorg. & Nucl. Chem. **26**, 1991.
Smith, B.F., G.D. Jarvinen, G.G. Miller, R.R. Ryan and E.J. Peterson, 1987, Solvent Extr. & Ion Exch. **5**, 895.
Smith, H.L., and D.C. Hoffman, 1956, J. Inorg. & Nucl. Chem. **2**, 243.
Stary, J., 1966, Talanta **13**, 421.
Street Jr, K., and G.T. Seaborg, 1950, J. Am. Chem. Soc. **72**, 2790.
Surls, J.P., and G.R. Choppin, 1957, J. Inorg. & Nucl. Chem. **4**, 62.
Tang, J., and C.M. Wai, 1986, Anal. Chem. **58**, 3233.
Thiyagarajan, P., H. Diamond and E.P. Horwitz, 1988, J. Appl. Crystallogr. **21**, 848.
Usuda, S., 1988, J. Radioanal. & Nucl. Chem. **123**, 619.
Usuda, S., N. Shinohara and H. Yoshikawa, 1987, J. Radioanal. Nucl. Chem. **109**, 353.
Vitorge, P., 1985, Report 1984, CEA-R-5270.
Vobecky, M., 1989, J. Radioanal. Nucl. Chem. **135**, 165.
Weaver, B., 1974, Solvent extraction in the separation of rare earths and trivalent actinides, in: Ion Exchange and Solvent Extraction, Vol. 6, eds J.A. Marinsky and Y. Marcus (Marcel Dekker, New York).
Weaver, B., and F.A. Kappelmann, 1968, J. Inorg. & Nucl. Chem. **30**, 263.
Werner, L.B., and I. Perlman, 1946, Manhattan Project Report BC-1.
Yan, J., and W. Ye, 1989, Zhongguo Xitu Wuebao **7**, 39.

Handbook on the Physics and Chemistry of Rare Earths
Vol. 18 – Lanthanides/Actinides: Chemistry
edited by K.A. Gschneidner, Jr., L. Eyring, G.R. Choppin and G.H. Lander

Chapter 122

COMPARATIVE THERMOCHEMICAL AND OXIDATION–REDUCTION PROPERTIES OF LANTHANIDES AND ACTINIDES

Lester R. MORSS
Chemistry Division, Argonne National Laboratory, Argonne, IL 60439, USA

Contents

Symbols 240
1. Introduction 240
2. Experimental thermodynamic properties 241
   2.1. Free atoms; free and hydrated (standard-state aqueous) ions 243
      2.1.1. Enthalpies of vaporization of metals 243
      2.1.2. Ionization energies 248
      2.1.3. Hydration enthalpies and entropies 249
      2.1.4. Standard-state enthalpies of formation of aqueous ions 254
      2.1.5. f→d transitions and the correlation function $P(M)$ 255
   2.2. Thermophysical properties of condensed systems 256
      2.2.1. Solids: heat capacities 256
      2.2.2. Aqueous ions: heat capacity, osmotic coefficient, entropy 256
   2.3. Thermochemical properties of compounds 257
      2.3.1. Sesquioxides 257
      2.3.2. Hydroxides 257
      2.3.3. Other oxides 260
      2.3.4. Halides 260
   2.4. Free-energy determinations 261
      2.4.1. Oxidation–reduction chemistry in aqueous solution 261
         2.4.1.1. Aqueous solution electrochemistry (uncomplexed ions) 261
         2.4.1.2. Aqueous solution electrochemistry and chemical oxidation (complexed ions) 267
         2.4.1.3. Radioelectrochemistry 267
         2.4.1.4. Pulse radiolysis evidence for dipositive and tetrapositive ions 267
         2.4.1.5. Evidence for An(VI) ions from β-decay of precursor ions in aqueous solution 267
      2.4.2. Reduction potential diagrams in aqueous solution 268
      2.4.3. Solution electrochemistry in non-aqueous solvents (including molten salts) 268
      2.4.4. Gas–solid equilibrium and vaporization measurements 270
      2.4.5. Solid-state electrochemistry 272
3. Estimated and calculated thermodynamic properties 272
   3.1. Synthesis under equilibrium conditions 272
   3.2. Thermal analysis 272
   3.3. Lattice-energy calculations and Born–Haber cycles: intra- and inter-group comparisons 272
   3.4. Correlations of electron-transfer and f→d spectra and reduction potentials 273

4. Lanthanide–actinide bonding and oxidation–reduction comparisons 274
4.1. Bonding in "ionic" systems 274
4.1.1. Oxides: covalency and acid–base effects 274
4.1.2. Binary and complex oxides 276
4.1.3. Binary and complex halides 277
4.2. Bonding in "covalent" systems: organometallics 278
4.2.1. Sigma bonding 278
4.2.2. Pi bonding 279
4.3. Bonding in metallic systems 279
4.4. Oxidation–reduction comparisons in "ionic" systems 280
4.4.1. Binary oxides and halides 280
4.4.2. Complex oxides and halides 282
4.5. Lanthanide–actinide oxidation–reduction comparisons in aqueous (uncomplexed, "standard-state" as well as "formal") solutions 282
References 286

Symbols

a	acidity parameter, defined in section 4.1.1 [eq.(7)]
CN	inner-sphere coordination number of an ion
Cp′	the functional group η^5-$(CH_3)_5C_5$, in which η^5 refers to all five carbon atoms in the cyclopentadienyl ring being bonded to a metal atom
I_n	ionization energy of $M^{(n-1)+} \rightarrow M^{n+}$
J	the overall magnetic quantum number of an atom or ion
K_{sp}^0	solubility product: equilibrium constant for solubility in water, e.g., eq.(3)
$P(M)$	promotion function defined in fig. 2
r	ionic radius as defined by Shannon (1976)
ΣI	sum of ionization potentials $I_1 + I_2 + \cdots + I_n$ for the ion M^{n+}
t	Goldschmidt tolerance factor defined in section 4.1.2
$\Delta_d E(q)$	energy difference between lowest energy levels of the $f^q d^1 s^2$ and $f^{q+1} s^2$ configurations, where $q = Z - 57$ (lanthanides) or $q = Z - 89$ (actinides)
$\Delta \bar{G}(O_2)$	partial molar Gibbs free energy of oxygen
$\Delta_{hyd}H(M)$	enthalpy of hydration of element M (kJ mol^{-1})
$\Delta_{subl}H(M)$	enthalpy of sublimation of element M (kJ mol^{-1})
α	rare-earth oxide phase $PrO_{1.72-2.00}$
β	rare-earth oxide phase $PrO_{1.833} = Pr_{12}O_{22}$
δ	rare-earth oxide phase $PrO_{1.818} = Pr_{11}O_{20}$
ε	rare-earth oxide phase $PrO_{1.800} = Pr_{10}O_{18}$
ϕ	rare-earth oxide phase $PrO_{1.50} = Pr_2O_3$
ι	rare-earth oxide phase $PrO_{1.714} = Pr_7O_{12}$
σ	rare-earth oxide phase $PrO_{1.50-1.70}$
ζ	rare-earth oxide phase $PrO_{1.778} = Pr_9O_{16}$

1. Introduction

This chapter reviews and compares the thermochemical properties of f-element ions in aqueous solution, in oxides (sesquioxides, dioxides, and complex oxides), in selected

halides (trichlorides, trifluorides and tetrafluorides) and in organometallic compounds. New insights based upon recent measurements are highlighted. The differences among lanthanide and actinide ions as a function of f-electron number and coordination environment are discussed.

In general, the two emphases of this chapter are (1) to correlate the energetics of ions that change their f-electron configuration smoothly and (2) to contrast energetics of reactions of 4f ions with those of 5f ions. We may generalize a recent concept enunciated by Johnson (1980) as follows: *The lanthanide elements are a series, and the actinide elements are a second series, that behave similarly in reactions in which the number of 4f or 5f electrons is conserved. The elements behave differently in reactions in which the number of 4f or 5f electrons changes.* We accept this principle for *intra*-series comparisons that conserve the number of *f* electrons ($4f^n \rightarrow 4f^n$ or $5f^n \rightarrow 5f^n$ reactions, such as coordination, complexation, dissolution and acid–base reactions). The principle does not apply to *inter*- series comparisons [e.g., we do not assume that the hydrolysis of Am^{3+}(aq) is the same as that of Nd^{3+}(aq), although both have nearly the same crystallographic radii]. We attempt wherever possible to identify *differences* between 4f and 5f reaction energetics. Thus we do not review lanthanide-only sets of data and we reject any comparison that merely assumes parallel $4f^n$–$5f^n$ energetics. In this way, covalency and acid–base differences of the two series are highlighted.

2. Experimental thermodynamic properties

A systematic understanding of the energetic relationships among free and condensed f-element species was developed by Brewer (1971, 1983a, b, 1987) and by Nugent et al. (1971, 1973a, b and Nugent (1975) to assign and to correlate the known free atom/ion energy levels as well as the 4f–5d (lanthanide) and 5f–6d (actinide) spectra in solids and in solution. Regularities and apparent irregularities among these energetic relationships (e.g., fig. 1) also provided insight and predictive value for the thermochemical properties of the di-, tri- and tetrapositive ions in solids and aqueous solution. These authors used the systematics of energetic relationships to predict properties for those species too unstable (in a chemical or nuclear sense) to be studied. A useful function, $P(M)$, was defined (Nugent et al. 1973b) for these heavy actinide ions Bk^{3+} through Lr^{3+}. This function is defined in fig. 2, is plotted in fig. 3, and is discussed in detail in section 2.1.5. The correlations shown in figs. 1 and 2 represent chemically meaningful uses of the term *valence*. The f^0, f^7 and f^{14} solid metals Y, La, Gd, Lu, Ac, Cm and (possibly) Lr are trivalent; ionic compounds containing their tripositive ions are also trivalent. Properties of these elements shown in figs. 1, 2 and 3 represent trivalent → trivalent reactions and thus fulfill Johnson's "conservation principle" above. Other properties represent divalent → trivalent reactions [e.g., Eu(s) → Eu(g)] and these reactions display unusual f-element chemistry. A reaction exhibiting a change of valence is an oxidation–reduction reaction in a generalized sense.

This section discusses and tabulates "best values" for important experimentally derived thermodynamic properties of free atoms and ions, aquo-ions, halides, dioxides, sesquioxides and tripositive hydroxides in an effort to characterize the properties of

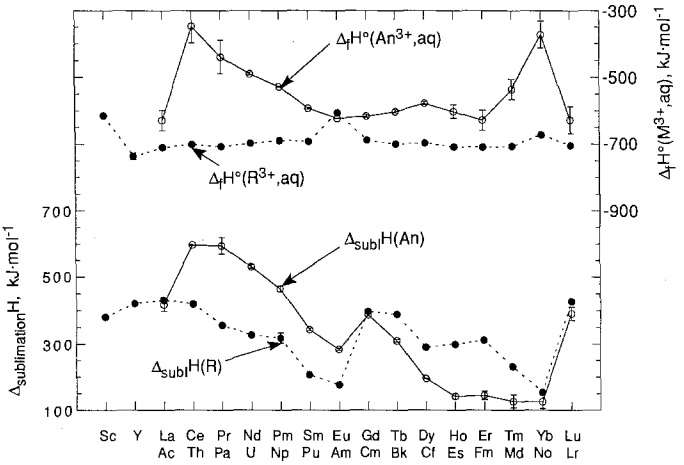

Fig. 1. Enthalpies of sublimation of rare earth and actinide metals and enthalpies of formation of their 3+ aquo-ions. Values of $\Delta_{subl}H$ for Md–Lr and $\Delta_f H^0$ [$Es^{3+}(aq)$–$Lr^{3+}(aq)$] are estimates.

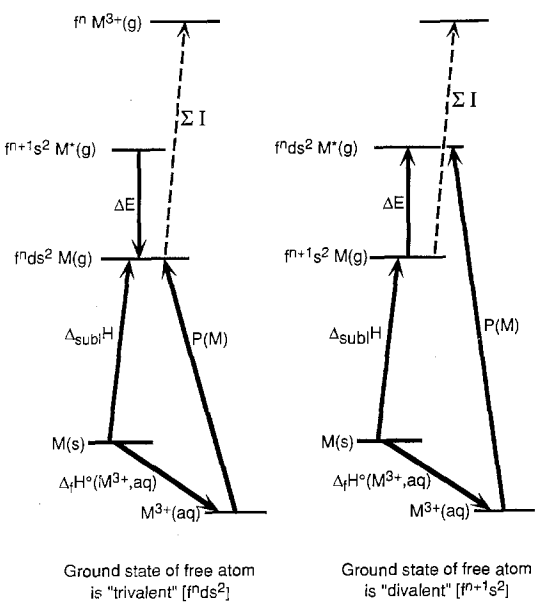

Fig. 2. Energy-level diagram illustrating the relationships among a metal M, the standard-state aqueous ion, the free ion, and the hydrated ion in dilute aqueous solution. The promotion function P(M) (section 2.1.5) is shown. Left-hand side: ground state of free atom M(g) is "trivalent" [$f^n ds^2$]; right-hand side: ground state of free atom M(g) is "divalent" [$f^{n+1}s^2$]. M*(g) refers to an excited state of M(g).

these species as a function of their f-element ions. Figure 2 shows the species (metals, free atoms, isolated ions and solvated ions), the energetics of transitions among these species on an energy-level scale, and the function P(M).

Bratsch and Lagowski (1985a, 1986) calculated enthalpies of formation of lanthanide and actinide aquo-ions and compounds. However, they used thermodynamic proper-

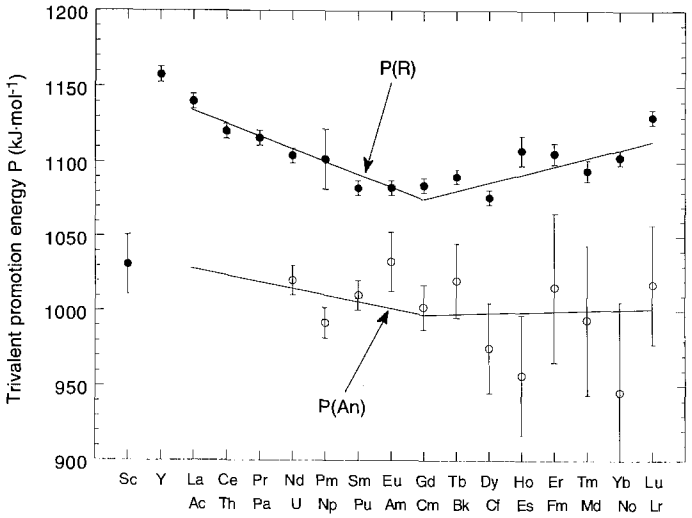

Fig. 3. *P*(M) function for lanthanide and actinide ions, representing the energetics of transition from a trivalent aquo-ion M^{3+} (aq) to a "trivalent" free atom $M(f^n ds^2)(g)$. Error limits and the nearly-horizontal lines (forming open V's and representing the f^0–f^7 and f^7–f^{14} regions) are the author's estimates.

ties for actinide free atoms and ions and condensed species that were derived from lanthanide thermochemical data (Bratsch and Lagowski 1985a, table IV) and assumed that trends in these properties parallel those for the lanthanide species (Bratsch and Lagowski 1986). Their assumption renders moot the issue of lanthanide–actinide differences, since it assumes that inter-series differences are essentially constant. Therefore, we utilize their free-ion thermodynamic properties where appropriate but *not* their thermodynamic properties for condensed species.

Thermochemical properties of scandium species, including Sc^{3+}(aq), have been evaluated by Travers et al. (1976). For completeness, the properties of scandium species are included in this chapter. Because the ionic radius of Sc^{3+} is much smaller than that of any other R^{3+}, its properties are not included in inter-series comparisons.

2.1. *Free atoms; free and hydrated (standard-state aqueous) ions*

Enthalpies and entropies of hydration, and standard-state enthalpies of formation, of *monoatomic ions* are discussed in this section. Thermophysical and thermochemical properties of *condensed systems* are found in sections 2.2 and 2.3. Standard-state entropies of ions are discussed in section 2.2.2. Free energies (reduction potentials, etc.) are discussed in section 2.4.

2.1.1. *Enthalpies of vaporization of metals*

The enthalpy of vaporization of a metal at 298 K $\{\Delta_{subl}H(M) = \Delta_f H^0(M,g)\}$, which is the standard-state enthalpy of formation of the metal vapor at 298 K, is determined (Pitzer and Brewer 1961) from the temperature coefficient of the vapor pressure of the

TABLE 1

Standard enthalpies, free energies of formation and standard entropies of important rare-earth and actinide species at 298 K and $p = 1$ atm ($\Delta_f H^0$ and $\Delta_f G^0$ in kJ mol^{-1}; S^0 in J mol^{-1} K^{-1}) (estimated values in parentheses)[a].

M	$\Delta_f H^0$ [M(g)][b]	$\Delta_f H^0$ [M^{2+}(aq)]	S^{0c} [M^{2+}(aq)]	$\Delta_f G^0$ [M^{2+}(aq)]	$\Delta_f H^0$ [M^{3+}(aq)]	S^{0c} [M^{3+}(aq)]	$\Delta_f G^0$ [M^{3+}(aq)]	$\Delta_f H^0$ [M^{4+}(aq)]	S^{0c} [M^{4+}(aq)]	$\Delta_f G^0$ [M^{4+}(aq)]
Sc	381.2[d]				−650[d]	255[d]	−623[d]			
Y	421.3				−736.5[c]	−249	707.5			
La	431.0		(7)		−709.4	−209	−688		–	
Ce	420.1		(6)		−700.4	(−200)[f]	−676	−580	−431	−510
Pr	356.9		(2)		−706.2	(−194)[f]	−681	(−439)	(−419)	(−371)
Nd	326.9	(−402)	(−4)	−419	−696.6	−206	−672	(−263)	(−419)	(−197)
Pm	(318)	(−390)	(−10)	(−406)	(−688)	(−200)	(−663)		(−420)	
Sm	206.7	(−504)	(−17)	−527	−691.1[g]	−207	−677		(−423)	
Eu	177.4	−527.8	−10	−541	−605.6	−216	−576		(−428)	
Gd	397.5		(−16)		−687.0	−219	−660		(−445)	
Tb	388.7		(−6)		−698.3[h]	−224	−668	(−443)	(−430)	(−369)
Dy	290.4	(−418)	(−7)	(−430)	−695.6	−229	−664	(−307)	(−427)	(−233)
Ho	300.6		(−8)		−707.2[h]	−229	−675		(−427)	
Er	311.9		(−11)		−708.1	−235	−673		(−430)	
Tm	232.2	(−442)	(−16)		−705.2	−236	−671		(−432)	
Yb	155.6	−530.4[h]	(−34)	−537	−670.5[h]	−241	−639[h]		(−435)	
Lu	427.6		–		−702.6	−264	−677		(−440)	
Ac	418	(−118)	(75)	(−142)	(−628)	(−199)	(−609)		–	
Th	597.1	(+161)	(39)		(−347)	(−186)	(−339)	−769.0	−417	−705
Pa	595[i]		(19)		(−439)	(−183)	(−431)	−622	(−402)	(−657)
U	531.4		(12)		−489.1	−190[j]	−476	−591.2	−417[j]	−530.9
Np	464.8		(2)		−527.2	(−185)	−515	−556.1	(−398)	
Pu	343.1		(−8)		−592	(−190)[k]	−577	−536	−402[j]	
Am	284.1		(−1)		−621.2[l]	(−199)	(−603)[l]	(−406)	(−402)	
Cm	387.4		(0)		−615	(−194)	(−594)	(−379)	(−408)	
Bk	310.0		(1)		−601[m]	(−194)	(−578)	(−483)	(−399)	
Cf	196		(0)		−577[n]	(−197)	(−552)	(−313)	(−395)	
Es	143[o]		(−1)		(−601)[c]	(−206)	(−571)	(−209)	(−393)	

Fm	146[p]		(−4)		(−627)[c]	(−215)	(−594)	(−165)	(−393)
Md	(128)[q]		(−9)		(−535)[c]	(−224)	(−501)		(−393)
No	(126)[q]	(−469)[r]	(−27)[r]	(−480)[r]	(−372)[r]	(−231)	(−342)[r]		(−395)
Lr	(391)				(−627)[c]	(−255)	(−593)		(−399)

[a] Unless otherwise noted, rare-earth entries are taken from Morss (1976, 1985); actinide entries from Fuger and Oetting (1976), Grenthe et al. (1992), Morss (1986) or Ward (1983).

[b] $\Delta_f H^0[M(g)] = \Delta_{subl} H$ of metal M.

[c] David (1986b). Since $\Delta_f G^0[M^{2+}(aq)]$ were calculated for $Nd^{2+}(aq)$, $Sm^{2+}(aq)$, $Eu^{2+}(aq)$, $Tm^{2+}(aq)$ and $Yb^{2+}(aq)$ from $\Delta_f G^0[R^{3+}(aq)]$ and $E^0(R^{3+}/R^{2+})$ and $\Delta_f H^0[R^{2+}(aq)]$ were calculated in the same cases from calorimetric measurements and estimates on RCl_2, some minor inconsistencies exist in reconciling $\Delta_f H^0$, $\Delta_f G^0$, and S^0 in these cases.

[d] Travers et al. (1976) and Wagman et al. (1982) list $\Delta_f H^0[Sc^{3+}(aq)] = -614.2$. O'Hare et al. (1987) measured $\Delta_{soln} H[Sc(s)]$ in very dilute HCl/HI as $-651.02 \pm 0.87\ kJ\ mol^{-1}$. This value should be very nearly $\Delta_f H^0[Sc^{3+}(aq)]$ and renders the value cited in this table [based upon the old work of Bommer and Hohmann (1941)] very doubtful. The values in this table are estimated from the measurements of O'Hare et al.

[e] Wang et al. (1988).

[f] Recalculated by J. A. Rard using known standard-state properties and best estimates of $S^0[MCl_3 \cdot 7H_2O(s), 298\ K]$.

[g] Newly reported value by Khanaev et al. (1987) is consistent: $-690.2 \pm 0.8\ kJ\ mol^{-1}$.

[h] Bettonville et al. (1987). Free energies calculated from ΔS and E^0 values.

[i] Kleinschmidt (1986).

[j] Fuger (1992).

[k] $S^0[Pu^{3+}(aq)]$ is an estimate because its calculation requires estimation of $S^o(PuCl_3 \cdot 6H_2O)$.

[l] Mondal et al. (1987).

[m] Fuger et al. (1981).

[n] Fuger et al. (1984).

[o] Kleinschmidt et al. (1984).

[p] Haire and Gibson (1989).

[q] Haire and Gibson (1989) recommend the same values as for $\Delta_f H^0$(Es–Fm).

[r] David et al. (1990).

TABLE 2

Electronic configurations (free atom or ion) and ionization energies (kJ mol^{-1}) of rare earths and actinides[a].

M	Config. [(M(g)]	$\Delta_d E(q)$[b]	$P(M)$[c]	I_1	Config. [$M^+(g)$]	I_2	Config. [$M^{2+}(g)$]	I_3	Config ($M^{3+}(g)$]	I_4	Config. [$M^{4+}(g)$]
Sc	$3d\,4s^2$		1031 ± 20							–	–
Y	$4d\,5s^2$		1158 ± 5	615.6	$5s^2$	1181	5s	1980	$4p^6$	5963	$5p^5$
La	$5d\,6s^2$	−181.8	1140 ± 5	538.1	$5d^2$	1067.1	5d	1850.4	$5p^6$	4819.5	$5p^5$
Ce	$5d^2\,6s^2$	− 57.0	1120 ± 5	534.3	$4f\,5d^2$	1047	$4f^2$	1948.8	4f	3546.7	$5p^6$
Pr	$4f^3\,6s^2$	+ 53.0	1116 ± 5	528.1	$4f^3\,6s$	1018	$4f^3$	2086.4	$4f^2$	3761.1	4f
Nd	$4f^4\,6s^2$	+ 80.9	1104 ± 5	533.1	$4f^4\,6s$	1035	$4f^4$	2132.4	$4f^3$	3899	$4f^2$
Pm	$4f^5\,6s^2$	$+96 \pm 12$	1102 ± 20	538.6	$4f^5\,6s$	1018	$4f^5$	2152	$4f^4$	3966	$4f^3$
Sm	$4f^6\,6s^2$	$+185 \pm 1$	1083 ± 5	544.5	$4f^6\,6s$	1068	$4f^6$	2258	$4f^5$	3995	$4f^4$
Eu	$4f^7\,6s^2$	$+300 \pm 1$	1083 ± 5	547.1	$4f^7\,6s$	1084.6	$4f^7$	2404	$4f^6$	4110	$4f^5$
Gd	$4f^7\,5d\,6s$	−131.0	1084 ± 5	593.4	$4f^7\,5d\,6s$	1166	$4f^7\,5d$	1990	$4f^7$	4245	$4f^6$
Tb	$4f^9\,6s^2$	+3.4	1090 ± 5	565.8	$4f^9\,6s$	1122	$4f^9$	2114	$4f^8$	3839	$4f^7$
Dy	$4f^{10}\,6s^2$	+ 90.5	1076 ± 5	573.0	$4f^{10}\,6s$	1126	$4f^{10}$	2200	$4f^9$	4001	$4f^8$
Ho	$4f^{11}\,6s^2$	+ 100.2	1108 ± 10	581.0	$4f^{11}\,6s$	1138	$4f^{11}$	2204	$4f^{10}$	4101	$4f^9$
Er	$4f^{12}\,6s^2$	+ 85.9	1106 ± 7	589.3	$4f^{12}\,6s$	1151	$4f^{12}$	2194	$4f^{11}$	4115	$4f^{10}$
Tm	$4f^{13}\,6s^2$	+ 157.0	1094 ± 7	596.7	$4f^{13}\,6s$	1163	$4f^{13}$	2285	$4f^{12}$	4119	$4f^{11}$
Yb	$4f^{14}\,6s^2$	+ 277.4	1104 ± 7	603.4	$4f^{14}\,6s$	1175.6	$4f^{14}$	2415	$4f^{13}$	4220	$4f^{12}$
Lu	$4f^{14}\,5d\,6s^2$	–	1130 ± 5	523.5	$4f^{14}\,6s^2$	1341	$4f^{14}\,6s$	2022.3	$4f^{14}$	4360	$4f^{13}$
Ac	$6d\,7s^2$	-292 ± 25	1046 ± 50		$7s^2$		7s	1823	$5f^0$		
Th	$6d^2\,7s^2$	-251 ± 25	944 ± 70	608.5[e]	$6d^2\,7s$		5f 6d or $6d^2$	1930	5f	2774[d]	$5f^0$
Pa	$5f^2\,6d\,7s^2$	−155.7	1034 ± 50		$5f^2\,7s^2$		$5f^2\,6d$	1930	$5f^2$	2991[d]	5f
U	$5f^3\,6d\,7s^2$	−84.0	1020 ± 10	597.6	$5f^3\,7s^2$	1148	$5f^4$ or $5f^3\,6d$	1881	$5f^3$	3145[d]	$5f^2$
Np	$5f^4\,6d\,7s^2$	−33.9	992 ± 10	604.5[e]	$5f^4\,6d\,7s$	1129	$5f^5$	1968	$5f^4$	3242[d]	$5f^3$
Pu	$5f^6\,7s^2$	+ 75.5	1011 ± 10	584.9	$5f^6\,7s$	1129	$5f^6$	2055	$5f^5$	3338[d]	$5f^4$
Am	$5f^7\,7s^2$	+ 127.8	1033 ± 20	576.4[e]	$5f^7\,7s$	1158	$5f^7$	2113	$5f^6$	3493[d]	$5f^5$
Cm	$5f^7\,6d\,7s^2$	− 14.5	1002 ± 15	580.9	$5f^7\,7s^2$	1196	$5f^8$	1997	$5f^7$	3551[d]	$5f^6$
Bk	$5f^9\,7s^2$	+ 109.4	1020 ± 25	601.0	$5f^9\,7s$	1187	$5f^9$	2103	$5f^8$	3435[d]	$5f^7$

Cf	$5f^{10}\,7s^2$	+202.3	975 ± 30	607.7	$5f^{10}\,7s$	1206	$5f^{10}$	2238	$5f^9$	3599[d]	$5f^8$
Es	$5f^{11}\,7s^2$	+213.0	957 ± 40		$5f^{11}\,7s$		$5f^{11}$	2335	$5f^{10}$	3734[d]	$5f^9$
Fm	$5f^{12}\,7s^2$	243 ± 25	1016 ± 50				$5f^{12}$	2364	$5f^{11}$	3792[d]	$5f^{10}$
Md	$(5f^{13}\,7s^2)$	331 ± 25	994 ± 50				$5f^{13}$	2470	$5f^{12}$	3840[d]	$5f^{11}$
No	$(5f^{14}\,7s^2)$	448 ± 38	946 ± 60				$5f^{14}$	2643	$5f^{13}$	3956[d]	$5f^{12}$
Lr	$(5f^{14}\,6d\,7s^2$ or $5f^{14}\,7_s^2 7p)$	–	1018 ± 40			–		2229	$5f^{14}$	4110[d]	$5f^{13}$

[a]Unless otherwise noted, rare-earth entries from Martin et al. (1974) or Morss (1985) and references therein; actinide entries (U–Cf) from Schoebrechts et al. (1989) and referenced therein; other actinides from Morss (1986) and references therein.

[b]$\Delta_d E$ denotes the difference between lowest energy levels of the $f^q\,d^1\,s^2$ and $f^{q+1}\,s^2$ configurations, where $q = Z - 57$ (lanthanides) (Brewer 1983a) or $q = Z - 89$ (actinides) (Brewer 1983b). For Ac, Th, and Fm–Lr, values are taken from Nugent et al. (1973b). When $\Delta_d E > 0$, $f^{q+1}\,s^2$ configuration lies lower in energy. When not given, uncertainties are smaller than 0.1 kJ.

[c]Calculated as in section 2.1.5. Error limits propagated from literature; some cases estimated.

[d]Bratsch and Lagowski (1986).

[e]Riegel et al. (1993), Trautmann (1994).

metal (referred to as the second law method) or from combination of free-energy functions and entropies (referred to as the third law method). Morss (1985) evaluated and listed a set of recommended enthalpies of sublimation of rare-earth metals. Ward (1983) published a parallel set for the actinide metals through Es. Ward's values were adopted by Morss (1986) and by Bratsch and Lagowski (1986). Except where noted, values from these references are given in table 1. Keller (1984) attempted to extend these values to Es, Fm and Md by interpreting thermochromatographic observations on tracer amounts of isotopes of these elements and by extrapolating these values to even heavier elements based on their expected ground-state electron configurations in metal and vapor. Haire and co-workers have measured the enthalpies of vaporization of Es (Kleinschmidt et al. 1984) and of Fm (Haire and Gibson 1989) by using dilute solid alloys of these elements in metallic Sm and Yb. The "best values" cited in table 1 are plotted in fig 1.

A crucial issue is to determine the valence (the number of electrons participating in metallic bonding) of each metal (i.e., the pure, solid metal at 298 K and 1 atm pressure). For example, most of the solid rare earths are trivalent metals (with $6s^2\,5d^1$ bonding) but europium metal is divalent ($6s^2\,5d^0$). Many of the gaseous atoms (table 2, second column, e.g., Pr, Nd, Pm, ...) are also divalent. (One electron of a filled s^2 subshell is readily promoted.) This situation was described and explained by Brewer (1971, 1983a, b, 1987) and has been further elaborated by Johansson and co-workers (Johansson 1978, Brooks et al. 1984) and by Gschneidner (1993). Haire and co-workers (Kleinschmidt et al. 1984, Haire and Gibson 1989) established that both Es and Fm metals are divalent and they predicted enthalpies of vaporization of Md and No to be the same (*ca.* 143 kJ mol^{-1}) based on their expected divalency.

2.1.2. *Ionization energies*

Ionization energies for removal of the first four electrons from all of the lanthanides and from the actinides Th, U and Pu have been derived from experimental measurements. Surface ionization and electron impact measurements yield ionization energies of free atoms. Emission spectra lead to ionization energies of free atoms and ions. The best set of lanthanide ionization potentials remains that by Martin et al. (1974, 1978). These have been cited by Morss (1985) and are reproduced in table 2. The same values were cited by Bratsch and Lagowski (1986). Morss (1986), Bratsch and Lagowski (1986) and others have derived ionization-potential sums from Born–Haber cycles on various actinide compounds. Schoebrechts et al. (1989) used the structural and thermochemical data on the isostructural series Cs_2NaMCl_6 to derive ionization energies and hydration enthalpies for several rare earths and for all of the actinides U–Cf and we have adopted these in table 2. Each of these ionization-potential sums derived from Born–Haber cycles assumes that covalency and ligand-field effects are small and similar for $4f^n$ and $5f^n$ ions. Larger covalency stabilization may exist for light actinide ions in oxides and halides but is ignored because we have no experimental way to assess its magnitude.

In this chapter, the symbol I_n refers to the process $M^{(n-1)+} \rightarrow M^{n+}$. (To avoid possible confusion, we point out that atomic spectroscopists use the symbol MI to refer to

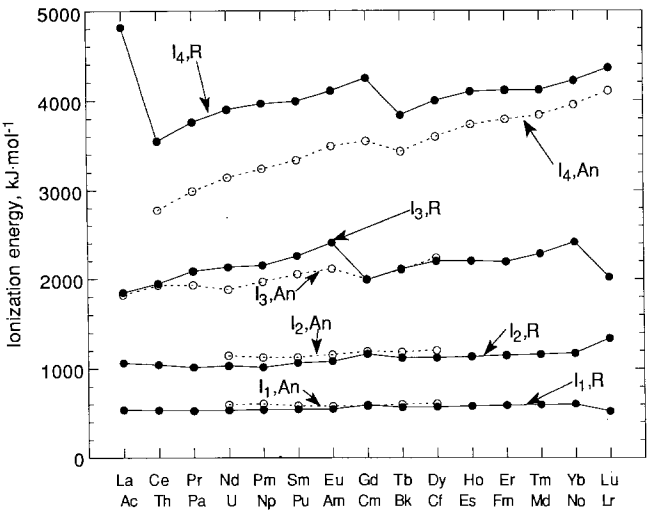

Fig. 4. Ionization energies of the lanthanides and actinides.

neutral M, MII to refer to M^+, etc., so that I_1 in this chapter refers to the energy expended to produce the transition MI to MII, etc.) Ionization energies are converted to enthalpies at 298 K as described by Wagman et al. (1982) in their Appendix 2.

In fig. 4 the first to fourth ionization energies of the lanthanides and actinides are plotted for comparison. It is evident that the half-filled shell effect is much less significant for the actinides than for the lanthanides. This diminished effect is caused by the greater radial extension of the 5f orbitals compared to the 4f orbitals and manifests itself in the easier accessibility of 4+ oxidation states of many actinides.

2.1.3. *Hydration enthalpies and entropies*

The hydration enthalpy for the ion $\Delta_{hyd}H(M^{n+})$ represents the enthalpy (usually at 298 K) released in the process $M^{n+}(g) \rightarrow M^{n+}(aq)$. Although not an experimental property, it can be calculated from the difference between the "energy levels" of these two experimentally accessible species. It has also been calculated by a Born-equation model such as that of Tremaine and Goldman (1979) that yields free energies up to 350°C using only the hydration number as a variable parameter or calculated from various Born-equation models as reviewed by David (1986b). After comparing the alternative models, David (1986b) published a recommended set of hydration enthalpies based upon a semi-theoretical model that incorporates the hydration-number change from nine to eight between Pm and Gd in the tripositive lanthanides and between Cm and Es in the tripositive actinides. (Here and elsewhere in this chapter An denotes actinium plus the actinides Th–Lr.) The values of David are reproduced in table 3 along with other values that have significant connection to experiment (e.g., a Born–Haber cycle or chromatographic separation behavior tie-point). David has also developed a hydration model that incorporates the second hydration sphere (David 1991). The enthalpies of hydration are also plotted in fig. 5 which shows nearly parallel

TABLE 3

Crystallographic ionic radii (Å), typical coordination number in solid and hydration enthalpies (kJ mol^{-1}) of the rare earth and actinide ions.

M	$r(M^{2+})$[a]	$CN(M^{2+})$[b]	$-\Delta_{hyd}H^0$ (M^{2+})[c]	$r(M^{3+})$[c]	$CN(M^{3+})$[b]	$-\Delta_{hyd}H^0$ (M^{3+})[d] David	Others	$r(M^{4+})$[c]	$CN(M^{4+})$[b]	$-\Delta_{hyd}H^0$ (M^{4+})[f]
Sc	—	—	—	0.745	6			—	—	—
Y	—	—	—	0.900	6	3640		—	—	—
La	1.304[g]	—	—	1.032	6	3372	3363	—	—	—
Ce	1.278	—	—	1.010	6	3420	3372	0.967	8	6390
Pr	1.253	6	1438	0.990	6	3453	3406	0.949	8	6469
Nd	1.225	6	1459	0.983	6	3484	3441	0.936	8	6528
Pm	1.206	6	1474	0.970	6	3520		0.925	8	6579
Sm	1.183	6	1493	0.958	6	3544		0.912	8	6639
Eu	1.166	6	1507	0.947	6	3575		0.903	8	6682
Gd	1.140[g]	6	—	0.938	6	3597		0.894	8	6726
Tb	1.119	6	1546	0.921	6	3631		0.886	8	6765
Dy	1.096	6	1566	0.912	6	3661	3654	0.874	8	6824
Ho	1.075	6	1585	0.901	6	3692		0.864	8	6875
Er	1.056	6	1602	0.890	6	3718		0.854	8	6926
Tm	1.038	6	1619	0.880	6	3742		0.844	8	6978
Yb	1.026	6	1631	0.868	6	3764	3794	0.835	8	7026
Lu		6	—	0.861	6	3777		0.827	8	7069
Ac	1.41[g]	6	—	1.12	6	3185		—	—	—
Th	1.36[g]	6	1362[g]	1.08	6	3262		1.048	8	6056
Pa	1.30[g]	—	—	1.05	6	3299		1.016	8	6184
U	1.27	—	—	1.025	6	3376	3408	0.997	8	6262
Np	1.24	—	—	1.011	6	3414	3442	0.980	8	6334
Pu	1.212	6	1470	0.995	6	3451	3455	0.962	8	6412
Am	1.194	6	1484	0.980	6	3486	3503	0.950	8	6465
Cm	1.164	6	1508	0.970	6	3512	3525	0.942	8	6501
Bk	1.145	6	1524	0.955	6	3548	3557	0.932	8	6546

Cf	1.125	6	1541	0.945	6	3573	3580	0.925	8	6579
Es	1.102	6	1561	0.934	6	3602		0.914	—	6630
Fm	1.083	6	1578	0.922	6	3631		0.906	—	6668
Md	1.064	6	1595	0.912	6	3659	3654[h]	0.897	—	6711
				0.904[h]						
No	1.052	6	1606	0.902	6	3685	3753[i]	0.889	—	6750
Lr		6		0.896	6	3701	3685[h]	0.881	—	6789
				0.889[h]						

[a] David (1986b). Values are estimates.

[b] These are common coordination numbers in solids, *not* hydration numbers in solution. They have been used to provide a conventional size parameter for calculation of hydration enthalpies. It is recognized that in many coordination compounds the 3+ ions are coordinated to eight or even more ligands, and that in aqueous solution the primary coordination sphere has nine water molecules for light 3+ ions and eight for heavy 3+ ions.

[c] David (1986b). $\Delta_{hyd}(H^+) = -1114\,kJ\,mol^{-1}$.

[d] Left entry: David (1986b). Right entry: Goldman and Morss (1975) or Schoebrechts et al. (1989). Value for Y^{3+} from Rizkalla and Choppin (1991) using equations of Bratsch and Lagowski (1985b); other values cited by Rizkalla and Choppin (1991) are intermediate between those shown in the two columns below. Reference is $\Delta_{hyd}(H^+) = -1114\,kJ\,mol^{-1}$.

[e] Ionic radii from Shannon (1976)(rare earths) or David (1986a, 1985, 1986b)(actinides, on Shannon scale). Many of David's values are estimates.

[f] David (1986b). Reference is $\Delta_{hyd}(H^+) = -1114\,kJ\,mol^{-1}$.

[g] f^n configuration. See table 2 for actual ground states.

[h] Brüchle et al. (1988): ionic radii normalized to Shannon (1976) scale; $\Delta_{hyd}H$ mean from three models, using $\Delta_{hyd}(H^+) = -1114\,kJ\,mol^{-1}$.

[i] Fourest et al. (1988).

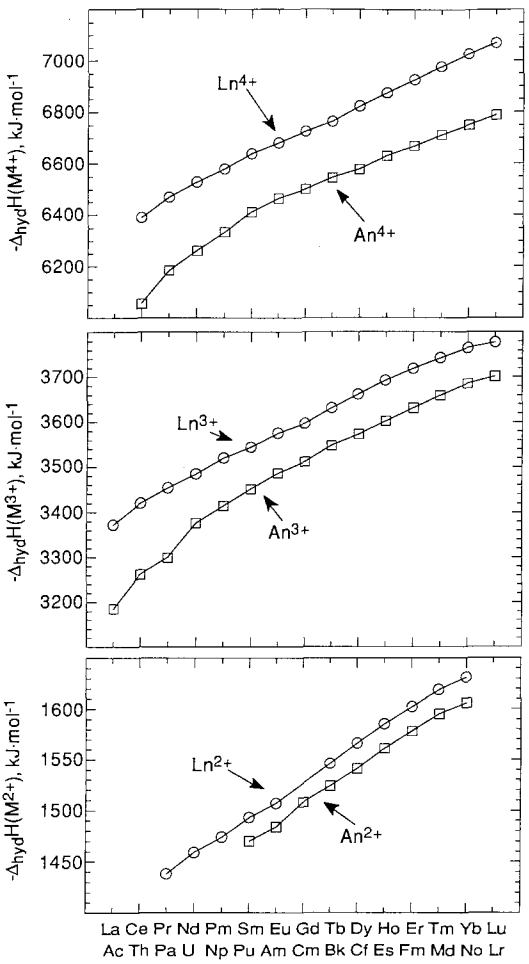

Fig. 5. Hydration enthalpies of lanthanide and actinide ions. Data from David (1986b).

lanthanide–actinide curves that diverge slightly at the lightest and heaviest ions. This phenomenon will be discussed again in section 4.5.

Hydration enthalpies have also been derived from a Born–Haber cycle (e.g., Morss 1971) for ions R^{3+} and An^{3+} if all other terms are known. Recently, this approach has been updated (Schoebrechts et al. 1989) with new lanthanide ionization potentials and has been extended to the actinide ions U^{3+}–Cf^{3+} using experimental results for the isostructural (cubic) elpasolites $Cs_2NaAnCl_6$. The reader is cautioned that these absolute hydration enthalpies require a reference to $\Delta_{hyd}(H^+)$, for which Schoebrechts et al. (1989) used the value of $-1091\,kJ\,mol^{-1}$ (Halliwell and Nyburg 1963) so as to be consistent with Morss (1971). David et al. (1985) independently derived $\Delta_{hyd}(H^+) = -1114\,kJ\,mol^{-1}$ as one least-squares parameter from 35 Born–Haber cycles using experimental properties and Brüchle et al. (1988) used this value also. Bratsch used

$\Delta_{hyd}(H^+) = -1105\,kJ\,mol^{-1}$ from Conway (1978). The values in table 3 are all consistent with $\Delta_{hyd}(H^+) = -1114\,kJ\,mol^{-1}$.

In an important study, Hoffman et al. (1988) found that Lr^{3+} solvent-extraction, ion-exchange and reverse-phase chromatography behavior is very similar to that of Er^{3+}. Subsequently, Brüchle et al. (1988) confirmed the ion-exchange behavior of Lr^{3+} with many more atoms of Lr^{3+}. Therefore, it appears that Lr^{3+} has separation behavior parallel to the heavy lanthanide ions, with a "shift" of $Z = 3$. They also found that Md^{3+} ion-exchange behavior nearly parallels that of Ho^{3+}, a "shift" of Z slightly more than 2. Using the R^{3+} ionic radii (CN6) of Templeton and Dauben (1954), they inferred the ionic radius of Md^{3+} to be 0.904 Å and that of Lr^{3+} to be 0.889 Å. Using the R^{3+} ionic radii (also CN6) of Shannon (1976) and the elution curves of Brüchle et al. (1988), we infer the ionic radius of Md^{3+} to be 0.889 Å and that of Lr^{3+} to be 0.904 Å. David (1986b) found a difference of 0.016 Å between the ionic radii of Md^{3+} and Lr^{3+}. Brüchle et al. (1988) calculated hydration enthalpies of Md^{3+} as -3654 and Lr^{3+} as $-3685\,kJ\,mol^{-1}$; one must remember that such calculations are dependent on model, ionic radius, etc.

Jia (1987) calculated lanthanide hydration enthalpies using a CNDO model for the first hydration sphere only and confirmed the transition from CN9 at Nd^{3+} to CN8 at Tb^{3+}. Miyakawa et al. (1988) calculated lanthanide hydration enthalpies based upon four structural models: nine-fold coordinated tricapped trigonal prism, and eight-fold coordinated cube, square antiprism, and dodecahedron. They compared their calculations to an early set of hydration enthalpies derived by Morss (1971) from a Born–Haber cycle treatment of experimental data on the isostructural elpasolite series $Cs_2NaLnCl_6$. Their comparison is consistent with nine-fold (tricapped trigonal prism) from La^{3+} to Tb^{3+} with a shift to the eight-fold (cube) model at Ho^{3+}. They also calculated that the free-energy difference between $Ce(OH_2)_9{}^{3+}$ and square-antiprism $Ce(OH_2)_8{}^{3+}$ is $3\,kJ\,mol^{-1}$ and correlated this difference with electronic excitation energies.

Hydration enthalpies of Ln^{2+} ions have also been calculated, e.g., by David (1986b), Bratsch and Lagowski (1985b) and Mikheev and Rumer (1988). David's self-consistent values have been used for hydration enthalpies of M^{2+}, M^{3+}, and M^{4+} in table 3. As mentioned earlier for ionization energies, any covalency effects for actinide hydration energies are masked in all of these calculations since they use a similar ionic model for lanthanide and actinide ions.

The hydration *entropy* for the ion $\Delta_{hyd}S^0(M^{n+})$ represents the standard entropy change (usually at 298K) for the process $M^{n+}(g) \rightarrow M^{n+}(aq)$. This property should reflect lanthanide–actinide differences because the final state represents the ion with all the water molecules in the primary and outer hydration spheres. Bratsch and Lagowski (1985b, table I) proposed a set of hydration parameters A_Y and r_x by which hydration entropies could be calculated for the lanthanides. Rizkalla and Choppin (1991, table 11) used these parameters to tabulate entropies of hydration for the lanthanides. However, it is not reasonable to extend these entropies for a lanthanide–actinide comparison because there are no experimental data from which independent actinide hydration entropy parameters A_Y and r_x can be calculated (see section 2.2.2 for experimental entropies of aqueous ions).

Hydration properties are also discussed by Rizkalla and Choppin (1992) and in the chapter by Rizkalla and Choppin (ch. 127) of this volume. For internal consistency, especially when used to calculate ionization enthalpies of the heavy actinides, hydration enthalpies of David (table 3, this chapter) on the absolute scale of $\Delta_{hyd}(H^+) = -1114\,kJ\,mol^{-1}$ were used to calculate ionization energies in table 2.

2.1.4. *Standard-state enthalpies of formation of aqueous ions*

The standard-state enthalpy of formation of an aqueous ion is a key thermochemical property. Often enthalpies of *solution* of compounds are measured and their enthalpies of *formation* are calculated from the enthalpies of solution of the compounds and of formation of aquo-ions. Thus (as is the case for some f elements), when a new measurement of enthalpy of solution of a metal is reported, the enthalpies of formation of many compounds of that element may have to be redetermined.

The standard-state enthalpy of formation of all of the aqueous rare-earth ions R^{3+} (except for Sc^{3+} and Pm^{3+}) and of aqueous Np^{3+}, Pu^{3+} and Am^{3+} have been typically determined at 298 K as follows using the metal, the trichloride, and thermochemistry in aqueous HCl: The enthalpies of solution of pure metal and pure trichloride in dilute HCl(aq) are measured at 298 K. From these measurements and auxiliary data the enthalpy of formation of the trichloride is calculated. The enthalpy of solution of pure trichloride in pure water at 298 K is also measured and is corrected to infinite dilution (the standard state for enthalpies of formation of electrolytes). Then $\Delta_f H^0[R^{3+}(aq)] = \Delta_f H^0[RCl_3(s)] + \Delta_{soln}H^0(RCl_3) - 3\Delta_f H^0[Cl^-(aq)]$. The literature through 1976, mostly using this method, was assessed by Morss (1976). In general the same values of $\Delta_f H^0[R^{3+}(aq)]$ were tabulated by Wagman et al. (1982); it should be pointed out that this monograph is identical to the NBS Technical Note 270 series [most of the lanthanide volume, Wagman and Evans (1971) was evaluated in the 1960's] with entries recalculated from calories to SI units. A few more recent data are included in Morss (1985) and that assessment (with the exception of Sc) is used for $\Delta_f H^0[M^{n+}(aq)]$ in table 1. Because of the importance in comparison of lanthanide and actinide(III) properties, the values of $\Delta_f H^0[M^{3+}(aq)]$ are plotted in fig. 1.

Thermodynamic measurements of scandium species were reviewed and properties were assessed by Travers et al. (1976). The most recent report is an enthalpy of very pure metal and ScI_3 in dilute HCl/HI(aq) and determination of $\Delta_f H^0[ScI_3(s)]$ (O'Hare et al. 1987). O'Hare et al. did not report or estimate $\Delta_f H^0[Sc^{3+}(aq)]$ but their measurement [enthalpy of solution in $\sim 2\,mol\,dm^{-1}HCl(aq) = -651\,kJ\,mol^{-1}$] implies that this datum is much more exothermic than assessed by Travers et al. (1976) and by Wagman et al. (1982) ($-614\,kJ\,mol^{-1}$); see table 1 and footnote d therein. For yttrium (Wang et al. 1988) a cycle has been developed for YCl_3, YBr_3, and YI_3 and HCl. Bettonville et al. (1987) published new enthalpies of formation of $Tb^{3+}(aq)$, $Ho^{3+}(aq)$, $Yb^{3+}(aq)$ and $Yb^{2+}(aq)$. A few other new measurements have appeared but their accuracy does not justify revision of any of the data, other than for Sc and Y. Hepler and Singh (1976) reviewed thermodynamic measurements of lanthanum species and assessed properties that are consistent with those of Wagman et al. (1982). Rard (1985) did the same for europium and his assessments are nearly identical with those of table 1. A table of lanthanide standard enthalpies of formation was recently published in this handbook (Rizkalla and Choppin 1991); they are referenced to a textbook (Johnson

1982) and in all cases differ significantly from other reviews. The values in table 1 of this chapter represent critically assessed values by this author, incorporating all appropriate literature references through 1992.

Among the actinides, measurements have been carried out that yield enthalpies of formation for U^{3+} from the enthalpy of oxidation of U^{3+} to U^{4+} by 0.5 M $HClO_4$(aq) as assessed by Fuger and Oetting (1976) and for Np^{3+}, Pu^{3+}, and Am^{3+} using chlorides and HCl(aq) as described in the previous paragraphs. Enthalpies of formation of Cm^{3+}(aq), Bk^{3+}(aq) and Cf^{3+}(aq) represent measured enthalpies of solution of the metals in HCl(aq) and estimates of enthalpies of solution of the respective trichlorides. For the actinide ions, the assessed values of Fuger and Oetting (1976) are cited in table 1, except for Am^{3+}, Bk^{3+} and Cf^{3+}, for which the new values and references are given in table 1.

Enthalpies of formation of the dipositive aquo-ions have been calculated as follows: Eu^{2+} from enthalpy of solution in water and of formation of $EuCl_2$ (Morss and Haug 1973); Nd^{2+}, Sm^{2+}, Dy^{2+} and Tm^{2+} from measured enthalpy of formation RCl_2 and estimate of its enthalpy of solution in water (Morss and McCue 1976; Morss and Fahey 1976). Other $\Delta_f H^0[M^{2+}(aq)]$ values were estimated from $\Delta_f G^0[M^{2+}(aq)]$ and ΔS for the reaction $M(s) + 2H^+(aq) = M^{2+}(aq) + H_2(g)$.

Enthalpies of formation of the tetrapositive aquo-ions have been calculated as follows: Ce^{4+} from Morss (1985), using enthalpies of reduction with H_2O_2, Fe^{2+} and U^{4+} and correcting for extensive hydrolysis; U^{4+} from UCl_4 cycles (Fuger and Oetting 1976, Grenthe et al. 1992); Np^{4+} from dissolution of Np metal in oxygen-saturated 1 M HCl(aq) (Fuger and Oetting 1976); Pu^{4+} from oxidation of Pu^{3+} with dichromate (Fuger and Oetting 1976); Am^{4+} and Cm^{4+} from cycles using the enthalpies of dissolution of AmO_2 (Morss and Fuger 1981) and CmO_2 (Morss et al. 1981); and Bk^{4+} from the $E^0(Bk^{4+}/Bk^{3+})$ and entropy estimates. Other $\Delta_f H^0[M^{4+}(aq)]$ values were calculated from $\Delta_f G^0[M^{4+}(aq)]$ and ΔS for the reaction $M(s) + 4H^+(aq) = M^{4+}(aq) + 2H_2(g)$.

2.1.5. f→d *transitions and the correlation function* P(M)

Nugent (1975) summarized the behavior of the energy differences $\Delta_d E(q)$ between lowest energy levels of the $f^q d^1 s^2$ and $f^{q+1} s^2$ configurations, where $q = Z - 57$ (lanthanides) or $q = Z - 89$ (actinides),

$$\Delta_d E(q) = W + (E - A')q - M(L)E^3(q) - P(S, L, J)\zeta_f(q), \qquad 0 \le q < 7, \qquad (1)$$

$$\Delta_d E(q) = W + (E - A')q - 9E^1(q) - M(L)E^3(q) - P(S, L, J)\zeta_f(q), \quad 7 \le q \le 13. \qquad (2)$$

Some of the terms, especially the term $(E - A')q$, change as a function of Z, and $\Delta_d E(q)$ shifts downward by $9E^1(q)$ at $q = 7$. Nugent (1975) listed $\Delta_d E(q)$ values in his table 6.1. Brewer (1983a, b) and Carnall and Crosswhite (1984) have analyzed the spectroscopic literature on the differences between the f^{q+1} and $f^q d$ configurations in atoms and ions. Values of $\Delta_d E(q)$, mostly from Brewer (1983a, b), are given in kJ mol^{-1} in the third column of table 2.

P(M) was defined by Nugent et al. (1973b) to explain the apparent irregularities in lanthanide-metal enthalpies of sublimation and lanthanide aquo-ion enthalpies of formation. P(M) is shown in fig. 2 on an energy-level scale; values are tabulated in

table 2 and plotted in fig. 3. When $\Delta E<0$, $P(M) = \Delta H_{subl} - \Delta_f H^0[M^{3+}(aq)]$; when $\Delta E>0$, $P(M) = \Delta H_{subl} + \Delta E - \Delta_f H^0[M^{3+}(aq)]$. P(M) also served to predict some parallel actinide properties, especially thermochemical properties of the heaviest actinides. A critical issue remains: Do the heavy actinides with electronic configuration $5f^8$–$5f^{14}$ have the same V-shaped P(M) as that calculated for the isoelectronic lanthanides Tb^{3+} through Lu^{3+} (Nugent et al. 1973b)? Since this issue could not be resolved because of the lack of adequate experimental information on these heavy actinide ions, Nugent et al. (1973b) assumed a V shape for the actinide P(M) parallel to that for the lanthanides. The approach was subsequently revised by David et al. (1978) and David (1986a,c) with a linear extension of the actinide P(M) to predict thermochemical properties of the heavy actinide ions Es^{3+} through Lr^{3+}. Morss (1986) used a V shape for the actinide P(M) with new results for Am, Bk and Cf species to systematize the thermochemical properties of oxides and halides.

Johansson (1978) and Brooks et al. (1984) utilized the energy difference (f→d transitions) between trivalent ($f^n ds^2$) and tetravalent ($f^{n-1} d^2 s^2$) cerium and other f-element metals to estimate thermochemical data for compounds. A similar approach has been used by Mikheev et al. (1986) and Spitsyn et al. (1985) to include the divalent as well as the tetravalent state. Again, a critical issue has been the behavior of the heavy actinides with respect to f→d transitions, and the need to utilize and to interpret the few experimental measurements on these actinides, which are discussed below (e.g., section 2.4.1.3). Johansson and Munck (1984) defined a function P^*(M) that removes the intershell multiplet coupling energy from the atomic reference state ($\Delta E_{coupling}$ is the energy difference between the baricenter and the lowest level of a multiplet). For the lanthanides P^*(M) is significantly smoother than P(M),·except for an anomaly at Yb that may be due to an error in experimental data. Unfortunately, Johansson and Munck (1984) point out that spectroscopic data on the heavy actinides are inadequate to correct P(M) to P^*(M) for the actinides.

Since 1986, the only new experimental datum is the enthalpy of sublimation of Fm (Haire and Gibson 1989). However, the electrochemical estimate of $E^0(Fm^{3+}/Fm)$ has a significant uncertainty in amalgamation energy. Because of this uncertainty, the uncertainty of extrapolation of the heavy actinide P(M) beyond Cf, and the inadequate knowledge of $\Delta E_{coupling}$ for the actinides, we do not attempt to use the actinide P(M) to estimate thermochemical properties of Es^{3+}(aq) through Lr^{3+}(aq). Figure 3 shows P(M) for rare-earth and actinide 3+ species, using the best available thermodynamic and spectroscopic data.

2.2. *Thermophysical properties of condensed systems*

2.2.1. *Solids: heat capacities*

There have been no significant actinide heat-capacity determinations since publication of the IAEA series (described in Fuger 1992) except for metallic compounds of the NaCl (B1) structure such as PuSb (Hall et al. 1991).

2.2.2. *Aqueous ions: heat capacity, osmotic coefficient, entropy*

The heat capacities and osmotic coefficients of aqueous solutions of some salts of most of the R^{3+} ions have been determined by Spedding and others (Rard 1985, 1987).

From heat capacities of electrolytes, limiting ionic heat capacities $C_p^0[R^{3+}(aq)]$ can be derived. Since there have been no parallel measurements for aqueous solutions of salts of any actinide ions An^{3+}, no comparisons can be made, although estimates have been made of $C_p^0[U^{3+}(aq)] = -64 \pm 22\,J\,mol^{-1}\,K^{-1}$ (Grenthe et al. 1992) and $C_p^0[Pu^{3+}(aq)] = -61\,J\,mol^{-1}\,K^{-1}$ (Lemire and Tremaine 1980). There is one measured actinide $C_p^0[Th^{4+}(aq)] = -1 \pm 11\,J\,mol^{-1}\,K^{-1}$ (Morss and McCue 1976) and there are two estimated actinide $C_p^0[U^{4+}(aq)] = -48 \pm 15\,J\,mol^{-1}\,K^{-1}$ (Grenthe et al. 1992) and $C_p^0[Pu^{4+}(aq)] = -63\,J\,mol^{-1}\,K^{-1}$ (Lemire and Tremaine 1980) but there are no data for any $R^{4+}(aq)$ ions.

Morss (1985, 1986) compiled tables of entropies of $M^{2+}(aq)$, $M^{3+}(aq)$, and $M^{4+}(aq)$ (M = R, An), using entropies derived from measured thermochemical properties wherever possible. For example, he used $S^0[Dy^{2+}(aq)] \approx -15 \pm 10\,J\,mol^{-1}\,K^{-1}$ (Morss and Fahey 1976); $S^0[Dy^{3+}(aq)] = -229 \pm 5\,J\,mol^{-1}\,K^{-1}$ [essentially the same as that of Wagman et al. (1982): $-231\,J\,mol^{-1}\,K^{-1}$]; and $S^0[Th^{4+}(aq)] = -424 \pm 4\,J\,mol^{-1}\,K^{-1}$ (Morss and McCue 1976). David (1986b) did likewise, using similar systematics. Differences between these authors' values are usually due to small differences in selected ionic radii or in interpolating or extrapolating properties using essentially the same model. We note that calculation of $S^0[Pu^{3+}(aq)]$ is based partly on experimental results but also that $S^\circ[Pu^{3+}(aq)]$ required an estimate of $S^0[PuCl_3 \cdot 6H_2O(s)]$.

2.3. *Thermochemical properties of compounds*

2.3.1. *Sesquioxides*

The thermochemical and thermophysical properties of the rare earth sesquioxides were critically evaluated in 1973 (Gschneidner et al. 1973). A systematic comparison of rare-earth and actinide sesquioxides was published in 1983 (Morss 1983). Thermodynamic properties of europium oxides were assessed by Rard (1985). Since then the enthalpies of formation of Am_2O_3 and Cf_2O_3 were determined by solution microcalorimetry. The $\Delta_f H^0[Am^{3+}(aq)]$ has been redetermined even more recently so the $\Delta_f H^0[Y^{3+}(aq)]$ has been corrected in table 4. Recently, the enthalpy of formation of Y_2O_3 was redetermined by combustion calorimetry (Lavut and Chelovskaya 1990) and independently by solution calorimetry (Morss et al. 1993). The latter determination took advantage of a determination of $\Delta_f H^0[Y^{3+}(aq)]$ that used very pure Y metal (Wang et al. 1988). Assessed values are listed in table 4.

Morss (1986) and Morss et al. (1987) correlated the thermochemistry of lanthanide and actinide sesquioxides by plotting enthalpy of solution as a function of ionic size. The enthalpies of formation and solution of all rare-earth and actinide sesquioxides are listed in table 4 and the enthalpies of solution are plotted in fig. 6. The enthalpies of solution follow separate correlation curves for the three crystal modifications of these oxides, which have metal–oxygen coordination of eight (hexagonal La_2O_3–Nd_2O_3), seven (monoclinic Sm_2O_3–Gd_2O_3) or six (cubic Pr_2O_3–Lu_2O_3). See section 4.1.1 for further discussion.

2.3.2. *Hydroxides*

Enthalpies of formation of lanthanum and neodymium hydroxides have been determined recently (Cordfunke et al. 1990, Morss et al. 1989) using crystalline hydrox-

TABLE 4

Enthalpies of formation and solution (in water) of sesquioxides, trichlorides and hydroxides at 298 K (kJ mol^{-1}) (see text for general references; estimated values in parentheses).

M	$\Delta_f H^0$ (M_2O_3, cubic)	$\Delta_{soln} H^0$ (M_2O_3, cubic)[a]	$\Delta_f H^0$ (MCl_3, hexagonal)	$\Delta_{soln} H^0$ (MCl_3, hexagonal)	$\Delta_f H^0$ [$M(OH)_3$(s)]	$\Delta_{soln} H^0$ [$M(OH)_3$(s)][b]
Sc	−1909[c]		−925[c]			
Y	−1932.8	−398	−1018.4[d, e]	−220[e]		−159
La	−1794[f]	−482[f]	−1073	−138	−1415.5	−151
Ce	−1796[f]	−462[f]	−1058	−144		
Pr	−1810[f]	−459[f]	−1059	−148	−1404[g]	−160
	−1810	−459				
Nd	−1808[f]	−442[f]	−1042	−156	−1403.7	−150
Pm	(−1813)	(−420)	(−1029)	(−160)		
Sm	−1824[h]	−416[h]	−1026	−166		
	−1828	−411				
Eu	−1651[h]	−418[h]	−936	−171	−1336.5[i]	−131
	−1663	−406				
Gd	−1816[h]	−416[h]	−1008	−180		
	−1827	−404				
Tb	−1865	−388	−1007[j]	−192[j]		
Dy	−1863	−386	−989[e]	−208[e]		
Ho	−1881	−390	−995[e]	−213[e]		
Er	−1898	recalc	−995[e]	−215[e]		
Tm	−1889	−380	−991[e]	−215[e]		
Yb	−1815	−392	−960[e]	−216[e]		
Lu	−1878	−384	−986[e]	−218[e]		
Ac	(−1756)	(−357)	(−1049)	(−105)		
Th						
Pa						
U	(−1456)	(−379)	−863.7	−124		
Np	(−1522)	(−389)	(−898)	(−130)		
Pu	(−1656)	(−385)	−960	−133		
Am	−1690	−400	−982	−139.6	−1371[g]	−108[g]
Cm	−1682	−406	(−974)	(−142)		
Bk	(−1694)	(−366)	(−952)	(−150)		
Cf	−1653	−358	(−925)	(−153)		
Es	(−1696)	(−353)	(−950)	(−154)		

[a] $\Delta_{soln} H^0 = 2\Delta_f H^0[M^{3+}(aq)] + 3\,\Delta_f H^0[H_2O(l)] - \Delta_f H^0[M_2O_3(s)]$.

[b] In dilute acid: $M(OH)_3(s) + 3H^+(aq) = M^{3+}(aq) + 3H_2O(l)$.

[c] Travers et al. (1976). $ScCl_3$ has the rhombohedral $FeCl_3$ structure; its enthalpy of solution does not correlate with that of any of the other rare-earth trichlorides.

[d] Wang et al. (1988).

[e] Monoclinic ($AlCl_3$ structure) trichloride.

[f] Hexagonal sesquioxide.

[g] Morss and Williams (1994).

[h] Monoclinic sesquioxide.

[i] Rard (1985), from solubility equilibrium and entropies.

[j] Orthorhombic ($PuBr_3$ structure) trichloride.

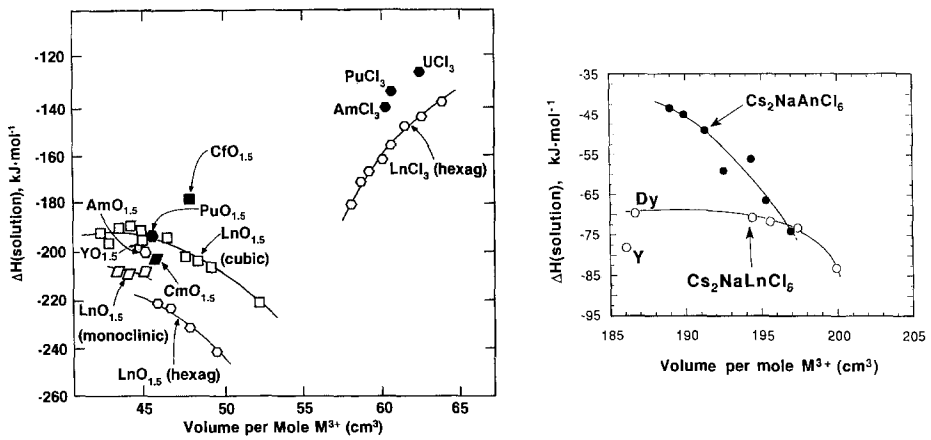

Fig. 6. Enthalpies of solution of rare-earth (open symbols) and actinide (shaded symbols) sesquioxides, trichlorides and elpasolites Cs_2NaMCl_6 as a function of molar volume (representing ionic size). The molar volumes were calculated from crystallographic unit cell parameters, normalized to one mole of M^{3+}. Smooth curves have been drawn through each class of compounds to guide the eye. In all cases the enthalpies of solution of actinide (III) compounds are less exothermic than those of structurally similar lanthanide (III) compounds.

ides. These measurements are important because they can be combined with measured entropies of crystalline hydroxides (Chirico and Westrum 1980) and other thermochemical properties to determine standard free energies of the reactions at 298 K,

$$La(OH)_3(s) = La^{3+}(aq) + 3\ OH^-(aq), \qquad \Delta G^0 = 123.3 \pm 2.0\ kJ\ mol^{-1}, \tag{3}$$

$$Nd(OH)_3(s) = Nd^{3+}(aq) + 3\ OH^-(aq), \qquad \Delta G^0 = 127.3 \pm 3.0\ kJ\ mol^{-1}. \tag{4}$$

The solubility product constants $K_{sp}^0 = \exp(-\Delta G^0/RT)$ are 2.5×10^{-22} and 5.0×10^{-23}, respectively. Prior K_{sp}^0 values from approaches to solubility equilibria on poorly crystallized precipitates were significantly larger (Baes and Mesmer 1976). One would expect the K_{sp}^0 measured from finely divided precipitates to be larger, rather than smaller, than that determined from well-crystallized solids used for calorimetry. However, Kragten and Decnop-Weever (1987) found $K_{sp}^0[La(OH)_3] = 1.6 \times 10^{-23}$ in the most recent study of a series of lanthanide–hydroxide equilibrium studies by the precipitation borderline method.

Rard's (1985) assessment of europium thermodynamics included $\Delta G^0 = 150.7 \pm 5.7\ kJ\ mol^{-1}$ ($K_{sp}^0 = 3.9 \times 10^{-27}$) for the similar solubility equilibrium of $Eu(OH)_3$. From this ΔG^0 and other thermodynamic properties he calculated $\Delta_f G^0[Eu(OH)_3(s)] = -1198.9 \pm 7.8\ kJ\ mol^{-1}$ and $\Delta_f H^0[EU(OH)_3(s)] = -1336.5 \pm 8.3\ kJ\ mol^{-1}$. Clearly, the calorimetric and equilibrium measurements for these hydroxides need to be reconciled. For actinide hydroxides approach-to-equilibrium measurements have been made; the scatter among measurements and estimates indicates that equilibrium may not have been reached (Morss 1992a). One calorimetric measurement of an actinide hydroxide enthalpy of formation has been made (table 4, Morss and Williams 1994) from which $K_{sp}^0[Am(OH)_3] = 7 \times 10^{-31}$ has been calculated. This K_{sp}^0 is significantly smaller than that of structurally similar $Nd(OH)_3$.

2.3.3. *Other oxides*

Morss's review of tetravalent f-element oxides (Morss 1983) included all the known dioxides (and estimates for the known CfO_2 and the unknown EsO_2) and the perovskites $BaMO_3$ (M = Ce, Pr, Tb, U). No new data have been reported for dioxides, but several additional perovskites have been studied (Goudiakas et al. 1990, Fuger 1992). The enthalpies of complexation of perovskites AMO_3(A = Ca, Sr, Ba),

$$AO(s) + MO_2(s) = AMO_3(s), \tag{5}$$

have been correlated with the volume changes of reaction (5) and with the structural Goldschmidt tolerance factor $t = (r_A + r_O)/[\sqrt{2}(r_M + r_O)]$ (Morss 1983, Morss and Eller 1989, Goudiakas et al. 1990).

A systematic effort to correlate enthalpies of complexation of hexavalent actinide oxides, e.g.,

$$2\,Na_2O(s) + UO_3(s) = Na_4UO_5(s), \tag{6}$$

in terms of molar volume changes and as a function of the alkali-metal or alkaline-earth oxide, was made by Morss (1982). Many new measurements have been completed since then and all of them are incorporated into an assessment by Fuger (1992) that classifies the alkali-metal and alkaline-earth oxides in terms of their basicities. This concept has been extended in section 4.1.1 with the development of a quantitative acid–base scale for all the binary oxides involved in these reactions. Hexavalent oxides are not compared in this chapter because there are no lanthanide oxides with oxidation state above 4+.

2.3.4. *Halides*

The thermochemistry of rare-earth trifluorides was summarized in Gmelin Handbuch (1976) and the thermochemistry of rare-earth tribromides and triiodides was summarized in Gmelin Handbuch (1978). The thermochemistry of trivalent rare-earth trichlorides was critically assessed by Morss (1976). Enthalpies of formation of most of the lanthanide tribromides were determined by Hurtgen et al. (1980). Thermodynamic properties for europium halides were assessed by Rard (1985). Only enthalpies of formation of Sc, Y, Dy and Tm triiodides have been redetermined since the classical work of Hohmann and Bommer (Morss and Spence 1992). A recent set of literature values of enthalpies of formation of rare-earth solid and gaseous trihalides has been published, accompanied by Born–Haber cycle estimated values for all trihalides (Struck and Baglio 1992).

All of the thermodynamic data on actinide halides were reviewed, assessed and tabulated by Fuger et al. (1983). More recent results on uranium are included in a survey of that element's thermochemistry (Grenthe et al. 1992). Among halides of transplutonium elements, enthalpies of formation have been determined only for $AmCl_3$ [Fuger et al. (1983), corrected in table 4 with new $\Delta_f H^0[Am^{3+}(aq)] = -621.2 \pm 2.0\,kJ\,mol^{-1}$, (Mondal et al., (1987)] and $CfBr_3$ (Fuger et al. 1990). Burgess and Kijowski (1981) have summarized most of the enthalpies of solution of rare-earth halides. Morss (1986) correlated enthalpies of solution of all trihalides with structure type and unit-cell volumes; in every class of compounds the enthalpies of solution of lanthanide trihalides are more exothermic than structurally similar actinide trihalides.

Some relevant data are compiled in table 4 and the enthalpies of solution are plotted in fig. 6. We note that, as is the case for sesquioxides, all enthalpies of solution of actinide trihalides are less exothermic than those of structurally similar lanthanide trihalides. See section 4.1.1 for further discussion.

$CfBr_3$ cannot be used in such a comparison since the structure (monoclinic) of the sample used for calorimetry is different from that of all the rare-earth tribromides studied thermochemically. Fuger et al. (1990) estimated enthalpies of formation of other tribromides using a plot of $[\Delta_f H^0[MBr_3(s)] - \Delta_f H^0[M^{3+}(aq)]$ versus M^{3+} ionic radius. Because that approximation does not take crystal structures into account, we will not attempt to incorporate $CfBr_3$ into a correlation of lanthanide versus actinide tribromides.

Enthalpies of formation of several rare-earth dichlorides (Morss and Fahey 1976) and of dysprosium diiodide (Morss and Spence 1992) have been published and have been used to calculate the aqueous reduction potentials $E^0(R^{3+}/R^{2+})$; see section 4.5 for details. Others (Kim and Oishi 1979, Johnson and Corbett 1970, Johnson 1974, 1977) have calculated enthalpies of formation and used them as part of a cycle to calculate aquo-ion properties; see section 3.3 for details.

Gibson and Haire (1988a,b) decomposed several lanthanide and actinide tetrafluorides thermally in a Knudsen effusion cell, carried out (1992) high-temperature fluorinations, and used mass spectrometry to identify the gaseous decomposition products (F_2 or MF_3) and the rate of change of pressure of these products with temperature. They showed that stability trends in the tetrafluorides differ slightly from those in the dioxides. These trends are discussed in sections 2.4.4 and 4.4.1. Similar studies have been carried out with trichlorides (Sapegin et al. 1984), tribromides, and triiodides but are not discussed further in this chapter.

2.4. *Free-energy determinations*

2.4.1. *Oxidation–reduction chemistry in aqueous solution*

There are several well-documented critical summaries of redox potentials in aqueous solution (Martinot and Fuger 1985, Morss 1985, Bratsch 1989). Recent measurements and assessments are emphasized in the following sections.

2.4.1.1. *Aqueous solution electrochemistry (uncomplexed ions).* Several new sets of electrochemical measurements have resulted in new aqueous reduction potentials for aquo-ions of uranium, neptunium and plutonium. These potentials are important for thermochemical and geochemical assessments. Fuger (1992, table 1) has evaluated the effect of each of these new potentials on those tabulated in the most recent IAEA compilation (Fuger and Oetting 1976). For the purposes of this chapter only the $E^0(U^{4+}/U^{3+}) = -0.568 \pm 0.010$ V (Bruno et al. 1990), $E^0(Np^{4+}/Np^{3+}) = 0.210 \pm 0.010$ V and $E^0(Pu^{4+}/Pu^{3+}) = 1.046 \pm 0.011$ V (Riglet et al. 1989) need to be considered. They have been incorporated in table 5. Fuger (1992) has used these potentials to calculate new values of $S^0[U^{3+}(aq)]$and $S^0[Pu^{4+}(aq)]$ that have been adopted in table 1. He notes, and we concur, that the $E^0(Np^{4+}/Np^{3+}) = 0.210 \pm 0.010$ V indicates that both $\Delta_f H^0[Np^{3+}(aq)]$ and $S^0[Np^{3+}(aq)]$ need experimental determination. These determinations will require calorimetric determination of $\Delta_{oxid'n} H^0[Np^{3+}$

TABLE 5
Reduction potentials (in Volts) for rare earths and actinides[a].

Acid solution – rare earths

+7	+6	+5	+4	+3	+2	0
				Sc^{3+}		Sc
				Y^{3+}		Y
				La^{3+}		La
			Ce^{4+}	Ce^{3+}		Ce
			(Pr^{4+})	Pr^{3+}	Pr^{2+}	Pr
			(Nd^{4+})	Nd^{3+}	Nd^{2+}	Nd
				Pm^{3+}	Pm^{2+}	Pm
				Sm^{3+}	Sm^{2+}	Sm
				Eu^{3+}	Eu^{2+}	Eu
				Gd^{3+}		Gd
			(Tb^{4+})	Tb^{3+}		Tb
			(Dy^{4+})	Dy^{3+}	Dy^{2+}	Dy
				Ho^{3+}	(Ho^{2+})	Ho
				Er^{3+}		Er

TABLE 5 (continued)

Acid solution – rare earths

+7	+6	+5	+4	+3	+2	0

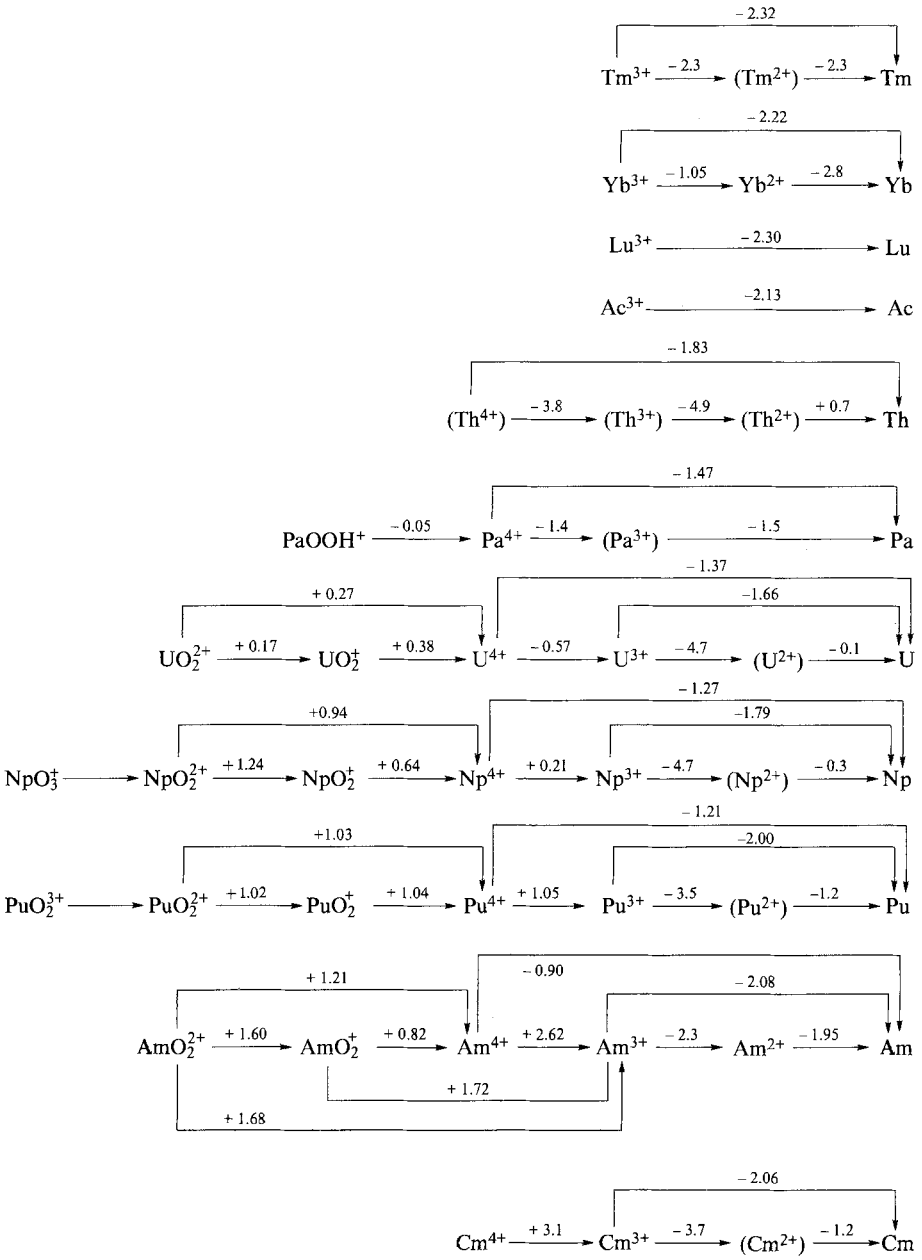

TABLE 5 (continued)

Acid solution – actinides

+7	+6	+5	+4	+3	+2	0

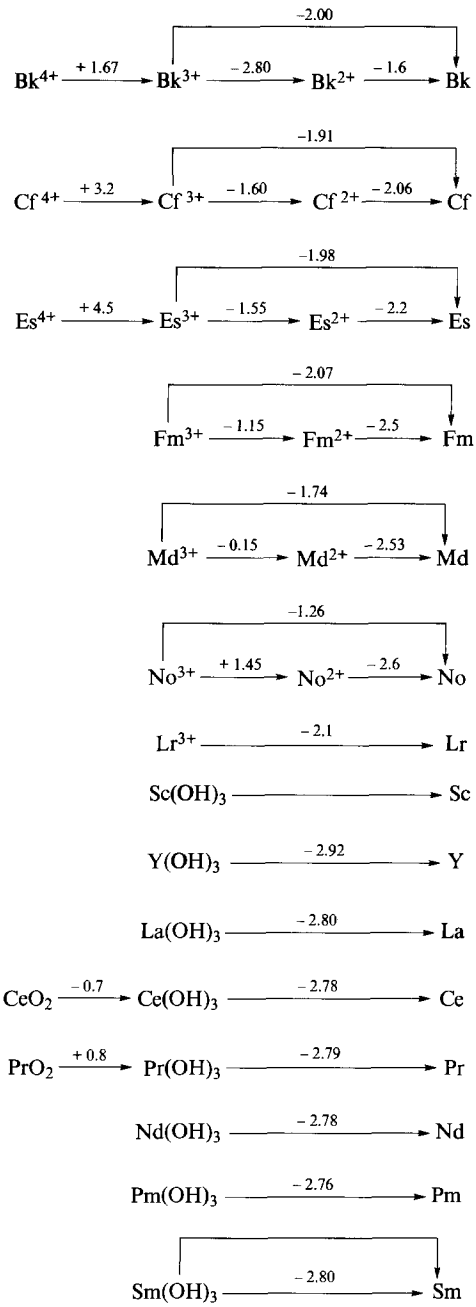

TABLE 5 (continued)

Basic solution – rare earths						
+ 7	+6	+5	+4	+3	+2	0

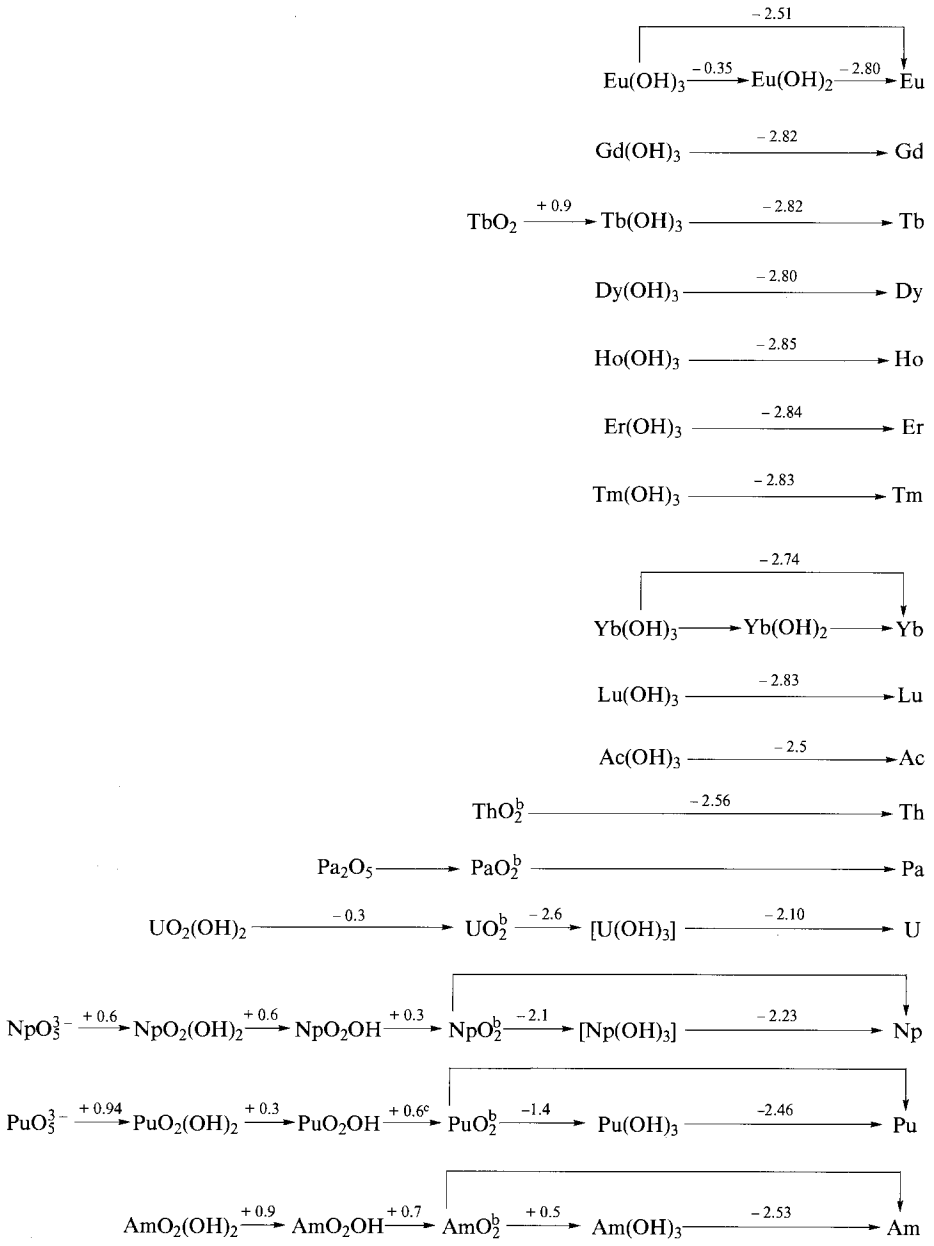

TABLE 5 (continued)

Basic solution – actinides

+7	+6	+5	+4	+3	+2	0
			$CmO_2^b \xrightarrow{+0.7} Cm(OH)_3$	$\xrightarrow{-2.53}$		Cm
			$BkO_2^b \xrightarrow{-0.8} Bk(OH)_3$	$\xrightarrow{-2.5}$		Bk
			$(CfO_2)^b \xrightarrow{+0.8} Cf(OH)_3$	$\xrightarrow{-2.4}$	$Cf(OH)_2$	Cf
				$Es(OH)_3 \xrightarrow{-2.5}$	$Es(OH)_2$	Es
				$Fm(OH)_3 \xrightarrow{-2.5}$	$Fm(OH)_2$	Fm
				$Md(OH)_3 \xrightarrow{-2.2}$	$Md(OH)_2$	Md
				$No(OH)_3 \xrightarrow{-1.6}$	$No(OH)_2$	No
				$Lr(OH)_3 \xrightarrow{-2.6}$		Lr

[a] Except for solid metals and hydroxide solids, all species in these diagrams are aqueous ions. Extremely unstable species in brackets.

[b] MO_2 assumed to be in equilibrium with, or slightly more stable than, "$M(OH)_4$", i. e., uncharacterized hydrous M(IV) oxide.

[c] Peretrukhin et al. (1993).

(aq) → Np^{4+} (aq)], of $\Delta_{soln}H^0[NpCl_3 \cdot 6H_2O\ (298\ K)]$ and of $S^0[NpCl_3 \cdot 6H_2O(298\ K)]$, each of which will be a demanding experimental undertaking.

Since there are no rare-earth ions of oxidation state higher than 4+, we do not discuss MO_2^+ or MO_2^{2+} thermodynamics. There have been assessments of these properties when M is U–Am (Fuger and Oetting 1976, Grenthe et al. 1992, Riglet et al. 1987).

2.4.1.2. *Aqueous solution electrochemistry and chemical oxidation (complexed ions).* Electrochemical and chemical (using ozone) oxidation of Pr(III) to Pr(IV) and Tb(III) to Tb(IV) has been carried out in concentrated, strongly basic aqueous carbonate solutions (Hobart et al. 1980, Varlashkin et al. 1985, Myasoedov et al. 1986). Other measurements and calculations (Nugent et al. 1973a, Morss 1985) on the $E^0(Ce^{4+}/Ce^{3+})$, $E^0(Pr^{4+}/Pr^{3+})$ and $E^0(Tb^{4+}/Tb^{3+})$ couples indicate that this basic complexing medium decreases the electrode (reduction) potential by 1.7 V, i.e., $E^0(Ce^{4+}/Ce^{3+}) = 1.72$ V and $E^{o\prime}(Ce^{4+}/Ce^{3+}) = +0.05$ V in basic carbonate. This decrease in potential means that the M^{4+} state is significantly stabilized by complexation. Similar studies have achieved electrochemical oxidation of Am(III) to Am(IV) (Hobart et al. 1982) and of Bk(III) to Bk(IV) (Morris et al. 1990) but *not* electrochemical or chemical oxidation of Cm(III) or Cf(III) (Hobart et al. 1983). More recently, however, Frenkel et al. (1986) and Myasoedov et al. (1986) reported partial (ca. 20%) oxidation of aqueous Cf(III)–2 M K_2CO_3 at pH 13.2 to a higher oxidation state, presumably Cf(IV).

Complexing by phosphotungstate in aqueous solution has achieved the oxidation of Pr(III) to Pr(IV), Tb(III) to Tb(IV), Am(III) to Am(IV) and Cf(III) to Cf(IV) (Volkov et al. 1981, Myasoedov 1982). The electrochemical measurements are consistent with a decrease of $E^0(M^{4+}/M^{3+})$ by about 1.0 V at pH 4–5. The successful oxidation of Cf(III) to Cf(IV) in phosphotungstate solution is inconsistent with a 1.0 V shift in E^0 and also with (at best) a partial oxidation of Cf(III) in basic carbonate solution, in which medium the 1.7 V shift in E^0 should make Cf(IV) much more accessible. Curium(III) has not been oxidized in either basic carbonate or phosphotungstate.

2.4.1.3. *Radioelectrochemistry.* Radioelectrochemistry has been used extensively to determine the oxidation–reduction behavior of heavy actinides. The earliest studies were those of Maly (1967), Maly and Cunningham (1967), Hulet et al. (1967), David (1970) and David et al. (1978). These pioneering studies have been summarized in papers by David (1986a) and Silva (1986). Most recently, radiocoulometry was used by David et al. (1990) to estimate the No^{2+}/No electrode potential as -2.49 ± 0.06 V.

2.4.1.4. *Pulse radiolysis evidence for dipositive and tetrapositive ions.* Pulse-radiolysis studies have been performed in aqueous solution to identify the 2+ ions Sm^{2+}, Eu^{2+}, Gd^{2+}, Tb^{2+}, Ho^{2+}, Ho^{2+}, Tm^{2+} and Yb^{2+} (Gordon et al. 1977), Am^{2+} and Cm^{2+} (Sullivan et al. 1976), Bk^{2+} (Sullivan et al. 1988) and Cf^{2+} (Sullivan et al. 1983), and the 4+ ions Am^{4+} and Cm^{4+} (Sullivan et al. 1976, Gordon et al. 1978). Pulse radiolysis was unsuccessful in oxidizing Cf^{3+} to Cf^{4+}(aq) (Sullivan et al. 1983). From these studies and from the reduction potential of e^-(aq), -2.86 V, and the oxidation potential of OH radical, + 2.65 V, these authors established limits for several standard electrode potentials. Because pulse radiolysis produces transient species that may not have relaxed to equilibrium conditions of hydration, they are not suitable for entry in table 5 as equilibrium E^0 values.

2.4.1.5. *Evidence for An(VI) ions from β^- decay of precursor ions in aqueous solution.* The isotope ^{242}Am decays by β^- emission to ^{242}Cm and the isotope ^{249}Bk decays by β-emission to ^{249}Cf. It is possible that the nuclear decay process conserves the elect-

rons, thereby making possible the conversion of AmO_2^{2+} into CmO_2^{2+} and of Bk^{4+} into Cf^{5+}. A claim has been made for synthesis of Cm (VI) as the result of ozonation of ^{242}Am solution in bicarbonate, followed by addition of $Na_4UO_2(CO_3)/K_2CO_3$ solution to coprecipitate tracer amounts of Cm(VI) with UO_2^{2+} in a $K_4(U,Cm)O_2(CO_3)_3$ precipitate (Peretrukhin et al. 1978). A claim has similarly been made for production of ~ 10% of Cf(V) as CfO_2^+ in aqueous carbonate solution, followed by coprecipitation with $Na_4UO_2(CO_3)_3$ (Kosyakov et al. 1982).

2.4.2. *Reduction potential diagrams in aqueous solution*

Since only a few standard aqueous electrode potentials $E^0(Ln^{3+}/Ln^{2+})$ have been determined electrochemically, others have been estimated [e.g., $E^o(Dy^{3+}/Dy^{2+})$ (Morss and Fahey 1976, Morss and Spence 1992)] from calorimetric measurements on their dichlorides or from spectroscopic correlations. The only experimental values of $E^0(An^{3+}/An^{2+})$ are from radioelectrochemical measurements on Fm–No (David 1986a) and coprecipitation studies (Mikheev 1988, 1992). Spectroscopic correlations of $E^0(An^{3+}/An^{2+})$ have also been made (section 3.4). These reduction potentials have been assessed for the rare earths (Morss 1985), for the lighter actinides (Martinot and Fuger 1985), and for the heavier actinides (David 1986a, Morss 1986). With the exception of uranium, neptunium and plutonium species [(Fuger 1992, table 1), discussed in section 2.4.1] and No^{2+} (discussed in section 2.4.1), these potentials are still valid. We note that the $E^0(An^{3+}/An)$ values depend on the $S^0[An^{3+}(aq)]$ which are referenced to a value for $Pu^{3+}(aq)$ that is based in part on experiment but also required estimation of $S^0[PuCl_3 \cdot 6H_2O(s)]$.

These potentials are compiled in reduction potential diagrams, often referred to as Latimer diagrams, in table 5. These are *formal potentials* measured in or calculated for 1.00 mol dm^{-3} $HClO_4(aq)$ or for another acid if no value in $HClO_4$ has been measured. In a few cases the formal potentials have been converted to *standard potentials* for incorporation into tables of standard thermodynamic properties using the specific ion interaction theory (Grenthe et al. 1992). Values in basic solution have been calculated using solubility equilibria (Morss 1985, 1986).

2.4.3. *Solution electrochemistry in non-aqueous solvents (including molten salts)*

Three classes of solvents are of interest for electrochemical properties of the f elements.

(1) Electrochemical behavior in simple molten salt systems such as $M-MCl_3$ showed evidence for M^{2+} where M denotes Ce, Pr and Nd (Bronstein 1969), but not when M is Pu (Johnson and Leary 1964). Many studies were carried out in the 1960's in support of molten salt fast breeder reactor technology; a recent review has been published (Willit et al. 1992). Very recent interest in actinide electrochemistry in molten salts is driven by "pyrochemical" electrorefining of spent reactor fuel in the Integral Fast Reactor program at Argonne National Laboratory. Recent actinide molten salt electrochemical and partitioning data have been published (Ackerman 1991, Ackerman and Settle 1992, 1993, Koyama et al. 1992) but they show no evidence for Np^{2+}, Pu^{2+} or Am^{2+}.

Molten salt systems offer a wide range of acidity ($AlCl_3$) and basicity (NaCl, *t*-butylpyridinium chloride) and thus stabilize low and high oxidation states in acidic

and basic solvents, respectively. Early papers describe many studies of lanthanides (Gilbert et al. 1978) and actinides (Gruen 1976) in molten salt systems. The M^{3+}/M^{2+} electrochemistry for M = Sm, Tm and Yb as well as the Np^{4+}/Np^{3+} electrochemistry were studied by Schoebrechts et al. (1983, Schoebrechts and Gilbert 1985) and correlated with Nugent's electron-spin correlation parameters. DeWaele et al. (1986) showed how acid–base relationships in $MCl–AlCl_3$ molten salts affect the $E(U^{4+}/U^{3+})$ potential. Martinot has reviewed the electrochemical properties of actinides (Martinot 1991) in molten salts.

Mikheev (1988, 1989, 1992) has obtained extensive evidence through cocrystallization that almost all the tripositive lanthanide (except for Sm, Eu, Tm and Yb) and actinide ions (U, Np, Pu, Cm, Bk) can be reduced and have $E^0(M^{3+}/M^{2+})$ in the neighborhood of -2.5 to -2.9 V. The lanthanide potentials are not consistent with the experimentally confirmed generalized f^q electron energetics scheme developed by Nugent (1975). The potentials are not consistent with potentials inferred from pulse-radiolysis studies (Sullivan et al. 1976, 1983, 1988). If the potentials $E^0(M^{3+}/M^{2+})$ proposed by Mikheev for uranium, -2.54 V, and plutonium, -2.59 V, at macroscopic concentrations (Mikheev et al. 1991) were correct, phase diagram studies and electrochemistry in molten salts should have revealed the ions U^{2+} and Pu^{2+}, but no evidence other than cocrystallization has been presented. In fact, the crystal chemistry of the "reduced" uranium halide NaU_2Cl_6 (Schleid and Meyer 1989) is consistent with U^{3+} ions and metallic electrons. The cocrystallization model (Mikheev and Merts 1990) may not be transferable to aqueous solution and thus Mikheev's $E^0(M^{3+}/M^{2+})$ potentials are not cited in table 5.

(2) Non-aqueous solvents such as dimethylsulfone do not react with many reducing- (H_2) or oxidizing (O_2, Cl_2) gases. They offer a wide range of redox potentials (e.g., the polarization window of hexamethylphosphoramide is 5.5 V). Herman and Rairden (1976) reviewed the electrochemistry of lanthanides in non-aqueous solvents. Martinot (1978) reviewed the electrochemical properties of actinides in non-aqueous solvents and has reported the reduction behavior of U^{4+} in non-aqueous solvents (Martinot et al. 1990).

Musikas and Myasoedov (1969) claimed the polarographic reduction of Am^{3+} to Am^{2+} in acetonitrile and inferred $E^0(Am^{3+}/Am^{2})= -2.2$ V. This claim and that for the corresponding $Cm^{3+}–Cm^{2+}$ reduction (David 1970) was challenged by Friedman and Stokely (1976), who attributed the polarographic wave to reduction of water and the $Am^{3+}–Am$ reduction. Nevertheless, the accepted $E^0(Am^{3+}/Am^{2+})= -2.3$ V is very close to that inferred by Musikas and Myasoedov. Kulyukhin et al. (1992) claim that the failure to see Am^{2+} in tetrahydrofuran solution in the presence of Nd^{2+} or Tm^{2+} is due to its reoxidation by radiochemically generated free radicals. Since the assessment of this chapter reports $E^0(Nd^{3+}/Nd^{2+})= -2.6$ V and estimates $E^0(Am^{3+}/Am^{2+})= -2.3$ V, we concur with the interpretation of Kulyukhin et al. (1992).

(3) Anhydrous HF (AHF) represents a robust (it is difficult to oxidize or reduce) solvent system, but experimental work with AHF is technically very demanding. Baluka et al. (1981) stabilized U(III) in highly acidic $HF–BF_3$. Barraclough et al. (1991) stabilized Sm(II), Eu(II) and Yb(II) in HF-superacid media. O'Donnell (1992)

has described the spectra of U(III), U(IV), Np(III) and Np(IV), as well as the disproportionation of U(III) to U(0) and U(IV) in this medium. Unfortunately, electrochemical measurements have not been done but it is evident that this acidic medium is not favorable for high oxidation states.

2.4.4. *Gas–solid equilibrium and vaporization measurements*

The partial molar Gibbs free energy of solution of oxygen in MO_{2-x}, $\Delta\bar{G}(O_2)$, has been determined for the MO_{2-x} systems [M denotes Ce (Bevan and Kordis 1964, Sørensen 1981), Pr (Hyde et al. 1966, Turcotte et al. 1971a), Tb (Hyde and Eyring 1965, Kordis and Eyring 1968, Inaba et al. 1981), U (Lindemer and Besmann 1985), Pu (Anon 1967), Am (Chikalla and Eyring 1967), Cm (Chikalla and Eyring 1969, Turcotte et al. 1973), Bk (Turcotte et al. 1971b, 1980) and Cf (Turcotte and Haire 1976)] by isobaric thermal analysis. These oxide phase diagrams have been well characterized: as PrO_2 is reduced, e.g., the phases are α ($PrO_{1.72-2.00}$), β ($PrO_{1.833} = Pr_{12}O_{22}$), δ ($PrO_{1.818} = Pr_{11}O_{20}$), ε ($PrO_{1.800} = Pr_{10}O_{18}$), ζ ($PrO_{1.778} = Pr_9O_{16}$), ι ($PrO_{1.714} = Pr_7O_{12}$), σ ($PrO_{1.50-1.70}$), and ϕ ($PrO_{1.50} = Pr_2O_3$). Figure 7a is a free energy versus temperature diagram of some of these phase boundaries. Unfortunately, these oxide systems display hysteresis (gain of oxygen occurs at lower temperature than loss of oxygen). An oxide with a stable 4+ state appears to the right of this diagram.

The partial molar Gibbs free energy of oxygen $\Delta\bar{G}(O_2)$ has been determined for the $UO_{2\pm x}$ system [recently reviewed by Lindemer and Besmann (1985)] although the hypostoichiometric region UO_{2-x} requires much higher temperatures than the hyperstoichiometric region UO_{2+x}. In addition, $\Delta\bar{G}(O_2)$ has been determined for $(M, M')O_{2-x}$ solid-solution systems, typically where the majority component M denotes U and the minority component M′ denotes La, Ce, Pu, etc. (Fujino 1988). Some of these results are superimposed in fig. 7b. The shifts in $\Delta\bar{G}(O_2)$ parallel the stability relationships between MO_2 and M_2O_3 shown in fig. 10c. In fact, $\Delta\bar{G}(O_2)$ of the solid solution $(U, Eu)O_{2-x}$ is displaced to $x < 0$ (suggesting that Eu^{2+} may even be present). As expected, $\Delta\bar{G}(O_2)$ of the solid solution $(U, Nb)O_{2\pm x}$ is displaced to $x > 0$. A very negative partial molar Gibbs free energy of oxygen represents an oxide that accepts oxygen readily: a solid solution of $(U, Nb)O_{2+x}$ enhances the hyperstoichiometric region, whereas a solid solution of $(U, La)O_{2-x}$ enhances the hypostoichiometric region. In other words, Nb^{5+} is an n-type (electron) donor and La^{3+} is a p-type (hole) donor in UO_2.

Many studies have been done to determine the partial molar free energy of oxygen in nonstoichiometric or doped UO_2 (see, e.g., Fujino 1988, Fujino and Miyake 1991). These studies provide insight into the effects of defects and of n- or p-type dopants into the thermodynamics of $UO_{2\pm x}$. The $UO_{2\pm x}$ system will not be discussed further because the UO_2–UO_3 region has no lanthanide parallel. We note that there are no data for U_2O_3–UO_2 or Np_2O_3–NpO_2 because the sesquioxides do not exist; even at 2200 °C there is a miscibility gap approximately from $UO_{0.02}$ to $UO_{1.75}$ (Martin and Edwards 1965). There have been many gas–solid equilibrium studies (e.g., Woodley 1981) on the Gibbs free energy of oxygen in $(A, B)O_{2-x}$ systems, where A and B represent Ce, Th, U and/or Pu.

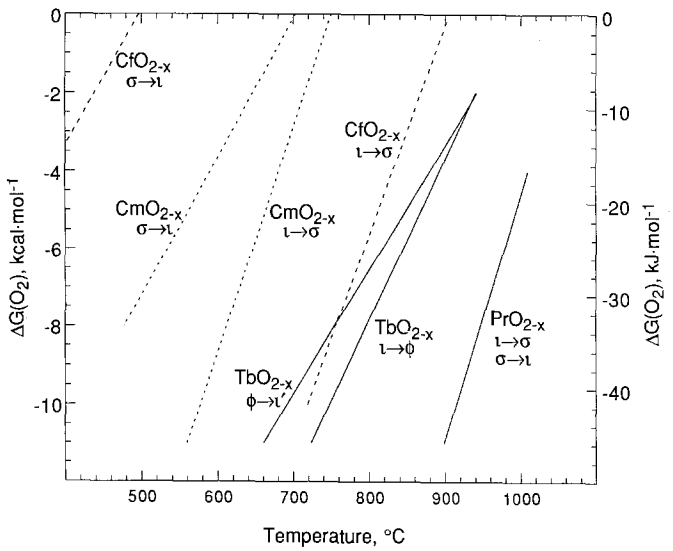

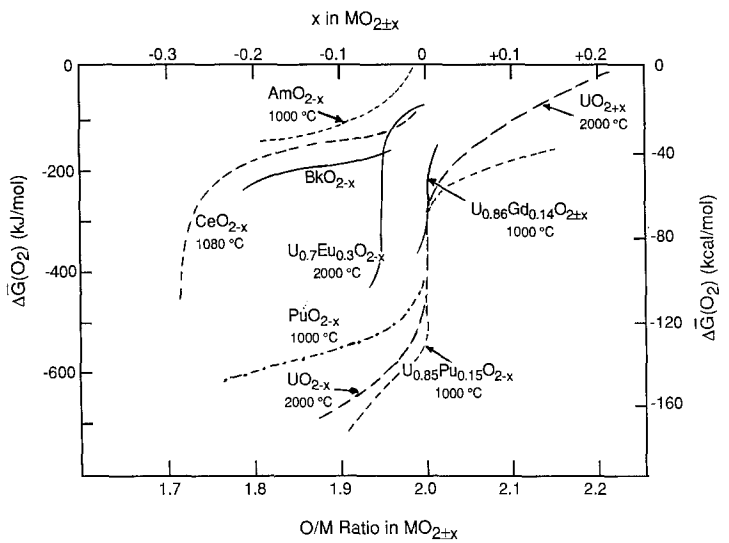

Fig. 7.(a) Free energy versus temperature diagram of some of the phase boundaries in the PrO_{2-x}, TbO_{2-x}, $^{248}CmO_{2-x}$ and CfO_{2-x} systems. The oxide with the most stable 4 + state (PrO_2) appears at the lower right of this diagram. Higher ($\iota \rightarrow \sigma$ or $\iota \rightarrow \phi$) and lower ($\sigma \rightarrow \iota$ or $\phi \rightarrow \iota'$) temperature transitions reflect hysteresis. The MO_{2-x} phases are $\iota(MO_{1.714} = M_7O_{12})$, ι' (metastable $MO_{\sim 1.7}$), $\sigma(MO_{1.50-1.70})$ and $\phi(MO_{1.50})$. (b) Partial molar Gibbs free energies of solution of oxygen $\Delta\bar{G}(O_2)$ above the systems $MO_{2\pm x}$ (M = Ce, U, Pu, Am, Bk) and some solid solutions in $UO_{2\pm x}$. $\Delta\bar{G}(O_2)$ is a differential property; it represents the free energy of addition of one mole of O_2(g) to a very large number of moles of $MO_{2\pm x}$. An oxide with stable higher oxidation state appears to the right of this diagram.

Gibson and Haire (1988a, b) (table 7) studied the congruent [$MF_4(g) \rightarrow MF_4(g)$] and incongruent [$MF_4(s) \rightarrow MF_3(g) + \frac{1}{2}F_2$ (g)] reactions for M = Ce, Am and Cm. These properties are compared in section 4.4.1.

2.4.5. *Solid-state electrochemistry*

Solid-state galvanic cells of the sort $(-)Sr|SrCl_2||BaCl_2||DyCl_2|Dy(+)$ have been used to determine free energies of reactions such as $DyCl_2 + Sr = SrCl_2 + Dy$ at elevated temperatures (Goryushkin et al. 1989). A second-law extrapolation yielded $\Delta_f H^0[DyCl_2(s, 298\,K)] = -676.4 \pm 2.5\,kJ\,mol^{-1}$, differing from the value of Morss and Fahey (1976), $-693 \pm 6\,kJ\,mol^{-1}$. We prefer calorimetric enthalpies (since the calorimetric reactions of these unstable salts are very well defined) to enthalpies derived from solid-state electrochemistry (where unidentified products may form at solid electrode surfaces).

Micro-scale solid-state electrochemistry is ideally suited to the parallel determination of high-temperature thermodynamic properties of transuranium oxides. The $UO_{2\pm x}$–MO systems (M denotes alkaline earth) have been thoroughly investigated (Fujino 1988). Solid-state electrochemistry of transuranium oxides have been reported only for PuO_{2-x} and $(U, Pu)O_{2\pm x}$ as reviewed in Anon (1967).

3. Estimated and calculated thermodynamic properties

3.1. *Synthesis under equilibrium conditions*

Partial oxidations of Nd^{3+} to Nd^{4+} and of Dy^{3+} to Dy^{4+} have been claimed in oxide matrices (Brauer and Kristen 1980) but a repeated synthesis of $BaCeO_3$: Dy failed to detect Dy^{4+} by Mössbauer spectroscopy (Soderholm et al. 1987). Syntheses of Nd^{4+} and Dy^{4+} and Dy^{4+} have been achieved in Cs_3MF_7, Cs_2RbMF_7, and Cs_2KMF_7; Raman spectra confirmed the presence of the tetravalent cations (Hoppe 1982).

Experiments to synthesize Es^{4+} compounds (EsF_4, EsO_{2-x}, $BaEsO_3$, Es^{4+} in CeF_4, Es^{4+} in TbF_4) have failed (Haire 1980, Beitz 1991). We do not consider these failures to be due to the high specific α radioactivity of $^{253}Es(t_{1/2} = 20.47\,d)$. We use these experiments to infer that the reduction potential $E^0(Es^{4+}/Es^{3+})$ is greater than those of Pr, Tb, Cm and Cf and perhaps comparable to those of Nd and Dy. Preparation of crystals of, e.g., Cs_3CeF_7 doped with Es and identification of the oxidation state of Es in such a highly basic matrix remains an unachieved challenge.

3.2. *Thermal analysis*

For a discussion of thermal analysis see section 2.4.4.

3.3. *Lattice-energy calculations and Born–Haber cycles: intra- and inter-group comparisons*

Many lattice-energy calculations have provided useful perspectives on solid-state reactions. The MAPLE concept (section 4.1.1) is often used as a way of judging if

crystal-structure determinations of binary and complex oxides are correct. The work of Catlow (Catlow and Mackrodt 1982) and his followers (e.g., Grimes 1992, Ball 1992) exemplify lattice-energy studies of uranium oxides and fission products in which a crystal lattice is divided into an inner region that may contain a defect and an outer region that extends to infinity (see additional discussion in sections 4.1.1 and 4.1.2).

At a time when little was known about ionization potentials of lanthanide ions as well as about thermochemistry of non-tripositive lanthanide species, Johnson (1969a) showed that differences in the third ionization potentials I_3 of the lanthanides are primarily responsible for many of their apparent oxidation–reduction anomalies. In a subsequent paper (Johnson 1969b) he compared and contrasted the relative stabilities of the di-, tri- and tetrapositive oxidation states of the lanthanides and actinides, pointing out how much less is the change in ionization potential for actinides than lanthanides at the half-filled shell (see fig. 4). He elaborated (Johnson 1974) on the first paper by systematizing the properties of the dipositive lanthanide ions in conjunction with those of the alkaline-earth metal ions.

Johnson and Corbett (1970) discussed the difference between the enthalpies of formation of DyI_2 and DyI_3 in terms of disproportionation reactions. Johnson's earlier treatment of the dipositive alkaline-earth and lanthanide ions (Johnson 1974) has recently been applied to the DyI_2–DyI_3 and $Dy^{2+}(aq)$–$Dy^{3+}(aq)$ enthalpy differences (Morss and Spence 1992).

The above cycles were applied only to rare earths. A simplified cycle, such as the $P(M)$ relationship, must be used for most actinides, since only the first ionization potentials have been derived from experiments for only a few actinides (Morss 1986).

3.4. *Correlations of electron-transfer and f → d spectra and reduction potentials*

This topic was fully developed spectroscopically by Vander Sluis and Nugent (1974), received its last comprehensive review by Nugent (1975), and was discussed in section 2.1.5. It is often considered (Nugent et al. 1971, 1973a, Johnson 1977, Ionova and Spitsyn 1978, Mikheev et al. 1985, Mikheev 1988) in predicting or correlating $E^0(M^{4+}/M^{3+})$ and $E^0(M^{3+}/M^{2+})$. When the $4f \rightarrow 5d$ excitation energy of an R^{3+} ion is small, an f electron in R^{3+} may be easily promoted into a d orbital and R^{3+} can be oxidized readily to R^{4+}. For example, the $4f^1 \rightarrow 5d^1$ excitation energy in $CeBr_3$ is at $32\,000\,cm^{-1}$ while the $4f^2 \rightarrow 4f^15d^1$ excitation energy in $PrBr_3$ is at $43\,800\,cm^{-1}$ (Nugent et al. 1971). Thus, the $Ce^{3+} \rightarrow Ce^{4+}$ oxidation is easier to achieve than is the $Pr^{3+} \rightarrow Pr^{4+}$ oxidation; i.e., $E^0(Ce^{4+}/Ce^{3+})$ is smaller than $E^0(Pr^{4+}/Pr^{3+})$. A parallel argument applies to $5f \rightarrow 6d$ excitation energies and $E^0(An^{4+}/An^{3+})$ values. Likewise $f \rightarrow d$ excitation energies in Ln^{2+} and An^{2+} spectra correlate well with $E^0(M^{3+}/M^{2+})$ (Mikheev et al. 1985). For those $M^{2+}(aq)$ with unknown $f \rightarrow d$ spectra the energetics of the free ion can be used (Brewer 1971): the $Cf^{3+} \rightarrow Cf^{2+}$ reduction represents the transition $5f^8 \rightarrow 5f^9$ and the $Es^{3+} \rightarrow Es^{2+}$ reduction represents the transition $5f^9 \rightarrow 5f^{10}$; the increase in $f \rightarrow d$ excitation energies as one passes from Cf^{2+} to Es^{2+} makes the "trivalent" configuration for Cf^{2+}, $5f^96d$, less favorable than that for Es^{2+}, $5f^{10}6d$.

4. Lanthanide–actinide bonding and oxidation–reduction comparisons

4.1. *Bonding in "ionic" systems*

In this section only coordination and complexing (sharing of electron pairs, i.e., acid–base effects) are considered. Oxidation–reduction comparisons (transfer of electrons) are made in sections 4.4 and 4.5.

4.1.1. *Oxides: covalency and acid–base effects*

Morss et al. (1987) noted that the enthalpies of solution of actinide sesquioxides are systematically less exothermic than enthalpies of solution of structurally similar lanthanide sesquioxides. Morss (1986, fig. 17.10) found similar behavior for all known trihalides. These enthalpies of solution for sesquioxides and hexagonal trichlorides are shown in fig. 6. The enthalpies of solution of An elpasolites $Cs_2NaAnCl_6$ (Schoebrechts et al. 1989) are also systematically less exothermic than enthalpies of solution of structurally similar Ln elpasolites, fig. 6. Since the enthalpy of solution of an ionic compound (e.g., MX_3) represents the difference between the lattice energy of the solid and the hydration enthalpy of the free ions (e.g., M^{3+} and $3X^-$), the smaller actinide enthalpies of solution mean either that actinide(III) compound lattice energies are *larger* than those of corresponding lanthanide(III) compounds, or that hydration enthalpies of actinide(III) ions are *smaller* than those of corresponding lanthanide(III) ions. This behavior is illustrated in fig. 8. It clearly represents a lanthanide–actinide bonding difference although it is speculative to attribute the smaller actinide enthalpy of solution to larger actinide compound lattice energies.

Aronson (1982) and Smith (1987) independently developed quantitative scales of solid oxide bonding energetics based upon the enthalpy of reaction of acidic oxides with basic oxides, following Pauling's electronegativity scale. Aronson calculated "pseudo-electronegativity" values for metal ions. Smith defined "acidity" parameters a for oxides, e.g., a(A) for an acidic oxide A and a(B) for a basic oxide B, in terms of the

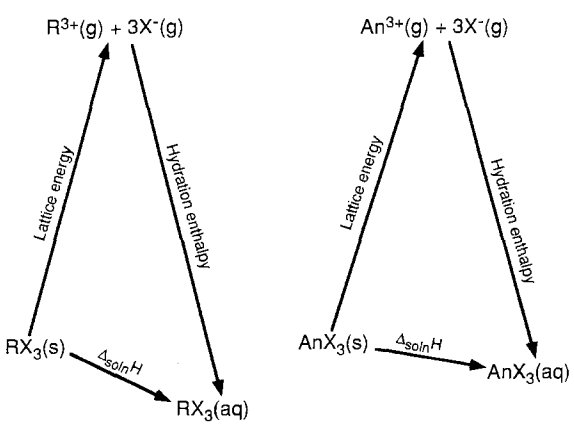

Fig. 8. Comparison of energetics of dissolution of an ionic lanthanide compound (trihalide shown in this example) versus an isostructural actinide compound. Note that the enthalpy of solution ($\Delta_{soln}H$) of the lanthanide compound is more exothermic than that of the actinide compound.

enthalpy of reaction of these oxides to form an oxo-salt,

$$a(\text{acidic oxide}) - a(\text{basic oxide}) = [-\Delta H^0(\text{reaction})]^{1/2}, \tag{7}$$

where ΔH^0(reaction) refers to reactions such as

$$SO_3(s) + CaO(s) = CaSO_4(s), \qquad \Delta H = -344.5\,\text{kJ mol}^{-1}, \tag{8}$$

$$H_2O(\ell) + CaO(s) = Ca(OH)_2(s), \quad \Delta H = -65.2\,\text{kJ mol}^{-1}. \tag{9}$$

As a reference for this scale, he assigned the acidity parameter of water as zero. Thus, $a(CaO) = (65.2)^{1/2} = 8.1$. Smith used 250 enthalpies of reactions with solid oxides (except for H_2O, SO_2, and N_2O_5) and found best values of a by least-squares analysis. The scale is normalized for oxide–oxide reactions such that the basic oxide transfers one mole of oxide to the acidic oxide. He applied this scale only to reactions in which there is a distinct oxo-anion in the salt (e.g., orthosilicates, orthophosphates, and

TABLE 6
Acidity parameters a for f-element oxides[a].

Sesquioxides behaving as bases			
Oxide	a_{Oxide}	Oxide	a_{Oxide}
Y_2O_3			
La_2O_3	−6.1	Ac_2O_3	
Ce_2O_3	−5.8		
Pr_2O_3	−5.8		
Nd_2O_3	−5.7	(U_2O_3)	
Pm_2O_3		(Np_2O_3)	
Sm_2O_3		Pu_2O_3	−6.9
Eu_2O_3		Am_2O_3	−5.6
Gd_2O_3		Cm_2O_3	−5.8
Tb_2O_3		Bk_2O_3	−4.5
Dy_2O_3		Cf_2O_3	−4.2
Er_2O_3		Es_2O_3	
Ho_2O_3			
Tm_2O_3			
YbO_3			
Lu_2O_3			

Oxides behaving as acids							
Oxide	a	Oxide	a	Oxide	a	Oxide	a
CeO_2		ThO_2	−3.8				
PrO_2		PaO_2		Pa_2O_5			
NdO_2		UO_2	−3.2	U_2O_5		UO_3	+3.8
		NpO_2		Np_2O_5		(NpO_3)	+4.2
		PuO_2	−3.5	Pu_2O_5		(PuO_3)	
		AmO_2					
		CmO_2					
		BkO_2					

[a] Acidity parameter as defined in section 4.1.1 (Smith 1987).

tungstates such as K_2WO_4 but not tungstates such as Ba_3WO_6). Except for some lanthanide sesquioxides, Smith did not focus on f-element oxides.

Using enthalpies of reaction including complex oxides, also called ternary or mixed oxides, such as $BaCeO_3$ [to calculate $a(CeO_2)$ as an acid] and $BaUO_4$ [to calculate $a(UO_3)$ as an acid] as well as the aqueous acid H_3O^+, we have calculated acidity parameters for f-element oxides on this scale. (The energetics of these complex oxides are discussed in section 4.1.2.) These acidity parameters are shown in table 6. They have the virtue of requiring no crystal structure determination to predict the stability of a complex oxide, but they are strictly empirical guides to solid-state reactions. Clearly, a more fundamental approach to the "non-Coulombic" contribution to crystal energies is needed in order to distinguish covalent or acid–base differences among 4f and 5f element oxides.

4.1.2. *Binary and complex oxides*

Kubaschewski (1972) collected and compared the enthalpies of formation of complex oxides from binary oxides. He did not offer any systematic correlation of these enthalpies with structural properties. Hoppe (1966, 1970a, b, 1975) developed the MAPLE concept (Madelung part of lattice energy) as a tool to guide the structural interpretation of bonding in complex oxides and halides. It requires as input parameters the unit cell of a compound and positions of all atoms, and it treats the crystal as an ionic array of point charges. If crystal structure determinations have been properly done, MAPLE calculations for a complex compound are within 2% (sometimes larger, sometimes smaller) of the MAPLE values of the binary (parent) compounds. Therefore, purely ionic-model calculations are not sufficiently sensitive to correlate quantitatively with the relatively small enthalpies of solid-state complexation.

There have been many other efforts to provide both theoretical and experimental underpinning of the energetics of solid oxides and halides. The perovskites AMO_3 (A denotes Ca, Sr, Ba; M many M^{4+} cations) are a very large class of complex oxides (Takayama-Muromachi and Navrotsky 1988) for which many lanthanide and actinide examples are known (Goudiakas et al. 1990). Takayama-Muromachi and Navrotsky (1988) separated the high-temperature enthalpy of complexation of many pervoskites into Madelung and non-Coulombic parts. They presented graphs of these two parts as a function of the Goldschmidt tolerance factor $t = (r_A + r_O)/[\sqrt{2}(r_M + r_O)]$, but they did not discuss lanthanide or actinide perovskites, nor did they offer a systematic interpretation of the non-Coulombic contribution to the energetics of perovskites.

The perovskites $SrLnO_3$ and $Ba(Ln, An)O_3$ are the most extensive and well characterized class of ternary oxides of the f elements. Morss and Eller (1989) characterized both the volume changes and enthalpy changes for the reaction

$$BaO(s) + MO_2(s) = BaMO_3(s) \tag{10}$$

in terms of the Goldschmidt tolerance factor t. Goudiakas et al. (1990) summarized all available thermochemical information about these oxides. Newer data have been published for $BaCmO_3$ and $BaCfO_3$ (Fuger 1992, Fuger et al. 1992). Enthalpies of complexation of all perovskites $SrMo_3$ and $BaMO_3$ correlate very well with t, but there are no group distinctions between lanthanide and actinide perovskites that might

reflect bonding influence of 5f electrons. The enthalpies of reaction (10) of two compounds ($BaPrO_3$ and $BaMoO_3$) did not correlate with t. $BaPrO_3$ appears to be more stable than predicted by correlation with t. There is no theoretical explanation for this discrepancy; Morss (1992b) has repeated the syntheses and enthalpy of formation measurements on both PrO_2 and $BaPrO_3$ with results essentially identical to those determined earlier. $BaMoO_3$ appears to be less stable than predicted by the correlation with t; this discrepancy cannot be attributed to the unusual stability of MoO_2 (through metal–metal bonding) because $SrMoO_3$ does not show a similar discrepancy.

Although there are no comparative theoretical studies of lanthanide and actinide perovskites, Ball (1992) has carried out computer modeling of ternary uranates, specifically comparing the known perovskite $BaUO_3$ with the unknown $CaUO_3$ and $SrUO_3$. The model is ionic; however, it is to a degree self-compensating [exaggeration of the ionic part of the lattice energy compensates for ignorance of the covalent part (Ball and Dickens 1991)]. Ball's results give enthalpies of reaction (10) for $CaUO_3$, $SrUO_3$ and $BaUO_3$ that agree qualitatively with experimental values (e.g., Goudiakas et al. 1990). Although this model is best for calculation of the energetics of defects, it does confirm that $BaUO_3$ is stable, and $CaUO_3$ and $SrUO_3$ are unstable with respect to the binary oxides. The lattice energy calculated for $BaUO_3$ by Ball (1992) differs by less than 2% from the lattice energy derived from a Born–Haber cycle. Although a small part of the total lattice energy, this difference is large in an absolute sense: 2.59 eV ($250\,kJ\,mol^{-1}$). Further, the calculated value for the enthalpy of reaction (10), $BaO(s) + UO_2(s) = BaUO_3(s)$, -0.21 eV $= -20\,kJ\,mol^{-1}$, is much less than the experimental enthalpy of complexation, $-57\,kJ\,mol^{-1}$ (Williams et al. 1984). Because these enthalpies of complexation are small with respect to the total lattice energy, lattice-energy calculations for complex oxides and halides cannot provide accurate enthalpies of complexation.

Fuger (1985, 1992) has summarized the experimental enthalpies of complexation of hexavalent actinide oxides with alkali-metal and alkaline-earth oxides in terms of the basicities of the alkali-metal and alkaline-earth oxides. Using Smith's (1987) acid–base oxide correlations (section 4.1.1), Morss and Williams (1992) placed these enthalpies on a quantitative scale to derive oxide acidity for UO_3.

4.1.3. *Binary and complex halides*

It has been noted (Morss 1986, fig. 17.10; this chapter, section 4.1.1 and fig. 3) that the actinide trihalides have less exothermic heats of solution than structurally similar lanthanide trihalides.

Fuger (1979) and Fuger et al. (1983) reviewed experimental thermodynamic data on complex halides of the f elements, almost all of which were limited to ternary An^{4+} chlorides. Jenkins and Pratt (1979) used an ionic model for lattice-energy calculation to place the energetics of formation of complex halides of d and f transition elements (from binary halides)

$$2ACl(s) + AnCl_4(s) = A_2AnCl_6(s) \qquad (11)$$

on a common basis. Complex halides of R^{4+} and An^{4+} (e.g., Cs_2CeCl_6 and Cs_2BkCl_6) had been synthesized earlier than 1979, whereas the binary halides (e.g., $CeCl_4$ and

$BkCl_4$) have not. Enthalpies of formation of some complex halides of An^{4+} were known but no enthalpies of formation of complex halides of R^{4+} were known. This situation is unchanged today. The enthalpies of reactions such as reaction (11) become more exothermic as the alkali metal A changes from Li → Cs and as the actinide changes from Th → Pu (Fuger 1979, Morss 1986, fig. 17.12). These trends can be interpreted using the Lewis acid–base concept (a Lewis base donates an electron pair to a Lewis acid). The alkali chloride basicity scale is LiCl (least basic) < NaCL < KCl < RbCl < CsCl (most basic) since Cs^+ has the largest ionic radius of alkali metal ions Li^+–Cs^+. The actinide tetrachloride acidity scale is $ThCl_4$ (least acidic) < $ThCl_4$ < $PaCl_4$ < UCl_4 < $NpCl_4$ < $PuCl_4$ < $BkCl_4$ (most acidic) since Bk^{4+} has the smallest An^{4+} ionic radius of the group Th^{4+}–Bk^{4+}. Unfortunately, there are no $LnCl_4$ compounds known, not even $CeCl_4$; although acid–base stabilization makes Cs_2CeCl_6 a marginally stable but easily synthesized compound, not even its enthalpy of formation has yet been reported. Therefore, it is not possible to make any systematic comparison of lanthanide(IV) versus actinide(IV) bonding in complex halides.

Among complex halides of R^{3+} and An^{3+}, the elpasolites Cs_2NaMCl_6 represent the one class of compounds for which thermochemical measurements have been made on both lanthanide and actinide examples (Morss 1971, Schoebrechts et al. 1989). Although $Cs_2NaNdCl_6$ and $Cs_2NaPuCl_6$ have essentially identical lattice parameters, as do $NdCl_3$ and $PuCl_3$, the enthalpy of complexation of the lanthanide chloride system

$$2CsCl(s) + NaCl(s) + NdCl_3(s) = Cs_2NaNdCl_6(s), \quad \Delta H = -46.4\,kJ\,mol^{-1}, \quad (12)$$

is significantly more exothermic than the enthalpy of complexation of the corresponding actinide chloride system

$$2CsCl(s) + NaCl(s) + PuCl_3(s) = Cs_2NaPuCl_6(s), \quad \Delta H = -38.5\,kJ\,mol^{-1}. \quad (13)$$

The chloride coordination number is nine in $NdCl_3$ and $PuCl_3$ but only six in $Cs_2NaNdCl_6$ and $Cs_2NaPuCl_6$. The enthalpy of the reversed reaction (13) is more exothermic (less endothermic) than that of reversed reaction (12); in this sense one may conclude that high coordination numbers (CN 9) as found in the UCl_3-type (trigonal) trichlorides are more favored by an actinide(III) ion than a lanthanide(III) ion of the same ionic radius.

It has already been noted (section 4.1.1) that the enthalpies of solution of actinide trihalides and elpasolites $Cs_2NaAnCl_6$ are systematically less exothermic than enthalpies of solution of structurally similar lanthanide compounds. This lanthanide–actinide bonding difference may be due to lattice energies that are larger for actinide compounds than for structurally similar lanthanide compounds (fig. 8).

4.2. *Bonding in "covalent" systems: organometallics*

4.2.1. *Sigma bonding*

Systematic studies have been carried out to determine the σ-bond disruption energies of lanthanide(III)-ligand σ bonds in systems such as $Cp'_2Sm–R$ and $Cp'_2Sm–X$ (Cp′ denotes $\eta^5-(CH_3)_5C_5$; R denotes alkyl, H; X denotes Cl, Br, I) (Nolan et al. 1989). Although σ-bonded trivalent actinide analogues are known, e.g., Cp_2BkCl_3 (Cp

denotes $\eta^5-C_5H_5$) (Marks and Streitwieser 1986), their radioactivity and small sample size have thus far precluded thermochemical measurements.

Beginning with the work of Bruno et al. (1983, 1986) and Sonnenberger et al. (1985), and most recently with the studies of Leal et al. (1992) and of Jemine et al. (1992), Th(IV)- and U(IV)-ligand σ-bond disruption enthalpies in systems such as Cp'_2Th-R_2 and Cp'_2Sm-X_2 have been determined. Since there are no parallel Ce(IV) bond disruption enthalpies, no quantitative comparison can be made with lanthanide(IV) compounds. These actinide(IV)-ligand σ bonds have strengths slightly less those of the lanthanide(III)-ligand σ bonds mentioned in the preceding paragraph: absolute bond disruption enthalpies are $D[(Me_3SiC_5H_4)_3U-I] = 261$ (Schock et al. 1988) and $D(Cp'_2Sm-I) = 290\,kJ\,mol^{-1}$ (Nolan et al. 1989).

4.2.2. *Pi bonding*

The cyclooctatetrene compounds $M(C_8H_8)$ have been synthesized when M is Ce, Th, Pa, U, Np, and Pu. There is significant covalency in the overlap of the (5f6d) uranium orbitals with the highest occupied molecular orbitals of $C_8H_8^{2-}$ in uranocene, apparently more so than in thorocene (Marks and Streitwieser 1986). The overall $Th-C_8H_8$ and $U-C_8H_8$ bond disruption energies have been determined from combustion calorimetry to be 494 ± 9 and $431 \pm 11\,kJ\,mol^{-1}$, respectively (Kuznetsov et al. 1986), making these bonds much stronger than either $U-C_5H_5$ bonds in $U(C_5H_5)_4$ ($247\,kJ\,mol^{-1}$) or $Fe-C_5H_5$ bonds in ferrocene ($297\,kJ\,mol^{-1}$) (Tel'noi et al. 1979).

4.3. *Bonding in metallic systems*

Eriksson et al. (1990) performed band-structure calculations that show how the ratios of the orbital and spin components of the magnetic moments μ_L/μ_S of 5f metallic compounds differ from the three-ion values. Since the free-ion values are appropriate for 4f metallic compounds, Lander (1992) defined this reduction of μ_L/μ_S as "metallic covalency". He determined this ratio in a series of actinide compounds AnSb and $AnFe_2$ by analysis of their magnetic form factor $f(Q)$, the angular dependence of the scattering of thermal neutrons. In confirmation of the calculations, μ_L/μ_S is significantly reduced in uranium intermetallics such as UFe_2 but less so in $PuFe_2$ in comparison with "ionic" compounds such as UO_2, $NpAs_2$, and Pu_2O_3.

High-pressure studies of f elements and intermetallic compounds have shown that interactions involving f electrons increase as the lanthanide or actinide atoms are forced closer together (Benedict 1987, Benedict et al. 1992). For example, at very high pressure americium metal "collapses" to a sequence of structures of the lighter actinide metals at lower pressure; this behavior implies that americium 5f electrons are becoming involved in bonding (itinerant) as the atoms are forced closer together. The cause of this phenomenon is that the lighter metal has more extended f orbitals, so that at higher pressure the heavier metal f orbitals resemble those of the lighter element. These high-pressure effects are more dramatic in the actinides than in the lanthanides, since the 5f orbitals play a much greater role in metallic bonding than do the 4f orbitals.

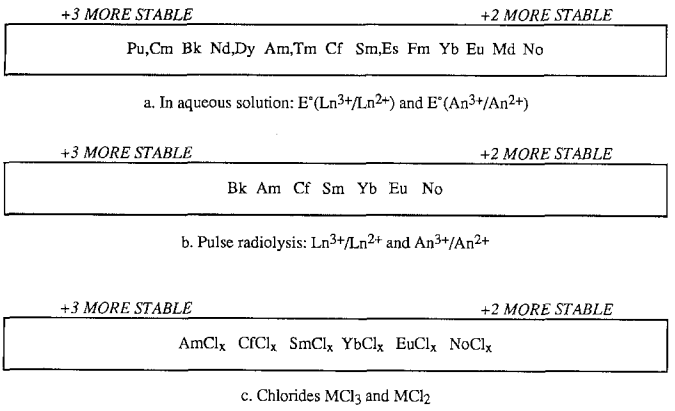

Fig. 9. Comparison of stabilities of 3 + /2 + lanthanide and actinide oxidation states (stable 3 + ions at left, stable 2 + ions at right).

4.4. *Oxidation–reduction comparisons in "ionic" systems*

4.4.1. *Binary oxides and halides*

It is fairly common for chemists to compare oxidation–reduction stability of solids, e.g., $MCl_3(s) = MCl_2(s) + \frac{1}{2}Cl_2(s)$, $MF_4(s) = MF_3(s) + \frac{1}{2}F_2(g)$ or $MO_2(s) = MO_{1.5}(s) + \frac{1}{4}O_2(g)$, using enthalpies of formation and entropy changes or using Knudsen-cell/mass spectrometer vaporization measurements. It is also possible to estimate oxidation–reduction relationships among solids using aqueous electrode potentials $E^0(M^{3+}/M^{3+})$ and $E^0(M^{4+}/M^{3+})$ (e.g., section 2.4.1) as a guide. Figure 9 compares the stability of M^{3+} and M^{2+} species in aqueous solution, aqueous pulse radiolysis, and solid chloride systems. There are no experimental thermochemical data for actinide (II) solids with which to make such a comparison more quantitative.

Table 7 is an attempt to make such a comparison quantitative for M^{4+}–M^{3+} reductions. For reactions involving no change of oxidation state, structural and magnetic entropy effects are the same for all reactions of the same stoichiometry involving adjacent f elements. However, these oxide and fluoride decomposition reactions do involve change of oxidation state, and magnetic entropy effects must be considered. These effects are greatest when comparing $Am^{4+} \rightarrow Am^{3+}$ and $Cm^{4+} \rightarrow Cm^{3+}$ reactions, where the magnetic $S = R\ln(2J+1)$ yields $\Delta S_{mag} = -14.9\,J\,K^{-1}\,mol^{-1}$ for Am and $+17.3\,J\,K^{-1}\,mol^{-1}$ for Cm. (We use free-ion J values). Gibson and Haire (1988a) used the well-studied PuF_4 and PuF_3 as references, for which $\Delta S_{mag} = +3.37\,J\,K^{-1}\,mol^{-1}$, so for $PuF_4(s) \rightarrow PuF_3(s) + \frac{1}{2}F_2(g)$ $\Delta S_{nonmag} = \Delta S_{observed} - \Delta S_{mag} = 147.25 + \frac{1}{2}(202.78) - 126.11 - 3.37 = 119.2\,J\,K^{-1}\,mol^{-1}$. The other ΔG entries in table 7 incorporate this ΔS_{nonmag} with ΔS_{mag} calculated for the specific reaction, assuming free-ion J values. The relative stabilities of MO_2 versus M_2O_3 and of MF_4 versus MF_3 are shown in fig. 10.

TABLE 7

Comparison of free energies of reduction of MO_2, MF_4, and $M^{4+}(aq)$ at 298 K (all values in kJ Mol^{-1} at 298 l estimated values in parentheses).

M	$MO_2(s) \rightarrow MO_{1.5}(s) + \frac{1}{4}O_2(g)$		$MF_4(s) \rightarrow MF_3(s) + \frac{1}{2}F_2(g)$		$M^{4+}(aq) + e^- \rightarrow M^{3+}(aq)$
	ΔH^{0a}	ΔG^{0b}	ΔH^{0c}	ΔG^{0b}	ΔG^0
Ce	191	172	243		−166
Pr	44		(42)		(−309)
Nd					(−473)
Tb	39		(79)		(−299)
Dy					(−550)
U	(357)	(341)	413	387	+50
Np	(313)	(298)	(345)	(324)	−14
Pu	228	208	260	237	−93
Am	86		(132)		−253
Cm	70		(90)		(−299)
Bk	(174)		(212)		−161
Cf	32 LRM		(70)		(−309)
	24 JF				
Es	(−85)		(54)		(−434)

[a] Morss (1985, 1986).

[b] Includes ΔS(magnetic), see text.

[c] Morss (1986), Gibson and Haire (1988c) and Grenthe et al. (1992).

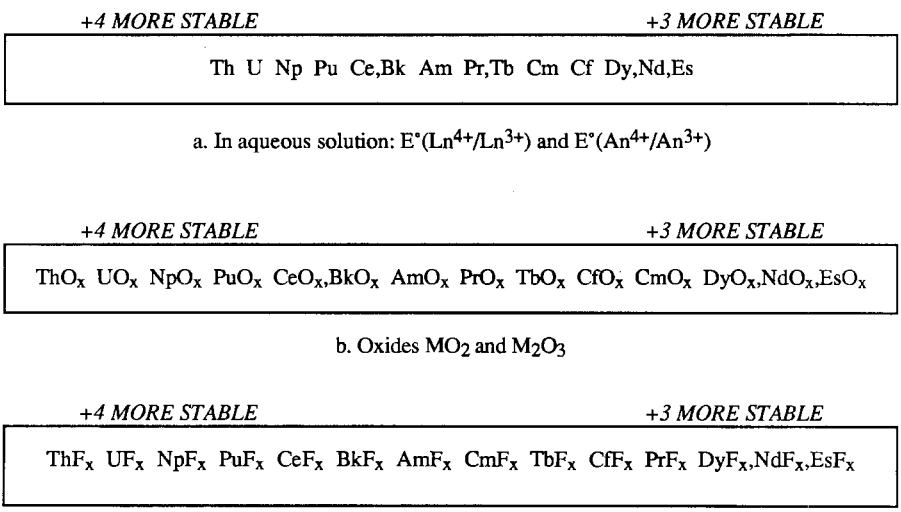

Fig. 10. Comparison of stabilities of 4 + /3 + lanthanide and actinide oxidation states (stable 4 + ions at left, stable 3 + ions at right).

4.4.2. *Complex oxides and halides*

Sections 4.1.2 and 4.1.3 compared complex oxides and halides with the binary (parent) compounds. In this section we attempt to show on a semiquantitative basis how complex oxides and halides favor high oxidation states, primarily because they represent acid–base reactions in which the presence of a basic oxides (e.g., BaO) or halide (e.g., CsCl) donates electron pairs (Lewis basicity) to the acidic (high charge density) f-element ion.

Complexation reactions of 4+ ions, reactions (10) and (11), are not oxidation–reduction reactions and have been interpreted above as acid–base reactions. Since those reactions are favorable, one may calculate the enthalpies of oxidation–reduction reactions such as

$$BaUO_3(s) + \tfrac{1}{2}O_2(g) \rightarrow BaUO_4(s) \qquad \Delta H = -307 \pm 10\,kJ\,mol^{-1}, \tag{14}$$

$$UO_2(s) + \tfrac{1}{2}O_2(g) \rightarrow UO_3(s) \qquad \Delta H = -139 \pm 3\,kJ\,mol^{-1}, \tag{15}$$

$$Cs_2NaPuCl_6(s) + \tfrac{1}{2}Cl_2(g) \rightarrow Cs_2PuCl_6(s) + NaCl(s)$$
$$\Delta H = -95 \pm 10\,kJ\,mol^{-1}, \tag{16}$$

$$PuCl_3(s) + \tfrac{1}{2}Cl_2(g) \rightarrow PuCl_4(s) \qquad \Delta H = -4 \pm 8\,kJ\,mol^{-1}. \tag{17}$$

ΔH of reaction (17) is an estimate since $PuCl_4(s)$ has not been synthesized; $\Delta_f H^0[PuCl_4(s)] = -964$ kJ is an estimate (Fuger et al. 1983). The dramatic difference in these enthalpies [Pu(IV) is more stable than Pu(III) in this complex chloride by $-95-(-4) = -91$ kJ or almost 1.0 V, in comparison with the binary chloride] shows how acid–base effects influence oxidation–reduction properties. As noted above, there are few known lanthanide(IV) complex halides and no thermodynamic data on even these few halides, so no quantitative comparison can be made. Nevertheless it does show how complexation effects by basic complexants make high f-element oxidation states attainable. Perhaps the most dramatic evidence of the enhancement of high oxidation state by a basic fluoride is the existence of the Nd(IV) and Dy(IV) compounds such as Cs_2(Cs, Rb, K) (Nd, Dy)Cl_7; these A_3RF_7 double fluorides are the only known Nd(IV) and Dy(IV) compounds.

4.5. *Lanthanide–actinide oxidation–reduction comparisons in aqueous (uncomplexed, "standard-state" as well as "formal") solutions*

Aqueous reduction potentials $E^0(M^{3+}/M^{2+})$ have been assessed from thermodynamic measurements and estimates as described in section 2.4.2. Among the actinides, dihalides of Am, Cf, and Es have been characterized but no thermochemical measurements have been made. The synthesis conditions are consistent with the $E^0(An^{3+}/An^{2+})$ values (Martinot and Fuger 1985). Within these limitations we compare the $E^0(Ln^{3+}/Ln^{2+})$ and $E^0(An^{3+}/An^{2+})$ in fig. 9. Similarly, some $E^0(M^{4+}/M^{3+})$ have been measured electrochemically and others estimated using thermochemical or spectroscopic measurements. We compare $E^{0\prime}(Ln^{4+}/Ln^{3+})$ with $E^{0\prime}(An^{4+}/An^{3+})$ in fig. 10. Note that $E^{0\prime}$ refers to a formal potential (as measured in 1 mol dm^{-3} acid solution, $HClO_4$ if available) rather than a standard potential (as

extrapolated from measurements in dilute electrolyte using a model such as the specific-ion theory (Riglet et al. 1989).

Johnson (1977) generalized the oxidation–reduction stability of the 2+ lanthanides with respect to the 3+ lanthanides as follows, comparing *adjacent* lanthanides to each other,

$$La < Ce < Pr < Nd < Sm < Eu \gg Gd < Tb < Dy > Ho > Er < Tb < Yb,$$

and the oxidation–reduction stability of the 4+ lanthanides with respect to the 3+ lanthanides as follows, again comparing adjacent lanthanides to each other,

$$Ce > Pr > Nd > Sm \text{ and } Gd \ll Tb > Dy > Ho.$$

In a similar fashion we generalize the oxidation–reduction stability of the 2+ actinides with respect to the 3+ actinides as follows, again comparing adjacent actinides to each other,

$$Am > Cm < Bk < Cf < Es < Fm < Md < No,$$

and the oxidation–reduction stability of the 4+ actinides with respect to the 3+ actinides as follows,

$$Th > Pa > U < Np < Pu > Am > Cm \ll Bk > Cf \gg Es.$$

Relative oxidation–reduction stability relationships, in which both the lanthanides and actinides are compared (stable high oxidation state on the left, stable low oxidation state on the right) in various media, are shown in figs. 9 and 10.

Although several energetic factors contribute to these oxidation–reduction stability relationships, the relationships primarily reflect dramatic changes in the third and fourth ionization energies (table 2) and the f→d energy level differences originally formulated by Jørgensen (1962) and elaborated more recently by Brewer (1971, 1983a, b), Nugent et al. (1971, 1973a) and Johnson (1977).

To illustrate how the third and fourth ionization energies dominate the energetics of f-element oxidation–reduction processes, three cycles will be considered. Only the first cycle, scheme I, includes f→d transitions inherent in the sublimation of metals. Scheme I represents the process of oxidation of the metal to the "normal" 3+ oxidation state,

$$M(s) + 3H^+(aq) \rightarrow M^3(aq) + \tfrac{3}{2}H_2(g). \tag{18}$$

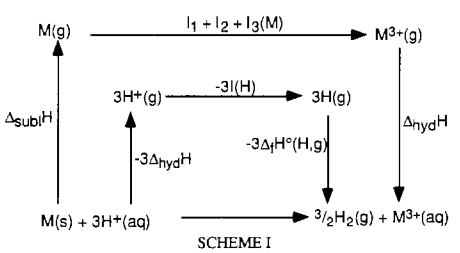

SCHEME I

The prominent terms $\Delta_{subl}H(M) + I_3(M) + \Delta_{hyd}H(M^{3+})$, the sums of which are shown in fig. 11, are responsible for variations in the energetics of reaction (18). It is evident

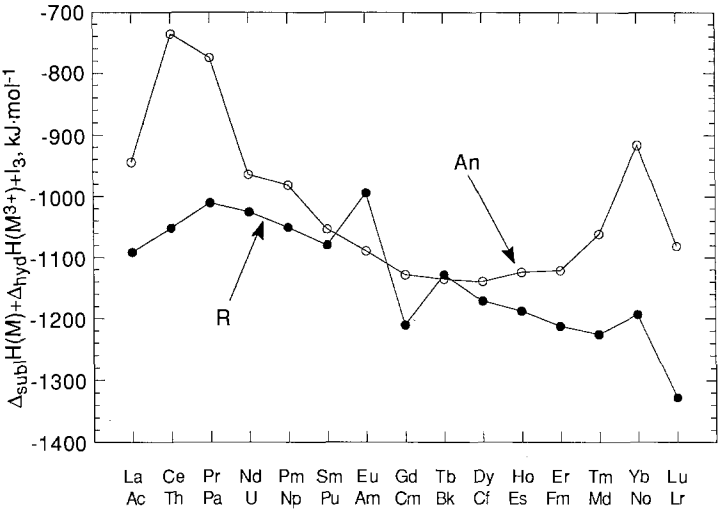

Fig. 11. Stability cycle for lanthanide–actinide $M \rightarrow M^{3+}(aq)$ energetics.

that these three terms are responsible for the trends in the stability of $M^{3+}(aq)$ with respect to the metal. $Eu^{3+}(aq)$ and $Yb^{3+}(aq)$ are notably destabilized because of their high I_3 values (partly compensated by small Δ_{subl}. The actinide points (open circles) that lie well above the lanthanide points (filled circles), e.g., Th^{3+}, Pa^{3+} and No^{3+}, represent very unstable 3+ ions with respect to oxidation (Th^{3+}, Pa^{3+}) or reduction (No^{3+}).

Scheme II represents the process of reduction of $M^{3+}(aq)$ to $M^{2+}(aq)$,

$$M^{3+}(aq) + H^{+}(aq) \rightarrow M^{2+}(aq) + \tfrac{1}{2}H_2(g). \tag{19}$$

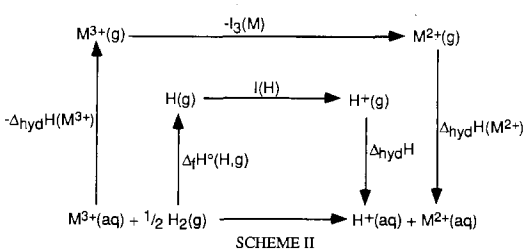

SCHEME II

(This cycle neglects f→d transitions.) This reduction is favored for No^{3+}, to a lesser extent for Eu^{3+}, and even less for other M^{3+} ions as shown in fig. 9.

The prominent terms are $\Delta_{hyd}H(M^{3+}) - \Delta_{hyd}H(M^{4+}) - I_4$, as summed in fig. 12. The crossover near Gd and Cm shows that the $E^0(M^{3+}/M^{2+})$ is unfavorable for light actinides but favorable for heavy actinides. I_3 is the term primarily responsible for the lanthanide–actinide difference.

Scheme III represents the process of reduction of $M^{4+}(aq)$ to $M^{3+}(aq)$,

$$M^{4+}(aq) + H^{+}(aq) \rightarrow M^{3+}(aq) + \tfrac{1}{2}H_2(g). \tag{20}$$

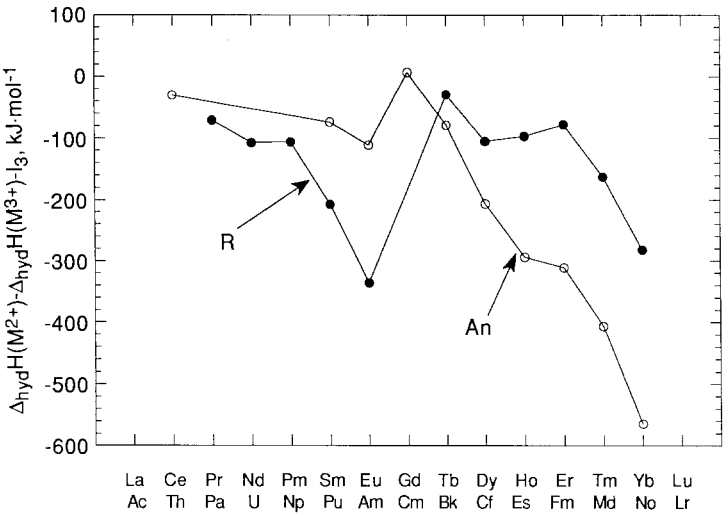

Fig. 12. Stability cycle for lanthanide–actinide $M^{3+}(aq) \rightarrow M^{2+}(aq)$ energetics.

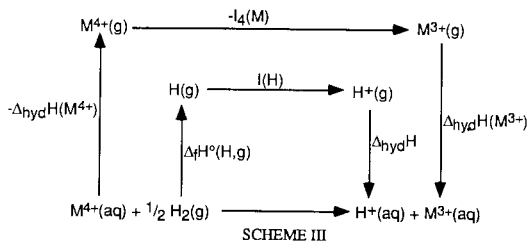

SCHEME III

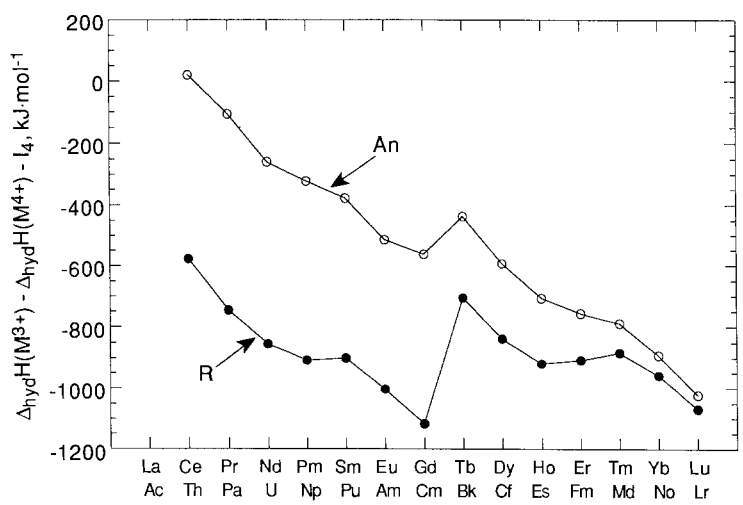

Fig. 13. Stability cycle for lanthanide–actinide $M^{4+}(aq) \rightarrow M^{3+}(aq)$ energetics.

This reduction is very favorable for most of the lanthanides but not so favorable for some actinides as shown in fig. 10.

The prominent terms are $\Delta_{hyd}H(M^{3+}) - \Delta_{hyd}H(M^{4+}) - I_4$, as summed in fig. 13. I_4 is the term primarily responsible for the lanthanide–actinide difference. The much smaller step between Cm and Bk (as compared to the large step from Gd to Tb) shows that the $E^0(M^{4+}/M^{3+})$ behavior is very different for the light lanthanides and actinides, but rather similar for the heavier halves of each series. We conclude that ionization energies I_3 and I_4 dominate the $3+/2+$ and $4+/3+$ oxidation–reduction reactions of the f-element ions in solutions and in compounds.

Acknowledgments

This work was supported in part by the US Department of Energy, Office of Basic Energy Sciences, Division of Chemical Sciences, under Contract W-31-109-ENG-38, and in part by the Alexander von Humboldt Foundation during tenure of the author as a US Senior Scientist awardee at the University of Hannover, Germany. The author thanks J.V. Beitz, G.R. Choppin, F. David, J.A. Rard and J.C. Sullivan for insightful improvements to the manuscript.

References

Ackerman, J.P., 1991, Ind. Eng. Chem. Res. **30**, 141.

Ackerman, J.P., and J.L. Settle, 1992, J. Alloys & Compounds **177**, 129.

Ackerman, J.P., and J.L. Settle, 1993, J. Alloys & Compounds **199**, 77.

Anonymous, 1967, The Plutonium–Oxygen and the Uranium–Plutonium–Oxygen Systems. A Thermochemical Assessment, IAEA Technical Reports Series, Vol. 67, STI/DOC/10/679 (IAEA, Vienna).

Aronson, S., 1982, J. Nucl. Mater. **107**, 343.

Baes Jr, C.F., and R.E. Mesmer, 1976, The Hydrolysis of Cations (Wiley, New York).

Ball, R.G.J., 1992, J. Mater. Chem. **2**, 641.

Ball, R.G.J., and P.G. Dickens, 1991, J. Mater. Chem. **1**, 105.

Baluka, M., N. Edelstein and T.A. O'Donnell, 1981, Inorg. Chem. **20**, 3279.

Barraclough, C.G., R.W. Cockman and T.A. O'Donnell, 1991, Inorg. Chem. **30**, 340.

Beitz, J.V., 1991, personal communication.

Benedict, U., 1987, The effect of high pressure on actinide metals, in: Handbook on the Physics and Chemistry of the Actinides, Vol. 5, eds A.J. Freeman and G.H. Lander (North-Holland, Amsterdam) ch. 3, pp. 227–269.

Benedict, U., S. Dabos-Seignon, J.P. Dancausse, M. Gensini, E. Gering, S. Heathman, H. Luo, J. Staun Olsen, L. Gerward and R.G. Haire, 1992, J. Alloys & Compounds **181**, 1.

Bettonville, S., J. Goudiakas and J. Fuger, 1987, J. Chem. Thermodyn. **19**, 595.

Bevan, D.J.M., and J. Kordis, 1964, J. Inorg. & Nucl. Chem. **26**, 1509.

Bommer, H., and E. Hohmann, 1941, Z. Anorg. Allg. Chem. **248**, 357, 373.

Bratsch, S.G., 1989, J. Phys. Chem. Ref. Data **18**, 1.

Bratsch, S.G., and J.J. Lagowski, 1985a, J. Phys. Chem. **89**, 3310.

Bratsch, S.G., and J.J. Lagowski, 1985b, J. Phys. Chem. **89**, 3317.

Bratsch, S.G., and J.J. Lagowski, 1986, J. Phys. Chem. **90**, 307.

Brauer, G., and H. Kristen, 1980, Z. Anorg. Allg. Chem. **456**, 41; **462**, 35.

Brewer, L., 1971, J. Opt. Soc. Am. **61**, 1101, 1666.

Brewer, L., 1983a, Systematics of the properties of the lanthanides, in: Systematics and the Properties of the Lanthanides, ed. S.P. Sinha (Reidel, Dordrecht) ch. 2, pp. 17–69.

Brewer, L., 1983b, High Temp. Sci. **17**, 1.

Brewer, L., 1987, J. Less-Common Met. **133**, 15.
Bronstein, H.R., 1969, J. Phys. Chem. **73**, 1320.
Brooks, M.S.S., B. Johansson and H.L. Skriver, 1984, Electronic structure and bulk ground state properties of the actinides, in: Handbook on the Physics and Chemistry of the Actinides, Vol. 1, eds A.J. Freeman and G.H. Lander (North-Holland, Amsterdam) pp. 153–259, and references therein.
Brüchle, W., M. Schädel, U.W. Scherer, J.V. Kratz, K.E. Gregorich, D. Lee, M. Nurmia, R.M. Chasteler, H.L. Hall, R.A. Henderson and D.C. Hoffman, 1988, Inorg. Chim. Acta **146**, 267.
Bruno, J., I. Grenthe and B. Lagerman, 1990, Acta Chem. Scand. **44**, 896.
Bruno, J.W., T.J. Marks and L.R. Morss, 1983, J. Am. Chem. Soc. **105**, 6824.
Bruno, J.W., H.A. Stecher, L.R. Morss, D.C. Sonnenberger and T.J. Marks, 1986, J. Am. Chem. Soc. **108**, 7275.
Burgess, J., and J. Kijowski, 1981, Adv. Inorg. Chem. Radiochem. **24**, 57.
Carnall, W.T., and H.M. Crosswhite, 1984, Report 84-90 (Argonne National Laboratory, Argonne, IL).
Catlow, C.R.A., and W.C. Mackrodt, 1982, in: Computer Simulation of Solids, eds C.R.A. Catlow and W.C. Mackrodt (Springer, Berlin) ch. 1.
Chikalla, T.D., and L. Eyring, 1967, J. Inorg. & Nucl. Chem. **29**, 2281.
Chikalla, T.D., and L. Eyring, 1969, J. Inorg. & Nucl. Chem. **31**, 85.
Chirico, R.D., and E.F. Westrum Jr, 1980, J. Chem. Thermodyn. **12**, 71, 311.
Conway, B.E., 1978, J. Solution Chem. **7**, 721.
Cordfunke, E.H.P., R.J.M. Konings and W. Ouweltjes, 1990, J. Chem. Thermodyn. **22**, 449.
David, F., 1970, Radiochem. & Radioanal. Lett. **5**, 279.
David, F., 1985, J. Nucl. Mater. **130**, 273.
David, F., 1986a, Oxidation–reduction and thermodynamic properties of curium and heavier actinide elements, in: Handbook on the Physics and Chemistry of the Actinides, Vol. 4, eds A.J. Freeman and C. Keller (North-Holland, Amsterdam) ch. 3.
David, F., 1986b, J. Less-Common Met. **121**, 27.
David, F., 1986c, J. Chim. Phys. **83**, 393.
David, F., 1991, in: Proc. Int. Symp. on Radiochemistry and Radiation Chemistry, February 4–7, 1991, Bhabha Atomic Research Center, Board of Nuclear Sciences, Government of India.
David, F., K. Samhoun, R. Guillaumont and N. Edelstein, 1978, J. Inorg. & Nucl. Chem. **40**, 69.
David, F., B. Fourest and J. Duplessis, 1985, J. Nucl. Mater. **130**, 273.
David, F., K. Samhoun, R.W. Lougheed, R.J. Dougan, J.F. Wild, J.H. Landrum, A.D. Dougan and E.K. Hulet, 1990, Radiochim. Acta **51**, 65.
DeWaele, R., L. Heerman and W. D'Olieslager, 1986, J. Less-Common Met. **122**, 319.
Eriksson, O., M.S.S. Brooks and B. Johansson, 1990, Phys. Rev. B **41**, 9087.
Fourest, B., F. David and E. Haltier, 1988, Lanthanide & Actinide Res. **2**, 393.
Frenkel, V.Ya., Yu.M. Kulyako, V.M. Chistyakov, I.A. Lebedev, B.F. Myasoedov, G.A. Timofeev and E.A. Erin, 1986, J. Radioanal. Nucl. Chem. Lett. **104**, 191.
Friedman, H.A., and J.R. Stokely, 1976, Inorg. & Nucl. Chem. Lett. **12**, 505.
Fuger, J., 1979, J. Phys. Colloq. (Paris) **40**, C4-207.
Fuger, J., 1985, J. Nucl. Mater. **130**, 253.
Fuger, J., 1992, J. Chem. Thermodyn. **24**, 337.
Fuger, J., and F.L. Oetting, 1976, The actinide aqueous ions, in: The Chemical Thermodynamics of Actinide Elements and Compounds, ed. F.L. Oetting (IAEA, Vienna) Part 2.
Fuger, J., R.G. Haire and J.R. Peterson, 1981, J. Inorg. & Nucl. Chem. **43**, 3209.
Fuger, J., V.B. Parker, W.N. Hubbard and F.L. Oetting, 1983, The actinide halides, in: The Chemical Thermodynamics of Actinide Elements and Compounds, ed. F.L. Oetting (IAEA, Vienna) Part 8.
Fuger, J., R.G. Haire and J.R. Peterson, 1984, J. Less-Common Met. **98**, 315.
Fuger, J., R.G. Haire, W.R. Wilmarth and J.R. Peterson, 1990, J. Less-Common Met. **158**, 99.
Fuger, J., R.G. Haire and J.R. Peterson, 1993, J. Alloys & Compounds **200**, 181.
Fujino, T., 1988, J. Nucl. Mater. **154**, 14.
Fujino, T., and C. Miyake, 1991, Phase relations, thermodynamics, and magnetic properties of fluorite-type solid solutions $M_yU_{1-y}O_{2\pm x}$ ($M = M^{4+}$, M^{3+}, M^{2+}) as a modification of UO_2, in: Handbook on the Physics and Chemistry of the Actinides, Vol. 6, eds A.J. Freeman and C. Keller (North-Holland, Amsterdam) ch. 4, pp. 155–240.

Gibson, J.K., and R.G. Haire, 1988a, Thermochim. Acta **1988**, 241.
Gibson, J.K., and R.G. Haire, 1988b, J. Less-Common Met. **144**, 123.
Gibson, J.K., and R.G. Haire, 1988c, J. Solid State Chem. **73**, 524.
Gibson, J.K., and R.G. Haire, 1992, J. Less-Common Met. **181**, 23.
Gilbert, B., V. Demarteau and G. Duyckaerts, 1978, J. Electroanal. Chem. **89**, 123.
Gmelin's Handbuch, 1976, Seltenerdelemente C3 (Springer, Berlin) pp. 75–96.
Gmelin's Handbuch, 1978, Seltenerdelemente C6 (Springer, Berlin) pp. 25–28, 164–169.
Goldman, S., and L.R. Morss, 1975, Can. J. Chem. **53**, 2695.
Gordon, S., J.C. Sullivan, W.A. Mulac, D. Cohen and K.H. Schmidt, 1977, in: Proc. 4th Tihany Symp. on Radiation Chemistry (Akademiai Kiado, Budapest) pp. 753–760.
Gordon, S., W.A. Mulac, K.H. Schmidt, R.K. Sjoblom and J.C. Sullivan, 1978, Inorg. Chem. **17**, 294.
Goryushkin, V.F., V.P. Podsevalov, S.A. Zalymova and A.I. Poshevneva, 1989, Zh. Fiz. Khim. **63**, 241 [Russ. J. Phys. Chem. **63**, 130].
Goudiakas, J., R.G. Haire and J. Fuger, 1990, J. Chem. Thermodyn. **22**, 577.
Grenthe, I., J. Fuger, R.J.M. Konings, R.J. Lemire, A.B. Müller, C. Nguyen-Trung and H. Wanner, 1992, Chemical Thermodynamics of Uranium (North-Holland, Amsterdam).
Grimes, R.W., 1992, Mater. Res. Soc. Symp. Proc. **257**, 361.
Gruen, D.M., 1976, in: Molten Salts, Electrochem. Soc., p. 204.
Gschneidner Jr, K.A., 1993, J. Alloys & Compounds **193**, 1.
Gschneidner Jr, K.A., N. Kippenhan and O.D. McMasters, 1973, Report IS-RIC-6 (Rare-Earth Information Center, Ames, IA).
Haire, R.G., 1980, personal communication.
Haire, R.G., and J.K. Gibson, 1989, J. Chem. Phys. **91**, 7085.
Hall, R.O.A., M.J. Mortimer and J.-C. Spirlet, 1991, Report AERE-R-13768 (Harwell Laboratory).
Halliwell, H.F., and S.C. Nyburg, 1963, Trans. Faraday Soc. **59**, 1126.
Hepler, L.G., and P.P. Singh, 1976, Thermochim. Acta **16**, 95.
Herman, H.B., and J.R. Rairden, 1976, in: Encyclopedia of Electrochemistry of the Elements, ed. A. Bard (Marcel Dekker, New York) ch. VI-2, pp. 33–62.
Hobart, D.E., K. Samhoun, J.P. Young, V.E. Norvell, G. Mamantov and J.R. Peterson, 1980, Inorg. & Nucl. Chem. Lett. **16**, 321.
Hobart, D.E., K. Samhoun and J.R. Peterson, 1982, Radiochim. Acta **31**, 139.
Hobart, D.E., P.G. Varlashkin, K. Samhoun, R.G. Haire and J.R. Peterson, 1983, Rev. Chim. Min. **20**, 817.
Hoffman, D.C., R.A. Henderson, K.E. Gregorich, D.A. Bennett, R.M. Chasteler, C.M. Gannett, H.L. Hall, D.M. Lee, M.J. Nurmia, S. Cai, R. Agarwal, A.W. Charlop, Y.Y. Chu, G.T. Seaborg and R.J. Silva, 1988, J. Radioanal. Nucl. Chem. **124**, 135.
Hoppe, R., 1966, Angew. Chem. **78**, 52; Int. Ed. **5**, 95.
Hoppe, R., 1970a, Angew. Chem. **82**, 7; Int. Ed. **9**, 25.
Hoppe, R., 1970b, Madelung constants as a new guide to the structural chemistry of solids, in: Advances in Fluorine Chemistry, Vol. 6, eds M. Stacey, J.C. Tatlow and A.G. Sharpe (Butterworths, London) p. 387.
Hoppe, R., 1975, The Madelung part of the lattice energy, MAPLE, as a guide in crystal chemistry, in: Crystal Structure and Chemical Bonding in Inorganic Chemistry, eds C.J.M. Rooymans and A. Rabenau (North-Holland, Amsterdam) pp. 127–161.
Hoppe, R., 1982, in: The Rare Earths in Modern Science and Technology, Vol. 3, eds G.J. McCarthy, H.B. Silber and J.J. Rhyne (Plenum Press, New York) p. 315.
Hulet, E.K., R.W. Lougheed, J.D. Brady, R.E. Stone and M.S. Coops, 1967, Science **158**, 486.
Hurtgen, C., J. Fuger and D. Brown, 1980, J. Chem. Soc. Dalton, p. 70.
Hyde, B.G., and L. Eyring, 1965, in: Rare Earth Research III, ed. L. Eyring (Gordon and Breach, New York) pp. 623–664.
Hyde, B.G., D.J.M. Bevan and L. Eyring, 1966, Philos. Trans. R. Soc. London A **259**, 583.
Inaba, H., A. Navrotsky and L. Eyring, 1981, J. Solid State Chem. **37**, 77.
Ionova, G.V., and V.I. Spitsyn, 1978, Radiokhimiya **20**, 196.
Jemine, X., J. Goffart, J.-C. Berthet and M. Ephritikhine, 1992, J. Chem. Soc. Dalton, p. 2439.
Jenkins, H.D.B., and K.F. Pratt, 1979, Prog. Solid State Chem. **12**, 125.
Jia, Y.-Q., 1987, Inorg. Chim. Acta **133**, 331.
Johansson, B., 1978, J. Phys. Chem. Solids **39**, 467.

Johansson, B., and P. Munck, 1984, J. Less-Common Met. **100**, 49.
Johnson, D.A., 1969a, J. Chem. Soc. A, p. 1525.
Johnson, D.A., 1969b, J. Chem. Soc. A, p. 1528.
Johnson, D.A., 1974, J. Chem. Soc. Dalton, p. 1671.
Johnson, D.A., 1977, Adv. Inorg. Chem. & Radiochem. **20**, 1.
Johnson, D.A., 1980, J. Chem. Educ. **57**, 475.
Johnson, D.A., 1982, Some Thermodynamic Aspects of Inorganic Chemistry, 2nd Ed. (Cambridge University Press, Cambridge).
Johnson, D.A., and J.D. Corbett, 1970, in: Les Elements des Terres Rares, Colloq. Int. du CNRS, No. 180 (CNRS, Paris). pp. 429–438.
Johnson, K.W.R., and J.A. Leary, 1964, J. Inorg. & Nucl. Chem. **26**, 103.
Jørgensen, C.K., 1962, Mol. Phys. **5**, 271.
Keller Jr, O.L., 1984, Radiochim. Acta **37**, 169.
Khanaev, E.I., T.P. Storozhenko and L.D. Il'ina, 1987, Zh. Fiz. Khim. **61**, 1776 [Russ. J. Phys. Chem. **61**, 926].
Kim, Y.-C., and J. Oishi, 1979, J. Less-Common Met. **65**, 199.
Kleinschmidt, P.D., 1986, J. Less-Common Met. **121**, 61.
Kleinschmidt, P.D., J.W. Ward, G.M. Matlack and R.G. Haire, 1984, J. Chem. Phys. **81**, 473.
Kordis, J., and L. Eyring, 1968, J. Phys. Chem. **72**, 2044.
Kosyakov, V.N., E.A. Erin, V.M. Vityutnev, V.V. Kopytov and A.G. Rykov, 1982, Radiokhimiya **24**, 551.
Koyama, T., T.R. Johnson and D.F. Fischer, 1992, J. Alloys & Compounds **189**, 37.
Kragten, J., and L.G. Decnop-Weever, 1987, Talanta **34**, 861.
Kubaschewski, O., 1972, High Temp.–High Pressures **4**, 1.
Kulyukhin, S.A., A.N. Kamenskaya and N.B. Mikheev, 1992, Radiokhimiya **34**, 147 [Sov. Radiochem. **34**, 117].
Kuznetsov, N.T., K.V. Kir'yanov, V.A. Mitin, V.G. Savast'yanoc and V.A. Bogdanvov, 1986, Radiokhimiya **28**, 709.
Lander, G.H., 1992, in: Actinide Chemistry: A Half Century, eds L.R. Morss and J. Fuger (American Chemical Society, Washington, DC) ch. 34, pp. 338–344.
Lavut, E.G., and N.V. Chelovskaya, 1990, J. Chem. Thermodyn. **22**, 817.
Leal, J.P., N. Marques, A. Pires de Matos, M.J. Calhorda, A.M. Galvao and J.A. Martinho Simoes, 1992, Organometallics **11**, 1632.
Lemire, R.J., and P.R. Tremaine, 1980, J. Chem. Eng. Data **25**, 361.
Lindemer, T.B., and T.M. Besmann, 1985, J. Nucl. Mater. **130**, 473.
Maly, J., 1967, Inorg. Chem. Nucl. Lett. **3**, 373.
Maly, J., and B.B. Cunningham, 1967, Inorg. & Nucl. Chem. Lett. **2**, 445.
Marks, T.J., and A. Streitwieser Jr, 1986, Organoactinide chemistry, in: The Chemistry of the Actinide Elements, 2nd Ed., eds J.J. Katz, G.T. Seaborg and L.R. Morss (Chapman & Hall, London) chs 22, 23, pp. 1547–1628.
Martin, A., and R.K. Edwards, 1965, J. Phys. Chem. **69**, 1788.
Martin, W.C., L. Hagan, J. Reader and J. Sugar, 1974, J. Phys. Chem. Ref. Data **3**, 771.
Martin, W.C., R. Zalubas and L. Hagan, 1978, Atomic Energy Levels: The Rare Earth Elements, NSRDS-NBS60 (National Bureau of Standards, Washington, DC).
Martinot, L., 1978, Actinides, in: Encyclopedia of Electrochemistry of the Elements, Vol. 8, ch. 2, ed. A. Bard (Marcel Dekker, New York).
Martinot, L., 1991, Molten salt chemistry of actinides, in: Handbook on the Physics and Chemistry of the Actinides, Vol. 6, eds A.J. Freeman and C. Keller (North-Holland, Amsterdam) ch. 4, pp. 241–279.
Martinot, L., and J. Fuger, 1985, in: Standard Potentials in Aqueous Solutions, eds A.J. Bard, R. Parsons and J. Jordan (Marcel Dekker, New York) ch. 21.
Martinot, L., D. Laeckmann, T. Materne and V. Müller, 1990, J. Less-Common Met. **163**, 185.
Mikheev, N.B., 1988, Radiokhimiya **30**, 297.
Mikheev, N.B., 1989, Naturwissenschaften **76**, 107.
Mikheev, N.B., 1992, in: Actinide Chemistry: A Half Century, eds L.R. Morss and J. Fuger (American Chemical Society, Washington, DC) ch. 45, pp. 469–480.
Mikheev, N.B., and E.R. Merts, 1990, Radiokhimiya **32**, 1 [Sov. Radiochem. **32**, 79].
Mikheev, N.B., and I.A. Rumer, 1988, Inorg. Chim. Acta **145**, 139.
Mikheev, N.B., I.A. Rumer and L.N. Auérman, 1985, Radiokhimiya **27**, 539 [Sov. Radiochem. **27**, 497].
Mikheev, N.B., V.I. Spitsyn, G.V. Ionova, L.N. Auerman and B.G. Korshunov, 1986, Radiokhimiya **28**, 82.
Mikheev, N.B., M.Z. Kazakevich and I.A. Rumer, 1991, Radiokhimiya **33**, 9 [Sov. Radiochem. **33**, 209].

Miyakawa, K., Y. Kaizu and H. Kobayashi, 1988, J. Chem. Soc. Faraday **84**, 1517.
Mondal, J.U., D.L. Raschella, R.G. Haire and J.R. Peterson, 1987, Thermochim. Acta **116**, 235.
Morris, D.E., D.E. Hobart, P.D. Palmer, R.G. Haire and J.R. Peterson, 1990, Radiochim. Acta **49**, 125.
Morss, L.R., 1971, J. Phys. Chem. **75**, 392.
Morss, L.R., 1976, Chem. Rev. **76**, 827.
Morss, L.R., 1982, in: Actinides in Perspective, ed. N. Edelstein (Pergamon Press, Oxford) pp. 381–407.
Morss, L.R., 1983, J. Less-Common Met. **93**, 301.
Morss, L.R., 1985, in: Standard Potentials in Aqueous Solutions, eds A.J. Bard, R. Parsons and J. Jordan (Marcel Dekker, New York) ch. 20.
Morss, L.R., 1986, in: The Chemistry of the Actinide Elements, 2nd Ed., eds J.J. Katz, G.T. Seaborg and L.R. Morss (Chapman & Hall, London) ch. 17, pp. 1278–1360.
Morss, L.R., 1992a, Mater. Res. Soc. Symp. Proc. **257**, 283.
Morss, L.R., 1992b, unpublished thermochemical measurements on PrO_2 and $BaPrO_3$.
Morss, L.R., and P.G. Eller, 1989, Radiochim. Acta **47**, 51.
Morss, L.R., and J.A. Fahey, 1976, in: Proc. 12th Rare Earth Research Conf., Vail, CO (Denver Research Institute, Denver, CO) pp. 443–450.
Morss, L.R., and J. Fuger, 1981, J. Inorg. & Nucl. Chem. **43**, 2059.
Morss, L.R., and H.O. Haug, 1973, J. Chem. Thermodyn. **5**, 513.
Morss, L.R., and M.C. McCue, 1976, J. Chem. Eng. Data **21**, 337.
Morss, L.R., and T.G. Spence, 1992, Z. Anorg. Allg. Chem. **616**, 162.
Morss, L.R., and C.W. Williams, 1992, Mater. Res. Soc. Symp. Proc. **257**, 283.
Morss, L.R., and C.W. Williams, 1993, J. Alloys & Compounds, to be published.
Morss, L.R., and C.W. Williams, 1994, Radiochim. Acta, in press.
Morss, L.R., J. Fuger, J. Goffart and R.G. Haire, 1981, Actinides 1981 Conference Abstract Book, Report LBL-12441 (Lawrence Berkeley Laboratory, Berkeley, CA) p. 263.
Morss, L.R., J. Fuger, J. Goffart, N. Edelstein and G.V. Shalimoff, 1987, J. Less-Common Met. **127**, 251.
Morss, L.R., C.M. Haar and S. Mroczkowski, 1989, J. Chem. Thermodyn. **21**, 1079.
Morss, L.R., P.P. Day, C. Felinto and H. Brito, 1993, J. Chem. Thermodyn. **25**, 415.
Musikas, C., and B.F. Myasoedov, 1969, Radiochem. Radioanal. Lett. **2**, 21.
Myasoedov, B.F., 1982, in: Actinides in Perspective, ed. N. Edelstein (Pergamon Press, Oxford) pp. 509–540.
Myasoedov, B.F., and C. Musikas, 1970, Radiokhimiya **12**, 856 [Sov. Radiochem. **12**, 826].
Myasoedov, B.F., I.A. Lebedev, P.L. Khizhnyak, G.A. Timofeev and V.Ya. Frenkel, 1986, J. Less-Common Met. **122**, 189.
Nolan, S.P., D. Stern and T.J. Marks, 1989, J. Am. Chem. Soc. **111**, 7844.
Nugent, L.J., 1975, Chemical oxidation states of the lanthanides and actinides, in: Int. Review of Science, Inorg. Chem., Series 2, Vol. 7, ed. K.W. Bagnall (Butterworths, London) ch. 6, pp. 195–219.
Nugent, L.J., R.D. Baybarz, J.L. Burnett and J.L. Ryan, 1971, J. Inorg. & Nucl. Chem. **33**, 2503.
Nugent, L.J., R.D. Baybarz, J.L. Burnett and J.L. Ryan, 1973a, J. Phys. Chem. **77**, 1528.
Nugent, L.J., J.L. Burnett and L.R. Morss, 1973b, J. Chem. Thermodyn. **5**, 665.
O'Donnell, T.A., 1992, in: Actinide Chemistry: A Half Century, eds L.R. Morss and J. Fuger (American Chemical Society, Washington, DC) ch. 22, pp. 213–224.
O'Hare, P.A.G., G.K. Johnson, I.R. Tasker, H.E. Flotow and C.W. Struck, 1987, J. Chem. Thermodyn. **19**, 77.
Peretrukhin, V.F., E.A. Erin, V.I. Dzyubenko, V.V. Kopytov, V.G. Polyukhov, V.Ya. Vasil'ev, G.A. Timofeev, A.G. Rykov, N.N. Krot and V.I. Spitsyn, 1978, Dokl. Akad. Nauk SSSR **242**, 1359.
Peretrukhin, V.F., F. David and A.G. Maslennikov, 1993, Actinides-93 conference paper 79, J. Alloys and Compounds, 1994, in press.
Pitzer, K.S., and L. Brewer, 1961, Revision of: Thermodynamics, 2nd Ed., G.N. Lewis and M. Randall (McGraw-Hill, New York).
Rard, J.A., 1985, Chem. Rev. **85**, 555.
Rard, J.A., 1987, J. Chem. Eng. Data **32**, 92.
Riegel, J., R. Deissenberger, G. Herrmann, S. Köhler, P. Sattelberger, N. Frautmann, H. Wendeler, F. Ames, H.-J. Kluge, F. Scheerer and F.-J. Urban, 1993, Appl. Phys. B **56**, 275.
Riglet, Ch., P. Vitorge and I. Grenthe, 1987, Inorg. Chim. Acta **133**, 323.
Riglet, Ch., P. Robouche and P. Vitorge, 1989, Radiochim. Acta **46**, 85.

Rizkalla, E.N., and G.R. Choppin, 1991, in: Handbook on the Physics and Chemistry of Rare Earths, Vol. 15, eds K.A. Gschneidner Jr and L. Eyring (North-Holland, Amsterdam) ch. 103, pp. 393–442.

Rizkalla, E.N., and G.R. Choppin, 1992, J. Alloys & Compounds **180**, 325.

Sapegin, A.M., A.V. Baluev and V.I. Evdokimov, 1984, Zh. Fiz. Khim. **58**, 2955 [Russ. J. Phys. Chem. **58**, 1792].

Schleid, T., and G. Meyer, 1989, Naturwissenschaften **76**, 118.

Schock, L.E., A.M. Seyam, M. Sabat and T.J. Marks, 1988, Polyhedron **7**, 1517.

Schoebrechts, J.-P., and B.P. Gilbert, 1985, Inorg. Chem. **24**, 2105.

Schoebrechts, J.-P., B.P. Gilbert and G. Duyckaerts, 1983, J. Electroanal. Chem. & Interfacial Electrochem. **145**, 127, 139.

Schoebrechts, J.-P., R. Gens, J. Fuger and L.R. Morss, 1989, Thermochim. Acta **139**, 49.

Shannon, R.D., 1976, Acta Crystallogr. A **32**, 751.

Silva, R.J., 1986, in: The Chemistry of the Actinide Elements, 2nd Ed., eds J.J. Katz, G.T. Seaborg and L.R. Morss (Chapman & Hall, London) ch. 13, pp. 1085–1117.

Smith, D.W., 1987, J. Chem. Educ. **64**, 480.

Soderholm, L., L.R. Morss and M.F. Mohar, 1987, J. Less-Common Met. **127**, 131.

Sonnenberger, D.C., L.R. Morss and T.J. Marks, 1985, Organometallics **4**, 352.

Sørensen, O.T., 1981, in: Nonstoichiometric Oxides, ed. O.T. Sørensen (Academic Press, New York) p. 17.

Spitsyn, V.I., V.G. Vokhmin and G.V. Ionova, 1983, Zh. Neorg. Khim. **28**, 1638 [Russ. J. Inorg. Chem. **28**, 925].

Spitsyn, V.I., V.G. Vokhmin and G.V. Ionova, 1985, Int. Rev. Phys. Chem. **4**, 57.

Struck, C.W., and J.A. Baglio, 1992, High Temp. Sci. **31**, 209.

Sullivan, J.C., S. Gordon, W.A. Mulac, K.H. Schmidt, D. Cohen and R. Sjoblom, 1976, Inorg. & Nucl. Chem. Lett. **12**, 599.

Sullivan, J.C., L.R. Morss, K.H. Schmidt, W.A. Mulac and S. Gordon, 1983, Inorg. Chem. **22**, 2338.

Sullivan, J.C., K.H. Schmidt, L.R. Morss, C.G. Pippin and C.W. Williams, 1988, Inorg. Chem. **27**, 597.

Takayama-Muromachi, E., and A. Navrotsky, 1988, J. Solid State Chem. **72**, 244.

Tel'noi, V.I., I.B. Rabinovich, M.R. Leonov, G.V. Solov'eva and N.I. Gramoteeva, 1979, Dokl. Akad. Nauk SSSR **245**, 1430.

Templeton, D.H., and C.H. Dauben, 1954, J. Am. Chem. Soc. **76**, 5237.

Trautmann, N., 1993, Appl. Phys., in press.

Trautmann, N., 1994, J. Alloys & Compounds, in press.

Travers, J.G., I. Dellien and L.G. Hepler, 1976, Thermochim. Acta **15**, 89.

Tremaine, P.R., and S. Goldman, 1979, J. Phys. Chem. **82**, 2317.

Turcotte, R.P., and R.G. Haire, 1976, in: Transplutonium Elements, eds W. Müller and R. Lindner (North-Holland, Amsterdam) p. 267.

Turcotte, R.P., J.M. Warmkessel, R.J.D. Tilley and L. Eyring, 1971a, J. Solid State Chem. **3**, 265.

Turcotte, R.P., T.D. Chikalla and L. Eyring, 1971b, J. Inorg. & Nucl. Chem. **33**, 3749.

Turcotte, R.P., T.D. Chikalla and L. Eyring, 1973, J. Inorg. & Nucl. Chem. **35**, 809.

Turcotte, R.P., T.D. Chikalla, R.G. Haire and J.A. Fahey, 1980, J. Inorg. & Nucl. Chem. **42**, 1729.

Vander Sluis, K.L., and L.J. Nugent, 1974, J. Opt. Soc. Am. **64**, 687.

Varlashkin, P.G., G.M. Begun and J.R. Peterson, 1985, J. Less-Common Met. **109**, 123.

Volkov, Yu.F., G.I. Visyashcheva, S.V. Tomilin, I.I. Kapshukov and A.G. Rykov, 1981, Sov. Radiochem. **23**, 195.

Wagman, D.D., and W.H. Evans, 1971, NBS Technical Note 270-6 (US Bureau of Commerce, Washington, DC).

Wagman, D.D., W.H. Evans, V.B. Parker, R.H. Schumm, I. Halow, S.M. Bailey, K.L. Churney and R.L. Nuttall, 1982, J. Phys. Chem. Ref. Data 11, Supplement 2.

Wang, Xiang-Yun, Jin Tian Zhu, J. Goudiakas and J. Fuger, 1988, J. Chem. Thermodyn. **20**, 1195.

Ward, J.M., 1983, J. Less-Common Met. **93**, 279.

Williams, C.W., L.R. Morss and I.-K. Choi, 1984, in: ACS Symposium Series, Vol. 246, eds G.S. Barney, J.D. Navratil and W.W. Schultz (American Chemical Society, Washington, DC) pp. 323–334.

Willit, J.L., W.E. Miller and J.E. Battles, 1992, J. Nucl. Mater. **195**, 229.

Woodley, R.E., 1981, J. Nucl. Mater. **96**, 5.

Handbook on the Physics and Chemistry of Rare Earths
Vol. 18 – Lanthanides/Actinides: Chemistry
edited by K.A. Gschneidner, Jr., L. Eyring, G.R. Choppin and G.H. Lander

Chapter 123

COMPARISON OF 4f AND 5f ELEMENT HYDRIDE PROPERTIES

John W. WARD and John M. HASCHKE
Los Alamos National Laboratory, Los Alamos, NM 87545, USA

Contents

Symbols 294
1. Introduction 294
2. Nature of the 4f and 5f elements and hydrides 295
   2.1. Electronic structure 295
   2.2. The early-actinide hydrides 296
   2.3. The "rare-earth-like" actinide hydrides 297
3. Phase and structural relationships 298
   3.1. New insights 298
      3.1.1. Results of X-ray diffraction, elastic neutron scattering and other techniques 301
      3.1.2. Other structure-related phenomena 310
   3.2. The alpha phase 310
4. Thermochemistry 313
   4.1. New rare-earth data 313
   4.2. New actinide data 318
5. Kinetics 320
   5.1. General observations 320
   5.2. Kinetics of bulk hydriding 321
   5.3. Mechanisms 325
   5.4. Rate data 327
6. Solid-state chemistry and physics 328
   6.1. Surface and near-surface properties 328
   6.2. Electronic-structure calculations 334
   6.3. Transport properties 338
      6.3.1. Electrical resistivity and related properties 338
         6.3.1.1. Rare earths 338
         6.3.1.2. Actinides 344
      6.3.2. Other transport-related properties 345
         6.3.2.1. Rare earths 346
         6.3.2.2. Actinides 349
   6.4. Magnetism 349
      6.4.1. General magnetic behavior 349
         6.4.1.1. The rare earths 349
         6.4.1.2. The actinides 350

6.4.2. Relationship of electrical resistivity and magnetism 351
6.4.3. Low-temperature heat capacities 352
6.5. Miscellaneous property measurements 354
6.5.1. Inelastic neutron scattering 354
6.5.2. NMR and EPR/ESR 356
6.6. Anomalous rare-earth systems 357
References 359

Symbols

C	hydride composition (H/M)	R	gas constant
C_p	heat capacity	ρ	electrical resistivity
ΔG_f^0	standard free energy of formation	ρ_m	magnetic resistivity
ΔH_f^0	standard enthalpy of formation	r	hydriding rate
ΔS_f^0	standard entropy of formation	T	temperature (°C or K as specified)
E_a	activation energy	T_C	ferromagnetic ordering (Curie) temperature
h	Planck's constant	T_1	spin–lattice relaxation time
M	lanthanide or actinide metal	T_2	spin–spin relaxation time
μ	magnetic moment	T_N	antiferromagnetic ordering (Néel) temperature
n	exponent defining the pressure dependence of the hydriding rate	Θ	fractional surface coverage by adsorbed species
ν	frequency	Θ_D	Debye temperature
P	H_2 pressure	x	hydride stoichiometry in the metal (α-phase) or cubic hydride regions
P_a	pressure below which the hydriding rate is controlled by the H_2 activity	y	hydride stoichiometry in the substoichiometric region below the trihydride
P_e	equilibrium H_2 pressure in the metal + hydride two-phase region		
P_i	pressure below which the hydriding rate is controlled by H_2 impingement		
P_s	pressure above which the surface is saturated by H_2		

1. Introduction

The last comprehensive review and evaluation of rare-earth hydride systems was published as part of this series by Libowitz and Maeland (1979). This chapter gives a good generic description of the phase behavior expected from various systems, as well as a basic introduction and explanation of the thermodynamic relationships and calculations relevant to a typical metal–hydrogen system. Methodologies for calculations and extensive data are presented and will not be repeated here.

During the decade prior to the preceding chapter, interest in the properties of rare-earth alloys for hydrogen-storage purposes generated a great deal of research activity. Preliminary data and discussion appear in the earlier chapter. Interest has since

lessened considerably, due in part to some of the sobering facts on reactivity, ultimate usefulness and costs, and also to ample availability of fossil fuels. An area of theoretical interest at that time was a continuing controversy as to whether hydrogens are "protonic", "atomic" or "hydridic" in nature, a question since laid to rest in favor of the latter by excellent studies.

New directions are evident in more recent investigations. Basic work in magnetism, electrical resistivity, neutron scattering, NMR and Mössbauer spectroscopy are documented by Libowitz and Maeland (1979). Since that time, solid-state physics and chemistry have been extremely active areas. The latest techniques and spectroscopies are often employed in combination to the extent that it is sometimes difficult to catalog a publication according to its major focus. Centers of expertise have emerged over the past twenty years at the Ames Laboratory, the Institut Hydrogene et Defauts dans les Metaux, the University Paris-Sud, and the ETH Zürich for the rare-earth hydrides, and at the Los Alamos National Laboratory and the Oakridge National Laboratory for actinide hydrides. Surface spectroscopies add a new dimension to our understanding, complemented often by advanced relativistic and fully self-consistent band-structure calculations. A large amount of new elastic and inelastic neutron scattering data gives new insight and precise data to the body of literature.

The bulk of older literature deals with structural determinations, *P-C-T* studies and heat-capacity measurements leading to thermodynamic data and phase relationships, but coverage of such studies is comparatively small in the present chapter. In addition to filling some gaps in the literature, most recent work confirms the results of previous structural and thermodynamic studies. However, as will be noted below, new and even startling observations are reported in the phase behavior of some systems that heretofore were thought to be consistent and well understood. The occurrence of mixed valence and intriguing electronic behavior in the Yb + H system deserves comment. A large body of literature has accumulated concerning the alpha phase (the region of hydrogen solubility in the metal) which, although not a "hydride" in the strict sense, is certainly a hydride precursor with implications for understanding higher composition phases.

A combined review of the rare-earth and actinide hydrides is appropriate. A reasonable literature on actinide–hydrogen systems now exists with an attendant realization that the 5f metals form fully rare-earth-like hydrides as well as totally unique hydride phases. This chapter concentrates on correlating the 4f and 5f metal–hydrogen systems and relies heavily on the most recent interpretations of the solid-state physics and chemistry.

2. Nature of the 4f and 5f elements and hydrides

2.1. *Electronic structure*

Electronic properties are an important determinant of hydride properties. Whereas the rare-earth 4f electrons are considered to already be localized in γ-cerium, the 5f actinide series is complex and produced great puzzlement in the early days. Thorium

and its compounds seemed to show a regular extension of the normal tetravalent behavior of Ti, Zr and Hf, thus beginning a new d-electron series. Unfortunately, radioactive actinium provides little help; the few measurements available show this element to be lanthanum-like with essentially the same metallic radius as La and having the trivalent state characteristic of Sc, Y and La. At protactinium, the broad-band, diffuse 5f electrons first dip below the Fermi level and give birth to a whole new chemistry and physics. Although the resulting research has been new and exciting and is presently rather well understood, those topics are not the province of this chapter, except as the data might apply to hydride systems.

In proceeding across the actinide series, two major and concomitant events occur: (1) more 5f electrons are added, and (2) the 5f bands narrow. As 5f electrons are added, they remain in the valence band and hybridize strongly with the s–d electrons. In contrast to their importance in the rare earths, s–d electrons contribute little to the chemistry and physics of the early actinide metals compared to the enormous influence of the 5f electrons. Narrowing of these bands as one proceeds across the series results finally in the onset of f-electron localization. This incipient localization produces a bewildering array of temperature- and structure-dependent properties at plutonium. Localization is percipitous and complete at americium, driven finally by spin polarization.

As one might expect, the physicochemical properties of the alloys and compounds of the actinide metals are as varied as any in the entire periodic table and include superconductors, magnets, heavy fermions and an array of valence states. The basic explanation is rather simple and given here because of its straightforward application to the hydride systems. Hill (1970) points out that most actinide compounds can be catalogued as to whether the 5f electrons are delocalized (bonding) or localized (essentially non-bonding) on the simple basis of lattice spacing. These so-called "Hill plots" are useful as a general guide; breakdowns appear for f–p bonded systems, but these refinements are not of concern here. Simply stated, if the lattice spacing is large, the 5f wave functions fall short of significant overlap and bonding reverts to much simpler s–d configurations characteristic of cubic or hexagonal symmetry. However, the 5f electrons exert influences in non-bonding areas such as magnetism, electron scattering and possible interaction with the hydrogen 1s electron. In the rare-earth hydrides, the effect of magnetic ordering on the conduction electrons is well documented.

Although the electronic behavior of the rare earths is more consistent than that of the actinides, important variations are encountered. The enhanced stabilities of electron configurations for divalent oxidation states prior to the half-filled and filled 4f configurations is well known. Strong alkaline-earth-like properties are manifest at Eu and appear in progressively lesser extents at Yb and Sm. The increased stability of tetravalent oxidation states at Ce, Pr and Tb apparently do not influence hydride properties.

2.2. *The early-actinide hydrides*

The early-actinide hydrides are diverse and unlike those observed for their rare-earth analogs. Ward (1985a) has provided an extensive review of the properties of the actinide

hydrides, through the Am + H system; Flotow et al. (1984) review the chemical thermodynamics of these hydrides. On the basis of fragmentary information from a microgram sample, actinium hydride is identified by Farr et al. (1961) as having a cubic lattice parameter of 5.670 ± 0.006 Å (cf. LaH_3: $a_0 = 5.663$). Thorium forms an apparently normal dihydride like those of Zr and Hf, but then forms Th_4H_{15}, a totally unexpected and unique superconductor. Possible influences of the 5f band are not obvious, but on closer examination the lattice constants are 17% larger than those for HfH_2, with an M–H distance typical of a *trivalent* metal.

The behavior of the Pa + H system is even stranger than that of Th. The hydrides of this element and uranium have cubic structures which have no counterparts in the periodic table. A study by Ward et al. (1984) provides a complete characterization of the *P-C-T* behavior of the system; a subsequent report by Haschke et al. (1985) includes thermodynamic values along with an interpretation of the pronounced hysteresis observed in *P-C* isotherms. At temperatures below 500 K, PaH_{3-x} ($0.1 \leq x \leq 1.7$) forms the bcc α-UH_3 structure, but unlike the stoichiometric uranium compound, the phase exists over an astonishingly large composition range. At higher temperatures, protactinium hydride forms the C15-type AB_2 Laves structure over the composition range $1.2 \leq H/Pa \leq 1.8$. Pa-atoms occupy both the A and B sites in the cubic lattice. As discussed by Ward et al. (1984), the structure is apparently stabilized by large Pa–H moieties on the A sublattice and small Pa atoms on the B sublattice in which major f–f overlap is implied by a Pa–Pa distance similar to that for the metal. The C15 phase is magnetic with moments attributed to the large A sublattice where f–f overlap should be nil and localization possible.

Upon further addition of hydrogen at high temperatures, a third protactinium hydride forms with sluggish kinetics and major hysteresis. This cubic phase exists over the $2.2 \leq H/Pa \leq 2.9$ composition range in a defect structure derived from that of A15-type β-UH_3, but pressures approaching 100 bar do not drive the composition to 3.0. In contrast, formation of stoichiometric β-UH_3 is rapid and facile. Metal atoms again play two roles (metal–hydrogen and metal–metal interactions) in the A15 hydrides for both Pa and U. Here again, both PaH_{3-x} and UH_3 are magnetic.

2.3. *The "rare-earth-like" actinide hydrides*

In remarkable contrast to the behavior of the early-actinide hydrides, the physicochemical properties of the transuranium phases are suddenly more rare-earth-like. As discussed earlier, the progressive narrowing of the 5f bands favors the stabilization of the fcc structure with the larger M–M distance; attendant localization can then occur and the f bands become "core-like" and magnetic. However, in contrast to the rare earths, the 5f electrons remain near the Fermi level and one can expect that effects such as scattering will then influence resistivity, neutron scattering and other properties.

In comparing and contrasting the rare-earth and late-actinide hydride systems, it should be noted that a shifted homologous relationship exists for the metals, as shown in fig. 1. As noted by Johansson (1975) and discussed by Ward (1985b), the heavy actinide metals relate to the beginning of the rare-earth series, rather than to the direct

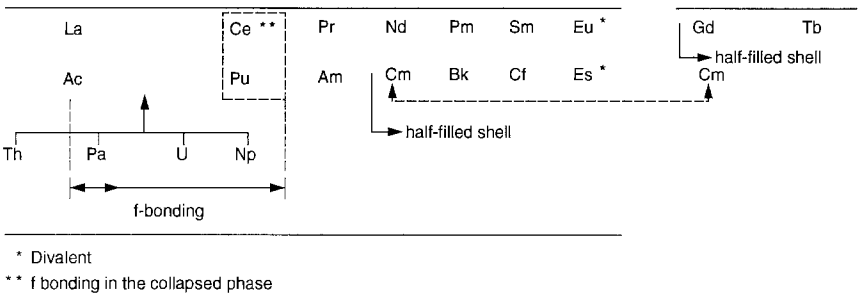

Fig. 1. Shifted homologous relationships between the lanthanide and actinide metals. The properties of Am through Es (metals without significant f-bonding) most closely mimic those for Pr through Eu; the half-filled shell gives Cm some properties like Gd. After Ward et al. (1986).

homologs. This relationship is quite remarkable and consistent, in terms of crystal structures, heats of vaporization and chemical properties, and extends easily to the divalency beginning at einsteinium compared to europium, and the ambivalence of both californium and samarium. It should be noted that the respective half-filled shell points cause an inconsistent perturbation to the model. (e.g., curium correlates to neodymium, but also in some ways to gadolinium).

Bearing this correlation in mind, one can immediately say that the hydrides of Np, Pu and Am are rare-earth-like with wide cubic solid solution ranges up to H/M = 2.7–2.8 and somewhat smaller lattice parameters. The hexagonal phase appears with regularity, unlike the behavior encountered for Ce, Pr and Nd. *P-C-T* data are not available for the Cm system and beyond, but relatively "normal" behavior is expected. As pointed out above, the large and simple lattices of the early rare earth and late-actinide hydride systems preclude f–f overlap. Since the "actinide contraction" is delayed as compared to the rare-earth contraction, phase relationships such as those seen for Gd hydride and beyond are not expected for the actinides.

It should be noted that the late-actinide hydrides react more easily and vigorously than any of the rare-earth counterparts. This effect, which is kinetic and not thermodynamic, is discussed in section 5. As an introduction to the new data and information to be presented, comparative trends for the rare-earth and late-actinide hydrides are summarized in table 1. It should be understood that "MH_2" simply implies a value at or near the phase boundary and that the temperature of the measurement is not unambiguously defined. For most systems, the phase-boundary composition is near $MH_{1.9 \pm \delta}$.

3. Phase and structural relationships

3.1. *New insights*

The rather simple view of hydride systems derived on the basis of early work must be revised. Experimental observations show that large lattice systems (La, Ce, Pr) form

TABLE 1
Comparative trends in the trivalent rare-earth and late-actinide hydrides.

Element M	MH_2/MH_3 phases (ambient)	Lattice constant MH_2 (Å)	Magnetic	Minimum M–H distance (Å)	ΔH_f^0 of MH_2 (kJ/mol)
La	fcc solid solution	5.66	no	2.45	−207.5
Ce	fcc solid solution	5.58	yes	2.42	−217.6
Pr	fcc solid solution	5.52	yes	2.39	−207.9
Nd	fcc solid solution (hexagonal)	5.46	yes	2.37	−211.3
Sm	fcc solid solution, hexagonal	5.37	no	2.33	−223.8
Gd	fcc solid solution, hexagonal	5.30	yes	2.32	−204.6
Tb	fcc solid solution, hexagonal	5.25	yes	2.32	−209.2
Dy	fcc solid solution, hexagonal	5.20	yes	2.32	−209.2
Ho	fcc solid solution, hexagonal	5.17	yes	2.32	−225.9
Er	fcc solid solution, hexagonal	5.12	yes	2.32	−223.8
Tm	fcc solid solution, hexagonal	5.09	yes	2.32	−225.1
Lu	fcc solid solution, hexagonal	5.03	no	2.32	−204.8
Ac	fcc solid solution	5.67	(no)	2.46	−???
Np	fcc solid solution, hexagonal	5.34	no	2.32	−111.6*
Pu	fcc solid solution, hexagonal	5.36	yes	2.32	−155.6
Am	fcc solid solution, hexagonal	5.35	no	2.32	−190.4
Cm	fcc solid solution, hexagonal	5.32	(yes)	2.32	(−187.0)
Bk	fcc solid solution, hexagonal	5.25	(yes)	2.32	−???
Cf	fcc solid solution, hexagonal	5.29	(yes)	2.32	−???

* For hypothetical $NpH_{2.0}$.

CaF_2-related cubic solid-solution phases starting near M/H = 2.0 and continuing to 3.0; substoichiometric LaF_3-related hexagonal trihydrides appear for the later rare-earth and the transuranium systems. In early descriptions, these extended solid solutions are cited as examples of classic nonstoichiometry. Although the upper phase boundary of the cubic phases vary with metallic element and conditions, a general conceptual model has been applied to all systems. The tetrahedral interstices (t-sites) in the ccp metal sublattice were formerly assumed to be fully occupied at the dihydride, but this is often (see below) not true. Higher stoichiometries were viewed as part of a continuous solid solution formed by random occupancy of vacant octahedral interstices (o-sites) in the dihydride structure. The o-site/M ratio of one leads to an upper limit of MH_3 for the phase and to a BiF_3-type structure. The structure of the hexagonal hydride is derived by formation of random hydrogen vacancies in the LaF_3-related parent.

Results of newer and more sensitive measurements suggest that the rare-earth and transuranium hydrides are similar to other systems with extended non-stoichiometric phases. For the cubic region, a close analogy is found to CaF_2-related systems having cation altervalence. Examples are provided by the M (III)–M (IV) oxides of Ce, Pr and Tb and the M (II)–M (III) fluorides of Sm and Eu are described in respective reviews by

Eyring (1979) and by Greis and Haschke (1982). As in the hydride systems, continuous solid solutions exist at high temperatures after the miscibility gap closes. In the oxide systems, this closure is between the CaF_2-related M_2O_3 and the CaF_2-type MO_2 phases. A similar gap closure is observed between the CaF_2-type MF_2 and LaF_3-related MF_3 phases. However, as discussed by Haschke et al. (1987), charge balance in the hydrides is apparently not accomplished by cation altervalence, but by progressively binding conduction-band electrons as hydridic states. This process is evidenced by a regular change from metallic to semiconducting behavior with increasing H/M and by a small decrease in lattice dimension with increasing composition.

Although the high-temperature oxide and fluoride solid solutions are readily obtained by quenching, equilibration of the product leads to precipitation of stoichiometric intermediate compositions. In these phases the metal ions exist as mixtures of oxidation states with structures derived by long-range anion ordering in a lower-symmetry lattice related to fluorite. As described by Eyring (1979), lattice-imaging microscopy shows that the oxide solid solution is formed by coherently intergrown microdomains of the ordered low-temperature phases. Evidence for a similar process involving layers composed of metal-fluoride clusters are reviewed by Greis and Haschke (1982). Variations in the stoichiometries and ratios of the domains provide a mechanism by which a continuously varying composition is attained at high temperature. Because of the intergrowth process, macroscopic properties such as thermodynamic activity and lattice parameter seem to vary continuously with composition as anticipated for an ideal solid solution.

A strong analogy between the hydrides and the oxides and fluorides is evident and suggests that the conceptual model described above should be reexamined. As outlined on the following section, recent measurements for the lanthanide and transuranium hydrides show that ordered hydride phases form in the cubic region at sub-ambient temperatures with various and often subtle lattice distortions and displacements of H atoms from so-called "normal" t-sites and o-sites. An important difference between the behavior of the hydrides and those of the oxides and fluorides is the temperatures at which order–disorder transitions occur leading to closure of the miscibility gaps. Because hydrogen mobility is high compared to that of oxygen or fluorine, hydride ordering is expected to occur at lower temperatures than for the oxides or fluorides. The extended hydride solutions existing above the disorder temperatures probably involve coherent intergrowth processes of domains or clusters. Closest-packed metal layers in both the cubic and hexagonal hydrides provide a coherent interface for intergrowth of those structures.

Significant progress has been made in defining the equilibria and structures of the α-phase and the cubic hydrides, but the picture is far from complete. The experimental difficulties of determining positional coordinates for hydrogen in polycrystalline samples and of conducting measurements at low temperature present substantial obstacles. Greis et al. (1981) has demonstrated that the rate of cooling is an important factor in forming ordered hydride phases. Relationships are sometimes confused, and it is not clear whether to discuss recent observations along with relevant experimental techniques or to consider each observation in a special section devoted to a technique. What follows is perhaps a hybrid, but topically leaning toward the latter.

3.1.1. *Results of X-ray diffraction, elastic neutron scattering and other techniques*

The phase and structural relationships of the lanthanide- and actinide-hydride systems are outlined here with relevant corollary evidence to provide a suitable background and preparation for some of the more esoteric discussions to follow. Historically, the first realizations of latent structural complexities appeared with the advent of more precise neutron-diffraction measurements in conjunction with new low-temperature capabilities. X-ray studies have been of limited utility because only metal atom positions are defined and only the near-surface regions of opaque heavy-metal hydrides are sampled. However, the influence of the H sublattice ordering upon the metal lattice can be deduced.

Neutron studies on the Ce + D system by Cheetham and Fender (1972) and continued by Titcomb et al. (1974) indicate that octahedral deuterium atoms are displaced from their ideal locations by as much as 0.3 Å along the {111} direction toward the t-sites. At higher hydrogen concentrations, previously filled t-sites are found to be vacant while o-sites are prematurely filled. Implications regarding the contraction of the lattice with increasing o-site occupancy will be considered later. Although incomplete occupation of t-sites at the supposed composition $CeD_{2.00}$ was not observed by these authors, such behavior is since well established for most lanthanide hydrides. Their low-temperature experiments foreshadow the later discovery of low-temperature ordering processes that are now well-established by a variety of experimental techniques.

Supporting observations were reported by other workers. Libowitz et al. (1972) not only observed a tetragonal distortion in $CeD_{2.75}$ by X-ray measurements near 252 K, but also documented a well-defined metal-to-semiconductor transition. Khatamian et al. (1980) studied $YD_{1.96}$ and $YD_{1.98}$ at room temperature and 11 K and found a reduced occupancy of t-sites, an enhanced occupation of o-sites and a diminution of the effect at 11 K. The implication of these observations is that thermal activation moves hydrogen atoms from the lower-energy t-sites to the higher-energy o-sites. Fedotov et al. (1982), studying the compositions $CeD_{2.26}$ and $CeD_{2.43}$, clearly establish the low-temperature ordering of octahedral hydrogens and the concomitant appearances of superlattice lines corresponding to two tetragonal domains (space groups $I4/mmm$ and $I4_1md$), with approximate doubling of the c-dimension of the unit cell. These authors report nearly 3% vacancies in the tetrahedral sublattice and displacements of D atoms from normal sites. In a related study, Anderson et al. (1980) used proton-NMR rigid-lattice second-moment measurements to show that the o-sites for $YH_{1.98}$ are already up to 15% occupied and the t-sites are then nearly 10% depopulated. The small lattice ($a_0 = 5.205$ Å) may favor this effect.

Bashkin et al. (1979) investigated the Nd-H system by differential thermal analysis (DTA) in the temperature range – 140 to 100°C. As shown in fig. 2, a T–C diagram constructed on the basis of their thermograms confirms the existence of several low-temperature phase fields and indicates a composition-dependent phase transition in the region $NdH_{2.65-2.75}$. The hexagonal phase was later confirmed for $NdH_{2.82}$. By invoking comparisons with neutron diffraction and resistivity data, the authors conclude that their observations result from low-temperature ordering in the octahedral sublattice. The relevance of their dome-shaped maxima to later results will become

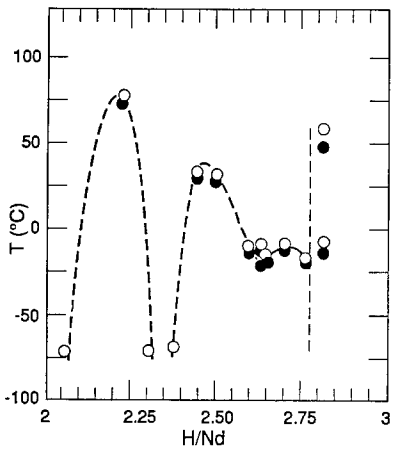

Fig. 2. T–C diagram for the Nd + H system constructed from differential thermal analysis (DTA) data for the temperature range − 140 to 100°C. Key: ● heating; ○ cooling; broken curve indicates approximate phase boundary. After Bashkin et al. (1979).

clear shortly. A further example is shown by the neutron-diffraction studies of Didisheim et al. (1980) for $LaH_{2.90}$. Assuming that the composition determined for this near-stoichiometric trihydride phase is accurate, the influence of vacancies appears to be small, but the displacement of H atoms in the {111} directions is detected. A phase transition is evident near 230 K.

Further complexities may be introduced by magnetic, electronic or even isostructural transitions. These effects are discussed in section 6, along with metal–semiconductor transition(s) appearing at high compositions. These rather murky waters have recently been greatly clarified by a combination of excellent X-ray studies and other techniques in the Laboratory for Solid-State Physics at the ETH, Zürich. A "generic" T–C diagram from the work of Boroch et al. (1989) on the La + H system is presented in fig. 3. Every point defines an in-situ X-ray result; the "two-dome" system clearly shows two dominant tetragonal regions and well-defined two-phase regions in addition to the normal cubic structure. With appropriate adjustments to the temperature and the composition scales, this diagram defines the expected behavior of the La, Ce, Pr systems, describes the Nd + H system to some extent, and correlates with what is presently known of the late-actinide hydrides. Another example is the work of Boroch and Kaldis (1987) on the Ce + H system. Detailed studies on this system are described by Boroch and Kaldis (1989), and Conder et al. (1989), who added high-resolution differential-scanning calorimetry (DSC) to their measurements. The DSC results reveal a further dimension of complexity in the phase diagrams below room temperature, with evidence for multiple non-stoichiometric phases or solid-solution regions.

Results for the early rare-earth systems are refined and extended with addition of neutron scattering results summarized by Conder et al. (1991). As shown in fig. 4, these incomplete measurements reveal rather complex phase diagrams with as many as nine microphases for La + H and more than ten for Ce + H. These painstaking studies were done with a precision in H/M of 0.005; thus, it is clear why earlier less-precise

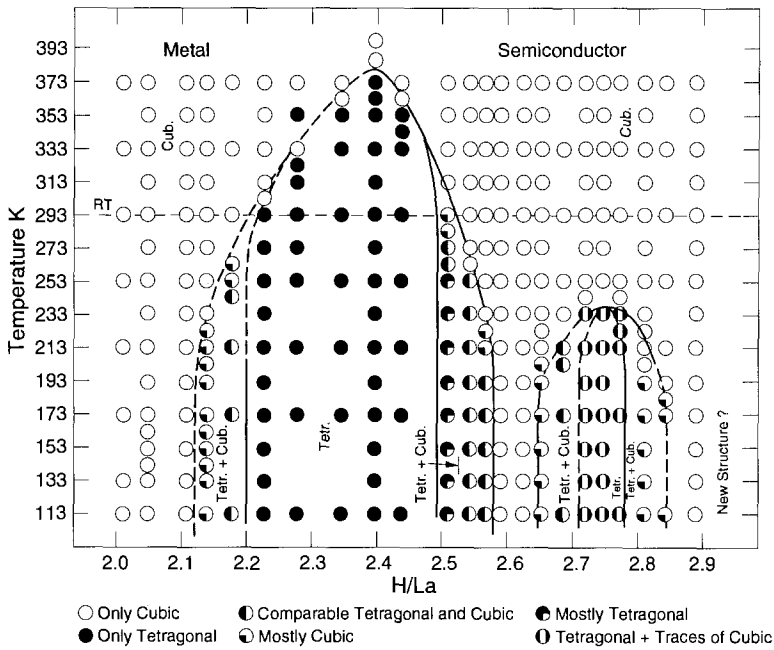

Fig. 3. Representative phase diagram for the early-lanthanide hydride systems based on X-ray diffraction data for La + H. The characteristic "double-humped" tetragonal phase fields may be compared with the DTA data in fig. 2. After Boroch et al. (1989).

measurements may have missed such fine detail. The neutron data obtained by these authors are generally in good agreement with the X-ray results and identify the I4 and $I4_1$ md space groups for tetragonal $CeH_{2.33}$ and $CeH_{2.43}$, respectively. Measurements in the higher composition regions show an additional tetragonal phase near H/M = 2.7–2.8 and another phase that apparently results from a distortion of cubic symmetry near the trihydride composition. As shown in fig. 4, extra diffraction lines could arise from residuals of the eutechtoid transformation beginning near room temperature (290 K for La + H, 305 K for Ce + H). These data confirm earlier neutron work indicating tetragonal phases, but show that these systems are still not well understood.

To briefly summarize the implications of this section with respect to the rare earths, we now realize that the low-temperature phase relationships are exceedingly complex and, as we shall see later, also provide a fertile area for resistivity, magnetic and crystal-field measurements as well as theoretical studies. The earlier papers can be drawn into reasonable agreement by examining fig. 4; cooling a hydride sample from ambient temperature at a given composition could give very different results than a similar experiment begun at a slightly different composition.

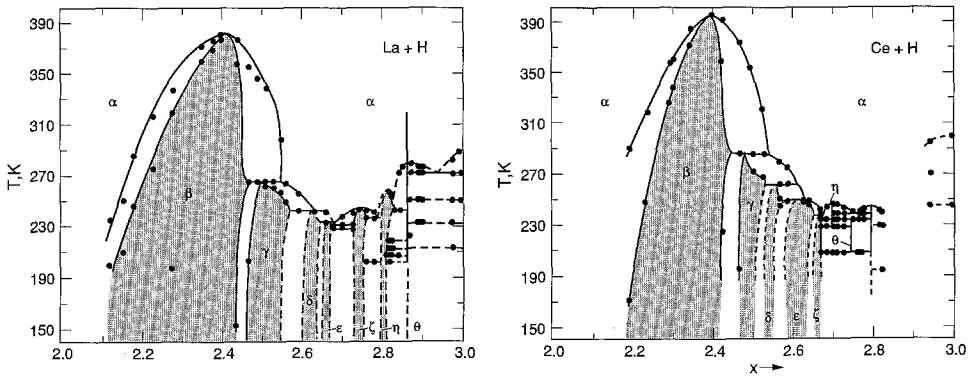

Fig. 4. Phase diagrams for the La + H (left) and Ce + H (right) systems derived from high-resolution differential-scanning calorimetric data. Multiple non-stoichiometric phases and/or solid-solution regions are shown. After Conder et al. (1989).

For actinide systems, Np + H and Pu + H are most thoroughly studied. Work by Haschke et al. (1987) on Pu + H suggest that multiple phases form in the continuous solid-solution region during hydrogen desorption studies at elevated temperatures. Stoichiometry ranges of these phases are indicated by linear regions in $\ln P$–C isotherms for the $1.8 \leq \mathrm{H/Pu} \leq 3.0$ range in fig. 5. Except for the III + IV field defining the cubic + hexagonal two-phase region, each segment defines a region of constant free energy change expected for a composition range having a closely related structure, and, as discussed by Ward (1985a), these apparent structures are formed by relatively rapid reaction above 400°C. Haschke et al. (1980) draw an analogy to the rare-earth fluoride systems of Sm and Eu, in which the phase behavior seems remarkably similar to that of the PuH_{2+x} system. As outlined in the review by Flotow et al. (1984), a metastable cubic solid-solution region apparently forms below 400°C for $\mathrm{H/Pu} \geq 2.7$. The metastable region is an extension of the stable cubic phase existing at lower compositions; the cubic trihydride composition is approached by careful addition of hydrogen and avoidance of heat spikes. Reaction in the cubic regime occurs essentially without hysteresis and with a remarkably constant entropy change characteristic of an ideal solution. Haschke and Hodges (1981) propose that the low-temperature cubic modification occurs because the metal atoms cannot easily move or reorder from a ccp to an hcp arrangement at low temperature. The question arises as to whether similar behavior could be induced in some rare-earth hydrides by such temperature/rate variations. However, none of these systems react readily at such low temperatures, and it would appear that the Pu + H system may be unique in this respect.

Elastic neutron scattering studies by Bartscher et al. (1985) on the compositions $\mathrm{D/Pu} = 2.25$, 2.33 and 2.65 show an apparent progressive depletion of t-sites (as compared to PuD_2) at the higher compositions. A displacement of octahedral deuteriums by 0.4 Å in the {111} direction is in agreement with observations noted

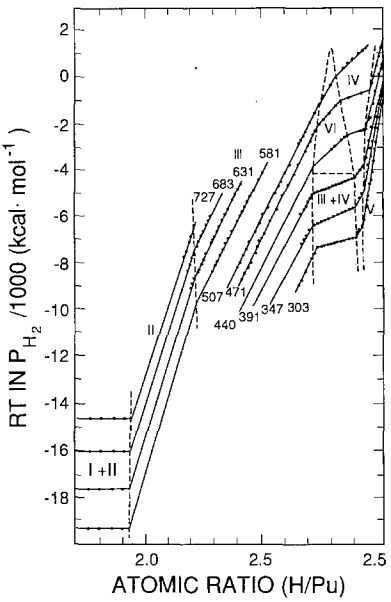

Fig. 5. $RT\ln P$ versus composition isotherms for Pu + H showing evidence for multiple partial molar free energy domains at high temperatures (T in kelvin). After Haschke et al. (1987).

above for certain rare-earth systems. A conceptual model based on vacancy clusters is proposed by Haschke et al. (1987) for interpreting t-site and o-site occupancy factors observed in this work. More recent neutron studies by Goldstone (1990) at the Los Alamos National Laboratory indicate a highly strained lattice, but show no evidence for distortion or tetragonal transformation(s). However, cooling rates and annealing times can be major factors in interpreting low-temperature data, as will be seen in the resistivity and magnetism discussions below. The "freeze-in" of hydrogens in cubic plutonium hydride at low temperatures seen in NMR results is reported by Cinader et al. (1976) and is evidenced by a broad lambda-type transition in the heat-capacity curve presented by Flotow et al. (1984). In any case, the low-temperature structural behavior of the Pu + H system remains to be fully characterized.

In contrast, the Np + H system, although unique in some ways, shows no unusual normal-to-high-temperature behavior. *P-C-T* measurements by Ward et al. (1987) are shown in fig. 6. These studies, using ultra-high-purity metal, resolved some discrepancies in earlier measurements and clearly defined for the first time a cubic-to-hexagonal two-phase region and an extremely narrow NpH_{3-x} phase. Most unusual for this system, as compared to all lanthanide systems and to the Pu + H and Am + H systems, is the sharp phase boundary near $NpH_{2.13}$. The data imply a thermodynamic equivalence of the o- and t-sites, while still in the (flat) plateau region above $x = 2.0$. As shown in table 2, cooling at this phase boundary composition produces a tetragonal phase similar to that shown in fig. 3, with the t-sites 11% vacant, even at 10 K. Thermal activation at the higher temperatures increases the population of the higher-energy o-sites, as discussed by Khatamian et al. (1980). The small lattice of $NpH_{2.13}$ may favor

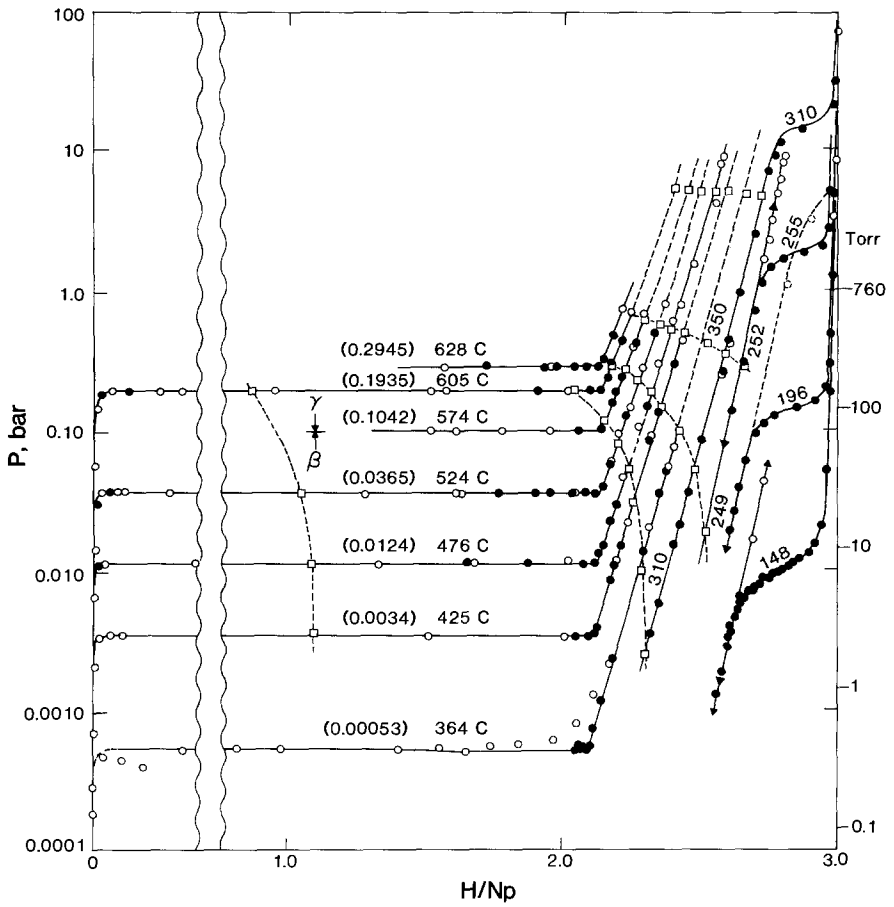

Fig. 6. *P–C–T* diagram for the Np + H system. Key: ○ hydriding, ● dehydriding; temperature ramp data at fixed H_2 moles. After Ward et al. (1987).

this effect because the degree of t-site depopulation for the early rare earth hydrides is much smaller (< 3% for $LaH_{2.0}$) than for yttrium (near 10% for $YH_{1.98}$) and the actinides. The same I4/mmm space group for $NpD_{2.13}$ is also assigned to the tetragonal phase at the $NpD_{2.65}$ composition, although there are subtle differences between these structures. In any case, the t-sites are nearly filled at the higher composition.

For the Np + H system the lattice expands upon further addition of hydrogen beyond the 2.13 phase boundary, in contrast to all other rare-earth hydride systems. This is because the minimum Np–H distance of 2.32 Å has already been reached at the phase-boundary composition (see table 1). The lattice parameter is smaller than that for SmH_2 as well as those for PuH_2 or AmH_2, suggesting that the "actinide contraction" does not really begin until PuH_2. Yet, as shown in fig. 6, the hexagonal phase does not appear until quite late and its stoichiometry range is quite narrow. The implications

TABLE 2
Neutron-diffraction data for neptunium deuterides.

Temperature (K)	Space group	Lattice parameter	Tetrahedral site occupancy	Octahedral site occupancy
		Fitted values for $NpD_{2.13}$		
10	I4/mmm	$a = 5.3337(3)$ $c = 10.6493(7)$	1.778(8)	0.352(8)
100	I4/mmm	$a = 5.3348(4)$ $c = 10.6522(8)$	1.774(8)	0.357(9)
200	I4/mmm	$a = 5.3349(4)$ $c = 10.6557(8)$	1.75(1)	0.376(9)
300	Fm3m	$a = 5.3324(4)$	1.72(1)	0.413(9)
		Fitted values for $NpD_{2.65}$		
10	I4/mmm	$a = 5.3337(4)$ $c = 10.6339(8)$	1.95(1)	0.70(1)
100	I4/mmm	$a = 5.3259(4)$ $c = 10.676(1)$	1.97(1)	0.68(1)
200	I4/mmm	$a = 5.3352(5)$ $c = 10.465(1)$	1.95(2)	0.70(2)
300	Fm3m	$a = 5.3361(3)$	1.95(1)	0.71(1)

of 5f-electron effects on the electronic and thermodynamic properties of this system will be considered in subsequent sections.

Neutron studies of rare-earth and actinide systems suggest that a similar ordered structure forms at low temperatures. A "generic" tetragonal lattice is shown in fig. 7a. Ordering of the octahedral hydrogens first occurs in the *c*-axis directions, and further ordering at still lower temperatures can result in additional isostructural and/or electronic transitions. Figure 7b shows typical elastic neutron diffraction data for $NpD_{2.65}$; superlattice lines begin to appear below 200 K. Additional peaks, seen at 10 K, may relate to the structure seen in the electrical-resistivity measurements discussed below.

Available structural and *P-C-T* data for the Am + H system have been reviewed and correlated by Ward (1985a). No solid-state property measurements have been made for this system, other than the recent resistivity measurements, to be discussed below. As note in table 1, the normal fcc and hexagonal phases have been identified by X-ray diffraction, although the *P-C-T* data were not sufficiently developed to delineate the latter phase. Note also that the heat of formation for AmH_2 is nearly equal that for a typical rare-earth hydride.

For the trans-americium systems only XRD data are reported for very small samples having unknown compositions. Nevertheless, results obtained with microgram quantities are quite remarkable and clearly establish the anticipated rare-earth-like proper-

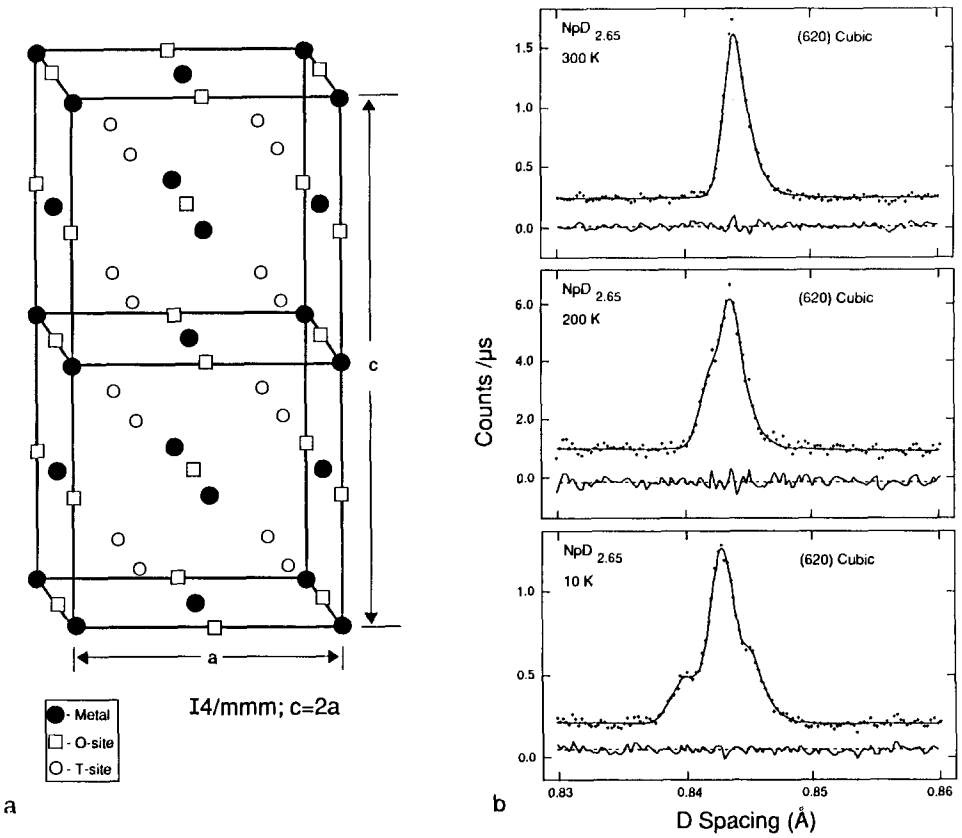

Fig. 7(a) Tetragonal lattice structure (I4/mmm, $c = 2a_0$) for $NpH_{2.65}$. The o-sites on the c-axis fill preferentially. After Ward et al. (1992). (b) Temperature dependence of neutron-diffraction data for the cubic (620) reflection of $NpH_{2.65}$. The 10 K peak shows an additional right shoulder in addition to the tetragonal (left) shoulder evident at 200 K. After Ward et al. (1992).

ties. Gibson and Haire (1985a) prepared both cubic CmH_{2+x} ($a_0 = 5.322$ Å) and hexagonal CmH_{3-y} ($a_0 = 3.77$ Å, $c_0 = 6.73$ Å) phases, the latter forming by a sluggish process typical of the earlier-actinide hydride systems. Gibson and Haire (1990) continued their studies on both the Am + H and Cm + H systems using Knudsen effusion mass spectrometry to estimate heats of formation.

Gibson and Haire (1985b) have also prepared microgram quantities of cubic BkH_{2+x} ($a_0 = 5.25$ Å) and hexagonal BkH_{3-y} ($a_0 = 3.73$ Å, $c_0 = 6.66$ Å) phases. The "actinide contraction" appears to continue, although the exact compositions are not known for these phases. Here the hexagonal phase forms rather easily, as is the case for the later lanthanide hydrides. Finally, Gibson and Haire (1985c) describe a cubic californium dihydride with an unexpectedly large lattice parameter ($a_0 = 5.29$ Å), but have been unable to prepare the trihydride. In discussing the physicochemical and thermochemical properties of californium metal in terms of the incipient trend of the

late actinides toward the divalency confirmed at einsteinium, Ward et al. (1986) draw an analogy to the Sm–Eu region in the rare earths, for which the trend is immediately broken by the stability of the half-filled shell. Gibson and Haire (1985c) propose a "reduced-valent" Cf to explain the expanded lattice; more likely; however, a mixed-valent system akin to that found recently for the Yb + H system is more likely (see section 6.6). In analogy to that system, the hexagonal Cf phase might form with sufficient hydrogen overpressure.

Examination of the trends established by the rare earths and actinides is instructive. Lattice parameters for the rare-earth-like actinide hydrides are summarized in table 3. A comparison of the formula volumes of all the lanthanide and actinide dihydrides by Gibson and Haire (1990) is shown in fig. 8. From this perspective it is obvious that NpH_2 is anomalously small and CfH_2 anomalously large. In any case, the non-metallic hexagonal phases are generally regular in terms of an actinide contraction and near-uniform c/a ratios.

TABLE 3
Lattice parameters for the late-actinide hydrides.

M	fcc MH_2	hex MH_{3-x}		c/a
	a_0(Å)	a_0(Å)	c_0(Å)	
Np	5.348	3.777	6.720	1.78
Pu	5.360	3.779	6.771	1.79
Am	5.344	3.764	6.763	1.80
Cm	5.322*	3.769	6.732	1.79
Bk	5.248*	3.726	6.663	1.79
Cf	5.285*	–	–	–

* Probably MH_{2+x}, x unknown.

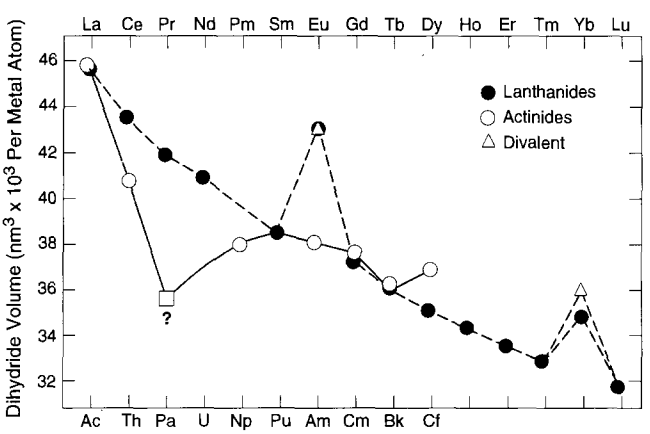

Fig. 8. Comparison of formula volumes for the lanthanide and actinide dihydrides showing volumes characteristic of divalent and trivalent metals. The mixed valence for Yb + H (see section 6.6) and possible analogous mixed valency for Cf + H are shown as Δ. After Gibson and Haire (1990).

3.1.2. *Other structure-related phenomena*

As noted before, it is difficult to assess individual and combined effects of stoichiometry, temperature, and electronic transitions. Whereas the tetrahedral hydrogens are usually considered in the framework of a strongly bound "rigid-lattice", the less-strongly bound octahedral hydrogens can move more easily throughout the lattice until temperatures below about 200 K are reached. As the o-sites fill, diffusion becomes increasingly difficult. However, ordering of the octahedral hydrogens at low temperatures apparently drives various related tetragonal transformations that depend on composition, but not on occurrence of concomitant metal-to-semiconductor transitions. The displacement of the octahedral hydrogens in the {111} directions toward t-sites not only indicates the presence of attractive forces but also implies that the two kinds of hydrogens are somehow electronically different. This is considered again in more detail in section 6. In any case, filling of o-sites causes the lattice to contract until H/M nears 2.3–2.4 (with the exception of Np + H, as just discussed). Beyond this point, the intra-o-site forces appear to become repulsive. Concomitant occurrence of metal to metal-to-semiconductor transitions adds to the confusion.

Stalinski (1985) attempts to draw some semblance of consistency to these various effects in a review article. Specific-heat measurements, once the domain primarily of thermodynamics, are sensitive to both structural transitions, electronic transitions (e.g., metal-to-semiconductor) and magnetic effects. Ito et al. (1983) describes a series of sharp anomalies for $LaH_{3.0}$ and $LaD_{3.0}$ in the range 200–300 K, indicative of multiple ordering transformations, displacements, etc.

Although NMR is primarily a tool for measuring hydrogen-diffusion rates and defining mechanisms, it provides a method for tracking certain structural transitions. For example, large effects accompany the "freezing out" or ordering of octahedral hydrogens, as discussed by Göring et al. (1980) for $LaH_{2.69}$ and described in earlier work by Cinader et al. (1976) for PuH_{2+x}. Applications of NMR to electronic structure, magnetic effects, metal-to-semiconductor transitions, and diffusion will be discussed in appropriate sections.

3.2. *The alpha phase*

One of the most vigorous areas of study at the moment is the behavior of hydrogen in the alpha phase, the region of hydrogen solubility in the metal before a hydride phase appears. The composition range of this region can be highly variable, ranging from nearly negligible for the actinide hydrides to very large for the rare earths ($\sim 21\%$ for Lu + H at 298 K). Reasons for this variability are not well understood although it seems to track with the metal melting point. The locations of the hydrogen atoms, the kinds of diffusion, the effects on solid-state properties, etc. are subjects of intensive investigation and are reasonable well understood.

Historically, results of studies on the alpha phase show a nearly exponential increase in recent years. Bonnet (1976) and Bonnet and Daou (1979) show that the addition of hydrogen to the hcp rare-earth metals results in a smooth, near-linear expansion of the lattice up to the saturation limit. Whereas the cell volumes for a number of metals expand at a similar linear rate ($\Delta V/V = 1.0 \times 10^3$/at.% H), the c/a ratio remains close to

those of the parent metals. Filling of the smaller t-sites in the lattice is postulated because of strain observed during thermal expansion, a result consistent with accompanying neutron studies. Tetrahedral-site occupancy is confirmed in channeling experiments by Danielou et al. (1981). Studies on the Tm + H system by Bonnet and Daou (1979) show that a curious condition occurs upon cooling; instead of precipitating hydride, certain systems form temperature-independent, constant-composition solid solutions. The authors prophetically postulated that some sort of hydrogen pairing must occur.

As discussed by Daou et al. (1981), a large and consistent resistivity anomaly occurs for the alpha phases. This behavior appears in the 160–180 K range and implies an ordering of the heretofore randomly distributed t-site atoms by a process that reduces the strain energy of the system. On the basis of diffuse neutron scattering results, Blaschko et al. (1985) show conclusively that the hydrogens order as second-neighbor pairs along the *c*-axis, as depicted in fig. 9a. Interstitial hydrogens pair in the C and B (triangles) tetrahedra separated by metal atoms; occupation of positions A and D is then precluded by repulsive effects.

Other observations at this and other laboratories provides strong supporting evidence for the existence of ordering. Neutron-spectroscopy studies of $Y(H)D_{0.18}$ by Anderson et al. (1986) show a soft anharmonic potential along the *c*-axis and a low-temperature splitting of the *c*-axis vibrational modes. Further refinements for the Y + H system by Anderson et al. (1988) show that hydrogen diffusion between adjacent

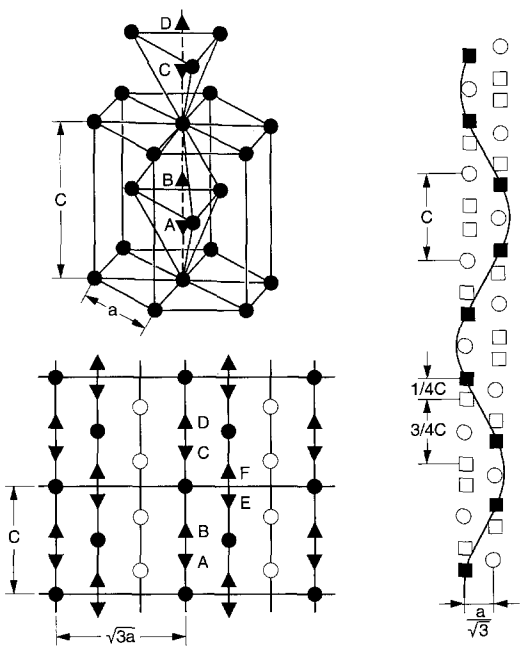

Fig. 9(a) Model for ordering of hydrogen pairs in the α-phase. Hydrogen occupies the C and B tetrahedra across the metal atom. Key: ● metal atom; ▲ t-site; ○ o-site. After Blaschko et al. (1985). (b) An example of the "chain" structure formed by H–M–H entities oriented in a typical lattice. ○ metal atom; □ unoccupied t-site; ■ occupied t-site. After Blaschko (1991) and Pleschiutschnig et al. (1991).

t-sites is an order of magnitude faster than the bulk diffusion rate. Similar results are reported for the Sc + H system by Udovic et al. (1990). The pairing phenomenon is now well-established for the Sc, Y, Dy, Ho, Er, Tm and Lu systems, which paradoxically have the smallest metal lattices and opt to form the stable low-temperature phase with short-range ordering (pairing) of the dissolved H atoms, instead of forming a hydride. A typical phase schematic is shown in fig. 10, for the Er, Tm and Lu systems.

Ordering in the alpha phase is predicted by calculation. In the first comprehensive theoretical study, Liu et al. (1989) use the self-consistent cluster model and the local-density approximation to successfully model the pairing mechanism. They identify an unusual double-well potential along the c-axis, with a barrier height of only 0.15 eV. The concept of comparatively rapid diffusion along the c-axis is consistent with a t–o-site barrier of 1.5 eV. The authors consider the NMR work of Lichty et al. (1989), who observed an anomalous change in the proton spin-lattice relaxation rate and interpreted the apparent lack of long-range order (between paired entities) as evidence of a disordered "proton-glass" system.

The French group has established a definite relation between the paired entities. As shown in fig. 9b, chains of hydrogen pairs form along the c-axis and become especially evident at the high hydrogen concentrations. Using diffuse neutron scattering, Pleschiutschnig et al. (1991) find recognizable relationships even at low concentrations ($x = 0.06$ and 0.08) for the Lu + D system. For $LuD_{0.19}$, the chain consists of three or four pairs with a periodicity of $\frac{3}{4}c$, as illustrated in fig. 9b. As discussed by Blaschko (1991), the particular "wave" of the chain is not unique; other similar structures are possible and fit the data well. The observed localized intensities, intensity ridges and ridge curvatures are well-reproduced. These inter-chain correlations show that the concept of a "proton-glass" in an amorphous or disordered sense cannot be correct. However, the origin of the periodic arrangement of $\frac{3}{4}c$ hydrogen pairs is not yet explained.

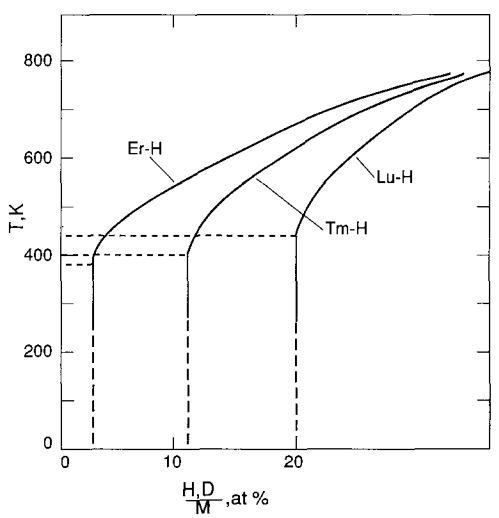

Fig. 10. Partial phase diagram for the α-solutions formed by Er + H, Tm + H and Lu + H. Low-temperature ordering and final compositions. After Burger et al. (1985).

Extension of internal-friction measurements to the alpha regions of Sc + H and Y + H by the French group provide evidence for ordering in other systems. Vajda et al. (1991) summarize this work along with earlier data on Lu + H. All three systems have a similar hydrogen-specific internal-friction peak (e.g., near 200 and 210 K for H and D in Sc, respectively) with activation energies for relaxation in the 0.54–0.61 eV range. Differences in the systems correlate with stiffness in the *c*-axis direction (Sc is most stiff) leading to concomitantly shorter chains. Relaxation is identified with a bulk rearrangement of occupied and vacant interstitial sites.

Another area of strong experimental interest is that of the mechanisms and paths for diffusion. Whereas low-temperature motion is through t-sites, higher-temperature motion is via t–o–t-site migration with no residence in the o-sites. There is some disagreement as to whether the motion is by hopping, by tunneling or by both processes; all possibilities describe the dynamics well. A detailed discussion of the general topic of diffusion is presented in section 6.3.2.

4. Thermochemistry

The thermochemical properties of the lanthanide-hydride systems have been well-catalogued by Libowitz and Maeland (1979). Heats, entropies and free energies of formation have been tabulated for both the dihydrides and dideuterides, as well as data for the La through Nd trihydrides and also the hydrogen-deficient hexagonal phases. Methods are described for typical calculations and are not repeated here. Thermodynamic data and thermal functions are presented by Flotow et al. (1984) and by Ward (1985a and b) for the hydrides of Th through Am. Newer data are reviewed here, and the values in table 1 reflect these updates.

4.1. *New rare-earth data*

The amount of new thermodynamic data produced since the summary of Libowitz and Maeland (1979) is disappointingly small. The values in table 1 are assembled for convenience and are weighted averages based on interpretations of the quality of the work in cases of disagreement. An example is provided by the La + H system. Uchida et al. (1979) measured hydrogen equilibrium pressures in the rage 10^{-4}–10^{1} mbar at temperatures from 773–1023 K, but do not describe the method of temperature measurement. High-purity hydrogen and extended sample outgassing were employed, but the working vacuum was only 10^{-6} mbar. Plateau pressures for the two-phase region involving hydrogen-saturated metal and hydride in equilibrium with hydrogen yield an average heat of formation $\Delta H_f^0 = -214 \pm 6$ kJ/mol H_2 equilibrium hydride. This is a rather high value in comparison to older results and can be compared to the work of Carstens (1981) who measured a value of $\Delta H_f^0 = -198.74$ kJ/mol H_2 (no limits given). His data for three hydrogen isotopes are given in table 4a, for the relationship $H(D,T)_2$ + La(sat. soln.) = LaH_2(solid) and for the solution of H(D, T) in the metal. However, Dantzer and Kleppa (1980) point out that heats of formation based on plateau pressure data cannot produce a correct ΔH_f^0 for stoichiometric MH_2 and note

TABLE 4a
Enthalpies and entropies of formation for $LaH(D,T)_2$.

Isotope	ΔH_f^0(kJ/mol)	ΔS_f^0(J/mol K)
H	−198.74	−142.25
D	−202.92	−148.11
T	−208.78	−153.13

TABLE 4b
Thermodynamic data for the alpha-phase region of La + H (D, T).

Isotope	ΔH^0(kJ/mol)	ΔS^0(J/mol K)
H	−71.13	−54.39
D	−71.13	−58.58
T	−66.94	−54.39

that the correct expression is

$$2/(2-\delta-x)\,[LaH_x(s)] + H_2(g) = 2/(2-\delta-x)\,[LaH_{2-\delta}(s)], \quad (1)$$

where x is the solubility of hydrogen in lanthanum and δ is a measure of hydride substoichiometry. These authors used a calorimetric-equilibrium method to measure the heat at 917 K. For a measured $x = 0.13$ and $\delta = 0.1$ (i.e., for $LaH_{1.9}$ at the phase boundary), they calculate $\Delta H_f^0 = -98.75$ kJ/mol for the plateau region, $\Delta H_f^0 = -68.20$ kJ/mol for the α-phase, and for the integration from $LaH_{1.9}$ to $LaH_{2.0}$, $\Delta H_f^0 = -28.35$ kJ/mol. The results for the α-phase compare favorably with values reported for the hydrogen isotopes in table 4b. By summing all experimental heat effects or by a complete Gibbs–Duhem integration of all the data, the average ΔH_f^0 for LaH_2 in both cases is -191.21 ± 1.26 kJ/mol.

Comparison of the measured pressures at 917 K for the three groups gives reasonable agreement; therefore the errors, if any, are not obvious. Several reasons are offered by Ward et al. (1987) who point out that hydrogen is no longer a good heat-transfer medium below about one torr pressure. In this pressure range, an internal thermocouple essentially imbedded in the sample may be as much as 30° cooler than that in contact with the pressure vessel. Thus, the mode of temperature measurement can be critial for pressures as low as those for the La + H system, and the resulting least-squares fit of the apparent plateau pressures can be skewed. Although hysteresis is probably not serious for the La + H system, slow diffusion and hindered movement of metal lattice atoms to equilibrium positions can be a factor at low temperatures. The nature of hysteresis has been considered in detail by Flanagan and Clewley (1982).

Another interesting example is the Sm + H system studied in the same laboratory by Uchida et al. (1979) and by Ohki et al. (1984) over the temperature ranges 773–1023 and 423–923 K, respectively. Ohki et al. (1984) extended earlier measurements to examine the cubic–hexagonal transition region and the hexagonal SmH_{3-y} phase. Whereas these authors found considerable hysteresis in the two-phase region $2.3 < H/Sm < 2.8$, more recent work by Wang et al. (1990), using ultra-high-purity material,

found a six-fold lower hysteresis effect. Their studies, over the temperature range 448–623 K in a UHV system, show the cubic–hexagonal plateau to extend from $2.5 < H/Sm <$ nearly 3.0; i.e., the hexagonal phase is very narrow, as shown in fig. 11. Furthermore, the hexagonal phase seems to disappear at higher temperature as it does for the Np + H system in fig. 6. Wang and co-workers attribute differences to less-than-accurate composition values by Ohki et al. (1984), and point out that their plateau pressures are lower at 573 K, but higher at 523 K, indicating some sort of systematic error and reemphasizing the importance of accurate temperatures for Van't Hoff plots. Their $\log P$ versus $1/T$ equation for the cubic–hexagonal region involving sub-stoichiometric SmH_{3-y} is

$$\log P(\text{bar}) = -(3400 \pm 200)/T + 5.90 \pm 0.20. \quad (2)$$

These authors discuss briefly the importance of sample purity and the manner in which the reaction is carried out, particularly in terms of the activation and subdivision of the sample. As shown by the comparison of thermodynamic values in table 5, the preferred dehydriding values of Ohki et al. (1984) are considerably different from those of Wang et al. (1990) who supply a detailed thermodynamic analysis showing that the system obeys regular solution theory.

Newer measurements for the early-lanthanide hydrides include those by Ohki et al. (1984) on the Ce + H system over the range 823–1023 K. Relatively sharp phase boundaries are observed up to 973 K for the metal-hydride plateau. Partial molar enthalpies for the CeH_{3-y} solid-solution region decrease rapidly with composition above the $CeH_{2.7}$ composition and tend toward zero at CeH_3. The suggestion that

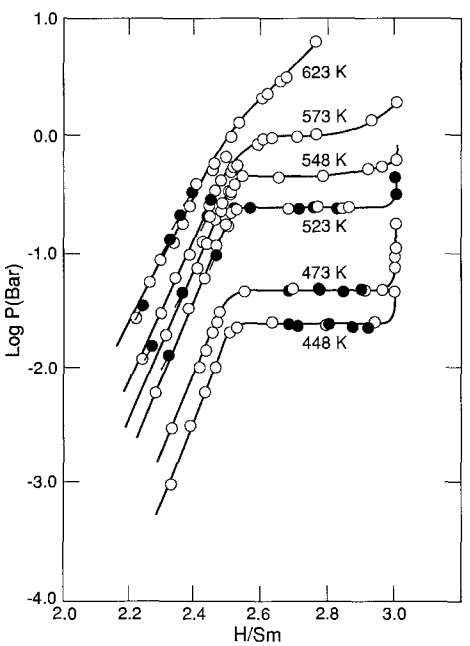

Fig. 11. P–C–T data for the cubic + hexagonal two-phase region of the Sm + H system. Key: ○ hydriding; ● dehydriding. Note the extremely narrow apparent range of the hexagonal phase. After Wang et al. (1990).

TABLE 5
Comparison of enthalpies and entropies for the reaction forming substoichiometric SmH_{3-y} from the hydrogen-rich cubic phase.

$-\Delta H^0$(kJ/mol H)	$-\Delta S^0$(J/mol K)	Temp. region (K)	Ref.
65.3 ± 4.0	113.0 ± 4.0	448–573	Wang et al. (1990)
74.6 ± 3.7	136.2 ± 6.8	523–623	Ohki et al. (1984)
79.6 ± 4.0	133.2 ± 6.7	523–623	Ohki et al. (1984)*

* Dehydriding.

sluggish kinetics observed for CeH_{3-y} arises from low reactivity of semiconductors with hydrogen is not supported by other measurements; rather, the rate is apparently limited by slow H transport through a lattice in which nearly all hydrogen sites are filled, a process that holds for both rare-earth and actinide systems.

The remaining early rare earth systems have also been investigated. Work published by Chernikov et al. (1987) for Ce + H, as well as for the Y + H and Er + H systems discussed later, does not show sharp phase boundaries, implying low sample purity. The calculated heat and entropy of formation for CeH_2 ($\Delta H_f^0 = -204.5$ kJ/mol and $\Delta S_f^0 = -147.1$ J/mol K) are in good agreement with results quoted in table 1. More recent work is reported by Ohki et al. (1989) on the PrH_2 + H and NdH_2 + H systems. For the first time, an incipient plateau observed during dehydriding of PrH_{3-y} implies existence of a phase change. Distinct plateaus found upon dehydriding of NdH_{3-y} confirm the earlier work of Mintz et al. (1974). Typical hysteresis appears with the dehydriding step providing faster kinetics, better-defined plateaus, and larger partial molar heats than the hydriding step. Calculated enthalpies and entropies are listed in table 6.

As noted earlier, the later lanthanide hydride systems generally have a broad cubic–hexagonal plateau region driven by the small cubic lattice and the need to accommodate additional hydrogen as the composition increases. Chernikov et al. (1987) measured plateaus for Er + H up to the dihydride composition, and report ΔH_f^0 for $ErH_2 = -203.3$ kJ/mol ($\Delta S_f^0 = -137.0$ J/mol K), a value considerably lower than the average of earlier results shown in table 1. The presence of highly curved phase boundaries indicate impure samples. Müller and Knappe (1982) report lattice parameters for the Tm + H and Tm + D systems, but supply no thermodynamic values. During dehydriding at 300°C, the cubic–hexagonal plateau extends from an H/M near 2.0 to 2.93.

TABLE 6
Enthalpies and entropies for the reaction forming MH_{3-y} phases of Pr and Nd from the hydrogen-rich cubic phase.

MH_{3-y}	ΔH_f^0(kJ/mol H_2)		ΔS_f^0(J/mol K)	
	hydr.	dehydr.	hydr.	dehydr.
PrH_{3-y}	−62.8	−88.6	−157	−181
NdH_{3-y}	−54.5	−89.9	−129	−170

As shown by results for the Lu + H system from Subramanian and Smith (1982) in fig. 12, the metal-cubic hydride plateaus become very short for the later elements. Lu forms the smallest of all the rare-earth hydrides and has the highest solubility in the α-phase, as noted in section 3.2. Pressure–composition isotherms are reproducible between runs, with minimal hysteresis except at the lowest temperature of 824°C. Phase boundaries and pressure equations thus determined are in excellent agreement with earlier work. Gibbs–Duhem integrations of the measured data and a small extrapolation to the LuH_2 composition give $\Delta H_f^0 = -204.8 \pm 1.9$ kJ/mol and $\Delta S_f^0 = -136 \pm 2$ J/mol K.

A recent study of the Y + H system by Chernikov et al. (1987) over the range 873–1273 K confirm an apparent inflection in the ln P–$1/T$ data at about 1100°C. Data for the low-temperature range agree very well with the earlier work of Yannopoulos et al. (1965) and with that of Lundin and Blackledge (1962) for high temperatures. For the dihydride, they report $\Delta H_f^0 = -224.5$ kJ/mol and $\Delta S_f^0 = -149.2$ J/mol K at 873–1073°C and $\Delta H_f^0 = -192.7$ kJ/mol and $\Delta S_f^0 = -119.4$ J/mol K for 1173–1273 K. The origin of the slope change is not yet understood. The boundary of the α-phase is at $H/Y = 0.37 \pm 0.02$ and that for the substoichiometric dihydride is at 1.90 ± 0.02. Results of an interesting series of experiments involving gradual oxygen contamination from 0.15 to 1.66 mass % Y_2O_3 shows that the hydrogen pressure rises in a regular manner until an oxide layer forms on the hydride surface and remains constant thereafter.

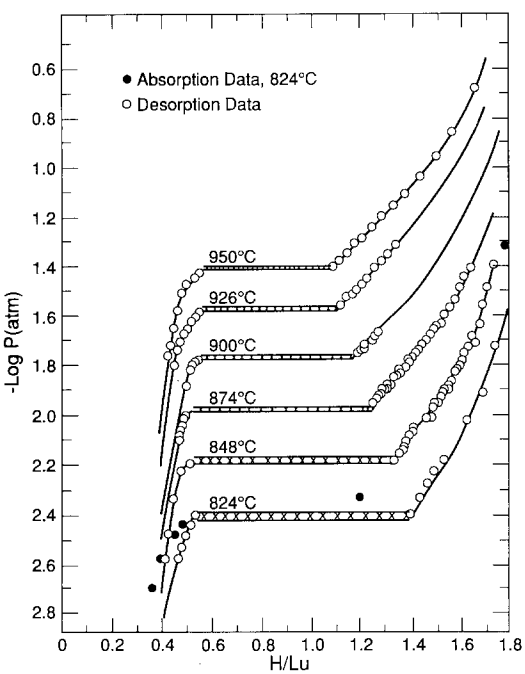

Fig. 12. P–C–T data for the α-phase + cubic two-phase region of the Lu + H system. The phase boundaries illustrate the extent of the α-phase and the narrow two-phase plateaus. Symbols are indicated on the figure. After Subramanian and Smith (1982).

4.2. *New actinide data*

Work on actinide-hydrogen systems through 1984 are assessed in detail by Ward (1985a). Additional relevant work has been published for the "rare-earth-like" transuranium systems of interest here. Ward et al. (1987) describe a new study on Np + H from 0.0005 to 70 bar pressure using doubly electrorefined Np metal. The P–C–T data are discussed above and are shown in fig 6. This experimental study resolved serious differences between two earlier reports, as reviewed by Ward (1985a) and by Flotow et al. (1984). For the reaction $0.94\ Np + H_2 = 0.94\ NpH_{2.13}$, the data are described by the equation

$$\ln P(\text{bar}) = 13.53 - 13421/T(\text{K}), \tag{3}$$

giving $\Delta H_f^0\ (NpH_{2.13}) = -118.8$ kJ/mol ($\Delta H^0 = -111.6$ kJ/mol of H_2) and $\Delta S_f^0\ (NpH_{2.13}) = -119.7$ J/mol K. Since the plateaus are flat and the phase boundaries are extremely sharp, the considerable population of o-sites below the odd phase boundary (see section 3.1.1 and table 2) implies a thermodynamic equivalence of o- and t-sites. Partial molar enthalpies and entropies are nearly constant over the cubic range; integral values calculated for the entire system are given in table 7. An anticipated maximum in 5f-electron effects observed for uranium and neptunium intermetallic compounds arises from the interplay of the number of 5f electrons versus bandwidth (see section 6). However, the unusually small heat of formation for NpH_2 and the extended plateau imply some 5f-electron influences, probably in Np(5f)–H(1s) interactions, but the Np–Np bond distance is large compared to 5f wave-function overlap. Note that the heat of formation for uranium hydride is even smaller (-84.6 kJ/mol H_2) than that for the neptunium phase.

The first truly rare-earth-like hydride behavior appears at plutonium. The dihydride exhibits a classical localized $5f^5$ magnetic moment (see section 6.4) and the lower phase boundary is near H/Pu = 1.9. However, other factors, such as the electrical resistivity, appear totally unrelated to the rare-earth hydrides (see section 6.3.1). A detailed publication by Haschke et al. (1987) summarizes the most recent understanding of the physicochemical and thermodynamic properties of the Pu hydrides. Data based on dehydriding studies lead to the revised high-temperature phase diagram shown in fig. 13. As noted in section 3.1.1, a metastable cubic modification apparently exists above $PuH_{2.7}$ at lower temperatures, along with the higher temperature results shown in figs. 5 and 13. Haschke (1981) and Flotow et al. (1984) thoroughly discuss and evaluate data for this metastable cubic modification, with values for $PuH_{1.9}$ corrected to

TABLE 7
Enthalpies and entropies of formation for neptunium hydrides.

Product	T(K)	ΔH_f^0 (kJ/mol product)	ΔS_f^0 (J/mol K product)
NpH_2	743	-111.6 ± 0.7	-112.4 ± 1.0
NpH_2	875	-122.9 ± 1.9	-125.5 ± 2.2
$NpH_{2.6}$	650	-138.5 ± 1.3	-144.1 ± 1.9
NpH_3	650	-153.9 ± 1.4	-174.0 ± 2.2

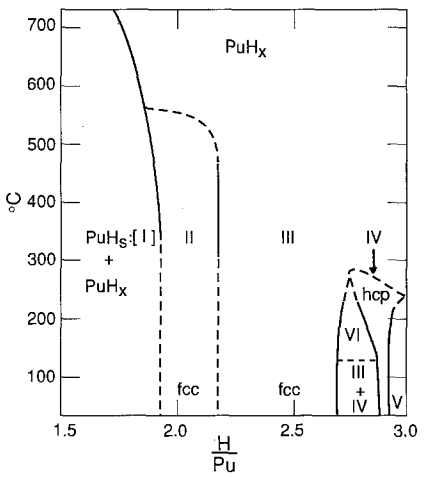

Fig. 13. The proposed phase diagram for the Pu + H system, showing the multiple domains suggested by the thermodynamic data in fig. 5. After Haschke et al. (1987).

298 K using experimental thermal functions. They also derive integral results for the higher compositions, commenting on the difficulties and approximations involved. For the plateau region, the composite equation for dehydriding is 1.11 Pu = 1.11 $PuH_{0.1} + H_2$, assuming the H/Pu limit for the α-phase is 0.1 (see below). The plateau pressures for H_2 and D_2 are defined by eqs. (4) and (5), respectively,

$$\ln P(H_2, \text{bar}) = 16.34 \pm 0.80 - (18975 \pm 175)/T(\text{K}), \tag{4}$$

$$\ln P(D_2, \text{bar}) = 15.70 \pm 0.02 - (17800 \pm 70)/T(\text{K}). \tag{5}$$

Enthalpies and entropies of formation for the extended-cubic-phase composition are given in table 8. For the stable high-temperature phases, Flotow et al. (1984) also derive thermodynamic data for compositions up to the trihydride by integrating the partial molar free energy data in fig. 5. For the phases identified in fig. 13, the average ΔS_f^0 per mol of H_2 is -136.8 ± 6.7 J/mol K for the cubic phase III and -182.4 ± 1.7 J/mol K for phase IV (hexagonal) and phase V, indicating a high degree of ordering. Integral values

TABLE 8
Enthalpies and entropies of formation for cubic plutonium hydrides at a median $T = 550$ K.

Product	ΔH_f (kJ/mol product)	ΔS_f (J/mol K product)
$PuH_{1.90}$	-155.6 ± 10.9	-138.5 ± 10.9
$PuH_{2.50}$	-190.4 ± 5.0	-175.7 ± 8.4
$PuH_{3.00}$*	-205.9 ± 4.6	-211.7 ± 11.7
$PuD_{1.90}$	-141.8 ± 1.7	-125.1 ± 3.8
$PuD_{2.50}$	-174.5 ± 4.2	-160.2 ± 7.5
$PuD_{3.00}$*	-189.1 ± 11.7	-188.3 ± 8.4

* Based on extrapolated partial molar free energy data.

for the hexagonal-related $PuH_{3.00}$ are $\Delta H_f^0 = -240.6$ kJ/mol and $\Delta S_f^0 = -271.5$ J/mol K at a median temperature of 461 K. These data may be compared with values for the high-stoichiometry cubic phase in table 8.

Heat capacities are measured by Oetting et al. (1984) for $PuH_{1.9}$ from 8 to 350 K and for $PuH_{2.0}$ from 340 to 670 K, using the 242 isotope. The low-temperature data join smoothly with the higher-temperature values and are described by the following equation (J/mol K),

$$C_p(PuH_{2.0}) = 47.307 - 0.1763(T, K) + 7.231 \times 10^{-4}(T, K)^2 - 5.845 \times 10^{-7}(T, K)^3. \quad (6)$$

Tabulated results and a detailed discussion are given in the paper.

A recent study on the narrow α-phase solubility region of Pu+H by Allen (1991) sheds interesting light on what may actually be occurring in these phases and related systems. Solubility data for hydrogen in solid and liquid Pu metal and solid delta-phase alloy complement earlier studies that defined equilibrium pressures and solubility limits summarized for the rare earths by Mueller et al. (1968) and Libowitz and Maeland (1979), and for the actinides by Ward (1985a and b). Detailed pressure-composition isotherms for the 475–825°C range show that H/Pu for the upper boundary of the solid and liquid solutions is continuous and varies exponentially with temperature. Observations are consistent with earlier results indicating markedly lower solubility limits for actinides than for rare earths. Extrapolation of the results shows the H/Pu values for the phase boundaries at 25 500 and 1000°C are 10^{-9}, 0.003 and 0.1, respectively. Data for the delta-phase alloy (1 mass % Ga) shows a higher solubility limit (H/Pu = 0.008 at 500°C) and a lower temperature dependence than for the unalloyed metal.

Integral thermodynamic values are derived for the α-phase by Allen (1991). The pressure-composition data are unanticipated and raise questions about the nature of the solution. Enthalpies of formation for the solid and liquid solutions are comparable with changes of about − 84 J for each 0.01 mol of H dissolved in the metal. As evidenced by the absence of a resolvable temperature dependence for the $\ln P$ versus H/Pu isotherms, the derived entropies of formatiom for the solutions are essentially zero. This result is inconsistent with a ΔS_f^o value near -130 ± 20 J/mol K H_2 observed for condensed hydride phases (see tables 4a, 7 and 8) and implies that the disorder of H atoms in solution with plutonium is comparable to that for gaseous H_2.

5. Kinetics

5.1. *General observations*

Kinetic studies of hydride formation are somewhat limited for both the rare earths and the actinides. Early work for the rare-earth elements is reviewed by Libowitz and Maeland (1979); work for the actinides is described in a recent review by Haschke (1991). In comparison to work on the acinides, kinetic studies on rare-earth hydriding are at present a dormant area. Only the U+H reaction is extensively investigated to

date, and definition of this system in this chapter should establish a foundation for future work with other reactions.

Results of kinetic studies suggest that the formation reactions of the rare-earth and actinide hydrides are similar multi-stage processess occurring with formation of adherent product layers on the metal surfaces. The reaction rate, r, is dependent on the surface area of the reacting metal, the hydrogen pressure P, and the temperature T. The value of r may be influenced by a variety of secondary parameters, including surface conditions, the process history of the metal, gas purity and the sample geometry.

Multi-stage reactions are described for the rare earths by Libowitz and Maeland (1979) and for the actinides by Haschke (1991). The four sequential stages are: (1) induction or nucleation, (2) acceleration, (3) bulk and/or linear reaction, and (4) deceleration to termination. The induction stage is associated with initiation or nucleation of microscopic reaction sites on the metal surface. During the acceleration stage, nucleation sites grow until the entire surface is covered by hydride. The bulk stage is typically a constant-rate process that generates the largest fraction of hydride and is frequently identified as the linear stage because the extent of reaction versus time curves are usually linear. However, data for both rare-earth and actinide systems at conditions for which the surface is highly activated suggest that the bulk stage is a two-step "paralinear" process in which the linear regime is preceded by a parabolic time-dependent region. The terminal stage is, of course, characterized by a steadily decreasing rate, as either the metal or the gas is consumed.

5.2. *Kinetics of bulk hydriding*

Similarities between the 4f and 5f elements are seen in their behavior during bulk hydriding, the only stage of the reaction that has been extensively studied. Data for both series of elements show that the area-normalized hydriding rate varies with T and P as shown by the following equation,

$$r\ (\mathrm{H_2}\ \text{consumed/unit area of metal}) = k\, \mathrm{e}^{-E_a/RT} P^n. \tag{7}$$

The temperature dependence is described by the Arrhenius term and the pressure dependence is defined by the pressure exponent n. Kinetic observations may appear inconsistent if r is simultaneously altered by both temperature and hydrogen pressure.

An understanding of the temperature–pressure interdependence is essential for interpreting the kinetics of bulk hydriding. Sufficient data for defining these relationships are available only for the U + H system; an in-depth analysis of this system can provide an example for the behaviors to be anticipated for other systems. Although numerous rate studies of U + H are described, this evaluation is based on reports by Bloch and Mintz (1981) and Powell et al. (1991). Experimental rate data from these studies are presented in fig. 14 as $\log r$ versus $\log P$ isotherms. Correlations of results from the two reports is, however, complicated by small differences in experimental temperatures and in observed rates. These differences are resolved in fig. 14 by combining data sets for 21 and 25°C and for 80 and 90°C into single isotherms for 23 ± 2 and 85 ± 5°C respectively, and by incorporating a five-fold increase in the values of r reported by Bloch and Mintz (1981). This modest adjustment in rate lies within the

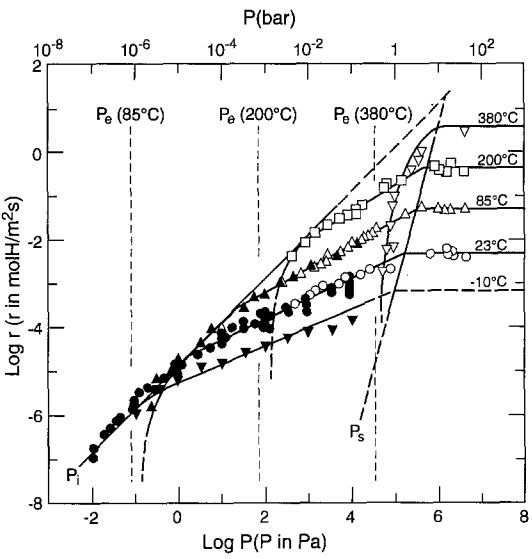

Fig. 14. $\log r$ versus $\log P$ isotherms for the $U + H_2$ reaction. Vertical lines show the equilibrium hydrogen pressures for the $U + UH_3$ two-phase region at the indicated isotherm temperatures. Data points measured by Bloch and Mintz (1981) are shown by open symbols; those derived from Powell et al. (1991) are shown by solid symbols.

bounds of the fifteen-fold change induced in r by Condon (1975) in studies where the annealing temperature of the metal was varied. Data points obtained from the study by Bloch and Mintz (1981) are indicated by open symbols and those derived from Powell et al. (1991) are shown as solid symbols.

The isotherms $\log r$ versus $\log P$ in fig. 14 show three regions with different pressure exponents defined by the slopes of the isotherms. At hydrogen pressures greater than a few bar, $n = 0$, showing that r is independent of P and dependent only on Tas shown by the spacing of the isotherms. At low pressures the curves converge to a single line with $n = 1$ and r depends only on P. At intermediate pressures the values of n are in the 0.5 ± 0.1 range, and r depends on both T and P. The differences in pressure exponent imply that r in each of the regions is controlled by a different kinetic process.

A fourth region of kinetic behavior is shown by the isotherms for 85, 200 and 380°C. In each case, r approaches zero as a limiting value of P is reached. As indicated by the vertical dashed lines, each limiting pressure is P_e, the temperature-dependent equilibrium pressure for the two-phase region in which hydrogen-saturated uranium coexists with the trihydride. P_e values are based on the equilibrium pressure equation recommended by Flotow et al. (1984). In all the temperature regimes, $\log r$ deviates from its pressure-related slope if $P < 10P_e$.

Each of the four kinetic regions observed in fig. 14 corresponds to control of the bulk hydriding rate by a separate process. The decrease in r as P approaches P_e is clearly thermodynamic in nature because r approaches zero as the thermochemical activity gradient driving the reaction approaches zero. As described by Haschke (1991), the approach to equilibrium gives rise to the rate decreases observed at high temperature in Arrhenius data for the U+H system under isobaric conditions. Unlike the $U-UH_3$ system, equilibrium pressures for the metal–hydride systems of the lanthanides and transuranium actinides are not in the 0.1 to 1 bar range frequently employed in hydride

preparation. Consequently, thermodynamic control may not be readily encountered with other elements.

The three kinetic regions with different pressure exponents correlate with the concentration of hydrogen on the surface of hydride-coated metal as defined by Langmuir adsorption theory. The dependence of the bulk rate on the hydrogen pressure parallels that of Θ, the fractional surface coverage. By varying P over many orders of magnitude as in fig. 14, the value of Θ for H_2 is forced to successively enter three regions of surface coverage described by a Langmuir isotherm: (1) a regime of negligible adsorption or bare surface at low pressure, where $n = 1$ and Θ is proportional to P, (2) a regime of moderate adsorption at intermediate pressures, where n assumes fractional values and Θ is proportional to P^n, and(3) a regime of complete coverage where $n = 0$ and $\Theta = 1$. These Langmuir regions correspond directly with the regions of pressure dependence in fig. 14 and facilitate their interpretation.

In the low-pressure region the effective surface concentration of hydrogen is zero and the hydriding rate is determined by the impingement of H_2 on the surface. According to kinetic theory the molecular collision frequency is proportional to $T^{-1/2}P$. The inverse square-root temperature dependence of r is imperceptible over a range in which T varies by a factor of two or three. As indicated by line P_i in fig. 14, the first-order pressure dependence is evidenced by coalescence of data for all isotherms as a temperature-independent set with unit slope. The observed rate for the $U + H_2$ reaction is, however, substantially less than the impingement frequency and shows that only one collision in 10^4 leads to product. Within the $n = 1$ region, the rates of all kinetic processes occurring in the solid phase are faster than the rate of effective collision with the surface. In addition to the concentration of active collision sites on the surface, the hydrogen pressure determines the collision frequency and r is independent of the Arrhenius term in eq. (7).

At high pressures, where $n = 0$ and $\Theta = 1$, the solid surface is saturated by H_2 and the hydriding kinetics are unaltered by changes in pressure. The rate is then controlled by a process occurring within the solid and depends only on temperature, as defined by the Arrhenius term. As fixed by the pressure-independent isotherms beyond the saturation boundary indicated by P_s in fig. 14, E_a for the rate-controlling process in the solid phase is 29 kJ/mol as determined by Bloch and Mintz (1981).

In the intermediate kinetic region between P_i and P_s, n and Θ assume fractional values and the bulk rate for $U + H_2$ is determined by a combination of condensed-phase and gas-phase properties. Both the Arrhenius and pressure terms in eq. (7) are required to define r and their combination leads to a complex situation. Values of n increase systematically with T from 0.40 at -10°C to 0.61 at 200°C, and measured E_a values increase regularly from zero at P_i to 29 kJ/mol at P_s. Θ and r increase with increasing P along an isothermal section, but their behavior is divergent along an isobaric section. Although increasing Tat constant P increases the rate, that increase is attenuated by a concurrent decrease in Θ. As discussed by Wicke and Otto (1962), the square-root pressure dependence indicates that hydride formation proceeds by a dissociative process involving formation of H atoms at the gas–solid interface.

Although the existence of four kinetic regions for the bulk stage of the $U + H_2$ reaction presents a somewhat confusing picture, the regions and their relationships are

delineated by the log P versus T kinetic diagram in fig. 15. The boundary lines in the diagram are defined using log P versis $1/T$equations for P_e from Flotow et al. (1984), by those derived for P_i and P_s in fig. 14, and by $P_a = 10P_e$. Ultimate thermodynamic control (no reaction) exists in the region where P is less than P_e. The equilibrium condition is bounded on the high-pressure side by a region of activity control at all temperatures. At pressures greater than P the rate-controlling process depends on T and P. Gas-phase (impingement) control occurs at low pressures and at temperatures less than 175–200°C. Reaction control by the condensed phase appears only at high pressures. Combined control by both gas-phase and condensed-phase behavior is confined to temperatures less than 400–425°C and pressures between P_i and P_s.

An understanding of the competition between gas-phase and condensed-phase properties for rate control is essential for correctly interpreting kinetic data. As discussed by Haschke (1991), measured E_a values for $U + H_2$ span a range from 8 to 33 kJ/mol and include several intermediate results. One must be concerned about the origin of such behavior and about identifying the correct value for E_a. In light of the preceding discussion, a range of activation energies between zero and about 30 kJ/mol is expected for measurements in the region of combined control. An excellent correlation is found between observed E_a values and experimental pressures. Although each E_a defines the temperature dependence for the test condition, only the pressure-independent value obtained for the saturated condition correctly defines E_a for the rate-

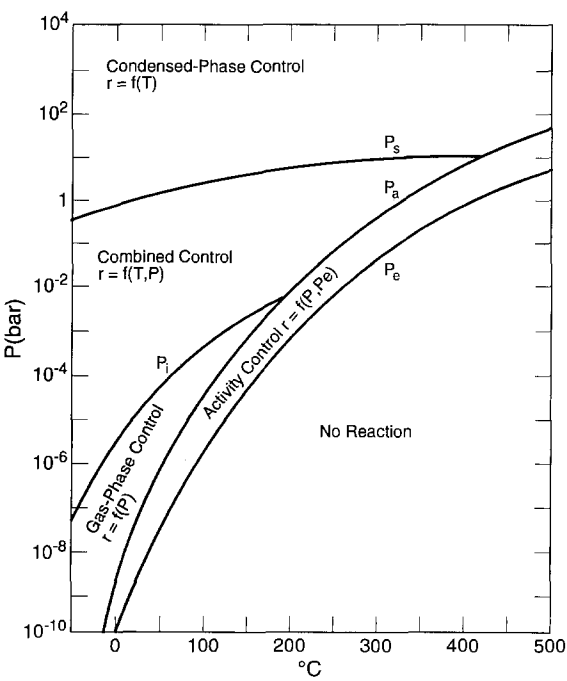

Fig. 15. Temperature–pressure regimes showing control by different kinetic processes for the $U + H_2$ reaction.

limiting process of the solid phase. A value of E_a should not be adopted for a mechanistic interpretation of reaction control unless the measurement is in a region where n is zero.

Results of Uchida et al. (1991) for the La + H_2 reaction also show pressure behavior consistent with Langmuir adsorption. Measurements at −196 and 25°C show that n is zero for bulk hydriding and imply that the solid surface is saturated at H_2 pressures as low as the 10^{-10} bar. Pressure exponents are also reported for dissolution of hydrogen in the clean La metal, and for metal with a preadsorbed oxygen film. As P increases, n for the reaction of oxide-coated metal changes from 1 to 0.5 across the miscibility range of the metal, and ultimately to $n = 0$ as the metal + hydride (bulk stage) region is entered.

Recent measurements of hydriding kinetics for plutonium power (0.2 to 0.3 m^2/g) by Stakebake (1992) show that the reaction is adsorption controlled at low pressures and reaction controlled at high pressures. Results for wide ranges of temperature (−41 to 350°C) and pressure (0.05 to 200 Torr) are consistent with earlier observations by Stakebake (1981) for a powdered delta-phase alloy. In addition to confirming that the rate is independent of temperature, the combined data show three regions of pressure dependence with $n = 1, \frac{1}{2}$ and 0 at low (< 0.5 Torr), intermediate and high ($P > 7$ Torr) pressures, respectively.

The kinetic regions identified for the bulk stage of U + H_2 are also anticipated for the bulk hydriding reactions of all the rare earths and later actinides. However, the pressure and temperature conditions at which these regions appear are expected to differ from element to element. At temperatures of interest, the P_e curves for other metal–hydrogen systems generally lie well below those for U + H. The locations of the various kinetic regions in P–T space also depend on other system-specific properties such as H_2 adsorption, physical state of the hydride, and the bulk reaction rate. Extensive data are needed to define the regions for each system, and certain areas may be experimentally inaccessible with normal procedures.

5.3. *Mechanisms*

Mechanistic evaluations of the hydriding process appear primarily in the actinide literature and the conclusions reached by various workers are diverse. Some investigators attempt to describe the entire multi-stage hydriding process using a model with a single rate-controlling step. Valid interpretations can only be based on extensive P–T data for a single kinetic region of a specific reaction stage.

Extent-of-reaction versus time isotherms are primary indicators of the reaction stage and mechanism. General observations for the rare earths by Libowitz and Maeland (1979) agree well with those reported for the actinides by Haschke (1991). Extent versus time curves frequently have sigmoidal shapes at low temperatures, but are parabolic or paralinear at high temperatures. Such observations are addressed by Gerard (1987), who concludes that the two shapes appear because of differences in nucleation behavior. A sigmoidal reaction isotherm is generated by nucleation and growth of isolated reaction sites on the metal surface. A parabolic curve is observed for a process in which the reaction initiates instantaneously on a totally activated surface.

The nucleation and growth processes are poorly characterized. Owen and Scudamore (1966) observed that nucleation of the $U + H_2$ reaction occurs at grain-boundary inclusions and at a second type of isolated surface site. Bedere and Sans (1983) present a mechanism for nucleation and growth. Recent work by Bloch et al. (1989) shows that initiation of $U + H_2$ is strongly dependent on thermal pretreatment of the sample, and involves desorption of hydroxyl groups and oxygen segregation.

A bulk gas–solid reaction typically forms an adherent product layer on the reactant surface and the rate is frequently controlled by diffusion of reactant through that layer. The rate of such a reaction decreases with increasing layer thickness and the integral rate equation for the process has a parabolic time dependence. Paralinear behavior is observed if spallation of the product initiates after the layer reaches a certain thickness. A region of linear time dependence is entered because the spallation process maintains a constant average thickness of product layer and results in a constant average rate. As discussed by Haschke (1991), a parabolic curve is not observed for a diffusion-controlled process if the reaction nucleates at isolated sites. Diffusion control occurs at the centers of the sites, but the parabolic dependence is masked by the accelerating kinetics of site growth and thus results in a sigmoidal reaction-extent versus time curve.

The rate of bulk hydriding in the pressure-independent kinetic region may be limited by any of the successive processes occurring in the condensed phase during reaction. Major steps include accommodation and dissociation of hydrogen at the solid–gas interface, transport of the atomic species through the surface layer of hydride, and formation of product at the hydride–metal reaction interface. The review by Haschke (1991) of rate-controlling steps proposed for $U + H_2$ by various workers shows a lack of consensus because each of the steps listed above is identified by one or more investigators as rate-controlling. Empirical and theoretical models are described and used to predict rate behavior beyond the experimental ranges, and as a basis for validating mechanistic interpretations. The results obtained using several such models to fit $\log r$ versus $\log P$ isotherms are compared by Powell et al. (1991).

Although the rate-controlling step for the bulk hydriding stage cannot be definitively identified and may differ from system to system, the appearance of parabolic curves for many elements suggests that hydriding is controlled by diffusion through the product layer. Rate versus time data presented by Powell (1989) for several rare earths and actinides show pronounced decreases in rate prior to attainment of the constant value, and strong evidence is found for diffusion control of $U + H_2$. Metallographic data presented by Bloch and Mintz (1981) show that a coherent hydride layer is present on the uranium surface during reaction. Activation energies of 26 and 35 kJ/mol meausred by Spalthoff (1961) and Grunzweig-Genossar et al. (1970), respectively, for hydrogen self-diffusion in uranium hydride, are in good agreement with the E_a derived for the pressure-independent kinetic region by Bloch and Mintz (1981). In evaluating $Th + H_2$ and $U + H_2$ kinetics, Haschke (1991) suggests that bulk hydriding of thorium is also controlled by diffusion and notes that the observed E_a for hydrogen self-diffusion depends on the stoichiometry (i.e., hydrogen-vacancy concentration) of the hydride and must be measured for the substoichiometric composition that coexists with the hydrogen-saturated metal during bulk hydriding.

5.4. *Rate data*

As shown by the results in table 9, the bulk hydriding rates of the rare earths and actinides lie in a range spanning four orders of magnitude. The rate for Pu is from Allen (1992) and the remaining values are derived by Powell (1989), who notes that the rates correlate well with the tendency of the metals to react with oxygen. Although other systematic trends are not evident, the highest rates appear for the early rare earths and the transuranium elements.

Results of rate measurements for certain elements in table 9 are described in other studies. Data for the Th+H, U+H and Pu+H systems are reviewed by Haschke (1991). The rate estimated for Th by extrapolating Arrhenius data to 25°C is a factor ten lower that measured by Powell (1989). Recent work includes the study of $La+H_2$ by Uchida et al. (1991); the pressure-independent rate observed by these authors for bulk reaction on clean metal films with a hydrogen-saturated ($n=0$) surface at 25°C is a factor of 10^4 less than that in table 9.

The discrepancy in the measured hydriding rates of La+H may originate from differences in the behavior of massive metal versus thin-film samples. Kinetic results are reported by Atkinson et al. (1976) for the reactions of several rare-earth metal films with hydrogen at low pressures (10^{-10} to 10^{-7} bar) and low temperatures (−196 to 100°C), conditions similar to those employed by Uchida et al. (1991) for the $La+H_2$ reaction. The initial sticking probabilities approach unity and the corresponding rates for Ce, Pr, Nd, Gd, Dy, Ho and Er are comparable to those reported for La, but are a thousand-fold larger than that for Sm. After remaining essentially constant across the metal–dihydride two-phase regions, the rates decrease sharply beyond the dihydride stoichiometries. Results reported for $Pu+H_2$ by Haschke et al. (1980) show that a similar decrease in r is not observed across the $PuH_{2.0}$–$PuH_{2.6}$ range. Differences observed between the hydriding kinetics of massive and powdered actinides are discussed by Haschke (1991).

TABLE 9
Bulk hydriding rates for rare earth and actinide elements at 0.10 bar hydrogen pressure and 25°C.

Element	Rate, mmol H/m²s
Pu	500 ± 60
Ce	22 ± 3
Nd	13 ± 2
La	5.0 ± 0.5
U	1.00 ± 0.05
Gd	0.7 ± 0.1
Y	0.5 ± 0.2
Th	0.040 ± 0.005

6. Solid-state chemistry and physics

As noted in the introduction, the majority of new work for the rare-earth and rare-earth-like actinide hydrides has been in the exciting areas of solid-state physics and chemistry. New and more precise techniques, especially in the area of surface science, improved low-temperature capabilities, and powerful computers for sophisticated electronic structure calculations, have encouraged many researchers to enter the field of hydride studies.

6.1. *Surface and near-surface properties*

Although the early and fundamental band-structure studies by Switendick (1970, 1971) (see also section 6.2) preceded the bulk of photoemission research, the major understanding of the electronic structure of hydrides, especially with regard to core-level effects, comes mostly from surface-science experiments. However, many of these experiments have also included parallel computational studies.

The basic concepts are well-illustrated by a series of studies performed at the University of Wisconsin Synchrotron Radiation Center to take advantage of both the tuneability and resolution of the synchrotron. Weaver et al. (1979b) published photoelectron spectra for ScH_2, YH_2 and LuH_2, comparing these results with an earlier optical absorption study by Weaver et al. (1979a) and a concomitant KKR self-consistent calculation by Peterman et al. (1979). In these optical absorption studies, carried out over the range $0.2 < h\nu < 5$ eV at 4.2 K, a consistent sharp rise in absorptivity appearing above 1.4 eV is interpreted as a screened-plasmon effect. Interband absorption becomes predominant above 1.5 eV. The photoelectron spectra agree with the early calculations by Switendick (1970, 1971) and show hydrogen-derived bonding bands from approximately 3 to 10 eV below the Fermi level, with a concomitant drastic decrease of d-band intensity in the conduction band. For LuH_2 the sharp $4f_{5/2,\,7/2}$ levels superimpose at -7.75 and -9.15 eV.

Studies of the $LaH_x (1.9 < x < 2.9)$ and $NdH_x (2.01 < x < 2.27)$ systems by Peterman et al. (1981) explore the effect of o-site filling. Photoelectron spectra for $LaH_{1.98}$, $LaH_{2.48}$ and $LaH_{2.89}$ are shown in fig. 16. Progressive depletion of the metal d- band with increasing composition is evident and nearly complete for the 2.89 (semiconducting) composition. For the so-called hydrogen-bonding band, a gradual shift to higher binding energy can be seen, along with a blurring out of structure at the lower photon energies. These peaks are attributed to low-angular-momentum states. Discussion of prior and concomitant band-structure calculations will be reserved for section 6.2. The spectra shown in fig. 16a, b and c are considered representative for most metallic dihydrides, with the caveats that the La + H system is single-phase cubic all the way to the trihydride, and that f-electron levels are superimposed for most of the other rare-earth and actinide systems.

Peterman et al. (1981) also extend optical spectroscopy measurements to include the LaH_x ($x = 1.9$, 2.04, 2.15, 2.36, 2.45, 2.63, 2.67 and 2.87) and NdH_x ($x = 2.01$, 2.21 and 2.27) systems. In addition to the sharp rise near 1.4 eV noted earlier, an octahedral feature appearing at about 0.4 eV increases steadily with increasing x and dominates

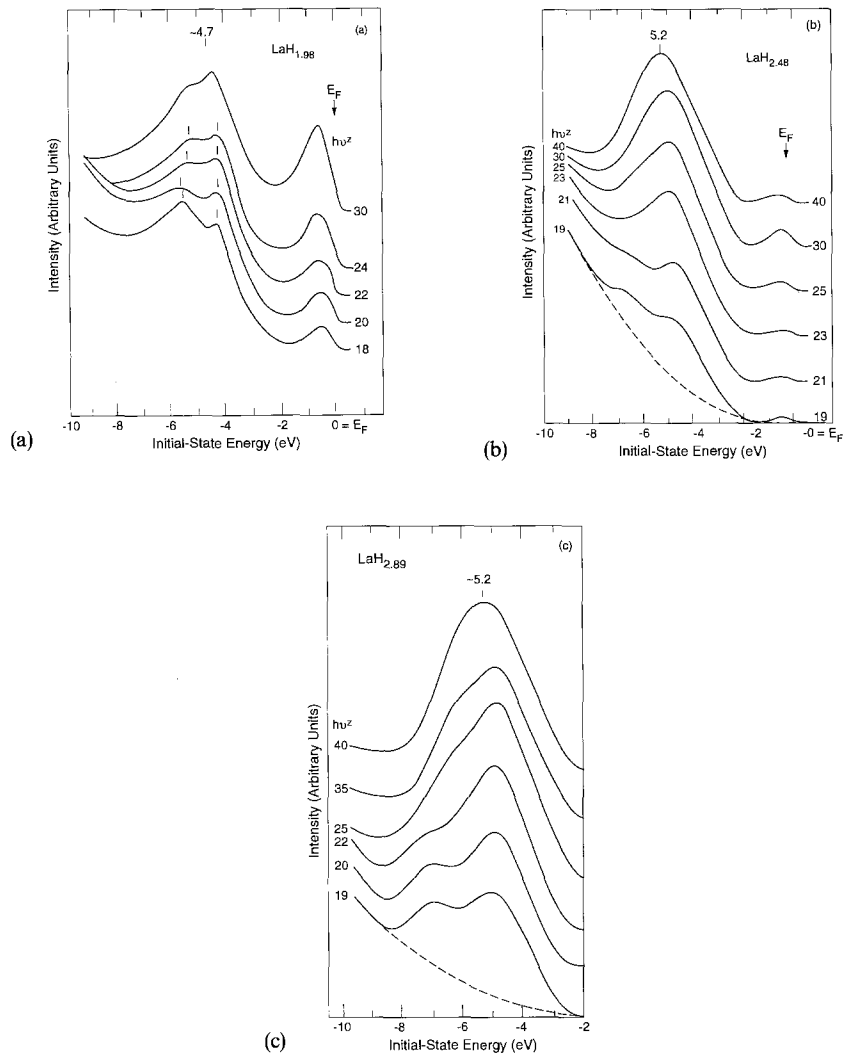

Fig. 16. Photoelectron spectra for (a) $LaH_{1.98}$, (b) $LaH_{2.48}$ and (c) $LaH_{2.89}$ showing progressive depletion of the conduction band with increasing composition. The behavior is typical for most rare-earth and actinide hydrides. After Peterman et al. (1981).

the spectrum at $x = 2.6$ as can be seen in fig. 17. Interband features also shift with concentration. Whereas a free-electron model fits the spectra for ScH_2 and YH_2 rather well, the fit is poor for $LaH_{1.90}$ because many o-sites are already occupied at the expense of t-sites, a phenomenon common to many rare-earth and actinide systems (see section 3.1). Optical absorption results are analyzed in great detail, but are beyond the scope of this chapter.

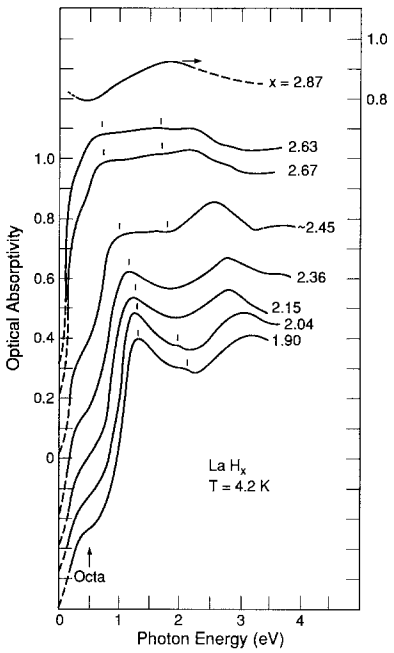

Fig. 17. Optical absorptivity data for several compositions in the La + H system. The rise of the o-site feature at about 0.4 eV is already evident at the phase boundary ($x = 1.90$), indicating a considerable occupancy of o-sites. After Peterman et al. (1981).

An extensive series of papers on photoelectron spectroscopy has come from Schlapbach and co-workers at the Laboratorium für Festkörperphysik ETH, Zürich. The first core-level data reported by Schlapbach and Scherrer (1982) for cleaved LaH_3 samples in UHV at 150 K show intense satellites on the low binding energy sides of the $3d_{5/2}$ and $3d_{3/2}$ peaks. These phenomena are explained as charge transfer shake-down screening of 3d core holes produced by the photoionization from the hydrogen-derived bonding band(s), with transfer of charge to a $4f^1$ level pulled below the bonding band. This explanation agrees with the observed data that include a chemical shift of about 3 eV relative to La metal as expected for charge transfer from La to hydrogen. Studies on the Ce + H system by Schlapbach and Osterwalder (1982) also show the disappearance of conducting states for $CeH_{2.9}$, as well as the intense 3d core-level satellites like those described for LaH_3. In addition, the Ce 4f peak is now superimposed about 2 eV below the Fermi level. More detail is supplied in a companion paper by Schlapbach et al. (1982).

A review paper by Osterwalder (1985) on the photoemission (both XPS and UPS) and inverse photoemission (BIS) results for Y, La, Ce, Pr and their hydrides includes extensive references. XPS valence-band spectra for the metals and hydrides are shown in fig. 18. The common features for all the systems are clear; however, XPS instruments cannot resolve the f-peaks as well as UPS spectrometers. A very important point discussed by Osterwalder is the concept of hybridization, particularly with the supposedly localized 4f states. The overlap of appropriate symmetries and energies can result in a complex picture, particularly in the generation of low-lying states that are

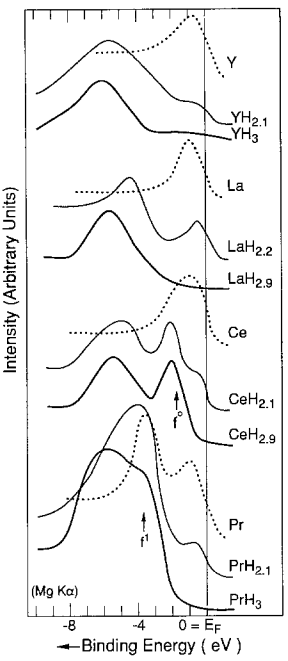

Fig. 18. Valence-band spectra for the La, Y, Ce and Pr and for their phase boundary and trihydride compositions. Data for the metals are shown by dotted lines. After Osterwalder (1985).

sometimes unexpected, but energetically favorable. Resonant photoemission experiments on LaH_2 by Peterman et al. (1983) show clearly a strong 4f-conduction band hybridization, in contrast to La metal. The effect becomes weaker as the 4f states become less extended at Ce and beyond. Influences on magnetic behavior are also important. For both the La + H (f bands initially above the Fermi level) and Ce + H (first and still fairly extended 4f level) systems, the screening just described is shown by Fujimori (1982) to involve strong hybridization of 4f levels with hydrogen 1s ligand orbitals, as mirrored in the enhancement of the photoemission satellites. This effect has major implications for the behavior of the actinide-hydride systems where the 5f levels are much broader and have energies in the midst of the conduction band.

Osterwalder (1985) introduces a very interesting and fascinatingly simple two-level hybridization model that readily explains observed spectra for both the metallic dihydrides and the semiconducting MH_{3-y} phases. The scheme, which is outlined in mathematical detail in two appendices, relates charge transfer to the position of the hydrogen-derived bonding band and considers the center of gravity of the metal d-band in relation to the position of the doubly occupied H 1s level. Since this separation is normally large, hybridization produces little mixing of states and a considerable amount of charge must be transferred from the metal to fully occupy the H 1s level, especially in approaching the trihydride composition. Alternatively, a smaller separation with more mixing from hybridization reduces the 1s character of the lower level and reduces the degree of charge transfer. The author notes that, while the levels are actually much broader than predicted, this simple model works rather well because the

actual selected states must have the proper symmetry. Although the real situation is rather complex, the qualitative success of the model is quite gratifying and provides a physically understandable picture of the processes in relation to band-structure calculations.

Photoelectron data are also reported for other early rare-earth hydrides. An extensive photoemission study of Pr, $PrH_{2.1}$ and a composition near PrH_3 is described by Fujimori and Osterwalder (1984) and in references cited by these authors. Initial versus final state effects and possible complications introduced by varying photoionization cross-sections are explored in detail. A large chemical shift between Pr and $PrH_{2.1}$ is related to major charge transfer from the metal to t-site hydrogens, but transfer is not detected for the trihydride. This observation agrees with the energy-band calculations of Misemer and Harmon (1982), which show the absence of charge transfer to o-site hydrogens. The two-level model of Osterwalder (1985) discussed above is relevant.

As an interesting sidelight to the properties of the early rare-earth hydrides, Schlapbach et al. (1986b) use UPS photoemission to show conclusively that a semiconductor-to-metal transition occurs *at the surface* of $LaH_{2.7}$ and $CeH_{2.7}$ below about 70 K. Significant d-electron charge reappears in a rather sharp peak near the Fermi level. The implication is that of a reduced concentration of H atoms in surface sites allows reconstruction to a more metallic configuration; i.e., the 5d states return from the bonding band to the conduction band. The effect seems to be independent of f-electron participation and proceeds in the direction of depopulating the higher energy o-sites upon cooling, as discussed in sections 3 and 4. Results by Schlapbach et al. (1987) for $GdH_{2.0}$ and $TbH_{2.2}$ in fig. 19 show a major low-temperature enhancement in

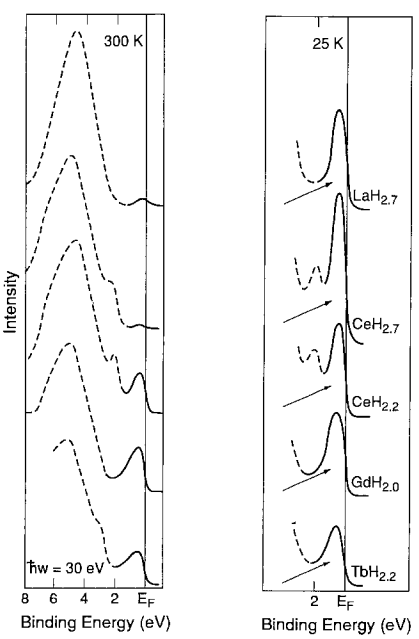

Fig. 19. UPS photoemission data for hydrides of La, Ce, Gd and Tb at binding energies near the Fermi level. Surface enhancement of d-character is seen (see text). After Schlapbach et al. (1987).

d character at the Fermi level, even for the dihydride. Since, as is discussed several times earlier, a considerable population of o-sites already exists in many systems at the dihydride composition, cooling tends to empty o-sites and refill t-sites (e.g., see table 2), making the material more metallic, irrespective of whether hydrogen moves from surface to bulk as the authors suggest.

Extensive photoemission data are not reported for the later-actinide hydrogen systems. Although nothing is available for Np + H, results are presented for Pu + H and Am + H. As shown in fig. 20, Ward et al. (1992) report valence band and 4f core-level spectra for PuH_x prepared by hydrogen implantation and with a presumed composition near $x = 2$. The huge $5f^5$ peak dominates the valence band spectrum and all but obscures the H-derived bonding band and any d or s contributions, even though the 5f electrons are apparently fully localized. In contrast to Pu metal where the 5f peak is pinned at the Fermi level, the peak for PuH_2 is shifted by over 2 eV to a higher binding energy. It should also be noted that the high XPS photon energy greatly enhances the 5f peak due to a favourable cross-section. UPS data do not exist for this system. In contrast to the highly asymmetric metal spectra, the core-level spectra are quite symmetric and similar to those for simple trivalent Pu compounds. The change is, however, quite remarkable, implying a radical transformation from 5f screening for the metal to primarily 6d screening for the hydride. Data are not reported for higher compositions.

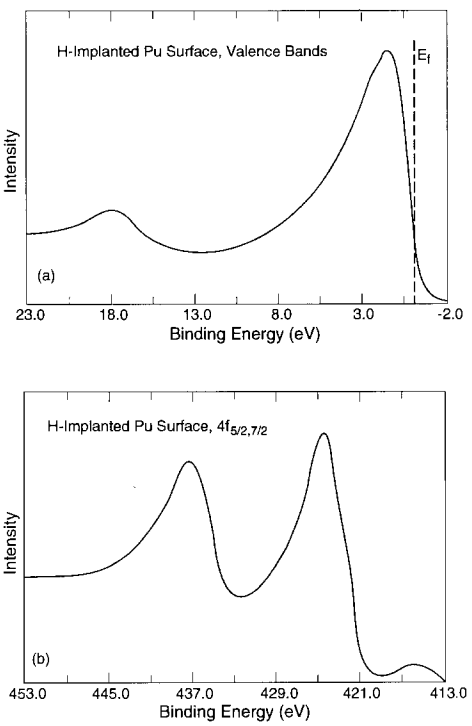

Fig. 20. Valence (upper) and core-level (lower) XPS spectra for plutonium hydride. A valence band shift of over 2 eV toward higher energy is seen relative to the metal. The symmetric core-level 4f peaks are characteristic of the Pu^{+3} ion with concomitant 6d screening. After Ward et al. (1992).

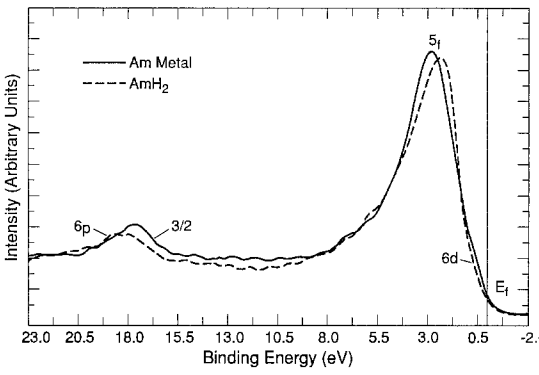

Fig. 21. Valence-band XPS spectra for Am metal and AmH_2 showing trivalence for both systems. Positive chemical shifts indicate electron transfer from metal to hydrogen. After Cox et al. (1992).

In a recent publication, Cox et al. (1992) presents photoemission data for Am metal and AmH_2. Both materials are expected to exhibit fully localized rare-earth-like spectra; nevertheless, as shown in fig. 21, the $5f^6$ peak distribution is still dominant with its centroid about 3 eV from the Fermi level. As with the rare earths, a reduced conduction-band intensity can be seen quite clearly. Positive chemical shifts for all the metal levels (4f, 5p, 4d and 3d) indicate electron transfer from the metal. As expected, the $6p_{3/2}$ binding energy for AmH_2 increases by about 0.6 eV, an amount similar to that found for Ce and Pr. Although the peak maximum for AmH_2 appears to shift to lower binding energies, the centroid is actually coincident with that for Am metal. In spite of these complications, cross-section effects and initial–final state considerations, the Am + H system is clearly the first unambiguously rare-earth-like actinide-hydride system. These observations are corroborated by resistivity measurements described in section 6.3.1.

6.2. *Electronic-structure calculations*

Even after years of study, the nature of the hydrogen atom and how it might change with hydride composition is not fully understood. Although the "protonic-versus-hydridic" controversy has been laid to rest (hydrogen is certainly not "protonic"), the question of "how hydridic?" remains and the details of charge transfer are still being discovered. The high metallic conductivity of the rare-earth hydrides (but *not* NpH_2 and PuH_2) is usually attributed to an enhancement of d character at the Fermi level as the non-conducting (scattering) d states are pulled down to form hydrogen-derived bonding bands. What happens as the o-sites begin to fill is, however, still a subject of much discussion.

As noted in section 6.1, the basic electronic structures of the metal hydrides are rather well delineated by the various photoemission studies. The abilities of various calculational methods to reproduce experimental data or even now to predict new results are remarkably good. One puzzlement has been at least partially removed by the realization that some artifical band-broadening must be introduced to better simulate experimental data, either because of intrinsic (i.e., real) electronic effects or because instruments have limited resolution.

A variety of calculational models have been used, and in general their sophistication and flexibility has increased steadily with time. A description of the methods is, however, beyond the aegis of this chapter. The initial use of self-consistency and subsequent introduction of relativistic effects and spin–orbit coupling resulted from increased computer power and from the codes themselves. In general, the existence of the low-lying hydrogen-derived bonding bands is identified by all calculations, although not necessarily with the correct energies and usually with insufficient broadening. The d-electron population in the metal conduction band, and its depopulation as hydrogen is added, are rather well-simulated. The ability to forecast the electronic structures of the empty states above the Fermi level is particularly valuable, especially in conjunction with the newer inverse photoemission capabilities. Results indicate that the empty states are mainly of d character.

Since most of the salient features concerning structure, electronic structure, bonding, and charge transfer are addressed earlier, particularly in section 6.1, emphasis here is placed on some of the more unique and perhaps still controversial results provided by theoretical calculations. Adequate references are, however, provided for the interested reader.

Results of early self-consistent calculations by Gupta (1978) on ErH_2 and by Peterman and Harmon (1979) on ScH_2 and YH_2 identify the major features noted for a dihydride. These include the typical overlapping metal–hydrogen bands, the concomitant diminution of the conduction band population with increasing hydrogen concentration, and the transfer of charge toward the t-site hydrogens. Sen Gupta and Chatterjee (1983, 1988) provide information on LaH_2, NdH_2 and more recently on SmH_2, showing the influence of the antibonding Γ_1 band. In the smaller lattice of SmH_2, this band begins to overlap the metal d states and results in a lower cohesive energy than for LaH_2, where the lower state is nearly filled. The authors use SmH_2 as an example to predict possible behavior for the later lanthanide dihydrides. See again the two-level hybridization model of Osterwalder (1985).

The first calculations for higher composition hydrides are presented by Gupta and Burger (1980), by Fujimori et al. (1980) and by Fujimori and Tsuda (1981). In detailed self-consistent calculations for both LaH_2 and LaH_3, Gupta and Burger (1980) recognize that the t-site and o-site hydrogens are non-equivalent, that the character of the complex hydrogen-derived bonding bands is not just H 1s-like and that the rigid-band model of charge transfer is only qualitatively applicable. Fujimori and Tsuda (1981), using the LCAO method, make computations on the CeH_2–CeH_3 system, promulgating the concept that the dihydride can be considered almost like a pseudo-metallic "element", with enhanced conductivity provided by "left-over" d-like conduction electrons. The concept, although overly simple, provides an understandable picture, including large charge transfer to t-site hydrogens, low resistivity, etc. The authors find shallow bonding levels between the third (o-site) hydrogen state and the remaining conduction electrons for CeH_2 as hydrogen is added, creating a new band between the valence and conduction bands. The implication is that the t-site and o-site hydrogens have sharply different properties. A band gap thus formed eventually leads to semiconducting properties with the composition range above $CeH_{2.7}$ being an n-type semiconductor as a result of hole-type donors in a defect band. [A somewhat

similar argument is offered by Libowitz et al. (1972) on the basis of resistivity measurements.] To a first approximation, calculations for $CeH_{2.75}$ in either a tetragonal or a cubic symmetry show that the gross electronic structure is basically unchanged. However, the calculated defect band seems too broad to support the Libowitz interpretation that the (narrow) defect band breaks up into localized states with the accompanying tetragonal distortion. Instead, an order–disorder transition is postulated at a critical defect concentration (H/Ce > 2.7), where electrons are localized in a higher-temperature disordered phase. A defect band forms in the lower-temperature ordered phase, giving rise to metallic conduction as postulated in the model by Anderson (1958).

In contrast, Kulikov (1982) calculates the band structures of LaH_2 and LaH_3, using self-consistent local-density functional theory. He stresses the importance and sensitivity of the choice for the crystal potential, finding incipient overlap between the conduction and valence bands for LaH_3. The concept leads to an excitonic insulator phase at low temperatures. The low-temperature phase is semiconducting, and the higher-temperature phase is metallic; i.e., the interpretation is opposite from that of Fujimori and Tsuda (1981).

Is LaH_{3-y} a semimetal or a semiconductor? A series of calculational studies undertaken by Misemer and Harmon (1982) attempt to provide more accurate insight into this problem. Their self-consistent calculations include relativistic corrections and spin–orbit coupling and confirm a large charge transfer to or towards the t-site hydrogens, with almost no transfer to the o-site hydrogens. The preferred coupling of the t-site orbitals (t_{2g} symmetry) in the {111} direction (tetrahedral symmetry) is well defined. In contrast, the o-sites are along the {100} direction that geometrically couple best to the e_g symmetry orbitals. In terms of bonding bands generated, both the geometric and electronic natures of these respective states become clear. The addition of the third band for LaH_3 partakes of the La e_g character, in agreement with the results of Fujimori and Tsuda (1981). The band structures and composite densities of states are shown in fig. 22. These calculations still do not define whether or not a true band gap develops for the trihydride (for the same complex reasons just discussed), but in any case the predicted gap should be quite small. Thus, the three sets of extended calculations for the La + H system presented here, although similar, result in at least semantic differences in the final interpretations, and the area remains one of considerable conjecture.

Mota (1985) and Mota and Borges da Costa (1987) take a radically different approach to formation of the third band appearing as the LaH_3 composition is approached. A model Hamiltonian is invoked to include major hybridization between metal d and hydrogen-derived s bands and to form the third band that appears in approaching the trihydride. A band gap that appears *between* the upper and the lower hydrogen-derived bonding bands provides an explanation for the metal/non-metal transition. Results published on Ce + H by Gilson et al. (1989) involve the same Hamiltonian and arguments as for La + H. However, the interpretation is in direct conflict with the work of Misemer and Harmon (1982) shown in fig. 22, and with photoemission results discussed in section 6.1. It is difficult to imagine that sufficient hybridization can occur to produce such a drastic change for these very large lattices. Unfortunately, little work

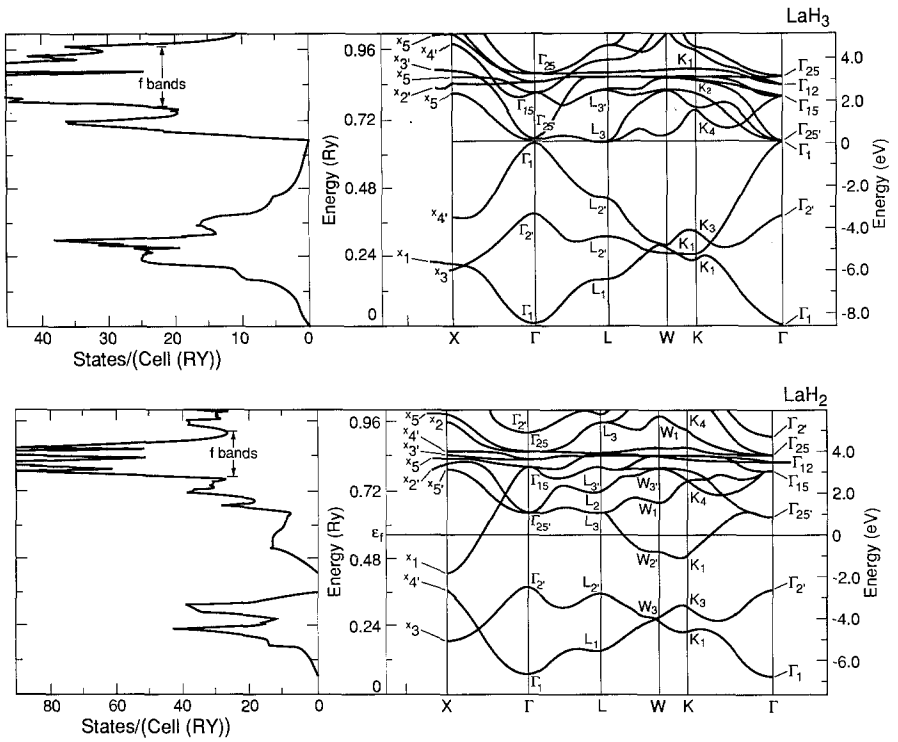

Fig. 22. Results of self-consistent band-structure calculations for LaH_2 (bottom) and LaH_3 (top). Depletion of conduction electrons at the Fermi level and large charge transfer toward t-site hydrogens is clearly seen in the LaH_3 curves. After Misemer and Harmon (1982).

has been done on the heavier (and smaller) lanthanide hydrides, other than that presented by Sen Gupta and Chatterjee (1988) for the Sm + H system, where significant overlap begins to be seen.

To date, only one relevant calculation is published for an actinide system. Eriksson et al. (1991) use the so-called "film linearized" muffin-tin orbital method (FLMTO) on Pu + H and Pu + O. Electronic structures of surface versus bulk configurations are addressed by this self-consistent method. The calculated density of states for PuH_2 shows strong hybridization of the metal 6d and H 1s states to form a broad bonding band about 7 eV below the Fermi level; i.e., in similar fashion to all the rare-earth systems discussed earlier. (The 5f electrons are considered to be localized, and do not appear in the densities of states.) In contrast to the results of Fujimori and Tsuda (1981) for Ce + H, these authors find little charge transfer to the hydrogen atoms. Although appreciable charge is lost by the Pu atom, the resultant charge distribution is concentrated in the interstitial region between the hydrogen atoms. This possibility was also proposed by Misemer and Harmon (1982) as an alternative interpretation for the observed spectra. The charge-density contour maps derived by Eriksson et al. (1991), using the latest and most sophisticated calculational codes, seem to confirm this

picture. Significant hybridization with ligand valence electrons is also seen and interpreted as giving rise to some covalency. Magnetic implications drawn from their spin-polarized results are considered in section 6.4.

6.3. *Transport properties*

Some of the most interesting and esoteric recent research is on low-temperature electrical resistivity. Measurements are frequently coupled with NMR, EPR and other newer experimental techniques. In combination with the phase, structural, surface and electronic results discussed earlier, results of these studies should give the reader a more clearly defined picture of hydride properties and their temperature dependence in the MH_2–MH_3 composition range.

6.3.1. *Electrical resistivity and related properties*

6.3.1.1. *Rare earths.* Most earlier resistivity studies were performed on thin metal films as they were progressively "titrated" with hydrogen. The results show changes from highly metallic properties for dihydrides to semiconducting behavior in approaching the trihydride. Since the resistivity rises steeply upon filling of the o-sites and random occupation supposedly begins to perturb the crystal field of the metal, the technique provides a method that equals or exceeds precise *P-C-T* measurements for defining the first hydride phase boundary, especially if kinetics are sluggish. However, as discussed in some detail earlier, sorting out the effects of phase transitions and/or various ordering phenomena as a function of composition and temperature is a difficult task. A recent and valuable addition is the ability to perform precise resistivity measurements down to liquid helium temperatures. Magnetic transitions (see section 6.4) intertwined in the data must be identified in resistivity studies. Finally, low-temperature specific-heat measurements provide valuable information and detail, and are included as needed in discussions of both resistivity and magnetism.

An excellent paper by Surplice and Kandasamy (1982) is recommended for those interested in phase boundary studies. Thin-film data are presented for Sc + H, Er + H and Yb + H, and comparison is made to earlier bulk studies and *P-C-T* measurements. The increases in resolution and in interpretation are quite revealing.

As noted previously, recent interest has concentrated on the MH_2–MH_3 region and especially on those effects seen as the temperature is lowered. As an introduction and brief overview, the study on Th, Er, Dy and Gd and their dihydrides by Burger et al. (1984) serves to delineate the comparison between the parent metal and the hydride at the beginning of the single phase region. It is particularly instructive to note the clear separation achieved between the (lower-temperature) acoustic-phonon coupling parameter and (higher-temperature) optical-phonon effects, which are both much smaller in the dihydrides than in the metals. Through comparison of the hydrides and the deuterides, the authors show that a well-defined (although small) coupling occurs with the optical phonons. This separation is possible, except for GdH_2, because the magnetic-ordering transition is drastically lowered for the dihydrides due to the reduction of condution electron-to-4f spin coupling. Comparative values, expected to

TABLE 10
Electron–phonon coupling parameters for rare-earth metals and their dihydrides.

		Tm	Er	Dy	Gd
$A\lambda^{ac}$ (μΩ cm/K) [metal]		0.175	0.19	0.125	–
Θ_E(K)	MH_2	1508	1485	1438	1392
	MD_2	1066	1050	1017	984
$A\lambda^{ac}$ (μΩ cm/K) [MH_2]		0.055	0.052	0.046	0.044
$A\lambda^{op}$ (μΩ cm/K) [MH_2]		0.0162	0.0172	0.0155	0.0143

be typical for most of the lanthanide dihydrides, are given in table 10, where $p(T) = A\lambda_t T$ and Θ_E is the calculated Einstein temperature.

For the following discussions, the results are conveniently presented according to the interests or emphases of a particular laboratory effort. Much recent work has come from various authors while at the Ames Laboratory. A wealth of information is available for the simplest rare earths (La and Ce) that have no high-temperature phase changes. The reader is directed to an excellent summary of work on the CeH_{2+x} system up to 1985, by Schlapbach et al. (1986a). In early NMR studies by Barnes et al. (1980), a clear transition at about 210 K is attributed to a metal-to-semiconductor transition. Also, a narrow band gap (~ 0.01 eV) appears below that temperature, as discussed at some length in sections 6.1 and 6.2. The authors also identify the off-center displacement of o-site atoms.

Heat-capacity studies on LaH_x and LaD_x ($2.5 < x < 3.0$) are described by Ito et al. (1982) and by Ito et al. (1983). Although mixed behavior is noted for intermediate compositions, four sharp anomalies at 211, 230.5, 233.5 and 274 K for LaD_3 indicate the existence of five phase modifications. Two broad peaks are observed for LaH_3 at 241 and 270 K; whereas the lowest transition for both $LaD_{3.0}$ and $LaH_{3.0}$ is assigned (but see below) to a semiconductor-to-metal transition upon warming, the others are attributed to location changes, ordering, structural transitions, etc. Puzzlement over the lack of peaks expected for cubic-to-tetragonal distortions at certain compositions are resolved by the work of Boroch et al. (1989) and Conder et al. (1989) as shown in figs. 3 and 4. The electronic specific heat coefficient for LaD_x ($2.76 < x < 3$) is essentially zero and indicates (as expected) a near-zero conduction-band population.

Shinar et al. (1988) measured the resistivities of LaH_x and CeH_x ($x > 2.70$) by an indirect Q-factor technique over the temperature range $120 < T < 500$ K. Composite data for $LaH_{2.90}$, $LaH_{2.80}$ and $LaH_{2.70}$ are shown in fig. 23. Because this method is not absolute, a resistivity ratio is used to normalize values to that for 295 K. A peak that becomes increasingly sharp at high compositions shows a transition from weakly metallic to semiconducting behavior with increasing temperature. This result is *reverse* of that normally expected, and opposite to what was derived by Ito et al. (1983) from heat-capacity data. At compositions above $LaH_{2.93}$ and $CeH_{2.82}$, the phases are semiconducting at all temperatures. The observed transitions clearly coincide with the structural ordering of o-site hydrogens described earlier. Whether or not a tetragonal distortion accompanies this ordering is sensitive to composition, as shown by fig. 3. The room-temperature resistivity increases rapidly with increasing x, as indicated in

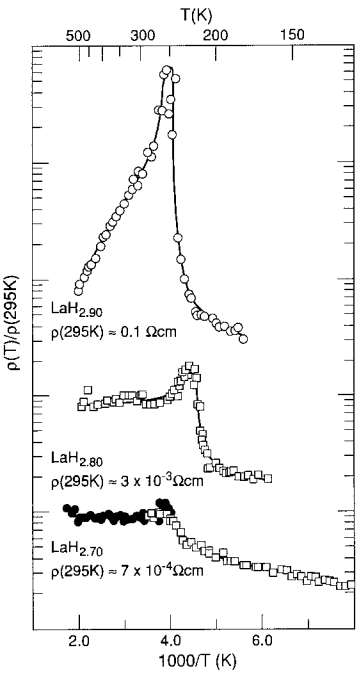

Fig. 23. Q-factor indirect resistivity data for the LaH_x system ($x = 2.70, 2.80, 2.90$), ratioed to 295 K. Transition from weakly metallic to semiconducting behavior is seen with *increasing* temperature. Note: symbols indicate data taken at various frequencies, over the range 4 to 44 MHz; all data are frequency insensitive. After Shinar et al. (1988).

fig. 23, and agrees with the disappearnce of d-like conduction electrons, as discussed in sections 6.1 and 6.2. Due to the extreme sensitivity of electronic properties near the trihydride composition, it is not known whether a small band gap appears (especially for CeH_x) or whether a gap-less but disordered metallic state is formed.

In the continuing series of reports from the Ames Laboratory, Kai et al. (1989) discuss more extensive and refined heat-capacity studies on LaD_x and LaH_x ($1.9 < x < 3.0$). Measured electronic specific heat coefficients ($mJ/mol\,K^2$) are $\gamma = 0.81 \pm 0.01$ for $LaH_2(D_2)$ and 0.038 ± 0.01 for $LaH_3(D_3)$, with Debye temperatures of $\Theta_D = 348 \pm 2$ and 381 ± 2 K, respectively. As in the work of Ito et al. (1982, 1983), four sharp peaks are observed for $LaD_{2.95}$, but at slightly different temperatures. Similar results were also quoted for samples at $x = 2.65, 2.75, 2.80$ and 2.90 where the cubic-to-tetragonal transition occurs, and all have a common peak at 250 K. These results and the lack of an observed cubic-to-tetragonal distortion for $x = 2.53$ correlate with the X-ray data in fig. 3. On the basis of the variation of the electronic specific heat coefficient with composition, special stabilities are proposed for compositions with $x = 2.25, 2.50$ and 2.75. For $x = 2.25$, the proposal seems somewhat nebulous because of the broad β-phase shown in fig. 4, but a positive relation is evident for the γ and η phases. Whether the δ and ε phases, near 2.62 and 2.66, respectively, should appear is, of course, a matter of conjecture. The authors present entropies of transition and provide an extensive discussion that includes comparisons of their experimental results with band-structure values.

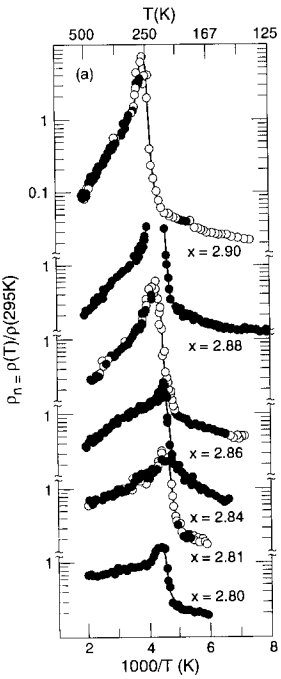

Fig. 24. Resistivity ratio results for LaH_x ($2.80 < x < 2.90$) showing the rapid localization of band states and concomitant drop in conductivity with increasing temperature. See note, fig. 23. After Shinar et al. (1990).

Recent work from the Ames Laboratory includes a resistivity study by Shinar et al. (1990). Measurements made over the 100 to 700 K range are intended to further investigate and elucidate the curious semiconductor-to-metallic transition that occurs with warming. According to a suggested mechanism, low-temperature ordered (o-site) states give rise to a defect band arising from the vacant o-sites and the associated electrons produce metallic conduction, as in the model by Anderson (1958). As discussed in section 6.2, the transition to more disordered o-site hydrogens at high temperatures localizes these band states and the conduction drops dramatically as shown in fig. 24. This interpretation agrees with the conclusions of Fujimori and Tsuda (1981) and Misemer and Harmon (1982); however, neither those studies nor that of Boroch et al. (1989), who present conflicting structural interpretations, are cited by the authors.

In the region where magnetic effects must be considered, a resistivity study on CeH_{2+x} ($0 < x < 0.01$) by Vajda et al. (1990) shows that the appearance of low-temperature anomalies related to magnetic transitions depends on whether the system is cooled slowly enough for ordering to occur. Both heavy-fermion and Kondo-lattice behaviors are inferred from the low-temperature results ($T < 20$ K) and a close competition between magnetic order and the Kondo effect is revealed by data from quenched versus slow-cooled samples.

Numerous and extensive studies on hydrides of the magnetic lanthanides are reported by the French group. Electrical-resistivity measurements for the PrH_{2+x} system ($0 < x < 0.75$) by Burger et al. (1988) show the strong reduction in carrier density with increasing x discussed earlier, and the authors identify both short-range

($x < 0.01$) and long-range ($x > 0.2$) ordering. Effects of rapid versus slow cooling are again delineated. Metallic magnetic ordering is completely quenched by hydride formation. In agreement with earlier observations, the mobility of o-sites hydrogens increases with increasing x up to the point where site blocking dominates.

Studies of the NdH_{2+x} system by Daou et al. (1992) explore in detail the effects of quenching versus slow cooling and give valuable insight into the relative weights of structural and magnetic ordering. Whereas a *ferromagnetic* transition occurs for NdH_{2+x} at 6.8 K, measurements for Nd metal by Senoussi et al. (1987) show an antiferromagnetic transition at 19 K. The transitions for all other rare-earth hydrides are antiferromagnetic and their magnetic transition temperatures are more than ten times smaller than for the pure metals. Since magnetic ordering produces a significant drop in spin-disorder resistivity, a minimum is also seen as the temperature is lowered toward a magnetic transition. The authors report detailed results on the quench-induced resistivities for various compositions, the dependence of these resistivities upon temperature and activation energies for hydrogen diffusion. Measurements were only made up to $x = 0.65$, because of sample instabilities implying appearance of the cubic NdH_{2+x} plus hexagonal NdH_{3-y} two-phase region at higher compositions. The existence of a high-composition plateau beginning near H/Nd = 2.6 is now confirmed by Ohki et al. (1989); a transition near $PrH_{2.8}$ is suggested. Since the resistivity of $Nd_{2.00}$ is only 0.18 μΩ cm, the magnetic resistivity term ρm and the onset of phonon scattering are well tracked. As the o-sites begin to fill, a more complex picture emerges in the form of short-range as well as long-range ordering, crystal-field effects, loss of symmetry, subtle phase transitions and distortions. At high x the complexity is of course magnified. Although further details about magnetic effects are given in section 6.4, this chapter provides a detailed analysis of how a rare-earth system *with magnetism* might behave and is recommended to the reader desiring a well-presented discussion.

Resistivity data are also reported for later rare earths. Data for the Sm + H system show again that short-range structural ordering begins as soon as o-sites begin to be occupied. Vajda et al. (1989a) have measured electrical resistivities up to $SmH_{2.26}$, and Daou et al. (1989) report concomitant lattice parameter and low-temperature thermal-expansion studies. The sharp magnetic transition seen at 9.6 K begins to diminish at $x > 0.16$, because the crystal-field levels of cubic symmetry are seriously perturbed by the random occupation of o-sites. The spin-disorder resistivity in the heavier hydrides of Gd, Tb, Dy, Ho and Er has been systematically evaluated by Daou et al. (1988a, b, c), and the Sm + H system is compared with Gd + H, where no crystal-field effect is expected (Gd^{+3} has only a pure spin moment). It is concluded that the so-called exchange integral term Γ is perhaps larger for the lighter rare earths, but measured values for T_N (9.6 K) and for the magnetic spin-disorder resistivity ρm (12 mΩ cm) are both larger than the expected values (6 K and 5.26 mΩ cm, respectively). The lattice parameter is a minimum size at about $SmH_{2.45}$, which is taken to be the beginning of the two-phase plateau leading to the hexagonal phase. However, this contraction is observed in all rare-earth-like MH_{2+x} systems, except for NpH_{2+x}, and signals that the minimum M–H distance of 2.32 Å has been reached. In any case,

the phase transition begins in this area, due to the strains produced by forcing more H atoms into the lattice. The NMR studies of Zogal and Drulis (1989) show two proton resonances, indicative of two phases with different hydrogen diffusion rates. Based on the analysis of the NMR and accompanying X-ray diffraction data, the two-phase boundaries are placed at 2.35 ± 0.05 and 2.95 ± 0.03.

The phase relationships defined for Sm + H by other techniques provide other bases for comparison. Results of X-ray diffraction studies by Greis et al. (1981) show that phase boundaries at high temperature are 2.35 and 2.76. These authors identify a tetragonal Sm_3H_7 ($SmH_{2.33}$) compound that forms upon slow cooling (a similar phase has been postulated for Pu + H). However, as shown by the data in fig. 11, the recent *P-C-T* studies by Wang et al. (1990) place the lower phase boundary at 2.55, in agreement with earlier studies; the upper boundary appears above H/Sm = 2.9. These discrepancies, although perhaps not major, show that the interpretation of electrical resistivity measurements can be difficult and highly dependent upon the temperature range, the method of cooling, and the accuracy and precision of the hydride composition. Since the span in H/Sm of the two-phase region is approximately 0.4 in several studies, composition errors seem likely. The best focus of a resistivity measurement might be to delineate magnetic transitions, a topic discussed in section 6.4.

Extensive work on the Tb + H system by the French group may serve as a model for the more magnetically complex late rare-earth hydrides. Resistivity data obtained on the $TbH_{1.93+x}$ phase by Vajda et al. (1985) show that an anomaly at about 150 K becomes more prominent with increasing x. This phenomenon is attributed to short-range ordering of H atoms on the o-sites, rather than to (or perhaps in addition to) a possible structural transformation. Analogy is drawn to ordering like that in the α-phase (see section 3.2) at similar temperatures; the introduction of hydrogens on o-sites is viewed as dissolution of hydrogen in MH_{2+x} solid phase. The work is extended by Daou et al. (1986), who explore in detail the technique of quenching in defects by rapid cooling, the effects of electron irradiation and the consequences of annealing by various paths. They suggest that ordering may occur in the {100} directions; i.e., across an intervening metal atom. Other resistivity work from this laboratory relates to magnetic transitions and the paramagnetic spin-disorder resistivity ρm, and is discussed later.

An interesting study by Daou et al. (1988b) explores the resistivity behavior of LuH_{2+x}. The insulating phase occurs already for x near 0.2, and large increases are observed in the residual resistivity and in the temperature contribution to the total resistivity as this composition is approached. Normalization of the data for various samples shows that the large difference observed with x as a function of temperature arise mainly from the phonon contribution to the resistivity. The variations in the residual resistivities are ascribed by the authors to admixture of the insulating phase possibly along grain boundaries of the metallic cubic phase. A so-called "percolation model" describes the process of conduction through and/or around the various paths in the two-phase mixture.

A recent paper by Vajda and Daou (1991) on the non-magnetic Y + H system shows for the first time a metal–semiconductor transition for $YH_{2.10}$ at 230 K. As in the

rare-earth systems, hydrogen ordering is again observed by applying the quench versus slow-cool technique. A further transition in the 60–80 K range is identified as very narrow-gap semiconducting behavior in this weakly metallic system.

6.3.1.2. *Actinides.* Resistivity studies on the Np + H, Pu + H and Am + H systems are summarized by Ward et al. (1992). Measurements were carried out on $NpH_{2.13}$ (the phase boundary composition), $Np_{2.33}$ and $NpH_{2.60}$. As shown in fig. 25a, $NpH_{2.13}$ and $NpH_{2.33}$ are rather poor conductors, but quite obviously metallic, although the

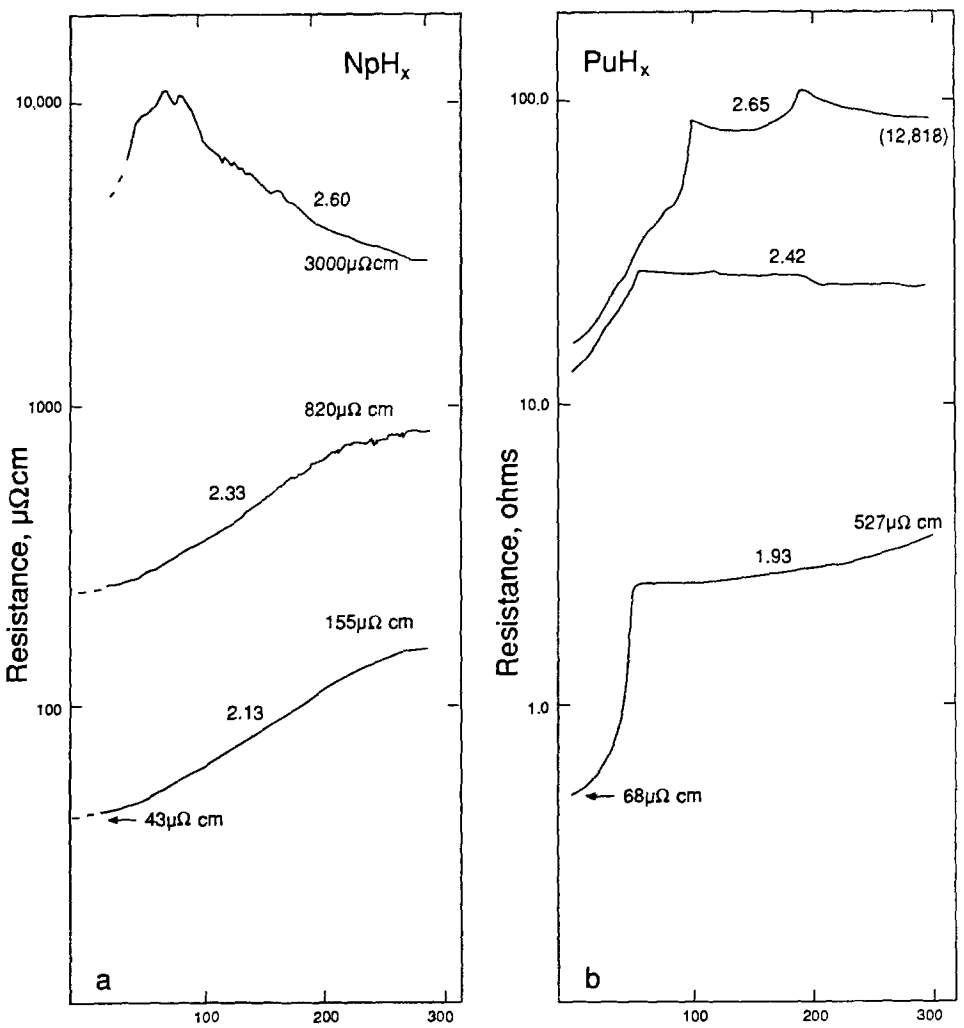

Fig. 25. Electrical resistivity data for the Np + D and Pu + H systems. (a) NpD_x ($x = 2.13$, 2.33 and 2.60); (b) PuH_x($x = 1.93$, 2.42, 2.65). After Ward et al. (1992).

amount of scattering introduced by the somewhat higher composition is quite large. In contrast, the 2.60 composition exhibits strong semiconducting behavior (see section 3.1.1) and has a cubic-to-tetragonal transition near 170 K, plus an as-yet unquantified semiconductor-to-metal transition in the neighborhood of 70 K. As noted earlier, this may correlate with the extra reflections seen in the neutron diffraction data at 10 K (see fig. 7b). Since the ground states of Np^{3+} and the neptunium hydrides are non-magnetic, the presence of a magnetic effect is doubtful. Proximity to the cubic–hexagonal two-phase region may also be a factor, as just considered in the Lu + H system, where a spectacular rise is observed; however, the relative curves for the Np and Lu hydrides do not correspond at all.

Based on the trend in the actinides towards more rare-earth-like behavior, the Pu + H system is expected to be more "normal". As discussed in sections 6.1 and 6.2, and alluded to in the discussion of early rare-earth hydride systems, Np (or Pu) (5f)–H(1s) interactions should be large, both due to the energy superposition and spatial distribution of the 5f band. However, the effect of 5f spatial extension should be small in the large Np (or Pu) + H lattices, and indeed plutonium hydride exhibits the classical $5f^5$ moment characteristic of a localized system. Nevertheless, as shown in fig. 25b, $PuH_{1.93}$ (phase-boundary composition) is less metallic than $NpH_{2.13}$, the sharp ferromagnetic transition at 60 K notwithstanding. Ordering of the o-site hydrogens is clearly evident for H/Pu at 2.42 and especially at 2.65 compositions. The higher composition exhibits a very high resistivity at room temperature and apparent semiconducting behavior, although not as spectacular as that for $NpH_{2.60}$. Again, proximity to the two-phase region may complicate the issue. As discussed below, magnetic transitions are sharply defined for all compositions including $PuH_{2.42}$, but are masked for $PuH_{2.65}$. The puzzling, and as-yet unexplained, observation is the very sharp transition for the 2.65 composition at about 110 K. The process has no magnetic component, and is not seen in neutron data. Satisfactory explanations are not given for the behavior of either Np + H or Pu + H. Although f–s scattering may be invoked, it is inconsistent with the complexity of Pu + H, a system which in theory should be simpler.

Excitement arises for the Am + H system because rare-earth-like behavior is finally seen. The 5f electrons finally become truly core-like, but remain relatively close to the Fermi level. Resistivity data for $AmH_{2.06}$ in fig. 26 shows that the hydride is more metallic than the parent metal at low temperatures and reaches a value less than 7 μΩ cm below 40 K. A well-defined but as-yet unexplained change of slope at 150 K implies some sort of transition that does not involve o-site hydrogens. Resistivity data are not available for any other transuranium hydride systems.

6.3.2. *Other transport-related properties*

Nuclear magnetic resonance (NMR) has been the major tool for assessing hydrogen motion in hydrides, because the t-site and o-site hydrogens exhibit markedly different diffusion rates, hopping frequencies and ordering temperatures. A good basic discussion of the technique is given by Seymour (1982). A more recent technique, quasi-elastic neutron scattering (QENS), enhances the ability to quantify hopping rates and diffusion paths.

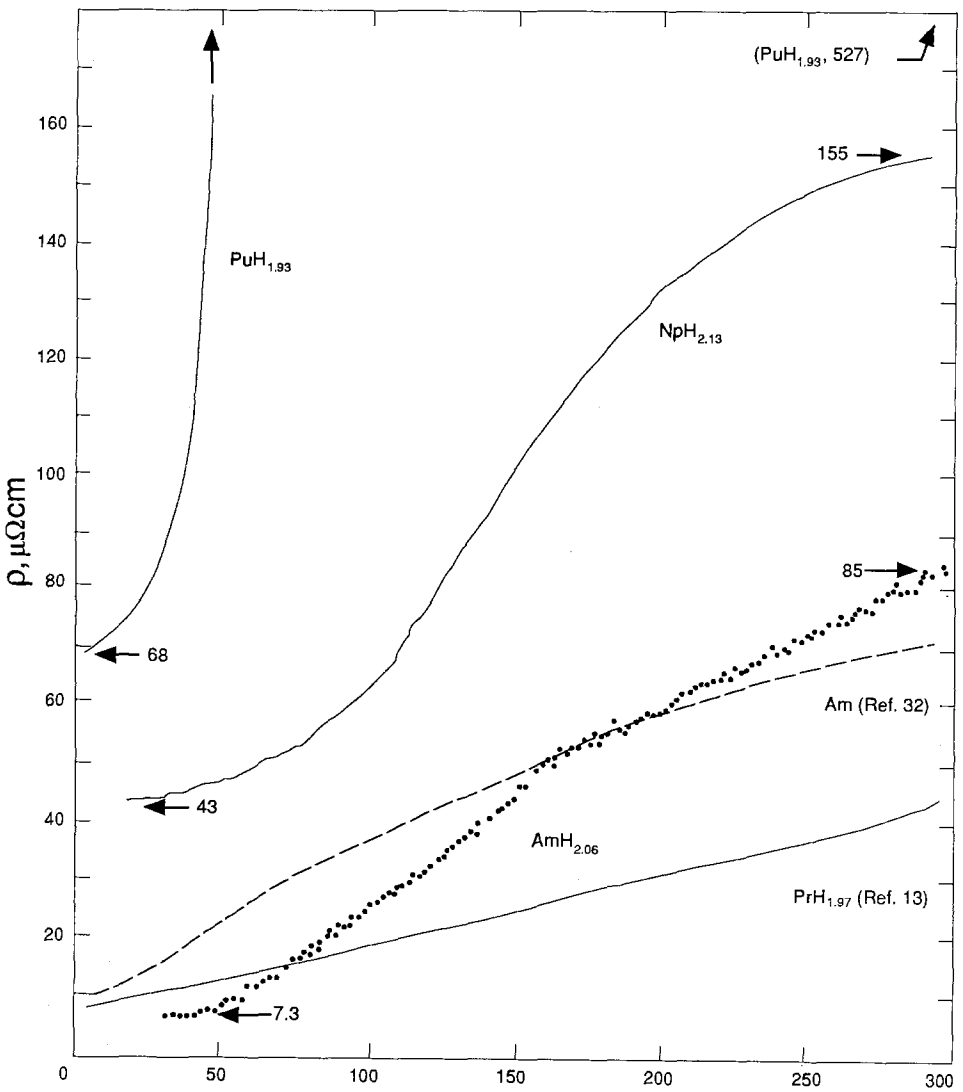

Fig. 26. Comparison of electrical resistivity data for $AmH_{2.06}$ (data points) with values for $PuH_{1.93}$, $NpH_{2.13}$ and $PrH_{1.97}$. After Ward et al. (1992).

6.3.2.1. *Rare earths.* Most of the diffusion data measured by NMR are for the hydrides and α-phases of the simpler, non-magnetic elements (La, Sc, Y and Lu). Kashaev et al. (1978) measured the proton magnetic relaxation for compositions near LaH_2 and LaH_3 over the −180 to 400°C range. The temperature dependence of the spin–lattice T_1 and spin–spin T_2 proton relaxation times show that the major contribution was from hopping diffusion, as evidenced by the modulation of dipole–dipole interactions. The contribution arising from interaction of protons with

the conduction electrons show that LaH_2 is metallic. For LaH_3, the conduction electrons are essentially gone and a very different relationship characteristic of a semiconductor is observed. Belyayev and Stepanov (1982) measured T_2 values for both LaH_x and NdH_x ($2 < x < 3$) over the range 150–400 K. The low-temperature ordering of o-site hydrogens causes non-uniform diffusion up to a temperature where the so-called t–o–t (tetrahedral-through-octahedral-to-tetrahedral) jumping mechanism begins. At this point diffusion becomes uniform; for $LaH_{2.29}$ the process appears above 380 K and has an activation energy of 0.107 ± 0.005 eV. Although similar qualitative results were seen for the Nd + H system, the data cannot be quantified, due to severe magnetic broadening. Borsa et al. (1982) look specifically at LaD_3, taking advantage of a deuterium electric quadrupole moment that couples to the electric-field gradient of the crystal. They postulated the existence of both hopping diffusion among the (newly discovered at that time) off-center o-site atoms and vacancy diffusion involving an estimated (but perhaps questionable) 3% vacancy concentration. The same activation energy is reported for both processes; the data show a large perturbation in T_1 data near 200 K, where electronic and/or structural transitions are seen (see section 6.3.1). It should be noted that the NMR work just discussed was completed during the times that lattice and electronic transformations (e.g., tetragonal distortions and metal–semiconductor transitions) were being discovered and catalogued.

A recurring anomaly is the apparent diminution of the jump rate at high temperatures. Richards (1987) postulates that increased vibrational amplitudes result in H–H repulsions that interfere with some diffusion paths. However, in discussing high-temperature NMR studies, Barnes (1989) points out that recent QENS studies such as the work on YH_2 by Stuhr et al. (1989) and by Barnfather et al. (1989) do not indicate any slowdown in diffusion. An excellent short review of the NMR technique as applied to diffusion is given, and a number of references are included. A two-state model similar to that for superionic conductors is proposed for the high-temperature anomaly. The model includes correlated motion of the H ions in the superionic state and a larger correlation time than classical diffusion. The existence of hydrogen clusters in the superionic mode is inferred but not proven. Some comparative hopping frequency values are given in table 11.

TABLE 11
Comparative hopping frequencies Γ_d^{-1} at the critical temperature for some hydrides and superionic conductors.

System	Critical temperature (K)	Γ_d^{-1} (10^{-10} s^{-1})
$Sc^1H_{1.88}$	1080	1.4
$^{45}ScH_{1.88}$	790	4.6
$Sc^2D_{1.82}$	950	0.20
$Y^1H_{1.98}$	950	0.20
$La^1H_{2.26}$	800	0.32
$Pb^{19}F_2$	700	2.5
$^7Li_{0.5}Al_{0.5}$	430	0.14
α-$^{45}ScH_{0.27}$	670	0.60

NMR data are presented for both the α-phase ($YH_{0.18}$) and the dihydride of yttrium in the study by Barnes (1989). For the α-phase, ^{89}Y signals are not found below 350 K, even though low-temperature ordering and pairing occurs in chains along the *c*-axis (see section 3.2). Although Blaschko et al. (1985) postulate three-dimensional ordering between chains, the NMR results imply inter-chain disorder that spreads out ^{89}Y and ^{1}H shifts and masks the ^{89}Y signal, even at 150 K. For the dihydride, a ^{89}Y doublet shows that the metal exist in two types of surroundings. Postulation of a hitherto unreported phase is supported by very recent work of Vajda and Daou (1991), who report for the first time several metal-to-semiconductor transitions and low-temperature ordering (see section 6.3.1.1).

Other studies of the α-phase are reported by Anderson et al. (1990) for the ScH_x system and by Barnes (1991) for the ScH_x, YH_x and LuH_x systems. The QENS analysis by Anderson et al. (1990) identify a fast hopping rate ($\sim 10^{12}\ s^{-1}$) involving a population of labile interstitial hydrogens; i.e., hydrogens not involved in short-range H–M–H low-temperature pairing (see fig. 9a). The behavior is attributed to a Kondo mechanism for rapid proton motion between nearly symmetric double wells between the metal atoms. Temporary puzzlements and disagreements arose during the last decade because such motion is too fast for NMR detection. This problem is recognized by Barnes (1991), who reports that *localized* motion occurs in Sc or Lu at hopping rates of the order of $10^8\ s^{-1}$ in the temperature range 10–100 K, as illustrated in fig. 27. Since the hydrogen concentration is so low, the dipolar field at the proton sites is dominated by the metal nuclei; the apparent divergence of the full curves identifies an electronic structure change between 160–200 K. Conversely, Y has a very small nuclear moment and localized motion rate is very small and barely distinguishable from the electronic contributions. Barnes (1991) discusses differential thermal analysis (DTA) results in terms of a classical over-barrier hopping, or possibly tunneling, process with a distribution of barrier heights. As postulated by Torgeson et al. (1991), the latter approach is relatively successful; however, close similarities to results observed for amorphous and disordered systems ("proton glasses") are also considered because they are examples of oscillating system involving two states.

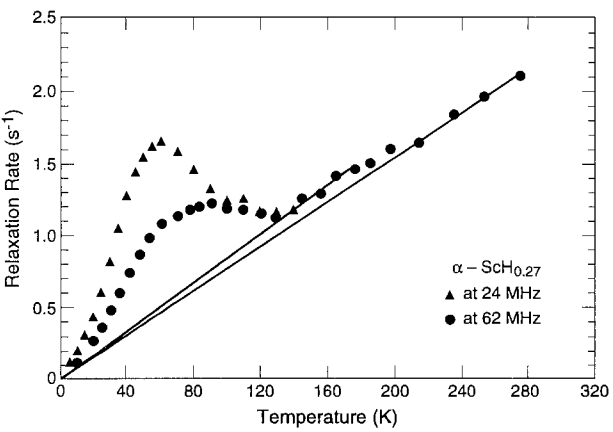

Fig. 27. Proton-resonance data for α-phase $ScH_{0.27}$ at 24 and 62 MHz. The two full curves show the electronic contribution above and below 170 K. After Barnes (1991).

QENS measurements on single crystals of the yttrium α-phase by Anderson et al. (1989) provides information on long-range and local diffusion rates. Fast hopping between neighbor t-sites are confirmed and an excellent discussion of data handling and interpretation is included.

6.3.2.2. *Actinides.* The only NMR work reported on a transuranium hydride system is that by Cinader et al. (1976) for Pu + H with H/Pu = 1.78, 2.35, 2.65 and 2.78, over the temperature range 77 – 300 K. For a composition in the plateau region (H/Pu = 1.78), a normal rigid lattice signature is observed near 90 K, as is the case for the higher compositions. At lower temperatures inhomogeneous broadening set in, characteristic of paramagnetic broadening. Both tetrahedral and octahedral line broadening are observed, with a much faster diffusion rate (as expected) for the o-site hydrogens. A new broad line observed for $PuH_{2.78}$ at 91 K is attributed to magnetic ordering. However, as noted by Ward et al. (1992) and discussed in section 6.3.1.2, the sharp resistivity inflection near 100 K (probably a related effect) shows no magnetic counterpart. Cinader et al. (1976) interpret their results in terms of a transferred hyperfine interaction model, rather than the more normal RKKY interaction model. They suggest that narrow-band d-type conduction electrons couple in normal fashion to the localized magnetic moments; i.e., the interpretation is consistent with the calculations presented by Eriksson et al. (1991).

6.4. *Magnetism*

Again, the problem is how to present a large amount of data taken by several techniques, upon a variety of systems. The choice has been made to review the techniques, considering the elements in row order, or in groups, as necessary.

6.4.1. *General magnetic behavior*

6.4.1.1. *The rare earths.* Most of the traditional magnetic measurements on rare-earth hydrides were made prior to the summary by Libowitz and Maeland (1979). Magnetic susceptibilities, moments, Weiss constants and ordering temperatures are well-catalogued. The reduction in ordering temperature upon withdrawal of coupling to the spins by the conduction electrons and upon forming the higher hydrides is well-understood. Recent refinements are in the categories of "why and how" and are primarily a consequence of newer and more sophisticated techniques and higher-purity materials. A large body of new information has accumulated.

Very little general magnetic work has been published during the last twenty-five years. Osterwalder et al. (1983) made both AC and high-field susceptibility measurements on the CeH_x ($1.8 < x < 3.0$) system over the 1.3–300 K temperature range. No ordering is observed for the 1.93 composition, but a sharp and very strong signal appearing at 4.2 K for the 2.43 composition is ascribed to ferromagnetism. $CeD_{3.0}$ is ordered at 2.4 K, and comparison neutron-diffraction measurements at 1.3 K showed this composition to be antiferromagnetic (AF) and to have long-range ordering of o-site deuteriums. The magnetic moment ($\mu_{Ce} = 0.64\mu_B$) is oriented in the {111} direction. The

low value with this orientation is imputed to be due to crystal-field effects. The expected tetragonal distortion near 290 K is shown by neutron results. The 2.43 composition is ordered ferromagnetically with a saturation moment of about $1.21\mu_B$, a value near that for a classical $4f^1$ electronic configuration. The introduction of o-site deuteriums is expected to produce more spherical symmetry and reduces the (strong) crystal-field splitting seen initially for the dihydride. A Γ_8 ground state is suggested for the Ce^{+3} ion.

Measurements are reported for the NdH_{2+x} system, which also forms the cubic hydride to high compositions. Carlin et al. (1982) clear up some discrepancies in older data by performing both AC susceptibility and DC magnetization measurements on the NdH_2 composition. They report a T_C of about 5.8 K, suggestive of long-range ferromagnetic order and confirmed by magnetization results. Onset of coercivity occurs near the same temperature. Curie–Weiss behavior is noted with an infinite field extrapolation moment value of 1.9 μ_B. Senoussi et al. (1987) extend measurements from $x = 0$ to 0.75 over the temperature range $1.5 < T(K) < 15$ at fields less than 15 kOe. Ferromagnetism is also reported for NdH_2, which also exhibits strong coercivity effects. At higher compositions, the long-range ferromagnetic ordering diminishes until spin-glass-like behavior appears at the highest composition. The authors attribute much of the results to local fluctuations in hydrogen concentration, resultant magnetic anisotropy and general random behavior influenced also by crystal-field effects.

Carlin et al. (1980) observe antiferromagnetic ordering in GdH_3 at 1.8 K. Since the metal orders near room temperature, this result demonstrates again the major change that occurs as conduction electrons are bound. Carlin and Krause (1981) also studied the DyH_2 and DyH_3 systems below 30 K by the AC mutual inductance method. DyH_3 orders antiferromagnetically at 3.2 K. The data are consistent with extensive short-range antiferromagnetic ordering and agree reasonably well with earlier work and with more recent Mössbauer and specific-heat measurements, but disagree with reports describing long-range order.

Flood (1978) has measured the magnetization and magnetic susceptibility of ErH_3, finding Curie–Weiss behavior from 4.2 to 2 K and evidence for an antiferromagnetic transition. The low-field effective moment is $6.77 \pm 0.27\mu_B$.

6.4.1.2. *The actinides.* Aldred et al. (1979) has measured magnetic susceptibilities for the compositions H/Np = 2.04, 2.67 and 3.0 at temperatures between 4 and 700 K. Evidence is not found for magnetism or magnetic ordering; however, a weak temperature dependence on the susceptibility is interpreted as a Np^{+3} ($5f^4$) non-magnetic ground state. The large Np–Np distance should preclude f–f overlap and the 5f electrons should be at least quasi-localized.

Quasi-localization becomes very clear for the Pu + H system. Ward (1983) has shown the Pu ion to be normally trivalent, with a nearly classical $5f^5$ moment. All compositions show sharp ferromagnetic transitions in contrast to earlier work on powders. The ordered moment ($\mu = 0.4\mu_B$) determined with neutron scattering by Bartscher et al. (1985) seemed a bit puzzling, but is now readily explained by Eriksson et al. (1991) as the result of anti-coupling of the d moments against the f moments. Magnetization data do not exist for actinide systems beyond Pu + H.

6.4.2. *Relationship of electrical resistivity and magnetism*

A large body of data has been accumulating in elucidating magnetic transitions via low-temperature resistivity measurements. Although this situation is already noted in section 6.3.1, a brief and more specialized addendum is given here. Where possible, results are presented in elemental order.

Burger et al. (1990a) compare the magnetic and related structural properties of several systems studies by low-temperature resistivity measurements. CeH_{2+x} is a special case due to conduction-electron hybridization, which modifies the exchange interaction Γ and leads to Kondo behavior. (In contrast, results for PrH_2 are more "normal".) Crystal-field effects can also introduce anomalies that may be superimposed on the expected reduction of the magnetic ordering temperature T_N by depopulation of the conduction band during formation of the hydrogen bonding bands at high compositions. As discussed previously, this corresponds to diminution of the RKKY interaction. However, this process, although the dominant one, is only one dimension of the fundamental changes that can occur with increasing x. Burger et al. (1990a) point out that the nature of the conduction electrons must also change from spd character in the metal to mostly d character for the hydrides.

The general relation of magnetic to structural ordering was already well-defined by earlier work. Studies on the TbH_{2+x} system by Vajda et al. (1987) show that a rather spectacular variation in $\rho(T)$ occurs for even small (0.045) values of x. The behavior is attributed to an incommensurate antiferromagnetic transition in addition to the expected commensurate one. This incommensurate transition is now confirmed by Arons and Schweizer (1982), using neutron-diffraction measurements. Additional effects of incommensurate ordering (apparent decrease of T_N with H disordering) are described in terms of modifications of the electronic structure by the opening of a new "superzone" boundary gap; e.g., by general modification of the electronic structure and the shape of the Fermi surface. The reader is referred to this paper for additional details.

In studying the DyH_{2+x} system, Vajda and Daou (1992) relate observed magnetic behavior to the effects of short-range or long-range ordering. For x near zero, well-defined magnetic transitions appear at 3.3 and 5.1 K, in agreement with earlier C_p work. Whereas the lower temperature is T_N, the point of normal commensurate antiferromagnetic ordering, the 5.1 K value is identified as an incommensurate antiferromagnetic ordering. These transitions are rapidly smeared out with increasing x, as short-range ordering appears in the hydrogen sublattice. However, as x increases further, a minimum appearing in the resistivity for $x > 0.3$ leads to a new magnetic feature at about 10.5 K and signals the appearance of longer-range ordering and attendant modification of both the magnetic and physical structures. The authors suggest a possible tetragonal modification, which agrees with the extensive information on such ordering discussed earlier. These results, summarized in fig. 28, illustrates the special sensitivity of resistivity measurements toward magnetic effects.

Another review paper by Daou et al. (1988a) considers the MH_{2+x} systems of Gd, Tb, Dy, Ho and Er in terms of magnetic properties and structural ordering. The order–disorder phenomenon at $x > 0$ becomes increasingly complex and begins to

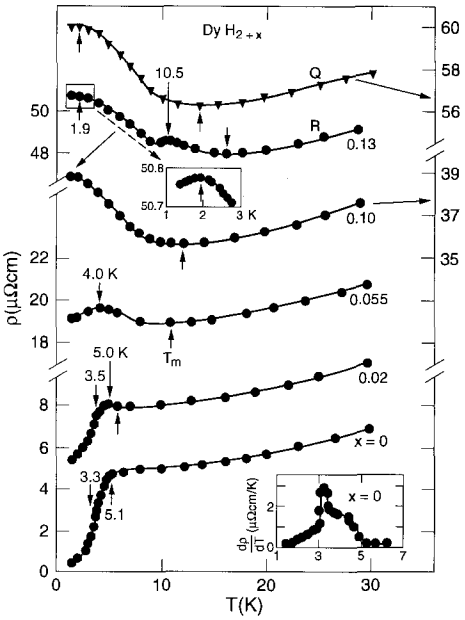

Fig. 28. Low-temperature electrical-resistivity data for DyH_{2+x} at several compositions. At $x = 0.13$, results for both rapid-cooled (curve Q) and slow-cooled (curve R) samples are shown. Magnetic contributions seen at low compositions are "smeared out" for $x \geq 0.10$; a new magnetic feature characteristic of longer-range ordering is seen at $x = 0.13$ (curve R). After Vajda and Daou (1992).

involve crystal-field theory, Kondo effects, etc. This appears to be the area and direction of the most recent research.

Finally, magnetic effects in the α-phase are also quite complex. The most interesting examples are in the high-solubility systems, such as Lu, Tm and Er. Tm, with a maximum solubility of 11 atom %, also exhibits magnetic transitions. Vajda et al. (1989b) present a detailed analysis, identifying earlier work with the later realization of the H–H pairing along the *c*-axis that occurs across the metal atoms with cooling/ordering. Whereas increasing the amount of dissolved hydrogen lowers T_N in a regular way by diminishing the contribution of the RKKY mechanism, a spectacular difference exists between the *b*-axis versus the *c*-axis resistivities. The *b*-axis data show the expected temperature and composition dependencies and a reasonably defined T_N. For the *c*-axis data, the residual resistivity increases so strongly with increasing H concentration that the expected resistivity drop due to magnetic ordering below 35 K is swamped for H/Tm > 0.05, and ρ_m is not seen. The *c*-axis data are shown in fig. 29. The authors successfully fit the body of data with exponential and/or polynomial expressions, from which residual, magnetic and phonon resistivity components can be deduced, and from which a rationale for the spin-disorder resistivity behavior is derived. In a related paper, Daou et al. (1988a) show that earlier heat capacity studies were probably made on H-contaminated (α-phase) Tm metal and that the α-phase exhibits an increasingly complex magnetic structure as the H content increases.

6.4.3. *Low-temperature heat capacities*

A reliable tool for detecting magnetic behavior is measurement of heat capacity. Many other phenomena, such as phase transformations, ordering, etc. are also seen.

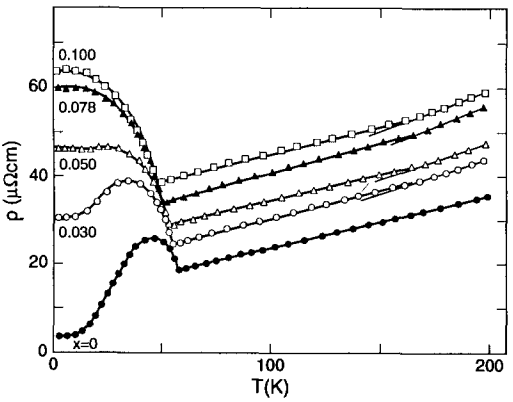

Fig. 29. c-axis resistivity data for α-phase LuH_x ($x = 0.030, 0.050, 0.078$ and 0.100). Symbols are identified on the figure. After Vajda et al. (1989a, b).

Crystal-field effects are sometimes detected, and thus it is difficult to place specific-heat studies in a single category. The references cited here are the more important ones related to magnetism, although overtones into other areas are evident.

Most of the specific heat work on the rare-earth hydrides has come from one laboratory, in the Institute of Low Temperature and Structure Research, Wroclaw. An early work with good references is that of Bieganski and Stalinski (1976), who summarize data for the dihydrides of Tb, Dy, Ho, Er and Nd, over the range 1.8–22 K. The C_p of non-magnetic and isostructural LaH_2 is subtracted from experimental data to highlight magnetic and crystal-field splitting effects. Exceptionally sharp γ-type anomalies corresponding to antiferromagnetic ordering appear for all systems except NdH_2, which orders ferromagnetically. Additional anomalies observed for the Tb and Dy dihydrides were not understood, but later identified by Vajda and Daou (1992) as incommensurate magnetic ordering. These results sometimes differ sharply from those of earlier magnetic susceptibility measurements, which seem to have missed these low-temperature transitions. The Neel temperatures are 16.06 ± 0.01, 3.30 ± 0.03, 5.2 ± 0.2 and 2.12 ± 0.03 K for the Tb, Dy, Ho and Er dihydrides, respectively.

The Sm + H system is studied by Opyrchal and Bieganski (1978) and by Bieganski and Drulis (1979), who find antiferromagnetic transitions at 6.75 ± 0.05 K for SmH_2 and at 25.8 ± 0.5 K for $SmH_{2.84}$. In both cases, crystal-field splitting (Schottky contributions) are noted and discussed. Drulis et al. (1984) describe an interesting study on the $TbH_{2\pm x}$ system ($x < 0.1$), finding sharp γ-type magnetic transitions at about 16 K for $TbH_{1.93}$ and $TbH_{2.01}$, but observing a radically different behavior for $TbH_{2.06}$. The 16 K transition is gone and new transitions appear at 36 and 42 K. These results may be compared with the electrical-resistivity measurements by Vajda et al. (1987) (see section 6.4.2) who find a large variation in ρ at $x = 0.045$. Drulis et al. (1984) analyze their TbH_x data in terms of crystal-field effects, calculating multiple level sequences to best fit the expected Schottky heat contribution. For the $x = 0.06$ data, a case is made for two non-equivalent Tb^{+3} ions; 70% see cubic symmetry, while the remainder are influenced by the o-sites and experience axial symmetry. In this scheme, a major fraction of the Tb^{+3} ions remain in the paramagnetic state and fit the observed

Schottky function. However, Vajda et al. (1987) have proposed an additional incommensurate antiferromagnetic transition to explain the large variation in resistivity.

The Polish group has reviewed the properties of the Ce, Pr and Nd higher hydrides and attempted to fit crystal-field parameters to the expected Schottky curves. For $CeH_{2.70}$ and $PrH_{2.65}$, Drulis and Bieganski (1979) observe specific heat anomalies that are attributed to possible metal-semiconductor transitions. Later work by Drulis and Stalinski (1982) recognizes the low-temperature cubic-to-tetragonal transitions seen with other methods, but still associates the structural changes with metal-semiconductor transitions. As discussed in detail above, these two effects are complex and extensive and may not be concurrent. In any case, the reduced crystal-field symmetry of the higher hydride compositions is recognized, with the observation that cubic symmetry again reappears near the stoichiometric trihydride compositions of the early rare earths. A detailed analysis of the PrH_x system ($x = 2.20$, 2.25, 2.41 and 2.50) by Drulis (1985) confirms early predictions that the Pr^{+3} ions exhibit a singlet ground state and thus explains the lack of magnetism in this system.

Only one specific-heat measurement is reported for a late actinide. Data presented by Oetting et al. (1984) for $PuH_{1.90}$ show a sharp magnetic inflection at 36.4 K. The result is in reasonable agreement with the transition seen at 44 K for the 1.93 composition in a magnetic study by Ward (1983), considering the observed sharp dependence of transition temperature on composition.

6.5. *Miscellaneous property measurements*

A host of special techniques are employed to study hydride systems (NMR, EPR/ESR, inelastic neutron scattering, etc.) and many have diverse applications and capabilities. Although it is almost impossible to catalog or even group techniques into specific disciplines, important data and interpretations of hydride behavior are found in several of these areas. A short review is included to present recent findings. Little, if any, Mössbauer work has been published since 1979, and that topic is not addressed.

6.5.1. *Inelastic neutron scattering*

Inelastic neutron scattering is a vital and developing field of research, spurred by the availability of the high-resolution pulsed neutron sources at several facilities. Applications of the technique include establishment of accurate crystal-field levels, analysis of optical phonons and differentiation of these lattice vibrations from crystal-field effects, as well as evaluation of certain magnetic phenomena.

The literature on hydride phonon spectra deduced from inelastic neutron scattering is well-documented and fairly consistent both in results and interpretation. The scattering technique is a most useful and unique tool for studying hydrogen vibration. A compilation of experimental phonon dispersion curves and phonon densities of states is published by Kress (1987). A well-defined optical t-site peak appears in the 100–120 meV range for most dihydrides. Acoustic data appear below 50 meV and are often not measured or not measurable in many experiments. Filling of o-sites produces a second optical peak near 80 meV. Substitution of D for H results in a consistent shift according to the square root of the H/D ratio. The increasing complexity of spectra at

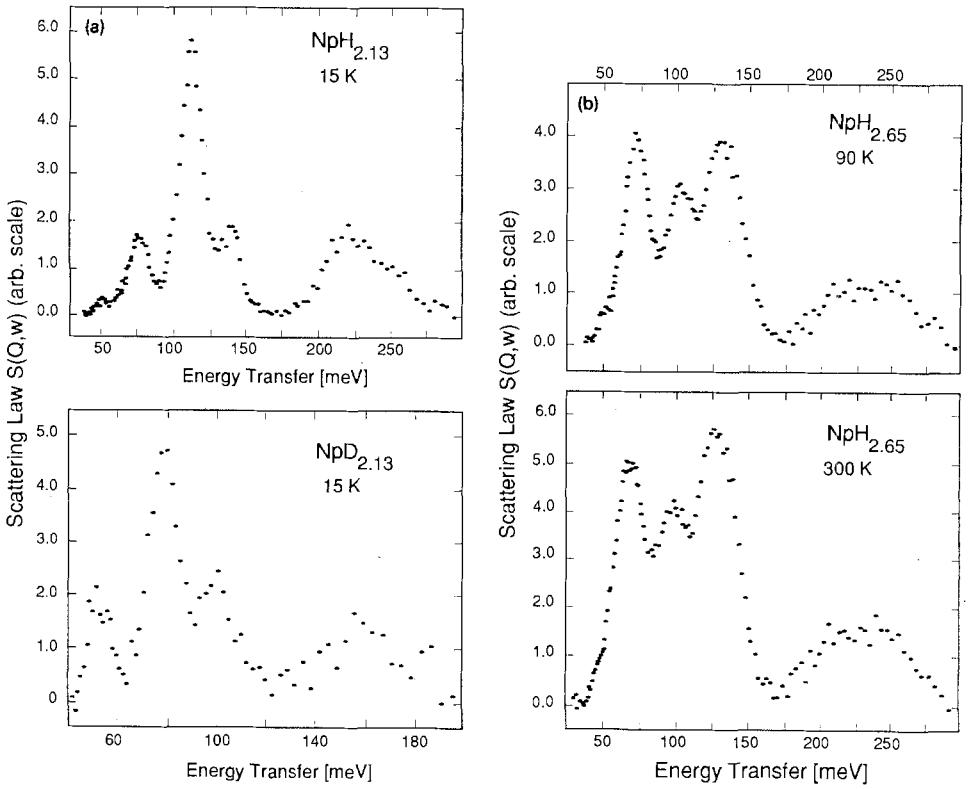

Fig. 30. Optical-phonon spectra from inelastic neutron scattering measurements on neptunium hydrides and deuterides. (a) Scattering law data for $NpH_{2.13}$ and $NpD_{2.13}$. (b) Scattering law data for $NpH_{2.65}$ at 90 K and room temperature. After Goldstone et al. (1989).

high composition is probably due to increased interaction of t-sites and o-sites, to the effects of inhomogeneity, to vacancies, etc. A typical example of phonon spectra for all hydride systems is shown by results of Goldstone et al. (1989) for the NpH(D) system in fig. 30a, b.

Numerous crystal-field studies are reported for the rare-earth hydrides. The time-of-flight inelastic scattering experiments by Vorderwisch et al. (1979) on CeD_x ($1.9 < x < 2.74$) show three distinct peaks attributed to crystal-field transitions (5.6, 12.6 and 18.5 meV) and provide evidence for t-site vacancies and non-cubic resultant symmetries. However, Glinka et al. (1979) and also Rowe and Rush (1978), using a $CeD_{2.12}$ single crystal, find only a single well-defined transition at 20 meV, in agreement with the expected Γ_7 doublet /Γ_8 quartet ground state. The apparent diagreement may be due to the more perfect stoichiometry of the single crystal as suggested by Vorderwisch et al. (1979), or to the presence of metallic cerium or contaminant causing angle-dependent structure in the time-of-flight data as proposed by Glinka et al. (1979).

Other crystal-field determinations include a study by Shamir and Shaked (1979) on DyD_2 that confirm the predicted $\Gamma_7-\Gamma_8$ transition (8 meV), and several studies on the Pr + D system. Earlier work by Knorr et al. (1978) clearly define the crystal-field splitting into Γ_1, Γ_3, Γ_4 and Γ_5, states, with major peaks at 21 and 41 meV among a host of phonon energies. Arons et al. (1987) used polarized neutrons to distinguish between crystal-field levels and phonon effects and showed that the 20 meV peak arises from the ground state at low temperatures. The 20 to 41 meV transitions are possible at room temperature, and thus increasing the observed intensity for the 20 meV peak. Finally, Burger et al. (1990b) used this crystal-field information to quantify the observed resistivity minimum in PrH_2 on the basis of a transition from the magnetic Γ_5 ground state to a non-magnetic Γ_1 excited state. The observed 20 and 41 meV peaks correspond to $\Gamma_5-\Gamma_4$ and $\Gamma_5-\Gamma_3$ transitions, respectively. It should be noted that this assignment for $PrH_{2.0}$ differs markedly from the incommensurate magnetic transitions found in the MH_{2+x} systems of Sm, Gd and Tb with $x > 0$.

The only scattering results for an actinide system are those measured by Goldstone et al. (1989) for the NpH(D) system in fig. 30a, b. The o-site peak at 74 eV is quite prominent because the lower phase boundary for the hydride is high ($x = 2.13$) and the o-site population is augmented by depletion of t-sites (see section 3.1.1). In addition to the two peaks corresponding to hydrogen on o- and t-sites, data for $NpH_{2.65}$ also show a third intermediate peak found for many high-composition rare-earth hydride systems. The third peak is persistent, but unexplained, and many authors suggest that it must be due to interaction of t-sites and o-sites. However, modeling by Vorderwisch et al. (1991) shows that the H_0-H_t interaction parameter must be increased by an unreasonably amount to account for the additional intensity of the third peak. Goldstone et al. (1989) suggest that the peak is due to the close proximity to the cubic–hexagonal two-phase region.

Considerable work is described on properties of α-phase solutions. Whereas the study by Anderson et al. (1986) on α-YH_x shows a single local-mode vibrational peak, results by Blaschko et al. (1988) reveal that a three-level structure persists even up to 300 K for the α-LuD_x, indicating that an appreciable amount of deuterium remains ordered even at room temperature. A large anisotropy of local-mode potentials at the tetrahedral interstice is found for both systems. A follow-up study by Pleschiutschnig et al. (1991) on the α-LuD_x system at lower concentrations ($x = 0.06, 0.08$) confirms the c-axis chain-like arrangement found at higher concentrations (see section 3.2). Although the chains are much shorter and the split level is missing (also for α-YH_x), diffuse neutron scattering clearly indicates that pairing persists, whether or not the local mode splitting is observed. Indications that a component of isolated or "labile" H atoms exists at high concentrations is confirmed in a recent and extensive study by Berk et al. (1991) on α-ScH_x and α-YH_x, where a fast local t-site hopping mode is observed. The authors develop a Kondo model of quantum hopping to describe the weak interactions of protons with the host-metal conduction electrons. The reader is referred to this paper for more detail.

6.5.2. *NMR and EPR/ESR*

Although application of NMR methods to magnetic and other non-diffusion studies such as spin–lattice mechanisms is not currently a major area of work, interesting and

TABLE 12
Crystal-field symmetry changes with site occupation for Er^{+3} in LaH_x.

Hydride composition (x)	Field symmetry (point charge model)
2.00	cubic
2.16	axial or tetragonal
2.33	tetragonal or axial
2.50	cubic or orthorhombic
2.66	tetragonal
2.83	tetragonal
3.00	cubic

fundamental data are reported on the Van Vleck paramagnet, TmH_2, by Winter et al. (1990) and Shaltiel et al. (1991a and b). For this unusual singlet ground state material, observed paramagnetic defects are attributed to deviations from ideal stoichiometry (rather than to impurities) or to damaged or strained areas. However, the influence of defects is supported by clear evidence that t-sites are unoccupied near MH_2 for many systems, with a concomitant slight early population of o-sites. Furthermore, results for PuH_x and NpH_x show a considerable *depopulation* of t-sites and anomalous filling of o-sites occurs at high compositions.

Electronic paramagnetic resonance (EPR), sometimes also defined as electron-spin resonance (ESR) is a particularly sensitive method for determining hydrogen site locations. Usually a small magnetic impurity (e.g., Er^{+3}) is introduced into a non-magnetic host lattice such as ScH_x, YH_x or LaH_x to probe the fields and the structure surrounding the impurity ion. A review of early data is published by Venturini (1981). In almost every case, the occupation of an o-site gives a clear signal in the form of an observed axial distortion; however, depletion of a t-site can complicate the interpretation. Although this story is well-established by other techniques such as neutron diffraction, ESR/EPR is especially sensitive in regions of low site occupancy. An interesting study by Drulis and Hoffmann (1985) on Er-doped LaH_x ($1.96 < x < 2.67$) shows a host of changing field symmetries during addition of hydrogen. Some of the data and assignments are given in table 12. In a companion piece to the NMR work just discussed, Shaltiel et al. (1991b) use the ESR method to confirm the NMR results for the Tm + H system and present an extensive discussion of possible exchange reactions and complexities in spin dynamics.

6.6. *Anomalous rare-earth systems*

Unlike the other rare earths, EuH_2 and YbH_2 form in the same orthorhombic (Pnma) structure as the alkaline-earth dihydrides. Only this dihydride is known for europium, but YbH_x can be driven, with sufficient hydrogen pressure, to form a cubic, metastable phase with a composition near $YbH_{2.25}$ ($a_0 = 5.192$ Å). Disagreements in the earlier literature and the realization that this phase apparently exhibits some very unusual properties at high compositions led to a flurry of studies during the past decade. In focusing on these phenomena, all results and techniques are condensed in this section.

The high-temperature behavior of ytterbium dihydride is unique among the rare earths and actinides. Studies by Haschke and Clark (1972) show that YbH_2 vaporizes to the gaseous elements by a congruent process like those observed for MgH_2 and CaH_2. This behavior stands in sharp contrast to the incongruent reactions of the other rare earths and actinides that form H_2 and condensed metal. Derived thermodynamic values ($\Delta H_{f\,0} = -179$ kJ/mol and $\Delta G_{f\,0} = -143$ kJ/mol) for YbH_2 are consistent with those of the alkaline earths.

Other unique properties are encountered at high H/Yb ratios. Bischof et al. (1983) prepared pure $YbH_{2.56}$ at 300°C and 120 atm, and point out that the unusually large lattice constant (see fig. 8) does not fit the rare-earth pattern and implies the coexistence of both Yb^{+2} and Yb^{+3} in the lattice. This constitutes the first occurrence of mixed valence in a rare-earth hydride. Accompanying optical emission measurements showed the material to be metallic, implying an unusual *homogeneously* mixed valence.

In an NMR and magnetic sysceptibility study, Zogal et al. (1984) confirm that the higher-composition phase obeys the Curie–Weiss law with $\mu_{eff} = 3.16\mu_B$, a value about 70% of that for the Yb^{+3} ion. The assumption of an equimolar Yb^{+2}/Yb^{+3} ratio satisfies the observed data. The mixed-valence concept is fully confirmed by Büchler et al. (1987) from photoemission data. The experimental and calculated Yb $3d_{5/2}$ spectra in fig. 31 clearly show the two valence states.

Using a diamond anvil cell, Staun Olsen et al. (1984) found a first-order phase transformation to a hexagonal phase at 15 GPa, with an accompanying 5.2% decrease in volume. The bulk modulus was found to be $B = 138$ GPa. Using a high-pressure method involing decomposition of AlH_3, Wakamori et al. (1986) synthesized hexa-

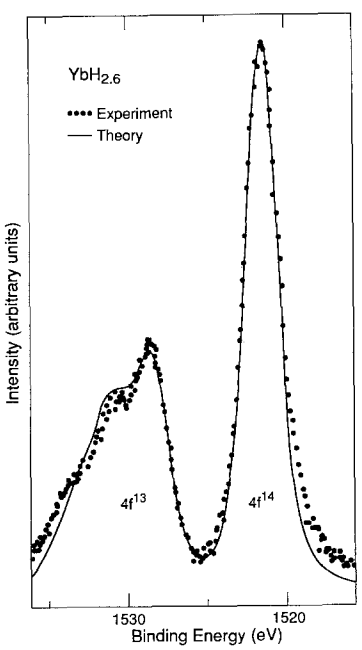

Fig. 31. Yb $3d_{5/2}$ XPS spectrum for $YbH_{2.6}$. The two electronic configurations ($4f^{13}$ and $4f^{14}$) correspond to the two valence states (3+ and 2+) of Yb in this hydride. After Büchler et al. (1987).

gonal $YbH_{2.96}$ by maintaining 250°C under 4.0 GPa for 30 min. Here almost the fully trivalent Yb^{+3} magnetic moment ($\mu_{eff} = 4.37\mu_B$) is realized.

Further improvements in experimental techniques and capabilities have also allowed several intermediate phases to be synthesized and characterized. H. Drulis et al. (1988) found a shoulder in the P–C isotherm at 235°C, corresponding to a rather narrow composition at H/Yb = 2.27–2.29, which confirms the existence of the fcc β' phase. M. Drulis et al. (1988) performed specific-heat measurements on $YbH_{2.25}$, $YbH_{2.37}$ and $YbH_{2.41}$, and analyze the data in terms of possible Kondo and crystal-field effects. For $YbH_{2.37}$, as an example, the electronic specific-heat reaches a value $\gamma = 589$ mJ/mol K at 2.48 K, making these legitimate heavy-fermion compounds. Data for the high-temperature cubic hydride obey the Curie–Weiss law with $\mu_{eff} = 3.82\mu_B$ and a paramagnetic Curie temperature of 68 K, the latter a clear indicator of a Kondo effect.

Although the unusual Yb + H system has yielded a wealth of experimental information and a fuller understanding of hydrides in general, little has been gained from studies of the Eu + H system. Attempts to prepare higher phases than the dihydride have been unsuccessful. However, Wortmann et al. (1986) were able to form Eu^{+3} in a matrix of SmH_{2+x} at low temperatures, following the radioactive decay of ^{153}Sm. The presence of hydrogen on more than three neighboring octahedral sites forces europium into the trivalent state.

References

Aldred, A.T., G. Cinader, D.J. Lam and L.W. Weber, 1979, Phys. Rev. B **19**, 300.

Allen, T.H., 1991, The Solubility of Hydrogen in Plutonium in the Temperature Range 475 to 825 Degrees Centigrade, Masters Thesis (University of Colorado, Denver, CO).

Allen, T.H., 1992, personal communication (Los Alamos National Laboratory, Los Alamos, NM).

Anderson, D.L., R.G. Barnes, D.T. Peterson and D.R. Torgeson, 1980, Phys. Rev. B **21**, 2625.

Anderson, I.S., J.J. Rush, T.J. Udovic and J.M. Rowe, 1986, Phys. Rev. Lett. **57**, 2822.

Anderson, I.S., N.F. Berk, J.J. Rush and T.J. Udovic, 1988, Phys. Rev. B **37**, 4358.

Anderson, I.S., D.K. Ross and J.E. Bonnet, 1989, Z. Phys. Chem. NF **164**, 923.

Anderson, I.S., N.F. Berk, J.J. Rush, T.J. Udovic, R.G. Barnes, A. Magerl and D. Richter, 1990, Phys. Rev. Lett. **65**, 1439.

Anderson, P.W., 1958, Phys. Rev. **109**, 1492.

Arons, R.R., and J. Schweizer, 1982, J. Appl. Phys. **53**, 2631.

Arons, R.R., J.W. Cable and R.M. Nicklow, 1987, J. Appl. Phys. **61**, 3423.

Atkinson, G., S. Coldrick, J.P. Murphy and N. Taylor, 1976, J. Less-Common Met. **49**, 439.

Barnes, R.G., 1989, Z. Phys. Chem. NF **164**, 841.

Barnes, R.G., 1991, J. Less-Common Met. **172–174**, 509.

Barnes, R.G., B.J. Beaudry, R.B. Creel, D.R. Torgeson and D.G. de Groot, 1980, Solid State Commun. **36**, 105.

Barnfather, K.J., E.F.W. Seymour, G.A. Styles, A.J. Dianoux; R.G. Barnes and D.R. Torgeson, 1989, Z. Phys. Chem. NF **164**, 935.

Bartscher, W., A. Boeuf, R. Caciuffo, J.M. Fournier, J.M. Haschke, L. Manes, J. Rebizant, F. Rustichelli and J.W. Ward, 1985, Physica B **130**, 530.

Bashkin, I.O., E.G. Ponyatovskii and M.E. Kost, 1979, Phys. Status Solidi b **91**, 401.

Bedere, D., and P. Sans, 1983, J. Less-Common Met. **91**, 33.

Belyayev, M.Yu., and A.V. Stepanov, 1982, Phys. Met. Metallogr. **54**, 80.

Berk, N.F., J.J. Rush, T.J. Udovic and I.S. Anderson, 1991, J. Less-Common Met. **172**, 496.

Bieganski, Z., and M. Drulis, 1979, Solid State Commun. **31**, 501.

Bieganski, Z., and B. Stalinski, 1976, J. Less-Common Met. **49**, 421.
Bischof, R., E. Kaldis and I. Lacis, 1983, J. Less-Common Met. **94**, 117.
Blaschko, O., 1991, J. Less-Common Met. **172–174**, 237.
Blaschko, O., G. Krexner, J.N. Daou and P. Vajda, 1985, Phys. Rev. Lett. **55**, 2876.
Blaschko, O., G. Krexner, L. Pintschovius, P. Vajda and J.N. Daou, 1988, Phys. Rev. B **38**, 9612.
Bloch, J., and M.H. Mintz, 1981, J. Less-Common Met. **81**, 301.
Bloch, J., E. Swissa and M.H. Mintz, 1989, Z. Phys. Chem. NF **164**, 1193.
Bonnet, J.E., 1976, J. Less-Common Met. **49**, 451.
Bonnet, J.E., and J.N. Daou, 1979, J. Phys. Chem. Solids **40**, 421.
Boroch, E., and E. Kaldis, 1987, Inorg. Chim. Acta **140**, 89.
Boroch, E., and E. Kaldis, 1989, Z. Phys. Chem. NF **163**, 117.
Boroch, E., K. Conder, Cai-Ru-Xiu and E. Kaldis, 1989, J. Less-Common Met. **156**, 259.
Borsa, F., R.G. Barnes, B.J. Beaudry and D.R. Torgeson, 1982, Phys. Rev. B **26**, 1471.
Büchler, S., L. Schlapbach, R. Monnier and L. Degiorgi, 1987, J. Phys. Colloq. (Paris) **48**, C9-947.
Burger, J.P., J.N. Daou, P. Vajda and A. Lucasson, 1984, J. Less-Common Met. **103**, 381.
Burger, J.P., J.N. Daou and P. Vajda, 1988, Philos. Mag. B **58**, 349.
Burger, J.P., J.N. Daou and P. Vajda, 1990a, J. Magn. & Magn. Mater. **90**, 110.
Burger, J.P., J.N. Daou and P. Vajda, 1990b, Z. Phys. B **80**, 233.
Carlin, R.L., and L.J. Krause, 1981, Chem. Phys. Lett. **82**, 323.
Carlin, R.L., R.D. Chirico, K.O. Joung, G.K. Shenoy and D.G. Westlake, 1980, Phys. Lett. A **75**, 413.
Carlin, R.L., L.J. Krause, A. Lambrecht and H. Claus, 1982, J. Appl. Phys. **53**, 2634.
Carstens, D.H.W., 1981, J. Phys. Chem. **85**, 778.
Cheetham, A.K., and B.E.F. Fender, 1972, J. Phys. C **5**, L35.
Chernikov, A.S., V.I. Savin, V.N. Fadeev, N.A. Landin and L.A. Izhvanov, 1987, J. Less-Common Met. **130**, 441.
Cinader, G., D. Zamir and Z. Hadari, 1976, Phys. Rev. B **14**, 912.
Conder, K., J. Schefer, E. Kaldis and Cai-Ru-Xiu, 1989, Z. Phys. Chem. NF **163**, 125.
Conder, K., L. Wang, E. Boroch and E. Kaldis, 1991, Eur. J. Solid State & Inorg. Chem. **28**(Suppl.), 487.
Condon, J.B., 1975, J. Phys. Chem. **79**, 392.
Cox, L.E., J.W. Ward and R.G. Haire, 1992, Phys. Rev. B **45**, 13239.
Danielou, R., J.N. Daou, E. Ligeon and P. Vajda, 1981, Phys. Status Solidi **67**, 453.
Dantzer, P., and O.J. Keppa, 1980, J. Solid State Chem. **35**, 34.
Daou, J.N., P. Vajda, A. Lucasson and P. Lucasson, 1981, Solid State Commun. **38**, 135.
Daou, J.N., P. Vajda, J.P. Burger and A. Lucasson, 1986, Phys. Status Solidi **98**, 183.
Daou, J.N., P. Vajda and J.P. Burger, 1988a, Phys. Rev. B **37**, 5236.
Daou, J.N., P. Vajda, J.P. Burger and D. Shaltiel, 1988b, Europhys. Lett. **6**, 647.
Daou, J.N., P. Vajda, G. Hilscher and N. Pillmayr, 1988c, J. Phys. Colloq. (Paris) C **8**, 49, 375.
Daou, J.N., P. Vajda and J.P. Burger, 1989, Solid State Commun. **71**, 1145.
Daou, J.N., J.P. Burger and P. Vajda, 1992, Philos. Mag. B **65**, 127.
Didisheim, J-J., K. Yum, P. Fischer, W. Haelg and L. Schlapbach, 1980, Phys. Lett. A **78**, 111.
Drulis, H., and K.P. Hoffmann, 1985, Z. Phys. Chem. NF **145**, 11.
Drulis, H., M. Drulis and W. Iwasieczko, 1988, J. Less-Common Met. **141**, 201.
Drulis, M., 1985, Z. Phys. Chem. NF **145**, 19.
Drulis, M., and Z. Bieganski, 1979, Phys. Status Solidi a **53**, 277.
Drulis, M., and B. Stalinski, 1982, Phys. Status Solidi a **69**, 385.
Drulis, M., J. Opyrchal and W. Borkowska, 1984, J. Less-Common Met. **101**, 211.
Drulis, M., H. Drulis and B. Stalinski, 1988, J. Less-Common Met. **141**, 207.
Eriksson, O., Y.G. Hao, B.R. Cooper, G.W. Fernando, L.E. Cox, J.W. Ward and A.M. Boring, 1991, Phys. Rev. B **43**, 4590.
Eyring, L., 1979, The binary rare earth oxides, in: Handbook on the Physics and Chemistry of Rare Earths, Vol. 3, eds K.A. Gschneidner Jr and L. Eyring (North-Holland, Amsterdam) ch. 27.
Farr, J.D., A.L. Giorgi, M.G. Bowman and R.K. Money, 1961, J. Inorg. & Nucl. Chem. **18**, 42.
Fedotov, V.K., V.G. Fedotov, M.E. Kost and E.G. Ponyatovskii, 1982, Sov. Phys. Solid State (E.T.) **24**, 1252.

Flanagan, T.B., and J.D. Clewley, 1982, J. Less-Common Met. **83**, 127.
Flood, D.J., 1978, J. Appl. Phys. **49**, 1495.
Flotow, H.E., J.M. Haschke and S. Yamauchi, 1984, in: The Chemical Thermodynamics of Actinide Elements and Compounds, Part 9. The Actinide Hydrides, ed. F.L. Oetting (IAEA, Vienna).
Fujimori, A., 1982, Phys. Rev. B **27**, 3992.
Fujimori, A., and J. Osterwalder, 1984, J. Phys. C **17**, 2869.
Fujimori, A., and N. Tsuda, 1981, J. Phys. C **14**, 1427.
Fujimori, A., F. Minami and N. Tsuda, 1980, Phys. Rev. B **22**, 3573.
Gerard, N., 1987, J. Less-Common Met. **131**, 13.
Gibson, J.K., and R.G. Haire, 1985a, J. Solid State Chem. **59**, 317.
Gibson, J.K., and R.G. Haire, 1985b, J. Less-Common Met. **109**, 251.
Gibson, J.K., and R.G. Haire, 1985c, Radiochim. Acta **38**, 193.
Gibson, J.K., and R.G. Haire, 1990, J. Phys. Chem. **94**, 935.
Gilson, A.R.L., A. Fazzio and R. Mota, 1989, Int. J. Quantum Chem. **23**, 709.
Glinka, C.J., J.M. Rowe, G.G. Libowitz and A.J. Maeland, 1979, J. Phys. C **12**, 4229.
Goldstone, J.A., 1990, personal communication (Los Alamos National Laboratory, Los Alamos, NM).
Goldstone, J.A., P. Vorderwisch, B. Cort, A.C. Lawson and J.W. Ward, 1989, Z. Phys. Chem. NF **164**, 1107.
Göring, R., B. Schnabaael and O.J. Zogal, 1980, Phys. Status Solidi **59**, K147.
Greis, O., and J.M. Haschke, 1982, Rare earth fluorides, in: Handbook on the Physics and Chemistry of Rare Earths, Vol. 5, eds K.A. Gschneidner Jr and L. Eyring (North-Holland, Amsterdam) ch. 45.
Greis, O., P. Knappe and H. Müller, 1981, J. Solid State Chem. **39**, 49.
Grunzweig-Genossar, J., M. Kuznietz and B. Meerovici, 1970, Phys. Rev. B **1**, 1958.
Gupta, M., 1978, Solid State Commun. **27**, 1355.
Gupta, M., and J.P. Burger, 1980, Phys. Rev. B **22**, 6074.
Haschke, J.M., 1981, USDOE Rep. RFP-3099.
Haschke, J.M., 1991, Actinide hydrides, in: Topics in f-Element Chemistry; Synthesis of Lanthanide and Actinide Compounds, Vol. 2, eds G. Meyer and L. Morss (Kluwer, Dordrecht) ch. 1.
Haschke, J.M., and M.R. Clark, 1972, High Temp. Sci. **4**, 386.
Haschke, J.M., and A.E. Hodges III, 1981, USDOE Report LBL-12441, p. 229.
Haschke, J.M., A.E. Hodges III, C.M. Smith and F.L. Oetting, 1980, J. Less-Common Met. **73**, 41.
Haschke, J.M., J.W. Ward and W. Bartscher, 1985, J. Less-Common Met. **107**, 159.
Haschke, J.M., A.E. Hodges III and R. Lucas, 1987, J. Less-Common Met. **133**, 155.
Hill, H.H., 1970, in: Plutonium 1970 and Other Actinides, ed. W.N. Miner (Nuclear Metallurgy, AIME, New York) Vol. 17, p. 1.
Ito, T., B.J. Beaudry and K.A. Gschneidner Jr, 1982, J. Less-Common Met. **88**, 425.
Ito, T., B.J. Beaudry, K.A. Gschneidner Jr and T. Takeshita, 1983, Phys. Rev. B **27**, 2830.
Johansson, B., 1975, Phys. Rev. B **11**, 2836.
Kai, K., K.A. Gschneidner Jr, B.J. Beaudry and D.T. Peterson, 1989, Phys. Rev. B **40**, 6591.
Kashaev, R.S., A.N. Gil'manov, F.F. Gubaidullin and M.E. Kost, 1978, Sov. Phys. Solid State **20**, 1.
Khatamian, D., W.A. Kamitakahara, R.G. Barnes and D.T. Peterson, 1980, Phys. Rev. B **21**, 2622.
Knorr, K., B.E.F. Fender and W. Drexel, 1978, Z. Phys. B **30**, 265.
Kress, W., 1987, Physics Data **26-1**, 226.
Kulikov, N.I., 1982, J. Less-Common Met. **88**, 307.
Libowitz, G.G., and A.J. Maeland, 1979, Hydrides, in: Handbook on the Physics and Chemistry of Rare Earths, Vol. 3, eds K.A. Gschneidner Jr and L. Eyring (North-Holland, Amsterdam) ch. 26.
Libowitz, G.G., J.G. Pack and W.P. Binnie, 1972, Phys. Rev. B **6**, 4540.
Lichty, L.R., J-W. Han, R. Ibanez-Meier, D.R. Torgeson, R.G. Barnes, E.F.W. Seymour and C.A. Sholl, 1989, Phys. Rev. B **39**, 2012.
Liu, F., M. Challa, S.N. Khanna and P. Jena, 1989, Phys. Rev. Lett. **63**, 1396.
Lundin, C.E., and J.P. Blackledge, 1962, J. Electrochem. Soc. **10**, 838.
Mintz, M.H., Z. Hadari and M. Bixon, 1974, J. Less-Common Met. **37**, 331.
Misemer, D.K., and B.N. Harmon, 1982, Phys. Rev. B **26**, 5634.
Mota, R., 1985, Can. J. Phys. **63**, 1576.
Mota, R., and J.A.T. Borges da Costa, 1987, Rev. Brasil. Fis. **17**, 165.
Mueller, W.M., J.P. Blackledge and G.G. Libowitz, 1968, Metal Hydrides (Academic Press, New York).

Müller, H., and P. Knappe, 1982, J. Less-Common Met. **87**, 59.
Oetting, F.L., A.E. Hodges III, J.M. Haschke and H.E. Flotow, 1984, J. Chem. Thermodyn. **16**, 1089.
Ohki, C., M. Tada, Y.C. Huang, Hi. Uchida and Ha. Uchida, 1984, J. Less-Common Met. **103**, 103.
Ohki, C., H. Uchida and Y.C. Huang, 1989, Z. Phys. Chem. NF **163**, 149.
Opyrchal, J., and Z. Bieganski, 1978, Solid State Commun. **26**, 965.
Osterwalder, J., 1985, Z. Phys. B **61**, 113.
Osterwalder, J., H.R. Ott, L. Schlapbach, J. Schefer and P. Fischer, 1983, J. Less-Common Met. **94**, 129.
Owen, J.W., and R.A. Scudamore, 1966, Corros. Sci. **6**, 461.
Peterman, D.J., and B.N. Harmon, 1979, Phys. Rev. B **20**, 5313.
Peterman, D.J., B.N. Harmon, J. Marchinao and J.H. Weaver, 1979, Phys. Rev. B **19**, 4867.
Peterman, D.J., J.H. Weaver and D.T. Peterson, 1981, Phys Rev. B **23**, 3903.
Peterman, D.J., J.H. Weaver, M. Croft and D.T. Peterson, 1983, Phys. Rev. B **27**, 808.
Pleschiutschnig, J., W. Schwarz, O. Blaschko, P. Vajda and J.N. Daou, 1991, Phys. Rev. B **43**, 5139.
Powell, G.L., 1989, Z. Phys. Chem. NF **164**, 1227.
Powell, G.L., W.L. Harper and J.R. Kirkpatrick, 1991, J. Less-Common Met. **172–174**, 116.
Richards, P.M., 1987, Phys. Rev. B **36**, 7417.
Rowe, J.M., and J.J. Rush, 1978, in: Neutron Inelastic Scattering, Vol. II (IAEA, Vienna) p. 303.
Schlapbach, L., and J. Osterwalder, 1982, Solid State Commun. **42**, 271.
Schlapbach, L., and H.R. Scherrer, 1982, Solid State Commun. **41**, 893.
Schlapbach, L., J. Osterwalder and H.C. Siegmann, 1982, J. Less-Common Met. **88**, 291.
Schlapbach, L., H.R. Ott, E. Felder, H. Rudigier, P. Thiry, J.E. Bonnet, Y. Petroff and J.P. Burger, 1986a, J. Less-Common Met. **130**, 239.
Schlapbach, L., J.P. Burger, P. Thiry, J.E. Bonnet and Y. Petroff, 1986b, Phys. Rev. Lett. **57**, 2219.
Schlapbach, L., J.P. Burger, J.E. Bonnet, P. Thiry and Y. Petroff, 1987, Surf. Sci. **189/190**, 747.
Sen Gupta, R., and S. Chatterjee, 1983, J. Phys. F **13**, 639.
Sen Gupta, R., and S. Chatterjee, 1988, Phys. Status Solidi b **148**, 579.
Senoussi, S., J.N. Daou, P. Vajda and J.P. Burger, 1987, J. Less-Common Met. **130**, 55.
Seymour, E.F.W., 1982, J. Less-Common Met. **88**, 323.
Shaltiel, D., H. Winter, E. Dormann, J.P. Burger, J.N. Daou, P. Vajda and A. Grayevsky, 1991a, J. Less-Common Met. **172–174**, 293.
Shaltiel, D., J.P. Burger, J.N. Daou, P. Vajda and A. Grayevsky, 1991b, Phys. Rev. B **43**, 6022.
Shamir, N., and H. Shaked, 1979, Phys. Lett. A **72**, 139.
Shinar, J., B. Dehner, B.J. Beaudry and D.T. Peterson, 1988, Phys. Rev. B **37**, 2066.
Shinar, J., B. Dehner, R.G. Barnes and B.J. Beaudry, 1990, Phys. Rev. Lett. **64**, 563.
Spalthoff, W., 1961, Z. Phys. Chem. NF **29**, 258.
Stakebake, J.L., 1981, J. Electrochem. Soc. **128**, 2383.
Stakebake, J.L., 1992, J. Alloys & Compounds **181**, 271.
Stalinski, B., 1985, Z. Phys. Chem. NF **145**, 1.
Staun Olsen, J., B. Buras, L. Gerward, B. Johansson, B. Lebech, H.L. Skriver and S. Steenstrup, 1984, Phys. Scr. **29**, 503.
Stuhr, U., M. Schlereth, D. Steinbinder and H. Wipf, 1989, Z. Phys. Chem. NF **164**, 929.
Subramanian, P.R., and J.F. Smith, 1982, J. Less-Common Met. **87**, 205.
Surplice, N.A., and K. Kandasamy, 1982, J. Phys. D **15**, 1117.
Switendick, A.C., 1970, Solid State Commun. **8**, 1463.
Switendick, A.C., 1971, Int. J. Quantum Chem. **5**, 459.
Titcomb, C.G., A.K. Cheetham and B.E.F. Fender, 1974, J. Phys. C **7**, 2409.
Torgeson, D.R., F. Borsa and I. Svare, 1991, Phys. Rev. B **43**, 7448.
Uchida, H., Y.C. Huang, M. Tada and K. Fujita, 1979, Z. Phys. Chem. NF **114**, 51.
Uchida, H., Y. Ohtani, T. Kawahata, H. Minamitani, N. Ninomiya, E. Fromm, N. Hosada and H.H. Uchida, 1991, J. Less-Common Met. **172–174**, 832.
Udovic, T.J., J.J. Rush, I.S. Anderson and R.G. Barnes, 1990, Phys. Rev. B **41**, 3460.
Vajda, P., and J.N. Daou, 1991, Phys. Rev. Lett. **66**, 3176.
Vajda, P., and J.N. Daou, 1992, Phys. Rev. B **45**, 9749.
Vajda, P., J.N. Daou, J.P. Burger and A. Lucasson, 1985, Phys. Rev. B **31**, 6900.
Vajda, P., J.N. Daou and J.P. Burger, 1987, Phys. Rev. B **36**, 8669.

Vajda, P., J.N. Daou and J.P. Burger, 1989a, Phys. Rev. B **40**, 500.

Vajda, P., J.N. Daou, J.P. Burger, G. Hilscher and N. Pillmayr, 1989b, J. Phys.: Condens. Matter **1**, 4099.

Vajda, P., J.P. Burger and J.N. Daou, 1990, Europhys. Lett. **11**, 567.

Vajda, P., J.N. Daou, P. Moser and P. Remy, 1991, J. Less-Common Met. **172–174**, 522.

Venturini, E.L., 1981, in: Nuclear and Electron Resonance Spectroscopies Applied to Materials Science, Vol. 74, eds F.J. Kaufmann and G.K. Shenoy (North-Holland, Amsterdam) p. 45.

Vorderwisch, P., S. Hautecler and J.B. Suck, 1979, Phys. Status Solidi b **94**, 569.

Vorderwisch, P., S. Hautecler and T. Lesmann, 1991, J. Less-Common Met. **172**, 231.

Wakamori, K., T. Nakamura and A. Sawaoka, 1986, J. Mater. Sci. **21**, 849.

Wang, L., K. Conder and E. Kaldis, 1990, Solid State Ionics **43**, 103.

Ward, J.W., 1983, J. Less-Common Met. **93**, 279.

Ward, J.W., 1985a, in: Handbook on the Physics and Chemistry of the Actinides, Vol. 3, eds A.J. Freeman and C. Keller (Elsevier, Amsterdam) ch. 1.

Ward, J.W., 1985b, in: Americium and Curium Chemistry and Technology, ed. N.M. Edelstein (Reidel, New York) p. 135.

Ward, J.W., J.M. Haschke, J. Rebizant and W. Bartscher, 1984, J. Less-Common Met. **100**, 195.

Ward, J.W., P.D. Kleinschmidt and D.E. Peterson, 1986, in: Handbook on the Physics and Chemistry of the Actinides, Vol. 4, eds A.J. Freeman and C. Keller (Elsevier, Amsterdam) ch. 7, pp. 352–356.

Ward, J.W., W. Bartscher and J. Rebizant, 1987, J. Less-Common Met. **130**, 431.

Ward, J.W., B. Cort, J.A. Goldstone, A.C. Lawson, L.E. Cox and R.G. Haire, 1992, in: Transuranium Elements. A Half Century, eds L.R. Morss and J. Fuger (ACS Books, Washington) ch. 39.

Weaver, J.H., R. Rosei and D.T. Peterson, 1979a, Phys. Rev. B **19**, 4855.

Weaver, J.H., D.T. Peterson and R.L. Benbow, 1979b, Phys. Rev. B **20**, 5301.

Wicke, E., and K. Otto, 1962, Z. Phys. Chem. NF **31**, 222.

Winter, H., D. Shaltiel and E. Dormann, 1990, J. Magn. & Magn. Mater. **87**, 181.

Wortmann, G., W. Thal, A. Mustachi and I. Nowik, 1986, J. Less-Common Met. **125**, 105.

Yannopoulos, L.N., R.K. Edwards and P.G. Wahlbaeck, 1965, J. Phys. Chem. **69**, 2510.

Zogal, O.J., and M. Drulis, 1989, Z. Phys. Chem. NF **163**, 303.

Zogal, O.J., K.P. Hoffmann, W. Petrynski, H. Drulis and B. Stalinski, 1984, J. Less-Common Met. **101**, 259.

Handbook on the Physics and Chemistry of Rare Earths
Vol. 18 – Lanthanides/Actinides: Chemistry
edited by K.A. Gschneidner, Jr., L. Eyring, G.R. Choppin and G.H. Lander

Chapter 124

LANTHANIDE AND ACTINIDE HALIDES

H.A. EICK
Department of Chemistry, Michigan State University, East Lansing, MI 48824-1322, USA

Contents

1. Introduction 366
2. Trivalent halides 368
   2.1. Synthesis 368
   2.2. Structural modifications at normal and elevated pressures 371
      2.2.1. Structure types preparable at normal pressures 371
      2.2.2. Pressure-induced structural transformations 375
   2.3. Mixed-cation and mixed-anion systems 378
      2.3.1. Multiple-cation systems 378
      2.3.2. Multiple-halide systems 378
      2.3.3. Halide and non-halide anion systems 380
         2.3.3.1. Fluorite-related cluster compounds 381
         2.3.3.2. Octahedral cluster compounds 383
      2.3.4. Mixed-cation systems 384
         2.3.4.1. MX_2–RX_3 systems 384
         2.3.4.2. AX–RX_3 systems 388
         2.3.4.3. Miscellaneous systems 392
3. Trihalide hydrates 393
4. Reduced halides MX_n, $n < 3$ 395
   4.1. Metallic halides 396
   4.2. Dihalides 397
   4.3. Mixed-dihalide systems 399
      4.3.1. Hydride-halide systems 401
      4.3.2. AX_n–MX_2 systems 402
   4.4. Cluster-stabilized reduced halides 402
5. Higher halides 403
   5.1. MX_4 compounds 403
   5.2. MX_n–$M'X_4$ systems 404
   5.3. AcX_6 systems 405
References 405

1. Introduction

The lanthanide and actinide halides remain an exceedingly active area of research; since 1980 they have been cited in well over 2500 Chemical Abstracts references, with the majority relating to the lanthanides. Lanthanide and actinide halide chemistry has also been reviewed numerous times. The binary lanthanide chlorides, bromides, and iodides were reviewed in this series (Haschke 1979). In that review, which included trihalides (RX_3), tetrahalides (RX_4), and reduced halides (RX_n, $n < 3$), preparative procedures, structural interrelationships, and thermodynamic properties were discussed. Hydrated halides and mixed metal halides were discussed to a lesser extent. The synthesis of scandium, yttrium and the lanthanide trihalides, RX_3, where X = F, Cl, Br, and I, with emphasis on the halide hydrates, solution chemistry, and aspects related to enthalpies of solution, were reviewed by Burgess and Kijowski (1981). The binary lanthanide fluorides and mixed fluoride systems, $AF - RF_3$ and $AF_2 - RF_3$, where A represents the group 1 and group 2 cations, were reviewed in a subsequent Handbook (Greis and Haschke 1982). That review emphasized the close relationship of the structures of these compounds to that of fluorite.

Additional areas of lanthanide halide chemistry that have been reviewed include the synthesis, phase studies, and structures of complex lanthanide halides – compounds formed between one or more group 1 cation and lanthanide element halides (Meyer 1982). Halides in combination with lanthanide elements in the II, III, and IV oxidation states were considered with the chemistry of the heavier halides being emphasized. More recently the reduced ternary lanthanide halides (Meyer 1983) and the reduced halides of the lanthanide elements were reviewed (Meyer 1988). The latter review considered lanthanides in which the formal oxidation state of the cation was ≤ 2 and included hydride halides, oxide halides, mixed-valence ternary halides, and reduced halide clusters. Corbett et al. (1987) discussed the structures and some bonding aspects of highly reduced lanthanide halides and compounds stabilized by a second-period element bound within each cluster, e.g., $Sc_7Cl_{12}B$, Sc_5Cl_6B, Y_2Cl_2C.

The synthesis of lanthanide and actinide compounds is the topic of a book edited by Meyer and Morss (1991). Topics that relate to halides, with the author(s) in brackets, include: "Lanthanide fluorides" [B.G. Müller], "Actinide fluorides" [N.P. Freestone], "Binary lanthanide(III) halides, RX_3, X = Cl, Br, and I" [G. Meyer], "Complex lanthanide(III) chlorides, bromides and iodides" [G. Meyer], "Conproportionation routes to reduced lanthanide halides" [J.D. Corbett], and "Action of alkali metals on lanthanide(III) halides: an alternative to the conproportionation route to reduced lanthanide halides" [G. Meyer and T. Schleid]. Meyer and Meyer (1992) reviewed lanthanide halides in which the valence of the lanthanide was considered unusual, with unusual being defined as compounds in which the "localized" valence of an atom differs from its oxidation number. A metallic halide such as LaI_2 [oxidation number (O) = +2; valence (V) = +3, since the $5d^1$ electron is delocalized in the conduction band] or a semiconducting halide such as Pr_2Br_5 (O = +2.5; V = +3) is "unusual" by this definition, but TmI_2 (O = +2; V = +2) is not. In this review synthesis, properties, and calculated electronic structures are considered with emphasis on praseodymium halides and hydrogen intercalation into lanthanide dihalides and "monohalides".

Comparable recent detailed reviews of the actinide halides could not be found. The structures of actinide fluorides, both binary fluorides and combinations of these with main-group elements with emphasis on lattice parameters and coordination polyhedra, were reviewed by Penneman et al. (1973). The chemical thermodynamics of actinide binary halides, oxide halides, and alkali-metal mixed salts were reviewed by Fuger et al. (1983), and while the preparation of high-purity actinide metals and compounds was discussed by Müller and Spirlet (1985), actinide-halide compounds were hardly mentioned. Raman and absorption spectroscopy of actinide tri- and tetrahalides are discussed in a review by Wilmarth and Peterson (1991). Actinide halides, reviewed by element, are considered in detail in the two volume treatise by Katz et al. (1986). The thermochemical and oxidation–reduction properties of lanthanides and actinides are discussed elsewhere in this volume [in the chapter by Morss (ch. 122)].

The goal of this chapter was to consider interrelationships, comparisons, and contrasts between lanthanide and actinide halide chemistry. Since the predominant oxidation state of the lanthanides is III with the IV, II, and lower oxidation states stable only in the solid state, while those of the actinides vary from II through VII, the region of commonality is limited to the III, the II, to cluster compounds, and to a lesser extent, the IV oxidation state. Reactions associated with higher oxidation states, some of which are mentioned at the end of this chapter, clearly contrast with lanthanide chemistry. The ionic radius plays an important role in the solid-state chemistry of the II and III oxidation states. Thus the phases observed in solid-state reactions, whether they involve a lanthanide or actinide cation, are determined predominantly by ionic size relationships. Since the (CN VI) radii for Ac(III) ions vary from 112 pm for Ac^{3+} to 95 pm for Cf^{3+}, while the (CN VIII) radii for R(III) vary from 116 pm for La^{3+} to 97.7 pm for Lu^{3+} (Ziółkowski, 1985), lanthanide/actinide solid-state divalent and trivalent halide chemistry must at times become almost indistinguishable.

All divalent, trivalent, and tetravalent chlorides, bromides, and iodides are hygroscopic and an appreciable solution chemistry has been characterized, but only aspects of solution chemistry that relate to hydrates are considered here. The solid-state chemistry of the lower oxidation states (to IV) of cations in combination with the F, Cl, Br, and I atoms, and combinations of these with main-group cations is considered. The numerous reactions some of these halides undergo with organic reagents and solvents are considered only to the extent they relate to solid-state chemistry.

The high level or radioactivity associated with the heavier actinides and the consequent micro quantities of reactants on which experiments must be made require special techniques for identification, and in some cases preclude use of a technique so commonly used for solid-state studies, X-ray diffraction. Thus spectroscopic techniques have played a more important role in the characterization of actinide solid-state chemistry than of lanthanide chemistry.

2. Trivalent halides

2.1. *Synthesis*

Although anhydrous lanthanide halides have long been synthesized from oxides by the ammonium halide/hydrohalic acid route (Taylor 1962), only recently has the reaction mechanism for halide synthesis been established definitively.

Lanthanide and actinide oxides react with NH_4HF_2 by different mechanisms and yield different reaction products. The greater stability of the higher oxidation state of the lighter actinides strongly influences the reaction mechanism. Patwe et al. (1989) note that NH_4HF_2 reacts with $RO_{1.5}$ and CeO_2, mixed in a 3:1 molar ratio, at room temperature. Sesquioxide reactants yielded $(NH_4)_3RF_6 \cdot 1.5H_2O$; CeO_2 yielded $(NH_4)_4CeF_8$. Although the reaction required three days for completion at room temperature, only 10 min was needed at 100°C. Upon heating, the fluorocomplexes decompose to RF_3. For R = La, the $1.5H_2O$ is lost initially, then between 150–225°C the $(NH_4)_3LaF_6$ intermediate decomposes first to NH_4LaF_4 and subsequently to LaF_3. For R = Ce, two intermediates are identified, $(NH_4)_2CeF_6$and NH_4CeF_5, the latter of which decomposes to the trihalide with the Ce^{4+} oxidizing the fluoride ion to F_2(g). The R = Y specimen, on the other hand, decomposed to YF_3 in a one step process. Intermediate phases were characterized only by thermal techniques. Rajeshwar and Secco (1977) had examined the lanthanum system previously and obtained comparable results; they did not examine the Ce system. These researchers utilized NH_4F as the fluorinating agent instead of NH_4HF_2 and examined the decomposition mode of the heavier lanthanides by thermal and X-ray powder diffraction techniques. They found that while the R = Pr, Nd, Sm–Tb specimens decompose through the intermediate NH_4RF_4, the R = Y, Dy–Lu follow a different mechanism in the presence of sufficient NH_4F. Two intermediates were reported: $(NH_4)_3R_2F_9$ and $NH_4R_2F_7$, the latter of which decomposed to RF_3. ARF_4 and AR_2F_7, where A denotes a group 1 cation such as Rb^+, are well characterized compounds (Meyer 1982), but the nanofluoride intermediate must be viewed with suspicion.

Wani et al. (1989) examined the mechanism whereby NH_4HF_2 reacts with UO_2, U_3O_8, and ThO_2 (mixture of 4 NH_4HF_2 : 1 g-atom actinide). Again, intermediates were determined only by thermal techniques. UO_2, like CeO_2, formed an $(NH_4)_4UF_8$ crystalline fluorocomplex upon being heated at 100°C. However, the subsequent decomposition mechanism differs from that found for cerium. The $(NH_4)_4UF_8$decomposes first to $(NH_4)_3UF_7$, an intermediate not observed in the cerium reaction, and then to the expected NH_4UF_5 intermediate which decomposes to the ultimate product, UF_4. This reaction illustrates the much greater thermal stability of uranium tetrafluoride. The oxide, U_3O_8, yielded the oxidefluoride, UO_2F_2. On the other hand, ThO_2 reacted at room temperature with NH_4HF_2 to yield $(NH_4)_4ThF_8 \cdot 2H_2O$. Upon heating intermediates $(NH_4)_2ThF_6 \cdot 2H_2O$ and $ThF_4 \cdot 2H_2O$ were obtained. The ultimate product was ThO_2, indicative that the H_2O remained continuously in the inner coordination sphere of thorium. This reaction shows the greater similarity of thorium to the group 4 rather than to the lanthanide elements.

Takashima et al. (1992) synthesized RF_3 from small powdered (400 mesh) RO_x specimens and F_2(g) and studied the reaction by thermogravimetric analysis under different gas pressure and heating conditions. La_2O_3, "Pr_6O_{11}", and "Tb_4O_7" react violently at room temperature and upon heating to 555°C yield pure RF_3; the remaining R begin to react at ~ 260°C. Products of the R = Ce, Sm, Y, and Ho–Lu reaction contained oxidefluoride. The rapid reaction rate of Pr and Tb is attributed to the mixed-valence state; that for La to the fluorination of hydroxide present on the oxide surface. Trivalent fluoride results from tetravalent oxide because of the thermal instability of the tetrafluorides. The fluorination of Nd_2O_3 is studied in detail and a mechanism is proposed. Adsorbed F_2(g) is assumed to dissociate into free radicals which substitute for oxide ions on the surface to form a NdF_3 surface layer. After the surface is coated with NdF_3, the mechanism becomes diffusion controlled.

Korczak and Mikołajczak (1983) emphasize that good lanthanide trifluoride crystals can only be obtained from oxide- and water-free reactants in a furnace with a large temperature gradient at a slow growth rate. They suggest purification of RF_3, R = La–Nd, by heating specimens confined in graphite crucibles in He 5 h at 90°C and 1 h at 550°C. They report low-temperature thermal-expansion coefficients, α (temperature range ~ 90–291 K). Greis and Cader (1985) also emphasize the impact of impurities, especially oxide impurities, on trifluoride properties. They synthesized very pure trifluorides by effecting dehydration under a stream of HF/N_2 at gradually incremented temperatures and confirmed resultant purity by analysis. They then determined phase-transition temperatures by DTA and map in a temperature–atomic-number plot the structure types exhibited by RF_3: $P\bar{3}c1$ and Pnma at low temperatures, $P6_3/mmc$ at $T > 1025$°C for the RF_3, R = La–Nd, Sm, and $P\bar{3}m1$ above $T > 1300$ K for the RF_3, R = Y, Er–Lu. The R = Sm, Eu, and Gd specimens transform from space group $P\bar{3}c1$ to Pnma at elevated temperatures. Synthesis of specific lanthanide divalent, trivalent, and tetravalent fluorides, and some mixed fluorides is discussed by Müller (1991).

Gibson and Haire (1988a) used Knudsen effusion-mass spectrometry to study the congruent vaporization of each component in a mixture of lanthanide trifluorides. By working with mixtures they could determine relative vapor pressures and enthalpies of vaporization more reliably than such values could be determined from independent measurements on the individual trifluorides. From these data they determined the enthalpies of vaporization relative to that of LuF_3. Their third-law derived data suggest a gradual increase in the enthalpy of vaporization with increasing size (decreasing Z), i.e., at 1225°C $\Delta(\Delta H_v^0)$ $[GdF_3(l)–LuF_3(l)] \approx 9\,kJ\,mol^{-1}$ and at 1125°C $\Delta(\Delta H_v^0)$ $[LaF_3(l)–LuF_3(l)] \approx 33\,kJ\,mol^{-1}$. Petzel et al. (1992) determined the enthalpies of vaporization of LaF_3 and LuF_3 by the Knudsen effusion mass-loss techniques and confirmed the trend reported by Gibson and Haire, obtaining at 1225°C $\Delta(\Delta H_v^0)$ $[LaF_3(l)–LuF_3(l)] = 25\,kJ\,mol^{-1}$.

Wilmarth et al. (1988a) synthesized AcF_3, Ac = Am, Cm, and Cf, by precipitating the insoluble trifluorides with HF from an aqueous solution of the trichloride ions. The hydrated trifluorides, confined in Ni boats, were first heated in a monel furnace at 300°C in one atmosphere of F_2(g) to remove oxidefluoride impurities and H_2O and then heated in vacuum to 600°C to decompose the tetrafluoride formed by reaction

with the F_2(g) to the trifluoride. Synthesis of specific actinide fluorides, and some mixed fluorides is discussed by Freestone and Holloway (1991).

Hölsä and Niinistö (1980) studied thermochemically the reaction of selected lanthanide sesquioxides (La, Gd, and Lu) with NH_4Br and of Y_2O_3 with NH_4X (X = F, Cl, Br, and I) and concluded that the reactions proceed in three stages. The first stage involves loss of water and the next two release of equal amounts of ammonia. They thus postulated formation of two intermediate compounds, $RX_3 \cdot 3NH_3$ and $RX_3 \cdot 1.5NH_3$, with the reaction becoming endothermic at 200–300°C and with oxidehalide formation being complete at 340–470°C. In contrast to the fluoride, chloride, and bromide reactions, that of Y_2O_3 with NH_4I yielded one endotherm and hence must proceed via simultaneous reactions.

Meyer and Ax (1982) verified the two-step reaction for chloride synthesis and determined the composition of the two intermediates by single-crystal X-ray diffraction. The first step of this reaction involves formation of the complex chloride, $(NH_4)_3RCl_6$, which is independent of the size of the R(III) ion. The second step involves decomposition of this complex ion to anhydrous RCl_3 through intermediates $(NH_4)_2RCl_5$ for R = La–Eu, and $NH_4R_2Cl_7$ for R = Gd–Yb, Y. Polonskii et al. (1982) also examined the NH_4Cl–La_2O_3 reaction by various thermochemical techniques and arrived at the same mechanistic scheme.

Gunsilius et al. (1987) used a different procedure to synthesize lanthanide chlorides from the oxides. They grew single crystals of the lanthanide chlorides – including $EuCl_3$ – by reaction of Al_2Cl_6 with the oxide and subsequent purification and crystal growth by chemical vapor transport. In this metathesis reaction Al_2Cl_6 is converted to AlOCl. The synthesis procedure worked equally well with the tetravalent lanthanide oxides, CeO_2, "Pr_6O_{11}", and "Tb_4O_7". In these cases RCl_3, AlOCl, and Cl_2(g) are the products. Although the procedure was not tested with actinide oxides, its versatility in reducing tetravalent lanthanides to the trivalent state suggests comparable success for actinides which do not have a tetrachloride thermodynamically stable at the synthesis temperature. The purification process involves vapor transport by the well-known vapor species, RAl_3Cl_{12}(g) and RAl_4Cl_{15}(g). The structures of RAl_3Cl_{12}, R = Tb, Dy, and Ho, were determined from single crystals and their decomposition to RCl_3 was followed in the high-temperature Guinier camera (Hake and Urland 1990); the transition occurred at $\sim$ 250°C.

Various synthesis procedures for anhydrous lanthanide bromides have also been investigated (Meyer et al. 1987). As with the chloride, the reaction proceeds via an intermediate complex ammonium salt when the haliding agent is NH_4Br. For R = La to Nd this salt is $(NH_4)_2RBr_5$, while for R = Eu to Lu, Sc, and Y it is $(NH_4)_3RBr_6$. The decomposition behavior of these salts varies with R; for R = Nd, Sm–Dy a second intermediate, $NH_4R_2Br_7$ forms in the 400–500°C temperature range; remaining R decompose directly to NH_4Br and RBr_3. These studies demonstrate that the reaction mechanism – the intermediates formed – depends principally upon cation size. Thus the reactions should proceed as well with heavier actinides as with lanthanides.

Single-crystalline $LaBr_3$ was also prepared by chemical vapor transport with Al_2Br_6 (Krämer et al. 1989). In this process, as with Al_2Cl_6, Al_2Br_6 reacts with La_2O_3 in a sealed tube under vacuum. When reaction is complete, the tube is moved to a two zone

furnace and the $LaBr_3$ product is deposited at the cooler end as single crystals. Zvarova (1979) reported that the tribromides of Lu, Yb, Tm, Gd, Eu, Sc, Ce, and the dibromides of Sr and Ba, were transported by Al_2Br_6, suggestive of the general applicability of this crystal growing procedure.

Meyer et al. (1985b) demonstrated the versatility of the ammonium halides as reactants for converting not only lanthanide and actinide oxides, but also the elements, a sulfide, or a phosphide, to the anhydrous halide at relatively low temperatures. The triammonium hexahalo-lanthanide or actinide complex can also be used as a reagent with R_2O_3 to give ROX, with R_2S_3 or $H_2S(g)$ to give RSX, or with LiCl to give complex ternary halides. They cite numerous examples of diverse reactions that can occur with NH_4X and $(NH_4)_3RX_6$ complexes as reactants at temperatures between 250° and ~ 500°C: redox, acid–base, decomposition, and metathesis reactions.

Wilmarth et al. (1988d) also synthesized previously unreported PmI_3 by reaction of HI with the trichloride or tribromide at ~ 400°C. They indicate that direct reaction with the sesquioxide always produced triiodide specimens containing oxideiodide impurities. Moyer (1978) compared some different triiodide synthesis routes for preparation of ScI_3 and DyI_3 and concluded that reaction between the element and iodine or mercuric iodide provided the highest yields under the conditions used. Iodination of ytterbium was examined by DTA by Molodkin et al. (1984) who found YbI_2 to form by direct combination of the elements at 738–778°C; and YbI_3 to form at 776–820°C.

Bonding in some lanthanide and actinide iodides was examined by ^{129}I Mössbauer spectroscopy. The spectra of ThI_4, UI_4, NpI_3, and PuI_3 were compared (Karraker 1987); Mössbauer parameters among the actinide iodides did not differ significantly. Comparison with ^{237}Np Mössbauer measurements on NpI_3 suggests that the $5p_z$ orbitals of the iodide ions contribute to the Np 6d orbitals. However, isomer shifts differed unexpectedly from those reported previously for LaI_3, GdI_3, and ErI_3; the $\delta = +0.25$ and 0.35 mm/s values for NpI_3 and PuI_3, respectively, compare to ~ -0.25 mm/s for RI_3.

2.2. *Structural modifications at normal and elevated pressures*

2.2.1. *Structure types preparable at normal pressures*

The structures of lanthanide and actinide trihalides at room temperature and pressure have been known for many years; six different modifications have been characterized. These modifications, together with coordination number, symmetry, and space group, are listed in table 1. The space group of the lighter RF_3 remained controversial with two different space groups proposed for LaF_3, primarily because of the inability to grow untwinned single crystals suitable for structural analysis. From a single-crystal neutron-diffraction structural analysis of LaF_3, Gregson et al. (1983) concluded that the correct space group was $P6_3cm$ and indicated further that this space group was retained upon heating to at least 650°C. However, Zalkin and Templeton (1985) recalculated the neutron single-crystal data of Gregson et al. (1983) in space groups $P6_3cm$ and $P\bar{3}c1$ with a structural model that accounted for the effects of twinning. They obtained the lower *R* factor in space group $P\bar{3}c1$. Maximov and Schulz

TABLE 1

Structural modifications of the trivalent halides. Normal temperature/pressure modifications are indicated in bold.

Structure type (space group)	LaF_3 ($P\bar{3}cl$)	YF_3 (Pnma)	UCl_3 ($P6_3/m$)	$PuBr_3$ (Cmcm)	$AlCl_3$ (C2/m)	$FeCl_3$ ($R\bar{3}$)	RhF_3 $R\bar{3}c$
Anion							
F	**La–Pm, Ac–Cm, Cf**	**Sm–Lu, Y, Cf**					
Cl			**La–Gd, Am–Cf** Tb	**Tb**, Gd, Dy–Yb Pr, Bk, Cf	**Dy–Lu, Y**		**Dy–Lu**
Br			**La–Pr** Nd	**Nd–Eu, Pu–Bk** Pr, Gd–Ho, Cf	**Cf, Es** Bk	**Gd–Lu, Y** Cf	
I				**La–Nd**, Pm, Sm, Gd, Tb, Am		**Pm, Sm, Gd–Lu, Y, Am, Cm, Cf**, Nd	
Coordination number	11(9)	9	9	8	6	6	6

(1985) collected both X-ray and neutron single-crystal data on an LaF_3 specimen and, like Zalkin and Templeton, considered twinning. They also concluded that the correct space group is $P\bar{3}c1$. Radaev et al. (1991) examined by neutron diffraction a large twinned single crystal of tysonite-type $La_{0.85}Sr_{0.15}F_{2.85}$ and achieved optimal refinement in space group $P\bar{3}c1$. They found the F-atom sites in the plane of the cations of this mixed-cation specimen (labeled F_3) to be fully occupied, those sites that in LaF_3 are displaced slightly from the cation layers to be split into two sites whose combined occupancy is unity, and the vacancies in the (F_1) tetrahedral anion sites to equal the nonstoichiometry as given by the formula.

Schubert (1989) points out that radius ratio considerations in LaF_3 would suggest coordination near LaF_8, and the LaF_3 structure should therefore be homeotypic with CaF_2. He then relates the LaF_3 structure to that of CaF_2, compares the displacements to those of related structures, e.g., CaF_2–YF_3 superstructures, and discusses crystal energetics. LaF_3 crystals were examined by DSC from 100–500 K; an anomaly which occurs in the C_p versus T curve is related to a phase transition in which the fluoride sublattice "fuses" (Aliev and Fershtat 1984). This phenomenon appears related to the high ionic conductivity of the tysonite-type fluoride phases.

A high-temperature polytype of $TbCl_3$, designated h-$TbCl_3$, was characterized by Gunsilius et al. (1988). This hexagonal modification, which is stable above ~ 520°C, was obtained upon heating $PuBr_3$-type $TbCl_3$. In this high-temperature structure the Tb^{3+} ions are coordinated octahedrally. The cell volume per Tb^{3+} ion is but slightly less than that of adjacent $DyCl_3$ which crystallizes in the rather inefficiently packed $AlCl_3$-type structure (see fig. 1). These authors also synthesized $TbCl_3$ in the UCl_3 modification. This apparently metastable modification forms when the oxide reacts with $AlCl_3$ and crystals are formed by vapor transport at ~ 300°C; if the temperature is increased to 400°C, the $PuBr_3$ modifications always results. The UCl_3-form transforms irreversibly to the $PuBr_3$ modification upon heating. In similar fashion, $PuBr_3$-type $DyCl_3$ results upon low-temperature vapor transport when $AlCl_3$ reacts with Dy_2O_3; a dysprosium analogue of h-$TbCl_3$ was not found (Urland and Hake 1989). Löchner (1988b) prepared the UCl_3 modification of $NdBr_3$ at temperatures between 110–115°C by carefully dehydrating a finely crystalline slurry of $NdBr_3 \cdot 6H_2O$ under a dynamic

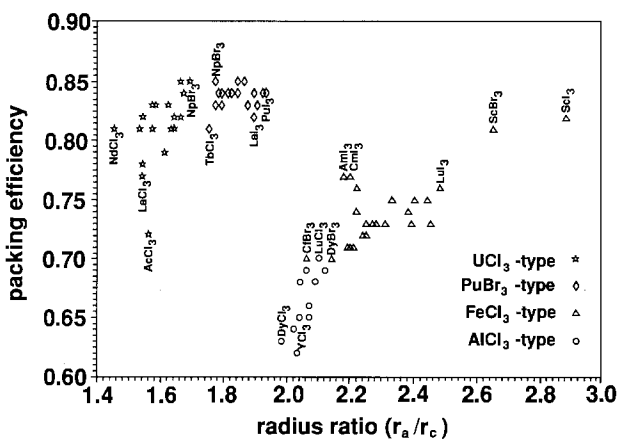

Fig. 1. A structure-field map of the lanthanide and actinide trihalides. Packing efficiency, determined from the sum of the (assumed spherical) volume calculated from the anion and cation radii divided by the actual volume derived from the lattice parameters, is plotted against radius ratio. Only those trihalides that mark the limits of the structure field are indicated.

vacuum. This metastable modification begins to transform into the normal $PuBr_3$-type modification at $\sim 140°C$. As expected, this hexagonal modification could not be prepared under high (~ 3.0 GPa) pressures.

Interrelationships among the various structural types have been discussed by Haschke (1979); transitions among modifications can generally be understood from radius-ratio considerations. Beck and Gladrow (1979) present a plot of space filling of lanthanide, actinide, and first-row transition-element trichlorides, tribromides and triiodides versus radius ratio. This plot demonstrates that the $AlCl_3$-type structure is packed least efficiently. A similar plot of packing efficiency versus radius ratio is presented in fig. 1. To construct this figure, cation radii were calculated with the second approach data of Ziółkowski (1985) for the coordination number of the cation in the structure-type assumed. Anion radii were held constant: Cl, 180 pm; Br, 191 pm, and I, 213 pm. The packiing efficiency (ordinate) was determined from sum of the (assumed spherical) volume calculated from the anion and cation radii divided by the actual volume derived from lattice parameters taken from literature cited herein, Brown (1968), or the CRYSTDAT database. Lanthanide and actinide trihalides (Ac–Es) for which lattice parameters could not be located are: $AcBr_3$, AcI_3, $BkBr_3$, BkI_3, $CfBr_3$, CfI_3, EsI_3, EuI_3, $PaBr_3$, and PaI_3. The abscissa was computed from the radii used in the calculations. Only those trihalides located either at or near the limit of the phase region are indicated in the figure. Note that two structural modifications of the same compound will have different radius ratios. Clustering of the different structural types is apparent; the figure illustrates the dominant effect of radius ratio in determining lanthanide and actinide halide structure types.

Igarashi and Mochinaga (1987) determined the melting points and molar volumes in the liquid state for RCl_3 compounds, R = La–Nd, Gd, Dy, and Y. They found the volume increase on melting of the hexagonal (UCl_3-type) chlorides to be more than 20%, while that for the monoclinic ($AlCl_3$-type) $DyCl_3$ and YCl_3 was less than 1%. These volume changes can be understood from the data presented in fig. 1. Atoms in the UCl_3-type structures with packing efficiencies of $\sim 85\%$ must expand due to thermal motion, whereas those in the $AlCl_3$-type structures with packing efficiencies of $\sim 65\%$ can rearrange upon fusion and more efficient packing compensate for increased thermal vibrations. Melting points of the chlorides studied are also compared with previously reported values. Mochinaga et al. (1991) studied the RCl_3 melts, R = La–Nd, Sm, Gd, and Dy, by X-ray diffraction and report in addition Raman spectra and electrical conductivity data. They conclude that in every melt six chloride ions, in octahedral coordination, surround the lanthanide cation. The average R^{3+}–Cl^{1-}–R^{3+} angle of about 130° estimated from the X-ray diffraction results suggests the presence of dimers or more complex polymeric anions in the melts.

Peterson et al. (1986a) showed that $PuBr_3$-type $BkCl_3$ and $CfCl_3$ could be prepared by quenching molten specimens; these are high-temperature modifications with transition temperatures near the melting points. In like fashion, slowly cooled $PrBr_3$ crystallized in the UCl_3-type structure, but molten $PrBr_3$ upon quenching yielded the orthorhombic $PuBr_3$-type modification (Wilmarth et al. 1989a). Both UCl_3- and $PuBr_3$-structural modifications of $BkCl_3$ preserve symmetry upon transformation to $CfCl_3$ through β^- decay, consistent with the behavior of $PuBr_3$-type $BkBr_3$.

Like its neighbors NdI_3 and SmI_3, PmI_3 is dimorphic (Wilmarth et al. 1988d). The as-synthesized product always exhibited the rhombohedral $FeCl_3$-type structure, but, as expected from packing efficiencies (fig. 1), heating this modification at a low temperature (275°C) converted it to the more dense $PuBr_3$-type modification. Lattice parameters for both modifications are presented in table 2.

2.2.2. *Pressure-induced structural transformations*

Since the structural modification adopted by the trihalides changes systematically with ionic radius and since the relatively "soft" halide ions undergo compression rather easily, lanthanide halide structures are pressure sensitive. Most lanthanide, numerous actinide, and several mixed lanthanide/actinide systems have been examined under elevated pressures, the typical effect of which is transformation to a more densely packed structure.

Peterson, Haire, and co-workers have demonstrated in a series of papers that by comparing the transitions observed for cations in an unknown structural modification to those of related ions in known structural modifications both absorption and Raman spectra can be used to determine the crystal structure of *f*-block element compounds. Their spectral technique is particularly utilitarian for those 5f elements for which either small specimen size or high levels of radioactivity preclude normal structural analysis by X-ray diffraction. Of course, they normally make spectral assignments in addition to determining crystal symmetries. Spectrophotometric and X-ray powder diffraction methods were used to demonstrate that the Cf daughter of ^{249}Bk in $^{249}BkBr_3$ has the same structure as the parent phase. Thus six-coordinate $AlCl_3$-type $BkBr_3$ generates upon β^- decay six-coordinate $CfBr_3$. In like fashion eight-coordinate $PuBr_3$-type $BkBr_3$ generates eight-coordinate $CfBr_3$, a structure-type that cannot be obtained by direct synthesis (Young et al. 1980). Subsequent synthesis of $CfBr_3$ specimens for calorimetric measurements by reaction of Cf_2O_3 with HBr also yielded specimens identified by both X-ray powder diffraction and spectroscopy as the monoclinic $AlCl_3$-form (Fuger et al. 1990), consistent with the previous report.

Beck and Gladrow (1983a), using high-pressure techniques, transformed the $AlCl_3$-type lanthanide trichlorides, $ErCl_3$–$LuCl_3$ into a quenchable ($R\bar{3}c$) RhF_3-type structure. At higher pressures of 1.5–4.0 GPa and temperatures of ~ 500–750°C, Beck and Gladrow (1979, 1983b) were able to convert the $FeCl_3$-type halides, SmI_3, GdI_3, TbI_3, $GdBr_3$–$HoBr_3$, $DyCl_3$–$TmCl_3$, and $YbCl_3$ into quenchable $PuBr_3$-type halides. They present both a structure-field diagram of the lanthanide chlorides, bromides, and iodides and plot against cation radii the temperature at which the high-pressure phases convert to the normal-pressure phases. Beck and Gladrow suggest the following order of packing efficiency with increasing pressure: $AlCl_3$ (C2/m)-type (least efficient space filling) < $FeCl_3$ ($R\bar{3}$)-type < UCl_3 ($P6_3/m$)-type < $PuBr_3$ (Cmcm)-type (most efficient space filling). The data presented in fig. 1 substantiate this arrangement. Consistent with this arrangement, Peterson et al. (1985) demonstrated that monoclinic ($AlCl_3$-type) $^{249}CfBr_3$ transformed irreversibly to the orthorhombic ($PuBr_3$-form) at pressures of 3.4 GPa. At a pressure of ~ 2 GPa, $FeCl_3$-type AmI_3 transforms irreversibly to the $PuBr_3$-type modification (Haire et al. 1985). Peterson et al. (1986b) examined the behaviour of UCl_3-type $NdCl_3$ under pressures up to 9.6 GPa by absorption spectro-

TABLE 2
Some recent crystallographic data for lanthanide/actinide or alkaline-earth substituted halides. RX_n, $2 < n \leq 3$.

Halide	Type	Symmetry	a(Å)	b(Å)	c(Å)	Angle	Reference
$Sr_9Nd_5Cl_{33}$	$Nd_{14}Cl_{33}$	$R\bar{3}$	12.908(6)	–	24.82(1)		[1]
$Sm_9Nd_5Cl_{33}$	$Nd_{14}Cl_{33}$	$R\bar{3}$	12.894(2)	–	12.425(3)		[1]
$Sm_{14}Cl_{33}$	$Nd_{14}Cl_{33}$	$R\bar{3}$	12.864(2)	–	12.36(4)		[2]
$Sr_9Eu_5Cl_{33}$	$Nd_{14}Cl_{33}$	$R\bar{3}$	12.854(4)	–	24.702(8)		[3]
$Sm_9Gd_5Cl_{33}$	$Nd_{14}Cl_{33}$	$R\bar{3}$	12.845(6)	–	12.347(4)		[3]
Ba_2LaCl_7	?		17.637(6)	–	12.495(5)		[4]
Ba_2SmCl_7	?		17.471(6)	–	12.351(6)		[4]
$Ba_9La_5Br_{33}$	$Nd_{14}Cl_{33}$	$R\bar{3}$	14.098(2)	–	26.678(6)		[4]
$Ba_9Nd_5Br_{33}$	$Nd_{14}Cl_{33}$	$R\bar{3}$	14.039(1)	–	26.477(4)		[4]
$NdCl_{2.31}(Nd_3Cl_7)$		I4/m	11.041(1)	–	21.209(2)		[5]
La_2Br_5	Pr_2I_5	$P2_1/m$	7.8909(6)	4.2489(4)	13.423(1)	$\beta = 91.60(1)°$	[6]
Pr_2Br_5	Pr_2I_5	$P2_1/m$	7.7438(4)	4.1533(3)	13.2706(9)	$\beta = 90.816(6)°$	[7]
$K_3Nd_3Br_{10}$		Pnma	13.2988(9)	9.2731(6)	8.3618(6)		[10]
$NdBr_3$	UCl_3	$P6_3/m$	7.938(5)		4.347(5)		[9,10]
$TbCl_3$	UCl_3	$P6_3/m$	7.3763(2)		4.0571(6)		[11]
$TbCl_3$	h-$TbCl_3$	$P4_2/mnm$	6.4251(4)		11.771(2)		[11]
$DyCl_3$	$PuBr_3$	Cmcm	3.8162(5)	11.815(2)	8.507(1)		[12]
PmI_3	$PuBr_3$	Cmcm	4.24(1)	13.93(7)	9.96(2)		[13]
PmI_3	$FeCl_3$	$R\bar{3}$	7.65(3)	–	21.1(1)		[13]

[1] Hodorowicz et al. (1987).
[2] Liu and Eick (1988).
[3] Olejak-Chodan et al. (1987b).
[4] Liu and Eick (1989a).
[5] Lumpp and Bärnighausen (1988).
[6] Krämer et al. (1989).
[7] Schleid and Meyer (1987a).
[8] Schleid and Meyer (1991).
[9] Löchner (1988b).
[10] Löchner (1988c).
[11] Gunsilius et al. (1988).
[12] Urland and Hake (1989).
[13] Wilmarth et al. (1988d).

scopy. They noted that the complexity of the absorption peaks decreased with increasing pressure, suggestive of a change to higher symmetry. Spectral changes were found to be reversible upon cycling the pressure. Maintaining the specimen under pressure for an extended time period did not result in further spectral changes. Since the changes did not occur abruptly, a higher-symmetry structure could not be postulated. Neither UCl_3-type $AmCl_3$ nor $CfCl_3$ could be converted to the $PuBr_3$-type structure under pressure. Since the volumes of UCl_3- and $PuBr_3$-type $CfCl_3$ are about the same, it is not surprising that a structure change does not occur even at pressures of 22 GPa. With $AmCl_3$ reversible spectral changes were observed, but they did not unequivocally demonstrate conversion to the more dense $PuBr_3$-type structure.

Wilmarth et al. (1988a) present Raman spectral data on the solid AcX_3 compounds, X = F, Cl, and I and Ac = Am, Cm, and Cf, and on $PuBr_3$. [See Wilmarth and Peterson (1991) for a review of the spectral assignments.] The similarities among the Raman spectra confirm structural assignments: LaF_3-type fluorides, UCl_3-type chlorides, $PuBr_3$-type $AmBr_3$ and $CmBr_3$, and $FeCl_3$-type $CfBr_3$ and AcI_3. $CfCl_3$ is dimorphic; it exhibits both UCl_3- and $PuBr_3$-type modifications. Raman active modes from the $PuBr_3$- and $FeCl_3$-type structural data are assigned. Two praseodymium compounds, PrX_3, X = Cl and Br, were examined by X-ray powder diffraction and absorption and Raman spectroscopy (Wilmarth et al. 1989a). With $PrCl_3$ exhibiting the UCl_3-type structure and $PuBr_3$ being dimorphic, the data illustrated clearly that both Raman and absorption spectra allow the different structure modifications to be distinguished. Wilmarth et al. (1989b) also examined by solid-state absorption and Raman phonon spectroscopy the effect of pressures up to ~ 26.0 GPa on PrX_3, X = Cl, Br and $NdBr_3$. Spectroscopic data indicate that UCl_3-type $PrCl_3$ transforms to the $PuBr_3$-form at pressures of ~ 15.5 GPa. This transformation decreases the cation coordination number, but is consistent with the packing efficiencies indicated in fig. 1. The UCl_3-type $PuBr_3$ undergoes a transition to $PuBr_3$-type $PrBr_3$ at ~ 11.0 GPa, and at still higher pressures undergoes absorption changes that suggest transformation to another unknown-type structure. While the $PuBr_3$-modification of $PrBr_3$ could be quenched upon release of pressure, that of the unknown structural modification could not be. $PuBr_3$-type $NdBr_3$ in like fashion also appears to undergo a comparable phase transformation to this unknown high-pressure modification. Wilmarth et al. (1988c) also examined the PmX_3, X = F, Cl, Br, and I compounds by Raman spectroscopy and made spectral assignments. Peterson et al. (1990) present absorption spectra of UCl_3-type $PrCl_3$, $PrBr_3$, $CfCl_3$, and Ce(Cf)Br_3; $PuBr_3$-type $PmBr_3$, PmI_3, $BkCl_3$, $BkBr_3$, $CfCl_3$, $CfBr_3$; and $AlCl_3$-type $CfBr_3$, $EsBr_3$, and Y(Cf)Cl_3 and Lu(Es)Cl_3. They compare the spectra of the pure halides with those of mixed halides and demonstrate again the similarity of the spectra of isostructural compounds. Comparing the spectra of the mixed cations whose crystal symmetry is known with those of unknown compounds, e.g., known Lu(Es)Cl_3 with unknown $EsBr_3$, they determined the crystal structure of the unknown, e.g., $EsBr_3$, unequivocally.

2.3. *Mixed-cation and mixed-anion systems*

2.3.1. *Multiple-cation systems*

Garton and Walker (1982) reported phase diagrams for the RCl_3–$R'Cl_3$ systems: R–R′ = Gd–Tb, Gd–Dy, Tb–Dy, Tb–Ho, and Dy–Ho. The $AlCl_3$-type Dy–Ho system exhibits continuous solid solution without an elevated temperature transformation. The Tb–Dy and Tb–Ho systems represent $PuBr_3$-type–$AlCl_3$-type systems and evidence continuous solid solution with polymorphism; the $PuBr_3$-type structure at lower temperatures transforms into the $AlCl_3$-type structure at elevated temperature. This transformation can be understood readily by noting that the $AlCl_3$-type structure is the least efficiently packed. The UCl_3–$PrBr_3$-type Gd–Tb and Gd–Dy systems, on the other hand, exhibit the expected UCl_3- and $PuBr_3$-type structures at lower temperatures, and, compatible with the previously discussed systems, the $PuBr_3$-type structure transforms to the less-efficiently packed $AlCl_3$-type structure at elevated temperature Blachnik and Enninga (1984) determined the enthalpies of mixing of $LaCl_3$–RCl_3, R = Gd, Y, and La at 927°C and noted that all the values were positive.

Several $R_{1-x}Gd_xF_3$ systems have been characterized to facilitate Gd^{3+} luminescence measurements. Brixner et al. (1991) examined the R = La system; two solid-solution regions separated by the expected two-phase area were identified. One prevailed for $0 \leq x \leq 0.5$ (hexagonal LaF_3-type) and the other for $0.75 \leq x \leq 1.0$ (orthorhombic YF_3-type). It is noteworthy that the smaller Gd^{3+} is more soluble in LaF_3 than is La^{3+} in GdF_3; the cell volume decreases almost monotonically with increasing Gd substitution, but remains practically invariant for La substitution. Blasse et al. (1989) studied the R = Y system; continuous (YF_3-type) solid solution prevailed.

Structures of two $RSnF_7$ compounds, R = Eu, Y, prepared for R = Eu by extended heating of the corresponding fluorides and for R = Y by heating, and then annealing, a mixture of YF_3, CuF_2, and metallic Sn, were confirmed by single-crystal techniques (Benner and Hoppe 1992). The monoclinic fluorides which are isotypic with $SmZrF_7$ are built from quadratic-antiprismatic RF_8 polyhedra and SnF_6-octahedra. The structure-type and lattice parameters of these and other compounds (R = La, Nd, Sm, Gd, Tb, Dy, Ho, Er, Tm, Yb, and Lu) were initially reported in 1989 (Grannec et al. 1989). The equilibrium phase diagram of the closely related LaF_3–ZrF_4 pseudobinary system was determined; only the line phase $LaZr_2F_{11}$ was detected (Aasland et al. 1992). Eutectic points were observed at 771 ± 1°C [at $X(LaF_3) = 0.23$] and 779 ± 2°C [$X(LaF_3) = 0.37$].

Numerous RAl_3Br_{12} compounds, R = La, Ce, Pr, Nd, Sm, Gd, were prepared by chemical transport and characterized structurally (Hake and Urland 1992). The structure is built of tetrahedrally coordinated Al and eight-coordinated R in a distorted square antiprismatic-dodecahedral arrangement.

2.3.2. *Multiple-halide systems*

Numerous lanthanide (III) chloride–bromide systems have been characterized. Again, the changes observed can be understood from radius ratio considerations. Most of these studies have been effected by confining the mixed halides in quartz or

Al_2O_3 containers, heating the mixture, and following the reaction by DTA and/or examining the reaction products by X-ray powder diffraction. However, Schulze and Urland (1991) synthesized single crystals of the mixed chloride–bromides, RBr_xCl_{3-x}, R = Ce, Pr, Sm, and Gd, by reacting the sesquioxides with $AlBr_3/AlCl_3$ mixtures in various ratios and determining the composition from single-crystal structural analyses. As expected from radius-ratio considerations (see fig. 1) the Ce, Pr, and Sm mixed halides crystallized in the UCl_3-type structure; that for Gd yielded the $PuBr_3$-type structure. Although compositions close to Br : Cl = 1 : 2 and 2 : 1 were achieved, anion ordering was not found.

The lanthanum and neodymium chloride–bromide systems were examined by Olejak-Chodan et al. (1987a). The lanthanum system exhibited complete solid solution as expected since both halides possess the UCl_3-type structure, but Vegard's law is not obeyed. In the neodymium system, which represents a UCl_3-type–$PuBr_3$-type mixture, a UCl_3-type solid-solution region prevailed to ~ 70 mol percent bromide. However, chloride solubility in the $PuBr_3$-type structure was severely limited. The chloride–bromide systems of gadolinium, terbium, and ytterbium (Olejak-Chodan et al. 1988) encompass the four structure types common to the heavier halides. With increasing tribromide mol percentage, the solid-solution phase regions observed are: R = Gd, UCl_3-, $PuBr_3$-, and $AlCl_3$-type regions; R = Tb, $PuBr_3$- and $AlCl_3$-type regions; and R = Yb, $AlCl_3$- and $FeCl_3$-type regions. Pure $TbBr_3$ specimens, even under extended annealing, yielded poor quality X-ray powder diffraction data; pure $TbBr_3$ appeared to be isostructural with $GdBr_3$ rather than $DyBr_3$. In each system the $AlCl_3$-type structure accommodated the largest solid-solution region. This observation is consistent with the data presented in fig. 1 since this structure, being packed least efficiently, can accommodate additional ions by only slight atomic rearrangements. No evidence for anion ordering was detected; lattice parameters for selected mixed phase compositions are reported.

Of particular interest was a study of the mixed quaternary $NdBr_3$–$TbCl_3$ system in which both parent phases exhibit the $PuBr_3$-type structure (Olejak-Chodan and Eick 1989). In contrast to the complete $PuBr_3$-type solid solution which was potentially possible, four structure types were observed. Expressed in mol percent $NdBr_3$: from 0 to ~ 12.5 and 52.5 to 100, $PuBr_3$-type solid solutions; from 5 to ~ 60, UCl_3-type solid solution; from ~ 15 to 50, $AlCl_3$-type solid solution; and from 7.5 to ~ 17, a high-temperature phase which could not be quenched. The phases observed, typical of most mixed cation and anion systems which involve trivalent lanthanides and actinides, can be understood on the basis of radius-ratio considerations. In this system coexistence of the UCl_3- and $AlCl_3$-type structure with increasing $NdBr_3$ content would certainly not intuitively be expected. However, $NdCl_3$ exhibits the UCl_3-type structure and $TbBr_3$ the $FeCl_3$-type structure. Thus the phases must be understood on some level of cation and anion mixing. The data for fig. 1 show that $NdBr_3$ lies close to the stability limit of the $PuBr_3$- and UCl_3-type structures; $TbBr_3$ lies close to the stability limit between the $FeCl_3$- and $AlCl_3$-type structures. Upon reaction substitution of chloride anions into $NdBr_3$ alters the radius ratio and moves the phase into the UCl_3-type region. Similarly, substitution of bromide anions into $TbCl_3$ changes the radius ratio, moving it out of the $PuBr_3$-type region and into the next ($AlCl_3$-type) region. As the concentration of the

bromide ion increases, radius ratios change such that both phases move back into the $PuBr_3$-type region, and solid solution prevails again. The later appearance (i.e., at ~ 15 mol% rather than the 5 mol% observed for the UCl_3-type structure) of the $AlCl_3$-type structure can also be understood from fig. 1. $TbCl_3$ lies close to the UCl_3 phase stability limit, so considerable bromide substitution is required to move the radius ratio across the entire phase region and the phase appears at a more bromine-rich concentration. The disappearance of the $AlCl_3$-type phase before that of the UCl_3-type is not readily apparent from the figure and probably reflects some level of ion preference, i.e., chloride-ion preference for Nd^{3+} cations.

Anhydrous 5–10 mol% $^{249}CfX_3$–RX_3 phases prepared by oxalate coprecipitation (Wilmarth et al. 1988b) with subsequent halogenation were examined by X-ray powder diffraction and absorption spectroscopy. Hexagonal UCl_3-type solid solutions were characterized for the X = Cl; R = La, Ce, and Sm mixtures, $PuBr_3$-type solid solution for $TbCl_3$ mixtures, and $AlCl_3$-type solid solutions for YCl_3 mixtures. X-ray powder diffraction data could not be obtained for the chloride mixtures which had high melting points; they reacted with the quartz container. $CeBr_3$–$CfBr_3$ mixtures were difficult to prepare; comparison of solubilities in the RCl_3–$R'Cl_3$ systems suggests the lack of Cf(III) solubility in $CeBr_3$ results more likely from ion size and not structure-type differences. Orthorhombic $PuBr_3$-type Cf(III)–$SmBr_3$ and Cf(III)–CeI_3 solid solutions were found, as were rhombohedral $FeCl_3$-type Cf(III)–$TbBr_3$, Cf(III)–YBr_3, and Cf(III)–YI_3 solid solutions.

Research on mixed trivalent chloride–iodide systems is limited. Beda et al. (1980) examined the $RCl_{3-x}I_x$, R = La, Gd, systems and in the lanthanum system characterized a UCl_3-type phase with a doubled *a* lattice parameter. A structural solution based upon X-ray powder diffraction data suggested the formula $La_4Cl_9I_3$ for this intermediate. An intermediate phase postulated for the R = Gd system was not characterized definitively.

2.3.3 *Halide and non-halide anion systems*

Sulfur and iodine. Beck and Strobel (1986) subjected various RSI compounds, R = Ce–Nd, Sm, Gd–Dy, to elevated temperatures (800°C) and pressures (0.5–4.0-GPa). Under normal pressures the R = Ce–Sm compounds exhibit the SmSI-type structure and the R = Gd–Dy compounds the GdSI-type structure. Under elevated pressure the R = Gd–Dy compounds transform to the SmSI-type structure, with GdSI itself transforming under additional pressure to the α-CeSI-modification. The R = β-Ce–Sm compounds convert to the α-CeSI modification.

Nitrogen and chlorine. By heating the appropriate stoichiometric mixture of GdN and $GdCl_3$ confined in a tantalum container and sealed under 1 atm of nitrogen in quartz ampoules, Simon and Koehler (1986) synthesized Gd_2Cl_3N and Gd_3Cl_6N. Synthesis of the former required heating at 750°C for five days; the latter heating at 610°C for three days. In Gd_3Cl_6N the gadolinium remains formally trivalent; electrons are not available for Gd–Gd bonding. The structure is not fluorite-related like that of the fluoride analogue, R_3F_6N; it contains Gd_6N_2 units built from two edge-sharing

Gd_4 tetrahedra which contain a centered nitrogen atom. Chloride anions which surround each Gd atom link the shared tetrahedra. The structure is related closely to that of Gd_2Cl_3N (Schwanitz-Schüller and Simon 1985) which contains NGd_4 tetrahedra linked via opposite edges to form infinite chains connected by chloride ions. In the Gd_3Cl_6N structure, two additional chloride ions cut the infinite chains in Gd_2Cl_3N into pieces of two edge-shared Gd_4 tetrahedra. These Cl^- ions are located above the opposite non-connecting tetrahedra edges. Additional structural changes include shifts of all other Cl^- ions and loss of N^{3-} ions from where the infinite chains of Gd_4 tetrahedra in Gd_2Cl_3N are cut. These nitrides are discussed by Meyer (1988). By including Y metal with the chloride and nitride reactants, Corbett and co-workers (Meyer et al. 1989b) synthesized an yttrium sesquichloride–nitride phase, β-Y_2Cl_3N, which is isostructural with the infinite cluster chain phase, Y_2Cl_3. The need for Y metal in the synthesis, as well as the black color of the crystals and the nitrogen occupancy factor determined from the structural analysis, indicate a nitrogen deficiency in the compound.

2.3.3.1. *Fluorite-related cluster compounds*

Nitrogen and fluorine. Fluorite-related compounds, RN_xF_{3-3x}, R = Ce and Pr, synthesized from pure nitride and trifluoride, were examined by neutron diffraction (Vogt et al. 1989). The large difference between the scattering lengths of fluorine and nitrogen allows anion site occupancies and overall composition to be determined. The structural refinement indicated that nitrogen and fluorine atoms were distributed statistically on the normal tetrahedral anion sites, but only fluorine atoms occupied the F″ and F‴ interstitial sites. The fluorine atom interstitials occupy the (x, x, x) positions of space group $Fm\bar{3}m$: F″ at $x = 0.41$ and to a lesser degree of occupancy, F‴ at $x = 0.32$. (The F‴ site represents anions relaxed from the normal tetrahedral sites.) The F′ position, $(\frac{1}{2}, x, x)$, is not occupied.

[*Fluorite-related cluster notation.* Studies on fluorite-related compounds have identified three kinds of interstitials. Two have the coordinates (x, x, x). One of these, designated F‴, with $x \approx 0.31$, is not a true interstitial in that it can be regarded as a normal anion that has relaxed from the $x = 0.25$ position. The second, designated F″, with $x = 0.41$, is a true interstitial, and corresponds to MF_9 or MF_{10} clusters. These clusters associate around a single anionic vacancy, 0 F′, have n F″ interstitials, and are designated [1 : 0 : n] clusters (see fig. 2). Since four F″ interstitial sites are located around any one F′ anionic vacancy, the maximum value of n is 4. A [1 : 0 : 3] cluster can be envisioned as a cubic arrangement of anions from which one anion is removed. The three faces adjacent to this vacant anion position are then capped, yielding a triangular arrangement of capping anions. A cation that was originally centered in the cube would then be ten-coordinated. The [1 : 0 : 4] cluster differs only slightly from the [1 : 0 : 3] cluster. An additional anion caps a cube adjacent to the anion vacancy such that a tetrahedral interstitial arrangement surrounds the vacancy (see fig. 2). The third kind of interstitial, designated F′, is located at $(\frac{1}{2}, x, x,)$ with $x \approx 0.37$, and corresponds to MF_8 square antiprisms associated with large clusters such as the cuboctahedral [8 : 12 : 0] (8 vacancies, 12 F′, and 0 F″ interstitials) or [8 : 12 : 1] (8 vacancies, 12 F′ ions, and 1 F″

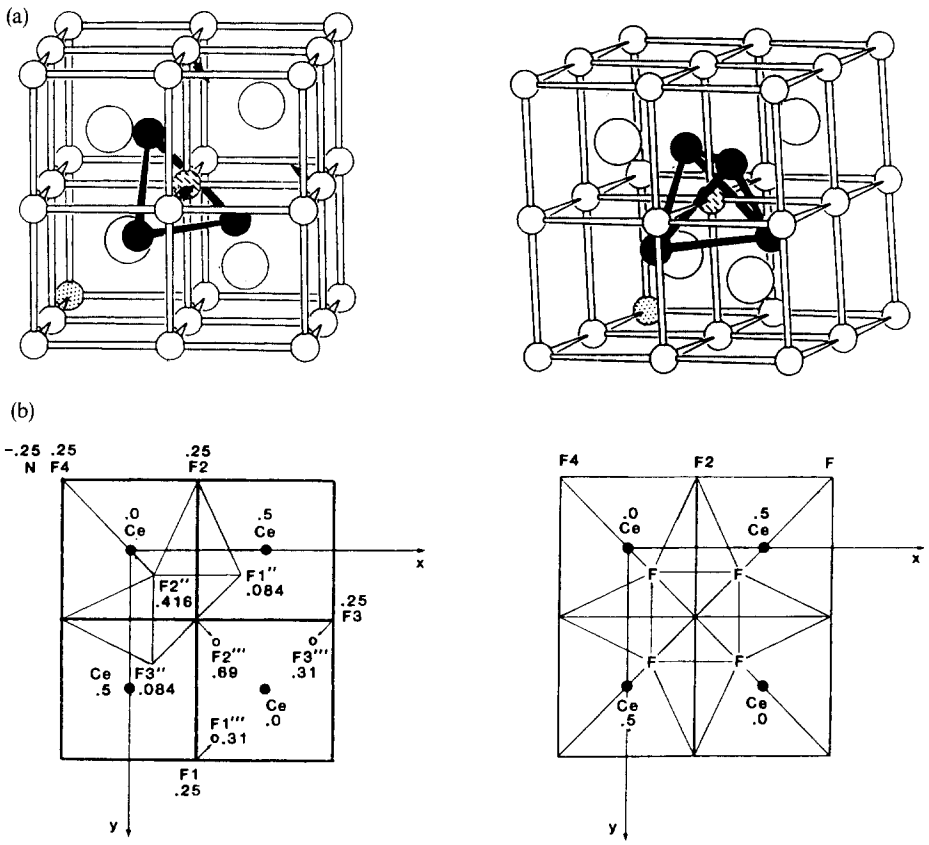

Fig. 2. (a) The [1:0:3] and [1:0:4] clusters in CeN_xF_{3-3x} and PrN_xF_{3-3x}. Small circles represent fluorine atoms (nitrogen atoms dotted) and large circles metal atoms. Full circles are fluorine interstitials in (x, x, x) $x = 0.41$ and dashed circles represent an anion vacancy at $(x, x, x) x = 0.25$. (b) The projection along [001] of fig. 2a. Arrows indicate relaxed fluoride positions of the anions (F'''). Numbers indicate heights in the z-coordinate. [From Vogt et al. (1989) with permission.]

interstitial), present in compounds such as tveitite (Bevan et al. 1982), β-U_4O_9 (Bevan et al. 1986), and KY_3F_{10} (Pierce and Hong 1973), among others.]

The neutron diffraction results on RN_xF_{3-3x} were interpreted in terms of [1:0:3] (1 V_F, O F′, and 3 F″) and [1:0:4] (1 V_F, O F′, and 4 F″) defect clusters within anion-excess fluorite related structures, and are depicted in fig. 2. The authors suggest a scheme whereby the [1:0:3] clusters might be arranged to maintain the stoichiometry. The R = La, Ce, Eu, Gd, and Tm systems were investigated previously (Pezat et al. 1976) and solid-solution limits, density as a function of composition, and powder X-ray diffraction data were collected. While the lattice parameters indicate global similarities among the systems, X-ray diffraction data can not differentiate between nitrogen and fluorine atoms. Other fluorite-related anion-excess lanthanide and actinide systems are discussed in section 2.3.4.1.

Oxygen and a halogen. Takashima and Kano (1987) synthesized mixed trivalent lanthanide oxidefluoride phases by fusing RF_3 and R'_2O_3 at 1100–1400°C to examine their electrical conducting properties. They report two homogeneous phases, one rhombohedral and stoichiometric ($RR'_2F_3O_3$) and the other tetragonal with a variable composition range ($R_xR'_{2-2x}F_{3x}O_{3-3x}$), $0.58 \leq x \leq 0.78$, and postulate a solid-state reaction pathway. These results are consistent with and expected from previous studies on the RF_3–R_2O_3 systems (Niihara and Yajima 1971). The tetragonal compounds which contained either Pr or Nd, or both, have high electrical conductivity ($> 10^{-2}$ $S\,cm^{-1}$ at 650°C).

Terada et al. (1988) synthesized extremely small particles of $La_{1-x}Nd_xOCl$ by a liquid phase process. The appropriate ratio of the pure chlorides was dissolved in methanol and NH_3(g) added to the solution. The homogeneous mixture of $La(OH)_3$, $Nd(OH)_3$, and NH_4Cl which resulted upon heating in air yielded particles of a few hundred angstroms in size. Ultimate particle size depended upon the heat-treatment temperature; powders treated at 400°C yielded a crystalline X-ray powder diffraction pattern. The hexagonal *c* lattice parameters vary linearly within the rather large error limits that result from the small particle size.

The similarities and differences between the actinides and lanthanide trihalides are apparent in their reactions with Sb_2O_3 (Brown et al. 1977a, b). The reaction typically yields the R(III) oxidehalide and appears generally applicable to all lanthanides and to most actinides, e.g., NpOI and PuOI. However, uranium yields the dioxide and unreacted trihalide. Comparable results would be expected for Th and Pa. Batsanov et al. (1983), using a shock wave generated by an explosive, synthesized numerous ROI compounds from the oxide, metal powder, and iodine. In contrast to values taken from the literature, lattice parameters of the shock-synthesized products varied smoothly with atomic number. Garcia et al. (1985), by hydrolysis of $(NH_4)_3YCl_6$ at temperatures of 270–500°C and use of a flux at ~ 450°C, synthesized the YOF modification of ROCl, R = Y, Ho, Er, and Tm and the SmSI (instead of the PbFCl) modification of HoOCl. Single crystals of ROBr, R = La and Sm, were grown with the corresponding anhydrous lanthanide bromide as flux; the method would seem to have general applicability (Haeuseler and Jung 1986).

2.3.3.2. *Octahedral cluster compounds. Carbon and a halogen.* Schwanitz-Schüller and Simon (1985) synthesized numerous gadolinium carbidebromide compounds, $Gd_2C_2Br_2$, Gd_2CBr_2, and $Gd_6C_2Br_7$, from $GdBr_3$, Gd, and carbon at 900–1050°C; compounds in some of which the oxidation state of the cation is formally lower than three (see Meyer 1988).

A gadolinium carbide fluoride, Gd_2CF_2, was prepared by heating at 1250°C between 2–3 weeks in a sealed Ta container under 1 bar Ar a mixture of GdF_3, powdered Gd (prepared by decomposing pulverized GdH_x under high vacuum), and C (from activated charcoal) (Mattausch et al. 1991). Synthesis composition and conditions were critical. The compound is isotypic with trigonal Gd_2CBr_2 and contains Gd_6 octahedra filled with C atoms and condensed via edge-sharing to form $[Gd_2C]$ layers separated by double layers of F^- ions. These ··FGdCGdF·· layers are held together by van der Waals forces. Subsequently the structure of holmium carbide fluoride, Ho_2CF_2,

synthesized in a manner comparable to that developed for the Gd analogue, was characterized by neutron diffraction (Cockcroft et al. 1992). Ho_2CF_2 is an insulator. Specific-heat and magnetic-susceptibility data are consistent with HoC_2F_2 undergoing an antiferromagnetic phase transition; a maximum occurs in the molar magnetic susceptibility at 4.6 K. Below $T_N = 3.7$ K Ho_2CF_2 transforms into an antiferromagnet with magnetic space group $P_a\bar{1}'$. The phase transition from the paramagnetic to the antiferromagnetic state is accompanied by a distortion of the lattice due to magnetoelastic effects.

Mattausch et al. (1992b) report the structure of an isomorph of $R_2C_2Br_2$, R = Gd and Tb, designated as 3s-$Gd_2C_2Br_2$ and synthesized by heating at 1050°C RBr_3, R activated as described above for the Gd_2CF_2 synthesis, and C confined in Ta under an Ar atmosphere. The C_2 units octahedrally surrounded by Gd atoms are condensed via edge sharing to form sheets which are separated by two layers of Br ions. In this variant three slabs of $BrGd(C_2)GdBr$ are stacked in the [103] direction until identity is achieved. For the R = Gd compound $T_N = 28(2)$ K; the paramagnetic Curie temperature, $\Theta = -20(2)$ K, and the effective magnetic moment is $7.8\mu_B$. Some $R_2C_2X_2$ compounds with R in the S electronic ground state, $Y_2C_2Br_2$, $Y_2C_2I_2$, $La_2C_2Br_2$, and $Lu_2C_{2-x}CI_2$ where found to be superconducting with $T_C \approx 6$ K (Simon et al. 1991). Reports of comparable actinide cluster compounds could not be found, but their existence seems likely.

2.3.4. *Mixed-cation systems*

2.3.4.1. MX_2–RX_3 *systems.* Podorozhnyi and Safonov (1983) effected a DTA and X-ray diffraction phase study of the HgX_2–RX_3 systems, X = Br and I, R = Ho and Dy, over the limited 0–30 mol% RX_3 range and reported complete immiscibility with no reaction between the components. Their results parallel those of Lasocha et al. (1990) on the $CaCl_2$–$YbCl_3$ system. In view of the similarity between the ionic radii of like-coordinated Hg^{2+} and Ca^{2+} [113 pm and 114 pm, respectively (Ziółkowski 1985)] this result might be expected. However, in view of the similarity of the ionic radii of Ca^{2+} and Yb^{2+}, the absence of a vernier-type phase in the Ca-containing system comparable to the long-known Yb_6Cl_{13}-type structure (Lüke and Eick 1982) is somewhat surprising. [See Meyer (1988) for a discussion of the vernier-type structure.] When the larger lanthanide and alkaline-earth elements Eu and Sr were mixed, the intermediate valent $Sr_9Eu_5Cl_{33}$ and Sr_4EuCl_{11} were obtained (Olejak-Chodan et al. 1987b). A similar result was obtained when $NdCl_3$ was substituted for $EuCl_3$ (Hodorowicz et al. 1987), and Sr_4DyCl_{11} is one of the first vernier-type group 2 cation-containing phases characterized (Bärnighausen 1976). Haire et al. (1978) synthesized Cf_4GdX_{11}, X = Cl, Br, vernier-type phases in which the actinide ion exhibited divalency; the ionic radius of Cf^{2+} is comparable to that of Sr^{2+} and Eu^{2+}. The vernier-type phases can be synthesized equally well for larger actinide and lanthanide elements, and their absence with calcium compounds suggests that with small ions differences between the group 2 and lanthanide cations become significant. Lattice parameters for some vernier-type phases are compiled in table 3.

TABLE 3
Crystallographic data for selected vernier-type halide phases not listed in Meyer (1982).

Halide	Symmetry	a(Å)	b(Å)	c(Å)	Angle	Reference
Nd_4Br_9	P11b	7.741(1)	30.165(5)	7.126(1)	$\gamma = 91.80(4)°$	Löchner (1988c)
Eu_4Cl_9	P11b	7.2335(5)	28.302(2)	6.7189(7)	$\gamma = 91.779(9)°$	Bachmann (1987)
Eu_5Cl_{11}	$P2_1/m$	7.214(2)	35.17(1)	6.775(2)	$\beta = 90.34(1)°$	Liu (1990)
Sr_4NdCl_{11}	$P2_1/m$	7.230(4)	35.29(2)	6.786(4)	$\beta \approx 90.00°$	Hodorowicz et al. (1987)
Sr_4EuCl_{11}	$P2_1/m$	7.220(2)	35.15(1)	6.790(4)	$\beta \approx 90.00°$	Olejak-Chodan et al. (1987b)
Cf_4GdCl_{11}	$P2_1/m$	7.130	34.83	6.685	$\beta = 90.24°$	Haire et al. (1978)
Cf_4GdBr_{11}	$P2_1/m$	7.619	36.97	7.040	$\beta = 90.18°$	Haire et al. (1978)

Petzel and Ahnen (1985) determined the phase diagram of the EuF_2–GdF_3 system by DTA and X-ray powder diffraction analysis of quenched specimens. They found the system eutectic with two extended solid-solution regions – cubic fluorite to approximately 44 mol% GdF_3, and hexagonal (tysonite-type) from 70 mol% GdF_3. Mixed EuF_2–LaF_3 samples were examined by X-ray powder diffraction and thermogravimetric analysis (Vinogradova-Zhabrova et al. 1990). Fluorite-type solid solution prevailed to 50 mol% LaF_3 and LaF_3-type solid solution spanned only the 92 to 100 mol% LaF_3 range. The cubic fluorite-type lattice parameter varied linearly with composition. The observations on solubility regions are consistent with behavior expected from the extensive studies of CaF_2–RF_3 systems, but the absence of superstructure reflections is surprising. Yoshimura et al. (1986) studied the SrF_2–LaF_3 system. The specimens were heated to 1300°C for a short time, annealed at 750°C for an extended time, and then quenched. Their experiments yielded only solid solutions. Because of the similar ionic radii of the cations, SrF_2 – and EuF_2 – RF_3 systems would be expected to behave similarly.

Greis and Cader (1986), on the other hand, identified phases of intermediate composition in these systems when the specimens were cooled slowly. They examined selected SrF_2–RF_3, R = La–Nd, Sm–Lu, and Y, mixtures in search of the intermediate phase, Sr_2RF_7, which was expected from previous studies of the AF_2–RF_3, A = Ca and Ba, systems. $Sr_xR_{1-x}F_{2+x}$ solid solutions were found when the specimens were quenched; superstructures were found when samples were heated at 1230°C and then cooled over a 14 day period. Superstructure reflections characteristic of the tetragonal Sr_2RF_7 phase were found for R = Sm–Lu, and Y. The superstructure cell, s, is related to the basic fluorite cell lattice parameter, a_F, as follows: $a_s = 0.5(10)^{1/2}\, a_F$; $c_s = 3a_F$. Rao et al. (1992) heated cold-pressed 1 : 2 mixtures of $BaF_2 : RX_3$ at 900°C and report lattice parameters of a product which was assumed to be BaR_2F_7. The R = La–Nd, exc. Pm phases were cubic; those for R = Sm, Gd, Tb, and Y were orthorhombic.

Laval and co-workers have examined numerous lanthanide and actinide fluorite-related structures. They prepared defect solid solutions of $Ca_{1-x}R_xF_{2+x}$, $x = 0.32$; R = La, Nd, Tb, Ho, Er, Yb, Lu, by heating the mixed fluorides in sealed Ni tubes at 1000°C for two days with subsequent quench and examining them by room tempera-

ture time-of-flight neutron diffraction (Laval et al. 1988b). Additionally $x = 0.32$ specimens for R = Er, Yb, Lu, and CaR_2F_7-related low-temperature superstructures, prepared as above but with different annealing conditions, were characterized by EXAFS (Laval et al. 1990). The defect $Ca_{1-x}La_xF_{2+x}$ ($0 \leq x \leq 0.38$) structure was also examined by neutron diffraction (Laval et al. 1989). These studies suggest the presence of two kinds of $\langle x, x, x \rangle$ interstitials whose numbers increase linearly with increasing dopant cation concentration: F‴ with $x \approx 0.31$ (the relaxed normal anion), and F″ with $x = 0.41$. These can be represented as [1:0:3] clusters. Phases for which [1:0:3] clusters (see page 383 for a description of cluster nomenclature) have been proposed include $Ca_{1-x}M^{IV}_xF_{2+2x}$, M^{IV} = Th, U (Laval et al. 1986), and $LaF_{1+2x}O_{1-x}$ (Laval et al. 1988a), among others. Thus in this $Ca_{1-x}R_xF_{2+2x}$ system the [1:0:3] cluster is the most stable observed, but at elevated temperatures a more dense [1:0:4] cluster might be present. Solid-state NMR would seem to be a useful tool for analysis of these mixed fluorite structures, but only one NMR analysis of a mixed CaF_2–LaF_3 system could be found (Sorokin 1992). In this study the chemical shift, δ_F, was reported to correlate linearly (with a correlation coefficient of 0.997) with interstitial fluoride ion concentration.

Laval et al. (1989, 1990) indicate that the principal factor that determines the nature of short-range order in anion-excess fluorites is the dopant cation size in comparison to the host cation size. With increasing dopant cation size the F′ interstitials prominent for small cations (Lu, Yb) are progressively replaced by F″ interstitials and relaxed F‴ anions. Large dopant cations (La–Tb) form small [1:0:3] clusters, while medium-sized and small dopant cations (Ho–Lu) form a mixture of small [1:0:3] clusters and large [8:12:1] cuboctahedral clusters with the number of the latter increasing with decreasing dopant cation size. Increasing numbers of [8:12:1] clusters lead to long-range ordering at low temperatures and to M_xF_{2x+5} superstructures.

The structure of Ca_2YbF_7, the $n = 15$ member of the homologous series (Ca, Yb)$_nF_{2n+5}$, was determined ab initio from the polyhedral model M_6X_{37} square-antiprism cluster, and experimentally from a single-crystal structural analysis (Ness et al. 1988, Bevan et al. 1988b). (A projection of the cuboctahedral [8:12:1] cluster onto the xy-plane is presented in fig. 3.) This structural solution demonstrated the pervasiveness of this cuboctahedral [8:12:n] cluster as a basic structural block of fluorite-related defect structures. Bevan et al. (1988a), using the square-antiprism cuboctahedral cluster (M_6X_{36} or M_6X_{37} if an anion is located in the center of the cluster) as a basis, discuss the crystal chemistry of numerous anion-excess fluorite-related phases and classify them into four distinct types:

(1) $R(III)_6F_{36}O$, in which O is located in the cuboctahedral cavity, e.g., $Nd_{14}Cl_{32+\delta}O_{1-\delta}$ (Eitel 1985);
(2) $R(II)R(III)_5F_{37}$ [or $Ca(II)R(III)_5F_{37}$], with F in the cuboctahedral cavity, e.g., $Nd_{14}Cl_{33}$ (Eitel 1985) or $Ca_9Yb_5F_{33}$ (Lechtenböhmer and Greis 1978);
(3) $M(II)_2(III)_4F_{36}$, in which the cuboctahedral cavity is empty, e.g., $BaCaLu_2F_{10}$ (Vedrine and Trottier 1979); and
(4) $R(III)_6F_{36}$, in which the cuboctahedral cavity is empty, e.g., KY_3F_{10} (Pierce and Hong 1973).

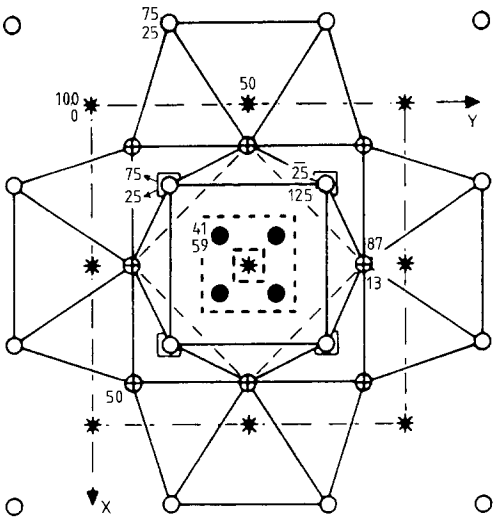

Fig. 3. Projection of an M_6X_{37} cuboctahedral [8:12:1] cluster (8 vacancies, 12 X′ anions, and 1 X″ anion) onto the xy plane (< 100 >). The cluster consists of an octahedral arrangement of six MX_8 square antiprisms sharing corners to enclose a cuboctahedron of X′ anions. The extra X″ anion is at the center. [From Laval et al. (1988b) with permission.]

They indicate further, with examples, that intergrowth of these structure types may occur. Bertaut et al. (1989) report using similarity operators to deduce the superlattice structure of these and related cuboctahedral compounds when the chemical formula is known.

Comparable anion clusters are reported for the light-lanthanide oxidefluoride phases (R = La–Nd). The $x = 0.35$ member of the tetragonal $LaF_{1+2x}O_{1-x}$ solid solution was examined by high-resolution time-of-flight neutron diffraction (Laval et al. 1988a). This tetragonal cell (space group P4/nmm) is related to the fluorite cell by the relationships $a_t = b_t = a_F\sqrt{2}/2$; $c_t = a_F$; oxygen and fluorine anions are ordered in planes perpendicular to the [111] and [001] fluorite axes. The defect structure in this system is basically the same as those observed for the homologous cubic fluorite related systems: $Ca_{1-x}R^{III}_xF_{2+x}$ (Laval et al. 1988b) and $Ca_{1-x}M^{IV}_xF_{2+2x}$, M^{IV} = Zr, U (Laval et al. 1987). In the latter system, where M^{IV} represents U and Zr, the larger U(IV) ion, over the composition range $0 \leq x \leq 0.195$, behaves similarly to the previously studied M^{IV} = Th system (Laval et al. 1986) and forms [1:0:3] clusters (no F′ interstitials) just as do the larger lanthanides. The smaller Zr^{4+} ion, on the other hand, forms $Ca_3Zr_3F_{37}$ [8:12:1] cuboctahedral clusters comparable to those of the smaller lanthanides. The ionic conductivity of $Ca_{1-x}Ac_xF_{2+2x}$, Ac = Th, U, solid solutions were determined (El Omari et al. 1991) and correlated with the short-range order present in these phases. Cluster formation is found comparable to that of the $Ca_{1-x}R_xF_{2+x}$, R = La–Gd, solid solution with [1:0:3] clusters in the composition range $0.01 \leq x \leq X_L$, where X_L represents the upper substitution limit. The uranium-substituted compound, with the larger number of vacancies, has better electrical properties.

Blachnik et al. (1985) examined selected MCl_2–RCl_3 systems, M = Sr, Ba, R = La, Sm, Gd, and Yb, by differential thermal analysis and derived the phase diagrams. They

reported compounds of the approximate compositions $BaRCl_5$, M_2RCl_7, Ba_3RCl_9, and probably Sr_4RCl_{11}, which decomposed peritectically. The Sr_2RCl_7 compounds, R = Sm, Gd, were indicated to be isotypic with a structure related to that of Sm_3Cl_7 which is now known to be a cluster-type compound [see Lumpp and Bärnighausen (1988) for the structure of "Nd_3Cl_7"]. The Sr_4RCl_{11} compounds were expected to be isotypic with vernier-type Sr_4DyCl_{11} (Bärnighausen 1976); phase assignments in the M = Sr, R = Yb system remined uncertain. The phase diagrams are comparable to those of RCl_2–RCl_3 systems with similar cation radius ratios. Enthalpy of mixing values, where measured, are exothermic with minima at approximately 65 mol% $SrCl_2$. Löchner and Blachnik (1988) subsequently reexamined the structures of the first three phases identified for these systems. Compositions of selected phases are found to be $(Sr, Sm)_{14}Cl_{32+x}$, $(Gd, Sr)_{14}Cl_{32+x}$, and $(Ba, Sm)_{15}Cl_{34+x}$, i.e., $M_nCl_{2n+5-\delta}$ phases. Consistent with the AF_2–RF_3 systems, all contain M_6X_{37} polyhedral (cuboctahedral) clusters. Lattice parameters reported for these phases are listed in table 2. Qiao and Xing (1991) report ternary phase diagrams for a few RCl_3–MCl_2–$MgCl_2$ and RCl_3–MCl_2–LiCl systems, R = La–Nd, M = Ca, Sr, derived by combining limited experimental data and computer calculations.

Liu and Eick (1989a) synthesized BaX_2–RX_3 phases which contained excess trihalide as part of their solvolytic decomposition studies: $Ba_9R_5Br_{33}$, R = La, Nd, and phases presumed from the above-cited phase studies to be "Ba_2RCl_7", R = La, Sm, but now known to be also M_6Cl_{37}-cluster based compounds. They noted that the *c* lattice parameters derived from powder data for the chloride compounds are comparable to those of the M_6X_{37} cluster compounds, but the *a* parameters are related by the factor $2^{1/2}$. Lattice parameters reported for these chloride phases are also listed in table 2, but should not be considered representative of the true unit cell. The understanding of cluster formation developed from the fluoride systems discussed above suggests that structures of all of these phases are based upon the M_6X_{37} cluster.

2.3.4.2. *AX–RX_3 systems.* As was indicated in the introduction, AX–RX_3 systems which contain a group 1 cation have been reviewed extensively. Consequently, only selected examples are included here. Structure types observed for the heavier halides in combination with K, Rb, and Cs include elpasolite-type A_3RX_6, K_2PrCl_5-type A_2RX_5, $Cs_3Cr_2Cl_9$-type $A_3R_2X_9$, and KDy_2Cl_7-type AR_2X_7. Blachnik and Enninga (1983), from thermochemical studies, constructed phase diagrams of the ACl–RCl_3 systems, A = Cu, Ag, and Tl, R = La, Gd, and Yb. The systems with A = Cu and Ag and R = La and Gd are eutectic, but those with R = Yb yielded peritectically decomposing A_3YbCl_6. The TlCl-containing systems, on the other hand, yielded Tl_2RCl_5 (R = La, Gd), TlR_2Cl_7 (R = Gd, Yb), and Tl_3RCl_6 (R = Gd, Yb) compounds typical of comparably sized A = group 1 cations. Seifert et al. (1985) reinvestigated the ACl–$LaCl_3$ systems, A = Na–Cs, and derived thermodynamic functions for the formation reactions. In addition to the expected A_2LaCl_5, A = K–Cs; A_3LaCl_6, A = Rb ($T > 452$°C), Cs; $A_2La_2Cl_7$, A = Rb, Cs; a UCl_3-type $KLa_{1.67}Cl_6$ was identified and its structure solved. In this phase, one K^+ substitutes for 0.33 La^{3+}; a comparable compound probably exists for A = Na. Seifert and Sandrock (1990) determined by DTA phase diagrams of ACl-$EuCl_3$ systems, A = Na–Cs, and reported lattice parameters and

thermochemical data on the numerous phases observed. Mattfeld and Meyer (1992) examined the $ACl-RCl_3$ systems, A = K, Rb, Cs, R = Y, Tb-Lu, and that of $(NH_4)_3YCl_6$, determining by X-ray single-crystal techniques the monoclinic structure of Rb_3YCl_6 (Cs_3BiCl_6-type). They also examined the $ACl-YCl_3$, A = NH_4, K, Rb, and Cs, systems by DTA and high-temperature X-ray powder diffraction and determined the temperature regions over which the three different A_3YCl_6 compounds (I, II, III) are stable. For A = K, $Rb_{0.67}K_{0.33}$, and NH_4, I is stable to $\sim 100°C$ and II (Cs_3BiCl_6-type) to $\sim 340°C$. For A = Rb and Cs, II is stable to $\sim 400°C$. Type III (cubic elpasolite) is stable at $T > \sim 340°C$ for A = K and $Rb_{0.67}K_{0.33}$, and at $T > \sim 400°C$ for A = Rb, and Cs. The type III A = NH_4 compound is stable only from $280° < T < 340°C$; $NH_4Y_2Cl_7$ forms above 340°C.

Other measurements have been made on Ag_3RCl_6 compounds. Staffel and Meyer (1988) synthesized the R = Dy–Lu, Y, and Sc compounds and measured thermal expansion. Lerch et al. (1990) characterized Ag_3YCl_6 structurally and determined its electrical conductivity from room temperature to the melting point; conductivity increases sharply at the transition temperature. Below its transition temperature of 350°C, Ag_3YCl_6 is isostructural with Na_3GdCl_6–I. Steiner and Lutz (1992) examined the related Li_3YCl_6 and found it to exhibit fast ionic conductivity and complicated order–disorder phase transitions.

Czjzek et al. (1992) demonstrated that monomethylammonium chloride would form a double salt with $YbCl_3$ to give a monoclinic structure with alternating $[YbCl_6]^{3-}$ octahedra and tetrahedrally arranged $[(CH_3NH_3)_4Cl]^{3+}$ units. The Yb^{3+} ion coordination sphere remains comparable to that in $YbCl_3$.

Numerous A_2RCl_5, A = In, NH_4, Rb, Cs, and (Cs and Rb), and a few A'_2PrX_5, A′ = In, K and Rb, X = Cl, Br, and I, were synthesized and characterized structurally by X-ray single-crystal techniques (Meyer et al. 1985a). These compounds are isotypic with either orthorhombic (Pnma) K_2PrCl_5 or orthorhombic (Pbnm) Cs_2DyCl_5. Lattice parameter data on Cs_2DyCl_5-type A_2RCl, $AA'RCl_5$ and K_2PrCl_5-type A_2RX_5, X = Cl, Br, I, are presented and a structure-field diagram is developed by plotting differing ΔV_m (molar volume) values. Khaidukov et al. (1990) synthesized K_2RF_5 compounds, R = Nd–Lu and Y, exc. Pm, from aqueous KF and the oxide at elevated temperatures and pressures. They report the orthorhombic lattice parameters and temperatures at which thermal transitions were observed by DTA. For the compounds, R = Tb–Lu, Y, complete decomposition to K_3RF_6 and KRF_4 occurred over the temperature range 500–580°C, with the decomposition temperature decreasing almost linearly with decreasing cation size. The R = Eu and Gd compounds decomposed to K_3RF_6 and KR_2F_7; lighter lanthanides did not decompose. Comparable compounds involving trivalent actinides would be expected, but few could be located in the recent literature.

Recent work on the $CsI-RI_3$ systems, R = Tb, Lu, yielded $Cs_3R_2I_9$ and Cs_3RI_6 compounds (Nechitailov et al. 1989), as would be expected from the review of Meyer (1982). $Cs_3Tm_2I_9$, synthesized by oxidation of Tm with HgI_2, is isostructural with $Cs_3Cr_2Cl_9$ (hexagonal, $P6_3/mmc$) (Wang et al. 1989). The structure of $Cs_3Ho_2Br_9$ was refined in space group $R\bar{3}c$ at numerous temperatures between 1.5 and 295 K with high-resolution neutron-diffraction data; the Br atoms evidenced anisotropic thermal

vibrations, the Cs and Ho atoms did not (Dönni et al. 1991). Long-range magnetic ordering was absent between 7 mk and room temperature. Metallinou et al. (1991) characterized the CsI - ScI_3 system by X-ray, DTA, DSC, and Raman spectroscopic techniques, obtaining spectra of both solid and melted specimens. The expected $Cs_3Sc_2I_9$ and Cs_3ScI_6 phases were observed. Molten mixtures for the concentration range 10–50 mol% ScI_3 appeared to exhibit the equilibrium, $[ScI_4]^{1-} + 2I^{1-} \rightleftharpoons [ScI_6]^{3-}$, with a dimeric species, $[Sc_2I_9]^{3-}$ possibly present. At 800°C the equilibrium vapor contained $CsScI_4(g)$ and $ScI_3(g)$.

Seifert and Yuan (1991) characterized the $ABr–LaBr_3$ (A = Na, K, Rb, Cs) system and provided thermochemical data. The A = Na system is eutectic. The A_2LaBr_5 (A = K, Rb, and Cs) compounds are stable at ambient temperature, but decomposed peritectically for A = Cs. At temperatures above ~430°C A_3LaBr_6 (A = Rb, Cs) crystallize in the cubic elpasolite structure common to the heavier lanthanides; at ambient temperature the monoclinic K_3MoCl_6-type structure prevailed, with A = Rb metastable. Cs_2LaBr_7 was stable over the limited 459–551°C range.

Although limited research on $AX–AcX_3$ mixed cation compounds, where A represents a group 1 element, could be found in the recent literature, work by Chudnovskaya et al. (1987) clearly suggested that such compounds could be synthesized. These workers examined the self luminescence of elpasolite-type $Cs_2NaLa(Am)Cl_6$ which contained 2.5 at. percent ^{243}Am and indicated no degradation in luminescence intensity over a four year period. Synthesis of the related elpasolite-type $Cs_2NaLu(Am)Cl_6$ which contained 5 mol% ^{243}Am was also indicated. More recently, the cubic $Fm\bar{3}m$ structure of Cs_2NaUCl_6 was determined by single-crystal techniques (Spirlet et al. 1988). Schoebrechts et al. (1989) synthesized numerous elpasolite-type cesium sodium actinide chlorides, $Cs_2NaAcCl_6$, Ac = U–Cf, and presented structural details, actinide ionization potentials, and hydration enthalpies. Different synthesis procedures were required: the Ac = U and Np complexes were prepared by fusing the appropriate molar mixture of $AcCl_3$, CsCl, and NaCl; the Ac = Am and Cf were synthesized from aqueous solution. Cubic lattice parameters of the actinides are compared with those of lanthanides. Enthalpies of solution were determined, using Fe^{3+} to oxidize the U^{3+} and Np^{3+} compounds rapidly and quantitatively. These enthalpies are combined with appropriate ancillary data and calculated lattice energies to derive third ionization potentials of the actinides and hydration enthalpies of their tripositive ions.

Zych and Drożdżyński (1991) synthesized A_2UBr_5, A = K, Rb, from UBr_4 dissolved in methylcyanide with a large excess of the group 1 bromide. The mixture was acidified with propionic acid and the U(IV) reduced with zinc amalgam. The precipitate which formed upon reduction, a methyl cyanide-hydrate, could be decomposed thermally in high vacuum to yield the anhydrous compounds; structural data were not presented. Solid-state absorption spectra taken from thin films and magnetic-susceptibility measurements are consistent with the presence of an U^{3+} cation. The authors indicate that the A = Cs compound can also be synthesized. Zych and Drożdżyński (1990) also synthesized $NH_4UBr_4 \cdot 1.5CH_3CN \cdot 6H_2O$ via the methylcyanide route. Upon decomposition in a high vacuum this complex salt converts to UBr_3.

$AUCl_4$, A = K, Rb, NH_4, were prepared from the tetrahydrate by thermal decomposition in high vacuum (Zych and Drożdżynski 1988). The monoclinic tetrahydrates of

the complex U(III) salt, $AUCl_4 \cdot 4H_2O$ were prepared from UCl_4 in methylcyanide solution to which the group 1 or ammonium salt and a small quantity of H_2O had been added. Reduction was effected with zinc amalgam. The $CsUCl_4 \cdot 4H_2O$ compound could not be prepared by this procedure, but was thought to be synthesized by mixing non-aqueous solutions of CsCl and UCl_4 and simultaneously effecting reduction with zinc amalgam (Karbowiak and Drożdżyński 1990). However, a subsequent structure determination showed that it was a trihydrate, $CsUCl_4 \cdot 3H_2O$, rather than a tetrahydrate (Krämer et al. 1991b). This monoclinic trihydrate structure appears unique. The uranium ion coordination is tricapped-trigonal prismatic; six chloride ions form the trigonal prism and three oxygen atoms cap the tetragonal faces. The prisms form an infinite zig-zag chain by sharing two chloride ions. In a subsequent report isostructural tetrachloride trihydrates, $AUCl_4 \cdot 3H_2O$, A = K, Rb, and NH_4 were synthesized (Karbowiak and Drożdżyński 1993). These latter compounds exhibited Curie–Weiss paramagnetism in the 100–300 K temperature range with derived effective magnetic moments of $3.7\mu_B$, $3.57\mu_B$, and $3.71\mu_B$, respectively, for the potassium, rubidium, and ammonium salts. IR absorption bands and electronic spectral data were also presented.

The fluorite-related $K_{1-x}R_xF_{1+2x}$ region of the $KF–RF_3$ (R = Pr–Er) systems were investigated for $0.66 < x < 0.75$ by X-ray and electron diffraction (Le Fur et al. 1988a) and the structure of $K_{0.265}Gd_{0.735}F_{2.47}$ was determined by single-crystal X-ray diffraction (Le Fur et al. 1988b). In $K_{0.265}Gd_{0.735}F_{2.47}$, the classic Gd_6F_{37} cuboctahedron (see section 2.3.4.1) is formed from six GdF_8 square antiprisms with an additional F anion in the center. These Gd_6F_{37} groups form chains within a fluorite-type matrix. A fluorite-related superstructure had been reported in this composition region for R = Ce, Nd, Sm, Eu, and Gd specimens heated at 700°C. These researchers also found a KHo_2F_7-type monoclinic compound, $(K_{0.33}R_{0.67}F_{2.33})$ for R = Tb–Er in specimens synthesized at 1000°C; they related it to the fluorite lattice, a_F, by the following transformations: $a \approx a_F\sqrt{6}$, $b \approx a_F\sqrt{2}$, $c \approx 3a_F/\sqrt{2}$, and $\beta = 125°$. Two other phases were also observed. The first, labelled A and found only for R = Eu and Gd (over the composition range $0.66 < x < 0.75$) after ten days treatment at 900°C, is an incommensurate modulated structure. It is bounded on each side by fluorite-related commensurate phases of orthorhombic symmetry. These two phases are related to fluorite by the relationships: $a \approx 2a_F$, $b \approx a_F\sqrt{2}$, and $c \approx 3a_F\sqrt{2}$; $a \approx 2a_F$, $b \approx a_F\sqrt{2}$, and $c \approx 4a_F\sqrt{2}$ The second, labelled B, was found for R = Pr, Nd, Sm, Eu, and Gd (over the composition range $0.66 < x < 0.70$) after treatment at 750–800°C for ten days. The wave vector which spans the incommensurate modulated structure is described. Phase B, a new compound of monoclinic symmetry, is related to the fluorite structure as

$$a \approx 2a_F\sqrt{3}, \quad b \approx a_F\sqrt{2}, \quad c \approx \tfrac{1}{2}a_F\sqrt{114} \quad \text{and} \quad \beta \approx 97°.$$

Champarnaud-Mesjard and Frit (1992) determined the structure of a high-temperature modification of $KScF_4$, an octahedral cis–trans layered compound which shows a close structural relationship to the compounds $TlAlF_4$ and KMF_4, M = Ga, In, Fe. Khaidukov et al. (1991) synthesized from an aqueous $KF–R_2O_3$ mixture at elevated temperatures and pressures numerous KRF_4 compounds, where R represents Y and all lanthanides except Tb, and reported lattice parameters. The R = La–Gd com-

pounds crystallize in the (Pmna) β-$KCeF_4$-type structure; the R = Dy–Lu compounds exhibit the $KErF_4$-type structure. From differential thermal data they deduce the high-temperature phase stability of the various compounds. The room temperature structures of KYF_4 and $KY_{0.95}Er_{0.05}F_4$ were determined in a single-crystal study by Le Fur et al. (1992a,b). The Y atoms are surrounded by seven F atoms in two environments, designated type I and type II. Type I coordination is described as badly distorted monocapped trigonal prismatic; type II as pentagonal bipyramidal. Two polyhedra of type I and type II share one of their equatorial edges to form Y_2F_{12} groups. These groups share one of their equatorial corners to form chains that run along one of the three trigonal directions. Cations are distributed in three layers perpendicular to the *c*-axis. In each layer chains of Y_2F_{12} groups alternate with chains of F edge-shared distorted cubes that surround the K atoms. The Er atoms are located only in the type II environment and are distributed among three sites which are characterized by the absence of F atoms in the [111] direction.

Köhler and Müller (1991) obtained a divalent samarium fluoroaluminate, $LiSmAlF_6$, by heating a confined mixture of the appropriate fluorides two days at ≤ 700°C. In contrast to the structure of the closely related strontium and calcium analogues in which the divalent cation is coordinated octahedrally, the Sm ion coordination is trigonal prismatic. Magnetic-susceptibility measurements show temperature dependence typical of divalent samarium.

2.3.4.3. *Miscellaneous systems. ROX-related compounds.* Corbett et al. (1986) demonstrated that RCl_3 added to R(R = Y, La, Nd, and Gd) which contained 1–5 atom% dissolved oxygen would be converted to ROCl and the metal oxygen content reduced to 0.1–0.2 atom% oxygen when the confined mixture was heated 1–2 weeks. This reaction also served to lower the dissolved oxygen content of elemental thorium, and was assumed to be a reaction general for all lanthanides.

Odink et al. (1992) intercalated the (hexagonal) layered SmSI-type YbOCl with pyridine (py) to obtain 3R structure-type $(py)_{0.1}YbOCl$ with a ~ 7 Å increase in the interlayer separation. The additional increase in the interlayer separation upon intercalation of 4-ethylpyridine and IR spectroscopic data support the conclusion that the lone pair of electrons on the nitrogen and the plane of the molecule are oriented perpendicular to the YbOCl layers.

Oxygen, a halogen, and a main group element. Phase diagrams for LaOI-AI(A = Na–Rb) systems determined by Tupoleva et al. (1988) by DTA and X-ray diffraction suggest formation of the peritectic phases A_2LaOI_3, A = Na–Rb, and $Rb_2La_3O_3I_5$. However, structural data were not presented.

Aurivillius (1984) synthesized and characterized single crystals of selected $R_xBi_{6-x}O_8Cl_2$, where $x = 1, 2, 3$, or 4, and R = Nd, Eu, and Gd. Some crystals in which the chloride anion was replaced by bromine were also examined. The structure is built from fluorite-like $[M_3O_4]^+$ blocks and single halogen layers. It can accommodate an extraneous oxygen atom and the Ce compound contained 8.5 rather than eight oxygen atoms. Interatomic distances suggest that the inert electron pairs on the bismuth atom are only moderately stereochemically active. Since the ionic radius of U^{3+} is about

10 pm larger than that of Bi^{3+} (Ziółkowski, 1985) and since an extra oxygen atom can be accommodated in the structure, actinide cations could probably be substituted for either the lanthanide or bismuth cations.

Schleid (1991) obtained an oxidesulfide-chloride, $Ce_4OS_4Cl_2$, as a by-product of the reaction of a 1 : 1 mixture of the $CeClH_{0.67}$ and S in molten NaCl. In this compound the Cl and S anions randomly occupy selected anion sites surrounding a ten- and an eight-coordinated Ce^{3+} cation. One oxide anion is in each coordination sphere. Using this same procedure and $YClH_{0.67}$ or $Na_{0.25}YClH_{0.75}$ and S in NaCl, he obtained single crystals of the previously reported D-type Y_2S and, when YOCl was an impurity, single crystals of Y_2OS_2 (Schleid 1992). Adaptations of this latter procedure yielded single crystals of different structural modifications of additional lanthanide sesquisulfides (Schleid and Lissner 1992) and for R = La–Nd, Sm, the complex oxidesulfide $R_{10}S_{14}O$ (Schleid and Lissner 1991).

The effects of substituting small amounts of fluoride and/or chloride ions for oxide ions in high T_C copper oxide superconducting systems continues to be an area of research. Recent examples include $Nd_2CuO_{4-x}F_x$ (Tighezza et al. 1992) and $YBa_2Cu_3O_xF_yCl_z$ (Sumiyama et al. 1991).

An interesting chloride-containing series of compounds, MRCuO$_3$Cl(M = Sr, Ca; R = Nd, Sm–Gd) crystallizes in a structure similar to that reported for $Nd_{1.4}Ce_{0.2}Sr_{0.4}CuO_4$. In this oxidehalide structure the R ion is located in a cubic-like arrangement of eight oxide ions while the M ion is surrounded by a capped square antiprism of four oxide and five chloride ions (Ramanujachary et al. 1991).

Crystalline fluorocarbonates, $Ba_2R(CO_3)_2F_3$ (R = Y, Gd), of interest for their potential application in optics, were synthesized hydrothermally from RF_3 and $BaCO_3$ in molten $Ba(NO_3)_2$ at 700°C and 216 MPa pressure (Mercier and Leblanc 1991). In these fluorocarbonates the Ba and R cations occupy the center of distorted BaO_5F_4 and RO_6F_3 Archimedean antiprisms monocapped on a square face. Two Ba-containing polyhedra are connected by an R-containing polyhedron to yield $Ba_2RO_{12}F_9$ blocks which are then connected to form infinite two-dimensional slabs.

3. Trihalide hydrates

A detailed study of the RF_3, R = La–Lu, exc. Pm, behavior in aqueous solutions was completed by Menon and James (1989). Solubilities and solubility products were determined by conductometric, potentiometric, and radiometric techniques as a function of pH. Stability constants for the mono- and difluorocomplexes in aqueous solution were also measured. The effect of precipitate aging was considered for DyF_3. Solubilities and pK_{sp} values of the RF_3 do not vary systematically with atomic number, but instead remain relatively constant, varying by no more than three units across the series, with values of 15.2 for LaF_3 and 14.4 for LuF_3.

Synthesis of $RI_3 \cdot nH_2O$ and the intermediates formed during dehydration in air were characterized for numerous R (Heiniö et al. 1980). For R = La–Ho, $n = 9$; for R = Y, Er–Lu, $n = 8$. The R = Tb, Dy, Ho, and Y iodides may crystallize in either form at room temperature, depending upon the ambient H_2O pressure. While reported

compositions differ little from earlier reports (Kwestroo and Van Hal 1976), structural details and decomposition behavior are presented. The orthorhombic nanohydrates decompose through various steps. The larger lanthanide iodides form, in sequence, the $n = 6$ and $n = 3$ hydrates, then RI_3, $2RI_3 \cdot ROI$, and finally an m $ROI \cdot R_2O_3$ product. The value of m is R dependent. The number of intermediate hydrates decreases with decreasing size of R; anhydrous RI_3 is stable over only a $\sim 5°C$ temperature range below 200°C. Decomposition in air of $YI_3 \cdot nH_2O$, determined as part of a study of iodide synthesis precursors for $YBa_2Cu_3O_{7-\delta}$, is reported to occur at 250°C (Baney et al. 1992).

Dehydration of $LaCl_3 \cdot 7H_2O$ was studied by various thermal analysis and thermogravimetric techniques (Gong et al. 1983). The dehydration mechanism was found to be H_2O vapor pressure dependent. With $p(H_2O) \approx 1-6$ Torr, $LaCl_3 \cdot 7H_2O \Rightarrow LaCl_3 \cdot 3H_2O \Rightarrow LaCl_3 \cdot 2H_2O \Rightarrow LaCl_3 \cdot H_2O \Rightarrow LaCl_3$. When $p(H_2O) \approx 10-100$ Torr, the $LaCl_3 \cdot 2H_2O$ phase is not observed; when $p(H_2O) \approx 150$ Torr, $LaCl_3 \cdot 3H_2O \Rightarrow LaCl_3 \cdot 5H_2O \Rightarrow LaCl_3 \cdot H_2O \Rightarrow LaCl_3$. The actinide hydrate, $UCl_3 \cdot 7H_2O$, was synthesized from UCl_4 dissolved in methylcyanide to which a small quantity of water and propionic acid had been added. Reduction of the U(IV) was effected in an inert atmosphere with liquid zinc amalgam (Drożdżyński 1985). The monoclinic heptahydrate appears isostructural with $LaCl_3 \cdot 7H_2O$. At low temperatures, the hydrate is stable in air, but above 15°C the loss of H_2O that occurs is followed by oxidation of the uranium. If the heptahydrate is heated slowly in a dynamic vacuum to remove most of the H_2O, and then at a higher temperature, pure UCl_3 can be prepared. A $UCl_3 \cdot CH_3CN \cdot 5H_2O$ mixed hydrate was also synthesized by Drożdżyński (1986) by modifying the procedure developed for synthesis of the heptahydrate (less water is added). Upon heating, the compound decomposes to an oxidechloride.

Acetate-chloride hydrates of samarium, (1) $[Sm(C_2H_3O_2)(H_2O)_6]Cl_2 \cdot H_2O$ and (2) $[Sm(C_2H_3O_2)_2(H_2O)_3]Cl$, were synthesized by slow evaporation of aqueous acetic-acid solutions of $SmCl_3 \cdot 6H_2O$ and SmOCl, respectively (Meyer et al. 1991). In both compounds the Sm^{3+} ions are nine-fold coordinated by oxygen; the chloride ions serve to achieve charge neutrality. The structure of the diacetate compound is characterized by one-dimensional infinite chains, $^1_\infty[Sm(C_2H_3O_2)_2(H_2O)_3]$, formed from two tridentate-bridging acetate groups. The structure of (1) was determined from the praseodymium analogue; the R ion is nine coordinated by oxygen from the six water molecules, a bidentate acetate group, and the bridging oxygen from a second acetate group (Schleid and Meyer 1990). The structure of (2) was determined from the europium analogue (Schleid and Meyer 1989).

An acetate-chloride hydrate of lanthanum, $[La_2Cl_3(C_2H_3O_2)_2(H_2O)_7]Cl$, was synthesized by reaction of the hydrated trichloride with dilute acetic acid or the sesquioxide with acetyl chloride. In this compound the La atom is coordinated by two chloride and seven oxygen ligands. This compound also is characterized by a one-dimensional infinite chain, $^1_\infty[La_2Cl_3(C_2H_3O_2)_2(H_2O)_7]^+$, connected to like chains by chloride ions which are surrounded by H_2O molecules (Schleid et al. 1991).

The compound, $U_2I_4(O\text{-i-pr})_4(HO\text{-i-pr})_2$, i-pr $= (H_3C)_2CH-$, was synthesized by desolvation of the product that resulted from the reaction of uranium metal turnings with iodine and 2-propanol (Van Der Sluys et al. 1992). In this compound two uranium

(IV) atoms six-coordinated (by two iodine and four oxygen atoms) edge-share oxygen atoms.

4. Reduced halides MX_n, $n < 3$

Structural details and phase equilibria of numerous intermediate valent halides were reviewed in this handbook (Haschke 1979). Intermediate valent compounds remain an area of exceedingly high activity. Lattice parameters of numerous phases which contain either a lanthanide or an actinide in an intermediate oxidation state, or an alkaline earth substituted for one of these elements, are listed in table 2.

Meyer and Schleid (1987) point out that many of the lanthanide(III) halides can be reduced by alkali metals either to binary or ternary lanthanide(II) compounds, or to more reduced halides stabilized by interstitials, e.g., $LuClH_x$ or $Cs_2Lu_7Cl_{18}C$. They emphasize that this metallothermic reduction procedure occurs at low temperatures and allows crystal growth from the melt. Meyer and Schleid (1991) and Corbett (1991) describe in detail synthesis procedures for reduced and heteroatom-containing halides. Mixed-valence $NaNd_2Cl_6$ and $NaPr_2Cl_6$ were synthesized from reaction of Na and the trichloride sealed in Ta tubes. Both of the NaR_2Cl_6 phases crystallize in the UCl_3-type structure. However, lattice parameter variations for the R = Pr compound are small, but consistent with inclusion of an Na^+ ion in the structure. On the other hand, those for the R = Nd specimen are appreciable and indicate both that an Na cation has been incorporated in the lattice and that an Nd^{3+} ion has been reduced to Nd^{2+} (Schleid and Meyer 1987b). Lumpp and Bärnighausen (1988) synthesized "Nd_3Cl_7" ($NdCl_{2.31}$) by heating a mixture of the tri- and dihalides sealed in Ta for an extended period of time. As expected for an element which can exhibit divalency in combination with halides, the tetragonal structure is based upon the fluorite-related Nd_6Cl_{37} cuboctahedron cluster. Procedures for synthesis of phase pure Eu_4Cl_9, Eu_5Cl_{11}, and $Eu_{14}Cl_{33}$ are reported (Liu and Eick 1991).

Löchner (1988b, c) completed a phase study of the Nd–$NdBr_3$ system by X-ray and thermochemical techniques and identified only CaF_2-type $NdBr_2$ and incongruently melting vernier-type Nd_4Br_9. Lattice parameters of this phase are listed in table 3. Schleid and Meyer (1991) heated an $NdBr_3$–K mixture confined in tantalum ampoules and obtained the mixed-valent $K_3Nd_3Br_{10}$. The structure contains one-dimensional infinite chains similar to that of trivalent K_2NdBr_5 with trans-edge-connected monocapped trigonal prisms.

Lyle and Westall (1985) point out that $EuBr_3$ loses bromine upon being heated above 190°C, yet retains the $PuBr_3$-type structure with the lattice parameters increasing slightly. Compositions $EuBr_x$, $2.84 \leq x \leq 3.0$, were characterized by Mössbauer spectroscopy and electrical conductivity techniques. Relaxation times, τ, were derived for the electron hopping process and activation energies were determined. Electron hopping is thermally activated and described as a process in which a 4f electron is promoted into the 5d6s conduction band for a characteristic time of the order of 10^{-6} s at 78 K. Europium trichloride behaves similarly (Ball et al. 1983).

To determine the enthalpy of formation of DyI_2, Morss and Spence (1992) synthesized a ~ 2 g specimen; mass analysis indicated a 94.5% DyI_2 and 4.7% DyI_3 yield.

Their procedure entailed heating stoichiometric quantities of sublimed Dy metal and I_2 at 680°C for 20 days.

4.1. *Metallic halides*

Meyer (1991) surveyed known metallic lanthanide halides and classified them into three categories with the formulas: RX_2, R'_xRX_3, and R_2X_5. The first category, RX_2, where X = I, has long been known to be metallic. However, $LaBr_2$ also shows metallic character. Single crystals of $LaBr_2$ and La_2Br_5 were prepared by reduction of $LaBr_3$ with Li in sealed Ta containers (Krämer et al. 1989). The $LaBr_2$ structure is composed of slabs of $LaBr_2$ in which the La atoms are in trigonal prismatic coordination. The La–Br distance of 3.07 Å suggests the presence of La^{3+} cations. Although octahedrally coordinated Li^+ interstitial ions were not located in the structural analysis, their presence cannot be ruled out definitively. Meyer (1991) also suggests that $PrCl_2$ is probably metallic. The CdI_2-type scandium iodide, $Sc_{0.93}I_2$, synthesized by reaction of liquid or gaseous ScI_3 with excess Sc metal at 550–870°C (McCollum et al. 1990) is also metallic. This is the only intermediate phase in the Sc–ScI_3 system; it decomposes at 892°C.

The second category of metallic halides, R_xRX_3, is typified by $PrCl_{2.33}$ (Meyer et al. 1989a), better designated $Pr_{0.29}PrCl_3$. This compound was synthesized by reduction of the trichloride with either elemental praseodymium or with lithium. The UCl_3-type structure of $PrCl_3$ is essentially retained with additional praseodymium atoms occupying octahedral interstices. X-ray powder data gave no evidence of a composition range for this reduced chloride. The compound is paramagnetic, consistent with Pr^{3+} ions. When Na was used as reductant, a non-metallic UCl_3-type $Na_{0.5}PrCl_3$ phase resulted. Meyer et al. (1989a) emphasize the structural differences between Pr_3Cl_7 ($PrCl_{2.33}$) and the fluorite-related R_6X_{37} cuboctahedron Nd_3Cl_7 ($NdCl_{2.31}$) (see page 397) structures. The cuboctahedron is ordinarily found when one of the elements assumes the divalent oxidation state; praseodymium remains trivalent.

The third category of metallic halides, R_2X_5, is typified by Pr_2Br_5, the existence of which was long-known from phase studies. Schleid and Meyer (1987a) synthesized Pr_2Br_5 through reaction of $PrBr_3$ with Li in sealed Ta containers and determined it to be isostructural with Pr_2I_5. On the basis of Pr–Br distances, they point out that the Pr atoms are trivalent and the compound therefore is best formulated as $(Pr^{3+})_2(Br^-)_5(e^-)$. In contrast to Pr_2Br_5 which becomes ferromagnetic at about 25 K, isostructural La_2Br_5 shows no magnetic ordering. The structures of Pr_2X_5, X = Br, I, were determined by neutron diffraction from 5 K to room temperature and electrical conductivity was measured over a 160°C temperature range by impedance spectroscopy (Krämer et al. 1991a). A positive paramagnetic Curie temperature, $\Theta_p \approx 40$ K, is calculated for both compounds. The praseodymium ion is also trivalent in both compounds; antiferromagnetic-ordering temperatures of 50(1) K and 37(1) K were determined for X = Br and I, respectively. A second magnetic phase transition observed in the X = Br sample at $T \approx 25$ K is attributed to different temperature dependence of the magnetic moments of the two inequivalent praseodymium sites; the directions of the magnetic moments differ in the two ordering regions. Both compounds are semiconductors. The electronic

band structures of Pr_2X_5, X = Br, I, as determined by extended Hückel calculations, show two narrow low-lying d bands, half occupied by two electrons per Pr_4X_{10} unit cell (Meyer and Hoffmann 1991). The authors concluded that as a result of large metal separations in the structure, only weak d interactions were present between metal atoms and the compounds could be viewed as Mott insulators. The antiferromagnetic and paramagnetic properties observed for Pr_2X_5 below and above T_N were also considered typical of Mott insulators.

Compounds related to Pr_2X_5 include Ce_2Br_5 (Krämer and Meyer 1991), in which interatomic distances suggest the cerium ions to be trivalent, and the numerous light-lanthanide diiodides. Lattice parameters of a few of these compounds are listed in table 2 (RX_n-compounds, $n > 2$) and table 4 (RX_2-compounds).

4.2. *Dihalides*

Liu and Eick solvolytically decomposed numerous reduced lanthanide halides with tetrahydrofuran (THF) or pyridine. Both of these solvents form complexes with the trivalent, but not the divalent cation. They found that mixed Ba(II)–R(III) compounds of the general composition $Ba_9R_5X_{33}$, X = Cl, Br and R = La, Sm or Nd, would undergo solvolytic decomposition with loss of RX_3, leaving the BaX_2 salt in a metastable anti-Fe_2P-type modification (Liu and Eick 1989a). Anti-Fe_2P-type BaI_2 had been synthesized previously at elevated pressures and temperatures (Beck 1983), but neither the chloride nor bromide could be prepared by this technique. However, by dehydrating $BaCl_2{\cdot}2H_2O$ in the temperature range 38–370°C, Hasse and Brauer (1978) prepared a mixture of the fluorite- and anti-Fe_2P-type modifications. The volume per formula unit of their anti-Fe_2P modification was slightly larger than that of the normal form. In contrast, the average volume per formula unit of the anti-Fe_2P-type modification prepared by solvolytic decomposition is about 1% smaller than that of the normal $PbCl_2$-type form, indicative that it is indeed a "high-pressure" modification. This anti-Fe_2P-type modification transforms slowly and irreversibly to the normal $PbCl_2$ form at temperatures in excess of 300–350°C.

A mechanism for this solvolytic decomposition reaction has been postulated (Liu and Eick 1991). The reaction is topochemical with the structure of the product controlled by symmetry and size considerations. Since the R_nCl_{2n+1} vernier structures are closely related to the fluorite structure (Haschke 1979), synthesis of fluorite-type modifications upon leaching is not surprising. However, when the $M_{14}X_{33}$ phase is leached either the fluorite or the anti-Fe_2P-type structure is obtained. If M represents Sm or Eu, and X = Cl, the fluorite modification is obtained. If M = Ba and La or Nd and X = Br, the anti-Fe_2P-type modification is obtained. The $M_{14}X_{33}$ and the fluorite structures both contain layers of cations and anions perpendicular to the three-fold axes. The anti-Fe_2P structure contains both cations and anions in the layers. Thus conversion of the $M_{14}Cl_{33}$ structure to the fluorite modification requires only in-layer movement of the unsolvated M^{2+} ions in the planes perpendicular to the three-fold axis. On the other hand, conversion to the anti-Fe_2P-type structure requires both in-plane and out-of-plane movement of the M^{2+} and Br^- ions. The latter motion results with larger cations which cannot fit easily in the planes. Reaction behavior is

TABLE 4
Selected dihalide crystallographic data.

Halide	Type	Symmetry	a(Å)	b(Å)	c(Å)	Reference
$Sc_{0.93}I_2$	CdI_2	$P\bar{3}m1$	4.0851(3)	–	6.9824(7)	[1]
GdI_2	2H-MoS_2	$P6_3/mmc$	4.075(1)	–	15.060(5)	[2]
$LaBr_2$	2H_2-MoS_2	$P6_3/mmm$	4.0988(4)	–	13.900(1)	[3]
LaI_2	Ti_2Cu	I4/mmm	3.912(1)		13.937(1)	[4]
SmI_2-II	$PbCl_2$	Pnma	11.208(6)	8.886(5)	4.579(4)	[5]
EuI_2-II	$PbCl_2$	Pnma	11.184(3)	8.893(2)	4.575(1)	[5]
NdI_2-II	$TiCu_2$	I4/mmm	3.848(1)		13.953(3)	[4]
NdI_2-III	CaF_2	$Fm\bar{3}m$	~ 7.688			[4]
SmI_2	SrI_2-IV	Pnma	12.290(8)	4.902(3)	8.421(7)	[6]
EuI_2	SrI_2-IV	Pnma	12.272(2)	4.8852(8)	8.363(1)	[6]
DyI_2	$CdCl_2$	$R\bar{3}m$	4.62(2)		20.86(3)	[7]
$SmCl_2$	CaF_2	$Fm\bar{3}m$	6.9827(5)			[8]
$EuCl_2$	CaF_2	$Fm\bar{3}m$	6.961(1)			[8]
$TmBr_2$	SrI_2	Pbca	7.1023(4)	13.8139(7)	7.3809(7)	[9]
NdClBr	$PbCl_2$	Pnma	9.208(3)	7.899(3)	4.623(2)	[10]
NdClI	$PbCl_2$	Pnma	9.468(2)	8.229(5)	4.772(2)	[10]
NdBrI	$PbCl_2$	Pnma	9.751(9)	8.432(7)	4.891(7)	[10]
EuBrI	$PbCl_2$	Pnma	9.824(2)	8.414(2)	4.856(1)	[11]
EuClI	$PbCl_2$	Pnma	9.395(3)	8.185(2)	4.691(2)	[11]
$KTmBr_3$	$GdFeO_3$	Pbnm	7.6069(4)	8.0668(4)	11.0542(6)	[9]
$KYbBr_3$	$GdFeO_3$	Pbnm	7.5906(4)	8.0440(4)	11.0317(6)	[9]
$RbTmBr_3$	$GdFeO_3$	Pbnm	7.8214(4)	8.0786(4)	11.2834(5)	[9]
$RbYbBr_3$	$GdFeO_3$	Pbnm	7.7995(4)	8.0512(4)	11.2551(5)	[9]
$CsTmBr_3$	$NaNbO_3$-II	P4/mbm	8.0817(4)		5.7452(3)	[9]
$CsYbBr_3$	$CaTiO_3$	$Pm\bar{3}m$	5.7165(3)			[9]
$RbTmI_3$	$GdFeO_3$	Pbnm	8.4768(6)	8.6198(7)	12.0798(9)	[9]
$RbYbI_3$	$GdFeO_3$	Pbnm	8.4729(7)	8.6100(8)	12.0670(9)	[9]
$CsTmI_3$	$GdFeO_3$	Pbnm	8.5724(6)	8.6854(8)	12.3342(9)	[9]
$CsYbI_3$	$GdFeO_3$	Pbnm	8.5806(6)	8.6714(5)	12.3282(8)	[9]
Rb_4YbI_6	K_4CdCl_6	$R\bar{3}c$	14.139		17.513	[9]

[1] McCollum et al. (1990).
[2] Bärnighausen (1984).
[3] Krämer et al. (1989).
[4] Beck and Schuster (1992).
[5] Beck (1979).
[6] Liu (1990).
[7] Morss and Spence (1992).
[8] Liu and Eick (1988).
[9] Schilling et al. (1922).
[10] Löchner (1988a).
[11] Hodorowicz et al. (1984).

consistent with the proposed mechanism. Reactions which yield the fluorite modification occur rapidly while those which produce the anti-Fe_2P modification occur slowly, consistent with the additional atomic rearrangement required.

The fluorite modification of RCl_2, R = Sm, Eu, were also synthesized by solvolytic decomposition of reduced lanthanide halide phases with THF (Liu and Eick 1988). This modification, which had previously been reported stable only at elevated temperatures, resulted when either the vernier-type R_nCl_{2n+1}, $n = 4-6$, or $R_{14}Cl_{33}$ cluster-type compound was leached. This fluorite modification has a lower density than the normal modification and transforms slowly and irreversibly to the normal modification when

heated in excess of $\sim 400°C$. Efforts to extend this work to $NdCl_2$ were unsuccessful. The mixed-valent $NdCl_{2.30}$ prepared by reduction of $NdCl_3$ with elemental Nd could not be decomposed by THF, presumably because of the presence of oxide impurities. Nor could an $YbCl_2$ compound be synthesized. Every intermediate-valent ytterbium chloride compound contained oxide, and consistent with the neodymium specimens, oxide-containing samples could not be decomposed by THF.

Beck and Schuster (1992) synthesized NdI_2 from NdI_3 and Nd and heated it at 400–500°C under pressures of 2–4 GPa. The structure of the high-pressure modification, which was determined by Rietveld refinement of X-ray powder diffraction data, is designated NdI_2-II and remained stable upon quenching. With NaF as an internal standard, high-pressure lattice parameters were determined by in situ X-ray measurements as a function of pressure. The pressure–temperature phase diagram for NdI_2 shows three modifications: $SrBr_2$-type at low temperatures ($< 50°C$) and all pressures examined; Ti_2Cu-type at $T > 150°C$ (pressure ≈ 1.5 GPa); and (probably) a CaF_2-type, designated NdI_2-III, at $T \sim 50°C$ and pressure ~ 4GPa. NdI_2-II is metallic; NdI_2-III is postulated to be semiconducting. Trends in the p–T phase diagram are rationalized on the basis of the band structures of the various modifications. A mechanism for the transformation is postulated.

Schilling et al. (1992) present lattice parameters for the dihalides $TmBr_2$, $YbBr_2$ (in both α-PbO_2- and SrI_2-type structures), TmI_2, and YbI_2. They obtained the dihalides by metallothermic reduction of the RX_3 salts, X = Br or I, with Li and Na. Liu (1990) synthesized a previously undescribed modification of MI_2, M = Sr, Sm, and Eu, designated the SrI_2-IV-type structure in accordance with the notation of Beck (1979), by dehydrating $MI_2 \cdot H_2O$ at 120°C in a high vacuum. The structure of this modification is related closely to that of the monohydrate and was solved by the Rietveld procedure from X-ray diffraction data (Liu and Eick 1989b). In this structure the oxygen coordination site remains vacant and iodide atoms relax slightly, so the modification is less dense than the normal diiodide. The SrI_2-I-type SmI_2 phase reported by Li and Wang (1985) upon dehydration of $SmI_2 \cdot H_2O$ or $SmI_2 \cdot 0.5H_2O$ at 170–240°C in a high vacuum is no doubt this SrI_2-IV-type structure.

4.3. *Mixed-dihalide systems*

Numerous lanthanide mixed dihalide systems have been characterized by fusing appropriate mixtures and examining the reaction product(s) by X-ray diffraction techniques. These systems are illustrated schematically in table 5. Recent comparable studies of actinide systems could not be found. Non-isomorphous parent phases usually produce either eutectic structures or two solid-solution regions with one or more different structure-type phase also present between these solid-solution regions (Davies and Navrotsky 1983). The expected behavior was observed in the majority of the systems. Löchner (1988a) characterized the $NdCl_2$–$NdBr_2$, $NdCl_2$–NdI_2, and $NdBr_2$–NdI_2 systems. The chloride and bromide compounds crystallize with $PbCl_2$-type structures while the iodide crystallizes in the $SrBr_2$-type structure. The expected continuous solid solution and solid-solution regions separated by a two-phase region, respectively, were observed. Anion ordering was observed in the chloride–bromide

TABLE 5

Structure types present in $Ln(X, X')_2$ systems. The "2" indicates a two-phase region. The anion compositions at which two-phase regions begin and terminate are listed beneath the structure types.

Cation (M)	MCl_2–MBr_2 system MCl_xBr_{2-x}	MCl_2–MI_2 system MCl_xI_{2-x}	MBr_2–MI_2 system MBr_xI_{2-x}	Reference
Nd	$PbCl_2$-type solid solution Anions ordered	$PbCl_2$, 2, $SrBr_2$ $x = 0.27, 0.22$	$PbCl_2$, 2, $SrBr_2$ $x = 0.20, 0.15$	Löchner (1988a)
Eu	UCl_3, 2, $PbCl_2$ $x = 0.15, 0.30$	$PbCl_2$, 2, $PbCl_2$, 2, *m*-EuI_2 $x = 1.9, 1.0, 1.0, \sim 0.0$	$SrBr_2$, 2, $PbCl_2$, 2, $EuBr_{0.4}I_{0.6}$, 2, SrI_2 $x = 1.8, 1.6, 0.7, 0.5, 0.1$	Hodorowicz et al. (1983a) Hodorowicz et al. (1984)
Yb	SrI_2-type solid solution	SrI_2, multiple (polytypes), CdI_2 $x = 0.2, 1.7$	Not studied	Voos-Esquivel and Eick (1987) Lasocha et al. (1988)
Ca/Yb		$CaCl_2$ and α-PbO_2, multiple (polytype), CdI_2 x values not meaningful		

system. Löchner noted that fluoride-containing systems could not be synthesized. Hodorowicz et al. (1983c) examined the layered PbFCl-type compounds, $Ca_{0.5}Sr_{0.5}$-FCl, $Ca_{0.5}Yb_{0.5}FCl$, and $Sr_{0.5}Eu_{0.5}FBr$, in search of cation ordering; none was found. It appears that a completely random solid solution of the cations can be made as long as the cation size limits fall within the range allowed for the PbFCl-type structure and the ion sizes are reasonably close to each other.

In contrast to the extended solid-solution regions observed in the neodymium mixed halide systems, the $EuCl_xI_{2-x}$ system shows minimal solid solution while that of $EuBr_xI_{2-x}$ shows multiple phases (Hodorowicz et al. 1983a, 1984). The $YbCl_2$–$YbBr_2$ system, as expected because of a common SrI_2-type structure, forms a continuous solid solution (Voos-Esquivel and Eick 1987). However, the $YbCl_xI_{2-x}$ system is much more complicated with polytypism prevalent (Lasocha et al. 1988). Over the region 15 to 80 mol% $YbBr_2$ a mixed anion 6R-polytype (space group, $R\bar{3}m$) and an iodide-saturated $YbCl_2$ phase coexisted. In addition, over the ~15–45 mol% bromide region a CdI_2-type phase of the composition $YbCl_{0.3}I_{1.7}$ could be identified. Although polytypism might be expected for the CdI_2-type structure common to YbI_2, the phases formed could not have been anticipated. Substitution of like-sized and comparably coordinating calcium for ytterbium (Lasocha et al. 1989) demonstrated that the complicated behavior of this system is related to the cation size and is not unique to ytterbium; this mixed cation/anion system exhibited, with increasing YbI_2 content, coexisting $CaCl_2$ and α-PbO_2-type phases, then coexisting $CaCl_2$-type, 6R-polytype, and unknown structure type phases, the latter with the approximate composition $Ca_3YbCl_6I_2$, then 6R-polytype and CdI_2-type YbI_2, and finally, only a solid solution of the YbI_2-structure. However, unlike the $CaCl_2$–YbI_2 system, that of $CaCl_2$–$YbCl_2$ shows two solid-solution regions: the first spans 0 to ~15 and the second ~55–100 mol% $YbCl_2$ (Lasocha et al. 1990).

Since the ionic radii of Ca(II) and Sr(II) are similar to those of Yb(II) and Eu(II), respectively, numerous mixed halides involving these alkaline-earth elements have also been examined. Upon addition of $EuCl_2$ to $SrCl_2$ a cubic solid-solution region prevailed to 50 mol% $EuCl_2$. A two-phase region separated this from the $PbCl_2$-type $EuCl_2$ (Olejak-Chodan et al. 1987b). This limited solubility is readily understood when the lattice parameter of the 50 mol% mixture, $a = 6.977(3)$ Å, is compared to the $a = 6.961(1)$ Å value reported for the fluorite-type metastable modification of $EuCl_2$ (see table 4).

4.3.1. *Hydride-halide systems*

Although lanthanide and actinide hydride-halides have long been known (Struss and Corbett 1978), they recently again became an active area of research. Hydride halides, $RX_2(H, D)_n$ were synthesized directly from RX_2 or from RX_2 and RH_n welded in Ta ampoules and heated under defined pressures of hydrogen (Michaelis et al. 1992a). Compounds that form under one atmosphere hydrogen pressure include: $CeBr_2H_{0.87}$, $CeI_2H_{0.90}$, $CeI_2D_{0.96}$, $GdI_2H_{0.97}$; all could be hydrogenated to $RX_2H_{1.00}$. $LaBr_2H_{0.90}$, upon dehydriding in dynamic vacuum, reverted to La and $LaBr_3$; GdI_2H_n, $0 < n < 1.0$, could be completely dehydrided to give GdI_2. The heavy atom structure in these RX_2H_n compounds is related to those found in MoS_2 and NbS_2 (Michaelis et al.

1992b). The hydrogen atoms as determined by neutron diffraction are located in positions that center the anionic prisms and the cationic triangles. Michaelis et al. (1992c) characterized GdI_2H_n and CeI_2H_n ($n \leq 1$) by numerous procedures: IR, diffuse reflectance spectra, magnetic susceptibility, electrical resistivity, and photoelectron spectroscopy. The Gd-containing samples are either insulating or semiconducting; compounds with $n = 1$ are colorless while those with $n < 0.9$ show metallic lustre. When $n \neq 1$, the bands ~ 1 eV below the Fermi edge are calculated to be populated. With decreasing H content they broaden and the density of states increases. CeI_2H_n exhibits a metal–semiconductor transition for $n \approx 0.33$.

Mattausch et al. (1992a) pointed out that YCl and YBr, previously described as "monohalides" (Mattausch et al. 1980), are in reality hydride halides YXH_n, X = Cl, Br, in which $0.7 \leq n \leq 1.0$. These hydride halides can be further hydrogenated in a hydrogen atmosphere to give colorless YXH_2. Although the lattice parameters changed only slightly as n in YXH_n was varied, the structure type changed from that of ZrBr at lower hydrogen concentrations to that of ZrCl at higher concentrations. Interconversion and loss of hydrogen upon heating were studied. Kremer et al. (1991) examined the origin of spin-glass behavior in $TbBrD_{0.7}$. In contrast to $TbBrD_{0.7}$, $TbBrD_{0.81}$ and $TbBrD_{0.88}$ undergo antiferromagnetic ordering, and $GdBrD_n$ undergoes antiferromagnetic ordering for all values of n. The authors attribute the different ordering behavior to random magnetic anisotropies that arise from the locally different crystal electric fields; Gd^{3+} has an S ground state while Tb^{3+} has a large L contribution to the total angular momentum, J.

4.3.2. *AX_n–MX_2 systems*

Schilling et al. (1992) synthesized perovskite-related ARX_3 structures, R = Tm and Yb, X = Br and I, through the metallothermic reduction of RX_3 with equimolar amounts of K, Rb, or Cs in Ta capsules (700–800°C, 7 d). They obtained $CsRI_3$, $RbRI_3$, and KRI_3 ($GdFeO_3$-type), $CsYbBr_3$ (cubic $CaTiO_3$-type), and $CsTmBr_3$ (tetragonal $NaNbO_3$-II-type) structures in addition to K_4CdCl_6-type Rb_4YbI_6. When Li or Na was the reductant, dihalide was the reaction product.

Köhler (1993) synthesized orange–red transparent single crystals of $SmAlF_5$ by heating 2:1:3 mixtures of SmF_3, Sm, and AlF_3 confined in niobium under Ar for 7–10 d at 750°C. The compound, which is isostructural with $BaTiF_5$, has linear chains of trans-corner sharing AlF_6 octahedra connected via corners to two additional AlF_6 octahedra. Isolated Al_2F_{10} bioctahedra are situated in a disordered arrangement between the chains.

4.4. *Cluster-stabilized reduced halides*

The bonding in Y_2Cl_3, and by analogy, in R_2Cl_3, R = Gd, Tb, was investigated by magic angle spinning NMR, electrical conductivity, and magnetic susceptibility measurements (Kremer et al. 1992). Y_2Cl_3 was confirmed to be a semiconductor with a band gap of 0.85(5) eV. The observed diamagnetic susceptibility confirmed that the excess valence electrons are involved in metal–metal bonding. The positive chemical shifts observed for the ^{89}Y NMR resonances are large and approach the magnitude of

typical Knight shift values detected for metallic compounds such as YH_2. Yee and Hughbanks (1992) developed a semi-localized description of the bonding in extended metal–metal-bonded systems. They used Y_2Cl_3 as the prototype compound and calculated its band structure.

Artelt et al. (1992) reduced RI_3, R = Er and Lu, with Cs in the presence of carbon in sealed Ta containers by the metallothermic technique and obtained as a by-product the quaternary electron-deficient cluster compounds: $Cs[Er_6C]I_{12}$ and $Cs_2Lu\ [Lu_6C]Cl_{18}$. The latter compound is isostructural with the zirconium hydride cluster compound, $Cs_2Zr[Zr_6H]Cl_{18}$ and contains $[Lu_6C]$ clusters edge-bridged by twelve chloride anions to form the $[Lu_6C]Cl_{12}$ units. Six additional chloride ions in the exo positions of the cluster provide octahedral coordination for the seventh Lu^{3+} cation; the Cs^+ ion occupies anti-cuboctahedral interstices within the chloride layers. The $[Er_6C]I_{12}$ unit of $Cs[Er_6C]I_{12}$ has a structural framework similar to that of $[Sc_6N]Cl_{12}$ in $Sc[Sc_6N]\ Cl_{12}$. Ruck and Simon (1992) produced in a reversible, topochemical reaction lanthanide carbide hydride halides, R_2XCH_n (R = Gd, Tb; X = Cl, Br, I; $n_{max} = 1$), by heating condensed cluster R_2XC compounds in hydrogen at 550°C. Upon addition of hydrogen the clusters change from the R_6X_{12}- to R_6X_8-type and the electrons gradually become localized in H-centered states giving rise to a metal–semiconductor transition. Artelt and Meyer (1993) also synthesized a quaternary reduced halide with isolated $[M_6(C_2)]$ clusters, $Cs_2[Pr_6(C_2)]I_{12}$, by heating at 850°C PrI_3, Cs, and C confined in Ta containers. The structure contains discrete Pr_6I_{12}-type clusters elongated to accommodate the C_2 units and connected via iodide ions. Internuclear C–C, M–C, and M–M distances in lanthanide clusters that contain C_2 units – layered clusters, chains, and those containing isolated double octahedra and isolated single octahedra are compared.

Reduced halide cluster compounds have also been characterized for thorium. Böttcher et al. (1991) synthesized and characterized extensively numerous thorium cluster compounds. In addition to those which contain a d-block transition element two, $Th_6Br_{15}H_7$ and $Th_6Br_{14}C$, contain only anions. Both compounds, whose structures are related closely to those of Nb_6F_{15} and Nb_6Cl_{14}, respectively, have $[Th_6Br_{12}]$ clusters with octahedral Th_6 cores and the H or C atom interstitial in the core. The structure of $Th_6Br_{15}D_7$ was determined by neutron diffraction. Neither compound is magnetic.

5. Higher halides

5.1. *MX_4 compounds*

Single-phase samples of actinide tetrafluorides, RF_4, R = U, Np, and Pu were synthesized, absorption spectra recorded at 298, ~77, and ~4 K in KBr pellets, the data interpreted, and a comparison of the computed energy levels made with published magnetic properties and heat-capacity measurements (Carnall et al. 1991). Gibson and Haire (1992) identified AmF_4 by mass spectrometry.

5.2. MX_n–$M'X_4$ systems

Gambino et al. (1989) determined the heat capacity of Na_2UBr_6 by differential scanning calorimetry over the temperature range 200–500°C. At elevated temperatures this compound undergoes a number of structural transitions that enhance ionic conductivity. A transition at 380°C which allows Na ions to move along the *z*-axis is reported to significantly increase the electrical conductivity. The structure of the related Na_2UI_6, also reported to be a fast-ion conductor, was determined by neutron diffraction (Małetka et al. 1992). It is closely related to that of Na_2UCl_6 (a', c'): $c = 3c'$; $a = a'/\sqrt{3}$, with I atoms in closely related positions, but with U atoms occupying empty holes in the Na atom planes.

Laligant et al. (1989) determined the crystal structure of long-known Li_3ThF_7 by X-ray ($T = 300$ K) and neutron ($T = 5$ K) powder diffraction. The structure, previously characterized as tetragonal and subsequently questioned, was found to be orthorhombic. The Li^+ ions are distributed randomly on three-fourths of the corresponding crystallographic sites and are arranged in a distorted octahedral coordination with the octahedra sharing edges to form layers which can be related to a defect NaCl-type structure. Thorium ions are in nine-fold coordination. El-Ghozzi et al. (1992) synthesized Li_4TbF_8 by heating LiF and TbF_3 or "Tb_4O_7" in F_2(g) and refined the orthorhombic structure by the X-ray Rietveld procedure. The compound Li_4TbF_8 is isostructural with Li_4UF_8; Tb ions are located in isolated, distorted Archimedean antiprisms that form in a three-dimensional network of octahedrally coordinated Li ions. Guillot et al. (1992) determined the magnetic properties of Li_2TbF_6, the only known ambient-pressure representative of the eight-coordinate high-pressure α-Li_2ZrF_6 structure, and confirmed the $4f^7$ configuration for Tb. Electronic structure and size relationships are presented to explain the absence of a corresponding eight-coordinate praseodymium compound.

The RF_3–TbF_4 system was examined for the majority of R. When RF_3–TbF_3 mixtures were fluorinated or $R_xTb_{1-x}F_3$ solid solutions and XeF_2 were heated in an autoclave, RF_3 and TbF_4 resulted (Brekhovskikh et al. 1989). If a mixture that contained the smaller lanthanides, R = Tb–Lu, Y, and Sc was heated at 400–450°C for an extended period of time, the compounds $R(TbF_5)_3$ which are isostructural with corresponding Zr and Hf analogues were formed. As would be expected, upon heating to a higher temperature (550–600°C), the tetravalent terbium oxidizes the fluoride ion to F_2(g), leaving the mixed-cation trifluoride, $R_{0.25}Tb_{0.75}F_3$. Gaweł (1987) examined the $LaCl_3$–UCl_4 system; the expected solid immiscibility with an eutectic near to 100 mol% UCl_4 was observed. Ouwerkerk (1985) discussed procedures needed to grow fluorite-type crystals of the solid-solutions AF_2–UF_4, A = Ca, Sr, Ba, and Pb, which contained minimal concentrations of U^{3+}.

The thermal decomposition of monoclinic (ZrF_4-type) CmF_4 and TbF_4 was characterized by a Knudsen cell–mass spectrometry technique (Gibson and Haire 1988b). Both compounds decompose to the trifluoride when heated in vacuum. Derived enthalpies of decomposition are: TbF_4, 23.7 ± 3.0 kcal mol^{-1}; CmF_4, 26.3 ± 2.0 kcal mol^{-1}. CmF_4 decomposes between 330 and 430°C; it is only slightly more stable to decomposition than is TbF_4.

5.3. AcX_6 systems

Room-temperature synthesis of RF_6, R = U, Np, and Pu, through reaction with KrF_2 and O_2F_2 or O_2F_2/HF has been reported (Asprey et al. 1986, and references therein). Treatment of AmO_2 with KrF_2 did not yield AmF_6 under the conditions studied. On the other hand, Fargeas et al. (1986), using a thermochromatographic technique in which the reaction products were separated immediately after formation in a tube in which a $\sim 950°C$ thermal gradient (-150–$800°C$) was maintained and analysis effected by radiochemical procedures, reported synthesis of trace amounts of both AmF_6 (0.04%) and CmF_6 (0.02%) when the fluorinating agent was a mixture of gaseous BF_3 and F_2. These workers also report the synthesis of numerous other high-valent oxidefluorides: NpO_3F, NpF_7, PuO_3F, AmF_5, $CmOF_3$, and EsF_4, but quantitative data relative to the yield were not presented. However, the work of Gibson and Haire (1992) casts doubt on the existence of both AmF_6 and CmF_6. Gibson and Haire treated the actinide elements U–Am with F_2, ClF_3, BF_3, and/or O_2 gases in platinum Knudsen cells and monitored the effusate by quadrupole mass spectrometry. They found no evidence of AmF_6. They report additional attempts to synthesize AmF_6. AmF_4 confined in a nickel reactor was exposed to F_2(g) at a pressure of 0.16 MPa and at temperatures up to 800°C in a system arranged such that volatiles were transported to a cold trap. In addition, a LiF–NaF–BeF_2 molten salt that contained $\sim$ 2wt.% AmF_4 was heated in a platinum Knudsen cell in the mass spectrometer at 525°C. In neither case was the elusive AmF_6 observed.

Absorption spectra of polycrystalline AUF_6, A = Li, α-Na, and Cs, were recorded at $T \leq 25°C$ (Hecht et al. 1986); the compounds have a common six-fold U–F coordination that approaches octahedral site symmetry for $LiUF_6$, but exhibits increasing trigonal distortion as the size of A increases.

Henche et al. (1993) synthesized a mixed R–U(VI)–oxidechloride, $R_3UO_6Cl_3$, R = La, Pr, and Nd, by heating [5–9 d, 800°C (1000°C for R = La)] stoichiometric quantities of ROCl, $R_2O_3(Pr_6O_{11})$, and U_3O_8 confined in quartz ampoules under a pressure of Cl_2(g). Single crystals were grown by chemical vapor transport with Cl_2(g) as the transport agent and the structure was determined. The uranium atom is coordinated in a trigonal prismatic arrangement by six oxygen atoms; the lanthanide is ten-coordinated by six oxygen and four chlorine atoms. The mixed metal system, $La_3(U_xW_{1-x})O_6Cl_3$, $0 \leq x \leq 1$, were also synthesized and the hexagonal lattice parameters determined.

References

Aasland, S., T. Grande and S. Julsrud, 1992, J. Non-Cryst. Solids **140**, 69–72.

Aliev, A.E., and L.N. Fershtat, 1984, Izv. Akad. Nauk USSR, Ser. Fiz.-Mat. Nauk (2), 76; Chem. Abstr. 101 : 98692d.

Artelt, H.M., and G. Meyer, 1993, Z. Anorg. Allg. Chem. **C19**, 1–6.

Artelt, H.M., T. Schleid and G. Meyer, 1992, Z. Anorg. Allg. Chem. **618**, 18–28.

Asprey, L.B., P.G. Eller and S.A. Kinkead, 1986, Inorg. Chem. **25**, 670–672.

Aurivillius, B., 1984, Chem. Scr. **24**, 125–129.

Bachmann, R., 1987, Ph.D. Dissertation (Universität Karlsruhe, Karlsruhe, Germany).

Ball, J., C.M. Jenden, S.J. Lyle and W.A. Westall, 1983, J. Less-Common Met. **95**, 161–170.

Baney, R.H., D.F. Bergstrom and B.H. Justice, 1992, Chem. Mater. 4, 984–987.

Bärnighausen, H., 1976, Mixed-valence rare-earth halides and their unusual crystal structures, in: Proc. Twelfth Rare Earth Research Conference, Vol. 1, ed. C. Lundin (Vail).

Bärnighausen, H., 1984, referred to by A. Kasten, P.H. Müller and M. Schienle, Solid State Commun. **51**, 919–922.

Batsanov, S.S., L.I. Kopaneva and G.D. Dorogova, 1983, Russ. J. Inorg. Chem. **28**(8), 1222, 1223.

Beck, H.P., 1979, Z. Anorg. Allg. Chem. **459**, 81–86.

Beck, H.P., 1983, J. Solid State Chem. **47**, 328–332.

Beck, H.P., and E. Gladrow, 1979, Z. Anorg. Allg. Chem. **453**, 79–92.

Beck, H.P., and E. Gladrow, 1983a, Z. Anorg. Allg. Chem. **498**, 75–84.

Beck, H.P., and E. Gladrow, 1983b, Z. Anorg. Allg. Chem. **502**, 178–184.

Beck, H.P., and M. Schuster, 1992, J. Solid State Chem. **100**, 301–306.

Beck, H.P., and C. Strobel, 1986, Z. Anorg. Allg. Chem. **535**, 229–239.

Beda, S., J.M. Haschke, L.S. Quayle and H.A. Eick, 1980, Mixed halide phases in the chloride–iodide systems of lanthanum and gadolinium, in: The Rare Earths in Modern Science and Technology, Vol. 2, eds G.J. McCarthy, J.J. Rhyne and H.B. Silber (Plenum Press, New York) pp. 51, 52.

Benner, G., and R. Hoppe, 1992, Eur. J. Solid State & Inorg. Chem. **29**, 659–677.

Bertaut, E.F., Y. Le Fur and S. Aléonard, 1989, Z. Kristallogr. **187**, 279–304.

Bevan, D.J.M., J. Strähle and O. Greis, 1982, J. Solid State Chem. **44**, 75–81.

Bevan, D.J.M., I.E. Grey and B.T.M. Willis, 1986, J. Solid State Chem. **61**, 1–7.

Bevan, D.J.M., S.E. Ness and M.R. Taylor, 1988a, Eur. J. Solid State & Inorg. Chem. **25**, 527–534.

Bevan, D.J.M., M.J. McCall, S.E. Ness and M.R. Taylor, 1988b, Eur. J. Solid State & Inorg. Chem. **25**, 517–526.

Blachnik, R., and E. Enninga, 1983, Z. Anorg. Allg. Chem. **503**, 133–140.

Blachnik, R., and E. Enninga, 1984, Thermochim. Acta **78**, 427–430.

Blachnik, R., G. Alberts and E. Enninga, 1985, Z. Anorg. Allg. Chem. **522**, 207–216.

Blasse, G., L.H. Brixner and G. Hyatt, 1989, Chem. Phys. Lett. **164**, 617–620.

Böttcher, F., A. Simon, R.K. Kremer, H. Buchkremer-Hermanns and J.K. Cockcroft, 1991, Z. Anorg. Allg. Chem. **598/599**, 25–44.

Brekhovskikh, M.N., A.I. Popov, Y.M. Kiselev, A.L. Il'inskii and V.A. Fedorov, 1989, Russ. J. Inorg. Chem. **34**(4), 573, 574.

Brixner, L.H., M.K. Crawford, G. Hyatt, W.T. Carnall and G. Blasse, 1991, J. Electrochem. Soc. **138**, 313–317.

Brown, D., 1968, Halides of the Lanthanides and Actinides (Wiley, New York).

Brown, D., L. Hall, C. Hurtgen and P.T. Mosley, 1977a, J. Inorg. & Nucl. Chem. **39**, 1466–1468.

Brown, D., C. Hurtgen and J. Fuger, 1977b, Rev. Chim. Miner. **14**, 189–198.

Burgess, J., and J. Kijowski, 1981, Adv. Inorg. Chem. Radiochem. **24**, 57–114.

Carnall, W.T., G.K. Liu, C.W. Williams and M.F. Reid, 1991, J. Chem. Phys. **95**, 7194–7203.

Champarnaud-Mesjard, J.C., and B. Frit, 1992, Eur. J. Solid State & Inorg. Chem. **29**, 161–170.

Chudnovskaya, G.P., Y.A. Barbanel' and Y.I. Gavrish, 1987, Dokl. Phys. Chem. **296**(4–6), 1041–1043.

Cockcroft, J.K., R.K. Kremer, Hj. Mattausch, N.P. Raju and A. Simon, 1992, J. Alloys & Compounds **183**, 241–251.

Corbett, J.D., 1991, Conproportionation routes to reduced lanthanide halides, in: Synthesis of Lanthanide and Actinide Compounds, eds G. Meyer and L.R. Morss (Kluwer, Dordrecht) pp. 159–174.

Corbett, J.D., J.D. Smith and E. Garcia, 1986, J. Less-Common Met. **115**, 343–355.

Corbett, J.D., D.S. Dudis, J.E. Ford, S-J. Hwu, G. Meyer and S. Wijeyesekera, 1987, J. Less-Common Met. **127**, 1–6.

CRYSTDAT Scientific Numeric Database Service, 1987, The National Research Council of Canada, Ottawa, Canada K1A OS2.

Czjzek, M., H. Fuess and I. Pabst, 1992, Z. Anorg. Allg. Chem. **617**, 105–109.

Davies, P.K., and A. Navrotsky, 1983, J. Solid State Chem. **73**, 259–267.

Dönni, A., P. Fischer, A. Furrer, J.K. Cockcroft and H.U. Güdel, 1991, J. Solid State Chem. **93**, 119–127.

Drożdżyński, J., 1985, Inorg. Chim. Acta **109**, 79–81.

Drożdżyński, J., 1986, Inorg. Chim. Acta **115**, 219–222.

Eitel, M., 1985, Doctoral Dissertation (Universität Karlsruhe).

El-Ghozzi, M., D. Avignant and J.C. Cousseins, 1992, Eur. J. Solid State & Inorg. Chem. **29**, 981–992.

El Omari, M., J.M. Reau, J. Senegas, J.P. Laval and B. Frit, 1991, J. Solid State Chem. **92**, 312–319.

Fargeas, M., B. Fremont-Lamouranne, Y. Legoux and J. Merini, 1986, J. Less-Common Met. **121**, 439–444.

Freestone, N.P., and J.H. Holloway, 1991, in: Synthesis of Lanthanide and Actinide Compounds, eds G. Meyer and L.R. Morss (Kluwer, Dordrecht) pp. 67–135.

Fuger, J., V.B. Parker, W.N. Hubbard and F.L. Oetting, 1983, in: The Actinide Halides, The Chemical Thermodynamics of Actinide Elements and Compounds, Vol. 8, eds V. Medvedev, M.H. Rand and E.F. Westrum Jr (International Atomic Energy Agency, Vienna).

Fuger, J., R.G. Haire, W.R. Wilmarth and J.R. Peterson, 1990, J. Less-Common Met. **158**, 99–104.

Gambino, M., P. Gaume and W. Szczepaniak, 1989, Ber. Bunsenges. Phys. Chem. **93**, 555–559.

Garcia, E., J.D. Corbett, J.E. Ford and W.J. Vary, 1985, Inorg. Chem. **24**, 494-498.

Garton, G., and P.J. Walker, 1982, Mater. Res. Bull. **17**, 1227–1234.

Gawel, W., 1987, Pol. J. Chem. **61**, 69–72.

Gibson, J.K., and R.G. Haire, 1988a, Thermochim. Acta **130**, 55–65.

Gibson, J.K., and R.G. Haire, 1988b, J. Solid State Chem. **73**, 524–530.

Gibson, J.K., and R.G. Haire, 1992, J. Alloys & Compounds **181**, 23–32.

Gong, Z., P. Chen, Z. Guo, J. Ma and Y. Chen, 1983, Huaxue Xuebao **41**(5), 391–396; Chem. Abstr. 99:186366w.

Grannec, J., P. Lagassie and L. Fournes, 1989, Mater. Lett. **9**, 33–37.

Gregson, D., C.R.A. Catlow, A.V. Chadwick, G.H. Lander, A.N. Cormack and B.E.F. Fender, 1983, Acta Crystallogr. B **39**, 687–691.

Greis, O., and M.S.R. Cader, 1985, Thermochim. Acta **87**, 145–150.

Greis, O., and M.S.R. Cader, 1986, J. Less-Common Met. **118**, 21–29.

Greis, O., and J.M. Haschke, 1982, Rare earth fluorides, in: Handbook on the Physics and Chemistry of Rare Earths, Vol. 5, eds K.A. Gschneidner Jr and L. Eyring (North-Holland, Amsterdam) pp. 387–460.

Guillot, M., M. El-Ghozzi, D. Avignant and G. Ferey, 1992, J. Solid State Chem. **97**, 400–404.

Gunsilius, H., W. Urland and R. Kremer, 1987, Z. Anorg. Allg. Chem. **550**, 35–40.

Gunsilius, H., H. Borrmann, A. Simon and W. Urland, 1988, Z. Naturforsch. **43b**, 1025–1028.

Haeuseler, H., and M. Jung, 1986, Mater. Res. Bull. **21**, 1291–1294.

Haire, R.G., J.P. Young, J.R. Peterson and R.L. Fellows, 1978, Absorption spectrophotometric and X-ray diffraction evidence for mixed-valence compounds in anhydrous halides of lanthanide–actinide mixtures, in: The Rare Earths in Modern Science and Technology, eds G.J. McCarthy and J.J. Rhyne (Plenum Press, New York) pp. 501–506.

Haire, R.G., U. Benedict, J.P. Young, J.R. Peterson and G.M. Begun, 1985, J. Phys. C **18**, 4595–4601.

Hake, D., and W. Urland, 1990, Z. Anorg. Allg. Chem. **586**, 99–105.

Hake, D., and W. Urland, 1992, Z. Anorg. Allg. Chem. **613**, 45–48.

Haschke, J.M., 1979, Halides, in: Handbook on the Physics and Chemistry of Rare Earths, Vol. 4, eds K.A. Gschneidner Jr and L. Eyring (North-Holland, Amsterdam) pp. 89–151.

Hasse, A., and G. Brauer, 1978, Z. Anorg. Allg. Chem. **441**, 181–195.

Hecht, H.G., J.G. Malm, J. Foropoulos and W.T. Carnall, 1986, J. Chem. Phys. **84**, 3653–3662.

Heiniö, O., M. Leskelä and L. Niinistö, 1980, Acta Chem. Scand., Ser. A **34**, 207–211.

Henche, G., K. Fiedler and R. Gruehn, 1993, Z. Anorg. Allg. Chem. **619**, 77–87.

Hodorowicz, E.K., S.A. Hodorowicz and H.A. Eick, 1983a, J. Solid State Chem. **49**, 362–367.

Hodorowicz, E.K., S.A. Hodorowicz and H.A. Eick, 1984, J. Solid State Chem. **52**, 156–162.

Hodorowicz, S.A., E.K. Hodorowicz and H.A. Eick, 1983b, J. Solid State Chem. **50**, 180–188.

Hodorowicz, S.A., E.K. Hodorowicz and H.A. Eick, 1983c, J. Less-Common Met. **93**, 415–418.

Hodorowicz, S.A., M. Olejak-Chodan and H.A. Eick, 1987, J. Solid State Chem. **71**, 205–213.

Hölsä, J., and L. Niinistö, 1980, Thermochim. Acta **37**, 155–160.

Igarashi, K., and J. Mochinaga, 1987, Z. Naturforsch. **42a**, 777–778.

Karbowiak, M., and J. Drożdżyński, 1990, J.

Less-Common Met. **163**, 159–164.
Karbowiak, M., and J. Drożdżyński, 1993, J. Alloys & Compounds **190**, 291–294.
Karraker, D.G., 1987, Inorg. Chem. **26**, 3816–3818.
Katz, J.J., G.T. Seaborg and L.R. Morss, eds, 1986, The Chemistry of the Actinide Elements, 2nd Ed. (Chapman and Hall, London).
Khaidukov, N.M., P.P. Fedorov, L.N. Dem'yanets, I.P. Zibrov and V.A. Malyusov, 1990, Russ. J. Inorg. Chem. (Engl. Transl.) **35**(3), 383–384.
Khaidukov, N.M., P.P. Fedorov and N.A. Abramov, 1991, Inorg. Mater. (Engl. Transl.) **27**(12), 2243–2246.
Köhler, J., 1993, Z. Anorg. Allg. Chem. **619**, 181–188.
Köhler, J., and B.G. Müller, 1991, Z. Anorg. Allg. Chem. **606**, 169–176.
Korczak, W., and P. Mikolajczak, 1983, J. Cryst. Growth **61**, 601–605.
Krämer, K., and G. Meyer, 1991, Eur. J. Solid State & Inorg. Chem. **28**, 523–528.
Krämer, K., T. Schleid, S. Schulze, W. Urland and G. Meyer, 1989, Z. Anorg. Allg. Chem. **575**, 61–70.
Krämer, K., G. Meyer, P. Fischer, A.W. Hewat and H.U. Güdel, 1991a, J. Solid State Chem. **95**, 1–13.
Krämer, K., G. Meyer, M. Karbowiak and J. Drożdżyński, 1991b, J. Less-Common Met. **175**, 347–352.
Kremer, R.K., W. Bauhofer, H. Mattausch and A. Simon, 1991, Eur. J. Solid State & Inorg. Chem. **28**, 519–522.
Kremer, R.K., Hj. Mattausch, A. Simon, S. Steuernagel and M.E. Smith, 1992, J. Solid State Chem. **96**, 237–242.
Kwestroo, W., and H.A.M. Van Hal, 1976, J. Inorg. & Nucl. Chem. **38**, 1019–1022.
Laligant, Y., A. LeBail, D. Avignant, J.C. Cousseins and G. Ferey, 1989, J. Solid State Chem. **80**, 206–212.
Lasocha, A., W. Lasocha and H.A. Eick, 1989, J. Solid State Chem. **80**, 222–226.
Lasocha, W., C.A. Voos-Esquivel, S.A. Hodorowicz, B.Y. Kim and H.A. Eick, 1988, J. Solid State Chem. **74**, 67–73.
Lasocha, W., A. Lasocha and H.A. Eick, 1990, J. Solid State Chem. **87**, 64–68.
Laval, J.P., A. Mikou, B. Frit and J. Pannetier, 1986, J. Solid State Chem. **61**, 359–368.
Laval, J.P., A. Mikou, B. Frit, G. Roult and J. Pannetier, 1987, Rev. Chim. Miner. **24**, 165–181.
Laval, J.P., A. Abaouz, B. Frit, G. Roult and W.T.A. Harrison, 1988a, Eur. J. Solid State & Inorg. Chem. **25**, 425–434.
Laval, J.P., A. Mikou, B. Frit and G. Roult, 1988b, Solid State Ionics **28–30**, 1300–1304.
Laval, J.P., A. Abaouz and B. Frit, 1989, J. Solid State Chem. **81**, 271–277.
Laval, J.P., A. Abaouz, B. Frit and A. Le Bail, 1990, J. Solid State Chem. **85**, 133–143.
Le Fur, Y., S. Aléonard, M.F. Gorius and M.T. Roux, 1988a, Z. Kristallogr. **182**, 281–290.
Le Fur, Y., S. Aléonard, M. Perroux, M.F. Gorius and M.T. Roux, 1988b, J. Solid State Chem. **72**, 173–180.
Le Fur, Y., N.M. Khaidukov and S. Aléonard, 1992a, Acta Crystallogr. C **48**, 978–982.
Le Fur, Y., N.M. Khaidukov and S. Aléonard, 1992b, Acta Crystallogr. C **48**, 2062–2064.
Lechtenböhmer, C., and O. Greis, 1978, J. Less-Common Met. **61**, 177–187.
Lerch, K., W. Laqua and G. Meyer, 1990, Z. Anorg. Allg. Chem. **582**, 143–150.
Li, X., and S-H. Wang, 1985, Chem. Abstr. **104**, 178089q (1986).
Liu, G, 1990, Ph.D. Dissertation (Michigan State University, East Lansing, MI 48824).
Liu, G., and H.A. Eick, 1988, Inorg. Chem. **27**, 2161–2163.
Liu, G., and H.A. Eick, 1989a, J. Less-Common Met. **149**, 47–53.
Liu, G., and H.A. Eick, 1989b, J. Less-Common Met. **156**, 237–245.
Liu, G., and H.A. Eick, 1991, J. Solid State Chem. **95**, 99–110.
Löchner, U., 1988a, in: 18th Rare Earth Research Conference, chairman L. Delong, Lake Geneva, WI, September 12–16, Abstract P3.20.
Löchner, U., 1988b, in: 18th Rare Earth Research Conference, chairman L. Delong, Lake Geneva, WI, September 12–16, Abstract P3.21.
Löchner, U., 1988c, Z. Kristallogr. **182**, 172, 173.
Löchner, U., and R. Blachnik, 1988, Z. Kristallogr. **183**, 207–212.
Lüke, H., and H. Eick, 1982, Inorg. Chem. **21**, 965–968.
Lumpp, A., and H. Bärnighausen, 1988, Z. Kristallogr. **182**, 174–177.
Lyle, S.J., and W.A. Westall, 1985, J. Less-Common Met. **106**, 109–116.
Maletka, K., P. Fischer, A. Murasik and W. Szczepaniak, 1992, J. Appl. Crystallogr. **25**, 1–5.
Mattausch, Hj., J.B. Hendricks, R. Eger, J.D. Corbett and A. Simon, 1980, Inorg. Chem. **19**, 2128–2132.

Mattausch, Hj., R. Eger and A. Simon, 1991, Z. Anorg. Allg. Chem. **597**, 145–150.

Mattausch, Hj., R. Eger, J.D. Corbett and A. Simon, 1992a, Z. Anorg. Allg. Chem. **616**, 157–161.

Mattausch, Hj., R.K. Kremer, R. Eger and A. Simon, 1992b, Z. Anorg. Allg. Chem. **609**, 7–11.

Mattfeld, H., and G. Meyer, 1992, Z. Anorg. Allg. Chem. **618**, 13–17.

Maximov, B., and H. Schulz, 1985, Acta Crystallogr. B **41**, 88–91.

McCollum, B.C., D.S. Dudis, A. Lachgar and J.D. Corbett, 1990, Inorg. Chem. **29**, 2030–2032.

Menon, M.P., and J. James, 1989, J. Chem. Soc., Faraday Trans. I **85**, 2683–2694.

Mercier, N., and M. Leblanc, 1991, Eur. J. Solid State & Inorg. Chem. **28**, 727–735.

Metallinou, M.M., L. Nalbandian, G.N. Papatheodorou, W. Voigt and H.H. Emons, 1991, Inorg. Chem. **30**, 4260–4264.

Meyer, G., 1982, Prog. Solid State Chem. **14**, 141–219.

Meyer, G., 1983, J. Less-Common Met. **93**, 371–380.

Meyer, G., 1988, Chem. Rev. **88**, 93–108.

Meyer, G., 1991, Eur. J. Solid State & Inorg. Chem. **28**, 473–478.

Meyer, G., and P. Ax, 1982, Mater. Res. Bull. **17**, 1447–1455.

Meyer, G., and H.-J. Meyer, 1992, Chem. Mater. **4**, 1157–1168.

Meyer, G., and L.R. Morss, 1991, Synthesis of Lanthanide and Actinide Compounds (Kluwer, Dordrecht) pp. 55–185.

Meyer, G., and T. Schleid, 1987, Inorg. Chem. **26**, 217–218.

Meyer, G., and T. Schleid, 1991, Action of alkali metals on lanthanide(III) halides: an alternative to the conproportionation route to reduced lanthanide halides, in: Synthesis of Lanthanide and Actinide Compounds, eds G. Meyer and L.R. Morss (Kluwer, Dordrecht) pp. 175–186.

Meyer, G., J. Soose, A. Moritz, V. Vitt and Th. Holljes, 1985a, Z. Anorg. Allg. Chem. **521**, 161–172.

Meyer, G., T. Staffel, S. Dötsch and T. Schleid, 1985b, Inorg. Chem. **24**, 3505–3507.

Meyer, G., S. Dötsch and T. Staffel, 1987, J. Less-Common Met. **127**, 155–160.

Meyer, G., T. Schleid and K. Krämer, 1989a, J. Less-Common Met. **149**, 67–71.

Meyer, G., H.-J. Meyer, N.L. Jones and J.D. Corbett, 1989b, Inorg. Chem. **28**, 2635–2637.

Meyer, G., A. Lossin and T. Schleid, 1991, Eur. J. Solid State & Inorg. Chem. **28**, 529–534.

Meyer, H.-J., and R. Hoffmann, 1991, J. Solid State Chem. **95**, 14–20.

Michaelis, C., Hj. Mattausch and A. Simon, 1992a, Z. Anorg. Allg. Chem. **610**, 23–27.

Michaelis, C., Hj. Mattausch, H. Borrmann, A. Simon and J.K. Cockcroft, 1992b, Z. Anorg. Allg. Chem. **607**, 29–33.

Michaelis, C., W. Bauhofer, H. Buchkremer-Hermanns, R.K. Kremer, A. Simon and G.J. Miller, 1992c, Z. Anorg. Allg. Chem. **618**, 98–106.

Mochinaga, J., Y. Iwadate and K. Fukushima, 1991, Mater. Sci. Forum **73–75**, 147–152.

Molodkin, A.K., A.M. Karagodina, A.G. Dudareva, A.G. Krokhina and V.S. Tupolev, 1984, Russ. J. Inorg. Chem. **29**(1), 14–17.

Morss, L.R., and T.G. Spence, 1992, Z. Anorg. Allg. Chem. **616**, 162–168.

Moyer, J.W., 1978, Proc. Electrochem. Soc. **78**, 147–162.

Müller, B.G., 1991, Lanthanide fluorides, in: Synthesis of Lanthanide and Actinide Compounds, eds G. Meyer and L.R. Morss (Kluwer, Dordrecht) pp. 55–66.

Müller, W., and J.C. Spirlet, 1985, Struct. Bonding (Berlin) **59–60**, 57–73.

Nechitailov, S.B., T.A. Babushkina, K.Y. Volgin and A.A. Boguslavskii, 1989, Russ. J. Inorg. Chem. (Engl. Transl.) **34**(12), 1809–1812.

Ness, S.E., D.J.M. Bevan and H.J. Rossell, 1988, Eur. J. Solid State & Inorg. Chem. **25**, 509–516.

Niihara, K., and S. Yajima, 1971, Bull. Chem. Soc. Jpn. **44**, 643–648.

Odink, D.A., K. Song and S.M. Kauzlarich, 1992, Chem. Mater. **4**, 906–911.

Olejak-Chodan, M., and H.A. Eick, 1989, J. Solid State Chem. **80**, 68–74.

Olejak-Chodan, M., S.A. Hodorowicz and H.A. Eick, 1987a, Lanthanide & Actinide Res. **2**, 3–8.

Olejak-Chodan, M., S.A. Hodorowicz and H.A. Eick, 1987b, Cryst. Res. Technol. **22**, 285–289.

Olejak-Chodan, M., W. Lasocha and H.A. Eick, 1988, J. Solid State Chem. **73**, 259–267.

Ouwerkerk, M., 1985, Mater. Res. Bull. **20**, 501–509.

Patwe, S.J., B.N. Wani, U.R.K. Rao and K.S. Venkateswarlu, 1989, Can. J. Chem. **67**, 1815–1818.

Penneman, R.A., R.R. Ryan and A. Rosenzweig, 1973, Structural systematics in actinide fluoride complexes, in: Structure and Bonding, Vol. 13,

eds J.D. Dunitz, P. Hemmerich, J.A. Ibers, C.K. Jørgensen, J.B. Neilands, R.S. Nyholm, D. Reinen and R.J.P. Williams (Springer, New York) pp. 1–52.

Peterson, J.R., J.P. Young, R.G. Haire, G.M. Begun and U. Benedict, 1985, Inorg. Chem. **24**, 2466–2468.

Peterson, J.R., J.P. Young, D.D. Ensor and R.G. Haire, 1986a, Inorg. Chem. **25**, 3779–3782.

Peterson, J.R., J.P. Young, R.G. Haire and U. Benedict, 1986b, Physica B **144**, 85–90.

Peterson, J.R., J.P. Young, W.R. Wilmarth and R.G. Haire, 1990, Appl. Spectrosc. **44**, 461–465.

Petzel, T., and Th. Ahnen, 1985, Thermochim. Acta **90**, 61–69.

Petzel, T., V. Marx, J. Potthast and Th. Ahnen, 1992, Thermochim. Acta **194**, 319–327.

Pezat, M., B. Tanguy, M. Vlasse, J. Portier and P. Hagenmuller, 1976, J. Solid State Chem. **18**, 381–390.

Pierce, J.W., and H.Y.P. Hong, 1973, Structural studies in the system KF–YF_3, in: Proc. Tenth Rare Earth Research Conf., eds C.J. Kevane and T. Moeller (National Technical Information Service, Springfield, VA) pp. 527–537.

Podorozhnyi, A.M., and V.V. Safonov, 1983, Russ. J. Inorg. Chem. **28**(12), 1812–1813.

Polonskii, A.V., N.V. Baryshnikov and V.R. Akhelik, 1982, Russ. J. Inorg. Chem. **27**(2), 302–303.

Qiao, Z.Y., and X.R. Xing, 1991, Mater. Sci. Forum **73–75**, 217–226.

Radaev, S.F., E.A. Krivandina, L.A. Muradyan, B.A. Maksimov, N.N. Bydanov, V.A. Sarin, B.P. Sobolev and V.I. Simonov, 1991, Sov. Phys. Crystallogr. (Engl. Transl.) **36**(2), 195–199.

Rajeshwar, K., and E.A. Secco, 1977, Can. J. Chem. **55**, 2620–2627.

Ramanujachary, K.V., M. Greaney, R.L. Fuller and M. Greenblatt, 1991, J. Solid State Chem. **93**, 263–266.

Rao, U.R.K., A.K. Tyagi, K.V. Muralidharan and R.M. Iyer, 1992, J. Mater. Sci. Lett. **11**, 435–436.

Ruck, M., and A. Simon, 1992, Z. Anorg. Allg. Chem. **617**, 7–18.

Schilling, G., C. Kunert, T. Schleid and G. Meyer, 1992, Z. Anorg. Allg. Chem. **618**, 7–12.

Schleid, T., 1991, Eur. J. Solid State & Inorg. Chem. **28**, 737–748.

Schleid, T., 1992, Eur. J. Solid State & Inorg. Chem. **29**, 1015–1028.

Schleid, T., and F. Lissner, 1991, J. Less-Common Met. **175**, 309–319.

Schleid, T., and F. Lissner, 1992, Z. Anorg. Allg. Chem. **615**, 19–26.

Schleid, T., and G. Meyer, 1987a, Z. Anorg. Allg. Chem. **552**, 97–102.

Schleid, T., and G. Meyer, 1987b, Inorg. Chim. Acta **140**, 113–116.

Schleid, T., and G. Meyer, 1989, Z. Naturforsch. **44b**, 1007–1010.

Schleid, T., and G. Meyer, 1990, Z. Anorg. Allg. Chem. **583**, 46–54.

Schleid, T., and G. Meyer, 1991, Eur. J. Solid State & Inorg. Chem. **28**, 591–596.

Schleid, T., A. Lossin and G. Meyer, 1991, Z. Anorg. Allg. Chem. **598–599**, 299–306.

Schoebrechts, J.-P., R. Gens, J. Fuger and L.R. Morss, 1989, Thermochim. Acta **139**, 49–66.

Schubert, K., 1989, J. Less-Common Met. **154**, 39–46.

Schulze, M., and W. Urland, 1991, Eur. J. Solid State & Inorg. Chem. **28**, 571–574.

Schwanitz-Schüller, U., and A. Simon, 1985, Z. Naturforsch. **40b**, 705–709.

Seifert, H.J., and J. Sandrock, 1990, Z. Anorg. Allg. Chem. **587**, 110–118.

Seifert, H.J., and Y. Yuan, 1991, J. Less-Common Met. **170**, 135–143.

Seifert, H.J., H. Fink and G. Thiel, 1985, J. Less-Common Met. **110**, 139–147.

Simon, A., and T. Koehler, 1986, J. Less-Common Met. **116**, 279–292.

Simon, A., Hj. Mattausch, R. Eger and R.K. Kremer, 1991, Angew. Chem. Int. Ed. Engl. **30**, 1188–1189.

Sorokin, N.I., 1992, Sov. Phys. Crystallogr. **37**(2), 270–271.

Spirlet, M.R., J. Rebizant, J. Fuger and J.P. Schoebrechts, 1988, Acta Crystallogr. C **41**, 1300–1301.

Staffel, T., and G. Meyer, 1988, Z. Anorg. Allg. Chem. **557**, 40–44.

Steiner, H.-J., and H.D. Lutz, 1992, Z. Anorg. Allg. Chem. **613**, 26–30.

Struss, A.W., and J.D. Corbett, 1978, Inorg. Chem. **17**, 965–969.

Sumiyama, A., Y. Oda and M. Takashima, 1991, Physica C **185–189**, 515–516.

Takashima, M., and G. Kano, 1987, Solid State Ionics **23**, 99–106.

Takashima, M., Y. Nosaka and T. Unishi, 1992, Eur. J. Solid State & Inorg. Chem. **29**, 691–703.

Taylor, M.D., 1962, Chem. Rev. **62**, 503–511.

Terada, S., Y. Hirai and K. Kubota, 1988, Solid State Ionics **68**, 567–569.

Tighezza, A., J.L. Rehspringer and M. Drillon, 1992, Physica C **198**, 209–214.

Tupoleva, A.L., A.G. Dudareva, A.K. Molodkin and A.I. Ezhov, 1988, Russ. J. Inorg. Chem. **33**(9), 1368–1371.

Urland, W., and D. Hake, 1989, Z. Kristallogr. **186**, 296.

Van Der Sluys, W.G., J.C. Huffman, D.S. Ehler and N.N. Sauer, 1992, Inorg. Chem. **31**, 1318–1319.

Vedrine, A., and D. Trottier, 1979, Acta Crystallogr. B **35**, 1536–1537.

Vinogradova-Zhabrova, A.S., L.D. Finkel'shtein, V.G. Bamburov, N.N. Efremova and M.P. Glazyrin, 1990, Inorg. Mater. **26**(2), 325–327.

Vogt, T., E. Schweda, J.P. Laval and B. Frit, 1989, J. Solid State Chem. **83**, 324–331.

Voos-Esquivel, C.A., and H.A. Eick, 1987, J. Solid State Chem. **67**, 291–296.

Wang, S.H., S.M. Luo, H.A. Eick, K. Krämer and G. Meyer, 1989, J. Less-Common Met. **155**, 45–48.

Wani, B.N., S.J. Patwe, U.R.K. Rao and K.S. Venkateswarlu, 1989, J. Fluorine Chem. **44**, 177–185.

Wilmarth, W.R., and J.R. Peterson, 1991, Characterization of selected solid-state actinide (and related) compounds via Raman and absorption spectrophotometry, in: Handbook on the Physics and Chemistry of the Actinides, Vol. 6, eds A.J. Freeman and C. Keller (North-Holland, Amsterdam) pp. 1–39.

Wilmarth, W.R., G.M. Begun, R.G. Haire and J.R. Peterson, 1988a, J. Chem. Phys. **89**, 4666–4670.

Wilmarth, W.R., J.P. Young, R.G. Haire and J.R. Peterson, 1988b, J. Less-Common Met. **143**, 183–193.

Wilmarth, W.R., G.M. Begun, R.G. Haire and J.R. Peterson, 1988c, J. Raman Spectrosc. **19**, 271–275.

Wilmarth, W.R., R.G. Haire, J.P. Young, D.W. Ramey and J.R. Peterson, 1988d, J. Less-Common Met. **141**, 275–284.

Wilmarth, W.R., G.M. Begun and J.R. Peterson, 1989a, J. Less-Common Met. **148**, 193–200.

Wilmarth, W.R., G.M. Begun, R.G. Haire, J.P. Young and J.R. Peterson, 1989b, Appl. Spectrosc. **43**, 1038–1045.

Yee, K.A., and T. Hughbanks, 1992, Inorg. Chem. **31**, 1620–1625.

Yoshimura, M., K.J. Kim and S. Sōmiya, 1986, Solid State Ionics **18–19**, 1211–1216.

Young, J.P., R.G. Haire, J.R. Peterson, D.D. Ensor and R.L. Fellows, 1980, Inorg. Chem. **19**, 2209–2212.

Zalkin, A., and D.H. Templeton, 1985, Acta Crystallogr. B **41**, 91–93.

Ziółkowski, J., 1985, J. Solid State Chem. **57**, 269–290.

Zvarova, T.S., 1979, Radiokhimiya **21**(5), 727–730; Chem. Abstract **92**, 87217x.

Zych, E., and J. Drożdżyński, 1988, J. Less-Common Met. **138**, 271–279.

Zych, E., and J. Drożdżyński, 1990, J. Less-Common Met. **161**, 233–238.

Zych, E., and J. Drożdżyński, 1991, Eur. J. Solid State & Inorg. Chem. **28**, 575–580.

Handbook on the Physics and Chemistry of Rare Earths
Vol. 18 – Lanthanides/Actinides: Chemistry
edited by K.A. Gschneidner, Jr., L. Eyring, G.R. Choppin and G.R. Lander

Chapter 125

COMPARISONS OF THE BINARY OXIDES

R.G. HAIRE
Oak Ridge National Laboratory, P.O. Box 2008, Oak Ridge, TN 37831-6375, USA

L. EYRING
Department of Chemistry and Biochemistry, Arizona State University, Tempe, AZ 85287-1604, USA

Contents

Symbols 414
1. The binary oxides of the lanthanide elements 415
  1.1. Introduction 415
    1.1.1. The purpose and scope 415
    1.1.2. The electronic configurations of the atoms and ions 415
    1.1.3. The oxidation states of the lanthanides in oxides 416
    1.1.4. Previous reviews 416
  1.2. The preparation of the lanthanide oxides 416
    1.2.1. The lower oxides 416
    1.2.2. The sesquioxides 418
    1.2.3. The dioxides 418
    1.2.4. The intermediate/homologous series of mixed-valent oxides 422
    1.2.5. Nonstoichiometric phases 424
    1.2.6. Hysteresis and pseudophase formation 426
    1.2.7. Single crystals 427
    1.2.8. Thin films 428
    1.2.9. Colloidal particles 428
  1.3. The structures of the lanthanide oxides 429
    1.3.1. The lower oxides 429
    1.3.2. The sesquioxides 429
    1.3.3. The dioxides 430
    1.3.4. The intermediate oxides 432
    1.3.5. The nonstoichiometric oxides 437
    1.3.6. High-pressure effects 438
    1.3.7. Special electron microscopic observation 438
  1.4. The thermodynamic properties of the lanthanide oxides 439
    1.4.1. The derived functions 439
    1.4.2. Equilibrium vaporization behavior 439
  1.5. Dynamic considerations 441
    1.5.1. The tarnishing of the lanthanide metals with oxygen 441
    1.5.2. Atomic transport 443
    1.5.3. The kinetics of phase reactions 444

1.6 Other physical properties 446
1.6.1. Magnetic characteristics 446
1.6.2. Electrical properties 446
1.6.3. Optical properties 448
1.6.4. Mechanical and thermomechanical properties 449
2. The binary oxides of the actinide elements 449
2.1. Introduction 449
2.2. Electronic configurations 452
2.3. Oxidation states 453
2.4. Actinide binary oxides 454
2.4.1. Lower oxides 454
2.4.2. Sesquioxides 455
2.4.3. Dioxides 456
2.4.4. Intermediate oxides 456
2.4.5. Higher oxides 457
2.5. Preparation of actinide oxides 457
2.5.1. General considerations 457
2.5.2. Preparation techniques 458
2.5.3. Stoichiometry considerations 459
2.5.4. Preparation of single crystals 459
2.6. Specific oxides of the actinide elements 460
2.6.1. Actinium oxides 460
2.6.2. Thorium oxides 460
2.6.3. Protactinium oxides 460
2.6.4. Uranium oxides 462
2.6.5. Neptunium oxides 463
2.6.6. Plutonium oxides 463
2.6.7. Americium oxides 464
2.6.8. Curium oxides 465
2.6.9. Berkelium oxides 466
2.6.10. Californium oxides 467
2.6.11. Einsteinium oxides 469
2.6.12. Transeinsteinium oxides 470
2.7. Thermodynamic properties of binary oxides 470
2.8. Magnetic properties of binary oxides 475
2.9. Other properties of binary actinide oxides 478
3. Comparison of the binary oxides of the lanthanide and actinide elements 479
3.1. General comparison 479
3.2. Thermodynamic and high-temperature behavior 489
3.3. Comparison of magnetic behavior 494
3.4. Concluding comments 496
References 498

Symbols

A-type (form)	a hexagonal form of the lanthanide/actinide sesquioxides	C-type (form)	a cubic form of the lanthanide/actinide sesquioxides
B-type (form)	a monoclinic form of the lanthanide/actinide sesquioxides	bcc	body-centered cubic
		fcc	face-centered cubic
		F	fluorite type

σ	a widely nonstoichiometric C-type-related phase	M19	$RO_{1.790\pm\delta}$
		V_O	vacant oxygen site
α	a widely nonstoichiometric fluorite-related phase	HREM	high-resolution electron microscope
ϕ	cubic C-type	MeV	million electron volts
θ	hexagonal A-type	O/M	oxygen/metal ratio
ι	$RO_{1.714\pm\delta}$	μ_B	magnetic moment in Bohr magnetons
ζ	$RO_{1.778\pm\delta}$		
ε	$RO_{1.800\pm\delta}$	$\mu_{eff}(\mu_B)$	effective magnetic moment in Bohr magnetons
δ	$RO_{1.818\pm\delta}$		
δ′	$RO_{1.806\pm\delta}$	L–S coupling model	magnetic moments calculated using simple coupling involving the L and S quantum numbers rather than the so-called intermediate coupling model
β	$RO_{1.833\pm\delta}$; (0), (1), (2), (3) refer to structural polymorphs		
π	$RO_{1.875\pm\delta}$; (0), (1), (2), (3) refer to structural polymorphs		

1. The binary oxides of the lanthanide elements

1.1. *Introduction*

1.1.1. *The purpose and scope*

It is our purpose to present a summary of the compounds formed with oxygen and the lanthanide and actinide elements in such a way as to facilitate comparisons and contrasts. It is hoped that for many readers this summary will, in itself, prove useful by presenting an updated account of some relevant research concerning the lanthanide and actinide oxides. Beyond this, it will be found that the oxides afford a substantial platform upon which to assemble a comparative collage of lanthanide/actinide chemistry.

1.1.2. *The electronic configurations of the atoms and ions*

The basis for the family relationships among the lanthanide elements themselves, and of periodic relationships that include the actinide elements, is their elemental and ionic electronic configurations. The fascinating story of the discovery and development of this truth can be found in several chapters in volume 11 of this *Handbook on the Physics and Chemistry of Rare Earths* (1988) and in the chapter by Seaborg (ch. 118) in this volume. The oxides provide a delicately sculpted model of the relationships between each element and other members of its series and also of the relationships between the two series. The electronic configurations for the ground state of the atoms and the relevant valence states of these elements are listed in table 1. The similarities and lack of congruence for the oxides of these two series is discussed in section 3.

Considerable attention has been paid to the electronic structures and valences of the rare-earth systems including the oxides. A full discussion of these aspects is outside our scope since they have been thoroughly considered in other places in this series (see Handbook on the Physics and Chemistry of Rare Earths Cumulative index, 1993).

TABLE 1
Properties of the lanthanide(III) ions (Westrum 1967).

Atomic number	Rare earth	Electronic configuration of (III ions)	Ground term	Experimental magnetic moment (μ_B)
57	La		$^1S_0$	0.00
58	Ce	$4f^1$	$^2F_{5/2}$	[2.56]
59	Pr	$4f^2$	$^3H_4$	3.55
60	Nd	$4f^3$	$^4I_{9/2}$	3.66
61	Pm	$4f^4$	$^5I_4$	[2.83]
62	Sm	$4f^5$	$^6H_{5/2}$	1.54
63	Eu	$4f^6$	$^7F_0$	3.51
64	Gd	$4f^7$	$^8S_{7/2}$	7.90
65	Tb	$4f^8$	$^7F_6$	9.63
66	Dy	$4f^9$	$^6H_{15/2}$	10.5
67	Ho	$4f^{10}$	$^5I_8$	10.5
68	Er	$4f^{11}$	$^4I_{15/2}$	9.5
69	Tm	$4f^{12}$	$^3H_6$	7.39
70	Yb	$4f^{13}$	$^2F_{7/2}$	4.34
71	Lu	$4f^{14}$	$^1S_0$	[0.0]

1.1.3. *The oxidation states of the lanthanides in oxides*

The combination of the lanthanide elements with oxygen results in a formal oxidation state of the metal atom that depends upon the chemical potential of oxygen and the different electronic conditions of the atoms within the compound. The oxidation state of the lanthanide atoms varies between (II), as in EuO, and (IV), as in CeO_2. All the lanthanides exhibit the (III) oxidation state in their oxide systems, as in La_2O_3. Furthermore, mixed-valence states exist in the series between these extremes both as stoichiometric and as nonstoichiometric compounds. Hund's first rule is followed in the lanthanide series which explains the stability of oxidation states other than three.

1.1.4. *Previous reviews*

A review of the binary lanthanide oxides has already appeared in an earlier volume of this series (Eyring 1979). A review of the "Seltenerdelemente" appeared in *Gmelin Handbuch der Anorganischen Chemie* (1974). The preparative methods and characterization of the many phases of the lanthanide oxides have recently been published (Eyring 1991). The structures and transformations of the rare-earth oxides have recently been reviewed (Schweda et al. 1991, Schweda 1992). Some aspects of these reviews are summarized and brought up-to-date here. A review of thermodynamic properties can be found in the chapter by Morss (ch. 122) in this volume.

1.2. *The preparation of the lanthanide oxides*

1.2.1. *The lower oxides*

All members of the lanthanide series occur as gas-phase RO molecules at high temperatures. However, condensation of the gaseous RO molecules does not, in any

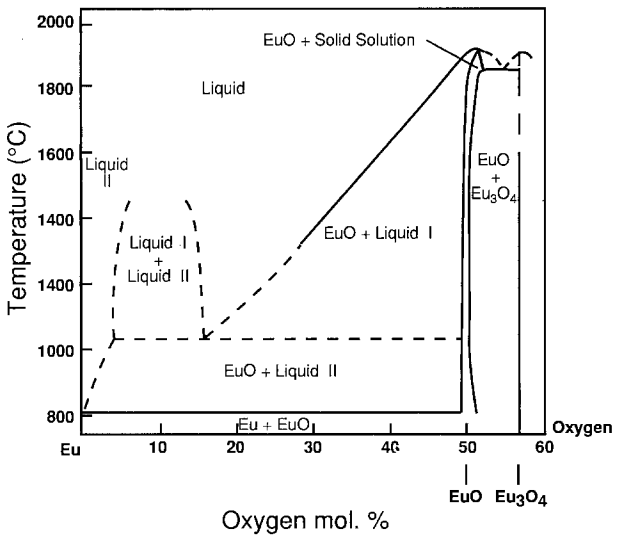

Fig. 1. Phase diagram in the $Eu-Eu_3O_4$ region (after Shafer et al. 1972).

instance, result in a solid of the same composition. Among the solid lanthanide compounds only EuO, Eu_3O_4, and probably YbO are preparable as stable phases at ordinary pressures (Eyring 1979). The other solid-state phases that reportedly have been produced at ordinary pressures appear to have been stabilized by impurities, notably nitrogen or carbon (Felmlee and Eyring 1968). The phase diagram for the $Eu-Eu_3O_4$ region is shown as fig. 1. (Shafer et al. 1972).

EuO can be prepared by the reduction of Eu_2O_3 with Eu metal at 800°C (Shafer 1965), with C (graphite) at 1600–1700°C (Achard 1960), with La at 1300–1500°C (Eick et al. 1956), or with EuH_2 at 800°C (Brauer and Schulz 1967). The oxyhalides of Cl, Br, and I are reduced by LiH in high vacuum at 600–800°C to yield good crystals of EuO (Bärnighausen 1966, Haschke and Eick 1969).

Eu_3O_4 can be prepared by reduction of an equal molar mixture of Eu_2O_3, EuOCl and LiH from which LiCl and H_2 are expelled at high temperatures (Bärnighausen 1966, Haschke and Eick 1968). Another method is to react EuO and Eu_2O_3 in the proper proportions and heat to 2050°C in an iridium container (Bedford and Catalano 1971). The thermodynamic conditions under which the lower oxides react or form are shown in fig. 2.

Calculations indicate that YbO is thermodynamically stable at low temperatures and at ambient pressure, and evidence for its existence has been found (Haschke and Eick 1970, Fishel et al. 1970).

Leger et al. (1980, 1981) have described the preparation, at high pressures, of the metallic monoxides for the elements from lanthanum to samarium and have determined their structure and conductivities. A negative $P\Delta V$ term in the free-energy expression makes it possible to synthesize the monoxides from a mixture of the metal and the sesquioxide under pressure. These monoxides can be maintained at normal pressures after preparation. The monoxides through NdO are metallic, golden-yellow compounds with the Ln atom being trivalent. SmO is metallic with a valence close to

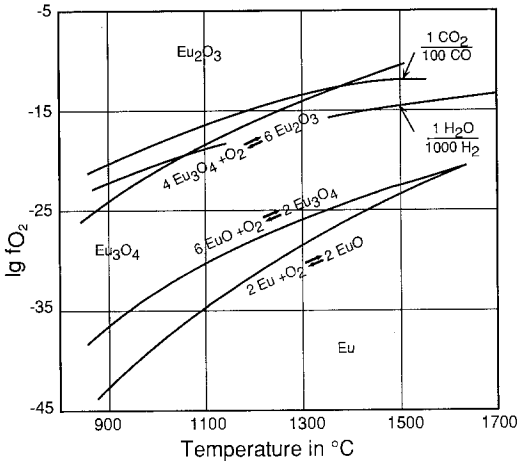

Fig. 2. Conditions for interactions of the lower oxides of europium (after Gmelin Handbuch der Anorganischen Chemie 1974).

three, while EuO and YbO are semiconductors with the lanthanide atom being divalent.

1.2.2. *The sesquioxides*

All the lanthanide elements form a sesquioxide. Although the sesquioxide can be synthesized by direct reaction of the elements, it is not a preferred method because the preparation of pure metals is difficult. The preferred method for all but Ce, Pr and Tb is by the decomposition of some compound precursor in air or oxygen. (In air CeO_2, $PrO_{1.83}$ and approximately $TbO_{1.75}$ are the compositions obtained.) Suitable precursors include hydroxides, nitrates, carbonates, formates, oxalates, acetates, citrates, chlorides and sulfates (Gmelin Handbuch der Anorganischen Chemie 1974, Eyring 1991). The most commonly used compounds are the oxalates and hydroxides. Table 2 indicates effective precursor decomposition temperatures. Even though the decomposition temperature is below 1000°C, this temperature should be attained and held for a few hours to assure the absence of H_2O and CO_2 in the final product. Conditions for preparing the sesquioxides of Ce, Pr and Tb from the decomposition reactions suggested in table 2 are given in table 3.

1.2.3. *The dioxides*

The highest established oxide (excluding peroxides) of the lanthanides is the dioxide, formed only by Ce, Pr and Tb. The phase diagrams for oxides higher than the sesquioxide are shown as figs. 3–5. Difficult-to-reduce CeO_2 is formed when its compounds are decomposed in oxygen at pressures in the millimeter range or higher. PrO_2 is formed slowly at temperatures around 300°C and oxygen pressures of one atmosphere (Hyde et al. 1965) and more rapidly at higher temperatures and oxygen pressures. It requires oxygen pressures in the range of 1000 atm at 300°C to form TbO_2. Conditions for preparing the dioxides are given in table 3.

PrO_2 and TbO_2 can also be formed by disproportionation when the oxides with O/M ratios between 1.5 and 2.0, obtained by the decomposition of precursors in air, are

TABLE 2
The formation of lanthanide sesquioxides from the thermal decomposition of their salts (Eyring 1991).

Product	*T*/*PC*, [ref.]/Type		
	Hydroxides	Nitrates(solid state)	Nitrates(from flux)
La_2O_3	840 [1]	780 [1, 2] 670 [3] 600 [4] A	650 [5] A
Nd_2O_3	830 [1]	810 [1] 830 [2] 660 [3] 600 [4] C	550 [5] A
Sm_2O_3	750 [1]	760 [1] 750 [2] 680 [3] C	430 [5] B
Eu_2O_3	720 [1]	760 [1] 670 [3] C	430 [5] B
Gd_2O_3	750 [1]	780 [1] 670 [3] C	430 [5] B
Dy_2O_3		730 [1] C	430 [5] C
Ho_2O_3		660 [1] C	430 [5] C
Er_2O_3	700 [1]	630 [1] C	430 [5] C
Tm_2O_3			430 [5]
Yb_2O_3	650 [1]	620 [1] C	430 [5] C
Lu_2O_3			430 [5] C
	Carbonates	Oxalates	Acetates
La_2O_3	850 [1] 830 [3, 8] A	830 [1] 800 [10, 11] 800 [3]	850 [1] A
Nd_2O_3	810 [1] 670 [8] 625 [4] C	760 [1] 735 [10, 11] 670 [3]	780 [1] C
Pm_2O_3		750 [12, 13]	
Sm_2O_3	620 [3] 650 [8] C	740 [1] 735 [10, 11] 630 [3]	
Eu_2O_3	750 [1] C	680 [1] 620 [10, 11] 630 [3]	750 [1] C

TABLE 2 (continued).

Product	*T*/*PC*, [ref.]/Type		
Gd_2O_3	700 [9]	740 [1]	
	620 [3]	700 [10, 11]	
		670 [3]	
Tb_2O_3	700 [9]	725 [11]	
Dy_2O_3	700 [9]	745 [11]	
Ho_2O_3	700 [9]	740 [1]	
		735 [10, 11]	
Er_2O_3	700 [9]	720 [1, 10, 11]	
Tm_2O_3	700 [9]	715 [11]	680 [1]
	C		C
Yb_2O_3	700 [1]	700 [1]	
		730 [11]	
Lu_2O_3		715 [11]	
	Fluorides	Chlorides	Sulfates
La_2O_3	1290 [3, 6]	1110 [3, 6]	1450 [3, 7]
	A	A	A
Nd_2O_3	1305 [3, 6]	990 [3, 6]	1400 [3, 7]
	A	A	A
Sm_2O_3	1265 [3, 6]	930 [3, 6]	1340 [3, 7]
	B	B + C	B
Eu_2O_3	1180 [3, 6]	895 [3, 6]	1330 [3, 7]
	B	C	B
Gd_2O_3	1240 [3,6]	865 [3, 6]	1280 [3, 7]
	C + B		B

[1] Glushkova and Boganov (1965)
[2] Wendlandt (1956)
[3] Stecura (1965)
[4] Ambrozhii and Luchnikova (1962)
[5] Brauer and Siegbert (1969)
[6] Wendlandt (1958a)
[7] Nathans and Wendlandt (1963)
[8] Ambrozhii et al. (1960)
[9] Head and Holley (1965)
[10] Wendlandt (1958b)
[11] Wendlandt (1959)
[12] Weigel and Scherer (1965)
[13] Wilson et al. (1963)

leached at room temperature by dilute acids. The advantage of this technique is that only simple equipment is required (Brauer and Pfeiffer 1963, Clifford 1964, Eyring 1979; Karnatak et al. 1985). Kang and Eyring (1988a, b) observed the disproportionation process utilizing high-resolution electron microscopic (HREM) techniques. It was clearly shown that the leaching process propagated from defects at the surfaces (e.g., emergence of dislocations) and proceeded inward, removing all metal species into solution as Ln^{+3} ions. This reduction of some of the metal atoms at the surface must

TABLE 3
The preparation of the oxides of Ce, Pr and Tb.

Oxide	Phase designation	Temp. (°C)	Reference for prep.	Oxygen pressure (Torr) or other gas
CeO_2	F	900	10	760
$Ce_{11}O_{20}$	δ	636	1	10^{-28}
		620	2	dry H_2 – 10^{-28}
$Ce_{62}O_{112}$	δ′	580	2	dry H_2
$Ce_{19}O_{34}$	M19	600	2	dry H_2
"$Ce_{10}O_{18}$"	ε	636	1	10^{-27}
		670	2	dry H_2
"Ce_9O_{16}"	ζ	715	1	$10^{-25.5}$
		730	2	dry H_2
Ce_7O_{12}	ι	971	1	$10^{-17.8}$
		840	2	dry H_2
Ce_2O_3	θ	900	2	dry H_2
	θ	700–800	9	$LiCeO_2 + CeO_2 + LiCl$ closed system
PrO_2	F	315	3	760
		450		3800
$Pr_{16}O_{30}$	π	240	8	38
$Pr_{12}O_{22}$	β	420	4	350
$Pr_{11}O_{20}$	δ	460 (Oxidation)	4	150
		465 (Reduction)	6	150
$Pr_{10}O_{18}$	ε	480	4	30
Pr_9O_{16}	ζ	560	4	10
Pr_7O_{12}	ι	850	4	10
Pr_2O_3	φ	550	10	H_2(flow)
Pr_2O_3	A	1000	10	10^{-6}
TbO_2	C	< 800°	5	10^6
$Tb_{12}O_{22}$	β(3)	800°	11	10^6
$Tb_{11}O_{20}$	δ	250	5	380
			7	
$Tb_{62}O_{112}$	δ′	535	5	380
Tb_7O_{12}	ι	695	7	13
Tb_2O_3	φ	650	10	H_2
	B	1000	10	vac. 10^{-6}

[1] Bevan and Kordis (1964)
[2] Knappe and Eyring (1985)
[3] Hyde et al. (1965)
[4] Hyde et al. (1966)
[5] Langley (unpublished)
[6] Lowe and Eyring (1975)
[7] Hyde and Eyring (1965)
[8] Otsuka et al. (1986)
[9] Bärnighausen and Schiller (1985)
[10] Eyring (1991)
[11] Kang et al. (1992b)

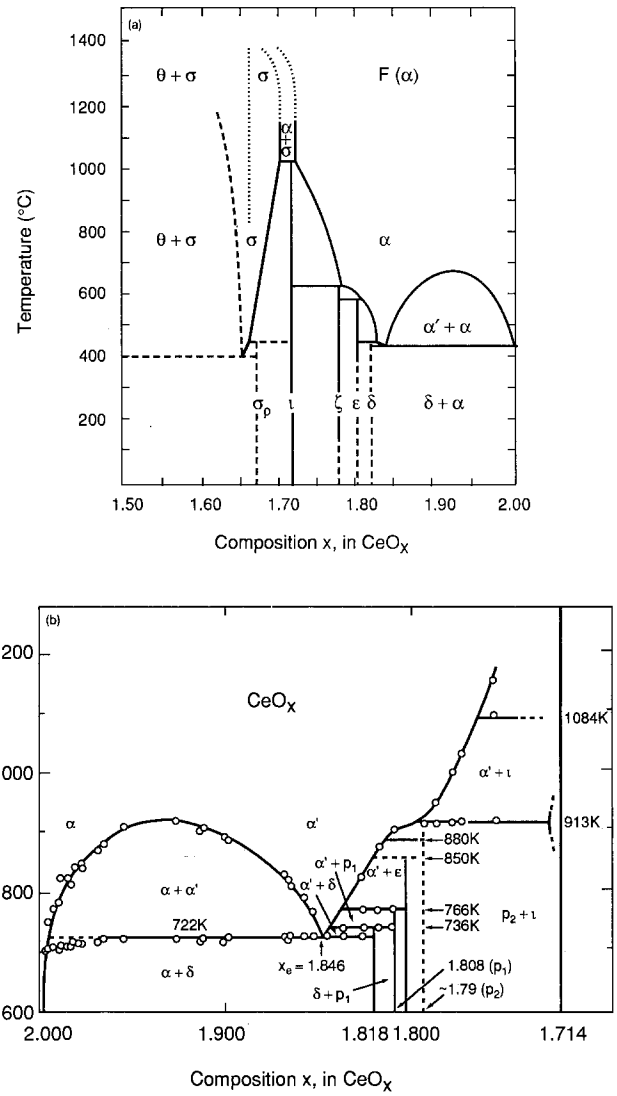

Fig. 3. (a) Phase diagram for the CeO_x–O_2 system (after Height and Bevan 1979, Kitayama et al. 1985). (b) Partial phase diagram for the CeO_2–O_2 system (after Ricken et al. 1984).

necessarily be accompanied by the transport of oxygen inward and electrons outward to the reaction surface. The overall effect is to produce LnO_2 crystals with re-entrant voids inward from the surface in every direction.

1.2.4. *The intermediate/homologous series of mixed-valent oxides*

As is evident from figs. 3–5, Ce, Pr and Tb form intermediate compounds of narrow composition ranges of which most, but not all, have compositions with the generic

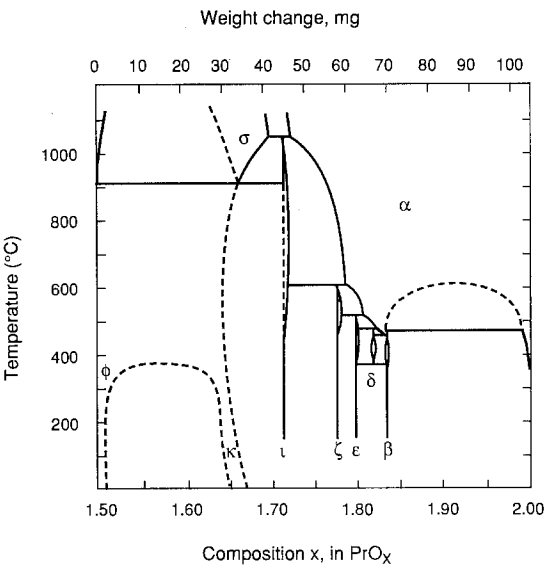

Fig. 4. Phase diagram for the PrO_x–O_2 system (after Turcotte et al. 1971a).

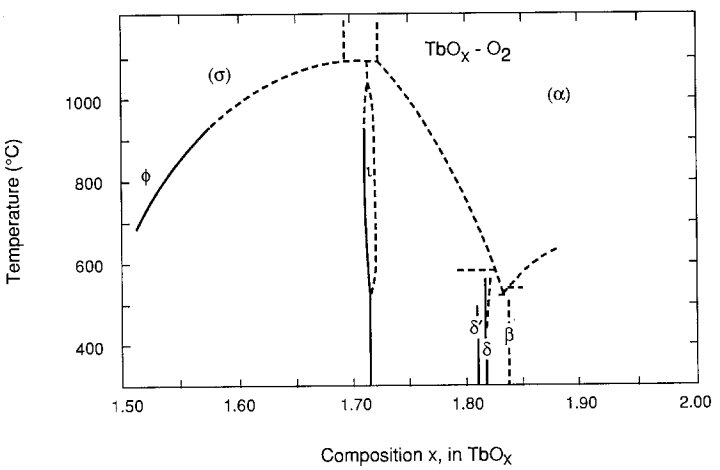

Fig. 5. Phase diagram for the TbO_x–O_2 system (after Tuenge and Eyring 1982).

formula R_nO_{2n-2} (n is an integer or infinity). The established values of n for the homologous series are, respectively, 4, (6), 7, (10), 11, and ∞ for Ce; 4, 7, 9, 10, 11, 12, 16 and ∞ for Pr; and 4, 7, 11, 12 and ∞ for terbium. Known intermediate phases of narrow composition not belonging to the homologous series are $Ce_{19}O_{34}$, $Ce_{62}O_{112}$ and $Tb_{62}O_{112}$. Table 3 indicates the conditions of temperature and oxygen pressure sufficient to produce each of the intermediate phases with $n = 7$–16. The references should be consulted for details.

There have been recent studies on the higher-oxide phase relationships particularly those of the cerium–oxygen system. Part of the phase diagram was clarified by Ricken et al. (1984) and by Riess et al. (1985) from heat capacity measurements and confirmed by Körner et al. (1989) by thermal expansion measurements. Two intermediate phases not belonging to the homologous series, $Ce_{19}O_{34}$ and $Ce_{62}O_{112}$, were observed independently from HREM observations by Knappe and Eyring (1985). The $n = 9$ phase reported earlier by Height and Bevan (1979) was not seen by either of these investigators nor was the $n = 10$ phase observed by Knappe and Eyring, although evidence of more ordered intermediate phases in the composition region $CeO_{1.818-1.714}$ were indicated in the electron diffraction patterns. More work must be done on this composition region in order to map out its obvious complexity.

The phase diagram of the praseodymium oxide system may need modification to include an $n = 16$ phase reported by Otsuka et al. (1986) from tensimetric kinetic observations of the evolution of X-ray powder diffraction patterns. Three polymorphs of this phase were confirmed by Kang et al. (1992a) from HREM studies of non-equilibrium quenching procedures and a review of previous results (Eyring and Kang 1991). However, it is not known whether or not this phase is metastable or should be added to the equilibrium phase diagram. In earlier kinetic and equilibrium studies (Hyde et al. 1965) $Pr_{16}O_{30}$ was not observed where it should have been if it were stable. In the study of quenched specimens by HREM (Kang et al. 1992a), the β(3) phase previously known for the TbO_x system was also observed in PrO_x. The unit cell content of this latter compound is $Pr_{48}O_{88}$.

1.2.5. *Nonstoichiometric phases*

All the single-phase regions discussed above have a finite range of composition that is accessible with careful manipulation of the preparative conditions. A marked additional feature of the phase diagrams of figs. 3–5 is the appearance of phases having a wide composition range at pressures and temperatures in excess of those required to form the ordered phases.

At these higher temperatures and pressures, depending on the system involved, these ordered intermediate phases disorder into one of two cubic, nonstoichiometric phases depending upon the composition (Hyde et al. 1966). The lower composition phase (σ) is derived from the C-type sesquioxide and the disordered phase of higher composition (α) is fluorite-type. The two disordered regions are separated by a narrow miscibility gap and each is itself possessed of a wide range of composition.

In the recent past, wide-range nonstoichiometric phases were commonly considered to be random solid solutions. Later, more and more were found to consist of closely spaced series of ordered structures (Bursill and Hyde 1972). The disordered phases in the rare-earth oxides are among the few wide-composition, nonstoichiometric equilibrium phases remaining and there are still questions about the structural details.

In order to prepare an oxide in this wide composition range, one must equilibrate the oxide at temperatures and oxygen pressures higher than those listed in table 3 for the intermediate compounds. Figure 6 epitomizes the intricacies of the praseodymium oxide system with more or less vertical or slanted single-phase regions, horizontal two-phase regions that show hysteresis. The nearly vertical lines mark the ordered

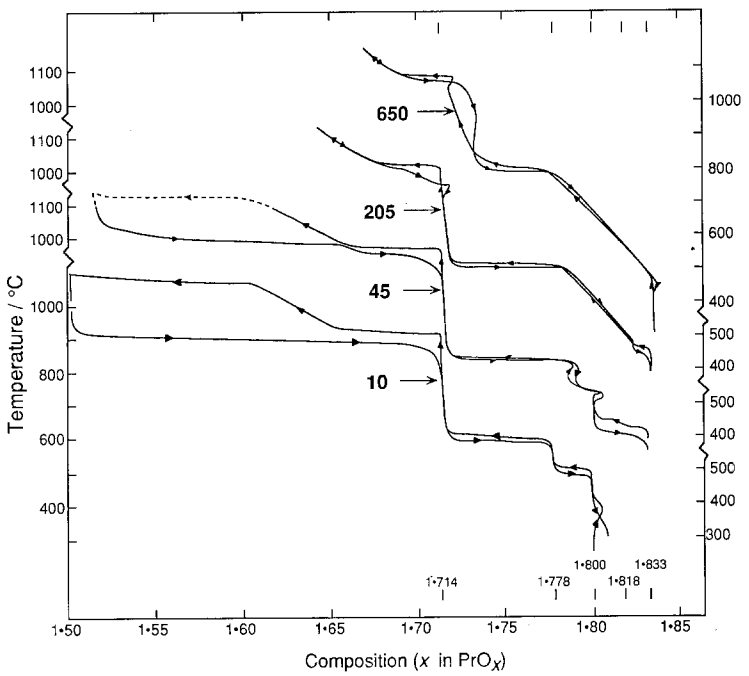

Fig 6. Representative isobaric runs in the PrO_x–O_2 system. The nominal oxygen pressure is indicated in Torr at each curve (from Hyde et al. 1966).

phases belonging to the homologous series. The unusual reversals observed at higher pressures indicate persistent metastability.

Recently a study of the CeO_x system at temperatures between 1000 and 1330°C has been carried out by Kitayama et al. (1985) that essentially extends the phase diagram of Height and Bevan (1979) (fig. 3a) to higher temperatures. This work confirms the continuation of a variable σ phase with a C-type structure (called by them Ce_3O_5) in the region $CeO_{1.65-1.70}$ and a miscibility gap of about 0.02 in composition width between the C-type region and a wide-range nonstoichiometric phase of fluorite structure, in agreement with previous suggestions. These new data are superimposed on the earlier phase diagram (fig. 3a) recommended by Height and Bevan (1979).

Lindemer (1986) has obtained an empirical fit to a wide range of published data on the CeO_x system to yield Gibbs free energies that unify the data and predict a consolute temperature of about 680°C to the two-phase, α′–α, region suggested by the data of Bevan and Kordis (1964). Lindemer suggests sufficient accuracy to allow useful thermodynamic data on grossly nonstoichiometric oxides in equilibrium with gaseous oxygen. They consider solid solutions of the dioxide end-member and the sesquioxide over the entire alpha region. This is a model not unlike that in the CeO_2–Y_2O_3 system studied by Wallenberg et al. (1989) where commensurate modulation of a C-type periodicity is apparent in the fluorite-related matrix of only 20% Y_2O_3. A caution is that, in this latter case, only the fluorite and C-type structures are involved. The CeO_x

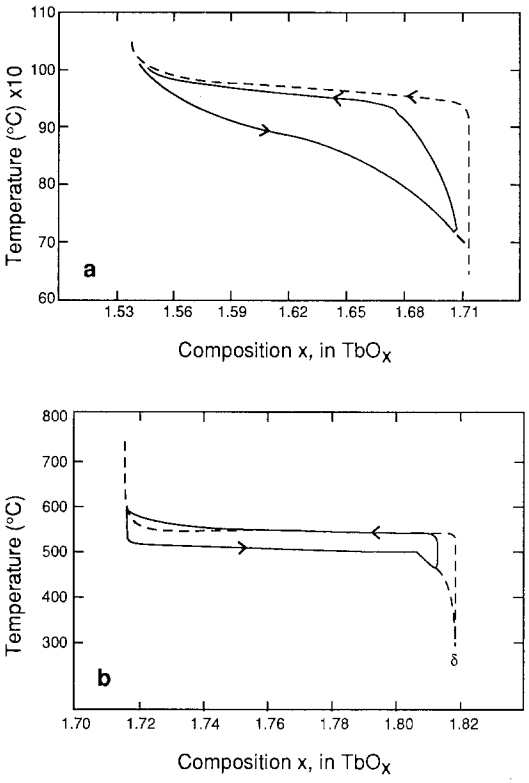

Fig. 7. Isobaric hysteresis loop for (a) the reaction $\frac{2}{7}\ Tb_7O_{12} \rightarrow Tb_2O_3 + \frac{3}{14}\ O_2(g)$ (dashed loop is the intrinsic hysteresis envelope), and (b) the reaction $\frac{7}{11}\ Tb_{11}O_{20} \rightarrow Tb_7O_{12} + \frac{4}{11}\ O_2$ (after Lowe and Eyring 1975).

system is quite different since one of the intermediate phases might be considered the end-member of the oxygen-poor side of the gap.

On the other hand, Benzakour et al. (1988) utilized Monte Carlo calculations to show that no satisfactory statistical treatment is available for $CeO_{1.7-2.0}$ due to inadequate knowledge of the physics of the system.

1.2.6. *Hysteresis and pseudophase formation*

A feature absent in the phase diagrams shown is that these oxide systems are reversible in the single-phase regions but show marked hysteresis in the two-phase regions, as can be easily seen in fig. 6. Figure 7 shows specific examples from the work of Lowe and Eyring (1975) of the hysteretic behavior in the $1-\phi$ and the $1-\delta$ regions of the TbO_x–O_2 system. The direction of approach to equilibrium must be taken into account when preparations are attempted.

In the hysteretic two-phase regions it is common to observe a linear approach to one side or the other as shown clearly in the lower curve in fig. 7a. This feature has been called a pseudophase and its nature requires further attention and explanation. The loop in fig. 7b indicates reversal of the temperature in the region between $Tb_{62}O_{112}$ and $Tb_{11}O_{20}$. Deviation of the hysteresis loop on the left where it rejoins the Tb_7O_{12} composition results from the residual $Tb_{62}O_{112}$, rather than from $Tb_{11}O_{20}$.

Thermodynamic and theoretical models for hysteresis and kinetics of phase reactions in the Pr and Tb oxide systems have been proposed. In the first study by Knittel et al. (1977) a model based on regular solution theory is developed and applied to hysteresis in the Pr and Tb oxide systems. Maren et al. (1984) modeled the Pr_7O_{12}–Pr_9O_{16} hysteretic reaction using a thermodynamic formalism. Models assuming both noninteracting and interacting domains were considered.

1.2.7. *Single crystals*

Single crystals of EuO, R_2O_3, CeO_2 and PrO_2 have been grown by means of special techniques that could, with substantial effort, be expanded to other oxides. EuO single crystals have been grown from a melt of Eu and Eu_2O_3 (Oliver et al. 1972). The crystals obtained have properties that depend strongly on the preparative conditions.

The sesquioxides of all the lanthanides except Ce, Pr and Tb can be grown from the melt and cooled in air. The structure of the product obtained varies over the series. La_2O_3 and Nd_2O_3 are usually found to be in the A-form, Sm_2O_3, Eu_2O_3 and Gd_2O_3 in the B-form, and the remainder in the C-form (see fig. 8). Similar results are obtained using the Verneuil or flame fusion techniques. If oxygen is excluded during cooling,

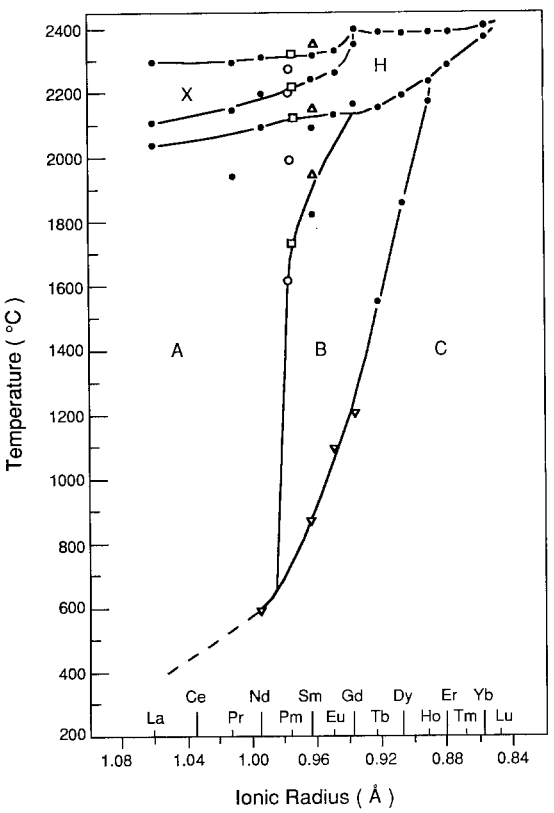

Fig. 8 Polymorphic transformation temperatures for the lanthanide sesquioxides (after Foex and Traverse 1966b, Warshaw and Roy 1961).

TABLE 4
Growth of lanthanide oxides single crystals.

Crystal	Method	Reference
EuO	Melt	Shafer et al. (1972)
CeO_2	Flux	Linares (1967)
CeO_2	Flux	Finch and Clark (1966)
CeO_2	Flux	Vinokurov et al. (1965)
PrO_2	Hydrothermal growth	McKelvy and Eyring (1983)
TbO_x	Hydrothermal growth	McKelvy and Eyring (1983) MacChesney et al. (1966)
$PrO_2(TbO_{1.818})$	Hydrothermal growth	Lowenstein et al. (1972)
Sm_2O_3(B-type)	Verneuil	Lejus et al. (1974)
Eu_2O_3	Flux	Drofenik et al. (1974)
R_2O_3	Verneuil	Lefever (1962) Lejus and Connan (1974) Popova and Zotkina (1967) Pastor and Pastor (1966)
R_2O_3	Reduction by alkali metals	Schleid and Meyer (1989)

Pr_2O_3 and Tb_2O_3 can be added to this list. In all these methods, severe problems of fracture are encountered as the crystals cool through any phase transformations. Some examples of crystal growth with references are recorded in table 4.

There are special problems in the growth of single crystals of the higher oxides. CeO_2 crystals are obtained from a wide variety of flux growth methods. PrO_2 is obtained hydrothermally and TbO_2 has been prepared only at very high oxygen pressures (see MacChesney et al. 1966, McKelvy and Eyring 1983). Single crystals of the intermediate oxides are obtained by adjusting their composition by annealing at appropriate temperatures and oxygen pressures. The sesquioxides of these three elements, grown by high-temperature methods, are not in the cubic form and they shatter when oxidized to the fluorite-related, higher oxides. The structural details are to be discussed later.

1.2.8. *Thin films*

Thin films of the oxides can be obtained by oxidation of evaporated or sputtered metallic films under suitable temperatures and oxygen pressures. The sesquioxides are the congruently vaporizing species, hence they can be prepared by direct vaporization. A low-temperature sol-gel technique, including annealing at elevated temperature in oxygen if required, could also be used to obtain thin films of the oxides.

1.2.9. *Colloidal particles*

Methods involving homogeneous precipitation of the hydroxycarbonate of the lanthanides followed by calcining can be utilized to obtain colloidal particles of binary or ternary lanthanide oxides with varied morphologies. This technique has been thoroughly described by Matijevi'c and by Hsu et al. (1988). Kang et al. (1992b) have

TABLE 5
Lattice parameters of NaCl-type lanthanide monoxides.

Monoxide	a (Å)	Reference
LaO	5.144 ± 0.005	Leger et al. (1981)
CeO	5.089 ± 0.005	Leger et al. (1981)
PrO	5.031 ± 0.005	Leger et al. (1981)
NdO	4.994 ± 0.005	Leger et al. (1981)
SmO	4.943 ± 0.005	Leger et al. (1981)
EuO	5.1439 ± 0.0018	Haschke and Eick (1969)
YbO	4.87	Fishel et al. (1970)

documented that production of monodispersed colloidal spheres of mixed lanthanides with either long-range or short-range order can be obtained by this technique.

1.3. *The structures of the lanthanide oxides*

The structural parameters and space group symmetries of the established lanthanide oxides are given in tables 5–12. Figures 9 and 23 contain plots of the lattice parameters of the sesquioxides and dioxides as a function of the atomic number. The lanthanide contraction is exhibited clearly in these plots.

1.3.1. *The lower oxides*

EuO and YbO crystallize in the NaCl-type structure. EuO is a red compound with $a = 5.1439$ Å (Haschke and Eick 1969). Eu_3O_4 is black with an orthorhombic structure having $a = 10.094$, $b = 12.068$ and $c = 3.500$ Å (Bärnighausen and Brauer 1962, Haschke and Eick 1968).

The monoxides prepared by applying high pressure to mixtures of metal and sesquioxide (see section 1.2.1) are NaCl-type up to about 25 GPa (Leger et al. 1981). Vedel et al. (1986) observed a rapid volume decrease in CeO with pressure (interpreted as an electronic instability) up to 3 GPa, followed by a continuing linear decline of much smaller slope up to 25 GPa. De and Chatterjee (1989) have used band calculations to show an increase in the valency of cerium in CeO from 3.0 to 3.26 with pressure.

1.3.2. *The sesquioxides*

Five polymorphic forms for the lanthanide sesquioxides have been identified. The temperature range of their stable existence is presented in fig. 8 (Foex and Traverse 1966a, b). More than one form is possible for all but lutetium, and all are potentially possible for the middle members. We concern ourselves here exclusively with the lower temperature A-, B- and C-forms. The A- and C-types are those most often encountered when the entire series is considered. The A-type, typical of the light lanthanide oxides formed at moderately elevated temperatures, is hexagonal. The lattice parameters for these oxides are given in table 6. The C-form structure is of the cubic bixbyite type related to a doubled-edge fluorite structure with one fourth of the oxygen sites vacated in a regular way. The lattice parameters for the C-type sesquioxides are given in table 7

TABLE 6
A-type structures of R_2O_3 ($P\bar{3}2/ml$, No. 164 I.T.) (after Schweda 1992).

Compound	a(Å)	c(Å)	Reference
La_2O_3	3.938	6.136	Aldebert and Traverse (1979)
Ce_2O_3	3.891(1)	6.059(1)	Bärnighausen and Shiller (1985)
Pr_2O_3	3.857(3)	6.016(5)	Hoekstra (1966)
Nd_2O_3	3.829(3)	6.002(5)	Boucherle and Schweizer (1975)
Pm_2O_3	3.802	5.954	Chikalla et al. (1972)

TABLE 7
C-type structures of R_2O_3 ($Ia\bar{3}$, No. 206 I.T.) (after Schweda 1992).

Compound	a(Å)	Reference
Pr_2O_3	11.152(2)	Sawyer et al. (1965b)
Nd_2O_3	11.080	Roth and Schneider (1960)
Pm_2O_3	10.99	Chikalla et al. (1972)
Sm_2O_3	10.934	Roth and Schneider (1960)
Eu_2O_3	10.869	Rau (1964)
Gd_2O_3	10.8122	Roth and Schneider (1960)
Tb_2O_3	10.7281(5)	Baenziger et al. (1961)
Dy_2O_3	10.6647	Roth and Schneider (1960)
Ho_2O_3	10.6065	Roth and Schneider (1960)
Er_2O_3	10.5473	Roth and Schneider (1960)
Tm_2O_3	10.4866	Roth and Schneider (1960)
Yb_2O_3	10.4342(4)	Schleid and Meyer (1989)
Lu_2O_3	10.3907	Roth and Schneider (1960)

and are plotted in fig. 9. The C-type sesquioxide of La has not been reported and that of Ce is not well established. From samarium, the C-type is known as the low-temperature form at ordinary pressures; for the oxides above Tb, the C-type is the most stable at any temperature for ordinary pressures. Both the A- and C-forms of Pr are well known. The A-type is the most common for Nd but the C-type has been observed. The intermediate members of the series can readily be prepared in any of the three forms [see Boulesteix (1982) for a detailed account of the stabilities and transformations among these three types].

The B-form sesquioxide is a monoclinic distortion of the A-form and the transformation of A- to B-form is displacive. Table 8 lists the lattice characteristics of the B-form sesquioxides. The heavier members of the group listed are nearly always found as C-form. The transformation of A- or B-form to the C-type is reconstructive, accounting for the integrity problems encountered on cooling after the crystal growth (see above). The structural relationships of the A-, B- and C-type sesquioxides juxtaposed against the fluorite structure are illustrated in fig. 10 (see Eyring and Holmberg 1963).

1.3.3. *The dioxides*

The dioxides of Ce, Pr and Tb (see table 9) crystallize in the fluorite structure type. The lattice parameters are $a = 5.4109$ Å (Height and Bevan 1979), $a = 5.3932$ Å

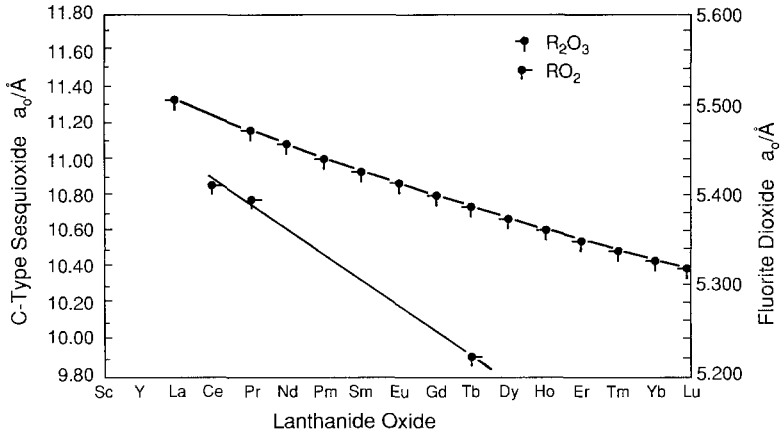

Fig. 9. Lattice parameters for the cubic rare-earth oxides (after Eyring 1979).

TABLE 8
B-type structures of R_2O_3 (C12/ml, No.12 I.T.) (after Schweda 1992).

Compound	a (Å)	b (Å)	c (Å)	β(°)	Reference
Pm_2O_3	14.22	3.65	8.91	100.1	Chikalla et al. (1972)
Sm_2O_3	14.1975 (9)	3.6273 (3)	8.8561 (5)	99.986 (5)	Schleid and Meyer (1989)
Eu_2O_3	14.1105	3.6021	8.808	100.037	Yakel (1978)
Gd_2O_3	14.061 (13)	3.566 (6)	8.760 (7)	100.10 (8)	Guentert and Mozzi (1958)
Tb_2O_3	14.04 (1)	3.541 (3)	8.725 (8)	100.00	Hoekstra (1966)
Dy_2O_3	13.97 (1)	3.519 (3)	8.661 (8)	100.06 (5)	Hoekstra (1966)
Ho_2O_3	13.90 (1)	3.492 (3)	8.59 (8)	99.98 (5)	Hoekstra (1966)
Er_2O_3	13.87 (1)	3.47 (3)	8.555 (8)	100.17 (5)	Hoekstra (1966)
Tm_2O_3	13.81 (1)	3.447 (3)	8.505 (8)	100.20 (5)	Hoekstra (1966)
Yb_2O_3	13.73 (1)	3.425 (3)	8.452 (8)	100.17 (5)	Hoekstra (1966)
Lu_2O_3	13.70	3.41	8.425	100.22	Hoekstra (1966)

(Sawyer et al. 1965b) and $a = 5.2156$ Å (Langley, unpublished work), respectively (plotted in fig. 9 and listed in table 9). The C-type and all the higher oxides considered are fluorite-related (see fig. 10). The parameters were determined on powders having particle diameters in the range of microns. However, Gamarnik (1988) found a monotonic increase in the unit cell parameter of CeO_2 thin films with grain size in the range of 25 nm and below, decreasing about one-half percent for the smallest sizes. This decrease was attributed to a reduction in the internal crystal pressure in the small crystals.

Duclos et al. (1988) studied the effect of pressure on CeO_2 up to 70 GPa. The volume of the CeO_2 was observed to decrease about 11% up to a loading of 31.5 GPa at which point a 7.5% volume decrease accompanied a transformation to an orthorhombic structure with $a = 5.457$ Å, $b = 6.521$ Å, $c = 3.427$ Å and $Z = 4$. The space group of this high-pressure form is Pnam. This transition was found to be unquenchable. The bulk modulus of CeO_2 reported from this study is 23 ± 10 GPa.

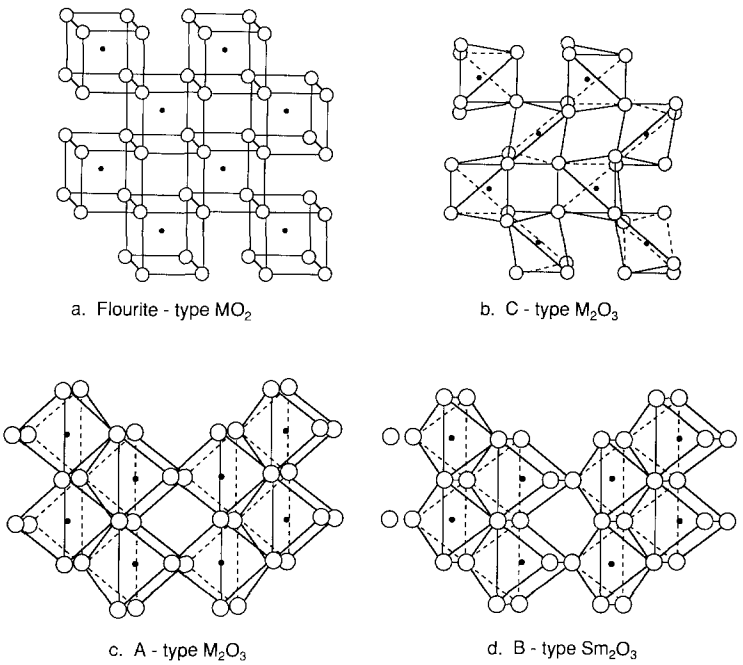

Fig. 10. Representations of (a) fluorite-type RO_2, (b) C-type R_2O_3, (c) A-type R_2O_3 and (d) B-type R_2O_3. The solid dots represent the metal atoms (after Eyring and Holmberg 1963).

TABLE 9
Lattice constants of the lanthanide dioxides.

	Fluorite type ($FM\bar{3}M$) (Å)	Orthorhombic (Pnam) (Å)	References
CeO_2	5.4109(3)	$a = 5.457$ $b = 6.521$ $c = 3.427$	Duclos et al. (1988)
PrO_2	5.3932(5)		Sawyer et al. (1965b)
TbO_2	5.2156(6)		Langley (unpublished)

1.3.4. *The intermediate oxides*

The intermediate oxides, whether or not they belong to the homologous series, have oxygen-deficient, fluorite-related structures. The structures have been solved for only seven of the homologous series (Ln_nO_{2n-2}) and for none of the other intermediate phases, such as $Tb_{62}O_{112}$. Among the cerium oxides, only the iota phase ($n = 7$) structure has been determined (Ray and Cox 1975a), although it is likely that the structure of the $n = 11$ phase is isostructural with $Tb_{11}O_{20}$. More structures have been determined in the praseodymium–oxygen system than in the other two. Those for $n = 7$ (Von Dreele et al. 1974), and for 9, 10 and 12(1) (Zhang et al. 1993a and Zhang et al.,

TABLE 10
Lattice constants of intermediate cerium oxides.

Composition	Lattice constants in Å						Relationship to fluorite*		
	a	b	c	α	β	γ	$2a$	$2b$	$2c$
Ce_7O_{12}	6.7997	6.7997	6.7997	99.4	99.4	99.4	$[21\bar{1}]$	$[\bar{1}21]$	$[1\bar{1}2]$[1, 2]
$Ce_{11}O_{20}$	6.750	9.900	6.750	90.00	99.21	96.30	$[21\bar{1}]$	$[\bar{1}32]$	$[1\bar{1}2]$[3]
$Ce_{19}O_{34}$	6.750	8.400	6.750	97.30	99.21	75.00	$[21\bar{1}]$	$[\bar{1}41]$	$[\bar{2}\bar{1}3]$[3]
$Ce_{62}O_{112}$	isomorphous with $Tb_{62}O_{112}$								

* After Schweda (1992)
[1] Ray and Cox (1975a)
[2] Ray and Cox (1975b)
[3] Knappe and Eyring (1985)

unpublished results) have been solved. Among the terbium oxides those for $n = 7$ and 11 have been determined (Zhang et al. 1993b). The known structures have all been determined from neutron powder diffraction information gathered according to the Rietveld method and processed utilizing the GSAS program (Larson and Von Dreele 1986). The lattice parameters are given in tables 10–12.

On the basis of the known unit cells, certain assumptions about the connectivities of the apparent defect clusters and symmetry considerations, the structures of the homologous series were proposed by Schweda et al. (1991). The cluster Ln_7O_{30}, consisting of the seven metal atoms surrounding two vacant oxygen sites along $\langle 111 \rangle_F$, and including all the other nearest-neighbor oxygens, was considered to be the characteristic structural element in all the Ln_nO_{2n-2} oxides. The $n = 7$ structure consists only of these clusters which also exist in the $n = 9$ and 10 members of the praseodymium oxide system but not in the others that are known.

The recent solution of the five additional structures in the homologous series enumerated above allows a much more general description of the structural principle governing these higher lanthanide intermediate oxides. An examination of tables 10–12 shows that all the members of the homologous series have one axis in common, namely $\frac{1}{2}\langle 21\bar{1} \rangle_F$. The series has two structural branches each with a common but different c-axis and with the b-axes depending on n. One structural branch, with one known exception, has primitive unit cells and odd n and usually low symmetry, while the other of even n has chemically twinned primitive unit cells typically with monoclinic symmetry.

The structural principle for the homologous series can be outlined as follows. The fluorite structure consists of an fcc array of Ln atoms in which all (and only) the tetrahedral intersticies are occupied with oxygen atoms. Metal atoms have oxygens at the corners of a coordination cube, while the oxygens are tetrahedrally coordinated with metal atoms. The intermediate phase compositions and structures are realized by the omission of oxygen atoms in a regular way. Except for small shifts away from the vacant oxygen sites (V_O) (about 0.18 Å), the metal atoms maintain their fcc positions. The six oxygen atoms nearest a vacant site move inward by about 0.3 Å. This leads to a cluster that can be formulated as $Ln_4O_6V_O$, which, together with a characteristic group,

TABLE 11
Lattice constants of intermediate praseodymium oxides.

Composition	Lattice constants in Å						Relationship to fluorite*		
	a	*b*	*c*	α	β	γ	2*a*	2*b*	2*c*
Pr_7O_{12}	6.7431(6)	6.7431(6)	6.7431(6)	99.306(6)	99.306(6)	99.306(6)	$[21\bar{1}]$	$[\bar{1}21]$	$[1\bar{1}2]$[1]
Pr_9O_{16}	6.7420(7)	8.715(1)	6.6732(7)	97.429(1)	100.000(1)	75.298(1)	$[21\bar{1}]$	[031]	$[1\bar{1}2]$[2]
$Pr_{11}O_{20}$	6.7	42.5	15.5	90.00	125.2	90.00[3]	$[21\bar{1}]$	$[\bar{1}32]$	$[1\bar{1}2]$[3]
$Pr_{16}O_{30}$ (π3)	6.67	30.82	15.41	90.00	125.3	90.00[4]	$[21\bar{1}]$	[088]	$[2\bar{3}3]$[2]
$Pr_{24}O_{44}$	6.6838(3)	11.5980(5)	12.8248(6)	90.00	99.975(5)	90.00[2]	$[21\bar{1}]$	[033]	$[2\bar{3}3]$[2]
$Pr_{40}O_{72}$	6.7358(4)	19.406(1)	12.8028(7)	90.00	100.214(1)	90.00	$[21\bar{1}]$	[055]	$[2\bar{3}3]$[2]

* After Schweda (1992)
[1] Von Dreele et al. (1974)
[2] Zhang et al. (1993a)
[3] Tuenge and Eyring (1979)
[4] Kang et al. (1992a)

TABLE 12
Lattice constants of intermediate terbium oxides.

Composition	Lattice constants in Å						Relationship to fluorite*		
	a	*b*	*c*	α	*β*	*γ*	2*a*	2*b*	2*c*
Tb_7O_{12}(ι)	6.5082(3)	6.5083(4)	6.5082(3)	99.3420(1)	99.3420(1)	99.3410(4)	$[21\bar{1}]$	$[\bar{1}21]$	$[1\bar{1}2]$[3]
$Tb_{11}O_{20}$(δ)	6.5099(2)	9.8298(6)	6.478(4)	90.019(2)	99.966(1)	95.886(1)	$[21\bar{1}]$	$[\bar{1}32]$	$[1\bar{1}2]$[3]
$Tb_{24}O_{44}$(β2)	6.4000	12.240	12.240	79.52	100.03	69.63	$[21\bar{1}]$	[233]	$[2\bar{3}3]$[2]
$Tb_{48}O_{88}$(β3)	6.700	23.200	15.500	90.00	125.25	90.00	$[21\bar{1}]$	[066]	$[0\bar{4}4]$[1]
$Tb_{62}O_{112}$(δ′)	13.800	16.200	12.100	121.0	107.4	100.10	$[\bar{1}05]$	$[\bar{4}\bar{4}\bar{2}]$	$[4\bar{2}0]$[1]
$Tb_{16}O_{30}$(π)	6.4	14.8	7.4	90.00	125.2	90.00[2]			

* After Schweda (1992)
[1] Kunzmann and Eyring (1975)
[2] Tuenge and Eyring (1982)
[3] Zhang et al. (1993b)

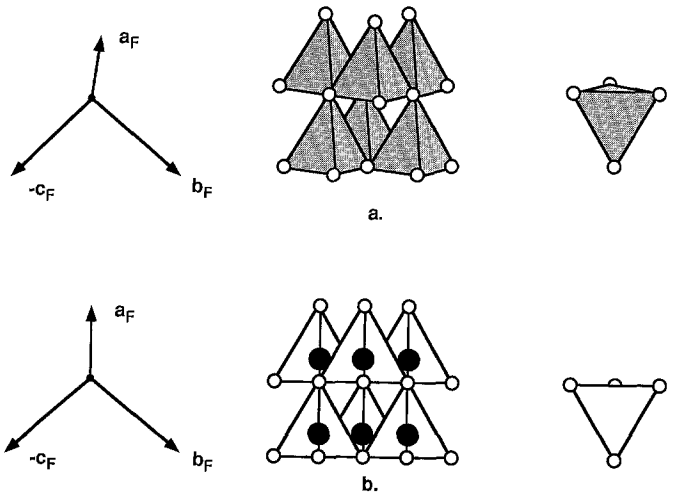

Fig. 11. Projections along [21$\bar{1}$] in (b) but tilted 5° in (a) showing the tetrahedrally coordinated vacant oxygen site and its immediate surroundings.

$Ln_{1/2}O$, of the fluorite structure make up all the intermediate oxide structures. This defect cluster and its environment are illustrated in fig. 11 (Hoskins and Martin 1976, Sørensen 1981). In the three Ln_7O_{12} structures, Pr_9O_{16} and $Pr_{10}O_{18}$, these defects are dimerized to give $LN_{7/2}O_6V_O$ clusters but in the other two known structures the defects are separated. The structures of the known intermediate oxides are shown projected along [2 1 $\bar{1}$] in fig. 12.

Upon examination of all the known structures, the following principles can be stated. (1) Vacancy cluster dimers of two types are found in the C-type sesquioxide. The one with vacant oxygen sites separated by $\frac{1}{2}\langle 1\,1\,1\rangle$ along $\langle 1\,1\,1\rangle$ occurs one third as often as those with vacant oxygen sites separated by $\frac{1}{2}\langle 1\,1\,0\rangle$. Only the former is found in the higher oxides and then only in $n = 7, 9$ and 10. (2) The tendency of the elementary clusters to associate decreases with their concentration. Dimers with the largest possible separation are found in Ln_7O_{12}, Pr_9O_{16} and $Pr_{10}O_{18}$ but are dissociated in $Tb_{11}O_{20}$ and $Pr_{12}O_{22}$. ($Pr_{11}O_{20}$ has a very large unit cell that is probably monoclinic.)

In structures where $n = 7$ or above, overlapping clusters are not observed, and maximum separation of the clusters occurs consistent with the composition, dimensions and symmetries of the unit cell. Furthermore, relaxation of the cation sublattice is observed to be maximized. In particular, although in the $n = 7$ structures double vacancies do occur along $\langle 1\,1\,1\rangle$, both across metal atoms and where no metal atoms separate them, the latter are not found in any other known structures, even for $n = 9$. The only intermediate compound reported for the actinide oxides is the iota phase, An_7O_{12} (see sections 2 and 3). However, efforts to prepare other phases have not been extensive. They might occur in the heavier oxides of the series from Pu to Es since these may possess both the 3+ and 4+ oxidation states. The structural principles appropri-

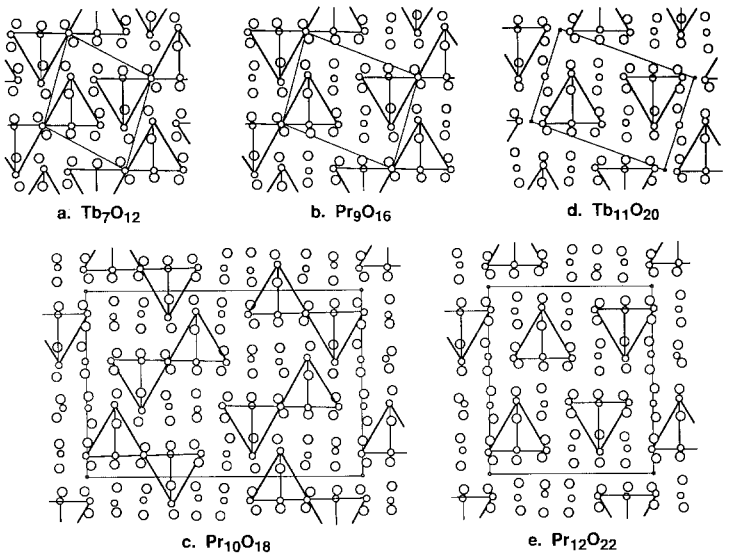

Fig. 12. Projections along $[21\bar{1}]$ of the structures of the five known members of the Ln_nO_{2n-2} homologous series: (a) Tb_7O_{12} and the corresponding Pr and Ce oxides, (b) Pr_9O_{16}, (c) $Tb_{11}O_{20}$, (d) $Pr_{10}O_{18}$, and (e) $Pr_{12}O_{22}$.

ate to fluorite-related, ordered phases of mixed higher valence could be further honed if they could be extended to the actinide series.

1.3.5. *The nonstoichiometric oxides*

As discussed above, and as is clearly shown in the phase diagrams (figs. 3–5), at higher temperatures and oxygen pressures, the regions of ordered intermediate phases of narrow composition give way to two phases of wide composition range separated by a miscibility gap. The nonstoichiometric phase of lower composition is labeled σ and has a C-type-related structure with a lattice constant that decreases with increasing oxygen composition. The disordered phase of higher composition, designated α, has a fluorite structure with decreasing lattice parameter as LnO_2 is approached.

In the PrO_x system, careful examination has revealed that the σ phase shows an unmixing at temperatures below 400°C into two C-type phases, ϕ and κ. The lattice parameter $a_C = 11.152$ Å is approximately $2a_F$, where a_F is the lattice parameter of the related fluorite phase. The intensities of the diffraction maxima that are derived from the doubling of the fluorite unit cell are diminished and modified with an increase in oxygen content. The unit cell of the C-type sesquioxide (fig. 10b) can be considered as consisting of eight fluorite unit cells from which one fourth of the oxygen atoms have been removed in an ordered way. All oxygens in nonintersecting strings along the four $\langle 1\,1\,1 \rangle$ directions are missing, (i.e., along the body diagonals of the RO_8 coordination cubes of the R atoms). Where the strings approach one another most closely, vacant oxygen sites are generated across the face diagonals of the RO_8 coordination cubes leaving all the R atoms six-coordinated and of two geometries. The face-diagonal

vacancies with the shortest vacancy–vacancy distances (which do not occur in any of the higher oxides) outnumber the body-diagonal vacancies by three to one. It is of great interest to discover the changes in the vacant oxygen sites across the σ phase and compare this development with the corresponding systems in the actinide series.

Isobaric studies of the α region of the PrO_x system in the composition range $1.778 < x < 1.833$ by Jenkins et al. (1970) showed that if isopleths were derived from the equilibrium isobaric data, four distinct regions of the α phase could be recognized. High-temperature X-ray studies also suggested the same complexity, especially at the lower temperatures of their existence. Subsequently, Lincoln et al. (1988) determined isopleths in the same region of the phase diagram and found that although the isopleths themselves did not show the breaks found in the derived isopleths of Jenkins et al., the isobars derived from their isopleths did indeed indicate four regions. On the basis of their study, Lincoln and his co-workers proposed that the subphases which appear to make up the nonstoichiometric α phase result from modulated, sometimes incommensurate, characteristic structures within each of the different α regions. This same phenomenon could cause the widespread pseudophase behavior observed in the two-phase regions of these systems in which a bivarient behavior is displayed when a disordered phase becomes ordered (see Hyde et al. 1966, Turcotte et al. 1971a,b). As the transition temperature for the α phase to any stable ordered intermediate structure is approached, modulations characteristic of the local composition might appear as the disorder–order boundary is crossed. The irregularities, largely in the form of stacking faults along certain characteristic directions, might become regular and characteristic of the particular ordered phase formed.

A recent study of PrO_2 irradiated in the microscope shows a rather complex behavior (Eyring and Kang 1991). Within a short time of irradiation, a modulation developed in the fluorite pattern that evolved into a new superstructure, later identified by Kang et al. (1992a) as the $n = 16$ member of the homologous series. As the observation continued, a new modulation gradually replaced the old then evolved into the ordered β phase. These structural changes have not previously been observed during dynamic change but are suggested by some thermodynamic events that are described below. This premonitory behavior may be typical of these nonstoichiometric phases as ordered regions are approached. Further studies, including the actinide oxides where possible, are required to sort out this curious behavior of widely nonstoichiometric compounds.

1.3.6. *High-pressure effects*

There have been a few studies of the effect of pressure on the sesquioxides. Sawyer et al. (1965a) found that under extreme pressure some of the C-type sesquioxides transformed to the A- or B-type. Hoekstra (1966) applied pressure to the whole series of sesquioxides and found the transformation of all of the C-type (Sm_2O_3 to Lu_2O_3) to the B-type. This transformation is consistent with the decreased molar volume of the B-type compounds. Lattice parameters are listed in table 8.

1.3.7. *Special electron microscopic observation*

The oxides of Ce, Pr and Tb have been studied *in situ* in an environmental cell (Schweda et al. 1987). Oxidation and reduction of the oxides was accomplished by

adjustment of the oxygen pressure and temperature of the sample within the environmental cell. Only the most stable of the intermediate phases were detected in these experiments. Furthermore, in nearly all instances the observed structures were those less oxidized than would have been expected from the equilibrium information available. It was believed that this discrepancy is accounted for as electron-beam-induced reduction.

Gasgnier et al. (1987) examined the behavior of oxide thin films of Ce, Pr and Tb contaminated with water and CO_2 subjected to the electron beam of an electron microscope. The reactions involved were complex and varied significantly from those made in the absence of the contaminants. They concluded that the electron beam impact itself resulted in beam-induced catastrophic events that could lead to unusual chemical effects. Earlier experiments (Gasgnier et al. 1986, 1987) had shown an unusual oxidation of the sesquioxides of Ce, Pr and Tb in the microscope vacuum during HREM observation. These results resemble a vapor phase leaching of the oxide resulting in a disproportionation of a surface reaction of the Knotek–Feibleman type (Knotek and Feibleman 1979) oxidation involving Auger emission, or a beam-induced reaction with residual OH or H_2O vapor.

In-situ high-resolution electron microscopic studies have provided insights at the atomic level into the structures and structural defects in the surface and thin-film regions of specimens. Kang et al. (1987) and Kang and Eyring (1992) have studied surface profiles and substructures in the CeO_2 and PrO_x systems. The dominance of the $\{1\ 1\ 1\}_F$ planes was established in the surface structures. Surface reconstruction was observed frequently to be related to the subsurface superstructures and defects.

The transformation of $Tb_{24}O_{44}$ to $Tb_{48}O_{88}$ through a partially ordered intermediate construction characterized by wavy fringes into which nuclei of the product phase emerged was followed in HREM by Kang et al. (1989).

1.4. *The thermodynamic properties of the lanthanide oxides*

1.4.1. *The derived functions*

The lanthanide oxides are among the most thermodynamically stable compounds. Their free energies of formation are in the range between those for Al_2O_3 and CaO as shown in fig. 13. Their melting points, which are in the vicinity of 2400°C, and their boiling points, of the order of 3900°C, are listed in table 13. The standard entropy, enthalpy and Gibbs free energies of the sesquioxides are tabulated in table 14. Table 15 lists the same quantities for the other lanthanide oxides. The phase diagrams discussed above show added thermodynamic information, especially phase relationships. For further thermodynamic information and comparisons with the actinide oxides the reader is referred to section three of this chapter and chapter 122 (by Morss) of this volume.

1.4.2. *Equilibrium vaporization behavior*

The thermodynamic properties of the gaseous oxide species have been recently reviewed in this series by Chandrasekharaiah and Gingerich (1989). The vapor species R, RO, R_2O, RO_2 and R_2O_2 are observed above the solid or molten oxides at high

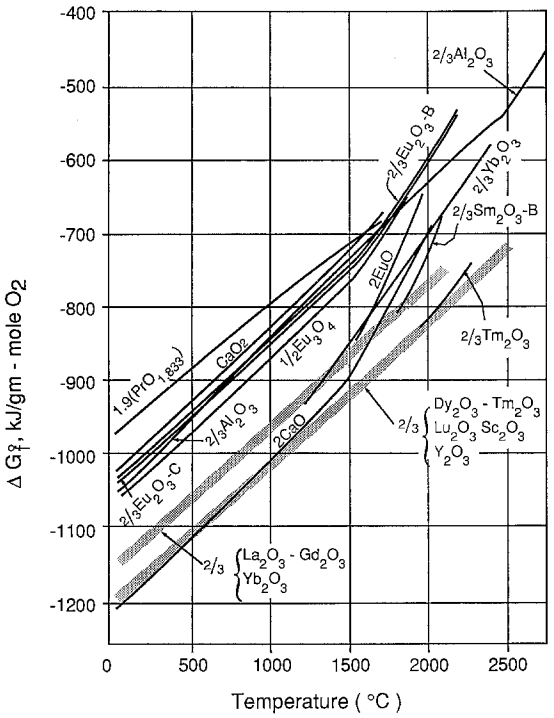

Fig. 13. The free energy of formation of the rare-earth oxides. Some common oxides are added for comparison. Dotted regions replace individual curves as indicated (after Gschneidner et al. 1973).

TABLE 13
The freezing and boiling points of the lanthanide sesquioxides.

Lanthanide oxide	Freezing point (°C)	Boiling point (°C)
La_2O_3	2256[1]	3620
	2304[2] ± 5	
Ce_2O_3	2210[3] ± 10	3730
Pr_2O_3	2183[1]	3760
Nd_2O_3	2233[1]	3760
Pm_2O_3	2320[4]	
Sm_2O_3	2269[1]	3780
Eu_2O_3	2291[1]	3790
Gd_2O_3	2339[1]	3900
Tb_2O_3	2303[1]	
Dy_2O_3	2228[1]	3900
Ho_2O_3	2330[1]	3900
Er_2O_3	2344[1]	3920
Tm_2O_3	2341[1]	3945
Yb_2O_3	2355[1]	4070
Lu_2O_3	2427[1]	3980

[1] Noguchi (1969)
[2] Sata (1966)
[3] Sata and Yoshimura (1968)
[4] Gibby et al. (1970)

TABLE 14
Some thermodynamic properties of the lanthanide sesquioxides.

Lanthanide oxide	S^0_{298} for R_2O_3[1] $Jk^{-1}mol^{-1}$ (est)	(obs)	S^0_{298} for metal 1 J/kmol	$-\Delta H^0_{298}$[2] kJ/mol	$-\Delta G^0_{298}$[2] kJ/mol
La_2O_3	127	128.0	57.07	1794$^+$	1706
Ce_2O_3	152		69.79	1796$^+$	1708
				1823$^+$	1735
Pr_2O_3	159	159	73.18	1823*	1735
Nd_2O_3	159	154.5	73.39	1808$^+$	1719
Pm_2O_3			[71.96]	[1813]	1724
Sm_2O_3	148	151	69.62	1824#	1736
				1828*	1740
Eu_2O_3	146		[71.1]	1651#	1560
				1663*	1572
Gd_2O_3	152	151	65.98	1816#	1730
				1827*	1741
Tb_2O_3	157		73.14	1865*	1776
Dy_2O_3	159	150	74.77	1863*	1772
Ho_2O_3	160	158	75.31	1881*	1792
Er_2O_3	157	153	73.30	1898*	1809
Tm_2O_3	153		72.68	1889*	1800
Yb_2O_3	144	133	[62.76]	1815*	1726
Lu_2O_3	109		[51.00]	1878*	1788

[1] Westrum (1967)
[2] Gschneidner et al. (1973)
$^+$ A-type
* C-type
# B-type

temperatures. Of these, RO is the most abundant and has been studied most completely. Tables 16 and 17 list some of the thermodynamic properties of the vapor species. Dulick et al. (1986) used crystal-field theory to identify the energy levels of low-lying states of the monoxides. These states were used to calculate the thermal functions from which dissociation energies could be derived leading to a model for promotion energies for the transition $4f^{n+1}\,5d^0 \rightarrow 4f^n\,5d^1$. These authors tabulate the lowest-energy electronic states of LnO, thermodynamic properties for LnO, and gaseous thermochemical equilibria including dissociation energies for LnO.

The vaporization thermodynamics of EuO and Eu_3O_4 have been reported by Haschke and Eick (1969, 1968). They found $\Delta G^0_f(298) = -581.6$ kJ/gfw for EuO and $\Delta G^0_f(298) = -2152$ kJ/gfw for Eu_3O_4. In each case the gaseous species was metal vapor and the solid product was the next higher oxide.

1.5. *Dynamic considerations*

1.5.1. *The tarnishing of the lanthanide metals with oxygen*

The high stability of the lanthanide oxides assures that the metal is unstable in the presence of oxygen. The tarnishing of the metals is facile, in most cases with a rapid rate

TABLE 15
Thermodynamic properties of other rare-earth oxides.

Oxide	S^0_{298} [1] ($J K^{-1} mol^{-1}$)	$-\Delta H^0_{298}$ [2] ($kJ mol^{-1}$)	$-\Delta G^0_{298}$ [2] ($kJ mol^{-1}$)
$CeO_{1.67}$	72.0		
$CeO_{1.72}$	69.0		
$CeO_{1.78}$	67.8		
$CeO_{1.81}$	67.8		
$CeO_{2.0}$	61.5	1089	1026
$PrO_{1.703}$	[79.9]	935.1	
$PrO_{1.717}$		937.2	
$PrO_{1.74}$	[80.3]		
$PrO_{1.804}$		947.7	
$PrO_{1.833}$	79.9	947.7	893.3
PrO_2	79.9	958	898.9
SmO	[65.7]		
EuO	[68.2]	597.9	569.0
Eu_3O_4		2255	2130
$TbO_{1.70}$		934.3	
$TbO_{1.72}$	80.8		
$TbO_{1.806}$		947.3	
$TbO_{1.81}$	81.2		
$TbO_{1.817}$		962.3	
$TbO_{1.975}$		970.7	
$TbO_{2.0}$	82.8	972	

$CeO_2(g)\ \Delta G^0_f = -13150 + 6.98\,T\,K^{-1}$

[1] Westrum (1967)
[2] Gschneidner et al. (1973)

TABLE 16
The Gibbs energy functions and the electronic statistical multiplicities for the rare-earth monoxides. Chandrasekharaiah and Gingerich (1989).

Monoxide	Electronic multiplicities	$-(G^0_T - H^0_0)/T$ ($J K^{-1} mol^{-1}$)			
		2000 K	2200 K	2400 K	2600 K
LaO	2	271.83	275.22	278.28	281.16
CeO	6	280.09	284.09	287.15	289.99
PrO	8	283.47	286.86	289.95	292.80
NdO	10	285.52	288.91	292.00	294.85
SmO	12	287.57	290.91	294.01	296.85
EuO	16	290.12	293.47	296.56	299.41
GdO	9	285.73	289.07	292.17	295.01
TbO	20	292.50	295.89	298.95	301.79
DyO	12	288.53	291.92	294.97	297.82
HoO	12	288.74	292.09	295.18	298.03
ErO	10	287.40	290.58	293.84	296.69
TmO	8	285.68	289.03	292.13	294.97
YbO	6	280.59	286.94	290.03	292.88
LuO	2	274.51	277.90	280.96	283.80

TABLE 17
The enthalpy of formation ($\Delta H^0_{f.0.}$) and the dissociation enthalpies (D^0_0) of rare-earth monoxides (kJ/mol)[a].

Monoxide	$-\Delta H^0_{f.0.}$	Dissociation enthalpy, D^0_0				
		a	b	c	d	e
LaO	121.0 ± 10.0	795 ± 9.6	797 ± 11	795 ± 9.6	794 ± 4.1	794.9 ± 10
CeO	117.0 ± 20.9	790 ± 17	801 ± 13	97 ± 9.6	786 ± 16.7	789 ± 10
PrO	133.9 ± 12.5	745 ± 9.5	743 ± 17	749 ± 9.6	736.4 ± 12.5	746.8 ± 10
NdO	125.5 ± 12.5	706 ± 12.5	698 ± 13	711 ± 9.6	698.7 ± 12.5	707 ± 10
SmO	117.0 ± 12.5	569 ± 9.6	567 ± 17	557 ± 9.6	569 ± 12.5	569 ± 10
EuO	46.0 ± 12.5	465 ± 15	479 ± 17	463 ± 9.6	468.6 ± 12.5	463.2 ± 10
GdO	66.9 ± 12.5	711 ± 12.5	710 ± 13	674 ± 9.6	711 ± 12.5	711.1 ± 10
TbO	54.4 ± 20.9	693 ± 21	704 ± 17	686 ± 9.6	690.4 ± 20.9	704.4 ± 10
DyO	75.3 ± 20.9	607 ± 21	611 ± 42	607 ± 9.6	610.8 ± 20.9	603 ± 10
HoO	54.4 ± 12.5	613 ± 9.6	607 ± 25	620 ± 9.6	602 ± 12.5	616.6 ± 10
ErO	37.7 ± 12.5	606 ± 9.6	604 ± 21	611 ± 9.6	602.5 ± 12.5	607.9 ± 10
TmO	31.4 ± 20.9	508 ± 9.6	507 ± 21	507 ± 9.6	510.5 ± 12.5	555.8 ± 10
YbO	−2 ± 21	401 ± 21	414 ± 8	406 ± 9.6	397.5 ± 20.9	355 ± 10
LuO	−8.4 ± 12.5	663 ± 9.6	671 ± 17	661 ± 9.6	665.3 ± 12.5	693 ± 10

[a] Chadrasekharaiah and Gingerich (1989)
[b] Pedley and Marshall (1983)
[c] Ackermann and Chandrasekharaiah (1975)
[d] Murad and Hildenbrand (1980)
[e] Huber and Herzberg (1979)

during which oxygen is dissolved in the metal, followed by a parabolic rate law during the build-up of a continuous oxide film through which oxygen must diffuse; then other mechanisms that depend on the nature and quality of the oxide diffusion barrier come into play. The composition of the oxide layer during the reaction is certainly dependent on the type and purity of the element involved and the conditions of the measurement. Some early experiments concerning this process were summarized by Eyring (1979).

1.5.2. *Atomic transport*

The fluorite-related lanthanide oxides exhibit unusual diffusional properties. The conventional rule-of-thumb is that atomic mobility in a solid does not become significant until one-half of the melting point temperature (the Tammann temperature) is reached. In these oxides this value is about 1200°C. At the Tammann temperature the metal atoms in lanthanide oxides just begin to become mobile as confirmed by the temperatures required for solid-state reactions. The oxygen substructure, to the contrary, is mobile below 300°C. This leads to a situation where equilibration and reaction must be considered for each substructure separately (see Bevan and Summerville 1979). This places the lanthanide oxides with fluorite-related structures in the category of fast-ion conductors along with, e.g., calcia-stabilized zirconia as indicated in table 18.

CeO_x has been used by Millot and de Mierry (1985) to test a new technique for determining chemical diffusion in nonstoichiometric oxides and to compare results with older methods. At 971°C the transport number for oxygen is one.

TABLE 18
Oxygen self diffusion in rare-earth oxides.

Compound	Activation energy (kJ/mol)	Temperature range (°C)	D_0 (cm^2/s)	D (1000 K)	Ref.
$Zr_{0.858}Ca_{142}O_{1.858}$	130.5	781–1097	1.8×10^{-2}	8.1×10^{-8}	[1]
Nd_2O_3(99.999%)	130	700–1000	1.3×10^{-4}	7.7×10^{-10}	[2]
Sm_2O_3(99.9%)	98.3	700– 950	9.2×10^{-6}	8.96×10^{-10}	[2]
Sm_2O_3(99.998%)	89.1	700–1000	6.0×10^{-6}	1.39×10^{-9}	[2]
Er_2O_3(99.999%)				10^{-14}	[2]
Pr_7O_{12}(low temp)	34.3	725– 930	9×10^{-8}	3.58×10^{-9}	[3]
Pr_7O_{12}(high temp)	79.70	725– 930	2.9×10^{-8}	1.65×10^{-9}	[3]

[1] Simpson and Carter (1966)
[2] Stone et al. (1968)
[3] Weber and Eyring (1970)

1.5.3. *The kinetics of phase reactions*

A discussion of the kinetics of reaction of oxygen with the rare-earth metals, or with their oxides, should be approached with the following in mind. The oxides of the rare-earth elements are among the most stable known. The oxidation paths in terms of the number and variety of intermediate steps that must be taken are complex. There are many possible intermediate configurations involving intergrowths of the end-members or the occurrence of behaviors that have been termed pseudophase formation where a material behaves as though it were a single phase of variable composition in a two-phase region. Structural modulation, either commensurate or incommensurate, may occur. Furthermore, a wide variety of interface constructions or defect clusters must exist. On a larger scale, extended defects such as stacking faults, dislocations, or interfacial boundaries can further complicate the reaction rates. This incomplete list of problems is certainly daunting and, in such complex systems, a true atomic mechanism cannot yet be promulgated. Nevertheless, it is useful where possible to arrive at phenomenological mechanisms from which physical quantities, such as activation energies, can be estimated to yield a useful base from which to attach knowledge gained from the observation of these reactions.

Nearly all of the information available on the kinetics of heterogeneous reactions with lanthanide oxides concerns the C-type sesquioxides or the fluorite-related higher oxides. As stated in the section above, in these materials oxygen mobility is very high, whereas, metal-atom movement is extremely limited below 1200°C. Table 19 suggests the type of experiments that were done and the phenomenological mechanisms proposed before 1980 (Eyring 1979).

Since 1980, much has been learned about the details of structure among the higher oxides of Ce, Pr and Tb. These details cause one to appreciate the importance of differentiating between a detailed mechanism and a phenomenological one. In this light, Inaba et al. (1980, 1981a), Sugihara et al. (1981a, b) undertook to describe the oxidation and reduction in the following reactions,

TABLE 19
Heterogeneous reactions in rare-earth oxides.

Reactant	Rate controlling mechanism	Activation energy (kcal/mol)	Temperature range (°C)	Oxygen pressure	D_{02} (cm/s) ($\times 10^4$)	D (100 K) ($\times 10^{10}$)	Ref.
$PrO_{2.00}$	Phase boundary	209	289– 347	vac			[1]
$PrO_{1.83}$	Phase boundary	113	265– 305	1 atm			[1]
$PrO_{1.78}$	Phase boundary	207	407– 493	vac			[2]
$PrO_{1.778}$	Phase boundary	67	464– 503	0.1–50 Torr			[4]
		C-type 105					
$PrO_{1.50}$	Phase boundary	A-type 209	240– 320	138 Torr			
$PrO_{1.714}$	Complex model	190	535– 570	1–7 Torr			[6]
Pr_7O_{12}	Complex model	314/255	655– 715	0–280 Torr			[7]
$PrO_{1.71}$	Diffusion	176	700– 970	vac			[2]
*$TbO_{1.82}$	Diffusion	174	383– 471	vac			[2]
*$TbO_{1.71}$	Diffusion	~ 167	570– 643	vac			[2]
$CeO_{1.818}$	Interstitially	~ 42	20– 40	1 atm, air			
$Tb_2O_{3+\delta}$	Diffusion with a phase boundary	~ 50	708– 806	20–150 Torr			[5]
Dy_2O_3	Diffusion with a moving boundary	100	1087–1235	air	0.163	5.27	[3]
Ho_2O_3	Diffusion with a moving boundary	170	1050–1274	air	71.8	8.26	[3]
Er_2O_3	Diffusion with a moving boundary	126	1060–1292	air	1.31	0.958	[3]
Tm_2O_3	Diffusion with a moving boundary	190	1015–1235	air	114.0	1.97	[3]
Lu_2O_3	Diffusion with a moving boundary	124	1020–1297	air	1.88	1.58	[3]

* Behavior deviates from diffusion-like mechanism in the early stages of reaction (modified diffusion behavior)

[1] Hyde et al. (1965)
[2] Kuntz and Eyring (1959)
[3] Berard et al. (1968)
[4] Sugihara et al. (1981b) see text
[5] Sugihara et al. (1981a) see text
[6] Inaba et al. (1980) see text
[7] Inaba et al. (1981a) see text

$$PrO_{1.714} + 0.032O_2 \rightarrow PrO_{1.778}, \quad (1)$$

$$\tfrac{1}{7}Pr_7O_{12} + (\tfrac{1}{7} - \tfrac{x}{2})O_2 \rightarrow PrO_{2-x}, \quad (2)$$

$$\tfrac{10}{9}Pr_9O_{16} + \tfrac{1}{9}O_2 \rightarrow Pr_{10}O_{18}, \quad \text{and} \quad (3)$$

$$\tfrac{7}{2}Tb_2O_{3+\delta} + (\tfrac{3}{4} - \tfrac{7}{4}\delta)O_2 \rightarrow Tb_7O_{12}. \quad (4)$$

These reactions represent changes including order–disorder, order–order and all require consideration of the complexities mentioned above. Only reaction (3) could be fitted to one of the popular phenomenological mechanisms (the phase-boundary controlled mechanism in which it is assumed that the reaction at a receding boundary is the rate-controlling step of the reaction). In all the other reactions it was necessary to concoct a more involved model taking into account hysteresis and the increasing pressure of oxygen required to supply the continuing reaction. For reactions (1) and (2), calorimetric measurements (Inaba et al. 1981b, c) were also made to help clarify the reaction mechanisms which had to take into account coherently intergrown crystals, etc. There remains much to be learned in describing the mechanisms of these reactions.

1.6. *Other physical properties*

1.6.1. *Magnetic characteristics*

The lanthanide atoms and their compounds have been the systems whose magnetic studies have made possible theoretical understanding (Van Vleck 1965). Extensive magnetic susceptibility measurements have been made on the lanthanide oxides, especially the sesquioxides, and they have been found to follow Van Vleck's theory rather well [see the study of Pr_2O_3 by Lejus et al. (1976)]. Neutron-scattering experiments have also been extensively used to determine the magnetic structure of oxides (Eyring 1979, Sinha 1978). A particular example is the investigation of the magnetic ground state of PrO_2 by Kern et al. (1984). In this comprehensive study they found that PrO_2 orders antiferromagnetically at 14 K with a type I magnetic structure as found in UO_2. After many other considerations they proposed the ground state of PrO_2 to be the Γ_8 quartet with the degeneracy lifted by a dynamic Jahn–Teller effect.

Some magnetic properties of the lanthanides are presented in section 3 in comparison with the actinides. Table 33 and fig. 27 should be consulted for specific electronic configurations and magnetic moments in each series.

Krill et al. (1980) measured some magnetic properties of the monoxides of Sm, Nd and Pr produced at high pressures and temperatures. These studies were made up to 40 kGauss between 1.4 and 300 K. For both NdO and PrO the thermal variation of the susceptibilities, and the lattice parameters agree with a trivalent state of their metal atoms. For SmO, on the other hand, a nearly trivalent state is to be expected from the crystallographic and X-ray absorption data. The magnetic susceptibility is mainly temperature independent.

1.6.2. *Electrical properties*

Because of the high potential use of EuO in electronic devices, its study has been extensive (Wachter 1979). Some physical properties, which depend very much on the

TABLE 20
Physical properties of EuO crystals.

Class or growth region	Initial composition mol.% oxygen	Crystallization temp.(°C)	Conductivity	Characterization IR	Stoichiometry
I	50–47	> 1890	Insulating 0.45–0.7 eV activation energy	Shows spectrum of Eu_3O_4	Contains Eu_3O_4 as second phase
II	47–44	1825–1890	Insulating 0.45–0.7 eV activation energy	Eu^{3+} absorption lines	Single phase EuO with Eu vacancies
III	44–42	1780–1825	–	Low absorption $\alpha < 3\,cm^{-1}$	Stoichiometric EuO
IV	42–35	1680–1780	Insulator–metal transitions 0.3 eV activation energy	Oxygen vacancy absorption	Contains oxygen vacancies
V	< 35	below ~ 1600	Metallic conductivity	Free-carrier absorption	Many oxygen vacancies

preparative conditions, are listed in table 20 (see Shafer et al. 1972). The electrical conductivity of the lanthanide sesquioxides has been studied and the results are summarized in table 21. The electrical properties of the higher oxides have also been studied. In these higher oxides, electron conductivity appears to be by a hopping mechanism. Oxygen-ion mobility and hence ionic conductivity is also appreciable in these oxides (Eyring 1979).

Inaba and Naito (1983a, b) made simultaneous measurements of the oxygen pressure, composition, and electrical conductivity for two-phase reactions in the praseodymium oxide system. First (1983a), they studied the two-phase region involving the iota and zeta phases and the hysteretic behavior in their transformation by the addition or loss of oxygen. They suggest that the predominant defects are neutral interstitial oxygen atoms and doubly charged oxygen vacancies. The model of conductivity they propose is electron hopping, with different mobilities, between praseodymium ions in well-ordered positions in the structure. Conductivity–composition diagrams confirm the hysteresis behavior.

In the second study (1983b), Inaba and Naito made a corresponding study of the phase transition between the ordered epsilon phase ($Pr_{10}O_{18}$) and the disordered α-phase (PrO_{2-x}). The defect species were considered to be the same as above. The conductivity was found to be governed by the concentration of seven-coordinated Pr ions where the most rapid hopping occurs. The model suggested that PrO_{2-x} ought better to be considered $PrO_{1.78+x}$. Hysteresis was again displayed in the conductivity measurements.

Arakawa et al. (1986) have studied the conductivity of thin-film praseodymium oxides as a function of both temperature and oxygen pressure. They observed an n- to

TABLE 21
Electrical transport characteristics of rare-earth oxides.

Oxide	$E_a(T > T_B)$(eV)*			
	Noddack and Walch (1959)	Subba Rao et al. (1970)	Wilbert et al. (1975) (ionic conduction)	2** $\sigma_{650°C} \times 10^9$ $(\Omega cm)^{-1}$
La_2O_3	1.05	1.05		1700
Ce_2O_3				
CeO_2	1.10			
Pr_2O_3		0.95		3450
Pr_6O_{11}	0.55			
PrO_2				
Nd_2O_3	0.97	1.15	0.87	1450
Sm_2O_3	1.17	1.28	1.28	880
Eu_2O_3	1.24	1.35	1.09–1.41	150
EuO				
Gd_2O_3	1.36	1.57	1.42	130
Tb_2O_3		0.95		200
"Tb_4O_7"	0.40			
TbO_2				
Dy_2O_3	1.39		2.28	
Ho_2O_3		1.61	1.89	160
Er_2O_3	1.40		1.29	
Tm_2O_3			1.65	
Yb_2O_3	1.53	1.61	1.49	50
Lu_2O_3			1.96	

* $E_a(T > T_B)$(eV) = activation energy in the temperature above the break in the curve.
** $\sigma_{650°C}$ = DC electrical conductivity at 650°C measured at P_{O_2} approx. 150 Torr.

p-type conduction transition at 630°C and found the activation energy to be 1.75 eV for p-type and 0.88 eV for n-type conduction. In the range of p-type behavior the pressure depencence was as $P_{O_2}{}^{1/4}$.

The electrical conductivity and oxygen-association pressure measurements have been carefully studied in the near-dioxide region (e.g., by Professor Blumenthal and his co-workers in a long series of papers, see, for example, Chang and Blumenthal (1988). and references therein). In this region there are serious problems with impurities, notably calcium. These are, for our purposes, considered as ternary phases and hence are not reviewed here.

1.6.3. *Optical properties*

The color of all the stoichiometric oxides are white or a light pastel except for PrO_2 and TbO_2, which are black or reddish-brown, respectively. The colors of the non-stoichiometric oxides are dark bluish for CeO_x, black for PrO_x, and dark brown for TbO_x. The substoichiometric sesquioxides of the lanthanides are all dark. The color is extremely sensitive to the deviation from stoichiometry, except in PrO_2 and TbO_2.

Some optical properties of the oxides have been mentioned by Eyring (1979). Volume 10 of this series is devoted entirely to the spectroscopic properties of the lanthanides and their compounds including some oxides, see especially chapter 71 (Röhler 1987).

1.6.4. *Mechanical and thermo-mechanical properties*

These properties have been considered in reviews by Gibson and Harvey (1966), Vier (1975) and Eyring (1979). Such properties as thermal expansion, elastic properties and volume change accompanying stoichiometric variation have been considered.

2. The binary oxides of the actinide elements

2.1. *Introduction*

As stated in the opening section of this chapter, the objective is to discuss and compare the solid-state chemistry and physics of the lanthanide and actinide element oxides. The topics of discussion have been limited to binary oxides of these elements. Therefore, a discussion of the many complex (ternary, mixed, etc.) oxide systems for these f elements, and oxides of actinides representing oxidation states above four that do not have lanthanide counterparts, are not present.

In section 3, a one-on-one comparison of behavior is given for the 4f- and the 5f-element binary oxides. Although there are some significant differences between the chemistry and the properties of the lanthanide and actinide series, most notably being in the chemistry of the earlier actinides, Pa–Pu, these f-element oxides also have many similarities. In some aspects these f-block elements have many unique features with respect to the other elements in the periodic table. Thus, a comparison of the trends and differences in the chemistry of the oxides of these two f series provides valuable insights into their position in the periodic table.

The actinides have been accepted as a 5f series of elements, comparable to the lanthanides as being a 4f series, even though one may contest whether or not the earlier members of the actinides are truly f elements. The actinide concept, which integrates the elements from atomic number 89 through 103 into the periodic table, makes the actinide series a sister series of the lanthanides. Thus, actinium is placed under lanthanum (although neither is truly an f element) and the subsequent members of each series follow these two elements to the end members, Lu and Lr. There is an implied actinide electronic homolog for each lanthanide element, even though each homolog pair may not have comparable chemistry and/or physical properties. A case in point is neodymium and uranium: the oxide chemistry of neodymium is essentially that of its sesquioxide, while with uranium the main oxides are UO_2, U_3O_8 or even UO_3, and the sesquioxide of uranium is not a known phase.

Another important, and perhaps confusing point, is that for each series of f elements the electronic configuration may be different in the gaseous state, in solution or in the solid state. This adds to the complexity noted above that an actinide homolog may not display the same electronic nature as its lanthanide homolog in a given situation.

In principle, each series is formed by successively adding an electron to an f orbital when progressing to the next higher member. This process is best approximated in the lanthanide series and deviates the most for the lighter actinide metals. The complexity of electronic configuration that is found for the elemental state of the actinides is carried over to the oxides, and it is, together with the differences between 4f- and 5f-orbitals (e.g., spatial extension, greater screening, etc.), mainly responsible for the differences between the behavior that is observed for the oxides of these two f series of elements.

As opposed to the lanthanide elements, all of which are found in nature except for Pm, less than half of the actinides are naturally occurring. The first six actinides, Ac through Pu, have been found in nature, although Np and Pu exist in only minute amounts as a result of "natural" neutron reactions in some uranium ores. Practicably, only Th and U are extracted from natural sources (small amounts of Pa have also been obtained). The remaining nine elements, Am through Lr, are available only as man-made materials. For these latter elements, there are many different isotopes that can be prepared by various synthetic, nuclear reactions. A discussion of all of these isotopes is beyond the scope of this chapter and the reader is referred to other sources (Seaborg and Loveland 1990, Ahmad and Fields 1986). However, it is pertinent in a discussion of actinide oxides to mention certain aspects of sources and specific isotopes of the actinides as they pertain to the solid-state science of the oxides.

In most instances, the first solid materials of the actinides that were studied were oxides, not only because the oxides of electropositive metallic elements are primary compounds, but also because oxides may have been the easiest compound to prepare, especially on the microscale.

In considering the solid-state chemistry of the actinide oxides, both the number of different isotopes and the quantities available for preparing oxides diminish when progressing across the series. For the practical aspect of preparing and studying oxides of the actinides, the information in table 22 concerning availability and lifetimes of specific isotopes is useful. Although many isotopes of these elements are known and can be synthesized, frequently the quantities generated are too small and too short-lived to be considered for solid-state oxide work.

Many of these actinide isotopes have been prepared in accelerators or cyclotrons, where picograms or only a few atoms are formed. It can be seen that for the Am–Lr elements, starting with Am, one has available grams (or even kg quantities of the Am-241 isotope), which changes to mg amounts for Cm, Bk or Cf isotopes satisfactory for basic studies (gram amounts of Cm-244 and up to $\frac{1}{2}$ gram of Cf-252 may be available but due to their radioactive nature are not satisfactory for basic studies), and then down to microgram amounts for Es. The quantities then further diminish until only a few atoms of short-lived Lr isotopes are available on a very limited basis. Not only are the quantities limited, but their radioactive nature and short half-lives hinder experiments and may even affect or limit the oxide stoichiometries attained. The reader is directed to other sources for a more complete discussion of actinide isotopes and their production (Seaborg and Loveland 1990) or of their separation and purification (Transplutonium Elements 1981).

TABLE 22
Primary isotopes of the actinides for solid-state studies.

Isotope	Quantities available	Half-lives	Decay mode	Remarks
Ac 227	milligram	21.8 y	β^-	Severe radiation problems due to daughters
Th-232	multi-kg	1.4×10^{10} y	α	Minor radiological problems
Pa-231	mg to g	3×10^4 y	α	Requires handling in a glove box; difficult chemistry (especially in purification); some radiation background encountered
U-238	multi-kg	4×10^9 y	α	Minor radiological problems
Np-237	multi-kg	2×10^6 y	α	Requires handling in a glove box; some radiation background encountered
Pu-239	multi-kg	2.4×10^4 y	α	Requires handling in a glove box; some radiation background encountered
Pu-242	multi-g	3.8×10^5 y	α	Requires handling in a glove box; some radiation background encountered
Am-241	multi-kg	4.3×10^2 y	α	Requires handling in a glove box; radiation limits work to 10–50 mg
Am-243	multi-g	7.4×10^3 y	α	Lower-specific activity than Am-241 but daughter product limits working quantities to Am-241 levels
Cm-244	multi-g	18 y	α	High radiation levels; self-irradiation damage to solids; operation in glove box limited to few mg
Cm-248	multi-mg	3.4×10^5 y(α)	α	Best readily available isotope for studies; neutron emission limits working quantities in glove box to 10–50 mg
Bk-249	few mg	320 d	β^-	High beta radiation field (low-energy β^-); $\simeq 3\%$ daughter in growth in three weeks (Cf-249)
Cf-249	few mg	351 y	α	High-energy gamma emitted; working qualities limited to few mg
Cf-252	g	2.6 y	α	Spontaneous neutron emission limits working quantities to few μg
Es-253	multi μg	20.5 d	α	Severe self-irradiation damage to solids; significant radiation field
Es-254	μg	276 d	α	Longer half-life than Es-253; limited amounts; radiation from Bk-250 daughter severe
Fm-255	ng	20 h	α	Quantities too small for most solid-state experimentation; rapid decay rate
Fm-257	pg	100 d	α	Limited quantities; essentially eliminates solid-state work
Md-258	≤ 0.1 pg	55 d	α	Limited quantities; essentially eliminates solid-state work
No-259	multiple atoms	1 h	α	Limited quantities; essentially eliminates solid-state work
Lr-260	few atoms	3 min	α	Limited quantities; essentially eliminates solid-state work

2.2. *Electronic configurations*

The electronic configurations of the actinide elements may provide insights into the properties of the element and/or its compounds; however, actual predictions of such properties can be very elusive. In many cases the configuration for the actual form of the material (or its initial and final configurations) controls the material's behavior, rather than the ground state of the element. However, the electronic configurations for the lighter actinides (Pa–Pu) can be used to explain or rationalize the differences in oxide formation/behavior between the different elements, as well as the variation in oxidation states exhibited by each element. Another contributing cause for differences in oxidation states for the 4f and 5f elements is the fact that the 5f electrons are more spatially extended and shielded from the nucleus than the 4f electrons; the 5f electrons are more accessible and similar in energy to the outer d and s electrons than are the 4f electrons.

The similarities and differences between the electronic configurations for the lanthanides and actinides (see tables 1 and 23) do provide some insights into the physics and chemistry of these two f series of elements. Beyond plutonium the actinides tend to be more lanthanide-like in behavior, although there are still notable differences between the two series of elements. For the actinide oxides whose solid-state properties have been studied (e.g., through Es_2O_3), one of the major differences is the greater ease

TABLE 23
Electronic configurations of actinide atoms, ions, and their common oxides.

Atomic number	Oxides formed	Element	Electronic configuration*					
			Atom	M(II)	M(III)	M(IV)	M(V)	M(VI)
89	Ac_2O_3	Ac	$5f^0\,6d^1\,7s^2$		$5f^0$			
90	ThO_2	Th	$5f^0\,6d^2\,7s^2$			$5f^0$		
91	PaO_2, Pa_2O_5	Pa	$5f^2 6d^1 7s^2$			$5f^1$	$5f^0$	
92	$UO_2, U_4O_9, U_2O_5,$ U_3O_8, UO_3	U	$5f^3\,6d^1 7s^2$			$5f^2$	$5f^1$	$5f^0$
93	NpO_2, Np_2O_5	Np	$5f^4\,6d^1\,7s^2$		$5f^4$	$5f^3$	$5f^2$	$5f^1$
94	Pu_2O_3, PuO_2	Pu	$5f^6\,7s^2$		$5f^5$	$5f^4$	$5f^3$	$5f^2$
95	$Am_2O_3, Am_7O_{12},$ AmO_2	Am	$5f^7\,7s^2$	$5f^7$	$5f^6$	$5f^5$	$5f^4$	$5f^3$
96	$Cm_2O_3, Cm_7O_{12},$ CmO_2	Cm	$5f^7\,6d^1\,7s^2$		$5f^7$	$5f^6$		
97	Bk_2O_3, BkO_2	Bk	$5f^9\,7s^2$		$5f^8$	$5f^7$		
98	$Cf_2O_3, Cf_7O_{12}, CfO_2$	Cf	$5f^{10}\,7s^2$	$5f^{10}$	$5f^9$	$5f^8$		
99	Es_2O_3	Es	$5f^{11}\,7s^2$	$5f^{11}$	$5f^{10}$			
100	(Fm_2O_3)	Fm	$5f^{12}\,7s^2$	$5f^{12}$	$5f^{11}$			
101	(Md_2O_3)	Md	$5f^{13}\,7s^2$	$5f^{13}$	$5f^{12}$			
102	$(NoO; No_2O_3)$	No	$5f^{14}\,7s^2$	$5f^{14}$	$5f^{13}$			
103	(Lr_2O_3)	Lr	$^+5f^{14}\,6d^1\,7s^2$		$5f^{14}$			

* Only the electrons outside the [Rn] core are given: data are for ground-state gaseous neutral atoms and charged ions.

$^+$ Non-relativistic configuration.

of forming their dioxides as compared to the formation of the lanthanide dioxides. The existence of dioxides for either series suggests intermediate oxides (compositions with O/M ratios intermediate to those in the sesquioxide and dioxide; e.g., the behavior of Ce, Pr and Tb oxides) may also form.

This difference in ability to form dioxides is most striking at the position of Cm, the electronic homolog of Gd. Both of these f elements have a f^7ds^2 outer configuration and it would seem logical that only the sesquioxide of each element would form, leaving a stabilized, half-filled f orbital. This behavior is observed in the case of Gd, which only forms a sesquioxide. However, with Cm it is also possible to form CmO_2, which would not be expected based on Cm being the homolog of Gd. Curium dioxide can be formed by heating its cubic sesquioxide in air or oxygen at 300–400°C. Further, whereas formation of TbO_2 should be easier to form than CmO_2 (on the basis of Tb attaining a half-filled 4f orbital), TbO_2 requires much stronger oxidizing conditions. Thus, electronic configurations can only serve as guides as to whether or not a particular oxide forms and to the oxidation states that may be attained.

2.3. *Oxidation states*

The wide variety of oxidation states known and/or reported for the actinides are portrayed in fig. 14. It is readily apparent that the actinides have more variable oxidation states than do their lanthanide counterparts; this is especially true for the lighter members of the actinide series. The different oxidation states shown in fig. 14 are not equally stable and the existence of some have not been independently substantiated. These variations for the actinides result from the close proximity of the energy levels for the 7s, 6d and 5f electrons. It is apparent that often the highest states for an element are not observed in their oxides; rather, these higher states are frequently found in solutions where additional stability is afforded by formation of complexes (often anionic complexes).

The formation of sesquioxides and dioxides for the actinides beyond Pu is more characteristic of the behavior of the lanthanides. The exceptional stability of the

Oxidation States of the Actinides

Ac	Th	Pa	U	Np	Pu	Am	Cm	Bk	Cf	Es	Fm	Md	No	Lr
												1?		
						(2)			2	2	2	2	2	
3	(3)	(3)	3	3	3	3	3	3	3	3	3	3	3	3
	4	4	4	4	4	4	4	4	(4)	4?				
		5	5	5	5	5	5?		5?					
			6	6	6	6	6?							
				7	(7)	7?								

( ) = unstable; ? = claimed but not substantiated

Fig. 14. Oxidation states of the actinides.

fluorite-type MO_2 structure is, together with the difference in electronic nature of the actinides, responsible for the formation of dioxides for the actinides from Th through Cf. This difference in the ease of formation of dioxides is especially evident for the transplutonium (more lanthanide-like) elements of the actinide series. Except for Bk, the tetravalent state for these transplutonium elements tends to be unstable in aqueous solutions (especially acidic solutions), although it is acquired in the dioxides.

It is worth mentioning the behavior of one ternary oxide system to expand on the discussion of the stability of the tetravalent state for the actinides. Stability for the IV state is offered in some complex oxides, e.g., $BaMO_3$ materials. In the case of Cf, its dioxide cannot be prepared in one atmosphere of air or pure oxygen, while the $BaCfO_3$ compound readily forms by heating in air. Isostructural $BaMO_3$ compounds for Am, Cm and Bk are also known; they are very stable thermally, and also form readily by heating the components in air. However, attempts to prepare either EsO_2 or $BaEsO_3$ have not been successful. Although this suggests that the stabilization of a ternary oxide was not sufficient to produce the Es(IV) state, a complicating factor in such studies has been the high self-irradiation field present with Es-253 (the isotope available in larger quantities), which may induce decomposition of a higher oxidation state. Interestingly, from an electronic consideration, Es(VI) would offer the stability of a half-filled 5f orbital and one could envision the existence of a gaseous species, such as EsF_6, as being possible although a solid compound would be less likely. There have been some chromatographic tracer studies aimed at generating volatile fluorides of the transplutonium elements; in one case both a gas and a condensed phase of EsF_4 was claimed (Jouniaux 1979).

Studies of oxides for members in the actinide series higher than Es have not been carried out and it is not likely that they will be forthcoming, mainly due to the scarcity of the elements. There is a tendency for lower oxidation states in the second half of the actinide series; one may speculate that the stability of the sesquioxides would predominate and that the formation of dioxides would not occur with these higher members.

2.4. *Actinide binary oxides*

In table 24 are shown the known condensed phase of actinide oxides. The similarity of the transplutonium oxides to known lanthanide type of oxides is obvious. The apparent absence of specific lanthanide-type of oxides beyond An_7O_{12} (e.g., the complex phases for intermediate oxides of the lanthanides) for the actinides may be real or may merely reflect that comparable in-depth studies for them have not been undertaken. The existence of higher oxides for the actinides, Pa–Np, reflect the differences in their electronic nature, as discussed above.

2.4.1. *Lower oxides*

All of the elements listed in table 24 are known or expected to have, under some conditions, gaseous monoxides at high temperatures; this is likely to be true for the transeinsteinium elements as well. However, even in the gaseous state, the stability of the monoxide relative to its dissociation to atomic vapor and oxygen changes across the series, so that with increasing Z in each series the monoxide tends to become less

TABLE 24
Established actinide oxides.

Actinium	Ac_2O_3
Thorium	ThO_2
Protactinium	PaO_2, Pa_2O_5
Uranium	$UO_2, U_4O_9, U_2O_5, U_3O_8, UO_3$
Neptunium	NpO_2, Np_2O_5
Plutonium	Pu_2O_3, PuO_2
Americium	$Am_2O_3, Am_7O_{12}, AmO_2$
Curium	$Cm_2O_3, Cm_7O_{12}, CmO_2$
Berkelium	Bk_2O_3, BkO_2
Californium	$Cf_2O_3, Cf_7O_{12}, CfO_2$
Einsteinium	Es_2O_3

stable. The only actinide monoxides that have been reported as existing as a separate condensed phase are AmO (Zachariasen 1949, Akimoto 1967) and BkO (Fahey et al. 1972). These compounds were reported to have been prepared on the microgram scale but their existence is still open to question. Many lanthanide monoxides that have been reported have subsequently been shown to be ternary phases involving nitrogen and/or carbon (Felmlee and Eyring 1968).

The stabilities of divalent Eu and Yb are expected to be greater than that of divalent Am or Bk. While EuO can be prepared in a more direct fashion (Eyring 1979), YbO may best be prepared using the reaction between the metal and sesquioxide under high pressure (Leger et al. 1980). This procedure has potential application for preparing actinic monoxides. Certainly fewer efforts have been made to prepare the actinide monoxides as compared to the lanthanide monoxides, except for the cases of U and Pu. From a speculative standpoint, condensed-phase actinide monoxides may be more probable for the actinide elements that exhibit a divalent state. Thus, it would seem that the monoxides for Am, Cf and the elements Es through No would have the highest potential for existence. Of these, Cf would be the most attractive monoxide to try to prepare. To date there has been no evidence for the existence of solid phases of CfO or EsO, although weighable amounts of solid dihalides have been prepared for both of these elements (Peterson and Baybarz 1972, Peterson et al. 1977, Fellows et al. 1978, Hulet et al. 1975, Wild et al. 1978).

2.4.2. *Sesquioxides*

If Ac is excluded from the actinide series (based on the absence of an f electron), the first member of the actinide series to form a condensed-phase sesquioxide is Pu. The Am–Es elements also form stable sesquioxides; presumably the Fm–Lr elements would also form sesquioxides. The sesquioxide is the most stable oxide for Cm, Cf, Es and likely would also be the most stable oxide for Fm, Md and Lr. The sesquioxide, or perhaps the monoxide, are the oxides expected for No. The Fm–Lr oxides have not been prepared or studied experimentally.

The actinide with the highest atomic number that has been studied in a solid phase is Es; the sesquioxide is its only known oxide phase. The scarcity of this element, and more importantly the intense self-irradiation from the Es-253 isotope which destroys rapidly the oxide matrix, may limit attaining higher oxygen stoichiometries. The structural identification of Es_2O_3 (Haire and Baybarz 1973) was only accomplished by using very small quantities (10–100 nanograms) and electron diffraction, which provided diffraction patterns in very short times as compared to conventional X-ray techniques.

Of the six known actinide sesquioxides (e.g., sesquioxides of Pu, Am, Cm, Bk, Cf and Es) only those of Cm, Cf and Es are resistent to air oxidation to ambient temperature. Due to the stability of their dioxides, the sesquioxides of Pu, Am and Bk readily take up oxygen, and require special storage (e.g., sealed containers) to avoid oxidation. All three oxides are oxidized readily when heated in oxygen-containing atmospheres below 1000°C. Above this temperature, oxygen is lost from AmO_2. Heating higher oxides of Cm or Cf in air or in vacuum above 900°C produces the sesquioxides.

The actinide sesquioxides have many similarities with the lanthanide sesquioxides, such as crystal structures (A, B and C forms), lattice parameters, etc., but there are also some significant differences. One notable difference is their melting points; it appears that the transcurium sesquioxides have significantly lower (several hundreds of degrees C) melting points and display a different melting point trend with Z than for comparable lanthanide sesquioxides. The similarities and differences of the two f-series' oxides are discussed in more detail in the following section.

2.4.3. *Dioxides*

All of the actinides from Th through Cf form isostructural dioxides (fluorite, fcc-type structure). The dioxide is the highest binary oxide known for Th, Pu, Am, Cm, Bk and Cf. The stability of these dioxides varies, with the order being Th > Pu > Bk > Am > Cm > Cf. The latter two dioxides, CmO_2 and CfO_2, begin to evolve oxygen when heated above 300°C and eventually yield sesquioxides. The dioxides of five of these six elements, with Cf being the exception, can be prepared by heating their sesquioxides in air or oxygen, although the dioxide of Cm requires careful treatment (long heating times at modest temperatures, 350–400°C, in high pressures, 100 atm, of oxygen). The formation of CmO_2 and the absence of a dioxide for Gd was discussed above in conjunction with electronic configurations, and is an interesting difference between these two elements having the same electronic configuration.

The preparation of the dioxides of Cf and Tb require stronger oxidizing conditions than does Cm. Attempts to prepare the dioxide of Es have not been successful, although claims have been made for the existence of a tetravalent oxidation state of Es in a vapor-condensed phase (see earlier section on oxidation states). Attempts to prepare the tetravalent state of Es as a complex oxide have also been negative (see section 3). Thus, Cf is the highest actinide in the series known to form a dioxide.

2.4.4. *Intermediate oxides*

Intermediate oxides, i.e., oxides displaying O/M stoichiometries between 1.5 and 2.0 (or oxides with oxygen stoichiometry between that for the sesquioxide and the dioxide), are common to both the actinide and lanthanides, although they are better established

for the lanthanides. Such intermediate oxides appear to be simpler systems with the actinides, perhaps only because of the more limited information and studies involving them. Very detailed studies have been performed on the intermediate oxides of Ce, Pr and Tb, which are the prime examples of this type of oxide system. Since both the lanthanides and actinides form intermediate oxides, they are also discussed in the section 3.

The four actinide oxide systems comparable to the lanthanide intermediate oxide systems are comprised of Am, Cm, Bk and Cf. Although Pu sesquioxide does take up oxygen to yield a hyper-stoichiometric oxide, and Pu dioxide can lose oxygen to give a sub-stoichiometric dioxide, very little is known about Pu oxides that are comparable to the lanthanide systems. The oxide systems of Am, Cm and Cf all form the stable An_7O_{12} oxide, which is isostructural with the comparable lanthanide phase. The absence of a known Bk_7O_{12} phase may be due to the extreme stability of BkO_2, which would make Bk_7O_{12} difficult to obtain experimentally. The stability of PuO_2 may create a similar situation for obtaining a Pu_7O_{12} phase.

2.4.5. *Higher oxides*

Only three actinides form oxides that have O/M stoichiometries greater than two; these are Pa, U and Np. Some "higher" oxide materials have been reported for Pu but these appear in reality to be oxyhydroxides (Weigel et al. 1986a, b). Attempts to prepare PuO_3 have not been successful. The formation and existence of oxides above the dioxide for these three actinides are in accord with their more complex electronic nature (e.g., the presence of itinerant f electrons and variable electronic configurations of similar energies).

Since the aim of this chapter is to compare the lanthanide and actinide binary oxides, and the lanthanides do not form oxides above the dioxide, the oxides of these lighter actinides are not discussed. However, it is worth mentioning which oxides are commonly observed with these lighter actinides. The oxides Pa_2O_5 and U_3O_8 are stable at elevated (800°C) temperatures in air while Np_2O_5 and UO_3 lose oxygen when heated above 400°C to form NpO_2 and U_3O_8. The highest oxygen stoichiometry in a binary oxide is obtained in UO_3.

2.5. *Preparation of actinide oxides*

2.5.1. *General considerations*

Once the existence of a new element had been established, the first experiments performed with it were likely to be done at the tracer level. It took considerable efforts to produce quantities of the element sufficient for solid-state studies, such as obtaining physical properties of its oxide(s). The lack of material is the reason for the void of information for the transeinsteinium elements.

Many of the studies of the actinides have required specialized preparative techniques and equipment, and in some cases very novel approaches have been used. The oxides of these elements were probably the first compounds to be prepared and studied due to their ease of preparation, their use in other syntheses, and the natural interest in the oxides as primary compounds. In general the oxides can be obtained by calcination in

air of several different materials; usually, the oxalates, hydroxides, nitrates, etc. The stoichiometry of the particular actinide oxide obtained after calcination depends on the specific element and/or the experimental conditions used.

2.5.2. *Preparation techniques*

When the quantity of the material that can be used is not of concern, classical methods of preparing the oxides are used. Thus, one may use the approach of precipitating an oxalate, and after washing and drying, calcine in air to obtain the oxide. Oxides of specific stoichiometry would be obtained by subsequent experimental treatment (e.g., hydrogen reduction of AmO_2 to obtain the sesquioxide). However, in many cases microtechniques are necessary for the preparation of actinide oxides. In some situations these techniques may require novel approaches to the preparation and study of the oxides. Such techniques may also limit the depth and accuracy of the study.

One such technique was the resin-bead technique. Here the actinide in solution was loaded on a cation ion-exchange resin of a selected size to hold one or more micrograms and this dried resin bead was carefully calcined to yield a small, single oxide particle containing about 1–2 micrograms of the actinide. Many actinide oxides have been characterized using this approach. This technique was not satisfactory for einsteinium oxides as the resin matrix was destroyed by the radiation from Es before it was calcined to a stable oxide particle. The term particle is important as it is not practical to consider handling/transporting only a few micrograms of oxide powder.

An approach similar to the resin-bead technique employed activated charcoal chunks in place of the beads. The actinide was sorbed on a chunk of charcoal, and after calcination in air to remove the carbon, a low-density oxide particle could be recovered (Haire 1982). This approach has been used with Es, but in general the procedure yielded less satisfactory particles than the resin technique.

Another novel technique for studying and characterizing very small amounts of oxides used an electron microscope and electron diffraction (Haire and Baybarz 1973). This approach was necessary for einsteinium oxide studies as the high specific activity of Es destroyed the crystalline matrix of the oxides before X-ray diffraction patterns could be obtained (e.g., 20 min). Using this technique, 10–100 nanograms of Es (or another lanthanide or actinide) oxide could be studied. With larger quantities of material (e.g., 20–100 micrograms) a preferred technique was to carry out micro oxalate precipitations in teflon molds to yield chunks of dried oxalates, which could be calcined quickly to the oxide. A large number of actinide and mixed actinide oxides in the form of individual multi-microgram particles have been prepared in this manner (Haire 1982).

The emphasis above has been on producing solid particulates of oxide that can be handled, transported, studied or used in subsequent syntheses. Many other approaches for other needs can be used and may be limited only by the needs and imagination of the investigators. For example, thin films of oxide can be readily generated by vaporizing metals and subsequently oxidizinng them on a substrate to the oxide.

An additional overview is given below for preparing specific actinide oxides, and discussions on the preparation of actinide oxides are also provided in a recent chapter on the subject (Morss 1991).

2.5.3. *Stoichiometry considerations*

The experimental conditions necessary to acquire a precise stoichiometry (i.e., O/M ratio) varies greatly with the particular actinide oxides. Establishing the stoichiometry is in itself not straightforward. For oxides of U, Np and Pu, many studies have been made regarding their stoichiometries and the O/M ratios are commonly discussed in terms of a few tenths of a percent. With the transplutonium oxides such precision is not available and stoichiometry data for them are not that well established. The particular oxide stoichiometries desired and the experimental conditions necessary to attain them are best discussed in terms of the oxides of each actinide. The nonstoichiometry in oxides has also been considered in terms of thermodynamics and bonding (Manes and Benedict 1985). In more practical terms, some generalities regarding stoichiometry are given below.

Hydrogen reduction in the temperature range of 600–1000°C is generally sufficient to provide PaO_2, UO_2, Pu_2O_3 (1500°C is required here), Am_2O_3, Cm_2O_3, Bk_2O_3 and Cf_2O_3. The sesquioxides of Cm and Cf are attainable by heating higher oxides to 1000°C and cooling in vacuum. The oxides generally obtained by heating salts (e.g., oxalates, nitrates, etc.) to 1000°C and cooling in air are ThO_2, Pa_2O_5, U_3O_8, NpO_2, AmO_2, Cm_7O_{12}, BkO_2, Cf_7O_{12} and Es_2O_3. Higher oxides of these elements, if they exist, normally require stronger oxidizing conditions (high-pressure oxygen, atomic oxygen) or controlled-temperature treatments.

A special aspect of oxide stoichiometry is the change in O/M ratio as a result of self-irradiation. Usually radiation reduces the O/M ratio and also produces crystal defects but in some instances oxidation may occur due to active materials generated by the radiation (e.g., atomic oxygen from radiation acting on oxygen). Unfortunately, radiation often "swells" the lattice parameters so that a damaged lattice and/or an oxide with less than stoichiometric oxygen content yield larger X-ray lattice parameters. Thus, attempts to determine O/M ratios of self-irradiated oxides by lattice parameters only can be ambiguous.

2.5.4. *Preparation of single crystals*

The preparation of single crystals of oxides in general requires larger quantities of material than the preparation of polycrystalline samples. Also the yield for the preparation of single crystals is often low; it is unusual to get a 75–100 percent yield of single crystals from preparations (a few percent is often considered satisfactory). The preparation of single crystals often involves luck as well as good experimental techniques! Since larger amounts (multi-grams) of material are normally required for growing single crystals of oxides, there have not been many successful efforts to grow single crystals of the transplutonium oxides. Single crystals of actinide oxides are therefore found mainly for the lighter members of the series, as these elements are available in larger quantities.

Several different techniques have been used to grow single crystals of Th, U, Np and Pu oxides (Muller and Spirlet 1985, Henrick and Behrens 1981, Finch and Clark 1965). One is hydrothermal growth using molten media. Single crystals of ThO_2 have been grown by this approach; e.g., techniques using either molten $Pb_2V_2O_7$ or a $Li_2O–2WO_3$ mixture. Single crystals of NpO_2 and PuO_2 have also been obtained in this way.

Another technique used for generating single crystals of oxides has been fused salt electrolysis. Crystals of UO_2, U_4O_9 and NpO_2 have been formed in this manner. Transport methods, which involve decomposition, transportation and then recombination, have also been employed for obtaining single crystals of NpO_2 and oxides of U; an example of this technique is using $TeCl_4$ as a carrying agent for the material (Spirlet 1980, Vogt 1982).

Vapor deposition is another method for making single crystals, and this has been used for ThO_2 (Laszlo et al. 1967) and for UO_2, U_4O_9 and U_3O_8 (Van Lierde et al. 1962). Controlled solidification of oxide melts, which requires that the oxide of interest be stable in the molten state, is another technique worth mentioning, and this approach has been used for ThO_2 and UO_2 (Spirlet and Vogt 1984). Finally, zone refining has had limited applications but has been employed in preparing single crystals of UO_2.

2.6. *Specific oxides of the actinide elements*

2.6.1. *Actinium oxides*

The chemistry of actinium has not been extensively studied due to its scarcity, radioactivity and the difficult nature of its decay products. Its chemistry should be very similar to that of lanthanium and therefore its white-colored sesquioxide is expected to be hexagonal (A-type; see table 25) (Weigel and Hauske 1977).

2.6.2. *Thorium oxides*

Thorium oxide chemistry is essentially that of ThO_2 (Katzin 1986). This white-colored oxide is stable as a fcc phase (fluorite) to its melting point (3390°C). Prolonged heating in vacuum at 2000°C causes darkening, supposedly indicating some loss of oxygen, but this "loss" is too small for analytical detection. A "lower" oxide (ThO; suggested composition), interstitial in nature, has been reported for thin films on Th metal. X-ray data (Ackermann and Rauh 1973a) suggested the material was a monoxide but the diffraction pattern indicated poor crystallinity and was not definitive. It is unlikely that, if ThO exists, it would exist in a bulk form. Vapor species such as ThO have been reported over ThO_2 and Th metal at elevated temperatures (Ackermann and Rauh 1973b, Neubert and Zmbov 1974, Hildenbrand and Murad 1974, Ackermann and Chandrasekharaiah 1974) and there have been several reports of hydrated oxide materials. Structural information for ThO_2 is provided in table 25. A more complete discussion of thorium and its oxides can be found in a review of the actinide elements (Katzin 1986).

2.6.3. *Protactinium oxides*

The oxide chemistry of Pa is more complex than that of Ac or Th oxides, in accord with the more complex energy levels and electronic nature of the element. There are essentially three stoichiometric binary oxides of Pa; PaO, PaO_2 and Pa_2O_5, although there are several other, variable oxide stoichiometries between the PaO_2 and Pa_2O_5 (Kirby 1986, Sellers et al. 1954, Stchouzkoy et al. 1966). In addition, there are some seven known crystal modifications of Pa_2O_5 (see table 25). The white-colored Pa_2O_5 is the oxide obtained when a variety of Pa salts (e.g., hydrated Pa_2O_5 or "hydroxide",

TABLE 25
Structural properties of actinide oxides.

Oxide	Symmetry	Space group structure type	Lattice parameters				Color
			a_0 (Å)	b_0 (Å)	c_0 (Å)	Angle (deg)	
Ac_2O_3	hexagonal-A	$P\bar{3}ml(La_2O_3)$	4.07		6.29		white
ThO_2	cubic	$Fm\bar{3}m(CaF_2)$		5.597			white
PaO_2	cubic	$Fm\bar{3}m$	5.509				black
Pa_2O_5	tetragonal		5.429		5.503		white
Pa_2O_5	hexagonal		3.82		13.22		white
UO_2	cubic	Fm3m	5.471				brown/black
α-U_2O_5	monoclinic		5.429		5.503	$\beta = 99.2$	black
β-U_2O_5	hexagonal		3.813		13.18		
γ-U_2O_5	monoclinic		5.410	5.481	5.410	$\beta = 90.49$	
α-U_3O_7	orthorhombic	Pmma	6.796	3.958	4.145		
α-U_3O_8	orthorhombic	C2mm	6.716	11.960	4.147		black
β-U_3O_8	orthorhombic	Cmcm	7.069	11.445	8.303		black
γ-UO_3	orthorhombic	Fddd	9.81	19.93	9.71		orange
A-UO_3	amorphous						orange
α-UO_3	orthorhombic	$P\bar{3}ml$	6.84	43.45	4.157		tan
β-UO_3	monoclinic	$P2_1$	10.34	14.33	3.910	$\beta = 99.03$	orange
γ-UO_3	orthorhombic	Fddd	9.813	19.93	9.711		yellow
δ-UO_3	cubic	$Pm\bar{3}m$	4.16				deep red
ε-UO_3	triclinic		4.002	3.841	4.165	$\alpha = 98.10$ $\beta = 90.20$ $\gamma = 120.17$	brick red
η-UO_3	orthorhombic	$P2_12_12_1$	7.511	5.466	5.224		brown
NpO_2	cubic	$Fm\bar{3}m$	5.433				green
Np_2O_5	monoclinic	$P2_{1/c}$	4.183	6.584	4.086	$\beta = 90.32$	dark brown
Pu_2O_3	hexagonal-A	$P\bar{3}ml$	3.841		5.958		tan
Pu_2O_3	cubic-C	$Ia3(Mn_2O_3)$		11.03			
PuO_2	cubic	$Fm\bar{3}m$	5.3960				green/brown/ black
AmO_2	cubic	Fm3m	5.374				black
Am_2O_3	hexagonal-A	$P\bar{3}ml$	3.817		5.971		tan
Am_2O_3	cubic-C	Ia3	11.03				reddish brown
Cm_2O_3	hexagonal-A	$P\bar{3}ml$	3.792		5.985		white
CmO_2	cubic	Fm3m	5.358				black
Cm_2O_3	monoclinic-B	$C2/m(Sm_2O_3)$	14.282	3.641	8.883	$\beta = 100.29$	white/lite green
Cm_2O_3	cubic-C	Ia3	11.002				white
Cm_7O_{12}	rhombohedral	$R\bar{3}$	10.184		9.448		black
BkO_2	cubic	Fm3m	5.3315				tan-brown
Bk_2O_3	hexagonal-A	$P\bar{3}ml$	3.754		5.958		light green
Bk_2O_3	monoclinic-B	C2/m	14.197	3.606	8.846	$\beta = 100.23$	pale green
Bk_2O_3	cubic-C	Ia3	10.887				tan
CfO_2	cubic	Fm3m	5.310				black
Cf_2O_3	hexagonal-A	$P\bar{3}ml$	3.72		5.96		pale green
Cf_2O_3	monoclinic-B	C2/m	14.121	3.592	8.809	$\beta = 100.34$	pale green
Cf_2O_3	cubic-C	Ia3	10.83				pale green
Cf_7O_{12}	rhombohedral	$R\bar{3}$	10.061		9.375		black
Es_2O_3	hexagonal-A	$P\bar{3}ml$	3.7		6.0		white
Es_2O_3	monoclinic-B	C2/m	14.1	3.59	8.80	$\beta = 100$	white
Es_2O_3	cubic-C	Ia3	10.766				

nitrate, etc.) are heated in oxygen or air above 650°C. The crystal form that is obtained for this oxide depends upon the temperature to which it has been heated (Roberts and Walter 1966, Stchouzkoy et al. 1964).

In the 1000–1500°C range frequently used in chemical laboratories, a hexagonal crystal form of Pa_2O_5 is obtained. Black PaO_2 (fluorite structure) is formed by hydrogen reduction of the higher oxide at temperatures above 1550°C. The oxides with O/M ratios between 2.0 and 2.5 can be obtained by selective oxidation of PaO_2 or reduction of Pa_2O_5. As in the case of ThO, a PaO film has been reported to form on the surface of Pa metal; but it is not likely that a bulk form of pure PaO can be prepared. A number of complex (ternary) oxides have been reported for Pa in addition to hydrated oxides and a hydrated peroxide of variable composition.

2.6.4. *Uranium oxides*

The uranium oxygen system is the most complex and best studied of the actinide oxides. There are a number of reviews of uranium oxides and two are suggested here (Weigel 1986, Cordfunke 1969, Gmelin Handbook of Inorganic Chemistry 1975, 1977, 1978, 1984, 1986). As might be expected due to the complexity of the uranium oxygen system, there have been some differences reported for the stoichiometries of its oxides. The range of binary oxides reported for U are the following: UO, UO_2, U_4O_9, $U_{16}O_{37}$, U_8O_{19}, U_2O_5, U_5O_{13}, $U_{13}O_{34}$, U_8O_{21}, $U_{11}O_{29}$, U_3O_8, $U_{12}O_{35}$ and UO_3. It is likely that some of these oxides do not form as separate phases; a particular oxide may also exhibit a range of oxygen compositions. Structural forms of several of the established oxides are listed in table 25. Several of these oxides also have very different crystal modifications.

The existence of a pure bulk phase of UO, although it has been reported, is probably not likely to exist as a separate, pure phase, as in the cases of the previous actinide oxides (Weigel 1986). The monoxide of uranium has been observed in the vapor state. The black/brown-colored oxide, UO_2, is well known and has the fluorite structure. It can be obtained by hydrogen reduction of higher uranium oxides at elevated temperatures (e.g., 800°C). This material has been reported to be able to accommodate a wide range of oxygen compositions while retaining its cubic lattice (e.g., up to $UO_{2.25}$, to which the U_4O_9 phase is assigned).

If UO_2 or U salts (e.g., nitrate, hydrated oxide "hydroxide", etc.) are heated in air or oxygen at 650–800°C, black U_3O_8 (O/M = 2.67) is formed. Two crystal modifications of this oxide have been reported (see table 25). This oxide is often used as a standard oxide for analytical purposes and classically contains both U(IV) and U(VI). A number of oxides between $UO_{2.25}$ and U_3O_8 have also been reported and require special preparative conditions. Their structures are given in table 25.

The highest oxide of U that is known is the yellow/orange UO_3. It can be prepared by different synthetic approaches, one being the treatment of lower oxides with high-pressure oxygen at modest temperatures (e.g., 300°C); another is the thermal decomposition of hydrated uranyl salts at temperatures below 650°C. In air, UO_3 loses oxygen when heated above 650°C to form U_3O_8. There are several different crystal modifications of UO_3 (see table 25).

2.6.5. *Neptunium oxides*

The complexity of actinide oxide systems begins to decrease after the uranium oxygen system, and neptunium oxides are far less complex than those of U (Fahey 1986). Little has been reported about NpO, except as a vapor species at high temperatures. Based on the nature of ThO, PaO, UO and PuO (see below), it would be expected that a NpO material might also be found on the surface of Np metal, but apparently it has not been reported. The most frequently encountered neptunium oxide is the olive-colored dioxide, which has a fluorite structure and is isostructural with the other actinide dioxides. The dioxide is formed when salts (e.g., nitrate, hydrous oxide "hydroxide", oxalate) are calcined in air or oxygen at 700–1000°C. Contrary to the uranium oxygen system, Np does not form an oxide above Np_2O_5; thus, neptunium oxides having stoichiometries as Np_3O_8 and NpO_3 are not known.

The Np_2O_5 oxide exhibits a very narrow compositional range and has limited thermal stability. It can be prepared by molten-salt techniques (Cohen 1963, Cohen and Walker 1964). The structural symmetry of Np_2O_5 is monoclinic but the angle (beta) is close to 90 degrees, so that samples of moderate to poor crystallinity can also be indexed as orthorhombic. An orthorhombic, hydrated oxide [$NpO_3 \cdot H_2O$ or $NpO_3(OH)_2$] is also known, and has been obtained by passing ozone through aqueous suspensions of Np(V) (Fahey 1986). The structural properties of Np oxides are listed in table 25.

2.6.6. *Plutonium oxides*

The existence of PuO has also been claimed, either as an impurity phase (Weigel et al. 1986a, Zachariasen 1949) or as material present on the surface of Pu metal. It has been reported as having an NaCl-type structure (see table 25). It was reported as a bulk phase prepared by reducing milligram amounts of PuOCl with Ba vapor at elevated temperatures, or by reduction of PuO_2 with Ba vapor. Other reported approaches for its preparation have been the controlled oxidation of molten Pu metal using stoichiometric quantitites of oxygen generated by decomposing known amounts of Ag_2O (Akimoto 1960), and by the reduction of PuO_2 with carbon (Weigel 1986). One problem with the latter approach is the formation of mixed systems as $PuC_xN_yO_z$ ($x + y + z = 1$; PuC and PuN are also cubic materials), where oxygen is only one of the components that combined with the Pu. The existence of PuO is known to form as a vapor species in the vaporization/decomposition of PuO_2.

A stoichiometric, tan-colored sesquioxide of Pu is known (hexagonal; A-type) and can be prepared by reducing PuO_2 at high temperatures (e.g., above 1500°C) with hydrogen, Pu metal or carbon. Two cubic forms of Pu sesquioxide are known, which have O/M ratios above 1.50. A hyperstoichiometric sesquioxide (bcc) with an O/M ratio of 1.515 is formed when PuO_2 is heated in vacuum to 1650–1800°C or reacted with carbon at above 1600°C. Another so-called sesquioxide with an O/M ratio of 1.61 and showing cubic symmetry is also known. It is obtained when PuO_2 is melted and rapidly cooled to room temperature.

The highest oxide of Pu is the dioxide. It can appear in various colors, from green to brown or black, which may reflect slightly different O/M ratios as well as particle sizes.

The stoichiometric dioxide (O/M = 2.00) is obtained by calcining a variety of salts (nitrate, oxalate, hydrated oxide "hydroxide", etc.) in air or oxygen to 800–1000°C. The structure of the dioxide is fcc (fluorite-type; see table 25). The O/M ratios of the dioxide are known to vary from 1.98 to 2.03, depending on the preparative route and specific treatment. The ignition of Pu sulfates has been reported to yield an O/M ratio as high as 2.09. The dioxide of Pu is very refractory in nature. Structural information for Pu_2O_3 and PuO_2 is given in table 25.

Efforts to prepare Pu oxides with O/M ratios above two have not been successful. Thus, neither PuO_3 nor Pu_3O_8 exist although many attempts have been made to prepare them. There does exist a hydrated oxide of the general formula, $PuO_3 \cdot 0.8H_2O$, prepared by passing ozone through suspensions of Pu "hydroxide". Attempts to dehydrate this material did not yield PuO_3; rather, both water and oxygen were lost to yield the dioxide (Campbell et al. 1968).

2.6.7. *Americium oxides*

As Am is considered to be the first of the "lanthanide-like" actinides, it would be expected that its oxide system would bear some resemblance to the oxide systems of the lanthanides. For Am, a monoxide, sesquioxide, a dioxide, and an oxide with an O/M ratio intermediate to that of the sesquioxide and dioxide have been reported. Although the quantity of Am has permitted extensive investigations of its oxide system, the number of studies is still small relative to the efforts that have been extended on the uranium and plutonium oxide systems. In part this is due to the more intense radioactive nature of Am but also to a decreased interest in its chemistry in contrast to those of U and Pu, whose applications in weapons and reactors promoted many detailed studies of those elements. However, the number of studies that have been carried out on the americium oxygen system is still large in comparison to the number of studies with higher actinides.

The existence of AmO has been reported by two researchers (Schultz 1976) but only on the microgram scale. This work led to reporting a lattice parameter for the compound (see table 25), yet the existence of AmO is still questioned. The preparative routes for AmO have included reaction of Am metal with stoichiometric amounts of oxygen (generated by decomposing Ag_2O) (Akimoto 1967); and as a phase formed inadvertently by exposure of americium hydrides at 300°C to air. An interesting approach for synthesis of AmO would be the high-pressure reaction between americium metal and Am_2O_3 as used for preparing lanthanide monoxides (Leger et al. 1980). However, the latter method would require precise control of the quantities of the starting materials to avoid the presence of secondary phase(s) (e.g., metal or sesquioxide).

Two crystal forms of Am_2O_3 (pink colored) have been reported (see table 25); a hexagonal (A-type) and a bcc (C-type) form. Which crystal form is obtained depends on the temperature of the preparation; the C-type is the low-temperature (less than 600°C) form. The A-type sesquioxide has been reported to be stable from 900 to 1500°C (Berndt et al. 1974). It appears that a B-form of this oxide does not exist; if it does, it has a very limited temperature range. Incorporation of small amounts of lanthanide oxides (e.g., Sm_2O_3) with Am_2O_3 can stabilize the monoclinic form of Am_2O_3 (Schultz 1976).

It has also been reported that self-irradiation transforms the C-form of the sesquioxide at room temperature to the A-form in about three years (Hurtgen and Fuger 1977).

The highest binary oxide of Am is its dioxide (black/brown) which is formed when calcining salts (e.g., nitrate, oxalate, hydroxide, etc.) of Am(III) in air or oxygen up to 900°C. Above this temperature the dioxide starts to lose oxygen. At 1000°C one report suggests that the oxygen pressure over the dioxide is about one atmosphere (Keller and Berndt 1976) while another states that, at this temperature, the O/M ratio is higher than 1.99 (Chikalla and Eyring 1967, 1968). The dioxide crystallizes in the fluorite (fcc) structure. Its lattice parameter is subject to expansion from self-irradiation (Hurtgen and Fuger 1977); the value given in table 25 is for freshly prepared samples with little or no self-irradiation damage.

Although there is no evidence for binary oxides above the dioxide (Coleman et al. 1963, Katz and Gruen 1949), there are several complex oxides where Am has an oxidation state above Am(IV) (Keller 1967, Morss 1982). Thus, Am follows Pu in having a value of 2.0 as its highest O/M stoichiometry in a binary oxide.

2.6.8. *Curium oxides*

Based on the behavior of curium's lanthanide homolog, Gd, curium would be expected to form only a sesquioxide. Curium forms a dioxide (a question exists if an O/M ratio of exactly 2.0 is reached; see below) as well as oxides having stoichiometries intermediate to those in the sesquioxide and dioxide. In addition, there has been a report of the formation of CmO on the surface of metals (Cunningham and Wallmann 1964).

The Cm_2O_3 (white) displays three crystal modifications, namely the A-, B- and C-type lanthanide structures as shown in table 23 (Eller and Pennemann 1986). A small uptake of oxygen can cause the oxide to acquire a tan to light brown appearance. The C-type (bcc) structure is the low-temperature form, which converts to the B-type (monoclinic) structure above 800°C, which in turn changes to the A-type (hexagonal) structure above 1600°C (Baybarz and Haire 1976). It is the C-type structure that is readily oxidized to higher oxides; the monoclinic form is very resistent to oxidation and the monoclinic to cubic transformation via temperature treatment is very difficult ("irreversible" transformation). The B to A and the A to B transformations occur more readily with temperature. Self-irradiation (especially noticeable with the more readily available, shorter-lived Cm-244 isotope) converts the C-form of the sesquioxide to the A-form (Wallmann 1964, Noe et al. 1970).

The dioxide (black) is prepared by oxidation of the cubic form of the sesquioxide at modest temperatures (300–400°C) in air or oxygen (preferably in high-pressure oxygen). Sufficient time (e.g., days; kinetics have not been established) should be allowed for the complete uptake of oxygen. The dioxide is thermally unstable above 400°C (Haug 1967) and with heating eventually yields the sesquioxide around 900°C. It has been reported that the dioxide is formed by calcining salts in oxygen (Asprey et al. 1955) followed by slow cooling. It is more likely that lower oxides (O/M = 1.5–2.0) of Cm are first produced, which are subsequently oxidized to the dioxide upon cooling in oxygen-containing atmospheres below 400°C.

The CmO_2 lattice parameter (fluorite structure; see table 25) is also affected by self-radiation (especially with Cm-244), which causes both the loss of oxygen and swelling of the lattice with time. The smallest parameter (potentially the highest O/M ratio) has been measured using the long-lived Cm-248 isotope (Noe and Fuger 1971). The Cm-248 isotope (normally obtained as a mixture having 3% Cm-246) has significantly lower radiation levels than Cm-244.

The question of the actual O/M ratio in CmO_2 is an important one. Magnetic data (see later section) yield moments that are too high (1.5 to 3.0 μB versus zero, as expected for an $5f^6$ electron core), which initially was interpreted to mean that the O/M ratio in the oxide was less than two. Several workers have tried different experiments to resolve this problem (Nave et al. 1983, Morss et al. 1989) and a theoretical evaluation of this problem has also been attempted (Goodman 1992). The simplest answer would be that the CmO_2 is nonstoichiometric (e.g., O/M < 2.00) but this is not a totally satisfactory explanation and is not supported by X-ray analyses of the oxides. Self-irradiation can lead to loss of oxygen in such oxides but the Cm-248 oxides should be relatively free of these effects over modest time periods.

Intermediate oxides of Cm that have stoichiometries between the sesquioxide and the dioxide have been reported (Noe and Fuger 1971, Stevenson and Peterson 1975). Oxides with O/M ratios of 1.50 to 1.65, 1.714 (Cm_7O_{12}), and 1.79 to 2.00 are the structural groupings (bcc, rhombohedral, and fcc, respectively) which have been reported. The curium oxygen system bears some resemblance to both the plutonium and praseodymium oxygen systems but additional work is needed on it.

From the above discussion of the sesquioxide phases and the oxidation behavior of Cm, it is obvious that some care must be exercised when attempting to prepare CmO_2. In calcining salts, one must avoid too high a temperature which would create the monoclinic form of the sesquioxide, while still heating to a sufficiently high temperature to fully decompose the salts or salt products (e.g., carbonate from the oxalate). It has been suggested (Haire 1982, Nave et al. 1983) that the best curium salt to use in this preparation is the nitrate since it decomposes below 600°C. After decomposition, the resulting curium oxide is cooled slowly to 400°C; it is then cooled very slowly (0.5 deg min^{-1}) with holding steps (days to weeks in the 300–400°C region) to room temperature while under oxygen pressure (e.g., 100 atm).

There have not been reports of binary or complex oxides where the Cm exists above the tetravalent state. There has been one unsubstantiated report of a ternary complex Cm salt ($LiCmO_3$) where a Cm(V) state was claimed (Weigel and Kohl 1985).

2.6.9. *Berkelium oxides*

The quantity of information available for the berkelium oxygen system is far less than that for the previous actinides, due mainly to the scarcity and the shorter half-life (325 days) of the Bk-249 isotope used in solid-state studies. The sesquioxide and the dioxide are the two well-established oxides of Bk, and the dioxide is much more stable than the dioxides of Cm and Am. This stability can be attributed in part to the fact that the Bk(IV) state results in a half-filled 5f state, as found for TbO_2. However, BkO_2 is much more stable and is formed more easily than is TbO_2.

There is a single report for the existence of BkO (Fahey et al. 1972) but, as in other reports of solid phases of actinide monoxides, evidence for it is not very definitive. The NaCl-type lattice parameter for the reported monoxide is given in table 25.

There are three crystallographic forms of the sesquioxide; the A-, B- and C-type rare-earth sesquioxide structures (Hobart and Peterson 1986). The low-temperature form is the C-type (cubic) sesquioxide, which is very susceptible to adding oxygen to form higher oxides of Bk, especially the dioxide. This C-type sesquioxide converts to the B-type, monoclinic sesquioxide at about 1200°C, which itself is converted to the A-type hexagonal form at 1742°C. As in the case of Cm sesquioxide, the B to C transition does not readily occur and is considered "irreversible". The melting point of the sesquioxide has been reported to be 1920°C (Baybarz and Haire 1976). The lattice parameters of these different forms of the sesquioxide are listed in table 25. The different crystallographic forms of the sesquioxide are pale green to off-white.

The sesquioxide is formed by reduction of the dioxide in hydrogen or CO/CO_2 atmospheres at elevated temperatures. Some care must be used to assure that reduction is complete (e.g., the O/M ratio reached is 1.50). The dioxide of Bk (black/brown) is readily obtained by decomposition of a variety of berkelium salts (e.g., nitrate, oxalate, etc.) in air or oxygen-containing atmospheres. In fact, precautions must be used to avoid the uptake of oxygen by the sesquioxide, even at room temperature. Heating lower oxides of Bk to 500°C in air is sufficient to produce the stoichiometric dioxide. The dioxide crystallizes in the fluorite structure (see table 25) and is isostructural with the earlier actinide dioxides.

A quantitative measurement of the oxygen dissociation pressures over berkelium oxides with O/M ratios from 1.5 to 2.0 has been reported (Turcotte et al. 1971b). A complication in this study was the ingrowth of the Cf-249 daughter, which necessitated an assumption about the behavior and influence of the californium oxide present and its effect on the decomposition pressure isotherms for the berkelium oxygen system. In the study it appeared that there was evidence for the existence of Bk_7O_{12}, although efforts to obtain X-ray data for this material were not successful. A probable oversimplification of the berkelium oxygen system (Turcotte et al. 1979) gives the following picture. The cubic sesquioxide can take up oxygen to reach an O/M ratio of 1.71, where a rhombohedral structure forms. Further uptake of oxygen (e.g., O/M = 1.8) would generate a fluorite structure, which can take up oxygen until the stoichiometric dioxide forms.

2.6.10. *Californium oxides*

There has been no evidence for the existence of a monoxide of Cf, although other compounds containing divalent Cf are known; e.g., dihalides (Haire 1986). It is possible that a monoxide can be attained by high-pressure reaction of californium metal and californium oxide, as has been used for the lanthanide monoxides (Leger et al. 1980) but this reaction has not been tried with Cf. An NaCl-type lattice parameter of 0.48–0.50 would be expected for the monoxide.

The known californium oxides are the sesquioxide (three structural forms), Cf_7O_{12} and the dioxide (Haire 1986). Crystallographic data for these forms are given in

table 25. The different crystal forms of the sesquioxide are all light green. The first structural form of Cf_2O_3 that was identified was the monoclinic, B-type (Green and Cunningham 1967). This form was followed by the identification of the cubic (C-type) form of the oxide (Copeland and Cunningham 1967). It was noted in that work that the C-type of Cf sesquioxide took up oxygen when heated in air, eventually giving a dark (brown/black) oxide. The cubic form of the sesquioxide can be oxidized by heating in air or oxygen to form Cf_7O_{12} (Turcotte and Haire 1976, Haire 1976).

The hexagonal (A-type) of the sesquioxide (Baybarz 1973, Baybarz and Haire 1976) is very difficult to prepare, as it only exists in a narrow phase region between the monoclinic form and the liquid (melting point reported to be 1750°C). This crystal form of Cf_2O_3 has also been obtained from old hexagonal forms of Bk_2O_3 after about five half-lives (97% transformation) following the beta decay of Bk-249 oxide. The transformation of the cubic form to the monoclinic form of sesquioxide occurs between 1100–1400°C and the transformation of the monoclinic form to the hexagonal form occurs at about 1700°C (Baybarz and Haire 1976).

The monoclinic to cubic transition for Bk_2O_3 also appears to be "irreversible", while the hexagonal–monoclinic transition is readily reversible. This transition behavior is typical for the first four transplutonium sesquioxides.

The preparation of californium dioxide (fluorite structure; see table 25) requires very strong oxidizing conditions. It is a black material. It has been prepared by heating the cubic form of the sesquioxide under high-pressure oxygen (e.g., 100 atm) or under atomic oxygen (Baybarz et al. 1972, Haire 1976). The latter is best used for small quantities (5–50 micrograms) and thin layers, since recombination of atomic oxygen on the surface layers precludes oxidation of bulk forms of the oxide.

The dioxide, or a slightly substoichiometric dioxide, is also produced when milligram quantities of the sesquioxide are stored for long periods in air or oxygen, presumably due to active oxygen species generated intimately around the oxide by the alpha radiation of Cf (Haire 1986). In contrast, with smaller samples (e.g., microgram amounts), self-irradiation appears to bring about the loss of oxygen (Baybarz et al. 1972). The stoichiometry of aged californium oxides is difficult to ascertain by X-ray analyses (e.g., values of the lattice parameter) since the parameters may change due either (or both) to the swelling or to an increase/decrease due to the loss/gain of oxygen. An earlier review of radiation effects is recommended with reference to this point (Fuger 1975).

Complex oxides, such as $BaCfO_3$ where Cf(IV) is stabilized by the lattice, can be readily formed by heating mixtures of the components in air (Haire and Bourges 1980, Fuger et al. 1993). The material is stable up to temperatures of at least 1000°C. In contrast, CfO_2 is thermally unstable above 400°C (Haire 1986).

A manometric and X-ray diffraction study of the californium oxide system for O/M ratios of $1.5 < O/Cf < 1.72$ (Turcotte and Haire 1976) established that Cf_7O_{12} was the stable oxide obtained by heating californium salts (e.g., nitrate, oxalate, etc.) in air or oxygen up to 750°C. At higher temperatures (950°C), oxygen is readily lost (especially in vacuum) to yield the sesquioxide. The stoichiometric sesquioxide can also be prepared by heating higher oxides of Cf in hydrogen or carbon monoxide atmospheres or in vacuum to 1000°C.

The californium oxygen system can be summarized as follows. The cubic sesquioxide can take up oxygen up to an O/M ratio of about 1.7, where Cf_7O_{12} forms (rhombohedral structure). This Cf_7O_{12} compound exists only over a narrow range of O/Cf values. For O/Cf ratios between 1.8 and 2.0, a fcc (fluorite) structure is observed; the lattice parameters for these products decrease with increasing O/Cf ratios. The californium oxygen system bears some resemblance to that of the terbium oxygen system, but the complex forms known for intermediate O/M ratios in the terbium oxygen system have not been identified in the californium oxygen system except for Cf_7O_{12}. Whether this is a real difference between the two systems, or merely signifies that the californium oxygen system has been studied in less detail, is not clear.

In a study of the berkelium oxygen system (Turcotte 1980) it was concluded that the growth of the Cf daughter in berkelium oxides gave different effects, depending upon the amount of Cf. For a Cf content up to 25 mol %, the Cf in the matrix was apparently oxidized to a dioxide; when the value reached 64 mol%, the Cf content controlled the Bk oxidation and the stoichiometry of the mixed cation product was limited to the stoichiometry of An_7O_{12}. The behavior of the mixed oxides is in accord with the behaviors known for the two pure oxide systems.

2.6.11. *Einsteinium oxides*

Due both to the scarcity of einsteinium, and the high specific activity of the only isotope (Es-253) available in sufficient quantities for solid-state studies, only a limited amount of data have been accumulated for this element's oxide system. The high specific activity of this isotope makes studies very difficult and rapidly destroys the oxide lattice; very likely it would cause the rapid loss of oxygen from higher oxides, should any form.

There has been no evidence for a monoxide of Es even though some divalent halides of Es (e.g., bromide, iodide) have been prepared and studied (Hulet 1986). The only known oxide of Es is its sesquioxide, which when freshly prepared is white. On standing in air at room temperature (the actual temperature may be higher due to self-heating) for hours to days, the oxide may attain a tan color. Although indicative of some oxygen uptake (e.g., O/Es > 1.5), this color change probably indicates the generation of color centers from self-irradiation. As the Bk-249 daughter grows in at a rate of about 3% per day, a mixed oxide system is quickly generated and Bk can also contribute to the tan color of the oxide. Attempts to prepare complex oxides (e.g., $BaEsO_3$) where the lattice may stabilize Es(IV), as has been done with Cf and other actinides, have not been successful (Haire and Bourges 1980).

The best characterized einsteinium oxide is the cubic (C-type) sesquioxide, prepared by calcining nanograms of a nitrate salt and rapidly analyzing the product by electron diffraction (Haire and Baybarz 1973). A monoclinic form of the sesquioxide was observed when thin films of einsteinium metal were oxidized in oxygen-containing atmospheres at temperatures of 800–1000°C (the direct oxidation of other actinide metals can also yield the monoclinic form of their sesquioxides at temperatures lower than that required for transformation of their C- to the B- forms). This low temperature for the monoclinic form of einsteinium sesquioxide is therefore not comparable to the established transition temperatures reported for the other actinide sesquioxides. The

hexagonal form of the einsteinium sesquioxide was generated following self-irradiation of the monoclinic sesquioxide. Both of these latter crystal forms of einsteinium sesquioxide were identified by electron diffraction (Haire 1985a, Hulet 1986).

Extrapolations for the einsteinium oxide transitions based on the lanthanide oxide and transplutonium oxide systems would suggest the C- to B-type transition for Es_2O_3 to be on the order of 1400°C, and the B- to A-type transition to be at least 1650°C. Lattice parameters for the three forms of einsteinium oxide are given in table 25.

2.6.12. *Transeinsteinium oxides*

There has not been any solid-state chemistry reported for pure "bulk" forms of the transeinsteinium elements, due to the small amounts of the elements that have been available and their short lives. The most abundant of these elements is Fm [nanograms of a very short-lived (20 h) Fm-255 isotope] and the above limitations have precluded studying its oxide. When reaching the end members of the actinide series, the availability of isotopes is a much greater problem; e.g., only a few atoms of a short-lived isotope of Lr can be produced.

Based on speculation, one would expect that the highest oxides formed by the transeinsteinium elements would be their sesquioxides, and the C-type structure would be the favored, or perhaps the only, structural form. A monoxide may become more probable for elements following Fm in the series due to the increased tendency toward divalent stability across the series; especially at No. The last member, Lr, almost certainly would form a sesquioxide, based on its filled 5f state ($5f^{14}$, like Lu in the lanthanide series).

2.7. *Thermodynamic properties of binary oxides*

The thermodynamic properties of the actinides are not as well established as those for the lanthanides, except for perhaps the elements U and Pu. These latter two actinides have a great deal of information available about them because of their applications in nuclear energy and weapons. It is also true that summaries of acitinide thermodynamics have not kept pace with experimental studies on these elements, perhaps because the experimental data tend to be somewhat more limited in scope and lacking in agreement than data available for nonradioactive materials.

There have been some reviews and discussions of thermodynamic properties of the actinides. One source of information is the International Atomic Energy Agency's reports (IAEA Rep. 1965, 1967) and reviews (Rand 1966, 1975, Wagman et al. 1981, Oetting 1967). In addition there are other discussions concerning the thermodynamics of the actinides for the reader to consider (Morss 1986, 1983, 1985, 1993).

For the monoxides in general, which have questionable or limited existence (see sections 1.2.1 and 2.4.1), thermodynamic calculations have shown that their stability is questionable. Even for the lanthanide monoxides, calculations have shown that these are only marginally stable (Morss 1986). In the case of CfO, Morss reports that this monoxide would be subject to disproportionating to metal and oxygen.

With regard to the actinide sesquioxides, excluding Ac_2O_3, the first sesquioxide occurs at Pu in the series and the last experimentally established sesquioxide is Es_2O_3.

TABLE 26
Experimental enthalpies of formation (a; kJ mol^{-1}) and standard entropies (b; J mol^{-1} K^{-1}) for actinide binary oxides.

An(III)*	An(IV)	An(V)	An(VI)
	ThO_2		
	$a = -1226.4$ (3.5)		
	$b =$ 65.23(0.20)		
	UO_2	$UO_{2.33}$	UO_3
	$a =$ 1085.0 (1.0)	$a = -1142.4$ (0.9)	$a = 1223.8$ (2.0)
	$b =$ 77.03(0.20)	$b =$ 83.51	$b =$ 96.11(0.40)
	NpO_2		
	$a = -1074.0$ (2.5)		
	$b =$ 80.3 (0.4)		
Pu_2O_3	PuO_2		
$a = -828(10)$	$a =$ 1056.2 (0.7)		
$b =$ 81.51(0.32)	$b =$ 66.13(0.26)		
Am_2O_3	AmO_2		
$a = -845(8)$	$a = -932.2$ (2.7)		
Cm_2O_3	CmO_2		
$a =$ 841.5(6.0)	$a = -911$ (6)		
Cf_2O_3	CfO_2		
$a = -826.5(5)$E	$a = -854(10)$		

*$\frac{1}{2}\Delta H_f^0$ (Am_2O_3(c))

Thus, one finds that the sesquioxides of Th, Pa, U and Np are thermodynamically unstable with regard to disproportionation to the metals and dioxide (Morss 1986). An overview of the enthalpies of formation and standard entropies for some binary actinide oxides are listed in table 26 (from Katz et al. 1986a). Morss (1986, see also ch. 122 in this volume) has described the cycle employed in obtaining the enthalpies of solution and formation for these oxides. The enthalpies of solution of the actinide oxides is expected to change slowly and smoothly as a function of ionic size of the metal ion. The enthalpies of formation of Am sesquioxide (Morss and Sonnenberger 1985), of Cm sesquioxides (Morss 1983), and of Cf sesquioxide (Morss et al. 1987, Haire and Gibson 1992) have been measured directly.

All of the actinides from Th through Cf form dioxides but several of these have not been studied thermodynamically, due in part to their instability and to limited availability (e.g., it is very difficult to prepare multi-milligrams of CfO_2 even though such quantities of the isotope are available). Plots of enthalpy of solution for the f elements have been established (Morss 1986) which permit estimating values for the other actinide dioxides. Although binary oxides above the dioxide stoichiometry are known for some of the actinides (Pa, U, Np), little thermodynamic data are available for these oxides.

The situation is different for complex oxide systems. Although this topic is beyond the scope of this chapter, one such case is worth mentioning. This deals with the $MAnO_3$ (M denotes an alkaline earth), perovskite-type compounds, which provide stability for the An(IV) oxidation state. Data for several lanthanide and for Am compounds of this type have been published (Goudiakas et al. 1990); data for Cm and

Cf compounds have been acquired recently (Fuger et al. 1993). A linear relationship exists between the heat of formation of these perovskite-type oxide systems and the Goldschmidt tolerance factor, which permits estimations for the enthalpies of formation of a number of homologous compounds of this type. From data of such Cf compounds, the enthalpy of formation of CfO_2 was estimated to be $-854 + 10$ kJ mol^{-1}, in good agreement with a value of -858 kJ mol^{-1} derived from interrelationships between the molar volumes of dioxides and their standard enthalpies of solution (Morss 1986). It has not been feasible to carry out such direct experimental measurements with CfO_2 and these indirect approaches have provided the only data of this type. Data for other actinide oxides can similarly be obtained by these indirect approaches.

Another aspect of the thermodynamics of actinide oxides is their high-temperature vaporization/decomposition behaviors. A considerable amount of work has been done on the Th through Pu oxide systems but only a limited effort on the transplutonium oxides. For this first group of oxides, the dioxides are the systems that are normally studied, although the Pu sesquioxide has also been examined. For the transplutonium oxides, it is generally the sesquioxides that are studied, as higher oxides decompose at relatively low temperatures to the sesquioxides (BkO_2 is an exception). Thus, both the sesquioxides and the dioxides of Pu and Bk can be studied at higher temperatures, although little is known about the thermal stability of BkO_2. For the lanthanides, such high-temperature behavior can be studied only for CeO_2.

The only thermodynamically stable solid oxide of Th is its dioxide; its monoxide disproportionates to the metal and dioxide. The vaporization behavior of ThO_2 has been investigated and the vapor species are ThO_2(g), ThO(g) and Th(g) (Ackermann and Rauh 1973b). The thermodynamic properties of ThO(g) have also been studied (Ackermann and Chandrasekharaiah 1974). The free energies of formation of the gaseous monoxide, dioxide and solid dioxide are given in table 27.

The thermodynamic behavior of protactinium oxides is not as well established as for the ThO_2 system. The free energy of formation of PaO_2(s) has been derived from carbothermic reductions. The entropy of formation of the dioxide is comparable to the other actinide dioxides (see table 27; data from Ackermann and Chandrasekharaiah (1974)]. A partial study of the reduction of Pa_2O_5 has also provided data for the protactinium oxide system (Kleinschmidt and Ward 1986).

The uranium oxygen system is complex and has been the topic of numerous studies. Part of the problem with the studies has been the exact stoichiometry of the phases being examined (see earlier discussion about the numerous oxide phases of U). Most efforts have dealt with the dioxide system and several reviews have been made (Ackermann and Chandrasekharaiah 1974 and references therein, Weigel 1986). The solid monoxide of uranium is at best metastable. Vaporization of the dioxide yields the following major species; U(g), UO(g), and UO_2(g). Discrepancies with regard to the free energy of formation of UO_3(g) – one of the species that has been seen over UO_{2+x}(s) – have been discussed.

The condensed oxides of Np have had only limited characterization, especially as compared to the uranium system. Early studies suggested that neptunium dioxide did not form superstoichiometric compositions, in contrast to the uranium system. The

TABLE 27
Thermodynamic values for actinide elements and their gaseous/solid oxides.

Material	ΔH_f^0(kJ mol^{-1})	ΔG_f^0(kJ mol^{-1})	S^0(J K^{-1} mol^{-1})
Ac (c)	0	0	[62(1)]
Ac (g)	[418(13)]	–	–
Ac_2O_3 (c)	[−1756(80)]		[67]
Th (c)	0	0	52.64
ThO (g)	−28(2)		240.0
ThO_2 (c)	−1226.4(3.5)	−1168.7	65.23(0.20)
ThO_2 (g)	497(3)	–	65.22
Pa (c)	0	0	55(1)
Pa (g)	370(26)	527	198
PaO_2 (c)	[−1109]	[−1044]	[77]
Pa_2O_5 (c)	–	–	[88]
U (c)	0	0	50.2
UO (c)	–	–	[68]
UO (g)	21	12	–
UO_2 (c)	−1085.0(1.0)	−1031.8	77.03(0.20)
UO_2 (g)			
UO_3 (c)	−1217.5(1.3)	−1140.6(1.3)	99.4(0.4)
UO_3 (g)	−816	–	–
Np (c)	0	0	50.3
Np (g)	465	421	198
NpO (c)	–	–	[69]
NpO (g)	–	–	
NpO_2 (c)	−1074(3)	−1022(3)	80.3(0.4)
NpO_2 (g)	–	–	–
NpO_3 (c)	[−1070(6)]	–	–
Np_2O_3 (c)	[−1522]	[−14483]	[160]
Pu (c)	0	0	54.46
Pu (g)	342(2)	305	177
PuO (c)	[365]	–	[76(6)]
PuO (g)	−92	−119	249
Pu_2O_3 (c, α)	[−836(11)]	[−795]	76
Pu_2O_3 (c, β)	[−1656]	[−1580]	163.0(0.6)
PuO_2 (c)	−1056.2(0.7)	−998.0(0.7)	66.13(0.26)
PuO_2 (g)	−422	–	–
Am (c)	0	0	55.4(2)
Am (g)	284(4)	242	194
AmO (g)			[86]
AmO_2 (c)	−573		[−92]
Am_2O_3 (c)	−1692(15)	–	[86]
Cm (c)	0	0	[72(1)]
Cm (g)	387.4(2.1)	350(2)	197.3
CmO (g)	122	−136	45
Cm_2O_3 (c)	−1682(12)	–	[161]
CmO_2 (c)	−911(6)		[87]
Bk (c)	0	0	[78 (1)]
Bk (g)	[310(6)]	–	200
Bk_2O_3 (c)	[−1694]	–	–
BkO_2 (c)	[−1021]	–	[89]
Cf (c)	0	0	[81 (1)]
Cf (g)	196(1)	–	–

TABLE 27 (continued)

Material	ΔH_f^0 (kJ mol^{-1})	ΔG_f^0 (kJ mol^{-1})	S^0 (J K^{-1} mol^{-1})
Cf_2O_3 (c)	−1653	–	–
CfO_2 (c)	[858]	–	–
Es (c)	0	0	[89]
Es (g)	133	–	–
Es_2O_3 (c)	[−1696]	–	–
EsO_2 (c)	[763]	–	–
Fm (c)	0	0	[91]
Fm (g)	[130]	–	–
Fm_2O_3 (c)	[−1694(86)]	–	–
Md (c)	0	0	[87]
Md (g)	[128(8)]	–	–
Md_2O_3 (c)	[−1535]	–	–
No (c)	0	0	[65]
No (g)	[126]	–	–
No_2O_3 (c)	[−1260]	–	–
Lr (c)	0	0	[55]
Lr (g)	[341]	–	–
Lr_2O_3 (c)	[−1766]	–	–

vaporization behavior of NpO_2 suggests that a substoichiometric composition is stable at temperatures over 2000 K and that an A-type sesquioxide of Np is precipitated upon cooling. Thermodynamic properties for Np oxides and the vaporization of neptunium monoxide and dioxide have been described (Ackermann et al. 1966a, b, Ackermann and Chandrasekharaiah 1974, 1975, Ackermann and Rauh 1975). With NpO_2, one observes NpO(g) and NpO_2(g) as the vapor species at high temperatures. Some pertinent thermodynamic values for neptunium oxides are given in table 27.

With the plutonium oxygen system, except for some hydrated materials, the highest oxides that forms is the dioxide. The dioxide exhibits extensive substoichiometry at high temperatures. The equilibrium vapor species for the plutonium oxygen system is made up of Pu(g), PuO(g) and PuO_2(g) at high temperatures (Weigel 1986, Baitles et al. 1969, Ackermann et al. 1966a, Ackermann and Chandrasekharaiah 1974). It appears that the congruently vaporizing composition is $1.9 > O/Pu > 1.8$, which is within the substoichiometric region of the dioxide phase between 1600–2400 K. An IAEA panel (Morss 1986) adopted a value of $82.4 + 4.2$ J mol^{-1} K^{-1} for the absolute entropy of PuO_2 at 298 K corrected for magnetic ordering; the latter has not been observed experimentally. Sandenaw (1963) measured an entropy of 68.2 J mol^{-1} K^{-1}. The data in table 27 for plutonium dioxide are revised without including the magnetic ordering. It has been determined (Morss 1986) that solid PuO is just unstable to disproportionation to Pu(l) and Pu_2O_3(s).

The number of vaporization studies that have been carried out on the oxides of Th, U and Pu is large compared to those performed on the transuranium oxides. At times the results of the studies on the lighter actinide oxides conflict with one another. These differences and the thermodynamics of these systems have been summarized (Acker-

mann and Chandrasekharaiah 1974, Ackermann and Thorn 1962, Ohse and Ciani 1968, Markin and Rand 1966, Ackermann et al. 1966b, Ackermann and Rauh 1975).

The quantity of high-temperature data for the transplutonium oxides is very limited, which is unfortunate as these are the actinides most like the lanthanides. Some vaporization data from a mixed $PuO_{1.6}/Am_2O_3$ system have indicated that the main mode of vaporization/decomposition for americium sesquioxide is via the generation of Am(g) and O_2(g) (Ackermann and Chandrasekharaiah 1974). This finding has been supported by other unpublished work (Kleinschmidt 1992, Haire 1992a). The solid monoxide of Am has been considered to be barely stable toward disproportionation in the solid phase and its existence as a gaseous species is reasonable. Based on the tendency toward divalency for higher members in the series, the monoxide would be expected to become the most prevalent vapor species.

A study of the americium dioxide system is complicated by the fact that the dioxide begins to lose oxygen above 1000°C and the stoichiometry of the resulting oxide phase becomes less certain. The enthalpy of formation of this dioxide has been estimated from a relationship of the enthalpies of formation of other actinide dioxides with the enthalpies of formation of the An^{+4} aquo ions (Morss 1986). The phase behavior and the partial molar free energy of oxygen over AmO_{2-x}(s) between 870 and 1170°C have been determined and these data have been used to yield the standard free energies, enthalpy and entropy of formation for the Am oxides (Chikalla and Eyring 1967).

The vaporization behavior for Cm sesquioxide has been reported (Smith and Peterson 1970). Mass-spectrometric data were not obtained in this study and the species were assigned based only on the systematics. The researchers believed these data support the congruent vaporization of Cm_2O_3 to yield CmO(g) and O(g). An enthalpy of vaporization of 1795 kJ mol^{-1} at 0 K was derived. Curium oxides with O/M ratios higher than 1.5 are not stable above 900°C (CmO_2 decomposes above 400°C), and therefore the vaporization processes of oxides having O/M ratios above 1.5 cannot be measured experimentally.

Data for berkelium oxides and the transcalifornium oxides are not published, although initial studies of BkO_2 have been carried out (Haire 1992a). Just as with curium oxides, californium oxides above the sesquioxide are not stable at temperatures where vaporization processes can be studied. Preliminary data for the vaporization/decomposition of Cf_2O_3 (Haire and Gibson 1992, Haire 1994) show that the process yields Cf(g) and O(g) as products, and has an enthalpy of decomposition of about 1025 kJ mol^{-1} at an average temperature of 1800 K. An enthalpy of formation of Cf_2O_3 of -1694 kJ mol^{-1} at 298 K was estimated, which agrees with a value of -1653 kJ mol^{-1} derived from solution calorimetry (Morss 1986). It is likely that transcalifornium sesquioxides through No would also vaporize/decompose via generation of atomic vapor and oxygen atoms (see section 3). For Lr_2O_3, the behavior would be expected to be more comparable to that reported for Cm_2O_3 (Haire 1994).

2.8. *Magnetic properties of binary oxides*

If the actinide series were characterized by the filling of the 5f shell with localized electrons across the series, the magnetic behavior of the actinides would be analogous

to that found for the lanthanides. In reality, many of the early actinides have itinerant 5f electrons which affect their magnetic behavior, since the magnetic properties arise from the spin and orbital angular momenta of unpaired electrons. If unpaired electrons are not present in a material (e.g., f electrons are involved in bonding), a magnetic moment would not be observed. In addition to the magnetic moments per se, one is also interested in the magnetic properties: in the behavior of a material as a function of temperature and in the existence of magnetic transitions (e.g., antiferromagnetic, paramagnetic, etc.).

The magnetic properties of the binary actinide oxides have been reviewed (Huray and Nave 1987, Edelstein and Goffart 1986, Huray et al. 1983b). Many of the early actinide oxides have itinerant electrons and display low or zero moments, depending on the oxidation state of the actinide in the oxide. There have been some detailed studies on UO_2, both as a pure oxide and as a dopant in ThO_2. Magnetic measurements have also been reported for NpO_2; above 60 K, the susceptibility of NpO_2 follows a Curie–Weiss law with a u_{eff} moment of about $3\mu_B$. PuO_2 exhibits temperature-independent paramagnetism between 4 and 1000 K. For the transplutonium oxides, the 5f electrons are localized; consequently a near free ion behavior is achieved and the materials exhibit paramagnetic moments.

The transplutonium oxides are useful for studying crystal-field effects or interactions, as the dioxides and the C-type sesquioxides have cubic symmetry and both oxide stoichiometries are available for most of the oxides. The magnetic behavior of these transplutonium oxides is compared with their lanthanide counterparts in section 3. The behavior of individual oxides is discussed briefly here and data are provided in table 28.

Trivalent americium oxides are expected to have a $5f^6$ core and therefore should display a zero moment. Due to the existence of low-lying excited electronic states, this zero moment is difficult to observe experimentally (Kannelakopulos et al. 1978). Measurements (Soderholm et al. 1986) of a pure A-type americium sesquioxide have indicated temperature-independent paramagnetism from 5 to 300 K. In other work, Karraker (1975a) studied AmO_2 between 2 and 97 K, but found two different regions that displayed Curie–Weiss behavior.

Curium sesquioxide has been studied by various groups (Nave et al. 1983, Morss et al. 1983). A trivalent curium ion should have a $5f^7$ free-ion moment of 7.92 (simple L–S coupling) or $7.55\,\mu_B$ based on intermediate coupling. These values are in accord with the range of values that have been measured (see table 28).

The dioxide of Cm presents another situation. The expected $5f^6$ core of Cm(IV) should produce a zero moment (as does the f^6 core of Am_2O_3), but a temperature-independent paramagnetic behavior has not been observed for CmO_2 to date (Nave et al. 1983). Thus Cm(IV) compounds in general show an anomalous temperature dependence and display moments ranging from $2–4\,\mu_B$ instead of the expected zero moment. The smallest measured moment reported for CmO_2 was $1.63\,\mu_B$. This sample had the smallest X-ray lattice parameter of the dioxide samples that have been studied, which suggests it had the highest O/M ratio (very close or equal to 2.00).

The simplest interpretion or explanation for a nonzero moment in CmO_2 would be nonstoichiometry due to the preparation difficulties or radiation damage and lower-

TABLE 28
Magnetic properties of actinide oxides.

Oxide (structure)	Configuration	$\mu_{eff}(\mu_B)$ (I.C.)	$\mu_{eff}(\mu_B)$	Θp(K)	Details
$Ac_2O_{3\ (hex)}$	f^0	–	–	–	Not studied
ThO_2 (fcc)	f^0	0	0	–	–
PaO_2 (fcc)	f^1	–	1.0	–	–
UO_2 (fcc)	f^2	–	3.7	–	–
NpO_2 (fcc)	f^3	–	3.0	–	Above 60 K
PuO_2 (fcc)	f^4	–	–	–	Exhibits TIP between 4–100 K
AmO_2 (fcc)	f^5	1.2	1.3	21	15–40 K (Γ_7)
			1.5	41	50–100 K (Γ_8)
Am_2O_3 (hex)	f^6	0	0	–	TIP 5–300 K
CmO_2 (fcc)	f^6	0	1.6–2.3	12–25	–
$BaCmO_3$ (fcc)	f^6	0	1.6–1.7	18–30	–
Cm_2O_3 (fcc)	f^7	7.6	8.2	+149	20–80 K
			7.9	+130	100–300 K
$^{244}Cm_2O_3$ (?)	f^7	7.6	6.1	22.5	2–50 K
Cm_2O_3 (mono)	f^7	7.6	7.5	72	100–300 K
Cm_2O_3 (mono)	f^7	7.6	7.7	130	50–300 K
Cm_2O_3 (bcc)	f^7	7.6	7.5	110	50–300 K
BkO_2 (fcc)	f^7	7.6	7.8	250	50–300 K (3% Cf)
BkO_2 (fcc)	f^7	7.6	8.1	224	50–300 K (3% Cf)
(BkO_2) ThO_2 (fcc)	f^7	7.6	7.7	12	10–95 K (Γ_6)
			5.8	−34	95–200 K (Γ_8)
Bk_2O_3 (bcc)	f^8	9.3	9.0	141	60–300 K (2% Cf)
CfO_2 (fcc)	f^8	9.3	9.1	70	100–340 K
$BaCfO_3$ (bcc)	f^8	9.3	9.2	210	100–340 K
Cf_7O_{12} (rhom)	$(40\%\, f^9 + 60\%\, f^{10})$	9.7	9.5	95	100–340 K
Cf_2O_3 (mono)	f^9	10.2	10.1	80	100–340 K
Cf_2O_3 (bcc)	f^9	10.2	9.8	115	100–340 K
Es_2O_3 (bcc)	f^{10}	10.3	10.5	53	4.2–180 K (13% Bk)

than-expected oxygen content, but this is not satisfactory based on X-ray and neutron diffraction data available for the samples studied. An alternative explanation would be an electronic configuration that deviates from the pure $5f^6$ state that is predicted for CmO_2. At the present time the reason for this nonzero moment for CmO_2 remains unanswered.

Beyond curium in the actinide series, the amount of magnetic data available becomes much smaller. Measurements for BkO_2 (Nave et al. 1983) and for BkO_2 in ThO_2 (Karraker 1975b) have been made and some work has been reported for studies of Bk_2O_3 (Huray and Nave 1987). The moments for the dioxide and the sesquioxide of Bk

are in fair agreement with the moments expected for these materials based on their electronic configurations (see table 28).

The magnetic behavior of Cf_2O_3, Cf_7O_{12} and $BaCfO_3$ have been reported (Moore et al. 1986). CfO_2 could not be prepared in significant quantities for magnetic measurement; the Cf(IV) state was attained instead in the $BaCfO_3$ compound. All three compounds exhibited Curie–Weiss behavior above 100 K and gave evidence for antiferromagnetic ordering. The moments for these oxides are in reasonable agreement with the expected values for them (see table 28). The moment of the Cf_7O_{12} compound was calculated using a weighted susceptibility based on the expected presence of the two oxidation states [e.g., 60% Cf(IV) and 40% Cf(III)].

A single magnetic measurement has been made on Es_2O_3 (Huray et al. 1983a). The moment for the latter material was in reasonably good agreement with that expected for a $5f^{10}$ configuration, considering the experimental difficulties incurred with the highly radioactive Es sample. Experimental magnetic data for higher members of the actinide series have not been, and likely will not be, measured.

2.9. *Other properties of binary actinide oxides*

It is worthwhile to mention briefly other aspects concerning the oxides. One area is the photoelectron spectrometry of the actinides covering the elements Ac through Es, which provides binding energies for selected electrons (Krause et al. 1988).

Another aspect is the electronic structure of the oxides. A recent report (Goodman 1992) has compared experimental results with two type of calculations (molecular orbital and traditional crystal field). In this latter work, the problem of the magnetic susceptibility of CmO_2 is discussed. The thermal diffusivity and conduction of Cm_2O_3 has also been reported and compared to data for ThO_2, UO_2 and PuO_2 (Gibby et al. 1970). The thermal expansion coefficient of CmO_2 using the Cm-248 isotope has been reported (Noe and Peterson 1972). Lattice defects in dioxides, both due to self-irradiation and from reactor irradiations, have been discussed (Kapshukov et al. 1976, Matzke 1976, Vallath 1976). A more extensive and general discussion of self-irradiation has been published (Fuger 1975).

The high-pressure behaviors and bulk moduli of the actinide dioxides ThO_2, PuO_2, AmO_2 (Dancausse 1991), UO_2 (Benedict et al. 1992a, b) and NpO_2 (Benedict et al. 1986) have been reported. The tendency is for the cubic (fluorite) structure to undergo a phase transition under pressure to yield a structure of orthorhombic symmetry. The bulk moduli, derived from such high-pressure studies of these dioxides, are all large: ThO_2, 252 GPa; UO_2, 207 GPa; NpO_2, 200 GPa; PuO_2, 367 GPa; and AmO_2, 280 GPa. These values indicate a "stiff" lattice which is not very compressible.

A review and a discussion of the electron paramagnetic resonance of the actinides has been published (Boatner and Abraham 1980). Discussions and references cited in this report are relevant to oxide systems.

Other aspects of the actinide oxides are discussed and the general properties and behavior of the actinide oxides compared to those of the lanthanide oxides in section 3.

3. Comparison of the binary oxides of the lanthanide and actinide elements

The objective of this section of the chapter is to compare the properties and behaviors of the binary oxides of the lanthanide and actinide elements. The trends and the differences between the binary oxides of each series of elements are reviewed but a discussion of the more complex (e.g., ternary or larger) oxides that these elements are known to form is excluded. Essentially this section offers a comparison of the monoxides, sesquioxides, dioxides and binary oxides with O/M ratios intermediate to those found in these three oxides. Since the lanthanide elements do not form oxides with higher O/M ratios than 2.0, actinide oxides with higher oxygen stoichiometries are not discussed in this section.

3.1. *General comparison*

The actinides are probably more like the lanthanides in their oxide forms than in the solid phases of their other compounds. This is especially true when considering the metallic states, where large deviations are apparent. If an actinide exists in a particular oxide stoichiometry (e.g., a sesquioxide), it is likely to have comparable chemical and physical behavior to that of a lanthanide sesquioxide that has a similar ionic radius. The first important point for these two series of oxides is whether a particular stoichiometry is formed by different members of each series.

A comparison of oxides is shown in fig. 15 which compares and summarizes, in a simple fashion, the oxide formation behavior for the two series of elements. It is obvious that, excluding the behavior of Pa, U and Np, the actinides show a greater tendency for variable oxide stoichiometries than do the lanthanides. The most striking difference (besides the fact that the elements Pa through U form oxides above the dioxide) is that all the actinides from Th through Cf form dioxides, while lanthanide dioxides are known only for Ce, Pr and Tb (the dioxides of Pr and Tb are more difficult to form). Only two oxide stoichiometries are shown for Ce and Pu in fig. 15. In reality, oxides with O/M ratios between 1.5 and 2.0 are known for both elements, although those for

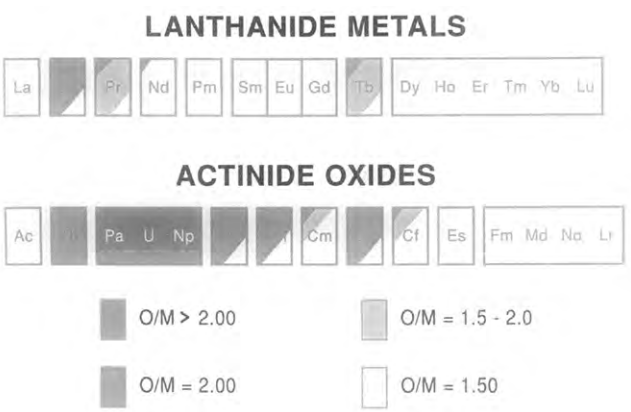

Fig. 15. Oxides of the lanthanides and actinides.

Pu are limited in scope. As mentioned in section two, the fact that Cm (the homolog of Gd) forms a dioxide is in itself surprising. The reason for the greater tendency for the actinides to form dioxides must be due, for the most part, to the larger spatial extension and energetics of their 5f orbitals.

Another significant difference between the two series is that, except for actinium (which like lanthnaium is not always considered the first member of its series) the earlier members of the actinide series (Th–Np) do not form sesquioxides. The first sesquioxide in the series occurs with Pu_2O_3. There are several good correlations between the sesquioxides of the first five transplutonium elements and those of the lanthanides, although these correlations involve a shift of the actinide with regard to a given lanthanide (see below).

Table 29 gives the electronic configurations for the lanthanide and actinide elements [configurations for gaseous atoms; configurations can be different in the solid state, see Brooks et al. (1984), Fournier and Manes (1985), Katz et al. (1986a), for their ions, and for their established solid oxides of a single oxidation state (intermediate valence states are excluded)]. Examination of these data can be informative, and give a feeling why each element forms a particular oxide. However, care must be used not to overextend the use of these configurations.

In the case of Ce (which forms both a sesquioxide and a dioxide) and Th (which essentially forms only a dioxide) there is a large difference in the stability of these nominally one f-electron elements, which is evident in their chemistry. With Cm, it is perhaps surprising that the stability of attaining a half-filled 5f orbital is not a controlling factor in the formation of oxides, as it appears to be in the case of Gd. Thus,

TABLE 29
Electronic configurations of f-block atoms and ions*.

Lanthanide series				Actinide series					
Element	Atom	M^{3+}	M^{4+}	Element	Atom	M^{+}	M^{2+}	M^{3+}	M^{4+}
La	$5d\,6s^2$			Ac	$6d\,7s^2$	$7s^2$	7s		
Ce	$4f\,5d\,6s^2$	$4f^1$		Th	$6d^2\,7s^2$	$6d\,7s^2$	$5f\,6d$	$5f^1$	
Pr	$4f^3\,6s^2$	$4f^2$	$4f^1$	Pa	$5f^2\,6d\,7s^2$	$5f^2\,7s^2$	$5f^2\,6d$	$5f^2$	$5f^1$
Nd	$4f^4\,6s^2$	$4f^3$		U	$5f^3 6d\,7s^2$	$5f^3\,7s^2$	$5f^3\,6d?$	$5f^3$	$5f^2$
Pm	$4f^5\,6s^2$	$4f^4$		Np	$5f^4\,6d\,7s^2$	$5f^5\,7s?$	$5f^5?$	$5f^4$	$5f^3$
Sm	$4f^6\,6s^2$	$4f^5$		Pu	$5f^6\,7s^2$	$5f^6\,7s$	$5f^6$	$5f^5$	$5f^4$
Eu	$4f^7\,6s^2$	$4f^6$		Am	$5f^7\,7s^2$	$5f^7\,7s$	$5f^7$	$5f^6$	$5f^5$
Gd	$4f^7\,5d\,6s^2$	$4f^7$		Cm	$5f^7\,6d\,7s^2$	$5f^7\,7s^2$	$5f^8$	$5f^7$	$5f^6$
Tb	$4f^9\,6s^2$	$4f^8$	$4f^7$	Bk	$5f^9\,7s^2$	$5f^9\,7s$	$5f^9$	$5f^8$	$5f^7$
Dy	$4f^{10}\,6s^2$	$4f^9$		Cf	$5f^{10}\,7s^2$	$5f^{10}\,7s$	$5f^{10}$	$5f^9$	$5f^8$
Ho	$4f^{11}\,6s^2$	$4f^{10}$		Es	$5f^{11}\,7s^2$	$5f^{11}\,7s$	$5f^{11}$	$5f^{10}$	$(5f^9)$
Er	$4f^{12}\,6s^2$	$4f^{11}$		Fm	$5f^{12}\,7s^2$	$(5f^{12}\,7s)$	$(5f^{12})$	$(5f^{11})$	(5^{10})
Tm	$4f^{13}\,6s^2$	$4f^{12}$		Md	$(5f^{13}\,7s^2)$	$(5f^{13}\,7s)$	$(5f^{13})$	$(5f^{12})$	$(5f^{11})$
Yb	$4f^{14}\,6s^2$	$4f^{13}$		No	$(5f^{14}7s^2)$	$(5f^{14}\,7s)$	$(5f^{14})$	$(5f^{13})$	$(5f^{12})$
Lu	$4f^{14}\,5d\,6s^2$	$4f^{14}$		Lr•	$(5f^{14}\,6d\,7s^2)$	$(5f^{14}\,7s^2)$	$(5f^{14}\,7s)$	$(5f^{14})$	$(5f^{13})$

* Configurations for electrons beyond the Rn core; data are for the ground-state gaseous atoms and charged ions.

• Nonrelativistic configurations.

curium forms a dioxide expected to have a $5f^6$ configuration at the expense of the stabilizing effect provided by having a half-filled f orbital.

In comparing berkelium and terbium, the situation with their configurations seems clearer; both form a half-filled f orbital in their dioxides, although there is a large difference in ease of formation and stability of these two dioxides. The dioxide of Bk is very stable and readily forms in air, whereas the formation of TbO_2 requires highly oxidizing conditions and TbO_2 is less stable thermally.

One final comparison can be made by looking at the oxides formed by Dy and Cf, which are electronic homologs. The oxide system of Dy is essentially that of Dy_2O_3, while with Cf, in addition to its sesquioxide, there are Cf_7O_{12} and CfO_2 (CfO_2 is difficult to form, as is TbO_2). Comparisons between other pairs of lanthanide and actinide oxides are also informative.

A useful comparison of the relative stabilities of the oxidation states for the two series of elements is obtained from examining oxidation–reduction potentials. Although, as in the case of electronic configurations, these potentials for predicting oxide formation must be used cautiously, and at best this is only qualitative in nature since many other factors play a role in determining the compounds that are formed (e.g., complexation). These potentials are best used for correlating the stabilities of species in solution. Comparative oxidation potentials for the lanthanide and actinides were published many years ago (Nugent et al. 1971) as shown in figs. 16 and 17; there have also been several other compilations of potentials for the actinides (Katz et al. 1986b, Samhoun and David 1976).

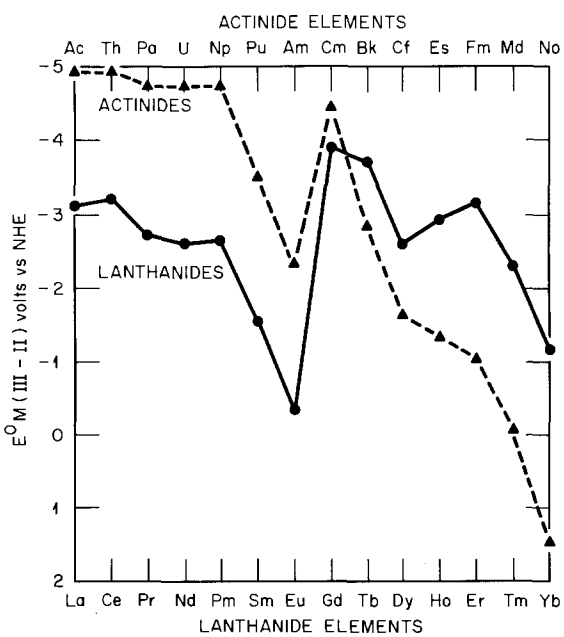

Fig. 16. Reduction potentials for the M(III)/(II) couples.

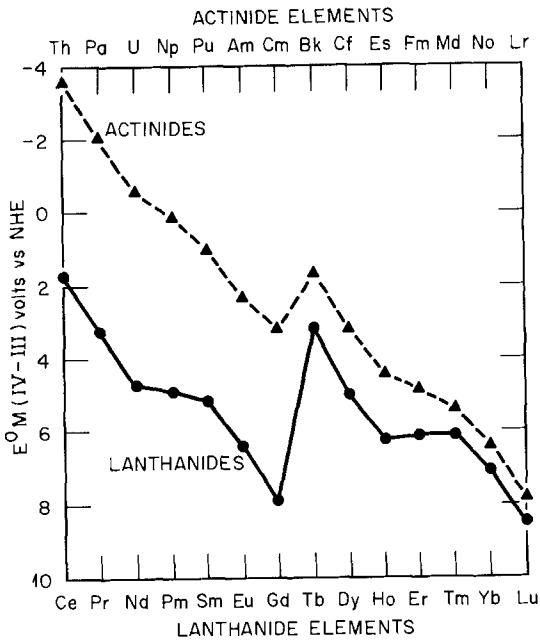

Fig. 17. Reduction potentials for the M(IV)/(III) couples.

With these oxidation potentials as a basis for comparison, examining the data in fig. 16 and assigning Eu as a reference f element for forming a divalent oxide (e.g., a monoxide), the first actinides expected to have stable monoxides would be Md and No. Although there have been reports (see section 2) of earlier actinides forming monoxides, it is questionable if a stable bulk form of a monoxide for these actinides actually exists. Three actinides, Cf, Es and Fm, show (III)/(II) couples close to that for Yb. It has been shown that YbO (see section 1) is much more difficult to prepare than EuO; on this basis, preparing the monoxides of Cf, Es or Fm (none of which have been reported to date) should be rather difficult and probably would require reactions between carefully controlled quantities of their oxides and their metals under pressure. However, solid dihalides of Yb are known and several dihalides of Cf and Es have been prepared, showing that this oxidation is a viable one for these two elements.

A qualitative picture can be formed by examining fig. 17, where the (IV)/(III) couples are shown for the lanthanides and actinides, and by assigning Pr and Tb as the reference lanthanides for formation of a dioxide. It would be expected that all the actinides before Es would form dioxides (which they do); curium and californium dioxides would only be marginally stable, and should be more difficult to prepare than the other actinides dioxides (which is also correct). Further, BkO_2 should be more stable than TbO_2, which is seen experimentally. For reference, the order of stability of the transplutonium and lanthanide dioxides has been determined to be: Bk > Ce > Am > Cm > Pr > Tb > Cf; this order is in agreement with that predicted from the curves in fig. 17.

TABLE 30
Comparison of selected radii of actinides and lanthanides.

Ion	Compound	Radius* nm × 10	Ion	Compound	Radius* nm × 10
La^{3+}	sesquioxide	1.018	Ac^{3+}	sesquioxide	1.016
Ce^{3+}	sesquioxide	1.018	Th^{3+}	–	–
Pr^{3+}	sesquioxide	1.008	Pa^{3+}	–	–
Nd^{3+}	sesquioxide	0.995	U^{3+}	–	–
Pm^{3+}	sesquioxide	0.976	Np^{3+}	–	–
Sm^{3+}	sesquioxide	0.964	Pu^{3+}	–	0.987
Eu^{3+}	sesquioxide	0.950	Am^{3+}	–	0.985
Gd^{3+}	sesquioxide	0.938	Cm^{3+}	–	0.979
Tb^{3+}	sesquioxide	0.920	Bk^{3+}	–	0.954
Dy^{3+}	sesquioxide	0.907	Cf^{3+}	–	0.949
Ho^{3+}	sesquioxide	0.894	Es^{3+}	–	0.928
Er^{3+}	sesquioxide	0.881	Fm^{3+}	–	–
Tm^{3+}	sesquioxide	0.869	Md^{3+}	–	–
Yb^{3+}	sesquioxide	0.858	No^{3+}	–	–
Lu^{3+}	sesquioxide	0.848	Lr^{3+}	–	–
Ce^{4+}	dioxide	0.898	Th^{4+}	dioxide	0.984
Pr^{4+}	dioxide	0.890	Pa^{4+}	dioxide	0.944
			U^{4+}	dioxide	0.929
			Np^{4+}	dioxide	0.913
			Pu^{4+}	dioxide	0.896
			Am^{4+}	dioxide	0.888
			Cm^{4+}	dioxide	0.886
Tb^{4+}	dioxide	0.817	Bk^{4+}	dioxide	0.870
			Cf^{4+}	dioxide	0.859
			Es^{4+}	–	–

* Radii derived from sesquioxide lattice parameters using an oxygen radius of 0.146 nm and adding 0.88 nm for covalent M–O bond character; six-coordinated metal ion. Radii derived from dioxide lattice parameters using the same oxygen radius, correcting for covalent character of M–O bond (+0. 010 nm) and for coordination numbers of eight to six (– 0.008 nm).

Assuming that the lanthanide and actinide dioxides are truly stoichiometric, a self-consistent and relative set of quadrivalent radii can be calculated from their lattice parameters. These radii are given in table 30. The actinide dioxides are known to have larger lattice parameters than their lanthanide electronic homologs. Thus, PuO_2 has a parameter similar to that for CeO_2, which is four elements to the left of samarium, the vertical 4f homolog of Pu. This is a greater shift than that observed with the sesquioxides (see below). Structurally, the dioxides of the lanthanides and actinides are isostructural, and crystallize in the fluorite-type, cubic (fcc) structure.

A similar approach can be taken in comparing the sesquioxides of both series, although some approximations must be considered (Templeton and Dauben 1957) in deriving radii from the sesquioxide lattice parameters. Radii based on these sesquioxides have also been compiled by others (Shannon 1976, Haire and Baybarz 1973). Trivalent radii for these f-element oxides are given in table 30. Radii and cubic lattice parameters are also plotted in fig. 18. Based on such radii, it can be seen that the

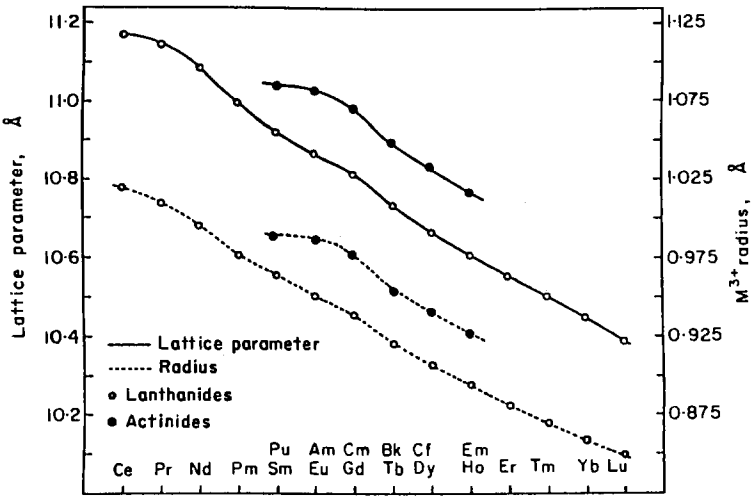

Fig. 18. Sesquioxide lattice parameters and ionic radii for the lanthanides and actinides.

actinide sesquioxides have larger parameters than their lanthanide electronic homologs; a particular actinide parameter or radius corresponds best to a lanthanide some two and one half elements to the left (earlier in the series) than the actinide's vertical homolog. Thus, americium and neodymium sesquioxides are more comparable than americium and europium sesquioxides. This relationship is useful for comparing the phase behavior, ionic radii and crystal lattice parameters of the lanthanide and actinide sesquioxides. The phase behaviors of the lanthanide and actinide sesquioxides having comparable radii are similar (e.g., that of Am and Nd).

The sesquioxides of the lanthanide and actinides are multiphasic. Figure 19 is a plot of phase formation as a function of temperature and radius of the lanthanide sesquioxides, and is based on a published plot (Chikalla et al. 1973, Schulz 1976). Included in a section of the plot are the radii for the first six actinide sesquioxides (Pu forms the first sesquioxide in the series if Ac is excluded) placed above comparable radii of the lanthanides, as opposed to their positions in the periodic table. If the very high temperature phases of the lanthanides (e.g., X, H phases) and the melting-point behaviors are excluded, there is a reasonable agreement between the expected and observed actinide sesquioxide behaviors based on radii. The X, H phases as such have not been reported for the actinide sesquioxides and there is a discrepancy with the melting points; the latter is discussed below.

From fig. 19, it would be expected that plutonium sesquioxide would form both a cubic and a hexagonal phase, and that curium and berkelium sesquioxides would both form cubic, monoclinic, and hexagonal phases. This is what is found experimentally. For americium sesquioxide, a cubic and a hexagonal phase would be expected, with a slight possibility that a monoclinic phase would also form. There has been some disagreement whether or not a pure Am monoclinic sesquioxide phase exists; there is a good probability that it does not. For californium and einsteinium sesquioxides, fig. 19 would predict the existence of a cubic and monoclinic phase for each; experimentally,

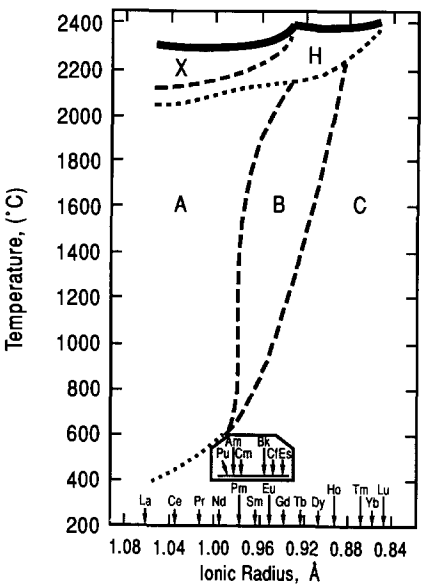

Fig. 19. Phase diagram of the lanthanide and actinide sesquioxides as a function of ionic radius.

both structure types as well as a hexagonal form (A type) are known for each of these elements. Whether the hexagonal boundary line "bends over" for the actinides or whether the californium and einsteinium sesquioxide hexagonal phases may even represent an actinide "H" phase is not clear. With einsteinium sesquioxide, both the hexagonal and monoclinic phases were observed as self-irradiation-induced phases in the initial cubic form of the oxide. A temperature phase diagram for the first six transplutonium sesquioxides is given in fig. 20. (Baybarz and Haire 1976), which can be compared to predictions based on radii that are shown in fig. 19.

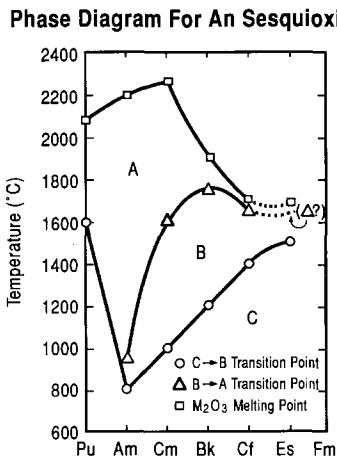

Fig. 20. Temperature–phase diagram for the actinide sesquioxides.

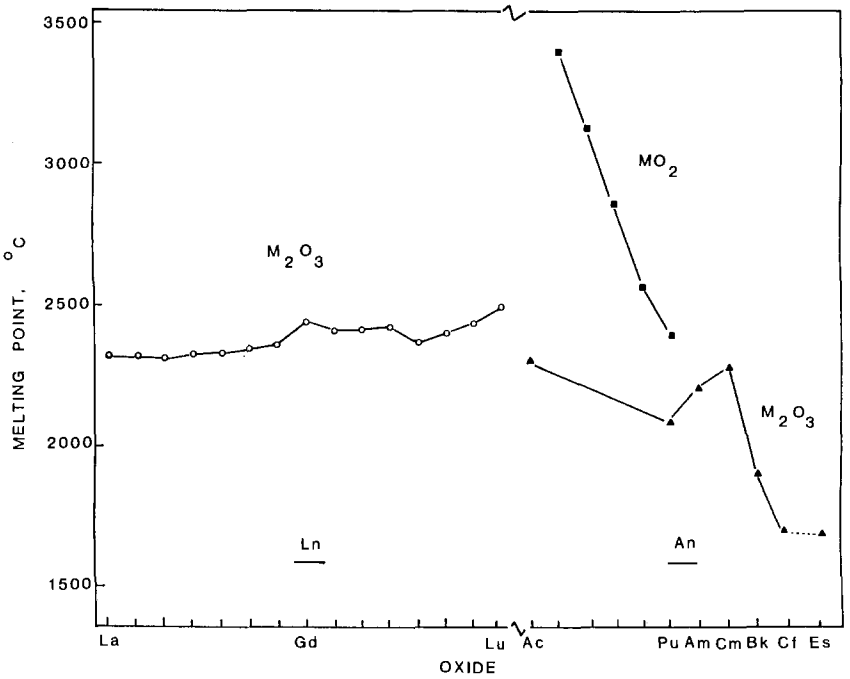

Fig. 21. Melting-point behavior of the lanthanide and actinide oxides.

There is a significant difference in both the value of melting points and their trend with Z for the lanthanide and actinide oxides. From the data in fig. 21 it can be seen that there is a uniform increase in the melting points of the lanthanide sesquioxides, except for a slight cusp at gadolinium sesquioxide (half-filled 4f shell). For the actinide sesquioxides, there is also an increase in the melting points from Pu to Cm (half-filled 5f shell); there appears an unexpected, sharp decrease for the subsequent actinide sesquioxides. There have been some questions raised as to whether or not the melting points for berkelium and californium sesquioxides are correct, due to the microscale method that was required to obtain these points (Schulz 1976). However, the same technique has given comparable melting points for curium sesquioxide to those determined by a more conventional method (Chikalla et al. 1971). These are the only values available for berkelium and californium sesquioxides; additional studies of the melting points have not been carried out since these values were reported many years ago. A value for the melting point of einsteinium sesquioxide has not been reported.

The melting points of the lanthanide and actinide dioxides are also given in fig. 21. For the lanthanides, the only dioxide sufficiently stable to permit a measurement of its melting point is CeO_2. The stability of the transplutonium dioxides also limits obtaining melting points for their dioxides, except for the possible case of BkO_2, for which a value has not been reported. The downward trend observed in fig. 21 for the

melting points of the actinide dioxides with increasing atomic number reflects the decreasing stability of the tetravalent oxidation state across the series.

A summary and a comparison of the different phases of the lanthanide and actinide sesquioxides is given in fig. 22 taken from Baybarz and Haire (1976), where the molecular volumes of the hexagonal, monoclinic and cubic forms are plotted. There is a considerable densification in going from the cubic (six coordinated) to the monoclinic (six and seven coordinated) and finally to the hexagonal (seven coordinated) forms of these oxides. It is evident that the monoclinic form has been observed at a larger molecular volume in the lanthanide sesquioxide series than in the actinide sesquioxide

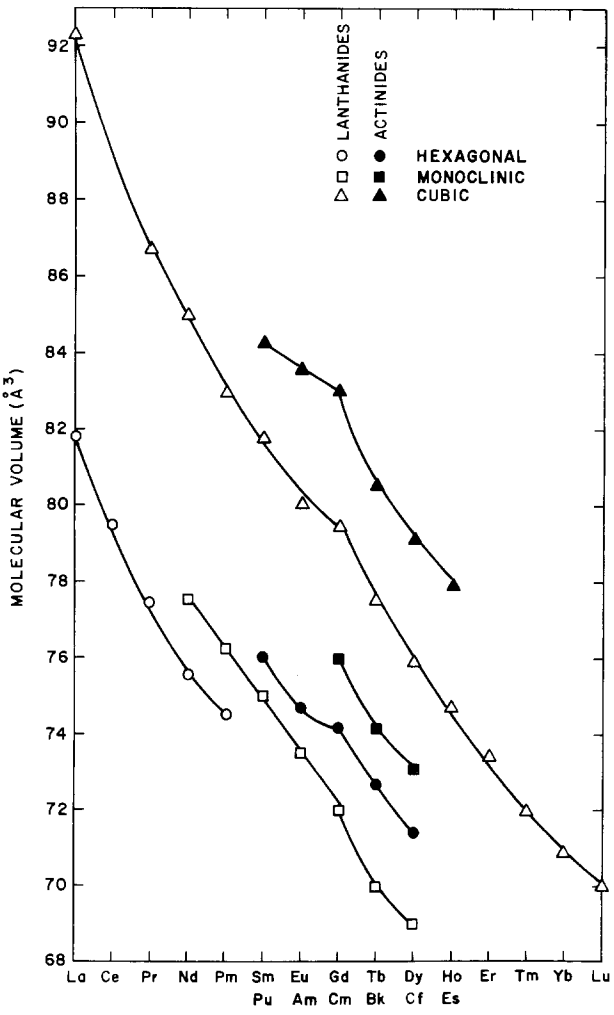

Fig. 22. Molecular volumes of the lanthanide and actinide sesquioxides.

series, which suggests that a monoclinic form of plutonium sesquioxide should exist. The latter has not been reported; its absence may be due to oxygen stoichiometry, as plutonium sesquioxide has a propensity for the uptake of oxygen to form higher oxides.

Another observation that can be made from fig. 22 is that the hexagonal structure appears to persist to a smaller molecular volume in the actinide series than in the lanthanide series (e.g., curium sesquioxide should be the highest member to form a hexagonal phase based on the lanthanide radius relationship). The hexagonal form of californium sesquioxide has a very narrow phase field and it is very difficult experimentally to retain this structural form of the sesquioxide at room temperature (e.g., to "quench-in" this form). This latter factor may have some bearing on this volume discrepancy (e.g., the volumes may be affected by the preparation). Finally, the volume data for the cubic forms of both series, the hexagonal forms of the actinides and the monoclinic forms of the lanthanides, all show a cusp at elements with half-filled shells.

The behavior and the structural details for the so-called intermediate oxides ($1.5 < O/M < 2.0$) are not as well established for the actinides as they have been for the lanthanides. Given the range of the above O/M ratios, the five actinides which qualify as potentially being able to exhibit such intermediate oxides are Pu through Cf. This limitation arises as Ac and the transcalifornium elements do not have known dioxides, and the first actinide sesquioxide appears at the position of Pu in the series.

In some cases, the behaviors of different intermediate oxides of the lanthanides have been used to assess the limited data available for such actinide oxides, and to assign phases to the actinide oxides. In general, these intermediate oxides can be viewed as oxygen-deficient fluorite structure (see section 1). A simplistic model for the actinide intermediate oxide phases would be the following: (a) a stoichiometric cubic sesquioxide ($O/M = 1.50$); (b) a cubic sesquioxide with some of the vacancies occupied by oxygen ($O/M = 1.5–1.7$) and showing variable lattice parameters; (c) an oxide phase corresponding to the R_nO_{2n-2} homologous series (rhombohedral, narrow stoichiometry range; e.g., Cf_7O_{12}); (d) a fcc substoichiometric dioxide ($O/M = 1.8–2.0$) phase with variable and larger parameters than the stoichiometric dioxide; and (e) the stoichiometric dioxide ($O/M = 2.00$).

Although a rhombohedral intermediate oxide phase has only been verified for Cm and Cf, in principle it may also exist for Pu, Am and Bk. Of these three, the plutonium oxygen system has been the most extensively studied and a rhombohedral intermediate oxide (e.g., Pu_7O_{12}) has not been reported. The stability of the dioxide of these three actinides may be contributing to the inability to obtain this particular intermediate phase (e.g., they are too easily oxidized to the dioxide). A study of the lanthanide systems (see section 1) provides a complete picture of the complexities that these intermediate oxide systems can exhibit. Whether or not these actinide oxide systems are more closely comparable to the lanthanide systems requires more extensive studies.

In fig. 23 plots are shown of the lattice parameters for the cubic sesquioxides and mononitrides of the lanthanides and actinides, and the atomic volumes for the metals of both series (Haire and Gibson 1992). The purpose of these plots is to point out that relationships (such as bonding, volumes of electronic homologs, etc.) between these series change considerably with the material being considered; i.e., the bonding involved in the oxides differs from that in the nitrides, which also varies from that in the

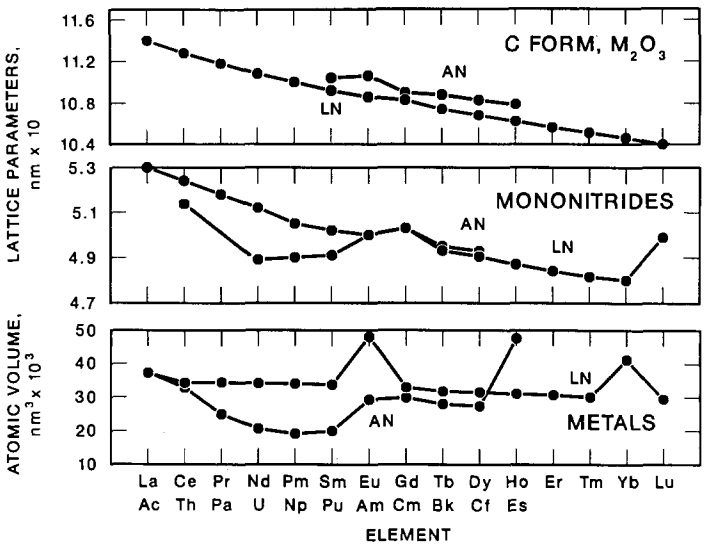

Fig. 23. Lattice parameters of the lanthanide and actinide sesquioxides and mononitrides, and the atomic volumes of the respective metals.

metals. As discussed earlier in connection with the sesquioxides, the actinide oxide parameters correspond to lanthanide oxide parameters about two elements earlier in the lanthanide series; with the transplutonium nitrides, the parameters of electronic homologs of each series are essentially the same. For uranium, neptunium and plutonium nitrides, one encounters a special case where there is additional bonding as compared to the transplutonium nitrides; this leads to much smaller parameters than expected for these lighter actinide nitrides. With the metals, the volumes of the actinides are all essentially smaller than their lanthanide homologs; it can be observed that the volumes of Am and Cm metals correspond most closely to those for Tm or Lu. Thus, there is a wide variation in the nature of the bonding between these three lanthanide and actinide materials; it is expected that the oxides are the most ionic.

3.2. *Thermodynamic and high-temperature behavior*

A review of the thermodynamic properties of the actinides and selected comparative data for the lanthanides have been given (Morss 1986). One experimental approach that has been frequently used for obtaining enthalpies of formation of the oxides has been through solution calorimetry, and many data have been acquired for the actinide oxides through Cf in the series. Elements with a higher Z than Cf are not amenable to this technique.

A cycle for yielding the enthalpy of solution of the lanthanide and actinide sesquioxides has been used and is described by Morss. A graphical approach (see fig. 24) has been devised using data for the different crystal forms of the lanthanide and actinide sesquioxides, which is useful for predictive purposes. The enthalpies of formation and

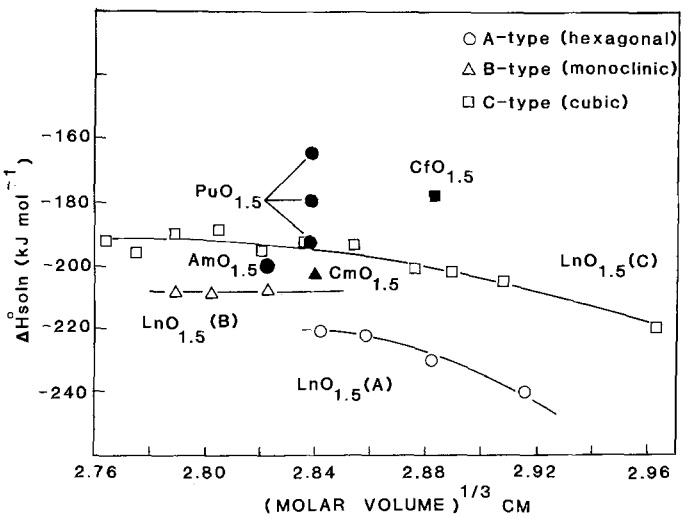

Fig. 24. The enthalpies of solution of actinide and lanthanide sesquioxides (three different values exist for plutonium sesquioxide).

solution for the different lanthanide and actinide sesquioxides are also given in table 31 taken from Morss (1986). From the data in fig. 24 it can be concluded that the actinide sesquioxides are slightly more stable than their respective, and structurally similar, lanthanide counterparts.

All of the actinides from Th through Cf form dioxides, whereas only three lanthanides, Ce, Pr and Tb, form dioxides. A correlation similar to that developed for the sesquioxides (using their enthalpy of solution and molar volume) has been devised from data for the dioxides (Morss 1986, Morss and Fuger 1981, Fuger 1982). This relationship provides both correlative and predictive capabilities, similar to that provided in fig. 24. One noted difference is that, for the dioxides, there does not appear to be a shift in the enthalpies for the elements in the two series, as is seen for the sesquioxides. The enthalpies of formation and solution for the dioxides are listed in table 31.

In terms of both the amount of data and the degree of understanding, the vaporization/decomposition behaviors of the lanthanide series are far better established than those of the actinide series, except for Th, U and Pu. Just as for the situation with intermediate oxide behavior, the high-temperature vaporization behavior of the actinides is often interpretated on the basis of the behaviors known for the lanthanide oxides. A comprehensive review of the lanthanide oxides has been given (Chandrasekharaiah and Gingerich 1989; see section 1). Since the only lanthanide dioxide that is sufficiently stable at temperatures where vaporization is encountered is CeO_2, a comparison between such high-temperature behavior for lanthanide and actinide oxides is essentially limited to that of the sesquioxides. With CeO_2, one finds that CeO and CeO_2 are the main vapor species encountered in vaporization studies, as is observed with the actinide dioxides (see section 2).

TABLE 31
Enthalpies of formation and solution of lanthanide and actinide oxides.

Lanthanide oxide	ΔH^0_{soln} (kJ mol^{-1})*	ΔH^0_f (kJ mol^{-1})*	Actinide oxide	ΔH^0_{soln} (kJ mol^{-1})*	ΔH^0_f (kJ mol^{-1})*
La_2O_3	−482$^+$	−1794$^+$	Ac_2O_3	(−1256)$^+$	(−1756)$^+$
Ce_2O_3	−462$^+$	−1796$^+$	Th no sesquioxide	–	–
Pr_2O_3	−446$^+$	−1828$^+$	Pa no sesquioxide	–	–
Nd_2O_3	−442$^+$	−1808$^+$	U_2O_3	(−379)$^+$	(−1456)$^+$
Pm_2O_3	(−420)	(−1813)	Np_2O_3	(−389)$^+$	(−1552)$^+$
Sm_2O_3	−423	−1828	Pu_2O_3	(−385)$^+$	(−1656)$^+$
Eu_2O_3	−412	−1663	Am_2O_3	−1233	−1690$^+$
Gd_2O_3	−410	−1827	Cm_2O_3	−1230	−1682
Tb_2O_3	−388	−1865	Bk_2O_3	−1202	(−1694)
Dy_2O_3	−386	−1863	Cf_2O_3	(−1154)	−1653
Ho_2O_3	−390	−1881	Es_2O_3	(−1192)	(−1696)
Er_2O_3	−378	−1898	Fm_2O_3	(−1184)	(−1694)
Tm_2O_3	−380	−1889	Md_2O_3	(−1020)	(−1534)
Yb_2O_3	−392	−1815	No_2O_3	(−740)	(−1260)
Lu_2O_3	−384	−1878	Lr_2O_3	(−1246)	(−1766)
CeO_2	−63	−1089	ThO_2	−115	−1226
PrO_2	−62	−958	PaO_2	(−851)	(−1109)
			UO_2	−78	−1085
			NpO_2	−54	−1074
			PuO_2	−52	−1056
			AmO_2	(−46)	−932
			CmO_2	(−41)	−911
TbO_2	−43	−972	BkO_2	(−36)	(−1021)
			CfO_2	(−27)	(−858)
			EsO_2	(−20)	(−763)

* cubic form of oxide
$^+$ hexagonal form of oxide
( ) estimated/calculated values

With the lanthanide sesquioxides, the high-temperature vapor species encountered above the molten or solid oxides range from R, RO, R_2O and R_2O_2. Thermodynamic properties of the lanthanide oxides have been given in section 1 and are therefore only reviewed briefly in this section for ease of comparison.

There appears to be two primary vaporization/decomposition modes for the lanthanide sesquioxides, which involve either the evolution of RO and oxygen, R and oxygen, or both metal bearing vapor species as shown below:

$$R_2O_3(s) \longrightarrow 2\,RO(g) + O(g) \quad \text{(lighter members)}$$

$$R_2O_3(s) \longrightarrow 2R(g) + 3O(g) \quad \text{(heavier members)}$$

In practice, the vaporization process often involves both reactions, as well as additional minor reactions that generate other species.

Concentrating only on these main reactions, for oxides where both processes are occurring as competitive reactions, it is possible to calculate ratios of the two

TABLE 32
Vapor species over selected lanthanide sesquioxides (species formed at 2000 K) (Parrish 1961).

	P(atm × 10^9)		
Ln_2O_3	Ln	LnO	Ln^+/LnO^+
Pr	< 10	100	0.1
Nd	< 5	50	< 0.1
Sm	3	3	1
Eu	70	9	8

metal-bearing vapor species that are generated. Some ratios (Parrish 1961) for selected lanthanides sesquioxides are given in table 32.

The major controlling factor in determining which vaporization/decomposition process occurs is the dissociation energy of the particular element's gaseous monoxide. The dissociation energies of these monoxides are known to vary irregularly across the lanthanide series and the monoxides tend to be the vapor products observed for the monoxides that have large dissociation energies. In general, the monoxide dissociation energies tend to decrease: (a) in progressing across the lanthanide series (greater f-electron occupancy); and (b) with a larger promotion energy for divalent–trivalent metallic states (promotion of an f electron to the conduction band; e.g., $f^n s^2 \rightarrow f^{n-1} ds^2$).

It might be expected that lanthanides which exhibit divalent states, like Eu and Yb, would be most likely to have their sesquioxides vaporize via the generation of monoxide vapor species. Instead these sesquioxides tend to form atomic vapor (e.g., R) species and oxygen due to the greater stability of R versus RO. Thus, for the sesquioxides of actinides with a greater tendency towards divalency or that are divalent metals (e.g., Cf, Es and Fm), the more likely it is that the vaporization mode of their sesquioxides is via generation of elemental vapor plus oxygen.

The first actinide sesquioxide encountered is plutonium sesquioxide (if actinium sesquioxide is excluded; vaporization data for it are not available) and Cf is the highest sesquioxide in the actinide series for which vaporization/decomposition data have been reported (Haire and Gibson 1992). Thus a comparison between the vaporization behaviors of the sesquioxides of the two f series can be made only between the lanthanides and the first six transneptunium oxides (Haire 1994).

In the case of plutonium sesquioxide, its vaporization has been reported to proceed mainly by the generation of PuO rather than via metal vapor (Ackermann et al. 1966a, b, Mulford and Lamar 1960). A limited amount of information has been published for americium sesquioxide (Ackermann et al. 1966a, b), although some unpublished data also exist for it (Kleinschmidt 1992, Haire 1992a). The vaporization mode for americium sesquioxide appears to be via the generation of atomic Am vapor and oxygen. In the case of curium sesquioxide, the actual vapor species have not been determined directly but rather from thermodynamic considerations (Smith and Peterson 1970) of high-temperature data for curium sesquioxide. From these data, it

has been reported that curium sesquioxide vaporizes via generation of CmO and oxygen. With californium sesquioxide, the mechanism has been reported to involve the production of Cf vapor and oxygen rather than CfO (Haire and Gibson 1992). From preliminary data for einsteinium sesquioxide, its vaporization/decomposition behavior is similar to that of californium sesquioxide. Preliminary data for berkelium sesquioxide indicate a mixture of atomic berkelium and berkelium monoxide vapor (Haire 1994).

The vaporization/decomposition behavior of these actinide sesquioxides is in accord with the tendencies expected using the behavior of the lanthanide sesquioxides in conjunction with properties of the actinide sesquioxides (e.g., dissociation energies of monoxides, metallic valence, promotion energies, etc.). In fig. 25 are given known dissociation energies of RO for the lanthanides (Chandrasekharaiah and Gingerich 1989) and for some the actinides (Ackermann and Chandrasekharaiah 1974). The values shown for californium and monoxides (Haire 1992a, b) is preliminary but demonstrates the expected trend of decreasing dissociation energies for higher actinides up to Lr. The dissociation energy for lawrencium monoxide would be expected to be larger and be similar in magnitude to that for lutetium monoxide.

The value for the dissociation energy of americium monoxide that is plotted appears to be too large and it is likely that the actual value may be smaller. From this plot it would be expected that the Fm–No sesquioxides would vaporize/decompose via atomic-metal vapor and oxygen. It appears that actinide monoxides having dissociation energies above 700 kJ mol^{-1} vaporize mainly via evolution of their monoxides while those having lower dissociation energies tend to favor vaporization via evolution of metal vapor and oxygen.

Another interesting correlation exists between the enthalpy of formation of the sesquioxides and the enthalpy of formation of the trivalent aquo ions, as shown in

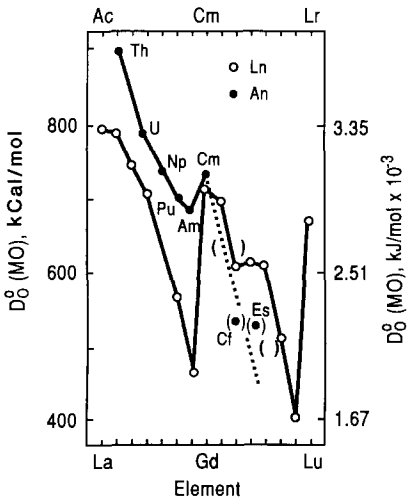

Fig. 25. Dissociation energies for the actinide and lanthanide monoxides.

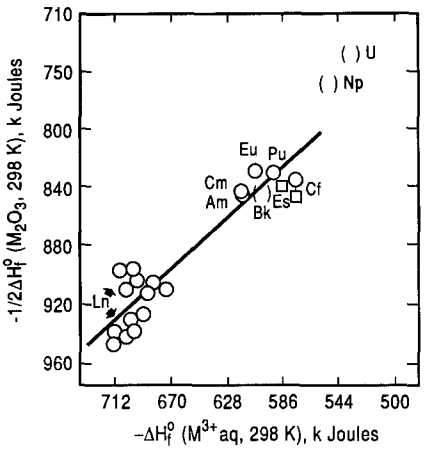

Fig. 26. The relationship between the enthalpies of formation of sesquioxides and the enthalpy of formation of the trivalent aquo ion.

fig. 26. As discussed above, the enthalpy of formation of the sesquioxide can be derived from the enthalpy of solution data for the oxides, or it can be calculated from the high-temperature decomposition of the oxides. The data shown are from the plot of Morss (1986) plus the Cf and Es values derived from high-temperature vaporizations (Haire and Gibson 1992, Haire 1994). Such a plot has use for actinides where high-temperature values can be obtained but where it may not be possible to determine their heat of solutions experimentally. The points shown for U, Np and Bk are calculated values, as the sesquioxides of U and Np are not known and experimental data are not available for berkelium sesquioxide.

3.3. *Comparison of magnetic behavior*

A complete comparison of the magnetic properties and behavior (e.g., magnetic structure, transitions, etc.) of the lanthanide and actinide oxides is beyond the scope of this chapter. Some information on these topics is given in sections 1 and 2 of the chapter. The main aspect addressed here is the general scope of the magnetic susceptibilities and the agreement of the magnetic moments with the so-called free-ion concept; i.e., the applicability of L–S coupling and Hund's rule for the f-element oxides. These concepts have been useful for the 4f elements for some time but only more recently have they been demonstrated for the more spatially extended electrons of the 5f series (Edelstein and Goffart 1986, Huray et al. 1983a, Huray and Nave 1987).

For the comparisons of the magnetic moments for the 4f- and 5f-element oxides, one is basically limited to comparing data for their sesquioxides and dioxides. Further, for the actinide series, the last member for which any information has been reported is Es. The 4f and 5f elements in well-defined ionic configurations have experimentally determined paramagnetic moments that are in reasonable agreement with theoretical moments that have been derived, based on the following assumptions. These are: (1) only highly localized f electrons contribute to the moments; and (2) the ground state is defined by Hund's rule and L–S or intermediate coupling. It is therefore of interest to

compare experimentally determined paramagnetic moments of the actinide oxides with the moments of the lanthanide oxides, as well as with the general pattern of moments for other ionic lanthanide materials.

A simplistic picture of the situation is to have a relationship between the effective moments of the f-element materials with the probable ion configuration. In this situation, localized f electrons in the metal would have the same moment as localized f electrons in a compound. The moment would depend on the number of such localized electrons regardless of the particular f-element's chemical form. Thus, the number of localized f electrons in Gd metal is seven ($4f^7$ with three electrons in a ds^2 conduction band), as it is in Cm metal ($5f^7$ configuration); there are also seven localized f electrons in both gadolinium and curium sesquioxides. Further, terbium and berkelium dioxides have seven localized f electrons. All six materials should have the same moment based on seven, unpaired "free-ion" electrons.

In fig. 27 plots are shown of some calculated effective moments based on probable electronic configurations of the lanthanides (L–S coupling and Hund's rule) (Huray et al. 1983a, Huray and Nave 1987). A perturbation may arise due to low-lying excited

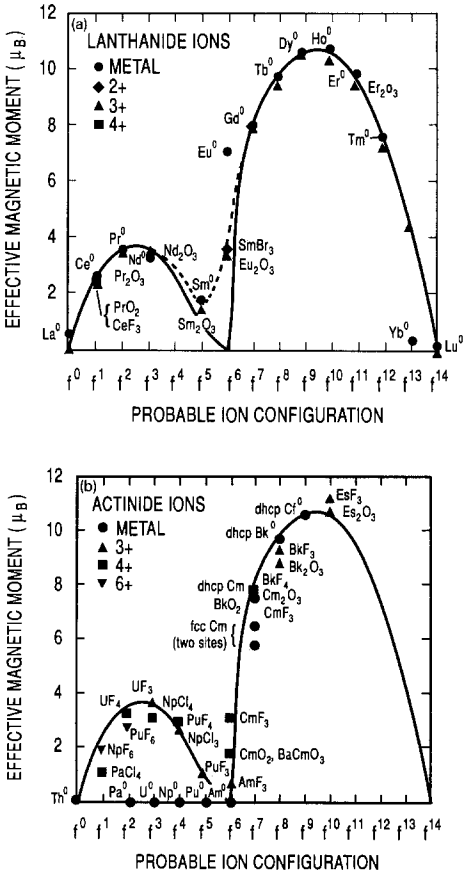

Fig. 27. Effective magnetic moments as a function of ion configuration for selected actinide and lanthanide materials.

states populated from thermal excitation (see dashed line). The experimental moments for some selected lanthanide and actinide materials in addition to moments for their oxides are also placed in this figure. In general, it can be seen that the lanthanide and actinide oxides give reasonably similar magnetic behavior with regard to their moments. Such a plot provides a summary of the magnetic moments for the two series of oxides.

A few additional comments concerning fig. 27 are worthwhile. The lighter actinide metals with nonlocalized f electrons display essentially zero moments. For thorium dioxide, a zero moment is also expected on the basis of the absence of f electrons. The situation with the dioxides of U and Pu is somewhat complex; e.g., experimental data for plutonium dioxide tend to support the electronic configuration expected for it but there is evidence that the 6d levels of this oxide may also be partially occupied. However, the halides of Pa, U and Np give reasonable agreement with the expected magnetic moments for the particular materials. Thus, the comparison of the magnetic moments of actinide oxides for a particular oxidation state seems to be best applied in the case of the transplutonium oxides. Table 33 (Huray and Nave 1987) provides a good summary of magnetic data for the transplutonium oxides.

3.4. *Concluding comments*

From the above discussions it should be clear that the lanthanides and the actinides series are not "mirror images". The elements of neither series reflect perfectly a series

TABLE 33
Comparative magnetic properties of lanthanide and actinide oxides.

Electronic configuration	Ground term	Saturated moment (I.C.)[a]	Rare-earth (III) ion	Experimental moments (μ_B)	Actinide (III) oxide	Experimental moment (μ_B)
f^0	$^1S_0$	0	La	0	Ac_2O_3	–
f^1	$^2F_{5/2}$	2.14	Ce	(2.56)	–	–
f^2	$^3H_4$	3.24	Pr	3.55	–	–
f^3	$^4I_{9/2}$	3.42	Nd	3.66	–	–
f^4	$^5I_4$	2.59	Pm	(2.83)	–	–
f^5	$^6H_{5/2}$	1.04	Sm	1.54	Pu_2O_3	1.0
f^6	$^7F_0$	0	Eu	3.51[b]	Am_2O_3	0
f^7	$^8S_{7/2}$	6.7	Gd	7.90	Cm_2O_3	7.5–7.9
f^8	$^7F_6$	9.0	Tb	9.63	Bk_2O_3	9.0
f^9	$^6H_{15/2}$	10.0	Dy	10.5	Cf_2O_3	9.8
f^{10}	$^5I_8$	10.0	Ho	10.5	Es_2O_3	10.5
f^{11}	$^4I_{15/2}$	9.0	Er	9.5	Fm_2O_3	–
f^{12}	$^3H_6$	7.0	Tm	7.39	Md_2O_3	–
f^{13}	$^2F_{7/2}$	4.0	Yb	4.34	No_2O_3	–
f^{14}	$^1S_0$	0	Lu	0	Lr_2O_3	–

[a] I.C. = intermediate coupling
[b] Low-lying excited state alters moment

that regularly adds a localized f electron when progressing to higher atomic numbers. The lanthanide series approximate this situation the closest; these elements and their compounds display very similar chemical behaviors, especially in the case of their oxides. The sesquioxide is the dominant oxide form for the lanthanide elements. Three different lanthanides form a dioxide, although CeO_2 is the only dioxide that readily forms in air atmospheres; PrO_2 and TbO_2 require special preparative conditions. It appears that EuO is the only divalent oxide (conflicting reports exist for YbO) that can be formed without special (e.g., high-pressure) preparative conditions.

The actinide series deviates the most from a regular filling of f orbitals, and the itinerant f electrons found in the early members give rise to a unique chemistry, which often is quite different from the chemistry observed for the lanthanides or the transplutonium elements. The early actinides generally exhibit higher oxidation states and more complex oxide behavior. It is only following plutonium in the series that the actinide oxides become more similar to the lanthanide oxides, in terms of oxidation states and structures. Even with the transplutonium elements, the prevalence of dioxides for the next four elements (Am–Cf) emphasizes a difference in behavior as compared to that for the lanthanides. The formation of curium dioxide, which destroys a half-filled f orbital, is especially striking in this regard. The sesquioxides of these transplutonium elements are more lanthanide-like and the sesquioxides of the two series share many crystal structures, exhibit similar phase behaviors, and display similar vaporization processes.

It is not feasible to consider conventional-type studies (structure, vaporization behavior, etc.) for the transeinsteinium oxides, given their scarcity and short lifetimes. Presumably their oxide chemistry would be very similar to that of the lanthanide oxides, especially for the trivalent oxidation state. However, there is an increased tendency for actinides in the second half of the series toward divalency. This suggests that the monoxides of the higher actinides (e.g., transeinsteinium elements) could be potentially more stable, perhaps approaching the stability of Eu monoxide. With No (element 102; homolog of Yb), the monoxide could be its most stable oxide.

Finally, the lanthanide oxides have been studied more thoroughly than the transplutonium oxides and it is possible that future studies of the latter oxides will determine further similarities between the chemistry and the physics of the oxides of these two series. One case may be the so-called intermediate oxides (e.g., oxides with O/M ratios between 1.5 and 2.0). It will require many careful studies in future years to elucidate the behavior of the actinide oxides to the present level of knowledge that is available for the intermediate oxides of the lanthanides.

Acknowledgements

One of the authors (RGH) acknowledges the sponsorship by the Division of Chemical Sciences, Office of Basic Energy Sciences, US Department of Energy under contract DE-AC05-840R21400 with Martin Marietta Energy Systems, Inc. LE gratefully acknowledges support from the National Science Foundation through Research Grant DMR-9114799.

References

Achard, J.C., 1960, Compt. Rend. **250**, 3025.

Ackermann, R.J., and M.S. Chandrasekharaiah, 1974, Thermodynamics of Nuclear Materials, Vol. 2 (IAEA, Vienna) p. 3.

Ackermann, R.J., and M.S. Chandrasekharaiah, 1975, Thermodynamics of Nuclear Materials, Vol. 2 (IAEA, Vienna) p. 1.

Ackermann, R.J., and E.G. Rauh, 1973a, J. Inorg. & Nucl. Chem. **35**, 3787.

Ackermann, R.J., and E.G. Rauh, 1973b, High Temp. Sci. **5**, 463.

Ackermann, R.J., and E.G. Rauh, 1975, J. Chem. Phys. **62**, 108; Thermodynamics **7**, 211.

Ackermann, R.J., and R.J. Thorn, 1962, Thermodynamics of Nuclear Materials (IAEA, Vienna) pp. **39**, 445.

Ackermann, R.J., R.L. Faircloth, E.G. Rauh and R.J. Thorn, 1966a, J. Inorg. & Nucl. Chem. **28**, 111.

Ackermann, R.J., R.L. Faircloth and M.H. Rand, 1966b, J. Phys. Chem. **70**, 3698.

Ahmad, I., and P.R. Fields, 1986, in: The Chemistry of the Actinide Elements, eds J.J. Katz, G.T. Seaborg and L.R. Morss (Chapman and Hall, New York) pp. 1649–1674.

Akimoto, Y., 1960, UCRL Report 9093 (US Atomic Energy Commission) p. 73.

Akimoto, Y., 1967, J. Inorg. & Nucl. Chem. **29**, 2650.

Aldebert, P., and J.P. Traverse, 1979, Mater. Res. Bull. **14**, 303.

Ambrozhii, M.N., and E.F. Luchnikova, 1962, Uch. Zap. Saratovsk. Univ. **75**, 11.

Ambrozhii, M.N., and E.F. Luchnikova, 1964, Chem. Abstr. **60**, 4783.

Ambrozhii, M.N., E.F. Luchnikova and M.I. Sidorova, 1960, Z. Neorg. Khim. **5**, 366 [Russ. J. Inorg. Chem. **5**, 176].

Arakawa, T., A. Kabumoto and J. Shiokawa, 1986, J. Less-Common Met. **115**, 281.

Asprey, L.B., F.H. Ellinger, S. Fried and W.H. Zachariasen, 1955, J. Am. Chem. Soc. **77**.

Baenzinger, N.C., H.A. Eick, H.S. Schuldt and L. Eyring, 1961, J. Am. Chem. Soc. **83**, 2219.

Baitles, J.E., J.W. Reishus and W.A. Shim, 1969, in: ANL Report 7575 (Argonne National Laboratory, Argonne, IL) pp. 77–82.

Bärnighausen, H., 1966, J. Prakt. Chem. **34**, 1.

Bärnighausen, H., and G. Brauer, 1962, Acta Crystallogr. **15**, 1059.

Bärnighausen, H., and G. Schiller, 1985, J. Less-Common Met. **110**, 385.

Baybarz, R.D., 1973, J. Inorg. & Nucl. Chem. **35**, 4149.

Baybarz, R.D., and R.G. Haire, 1976, J. Inorg. & Nucl. Chem. Suppl. 1976, pp. 7–12.

Baybarz, R.D., R.G. Haire and J.A. Fahey, 1972, J. Inorg. & Nucl. Chem. **34**, 557.

Bedford, R.G., and E. Catalano, 1971, J. Solid State Chem. **3**, 112.

Benedict, U., S. Dabos, C. Dufour, J.-C. Spirlet and M. Pagés, 1986, J. Less-Common Met. **121**, 461.

Benedict, U., S. Dabos-Seignon, S. Heathman, J.-P. Dancausse, M.M. Gensini, E. Gering and J.-C. Spirlet, 1992a, in: Transuranium Elements: A Half Century, eds L.R. Morss and J. Fuger (American Chemical Society, Washington, DC) pp. 396–403.

Benedict, U., S. Dabos-Seignon, J.-P. Dancausse, M.M. Gensini, E. Gering, S. Heathman, L. Luo, J. Staun Olsen, L. Gerward and R.G. Haire, 1992b, J. Alloys & Compounds **181**, 1.

Benzakour, M., R. Tetot and G. Boureau, 1988, J. Phys. Chem. Solids **49**, 381.

Berard, M.F., C.D. Wirkus and D.R. Wilder, 1968, J. Am. Ceram. Soc. **51**, 643.

Berndt, U., R. Tanamar, D. Maier and C. Keller, 1974, Inorg. & Nucl. Chem. Lett. **10**, 315.

Bevan, D.J.M., and J. Kordis, 1964, J. Inorg. & Nucl. Chem. **26**, 1509.

Bevan, D.J.M., and E. Summerville, 1979, Mixed rare earth oxides, in: Handbook on the Physics and Chemistry of Rare Earths, Vol. 3, eds K.A. Gschneidner Jr and L. Eyring (North-Holland, Amsterdam) pp. 401–524.

Boatner, L.A., and M.M. Abraham, 1980, ORNL Report 77–89 (Oak Ridge National Laboratory, Oak Ridge, TN).

Boucherle, J.X., and J. Schweizer, 1975, Acta Crystallogr. B **31**, 2745.

Boulesteix, C., 1982, Defects and phase transformation near room temperature in rare earth sesquioxides, in: Handbook on the Physics and Chemistry of Rare Earths, Vol. 5, eds K.A. Gschneidner Jr and L. Eyring (North-Holland, Amsterdam) pp. 321–386.

Brauer, G., and B. Pfeiffer, 1963, J. Less-Common Met. **5**, 171.

Brauer, G., and N. Schulz, 1967, J. Less-Common Met. **13**, 231.

Brauer, G., and A. Siegbert, 1969, Z. Anorg. Allgem. Chem. **371**, 263, 268, 271.

Brooks, M.S.S., B. Johansson and H.L. Skriver, 1984, in: Handbook on the Physics and

Chemistry of the Actinides, Vol. 1, eds A.J. Freeman and G.H. Lander (North-Holland, Amsterdam) pp. 153–270.

Bursill, L.A., and B.G. Hyde, 1972, Crystallographic shear in the higher titanium oxides: structure, texture, mechanisms and thermodynamics, in: Progress in Solid State Chemistry, Vol. 7, eds H. Reiss and J.O. McCaldin (Pergamon Press, Oxford) pp. 177–253.

Campbell, G.M., L.J. Mullins and J.A. Leary, 1968, Thermodynamics of Nuclear Materials, STI Pub., Vol. 162 (IEAE, Vienna) p. 75.

Chandrasekharaiah, M.S., and K.A. Gingerich, 1989, Thermodynamic properties of gaseous species, in: Handbook on the Physics and Chemistry of Rare Earths, Volume 12, eds K.A. Gschneidner Jr and L. Eyring (North-Holland, Amsterdam) pp. 409–431.

Chang, E.K., and R.N. Blumenthal, 1988, Solid State Chem. **72**, 330, and references therein.

Chikalla, T.D., and L. Eyring, 1967, J. Inorg. & Nucl. Chem. **29**, 2281.

Chikalla, T.D., and L. Eyring, 1968, J. Inorg. & Nucl. Chem. **30**, 133.

Chikalla, T.D., C.E. McNeilly, J.L. Bates and J.J. Rasmussen, 1971, USAEC Rept. BNWI-SA 3818 (US Atomic Energy Commission, Washington, DC).

Chikalla, T.D., C.E. McNeilly and F.P. Roberts, 1972, J. Am. Chem. Soc. **55**, 428.

Chikalla, T.D., C.E. McNeilly, J.L. Bates and J.J. Rasmussen, 1973, in: Proc. Int. Colloq. on High-Temperature Phase Transfers (Centre National Recherche Scientifique, Paris) No. 205.

Clifford, A.F., 1964, A joint report on the simultaneous independent work in three laboratories on the solvolytic disproportionation of intermediate higher oxides, in: Rare Earth Research II, ed. K. Vorres (Gordon and Breach, New York) pp. 45–50.

Cohen, D., 1963, Inorg. Chem. **2**, 866.

Cohen, D., and A.J. Walker, 1964, J. Chem. Soc., p. 2696.

Coleman, J.S., T.K. Keenan, L.H. Jones, W.T. Carnall and R.A. Penneman, 1963, Inorg. Chem. **2**, 58.

Copeland, J.C., and B.B. Cunningham, 1967, J. Inorg. & Nucl. Chem. **31**, 733.

Cordfunke, E.H.P., 1969, The Chemistry of Uranium (Elsevier, Amsterdam) pp. 63–97.

Cunningham, B.B., and J.C. Wallmann, 1964, J. Inorg. & Nucl. Chem. **26**, 271.

Dancausse, J.-P., 1991, Thesis (University of Paris, Orsay, Oct. 16, 1991).

De, S.K., and S. Chatterjee, 1989, J. Phys.: Condens. Matter **1**, 1169.

Drofenik, M., L. Golic and D. Kolar, 1974, J. Cryst. Growth **21**, 170.

Duclos, S.J., Y.K. Vohra, A.L. Ruoff, A. Jayaraman and G.P. Espinosa, 1988, Phys. Rev. B **38**, 7755.

Dulick, M., E. Murad and R.F. Barrow, 1986, J. Chem. Phys. **85**, 385.

Edelstein, N.M., and J. Goffart, 1986, in: The Chemistry of the Actinide Elements, eds J.J. Katz, G.T. Seaborg and L.R. Morss (Chapman and Hall, New York) pp. 1361–1388.

Eick, H.A., N.C. Baenzinger and L. Eyring, 1956, J. Am. Chem. Soc. **78**, 5147.

Eller, P.G.E., and R.A. Penneman, 1986, in: The Chemistry of the Actinide Elements, eds J.J. Katz, G.T. Seaborg and L.R. Morss (Chapman and Hall, New York) p. 974.

Eyring, L., 1979, The binary rare earth oxides, in: Handbook on the Physics and Chemistry of Rare Earths, Vol. 3, eds K.A. Gschneidner Jr and L. Eyring (North-Holland, Amsterdam) pp. 337–399.

Eyring, L., 1991, The binary lanthanide oxides: synthesis and identification, in: Synthesis of Lanthanide and Actinide Compounds, eds G. Meyer and L.R. Morss (Kluwer Academic Publishers, Dordrecht) pp. 187–224.

Eyring, L., and B. Holmberg, 1963, Ordered phases and nonstoichiometry in the rare earth oxide systems, in: Advances in Chemistry, Vol. 39, ed. R.F. Gould (American Chemical Society, Washington, DC) p. 46.

Eyring, L., and Z.C. Kang, 1991, Eur. J. Solid State & Inorg. Chem. **28**, 459.

Fahey, J.A., 1986, in: The Chemistry of the Actinide Elements, eds J.J. Katz, G.T. Seaborg and L.R. Morss (Chapman and Hall, New York) pp. 443–498.

Fahey, J.A., J.R. Peterson and R.D. Baybarz, 1972, Inorg. & Nucl. Chem. Lett. **8**, 101.

Fellows, R.L., J.R. Peterson, J.P. Young and R.G. Haire, 1978, in: The Rare Earths in Modern Science and Technology, Vol. 1, eds G.J. McCarthy and J.J. Rhyne (Plenum Press, New York) pp. 493–499.

Felmlee, T.L., and L. Eyring, 1968, Inorg. Chem. **1**, 660.

Finch, C.B., and G.W. Clark, 1966, J. Appl. Phys. **37**, 3910.

Finch, C.C., and G.W. Clark, 1965, J. Appl. Phys. **36**, 2143; J. Cryst. Growth **6**, 246.

Fishel, N.A., J.M. Haschke and H.A. Eick, 1970, Inorg. Chem. **9**, 413.

Foex, M., and J.P. Traverse, 1966a, Rev. Int. Hautes Temp. Refract. **3**, 429.

Foex, M., and J.P. Traverse, 1966b, Bull. Soc. Fr. Mineral. Cristallogr. **89**, 184.

Fournier, J.M., and L. Manes, 1985, in: Actinides – Chemical and Physical Properties, ed. L. Manes (Springer, Berlin) pp. 1–56.

Fuger, J., 1975, in: Lanthanides and Actinides, 1980, MTP Int. Review of Science, Inorg. Series II, Vol. 7, eds. H.J. Emeleus and K.W. Bagnall (Butterworths, London) pp. 151–194.

Fuger, J., 1982, in: Actinides in Perspective, ed. N.M. Edelstein (Pergamon Press, Oxford) pp. 409–431.

Fuger, J., R.G. Haire and J.R. Peterson, 1993, J. Alloys & Compounds **200**, 181.

Gamarnik, M.Ya., 1988, Sov. Phys. Solid State **30**, 808.

Gasgnier, M., G. Schiffmacher, P. Caro and L. Eyring, 1986, J. Less-Common Met. **116**, 31.

Gasgnier, M., G. Schiffmacher, D.R. Svoronos and P. Caro, 1987, Inorg. Chem. Acta **140**, 79.

Gibby, R.L., C.E. McNeilly and T.D. Chikalla, 1970, J. Nucl. Mater. **34**, 299.

Gibson, J.A., and G.S. Harvey, 1966, Properties of Rare Earth Metals and Compounds, Tech. Rept. AFML-TR-65–430 (Battelle Memorial Institute).

Glushkova, V.B., and A.G. Boganov, 1965, Izv. Akad. Nauk SSSR Ser. Khim., p. 1131; Bull. Acad. Sci. USSR Div. Chem. Sci., pp. 1101, 1104.

Gmelin Handbook of Inorganic Chemistry, Suppl. Ser., Uranium, 1975–1986, 1975, C3; 1977, C1; 1978, C2; 1984, C4; 1986, C5 (Springer, Berlin).

Gmelin's Handbuch der Anorganischen Chemie, 1974, Selternerdelemente, Teil Cl, Sc, Y, La und Lanthanide Oxide (Springer, Berlin).

Goodman, G.L., 1992, J. Alloys & Compounds **181**, 33.

Goudiakas, J., R.G. Haire and J. Fuger, 1990, J. Chem. Thermodyn. **22**, 577.

Green, J.L., and B.B. Cunningham, 1967, J. Inorg. & Nucl. Chem. **3**, 343.

Gschneidner Jr, K.A., and L. Eyring, eds, 1988, Handbook on the Physics and Chemistry of Rare Earths, Vol. 11 (North-Holland, Amsterdam).

Gschneidner Jr, K.A., and L. Eyring, eds, 1993, Handbook on the Physics and Chemistry of Rare Earths, Cumulative Index to Volumes 1–15 (North-Holland, Amsterdam).

Gschneidner Jr, K.A., N. Kippenhan and O.D. McMasters, 1973, Thermochemistry of the Rare Earths, Report IS-RIC-6 (Iowa State University, Ames, IA).

Guentert, O.J., and R.L. Mozzi, 1958, Acta Crystallogr. **11**, 746.

Haire, R.G., 1976, in: Proc. Rare Earth Research Conf., Vol. 2, ed. C.E. Lundin (Denver Research Institute, Denver, CO) pp. 584–593.

Haire, R.G., 1982, in: Actinides in Perspective, ed. N.M. Edelstein (Pergamon Press, New York) pp. 309–342.

Haire, R.G., 1985a, J. Less-Common Met. **121**, 379.

Haire, R.G., 1986, in: The Chemistry of the Actinide Elements, eds J.J. Katz, G.T. Seaborg and L.R. Morss (Chapman and Hall, New York) pp. 1025–1070.

Haire, R.G., 1992a, abstract, Rare Earth Research Conference, Lexington, KY, 1992; unpublished work.

Haire, R.G., 1992b, in: Proc. 4th Int. Symp. on Advanced Nuclear Energy Research, Mito, Japan, February 5–7, 1992, JAERI-M 92–207.

Haire, R.G., 1994, J. Alloys & Compounds, in press.

Haire, R.G., and R.D. Baybarz, 1973, J. Inorg. & Nucl. Chem. **35**, 489.

Haire, R.G., and J. Bourges, 1980, Journées des Actinides, May 27–28, Stockholm, Sweden, p. 19.

Haire, R.G., and J.K. Gibson, 1992, in: Transuranium Elements – A Half Century, eds L.R. Morss and J. Fuger (American Chemical Society, Washington, DC) p. 436.

Haschke, J.M., and H.A. Eick, 1968, J. Phys. Chem. **72**, 4235.

Haschke, J.M., and H.A. Eick, 1969, J. Phys. Chem. **73**, 374.

Haschke, J.M., and H.A. Eick, 1970, Inorg. Chem. **9**, 851.

Haug, H., 1967, J. Inorg. & Nucl. Chem. **29**, 2753.

Head, E.L., and C.E. Holley Jr, 1965, The preparation and thermal decomposition of the carbonates of Tb, Dy, Ho, Er, Tm, Yb, Lu, Y and Sc, in: Rare Earth Research, Vol. III, ed. L. Eyring (Gordon and Breach, New York) pp. 707–744.

Height, T.M., and D.J.M. Bevan, 1979, private communication.

Henrick, C.C., and R.G. Behrens, 1981, J. Cryst. Growth **51**, 183.

Hildenbrand, D.L., and E. Murad, 1974, J. Chem. Phys. **61**, 1232.

Hobart, D.E., and J.R. Peterson, 1986, in: The Chemistry of the Actinide Elements, eds J.J. Katz, G.T. Seaborg and L.R. Morss (Chapman and Hall, New York) pp. 989–1024.

Hoekstra, H.R., 1966, Inorg. Chem. **5**, 754.

Hoskins, B.F., and R.L. Martin, 1976, J. Chem. Soc. Dalton Trans., p. 677.

Hsu, W.P., L. Rönnquist and E. Matijević, 1988, Langmuir **4**, 31.

Huber, K.P., and G. Herzberg, 1979, Molecular Spectra and Molecular Structure IV, Constants of Diatomic Molecules (Van Nostrand, Princeton, NJ).

Hulet, E.K., 1986, in: The Chemistry of the Actinide Elements, eds J.J. Katz, G.T. Seaborg and L.R. Morss (Chapman and Hall, New York) pp. 1071–1084.

Hulet, E.K., J.F. Wild, R.W. Lougheed and W.N. Hayes, 1975, Radiokhimiya **17**, 632.

Huray, P.G., and S.E. Nave, 1987, in: Handbook on the Physics and Chemistry of the Actinides, eds A.J. Freeman and G.H. Lander (North-Holland, Amsterdam) pp. 311–372.

Huray, P.G., S.E. Nave and R.G. Haire, 1983a, J. Less-Common Met. **93**, 293.

Huray, P.G., S.E. Nave, R.G. Haire and J.R. Moore, 1983b, Inorg. Chim. Acta A **3**, 120.

Hurtgen, C., and J. Fuger, 1977, Inorg. & Nucl. Chem. Lett. **13**, 179.

Hyde, B.G., and L. Eyring, 1965, On phase equilibria and phase reactions in RbO_x–O_2 and related systems, in: Rare Earth Research, Vol. III, ed. L. Eyring (Gordon and Breach, New York) pp. 623–664.

Hyde, B.G., E.E. Garver, U.E. Kuntz and L. Eyring, 1965, J. Phys. Chem. **69**, 1667.

Hyde, B.G., D.J.M. Bevan and L. Eyring, 1966, Philos. Trans. R. Soc. London A **259**, 583.

IAEA Report, 1965, Tech. Rep. Series No. 39 (IAEA, Vienna).

IAEA Report, 1967, Tech. Rep. Series No. 79 (IAEA, Vienna).

Inaba, H., and K. Naito, 1983a, J. Solid State Chem. **50**, 100.

Inaba, H., and K. Naito, 1983b, J. Solid State Chem. **50**, 111.

Inaba, H., S.P. Pack, S.H. Lin and L. Eyring, 1980, J. Solid State Chem. **33**, 295.

Inaba, H., S.H. Lin and L. Eyring, 1981a, J. Solid State Chem. **37**, 58.

Inaba, H., S.P. Pack, S.H. Lin and L. Eyring, 1981b, J. Solid State Chem. **37**, 67.

Inaba, H., A. Navrotsky and L. Eyring, 1981c, J. Solid State Chem. **37**, 77.

Jenkins, M.S., R.P. Turcotte and L. Eyring, 1970, in: The Chemistry of Extended Defects in Non-Metallic Crystals, eds L. Eyring and M. O'Keeffe (North-Holland, Amsterdam) pp. 36–53.

Jouniaux, B., 1979, The Study of the Thermochromatography of the Transuranium Element Fluorides, Thesis IPNO-79–05 (University of Paris).

Kang, Z.C., and L. Eyring, 1988a, J. Solid State Chem. **75**, 52.

Kang, Z.C., and L. Eyring, 1988b, J. Solid State Chem. **75**, 60.

Kang, Z.C., and L. Eyring, 1992, J. Alloys & Compounds **181**, 483.

Kang, Z.C., L. Eyring and D.J. Smith, 1987, Ultramicroscopy **22**, 71.

Kang, Z.C., C. Boulesteix and L. Eyring, 1989, J. Solid State Chem. **81**, 96.

Kang, Z.C., J. Zhang and L. Eyring, 1992a, Aust. J. Chem. **45**, 1499.

Kang, Z.C., Ting Zhen Li and L. Eyring, 1992b, J. Alloys & Compounds **181**, 477.

Kannelakopulos, B., E. Aderhold, E. Dornberger, W. Müller and R.D. Baybarz, 1978, Radiochim. Acta **25**, 89.

Kapshukov, I.I., L.V. Sudakov, E.V. Shimbarev, A.Yu. Baranov and G.N. Yakovev, 1976, in: Plutonium 1975 and Other Actinides, eds. H. Blank and R. Lindner (North-Holland, Amsterdam) pp. 861–869.

Karnatak, R.C., M. Gasgnier, H. Dexpert, J.M. Esteva, P. Caro and L. Albert, 1985, J. Less-Common Met. **110**, 377.

Karraker, D.G., 1975a, J. Chem. Phys. **63**(7), 3174.

Karraker, D.G., 1975b, J. Chem. Phys. **62**(4), 1444.

Katz, J.J., and D.M. Gruen, 1949, J. Am. Chem. Soc. **71**, 2106.

Katz, J.J., L.R. Morss and G.T. Seaborg, 1986a, in: The Chemistry of the Actinide Elements, eds J.J. Katz, G.T. Seaborg and L.R. Morss (Chapman and Hall, New York) pp. 1121–1196.

Katz, J.J., L.R. Morss and G.T. Seaborg, 1986b, in: The Chemistry of the Actinide Elements, eds J.J. Katz, G.T. Seaborg and L.R. Morss (Chapman and Hall, New York) pp. 1142–1144.

Katzin, L.I., 1986, in: The Chemistry of the Actinide Elements, eds J.J. Katz, G.T. Seaborg and L.R. Morss (Chapman and Hall, New York) pp. 41–101.

Keller, C., 1967, in: Lanthanide and Actinide Chemistry, ed. R.F. Gould (American Chemical Society, Washington, DC) pp. 228–247.

Keller, C., and U. Berndt, 1976, in: Transplutonium Elements, eds W. Müller and R. Lindner (North-Holland, Amsterdam) pp. 85–93.

Kern, S., C.-K. Loong, J. Faber Jr and G.H. Lander, 1984, Solid State Commun. **49**, 295.

Kirby, H.W., 1986, in: The Chemistry of the Actinide Elements, eds J.J. Katz, G.T. Seaborg and L.R. Morss (Chapman and Hall, New York) pp. 102–168.

Kitayama, K., K. Nojiri, T. Sugihara and T. Katsura, 1985, J. Solid State Chem. **56**, 1.

Kleinschmidt, P.D., 1992, unpublished work (Los Alamos National Laboratory, Los Alamos, NM).

Kleinschmidt, P.D., and J.W. Ward, 1986, J. Less-Common Met. **112**, 61.

Knappe, P., and L. Eyring, 1985, J. Solid State Chem. **58**, 312.

Knittel, D.R., S.P. Pack, S.H. Lin and L. Eyring, 1977, J. Chem. Phys. **67**, 134.

Knotek, M.L., and P.J. Feibelman, 1979, Surf. Sci. **90**, 78.

Körner, R., M. Ricken and J. Nölting, 1989, J. Solid State Chem. **78**, 136.

Krause, M.O., R.G. Haire, O. Okeski-Rahkonen and J.R. Peterson, 1988, J. Electron Spectroscopy and Related Phenomena **47**, 215, and references therein.

Krill, G., M.F. Ravet, J.P. Kappler, L. Abadli, J.M. Leger, N. Yacoubi and C. Loriers, 1980, Solid State Commun. **33**, 351.

Kuntz, U.E., and L. Eyring, 1959, Diffusion of oxygen in rare-earth oxides, in: Kinetics of High Temperature Processes, ed. W.D. Kingery (Wiley, New York) p. 50.

Kunzmann, P., and L. Eyring, 1975, J. Solid State Chem. **14**, 229.

Langley, R.H., unpublished work.

Larson, A.C., and R.B. Von Dreele, 1986, (GSAS) LANL Report # LA-UR 86–748.

Laszlo, T.S., P.J. Sheehan and R.E. Gannon, 1967, J. Phys. Chem. Solids **28**, 313.

Lefever, R.A., 1962, Rev. Sci. Instrum. **33**, 1470.

Leger, J.M., N. Yacoubi and J. Loriers, 1980, in: The Rare Earths in Modern Science and Technology, Vol. II, eds G.J. McCarthy, J.J. Rhyne and H.B. Silber (Plenum Press, New York) pp. 203–208.

Leger, J.M., N. Yacoubi and J. Loriers, 1981, J. Solid State Chem. **36**, 261.

Lejus, A.M., and J.P. Connan, 1974, Rev. Int. Hautes Temp. Refract. **11**, 215.

Lejus, A.M., J.C. Bernier and R. Collongues, 1974, Rev. Int. Hautes Temp. Refract. **11**, 183.

Lejus, A.M., J.C. Bernier and R. Collongues, 1976, J. Solid State Chem. **16**, 349.

Linares, R.C., 1967, J. Phys. Chem. Solids **28**, 1285.

Lincoln, F.J., J.R. Sellar and B.G. Hyde, 1988, J. Solid State Chem. **74**, 268.

Lindemer, T.B., 1986, CALPHAD **10**, 129.

Lowe, A.T., and L. Eyring, 1975, J. Solid State Chem. **14**, 383.

Lowenstein, M.Z., L. Kihlborg, K.H. Lau, J.M. Haschke and L. Eyring, 1972, in: Proc. 5th Mater. Res. Symp. on Solid State Chemistry, NBS Pub. 364, eds R.S. Roth and S.J. Schneider Jr (National Bureau of Standards, Washington, DC) p. 343.

MacChesney, J.B., H.J. Williams, R.C. Sherwood and J.F. Potter, 1966, J. Chem. Phys. **44**, 596.

Manes, L., and U. Benedict, 1985, in: Actinides – Chemical and Physical Properties, Structure and Bonding Series, Vol. 59/60, ed. L. Manes (Springer, Berlin) pp. 75–126.

Maren, A., S.H. Lin, R.H. Langley and L. Eyring, 1984, J. Solid State Chem. **53**, 329.

Markin, T.L., and M.H. Rand, 1966, in: Thermodynamics, Vol. 1 (IAEA, Vienna) p. 145.

Matijević, E., and W.P. Hsu, 1987, J. Colloid & Interf. Sci. **118**, 506.

Matzke, Hj., 1976, in: Plutonium 1975 and Other Actinides, eds. H. Blank and R. Lindner (North-Holland, Amsterdam) pp. 801–832.

McKelvy, M., and L. Eyring, 1983, J. Cryst. Growth **62**, 635.

Millot, F., and P. de Mierry, 1985, J. Phys. Chem. Solids **46**, 797.

Moore, J.R., S.E. Nave, R.G. Haire and P.G. Huray, 1986, J. Less-Common Met. **121**, 187.

Morss, L.R., 1982, in: Actinides in Perspective, ed. N.M. Edelstein (Pergamon Press, Oxford) pp. 381–407.

Morss, L.R., 1983, J. Less-Common Met. **93**, 301.

Morss, L.R., 1985, in: Americium and Curium Chemistry and Technology, eds N.M. Edelstein, J.D. Navratil and W.W. Schultz (Reidel, Dordrecht) pp. 135–146.

Morss, L.R., 1986, in: The Chemistry of the Actinide Elements, eds J.J. Katz, G.T. Seaborg and L.R. Morss (Chapman and Hall, New York) pp. 1278–1360.

Morss, L.R., 1991, in: Synthesis of Lanthanide and Actinide Compounds, eds G. Meyer and

L.R. Morss (Kluwer Academic Publishers, Dordrecht) pp. 237–250.
Morss, L.R., 1994, ch. 122, this volume.
Morss, L.R., and J. Fuger, 1981, J. Inorg. & Nucl. Chem. **43**, 2059.
Morss, L.R., and D.C. Sonnenberger, 1985, J. Nucl. Mater. **130**, 266.
Morss, L.R., J. Fuger, J. Geoffart and R.G. Haire, 1983, Inorg. Chem. **22**, 1993.
Morss, L.R., J. Fuger, J. Geoffart, N.M. Edelstein and G.V.J. Shalimoff, 1987, J. Less-Common Met. **127**, 251.
Morss, L.R., J.W. Richardson, C.W. Williams, G.H. Lander, A.C. Lawson, N.M. Edelstein and G.V.J. Shalermoff, 1989, J. Less-Common Met. **156**, 273.
Mulford, R.N.R., and L.E. Lamar, 1960, in: Plutonium 1960, eds E. Grison, W.B.H. Lord and R.D. Fowler (Cleaver-Hume, London) pp. 411–429.
Müller, W., and J.-C. Spirlet, 1985, in: Actinides – Chemical and Physical Properties, ed. L. Manes (Springer, Berlin) pp. 57–74.
Murad, E., and D.L. Hildenbrand, 1980, J. Chem. Phys. **73**, 4005.
Nathans, M.W., and W.W. Wendlandt, 1963, J. Inorg. & Nucl. Chem. **24**, 869.
Nave, S.E., R.G. Haire and P.G. Huray, 1983, Phys. Rev. B **28**, 2317.
Navratil, J.D., and W.W. Schultz, eds, 1981, Transplutonium Elements, ACS Symposium Series, Vol. 161 (American Chemical Society, Washington, DC) multiple chapters therein.
Neubert, A., and K.F. Zmbov, 1974, High Temp. Sci. **6**, 303.
Noddack, W., and H. Walch, 1959, Z. Phys. Chem. **211**, 194.
Noe, M., and J. Fuger, 1971, Inorg. & Nucl. Chem. Lett. **7**, 421.
Noe, M., and J.R. Peterson, 1972, Inorg. & Nucl. Chem. Lett. **8**, 897.
Noe, M., J. Fuger and G. Duyckaerts, 1970, Inorg. & Nucl. Chem. Lett. **6**, 111.
Noguchi, T., 1969, High temperature phase studies with a solar furnace, in: Advances in High Temperature Chemistry, Vol. 2, ed. L. Eyring (Academic Press, New York) pp. 235–262.
Nugent, L.J., R.D. Baybarz, J.L. Burnett and J.L. Ryan, 1971, J. Inorg. & Nucl. Chem. **33**, 2503.
Oetting, F.L., 1967, Chem. Rev. **67**, 261.
Ohse, R.W., and V. Ciani, 1967, in: Thermodynamics of Nuclear Materials (IAEA, Vienna) p. 548.
Oliver, M.R., J.D. Dimmock, A.L. McWhorter and T.B. Reed, 1972, Phys. Rev. B **5**, 1087.
Otsuka, K., M. Kunitomi and T. Saito, 1986, Inorg. Chem. Acta **115**, L31.
Parrish, M.B., 1961, J. Chem. Phys. **34**, 1079.
Pastor, R.C., and A.C. Pastor, 1966, Mater. Res. Bull. **1**, 275.
Pedley, J.B., and E.M. Marshall, 1983, J. Phys. & Chem. Ref. Data **12**, 967.
Peterson, J.R., and R.D. Baybarz, 1972, Inorg. & Nucl. Chem. Lett. **8**, 423.
Peterson, J.R., R.L. Fellows, J.P. Young and R.G. Haire, 1977, Rev. Chim. Miner. **14**, 172.
Popova, A.A., and V.B. Zotkina, 1967, Sov. Phys. Dokl. **11**, 553.
Rand, M.H., 1966, At. Energy Rev. **4**(I), 7–51.
Rand, M.H., 1975, At. Energy Rev. **5**, 7–85.
Rau, R.C., 1964, X-ray crystallographic studies of europium oxides and hydroxides, in: Rare Earth Research, Vol. II, ed. K. Vorres (Gordon and Breach, New York) pp. 117–134.
Ray, S.P., and D.E. Cox, 1975a, J. Solid State Chem. **15**, 333.
Ray, S.P., and D.E. Cox, 1975b, J. Solid State Chem. **15**, 344.
Ricken, J., J. Nölting and I. Riess, 1984, J. Solid State Chem. **54**, 89.
Riess, I., M. Ricken and J. Nölting, 1985, J. Solid State Chem. **57**, 314.
Roberts, L.E., and A.J. Walter, 1966, in: Physico-Chimie du Proactinum, Orsay, 2–8 July 1965, eds G. Bouissieres and R. Muxart (Centre National de la Recherche Scientifique, Paris) pp. 51–59.
Röhler, J., 1987, X-ray absorption and emission spectra, in: Handbook on the Physics and Chemistry of Rare Earths, Vol. 10, eds K.A. Gschneidner Jr, L. Eyring and S. Hüfner (North-Holland, Amsterdam) pp. 453–545.
Roth, R.S., and S.J. Schneider, 1960, J. Res. Natl. Bur. Standards **64A**, 309.
Samhoun, K., and F. David, 1976, in: Transplutonium Elements, eds W. Müller and R. Lindner (North-Holland, Amsterdam) pp. 297–303.
Sandenaw, T.A., 1963, J. Nucl. Mater. **10**, 165.
Sata, T., 1966, Rev. Hautes Temp. & Refract. **3**, 337.
Sata, T., and M. Yoshimura, 1968, J. Ceram. Assoc. Jpn. **76**, 30.
Sawyer, J.O., B.G. Hyde and L. Eyring, 1965a, Inorg. Chem. **4**, 426.
Sawyer, J.O., B.G. Hyde and L. Eyring, 1965b, Bull. Soc. Chim. France, p. 1190.

Schleid, T., and G. Meyer, 1989, J. Less-Common Met. **149**, 73.

Schultz, W.W., 1976, The Chemistry of Americium, Report TID 26971 (ERDA, Oak Ridge).

Schweda, E., 1992, Rare earth oxides, in: Diffusionless Phase Transition and Related Structures in Oxides, ed. C. Boulesteix (Trans Tech. Publications, Zurich, Switzerland) p. 187.

Schweda, E., Z.C. Kang and L. Eyring, 1987, J. Microscopy **145**, 45.

Schweda, E., D.J.M. Bevan and L. Eyring, 1991, J. Solid State Chem. **90**, 109.

Seaborg, G.T., and W.D. Loveland, 1990, in: The Actinide Elements Beyond Uranium (Wiley, New York) pp. 7–65, 217–263.

Sellers, P.A., S. Fried, R.E. Elson and W.H. Zachariasen, 1954, J. Am. Chem. Soc. **76**, 5935.

Shafer, M.W., 1965, J. Appl. Phys. **36**, 1145.

Shafer, M.W., J.B. Torrance and T. Penney, 1972, J. Phys. Chem. Solids **33**, 2251.

Shannon, R.D., 1976, Acta Crystallogr. A **32**, 751.

Simpson, L.A., and R.E. Carter, 1966, J. Am. Ceram. Soc. **49**, 139.

Sinha, S.K., 1978, Magnetic structures and inelastic neutron scattering: Metals, alloys and compounds, in: Handbook on the Physics and Chemistry of Rare Earths, Vol. 1, eds K.A. Gschneidner Jr and L. Eyring (North-Holland, Amsterdam) pp. 489–590.

Smith, P.K., and D.E. Peterson, 1970, J. Chem. Phys **52**(10), 4963.

Soderholm, L., N.M. Edelstein, L.R. Morss and G.V.J. Shalimoff, 1986, J. Magn. & Magn. Mater. **54–57**, 597.

Sørensen, O.T., 1981, in: Nonstoichiometric Oxides, ed. O.T. Sørensen (Academic Press, New York) p. 17.

Spirlet, J.-C., 1980, J. Cryst. Growth **49**, 171.

Spirlet, J.-C., and O. Vogt, 1984, in: Handbook on the Physics and Chemistry of the Actinides, eds A.J. Freeman and G.H. Lander (North-Holland, Amsterdam) pp. 79–152.

Stchouzkoy, T., H. Pezerat, G. Bouissieres and R. Muxart, 1964, C.R. Acad. Sci. (Paris) **259**, 3016.

Stchouzkoy, T., A. Rezerat and R. Muxart, 1966, in: Physico-Chimie du Proactinium, Orsay, 2–8 July 1965, eds G. Bouissieres and R. Muxart (Centre National de la Recherche Scientifique, Paris) pp. 61–77.

Stecura, S., 1965, US Bureau of Mines Report Invest. 6616 1/47, p. 7; 1966; Chem. Abstr. **64**, 16736.

Stevenson, J.N., and J.R. Peterson, 1975, J. Microchem. **20**, 213.

Stone, G.D., G.R. Weber and L. Eyring, 1968, in: Mass Transport in Oxides, eds J.B. Wachtman Jr and A.D. Franklin, NBS Special Publication No. 296 (National Bureau of Standards, Washington, DC) p. 179.

Subba Rao, G.V., S. Ramdas, P.N. Mehrotra and C.N.R. Rao, 1970, J. Solid State Chem. **2**, 377.

Sugihara, T., S.H. Lin and L. Eyring, 1981a, J. Solid State Chem. **40**, 189.

Sugihara, T., S.H. Lin and L. Eyring, 1981b, J. Solid State Chem. **40**, 226.

Templeton, D.H., and C.H. Dauben, 1957, J. Am. Chem. Soc. **76**, 5237.

Tuenge, R.T., and L. Eyring, 1979, J. Solid State Chem. **29**, 165.

Tuenge, R.T., and L. Eyring, 1982, J. Solid State Chem. **41**, 75.

Turcotte, R.P., 1980, J. Inorg. & Nucl. Chem. **42**, 1735.

Turcotte, R.P., and R.G. Haire, 1976, in: Transplutonium Elements, eds W. Müller and R. Lindner (North-Holland, Amsterdam) pp. 267–277.

Turcotte, R.P., J.M. Warmkessel, R.J.D. Tilley and L. Eyring, 1971a, J. Solid State Chem. **3**, 265.

Turcotte, R.P., T.D. Chikalla and L. Eyring, 1971b, J. Inorg. & Nucl. Chem. **33**, 3749.

Turcotte, R.P., T.D. Chikalla, R.G. Haire and J.A. Fahey, 1979, J. Inorg. & Nucl. Chem. **42**, 1729.

Vallath, D., 1976, in: Plutonium 1975 and Other Actinides, eds H. Blank and R. Lindner (North-Holland, Amsterdam) pp. 843–850.

Van Lierde, W., R. Strumane, E. Smets and S. Amelinckx, 1962, J. Nucl. Mater. **5**, 250.

Van Vleck, J.H., 1965, The magnetic history of rare earths, in: Rare Earth Research, Vol. III, ed. L. Eyring (Gordon and Breach, New York) p. 3.

Vedel, I., A.M. Redon and J.M. Leger, 1986, J. Phys. C **19**, 3549.

Vier, D.T., 1975, Thermal and Other Properties of Refractories, in: Report LA-5937-MS (Los Alamos National Laboratory, Los Alamos, NM).

Vinokurov, I.V., Z.N. Zoon and V.A. Ioffe, 1965, Sov. Phys. Solid State **7**, 814.

Vogt, O., 1982, in: Actinides in Perspective, ed. N.M. Edelstein (Pergamon Press, New York) pp. 289–308.

Von Dreele, R.B., L. Eyring, A.L. Bowman and J.L. Yarnell, 1974, Acta Crystallogr. B **31**, 971.

Wachter, P., 1979, Europium chalcogenides: EuO, EuS, EuSe and EuTe, in: Handbook on the Physics and Chemistry of Rare Earths, Vol. 2, eds K.A. Gschneidner Jr and L. Eyring (North-Holland, Amsterdam) pp. 507–574.

Wagman, D.D., W.H. Evans, V.B. Parker, R.H. Schumm and R.L. Nuttall, 1981, US Bureau of Standards Technical Note 279–8 (US Printing Office, Washington).

Wagman, D.D., W.H. Evans, V.B. Parker, R.H. Schumm and R.C. Nuttall, 1982, J. Phys. & Chem. Ref. Data **11**, Suppl. 2.

Wallenberg, R., R. Withers, D.J.M. Bevan, J.G. Thompson, P. Barlow and B.G. Hyde, 1989, J. Less-Common Met. **156**, 1.

Wallmann, J.C., 1964, J. Inorg. & Nucl. Chem. **26**, 2053.

Warshaw, I., and R. Roy, 1961, J. Phys. Chem. **65**, 204.

Weber, G.R., and L. Eyring, 1970, in: Int. Colloq. of CNRS, no. 180, Vol. 1, the Rare Earth Elements, May 1969, Paris–Grenoble (CNRS, Paris) p. 179.

Weigel, F., 1986, in: The Chemistry of the Actinide Elements, eds J.J. Katz, G.T. Seaborg and L.R. Morss (Chapman and Hall, New York) pp. 169–442.

Weigel, F., and H. Hauske, 1977, J. Less-Common Met. **55**, 243.

Weigel, F., and R. Kohl, 1985, in: Americium and Curium Chemistry and Technology, eds N.M. Edelstein, J.D. Navratil and W.W. Schultz (Reidel, Dordrecht) pp. 159–192.

Weigel, F., and V. Scherer, 1965, Radiochim. Acta **4**, 197.

Weigel, F., J.J. Katz and G.T. Seaborg, 1986, in: The Chemistry of the Actinide Elements, eds J.J. Katz, G.T. Seaborg and L.R. Morss (Chapman and Hall, New York) pp. 680–705.

Wendlandt, W.W., 1956, Anal. Chim. Acta **15**, 435.

Wendlandt, W.W., 1958a, J. Inorg. & Nucl. Chem. **5**, 118.

Wendlandt, W.W., 1958b, Anal. Chem. **30**, 58.

Wendlandt, W.W., 1959, Anal. Chem. **31**, 408.

Westrum Jr, E.F., 1967, Developments in chemical thermodynamics of the lanthanides, in: Advances in Chemistry, Vol. 71, ed. R.F. Gould (American Chemical Society, Washington, DC) pp. 25–50.

Wilbert, Y., N. Dherbomeg and H. Breuil, 1975, Acad. Sci. Paris, Ser. C **280**, 465.

Wild, J.F., E.K. Hulet, R.W. Lougheed, W.N. Hayes, J.R. Peterson, R.L. Fellows and J.P. Young, 1978, J. Inorg. & Nucl. Chem. **40**, 811.

Wilson, A.S., F.P. Roberts and E.J. Wheelwright, 1963, Nature **198**, 580.

Yakel, H.L., 1978, Acta Crystallogr. B **35**, 564.

Zachariasen, W.H., 1949, Acta Crystallogr. **2**, 388.

Zhang, J., R.B. Von Dreele and L. Eyring, unpublished results.

Zhang, J., Z.C. Kang and L. Eyring, 1993a, J. Alloys & Compounds **192**, 57.

Zhang, J., R.B. Von Dreele and L. Eyring, 1993b, J. Solid State Chem. **104**, 21.

Handbook on the Physics and Chemistry of Rare Earths
Vol. 18 – Lanthanides/Actinides: Chemistry
edited by K.A. Gschneidner, Jr., L. Eyring, G.R. Choppin and G.H. Lander

Chapter 126

f-ELEMENT SPECIATION IN STRONGLY ACIDIC MEDIA: LANTHANIDES AND MID-ACTINIDE METALS, OXIDES, FLUORIDES, AND OXIDE FLUORIDES IN SUPERACIDS

Scott A. KINKEAD, Kent D. ABNEY
Isotope and Nuclear Chemistry Division, Los Alamos National Laboratory, Los Alamos, NM 87545, USA;

Thomas A. O'DONNELL
Department of Chemistry, University of Melbourne, Parkville, Victoria, 3052, Australia

Contents

1. Introduction 508
2. Discussion 508
  2.1. Lanthanides 508
  2.2. Actinide metals 510
  2.3. Actinide halides 512
  2.4. Actinide (IV) oxides 513
    2.4.1. Uranium, neptunium and plutonium dioxide 513
    2.4.2. Americium dioxide 515
  2.5. Uranium (VI) oxides 515
    2.5.1. Uranium trioxide 515
    2.5.2. Uranium sesquioxide (U_3O_8) 516
  2.6. Reactions of An (IV) with An (VI) in superacid media 516
  2.7. Uranium (VI) oxyfluorides 518
    2.7.1. Uranium oxide tetrafluoride 518
    2.7.2. Uranyl fluoride 519
  2.8. Thermogravimetric studies of uranium and thorium fluoroantimonates 520
  2.9. Cyclic-voltammetry studies of U, Np, Pu and Am-fluorosulfonates in HSO_3F/SbF_5 522
3. Conclusions 523
Appendix: Experimental procedures 524
References 526

1. Introduction

The powerful proton acidity produced by the combination of strong Lewis acids and anhydrous hydrogen fluoride or fluorosulfuric acid (media generally referred to as "superacids") have been known for more than thirty years (Olah et al. 1985, Gillespie and Peel 1973). Because of their extreme acidity, superacids such as HF/SbF_5 or HSO_3F/SbF_5 (also known as magic acid) have been used by inorganic and organic chemists to stabilize such electrophilic species as carbocations and polyhalogen or polychalcogen cations (e.g., I_3^+) in solution. One of the major advantages of the use of superacids as solvents in the characterization of unusual species – inorganic *and* organic – is the unprecedented solubility of common and unusual moieties in this media, making appreciable concentrations readily available for spectroscopic study. In actinide and lanthanide chemistry, these superacids dissolve more different compounds, more rapidly, and to a higher final metal concentration, than any other known solvent. Of the lanthanide and mid-actinide compounds studied, only the tetrafluorides of thorium, uranium, neptunium, and plutonium lack any appreciable solubility (i.e., greater than 10^{-2} M) in these solvents. While refractory compounds such as dioxides – which are highly soluble in superacids – lose oxygen from the actinide coordination shell, uranyl compounds (and presumably neptunyl and plutonyl compounds) retain the UO_2^{2+} configuration. A second feature of superacids is their strongly electrophilic nature, thereby rendering most metals and many nonmetals soluble as cationic species, typically with a fluorosulfate, hexafluoroantimonate, or polyfluoroantimonate anion. The property of superacids which stabilizes strong electrophiles also allows unprecedented observation and study of unusual oxidation states. Spectral characterization of such compounds, usually by UV-visible (and occasionally near-IR) spectroscopy, displays features of the superacid solvent coordination which are distinct from those observed in either aqueous acids or bases or molten salts. Typically these are manifested as substantial shifts in the position of *d–f* or *d–d* transitions of the order of 100–1000 cm^{-1} relative to those in aqueous media. Lanthanide spectra are unusual in this respect, since electronic spectra of the rare earths obtained in superacids, aqueous acids and in crystalline LaF_3 are nearly identical in peak position and relative magnitude of absorbances, indicating very similar coordination and electronic structure. This chapter reviews the reported chemistry of the lanthanides as well as thorium, uranium, neptunium, plutonium, and americium in these strongly acidic media.

2. Discussion

2.1. *Lanthanides*

Although lanthanides are well-characterized in the solid state in divalent (e.g., Sm, Eu, Tm, and Yb) and tetravalent (e.g., Ce, Tb, Pr, and less commonly Nd and Dy) oxidation states, the "normal" oxidation state of these elements in aqueous solution is the trivalent. While the rare earths are similar in their redox behavior to the late

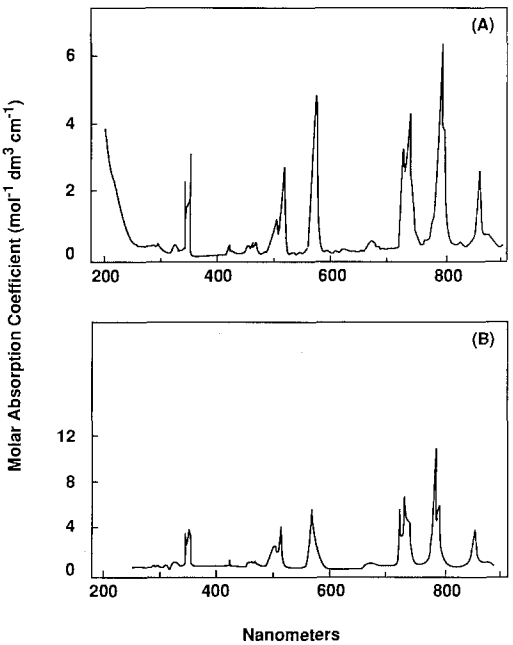

Fig. 1. UV-visible spectra of Nd(III) in (A) 5 M HF/SbF_5; and (B) 1 M $HClO_4$. Reprinted with permission from (O'Donnell 1992) as on p. 29.

actinides (Cm–Lr), they are vastly different from the mid-actinides Th–Am which exhibit stable valences of III to VII in aqueous media. As an additional contrast to the actinides, the electronic spectra of the lanthanides are relatively insensitive to media (i.e., aqueous versus nonaqueous or doped into crystalline LaF_3) or to anion (e.g., Cl^-, ClO_4^-, or SbF_6^-). This is illustrated for the case of neodymium(III) in HF/SbF_5 and aqueous (1 M) perchloric acid, shown in fig. 1 (O'Donnell 1992). As is shown in table 1 by the values of the peak positions and intensities of Nd(III) in aqueous and superacid media, as well as NdF_3 doped into LaF_3, peak positions vary by less than 5 nm indicating a similarity in the ionic/covalent nature of the lanthanide ion as well as the coordination sphere surrounding the ion. For comparison, uranium and neptunium differ

TABLE 1
Major peak positions of neodymium (III) in various media (O'Donnell 1992).

Anhydrous HF/–5 M SbF_5		H_2O–1 M $HClO_4$		LaF_3	
λ(nm)	E(cm^{-1})	λ(nm)	E(cm^{-1})	λ(nm)	E(cm^{-1})
861	11 600	862	11 600	865	11 560
791	12 460	793	12 610	794	12 590
735	13 610	736	13 590	740	13 510
572	17 500	575	17 390	575	17 390
519	19 270	520	19 230	522	19 160
507	19 720	510	19 610	512	19 530
351	28 490			354	28 250
344	29 070			345	29 000

by as much as 20 nm, still far less than the shifts of 25 to 150 nm (depending on band positions) observed for typical *d*-transition metals in anhydrous HF or aqueous acid.

Structural characterization (X-ray crystallography) of the aqueous lanthanide compounds $Nd(BrO_3)_3 \cdot 9H_2O$ and $La(OSO_3C_2H_5)_3 \cdot 9H_2O$ reveals nine-fold coordinated (tricapped trigonal prismatic) aquo ions (Albertson and Elding 1977, Sikka 1969, Fitzwater and Rundle 1959, Hubbard et al. 1974, Broach et al. 1979). Studies of lanthanide coordination in solution, including X-ray diffraction studies of concentrated aqueous Ln^{3+} solutions (Smith and Wertz 1975, 1977, Habenschuss and Spedding 1979a, b, 1980), are not entirely conclusive with respect to the coordination number of the ion, but suggest that at least in dilute solutions the coordination number is at least eight and probably nine in the early members of the series and decreases along the series to eight as the ionic radius decreases through lanthanide contraction. Given the established nine-fold coordination of trivalent Nd in the solid state, and the likelihood of nine-coordinate Nd^{3+} existing in solution, it is entirely possible that superacid solutions also exist in high coordination numbers such as eight or nine. The nearly identical electronic spectra observed for Nd^{3+} irrespective of matrix (i.e., superacids, aqueous acid, and doped into lanthanum fluoride) either supports such a hypothesis or suggests that the electronic spectra of lanthanides are not only insensitive to the coordinated species but also to the coordination number as well, a conjecture unsupported by data.

With the exception of cerium, which is easily oxidized to the tetravalent state, lanthanides invariably occur as trivalent species in aqueous media. Lanthanide(III) cations were generated in HF for spectroscopic investigation by treating solid LnF_3 with HF and the weak Lewis acid BF_3 (Barraclough et al. 1977). Sm^{2+}, Eu^{2+}, and Yb^{2+} have been characterized spectroscopically by treating the metals with anhydrous HF (Barraclough et al. 1991). Gilbert and co-workers (1978) produced stable solutions of Eu(II), Yb(II), and Sm(II) in molten salts by voltammetric reduction of the three lanthanides in oxidation state(III) in acidic chloroaluminates ($AlCl_3$: NaCl, 60 : 40 at 175°C). Members of this same group reported spectroscopic and electrochemical behavior of Yb(III)–Yb(II) and Sm(III)–Sm(II) (Schoebrechts et al. 1983a) and of Eu(III)–Eu(II) and Tm(III)–Tm(II) (Schoebrechts et al. 1983b) in acidic room temperature melts ($AlCl_3$: 1-*n*-butylpyridinium chloride, $>60 : <40$).

2.2. *Actinide metals*

While actinide metals are easily soluble in some mineral acids such as HCl and $HClO_4$, they are typically found in solution in valences IV to VI. However, Baluka and co-workers first reported in 1981 that dissolution of U and Np metals in superacids produces initially trivalent actinides (Baluka et al. 1981). The UV-visible spectra of the U and Np solutions, shown in fig. 2, are characteristic of the trivalent actinides found in aqueous acidic or basic systems. Avens and colleagues (1988) have dissolved both Pu and Am metal and observed trivalent species by UV-visible spectroscopy. The stability of oxidation state (III) for U, Np and Pu is all the more striking especially in light of the lower stability of the series U (III)–Pu (III) relative to higher oxidation states; e.g., trivalent uranium (III) is able to reduce water under normal conditions. In addition to the unusually low oxidation state obtained, another feature of actinide dissolution in

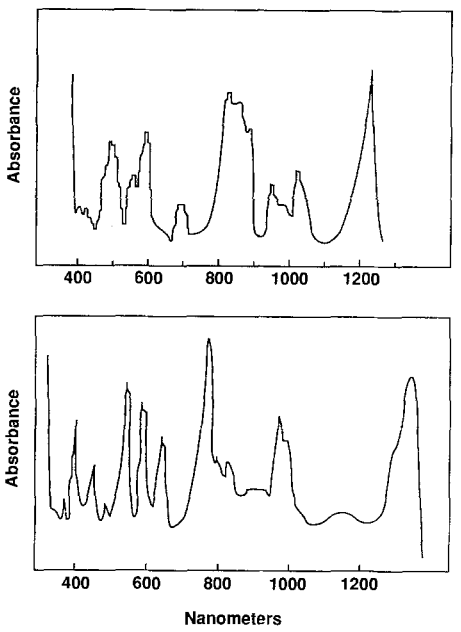

Fig. 2. (a) UV-visible spectra of U(III) in HF/BF_3 and (b) Np(III) in HF/AsF_5. Reprinted with permission from (O'Donnell 1992 b).

superacids is the high concentration of actinides which are obtained. For example, 0.155 g (0.916 mmol) of Np metal dissolves in 2.9 g of HF containing 2.35 g (7 mol%) SbF_5, although complete dissolution at ambient temperature takes on the order of weeks. The final concentration of neptunium in solution after several days is in excess of 0.3 M, a surprisingly large amount considering the usual concentrations obtained from mineral acid dissolution (typically less than 0.1 M). For comparison, this equates to over 70 g Np/liter of solution. In the dissolution of neptunium metal, the only neptunium species observed in HF/SbF_5 was Np(III), which agrees well with Baluka's observation (Baluka et al. 1981). At the completion of the dissolution, evaporation of the solvent afforded a light-blue solid. In fact, the upper limits of actinide concentration in superacids is not known: solutions of U and Pu in HF/SbF_5 in excess of 0.5 M have been obtained.

Although U, Np, Pu, and Am metals react easily to form solutions in superacids at ambient temperature, the same cannot be said for thorium metal. In fact, thorium metal incurred no weight change after either refluxing in magic acid for hours or standing in HF/SbF_5 for several months. This is consistent with observations that Th does not exist in fluoride media in oxidation states lower than (IV) and that the very high lattice energy of ThF_4 would hinder dissolution even in superacids.

When actinide metals are oxidized as they dissolve in HF/BF_3, hydrogen gas is evolved (Baluka et al. 1981, Avens et al. 1988), while in HF/SbF_5, there is evidence that antimony metal (Tarnero 1967), SbF_3, hydrogen, or one of several SbF_3/SbF_5 complexes – previously characterized by Gillespie and co-workers (Birchall et al. 1973) or Passmore and co-workers (Shantha Nandana et al. 1985, 1987) – may form. For instance, in the dissolution of Pu metal (see appendix) at different times evidence for all

of these products can be observed. The difference in observations may be a result of differences in the concentration of the Lewis acid in HF and of the differing kinetics for various competing reactions. Thus, in superacid solutions containing high mol ratios of actinide to SbF_5, reduction of Sb^{+5} to Sb^{+3} and subsequently to Sb^0 may be kinetically more labile than reduction of HF to H_2, and therefore may occur more rapidly. Although it takes place more slowly, the subsequent reaction of Sb metal with HF to form SbF_3 and liberate H_2 may nevertheless occur for thermodynamic reasons. Finally, the SbF_3 formed is sufficiently basic to form a complex with any Lewis acid remaining in the superacid. A variety of complexes formulated as $n SbF_3 \cdot m SbF_5$ ($n = 1, 2, 3, 6$; $m = 1, 3, 4, 5$) have been identified structurally from reactions of SbF_5 with Sb, SbF_3, or various reducing agents by the groups referenced above. A possible overall sequence of reactions may be as follows:

$$5An^0 + 3SbF_5 \xrightarrow{\text{anhydrous HF}} 5An^{+3}_{solv.} + 3Sb^0\downarrow, \tag{1}$$

$$3Sb^0 + 9HF \longrightarrow 3SbF_3 + \tfrac{9}{2}H_2\uparrow, \tag{2}$$

$$SbF_3 + nSbF_5 \xrightarrow{\text{anhydrous HF}} SbF_3 \cdot nSbF_5\downarrow. \tag{3}$$

2.3. *Actinide halides*

Whereas U(III) has been shown to be stable indefinitely in weakly acidic HF (HF/BF_3), its instability towards base-induced disproportionation has been strikingly

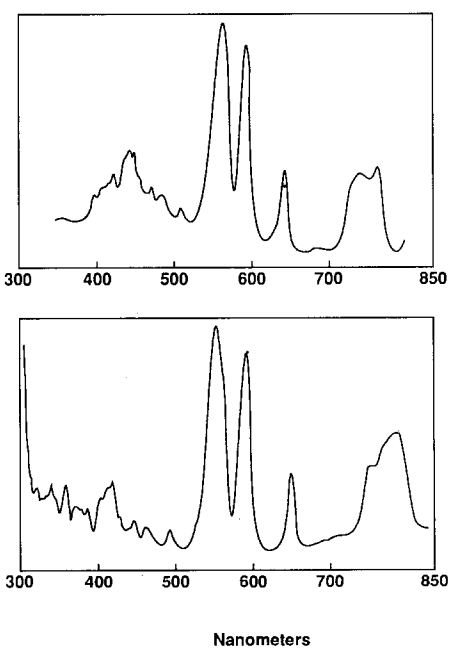

Fig. 3. UV-visible spectrum of $PuCl_3$ in HF/SbF_5 (top) and HSO_3F/SbF_5 (bottom).

demonstrated by O'Donnell (1987). Upon successive addition of the Lewis base NaF in HF to a solution of U(III) in superacid, UF_4 and either metallic uranium particles or – rarely – even a mirror of uranium metal precipitates. In our laboratories, when we treated a blue solution of Pu(III) – obtained from dissolution of metal – in HF/SbF_5 with a solution of NaF in anhydrous HF, only a lavender solid, indicative of Pu(III), precipitates (Avens and Abney 1988). We found no evidence for the formation of Pu metal or PuF_4 under such conditions. While this experiment has not been confirmed, this evidence supports the suggestion of O'Donnell (Barraclough et al. 1977, Baluka et al. 1981, Burns et al. 1981) that U(III) is far less stable (to disproportionation) than Pu(III) and presumably Np(III) due to the increasing f-element (i.e., lanthanide-like) character of the later actinides, and the corresponding decrease in d-element (transition-metal-like) character from U to Pu in higher valences.

To confirm the identity of the Pu species from metal dissolution, Avens et al. (1988) dissolved $PuCl_3$ in both HSO_3F/SbF_5 and HF/SbF_5. The resulting UV spectrum, shown in fig. 3, confirms that, indeed, Pu(III) results from the dissolution of metal. An additional feature of this experiment is that SbF_3 and complexes arising from oxidation of Pu metal are absent.

2.4. *Actinide(IV) oxides*

2.4.1. *Uranium, neptunium and plutonium dioxide*

While Baluka et al. (1981) showed that the tetrafluorides of uranium, neptunium and plutonium are only sparingly soluble in HF/BF_3 (0.02 M in [U]), even after extended periods of time, Avens et al. (1988) found that UO_2, NpO_2, and PuO_2 are extremely soluble in both HF/SbF_5 and HF/AsF_5 mixtures. In routine actinide processing, dissolution of the highly refractory actinide dioxides to produce even low concentrations (0.1 M) requires cascade dissolution in refluxing concentrated HNO_3/10% HF for days. It is therefore surprising that even uranium dioxide fired at temperatures in excess of 1000°C for over 24 hours dissolves in a matter of hours at ambient temperature in HF/SbF_5 to final concentrations in excess of 0.5 M uranium. Apparently, the solubility of uranium, neptunium, and plutonium are affected not only by the oxidation state, but also by the coordination number of the actinide, and more importantly, by the availability of moieties such as oxygen in the solid to react with the solvent. It seems likely that the oxygen atoms bound to an actinide are far more susceptible than fluorine atoms to attack by either HF, H_2F^+, or SbF_5, leading to formation of the hydronium salt and fluorination of the uranium. Dissolution of the tetrafluorides, which have very large lattice energies, requires removal of U atoms as HF-solvated U(IV) cations. However, O atoms are successfully abstracted from the dioxides by protonation, forming OH^-, H_2O, and H_3O^+ in turn. The latter is known to occur in HF/SbF_5 as the formal entity $(H_3O^+)(SbF_6^-)$. In either case, UF_2^{2+} and SbF_6^- ions are formed. The reaction for the dissolution of UO_2 by HF/SbF_5 is very much more thermodynamically favorable than that for UF_4.

The dissolution of actinide metal dioxides proceeds according to reaction 4 where the dissolution rate increases from Th to Pu. Based upon studies by O'Donnell (1992), it is highly likely that, at least for the case of uranium, a solvated fluoro-actinide cation,

such as $(UF_2^{2+})(SbF_6^-)_2$, is formed in highly acidic solution. Although spectral data strongly suggest that a cationic fluorocomplex also exists for Np and Pu, the lack of supporting data (i.e., structural data, results of electromigration experiments) renders the situation less clear for these elements. In addition, increasing similarities of the UV-visible spectra in superacids and in aqueous media (Baluka et al. 1981, Avens et al. 1988) for these elements may indicate different cationic species than the fluorocation UF_2^{2+} for these elements or, as has been suggested for the lanthanides (O'Donnell 1992), a decreasing sensitivity of the metal to the nature of the coordinating ligand. As shown by several analytical techniques, the dissolution reaction also results in the formation of stable group 15 oxonium salts:

$$AnO_2 + \text{xs}\ HF/SbF_5 \longrightarrow AnF_4 \cdot 2SbF_{5(solv)} + 2(H_3O^+)(SbF_6^-)_{(solv)} \quad [An = Th, U, Np, Pu]. \tag{4}$$

Both solution and solid-state vibrational spectroscopy have been employed to characterize the reaction shown above. In addition, X-ray powder diffraction of the recovered solids from the uranium experiment shows the presence of both $(H_3O^+)(SbF_6^-)$ and $UF_4 \cdot 2SbF_5$. Raman spectroscopy of the solid mixture after vacuum removal of the solvent features bands at 667, 561, and 295 cm^{-1} due to the ν_1, ν_2, and ν_5 stretching and bending modes of SbF_6^-, respectively. The infrared spectrum of the solid also shows a broad band at 3058 cm^{-1} (ν_3) and a sharp band at 1623 cm^{-1} (ν_4) due to the (H_3O^+) moiety. Little difference between the spectra reported for pure $(H_3O^+)(SbF_6^-)$ (Christe et al. 1984) and our heterogeneous mixtures was observed. Therefore,

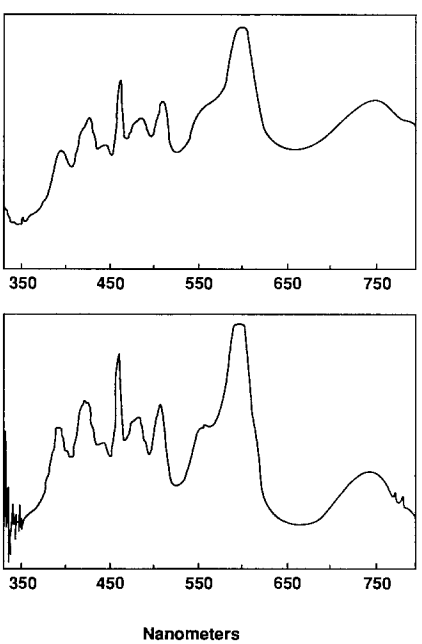

Fig. 4. UV-visible spectrum of UF_4 (top) and UO_2 (bottom) in HF/SbF_5.

no An–F stretching and bending modes, where An is Th, U, Np, or Pu, could be uniquely assigned since those modes must underlie the Sb–F modes and/or are weak scatterers.

The UV-visible spectrum of the green solution resulting from UO_2 and UF_4 dissolution, shown in fig. 4, displays bands characteristic of U(IV), and is similar to the spectrum obtained by others for UF_4 in HF/AsF_5 (Baluka et al. 1981). Removal of the HF/SbF_5 solvent under vacuum provided a mixture of green uranium substrate and colorless oxonium crystals. Analysis of the green material established the formula $UF_4 \cdot 2SbF_5$, which formally contains the UF_2^{2+} ion found by O'Donnel (1992) from dissolution of UF_4.

Determination of the structure of the colorless crystals isolated from the dissolution of UO_2 in HF/SbF_5 by X-ray diffraction has revealed the material to be $(H_3O^+)(SbF_6^-)$ (Larson et al. 1991) providing further confirmation for reaction 4. Evidence for the oxonium salt, $(H_3O^+)(SbF_6^-)$, as well as other reaction products was also found in the X-ray powder diffraction pattern and was consistent with the results of the Raman, infrared and thermogravimetric (vide infra) investigations of the resulting residues. The reflection indices were identical to those of pure $(H_3O^+)(SbF_6^-)$ reported by Christe et al. (1984).

2.4.2. *Americium dioxide*

Although the dissolution of AmO_2 in superacid is more rapid than even that of PuO_2, the reaction does not, in contrast to the earlier actinides, lead to a solution of Am(IV). Instead, dissolution of AmO_2 in either HF/SbF_5 or HSO_3F/SbF_5 results in reduction of the dioxide to a complex of Am(III) (Avens and Abney 1988). This is further evidence for the increasing f-element character of the later actinides, as well as the tendency of superacids to favor lower oxidation states. Reduction of Am(IV) to Am(III) in magic acid may be accompanied by formation of a volatile oxidation product such as O_2 since no solid oxidation product was found. The presence of Am(III) in both HF/SbF_5 and HSO_3F/SbF_5 was confirmed by comparison of the UV-visible spectrum, shown in fig. 5, with that of Am(III) in $HClO_4$ (Keenan 1959).

2.5. *Uranium (VI) oxides*

The chemistry of uranium trioxide and sesquioxide (U_3O_8) in superacids is characterized by incomplete fluorination rather than oxidation thus forming oxide fluoride-containing species such as solvated UO_2F_2. This contrasts with the case of uranium dioxide which undergoes complete fluorination to form the fluorocation UF_2^{2+} in the compound $UF_4 \cdot 2SbF_5$, and uranium metal which undergoes oxidation to U(III). Thus, dissolution of higher uranium oxides and oxide fluorides provides yellow or green solutions indicative of uranium (VI) complexes.

2.5.1. *Uranium trioxide*

Dissolution of UO_3 in HF/SbF_5 is complete within minutes of adding the superacid, giving a yellow solution. After removal of the solvent, weight gains of the solid suggest that six or more equivalents of SbF_5 may be associated with the complex

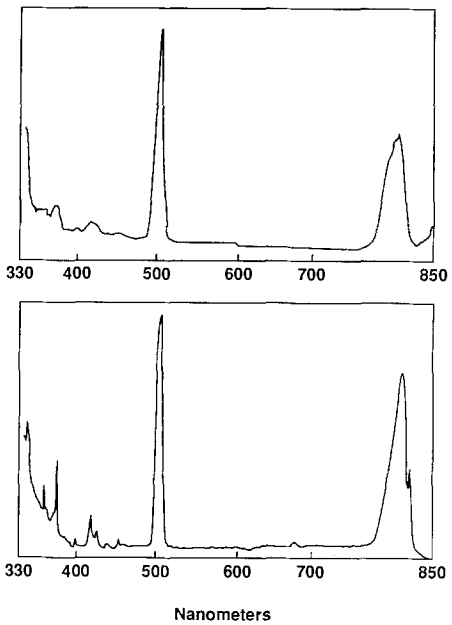

Fig. 5. UV-visible spectrum of Am(III) from AmO_2 dissolution in 5% SbF_5/HF (top) and 25% SbF_5/HSO_3F (bottom).

in the form of either SbF_6^-, $Sb_2F_{11}^-$, $Sb_3F_{16}^-$, or as lattice solvate. Direct evidence for UO_2^{2+} formation is found in the vibrational spectra of the solution, where the Raman-active symmetric UO_2^{2+} stretch is observed at 925 cm^{-1} and the infrared-active asymmetric stretch is observed at 1013 cm^{-1}. In addition, the UV-visible solution spectrum is identical to those observed for solutions of other uranyl compounds. Therefore we believe dissolution of UO_3 in HF/SbF_5 proceeds as follows:

$$UO_3 + 3HF + (3+n)SbF_5 \longrightarrow (UO_2^{2+})(SbF_6^-)_2 \cdot nSbF_5 + (H_3O^+)(SbF_6^-) \quad (5)$$

2.5.2. *Uranium sesquioxide (U_3O_8)*

Like the dioxide, U_3O_8 dissolves in HF/SbF_5 with stirring at ambient temperature in a matter of hours to give a blue–green solution. Inasmuch as U_3O_8 is a mixture of uranium(IV) and uranium(VI) oxides, it is not surprising that the UV-visible spectrum of this solution displays features characteristic of both uranium valences. UV-visible spectra of both UO_3 and U_3O_8 are shown in fig. 6.

2.6. *Reactions of An (IV) with An (VI) in superacid media*

As we have shown, the dissolution of UO_2 or UF_4 in HF/SbF_5 produces a blue–green solution typical of U(IV), whereas the dissolution of U(VI) species such as UOF_4 or UO_2F_2 (vide infra) provides orange or yellow solutions characteristic of the U(VI) oxidation state. While redistribution reactions occur fairly rapidly for some U(VI) species, both UO_2^{2+} and the U(IV) oxidation state are indefinitely

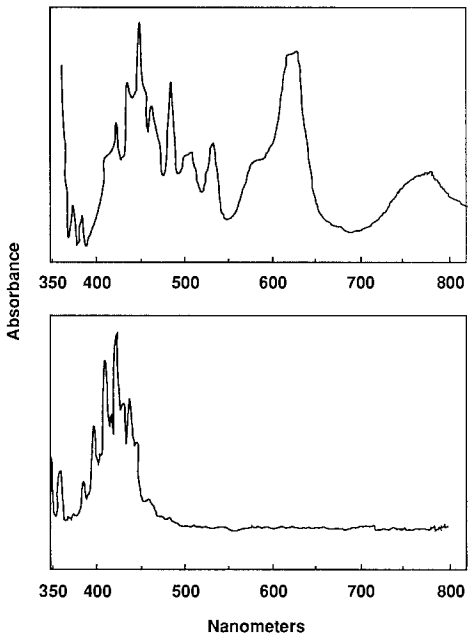

Fig. 6. UV-visible spectrum of U_3O_8 (top) and UO_3 (bottom) in HF/SbF_5.

stable in superacid media. In fact, from the dissolution of uranium sesquioxide, U_3O_8, we can see that the two species coexist without reaction. Therefore, we found it extremely interesting that treatment of a superacid solution of U(IV) from UO_2 or UF_4 with UF_6 results in a *con*proportionation reaction, producing two equivalents of a blue U(V) species.The only other report of such a reaction of uranium was the observation of Bennett and Ferris (1974) of the conproportionation of UF_4 and UF_6 in molten salts. The existence of the U(V) oxidation state has been confirmed by UV-visible absorption spectroscopy shown in fig. 7, in comparison with the reported spectrum of UCl_5 in $AlCl_3$ (Gruen and McBeth 1968). Based on product weight gains, the final product of the reaction of UF_6 with UF_4 is $UF_5 \cdot 2SbF_5$, which has been previously characterized by Bougon and Charpin (1979), and Sawodny and Rediess

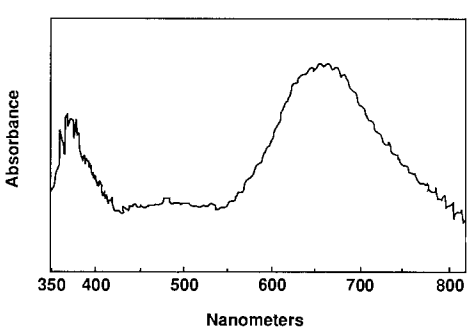

Fig. 7. UV-visible spectrum of U(V) resulting from the reaction of UF_6 with UO_2 in HF/SbF_5.

(1980). The stability, and lack of oxidizing character of UO_2^{2+} relative to UF_6 in solution may explain the difference in conproportionation of UF_2^{2+} with UO_2^{2+} and with UF_6.

By contrast, treatment of a solution of Pu(IV) in HF/SbF_5 with PuF_6 resulted only in a solution of Pu(IV). This result may be explained by another experiment in which PuF_6 spontaneously reduced in the strong-acid HF/SbF_5 to Pu(IV) and presumably fluorine gas. Nevertheless, additional studies are needed to further characterize these reactions as well as to explore whether the analogous reactions for Np occur.

2.7. *Uranium (VI) oxyfluorides*

2.7.1. *Uranium oxide tetrafluoride*

The chemistry of uranium oxide tetrafluoride (UOF_4) in superacids has been thoroughly studied by Holloway and co-workers (Bougon et al. 1978, 1979, Holloway et al. 1983). Due to the limited solubility of UOF_4 in HF or HF-based superacids, and also because such UOF_4 solutions are unstable, undergoing redistribution reactions with time to form UO_2^{2+} and UF_6, these compounds are best prepared by direct reaction of UOF_4 and the Lewis acid in the absence of anhydrous HF. UOF_4 is known to form three discrete complexes with SbF_5 of the formula $UOF_4 \cdot nSbF_5$ where $n = 1-3$ (Bougon et al. 1978). The intermediate product, $UOF_4 \cdot 2SbF_5$, can also be prepared by vacuum decomposition of $UOF_4 \cdot 3SbF_5$ at 60–70°C. After vacuum removal of the reactants and solvent, the X-ray structure of the solid $UOF_4 \cdot 2SbF_5$ adduct was determined, revealing a covalent structure of heptacoordinated (approximately pentagonal bipyramidal) uranium bridged through the five equatorial fluorine atoms to two SbF_5 moieties, each in turn connected by fluorine bridges to adjacent uranium atoms. The remaining two atoms, one oxygen and one fluorine, bound axially to the uranium, are unbridged and indistinguishable in the structure. Not surprisingly, there is no evidence for a contribution from an ionic UOF_3^+ species, since such a species would probably be extremely electrophilic. Investigation of the UOF_4/SbF_5 system in solution by ^{19}F NMR shows fluorine exchange between SbF_5 and UOF_4, although no signals arising from ionic SbF_6^- were observed (Bougon et al. 1979). This is supported by the solid phase and solution vibrational data where a shift of the U=O stretching frequency to higher wavenumbers occurred; however, no bands attributable to SbF_6^- or $Sb_2F_{11}^-$ were observed. Obviously, the uranium–oxygen bonds are weakened through delocalization of electrons to the coordinated SbF_5, but remain reasonably strong, since formation of UF_6 and $UO_2F_2 \cdot nSbF_5$ is slow.

In weaker superacids, e.g., HF/TaF_5 and HF/NbF_5, only the 1:3 complex appears to be appreciably stable in the solid phase (Holloway et al. 1983). Upon varying the stoichiometry and reaction conditions to those suited for the preparation of $UOF_4 \cdot 2SbF_5$ and $UOF_4 \cdot SbF_5$, only the 1:3 complexes, unreacted UOF_4, and UO_2^{2+} species were obtained. Both complexes are insoluble in or react with common ^{19}F NMR solvents, preventing satisfactory solution NMR studies. An interesting aspect of UOF_4 chemistry is that it does not form adducts with AsF_5, either alone or in anhydrous HF, even under conditions of prolonged exposure to elevated temperatures (40°C for 12 hours) (Holloway et al. 1983). With BiF_5 in HF, only a 1:2 complex

($UOF_4 \cdot 2BiF_5$) is formed. After extended exposure to HF/BiF_5 the vibrational spectra of $UOF_4 \cdot 2BiF_5$ shows only a weak band due to the uranyl component (ca. 928 cm^{-1}), indicating a greater solvolytic stability than the NbF_5 or TaF_5 adducts.

Both the oxide tetrafluorides of neptunium (Drobyshevskii et al. 1975, Peacock and Edelstein 1976) and plutonium (Burns and O'Donnell 1977) are known, although their chemistry in superacid media has been explored only in a limited sense. It is interesting to note, however, that UOF_4 and $NpOF_4$ are stable in anhydrous HF (in the absence of Lewis acids), but $PuOF_4$ is observed to undergo redistribution in HF even in the absence of Lewis acids to give PuO_2F_2 and PuF_6.

2.7.2. *Uranyl fluoride*

In contrast to the unstable superacid solutions of UOF_4, dissolution of UO_2F_2 in HF/AsF_5 and HF/SbF_5 affords extremely stable solutions of UO_2^{2+} (Fawcett et al. 1982). The spectrum of UO_2^{2+} in HF/AsF_5 shows much better resolution than in aqueous $HClO_4$ (Barraclough et al. 1981). Upon removal of the HF solvent and excess SbF_5 from the HF/SbF_5 system, a solid of composition $UO_2F_2 \cdot 3SbF_5$ is found. Thermal decomposition of this salt begins at 125°C with the liberation of SbF_5 and formation of $UO_2F_2 \cdot 2SbF_5$; which in turn decomposes to UO_2F_2 and SbF_5 at 245°C. Structural characterization of the $UO_2F_2 \cdot 3SbF_5$ adduct shows a polymeric system of six- and eight-membered rings composed of pentagonal bipyramidal uranium atoms connected by two of the equatorial bridging fluorine atoms to two SbF_6^- octahedra and by three equatorial bridging fluorine atoms to two $Sb_2F_{11}^-$ groups. As with the similar UOF_4 compound, the two axial ligands – both oxygen atoms in this case – are nonbridging. Like UO_2F_2, the oxygen atoms in the uranyl ion are nearly linear ($\angle$ O–U–O = 179.3(1.3)°), although from crystallographic measurements and infrared spectroscopy the U—O bond distance is somewhat shorter (1.68(3) Å versus 1.74(2) Å for UO_2F_2). The frequency of the asymmetric UO_2 stretch increases from 990 cm^{-1} for UO_2F_2 to 1004 cm^{-1} for $UO_2F_2 \cdot 2SbF_5$ to 1012 cm^{-1} for $UO_2F_2 \cdot 3SbF_5$, and is consistent with a lowering of the electron density on the uranium atom by the additional Lewis acid.

The instability of UOF_4 in HF/SbF_5 with respect to molecular rearrangement has lead to isolation of a third UO_2F_2/SbF_5 adduct (Holloway et al. 1982). When previously prepared $UOF_4 \cdot 2SbF_5$ is treated with anhydrous HF for eight or more hours the solution changes color from orange to yellow. Eventually, UF_6 precipitates and can be removed under vacuum along with the solvent. Elemental analysis of the remaining colorless solid supports the formula $UO_2F_2 \cdot 4SbF_5$. The fact that $UO_2F_2 \cdot 3SbF_5$ is not formed even in dilute solutions of $UOF_4 \cdot 2SbF_5$ in HF/SbF_5, and the fact that $UO_2F_2 \cdot 4SbF_5$ cannot be prepared from UO_2F_2 and SbF_5 directly suggests that the SbF_6^- and $Sb_2F_{11}^-$ coordination sphere surrounding UOF_4 in the solid persists even in solution,

$$2[UOF_4 \cdot 2SbF_5]_{(solv)} \xrightarrow{\text{anhydrous HF/SbF}_5} UF_6 + UO_2F_2 \cdot 4SbF_{5(solv).} \quad (6)$$

Under vacuum, $UO_2F_2 \cdot 4SbF_5$ thermally decomposes at 70°C to volatile SbF_5 and the previously discussed complex $UO_2F_2 \cdot 3SbF_5$. In all of these species, coordination

and subsequent reaction of HF with UOF_4 may occur since features of the vibrational spectra and powder diffraction pattern indicative of $(H_3O^+)(SbF_6^-)$ are evident even when rigorously dried HF is employed.

2.8. *Thermogravimetric studies of uranium and thorium fluoroantimonates*

One method of determining the approximate stoichiometry of reaction 4 above involved thermogravimetric analysis (TGA) on the solids after vacuum removal of all volatiles at ambient temperature. Observed weight gains for the reaction with UO_2 suggest that residues isolated after the vacuum drying process have a formula of $UF_2^{2+}\cdot(SbF_6^-)_2$ [occasionally $UF_2^{2+}\cdot(Sb_2F_{11}^-)_2$] with two equivalents of oxonium salt, $(H_3O^+)(SbF_6^-)$, also being formed. Variation of the $SbF_5:UO_2$ ratio from 10:1 to 65:1 does not significantly alter the apparent weight of the resulting residue after drying.

Analysis (TGA) of the HF/SbF_5 dissolution products has been performed and supports the $AnF_4\cdot 2SbF_5 + 2(H_3O^+)(SbF_6^-)$ formulation for both U and Th systems. A typical TGA run is shown in fig. 8. Equations (7)–(11) indicate the possible – through by no means certain – processes occurring during the stepwise thermal decomposition of the uranium salt,

$$UF_4\cdot 2SbF_5 + 2(H_3O^+)(SbF_6^-) \xrightarrow{<140^\circ C} UF_4\cdot 2SbF_5(s) + 2SbOF_3(s) + 6HF(g), \tag{7}$$

$$UF_4\cdot 2SbF_5 + 2SbOF_3 \xrightarrow{<240^\circ C} UF_4(s) + 2SbF_5(g) + 2SbOF_3(s), \tag{8}$$

$$UF_4 + 2SbOF_3 \xrightarrow{<350^\circ C} UF_4(s) + SbO_2F(s) + SbF_3(g) + F_2(g), \tag{9}$$

$$UF_4 + SbO_2F \xrightarrow{>400^\circ C} UO_2(s) + SbF_5(g). \tag{10}$$

The net reaction is

$$UF_4\cdot 2SbF_5 + 2(H_3O^+)(SbF_6^-) \longrightarrow UO_2(s) + 3SbF_5(g) + SbF_3(g) + 6HF(g) + F_2(g). \tag{11}$$

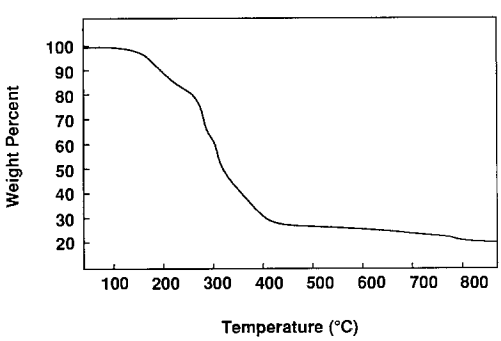

Fig. 8. Thermogravimetric analysis curve of $UF_4\cdot 2SbF_5 + 2(H_3O^+)(SbF_6^-)$

TABLE 2
Results of the thermogravimetric analysis of $UF_4 \cdot 2SbF_5 + 2(H_3O^+)(SbF_6^-)$

	Final weight	
	Theoretical	Experimental
Rxn(7)	90.4%	92.5%
Rxn(8)	56.0%	60.1%
Rxn(9)	38.7%	31.8%
Rxn(10)	21.5%	21.6%

The final weight percent at 800°C for the pyrolysis shown in fig. 8 was 21.6% as compared to a theoretical value of 21.5% for the high-temperature reactions which follow. Although a formulation of $(UF_4 \cdot 2SbF_5)$ and $2(H_3O^+)(SbF_6^-)$ agrees with the weight gain and TGA results, in one dissolution experiment the formula $UF_4 \cdot 4SbF_5$ was determined from single-crystal X-ray diffraction of a set of blue–green crystals (O'Donnell 1992a). The overall results of the TGA analyses for reaction 4 containing U or Th are shown in table 2.

The reactions (7)–(11), although speculative, are supported by several observations. First, the identity of the final pyrolysis product was suggested by its black color and confirmed by the X-ray powder diffraction pattern. The formation of SbF_3 in reaction (9) was identified by its X-ray powder diffraction pattern where the thermolysis was quenched below 350°C. Residual gas analysis (RGA) by quadrupole mass spectroscopy of the volatile products at 240°C also confirmed the presence of SbF_n fragments from SbF_5 and/or SbF_3. The high-temperature decomposition of $(H_3O^+)(SbF_6^-)$ by itself does not proceed by simple dissociation to HF, H_2O and SbF_5 since in the RGA of pure $(H_3O^+)(SbF_6^-)$, no SbF_4^+ or SbF_5^+ fragments were observed as are seen for pure SbF_5. The exact decomposition mechanism of $(H_3O^+)(SbF_6^-)$ is uncertain and formation of $SbOF_3$, SbO_2F, and F_2 (and other antimony oxides) are highly speculative, especially in light of the small sample size and possible wall reactions. For instance, atmospheric moisture present during the decomposition of $SbOF_3$ will likely lead to the formation of HF instead of F_2.

The TGA of the product isolated from the ThO_2 dissolution reaction is also consistent with the high-temperature decomposition reactions reported above. The

TABLE 3
Thermogravimetric analysis of $ThF_4 \cdot 2SbF_5 + 2(H_3O^+)(SbF_6^-)$.

	Weight loss	
	Theoretical	Experimental
Rxn(12)	65.4%	76.4%
Rxn(13)	55.8%	54.7%
Rxn(14)	38.4%	34.7%
Rxn(15)	21.1%	19.3%

theoretical versus experimental weight changes for the decomposition of $ThF_4 \cdot 2SbF_5$ and $2(H_3O^+)(SbF_6^-)$ are reported in table 3. Weight losses in the TGA are consistent with the following reactions:

$$ThF_4 \cdot 2SbF_5 + 2(H_3O^+)(SbF_6^-) \xrightarrow{<200°C} ThF_4(s) + 2(H_3O^+)(SbF_6^-) + 2SbF_5(g), \quad (12)$$

$$ThF_4 + 2(H_3O^+)(SbF_6^-) \xrightarrow{<310°C} ThF_4 + 2SbOF_3(s) + 6HF(g), \quad (13)$$

$$ThF_4 + 2SbOF_3 \xrightarrow{<500°C} ThF_4 + SbO_2F(s) + SbF_3(g) + F_2(g), \quad (14)$$

$$ThF_4 + SbO_2F \xrightarrow{>500°C} ThO_2(s) + SbF_5(g). \quad (15)$$

The net reaction is

$$ThF_4 \cdot 2SbF_5 + 2(H_3O^+)(SbF_6^-) \longrightarrow ThO_2(s) + 3SbF_5(g) + SbF_3(g) + 6HF(g) + F_2(g). \quad (16)$$

Like the analogous uranium experiment, X-ray diffraction, vibrational spectroscopy, and RGA techniques were used to identify many of products of the ThO_2 dissolution as well as the high-temperature TGA decomposition products.

2.9. *Cyclic-voltammetry studies of U, Np, Pu and Am-fluorosulfonates in HSO_3F/SbF_5*

We have established the electrochemical range for a 1:4 SbF_5:HSO_3F (25% magic acid) superacid mixture as +2.5 to −0.5 V versus copper on a glassy carbon electrode. For a 1:1 SbF_5:HSO_3F (100% magic acid) superacid mixture the electrochemical range was determined to be +3.0 to 0.0 V. The selection of 100% or of 25% magic acid as the solvent was based upon the electrochemical region of interest and the wave under investigation.

The cyclic voltammetry investigation of U, Np, Pu and Am in magic acid revealed a single wave attributable to the An(III/IV) couple only for U, Np, and Pu. The An(III)/An(IV) potential for Pu was observed at +1.66 V, for Np at +0.66 V, and −0.2 V for U. Thus, the ease of electrochemical oxidation increases from Pu(III) to Np(III) and finally to U(III), as would be expected from the known chemical behavior of these actinides. Unfortunately, the An(IV)/An(V) of U, Np, and Pu redox waves lie outside the useable solvent range for magic acid. This is especially disappointing in the case of uranium where Bougon has isolated U(V) complexes of the type $UF_3(SO_3F)_2$ (Masson et al. 1978). It is therefore surprising that the uranium(IV)/(VI) conproportionation reaction to form U(V) is observed in the superacid HF/SbF_5. The Am(III)/Am(IV) potential unfortunately also must lie outside the solvent range, which is consistent with the fact previously reported that AmO_2 spontaneously reduces to Am(III) in superacids.

3. Conclusions

When solutions are generated from compounds already in oxidation state(III), e.g., LnF_3, lanthanides exist in superacid solutions as Ln^{3+} cations, with spectra, and therefore probably solvent coordination, very similar to those in water. When the metals are reacted with superacids and also in acidic melts, the resulting Ln^{2+} cations are very much more stable than in aqueous media.

The chemistry of the mid-actinide metals (zero valent) in superacid chemistry is characterized by rapid dissolution and formation of solvated M^{3+} cations. The final reduction products of these reactions is uncertain, but may be speculated as being H_2 for HF-based superacids and SO_2 for HSO_3F solutions. While the dissolution of the metals occurs with oxidation/reduction reactions, with the exception of americium the dissolution of the dioxides proceeds with the formation of completely solvated fluoroactinide cations and $(H_3O^+)(SbF_6^-)$ with no change in the actinide oxidation state. Since Am (III) is expected to be the favored oxidation state in superacid media, it is not surprising that AmO_2 is reduced to Am(III) in both HF/SbF_5 and HSO_3F/SbF_5. These observations are consistent with the cyclic-voltammetry studies performed in magic-acid media where it has been observed that the resistance to oxidation for the (III/IV) potential increases from U to Pu and is above the solvent range for Am. Investigations by O'Donnell's group suggest that in solution in HF or in other superacids containing free F^- ions, solvated AnF_2^{2+} is formed from both dioxides and tetrafluorides of uranium (the situation is less clear for the other mid-actinides), whereas other groups have found evidence in the solid state for the existence of $AnF_4 \cdot nSbF_5$ ($n = 2,4$) complexes. The chemistry of the U(VI) oxide fluoride, UOF_4, is dominated by the redistribution of the oxide and fluoride ligands to form the more stable compounds $UO_2F_{2(solv)}$ and UF_6. In addition, the U(VI) oxidation state appears to be indefinitely stable in superacid media when present as UO_2^{2+} and, of course, as UF_6. Finally, it has been observed that it is possible to form U(V) species in solution by the conproportionation reaction of U(IV) fluorocations with UF_6.

Acknowledgements

The authors gratefully acknowledge the US Department of Energy's Transplutonium Element Production Program for providing the americium and the contribution of Dr. Wayne Smith (Nuclear Materials Technology Division) for assistance with the cyclic-voltammetry experiments. Drs. Larry R. Avens and P. Gary Eller performed many of the experiments with neptunium and plutonium metal and oxides including the dissolution of AmO_2. This work was supported by the US Department of Energy, Offices of Defense Programs and Nuclear Material Production.

Appendix

Experimental procedures

Because of the corrosiveness and moisture-sensitivity of superacids and actinide and rare-earth compounds treated with these materials, some introduction to the experimental details of this area of chemistry is warranted. Interested persons are urged to consult such standard textbooks as the one by Shriver and Drezdzon (1986).

Materials

[**Caution**: anhydrous HF, antimony pentafluoride, HSO_3F/SbF_5, and HF/SbF_5 mixtures are extremely corrosive and reactive materials. Superacids mixed with strong oxidizers such as xenon hexafluoride, krypton difluoride, or dioxygen difluoride (O_2F_2) should be handled only in metal or synthetic sapphire containers since these mixtures can react vigorously with even fluorocarbon plastic apparatus. Appropriate protective equipment (e.g., gloves, face shields and safety glasses) should always be used when handling these materials outside of gloveboxes. Superacids react violently with water and organic materials, producing copious HF fumes and heat, and should be treated with respect. Excess or spent acid should be neutralized by slowly pouring onto activated alumina (followed by neutralization with aqueous Na_2CO_3 or $NaHCO_3$) or soda lime in a fume hood, and the apparatus and residues rinsed with $CF_2ClCFCl_2$ (Freon 113) prior to neutralization with water or base. Mild skin burns resulting from exposure to superacids may be treated topically with commercial calcium gluconate salve or quaternary ammonium solutions (i.e., Hyamine ™); eye or inhalation injuries, or severe skin burns should be immediately seen by a doctor.]

Anhydrous HF (Matheson) typically contains 0.5–1% water and can be dried with K_2NiF_6, BiF_5, or elemental fluorine prior to use. Antimony pentafluoride (Aldrich, Ozark-Mahoning ATO) and fluorosulfuric acid (Aldrich) were distilled under vacuum in all-glass apparatus prior to use. Magic acid, 25% and 100% (Aldrich, 1:4 and 1:1 SbF_5:HF, respectively), were used as received without further purification. Thorium, uranium, neptunium, and plutonium metals, oxides, fluorides, and oxide fluorides were either supplied by or prepared from materials supplied by the Nuclear Materials Division, Los Alamos National Laboratory. Americium oxide ($^{243}AmO_2$) was made available through the US Department of Energy's Heavy Elements Production Program.

Apparatus

Experiments employing anhydrous HF or HF/SbF_5 mixtures were conducted in apparatus made of metal (typically nickel or Monel™), Kel-F™, sapphire, or teflon PFA™, with the latter two the most satisfactory from the standpoint of corrosion. Magic-acid solutions could be safely handled in glass apparatus although some etching of the glass occurred with time. UV-visible spectra of magic-acid solutions were recorded in quartz cuvettes while those of HF/SbF_5 solutions were recorded in 1/2″ or 3/8″ PFA tubes which have approximately the same UV cutoff as borosilicate glass (~350 nm). Thermogravimetric analyses were performed on a thermal analyzer moun-

ted in an inert atmosphere glovebox. Infrared spectra of solid residues were obtained by pressing the solid residues between silver chloride plates on an FTIR spectrometer. Raman spectra of solid residues were obtained by sealing the solids in glass capillaries under inert atmosphere. The irradiating laser line selected depended on the presence of fluorescent impurities and sensitivity to decomposition in the laser beam.

The electrochemical measurements were made using a standard three-electrode cell configuration. The counter electrode was a platinum wire and the working electrode was a platinum wire or a glassy carbon disk sealed in Kel-F (Bioanalytical Systems). Since the carbon electrode gave a slightly wider potential window and fewer extraneous peaks in background scans, all of the voltammograms reported in this chapter were done with the carbon electrode. The reference electrode was a copper wire inserted in a thin glass tube containing the acid solution, separated from the bulk solution by a fine porosity glass frit. The acid slowly attacked the frit rendering it unusable after a few experiments. Theoretically the copper wire formed only a quasi-reference electrode since no copper ion was introduced into the reference compartment; however, during the experiment some of the copper reacted leaving a pale green insoluble salt in the bottom of the container. The concentration of copper ions was dictated by the solubility of this salt and was essentially fixed since the composition of this solvent did not change. In that sense it behaved quite similarly to a standard aqueous calomel electrode. There was never any measurable drift in electrode potential during the course of an experiment.

Voltammetric measurements were carried out in a small H-cell with a medium porosity glass frit separating the two compartments. The working compartment contained the metal or salt of interest that had been previously dissolved in a given acid solution. The auxiliary compartment contained only the pure acid. Each side held approximately 20 ml total volume. The electrodes were held in position with teflon caps.

Example procedure

Dissolution of plutonium metal. In a glovebox fitted for transuranic chemistry under inert atmosphere, a 0.155 g Pu metal coupon (0.648 mmol) and a small teflon-coated stirring bar are placed in a PFA tube closed at one end. A teflon PFA valve (Galtek®, Inc.) equipped with a compression tube fitting is attached to the tube and the fitting tightened until leak-tight. The reactor is attached to an all-metal and teflon PFA vacuum line, evacuated, and 0.815 g (3.76 mmol) SbF_5 and 1.633 g (81.6 mmol) anhydrous HF distilled in. Upon warming to room temperature, a black solid formed on the surface of the metal coupon, which eventually broke loose and dissolved. As the Pu coupon dissolved, a blue color characteristic of Pu(III) developed, colorless crystals eventually formed which later analyses (i.e., TGA) were suggested to be an $SbF_3 \cdot n SbF_5$ complex; and late in the dissolution a noncondensable gas evolved from the solution. The transparency range of teflon PFA to UV light (wavelength cutoff approximately 350 nm) permitted nearly continuous observation of the UV-visible spectrum of the solution through a spectroscopy dropout in the glovebox. The crystals could be partially separated from the solution by inverting the tube and attaching another tube

with a valve. When the valves were cracked open to allow a slow trickle of superacid, nearly all of the colorless crystals remained in the first tube for further analysis. Filtration through a PTFE filter material (e.g., Zytex) also served to separate the crystalline material. The solvent could then be removed from the Pu(III) in the lower tube by vacuum.

References

Albertsson, J., and I. Elding, 1977, Acta Crystallogr. B **33**, 1460.

Avens, L.R., and K.D. Abney, 1988a, private communication.

Avens, L.R., and K.D. Abney, 1988b, unpublished data.

Avens, L.R., P.G. Eller, L.B. Asprey, K.D. Abney and S.A. Kinkead, 1988, J. Radioanal. Nucl. Chem. **123**, 707.

Baluka, M., N.M. Edelstein and T.A. O'Donnell, 1981, Inorg. Chem. **20**, 3279.

Barraclough, C.G., R.W. Cockman and T.A. O'Donnell, 1977, Inorg. Chem. **16**, 673.

Barraclough, C.G., R.W. Cockman and T.A. O'Donnell, 1981, Inorg. & Nucl. Chem. Lett. **17**, 83.

Barraclough, C.G., R.W. Cockman and T.A. O'Donnell, 1991, Inorg. Chem. **30**, 340.

Bennett, M.R., and L.M. Ferris, 1974, J. Inorg. & Nucl. Chem. **36**, 1285.

Birchall, T., P.A.W. Dean, B. Della Valle and R.J. Gillespie, 1973, Can. J. Chem. **15**, 667.

Bougon, R., and P. Charpin, 1979, J. Fluorine Chem. **14**, 235.

Bougon, R., J. Fawcett, J. Holloway and D.R. Russell, 1978, C.R. Acad. Sci. (Paris) **287C**, 423.

Bougon, R., J. Fawcett, J.H. Holloway and D.R. Russell, 1979, J. Chem. Soc. Dalton Trans., p. 1881.

Broach, R.W., J.M. Williams, G.P. Felcher and D.G. Hinks, 1979, Acta Crystallogr. B **35**, 2317.

Burns, R.C., and T.A. O'Donnell, 1977, Inorg. & Nucl. Chem. Lett. **13**, 657.

Burns, R.C., T.A. O'Donnell and C.H. Randall, 1981, J. Inorg. & Nucl. Chem. **43**, 1231.

Christe, K.O., P. Charpin, E. Soulie, R. Bougon, J. Fawcett and D.R. Russell, 1984, Inorg. Chem. **23**, 3756.

Drobyshevskii, Yu.V., V.F. Serik and V.B. Sokolov, 1975, Dokl. Akad. Nauk SSSR **225**, 1079.

Fawcett, J., J.H. Holloway, D. Laycock and D.R. Russell, 1982, J. Chem. Soc. Dalton Trans., p. 1355.

Fitzwater, D.R., and R.E. Rundle, 1959, Z. Kristallogr., Kristallgeom., Kristallphys., Kristallchem. **112**, 362.

Gilbert, B., V. Demarteau and G. Duyckaerts, 1978, J. Electroanal. Chem. **89**, 123.

Gillespie, R.J., and T.E. Peel, 1973, J. Am. Chem. Soc. **95**, 5173.

Gruen, D.M., and R.L. McBeth, 1968, Inorg. Chem. **8**, 2625. See also O'Donnell (1992).

Habenschuss, A., and F.H. Spedding, 1979a, J. Chem. Phys. **70**, 2797.

Habenschuss, A., and F.H. Spedding, 1979b, J. Chem. Phys. **70**, 3758.

Habenschuss, A., and F.H. Spedding, 1980, J. Chem. Phys. **73**, 442.

Holloway, J.H., D. Laycock and R. Bougon, 1982, J. Chem. Soc. Dalton Trans., p. 1635.

Holloway, J.H., D. Laycock and R. Bougon, 1983, J. Chem. Soc. Dalton Trans., p. 2303.

Hubbard, C.R., C.O. Quicksall and R.A. Jacobson, 1974, Acta Crystallogr. B **30**, 2613.

Keenan, T.K., 1959, J. Chem. Educ. **36**, 27.

Larson, E.M., K.D. Abney, A.C. Larson and P.G. Eller, 1991, Acta Crystallogr. B **47**(2), 206.

Masson, J.P., C. Naulin, P. Charpin and R. Bougon, 1978, Inorg. Chem. **17**, 1858.

O'Donnell, T.A., 1987, Chem. Soc. Rev. **16**, 1.

O'Donnell, T.A., 1992a, Superacids and Acidic Melts as Inorganic Reaction Media (VCH, New York) used with permission.

O'Donnell, T.A., 1992b, in: Transuranium Elements: A Half Century, eds L.R. Morss and J. Fuger (American Chemical Society, Washington, DC).

Olah, G.A., G.K.S. Prakash and J. Sommer, 1985, Superacids (Wiley, New York).

Peacock, R.D., and N. Edelstein, 1976, J. Inorg. & Nucl. Chem. **38**, 771.

Sawodny, W., and K. Rediess, 1980, Z. Anorg. Allg. Chem. **469**, 81.

Schoebrechts, J.P., B.P. Gilbert and G. Duyckaerts, 1983a, J. Electroanal. Chem. **145**, 127.

Schoebrechts, J.P., B.P. Gilbert and G. Duyckaerts, 1983b, J. Electroanal. Chem. **145**, 139.

Shantha Nandana, W.A., J. Passmore and P.S. White, 1985, J. Chem. Soc. Dalton Trans., p. 1623.

Shantha Nandana, W.A., J. Passmore, P.S. White and C-M. Wong, 1987, J. Chem. Soc. Dalton Trans., p. 1989.

Shriver, D.F., and M.A. Drezdon, 1986, The Manipulation of Air-Sensitive Compounds, 2nd Ed. (Wiley–Interscience, New York) p. 227.

Sikka, S.K., 1969, Acta Crystallogr. A **25**, 621.

Smith, L.S., and D.L. Wertz, 1975, J. Am. Chem. Soc. **97**, 2365.

Smith, L.S., and D.L. Wertz, 1977, J. Inorg. & Nucl. Chem. **39**, 95.

Tarnero, M., 1967, Report CEA-R-3205, 49, French Atomic Energy Agency.

Handbook on the Physics and Chemistry of Rare Earths
Vol. 18 – Lanthanides/Actinides: Chemistry
edited by K.A. Gschneidner, Jr., L. Eyring, G.R. Choppin and G.H. Lander

Chapter 127

LANTHANIDES AND ACTINIDES HYDRATION AND HYDROLYSIS

Emil N. RIZKALLA and Gregory R. CHOPPIN
Florida State University, Department of Chemistry, Tallahassee, FL 32306-3006, USA

Contents

1. Introduction 529
2. Hydration studies 531
2.1. Solid-state hydrates 531
2.2. Hydrated cations in solution 534
2.2.1. Experimental data 534
2.2.2. Thermodynamic and theoretical studies 540
3. Hydrolysis 547
4. Summary and conclusions 554
References 555

1. Introduction

Knowledge of the properties of hydrated ions is of fundamental importance to understand the chemistry of these ions in aqueous solutions. The fact that many f-element salts which have relatively large lattice energies are fairly soluble in water is a reflection of the strength of the interactions between the metal cations and water molecules. In turn, this strong hydration competes with complexation by a ligand as the process of complexation involves the displacement of one or more water molecules by a ligand.

For cations in aqueous solution, a model which uses four structurally different zones of solvation about the cation (Burgess 1978) can serve to illustrate some important aspects. Zone A is the primary solvation shell in which water molecules are directly bonded to the metal ion. The number of water molecules in this zone, N, defines the primary hydration number. Zone B represents the extended sphere in which an additional number of water molecules are influenced by the charge field of the cation. The number of water molecules in this zone, designated by H, is strongly dependent on

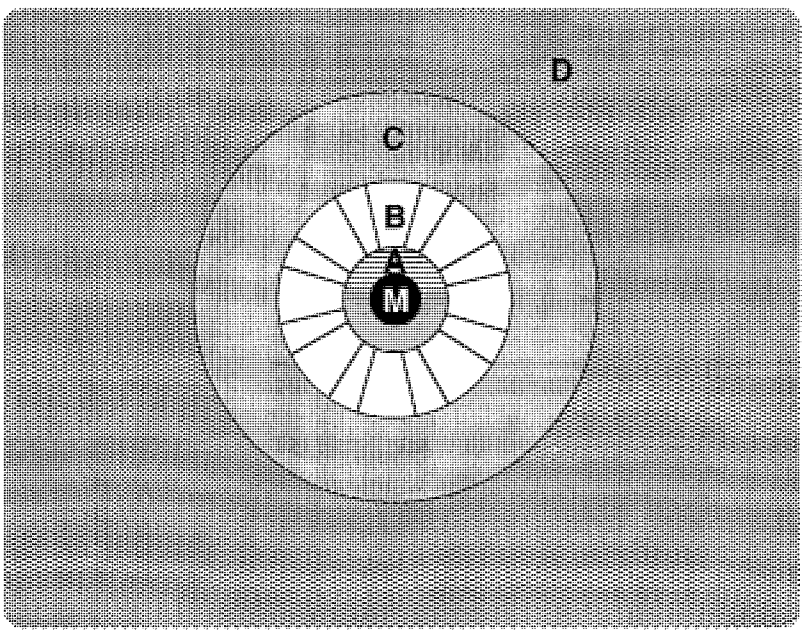

Fig. 1. Hydration zones of a cation in solution. ● Metal cation; Zone A, the primary hydration sphere; zone B, the secondary hydration sphere; zone C, the disordered water; zone D, the bulk water.

the charge density of the cation. The total number of water molecules of hydration, h, is equal to $H + N$ (Impey et al. 1983). In the outermost zone, D, the water has the hydrogen-bonded structure of bulk water while zone C is a disordered region in which the cation-oriented waters of zone B compete with the bulk structure of D. A schematic representation of this model is given in fig. 1. A requirement for such a model is that the solutions be sufficiently dilute that there be a zone D (i.e., the cations are sufficiently separated that their B and C zone do not overlap). Of course, the concept of defined zones is a formality although a distinction between zones A and B can sometimes be made when there is a slow rate of solvent exchange for the water molecules between these zones. The net ordering is the difference between the number of water molecules in zones A + B and the number of water molecules in zone C. Ions with low charge densities act as net structure breakers (zones A + B < zone C) and those of high charge densities act as net structure makers (zones A + B > zone C).

Solvation in mixed solvents may be described similarly; however, the compositions of the four zones would differ markedly as a result of the differences in cation–solvent and solvent–solvent interactions.

Classical measurements such as ion mobilities, apparent hydrated radii, enthalpies and entropies of solution, etc. fail to provide an explicit distinction between water molecules in zones A and B. Methods which can probe the primary hydration sphere of a cation include optical spectroscopy, nuclear magnetic resonance, electron spin resonance, extended X-ray absorption fine structure (EXAFS), X-ray diffraction and

neutron scattering measurements. The principles and limitations of the individual techniques when applied to lanthanide cations have been reviewed recently (Rizkalla and Choppin 1991).

This chapter discusses recent developments in solvation dynamics and thermodynamics of f-element cations and the hydrolytic tendencies of these ions in aqueous media. Direct comparisons are made for the trivalent cations of the lanthanides and actinides while the data for the other oxidation states of the actinides are reviewed to assess the effects of charge density and structure on hydration and hydrolysis. Since the lanthanides were reviewed recently, major attention is given to the actinides and the similarities and differences in their behavior with that of the lanthanides.

2. Hydration studies

2.1. *Solid-state hydrates*

The structural aspects of solid hydrated coordination compounds have been reviewed for the actinides by Bombieri and De Paoli (1985) and for the lanthanides by Rizkalla and Choppin (1991). Problems associated with the radioactivity of the transuranium elements have usually limited solid-state studies to thorium (the IV state) and uranium (the IV and VI states). The coordination numbers and geometries vary significantly with both the metal-ion oxidation state and the ligand denticity (Kepert 1982). While structural investigations of trivalent hydrated actinides have not been reported, they would be expected to resemble closely the structure of the known lanthanide hydrates. Lanthanide bromates (Helmholz 1939, Singh 1944, Sikka 1969, Albertsson and Elding 1977), trifluoromethylsulfonates (Lincoln 1986, Harrowfield et al. 1983a, Santos et al. 1985, Chatterjee et al. 1988) and ethylsulfates (Fitzwater and Rundle 1959, Hubbard et al. 1974, Broach et al. 1979, Albertsson and Elding 1977, Gerkin and Reppart 1984) form enneahydrates with hexagonal symmetries. The cation is coordinated to an oxygen of each of the nine water molecules, forming a tricapped trigonal prism (TCTP) (Broach et al. 1979, Mackay et al. 1977). However, depending on the anion, structural differences exist which have been attributed to hydrogen-bonded networks in the crystal lattice (Albertsson and Elding 1977, Harrowfield et al. 1983a). In the ethylsulfate and trifluoromethylsulfonate structures, the six prismatic oxygens (O_p) form a regular trigonal prism. The three capping oxygen (O_c) lie in the mirror plane, forming an equatorial triangle that is rotated slightly about the C_3 axis from the D_{3h} position of an ideal TCTP geometry. The result is a C_{3h} symmetry.

The difference between the Ln–O_p and the Ln–O_c bond lengths in these complexes (table 1) has been examined with point-on-a-sphere repulsion calculations (Harrowfield et al. 1983a). In the minimum-energy TCTP geometry obtained by these calculations, the four nearest interligand distances for a capping ligand were, on average, shorter than those for a prismatic ligand. This led to the prediction that the capping ligands experience an excess steric repulsion which is alleviated by an increase in the metal to ligand bonds. Molecular mechanics calculations (Hay 1991) yielded a regular TCTP geometry of D_{3h} symmetry as the minimum-energy conformation of the oxygen atoms.

TABLE 1
Metal–oxygen distances in TCTP lanthanide hydrates.

Species*	Ln–O (capping) (Å)	Ln–O (prismatic) (Å)	r_{Ln}^{3+} (Å)
$[La(H_2O)_9]A_3$	2.62	2.52	1.22
$[Gd(H_2O)_9]A_3$	2.55	2.40	1.11
$[Lu(H_2O)_9]A_3$	2.50	2.29	1.03
$[Y(H_2O)_9]A_3$	2.53	2.34	1.08
$[Pr(H_2O)_9]B_3$	2.59	2.47	1.05
$[Ho(H_2O)_9]B_3$	2.47	2.37	1.07
$[Er(H_2O)_9]B_3$	2.52	2.32	1.06
$[Yb(H_2O)_9]B_9$	2.52	2.32	1.04
$[Y(H_2O)_9]B_3$	2.52	2.37	1.08
$[Pr(H_2O)_9]C_3$	2.52	2.49	1.18
$[Sm(H_2O)_9]C_3$	2.55	2.46	1.13
$[Yb(H_2O)_9]C_3$	2.43	2.32	1.04

* $A = CF_3SO_3^-$; $B = EtOSO_3^-$; $C = BrO_3^-$.

This calculated conformation is similar to the observed structures in that both contain regular trigonal prisms and have identical orientations of the capping hydrogens but differ in the positioning of the O_c atoms and the orientation of the prismatic hydrogens. The structural differences represent distortions from the calculated conformation to achieve optimum hydrogen bonding in the crystal lattice. Except for Lu(III), the values of the calculated and observed Ln–O_p and Ln–O_c bond lengths are accurate to ± 0.02 Å and O–Ln–O bond angles to $\pm 3°$ over the entire lanthanide series (Hay 1991). The strain energy increased from -21.1 kJ mol^{-1} for La(III) to $+18.0$ kJ mol^{-1} for Lu(III) which was attributed to increased (unfavorable) oxygen–oxygen steric interactions as the size of the metal ion decreases.

In the case of bromate salts, the structure was symmetrical with a D_{3h} point group. Calculations to minimize the conformation using the input coordinates of the observed structure gave a D_{3d}, rather than the expected D_{3h} symmetry, which was due to rotations about the Ln–O_p bonds as well as to hydrogen-bonding effects (Hay 1991).

In $Ln(BrO_3)_3 \cdot 9H_2O$ (Ln denotes Eu or Tb) (Moret et al. 1991) the metal-ion site symmetry is lowered from D_{3h} to C_{3v} as the metal-oxygen distances change when the temperature is decreased from 295 to 200 K. These observations agreed with high-resolution and polarized luminescence spectra of $Eu(BrO_3)_3 \cdot 9D_2O$ which indicated a gradual decrease in symmetry around the Eu(III) ion as the temperature was decreased. These spectra indicated the presence of several distinct metal-ion sites at lower temperatures (Moret et al. 1991).

An example of actinide solids is the structure of $Th(NO_3)_4 \cdot 5H_2O$ which was determined by X-ray (Ueki et al. 1966) and neutron diffraction (Taylor et al. 1966). The Th(IV) atom was shown to be surrounded by eleven oxygen atoms in an irregular icosahedron. The structure has a polar arrangement (fig. 2) with the four bidentate

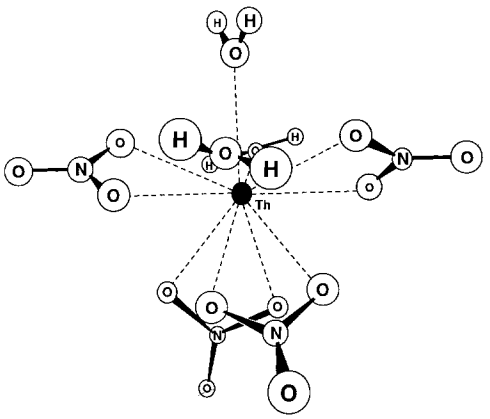

Fig. 2. Oxygen arrangement around the thorium atom in $Th(NO_3)_4 \cdot 5H_2O$ as viewed in the *b* direction.

nitrates bound about one hemisphere and three of the water molecules capping the coordination sphere.

The linear dioxo actinide cations have no analogs in the lanthanides but their structure reflects the steric effects of such cations. The only structure reported for a binary UO_2^{2+} hydrate is that of $[UO_2(H_2O)_2]^{2+}X$ [X is $(B_{12}H_{12}^{2-})$ (Mikhailov et al. 1982) or $(ClO_4^-)_2$ (Alcock and Esperas 1977)]. The cation has a characteristic pentagonal bipyramidal geometry with some slight deviations attributable to different degrees of hydrogen bonding. The average distance of the O(uranyl) to O(aqua) is 2.98 Å which is close to the expected non-bonding O···O contact distance, indicating that $[UO_2(H_2O)_5]^{2+}$ has the maximum possible hydration number. Metal solvates such as $[UO_2(DMSO)_5]^{2+}$ (Harrowfield et al. 1983b) also have five solvent molecules in the coordination sphere but shorter U–O(DMSO) bond distance due to the stronger basicity of the oxygen donor in the DMSO molecule.

Mixed hydrates with monodentate ligands [e.g., $[UO_2(H_2O)(urea)_4]^{2+}$ (Dalley et al. 1972)] have a similar structure to that of binary hydrates. Inclusion of bidentate ligands in the equatorial plane can lead to expansion of the coordination number of the uranyl ion to six (Dalley et al. 1971, Taylor and Mueller 1965, Hall et al. 1965, Bombieri et al. 1976, Eller and Penneman 1976, Ritger et al. 1983), as in the structure of the neutral $[UO_2(H_2O)_2(NO_3)_2]$ unit. The U–O (water) distances in these compounds ranges from 2.42 to 2.47 A.

Perry et al. (1980) isolated the dimeric complex $[UO_2(NO_3)_2(H_2O)]_2 \cdot 2C_3H_4N_2$ ($C_3H_4N_2$ is imidazole) in which water acts as a bridging ligand. In each unit, the uranium atom is in the center of a distorted hexagonal bipyramid geometry with the two uranyl oxygens at the apices. The O–U–O axis is nearly perpendicular to the distorted equatorial plane. The slight twist of the nitrate group out of this plane reflects some crowding in the coordination about UO_2^{2+}. The U–OH_2 distances are approximately 0.07–0.12 Å shorter than the U–O distances for a non-bridging solvate water.

2.2. *Hydrated cations in solution*

2.2.1. *Experimental data*

Few experimental results on the hydration of actinide ions have been reported. Literature values for hydration of the trivalent actinide cations has been derived from analogy to the experimental data of lanthanide ions. Perhaps the most comprehensive set of lanthanide-cation data is that from diffraction measurements by Habenschuss and Spedding (1979a, b, 1980). The radial distribution functions (RDF) for concentrated lanthanide chloride solutions were interpreted as reflecting three distinct zones at ca. 2.5, 3.0 and 5.0 Å corresponding to Ln–H_2O, H_2O–H_2O and Cl–H_2O interactions, respectively. The resolution of the first peak in the RDF was based on the assumption of a gaussian distribution from which the average Ln–H_2O coordination was calculated. Table 2 summarizes these results together with those obtained from neutron diffraction measurements (Narten and Hahn 1982, Annis et al. 1985, Cossy et al. 1989, Helm and Merbach 1991). The data are consistent with formation by the early lanthanides (La–Nd) of an isostructural series with coordination number nine in a TCTP structure. The later members (Tb–Lu) form a second series with coordination

TABLE 2
Lanthanide hydration data obtained from diffraction measurements.

Cation	Ln–O distance (Å)	Hydration number	Method	Reference†
La	2.58	9.1	X-ray	a
Pr	2.54	9.2	"	a
Nd	2.51	8.9	"	a
	2.48	8.5	Neutron diffraction	b
	1.00*	9.0	"	g
	1.00**	6.0	"	g
		3.0		
	0.30	8.9	"	g
Sm	2.47	8.8	X-ray	c
	1.00	8.5	Neutron diffraction	g
Eu	2.45	8.3	X-ray	c
Tb	2.41	8.2	"	d
Dy	2.37	7.4	Neutron diffraction	e
	1.00	8.0	"	f, g
	0.30	8.0		f, g
	2.40	7.9	X-ray	d
Er	2.37	8.2	"	d
Tm	2.36	8.1	"	d
Yb	1.00	7.9	Neutron diffraction	f, g
Lu	2.34	8.0	X-ray	d

* Estimated with the assumption that all water molecules have the same distance.

** Obtained with the assumption of an hydration geometry with water molecules at two different distances from the metal ion; the ratio of the areas of these two sites was fixed to 2:1.

† (a) Habenschuss and Spedding (1979b); (b) Narten and Hahn (1982); (c) Habenschuss and Spedding (1980); (d) Habenschuss and Spedding (1979a); (e) Annis et al. (1985); (f) Cossy et al. (1989); (g) Helm and Merbach (1991)

number eight in a square prismatic structure. The hydrated ions in the middle of the series were assumed either to have structures that represented some transition between those of the two major groups or to exist in an equilibrium mixture of these two structures.

The broad peaks, observed in the neutron diffraction measurements of the light elements, indicate unequal metal–oxygen distances for the water molecules in the first coordination shell presumably due to the formation of a TCTP structure similar to that present in the solid-state hydrates. The broadening of the peaks in Sm(III) solution was attributed to the superposition of three strongly overlapping gaussians, one corresponding to the eight equidistant water molecules in the first sphere and two due to the water molecules in the primary hydration sphere when $C = 9$ as these are not all equivalent. These conclusions were also supported by the extended X-ray absorption fine structure (EXAFS) measurements of concentrated aqueous lanthanide perchlorates (Yamaguchi et al. 1988). In both liquid and glassy states, the hydration number is approximately nine for the light elements and eight for the heavy lanthanides with a transition between these hydration numbers occurring from Sm(III) to Gd(III). The average Debye–Waller factor of the $Ln-OH_2$ bonds for the light rare earth ions calculated by the use of a symmetric shell model was larger than that for the heavy ions, consistent with the presence of different $Ln-OH_2$ distances within the hydrated species. A better least-squares fit of the EXAFS data of the light elements was obtained when a model based on six short and three long Ln–O bonds in the first hydration sphere was employed.

The use of fluorescence lifetime studies to evaluate the primary hydration number of Eu(III) and Tb(III) in perchlorate solution has been reviewed recently (Rizkalla and Choppin 1991). Values of 9.6 ± 0.5 for Eu(III) and 9.0 ± 0.5 for Tb(III) led to the proposal that hydration numbers are ten for La–Nd and nine for Tb–Lu (Horrocks and Sudnick 1979).

The X-ray techniques have limited applications in actinide systems because the high concentration required for the measurements (ca. 2–3 M) does not allow study of elements for which only isotopes of high specific radioactivity are available. Beitz (1991) calculated the hydration number of some curium complexes using luminescence lifetime measurements and assuming a hydration number of nine of the free ion. Electrophoretic measurements using tracer concentrations (Lundqvist 1981, Lundqvist et al. 1981) have provided estimates of the hydrated radii (r_h) for Eu, Am, Cm, Cf, Es, Fm and Md from Stokes' law. The hydrated radii were used, in turn, to calculate hydration numbers, h, by dividing the volume of the hydrated sphere by the volume of a water molecule ($\simeq 30$ Å^3). Since the volume occupied by the bare metal ion is small [2–5 Å^3 for Ln(III) and An(III)], it was neglected in comparison with the volume of the water molecules. The results are listed in table 3.

Generally, the values of h differ somewhat with different methods of calculation, but they consistently show an increase in h of 10–20% throughout the lanthanide series (Bertha and Choppin 1969). Thus, hydration numbers range from 9.0–11.0 and 12.8–13.9 as calculated from partial molal volumes (Padova 1967) and conductivity (Choppin and Graffeo 1965) measurements. Under similar experimental conditions, the relative values of h for An(III) ions and Eu(III) indicate that actinide ions are more

TABLE 3
Hydration numbers and hydration radii of trivalent actinide and lanthanide ions obtained by electrophoresis and diffusion measurements (Lundqvist et al. 1981, Fourest et al. 1984, David 1986).

Ln^{3+}	r_h (Å)	h	An^{3+}	r_h (Å)	h	N
La	4.51	12.8				
Ce	4.51	12.8				
	4.53	12.7*				
Pr	4.52	12.9				
Nd	4.53	13.0				
Sm	4.55	13.2				
Eu	4.58	13.4	Am	4.60	13.6	
	4.58	13.3*		4.51	12.6*	9.0
Gd	4.60	13.6	Cm	4.69	14.4	
	4.69	14.2*		4.55	13.0	8.9
Tb	4.67	14.0*				
Dy	4.65	14.0	Cf	4.90	16.4	
				4.64	13.8*	8.2
Ho	4.62	13.8	Es	4.92	16.6	
				4.68	14.1*	8.0
Er	4.64	13.9	Fm	4.95	16.9	
Tm	4.65	14.0	Md	4.88	16.2	
	4.67	14.1*				
Yb	4.65	14.0				
	4.67	14.1				

* Data obtained from diffusion measurements.

hydrated than lanthanide ions of similar ionic radii. Such a difference was attributed to differences in the shielding properties of the 4f and 5f electrons (Lundqvist et al. 1981).

Diffusion measurements were also used to estimate the overall hydration numbers of the trivalent Am, Cm, Cf and Es ions (Fourest et al. 1982, 1983, 1984, 1988, Latrous et al. 1982). The "open-end capillary" method was claimed to have an accuracy better than 1% for γ-emitters and 1–2% for α-emitters. The results are included in table 3. Comparison of the data obtained by the electrophoretic and the diffusion methods reflect the uncertainty of the measurements; e.g., the individual h values for the Ln(III) cations are roughly the same for both methods while those for the An(III) cations from the diffusion measurements are lower than those from electrophoresis.

Assuming that the interaction between the primary hydration sphere and the secondary water molecules of hydration are strongly electrostatic for both f-element series, Fourest et al. (1984) were able to estimate the inner-sphere hydration numbers of the trivalent actinide ions by interpolation using the values for the lanthanide elements (Habenschuss and Spedding 1979a, b, 1980). The interpolated values are listed in the last column of table 3 and shown in fig. 3.

The increase of the net hydration, h, with decreasing ionic radii, r, for both the 4f and 5f elements (Fourest et al. 1984) shown in fig. 4 can be attributed to the increase in the surface charge density as the atomic number increases. The break in the lanthanide series for the ions from Nd to Gd is also observed for other bulk physical data such as

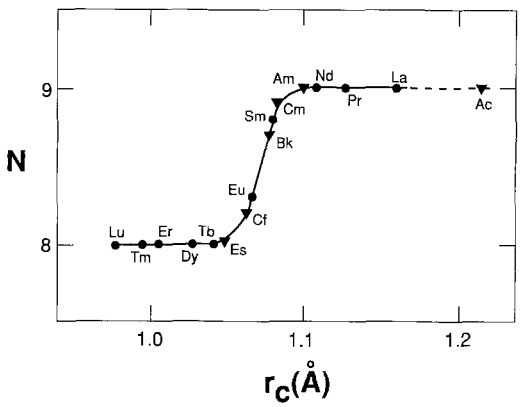

Fig. 3. S-shaped variation of the primary hydration number, N, for some trivalent lanthanides and actinides, versus r_c (coordination number is eight): (●) Values given by Habenschuss and Spedding (1979a, b, 1980); (▼) Interpolated values.

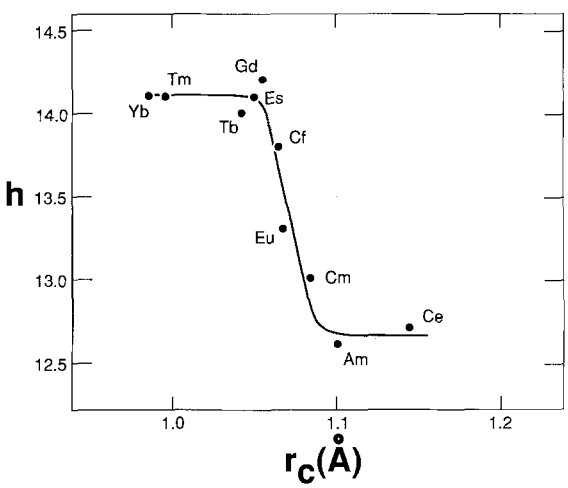

Fig. 4. S-shaped variation of the overall hydration number, h, derived from diffusion measurements, as a function of crystallographic radius, r_c ($C = 8$) for some trivalent 4f and 5f ions.

apparent molal volumes (Spedding et al. 1966b, 1975b), relative viscosities (Spedding and Pikal 1966, Spedding et al. 1975a), apparent molal heat capacities (Spedding and Jones 1966), heats of dilution (Spedding et al. 1966a), and electrical conductance (Spedding et al. 1974). For the actinide elements, this discontinuity is shifted to Bk–Cf.

The information relating to solvation numbers of tetravalent actinide ions is rather sparse. From NMR peak area, an estimate of the hydration number of Th(IV) in an aqueous-acetone solution of $Th(ClO_4)_4$ at $-100°C$ indicated a value of nine (Butler and Symons 1969, Fratiello et al. 1970b) whereas an indirect NMR linewidth method gave a hydration number of ten (Swift and Sayre 1966). An entirely different method for the estimation of hydration numbers from conductivity measurements has been proposed and developed by Gusev (1971, 1972, 1973). The dependence of conductance on concentration in acidic solutions of metal salts shows the pattern given in fig. 5.

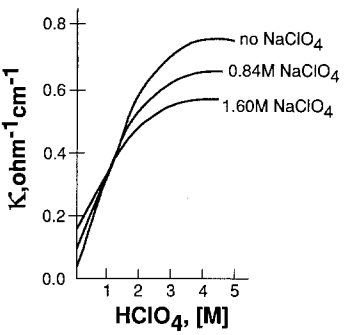

Fig. 5. The dependence of the conductance on the concentration of perchloric acid in $NaClO_4$–$HClO_4$ solutions (Gusev 1971, 1972, 1973).

Gusev assumed that the point of intersection indicates the absence of free (i.e., non-solvating) water, so there is minimal proton transport through the solution. The water : cation mole ratio at that point is presumably the hydration number of the cation, including both primary and secondary solvation. This method gave a value of $h = 20$ for Th(IV) which can be compared to the value of 22 obtained from compressibility measurements (Bockris and Saluja 1972a, b, 1973) based on the lower compressibility of solvated solvent molecules (Passynski 1938) as a result of electrostriction.

Reviews of the available evidence pertaining to hydration numbers of U(IV) and Np(IV) have suggested that two forms of each of these aquo ions may exist, differing in geometry and possibly in coordination number (Rykov et al. 1971, Sullivan et al. 1976). Radial distribution curves from X-ray measurements on uranium(IV) perchlorate solutions indicate a primary hydration number of eight for the U(IV) cation with no perchlorate in the primary coordination sphere (Pocev and Johansson 1973).

Hydration studies for higher oxidation state actinides are reported for some AnO_2^{2+} salts (UO_2^{2+} or NpO_2^{2+}) but not for any AnO_2^{+} systems. The Raman spectra of aqueous uranyl solutions were interpreted to show the presence of six water molecules coordinated in the primary plane perpendicular to the O–U–O axis (Sutton 1952). However, similar hydration numbers have been obtained by methods in which the secondary hydration shell may also contribute to the value. For example, the activity coefficient measurements suggest a hydration number of 7.4 [relative to an assumed hydration number of zero for Cs(I) (Hinton and Amis 1971)]. Similarly, a hydration number of seven has been derived from Gusev's conductivity method (Gusev 1971, 1972, 1973).

Solvation of f-element cations in mixed aqueous solvents has been studied using the fluorescence technique. With Eu(III) ion as a probe (Tanaka et al. 1988, Lis and Choppin 1991), in water–acetone, water–acetonitrile and water–1,4-dioxane, the first solvation sphere is occupied exclusively by water molecules even at bulk-phase mole fractions of water as low as 0.1 (fig. 6, curve I). However, in solvents with more basic donors such as DMSO (DMSO is dimethylsulphoxide), the metal ion is preferentially solvated by DMSO even for very low mole fractions of DMSO in the solvent (curve II, fig. 6). Less regular behavior can be expected for systems in which (a) strong interactions exist between the components of the solvent mixture or between the coordinated

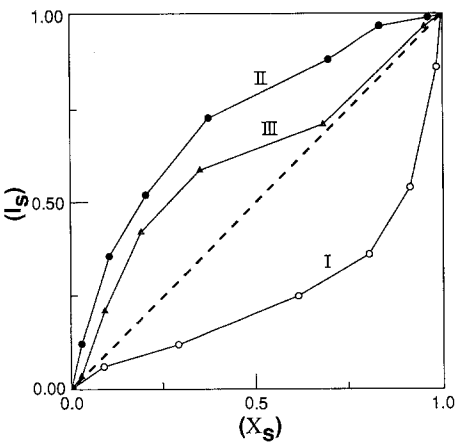

Fig. 6. Relationship between the mole fraction in the first hydration sphere (I_s) and the mole fraction in the bulk (X_s). (I) water + methanol; (II) water + DMSO; (III) water + DMF.

and bulk solvent molecules, and (b) the steric barrier increases markedly with the degree of solvation. Such an irregular pattern is observed for solvation by DMF–water mixtures (DMF is dimethylformamide). In this case, Eu(III) is preferentially solvated by DMF when the mole fraction of DMF is < 0.7. At higher mole fractions, the DMF is present in the solvation sphere in about the same mole fraction as in the bulk phase which may reflect the effect of steric crowding by the large DMF molecules.

Solvation of UO_2^{2+} ions in water–acetone and water–dioxane mixtures was studied by ultrasound and ^{1}H-NMR techniques and the estimated hydration numbers given in table 4 (Ernst and Jezowska-Trzebiatowska 1975a, b). The results indicate a decrease in the hydration numbers with increasing dioxane concentration. This was attributed to a probable partial replacement of waters of hydration by the organic solvent although inner-sphere complexation by the anion would also reduce the hydration number.

TABLE 4
Hydration numbers of AnO_2^{2+} ions in aqueous and mixed solvents.

Salt	Medium	Method	h	Reference*
UO_2SO_4	Water	ultrasound	10.3	a
$UO_2(NO_3)_2$	Water	"	11.9	a
UO_2SO_4	dioxane–water (20%)	"	6.3	a
$UO_2(NO_3)_2$	dioxane–water (20%)	"	6.3	a
UO_2SO_4	dioxane–water (45%)	"	4.8	a
$UO_2(NO_3)_2$	dioxane–water (45%)	"	5.8	a
$UO_2(ClO_4)_2$	acetone–water	PMR	4.0	b
$UO_2(NO_3)_2$	acetone–water	PMR	2.0	b
$UO_2(ClO_4)_2$	acetone–water	PMR	6.0	c
$UO_2(NO_3)_2$	acetone–water	PMR	6.0	c
UO_2Cl_2	acetone–water	PMR	6.0	c
NpO_2^{2+}	acetone–water	PMR	6.0	d

* (a) Ernst and Jezowska-Trzebiatowska (1975a); (b) Fratiello et al. (1970a); (c) Ernst and Jezowska-Trzebiatowska (1975b); (d) Shcherbakov and Jorga (1977).

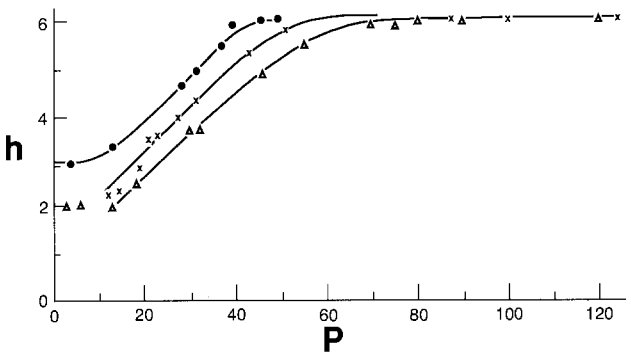

Fig. 7. Dependence of the average number of coordinated water molecules on the molar ratio, P, for aqueous acetone solutions of uranyl perchlorate (•), chloride (X), nitrate (▲).

These results are in broad agreement with the low-temperature PMR measurements for both UO_2X_2 (X is ClO_4^-, Cl^- and NO_3^-) (Shcherbakov and Shcherbakova 1976, Fratiello et al. 1970a) and NpO_2^{2+} (Shcherbakov and Jorga 1977) compounds (see table 4). For uranyl, the average numbers of bound waters were shown to increase with increasing molar ratio ($= [H_2O]/[UO_2^{2+}]$) to a limiting value of six at values ranging from 40 to 70 depending on the anion (Shcherbakov and Shcherbakova 1976, Shcherbakov and Jorga 1977). The stronger the complexing ability of the anion, the higher the ratio required to reach maximum aquation (fig. 7).

Solvation numbers of actinide cations in non-aqueous media are almost an unexamined field. FT-IR investigations of the homologous solvates $[Ln(NO_3)_3(DMSO)_n]$ in anhydrous acetonitrile (Bünzli et al. 1990) indicated a change in coordination number in the middle of the series [ca. Eu(III)] from nine to eight with increasing atomic number. In the presence of large excess of DMSO($[DMSO]_t/[Ln]_t = 6$), the coordination numbers can be increased by one unit. NMR spectroscopy and crystal stoichiometries have indicated a solvation number of two for the uranyl cation in pure TBP (TBP is tributylphosphate). The overall coordination number in this case should include two for TBPs coordination and four for the bidentate nitrate coordination (Siddall and Stewart 1967).

2.2.2. *Thermodynamic and theoretical studies*

The thermodynamic properties of the f-elements and their compounds for oxidation states II to IV for the lanthanides and II to VI for the actinides has been reviewed comprehensively by several authors (Morss 1976, Fuger and Oetting 1976, Fuger 1982, Bratsch and Lagowski 1985a, b, 1986, David 1986). Calorimetric measurements of the heats of formation of the trivalent actinide cations are limited to those cations available in macroscopic quantities and with isotopes of relatively low specific radioactivity such as Pu(III) (Hinchey and Cobble 1970, Smith et al. 1981), Am(III) (Fuger et al. 1972), Cm(III) (Fuger et al. 1975, Morss et al. 1983), Bk(III) (Fuger and Haire 1975, Fuger et al. 1981) and Cf(III) (Fuger et al. 1984). Heats of formation of the hexavalent UO_2^{2+} (Coulter et al. 1940) and NpO_2^{2+} (Brand and Cobble 1970) ions were also determined. Data on other species were estimated from various ionic models.

David et al. (1985) proposed a general expression for the calculation of the absolute enthalpy of hydration, ΔH^0_{hyd}, based on a semiempirical model of Bockris and Reddy (1970). The hydration enthalpy is related to the crystallographic radii, R, the hydration number, n, and the ionic charge, z,

$$\Delta H^0_{hyd} = \alpha z^2 (R + 2R_w)^{-1} + \beta z n (R + R_w)^{-2} + \gamma z n (R + R_w)^{-3} + \delta z^2 n (R + R_w)^{-4} + W + P(-1)^z, \quad (1)$$

TABLE 5
Gibbs free energies of formation of the gaseous and hydrated actinide ions.

Element	Gas phase [a, b, c]				Aquo ions [a, b, d]				
	+2	+3	+4	+6	+2	+3	+4	+5	+6
Ac	2007	3832	----		−167	−614	----		
Th	2253	4182	6960		−148[e]	−314	−704		
Pa	2205	4136	7128		−160[e]	−411	−606	−1050	
U	2184	4114	7259	1177	−63	−477	−539	−969	−953
Np	2118	4115	7357		−149	−516	−497	−915	−796
Pu	1995	4095	7432		−291	−571	−475	−850	−757
Am	1944	4110	7598		−360	−590	−356	−741	−587
Cm	2097	4144	7700		−223	−586	−298		
Bk	2034	4186	7622		−301	−574	−416		
Cf	1945	4222	7822		−405	−563	−250		
Es	1930	4256	7990		−433	−554	−116		
Fm	1930	4285	8076		−445	−547	−61		
Md	1930	4379	8219		−458	−476	+51		
No	1923	4523	8477		−476	−351	+282		
Lr	2125	4347	8452		−291	−546	+233		

[a] kJ mol^{-1}; [b] Bratsch and Lagowski (1986); [c] calculated for the lowest energy ground state; [d] Marcus and Loewenschuss (1986); [e] corrected for LFSE.

Element	ΔG^{0a}_h			
	+2	+3	+4	+6
Ac	−1272	−3093	-----	
Th	−1499	−3143	−5860	
Pa	−1463	−3194	−5930	
U	−1345	−3238	−5994	−1228
Np	−1365	−3278	−6050	
Pu	−1384	−3313	−6105	
Am	−1402	−3347	−6150	
Cm	−1418	−3377	−6194	
Bk	−1433	−3407	−6234	
Cf	−1448	−3432	−6268	
Es	−1461	−3457	−6302	
Fm	−1473	−3479	−6333	
Md	−1486	−3502	−6364	
No	−1497	−3521	−6391	
Lr	−1514	−3540	−6415	

[a] kJ mol^{-1}

where W is the sum of the work done to break the hydrate cluster structure and the work to condense one water molecule while R_w is the radius of water molecule (1.38 Å). The numerical values of the coefficients (α, β, etc.) of eq. (1) were computed using precise hydration enthalpies of 35 mono-, di-, tri- and tetravalent ions (David et al. 1985). The calculations were based on the assumption that n is four for monovalent, six for divalent, and eight for trivalent and tetravalent cations. The estimated error between experimental and calculated enthalpies from this equation is ca. 0.4–0.5%.

Alternatively, Bratsch and Lagowski (1985a, b, 1986) proposed an ionic model to calculate the thermodynamics of hydration ΔG^0_h, ΔH^0_h and ΔS^0_h using standard thermochemical cycles. This model is based on the knowledge of the values of quantities such as the enthalpy of formation of the monoatomic gas $[\Delta H^0_f(M_g)]$, the ionization potential sum for the oxidation state under consideration and the crystal ionic radius of the metal ion. This approach, however, is difficult to apply for the actinides since the ionization potentials are, for the most part, unavailable. To overcome this problem, the authors "back-calculated" an internally consistent set of "thermochemical" ionization potentials from selected thermodynamic data (Bratsch and Lagowski 1986). The general set of equations developed are:

$$\Delta H^0_h(M^{z+}) = \Delta H^0_f(M^{z+}_{aq}) - \Delta H^0_f(M^{z+}_g) + z[\Delta H^0_f(H^+_g) + \Delta H^0_h(H^+_{aq})], \tag{2}$$

$$\Delta S^0_h(M^{z+}) = S^0(M^{z+}_{aq}) - S^0(M^{z+}_g) + z[S^0(H^+_g) + \Delta S^0_h(H^+_{aq})], \tag{3}$$

$$\Delta G^0_h(M^{z+}) = \Delta G^0_f(M^{z+}_{aq}) - \Delta G^0_f(M^{z+}_g) + z[\Delta G^0_f(H^+_g) + \Delta G^0_h(H^+_{aq})]. \tag{4}$$

In these equations, the reference states of H^+_{aq} is equal to -1091 ± 10 kJ (Hallinwell and Nyburg 1963) and the functions $\Delta H^0_f(e^-_g)$ and $\Delta G^0_f(e^-_g)$ are equal to zero. A list of the calculated Gibbs free energies and enthalpies of hydration for the actinide elements are given in tables 5 and 6. The corresponding values of the lanthanide elements are listed in our earlier review (Rizkalla and Choppin 1991). The trends in these parameters across the two series of elements are esssentially the same with the standard enthalpy and Gibbs free energy of formation of U(IV) more negative than anticipated due to the ligand-field stabilization energy (LFSE). The spectroscopic analysis of Nugent et al. (1973a, b) and the standard electrode potential compiled by Mikheev (1984) showed that the LFSE (M^{2+}_{aq}, $6d^1$) is greater than the LFSE of the corresponding lanthanide (M^{2+}_{aq}, $5d^1$). It should be noted that the values of Bratsch and Lagowski (1986) in tables 5 and 6 used LFSE values for (M^{2+}_{aq}, $6d^n$) of 140 and 200 kJ mol^{-1}, respectively, for $n = 1$ and 2 which are the values of the lanthanide ions.

The absolute entropies for the gaseous ions are calculated from statistical mechanics (Johnson 1982) by

$$S^0(M^{z+}_g) = 1.5R\ln(\text{at wt.}) + R\ln(2J+1) + 108.745. \tag{5}$$

The values of the entropies of the aquo actinide ions were obtained by interpolation from the dependence of the corrected entropy term, S^0_c of the lanthanides on ionic radii (fig. 8) where

$$S^0_c = S^0(M^{z+}_{aq}) - S_e - S_M. \tag{6}$$

These correlated values are claimed to be dependent on the structure of the aquo ion

TABLE 6

Standard enthalpies of formation of the gaseous and hydrated actinide ions (data between brackets denote experimental data).

Element	Gas phase[a, b]				Aquo ions[a, c]				
	+2	+3	+4	+6	+2	+3	+4	+5	+6
Ac	2055	3885	----		−124	−633	----		
Th	2306	4242	7022		−113	−327	−766		
Pa	2261	4197	7194		−130	−423	−664	−677	
U	2240	4176	7327	1210	−35	−489	−595	−1032	(−1019)
Np	2173	4177	7425		−124	−528	−553	−978	−861
Pu	2044	4154	7498		−270	−587	−534	−915	−822
						(−592)			
Am	1998	4165	7664		−338	−608	−414	−805	−652
						(−617)			
Cm	2147	4199	7756		−205	−608	−364		
						(−615)			
Bk	2083	4241	7682		−285	−597	−480		
						(−601)			
Cf	1994	4277	7882		−389	−587	−314		
						(−577)			
Es	1976	4308	8048		−420	−584	−182		
Fm	1976	4337	8135		−433	−580	−127		
Md	1976	4432	8279		−446	−510	−13		
No	1969	4580	8542		−464	−382	+223		
Lr	2176	4402	8518		----	−581	+175		

[a] kJ mol^{-1}; [b] Bratsch and Lagowski (1986); [c] Marcus and Loewenschuss (1986).

Element	ΔH_h^{0a}			
	+2	+3	+4	+6
Ac	−1317	−3224	-----	
Th	−1557	−3275	−6063	
Pa	−1529	−3326	−6133	
U	−1413	−3371	−6197	−1345
Np	−1435	−3411	−6253	
Pu	−1452	−3447	−6307	
Am	−1474	−3479	−6353	
Cm	−1490	−3513	−6395	
Bk	−1506	−3544	−6437	
Cf	−1521	−3570	−6471	
Es	−1534	−3598	−6505	
Fm	−1547	−3623	−6537	
Md	−1560	−3648	−6567	
No	−1571	−3668	−6594	
Lr	-----	−3689	−6618	

[a] kJ mol^{-1}.

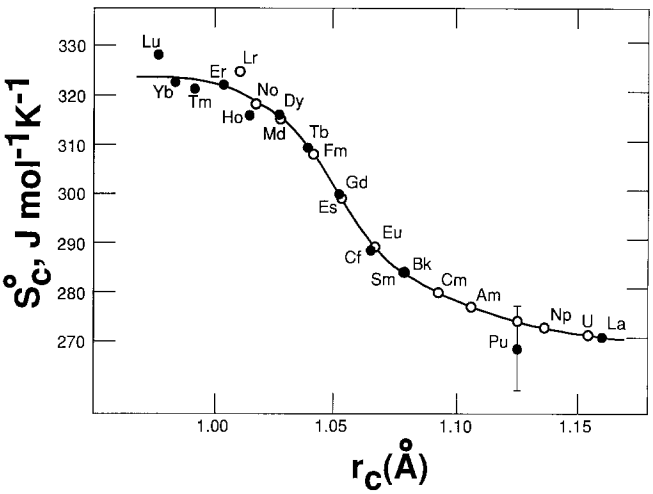

Fig. 8. Variation of the "corrected entropy", S_c, with r_c the tripositive crystallographic radius ($C = 8$): • experimental data for Ln(III) and Pu(III) ions; ○ interpolated actinide data.

only (David et al. 1985). A justification of this approach is provided by the fair agreement of the calculated value of S^0 of Pu(III) and that obtained from experimental data (Fuger and Oetting 1976). A summary of these values is given in table 7. Similarly, the hydration entropies of the divalent and tetravalent actinides were obtained from the pertinent data on the divalent alkaline earths and Th(IV) (Morss and McCue 1976) and Ce^{4+} (Morss 1976).

Differences in lanthanide and actinide hydration thermodynamics have been discussed by Bratsch and Lagowski (1986) who attributed the differences to relativistic effects in the actinides which cause changes in the energies of the s, p, d, and f orbitals. For example, the first and second ionization potentials of the electrons of the 7s state of the actinides are higher than those of the 6s state of the lanthanides whereas the third ionization potentials are similar for both families and the fourth ionization potential is lower for the actinides than the lanthanides. The small decrease in IP_3 and IP_4 for the f^7 configuration in the actinides results in smooth variations in the relative stabilities of the adjacent oxidation states across the actinide series while the greater spatial extension of the 5f orbitals increases the actinide susceptibility to environmental effects (Johnson 1982).

Nugent et al. (1973a, b) proposed the following correlation as a basis for comparison of the actinide and lanthanide thermodynamics:

$$P(\mathrm{M}) = \Delta H_f^0(\mathrm{M_g}) + \Delta E(\mathrm{M}) - \Delta H_f^0(\mathrm{M_{aq}^{3+}}), \tag{7}$$

where $\Delta E(\mathrm{M})$ is the promotion energy from the ground-state electron configuration to the $f^q d^1 s^2$ configuration where q varies from 0 (La, Ac) to 14 (Lu, Lr). ΔE is approximately zero or near zero for La, Ce, Gd, and Lu, and for Ac, Pa, U, Np, Cm, and

TABLE 7
Standard entropies of formation of the gaseous and hydrated actinide ions.

Element	Gas phase[a, b, c, d]						Aquo ions[a, e]			
	+2	+3	+4	+5	+6	+2	+3	+4	+5	+6
Ac	182	176	---			75	−199	----		
Th	190	192	177			39	−186	−417		
Pa	197	195	192			19	−183	−402	−21	
U	197	196	195	275	258	12	−183	−399	−26	−98
Np	192	195	196	280	273	2	−185	−398	−21	−94
Pu	177	192	196	281	277	−8	−190	−399	−21	−92
Am	195	177	192	>271	278	−1	−199	−402	−21	−88
Cm	199	195	178			0	−194	−408	−25	−88
Bk	201	199	195			1	−194	−399	−30	
Cf	201	201	199			0	−197	−395	−22	
Es	201	201	201			−1	−206	−393		
Fm	199	201	202			−4	−215	−393		
Md	195	199	201			−9	−224	−393		
No	178	195	199			−27	−231	−395		
Lr	184	178	195			---	−255	−399		

[a] $J K^{-1} mol^{-1}$; [b] Bratsch and Lagowski (1986); [c] calculated for the lowest energy ground states; [d] Marcus and Loewenschuss (1986); [e] David (1986).

Element	$\Delta S_h^{0\,a}$				
	+2	+3	+4	+5	+6
Ac	−151	−441	----		
Th	−195	−444	−682		
Pa	−222	−444	−682		
U	−229	−445	−682	−323	−400
Np	−234	−446	−682	−323	−411
Pu	−229	−448	−683	−324	−413
Am	−240	−442	−682	<−314	−410
Cm	−243	−455	−674		
Bk	−244	−459	−682		
Cf	−245	−464	−682		
Es	−246	−473	−682		
Fm	−247	−482	−683		
Md	−248	−489	−682		
No	−249	−492	−682		
Lr	----	−499	−682		

[a] $J K^{-1} mol^{-1}$.

Lr. For the other f-elements, it is positive and the values are accurately known from spectroscopic measurements (Bratsch 1983).

A plot of the lanthanide $P(M)$ values versus q is roughly V-shaped with a break at gadolinium (Nugent et al. 1973a,b). The deviation from this plot was attributed to a "tetrad" effect (Nugent 1970, Fidelis and Mioduski 1981). Similarly, the light actinides fall on a separate but parallel plot (Nugent et al. 1973a, b). Assuming a parallelism

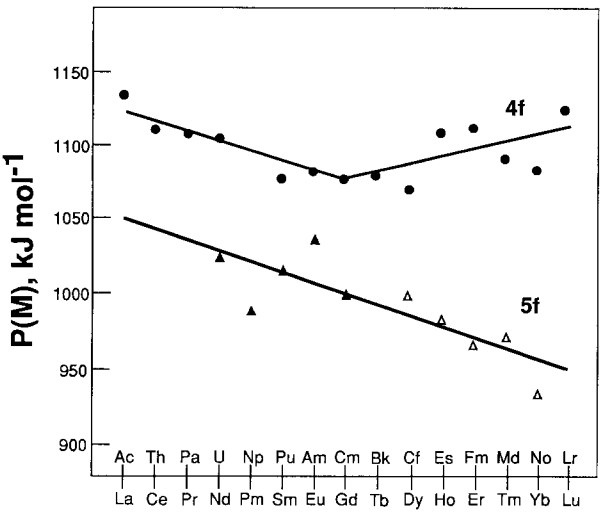

Fig. 9. Plot of $P(M)$ against atomic number Z for the lanthanide and actinide series: • 4f experimental data; ▲ 5f experimental data; △ 5f extrapolated data.

throughout both series (including a break at $q = 7$), the values of $\Delta H_f^0(M_{aq}^{3+})$ were predicted for the heavy elements.

Subsequent electro- and thermochemical analysis prompted David et al. (1978) to re-evaluate the actinide $P(M)$ function. They found that $P(M)$ varies linearly with q confirming the differences between heavy lanthanides and actinides (David et al. 1978) (fig. 9).

Bratsch and Lagowski (1986) explained this anomaly as follows. According to their model,

$$\Delta H_f^0(M_{aq}^{3+}) = \Delta H_f^0(M_g^{3+}) - \frac{613.4}{r_{M^{3+}} + 0.0784} - 1293.6.$$

$$= \Delta H_f^0(M_g) + \sum_1^3 IP(M) - \frac{613.4}{r_{M^{3+}} + 0.0784} - 1275.0. \quad (8)$$

Combining eqs. (7) and (8) gives

$$P(M) = \Delta E(M) - \sum_1^3 IP(M) + \frac{613.4}{r_{M^{3+}} + 0.0784} - 1275.0. \quad (9)$$

According to eq. (9), lanthanides and actinides are expected to fall in separate (parallel) plots since $\Delta E(M) - \Sigma_1^3 IP(M)$ are not identical for a lanthanide and an actinide with the same q value. Also, the lanthanide $P(M)$ function is V-shaped as a result of the break in ionic radius at $q = 7$. The lack of a significant break in the actinides at curium accounts for the observed linearity (Spitsyn et al. 1983).

Extensive data for thermodynamics of hydration of the actinyl ions are limited to UO_2^{2+}. Comparison of ΔH_h^0 and ΔS_h^0 with typical di- and tripositive ions indicated that

the enthalpy of hydration of the actinyl(VI) cations is comparable to those of the dipositive ions whereas the entropy of hydration is somewhat between that of di- and tripositive ions (Marcus and Loewenschuss 1986). These authors assigned the increase in entropy to the large effective charge on the uranium center (+3.3). The nonspherical symmetry of the uranium atom caused by the shielding effect of the axial uranyl oxygens results in a lower hydration entropy than those of the typical trivalent cations. However, the primary sphere interactions from the charge–dipole effects are strong, causing more extensive but weaker secondary hydration. As a result, the net enthalpy of hydration, is more similar to that of divalent than to trivalent cations.

3. Hydrolysis

Hydrolysis reactions occur for the f-elements in near-neutral solutions in the III, IV, and VI oxidation states and often predominate over other complexation reactions in solution. Hydrolysis of these elements in the II and V states occur for pH ≥ 8. The hydrolysis reactions can be expressed by the general reaction

$$n\mathrm{M(OH_2)}_q^{z+} \longleftrightarrow \mathrm{M}_n(\mathrm{OH})_q^{nz-q} + q\mathrm{H}^+ \quad (\mathrm{M} = \mathrm{Ln}^{z+} \text{ or } \mathrm{An}^{z+}),$$

$$^*\beta_{qn} = [\mathrm{M}_n(\mathrm{OH})_q^{nz-q}][\mathrm{H}^+]^q/[\mathrm{M}^{z+}]^n. \tag{10}$$

$^*\beta_{qn}$ increases with increasing cationic charge density. At the simplest level, this behavior can be ascribed to the influence of the positive charge of the metal ion polarizing the water molecule(s) sufficiently to release the proton(s). The strength of hydrolysis follows the order

$$\mathrm{M}^{4+} > \mathrm{MO}_2^{2+} > \mathrm{M}^{3+} > \mathrm{MO}_2^{+} > \mathrm{M}^{2+}.$$

This is consistent with other thermodynamic data which indicate effective central charges on the actinide atoms in the actinyl(V) and actinyl(VI) ions greater than the formal ionic charges of +1 and +2, respectively. In other words, these ions act as stronger Bronsted acids than ions which possess spherical symmetry of the same net cationic charge. Estimates of these charges were about +2.2 and +3.3 for both classes, respectively (Choppin and Rao 1984).

Various techniques have been used to study the speciation and the precipitation of trivalent ions in aqueous medium. Among these are pH, extraction, and oscillopolarographic measurements. The data provide conclusive evidence for the formation of polynuclear as well as mononuclear hydroxo complexes although the agreement between different sets of measurements are relatively poor due to the problems associated with the low solubility of these complexes. A summary of the data for actinide ions is given in table 8A. Those of the lanthanides are listed elsewhere (Rizkalla and Choppin 1991). For an internally consistent set of lanthanide data (Kragten and Decnop-Weever 1978, 1979, 1980, 1982, 1983a, b, 1984, 1987), the values of $^*\beta_{11}$ were found to decrease with increasing atomic number as a result of cation contraction.

Based on this argument, the hydrolysis constants for actinides would be expected to be slightly more negative than those for the isoelectronic lanthanides. This is seen in

TABLE 8
Hydrolysis constants of mononuclear actinide complexes.
A: Trivalent ions.

Species	T (°C)	Medium	Method	$\log {}^{*}\beta_{qn}$	Reference*
$Np(OH)^{2+}$	25	0.3 M $NaClO_4$	pH	-7.43 ± 0.12	a
$Pu(OH)^{2+}$	25	1.0 M $NaClO_4$	pH	-5.53	b
	23	0.2 M $LiClO_4$	dis	-3.80 ± 0.2	c
	25	0.1 $HClO_4$		-7.08	d
		0.069 M $HClO_4$	pH	-7.25	e
	25	0		-6.95	f
$Am(OH)^{2+}$	25	1.0 M $NaClO_4$	sol	-7.03 ± 0.05	b
	25	1.0 M $NaClO_4$	ex	-7.50 ± 0.3	g
	21	0.7 M NaCl	ex	-7.54 ± 0.2	h
	25	0.5 M(H, NH_4) ClO_4	ex	-6.80 ± 0.3	i
	23	0.1 M $LiClO_4$	ex	-5.92	j
	23	0.1 M $LiClO_4$	ex	-5.30 ± 0.1	k
		0.1 M $NaClO_4$	sol	-7.68	l
		0.1 M $NaClO_4$	sol	-7.93	m
	25	0.1 M $HClO_4$		-5.88	d
		0.1 M $NaClO_4$	sol	-6.34 ± 0.83	n
	24	0.035 M	pH	-7.0	o
	10	0.005 M KCl	mig	-2.70 ± 0.03	p
	25	0.005 M(H, NH_4) ClO_4	mig	-3.3 ± 0.1	q
$Am(OH)_2^+$		0.2 M $NaClO_4$	ex	-14.76	r
		0.1 M $NaClO_4$	sol	-16.56	l
		0.1 M $NaClO_4$	sol	-14.77	m
		0.1 M $NaClO_4$	sol	-13.64 ± 0.63	n
	25	0.005 M NH_4ClO_4	mig	-7.1	q
		0.003 M $CaCl_2$		-16.62	s
		0	sol	-17.1 ± 0.5	t
$Am(OH)_3$		0.1 M $NaClO_4$	sol	-24.84	l
		0.1 M $NaClO_4$	sol	-24.71	m
$Cm(OH)^{2+}$	23	0.1 M $LiClO_4$	ex	-5.92 ± 0.13	j
	23	0.1 M $LiClO_4$	ex	-5.40 ± 0.1	u
		0.1 M $LiClO_4$	ex	-5.93	v
		0.1 M KCl		-7.68	w
	25	0.005 M NH_4ClO_4	mig	-3.40 ± 0.2	q
		0.005 M KCl	mig	-2.70 ± 0.1	x
$Cm(OH)_2^+$	25	0.005 M NH_4ClO_4	mig	-9.1 ± 0.3	q
$Bk(OH)^{2+}$	23	0.1 M $LiClO_4$	ex	-5.66	j
$Cf(OH)^{2+}$	23	0.1 M $LiClO_4$	ex	-5.62	j
	23	0.1 M $LiClO_4$	ex	-5.05	k
$Es(OH)^{2+}$	23	0.1 M $LiClO_4$	ex	-5.14	k
$Fm(OH)^{2+}$	23	0.1 M $LiClO_4$	ex	-3.8 ± 0.2	k

* (a) Mefod'eva et al. (1974); (b) Nair et al. (1982); (c) Hubert et al. (1975); (d) Smith and Martell (1976); (e) Kraus and Dam (1949a); (f) Kraus and Dam (1949b); (g) Lundqvist (1982); (h) Caceci and Choppin (1983); (i) Rao et al. (1987); (j) Desire et al. (1969); (k) Hussonnois et al. (1973); (l) Silva (1983); (m) Bernkopf (1984); (n) Kim et al. (1984); (o) Korotkin (1973); (p) Marin and Kikindai (1969); (q) Schalinates and Stepanov (1972); (r) O'Connor (1944); (s) Rai et al. (1982); (t) Rai et al. (1983); (u) Hussonnois et al. (1976); (v) Guillaumont et al. (1969); (w) Edelstein et al. (1983); (x) Marin et al. (1968).

TABLE 8 (continued)
B:Tetravalent ions.

Species	T (°C)	Medium	Method	$\log {}^*\beta_{qn}$	Reference*
$Th(OH)^{3+}$	25	3.0 M NaCl	pH	-5.0	a
	0	1.0 M $NaClO_4$	pH	-4.3 ± 0.02	a, b
	25	1.0 M $NaClO_4$	pH	-4.3	c
	25	1.0 M $NaClO_4$	pH	-4.23 ± 0.02	b
	95	1.0 M $NaClO_4$	pH	-2.29 ± 0.02	b
	25	0.5 M $NaClO_4$	cix, pH	-2.36 ± 0.07	d
	25	0.5 M $NaClO_4$	pH	-4.26	e
	25	0.3 M $NaClO_4$	pH	-4.12	e
	25	0.1 M $NaClO_4$	pH	-4.00	e
	8	0.1 M $NaClO_4$	sol, pH	-4.60	f
	25	0.05 M $NaClO_4$	pH	-3.92	e
		0.05 M		-3.15 ± 0.07	g
	rt	var	pH	-3.6	h
	20	0	pH	-3.61	i
$Th(OH)_2^{2+}$	25	1.0 M		-7.69	j
	25	0		-6.9	j
$Pa(HO)^{3+}$	25	3.0		-0.14	j
	25	0		0.80	j
$Pa(OH)_2^{2+}$	25	3.0		-0.52	j
	25	0		0.0	j
$Pa(OH)_3^+$	25	3.0		-1.84	j
$Pa(OH)_4$	25	3.0		-5.32	j
$U(OH)^{3+}$	25	3.0 M $NaClO_4$	pH	-2.1 ± 0.15	k
	25	3.0 M $NaClO_4$	sp	-1.65 ± 0.05	l
	25	2.0 M $NaClO_4$	pH, sp	-1.68	m
	25	2.0 M $NaClO_4$	sp	-1.63	n
	20	1.0 M $NaClO_4$	sp	-1.57	o
	25	1.0 M $NaClO_4$	sp	-1.56	n
	25	0.5 M $NaClO_4$	sp	-1.54	n
	10	0.5 M $NaClO_4$	sp	-1.90	p
	25	0.5 M $NaClO_4$	sp	-1.46	p
		$\Delta^*H = 46.9$ kJ/mol; $\Delta^*S = 130$ J/K/mol			
	43	0.5 M $NaClO_4$	sp	-1.00	p
	15	0.19 M $HClO_4$	sp	-1.38	q
	20	0.19 M $HClO_4$	sp	-1.24	q
	25	0.19 M $HClO_4$	sp	-1.12	q
		$\Delta^*H = 44.8 \pm 4.2$ kJ/mol			
	25	0.11 M $NaClO_4$	sp	-1.22	n
	10	0	sp	-1.12	n
	25	0	sp	-0.68	n
		$\Delta^*H = 49.0$ kJ/mol; $\Delta^*S = 151$ J/K/mol			
	25	0	sp	-1.11	n, s
	25	0	sp	-0.47	t

TABLE 8 (continued)

Species	T (°C)	Medium	Method	$\log {}^*\beta_{qn}$	Reference*
	21	0	sol	-0.50	u
	43	0	sp	-0.18	n
	50	0	sp	0.18 ± 0.07	t
	75	0	sp	0.76 ± 0.03	t
	100	0	sp	1.00 ± 0.03	t
	125	0	sp	1.27 ± 0.03	t
	150	0	sp	1.83 ± 0.04	t
$Np(OH)^{3+}$	25	2.0 M $NaClO_4$	pH, sp	-2.30 ± 0.03	m
$Np(OH)_2^{2+}$	25	1.0 M $HClO_4$	ex	-0.50	v
		0.001 M $HClO_4$	pulse radiolysis	-0.47	w
$Pu(OH)^{3+}$	15	2.0 M $LiClO_4$	red	-1.41 ± 0.02	x
	15	2.0 M $NaClO_4$	sp	-1.90	y
	25	2.0 M $LiClO_4$	red	-1.27 ± 0.01	x
	25	2.0 M $NaClO_4$	sp	-1.73 ± 0.01	z
	34	2.0 M $LiClO_4$	red	-1.06 ± 0.02	x
	25	1.11 M NaCl	sp	-1.55 ± 0.11	aa
	25	1.00 M $NaClO_4$	red	-1.51	bb
				-1.54	cc
		1.00 M $LiClO_4$	ex	-0.45	dd
		1.00 M $NaClO_4$		-1.50	ee
	25	0.5 M $NaClO_4$	sp	-1.65 ± 0.02	ff
	25	0.5 M $NaClO_4$	sp	-1.60 ± 0.05	n
	25	0.5 M $NaClO_4$	sp	-1.72 ± 0.05	n, y
	23	0.19 $LiClO_4$		-1.96	z
		0.06 $LiClO_4$	sp	-1.48	z
$Pu(OH)_2^{2+}$		1.00 M $LiClO_4$	ex	-0.75	dd
	rt	1.00 M $NaClO_4$		-3.2	ee
$Pu(OH)_3^{+}$		1.00 M $LiClO_4$	ex	-3.3	dd
	rt	1.00 M $NaClO_4$		-6.3	ee
$Pu(OH)_4$		1.00 M $LiClO_4$	ex	-6.3	dd
	rt	1.00 M $NaClO_4$		-11.9	ee

* (a) Hietanen and Sillen (1968); (b) Baes et al. (1965); (c) Kraus and Holmberg (1954); (d) Beran (1967); (e) Pan and Hseu (1955); (f) Nabivanets and Kudritskaya (1964); (g) Usherenko and Skorik (1971); (h) Kaspar (1941); (i) Kisiak and Stefanowicz (1971); (j) Smith and Martell (1976); (k) Hietanen (1956); (l) Grenthe et al. (1989); (m) Sullivan and Hindman (1959); (n) Kraus and Nelson (1950); (o) McKay and Woodhead (1964); (p) Kraus and Nelson (1955); (q) Betts (1955); (s) Solovkin et al. (1967); (t) Nikolceva (1978); (u) Rai et al. (1990); (v) Duplessis and Guillaumont (1977); (w) Schmidt et al. (1980); (x) Rabideau (1957); (y) Rabideau and Kline (1960); (z) Cleveland (1968); (aa) Hindman (1949); (bb) Rabideau and Lemons (1951); (cc) Davydov (1972); (dd) Metivier and Guillaumont (1976); (ee) Lierse (1985); (ff) Kraus and Nelson (1949).

the comparison of Eu(III) and Am(III) values (Caceci and Choppin 1983). The most common polynuclear hydroxides detected for trivalent lanthanides are those of the 2:2 and the 3:5 types. Although none have been reported for trivalent actinides, presumably, these ions also form hydrolytic polymers at similar cationic concentration and ionic strength as the Ln(III) cations.

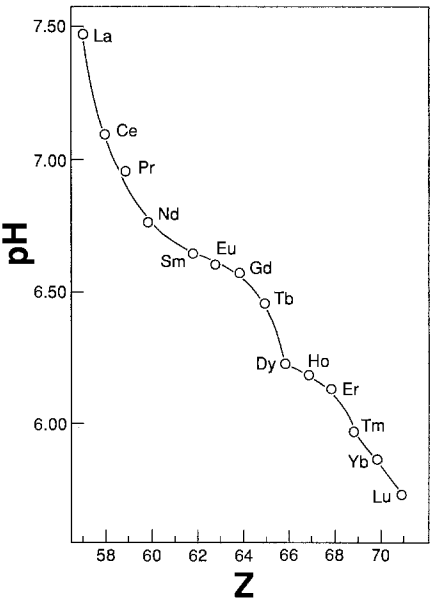

Fig. 10. Plot of the pH of the onset precipitation as a function of the atomic number across the lanthanide series.

The mechanism of hydrolysis and oleation for the Ln^{3+} elements was studied by Suzuki et al. (1986) who measured the onset of precipitation of $Ln(OH)_3$ by an optical scattering technique. To avoid local concentration effects, the hydroxide ion was generated electrolytically. The pH values for the initiation of precipitation ranged from 5.7 to 7.5 and are plotted versus r in fig. 10. The S-shaped relationship was associated, again, with the change in hydration number between the heavy and light elements (vide infra).

Hydrolysis studies of the tetravalent cations are limited to Ce and the light (Pa, Th, U, and Pu) actinides (tables 8B and 9). Only in strong acid media do the tetravalent ions exist free of hydrolysis. Similarly, only at very low concentrations are mononuclear hydroxides of significance. For Ce(IV), stability constants have been determined for bi-, ter-, tetra-, and dodeca-cerium units and for species with molecular weights as large as 40,000 (Hardwick and Robertson 1951, Danesi 1967, Louwrier and Steemers 1976). X-ray measurements of thorium and uranium solutions show polynuclear complexes built from

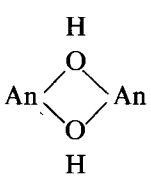

units with an An–An distance of 3.95 Å (Bovin 1974, Johansson 1968) and 4.00 Å (Katz and Seaborg 1957, Pocev and Johansson 1973) for Th and U, respectively. As

TABLE 9
Hydrolysis constants of polynuclear actinide complexes.

Species	T (°C)	Medium	Method	$\log {}^*\beta_{qn}$	Reference*
$Th_2(OH)_2^{6+}$	25	4.0 M $NaNO_3$	pH	− 5.5	a
	25	3.0 M NaCl	pH	− 4.70 ± 0.05	b
	0	1.0 M $NaClO_4$	pH	− 5.6 ± 0.02	b, c
	25	1.0 M $NaClO_4$	pH	− 4.70	d
	25	1.0 M $NaClO_4$	pH	− 4.61 ± 0.02	c
	90	1.0 M $NaClO_4$	pH	− 2.55 ± 0.03	c
	20	var.	pH	− 4.56	e
	25	0	sol	− 5.40	f
$Th_2(OH)_3^{5+}$	25	3.0 M NaCl		− 8.70	g
$Th_4(OH)_8^{8+}$	25	1.0		−19.2	g
$Th_6(OH)_{14}^{10+}$	25	3.0 M NaCl		−36.4	g
$Th_6(OH)_{15}^{9+}$	25	1.0		−37.2	g
	25	3.0		−16.6	g
$U_6(OH)_{15}^{9+}$	25	0		−17.2	g

* (a) Danesi et al. (1968); (b) Hietanen and Sillen (1968); (c) Baes et al. (1965); (d) Kraus and Holmberg (1954); (e) Lefebre (1958); (f) Higashi (1959); (g) Smith and Martell (1976).

hydrolysis proceeds, the degree of polymerization increases rapidly such that before the average number of ionized protons per An ion reaches three, the number of An ions in the hydrolyzed cluster exceeds 100, resulting in a decrease in the kinetic rate of equilibration.

The hydrolysis of Pu (IV) can result in the formation of polymers which are rather intractable to reversal to simpler species. This has led often to incorrect conclusions about the nature of the plutonium species present and the validity of their equilibrium constants. The kinetics of depolymerization take a different course as the polymer ages such that while freshly prepared hydroxides are easily decomposed, aged polymers require quite rigorous conditions. A reasonable model for this process involves initial formation of aggregates with OH bridging which dehydrate with aging (Choppin 1983).

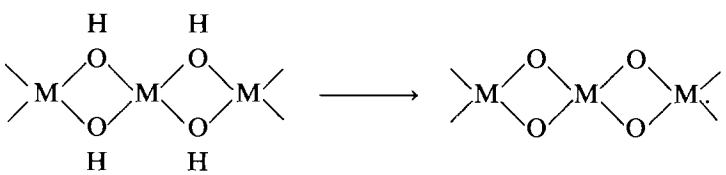

The relative percentages of oxo and hydroxo bridging presumably are the major factors in the inertness of the polymer.

The tendency to disproportionate by UO_2^+ and PuO_2^+ and the strong oxidation properties of AmO_2^+ have led to few hydrolytic studies of these cations. The values of $\log {}^*\beta_{11}$ for NpO_2^+ (ca. − 8.85 at $I = 0$) (Baes and Mesmer 1976, Schmidt et al. 1980))

are in good accordance with predictions based on an effective charge of +2.2 and can serve as a measure for the other AnO_2^+ species.

Most of the hydrolytic studies of the hexavalent actinides have been concerned with UO_2^{2+}. The recommended hydrolysis constants for the formation of $[UO_2(OH)^+]$, $[UO_2(OH)_2]$ (Choppin and Mathur 1991), and $[(UO_2)_2(OH)_2^{2+}]$ (Baes and Mesmer 1976) at 1.0 M ionic strength are -5.72 ± 0.07, -11.78 ± 0.09 and -5.89, respectively, and the enthalpy of formation of the dimer was found to be -68.1 ± 10.0 kJ/mol (Choppin et al. 1991).

Polynuclear complexes are formed at pH values above two (Rabinowitch and Belford 1964) although thermodynamic data do not allow choice between

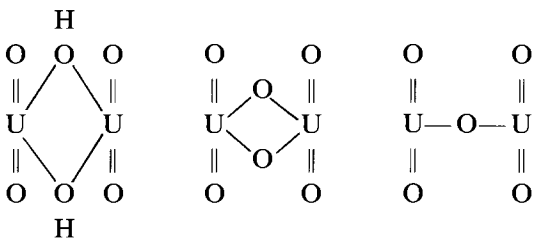

(I) (II) (III)

(Mavrodin-Tarabic 1973, 1974). This tendency of hydrolytic polymerization varies strongly across the series UO_2^{2+}, NpO_2^{2+}, and PuO_2^{2+}. Based on the measured values of $\log {}^*\beta_{11}$ and $\log {}^*\beta_{22}$ for NpO_2^{2+} (-5.14 and -6.66) and PuO_2^{2+} (-5.98 and -8.50) hydrolysis (Baes and Mesmer 1976), the following pH values (table 10) were estimated for 1 : 1 monomer : polymer formation at different levels of free AnO_2^{2+} concentration (Choppin et al. 1991).

An additional interesting aspect is found in the higher resistivity of alkaline solutions of PuO_2^{2+} to precipitation as compared to UO_2^{2+}. This anomaly cannot be attributed to changes in the effective charges of the actinide atoms alone [+3.2, +3.0, and +2.9 for UO_2^{2+}, NpO_2^{2+}, and PuO_2^{2+}, respectively (Choppin and Rao 1984)] raising questions about the validity of the proposed hydrolytic schemes. Madic et al. (1984), from a Raman spectral study of PuO_2^{2+} at different pH values, proposed that the hydrolytic scheme of PuO_2^{2+} is different from that of UO_2^{2+}. The PuO_2^{2+} spectra has four peaks at

TABLE 10
pH values required to achieve 50% polymerization.

$[MO_2^{2+}]_{total}$ M	pH		
	UO_2^{2+}	NpO_2^{2+}	PuO_2^{2+}
10^{-1}	3.45	3.84	4.76
10^{-3}	4.46	4.94	5.87
10^{-5}	5.56	6.54	7.51

833, 817, 826 and 805 cm^{-1} whose relative intensities vary with the pH of the medium. The analogous spectra of hydrolyzed U(VI) solutions displayed three bands at 869, 851 and 836 cm^{-1}. The difference in the number of bands was attributed to differences in speciation. For UO_2^{2+}, the three stretching frequencies were assigned to UO_2^{2+}, $(UO_2)_2(OH)_2^{2+}$ and $(UO_2)_3(OH)_5^+$, respectively, whereas for PuO_2^{2+} the bands were attributed to $(PuO_2)^{2+}$, (833 cm^{-1}), $(PuO_2)_2(OH)_2$ (817 cm^{-1}), and $(PuO_2)_4(OH)_7^+$ (826 and 805 cm^{-1}). At high pH values (ca. 13–14), a new band of unknown origin was observed at 794 cm^{-1}. A comparison of the potentiometric curves of PuO_2^{2+} obtained by forward titration with NaOH and back titration with $HClO_4$ indicated a hysteresis effect with large drifts in the pH of the back-titration curve (Kraus and Dam 1949a). Madic et al. (1984) and Schedin (1975) attributed this to a slow disintegration of the large (4,7) aggregates relative to its rate of formation.

In the case of NpO_2^{2+} ion, only the hydroxo dimer complex was identified (by Raman spectrometry) (Madic et al. 1984).

4. Summary and conclusions

Understanding of the processes and thermodynamics of hydration and hydrolysis is a necessary background to understanding complexation of f-block elements. As such, this chapter has a relationship to the topics covered in the chapter by Choppin and Rizkalla (Ch. 128) in this volume.

In their trivalent state, both families seem to share many hydration and hydrolytic characteristics. The solid hydrates of the lanthanides adopt either the tricapped trigonal prismatic structure or the square antiprismatic structure with coordination numbers nine and eight for the light and heavy elements, respectively, with a transitional region in the middle of the series. X-ray scattering, neutron diffraction and diffusion measurements for lanthanide and actinide solutions support such structures in both series although they differ in the transitional regions. For the lanthanides, the break occurs between Nd and Gd, while for the actinides it occurs between Bk and Cf. This difference suggests that the hydration number is sensitive to variations in size parameters but is not dependent on the electronic configuration of the ion.

Bulk data of solvation of tetravalent cations supports octa-coordination in the first hydration sphere whereas the actinyl(VI) cations seem to favor hexa-coordination in the plane perpendicular to the axial actinyl group. The trends in the thermodynamic parameters of hydration across the actinide series are essentially similar to those observed for the lanthanide ions and the small differences can be attributed to relativistic effects in the actinides which causes changes in the relative energies of the s, p, d, and f orbitals.

Hydrolytic behavior of trivalent actinides copies that of the analogous lanthanides of the same ionic size. For higher valent actinides the trend in hydrolytic tendencies across a homologous series [e.g., U(VI), Np(VI), and Pu(VI)] is not clearly understood. The anomalies associated with Pu(VI) hydrolysis may be related to a decreased tendency to polymerization [relative to that of U(VI) and Np(VI)].

Acknowledgements

Preparation of this manuscript was assisted by a grant from the USDOE-OBES Division of Chemical Sciences.

References

Albertsson, J., and T. Elding, 1977, Acta Crystallogr. B **33**, 1460.

Alcock, N.W., and S. Esperas, 1977, J. Chem. Soc. Dalton Trans., p. 893.

Annis, B.K., R.L. Hahn and A.H. Narten, 1985, J. Chem. Phys. **82**, 2086.

Baes Jr, C.F., and R.E. Mesmer, 1976, The Hydrolysis of Cations (Wiley, New York).

Baes, C.F., J. Norman, H.-J. Meyer and C.E. Roberts, 1965, Inorg. Chem. **4**, 518.

Beitz, J.V., 1991, Radiochim. Acta **52/53**, 35.

Beran, M., 1967, Collect. Czechosl. Chem. Commun. **32**, 1368.

Bernkopf, M.F., 1984, Dissertation (Technical University, München).

Bertha, S.L., and G.R. Choppin, 1969, Inorg. Chem. **8**, 613.

Betts, R.H., 1955, Can. J. Chem. **33**, 1775.

Bockris, J.O'M., and A.K.D. Reddy, 1970, Modern Electrochemistry, Vol. 1 (Plenum Press, New York).

Bockris, J.O'M., and P.P.S. Saluja, 1972a, J. Phys. Chem. **76**, 2140.

Bockris, J.O'M., and P.P.S. Saluja, 1972b, J. Phys. Chem. **76**, 2298.

Bockris, J.O'M., and P.P.S. Saluja, 1973, J. Phys. Chem. **77**, 1598.

Bombieri, G., and G. De Paoli, 1985, in: Handbook on the Physics and Chemistry of the Actinides, Vol. 3, eds A.J. Freeman and C. Keller (North-Holland, Amsterdam) ch. 3.

Bombieri, G., G. De Paoli, A. Cossol and A. Immirzi, 1976, Inorg. Chim. Acta **18**, L23.

Bovin, J.O., 1974, Acta Chem. Scand. **28A**, 723.

Brand, J.R., and J.W. Cobble, 1970, Inorg. Chem. **9**, 912.

Bratsch, S.G., 1983, Chem. Phys. Lett. **98**, 113.

Bratsch, S.G., and J.J. Lagowski, 1985a, J. Phys. Chem. **89**, 3310.

Bratsch, S.G., and J.J. Lagowski, 1985b, J. Phys. Chem. **89**, 3317.

Bratsch, S.G., and J.J. Lagowski, 1986, J. Phys. Chem. **90**, 307.

Broach, R.W., J.M. Williams, G.P. Felcher and D.G. Hinks, 1979, Acta Crystallogr. B **35**, 2317.

Bünzli, J.-C.G., J.-P. Metabanzoulou, P. Froidevaux and L. Jin, 1990, Inorg. Chem. **29**, 3875.

Burgess, J., 1978, Metal Ions in Solution (Ellis Horwood, Chichester).

Butler, R.N., and M.C.R. Symons, 1969, Trans. Faraday Soc. **65**, 945.

Caceci, M.S., and G.R. Choppin, 1983, Radiochim. Acta **33**, 101.

Chatterjee, A., E.N. Maslen and K. Watson, 1988, Acta Crystallogr. B **44**, 381, 386.

Choppin, G.R., 1983, Radiochim. Acta **32**, 43.

Choppin, G.R., and A. Graffeo, 1965, Inorg. Chem. **4**, 1254.

Choppin, G.R., and J.N. Mathur, 1991, Radiochim. Acta **52/53**, 25.

Choppin, G.R., and L.F. Rao, 1984, Radiochim. Acta **37**, 143.

Choppin, G.R., L.F. Rao, E.N. Rizkalla and J.C. Sullivan, 1991, unpublished results.

Cleveland, J.M., 1968, Inorg. Chem. **7**, 874.

Cossy, C., A.C. Barnes, J.E. Enderby and A.E. Merbach, 1989, J. Chem. Phys. **90**, 3254.

Coulter, L.V., K.S. Pitzer and W.M. Latimer, 1940, J. Am. Chem. Soc. **62**, 2845.

Dalley, N.K., M.H. Mueller and S.H. Simonsen, 1971, Inorg. Chem. **10**, 323.

Dalley, N.K., M.H. Mueller and S.H. Simonsen, 1972, Inorg. Chem. **11**, 1840.

Danesi, P.R., 1967, Acta Chem. Scand. **21**, 143.

Danesi, P.R., M. Magini, S. Margherita and G. D'Alessandro, 1968, Energia Nucl. **15**, 335.

David, F., 1986, J. Less-Common Met. **121**, 27.

David, F., K. Samhoun, R. Guillaumont and N.M. Edelstein, 1978, J. Inorg. & Nucl. Chem. **40**, 69.

David, F., B. Fourest and J. Duplessis, 1985, J. Nucl. Mater. **130**, 273.

Davydov, Yu.P., 1972, Dokl. Akad. Nauk Belorus. SSR **16**, 524.

Desire, B., M. Hussonnois and R. Guillaumont,

1969, C.R. Acad. Sci. (Paris) Ser. II **269**, 448.
Duplessis, J., and R. Guillaumont, 1977, Radiochem. & Radioanal. Lett. **31**, 293.
Edelstein, N.M., J. Bucher, R.J. Silva and H. Nitsche, 1983, Report LBL 14996 (Lawrence Berkeley Laboratory, Berkeley, CA).
Eller, P.G.E., and R.A. Penneman, 1976, Inorg. Chem. **15**, 2439.
Ernst, S., and B. Jezowska-Trzebiatowska, 1975a, J. Phys. Chem. **79**, 2113.
Ernst, S., and B. Jezowska-Trzebiatowska, 1975b, J. Phys. Chem. **256**, 5330.
Fidelis, I.K., and T.J. Mioduski, 1981, in: Structure and Bonding, Vol. 47, ed. M.J. Clark (Springer, New York).
Fitzwater, D.R., and R.E. Rundle, 1959, Z. Kristallogr. **112**, 362.
Fourest, B., J. Duplessis and F. David, 1982, C.R. Acad. Sci. (Paris) Ser. II **294**, 1179.
Fourest, B., J. Duplessis and F. David, 1983, J. Less-Common Met. **92**, 17.
Fourest, B., J. Duplessis and F. David, 1984, Radiochim. Acta **36**, 191.
Fourest, B., F. David and E. Haltier, 1988, Lanthanide & Actinide Res. **2**, 393.
Fratiello, A., V. Kubo, R.E. Lee and R.E. Schuster, 1970a, J. Phys. Chem. **74**, 3726.
Fratiello, A., R.E. Lee and R.E. Schuster, 1970b, Inorg. Chem. **9**, 391.
Fuger, J., 1982, in: Actinides in Perspective, ed. N.M. Edelstein (Pergamon Press, New York) p. 409.
Fuger, J., and R.G. Haire, 1975, J. Inorg. & Nucl. Chem. **37**, 1725.
Fuger, J., and F.L. Oetting, 1976, The Chemical Thermodynamics of Actinide Elements and Compounds, Part 2 (IAEA, Vienna).
Fuger, J., J.C. Spirlet and W. Müller, 1972, Inorg. & Nucl. Chem. Lett. **8**, 709.
Fuger, J., J. Reul and W. Müller, 1975, Inorg. & Nucl. Chem. Lett. **11**, 265.
Fuger, J., R.G. Haire and J.R. Peterson, 1981, J. Inorg. & Nucl. Chem. **43**, 3209.
Fuger, J., R.G. Haire and J.R. Peterson, 1984, J. Less-Common Met. **98**, 315.
Gerkin, R.E., and W.J. Reppart, 1984, Acta Crystallogr. C **40**, 781.
Grenthe, I., G. Bidoglio and N. Omenetto, 1989, Inorg. Chem. **28**, 71.
Guillaumont, R., C. Ferreira de Miranda and M. Galin, 1969, C.R. Acad. Sci. (Paris) Ser. C **268**, 140.
Gusev, N.I., 1971, Russ. J. Phys. Chem. **45**, 1268, 1455, 1575.
Gusev, N.I., 1972, Russ. J. Phys. Chem. **46**, 1034, 1657.
Gusev, N.I., 1973, Russ. J. Phys. Chem. **47**, 52, 184, 687, 1309.
Habenschuss, A., and F.H. Spedding, 1979a, J. Chem. Phys. **70**, 2797.
Habenschuss, A., and F.H. Spedding, 1979b, J. Chem. Phys. **70**, 3758.
Habenschuss, A., and F.H. Spedding, 1980, J. Chem. Phys. **73**, 442.
Hall, D., A.D. Rae and T.N. Waters, 1965, Acta Crystallogr. **19**, 389.
Hallinwell, H.F., and S.C. Nyburg, 1963, Trans. Faraday Soc. **59**, 1126.
Hardwick, T.J., and E. Robertson, 1951, Can. J. Chem. **29**, 818.
Harrowfield, J.McB., D.L. Kepert, J.M. Patrick and A.H. White, 1983a, Aust. J. Chem. **36**, 483.
Harrowfield, J.McB., D.L. Kepert, J.M. Patrick, A.H. While and S.F. Lincoln, 1983b, J. Chem. Soc. Dalton Trans., p. 393.
Hay, B.P., 1991, Inorg. Chem. **30**, 2876.
Helm, L., and A.E. Merbach, 1991, Eur. J. Solid State & Inorg. Chem. **28**, 245.
Helmholz, L., 1939, J. Am. Chem. Soc. **61**, 1544.
Hietanen, S., 1956, Acta Chem. Scand. **10**, 1531.
Hietanen, S., and L.G. Sillen, 1968, Acta Chem. Scand. **22**, 265.
Higashi, S., 1959, Bull. Inst. Chem. Res., Kyoto Univ. **37**, 200.
Hinchey, R.J., and J.W. Cobble, 1970, Inorg. Chem. **9**, 922.
Hindman, J.C., 1949, Nat. Nuclear Energy Serv., IV-14B, 370 (McGraw-Hill, New York).
Hinton, J.F., and E.S. Amis, 1971, Chem. Rev. **71**, 627.
Horrocks Jr, W.deW., and D.R. Sudnick, 1979, J. Am. Chem. Soc. **101**, 334.
Hubbard, C.R., C.O. Quicksall and R.A. Jacobson, 1974, Acta Crystallogr. B **30**, 2613.
Hubert, S., M. Hussonnois and R. Guillaumont, 1975, J. Inorg. & Nucl. Chem. **37**, 1255.
Hussonnois, M., S. Hubert, L. Billard and R. Guillaumont, 1973, Radiochim. & Radioanal. Lett. **15**, 47.
Hussonnois, M., S. Hubert, L. Billard and R. Guillaumont, 1976, in: Transplutonium Elements, eds W. Muller and R. Lindner (North-Holland, Amsterdam) p. 109.
Impey, R.W., P.A. Madden and I.R. McDonald, 1983, J. Phys. Chem. **87**, 5071.
Johansson, G., 1968, Acta Chem. Scand. **22**, 399.
Johnson, D.A., 1982, Some Thermodynamic Aspects of Inorganic Chemistry, 2nd Ed.

(Cambridge University Press, London).
Kaspar, J., 1941, Thesis (Johns Hopkins University, Baltimore, MD).
Katz, J.J., and G.T. Seaborg, 1957, The Chemistry of Actinide Elements (Methuen, New York).
Kepert, D.L., 1982, Inorganic Stereochemistry (Springer, Berlin).
Kim, J.I., M.F. Bernkopf, Ch. Lierse and F. Koppold, 1984, in: Geochemical Behavior of Disposed Radioactive Waste, ACS Symp. Ser., Vol. 246, eds G.S. Barney, J.D. Navratil and W.W. Schultz (American Chemical Society, Washington, DC).
Kisiak, S., and T. Stefanowicz, 1971, Rocz. Chem. **45**, 1801.
Korotkin, Yu.S., 1973, Radiokhim. **15**, 766.
Kragten, J., and L.G. Decnop-Weever, 1978, Talanta **25**, 147.
Kragten, J., and L.G. Decnop-Weever, 1979, Talanta **26**, 1105.
Kragten, J., and L.G. Decnop-Weever, 1980, Talanta **27**, 1047.
Kragten, J., and L.G. Decnop-Weever, 1982, Talanta **29**, 219.
Kragten, J., and L.G. Decnop-Weever, 1983a, Talanta **30**, 131.
Kragten, J., and L.G. Decnop-Weever, 1983b, Talanta **30**, 134.
Kragten, J., and L.G. Decnop-Weever, 1984, Talanta **31**, 731.
Kragten, J., and L.G. Decnop-Weever, 1987, Talanta **34**, 861.
Kraus, K.A., and J.R. Dam, 1949a, in: Transuranium Elements, eds G.T. Seaborg, J.J. Katz and W.M. Mannings (McGraw-Hill, New York) p. 466.
Kraus, K.A., and J.R. Dam, 1949b, Nat. Nucl. Energy Ser., Div. IV, Vol. 14B, p. 466.
Kraus, K.A., and R.W. Holmberg, 1954, J. Phys. Chem. **58**, 325.
Kraus, K.A., and F. Nelson, 1949, J. Am. Chem. Soc. **71**, 2517.
Kraus, K.A., and F. Nelson, 1950, J. Am. Chem. Soc. **72**, 3901.
Kraus, K.A., and F. Nelson, 1955, J. Am. Chem. Soc. **77**, 3921.
Latrous, H., J. Oliver and M. Chemla, 1982, Radiochim. & Radioanal. Lett. **53**, 81.
Lefebre, J., 1958, J. Chim. Phys. **55**, 227.
Lierse, Ch., 1985, Dissertation (Institut für Radiochemie, Technische Universität, München).
Lincoln, S.F., 1986, Adv. Inorg. & Bioinorg. Mechanisms **4**, 217.
Lis, S., and G.R. Choppin, 1991, Anal. Chem. **63**, 2542.
Louwrier, K.P., and T. Steemers, 1976, Inorg. & Nucl. Chem. Lett. **12**, 185.
Lundqvist, R., 1981, Acta Chem. Scand. A **35**, 31.
Lundqvist, R., 1982, Acta Chem. Scand. A **36**, 741.
Lundqvist, R., E.K. Hulet and P.A. Baisden, 1981, Acta Chem. Scand. A **35**, 653.
Mackay, A.I., I.I. Finney and R. Gotoh, 1977, Acta Crystallogr. A **33**, 98.
Madic, C., G.M. Begun, D.E. Hobart and R.L. Hahn, 1984, Inorg. Chem. **23**, 1914.
Marcus, Y., and A. Loewenschuss, 1986, J. Chem. Soc. Faraday Trans. I **82**, 2873.
Marin, B., and T. Kikindai, 1969, C.R. Acad. Sci. (Paris) C **268**, 1.
Marin, B., T. Kikindai and D. Gourisse, 1968, CEA (France), 332-1044.
Mavrodin-Tarabic, M., 1973, Rev. Roum. Chim. **18**, 73.
Mavrodin-Tarabic, M., 1974, Rev. Roum. Chim. **19**, 1461.
McKay, H.A.C., and J.L. Woodhead, 1964, J. Chem. Soc., p. 717.
Mefod'eva, M.P., N.N. Krot, T.V. Afans'eva and A.D. Gelman, 1974, Izv. Akad. Nauk SSSR, Ser. Khim. **10**, 2370.
Metivier, H., and R. Guillaumont, 1976, J. Inorg. & Nucl. Chem. Suppl., p. 179.
Mikhailov, Yu.N., A.S. Kanishcheva, L.A. Zemskova, V.A. Mistryukov, N.T. Kuznetsov and K.A. Solintsev, 1982, Russ. J. Inorg. Chem. **27**, 343.
Mikheev, N.B., 1984, Inorg. Chim. Acta **94**, 241.
Moret, E., F. Nicolo and J.-C.G. Bünzli, 1991, J. Less-Common Met. **71**, 273.
Morss, L.R., 1976, Chem. Rev. **76**, 827.
Morss, L.R., and X.X. McCue, 1976, J. Chem. Eng. Data **21**, 337.
Morss, L.R., J. Fuger, J. Goffart and R.G. Haire, 1983, Inorg. Chem. **22**, 1993.
Nabivanets, B.I., and L.N. Kudritskaya, 1964, Ukr. Khim. Zh. **30**, 891.
Nair, G.M., K. Chander and J.K. Joshi, 1982, Radiochim. Acta **30**, 37.
Narten, A.H., and R.L. Hahn, 1982, Science **217**, 1249.
Nikolceva, N., 1978, Tzv. Sib. Otd. Akad. Nauk SSSR, Ser. Khim. **N4**, g1.
Nugent, L.J., 1970, J. Inorg. & Nucl. Chem. **32**, 3485.

Nugent, L.J., R.D. Baybarz, J.L. Burnett and J.L. Ryan, 1973a, J. Phys. Chem. **77**, 1528.
Nugent, L.J., J.L. Burnett and L.R. Morss, 1973b, J. Chem. Thermodyn. **5**, 665.
O'Connor, P.R., 1944, Metallurgical Project Report CN-2083 (Chicago).
Padova, J., 1967, J. Phys. Chem. **71**, 1967.
Pan, K., and T.M. Hseu, 1955, Bull. Chem. Soc. Jpn. **28**, 162.
Passynski, A., 1938, Acta Phys. Chim. **8**, 385.
Perry, D.L., H. Ruben, D.H. Templeton and A. Zalkin, 1980, Inorg. Chem. **19**, 1067.
Pocev, S., and G. Johansson, 1973, Acta Chem. Scand. **27**, 2146.
Rabideau, S.W., 1957, J. Am. Chem. Soc. **79**, 3675.
Rabideau, S.W., and R.J. Kline, 1960, J. Phys. Chem. **64**, 680.
Rabideau, S.W., and J.F. Lemons, 1951, J. Am. Chem. Soc. **73**, 2895.
Rabinowitch, E., and R.L. Belford, 1964, Spectroscopy and Photochemistry of Uranyl Compounds (Pergamon Press, New York) ch. 2.
Rai, D., R.G. Strickert, D.A. Moore and J.L. Ryan, 1983, Radiochim. Acta **33**, 201.
Rai, D., A.R. Felmy and J.L. Ryan, 1990, Inorg. Chem. **29**, 260.
Rai, D.K., R.G. Strickert and D.A. Moore, 1982, Report PNL-SA 10635 (Pacific Northwest Laboratory).
Rao, V.K., G.R. Mahajan and P.R. Natarajan, 1987, Inorg. Chim. Acta **128**, 131.
Ritger, P.L., J.H. Burns and G. Bombieri, 1983, Inorg. Chim. Acta **77**, L217.
Rizkalla, E.N., and G.R. Choppin, 1991, in: Handbook on the Physics and Chemistry of Rare Earths, Vol. 15, eds K.A. Gschneidner Jr and L. Eyring (North-Holland, Amsterdam) ch. 103.
Rykov, A.G., V.Ya. Vasil'ev and N.B. Blokhin, 1971, Russ. J. Inorg. Chem. **16**, 1539.
Santos, C.O.P., E.E. Castellano, L.C. Machado and G. Vencentini, 1985, Inorg. Chim. Acta **110**, 83.
Schalinates, A.B., and A.V. Stepanov, 1972, Radiokhim. **14**, 280.
Schedin, U., 1975, Acta Chem. Scand. Ser. A **29**, 333.
Schmidt, K.H., S. Gordon, R.C. Thompson and J.C. Sullivan, 1980, J. Inorg. & Nucl. Chem. **42**, 611.
Shcherbakov, V.A., and E.V. Jorga, 1977, Chem. Abstr. **87**, 142076z.
Shcherbakov, V.A., and L.L. Shcherbakova, 1976, Radiokhimiya **18**, 207.
Siddall, T.H., and W.E. Stewart, 1967, Inorg. & Nucl. Chem. Lett. **3**, 279.
Sikka, S.K., 1969, Acta Crystallogr. A **25**, 621.
Silva, R.J., 1983, Report LBL-16690 (Lawrence Berkeley Laboratory, Berkeley, CA).
Singh, S., 1944, Z. Kristallogr. **105**, 384.
Smith, C.M., G.E. Bixby and F.L. Oetting, 1981, J. Inorg. & Nucl. Chem. **43**, 1555.
Smith, R.M., and A.E. Martell, 1976, Critical Stability Constants, Vol. 4 (Plenum Press, New York).
Solovkin, A.S., Z.N. Tsvetkova and A.I. Ivantsov, 1967, Zh. Neorg. Khim. **12**, 626.
Spedding, F.H., and K.C. Jones, 1966, J. Phys. Chem. **70**, 2450.
Spedding, F.H., and M.J. Pikal, 1966, J. Phys. Chem. **70**, 2430.
Spedding, F.H., D.A. Csejka and C.W. Dekock, 1966a, J. Phys. Chem. **70**, 2423.
Spedding, F.H., M.J. Pikal and B.O. Ayers, 1966b, J. Phys. Chem. **70**, 2440.
Spedding, F.H., J.A. Rard and V.W. Saeger, 1974, J. Chem. Eng. Data **19**, 373.
Spedding, F.H., L.E. Shiers and J.A. Rard, 1975a, J. Chem. Eng. Data **20**, 66.
Spedding, F.H., L.E. Shiers, M.A. Brown, J.L. Derer, D.L. Swanson and A. Habenschuss, 1975b, J. Chem. Eng. Data **20**, 81.
Spitsyn, V.I., V.G. Vokhmin and G.V. Ionova, 1983, Zh. Neorg. Khim. **28**, 1638.
Sullivan, J.C., and J.C. Hindman, 1959, J. Phys. Chem. **63**, 1332.
Sullivan, J.C., S. Gordon, D. Cohen, W.A. Mulac and K.A. Schmidt, 1976, J. Phys. Chem. **80**, 1684.
Sutton, J., 1952, Nature **169**, 235.
Suzuki, Y., T. Nagayama, M. Sekini, A. Mizuno and K. Tamaguchi, 1986, J. Less-Common Met. **126**, 371.
Swift, T.J., and W.G. Sayre, 1966, J. Chem. Phys. **44**, 3567.
Tanaka, F., Y. Kawasaki and S. Yamashita, 1988, J. Chem. Soc. Faraday Trans. I **84**, 1083.
Taylor, J.C., and M.H. Mueller, 1965, Acta Crystallogr. **19**, 536.
Taylor, J.C., M.H. Mueller and R.L. Hitterman, 1966, Acta Crystallogr. **20**, 842.
Ueki, T., A. Zalkin and D.H. Templeton, 1966, Acta Crystallogr. **20**, 836.
Usherenko, L.N., and N.A. Skorik, 1971, Radiokhimiya **13**, 646.
Yamaguchi, T., M. Nomura, H. Wakita and H. Ohtaki, 1988, J. Chem. Phys. **89**, 5153.

Handbook on the Physics and Chemistry of Rare Earths
Vol. 18 – Lanthanides/Actinides: Chemistry
edited by K.A. Gschneidner, Jr., L. Eyring, G.R. Choppin and G.H. Lander

Chapter 128

SOLUTION CHEMISTRY OF ACTINIDES AND LANTHANIDES

Gregory R. CHOPPIN and Emil N. RIZKALLA
Chemistry Department, The Florida State University, Tallahassee, FL 32306–3006, USA

Contents

1. Introduction 559
2. Oxidation states 561
3. Bonding in lanthanides and actinides 563
   3.1. Mössbauer studies 567
   3.2. Calorimetric studies 568
   3.3. Solvent extraction and synergistic studies 570
4. Complexation studies 571
   4.1. Inner- and outer-sphere complex formation 571
   4.2. Structure of the inner-sphere complexes 573
   4.3. Kinetics 580
      4.3.1. Redox reactions 580
      4.3.2. Substitution reactions 582
5. Summary and conclusions 585
References 586

1. Introduction

The strong similarity in the solution chemistry of the 4f and the 5f elements is most evident for the trivalent oxidation state of both families. The discovery experiments of the transplutonium actinides depended directly on this similarity as it allowed very accurate predictions of the chemical properties of the "to-be-discovered" elements. However, the actinide series is not an exact analog of the lanthanide elements. For example, while the stability of the trivalent oxidation state is a primary characteristic of all the lanthanide elements, trivalency is not the most stable state for the actinide elements of $Z = 90$–94 and 102. The greater stability of $No^{2+}_{(aq)}$ relative to $No^{3+}_{(aq)}$ is not observed in the 4f analog although Yb^{2+} can be present in reducing systems. Such differences are related to the differences in the relative energies of the (n)f, $(n+1)$d and $(n+2)$s orbitals when $n = 4$ (Ln) and 5 (An).

In both families of elements, the cations are typical hard acids. Their outermost electronic configuration resembles that of the closed-shell systems (e.g., inert gases, alkali, and alkaline-earth cations) as the inner f orbitals are largely or completely unavailable for bond formation. There is evidence for covalent bonding in actinide chemistry in the formation of the actinyl ions, AnO_2^+ and AnO_2^{2+}, in which both f and d orbitals participate in the An–O bonds, but the extent and even the existence of covalency in the bonding of simple An^{n+} species is a subject of controversy. The presence of a slight amount of covalency in lanthanide bonds has been attributed to involvement of the lanthanide 6s orbitals rather than of the 4f orbitals (Lewis et al. 1962). Differences in interactions with soft donor atoms have been the basis of a

TABLE 1
Effective ionic radii [data from Shannon (1976) and David (1986)] of lanthanide and actinide ions.

Ion	Ionic radius (Å)			Ion	Ionic radius (Å)	
	CN = 6	CN = 8	CN = 9		CN = 6	CN = 8
			Trivalent ions			
La	1.032	1.160	1.216	Ac	1.12	1.26
Ce	1.010	1.143	1.196			
Pr	0.990	1.126	1.179	Pa	1.05	1.20
Nd	0.983	1.109	1.163	U	1.028	1.160
Pm	0.970	1.093	1.144	Np	1.011	1.141
Sm	0.958	1.079	1.132	Pu	0.995	1.123
Eu	0.947	1.066	1.120	Am	0.980	1.106
Gd	0.938	1.053	1.107	Cm	0.970	1.094
Tb	0.923	1.040	1.095	Bk	0.955	1.077
Dy	0.912	1.027	1.083	Cf	0.945	1.066
Ho	0.901	1.015	1.072	Es	0.934	1.053
Er	0.890	1.004	1.062	Fm	0.922	1.040
Tm	0.880	0.994	1.052	Md	0.912	1.028
Yb	0.868	0.985	1.042	No	0.902	1.017
Lu	0.861	0.977	1.032	Lr	0.896	1.010
			Tetravalent ions			
Ce	0.87	0.97		Th	0.932	1.048
Pr	0.85	0.96		Pa	0.906	1.016
Tb	0.76	0.88		U	0.889	0.997
				Np	0.874	0.980
				Pu	0.859	0.962
				Am	0.848	0.950
				Cm	0.841	0.942
				Bk	0.833	0.932
			Pentavalent and hexavalent ions			
PaO_2^+	0.78			UO_2^{2+}		0.73
UO_2^+	0.76			NpO_2^{2+}		0.72
NpO_2^+	0.75			PuO_2^{2+}		0.71
PuO_2^+	0.74					

proposal for a greater degree of covalency in the bonding of An(III) relative to that of Ln(III) (see section 3).

The hard-acid nature of both series of elements is seen in their aqueous solution chemistry where actinide and lanthanide cations complex preferentially with hard bases such as fluoride anions or oxygen donor ligands. The absence of significant variation in ligand-field effects in the formation of these complexes in solution allows correlation of the trends in complexation thermodynamics and kinetics within both series with changes in cationic radii and effective cationic charges. The predominantly ionic character of the bonding in these complexes is reflected in a wide range of coordination numbers (four to twelve) and of symmetries as these are the result of steric and electrostatic factors with little or no evidence of bond-overlap constraints.

One aspect of similarity in the two series is the contraction of the ionic radii with increasing atomic number. For any oxidation state, the ionic radii decrease regularly along the series, due to the increase of the nuclear electric field. The variations of r_M with atomic number for the same coordination number are parallel for the lanthanides and actinides and the difference $(r_{Ln} - r_{An})$ is essentially constant from Am^{3+} to Cf^{3+} (David et al. 1985). This property allows extrapolation to obtain the values of ionic radii of the heaviest actinide elements which have not been measured (table 1) (David 1986).

2. Oxidation states

Most neutral lanthanide atoms have the electronic configuration, $4f^{n+1}\,5s^2\,5p^6\,6s^2$, and lose one 4f and the $6s^2$ electrons to form the characteristic $+3$ cations [the sum of the first three ionization energies changes over the series from 36 to 44 eV (Faktor and Hanks 1969)]. The 4f electrons are sufficiently shielded from the environment by the 5s and 5p orbitals that their contribution to valence forces is negligible. In a few cases, the energy difference between the 4f and 5d electrons is sufficiently small that changes in the environment about the cation can lead to promotion of a 4f electron to the valence shell (5d orbital). This results in formation of the tetravalent ions as in the case of Ce(IV). Alternately, the result may be the transfer of the 5d electron to a 4f orbital, leading to the formation of divalent ions (e.g., Sm^{2+}, Eu^{2+} and Yb^{2+}).

The lighter actinide elements exhibit an unusually broad range of oxidation states. The 5f electrons are much more delocalized and are energetically closer to the valence (6d and 7s) electrons (Freeman and Darby 1974, Freeman 1980, Johansson et al. 1980) than are the 4f electrons. This means smaller promotion energies of the $5f \rightarrow 6d$ transitions which results in the observed range of oxidation states. Thus, the lighter actinide ions exhibit an intermediate character between the transition elements (in which electronic and magnetic properties are satisfactorily understood in terms of delocalized or exchanged s and d valence electrons) and the lanthanide elements (in which the localized 4f electrons are essentially unaffected by chemical bonding). With the progressive filling of the 5f orbitals and the increase in the nuclear charge, the energy difference between the 5f orbitals and the outer orbitals increases. As a consequence, the 5f electrons become more localized and their participation in bonding becomes less

TABLE 2
The oxidation states of the f elements. The most common states are underlined, unstable states are listed in parentheses.

4f elements														
La	Ce	Pr	Nd	Pm	Sm	Eu	Gd	Tb	Dy	Ho	Er	Tm	Yb	Lu
		(2)	(2)		2	2			(2)	(2)		(2)	2	
3	3	3	3	3	3	3	3	3	3	3	3	3	3	3
	4	4	(4)					4	(4)					

5f elements														
Ac	Th	Pa	U	Np	Pu	Am	Cm	Bk	Cf	Es	Fm	Md	No	Lr
						(2)			(2)	(2)	2	2	2	
3	(3)	(3)	3	3	3	3	3	3	3	3	3	3	3	3
	4	4	4	4	4	4	4	4	(4)					
		5	5	5	5	5								
			6	6	6	6								
				7	7									

likely. This localization explains the marked stabilization of the trivalent oxidation state for the heavier actinides. A survey of the oxidation states in aqueous solution is presented in table 2.

In general, lower oxidation states are stabilized by acidic conditions, while higher oxidation states are favored by basic media. A point of difference between divalent lanthanides and actinides is that Eu^{2+} ($4f^7$) is more stable [the standard potential of the Eu^{3+}/Eu^{2+} couple is -0.35 V (Rard 1985)] than Yb^{2+} ($4f^{14}$) [E^0 (Yb^{3+}/Yb^{2+}) $= -1.05$ V (Morss 1994)] whereas Am^{2+} ($4f^7$) is less stable than No^{2+} ($4f^{14}$) (Penneman and Mann 1972, Penneman et al. 1971). In fact, Am^{2+} does not exist as a stable species in aqueous solution in spite of its half-filled structure. Pulse-radiolysis measurements indicate that its half life in solution is about 5 ms (Sullivan et al. 1976).

Comparison of the tetravalent states of the two families is more limited. Tetravalent cations can be obtained for a number of the actinide elements, although the (IV) state is quite unstable for the heaviest members of the series (Sullivan et al. 1976, Propst and Hyder 1970). The chemistry of the An(IV) species shows a general resemblance to that of Ce(IV). The rate of reduction follows the order $Bk^{4+} < Am^{4+} < Cm^{4+} < Cf^{4+}$ which resembles the order of thermodynamic stability as predicted from the reduction potentials of the M^{4+}/M^{3+} couples (Nugent et al. 1971).

The pentavalent and hexavalent actinides, AnO_2^+ and AnO_2^{2+}, are unique species with linear structures and very strong M–O bonds. The heptavalent oxidation states can be obtained by vigorous oxidizing agents in strongly complexing agents (Spitsyn 1985). Disproportionation reactions such as

$$2\,An^{VI} \rightarrow An^{VII} + An^{V} \quad (An = Np \text{ or } Am)$$

occur in strongly alkaline media (> 50% in 15 M NaOH). Equilibrium of this dispro-

portionation reaction of An^{VI} is established very rapidly, which is evidence of a similar structure for the An^{V}, An^{VI} and An^{VII} ions in alkaline solutions (presumably, the linear O=An=O).

The "effective charges" of the penta- and hexavalent actinyl ions were estimated from thermodynamic data using an extended Born equation (Choppin 1983b, Choppin and Rao 1984). The results obtained were +2.0, +3.3, +3.1 and +3.0 for NpO_2^{2+}, UO_2^{2+}, NpO_2^{2+} and PuO_2^{2+}, respectively. An alternative method of estimating these charges is based on an iterative manipulation of the relationships (Clarke and Rizkalla 1976)

$$I_{O-An} = 1 - e^{-0.25(X_O - X_{An})},$$

$$q = Q + n\sum I_{O-An},$$

where X_O (=3.5) and X_{An} ($\simeq$2.1) are the electronegativities of the oxygen and the actinide atoms, respectively; q is the effective charge of each atom, Q is the formal charge (+1 and +2 for penta- and hexavalent actinyls, respectively) and n is the bond order. The calculated value for the central metal atom in NpO_2^+ and UO_2^{2+} is +2.20 and +3.30, respectively, in good agreement with those listed above. These values also agree with theoretical calculations (Welch and Ellis 1976, Pershina 1992, Denning 1992).

Since the present chapter focuses on the similarities and differences in the coordination chemistry of the lanthanides and actinides, major attention is given to the solution chemistry of the common oxidation states (+2, +3 and +4) and consideration of the higher oxidation states is included only when relevant to the general discussion.

3. Bonding in lanthanides and actinides

Ligand fields of different symmetries result in different splitting patterns of the f orbitals (Friedman et al. 1964). For example, a cubic field leads to two sets of triply degenerate orbitals (t_{1u} and t_{2u}) and a non-degenerate (a_{2u}) orbital. Unsymmetrical electron occupancy of these orbitals cause further splitting of the triply degenerate sets. However, the magnitude of these CF splittings are small (ca. $\leqslant 200\,cm^{-1}$).

Weak covalency in the interactions of the f-element cations with ligands was proposed based on the resemblance between the nephelauxetic series of ligands for lanthanide and actinide ions and that for the d-transition-metal ions (Jorgenson 1957, Jorgenson et al. 1964, Sinha 1965, 1966, Sinha and Schmidtke 1965, Yatsimirskii and Kostromina 1964). The nephelauxetic scale was developed using the relationship:

$$1 - \beta = (\bar{\nu}_{aquo} - \bar{\nu}_{complex})/\bar{\nu}_{aquo},$$

where $\bar{\nu}$ is the maximum wave number of the absorption band of the Ln(III) ion. This assumes that each J value of a $4f^n$ configuration is linearly dependent on the radial integral. Based on this assumption, $\Delta\bar{\nu}/\bar{\nu}_{aquo}$ of all bands of the same lanthanide complex should be identical [$\bar{\nu}$ is the wave number of the maximum of the absorption band of the f-element ion and $\Delta\bar{\nu} = (\bar{\nu}_{aquo} - \bar{\nu}_{complex})$]. However, this is not in agreement with experimental observations (Dutt and Rahut 1970). Perturbations in electronic

spectra upon complexation were interpreted in terms of a partial charge transfer mixed into the f^n configuration. This interpretation seemed to be supported by a linear dependency of the oscillator strength of hypersensitive transitions on the net ligand basicity (Choppin et al. 1966, Gupta and Rohatgi 1970, Henrie et al. 1976). Mason et al. (1974) proposed that these spectral perturbations are due to coulombic correlation of dipoles induced in the ligands by the transition quadrupole moment of the metal ion.

Paramagnetic and diamagnetic shifts of the ^{17}O-NMR signal in aqueous solutions of the lanthanide ions were attributed by Shulman and Wyluda (1959) to electron transfer from the oxygen atom of the hydration water to the lanthanide ion. In contrast, Lewis et al. (1962) interpreted these shifts as arising from the isotropic part of the indirect-contact hyperfine interaction of the unpaired lanthanide electrons with the oxygen nuclear charge through a configuration interaction. The dependence of the magnitude of the shift on the number of the 4f electrons was interpreted as evidence for very weak covalent interaction between the oxygen 2s orbitals (or a linear combination of the 2s + 2p orbitals) and the lanthanide 6s orbital with the 4f, 5d and 6p orbitals playing, at most, a minor role in this bonding (Lewis et al. 1962).

Magnetic-susceptibility measurements of polyaminocarboxylate complexes agreed with a model of predominantly ionic interactions (Möeller and Horwitz 1959). Additional evidence for the ionic nature of the bonding in the f-element complexes is found in the linear correlation of the log of the stability constant for complexation, $\log \beta_{101}$, of a particular lanthanide with the ligand basicity (as measured by the acid constants) (Choppin 1983a) (fig. 1). This correlation holds over a wide acid range of ligand $\sum pK_a$ values for M(III) and M(IV) cations (M = An and Ln) as well as for AnO_2^+ and AnO_2^{2+}, provided that no strong steric effects are involved in the complexation.

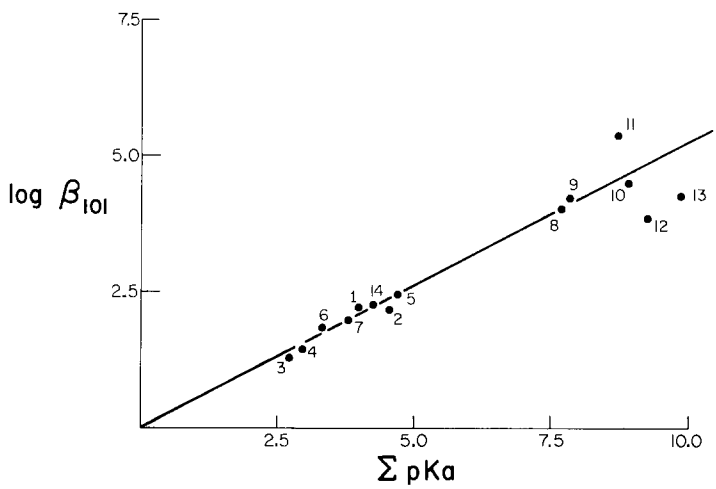

Fig. 1. Relationship between the stability constant, $\log \beta_{101}$, for the formation of Sm(III) complexes and the acid constant, $\sum pK_a$ of the ligand: 1. benzoate; 2. acetate; 3. chloroacetate; 4. iodoacetate; 5. propionate; 6. 3-nitrobenzoate; 7. 3-fluorobenzoate; 8. phthalate; 9. malonate; 10. diethylmalonate; 11. CPD; 12. trans-CHeDC; 13. cis-CHeDC; 14. p-methoxybenzoate.

The ionic model was tested by using an "extended" Born equation to calculate the free-energy change of interaction of lanthanide ions with acetate ligands (Münze 1972). The equation, in addition to the Born term, includes a "cratic" term to account for the change in the number of species upon complexation and an activity coefficient term to account for the experimental ionic strength:

$$\Delta G_{101} = \frac{Ne^2 Z_1 Z_2}{418.7 D_e d_{12}} - v\,RT \ln 55.51 + RT \sum \ln f(I),$$

where ΔG_{101} is the free energy of complexation of ML, N is Avogadro's number, e is the unit charge (4.80×10^{-10} esu), Z_1 and Z_2 are the ionic charges of the metal and the ligand, respectively, D_e is the "effective" dielectric constant, d_{12} is the distance between charge centers, v is the change in the number of reacting species and

$$\sum \ln f(I) = -[(\Delta Z^2)\, 0.511 I^{1/2}/(1 + B\mathring{a}I^{1/2})] - CI^{1/2} - DI,$$

with $\Delta Z^2 = [Z_{ML}^2 - (Z_M^2 + Z_L^2)]$; $\mathring{a} = 4.3$, $B = 0.33$, $C = 0.75$, $D = -0.15$ (Choppin and Unrein 1976).

As proposed by Münze, the equation used a temperature-dependent dielectric constant. However, in subsequent use (Choppin 1980), the dielectric constant was treated as a variable parameter dependent on the cationic charge. The values 80, 57 and 41 were estimated for D_e for complexation involving Ca^{2+}, Ln^{3+}, and Th^{4+}, respectively. Using these values, it was possible to calculate the variation of ΔG_{101} as a function of d_{12}. The results of the calculations are shown as the full curves in fig. 2 for metal-fluoride complexation while the points show the experimental data. The agreement between experimental data and the calculations was taken to support a model of strongly ionic nature in the bonding of fluoride anions to both lanthanide and actinide cations.

The same equation has been used successfully (fig. 3) to calculate the free energy of complexation of lanthanide and actinide ions by a variety of organic ligands ranging from monocarboxylates such as acetate to polyfunctional anions such as DTPA (Choppin 1983b). In these systems, an "effective anionic charge" Z_2, is set proportional to the acid constant of the carboxylate groups (i.e., to $\sum pK_a$ for polydentate ligands).

Careful inspection of the experimental data provides evidence for differences in the relative complexation strength of analogous members of the two families of f elements with the same ligands. As shown in fig. 4, the slope of $\log \beta_{AmL}$ versus $\log \beta_{NdL}$ [$r_{AmL} \simeq r_{NdL}$(from Shannon 1976)] has a value of approximately 1.1 rather than 1.0. This slight enhancement in stability of the actinide complexes may be a reflection of a slightly enhanced covalency. Several studies have sought to ascertain whether such a covalent effect is, indeed, present. Observations based on the pattern of the elution curves of actinide and lanthanide elements from columns of ion-exchange resin using chloride (Diamond et al. 1954) and thiocyanate (Surls and Choppin 1957) as the eluting solution have been interpreted as reflecting stronger An–Cl and An–N interactions. Subsequently, this was attributed to participation of the 6d and/or 7s orbitals rather than f orbitals in the bonding (Jorgenson 1980). Other studies involved synergistic reactions in solvent extraction with soft donors, calorimetric measurements of the enthalpy changes for complexation and Mössbauer chemical shifts of complexes.

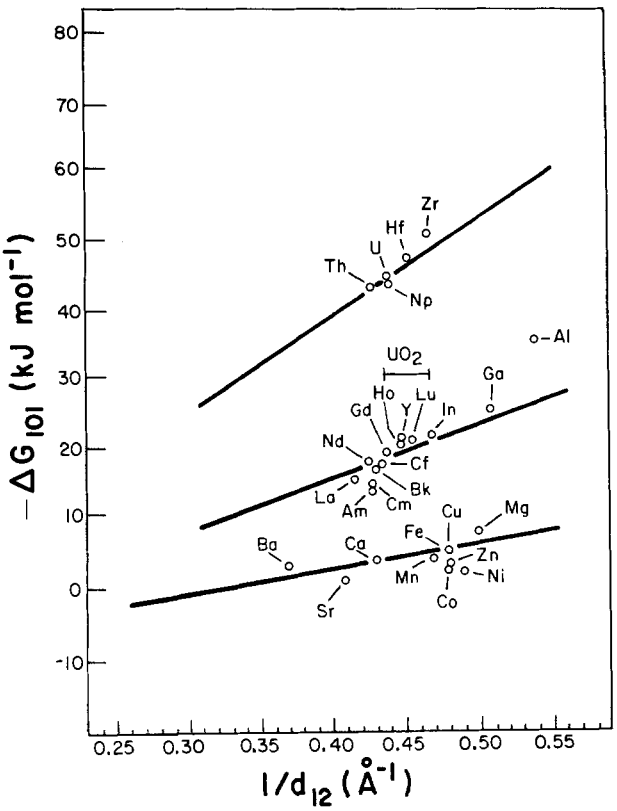

Fig. 2. The correlation of experimental values of $-\Delta G$ for formation of MF complexes with values calculated by the extended Born equation. The full curves show the calculated values as a function of $1/d_{12}$.

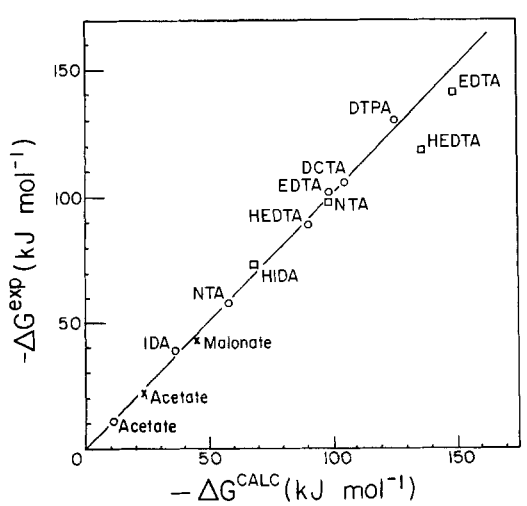

Fig. 3. Comparison of the $-\Delta G$ calculated using the extended Born equation and those obtained experimentally: ○ = Eu(III); × Th(IV); □Np(IV). The full curve has a slope of 1.

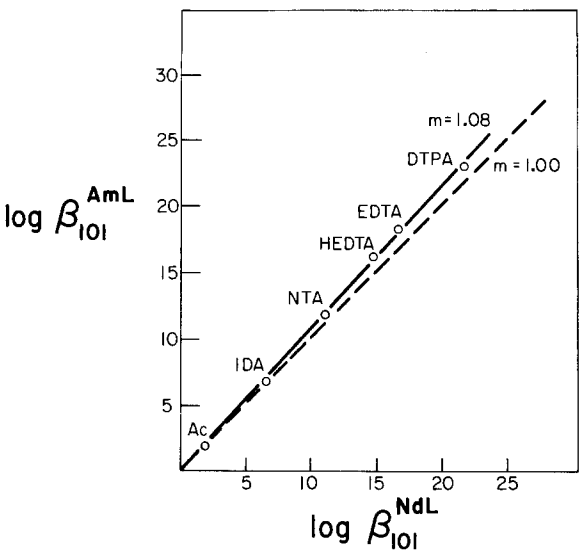

Fig. 4. Correlation of $\log\beta_{AmL}$ with $\log\beta_{NdL}$ for acetate and a series of aminocarboxylate ligands.

3.1. *Mössbauer studies*

Mössbauer chemical shifts of ^{151}Eu, ^{243}Am and ^{237}NP crystalline compounds show an increase in the range of shift values as the oxidation state is increased (fig. 5) (Friedt 1983). Relative to the lanthanide resonances, the spread of shift values for complexes of a particular oxidation state is significantly larger for the actinide cations and is comparable to that of the 4d- and 5d-transition-metal compounds (Greenwood and Gibb 1971, Friedt and Danon 1979). These observations were interpreted as qualitative evidence of covalency in the bonding of the compounds of Np and Am, due to mixing of 5d, 6d, and 7s orbitals. Some support for this interpretation was obtained from molecular cluster calculations which indicate large occupation numbers for these orbitals in comparison to the nominal values for ionic systems (Freeman and Ellis 1978, Koelling et al. 1976, Welch and Ellis 1976).

For a given valence state, the isomer shift, δ_{IS}, for actinide compounds was found to increase with increased electronegativity of the ligand, provided that the coordination number and the cluster geometry remain constant (Friedt and Danon 1979, Friedt et al. 1978). This correlation was explained by electron transfer from the ligand to the metal through the covalent interaction. The slope of the correlation line is almost zero for the trivalent state but increases as the cationic charge increases. This may reflect an increase in the degree of covalency with oxidation state.

Mössbauer measurements of ^{129}I in solid NpI_3, PuI_3, ThI_4 and UI_4 (Karraker 1987) showed essentially constant isomer shifts (δ_{IS} = 0.24, 0.35, 0.23 and 0.32 mm/s, relative to the reference zinc telluride (^{129}Te) for the four compounds, respectively) with no significant difference between tri- and tetravalent compounds. Comparison of these results to those reported for the LaI_3, GdI_3 and ErI_3 compounds (Da Costa et al. 1970, 1971) indicate large differences in the isomer shifts of the lanthanides and actinides; e.g.,

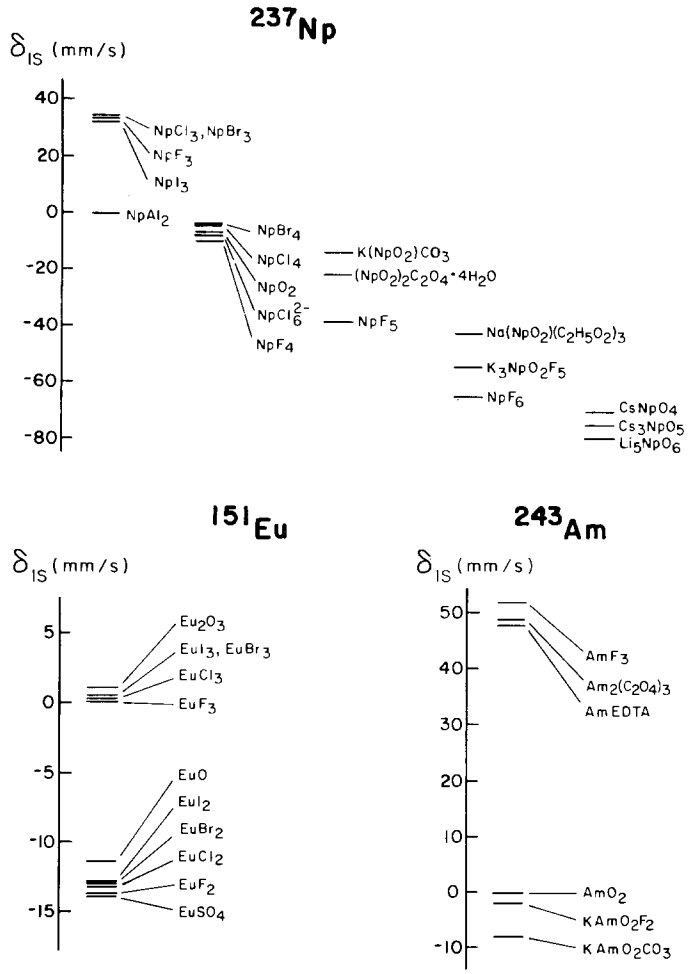

Fig. 5. Mössbauer shift data for Eu, Am, and Np compounds.

for the lanthanide iodides, δ_{IS} is approximately -0.25 mm/s. The difference of 0.5–0.60 mm/s between the two series of trivalent ions was interpreted as evidence of a greater degree of covalency in the bonding of the 5f elements relative to that of the 4f group

3.2. *Calorimetric studies*

If there is greater covalency in the bonding of actinide cations relative to that of lanthanides of the same oxidation state and ionic radius, it can be expected to be manifested in a more exothermic enthalpy of the metal–ligand bonds. For bonding to softer donor atoms such as nitrogen, this effect should be enhanced. To overcome the

difficulty of displacing the hard oxygen donors of the solvating water molecules from the primary coordination sphere of the cations in aqueous solution, donor ligands which have both hard and softer donors, such as the aminopolycarboxylates, were used in the investigation of enthalpy differences. For such ligands, the "hard" carboxylate interactions result in loss of solvate waters. The interaction of the metal with the softer donors would be reflected in a more negative (or less positive) enthalpy with little or no difference in the entropy changes. The metal–nitrogen enthalpy contribution can be estimated by:

$$\delta\Delta H_N = \Delta H_{101} - n\Delta H_{OAc}$$

In this equation, n is the number of binding carboxylates in the ligand and ΔH_{OAc} is the enthalpy change for the formation of the 1:1 metal–acetate complex. This assumes that each metal–carboxylate interaction causes the same enthalpy change as acetate complexation (Choppin et al. 1977). The residual enthalpy, $\delta\Delta H_N$, should include the extra exothermicity due to any covalency in the M–N bonding. In a test of this argument, values of $\delta\Delta H_N$ for AmL and CmL complexes versus $\delta\Delta H_N$ of the corresponding EuL complex for a number of aminocarboxylate ligands (Choppin et al. 1987, Rizkalla et al. 1989) were found to have slopes of unity, indicating no apparent differences in M–N bonding between Am(III), Cm(III) and Eu(III) outside the experimental uncertainties.

Musikas (1985) has drawn attention to the use of complexation by softer ligands to obtain improved group separations of trivalent lanthanides from trivalent actinides. Such separations have been attributed to an enhanced covalency in the actinide–ligand complex. The selectivity between analogous actinide–lanthanide pairs by a ligand was compared using the selection factor, S_f, defined by

$$S_f = (\Delta G_{An} - \Delta G_{Ln})/0.5\,(\Delta G_{An} + \Delta G_{Ln}).$$

Some typical S_f values for the Am(III)–Eu(III) complex pairs are listed in table 3. Also listed is the selection factor, S_f', which is calculated using ΔH_{An} and ΔH_{Ln} instead of the

TABLE 3
Selection factors for selected pairs of Am(III) and Eu(III) 1:1 complexes.

Ligand	S_f	S_f'	No. of M–O bonds	No. of M–N bonds	Ref.
F^-	-0.29 ± 0.02	-0.33 ± 0.17	0	0	a
Ac^-	0.03 ± 0.02	-0.04 ± 0.15	1	0	b, c
IDA^{2-}	0.06 ± 0.01	0.12 ± 0.37	2	1	b, d
NTA^{3-}	0.00 ± 0.01	0.51 ± 0.38	3	1	b, e
$EDTA^{4-}$	0.03 ± 0.01	0.10 ± 0.08	4	2	b, e
$DCTA^{4-}$	0.01 ± 0.01	0.54 ± 0.21	4	2	b
$TMDTA^{4-}$	-0.01 ± 0.01	-0.02 ± 0.12	4	2	b
N_3^-	0.16 ± 0.01	-0.11 ± 0.59	0	1	f
Phen	0.69		0	2	g
TPTZ	0.38		0	3	g

(a) Choppin and Unrein (1976); (b) Rizkalla et al. (1989); (c) Martell and Smith (1977); (d) Martell and Smith (1974); (e) Choppin and Schneider (1970); (f) Choppin and Barber (1989); (g) Musikas (1985).

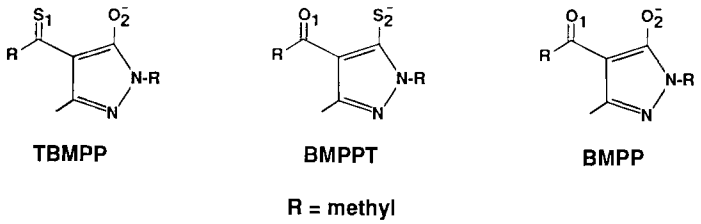

Fig. 6. Structures of TBMPP, BMPPT, and BMPP.

ΔG values. The data in table 3 indicate that hard base ligands with high electronegativity (e.g., F^- ion) interact more favorably with lanthanide cations whereas softer donors (i.e., N) have larger relative affinities toward actinide ions. These observations are consistent with slightly greater covalent interactions for actinides compared to lanthanides of comparable radius. It is interesting to note that while IDA, NTA, EDTA and DCTA have positive S'_f factors, the value for trimethylenediaminetetraacetate is negative. This is consistent with previous thermodynamic and PMR studies which showed a weakening in the metal–nitrogen interaction upon expansion of the size of the chelate ring from 5 (EDTA) to 6 (TMDTA) (Muscatello et al. 1989).

3.3. *Solvents extraction and synergistic studies*

Ligands with soft sulfur donors (fig. 6) such as TBMPP (4-thiobenzoyl-2, 4-dihydro-5-methyl-2-phenyl-3H-pyrazol-3-one) and its isomer BMPPT (4-benzyl-2, 4-dihydro-5-methyl-2-phenyl-3H-pyrazol-3-thione) (fig. 6) have been studied as extractants to enhance separation between lanthanides and actinides (Smith et al. 1987, 1989). The BMPPT ligand extracted neither Am(III) nor Eu(III) in the absence of TOPO (tri-n-isooctylphosphine oxide) but its isomer TBMPP extracted Am(III) to a small extent. For both ligands, good extraction was achieved when TOPO was also present with a larger separation factor for Am from Eu for the BMPPT isomer. Semi-empirical extended Hückel calculations and *ab initio* calculations for these anions and their oxygen analog (table 4) gave a greater charge density for the pyrazol-sulfur in BMPPT.

TABLE 4
Comparisons of atomic charges from ab initio and extended Hückel calculations.

Ligand		Charges	
		Ab initio	Extended Hückel
BMPP	O_1	−0.417	−1.256
	O_2	−0.332	−1.215
BMPPT	O_1	−0.343	−1.165
	S_2	−0.296	−1.177
TBMPP	S_1	−0.378	−1.211
	O_2	−0.230	−1.064

This presumably results in greater covalent interactions with Am(III) and may explain the increased separation factor for BMPPT + TOPO. The molecular structure of $UO_2(BMPP)_2(DMSO)$ (BMPP is 4-benzoyl-2, 4-dihydro-5-methyl-2-phenyl-3H-pyrazol-3-one) (Ryan and Jarviven 1987) showed that the U–O distances are shorter for the oxygen on the pyrazole ring than for the benzoyl oxygen, indicating a larger charge density on the former. Musikas (1985) found that in dithiophosphoric acid systems the Am(III)/Eu(III) separation is not only influenced by the nature of the soft ligand but also by the metal-to-ligand distance, which varies with the stereochemistry of the auxiliary ligand.

Measurements using the soft donor triisobutylphosphine sulfide (TIBPS) in the presence of thenoyltrifluoroacetone (TTA) showed no preferential extraction of Am(III) over Eu(III) (Wharf et al. 1990).

In summary, calorimetric data for complexation of Am(III), Cm(III) and Eu(III) with polyaminocarboxylates indicated no significant differences in the Eu–N and An–N bond strengths. Free energy, synergistic extraction, Mössbauer and spectral measurements suggest a small degree of enhanced covalency in the binding of trivalent actinides to soft donors as compared to that of lanthanides. Mössbauer-shift data indicate that the degree of covalency is quite small for trivalent elements but increases with the cationic oxidation state. All the data are consistent with the cations of both families in aqueous solutions forming predominantly ionic compounds.

4. Complexation studies

4.1. *Inner- and outer-sphere complex formation*

The structures of the solvated f-element cations and of their complexes in solution have been the subject of a large number of investigations. Most methods, however, are capable of providing only indirect evidence on the nature and structures of weak complexes in solution; e.g., data from thermodynamic (Choppin 1980), ultrasonic (Reidler and Silber 1974, Silber and Zhang 1991, Silber et al. 1972, 1990), UV-vis (Bünzli and Vucovic 1984, Bünzli and Yersin 1984) and FT-IR (Bünzli and Mabillard 1986a, b, Bünzli et al. 1982a, b, 1987, 1990) measurements. Direct structural information can be gained from NMR (Choppin 1980, Bünzli et al. 1987), luminescence (Breen and Horrocks 1983, Bünzli and Yersin 1984, Rizkalla and Choppin 1991b), X-ray diffraction (Habenschuss and Spedding 1978, 1979a, b, 1980, Johansson and Yokoyama 1990), EXAFS (Yamaguchi et al. 1988) and neutron diffraction (Narten and Hahn 1982, 1983, Annis et al. 1985, Cossy et al. 1987, 1989). The latter is based on the use of scattering measurements from two solutions containing the same complex of metal ions of different scattering powers so the RDF can be used to determine the metal–ligand interactions. Examination of the halide systems using solution X-ray diffraction (Brady 1960) revealed that the shortest Ln–Cl and Ln–I distances are 4.6 and 5.4 Å, respectively, indicating the presence of solvent-separated ion pairs. Habenschuss and Spedding (1970, 1979a, b, 1980) also found no evidence from X-ray diffraction for inner-sphere complex formation using concentrated chloride solutions (ca.

3 M). These results were disputed by other investigators (Johansson and Yokoyama 1990, Smith and Wertz 1975, Steele and Wertz 1976, 1977) who suggested that inner-sphere chloride complexation is present in concentrated chloride solutions (ca. 1 to 3 M).

Luminescence spectra of solutions containing 0.01 M $Eu(ClO_4)_3$ and varying amounts of NaCl (1–5 M) had a peak centered at 579.04 nm ($^7F_0 \rightarrow {}^5D_0$ transition) which increases in intensity with increasing halide concentration. This was taken as evidence for inner-sphere complexation with chloride ions (Breen and Horrocks 1983). The isomer shift data obtained from ^{151}Eu-Mössbauer measurements in the glassy state (Greenwood et al. 1971) supported these conclusions and were interpreted as indicating inner-sphere coordination at concentrations of chloride ions greater than 1 M. Thermodynamic (Marcus 1966), spectroscopic (Choppin et al. 1966) ^{139}La-NMR shift (Rinaldi et al. 1979) and ultrasonic absorption (Reidler and Silber 1974) data in solutions provide strong evidence for a strong dominance of outer-sphere complexation at chloride solutions ≤ 1 M.

It has been proposed (Choppin and Strazik 1965, Choppin and Ensor 1977, Khalili et al. 1988) that the thermodynamic parameters of complexation can be used as a criterion for evaluation of inner- versus outer-sphere complexation. For outer-sphere complexes, the primary hydration sphere is minimally perturbed. As a result, an exothermic enthalpy results from the cation + ligand interaction while the entropy change can be expected to be negative since the ordering of ionic charges is not accompanied by a compensatory disordering of the hydration sphere. By contrast, when inner-sphere complexes are formed, the primary hydration is sufficiently disrupted that its contribution exceeds that of the cation + ligand interaction and the result is an endothermic enthalpy and a positive entropy change. These considerations have led for trivalent lanthanides and actinides in their 1:1 complexes (i.e., ML) to assignment of predominantly outer-sphere character with Cl^-, Br^-, I^-, ClO_3^-, NO_3^- and sulfonate and of inner-sphere character with F^-, IO_3^- and SO_4^{2-} (Choppin 1971). The experimental stability constant, β_{exp} is related to β_{os} and β_{is} by

$$\beta_{exp} = \beta_{is} + \beta_{os},$$

where β_{is} and β_{os} are the stability constants for inner- and outer-sphere formation, respectively. The effect of cationic charge on the equilibrium between inner- and outer-sphere complexation by the halate and chloroacetate anions has been investigated (Choppin et al. 1991, Rizkalla et al. 1990). In the case of halate systems, the entropy for the monochlorate ($pK_a = -2.7$) was considered to indicate 100% outer-sphere character while that of the monoiodate ($pK_a = 0.7$) led to assignment of a predominantly inner-sphere character. The data for the 1:1 europium bromate (pK_a for BrO_3^- is -2.3) complex was interpreted to show a mixed nature with an outer-sphere character more dominant. Values of 40, 70, 80 and 85% ($\pm$ 10%) were estimated as the percent of outer-sphere character for the 1:1 bromate complexes of Ca^{2+}, Eu^{3+}, UO_2^{2+} and Th^{4+}, respectively. These estimates of a greater degree of outer-sphere nature in the $UO_2XO_3^+$ and $ThXO_3^{3+}$ complexes relative to $EuXO_3^{2+}$ are consistent with increased outer-sphere nature with cationic charge (recall that U in UO_2^{2+} is $\sim +3.3$).

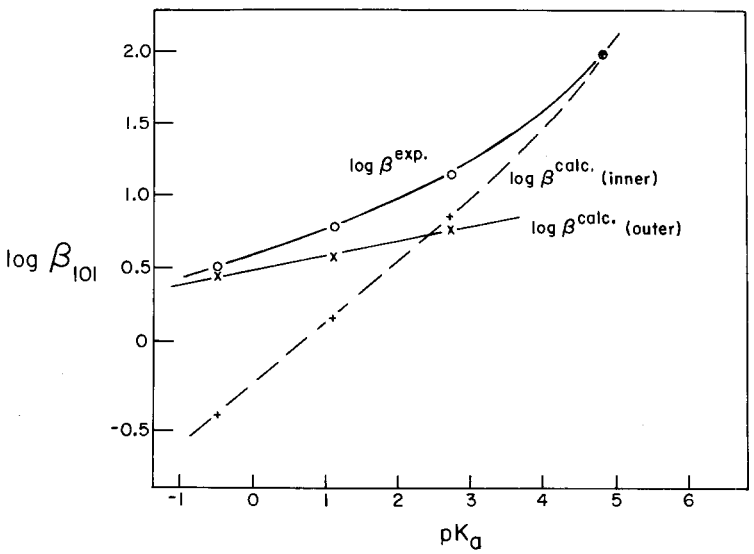

Fig. 7. Relationship between $\log\beta_{exp}$, $\log\beta_{is}$ and $\log\beta_{os}$ and the pK_a for the ligands $Cl_nCH_{3-n}COO^-$ (n=O–3).

The complexes of $Cl_nCH_{3-n}CO_2^-$ ligands were studied by ^{139}La-NMR spectroscopy (Rinaldi et al. 1979). The shift data provided estimates for inner-sphere character of 100% ($LaAc^{2+}$), 50% ($LaClAc^{2+}$), 22% ($LaCl_2Ac^{2+}$) and 0% ($LaCl_3Ac^{2+}$). These fractions agreed well with those calculated from thermodynamic data for Eu(III) and Am(III) (Choppin 1980, 1983b) using the extended Born equation (see section 3).

Figure 7 shows the relationship for 1:1 complexes between $\log\beta_{exp}$, $\log\beta_{is}$, and $\log\beta_{os}$, as a function of the ligand pK_a value. For trivalent f elements, outer-sphere complexation is dominant for 1:1 complexation with alkyl carboxylate ligands of p$K_a \leq 2$ with the degree of inner-sphere character increasing with the pK_a. A similar study of complexation by the simple alkyl monocarboxylate ligands with NpO_2^+, Eu^{3+} (or Am^{3+}), UO_2^{2+} and Th^{4+} (Khalili et al. 1988, Choppin et al. 1992b, Rizkalla et al. 1990) indicated that formation of equal amounts of inner- and outer-sphere character in the 1:1 complex would be found for ligand pK_a values of about 1.1, 3.3, 3.4 and 4.2, respectively. As with the halates, increased cation charge density favors outer-sphere formation. By contrast, an increased anionic charge of the carboxylate ligand favors an increase in inner-sphere character. The increased charge density of the cations results in stronger hydration whereas, for the lesser hydrated anions, the effects of dehydration upon complexation is less important.

4.2. *Structure of the inner-sphere complexes*

Knowledge of the structural characteristics of actinide and lanthanide complexes in solution has increased significantly in the past two decades with the observation of a

wide variety of coordination numbers and symmetries. This structural versatility arises from the lack of strong crystal-field effects (vide infra) for the 4f and 5f electronic configurations as well as from the large ionic radii of these metal ions. The ionic character of the bonding in the complexes leads to the variety of coordination numbers and symmetries as these are determined by steric and electrostatic factors. The most fundamental f element complexes in solution can be considered to be the aquated cations which are discussed in the following section.

The complexation reactions usually proceed by the Eigen mechanism (Diebler and Eigen 1959, Eigen 1963, Eigen and Tamm 1962). This mechanism involves two steps, the rapid formation of an outer-sphere association complex (i.e., an ion pair) and the subsequent rate-determining step in which the ligand displaces one or more water molecules,

$$M(H_2O)_x^{n+} + L \rightleftharpoons M(H_2O)_x^{n+}\text{--}L \longrightarrow M(H_2O)_{x-1}L^{n+} + H_2O.$$

The actual ligand interchange step may be dissociative or associative in character. For multidentate ligands (L–L), the associative steps with replacement of two coordinated waters can be represented as

$$M\begin{matrix}OH_2\\OH_2\end{matrix} + L\text{–}L \longrightarrow M\begin{matrix}OH_2\\L\text{–}L\end{matrix} \rightleftharpoons M\begin{matrix}L\\L\end{matrix}.$$

In the absence of any steric constraints, the establishment of the first bond generally, but not always, leads to rapid ring closure. As the chain distance separating the two donor atoms of the ligand increases, the rate (or probability) of ring closure decreases (Wilkins 1974, Burgess 1978). This is reflected in a decrease in $\log \beta_{101}$ and a deviation from linearity in plots of $\log \beta_{101}$ versus $\sum pK_a$. In some systems it is uncertain whether this increase in donor separation is accompanied by a change from chelation to monodentation. Luminescence lifetime measurements of Eu(III) were used to study the change in hydration upon complexation with dicarboxylate ligands $^-OOC(CH_2)_n$–COO^- ($n = 1$ to 4) (Barthelemy and Choppin 1989). The data indicated that malonate behaves strictly as a bidentate ligand whereas the release of $\simeq 1.5$ molecules of water in succinate, glutarate and adipate complexation was interpreted as reflecting equilibrium between a mixture of mono- and bidentate complex species.

The increased strain in chelation with ring expansion is also reflected in the complexation entropy. The dependence of the entropy change for the overall reaction,

$$Sm^{3+} + H_2L \rightleftharpoons SmL^+ + 2H^+$$

on ring size, defined as ΔS^*_{101}, is shown in fig. 8 (Choppin et al. 1986). The data for the dicarboxylic alicyclic ligands with the structures 1,4-cyclohexane- (CHDCA), 1,1-cyclopropane- (CPD), cis-4-cyclohexene-1,2- (cis-CHeDC) and trans-4-cyclohexene-1,2- (trans-CHeDC) (Rizkalla et al. 1991) are included to illustrate the effect of ligand rigidity on metal chelation. The decrease in ΔS^*_{101} with increased chain length was attributed to an increased loss of configurational entropy in the alkyl chain. By contrast, the greater ΔS^*_{101} value for the CHDCA complexation (ca. 40 J K^{-1} mol^{-1})

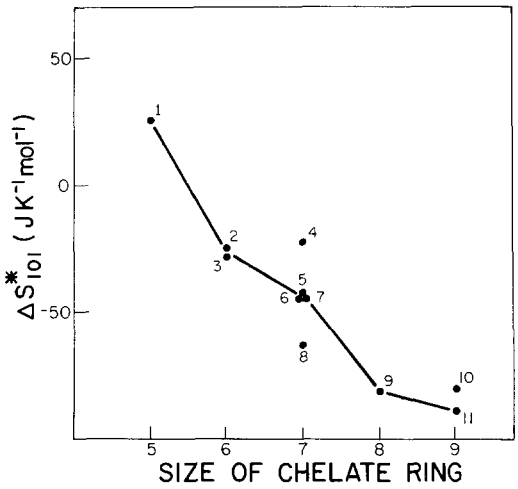

Fig. 8. Variation of the entropies of complexation ΔS^*_{101} of Sm(III) with various dicarboxylate ligands: 1. oxalate; 2. CPD; 3. malonate; 4. cis-CHeDC; 5. maleate; 6. succinate; 7. phthalate; 8. trans-CDeDC; 9. gluturate; 10. 1, 4-CHDCA; 11. adipate.

was taken as reflecting the favorable geometric orientation for chelation by the boat structure of this ligand compared to that of ligands with an alkyl chain which have no such inherently favored structure for a chelate ring. Deviation in the entropy of complexation due to configurational changes upon complexation were also observed in the systems with cis- and trans-CHeDC ligands. The twisted structure necessary for favorable carboxylate orientation in both complexes requires ca. 5.5 kJ/mol to overcome the energy barrier hindering the change from the original half-boat or half-chair configuration.

The trends for the complexes of the dioxoactinide and the tetravalent cations are remarkably similar to those for the complexes of the trivalent 4f cations as seen from the relationship of $\log \beta_{101}$ versus ring size in fig. 9. The presence of axial oxygens in UO_2^{2+} which are perpendicular to the plane of complexation seems to have very little, if any, influence on the chelation with the simple alkyl dicarboxylates.

The enhanced stability of the five-membered chelate rings relative to those of larger size is also apparent in the trend of the thermodynamic parameters for the complexation of trivalent cations by a homologous series of polyaminocarboxylate ligands (Rizkalla et al. 1988, 1989, Choppin and Muscatello 1985). These systems were analyzed, as described in section 3.2, in terms of $\delta\Delta H_n$ where

$$\delta\Delta H_n = \Delta H_{101} - n\Delta H_{101}(MAc^{2+}),$$

where n denotes the number of carboxylate groups, and ΔH_{101} the enthalpy change for complexation of MAc^{2+} (Ac = acetate). Expanding the chelate ring size from five to six in the case of lanthanide complexation by ENDPDA (ethylenediaminedi-3-propionate-diacetate) and actinide complexation by TMDTA (trimethylenediaminetetraacetate) or to seven for complexation by TMEDTA (tetramethylenediaminetetraacetate) was accompanied by a sharp decrease in the $\delta\Delta H$ values relative to those of the EDTA complex. This can be attributed to a weakening in the M–N bond associated with the

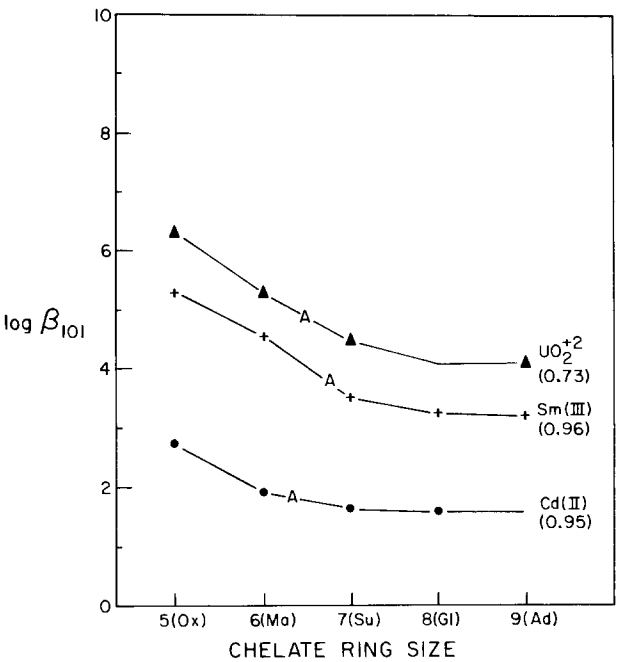

Fig. 9. The dependence of $\log \beta_{101}$ for Cd^{2+}, Sm(III) and UO_2^{2+} chelates on the ring size. The symbol A shows the value of $\log \beta_{102}$ for the diacetate complexation.

increase in chelate-chain length. Support for these conclusions was obtained from the differences of the ^{1}H-NMR spectra for ENDPDA and TMEDTA as compared to that of EDTA. The AB quartet pattern observed for the acetate protons of EDTA complexes (Day and Reilley 1964, Baisden et al. 1977, Choppin et al. 1982) was interpreted in terms of short-lived M–O bonds and long-lived M–N bonds (on the NMR time scale of ca. 10^{-4}–10^{-7} s). The M–N bond lifetime increases with increased metal charge density. For ENDPDA chelates, the change from a singlet (short M–N lifetime) to a quartet (long M–N lifetime) pattern requires a higher metal-ion charge density than for the EDTA complexes, showing that the metal–nitrogen interactions are weaker in the ENDPDA complexes. Measurements of the TMDTA and TMEDTA complexes also indicated that the Ln–N lifetime decreases (i.e., the M–N bond weakens) as the size of the ring ($\overline{\text{N–M–N}}$) increases.

The geometric structures of rigid complexes in solution can be determined from magnetic-resonance shift data. In the ML complex (L is benzene-1,2-dioxyacete), the metal was bound to the two ether oxygens ($d_{\text{Ln-O}} = 2.20$ Å) and to an oxygen of each of the carboxylate groups ($d_{\text{Ln-O}} = 2.10$ Å), all in the same plane (Kullberg and Choppin 1977). In the ML_2^- species, the metal–ether oxygen distances increased significantly (2.70 Å), indicating very weak Ln–O (ether) interaction. In these ML_2^- complexes, the metal ion was in the center of the plane of four oxygen donors from the four carboxylate groups formed by a perpendicular arrangement of the two ligands. These changes in the structural features minimize the electrostatic repulsions between the ligands and illustrate the geometrical flexibility in the f element systems. By contrast to the

lanthanide systems, the thermodynamic and NMR shift data for UO_2^{2+} (Rao and Choppin 1990) and NpO_2^+ (Choppin et al. 1992a, b) complexation are consistent with metal binding to the carboxylate oxygens with no significant interaction with the ether oxygens. This was attributed to steric interference between the axial actinyl oxygens and the oxygens of the ligand.

The molecular conformation of the solid sodium (benzene-1,2-dioxydiacetato) lanthanate(III) tetra-hydrate, $NaLaL_2 \cdot 4H_2O$, does not duplicate the structure found in solution for the LnL_2^- anion (Kerfoot et al. 1979). In aqueous solution, the sodium ion is not directly associated with the LnL_2^- complex whereas in the crystal it must be in close proximity. This results in a change in the coordination polyhedron about the lanthanum ion to an approximately s-bicapped square antiprism. In the solid, the two ligands show some puckering of the oxyacetate arms in contrast to the near planarity of the ligands in solution; the dihedral angle between both ligands decreases from ca. 90° in solution to 30° in the crystalline form.

Duplications of solid and solution structures have been noted in a few cases such as the tris(dipicolinato) lanthanate(III) complex (Donato and Martin 1972, Desreux and Reilley 1976, Albertsson 1970, 1972a–c). The D_3 symmetry determined by ^{1}H-NMR measurements is essentially similar to the symmetry observed by X-ray structure analyses of the solid chelates. The coordination polyhedron of the metal ion is a tricapped trigonal prism with the nitrogen donors occupying the capped positions. However, the bis-dipicolinatolanthanide complexes differ in solution and solid. NMR studies of the bis-dipicolinatolanthanide chelates (Ln = Ce–Dy) (Williams 1982) indicated a structure with three water molecules bonded to the central metal ions, with the two tridentate dipicolinato anions filling the coordination sphere. In crystalline $[La(DP)(HDP)(H_2O)_2] \cdot 4H_2O$, the lanthanum ion is nona-coordinate with a monocapped antiprism structure (Guerriero et al. 1987). One carboxylate oxygen of the dipicolinate ligand is shared between the neighboring lanthanum polyhedron, resulting in the formation of a polymeric chain.

Trivalent actinide ions are expected to form complexes with solution structures similar to those of the corresponding lanthanides of comparable ionic radii. Although no reports are known on the structure of trivalent actinides in solution, X-ray measurements of solid $U(HCOO)_3$ and $Pu(HCOO)_3$ indicate that the crystals are isomorphous with $Nd(HCOO)_3$ and other lanthanides (Pabst 1943, Mayer et al. 1962, Jezowska-Trzebiatowska and Drozdzynski 1969). The monoclinic tris-oxalato complexes of the Pu^{3+}, Am^{3+} and Cm^{3+}, $An_2(C_2O_4)_3 \cdot 10H_2O$, are similar to those of the lanthanides (Jenkins et al. 1963, Chackraburtty 1963, Scherer and Fochler 1968).

Th(IV) and U(IV) form insoluble $An(DP)_2 \cdot 4H_2O$ (DP is dipicolinato anion) chelates (Degetto et al. 1978). In the presence of bulky cations such as $[Ph_4As]^+$, tris-chelates of the type $(Ph_4As)_2[An(DP)_3] \cdot H_2O$ ($An = Th^{4+}$ or U^{4+}) were isolated (Degetto et al. 1978, Baracco et al. 1974). The coordination polyhedron of the bis-chelate has a bicapped square antiprismatic structure with an oxygen of each carboxylate group and four oxygens of the waters of crystallization occupying the antiprismatic corners and two nitrogen atoms located outside the midpoints of the two opposite rectangular faces of the prism. The N–An–N angle is almost linear (179°). The same ligand arrangement was duplicated approximately in $UO_2(DP)_2P \cdot 6H_2O$ (P is

the α-picolinate anion) (Cousson et al. 1991) with the uranyl axial oxygens completing the coordination sphere.

Interest in developing new lanthanide and actinide reagents has led to the synthesis of many new macrocyclics derived from cyclic polyaza and mixed polyaza–polyoxa ligands (Bünzli and Wessner 1984, Bombieri 1987, Vallarino 1989), and from cyclic and open-chain polycatecholates (Raymond et al. 1984).

Based on the similarity in radii and acidity of Pu(IV) and Fe(III), Raymond et al. (1984) proposed a biomimitic approach involving design of polycatecholates for Pu(IV) complexation which would be similar in structure to the siderophores*, highly specific iron-sequestering agents. Single crystals of the isoelectronic, isomorphous $Na_4[M(C_6H_4O_2)_4]\cdot 21H_2O$ [M = Th(IV), U(IV), Ce(IV) and Hf(IV)] compounds consists of discrete $[M(C_6H_4O_2)_4]^{4-}$ dodecahedron, a hydrogen-bonded network of waters of crystallization and sodium ions, each of which is bonded to two catecholate oxygens and four water oxygens. The structure of $Na_5[Gd(C_6H_4O_2)_4]\cdot 19H_2O$ is almost isomorphous with that of the complex of the tetravalent elements. Four 2,3-dihydroxybenzoic acid groups attached to a series of linear and cyclic tetraamines via amide linkages were prepared and their interaction with tri- and tetravalent actinides and lanthanides investigated.

The complexing agent, NN′-diheptyl-NN′-6,6-tetramethyl-4,8-dioxaundecane diamide, was used to develop a uranyl-specific ion electrode (Senkyr et al. 1979, Bertrand et al. 1983). The electrode showed good specificity over a limited range of pH for UO_2^{2+} and PuO_2^{2+} for a greater than ten-fold excess of +2 and +3 cations and a 100-fold excess of NpO_2^+, but had interference by Th^{4+} when its concentration exceeded that of the AnO_2^{2+} ions.

The solid-state structural analysis of $Eu(DOTA)^-$ (DOTA is 1,4,7,10-tetraazacyclotetradecane-1,4,7,10-tetraacetic acid) indicates that the chelate is strained, resulting in variable Eu–N bond lengths (Spirlet et al. 1984a). The Eu^{3+} cation must be too large to fit into the square conformation of the tetraazadodecane ring. Conformational studies of $La(DOTA)^-$, $Pr(DOTA)^-$ and $Eu(DOTA)^-$ by NMR indicated that these complexes have similar free energies of activation for the interconversion of the ethylenediamine protons between two staggered conformations. The complexes have axial symmetry (C_4) with a single water molecule located near the main symmetry axis on the same side of the carboxylate groups. The whole structure is rigid within the NMR time frame (Desreux 1980). Even the acetate groups remain bonded within that time frame, in contrast to the linear aminocarboxylate complexes in which the bonds of the lanthanide-acetate arms are short-lived on the NMR time scale (Baisden et al. 1977). The smaller, heavy lanthanides form stronger chelates, possibly because the diameter of the metal ion provides a better fit to the cavity size of the polyaza ring (Desreux 1980). For example, although the difference in ionic radius between Sm^{3+} and Gd^{3+} is $\simeq 0.02$ Å, the increase in $\log \beta_{101}$ is approximately two orders of magnitude (Cacheris et al. 1987). This may be, however, too simple a correlation. For example,

* Siderophores typically contain hydroxamate or catecholate functional groups which are arranged to form an octahedral cavity the exact size of a ferric iron.

although the cavity size is increased in TETA (TETA is 1,4,8,11-tetraazacyclotetradecane-1,4,8,11-tetraacetic acid), insignificant changes are found between TbTETA and TbDOTA in the metal–donor-atom distances (Spirlet et al. 1984b). The greater flexibility of the TETA ring compared to that of the DOTA ring allows TETA to wrap itself around the lanthanide ion more effectively.

Structural studies involving actinide complexation by these cyclic ligands are lacking in the literature. Thermodynamic studies of lanthanide and actinide complexation using these somewhat rigid ligands with four nitrogen donors might provide better insight into the differences in covalency of the f element–donor interactions. Unfortunately the slow kinetics in the complexation by the polyaza ligands has been a barrier to the direct calorimetry required for sufficiently accurate ΔH_{101} values.

The major distinction between lanthanides and actinides in the ability of the 5f elements to form linear dioxo cations has been discussed (section 2). These dioxo cations have the unique property of interacting with themselves and with tri- or higher-valent cations to form "cation–cation" complexes (Sullivan et al. 1961). Spectrophotometric, EMF and proton-relaxation measurements of Np(V) + U(VI) solutions (Sullivan et al. 1961) demonstrated the existence of specific interaction between the two cations with the formation of a 1:1 complex. Rykov and Frolov (1972a, b, 1975) proposed that the interaction between these cations is due to an electron transfer. This interpretation was invalidated by the absence of a solvated electron signal in the EPR spectrum in the vicinity of $g = 2.0023$ (free-electron gyromagnetic ratio) (Madic et al. 1979). The presence of magnetic splitting in the Mössbauer spectrum of the Np(V)–Cr(III) complex sorbed on Dowex-50 cation exchanger and the lack of such splitting in the corresponding Np(V)–Rh(III) complex (Karraker and Stone 1977) were interpreted as consistent with an inner-sphere structure of the type $[(H_2O)_5M^{III}\text{-}O\text{-}Np\text{-}O]^{4+}$ (Sullivan 1964, Murmann and Sullivan 1967). These authors had inferred such an inner-sphere structure from kinetic measurements of the reaction

$$\text{Np(V)Cr(III)} \xrightarrow{k} \text{Np(V)} + \text{Cr(III)}.$$

A more recent thermodynamic study obtained negative entropies and enthalpies of complexation for these reactions which seems to reflect a greater degree of hydration of the complex ion than of the individual reactants (Stout et al. 1993). This is plausible since the total positive charge of the complex leads to a higher local charge density than that of the separate reactants, which could result in an increased net ordering of the solvent molecules about the complex. Proposed structures are given in fig. 10.

Wide-angle X-ray scattering measurements (Guillaume et al. 1983) showed that the distance separating the metal centers U and Np in their U(VI)–Np(V) aqueous complex is approximately 4.2 Å, which is comparable to the value of 3.9 Å of U–U

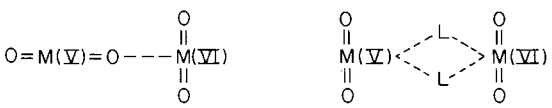

Fig. 10. Proposed structures of the "cation–cation" complexation.

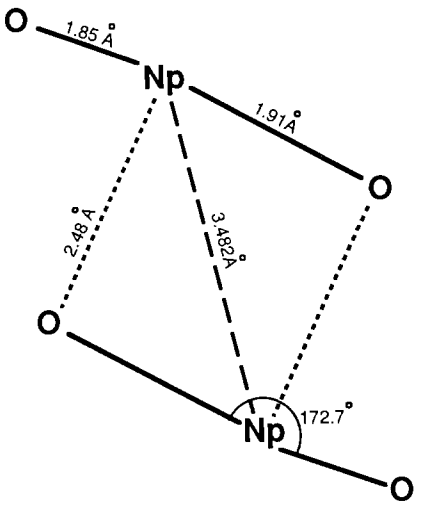

Fig. 11. Neptunyl–neptunyl dimer unit in $Na_4(NPO_2)_2C_{12}O_{12} \cdot 8H_2O$.

distance measured by the same technique for dilute, hydrolyzed UO_2^{2+} solution (Musikas and Narten 1978), and also with that measured for solid polymers of hydrolyzed UO_2^{2+} species (Aberg 1969, 1970). This prompted the suggestion that the metal ion in these complexes are not directly bound to each other but rather bridged as shown in fig. 10 in which L is H_2O or another bridging anion in solution. However, X-ray structural analysis of $Na_4(NpO_2)_2C_{12}O_{12} \cdot 8H_2O$ (Cousson et al. 1984) ($C_{12}O_{12}$ is benzenehexacarboxylate) indicated the presence of neptunyl dimers in the lattice (fig. 11) with the relatively short Np–Np distance of 3.48 Å and a distortion in the O–Np–O angle (172.7°). A magnetic transition at ca. 10 K detected in the measurement of magnetic susceptibility and the presence of a very strong magnetic field in the Mössbauer spectrum of ^{237}Np at 4.2 K (Nectoux et al. 1984) indicated some Np–Np interaction.

4.3. *Kinetics*

It is not intended in this section to provide a comprehensive review of kinetic data of lanthanide and actinide complexation reactions; the reader may consult other reviews (e.g., Lincoln 1986, Nash and Sullivan 1986). Here, we briefly outline the main conclusions with emphasis on those which shed light on differences and similarities between the two groups of f elements.

4.3.1. *Redox reactions*

The reactions of the dipositive lanthanide ions Sm(II), Yb(II) and Eu(II) with a number of non-metallic elements (Faraggi and Tendler 1972) and with Co(III), Ru(III) and Cr(III) complexes (Faraggi and Feder 1973, Christensen et al. 1973) have rate constants which follow the order Sm(II) > Yb(II) > Eu(II) and are independent of the oxidant electronic structure. This sequence agrees with that of the Ln^{II}/Ln^{III} reduction potentials, -1.55, -1.05, and -0.35 V, respectively (Morss 1994).

Evidence is strong for the prevalence of inner-sphere mechanisms in reactions in which Eu(II) ix oxidized (Fan and Gould 1974). This reduction of the isomer of $[Co(NH_3)_5(SCN)]^{2+}$, with a Co–S bond, was found to be much faster than the reduction of the isomer with Co–N bond (Adegite and Kuku 1976). This would be consistent with the greater affinity of Eu interaction with an N donor in the Co–S isomer compared to Eu–S interaction in the Co–N isomer. The rate of reduction of $[(NH_3)_5Co^{III}R]$ by Eu(II) ion was also greatly accelerated when R was an α-hydroxy acid or α-alkoxy acid as compared to complexes with R is α-mercapto substituent (Fan and Gould 1974).

The redox chemistry of Am(II), Cm(II) and Cf(II) has been studied by pulse-radiolysis techniques. The relative stability of these divalent actinides is Cf(II) > Am(II) > Cm(II). There is no obvious correlation in this order and the electronic configurations or the ionic radii of these elements (Nash and Sullivan 1986).

A comparison of the second-order rate constants for the reaction (Gordon et al. 1978)

$$M(III) + e^-_{aq} \longrightarrow M(II) \quad (M = Am \text{ or } Sm)$$

shows that Sm(III) reduces 100-times faster than Am(III). Factors normally assumed to control the reactions with hydrated electrons are the charge, ionic radii and formal potential [1.5 V for Am(II)/Am(III) and 1.56 V Sm(II)/Sm(III) couples (Hart and Anbar 1970)]. Obviously, in all three cases, the difference in the values for Sm(III) and Am(III) is insufficient to account for such a large difference in the rate constants. A greater covalent contribution by the 5f orbitals to the bonding was postulated as the cause of an increase in the free energy of formation of the activated complex of Am compared to that of Sm, resulting in a decrease in the rate of reduction of the Am complex (Gordon et al. 1978).

Oxidation of NpO_2^+ (Ekstrom and McLaren 1972), Pu^{4+} (Ekstrom and McLaren 1971) and U^{4+} (Eltantawy and Abu-Shady 1973) by Ce^{4+} was investigated in dilute-acid media. The reaction rates were interpreted in terms of a two-step mechanism,

$$An(OH)^{3+} + Ce(OH)^{3+} \xrightarrow{\text{slow}} AnO_2^+ + Ce^{3+} + 2H^+,$$

$$AnO_2^+ + Ce(OH)^{3+} \xrightarrow{\text{fast}} ANO_2^{2+} + Ce^{3+}.$$

Reactions involving An–O bond formation (step 1) are much slower than those involving simple electron exchange (step 2). Similar two-step mechanisms were proposed for the reactions of $Pu^{3+} + NpO_2^{2+}$ (Fulton and Newton 1970) and $Np^{3+} + UO_2^{2+}$ (Newton 1970); e.g.,

$$Pu^{3+} + NpO_2^{2+} \underset{}{\overset{\text{fast}}{\rightleftharpoons}} Pu^{4+} + NpO_2^+,$$

$$Pu^{3+} + NpO_2^+ \xrightarrow{\text{slow}} Pu^{4+} + Np^{4+}.$$

Comparison of the rate constants for the reaction of $[(NH_3)_5CoX]^{2+}$ with U^{3+} ($X = N_3^-$, F^-, Cl^-, Ac^-, Br^-, CN^-, NCS^-, or NH_3) led to the conclusion that the reactions proceed by an inner-sphere mechanism. The activation parameters for the analogous reaction of Np^{3+} with $(NH_3)_5RuX^{3+}$ ($X = H_2O$ and others) (Epenson and Wang 1970, Lavallee et al. 1973) supported this proposal, indicating that the formation of a seven-coordinate Ru(III) intermediate is involved. Other bridging ligands such as SO_4^{2-}, ClO_4^-, Cl^-, etc. have an accelerating effect on the reaction rate. This was attributed to a reduction in the cation–cation electrostatic repulsion through the formation of the intermediate $An^{3+} \ldots X^{t-1} \ldots M^{m+}$.

The reactions of the disproportionation of An^{4+} and AnO_2^+ cations have interesting aspects. Here, it is sufficient to note that when they involve metal–oxygen bond formation or bond breaking, they are slow; e.g.,

$$2An^{4+} + 2H_2O \longrightarrow An^{3+} + AnO_2^+ + 4H^+,$$

$$2AnO_2^+ + 4H^+ \longrightarrow An^{4+} + AnO_2^{2+} + 2H_2O.$$

However, when only electron exchange is involved in the redox, the reactions are fast; e.g.,

$$AnO_2^+ + An^{4+} \longrightarrow AnO_2^{2+} + An^{3+}.$$

4.3.2. *Substitution reactions*

Substitution reactions normally are quite rapid for complexes of both families of the f elements, reflecting the ionic nature of the bonding. Farrow and Purdie (1974) have attempted to correlate rate data for metal-complex formation obtained by transient relaxation methods with those obtained by the ultrasound absorption technique. A relaxation signal at a relatively low frequency for the Sm(III)-malonate system was attributed to rate-determining ring-closure step. The reaction was assigned the mechanism

$$Sm^{3+} + {}^-OOCCH_2COO^- \underset{k_{-1}}{\overset{k_1}{\rightleftharpoons}} [SmOOCCH_2COO]^- \underset{k_{-2}}{\overset{k_2}{\rightleftharpoons}}$$

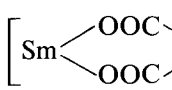

The values of $\log k_1$ and $\log k_2$ are 8.85 and 7.70, respectively. Similar conclusions were reached for the tartrate (Yun and Bear 1976), anthranilate (Silber et al. 1969) and picolinate (Erikson et al. 1987) complexation and for mixed-complex formation involving Ln(EDTA)(X) where X is a picolinate (Ekstrom et al. 1980) or a 5-sulfosalicylate anion (Ekstrom et al. 1981). The kinetic parameters for the overall reactions of these systems (Erikson et al. 1987) were consistent with the Diebler – Eigen mechanism (diebler and Eigen 1959, Purdie and Farrow 1973),

$$M(H_2O)_n^{3+} + L\text{–}L \underset{}{\overset{K_{os}}{\rightleftharpoons}} [M(H_2O)_n(L\text{–}L)]^{3+}$$

$$[M(H_2O)_n(L\text{–}L)]^{3+} \underset{k_{-1}}{\overset{k_1}{\rightleftharpoons}} [(H_2O)_{n-1}M\text{–}L\text{–}L]^{3+} + H_2O.$$

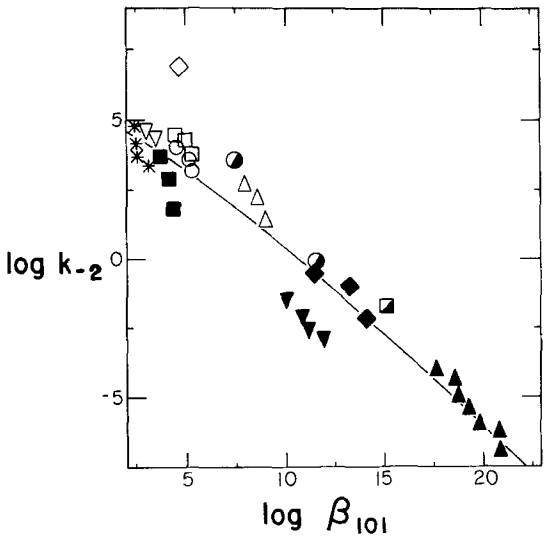

Fig. 12. Rate constant for the lanthanide-chelate ring-opening step as a function of the stability constant for several carboxylate ligands.

This is followed by the rate-determining ring-closure step,

$$[(H_2O)_{n-1}M\text{–}L\text{–}L]^{3+} \underset{k_{-2}}{\overset{k_2}{\rightleftharpoons}} \left[(H_2O)_{n-2}M\begin{matrix}L\\|\\L\end{matrix}\right]^{3+} + H_2O,$$

where,

$$k_f = K_{os}k_1k_2/(k_{-1} + k_2),$$

and

$$k_r = k_{-1}k_{-2}/(k_{-1} + k_2).$$

Assuming that $k_{-1} \gg k_2$, it follows that

$$k_f = K_{os}K_1K_2 \quad \text{and} \quad k_r = k_{-2}.$$

The values of $\log k_{-2}$ for these systems are plotted as a function of $\log \beta_{101}$ in fig. 12. Also included in this plot are the data of cyclohexanediaminetetraacetate (DCTA) (Nyssen and Margerum 1970, Möeller and Hseu 1962), 1, 7-diaza-4, 10, 13-trioxacyclopentanedecane-N, N′ -diacetate (K_{21}DA) (Chang et al. 1985, Sekhar and Chang 1986), diethylenetriaminepentaacetate (DTPA) (Brücher and Laurenczy 1981, Möeller and Thomson 1962) and EDTA (Ryhl 1972) complexation. The slope of ca. 0.6 was interpreted as reflecting a degree of bonding to the entering water molecule (Erikson et al. 1987). Using a modified Marcus equation (Cohen and Marcus 1968),

$$\Delta G^{\#} = W^r + \Delta G_0^{\#}(1 + \Delta G/4\Delta G_0^{\#})^2,$$

the values -39 ± 30 and 79 ± 30 kJ/mol were estimated for W^r and $\Delta G_0^{\#}$, respectively (W^r is the energy required to bring the reactants together in the precursor complex and $\Delta G_0^{\#}$, is the intrinsic energy barrier). In agreement with these conclusions, the ligand

exchange reaction of Nd(DTPA) + DTPA* was assigned a partially dissociative (D_A) mechanism (Asano et al. 1970) while that of Lu(DTPA) exchange was assigned a fully dissociative (D) mechanism.

The rate of the metal-ion exchange for the trivalent ions (Am, Cm, Bk, Cf and Eu) with $EuEDTA^-$ (Choppin and Williams 1973, Williams and Choppin 1974, D'Olieslager et al. 1970) and (Ce, Eu and Am) with $LaEDTA^-$ (D'Olieslager and Choppin 1971) was studied using radiotracer techniques. The exchange was found to be a first-order reversible reaction and both the forward (k_f) and the reverse (k_r) rate constants contained an acid-dependent and an acid-independent term,

$$k_f = k_A[LnEDTA^-][M^{3+}][H^+][Ln^{3+}]^{-1} + k_B[LnEDTA^-][M^{3+}],$$

and

$$k_r = k_C[H^+][MEDTA^-] + k_D[Ln^{3+}][MEDTA^-] (M \text{ is } Ln^{3+} \text{ or } An^{3+}).$$

The metal-catalyzed exchange reaction can be represented schematically as follows,

$$LnY + \rightleftharpoons Ln{\equiv}Y{-}M \rightleftharpoons (Ln{=}Y{=}M)^* \rightleftharpoons Ln{-}Y{\equiv}M \rightleftharpoons Ln + MY,$$

where (Ln=Y=′M)* is the unstable intermediate binuclear complex. The lines between Y and the cations indicate the number of carboxylate groups bound to the metal. For the acid-catalyzed mechanism, it was proposed that the first step is a rapid protonation of one of the carboxylate groups of the EDTA complex. The slow step is either (1) the dissociation of a second carboxylate group from the metal ion or (2) the transfer of a proton from the carboxylate oxygen to the nitrogen. Schematically, this mechanism is

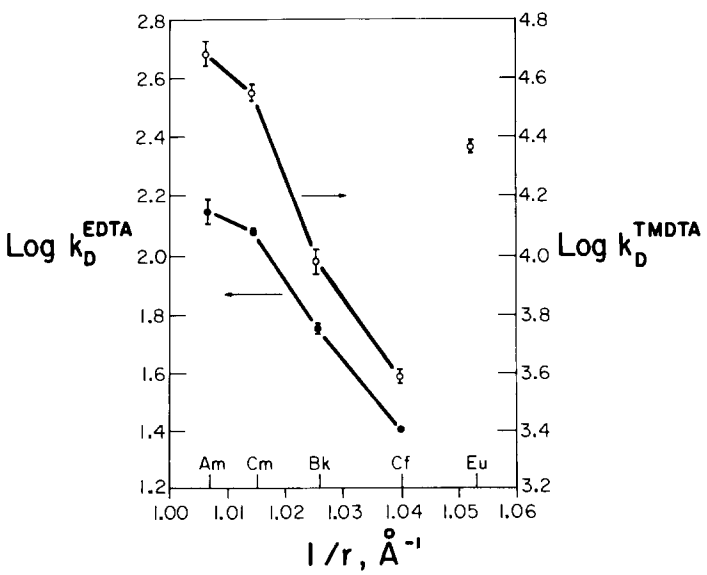

Fig. 13. Plots of the rate constants of the acid-dependent dissociation pathway of AnY^- versus $1/r$.

described by:

$$\mathrm{LnY + H} \overset{\text{fast}}{\rightleftharpoons} \mathrm{LnYH} \xrightarrow{\text{slow}} \mathrm{(LnYH)^*} \xrightarrow[(X-1)\mathrm{H^+}]{\text{fast}} \mathrm{Ln + H_xY + M}$$

$$\mathrm{MY + H} \overset{\text{fast}}{\rightleftharpoons} \mathrm{(MYH)^*} \xleftarrow{\text{slow}} \mathrm{(MYH)}$$

Similar conclusions were reached for the dissociation reaction of Am, Cm, Bk, Cf and Eu chelates of TMDTA (TMDTA is trimethylenediamine-NN′-tetraacetic acid) (Muscatello et al. 1989) and $AmDCTA^-$ (Sullivan et al. 1978).

Since the bonding in these chelates is strongly electrostatic, the rate is expected to be proportional to the charge density of the metal cation for a given ligand. Figure 13 illustrates this dependency for the EDTA and TMDTA chelates. As seen from these plots, the relative dissociation of an EDTA chelate is two orders of magnitude slower than that of the corresponding TMDTA complex. The rates for EuENDPDA dissociation were found also to be faster than that for EuEDTA (Rizkalla and Choppin 1991a). This enhancement is most likely due to the lability associated with the greater size of the

 and  rings in the ENDPDA and TMDTA complexes, respectively. A lower reaction rate of the dissociation of LnDCTA chelates is attributable to the greater stereochemical rigidity of the ligand anion.

The dissociation kinetics of Th(IV), U(IV), Np(IV) and Pu(IV) chelates with DCTA and DTPA have been reported (Nikitina et al. 1979). The rates of dissociation of the DTPA complexes were reported to be larger than for the corresponding DCTA complexes. Assuming that the operative mechanism for the dissociation of these chelates is similar to that of the trivalent-metal chelates, it would be expected that the rate of dissociation follows the order of decreasing ionic radii, i.e., Th > U > Np > Pu; however, this is not the sequence observed. At this time, no acceptable explanation has been offered for the observed sequence.

5. Summary and conclusions

This chapter has attempted to provide some understanding of the similarities and differences of the solution chemistry of the lanthanide and the actinide families of elements. The data reviewed support a model of dominant ionic interaction for both series of elements with various ligands. However, a slight enhancement in the stabilities of the 5f complexes is often observed and may be due to a slightly greater degree of covalency in the bonding of the actinide elements. This effect was found to increase with cationic charge and has not been definitely associated with the involvement of 5f orbitals.

Thermodynamic, NMR, and luminescence measurements provide information on the factors that contribute to the formation of outer- and/or inner-sphere complexation

in both families. The influence of cationic charges and ligand basicity on the nature of the complexes was discussed. Thermodynamic parameters are also used to understand the pattern in stabilities associated with differences in the size of chelate rings for these hard-acid cations. Although the 4f elements lack the rich redox chemistry of the 5f series, when a broad scope of solution chemistry is considered, the similarities in the behavior of the trivalent cations of the two families are much greater than the differences. The study of the behavior of these elements in aqueous solution has progressed rapidly in the last several decades and has served to show there is still much fruitful research to be done.

Acknowledgement

The preparation of this chapter was assisted by a grant from the USDOE-OBES Division of Chemical Sciences.

References

Aberg, M., 1969, Acta Chem. Scand. **23**, 791.
Aberg, M., 1970, Acta Chem. Scand. **24**, 2901.
Adegite, A., and T.A. Kuku, 1976, J. Chem. Soc. Dalton Trans., p. 158.
Albertsson, J., 1970, Acta Chem. Scand. **24**, 1213.
Albertsson, J., 1972a, Acta Chem. Scand. **26**, 985.
Albertsson, J., 1972b, Acta Chem. Scand. **26**, 1005.
Albertsson, J., 1972c, Acta Chem. Scand. **26**, 1023.
Annis, B.K., R.L. Hahn and A.H. Narten, 1985, J. Chem. Phys. **82**, 2086.
Asano, T., S. Okada and S. Tanigushi, 1970, J. Inorg. & Nucl. Chem. **32**, 1287.
Baisden, P.A., G.R. Choppin and B.B. Garrett, 1977, Inorg. Chem. **16**, 1367.
Baracco, L., G. Bombieri, S. Degetto, E. Forsellini, R. Graziani and G. Marangoni, 1974, Inorg. & Nucl. Chem. Lett. **10**, 1045.
Barthelemy, P.P., and G.R. Choppin, 1989, Inorg. Chem. **28**, 3354.
Bertrand, P.A., G.R. Choppin, L.F. Rao and J.-C.G. Bünzli, 1983, Anal. Chem. **55**, 364.
Bombieri, G., 1987, Inorg. Chim. Acta **139**, 21.
Brady, G.W., 1960, J. Chem. Phys. **33**, 1079.
Breen, P.J., and W.DeW. Hofrocks Jr, 1983, Inorg. Chem. **22**, 536.
Brücher, E.B., and G Laurenczy, 1981, J. Inorg. & Nucl. Chem. **43**, 2089.
Bünzli, J.-C.G., and C. Mabillard, 1986a, Inorg. Chem. **25**, 2750.
Bünzli, J.-C.G., and C. Mabillard, 1986b, J. Less-Common Met. **126**, 379.
Bünzli, J.-C.G., and M.M. Vucovic, 1984, Inorg. Chim. Acta **95**, 105.
Bünzli, J.-C.G., and D. Wessner, 1984, Coord. Chem. Rev. **60**, 191.
Bünzli, J.-C.G., and J.-R. Yersin, 1984, Inorg. Chim. Acta **94**, 301.
Bünzli, J.-C.G., J.-R. Yersin and C. Mabillard, 1982a, Inorg. Chem. **21**, 1471.
Bünzli, J.-C.G., C. Mabillard and J.-R. Yersin, 1982b, Inorg. Chem. **21**, 4214.
Bünzli, J.-C.G., A.E. Merbach and R.M. Nielson, 1987, Inorg. Chim. Acta **139**, 151.
Bünzli, J.-C.G., J.-P. Metabanzoulou, P. Froidevaux and L. Jin, 1990, Inorg. Chem. **29**, 3875.
Burgess, J., 1978, Metal Ions in Solution (Ellis Horwood, Chichester).
Cacheris, W.P., S.K. Nickle and A.D. Sherry, 1987, Inorg. Chem. **26**, 958.
Chackraburtty, D.M., 1963, Acta Crystallogr. **16**, 834.
Chang, C.A., V.O. Ochaya and V.C. Sekhar, 1985, J. Chem. Soc. Chem. Commun., p. 1724.
Choppin, G.R., 1971, Pure & Appl. Chem. **27**, 23.
Choppin, G.R., 1980, in: Lanthanide and Actinide

Chemistry and Spectroscopy, ed. N. Edelstein, ACS Symposium Series, Vol. 131 (American Chemical Society, Washington, DC).
Choppin, G.R., 1983a, J. Less-Common Met. **93**, 323.
Choppin, G.R., 1983b, Radiochim. Acta **32**, 43.
Choppin, G.R., and D.W. Barber, 1989, J. Less-Common Met. **149**, 231.
Choppin, G.R., and D.D. Ensor, 1977, J. Inorg. & Nucl. Chem. **39**, 1226.
Choppin, G.R., and A.C. Muscatello, 1985, Inorg. Chim. Acta **109**, 67.
Choppin, G.R., and L.F. Rao, 1984, Radiochim. Acta **37**, 143.
Choppin, G.R., and J.K. Schneider, 1970, J. Inorg. & Nucl. Chem. **32**, 3283.
Choppin, G.R., and W.F. Strazik, 1965, Inorg. Chem. **4**, 1250.
Choppin, G.R., and P.J. Unrein, 1976, in: Transplutonium Elements, eds W. Muller and R. Lindner (North-Holland, Amsterdam).
Choppin, G.R., and K.R. Williams, 1973, J. Inorg. & Nucl. Chem. **35**, 4255.
Choppin, G.R., D.E. Henrie and K. Buijs, 1966, Inorg. Chem. **5**, 1743.
Choppin, G.R., M.P. Goedken and T.F. Gritmon, 1977, J. Inorg. & Nucl. Chem. **39**, 2025.
Choppin, G.R., P.A. Baisden and E.N. Rizkalla, 1982, in: The Rare Earth in Modern Science and Technology, Vol. 3, eds G. McCarthy, H.B. Silber and K. Rhyne (Plenum Press, New York) p. 187.
Choppin, G.R., A. Dadgar and E.N. Rizkalla, 1986, Inorg. Chem. **25**, 3581.
Choppin, G.R., E.N. Rizkalla and J.C. Sullivan, 1987, Inorg. Chem. **26**, 2318.
Choppin, G.R., L.F. Rao, E.N. Rizkalla and J.C. Sullivan, 1992a, Radiochim. Acta **57**, 173.
Choppin, G.R., F.I. Khalili and E.N. Rizkalla, 1992b, unpublished results.
Christensen, R.J., J.H. Espenson and A.D. Butcher, 1973, Inorg. Chem. **12**, 564.
Clarke, T.A., and E.N. Rizkalla, 1976, Chem. Phys. Lett. **37**, 523.
Cohen, A.O., and R.A. Marcus, 1968, J. Phys. Chem. **72**, 4249.
Cossy, C., L. Helm and A.E. Merbach, 1987, Inorg. Chim. Acta **139**, 147.
Cossy, C., A.C. Barnes, J.E. Enderby and A.E. Merbach, 1989, J. Chem. Phys. **90**, 3254.
Cousson, A., S. Dabos, H. Abazli, F. Nectoux, M. Pagés and G.R. Choppin, 1984, J. Less-Common. Met. **99**, 233.
Cousson, A., J. Proust and E.N. Rizkalla, 1991, Acta Crystallogr. C **47**, 2065.
Da Costa Jr, M.I., E.F.R. Fraga and T. Sonnino, 1970, J. Chem. Phys. **52**, 1611.
Da Costa Jr, M.I., P.D.R. Andrade and P. Viccaro, 1971, J. Rev. Brasil Fis. **1**, 337.
David, F., 1986, J. Less-Common Met. **121**, 29.
David, F., B. Fourest and J. Duplessis, 1985, J. Nucl. Mater. **130**, 273.
Day, R.J., and C.N. Reilley, 1964, Anal. Chem. **36**, 1073.
Degetto, S., L. Baracco, R. Graziani and E. Celon, 1978, Trans. Met. Chem. **3**, 351.
Dennig, R.G., 1992, private communication.
Desreux, J.F., 1980, Inorg. Chem. **19**, 1319.
Desreux, J.F., and C.N. Reilley, 1976, J. Am. Chem. Soc. **98**, 2105.
Diamond, R.M., K. Street Jr and G.T. Seaborg, 1954, J. Am. Chem. Soc. **76**, 1461.
Diebler, H., and M. Eigen, 1959, Z. Phys. Chem. (Frankfurt) **20**, 229.
D'Olieslager, W., and G.R. Choppin, 1971, J. Inorg. & Nucl. Chem. **33**, 127.
D'Olieslager, W., G.R. Choppin and K.R. Williams, 1970, J. Inorg. & Nucl. Chem. **32**, 3605.
Donato Jr, H., and R.B. Martin, 1972, J. Amer. Chem. Soc. **94**, 4129.
Dutt, N.K., and S. Rahut, 1970, J. Inorg. & Nucl. Chem. **32**, 2905.
Eigen, M., 1963, Ber. Bunsenges. Phys. Chem. **67**, 753.
Eigen, M., and K. Tamm, 1962, Z. Elektrochem. **66**, 93, 107.
Ekstrom, A., and A. McLaren, 1971, J. Inorg. & Nucl. Chem. **33**, 3511.
Ekstrom, A., and A. McLaren, 1972, J. Inorg. & Nucl. Chem. **34**, 2015.
Ekstrom, C.G., L. Nilsson, I.A. Duncan and I. Grénthe, 1980, Inorg. Chim. Acta **40**, 91.
Ekstrom, C.G., L. Nilsson and I. Grénthe, 1981, Inorg. Chim. Acta **48**, 145.
Eltantawy, Y.A., and A.I. Abu-Shady, 1973, Z. Phys. Chem. (Frankfurt) **84**, 225.
Erikson, T.E., I. Grénthe and I. Paigdomenech, 1987, Inorg. Chim. Acta **126**, 131.
Espenson, J.H., and R.T. Wang, 1970, J. Chem. Soc. Chem. Commun., p. 207.
Faktor, M.M., and R. Hanks, 1969, J. Inorg. & Nucl. Chem. **31**, 1649.
Fan, F.-R.F., and E.S. Gould, 1974, Inorg. Chem. **13**, 2639.
Faraggi, M., and A. Feder, 1973, Inorg. Chem. **12**, 236.

Faraggi, M., and Y. Tendler, 1972, J. Chem. Phys. **56**, 3287.
Farrow, M.M., and N. Purdie, 1974, Inorg. Chem. **13**, 2111.
Fluck, E., and V.I. Goldanskii, 1974, in: The Actinides: Electronic Structure and Related Properties, Vol. 2, eds A.J. Freeman and J.B. Darby Jr (Academic Press, New York) p. 196.
Freeman, A.J., 1980, Physica B **102**, 3.
Freeman, A.J., and J.B. Darby Jr, eds, 1974, The Actinides: Electronic Structure and Related Properties, Vol. 2 (Academic Press, New York).
Freeman, A.J., and D.E. Ellis, 1978, in: Mössbauer Isomer Shifts, eds G.K. Shenoy and F.E. Wagner (North-Holland, Amsterdam) p. 111.
Friedman, H.G., G.R. Choppin and D.G. Feuerbacker, 1964, J. Chem. Ed. **41**, 354.
Friedt, J.M., 1983, Radiochim. Acta **32**, 105.
Friedt, J.M., and J. Danon, 1979, Modern Physics in Chemistry (Academic Press, London) p. 196.
Friedt, J.M., G.K. Shenoy and M. Pagés, 1978, J. Phys. & Chem. Solids **39**, 1313.
Fulton, R.B., and T.W. Newton, 1970, J. Phys. Chem. **74**, 1661.
Gordon, S., W.A. Mulac, K.H. Schmidt, R.K. Sjoblom and J.C. Sullivan, 1978, Inorg. Chem. **17**, 294.
Greenwood, N.N., and T.C. Gibb, 1971, Mössbauer Spectroscopy (Chapman and Hall, London).
Greenwood, N.N., G.E. Turner and A. Vertes, 1971, Inorg. & Nucl. Chem. Lett. **7**, 389.
Guerriero, P., U. Casellato, S. Sitran, P.A. Vigato and R. Graziani, 1987, Inorg. Chim. Acta **133**, 337.
Guillaume, B., R.L. Hahn and A.H. Narten, 1983, Inorg. Chem. **22**, 109.
Gupta, S.K., and K.K. Rohatgi, 1970, J. Inorg. & Nucl. Chem. **32**, 2247.
Habenschuss, A., and F.H. Spedding, 1978, Cryst. Struct. Commun. **7**, 535.
Habenschuss, A., and F.H. Spedding, 1979a, J. Chem. Phys. **70**, 2797.
Habenschuss, A., and F.H. Spedding, 1979b, J. Chem. Phys. **70**, 3758.
Habenschuss, A., and F.H. Spedding, 1980, J. Chem. Phys. **73**, 442.
Hart, E.J., and M. Anbar, 1970, The Hydrated Electron (Wiley, New York).
Henrie, D.E., R.L. Fellows and G.R. Choppin, 1976, Coord. Chem. Rev. **18**, 199.
Jenkins, I.L., F.H. Moore and M.L. Waterman, 1963, 1382.
Jezowska-Trzebiatowska, B., and J. Drożdżyński, 1969, J. Inorg. & Nucl. Chem. **31**, 727.
Johansson, B., H.L. Skriver, M. Martensson, O.K. Andersen and D. Glotzel, 1980, Physica B **102**, 12.
Johansson, G., and H. Yokoyama, 1990, Inorg. Chem. **29**, 2460.
Jørgensen, C.K., 1957, Acta Chem. Scand. **11**, 1981.
Jørgensen, C.K., 1980, Isr. J. Chem. **19**, 174.
Jørgensen, C.K., R. Pappalardo and E. Ritterhaus, 1964, Z. Naturforsch. a **19**, 424.
Karraker, D.G., 1987, Inorg. Chem. **26**, 3816.
Karraker, D.G., and J.A. Stone, 1977, Inorg. Chem. **16**, 2979.
Kerfoot, H.B., G.R. Choppin and T.H. Kistenmacher, 1979, Inorg. Chem. **18**, 787.
Khalili, F.I., G.R. Choppin and E.N. Rizkalla, 1988, Inorg. Chim. Acta **143**, 131.
Koelling, D.D., D.E. Ellis and R.J. Bartlett, 1976, J. Chem. Phys. **65**, 3331.
Kullberg, L., and G.R. Choppin, 1977, Inorg. Chem. **16**, 2926.
Lavallee, D.K., C. Lavallee, J.C. Sullivan and E. Deutsch, 1973, Inorg. Chem. **12**, 570.
Lewis, W.B., J.A. Jackson, J.F. Lemons and H. Taube, 1962, J. Chem. Phys. **36**, 694.
Lincoln, S.F., 1986, Adv. Inorg. & Bioinorg. Mechanisms **4**, 217.
Madic, C., B. Guillaume, J.C. Morisseau and J.P. Moulin, 1979, J. Inorg. & Nucl. Chem. **41**, 1027.
Marcus, Y., 1966, J. Inorg. & Nucl. Chem. **28**, 209.
Martell, A.E., and R.M. Smith, 1974, Critical Stability Constants, Vol. 1 (Plenum Press, New York).
Martell, A.E., and R.M. Smith, 1977, Critical Stability Constants, Vol. 3 (Plenum Press, New York).
Mason, S.F., R.D. Peacock and B. Stewart, 1974, Chem. Phys. Lett. **29**, 149.
Mayer, I., M. Steinberg, F. Feigenblatt and A. Glasner, 1962, J. Phys. Chem. **66**, 1737.
Moeller, T., and E.P. Horwitz, 1959, J. Inorg. & Nucl. Chem. **12**, 49.
Moeller, T., and T.M. Hseu, 1962, J. Inorg. & Nucl. Chem. **24**, 1625.
Moeller, T., and L.C. Thomson, 1962, J. Inorg. & Nucl. Chem. **24**, 499.
Morss, L.R., 1994, this volume, ch. 122, pp. 262–263.
Münze, R., 1972, J. Inorg. & Nucl. Chem. **34**, 661.
Murmann, K., and J.C. Sullivan, 1967, Inorg. Chem. **6**, 892.

Muscatello, A.C., G.R. Choppin and W. D'Olieslager, 1989, Inorg. Chem. **28**, 993.
Musikas, C., 1985, in: Actinide/Lanthanide Separations, eds G.R. Choppin, J.D. Navratil and W.W. Schulz (World Scientific, Singapore) p. 19.
Musikas, C., and A.H. Narten, 1978, Inorg. & Nucl. Chem. Lett. **14**, 283.
Narten, A.H., and R.L. Hahn, 1982, Science **217**, 1249.
Narten, A.H., and R.L. Hahn, 1983, J. Phys. Chem. **87**, 3193.
Nash, K.L., and J.C. Sullivan, 1986, Adv. Inorg. & Bioinorg. Mechanisms **4**, 185.
Nectoux, F., H. Abazli, J. Jové, A. Cousson, M. Pagés, M. Gasperin and G.R. Choppin, 1984, J. Less-Common Met. **97**, 1.
Newton, T.W., 1970, J. Phys. Chem. **74**, 1655.
Nikitina, S.A., T.A. Dem'yanova, A.V. Stepanov, A.A. Lipeoskii and M.A. Nemtsova, 1979, J. Radioanal. Chem. **51**, 393.
Nugent, L.J., R.D. Baybarz, J.L. Burnett and J.L. Ryan, 1971, J. Inorg. & Nucl. Chem. **33**, 2503.
Nyssen, G.A., and D.W. Margerum, 1970, Inorg. Chem. **9**, 1814.
Pabst, A., 1943, J. Chem. Phys. **11**, 145.
Penneman, R.A., and J.B. Mann, 1972, J. Inorg. & Nucl. Chem., Proc. Moscow Symp. Transuranium Elements, eds V.I. Spitsyn and J.J. Katz (Pergamon Press, Oxford) p. 257.
Penneman, R.A., J.B. Mann and C.K. Jørgensen, 1971, Chem. Phys. Lett. **8**, 321.
Pershina, V., 1992, private communication.
Propst, R.C., and L. Hyder, 1970, J. Inorg. & Nucl. Chem. **32**, 2205.
Purdie, N., and M.M. Farrow, 1973, Coord. Chem. Rev. **11**, 189.
Rao, L.F., and G.R. Choppin, 1990, Inorg. Chem. **29**, 3589.
Rard, J.A., 1985, Chem. Rev. **85**, 555.
Raymond, K.N., G.E. Freeman and M.J. Koppel, 1984, Inorg. Chim. Acta **94**, 193.
Reidler, J., and H.B. Silber, 1974, J. Phys. Chem. **78**, 424.
Rinaldi, P.L., S.A. Khan, G.R. Choppin and G.C. Levy, 1979, J. Am. Chem. Soc. **101**, 1350.
Rizkalla, E.N., and G.R. Choppin, 1991a, J. Coord. Chem. **23**, 33.
Rizkalla, E.N., and G.R. Choppin, 1991b, in: Handbook on the Physics and Chemistry of Rare Earths, Vol. 15, eds K.A. Gschneidner Jr and L. Eyring (North-Holland, Amsterdam) ch. 103.
Rizkalla, E.N., C. Niu and G.R. Choppin, 1988, Inorg. Chim. Acta **146**, 135.
Rizkalla, E.N., J.C. Sullivan and G.R. Choppin, 1989, Inorg. Chem. **28**, 909.
Rizkalla, E.N., F. Nectoux, S. Dabos-Seignon and M. Pagés, 1990, Radiochim. Acta **51**, 151.
Rizkalla, E.N., G.R. Choppin and S. Lis, 1991, unpublished results.
Ryan, R.R., and G.D. Jarvinen, 1987, Acta Crystallogr. C **43**, 1295.
Ryhl, T., 1972, Acta Chem. Scand. **26**, 3955.
Rykov, A.G., and A.A. Frolov, 1972a, Radiokhimiya **14**, 709.
Rykov, A.G., and A.A. Frolov, 1972b, Radiokhimiya **14**, 717.
Rykov, A.G., and A.A. Frolov, 1975, Radiokhimiya **17**, 187.
Scherer, V., and M. Fochler, 1968, J. Inorg. & Nucl. Chem. **30**, 1433.
Sekhar, V.C., and C.A. Chang, 1986, Inorg. Chem. **25**, 2061.
Senkyr, J., D. Ammann, P.C. Meier, W.E. Morf, E. Pretsch and W. Simon, 1979, Anal. Chem. **51**, 786.
Shannon, R.D., 1976, Acta Crystallogr. A **32**, 751.
Shulman, R.G., and B.J. Wyluda, 1959, J. Chem. Phys. **30**, 335.
Silber, H.B., and Y. Zhang, 1991, Eur. J. Solid State & Inorg. Chem. **28**, 267.
Silber, H.B., R.D. Farina and J.H. Swinehart, 1969, Inorg. Chem. **8**, 819.
Silber, H.B., N. Scheinin, G. Atkinson and J.J. Grecsek, 1972, J. Chem. Soc., Faraday Trans. I **68**, 1200.
Silber, H.B., R. Bakhshandehfar, L.A. Contraras, F. Gaizer and M. Gonsalves, 1990, Inorg. Chem. **29**, 4473.
Sinha, S.P., 1965, J. Inorg. & Nucl. Chem. **27**, 115.
Sinha, S.P., 1966, Spectrochim. Acta **22**, 57.
Sinha, S.P., and H.H. Schmidtke, 1965, Mol. Phys. **10**, 7.
Smith, B.F., G.D. Jarvinen, G.G. Miller, R.R. Ryan and E.J. Peterson, 1987, Solv. Extr. & Ion Exch. **5**, 895.
Smith, B.F., G.D. Jarvinen, M.M. Jones and P.J. Hay, 1989, Solv. Extr. & Ion Exch. **7**, 749.
Smith, L.S., and D.L. Wertz, 1975, J. Am. Chem. Soc. **97**, 2365.
Spirlet, M.R., J. Rebizant, J.F. Desreux and

M.F. Loncin, 1984a, Inorg. Chem. **23**, 359.
Spirlet, M.R., J. Rebizant, M.F. Loncin and J.F. Desreux, 1984b, Inorg. Chem. **23**, 4278.
Spitsyn, V.I., 1985, Russ. J. Radiochem. **27**, 221.
Steele, M.L., and D.L. Wertz, 1976, J. Am. Chem. Soc. **98**, 4424.
Steele, M.L., and D.L. Wertz, 1977, Inorg. Chem. **16**, 1225.
Stout, B.E., G.R. Choppin, F. Nectoux and M. Pagés, 1993, Radiochim. Acta **69**, 65.
Sullivan, J.C., 1964, Inorg. Chem. **3**, 315.
Sullivan, J.C., J.C. Hindman and A.J. Zielan, 1961, J. Am. Chem. Soc. **83**, 3373.
Sullivan, J.C., S. Gordon, W.A. Mulac, K.H. Schmidt, D. Cohen and R.K. Sjoblom, 1976, Inorg. & Nucl. Chem. Lett. **12**, 599.
Sullivan, J.C., K.L. Nash and G.R. Choppin, 1978, Inorg. Chem. **17**, 3374.
Surls, J.P., and G.R. Choppin, 1957, J. Inorg. & Nucl. Chem. **4**, 62.
Vallarino, L.M., 1989, J. Less-Common Met. **149**, 121.
Welch, P.E., and D.E. Ellis, 1976, J. Chem. Phys. **65**, 2387.
Wharf, R.M., G.R. Choppin and D.J. Pruett, 1990, Solv. Extr. & Ion Exch. **8**, 615.
Wilkins, R.G., 1974, The Study of Kinetics and Mechanisms of Reactions of Transition Metal Complexes (Allyn and Bacon, Boston).
Williams, K.R., and G.R. Choppin, 1974, J. Inorg. & Nucl. Chem. **36**, 1849.
Williams, R.J.P., 1982, Structure and Bonding, Vol. 50 (Springer, Berlin) p. 79.
Yamaguchi, T., M. Numora, H. Wakita and H. Ohtaki, 1988, J. Chem. Phys. **89**, 5153.
Yatsimirskii, K.B., and N.A. Kostromina, 1964, Russ. J. Inorg. Chem. **9**, 971.
Yun, S.S., and J.L. Bear, 1976, J. Inorg. & Nucl. Chem. **38**, 1041.

Handbook on the Physics and Chemistry of Rare Earths
Vol. 18 – Lanthanides/Actinides: Chemistry
edited by K.A. Gschneidner, Jr., L. Eyring, G.R. Choppin and G.H. Lander

Chapter 129

THE BIOCHEMISTRY OF THE f-ELEMENTS

John R. DUFFIELD
Department of Chemistry, The Manchester Metropolitan University, Manchester M1 5GD, UK;

David M. TAYLOR
Institute for Pharmacology (Toxicology), University of Heidelberg, W-6900 Heidelberg, Germany; and School of Chemistry and Applied Chemistry, University of Wales College of Cardiff, Cardiff CF1 3TB, UK;

David R. WILLIAMS
School of Chemistry and Applied Chemistry, University of Wales College of Cardiff, Cardiff CF1 3TB, UK

Contents

1. Introduction 592
1.1. A brief overview of germane aspects of lanthanide and actinide chemistry 592
1.2. Properties of the lanthanide elements 593
1.2.1 Absorption of radiant energy 594
1.2.2 Luminescence behaviour 594
1.2.3 Paramagnetism 594
1.3. Properties of the actinide elements 595
1.4. Actinide reduction–oxidation behaviour 596
1.5. Reduction–oxidation equilibria 597
1.6. Why study actinide biochemistry? 597
1.7. Actinide complexation phenomena including hydrolysis reactions 598
1.8. Hydrolysis 598
2. Route of entry of actinides into man 599
2.1. Initial physicochemical form on route of entry 599
2.2. Gastrointestinal uptake 600
2.3. Exposure by inhalation 601
2.4. Absorption through intact skin 602
2.5. Absorption from wounds 602
3. Biodistribution and biokinetics of the f elements 603
4. Biochemistry in the body compartments 605
4.1. Reactions in blood plasma 605
4.1.1. Binding to transferrin 606
4.1.1.1. The mechanisms of actinide/lanthanide binding to transferrin may not be the same as that for iron(III) 608

4.1.1.2. The differences may be due to changes in protein conformation upon metal ion binding 608
4.1.2. Binding to albumin 609
4.2. Low molecular mass fractions 610
4.3. Chemical speciation modelling 610
4.4. Reactions with cellular and other proteins 611
4.4.1. Reactions with ferritin 611
4.4.2. Reactions with bone proteins 612
4.4.3. Reactions with other proteins 612
4.5. Interactions between f elements and chelators in vivo 613
5. Lanthanides as actinide analogues for biokinetic studies 616
6. Conclusion 617
References 617

1. Introduction

In spite of the fact that the f-block elements, the members of the lanthanide and actinide transition series, have no known essential role in life processes (Williams 1988), they pose some of the most fascinating, challenging and important chemical and biochemical problems of all the inorganic elements of the periodic table.

The reasons for this, primarily, stem from the properties conferred by their outer-electron configurations and associated energy levels coupled with their chemical toxicities, which are low for the lanthanides, and with their radiotoxicities, which are a major problem for the actinides. Unfortunately, in the latter case, relatively straightforward issues may become obscured because of the public and political concern generated over radioactive waste and the effects of nuclear weapon fallout. This is not the place to discuss such issues but clear and well-argued scientific methodology can only help to allay the concerns, and correct the misapprehensions, of all but the most intransigent of individuals.

This and following sections aims to highlight important aspects of lanthanide and actinide chemistry which impinge upon and govern biochemical considerations and interactions.

1.1. *A brief overview of germane aspects of lanthanide and actinide chemistry*

In recent years the scientific literature reporting and reviewing aspects of lanthanide and actinide chemistry, and biochemistry, has expanded to a great extent, reflecting the importance and challenge represented by these elements. Because of this, the literature cited here has been restricted to that judged to be most relevant, significant and timely in the subject area. With respect to actinide chemistry three publications have proved to be most informative and useful as sources (Katz et al. 1986a, Seaborg and Loveland 1990a, National Research Council 1983).

Many aspects of lanthanide and actinide chemistry and biochemistry overlap and common themes can be identified in both chemical and biological systems. In addition, due in part to actinide-element radiotoxicity, much effort has been, and is being,

expended on elucidating the prospects of using lanthanide elements as realistic chemical analogues and biomimetic agents for the actinide elements (Delgarno 1988, Krauskopf 1986, Choppin 1986, Evans 1990). It is useful, therefore, to consider the biochemistry of the f-elements in terms of a "compare and contrast" type of approach. First, however, for the sake of clarity the basic and important physicochemical properties of the lanthanide and actinide elements will be considered separately.

1.2. *Properties of the lanthanide elements*

The lanthanide transition series starts with lanthanum (atomic number 57) and continues through to lutetium (atomic number 71). Some pertinent chemical properties are given in table 1. Here it can be seen that progress along the transition series involves successive filling of the 4f atomic orbitals. It is also apparent that the lanthanide ionic radii for the Ln^{3+} ion* decrease with increasing atomic number, an observation known as the lanthanide contraction. It is the convergence/confluence of these intrinsic properties which account for the biological significance and potential usefulness of the lanthanides even though no essentiality of the elements for life has been demonstrated. These properties and their significance have been reviewed extensively in two recent books (Evans 1990, Bünzli and Choppin 1989) and numerous review articles and scientific papers (Suzuki et al. 1989, Meares and Wensel 1984, Hider and Hall 1991,

TABLE 1
Electron configuration and ionic radius data for the lanthanide elements.

Lanthanide	Atomic number	Electron configuration		Ionic radius (nm)
		Ground state (Ln^0)	Ionic (Ln^{3+})	(coordination number = 6)
Lanthanum[a] (La)	57	[Xe] $5d^1\,6s^2$	[Xe]	0.1032
Cerium (Ce)	58	[Xe] $4f^2\,6s^2$	[Xe] $4f^1$	0.101
Praseodymium (Pr)	59	[Xe] $4f^3\,6s^2$	[Xe] $4f^2$	0.099
Neodymium (Nd)	60	[Xe] $4f^4\,6s^2$	[Xe] $4f^3$	0.0983
Promethium[b] (Pm)	61	[Xe] $4f^5\,6s^2$	[Xe] $4f^4$	0.097
Samarium (Sm)	62	[Xe] $4f^6\,6s^2$	[Xe] $4f^5$	0.0958
Europium (Eu)	63	[Xe] $4f^7\,6s^2$	[Xe] $4f^6$	0.0947
Gadolinium (Gd)	64	[Xe] $4f^7\,5d^1\,6s^2$	[Xe] $4f^7$	0.0938
Terbium (Tb)	65	[Xe] $4f^9\,6s^2$	[Xe] $4f^8$	0.0923
Dysprosium (Dy)	66	[Xe] $4f^{10}\,6s^2$	[Xe] $4f^9$	0.0912
Holmium (Ho)	67	[Xe] $4f^{11}\,6s^2$	[Xe] $4f^{10}$	0.0901
Erbium (Er)	68	[Xe] $4f^{12}\,6s^2$	[Xe] $4f^{11}$	0.0890
Thulium (Tm)	69	[Xe] $4f^{13}\,6s^2$	[Xe] $4f^{12}$	0.0880
Ytterbium (Yb)	70	[Xe] $4f^{14}\,6s^2$	[Xe] $4f^{13}$	0.0868
Lutetium (Lu)	71	[Xe] $4f^{14}\,5d^1\,6s^2$	[Xe] $4f^{14}$	0.0861

[a] Moderately toxic.
[b] Toxic due to radioactivity.

*Throughout this chapter, Ln is used as a generic term for a lanthanide element whilst An is used correspondingly for an actinide element.

Sherry 1989, Lauffer 1987, Williams 1982), but it is worthwhile reiterating some of the salient features.

As outlined above, progress along the lanthanide series from element to element is characterised by successive filling of the 4f level of atomic orbitals. It should be noted and emphasised, however, that these are not the outermost atomic orbitals, as all of the lanthanides possess filled 5s, 5p and 6s orbitals, whilst some members of the series, namely lanthanum, gadolinium and lutetium, have one electron each in a 5d orbital. Thus, upon ionisation to give Ln^{3+} ions, the electrons in the 4f levels remain relatively unaffected and the properties they confer upon the lanthanide in question are undiminished. This is substantially the case even upon complexation of the Ln^{3+} ions. It is the electrons in these 4f levels and the transitions thereof which give the lanthanides their intrinsic spectroscopic and magnetic properties allowing them to be used as chemical and biochemical probes (vide infra).

1.2.1. *Absorption of radiant energy*

Due to electron transitions within the 4f level, all of the lanthanide (Ln^{3+}) ions, with the exception of lanthanum (III) and lutetium (III) which have closed-shell configurations, absorb radiation at ultraviolet or visible wavelengths of the electromagnetic spectrum. Absorptivities are not high, however, and because of shielding the absorption spectra do not, on the whole, show significant changes upon complexation of the Ln^{3+} ion.

1.2.2. *Luminescence behaviour*

This is most prominent for terbium (III) and europium (III) ions which are commonly used as luminescence probes utilising energy transfer to and from chelated metal ions (Evans 1990, Meares and Wensel 1984).

1.2.3. *Paramagnetism*

The lanthanide elements exhibit high magnetic moments due to the number of unpaired electrons in the 4f orbitals. This makes them of great practical value with respect to nuclear magnetic resonance (NMR) spectroscopy. Gadolinium(III) complexes, especially, make good NMR contrast agents because of their high magnetic moments coupled with good relaxation efficiency. This latter area of study and application has been the subject of an extensive review by Lauffer (Lauffer 1987).

The utilisation of the intrinsic properties of the lanthanides and their complexes, as described briefly above, in biological and biochemical studies have been reviewed concisely by Williams (1982).

They include the following

(1) Lanthanides can be used as heavy-atom "stains" in electron microscopy or X-ray diffraction studies.

(2) Thermodynamic properties of metal-ion binding sites, e.g., for calcium(II)*, can be elucidated through competition or exchange reactions with Ln^{3+} ions.

*Calcium, one of the most important and ubiquitous of the essential elements, has very few chemical properties which can be used to probe its biochemistry *in situ*. The lanthanides, as Ln^{3+} ions, make almost ideal biomimetic agents for calcium (II) as they are chemically hard and exhibit a range of ionic radii which encompass that of the Ca^{2+} ion (Evans 1990).

(3) Kinetic properties of biochemical reactions involving metal ions can likewise be investigated and mechanistic information gained.
(4) Fine-structural features of biological systems may be researched and defined using NMR, ESR or energy transfer leading to fluorescence.

Further applications inlude in vivo targeting and localisation of tumours using appropriate lanthanide-ion complexes (Hider and Hall 1991, Lauffer 1987).

1.3. *Properties of the actinide elements*

Table 2 shows electron-configuration and ionic-radius data relating to the elements of the actinide series. As for the lanthanides, so for the actinides in that progress along the series involves successive filling of the f level, in this case the 5f level. One important difference is that the 5f electrons are shielded to a greater extent from the nucleus of the atom than are the equivalent 4f electrons in the lanthanide series. Thus, the energy differences between the 5f, 6d and 7s electrons are less than those between the 4f, 5d and 6s electrons of the lanthanides. The resultant close proximity of the 5f, 6d and 7s energy levels in the actinide series militates towards multiple valence states for the actinide ions, particularly in the first half of the series (Katz et al. 1986b). This is in contrast to

TABLE 2
Electron configuration and ionic radius data for the actinide elements.

Actinide	Atomic number	Electron configuration [1, 2]*		Ionic radius of An^{3+} and An^{3+} ions (nm)		
		Ground state	Most stable aquo ion	[1, 2]	[3]	[4]
Actinium (Ac)	89	$[Rn]\,6d^1\,7s^2$	Ac^{3+} : [Rn]	0.112	0.1119	0.118
Thorium (Th)	90	$[Rn]6d^2\,7s^2$	Th^{4+} : [Rn]	0.094	0.0972	0.099
Protactinium (Pa)	91	$[Rn]\,5f^2\,6d^1\,7s^2$	PaO_2^+ : $[Rn]5f^0$	–	–	–
Uranium (U)	92	$[Rn]\,5f^3\,6d^1\,7s^2$	UO_2^{2+} : $[Rn]\,5f^0$	–	–	–
Neptunium (Np)	93	$[Rn]\,5f^4\,6d^1\,7s^2$	NpO_2^+ : $[Rn]\,5f^2$	–	–	–
Plutonium (Pu)	94	$[Rn]\,5f^6\,7s^2$	Pu^{4+} : $[Rn]\,5f^4$	0.086	0.0887	0.093
Americium (Am)	95	$[Rn]\,5f^7\,7s^2$	Am^{3+} : $[Rn]\,5f^6$	0.0975	0.0982	0.107
Curium (Cm)	96	$[Rn]\,5f^7\,6d^1\,7s^2$	Cm^{3+} : $[Rn]\,5f^7$	0.097	0.097	0.099
Berkelium (Bk)	97	$[Rn]\,5f^9\,7s^2$	Bk^{3+} : $[Rn]\,5f^8$	0.096	0.0949	0.098
Californium (Cf)	98	$[Rn]\,5f^{10}\,7s^2$	Cf^{3+} : $[Rn]\,5f^9$	0.095	0.0934	0.098
Einsteinium (Es)	99	$[Rn]\,5f^{11}\,7s^2$	Es^{3+} : $[Rn]\,5f^{10}$	0.094	0.0925	0.098
Fermium (Fm)	100	$[Rn]\,5f^{12}\,7s^2$	Fm^{3+} : $([Rn]\,5f^{11})$	–	–	0.097
Mendelevium (Md)	101	$([Rn]\,5f^{13}\,7s^2)$	Md^{3+} : $([Rn]\,5f^{12})$	–	0.0896	0.096
Nobelium (No)	102	$([Rn]\,5f^{14}\,7s^2)$	No^{2+} : $([Rn]\,5f^{14})$	0.105	–	0.113
Lawrencium (Lr)	103	$([Rn]\,5f^{14}\,6d^1\,7s^2)$	Lr^{3+} : $([Rn]\,5f^{14})$	–	0.0882	0.094

*() Electronic structures predicted.

References to table

[1] Shannon (1976).
[2] Katz et al. (1986c).
[3] Seaborg and Loveland (1990).
[4] Emsley (1989).

Comments

References [1] and [2] refer to a co-ordination number of six for the ionic radii quoted above.
References [3] and [4] give no indication as to relevant co-ordination numbers for ionic radii. Both refer to other reference works as sources.

the lanthanide elements for which the trivalent state is the most stable oxidation state under equivalent conditions (see table 3).

1.4. *Actinide reduction–oxidation behaviour*

From table 3, it can be seen that for the actinides in the first half of the transition series a multiplicity of valence states are possible, whilst those in the second half have a more restricted number of valence states available and have more in common with the lanthanide elements. This multiplicity of oxidation states can lead to some extremely complicated solution chemistry, but, fortunately, all of the actinides have one oxidation state which is dominant under fairly well-defined solution conditions. As a result, actinide redox behaviour is understood to a reasonable extent under physiological conditions although there are exceptions as will be discussed. It is, however, worthwhile discussing, briefly, general actinide reduction–oxidation behaviour because valence states which dominate in the environment and which impinge on biochemical/biological systems may not dominate under physiological conditions.

In general, four oxidation states from III to VI, characterised by the An^{3+}, An^{4+}, AnO_2^{+} and AnO_2^{2+} ions, respectively, can exist for some if not all of the actinides, the dominant ionic form being shown in table 2 and highlighted in table 3. Under extreme solution conditions the presence of a +7 oxidation state, corresponding to the AnO_5^{3-} ion, has been reported but this is certainly not relevant to physiological conditions. Of

TABLE 3
Lanthanide and actinide oxidation states in solution.

Number of f electrons	Valence state and associated ion type									
	Lanthanide series			Actinide series						
	II	III	IV	I	II	III	IV	V	VI	VII
0		**La^{3+}**	Ce^{4+}			**Ac^{3+}**	**Pu^{4+}**	**PaO_2^{+}**	**UO_2^{2+}**	NpO_5^{3-}
1		**Ce^{3+}**	Pr^{4+}			(Th^{3+})	Pa^{4+}	UO_2^{+}	NpO_2^{2+}	(**PuO_5^{3-}**)
2		**Pr^{3+}**	Nd^{4+}			(Pa^{3+})	U^{4+}	NpO_2^{+}	PuO_2^{2+}	AmO_5^{3-}?
3		**Nd^{3+}**				U^{3+}	Np^{4+}	PuO_2^{+}	AmO_2^{2+}	
4	Nd^{2+}	**Pm^{3+}**				Np^{3+}	**Pu^{4+}**	AmO_2^{+}	CmO_2^{2+}?	
5		**Sm^{3+}**				Pu^{3+}	Am^{4+}	CmO_2^{+}?		
6	Sm^{2+}	**Eu^{3+}**				**Am^{3+}**	Cm^{4+}			
7	Eu^{2+}	**Gd^{3+}**	Tb^{4+}		(Am^{2+})	**Cm^{3+}**	Bk^{4+}	CfO_2^{+}?		
8		**Tb^{3+}**				**Bk^{3+}**	(Cf^{4+})			
9		**Dy^{3+}**				**Cf^{3+}**	Es^{4+}?			
10	Dy^{2+}	**Ho^{3+}**			(Cf^{2+})	**Es^{3+}**				
11		**Er^{3+}**			(Es^{2+})	**Fm^{3+}**				
12		**Tm^{3+}**			Fm^{2+}	**Md^{3+}**				
13	Tm^{2+}	**Yb^{3+}**			Md^{2+}	No^{3+}				
14	Yb^{2+}	**Lu^{3+}**		Md^{1+}?	**No^{2+}**	**Lr^{3+}**				

Comments: Cations shown in bold type represent the most stable oxidation state and species for that element.
Species shown in parentheses ( ) are unstable.
Species of questionable or unconfirmed existence are shown thus: ?

the actinides, and other elements in the periodic table, plutonium is unique in that, under appropriate conditions, it can exist in all four of its lower oxidation states simultaneously (Cleveland 1970). However, under physiological conditions the plutonium(IV) valence state is stabilised (Taylor 1973a).

1.5. *Reduction–oxidation equilibria*

In certain aqueous environments the dominant valence state of an actinide may differ from that observed under in vivo conditions. For example, in sea water plutonium exists predominantly in the V and/or VI oxidation states (Watters et al. 1980, Orlandini et al. 1986), whereas in the body the IV valence state is stabilised (Taylor 1973a). An understanding of the kinetics of reversibility amongst redox states is important, therefore, in understanding and modelling (see later) actinide chemistry. Briefly, it can be stated that redox equilibria are reversible if they do not involve the subsequent removal of products from back reactions as is, generally, the case for Pu(IV). From a kinetic viewpoint, reversibility amongst redox states is rapid if the redox equilibria do not involve the making or breaking of chemical bonds. Therefore, equilibration between An^{3+}/An^{4+} and AnO_2^{+}/AnO_2^{2+} redox couples is rapidly achieved whilst equilibration between couples of the type An^{4+}/AnO_2^{+} is much slower.

1.6. *Why study actinide biochemistry?*

Before going on to consider the biochemistry of the actinides it is worth pausing to put the subject into perspective by musing upon the *raison d'etre* for studying actinide metabolism and biochemistry in the first place.

All of the actinide elements are radioactive and those radioisotopes which decay via alpha-particle emission may represent a significant hazard to health following their incorporation. In addition, the actinide elements are intrinsic to the nuclear fuel cycle both as components and as waste products. Thus, there is a risk of occupational exposure to certain categories of worker in the nuclear industry, to scientists undertaking research into the actinides and to the general public through accidental discharge into the environment (Duffield and Williams 1986). It is important, therefore, to understand actinide metabolism so that predictions can be made concerning retention and distribution in the body for the purposes of making radiological risk assessments (ICRP 1986, Taylor et al. 1989). Furthermore, the actinides are exogenous elements which have no specific or essential role in normal biochemistry. As a result, the human body has no regulatory mechanisms for sensing the presence of actinide elements in order to facilitate their quantitative excretion and significant amounts of ingested or incorporated material may be retained and deposited either at primary or secondary deposition sites (Taylor 1989a).

For non-radioactive heavy metals such immobilisation may well negate or reduce the effects of chemical toxicity. However, immobilisation does not negate radiotoxic effects and, in fact, may exacerbate them by leading to alpha-particle emission within cells near chromosomal or nuclear material. In situations like these, human intervention using chelation therapy is required, the success of which involves targeting the

chelating agent of choice to the actinide(s) in question (Duffield and Taylor 1986). This can only be achieved from a detailed understanding of actinide chemistry and biochemistry.

1.7. *Actinide complexation phenomena including hydrolysis reactions*

In the environment and body the physicochemical forms* of actinides are controlled and stabilised, to a large extent, by the presence of complexing ligands and groups (Duffield and Taylor 1986, Bulman 1978, 1980a). In biochemical systems, such moieties can range from solvent molecules to low molecular mass ligands to proteins and may include surface complexation and sorption sites associated with bone surfaces (Duffield and Taylor 1986). Therefore, an important thrust of actinide biochemistry has been, and is, to understand and elucidate the thermodynamics and kinetics of actinide binding to complexing groups.

The actinide ions, in whatever valence state, are classed as "hard" under Pearson's HSAB (hard and soft acids and bases) scheme (Pearson 1972). Oxygen-containing donor groups are, therefore, the preferred complexing moieties. In addition, bonding is predominantly ionic in character (Seaborg and Loveland 1990b). With respect to oxidation state the normal order of complexing is

$$An^{4+} > AnO_2^{2+} > An^{3+} > AnO_2^{+}.$$

At first sight this order of binding strength may seem surprising in that the VI valence state is bound more strongly than the III, but studies indicate that the effective charge on AnO_2^{2+} approximates to 3.3 (Choppin 1983).

1.8. *Hydrolysis*

Actinide-ion hydrolysis has been reviewed extensively and data is available from a wide range of sources (Baes Jr and Mesmer 1976, 1981, Phillips 1982, Smith and Martell 1976).

In general, the hydrolytic behaviour of the actinides is very complicated and, in spite of much effort, is still poorly understood with respect to both thermodynamic and kinetic factors (Waters et al. 1991). The presence of mixed hydroxy-carbonate-actinide species has been shown in solutions from which carbon dioxide has not been excluded and so there is a strong possibility that some equilibrium hydrolysis data has been "contaminated" by the presence of carbonate (Bernkopf and Kim 1984, Kim 1986). For certain of the actinides, particularly uranium, it is probable that ternary hydroxy-carbonate species exist in vivo (Bulman 1980b).

In the absence of strongly complexing ligands such as citrate or nitrilotriacetate (NTA) and at only moderately acidic pH values, hydrolysis reactions may lead to the formation of polymeric hydroxy species for An^{4+} ions (Taylor 1973a, b). These species may be colloidal in nature and whilst their presence may be confirmed, thermodynamic

*Otherwise known as *chemical speciation.*

data describing their formation is not available. With respect to predicting possible reactions this is a serious omission in our knowledge. It is noteworthy that some of the earlier studies on plutonium (IV) metabolism and biochemistry may have been marred by the unintentional use of colloidal solutions rather than of solutions in which plutonium was present in a "known" physicochemical form.

At higher actinide concentrations and in the absence of complexing agents precipitation of amorphous An(IV) hydroxides with subsequent aging to oxides occurs (Duffield et al. 1991, Morss 1986).

It is unlikely that hydrolysis reactions occur to any appreciable extent under physiological conditions in, e.g., blood plasma or any biological fluid containing strongly complexing groups. However, such reactions are important with regard to the formation and dissolution of hydroxides and oxides to which some individuals may be exposed, e.g., via inhalation of plutonium (IV) oxides (Stradling et al. 1978, Morrow et al. 1967, Cooper et al. 1978), curium oxides (Guillmette and Kanapilly 1988) or mixed oxides (Briant and Sanders 1987). Subsequent biochemistry in such cases may well be a function of the initial chemical form in which the actinide is presented as well as of the route by which the individual has become contaminated.

2. Route of entry of actinides into man

As mentioned in the previous section, the route of entry can be critical with respect to distribution and longer-term effects of actinide exposure (ICRP 1972). Four potential routes can be identified by which exposure and incorporation can occur (Brown 1988).

(1) Gastrointestinal uptake from contaminated foodstuffs or by dust particles taken in through the nose or mouth (*enteral exposure*).
(2) Inhalation of contaminated material or of actinide-compound aerosols and solids forms (*inhalation exposure*).
(3) Absorption through the skin (*percutaneous exposure*).
(4) Via cuts, wounds, burns and abrasions (*parenteral exposure* if by injection).

In the case of uptake via inhalation and/or wounds, and depending upon the initial chemical form the element(s), the lungs and/or wound site may be designated as a *primary deposition site* from which the actinide(s) will be transported to a *secondary deposition site.*

2.1. *Initial physicochemical form and route of entry*

It is most important to consider the initial chemical form in which an actinide is presented to an individual as this will to a large extent, and depending upon the route of entry, determine whether or not the element in question is bioavailable* (Barnett et al. 1989, Cooper 1986, Nenot and Stather 1979).

*The term *bioavailability* is used to denote the ability of an element to undergo gastrointestinal absorption and then to take part in the normal biochemical processes of transport, metabolism, storage and excretion.

2.2. *Gastrointestinal uptake*

Uptake of actinides *via* the oral route is perceived to be a major possible route of exposure for members of the general public and much experimental effort has gone into elucidating the factors controlling uptake (absorption) across the gut membranes into the body compartments (ICRP 1972, 1986, Bulman 1980, Taylor et al. 1986, Sullivan et al. 1985, 1986, La Touche et al. 1987). Furthermore, a number of studies and compilations have studied and quantified the uptake of actinides from a wide range of compounds in a variety of animal models (ICRP 1986, Popplewell et al. 1991a, Gilbert et al. 1988, Coughtrey et al. 1985, Long 1987, Johnson and Lamothe 1989, Bishop et al. 1989). Overall absorption is low and recommendations of f_1 values* (fractional absorption values) to be used in assessments have been put forward in ICRP publication no. 48 (1986) (Taylor 1989b). These are summarised in table 4.

Within table 4, it can be seen that with respect to occupational exposure compounds are divided into different types; on one level this is a reflection of their solubility. Thus, insoluble compounds like oxides have a very low fractional absorption indicating that their potential for passage into the body is low. This is because their initial physicochemical form renders them unsuitable for absorption.

TABLE 4

Fractional absorption values proposed, in ICRP publication no. 48 (1986), for the gastrointestinal uptake of actinide compounds.

Actinide element	Type of exposure, and compound type	f_1-value, $\times 10^4$
Plutonium	Occupational exposure	
	oxides (excluding "polydisperse" oxides)	0.1
	nitrates	1
	other compounds or unknown mixtures	10
	Population exposure (via food chains)	
	all compounds	10
Neptunium	Occupational and population exposure	
Americium	all compounds	10
Curium		
Californium		

Comments: ICRP Publication no. 48 is probably the most authoritative document with respect to gastrointestinal uptake of actinide elements. However, further information can be found in several other compilations and a number of more recent research papers, see text for details of references.

* In defining exposure via the gastrointestinal route it is very important to have a clear understanding of the accepted nomenclature: when a substance enters the gastrointestinal tract, a fraction of the substance passes through the intestinal mucosal cells and enters the bloodstream. This fraction of the ingested substance which is transferred into the blood is the *"fractional absorption"*. A certain fraction of the absorbed material is *excreted* in the urine and in the faeces (*via* the bile). The material remaining is that *retained*. When the retention in the total body, minus the gastrointestinal tract, is measured at some given time after ingestion, the measured *"fractional retention"* is smaller than the fractional absorption by the amount excreted (ICRP 1986).

Compounds such as those of the actinides with EDTA, on the other hand, may be more soluble and be absorbed more readily. However, as they do not dissociate in the blood and are excreted readily they are not retained and are not bioavailable (Duffield and Williams 1989a).

Certain of the actinide compounds, e.g., plutonium citrate complexes, are soluble, are absorbed (although even here absorption is very low) and dissociate in the body giving a relatively high fractional retention so that actinides in these initial physicochemical forms are bioavailable to a measurable extent.

Finally, it should be noted that gastrointestinal uptake cannot be considered to be purely a function of actinide speciation or initial physicochemical form. The physiological state of the individual should always be considered, e.g., with respect to fasting state or iron-deficiency status, as this may increase the f_1 value by an order of magnitude (Taylor 1989b, Sullivan and Ruemmler 1988).

2.3. *Exposure by inhalation*

Inhalation of actinide compounds is an important route of exposure which has received much study and research (ICRP 1979, 1986, Nenot and Stather 1979, Task Group on Lung Dynamics 1966, Morgan et al. 1988). Once again the initial physicochemical form of the actinide governs to a significant extent the subsequent mobilisation and rate of transport of the actinide from the primary deposition site(s) in respiratory regions to the sites of secondary deposition within the body. In addition, the initial form, particularly particle/aerosol size, also affects the area in the respiratory region in which primary deposition occurs. For the purposes of metabolic modelling, four regions of the respiratory tract have been identified and designated as compartments:

(1) the nasal passage (N-P);
(2) the tracheobronchiolar region (T-B);
(3) the pulmonary parenchyma (P); and
(4) the lung-associated lymph nodes.

A full discussion of the deposition and lung clearance characteristics of the actinides is beyond the scope of this chapter, but the subject area has been comprehensively and clearly reviewed in ICRP publication no. 48 (1986). It is germane, however, to consider some of the lung clearance characteristics determined by the initial physicochemical form of the actinide as this is vital to the targeting of subsequent chelation therapy and other modes of intervention.

In order to make radiological assessments following exposure and to prescribe some therapeutic treatment or other, the mobilisation and transport of actinides from the respiratory tract must be considered. With regard to this, three classes of compound can be identified which are of importance and which control mobilisation and transport (ICRP 1980):

(1) Class D – compounds in this category show a minimal retention and are cleared with a half-time of less than ten days;

(2) Class W – these have a moderate retention and are cleared with a half-time in between 10 and 100 days; and
(3) Class Y – compounds of this type are retained strongly with clearance half-times in excess of 100 days.

Thus, the classes effectively depend upon the rate(s) at which an actinide is leached from a primary deposition site into the bloodstream. The classification is useful, therefore, in considering mobilisation of actinide compounds from all routes of entry and some illustrative data is summarised in table 5.

2.4. *Absorption through intact skin*

This area of actinide biochemical/biological research has been relatively poorly researched (ICRP 1986). However, absorption of commonly encountered actinide compounds appears to be low. Absorption of plutonium from dilute aqueous acid does not exceed 0.01% during the first hour following contamination, whilst plutonium present in an organic solvent and complexed with tributylphosphate was absorbed to a slightly greater and more rapid extent, i.e., 0.04% in fifteen minutes (Wilson 1956).

From a chemical viewpoint, significant absorption of actinides via the percutaneous route would probably require the presence of a stable and lipophilic actinide complex.

2.5. *Absorption from wounds*

This has been the subject of considerable effort over recent years and a large body of data has accrued, see, e.g., (ICRP 1972, 1986, Nenot and Stather 1979). Once again migration of the actinide element from wound site to secondary deposition site appears

TABLE 5
Transport and mobilisation characteristics of actinide compounds from primary sites of deposition.

Compound classification	Chemical type and examples	Characteristics and comments
Y (years)	Highly insoluble compounds, e.g., high fired oxides	These are retained largely at the initial deposition site, in a wound or lung. Mobilisation/leaching is slow with half-times in excess of 100 days. This may be facilitated by physical break-up of particles due radioactive recoil effects (Nenot and Stather 1979). Treatment may involve lung lavage or washing and physical excisement of wounds. Absorption by gastrointestinal uptake is low (see table 4).
W (weeks)	Labile salts and complexes, e.g., nitrates, chlorides	The complex/salt tends to dissociate at the deposition site. This may lead to precipitation of the actinide, in the absence of strongly complexing ligands, to give amorphous actinide hydroxides. This will be leached slowly from the deposition site with half-times in the region of 10 to 100 days.
D (days)	Relatively non-labile and soluble actinide complexes, e.g., with EDTA.	Transport from the deposition site is rapid and quantitative with half-times of less than 10 days. Depending upon the complex, excretion may be significant.

to be a function of the initial physicochemical form. This assertion is supported by data obtained from an accidental exposure in 1976 in which an individual was extensively contaminated following the explosion of an ion-exchange column loaded with ^{241}Am, and in which the actinide was present in a variety of physical forms, e.g., adsorbed on to glass and metal debris (Palmer and Rieksts 1983).

Recent work has investigated the possibilities of modelling the speciation chemistry of actinides in wound fluids (Lunn 1990). This theoretical work supports the views expressed above that the initial physicochemical form determines the rate of mobilisation from the wound site. Thus, oxides are dissolved in wound fluids to a negligible extent even in the presence of strong chelators such as diethylenetriaminepentaacetate (DTPA). This may have important implications with respect to treatment of wound-contamination incidents where surgical excision is often combined with chelation therapy and wound washing with DTPA (Carbaugh et al. 1989).

Further work by Piechowski et al. (1989) has proposed a metabolic model to assess internal exposure following a wound contamination incident. Results indicate that the internal contamination was a result of activity which passed through vascular injuries at the time of the incident and support the conclusion that chelation therapy should be started immediately whilst the decision to excise tissue may be resolved in a more leisurely and composed manner.

3. Biodistribution and biokinetics of the f elements

Following resorption into the systemic circulation, the actinide and lanthanide elements are deposited predominantly in the skeleton and liver with rather smaller amounts being deposited in muscle, spleen, lungs and gonads. For the actinides and for some lanthanide radionuclides, this tendency to deposit heavily in bone carries with it the risk of induction of bone tumours, predominantly osteosarcoma (Duffield and Williams 1986). The tissue distribution of plutonium, as an example for the f elements in general, in the tissues of humans, rats and dogs at periods ranging from 5 to 30 days after intravenous injection is compared in table 6. For each species the retention in the

TABLE 6

The comparative distribution of plutonium in human, beagle and rat tissues after intravenous injection of ng amounts of ^{239}Pu. The data are expressed as % of the injected dose.

Tissue	Human 5d (Langham et al. 1951)	Beagle 30d (Vaughan et al. 1973)	Rat 14d (Taylor et al. 1983)
Skeleton	65	38	72
Liver	12	47	5
Spleen	0.9	0.8	0.1
Lung	1.5	0.5	0.08
Kidney	0.5	0.9	0.4
Testes	0.08	–	0.1
Muscle	6	8	1.3

tissues shown does not decrease dramatically between 5 and 30 days post-injection.

Durbin (1962) noted that for both lanthanides and actinides the skeletal uptake tended to increase with decreasing ionic radius, from about 10% to over 60% of the resorbed element, whereas liver uptake decreased, within the same range, with increasing ionic radius. The skeletal retention of the actinides and lanthanides in experimental animals appears to be long, equalling or even exceeding the natural life expectancy of the animal (Taylor 1983). The retention in animal liver shows quite wide species variation from relatively rapid clearance in rat or mouse to near complete retention in hamster or beagle. The available human information suggests that the skeletal retention is also prolonged, the estimates of the retention half-time for plutonium, e.g., ranging from about 20 years (Taylor 1985) to over 100 years (Langham et al. 1951). For radiation protection purposes the International Commission on Radiological Protection (ICRP publication no. 19, 1972) assumes a half-life of 50 years for actinides in the human skeleton. The half-time of retention of Am(III) or Pu(IV) in human liver may be as little as perhaps four-eight years, or as long as 20 years (Taylor 1984). For radiation protection purposes, ICRP publication no. 19 (1972) assumes a half-time of 20 years for the retention of actinides in human liver.

Little information is available from animal studies on the long-term retention of lanthanides, and human data are almost entirely lacking. Recently small-scale studies of the biokinetics of yttrium, which may be regarded analogues of the trivalent lanthanides, have been started in human volunteers who were given intravenous injections of ^{88}Y citrate. The preliminary results for the first 200 days post-injection, obtained using whole body counting and excreta analysis, indicate that about 22% of the ^{88}Y is lost by excretion and 78% is retained with a half-time of about 2.5 years. This half-time may perhaps increase as the studies are continued for a longer period (Bailey 1989).

Perhaps the only other tissues of concern with respect to the deposition of actinides or lanthanides in humans are the testes and ovaries, since the possibility of genetic damage or of cancer transmission to children cannot be excluded. The studies with plutonium, and to a lesser extent americium and curium, suggest that testicular uptake is low, perhaps $< 0.03\%$ of the resorbed element, and that deposition in the ovaries is even lower, $< 0.01\%$. However, the studies in every species examined, except monkeys, suggests that the retention of actinides in the gonads is essentially infinite (ICRP 1986).

The prolonged retention of the f elements in the human and animal body results from the very limited capacity of the body to excrete elements such as plutonium, americium and curium, although others such as neptunium may be more mobile. The excretion of actinides from the mammalian body was reviewed recently by Taylor (1991) in relation to the use of chelating agents to accelerate their elimination. Table 7 shows the urinary excretion of plutonium during the first four days after intravenous injection of plutonium, curium, neptunium and yttrium (as a lanthanide analogue) into human volunteers. For all the elements studied in man, the urinary excretion route appears to predominate. The limited studies which have been published indicate that plutonium and, perhaps, other f elements are eliminated in the urine as citrate complexes (Taylor 1991). The differences in the urinary excretion of neptunium, plutonium, curium or yttrium shown in table 7 do not appear to show any simple

TABLE 7
The cumulative urinary excretion (expressed as % of the injected dose) of some f elements at four days after intravenous injection into human volunteers.

	Neptunium	Plutonium	Curium	Yttrium
Mean	30.0	0.8	7.4	0.8
SD	±7.7	±0.3	±0.8	–
No. of subjects	5	13	5	2
Reference	(Popplewell et al. 1991b)	(Langham et al. 1951)	(Popplewell et al. 1991b)	(Bailey 1989)

relationship to either ionic radius or to the stability of the citrate, or other low molecular weight complexes.

4. Biochemistry in the body compartments

4.1. *Reactions in blood plasma*

After entry into the body by whatever route, transport of actinides or lanthanides to secondary deposition sites is mainly *via* the plasma in the bloodstream. Within this body compartment it is convenient to consider the f element as being partitioned between three (or perhaps four) fractions which are in equilibrium with one another and which are responsible for transport and intracellular uptake. For reasons which will become apparent it is appropriate to illustrate this concept using the partitioning of the essential element iron, as iron(III), as an example, as shown in fig. 1 (May and Williams 1980).

It can be seen that the metal ion, Fe^{3+} in this case, is partitioned between three fractions which exist in a labile and thermodynamic equilibrium with one another. There is a fourth fraction in which the metal is bound inertly and which is not readily exchangeable with the other three fractions. This latter fraction can be thought of as a storage compartment.

With respect to metal transport, it is the three labile compartments which are of interest. Transferrin, the protein which is responsible for transporting iron(III) into and

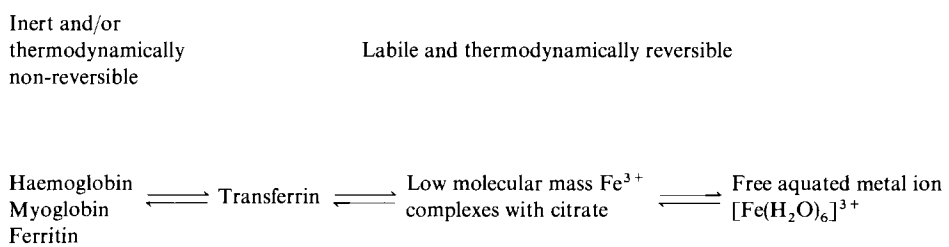

Fig. 1. Intert and labile forms of metal ions in vivo.

out of cells via receptor-mediated endocytosis (Dautry-Varsat 1986, May Jr and Cautrecasas 1985, Wileman et al. 1985), appears to play a major role in *f*-element transport within the bloodstream. Interestingly, many of the characteristics of transferrin metal-ion binding, transport and cellular uptake have been probed using Ln^{3+} ions and their complexes (Luk 1971, O'Hara and Bersohn 1982, Messori et al. 1986, O'Hara and Koenig 1986).

4.1.1. *Binding to transferrin*

Transferrin is a glycoprotein with a molecular mass of about 80 kDa which contains about 800 amino acid residues (Aisen and Listowsky 1980). The protein is bilobular with one metal binding site in each lobe. These metal binding sites are designated the N- and C-terminal sites, each contains two tyrosine, one histidine and one aspartic acid residues which appear to be involved in the metal binding; a third tyrosine residue may also participate in the binding of some metals (Harris et al. 1981). The biochemical significance or equivalence of these two binding sites is not clear, although at pH 7.4 the formation constant for the Fe(III) complex with the C-terminal site is about six times greater than that for the N-terminal site (Baldwin and Egan 1987).

In addition to binding and transporting Fe^{3+} ions, transferrin is also responsible for binding certain of the actinide and lanthanide ions *in viva*, much evidence having been gleaned from animal studies by Taylor et al. (1987) and Taylor (1991). These studies have shown transferrin to bind ^{239}Pu, ^{237}Np, ^{233}Pa in rat plasma. Evidence for Th(IV) binding to transferrin has been obtained (Duffield and Taylor 1986) with indications that this protein also binds Am^{3+}, Cm^{3+}, Eu^{3+}, Gd^{3+} and Yb^{3+} in plasma (Taylor et al. 1991). In fact the "...remarkable similarity in the interactions of plutonium, neptunium and protactinium with proteins and other ligands *in vivo*..." (Taylor et al. 1987) has prompted Taylor and his colleagues to suggest that, under physiological conditions, neptunium and protactinium are stabilised and bound as Np^{4+} and Pa^{4+} ions, respectively, rather than as the normally more stable NpO_2^+ and PaO_2^+ ions. This is of interest as reduction of Np(V) and Pa(V) to Np(IV) and Pa(IV) involves breaking of metal-oxygen bonds and re-organisation of the inner solvation layer in a reduction process which is essentially irreversible (Seaborg and Loveland 1990a). Much more work is needed on this aspect of actinide biochemistry. Studies by Stevens et al. (1980) have indicated that transferrin is also responsible for the transport of uranium, injected as U(VI) citrate into the blood of beagle dogs. In this latter study it is presumed that the uranium (VI) is bound as the UO_2^{2+} ion.

UV-difference spectroscopy, and other studies *in vitro* with plutonium (IV), thorium(IV) and a number of trivalent lanthanides, have demonstrated that, like iron, two lanthanide or actinide metal atoms are bound per transferrin molecule (Duffield and Taylor 1986, Taylor et al. 1991, Zak and Aisen 1988). Saturation of the lanthanide- or actinide-containing transferrin with excess iron results in a liberation of the f element, thus suggesting that these metals are binding to the two iron-binding sites on the transferrin molecule (Taylor et al. 1991). These studies have also shown that bicarbonate is necessary, as a synergistic anion, for the binding of actinides and lanthanides to transferrin.

Comparative studies *in vitro* and *in vivo* have demonstrated the binding of americium, curium, europium, gadolinium and ytterbium to transferrin; however, *in*

vivo less than 20% of the total metal in the plasma appears to be bound to transferrin (Taylor et al. 1991, Cooper and Gowing 1981). On the basis of a spectroscopic and thermodynamic study of the binding of gadolinium to human serum transferrin *in vitro*, Zak and Aisen (1988) have suggested that transferrin may not be an important carrier protein for gadolinium *in vivo* because of the formation in the blood plasma of non-binding carbonato complexes of Gd(III), this same phenomenon may also explain the low proportion of americium, curium, europium and ytterbium bound to transferrin *in vivo*.

In vitro studies of lanthanide and actinide binding to transferrin can yield useful information about the binding characteristics and about the stability of the binding. Zak and Aisen (1988) used UV-difference spectroscopy, electron paramagnetic resonance (EPR) titration, EPR-difference spectroscopy, gel electrophoresis and equilibrium dialysis to study the binding of gadolinium to human serum transferrin. From these studies they concluded that at pH 7.4 only one Gd(III) atom was bound per transferrin molecule and that this represents specific binding to the C-terminal metal-binding site in the transferrin molecule. Other spectroscopic studies have suggested that at pH 8.5 two Gd(III) atoms were bound per transferrin molecule (O'Hara and Koenig 1986), while other UV-difference spectroscopic studies have yielded data which would be consistent with the binding of either one or two atoms of Gd(III), Eu(III) or Yb(III) to human transferrin (Taylor et al. 1991). In a study of thorium complexation by transferrin in vitro, Harris et al. (1981) drew attention to the fact that there is evidence that the N-terminal binding site is slightly smaller than the C-terminal site and that while Th(IV) could fit easily into the C-terminal site, it might be of borderline size with respect to entry into the N-terminal site. Such asymmetric binding might also occur with Eu(III) (Harris et al. 1981). Plutonium(IV) with its slightly smaller radius would be more likely to fit easily into both binding sites, which agrees with the observation of Duffield and Taylor (1987) that two Pu(IV) atoms appeared to bind to one transferrin molecule.

Data on values for the formation constants for actinide and lanthanide complexes with transferrin are relatively sparse. Harris (1986) reported conditional values for the equilibrium formation constants of Nd(III)– and Sm(III)–transferrin complexes, based on UV-difference spectra measurements at pH 7.4 in 10 mM HEPES buffer containing only 0.2 mM bicarbonate. The results of titrations of apotransferrin with the metal chelates and of the metal–transferrin complex with free ligand gave close agreement for the values of the formation constant for the binding of one metal atom. However, for the binding of the second metal atom the agreement was less good and larger standard deviations were observed. This latter was interpreted as evidence for weaker binding to the N-terminal site and for competition from the formation of lanthanide–carbonato complexes. The values obtained for the formation constants are shown in table 8.

Using the data for 88 low molecular weight ligands, Harris (1986) constructed a linear free-energy relationship (LFER) between Sm(III) and Nd(III) and used this, together with the ionic radii of the metals, to derive formation constants for Am(III) and Cm(III). These derived constants are also shown in table 8.

Zak and Aisen (1988) measured the formation constant for the binding of Gd(III) to the C-terminal site of human serum transferrin and derived a value which lies between that of Sm(III) and Nd(III), table 8. Recently, Yule (1991) has used UV-difference

TABLE 8
Formation constants for trivalent lanthanide and actinide complexes with human serum transferrin.

Element	Ionic radius (pm)	Log K_1	Log K_2	Reference
Nd(III)	98	6.09 ± 0.15	5.04 ± 0.46	[1]
Sm(III)	96	7.13 ± 0.24	5.39 ± 0.32	[1]
Gd(III)	94	6.83	–	[2]
Am(III)	98	6.3 ± 0.7	–	[1]
Cm(III)	97	6.5 ± 0.8	–	[1]

[1] Taylor (1985).
[2] Vaughan et al. (1973).

spectroscopy and ultrafiltration to derive a provisional conditional stability constant for Pu(IV) of log β of 21.1 ± 0.7.

The observations described above have important implications with regard to actinide/lanthanide distributions within the body. It is apparent that in binding to transferrin, the f elements are participating in certain aspects of the iron transport pathways in vivo. However, no plutonium, e.g., is found within red blood cells following incorporation and there is no unequivocal evidence that plutonium and the other actinides or lanthanides are transported into cells via transferrin-receptor-mediated endocytosis (Duffield and Taylor 1986). This, too, is a puzzling aspect of f-element-transferrin chemistry and biochemistry which needs more study.

A number of explanations can be advanced which may explain the apparent dichotomy of f-element binding to transferrin and the imperfect participation in the iron metabolic pathways.

4.1.1.1. *The mechanisms of actinide/lanthanide binding to transferrin may not be the same as that for iron(III).* Spectroscopic studies by Duffield and Taylor (1987) have shown the fine details of Pu(IV) and Th(IV) binding to transferrin to be very similar to that of Fe(III).

(1) One mole of transferrin binds two moles of Pu(IV) in a specific fashion implying that plutonium binds at the same sites as Fe(III). The same is true for Th(IV).
(2) Fe(III) binding to transferrin requires stabilisation with a synergistic anion, carbonate or bicarbonate. Binding of Pu(IV) also requires such a synergistic anion.

4.1.1.2. *The differences may be due to changes in protein conformation upon metal ion binding.* It is known that the conformation of transferrin changes upon binding with iron (Duffield and Taylor 1987 and references contained therein). This may be critical regarding subsequent binding of metal–transferrin complexes to cell surface receptors prior to internalisation by receptor-mediated endocytosis. Recent studies using small-angle X-ray scattering studies of metal–transferrin solutions support this view Grossmann et al. (1991). Following iron binding the transferrin molecule has been

shown to contract due to closure of the interdomainal clefts but no such closure is seen on binding hafnium(IV), a metal which may be regarded as a plutonium analogue (Birnbaum et al. 1970).

4.1.2. *Binding to albumin*

In contrast to the quite extensive interest in the binding of the f elements to transferrin, less attention appears to have been paid to their binding to albumin, even though this protein may be more important than transferrin for transporting some trivalent f elements in vivo.

Spectroscopic studies of the binding of neodymium(III) and gadolinium(III) to bovine serum albumin (BSA) have suggested that the lanthanides bind only through carboxyl groups and that there are four binding sites per albumin molecule (Birnbaum et al. 1970, Reuben 1971). Shahid et al. (1982) have shown that lanthanide binding to BSA or to human serum albumin (HSA) induces conformational changes in a manner analogous to the change in the protein's structure which occurs upon lowering the pH. The effectiveness in producing this conformational change was found to lie in the order

$$Lu^{3+} < Tb^{3+} < Nd^{3+} < La^{3+}.$$

Shahid et al. ascribe the conformational changes to the neutralisation of negative charges on the protein resulting from H^+ or lanthanide ions to carboxyl groups. Ca^{2+} neither produced this conformational change nor showed any evidence of competing for the lanthanides at the carboxyl sites (Shahid et al. 1982, Reuben and Luz 1976).

Schömacker et al. (1988) labelled human blood serum with ^{169}Yb *in vitro* and showed, by alcohol fractionation at low temperature, that 95% of the radioactivity was associated with the albumin. Equilibrium dialysis studies in vitro using HSA–lanthanide solutions or whole human serum yielded values for the association constant for the lanthanide–albumin complex ranging, with increasing atomic number and decreasing ionic radius, from $\log K_{pr} = 4.7$ for Ce to $\log K_{pr} = 9.5$ for Yb, table 9.

Actinide binding to albumin appears to have attracted little attention. Chipperfield and Taylor (1970) using gel chromatography concluded that plutonium binding to

TABLE 9
Association constants of lanthanide–human serum albumin complexes.

Atomic No.	Element	Radius (pm)	Log K_{pr}
58	Cerium	101	4.90 ± 0.03
60	Neodymium	98	5.39 ± 0.03
63	Europium	95	6.41 ± 0.02
66	Dysprosium	91	7.40 ± 0.002
67	Holmium	89	7.62 ± 0.003
68	Erbium	88	8.85 ± 0.01
69	Thulium	87	8.90 ± 0.03
70	Ytterbium	86	9.54 ± 0.01

Association constants from Schömacker et al. (1988). Ionic radii from Shannon (1976).

human serum albumin was weak, with only about 1% of the metal being recovered in protein bound form at pH 7.4.

The physiological result of the binding of the non-essential lanthanide and actinide metals to albumin, or transferrin, in the blood plasma may well be that the metals are held in a form in which they are virtually unable to penetrate the cell membrane in ionic form thus limiting cellular uptake and also the ability to cause harmful effects by interaction with essential enzymes or other proteins. Thus for the non-essential f elements, protein binding may be regarded as part of a protective mechanism against chemical toxicity.

4.2. *Low molecular mass fractions*

From fig. 1 it can be seen that in addition to the labile protein-bound fraction, metal–transferrin complexes in the case of actinides, there is also a low molecular mass fraction in which metal ions are bound to, and transported with, ligands such as the anions of amino and carboxylic acids. For the hard cations of the actinide elements, these complexing agents are predominantly carboxylic acids (from the citric acid cycle) (Duffield and Taylor 1986, Popplewell et al. 1975, Duffield et al. 1984, Metivier 1973) or inorganic anions such as carbonate, e.g., for uranium(VI) (Stevens et al. 1980).

It has been suggested that the low molecular mass complexes in blood plasma may be responsible, at least partially, for the transport and cellular uptake of transition-metal ions by passive diffusion (May 1980). This implies that the lipophilicity and the charge of the predominant low molecular mass complex species formed in blood plasma *in vivo* plays a dominant role in determining the distribution of the metal ion amongst the different body compartments. Therefore, a knowledge of the low molecular mass *chemical speciation* of actinides and lanthanides may be considered indispensible to understanding, rationalising and predicting f-element transport in the body.

Unfortunately, because of the lability of the equilibrium in the interactions of the proteins and low molecular mass complexes indicated in fig. 1, it is difficult to determine the exact chemical speciation in such systems experimentally. Separation of fractions by mass, using, e.g., size-exclusion chromatography, upsets the equilibria under study so that results must be treated with great caution. As a result of this experimental uncertainty, computer-assisted methods have been developed which allow prediction of the chemical speciation pertaining to the low molecular mass fraction (May 1980, May et al. 1977, May and Williams 1977, Duffield and Williams 1989b).

4.3. *Chemical speciation modelling*

Much has been written concerning the use of computers to model chemical speciation occurring in equilibrium systems (see, e.g., Duffield and Williams 1986) and so only a brief summary of this topic is given here.

To model the chemical speciation of a given element in a given system, the following are required.

(a) Input describing the system under study including component identities, total

analytical concentrations of components and system parameters such as pH and reduction potential values.
(b) A computer program which can be used to calculate the equilibrium distributions of complex species in the aqueous phase and also in the presence of solid phases. These are based on the laws of mass balance and of mass action.
(c) A thermodynamic database containing equilibrium constants describing *all relevant interactions* in the system under study.

Of the above requirements, the latter [part (c)] is probably the most contentious as the quality of equilibrium data is variable in the extreme (Waters et al. 1991).

It is the quality, applicability and relevance of this data which primarily affects the accuracy of speciation calculations. This area has been the subject of extensive review in recent years and its importance cannot be overstated (Duffield et al. 1991, 1991a, b). With good quality equilibrium data and carefully stated assumptions, it is possible to rationalise actinide-distribution characteristics and predict the efficiency of chelation therapy regimens (Duffield and Taylor 1986, Duffield et al. 1984).

4.4. *Reactions with cellular and other proteins*

Studies with various actinides, following their injection into experimental animals, have shown that after entry into the cells of liver, spleen, kidney and testes, and probably also in other tissues, the metals interact with the subcellular organelles and with the intracellular proteins (Duffield and Taylor 1986). Immediately after entry into the cell the actinides react first with the cytosolic proteins and are then transferred into the membrane-bounded lysosomes within the cell. The rate of transfer to the lysosomes is fastest for americium and curium and slowest for plutonium. In rat or hamster liver plutonium is associated first with an unidentified protein – "Protein X" – with a molecular mass of 150 (hamster) and 200 kDa (rat) (Neu-Mueller 1988), and then subsequently with the iron-storage protein ferritin. In contrast, americium and curium are rapidly bound to ferritin, without any apparent binding to protein X. Within the lysosomes ferritin appears to be the important binding species (Duffield and Taylor 1986). Much less is known concerning the subcellular distribution of lanthanides, but comparative studies using ^{144}Ce and ^{239}Np, ^{239}Pu and ^{241}Am confirm the importance of the lysosomes as a deposition site for lanthanides and actinides (Seidel et al. 1986).

4.4.1. *Reactions with ferritin*

In vivo studies with plutonium, americium and curium have demonstrated that the elements become associated with the iron-storage protein ferritin, following their uptake, probably by pinocytosis, into liver cells, especially in reticuloendothelial cells (Taylor 1973a, b). With plutonium this binding to ferritin appears to be stronger than that to transferrin (Taylor 1973a). The nature of the binding of actinides to ferritin has not been investigated but the adsorption of hydrolysed species onto the hydrated iron–oxide complex in the protein has been suggested for americium and curium, and might also apply to plutonium (Taylor 1973a, b). More recent studies have shown that neptunium and protactinium may also be associated with ferritin in vivo (Taylor et al. 1987).

As mentioned above, lanthanide elements also become deposited in liver, where they are known to be deposited within lysosomal structures (Seidel et al. 1986). Although clear evidence for association of the elements with ferritin in the liver cells has not been reported, such an association would be expected on the basis of *in vitro* studies of lanthanide binding to ferritin. Luminescence and X-ray crystallographic studies have demonstrated that Tb^{3+} ions bind to one apoferritin molecule and thereby inhibit the subsequent uptake of Fe^{2+} (Macara et al. 1973, Stefanini et al. 1983, Banyard et al. 1978).

4.4.2. Reactions with bone proteins

The idea that proteins might play a role in the fixation of yttrium, americium and plutonium in bone was proposed by Vaughan and her colleagues (Williamson and Vaughan 1967) who had observed in autoradiographs that these elements appeared to deposit in the osteoid layer on the bone surfaces. Herring (1969) and Williams and Peacocke (1967) subsequently isolated and characterised a number of glycoproteins from bovine bone. The actinide-binding properties of some of these proteins were investigated by Chipperfield and Taylor [see Taylor 1973a, b for detailed references] who showed that plutonium indeed bound quite strongly to the fractions designated bone sialo-protein, glycoproteins I and II and to bone chondroitin sulphate, but americium and curium bound much less strongly (Taylor 1973b). The biological significance of actinide binding to these bone glycoproteins is not known, but since these proteins appear to be located on bone surfaces near to the radiosensitive osteoprogenitor cells, preferential binding of ^{239}Pu could help to explain the greater ability of this nuclide, in comparison to ^{241}Am or ^{244}Cm, to induce bone tumours (Taylor 1986).

4.4.3. *Reactions with other proteins*

In vivo studies of the reactions of f elements with other specific intracellular proteins do not appear to have been reported, but extensive *in vitro* investigation of the binding, and the effects of binding, of lanthanides to enzymes and other proteins have been published. Not surprisingly there has been little interest in the study of actinide interactions with such proteins.

The interactions of various lanthanides with a very wide range of proteins has been recently reviewed in depth by Evans (1990). The range of proteins which have been investigated is large and includes such enzymes as the trypsins, elastase, collagenases, amylase, nucleases, ATPases, phospholipase-A_2 and acetylcholinesterase, the contractile proteins actin and myosin and molecular oxygen carriers such as haemocyanin. These studies have confirmed that the major ligand for Ln^{3+} ions is the carboxyl group, with additional coordination occurring through carbonyl and hydroxyl oxygens. Often the lanthanides occupy Ca^{2+} ion binding sites on proteins. X-ray crystallographic studies have shown that in proteins such as calmodulin, Ca^{2+} replacement by Ln^{3+} can occur isomorphously. However, Ln^{3+} ions may also bind to sites on proteins which are not known to bind calcium or any other metal. Because of their higher charge-to-volume ratio, Ln^{3+} ions usually have higher affinities for proteins than Ca^{2+}. The affinities of the Ln^{3+} ions vary widely but in general they increase with decreasing

hydration of the sequestered lanthanide ion and with increasing cationic charge at the binding site.

The biochemical effects of Ln^{3+} binding to proteins include both inhibition and activation, as well as stabilisation of enzymes.

Lanthanide binding to proteins and other biomolecules can make very important contributions to structural and functional analyses. Techniques such as luminescence and NMR spectroscopy can help to provide detailed structural information and/or permit the identification of amino acids in the vicinity of binding sites, the estimation of hydration numbers of sequestered Ln^{3+} ions and, where more than one metal-binding site exists, interionic distances. At the functional level Ln^{3+} binding can also provide valuable information, e.g., the fact that Ln^{3+} ions are better cofactors than Ca^{2+} for the activation of trypsinogen to trypsin points to a "charge-masking" role for metal ions in this reaction (Evans 1990).

In addition to protein studies, Ln^{3+} ion binding to other types of biomolecules in vitro can also provide valuable structural and other information. The molecules investigated include nucleic acids, phospholipids and phospholipid model membranes, porphyrins, vitamin B_{12} and high-density lipoproteins [see Evans 1990 for reviews].

4.5. *Interactions between f elements and chelators in vivo*

Because of the high radiotoxicity of the actinides and a widespread interest in the possible use of lanthanide radionuclides as diagnostic or therapeutic agents in clinical medicine, the ability of chelators to modify the biokinetics of f elements in the body has been widely studied. In the nuclear-energy industry, the interest has been predominantly in the development of chelators which could be used therapeutically in the case of an accident involving contamination with plutonium or americium to enhance the naturally slow rate of elimination of these elements from the body and thereby reduce the risk of long-term radiation injury. This aspect of chelation therapy has recently been reviewed in depth by Taylor (1991). Since the work on the effects of chelators on lanthanide interactions *in vivo* has been reviewed recently by Evans (1990), both aspects are discussed only briefly here.

For the treatment of internal contamination by plutonium or americium the current agent of choice is the polyaminopolycarboxylic acid, diethylenetriaminepentaacetic acid (DTPA), which is administered by slow intravenous injection as the $CaNa_3DTPA$ salt. For prolonged treatment the less toxic, but also slightly less effective, $ZnNa_3DTPA$ salt may be used.

Diethylenetriaminepentaacetic acid forms very stable chelates with the actinide and transuranium metals with values of $\log \beta$ ranging from about 22 to 30. The ability of DTPA to mobilize plutonium from the transferrin complex has been demonstrated by *in vitro* studies (Duffield et al. 1986). These studies demonstrated the influence of the chemical environment on the release of the metal by DTPA. When the release of plutonium from the transferrin complex in 20 mM TRIS-HCl buffer containing 130 mM NaCl was studied, the results showed a maximum plutonium release of ca. 86%, achieved with DTPA : transferrin molar ratios > 10. This corresponded to a

DTPA : Pu ratio of > 1000. In contrast, when the release of plutonium from the transferrin complex in rat serum was investigated, only about 20% of the plutonium was released at a DTPA : transferrin ratio of 100, corresponding to a DTPA : Pu ratio of 10^4.

Numerous studies in experimental animals, predominantly in rats and mice, have shown that DTPA can be very effective in accelerating the excretion of injected plutonium, but that the effectiveness decreases rapidly with the time lapse between the contamination and the start of treatment. The maximum effect is seen only when treatment is commenced within a few minutes of contamination, i.e., while the concentrations of plutonium in the blood and easily accessible body fluids are high. However, significant reduction in the retention of plutonium and, especially of the trivalent actinides such as ^{241}Am, may be achieved even when the start of treatment is delayed for several weeks (Taylor 1991). One disadvantage of DTPA, as indeed with all the currently available chelators, is that they are of only very limited effectiveness in mobilizing transuranium elements which have already been deposited in the bone. Thus a principal aim of decorporation therapy must be to limit the extent of deposition in bone which generally means that, in the event of an accident involving significant contamination, treatment must be commenced as rapidly as possible.

The human experience in the use of DTPA for the treatment of human contamination with transuranium elements was reviewed by Volf (1978). The most important case to date was the so-called 1976 Hanford americium exposure incident, in which a process worker was severely contaminated, on the face and upper body, with soluble and insoluble ^{241}Am, and with heavily contaminated foreign bodies, as a result of the explosion of an ion-exchange column in a glove box (Thompson 1983). There was a very high degree of contamination, some tens of MBq, it was possible to start DTPA therapy about two hours after the incident, initially with $CaNa_3DTPA$, and subsequently with the less toxic Zn salt. The course of DTPA therapy extended over a period of some four years during which time 583 g of DTPA were administered intravenously without any ill effects. The patient excreted a total of 41 MBq of ^{241}Am in his urine and faeces before he died, from the complications of long-standing heart disease, in 1987 (Breitenstein and Palmer 1989). This spectacular, and, hopefully, unique case, is the only published incident in which it can be stated with near certainty that the treatment with DTPA was life-saving. With the degree of internal contamination, without treatment, the radiation damage from the deposition of ^{241}Am in the liver would have led to death within a few months from liver failure.

The animal studies, and the limited human data, have shown that DTPA is most effective for the removal of plutonium and the trivalent actinides and appears to be much less effective for the removal of ^{237}Np or ^{233}Pa.

A serious practical disadvantage is the need to administer the DTPA intravenously by slow injection, or by infusion for maximum effectiveness. This requirement may delay the start of treatment if no qualified person is immediately available to give an intravenous injection. Further, experience has shown that the treatment needs to be continued for many months or years; long-term intravenous treatment may be unpleasant for the patient, and is quite demanding on medical resources. Thus there has been considerable interest in the possibilities of the other routes of treatment. For continuation therapy, after the first few weeks, oral treatment would be very useful. The

absorption of $CaNa_3DTPA$ from the gastrointestinal tract is small, $< 5\%$ (Foreman 1960), but studies in animals showed that administration of $ZnNa_3DTPA$ in drinking water was very effective in removing plutonium, americium or thorium from rats, when administered in daily doses of about three times greater than a single injected dose of $CaNa_3DTPA$ (Taylor 1991).

Other types of chelator. An elegant approach was pioneered by Raymond and his colleagues at the University of California, Berkeley (Raymond and Smith 1981). The concept underlying this approach was the apparent chemical similarities between Fe(III) and Pu(IV) membrane. Noting that catechoylamide residues played an important role in the biological iron chelators called siderophores, Raymond and his colleagues developed a series of compounds designed to have the correct steric dimensions to form stable complexes with Pu(IV), but not with Fe(III) or the trivalent actinides. Of these "actinide-specific" compounds, perhaps the most interesting was the linear tetracatechoylamide known as 3,4,3-LICAM(C). In vitro studies have shown that LICAM(C) is about 500 times more efficient than $Na_3CaDTPA$ in mobilizing plutonium from transferrin in serum. The early in vivo studies with LICAM(C) showed that for treatment beginning at 30 min after Pu(IV) injection, LICAM(C) was much more effective than CaDTPA in enhancing the elimination of plutonium in beagles and in mice. Later studies, using rats, hamsters and baboons indicated that at longer time intervals after contamination, LICAM(C) was no more, or even less effective than $Na_3CaDTPA$ in mobilizing plutonium. These studies also revealed a two- to ten-fold increase in the retention of plutonium in the kidney following LICAM(C) treatment. Thus, despite its early promise, the potential of LICAM(C) for human therapy is very limited. Nevertheless, this approach was important and has led to the synthesis of further compounds of apparent high effectiveness in animals.

The hydroxamic acid derivative known as Desferrioxamine B methane sulphonate (DFOA), a selective chelator for iron which has been widely used for the treatment of iron overload in man, is effective, either alone or in combination with $Na_3CaDTPA$, for the removal of plutonium from rats. However, the compound is ineffective for the removal of americium and the effectiveness for the removal of plutonium was limited to very short times after injection [see Taylor 1991 for references].

Raymond and his colleagues (White et al. 1988) have investigated a number of new sequestering agents based on polydentate oxohydroxypyridinecarboxylate ligands. Some of these appear to be of considerable interest; e.g., one compound, code-named DFO-HOPO, on an equimolar basis, reduced the retention of newly deposited tissue plutonium to a greater extent than any agent previously tested. Further it was active when administered orally (Stradling et al. 1991). Recent research suggests that the synthesis of even more effective compounds of acceptably low toxicity is likely in the near future.

In contrast to the actinides, interest in chelation therapy for radiolanthanide contamination has been very limited. However, there has been interest in the biological behaviour of lanthanides administered as complexes with DTPA or with EDTA. This interest has been directed principally to the possible applications of radioactive lanthanides, such as ^{169}Yb-DTPA, for the scintigraphic localization of tumours, or of

^{90}Y-DTPA for radiotherapeutic purposes (Evans 1990). There is also interest in the use of the paramagnetic lanthanide complexes, e.g., Gd(III)-DTPA, as "contrast enhancers" in clinical magnetic resonance (NMR) and in computer tomographic imaging (CT). For these purposes it is necessary for the biological stability of the chelate to be so high that the lanthanide ion does not dissociate from the chelator, which appears to be achieved when the log β for the Ln-DTPA complex is > 18. For such strong complexes the undissociated complex remains in the extracellular fluids with virtually no deposition in liver, skeleton or soft tissues (Evans 1990).

5. Lanthanides as actinide analogues for biokinetic studies

Because of the high radiotoxicity of most of the actinide nuclides, only very limited studies of the biokinetics of plutonium and other important actinides are possible in human volunteers. As our information about the long-term retention of actinides is limited, there is interest in the possible use of stable lanthanide elements as surrogates for the actinides for long-term biokinetic studies in humans. The aim of such studies is to inject appropriate stable isotopes of lanthanides such as cerium, europium, and gadolinium into human volunteers and then to measure the excretion of the lanthanide in urine and faeces by mass spectrometry, charged-particle activation analysis or similar methods. Also, limited human studies can also be carried out using small doses of appropriate lanthanide radionuclides (Bailey 1989).

For the trivalent actinides the choice of a lanthanide surrogate is relatively easy. For example, based on electron configuration and ionic radius europium and gadolinium could serve as surrogates for americium and curium, respectively, tables 1 and 2. For the tetravalent actinides, thorium and plutonium, the choice is more difficult, Ce(IV) is a possible surrogate for Th(IV) or Pu(IV). The ionic radius of Ce(IV), 0.087 nm, is comparable with that of Pu(IV), however, it is considerably smaller than that of Th(IV), 0.094. However, a more serious problem is that Ce(IV) is not the most stable valency for cerium in solution and in vivo studies (Durbin 1962) indicate that the skeletal cerium deposition is lower than that of plutonium while the liver uptake is greater. Taylor and co-workers (Taylor et al. 1983, Birnbaum et al. 1970) have used hafnium(IV) as a plutonium analogue for both biodistribution and kinetic studies as well as for studies of its binding to transferrin.

Europium and gadolinium show in vivo deposition in the skeleton of rats which is broadly comparable to that of americium and curium. However, the liver deposition of the two actinides appears to be almost double that of the two lanthanides (Durbin 1962). In the blood plasma in vivo (as discussed earlier) europium, gadolinium, americium and curium associate with transferrin to about 20% and the stability constants for their transferrin complexes appear to be similar, table 8. The long-term retention of the lanthanides in bone does not appear to have been studied in similar depth to that of the actinides, but animal studies appear to suggest that lanthanide retention time in bone may be a little shorter than for the actinides. By contrast, liver retention appears to be comparable for actinides and lanthanides, at least in rats and mice (Evans 1990). Although care will be needed in the interpretation of the data, it does

seem likely that human studies using lanthanides as actinide surrogates can provide valuable information about biokinetics in humans.

6. Conclusion

Although the f elements have no known essential biochemical or physiological role in the body, and some of the actinides are the most highly radiotoxic elements known to mankind, the study of their interactions with the components of biological systems has provided fascinating and valuable data about the behaviour of readily hydrolysable metal ions in biological systems, as well as fundamental information on interactions with various types of protein. While the actinides will always remain potentially harmful to *homo sapiens*, some of the lanthanides, in small amounts, are proving to be valuable probes for many biochemical systems, especially those involving Ca^{2+} ions, and lanthanide chelates are of increasing value in clinical medicine, both for diagnosis and therapy.

References

Aisen, P., and I. Listowsky, 1980, Ann. Rev. Biochem. **49**, 357–393.

Baes Jr, C.F., and R.E. Mesmer, 1976, The Hydrolysis of Cations (Wiley, New York).

Baes Jr, C.F., and R.E. Mesmer, 1981, Am. J. Sci. **281**, 935–962.

Bailey, M.R., 1989, in: Radiation Protection – Theory and Practice, 4th Int. Symp. (Society for Radiation Protection, Malvern, UK) pp. 445–448.

Baldwin, D.A., and T.J. Egan, 1987, South Afr. J. Sci. **83**, 22–31.

Banyard, S., D.K. Stammers and P.M. Harrison, 1978, Nature **271**, 282–284.

Barnett, M.I., J.R. Duffield, D.A. Evans, J.A. Findlow, B. Griffiths, C.R. Morris, J.A. Vesey and D.R. Williams, 1989, Modelling bioavailability as a function of speciation using physicochemical data and computers, in: Nutrient Availability: Chemical and Biological Aspects, eds D. Southgate, I. Johnson and G.R. Fenwick (Royal Society of Chemistry, London) pp. 97–99.

Bernkopf, M.F., and J.I. Kim, 1984, Hydrolysis Reactions and Carbonate Complexation of Trivalent Americium in Natural Aquatic Systems, Inst. for Radiochem., Report No. RCM-02884 (Technical University of Munich, Munich). In German.

Birnbaum, E.R., J.E. Gomez and D.W. Darnall, 1970, J. Am. Chem. Soc. **92**, 5287, 5288.

Bishop, G.P., C.J. Beetham and Y.S. Cuff, 1989, Review of Literature for Chlorine, Technetium and Neptunium, Nirex Safety Studies, NSS/R193 (Harwell, UK).

Breitenstein, B.D., and H.E. Palmer, 1989, Radiat. Prot. Dosim. **26**, 317–322.

Briant, J.K., and C.L. Sanders, 1987, Health Phys. **53**, 365–375.

Brown, V.K., 1988, Acute and Sub-Acute Toxicology (Edward Arnold, London) pp. 11–24.

Bulman, R.A., 1978, Struct. & Bonding **34**, 39–77.

Bulman, R.A., 1980a, Coord. Chem. Rev. **31**, 221–250.

Bulman, R.A., 1980b, Coord. Chem. Rev. **31**, 235.

Bünzli, J.-C.G., and G.R. Choppin, 1989, Lanthanide Probes in Life, Chemical and Earth Sciences: Theory and Practice (Elsevier, Amsterdam).

Carbaugh, E.H., W.A. Decker and M.J. Swint, 1989, Rad. Prot. Dosim. **26**, 345.

Chipperfield, A.R., and D.M. Taylor, 1970, Eur. J. Biochem. **17**, 581–585.

Choppin, G.R., 1983, Radiochim. Acta **32**, 43.

Choppin, G.R., 1986, J. Less-Common Met. **126**, 307–313.

Cleveland, J.M., 1970, The Chemistry of Plutonium (Gordon and Breach, New York).

Cooper, J.R., 1986, The influence of speciation on the gastrointestinal uptake of elements, in: Speciation of Fission and Activation Products in the Environment, eds R.A. Bulman and J.R.

Cooper (Applied Science Publishers, Barking) pp. 162–174.

Cooper, J.R., and H.S. Gowing, 1981, Int. J. Radiat. Biol. **40**, 569–572.

Cooper, J.R., G.N. Stradling, H. Smith and S.E. Breadmore, 1978, Biochem. Soc. Trans. **6**, 972–975.

Coughtrey, P.J., D. Jackson and M.C. Thorne, 1985, in: Radionuclide Distribution and Transport in Terrestrial and Aquatic Ecosystems, Vol. 6, A Compendium of Data (A.A. Balkema, Rotterdam).

Dautry-Varsat, A., 1986, Biochimie **68**, 375–381.

Delgarno, B.G., 1988, The distribution and uptake or rare-earth elements in the food chain and their use as analogues for the transuranic elements: A literature review, Technical Report AERE-R-13220 (UKAEA, Harwell, UK).

Duffield, J.R., and D.M. Taylor, 1986, The biochemistry of the actinides, in: Handbook on the Physics and Chemistry of the Actinides, Vol. 4, eds A.J. Freeman and C. Keller (Elsevier, Amsterdam) pp. 129–157.

Duffield, J.R., and D.M. Taylor, 1987, Inorg. Chim. Acta **140**, 365–367.

Duffield, J.R., and D.R. Williams, 1986, Chem. Soc. Rev. **15**, 291–307.

Duffield, J.R., and D.R. Williams, 1989a, Toxicol. Environm. Chem. **22**, 17–25.

Duffield, J.R., and D.R. Williams, 1989b, Chem. Br. **25**, 375–378.

Duffield, J.R., P.M. May and D.R. Williams, 1984, J. Inorg. Biochem. **20**, 199–214.

Duffield, J.R., D.M. Taylor and S.A. Proctor, 1986, Int. J. Nucl. Med. Biol. **12**, 483–487.

Duffield, J.R., J.R. Johns, F. Marsicano and D.R. Williams, 1991, Polyhedron **10**, 1121–1129.

Duffield, J.R., F. Marsicano and D.R. Williams, 1991a, Polyhedron **10**, 1105–1111.

Duffield, J.R., M. Waters, F. Marsicano and D.R. Williams, 1991b, Polyhedron **10**, 1113–1120.

Durbin, P.W., 1962, Health Phys. **8**, 665–671.

Emsley, J., 1989, The Elements (Clarendon Press, Oxford).

Evans, C.H., 1990, Biochemistry of the Lanthanides (Plenum, New York).

Gilbert, R.O., D.W. Engel, D.D. Smith, J.H. Shinn, L.R. Anspaugh and G.R. Eisele, 1988, Health Phys. **54**, 323–335.

Großmann, G., M. Neu, E. Pantos, R.W. Evans, P.F. Lindley, D.M. Taylor, H. Appel, F. Schwab, W.-G. Thies and S.S. Hasnain, 1991, X-ray solution scattering studies reveal metal-induced conformational changes in transferrins. Poster, Fifth International Conference on Bioinorganic Chemistry, Oxford, August 1991.

Guillmette, R.A., and G.M. Kanapilly, 1988, Health Phys. **55**, 911–925.

Harris, W.R., 1986, Inorg. Chem. **25**, 2041–2045.

Harris, W.R., C.J. Carrano, V.L. Pecoraro and K.N. Raymond, 1981, J. Am. Chem. Soc. **103**, 2231–2237.

Herring, G.M., 1969, Bibl. Nutr. Dieta (Basel) **13**, 147–154.

Hider, R.C., and A.D. Hall, 1991, Clinically useful chelators of tripositive elements, in: Progress in Medicinal Chemistry, Vol. 28, eds G.P. Ellis and G.B. West (Elsevier, Amsterdam) pp. 41–173.

ICRP, 1972, The Metabolism of Compounds of Plutonium and Other Actinides, ICRP Publication 19 (Pergamon Press, Oxford).

ICRP, 1979, Limits for Intake of Radionuclides by Workers, ICRP Publication 30, Part 1, Annals of the ICRP, Vol. 2, nrs 3/4 (Pergamon Press, Oxford).

ICRP, 1980, Biological Effects of Inhaled Radionuclides, ICRP Publication 31, Annals of the ICRP, Vol. 4, nrs 1/2 (Pergamon Press, Oxford).

ICRP, 1986, The Metabolism of Plutonium and Related Elements, Publication 48, Ann. ICRP, 16(2/3).

Johnson, J.R., and E.S. Lamothe, 1989, Health Phys. **56**, 165–168.

Katz, J.J., G.T. Seaborg and L.R. Morss, eds, 1986a, The Chemistry of the Actinide Elements, 2nd Ed. (Chapman and Hall, London) 2 volumes.

Katz, J.J., G.T. Seaborg and L.R. Morss, eds, 1986b, The Chemistry of the Actinide Elements, 2nd Ed., Vol. 2 (Chapman and Hall, London) p. 1137.

Katz, J.J., L.R. Morss and G.T. Seaborg, 1986c, Summary and comparative aspects of the actinide elements, in: The Chemistry of the Actinide Elements, Vol. 2, eds. J.J. Katz, G.T. Seaborg and L.R. Morss (Chapman and Hall, London) ch. 14, p. 1165.

Kim, J.I., 1986, Transuranic elements in natural aquatic systems, in: Handbook on the Physics and Chemistry of the Actinides, Vol. 3, eds A.J. Freeman and C. Keller (Elsevier, Amsterdam) p. 420.

Krauskopf, K.B., 1986, Chem. Geol. **55**, 323–335.

La Touche, Y.D., D.L. Willis and O.I. Dawydiak, 1987, Health Phys. **53**, 147–162.

Langham, W.H., S.H. Bassett, P.S. Harris and

R.E. Carter, 1951, United States Atomic Energy Commission Document La-1151. Reprinted 1980, Health Phys. **38**, 1031–1060.

Lauffer, R.B., 1987, Chem. Rev. **87**, 901–927.

Long, S.E., 1987, Uranium and Human Diet: A Literature Review, AERE R 12810 (Harwell, UK).

Luk, C.K., 1971, Biochem. **10**, 2838–2843.

Lunn, H., 1990, Chemical Speciation of Wound Fluids, PhD Thesis (University of Wales).

Macara, I.G., T.G. Hoy and P.M. Harrison, 1973, Biochem. J. **135**, 785–789.

May, P.M., 1980, Computer Applications in Bioinorganic Chemistry (University of St. Andrews).

May, P.M., and D.R. Williams, 1977, FEBS Lett. **78**, 134.

May, P.M., and D.R. Williams, 1980, The inorganic chemistry of iron metabolism, in: Iron in Biochemistry and Medicine, Vol. II, eds A. Jacobs and M. Worwood (Academic Press, London) pp. 1–28.

May, P.M., P.W. Linder and D.R. Williams, 1977, J. Chem. Soc. Dalton Trans., p. 588.

May Jr, W.S., and P. Cautrecasas, 1985, J. Membrane Biol. **88**, 205–215.

Meares, C.F., and T.G. Wensel, 1984, Acc. Chem. Res. **17**, 202–209.

Messori, L., R. Monnanni and A. Scozzafava, 1986, Inorg. Chim. Acta **124**, L15–L17.

Metivier, H., 1973, A Contribution to the Study of Tetravalent Plutonium Hydrolysis and Complexation by Acids of Biological Interest, Rapport CEA-R-4477 (CEN-Saclay, Gif-sur-Yvette, France). In French.

Morgan, A., A. Black, D. Knight and S.R. Moores, 1988, Health Phys. **54**, 301–310.

Morrow, P.E., F.R. Gibb, H. Davies, J. Mitola, D. Wood, N. Wraight and H.S. Campbell, 1967, Health Phys. **13**, 113–133.

Morss, L.R., 1986, in: The Chemistry of the Actinide Elements, Thermodynamic Properties, Vol. 2, 2nd Ed., eds J.J. Katz, G.T. Seaborg and L.R. Morss (Chapman and Hall, London) ch. 17, p. 1288.

National Research Council, 1983, Opportunities and Challenges in Research with Transplutonium Elements (National Academy Press, Washington, DC).

Nenot, J.C., and J.W. Stather, 1979, The Toxicity of Plutonium, Americium and Curium (Pergamon Press, Oxford).

Neu-Mueller, M., 1988, Vergleichende Untersuchungen zur Stoffwechsel von Eisen und Plutonium in Hepatocytes, Dr. sci. hum. Thesis (University of Heidelberg).

O'Hara, P.B., and R. Bersohn, 1982, Biochem. **21**, 5269–5272.

O'Hara, P.B., and S.H. Koenig, 1986, Biochem. **25**, 1445–1450.

Orlandini, K.A., W.R. Penrose and D.M. Nelson, 1986, Marine Chem. **18**, 49–57.

Palmer, H.E., and G.A. Rieksts, 1983, Health Phys. **45**, 893–910.

Pearson, R.G., 1972, Hard and Soft Acids and Bases (Dowden, Hutchinson and Ross, Pennsylvania).

Phillips, S.L., 1982, Hydrolysis and Formation Constants at 25°C, Report LBL-14313 (Lawrence Berkeley Laboratory).

Piechowski, J., D. Cowadone, J. Tourte, M.H. Cauquil, P. Raynaud, J.C. Harduin, P. Thomas and Y. Chaptinel, 1989, Rad. Prot. Dosim. **26**, 265.

Popplewell, D.S., G.N. Stradling and G.J. Ham, 1975, Rad. Res. **62**, 513.

Popplewell, D.S., J.D. Harrison and G.J. Ham, 1991a, Health Phys. **60**, 797–805.

Popplewell, D.S., J.D. Harrison and G.J. Ham, 1991b, Health Phys. **60**, 797–805.

Raymond, K.N., and J.L. Smith, 1981, Struct. Bonding (Berlin) **43**, 159–186.

Reuben, J., 1971, Biochemistry **10**, 2834–2838.

Reuben, J., and Z. Luz, 1976, J. Phys. Chem **80**, 1357–1369.

Schömacker, K., D. Mocker, R. Münze and G.-D. Beyer, 1988, Appl. Radiat. Isotopes **39**, 261–264.

Seaborg, G.T., and W.D. Loveland, 1990a, The Elements Beyond Uranium (Wiley, New York) p. 82.

Seaborg, G.T., and W.D. Loveland, 1990b, The Elements Beyond Uranium (Wiley, New York) p. 91.

Seidel, A., M. Wiener, E. Krüger, R.E. Wirth and H. Haffner, 1986, Nucl. Med. Biol. **13**, 515–518.

Shahid, F., J.E. Gomez, E.R. Birnbaum and D.W. Darnall, 1982, J. Biol. Chem. **257**, 5618–5622.

Shannon, R.D., 1976, Acta Crystallogr. A **32**, 751–767.

Sherry, A.D., 1989, J. Less-Common Met. **149**, 133–141.

Smith, R.M., and A.E. Martell, 1976, Critical Stability Constants, Vol. 4, Inorganic Complexes (Plenum Press, New York).

Stefanini, S., E. Chiancone, E. Antonini and

A. Finazzi-Agro, 1983, Arch. Biochem. Biophys. **222**, 430–434.

Stevens, W., F.W. Bruenger, D.R. Atherton, J.M. Smith and G.N. Taylor, 1980, Rad. Res. **83**, 109–126.

Stradling, G.N., B.W. Loveless, G.J. Ham and H. Smith, 1978, Health Phys. **35**, 229–235.

Stradling, G.N., S.A. Gray, J.C. Moody, A. Hodgson, K.N. Raymond, P.W. Durbin, S.J. Rodgers, D.L. White and P.N. Turowski, 1991, Int. J. Radiat. Biol. **59**, 1269–1277.

Sullivan, M.F., B.M. Miller, P.S. Ruemmler and J.L. Ryan, 1985, Health Phys. **48**, 61–73.

Sullivan, M.F., P.S. Ruemmler, J.L. Ryan and R.L. Buschbom, 1986, Health Phys. **50**, 223–232.

Sullivan, M.S., and P.S. Ruemmler, 1988, Health Phys. **54**, 311–316.

Suzuki, Y., H. Saitoh, Y. Kamata, Y. Aihara and Y. Tateyama, 1989, J. Less-Common Met. **149**, 179–184.

Task Group on Lung Dynamics, 1966, Health Phys. **12**, 173–207.

Taylor, D.M., 1973a, Chemical and physical properties of plutonium, in: Handbook of Experimental Pharmacology, Vol. 36, eds H.C. Hodge, J.N. Stannard and J.B. Hursh (Springer, Berlin) p. 339.

Taylor, D.M., 1973b, Chemical and physical properties of the transplutonium elements, in: Handbook of Experimental Pharmacology, Vol. 36, eds H.C. Hodge, J.N. Stannard and J.B. Hursh (Springer, Berlin) pp. 717–738.

Taylor, D.M., 1983, Health Phys. **45**, 768–772.

Taylor, D.M., 1984, in: Radiation Risk Protection, 6th Int. Radiation Protection Association Congr., Berlin, pp. 431–434.

Taylor, D.M., 1985, in: Metals in Bone, ed. N.D. Priest (MTP Press/CEC, Lancaster, UK) pp. 221–228.

Taylor, D.M., 1986, The comparative carcinogenicity of ^{239}Pu, ^{241}Am and ^{244}Cm in the rat. in: Life-span Radiation Effects Studies in Animals: What can they tell us?, CONF-830951, eds R.C. Thompson and J.A. Mahaffey (USDOE, OSTI, Springfield, VA) pp 404–412.

Taylor, D.M., 1989a, Sci. Total Environ. **83**, 217–225.

Taylor, D.M., 1989b, Rad. Prot. Dosim. **26**, 137–140.

Taylor, D.M., 1991, Acceleration of the natural rate of elimination of transuranium elements from the mammalian body, in: Handbook on the Physics and Chemistry of the Actinides, Vol. 6, eds A.J. Freeman and C. Keller (North-Holland, Amsterdam) ch. 11.

Taylor, D.M., M. Lehmann, F. Planas-Bohne and A. Seidel, 1983, Rad. Res. **95**, 339–358.

Taylor, D.M., J.R. Duffield and S.A. Proctor, 1986, The chemical forms of plutonium in the gastrointestinal tract, in: Speciation of Fission and Activation Products in the Environment, eds R.A. Bulman and J.R. Cooper (Applied Science Publishers, Barking) pp. 208–212.

Taylor, D.M., A. Seidel, F. Planas-Bohne, U Schuppler, M. Neu-Mueller and R.E. Wirth, 1987, Inorg. Chim. Acta **140**, 361–363.

Taylor, D.M., C.W. Mays, G.B. Gerber and R.G. Thomas, eds, 1989, Risks from Radium and Thorotrast, Report 21 (British Institute of Radiology (BIR), London), Editorial, p. vii.

Taylor, D.M., J.R. Duffield, D.R. Williams, L. Yule, P.W. Gaskin and P. Unalkat, 1991, Eur. J. Solid State & Inorg. Chem. **28**, 271–274.

Thompson, R.C., 1983, Health Phys. **45**, 837–845.

Vaughan, J.M., B. Bleaney and D.M. Taylor, 1973, Distribution, excretion and effects of plutonium as a bone-seeker, in: Handbook of Experimental Pharmacology, Vol. 36, eds H.C. Hodge, J.N. Stannard and J.B. Hursh (Springer, Berlin) pp. 349–502.

Volf, V., 1978, Treatment of incorporated transuranium elements, WHO-IAEA Tech. Rept. Ser., Vol. 184.

Waters, M., J.R. Duffield, P.J.F. Griffiths and D.R. Williams, 1991, Final Report on the UW Contribution to the CHEMVAL Project. School of Chemistry and Applied Chemistry (University of Wales, College of Cardiff, P.O. Box 912, Cardiff, CF1 3TB, UK).

Watters, R.L., D.N. Edgington, T.E. Hakonson, W.C. Hanson, M.H. Smith, F.W. Whicker and R.E. Wildung, 1980, Synthesis of the research literature, in: Transuranic Elements in the Environment, ed. W.C. Hanson (Technical Information Centre, U.S. Department of Energy, Washington) p. 13.

White, D.L., P.W. Durbin, N. Jeung and K.N. Raymond, 1988, J. Med. Chem. **31**, 11–18.

Wileman, T., C. Harding and P. Stahl, 1985, Biochem. J. **232**, 1–14.

Williams, D.R., 1988, Bioinorganic pharmacy – metal complexation and metal side-effects in drug design, in: Smith and Williams' Introduction to the Principles of Drug Design, 2nd Ed., ed. H.J. Smith (Butterworths, London) pp. 159–190.

Williams, P.A., and A.R. Peacocke, 1967, Biochem. J. **105**, 1177–1185.
Williams, R.J.P., 1982, Struct. & Bonding **50**, 79–119.
Williamson, M., and J.M. Vaughan, 1967, Nature **215**, 711–714.
Wilson, R.H., 1956, Decontamination of Human Skin after Immersion in a Plutonium Solution, Operation Report HW-42030 (Hanford Atomic Products).
Yule, L., 1991, Ph.D. Thesis (University of Wales).
Zak, O., and P. Aisen, 1988, Biochemistry **27**, 1075–1080.

SUBJECT INDEX

A-form 427, 429, 463
ab initio techniques 32, 43
absolute entropies for gaseous ions 542
absorption spectra 161, 177, 184
absorption spectrum of
– aquated Am^{3+} 166
– aquated Bk^{3+} 168
– aquated Ce^{3+} 162
– aquated Cf^{3+} 169
– aquated Cm^{3+} 167
– aquated Dy^{3+} 169
– aquated Er^{3+} 171
– aquated Es^{3+} 170
– aquated Eu^{3+} 166
– aquated Gd^{3+} 167
– aquated Ho^{3+} 170
– aquated Nd^{3+} 163
– aquated Np^{3+} 164
– aquated Pm^{3+} 164
– aquated Pr^{3+} 162
– aquated Pu^{3+} 165
– aquated Sm^{3+} 165
– aquated Tb^{3+} 168
– aquated Tm^{3+} 171
– aquated U^{3+} 163
– aquated Yb^{3+} 172
Ac(c) 473
Ac(g) 473
Ac-227 451
AcH 97
Ac_2O_3 452, 455, 461, 473, 477, 491
acetonitrile 540
acetylacetone 202
acid–base effects in oxides 274
acidic organophosphorus extractants 211, 213
acidity parameters in oxides 275
actinide atoms in actinyl(V) and actinyl(VI) ions 547
actinide binary oxides 449, 454
– enthalpies of formation 471
actinide cations 540
actinide concept, first open publication 7
actinide dioxides
– bulk modulus 478
– enthalpies of formation 475
– high-pressure behavior 478
actinide hexahalides 405
actinide hydrides 297
actinide ions
– gaseous 541, 543
– hydrated 541, 543
actinide metals 248, 510
actinide oxides 450, 455
– color 461
– lattice parameters 461
– magnetic properties 477
– space group structure type 461
– symmetry 461
– thermodynamics 472
actinide sesquioxides 257
actinide trihalides 371
actinide–lanthanide tetrahalides 403
actinides
– ability to form dioxides 453
– availability 450
– broad range of oxidation states (+2 to +7 in solution) 19
– half-lives 451
– isotopes
– – for solid-state study 451
– – lifetimes 450
– natural occurrence 450
– oxidation states 453
– quantities available 450, 451
– reactions with cellular and other proteins 611
– route of entry into man 599
– – gastrointestinal uptake 600
– – inhalation 601
actinium 16, 198, 460
actinium oxides 460
actinocenes 139
actinyl ions 546
actinyl (VI) 547
activation parameters 582
air oxidation 456
albumin 609
alkaline earth–lanthanide dihalides 399
alkyl pyrocatechol extractants 221
alkylene phosphine dioxides 29
α-bromocaprate 230

α-hydroxyisobutyric acid 226
α phase 437
– four distinct regions 438
– solubility behavior 310–313
α-UO_3 461
α-U_2O_5 461
α-U_3O_7 461
α-U_3O_8 461
Am 16, 455, 457
Am(c) 473
Am(g) 473
Am metal 510
Am^{2+}
– half life in solution 562
Am-241 451
Am-243 451
Am dioxide 465
Am/Eu separation factors 223, 230, 231, 234
Am(II) 581
AmO_x 452, 455, 464
AmO 455, 464
AmO(g) 473
AmO_2 459, 461, 477, 491, 515
AmO_2(c) 473
Am_2O_3 459, 461, 464, 477, 491
Am_2O_3(c) 473
$Am(OH)_3$ 259
amalgamation energy 256
amine extractants 210
amines 202
aminocarboxylate ligands 569
aminopolycarboxylates 569
ammonium α-hydroxyisobutyrate 226
An^{4+} aquo ions, enthalpies of formation 475
AnO_2^+ 560
AnO_2^{2+} 538, 560
An_7O_{12} 454, 457
anhydrous HF 524
– as solvent 269
anion exchange 203
anomalous temperature dependence of Cm(IV) compounds 476
antimony pentafluoride 524
apparent hydrated radii 530
apparent molal heat capacities 537
apparent molal volumes 537
application of quaternary amines to lanthanide/actinide group separation 210
aquated ions 161, 189
aqueous ions, heat capacities 256
aqueous Np^{3+}, Pu^{3+}, Am^{3+} 254
aqueous rare-earth ions R^{3+} 254
aqueous reduction potentials 282
aquo ions, enthalpies of formation 494
atomic theory 173
atomic transport 443
atoms and ions 415
augmented Hessian method 48

B-form 427, 429
$BaCfO_2$ 477
$BaCfO_3$ 454, 468
$BaCmO_3$ 477
$BaEsO_3$ 454, 469
$BaMO_3$ 454
basic relativistic quantum techniques 40
bastnasite 198
benzo-15-crown-5 217
4-benzoyl-2,4-dihydro-5-methyl-2-phenyl-3H-pyrazol-3-thione (BMPPT) 230
β-diketones 202, 211
β-UO_3 461
β-U_2O_5 461
β-U_3O_8 461
BiF_5 519
bifunctional extractants 208
binary lanthanide oxides 428
binary or ternary lanthanide (II) compounds 395
binary oxides of actinide elements 449
binary oxides of lanthanide elements 415
bioavailability 599
biodistribution of f elements 603
biokinetics of f elements 603
Biorex 70 202
1,13-bis(8-quinolyl)-1,4,7,10,13-pentaoxatridecane (Kryptofix-5, or K-5) 217
bismuth phosphate 200
Bk 16
Bk(c) 473
Bk(g) 473
Bk-249 451
BkO_x 452, 455, 466, 467
BkO 455, 467
BkO_2 457, 459, 461, 466, 467, 477, 491
BkO_2(c) 473
Bk_2O_3 459, 461, 477, 491
Bk_2O_3(c) 473
Bk_7O_{12} 457, 467
boiling points of lanthanide sesquioxides 440
bond disruption enthalpies 279
bond lengths
– LaH, AcH, TmH, LuH, LrH 96
– of rare-earth monofluorides 108
bonding in metallic systems 279
Born–Haber cycles 272
Born equation 565

Breit interaction 40
bulk modulus of actinide oxides 478

CASSCF 48
C-form sesquioxides 427, 429, 444
calculated and experimental states of CeO 116
calculated and experimental states of LaO 112
calculated relativistic U–O bond lengths 137
calorimetric data for complexation 571
calorimetric measurements 540, 565
calorimetric studies 568
carbamoylmethyl phosphonates 208
carbamoylmethylphosphine oxides 208
carbamoylphosphonates 208
carbonate 267
carboxylic acids 202
cascade dissolution 513
cation radii 200, 205, 206
cation–cation complexes 579
Ce 16
CeO 111, 429, 442, 443
$CeO_{1.67}$ 442
$CeO_{1.72}$ 442
$CeO_{1.78}$ 442
$CeO_{1.81}$ 442
$CeO_{1.818}$ 445
$CeO_{2.0}$ 442
CeO_2 421, 428, 432, 439, 442, 448, 491
Ce_2O_3 421, 440, 441, 448, 491
Ce_7O_{12} 421, 433
Ce_9O_{16} 421
$Ce_{10}O_{18}$ 421
$Ce_{11}O_{20}$ 421, 433
$Ce_{19}O_{34}$ 421, 423, 424, 433
$Ce_{62}O_{112}$ 421, 423, 424, 433
cellular and other proteins 611
Cf 16, 455, 457, 467
Cf(c) 473
Cf(g) 473
Cf-249 451
Cf-252 451
Cf(II) 581
Cf–O system 469
Cf daughter in berkelium oxides 469
Cf monoxide 467
CfO_x 452, 455, 467
– magnetic behavior 478
CfO_2 456, 461, 467, 477, 491
CfO_2(c) 474
Cf_2O_3 459, 461, 477, 491
– structural forms 468
Cf_2O_3(c) 473
Cf_7O_{12} 459, 461, 467, 477
CfO_x, $1.5 < x < 1.72$ 468
chelating ligands 211
chelators 613
chemical diffusion in nonstoichiometric oxides 443
chemical properties of elements 104 through 112 21
chemical properties of the heaviest elements
– neptunium, plutonium 5
– study in transuranium elements 3, 4
chemical speciation 598
– modelling 610
chemistry of hahnium 21
– in aqueous solution 23
chemistry of rutherfordium 21
– in aqueous solution 22
– influence of relativistic valence electrons 22
chloride complexes of rutherfordium 22
cluster compounds 383
cluster-stabilized reduced halides 402
Cm 16, 457
Cm(c) 473
Cm(g) 473
Cm-244 451
Cm-248 451
Cm(II) 581
Cm(IV) 476
CmO_x 452, 455, 465
CmO(g) 473, 475
CmO_2 456, 461, 465, 466, 473, 476, 477, 491
Cm_2O_3 459, 461, 465, 473, 477, 491
– vaporization 475
Cm_7O_{12} 461, 466, 559
$^{244}Cm_2O_3$ 477
Cm sesquioxide 475
cocrystallization 269
colloidal particles of oxides 428
comparison of the binary oxides 479
completion of actinide series by 1961 16
completion of 5f shell at lawrencium (element 103) 17
complex exchange potentials 51
complex halides 277
complex oxides 276
complex oxides and halides 282
complexation 267
complexing by phosphotungstate 267
compounds of oxidation states of actinide elements 19
conductivity 535
conductivity measurements 537, 538
configuration interaction 48
– first-order, for ScH 58
configurational entropy 574
conproportionation reaction 517

constants for excited states of CeO 115
constants for low-lying states of CeO 113
contraction of orbital radius 35
contraction of outer 6s orbital 35
contraction radii 561
coordination numbers 531, 561, 574
coordination polyhedron 577
coprecipitation 200
coupled-cluster method 49
coupled-electron pair formalism 49
covalency 274, 560, 563, 565, 567–569, 571, 585
covalency in the actinides 205
covalent bonding 560
covalent interactions 564, 567, 570, 571
Cowan–Griffin approximation 43
crown ether extractants 216
crown ethers 202
crystal-field calculations 478
crystal-field effects 476, 574
crystal-field parameters 173
crystal fields 353–357
cubic field 563
cubic rare-earth oxides, lattice parameters 431
Curie–Weiss behavior 476
cyclic and linear polyethers 216
cyclic polyaza 578
cyclic voltammetry 522
cyclooctatetrene compounds, uranocene 279

DHDECMP 208
DMF–water 539
DMSO 538
DOTA (1, 4, 7, 10-tetraazacyclotetradecane-1, 4, 7, 10-tetraacetic acid) 578
D_e of Pb_2 34
DTPA (diethylenetriaminepentaacetic acid) 227, 613
D_e values of schematic Cu_2, Ag_2, Au_2 39
Darwin Hamiltonian 42
Davidson method 48
dehydration 203
δ-UO_3 461
$^2\Delta$–$^4\Delta\Phi$ energy separations of TiH, ZrH and HfH 88
derived thermodynamic functions 439
desferrioxamine B 615
di-cyclohexano-18-crown-6 217
di-thio-substituted HDEHP 230
1, 10-diaza-4, 7, 13, 16-tetraoxacyclooctadecane-*N, N′*-diacetic acid (DACDA) 216, 217
1, 7-diaza-4, 10, 13-trioxacyclopentadecane-*N, N′*-diacetic acid (DAPDA) 216
dibenzoyl methane 215
dicarboxylate ligands 574
5, 7-dichloroxine 214
dielectric constant of the diluent 224
diethylenetriaminepentaacetic acid (DTPA) 227, 613
diffusion measurements 536
diffusion; NMR 345–349
dihalides 397
diluent effects 221
diluents 204, 223
dimeric complex 533
dioxides 260, 418, 430, 453, 456, 467, 482
– order of stability 482
dioxygen difluoride 524
dipole-allowed transition of YCl 104
dipole moment per unit M–H distance for ScH, YH and LaH 67
dipole moments
– for low-lying states of YH_2 60
– HfH_2 92
– LaH_2 80
– ZrH_2 95
dipositive aquo-ions 255
Dirac–Fock orbital energies 35
Dirac–Fock trend 38
Dirac–Hartree–Fock (DHF) equation 44
Dirac–Hartree–Fock (DHF) orbital energies of Cu, Ag, Au 38
Dirac–Slater multiple $X\alpha$ method 43
Dirac equation 40
Dirac Hamiltonian 40, 41
disproportionation 418, 512, 582
– by PuO_2^+ 552
– by UO_2^+ 552
– reactions 562
dissociation energies
– of monoxides 493
– of rare-earth monofluorides 109
dissociation enthalpies of rare-earth monoxides 443
dissociation kinetics 585
dissociation relationships for low-lying states of LaH^+ 68
divalent actinides 544
divalent ions 561
divalent lanthanides in superacids 510
dominant oxidation states for light actinides 204
Dowex A-1 202
Dy 16
Dy^{4+} 272
DyO 127, 442, 443
Dy_2O_3 419, 420, 430, 431, 440, 441, 445, 448, 491

ECP and all-electron results for ScH 59
ECP method 43
EXAFS (X-ray absorption fine structure) 530, 535
early papers on electronic structure of the heaviest elements 2, 3
effect of aqueous complex formation on distribution ratios and separation factors 224
effect of diluent 223
effect of pressure on CeO_2 431
effective central charges 547
effective charges 563
effective ionic radii 560
effective-operator Hamiltonian 173
Eigen mechanism 574
Einstein energy expression 40
einsteinium 16
einsteinium oxides 469
electrical conductance 537
electrical properties 447
electrical transport in rare-earth oxides 448
electron diffraction 458
electron microscopic observation 438
electron paramagnetic resonance 478
electron spin resonance 530
electron-transfer spectra 273
electronic assignments of PrO 119
electronic configurations 51, 246, 415, 452, 480, 496
– for actinide atoms, ions, and their common oxides 452
– for elements actinium to curium, inclusive (1949) 9
– for f-block atoms and ions 480
– for gaseous atoms of actinide and lanthanide elements (1963) 16
– for (III) ions 416
electronic homologs 481
electronic spectra of the lanthanides 509
electronic states
– of LaO 111
– of lanthanide oxides 110
– of M@C_{60} (M = La, Eu, Eu^+, U, U^+) 148–150
electronic structure 29, 334–337
– of lanthanide hydrides 52
electronic structure and chemical properties of a "superactinide" group 18
electronic transitions of PrO 118
electrophoretic measurements 535
element 106 21
elements 95 and 96
– announcement on "Quiz Kids" programme 7
– identification of isotopes 7
– names americium (Am) and curium (Cm) announced 9
elements Am–Es 455
elements Fm–Lr 455
elpasolites 274, 278
energies and constants of DyO 127
energies and equilibrium structures for YH_2 59
energies of molecular states of PrO 120
energies of molecular states of TmO 132
energy gap 185, 188
energy-gap law 185, 187
energy-level diagrams
– Ce^{+2} 112
– DyO 128
– HoO 130
– LaF 102
– Pr^{+2} 122
– PrO 118, 121
– SmO 123
– TmO 133
– YCl 105
– YbO 135
energy separations
– HfH_2 90
– Ti, Zr, Hf 89
– Zn, Cd, Hg 40
enthalpies of complexation 282
enthalpies of formation
– for U^{3+} 255
– of actinide binary oxides 471
– of actinide dioxides 475
– of An^{+4} aquo ions 475
– of aquo ions 494
– of lanthanide and actinide oxides 491
– of monoatomic gas 542
– of rare-earth monoxides 443
– of sesquioxides 494
enthalpies of solution 254, 260
– of lanthanide and actinide oxides 491
– of sesquioxides 490
enthalpies of vaporization 243
enthalpy of hydration 547
entropies of aquo actinide ions 542
entropy 256, 572
entropy of complexation 575
entropy of hydration 547
entropy of PuO_2 474
environmental cell 438
ε-UO_3 461
equilibrium vapor species of plutonium oxide system 474
Er 16
ErO 442, 443

Er_2O_3 419, 420, 430, 431, 440, 441, 444, 445, 448, 491
Es 455, 456
Es(c) 474
Es(g) 474
Es^{4+} 272
Es-253 451
Es-254 451
EsO 469
EsO_2 454, 491
Es_2O_3 452, 455, 459, 461, 469, 474, 477, 478, 491
EsO_2(c) 474
η-UO_3 461
ethers 202
2-ethyl(hexyl)phenylphosphonic-acid 228
Eu 16
Eu^{2+} 510, 562
Eu^{3+} 572, 573
Eu(II) 580
EuO 121, 417, 428, 429, 442, 443, 447, 448
Eu_2O_3 419, 420, 428, 430, 431, 440, 441, 448, 491
Eu_3O_4 417, 429, 442
experimental magnetic moment 416
exposure to actinides by inhalation 601
extraction chromatography 213, 227
extraction from alkaline and carbonate media 220

$5f^6$ core 476
$^7F_0 \rightarrow {}^5D_0$ transition 572
f-electron bonding 297
5f electron shell "actinide" series 15
f^2 electronic states of uranocene 143
$5f^2$ electronic states of uranocene 141
5f-orbitals 450
f^3 states of $Np(C_8H_8)_2$ 144
f^3 states of $Pu(C_8H_8)_2$ 145
FT-ICR mass spectra
– of fullerenes containing up to 3 La atoms 152
– of hot-toluene extract of fullerene 151
FT-IR investigations 540
$f \rightarrow d$ excitation energies for the electronic states of uranocene 143
$f \rightarrow d$ spectra 273
$5f \times 6d$ states of uranocene 142
$f \rightarrow d$ transitions 255, 256
$5f \rightarrow 6d$ transitions 561
fermium 198
ferritin 611
filling of 5g, 6f shells 18
fluorescence 184, 186, 187, 190, 191, 538
fluorescence lifetime 535
fluorescence quantum yield 185
fluorite-related cluster compounds 381, 383
fluorite-related lanthanide oxides 443
fluorite structure type 430
Fm 16
Fm(c) 474
Fm(g) 474
Fm-255 451
Fm-257 451
Fm–Lr oxides 455
Fm_2O_3 452, 474, 491
four-component spinor 41
fourth group atoms 34
fractional absorption 600
fractional crystallization 200
fractional retention 600
free energies and enthalpies of hydration for the actinide elements 542
free energies of formation 541
– of rare-earth oxides 440
free energy of solution 270
free-ion states 174
freezing points of lanthanide sesquioxides 440

γ-UO_3 461
γ-U_2O_5 461
gastrointestinal uptake of actinides 600
Gd 16
GdO 124, 442, 443
Gd_2O_3 419, 420, 430, 431, 440, 441, 448, 491
geometries 531
geometries and energies of linear states of HfH_2 91
geometries and energies of low-lying states
– HfH_2 90
– LaH_2 77
– LaH_2^+ 73
– ScH_2 62
geometries and energy separations of bent electronic states of ZrH_2 94
Gibbs energy functions of rare-earth monoxides 442
graphical-unitary group approach 48
ground-state properties of lanthanide hydrides 99
ground term 416, 496
growth of lanthanide single crystals 428

^{1}H-NMR 539, 576, 577
HDNNS 230
hahnium 21
– relativistic effects 25
halate systems 572
half-filled shell effect 249

halide and non-halide anion systems 380
halide complexation of hahnium 23
hard-acid nature 561
Hartree–Fock calculations 35
hassium 21
heats of dilution 537
heats of formation 540
heaviest elements 4
heptavalent oxidation states 562
heterogeneous reactions in rare-earth oxides 445
hexamethylphosphoramide 269
hexavalent actinides 562
HfH 80
HfH_2 89
high-pressure behavior 478
high-pressure effects 438
high-pressure studies 279
high-temperature vapor species 491
higher composition (α) 424
higher oxidation states 562
higher oxides 447
– of Ce, Pr, Tb 444
higher oxides (O/M stoichiometries greater than 2) 457
Ho 16
HoO 128, 442, 443
Ho_2O_3 419, 420, 430, 431, 440, 441, 445, 448, 491
Hobenberg–Kohn theorem 50
Hund's rule 494
hydrated cations 534
hydrated ions 529
hydrated Pa_2O_5 460
hydration 190, 538
hydration enthalpies 249–252, 541, 542
hydration entropies 253, 544
hydration number 538, 539
hydration zones 530
hydride halides 401
hydrogen reduction 459
hydrolysis 190, 547
– order 547
hydrolysis constants
– actinides 547
– mononuclear actinide complexes 548
– polynuclear actinide complexes 552
hydrolysis studies of tetravalent cations 551
hydrolyzed U(VI) 554
hydroxo complexes 547
hypersensitive bands 182
hypersensitive transitions 180, 564
hyperstoichiometric sesquioxide 463
hypothesis of "actinide series" 5
hysteresis 426

(III)/(II) couples 482
INDO-SCI energy separation of Kotzian et al. for GdO 126
INDO/CI method 43
IPs of Cu, Ag, Au 39
(IV)/(III) couples 482
inelastic neutron scattering 354–357
inert-pair effect 31
inner-sphere character 573
inner-sphere complex formation 571, 572, 585
inner-sphere hydration numbers 536
inner-sphere mechanisms 581, 582
inner-sphere structure 579
inorganic-ion exchangers 202
interactinide separation factors 232
interactinide separations 232
interactions of lower oxides of europium 418
interlanthanide separation factors 232
interlanthanide separations 232
intermediate cerium oxides, lattice constants 433
intermediate neglect of differential overlap 52
intermediate oxides 432, 453
– of Cm 466
intermediate oxides (O/M stoichiometries between 1.5 and 2.0) 456
intermediate praseodymium oxides, lattice constants 434
intermediate terbium oxides, lattice constants 435
intermediate-valent halides 395
intermediate/homologous series 422
intra-group separations 206, 231
ion configuration 495
ion exchange 199, 200
ion mobility 190
ionic bonding 561
ionic character 574
ionic radii 205, 250, 251, 484
ionic radii of actinides and lanthanides 483
ionic UOF_3^+, no evidence for contribution 518
ionization energies 246, 248, 561
ionization potentials 273, 542, 544
isobaric hysteresis loop 426
isobaric runs, PrO_x–O_2 425
isopropyltropolone 202
isotopes 450

Judd–Ofelt theory 179, 180, 187

Kahn–Baybutt–Truhlar form 45
ketones 202
kinetic-based separations 201
kinetics; mechanisms 321–327
kinetics of phase reactions 444
Klein–Gordon equation 40

known members of Ln_nO_{2n-2} homologous series 437
Kohn–Sham orbitals 51
krypton difluoride 524

LFSE 542
3, 4, 3-LICAM(C) 615
LIX 51 215
LIX 54 215
L–S coupling 494
La 16
^{139}La-NMR 573
^{139}La-NMR shift 572
$[La(DP)(HDP)(H_2O)_2]\cdot 4H_2O$ 577
LaF 101
LaF–LuF 106
LaH 63
LaH^+ 67
LaH_2 73
LaH_2^+ 71
LaO 111, 429, 442, 443
La_2O_3 419, 420, 440, 441, 448, 491
lactic acid 227
lantanide chlorides 370
lanthanide and actinide azide complexes 229
lanthanide and actinide hydration thermodynamics 544
lanthanide and actinide molecules 29
lanthanide and actinide perovskites 276
lanthanide and actinide tetrafluorides 261
lanthanide bromides 370
lanthanide chlorides 370
lanthanide contraction 31, 88
lanthanide coordination 510
lanthanide dioxides, lattice constants 432
lanthanide elements 415, 542
lanthanide fluoride coprecipitation 200
lanthanide fluorides 369
lanthanide halide cluster stabilized by non-metals 402
lanthanide hydrates 531
lanthanide (III) mixed halides 378
lanthanide metals, tarnishing 441
lanthanide oxides
– structures 429
– thermodynamic properties 439
lanthanide sesquioxides 419, 427, 447
– freezing and boiling points 440
– thermodynamic properties 441
lanthanide/actinide contraction 206
lanthanide/actinide separation
– by difference in reaction kinetics 235
– role of covalence 225
lanthanide/actinide separation factors 229
lanthanides 547
lanthanides and actinides inside carbon cages ($M@C_n$, $M@C_n^+$) 146
lanthanum and neodymium hydroxides 257
lattice constants 299, 307, 309
– of intermediate cerium oxides 433
– of intermediate praseodymium oxides 434
– of intermediate terbium oxides 433
– of lanthanide dioxides 432
lattice-energy calculations 272
lattice parameters
– for actinide oxides 461
– for cubic rare-earth oxides 431
– for NaCl-type lanthanide monoxides 429
– for sesquioxides 484, 489
$LiCmO_3$ 466
ligand-field theory 50
ligand fields 563
linear dioxo actinide cations 533
linear-equation method 48
Ln_nO_{2n-2} 432
local-density functional (LDF) method 50
low molecular mass fractions 610
low-temperature electric resistivity 338–347, 351–353
low-temperature heat capacity 339, 352–354, 359
low-temperature magnetic behavior 341, 349–352
lower composition phase (σ) 424
lower oxidation states 562
lower oxides 416, 429, 454
Lr 16
Lr(c) 474
Lr(g) 474
Lr-260 451
LrH 97
LrO 493
Lr_2O_3 452, 470, 474, 491
Lu 16
LuH 97
LuO 442, 443, 493
Lu_2O_3 419, 420, 430, 431, 440, 441, 445, 448, 491
luminescence 184, 187–189, 192, 572, 574, 585
luminescence lifetime 535
luminescence spectra 185

M^+ 480
M^{2+} 480
M^{3+} 480
M^{4+} 480
MAPLE (Madelung part of lattice energy) 272, 276
$MAnO_3$ 471

M(I)–M(IV) mixed halides 404
M(II)–M(IV) mixed halides 404
macrocyclics 578
magic acid 508
magnetic behavior 494
– of $BaCfO_3$ 478
– of transplutonium oxides 476
magnetic characteristics 446
magnetic data 477
magnetic measurements 476
– on Es_2O_3 478
magnetic moments 494, 495
magnetic properties
– of actinide oxides 477
– of binary oxides 475
– of lanthanide and actinide oxides 496
magnetic susceptibilities 494
mass–velocity effect 33, 42
Md(c) 474
Md(g) 474
Md-258 451
Md_2O_3 452, 474, 491
meitnerium 21
melting point 486
mendelevium 16
metal-ion exchange 584
metallic bonding 248
metallic reduced halides 396
metallic valence 493
metallurgical laboratory of the university of Chicago 4
Mischmetal 198
mixed-anion dihalides 283
mixed aqueous media 217
mixed aqueous solvents 538
mixed-cation dihalides 399
mixed-cation systems 384
mixed-cation trihalide systems 378
mixed-dihalide systems 399
mixed divalent–trivalent halide systems 384
mixed univalent–trivalent halide systems 388
mixed-valent oxides 422
mixtures of o-phenanthroline and nonanoic acid 230
mobilities 530
modelling of chemical speciation 610
modified coupled-pair formalism 49
molecular orbital calculations 478
molocular mechanics calculations 531
molten salts 268
moment 476, 496
monazite 198
mono-alkyl acid phosphorus extractants 214
mononuclear hydroxo complexes 547
monoxides 455
– dissociation energies 493
Morse potentials for LaH, LuH AcH 98
Mössbauer chemical shifts 565, 567
Mössbauer measurements 567, 571, 572
Mössbauer spectrum 579, 580
μ_{eff} 477
muffin-tin method 50
Mulliken-population analysis
– HfH 82
– HfH_2 92
– LaH^+ 71
– LaH_2 79
– LaH_2^+ 75
– ScH_2 63
– YH 56
– YH_2 61
– ZrH 86
multiple-scattering $X\alpha$ method 50

N-benzoyl-N-phenylhydroxylamine 212
NH_4SCN 209
NMR (nuclear magnetic resonance) 537, 585
NMR shift data 577
NaCl-type lanthanide monoxides, lattice parameter 429
NaCl-type structure 429
$Na_4(NpO_2)_2C_{12}O_{12}\cdot 8H_2O$ 580
NaSCN 220
natural orbitals 48
Nd 16
Nd^{4+} 272
NdF_3 509
NdO 429, 442, 443
Nd_2O_3 419, 420, 430, 440, 441, 444, 448, 491
nephelauxetic scale 563
neptunyl dimers 580
neutral organophosphorus compounds 202
neutral organophosphorus extractants 207
neutron diffraction 571
neutron diffraction measurements 535
neutron scattering 531
nielsbohrium 21
nitrogen and chlorine 380
nitrogen and fluorine 381
No 455, 470
No(c) 474
No(g) 474
No-259 451
NoO_x 452
No_2O_3 474, 491
nobelium 16
non-aqueous solvents 268

nonradiative decay 184, 187–189, 192
nonstoichiometric oxides 437
nonstoichiometric phases 424
nonstoichiometry in oxides 459
nonzero moment 476
Np 16, 198
Np(c) 473
Np(g) 473
Np metal 510
Np-237 451
Np(IV) 537
NpO_x 452, 455, 463
– thermodynamic properties 474
NpO 463
NpO(c) 473
NpO(g) 473
NpO_2 457, 459–461, 477, 491, 513
NpO_2^+ 573
NpO_2^{2+} 538
NpO_3 463
Np_2O_3 473, 491
Np_2O_5 457, 461, 463
Np_3O_8 463
NpO_2(c) 473
NpO_3(c) 473
NpO_2(g) 473
$NpO_3 \cdot H_2O$ 463
$NpO_3(OH)_2$ 463
NpO tetrafluorides 519
nuclear magnetic resonance 530

O/M ratio in CmO_2 466
observed electronic transitions of PrO 117
observed low-energy states of SmO 122
one-center Dirac–Fock method 47
optical properties 448
optical spectroscopy 530
orbital binding energies of atoms Hf through Bi 36
orbital energies of valence s electrons of radii Cu, Af, Au, Zn, Cd, Hg 37
organometallics, sigma bonding 278
organophosphorus compounds 202
oscillator strength 179
osmotic coefficient 256
outer-sphere association complex 574
outer-sphere complex formation 571, 572, 585
overall hydration numbers 536
oxalates, nitrates 459
oxidation of sesquioxides 439
oxidation potentials 481
oxidation state (III) for U, Np and Pu 510
oxidation states
– of actinide elements actinium to lawrencium, inclusive (1986) 20
– of actinides 453
– of lanthanides in oxides 416
oxidation–reduction comparisons 280
oxidation–reduction stability relationships 283
oxide systems 478
oxides 428, 448, 450, 457, 459, 478, 486, 496
– of Dy, Cf 481
– preparation by heating salts 459
oxines 211
oxonium salts 514
oxygen and a halogen 383
oxygen dissociation pressures 467
oxygen self-diffusion in rare-earth oxides 444

PUREX 205
P–C–T data 306, 307
Pa(c) 473
Pa(g) 473
Pa-231 451
PaO_x 452, 455, 460
PaO 462, 463
PaO_2 459, 461, 473, 477, 491
Pa_2O_5 457, 459, 461, 473
Paraisen–Parr–Pople method 52
partial molal volumes 535
partial phase diagram of CeO_2–O_2 422
Pauli terms 43
Pauli two-component spinors 45
pentagonal bipyramidal geometry 533
pentavalent actinides 562
perchlorate effect 219
Periodic Table
– futuristic 24, 25
– just prior to World War II 1, 2
– modern 24, 25
– showing heavy elements as members of an actinide series (1949) 13
– showing heavy elements as members of an actinide series (1945, arrangement by G.T. Seaborg) 8
perovskites 276
phase diagrams
– CeO_x–O_2 422
– Eu–Eu_3O_4 417
– PrO_x–O_2 423
– sesquioxides 485
– TbO_x–O_2 423
phase reactions, kinetics 444
phase relationships 301–303, 319, 357, 358
phenomenological mechanisms 444
1-phenyl-3-methyl-4-acyl-5-pyrazolones 211

1-phenyl-3-methyl-4-benzoyl-5-pyrazolone (PMBP) 215
1-phenyl-3-methyl-4-trifluoroacetyl-5-pyrazolone 217
Phillips–Kleinman approximation 43
phosphates 202, 208
phosphinates 202, 208
phosphine oxides 202, 208
phosphonates 202, 208
photochemistry 191
photoelectron spectrometry 478
physical properties of EuO 447
pi bonding 279
P(M) 241, 255
Pm 16
Pm_2O_3 419, 430, 431, 440, 441, 491
polarographic reduction of Am^{3+} 269
polarographic reduction of Cm^{3+} 269
polyaminocarboxylate complexes 564
polyaminocarboxylates 571, 575
polyatomic oxides and complexes 136
polyaza–polyoxa 578
polycatecholates 578
polymorphic transformation 427
polynuclear complexes 553
polynuclear hydroxo complexes 547
potential-energy curves
– LaH 64
– LaH^+ 69
– LaH_2^+ 72
– YH 54
potential-energy surfaces
– HfH 81
– HfH_2 90
– LaH_2 76
– ScH_2 62
– YH_2 60
– ZrH 84
– ZrH_2 93, 94
Pr 16
Pr–O system 447
PrO_x 439
PrO 114, 429, 442, 443
$PrO_{1.50}$ 445
$PrO_{1.703}$ 442
$PrO_{1.71}$ 445
$PrO_{1.714}$ 445
$PrO_{1.717}$ 442
$PrO_{1.74}$ 442
$PrO_{1.778}$ 445
$PrO_{1.78}$ 445
$PrO_{1.804}$ 442
$PrO_{1.83}$ 445
$PrO_{1.833}$ 442
$PrO_{2.00}$ 445
PrO_2 418, 421, 428, 432, 442, 448, 491
Pr_2O_3 421, 430, 440, 441, 448, 491
Pr_6O_{11} 448
Pr_7O_{12} 421, 434, 445
– high and low temperatures 444
Pr_9O_{16} 421, 434, 437
$Pr_{10}O_{18}$ 421, 437
$Pr_{11}O_{20}$ 421, 434
$Pr_{12}O_{22}$ 421, 437
$Pr_{16}O_{30}$ 421, 434
$Pr_{24}O_{44}$ 434
$Pr_{40}O_{72}$ 434
$PrO_2(TbO_{1.818})$ 428
precipitation 553
precipitation of $Ln(OH)_3$ 551
precipitation/coprecipitation 200
predicted and observed energy levels of YH 56
predicted properties of transcurium elements (1949) 15
prediction that element 96 is difficult to oxidize 6
predictions for electronic structures of some transactinide elements 18
preparation of actinide oxides 457
preparation of lanthanide oxides 416
preparation of oxides of Ce, Pr, Tb 421
preparation of single crystals 459
preparation techniques 458
pressure-induced structural transformations 375
primary hydration 547
primary hydration number 535
primary hydration sphere 530, 536, 572
primary solvation shell 529
projections along $[21\bar{1}]$ 437
promotion energies 493, 544
properties of binary actinide oxides 478
properties of the lanthanide(III) ions 416
protactinide series 3
protactinium 16, 198
protactinium oxides 460
– thermodynamic behavior 472
pseudo-orbital 45
pseudophase formation 426
Pu 16, 198
– correlation of chemical properties with atomic structure 4
Pu(c) 473
Pu(g) 473
Pu metal 510
Pu-239 451
Pu-242 451
Pu–O system 474
$PuCl_3$ 513
PuF_6 518

Pu(III) 513
Pu(IV) polymers 552
PuO_x 452, 455, 463
PuO 463
PuO(c) 473
PuO(g) 473
PuO_2 461, 464, 473, 474, 477, 491, 513
– temperature-independent paramagnetism 476
PuO_3 464
Pu_2O_3 459, 461, 463, 464, 473, 480, 491
Pu_3O_8 464
Pu_7O_{12} 457
$PuO_3 \cdot 0.8H_2O$ 464
$PuOF_4$, redistribution in HF 519
PuO tetrafluorides 519
pulse radiolysis 267, 269
pyrazolones 202, 211

qualitative representation of electronic binding energies in the heaviest elements 11
quasi-relativistic model potentials 46

R_2O_3 428
– A-type structures 430, 432
– B-type structures 431, 432
– C-type structures 430, 432
R_nO_{2n-2} 423
R_e values of $^2\Delta_{3/2}$ states of NiH, PdH, PtH 39
radial distribution functions (RDF) 534
radial expectation values for Hf, Re, Au, Hg, Tl, Pb, Bi 36
radioelectrochemistry 267
Raman spectra 538
Raman spectral study of PuO_2^{2+} 553
rare-earth dichlorides 261
rare-earth hydrides 296, 297
rare-earth metals 248
rare-earth monoxides
– dissociation enthalpies 443
– enthalpy of formation 443
– Gibbs energy functions 442
rare-earth oxides
– electrical transport in 448
– free energy of formation 440
– heterogeneous reactions in 445
– oxygen self-diffusion 444
– thermodynamic properties 442
rare-earth sesquioxides 257
rare-earth trifluorides 260
rare-gas structure at element 118 18
reaction mechanism for halide synthesis 368
reactivity of high spin state Ir 35
redistribution reactions 518
reduced halides stabilized by interstitials 395
reduction 467
reduction of PuO_2 463
reduction potential diagrams 268
reduction potentials 261–266
– for M(III)/(II) couples 481
– for M(IV)/(III) couples 482
relative viscosities 537
relativistic effective core potential 31
relativistic effects 29, 544
relativity and lanthanide contraction 35
representations of fluorite-type RO_2 432
resin-bead technique 458
route of entry of actinides into man 599
rutherfordium 21
– relativistic effects 25

6s 544
7s 544
SCF, CASSCF, CI, RCI methods 47
S^0 of Pu(III) 544
saddle points in potential-energy surfaces
– HfH_2 91
– LaH_2 77
– LaH_2^+ 73
salt effects in solvent extraction 218
saturated moment 496
SbF_3/SbF_5 complexes 511
Sc 243
ScH 52
ScH_2 59
Sc species 254
Schrödinger equation 40
secondary hydration 547
secondary hydration sphere 530
selected lanthanide and actinide polyatomics 135
selection factors 569
self-irradiated oxides 459
semi-empirical techniques 32
separation factors 211–214, 216, 220–222, 231, 570
sesquioxide of uranium 449
sesquioxides 418, 429, 453, 455, 456, 460, 467, 469–471, 492
– enthalpies of formation 494
– enthalpies of solution 490
– first occurrence in actinide series 480
– lattice parameters 484, 489
– molecular volumes 487
– – cubic forms 487
– – hexagonal forms 487
– – monoclinic forms 487
– phase diagrams 485
siderophores 578
σ phase 437

single crystals 427
– preparation 459
– – fused salt electrolysis 460
– – hydrothermal growth 459
– – vapor deposition 460
Slater local-exchange approximation 50
Sm 16
Sm^{2+} 510
Sm(II) 580
SmO 118, 429, 442, 443
Sm_2O_3 419, 420, 428, 430, 431, 440, 441, 444, 448, 491
small and large components of $6s_{1/2}$ spinor of Pb atom 42
small-angle neutron scattering (SANS) 224
sodium (benzene-1, 2-dioxydiacetato) lanthanate(III) tetra-hydrate 577
soft-donor synergist 4, 7-diphenyl-1, 10-phenanthroline (DPPHEN) 231
soft donors 571
soft sulfur donors 570
solid-state chemistry 450
solid-state electrochemistry 272
solid-state hydrates 531
solid-state studies 451, 531
solids, heat capacities 256
solubility of uranium, neptunium and plutonium 513
solubility product constants 259
solvated fluoro-actinide 513
solvating ligands 202
solvation 538
– of UO_2^{2+} 539
solvation number 540
solvent extraction 199, 200, 570
specific oxides of the actinide elements 460
spectra of YD and YH 55
spectroscopic analysis 542
spectroscopic constants
– of EuO 124
– of GdO 125
– of HoO 129
– of LaF 102
– of lanthanide hydrides 100
– of low-lying states
– – HfH 81, 82
– – LaH^+ 69
– of TiH 87
– of UF^- 106
– of YCl 103
– of YbO 134
spectroscopic properties
– of LaH 65
– of low-lying electronic states of YH 53
– of ZrH 83
spin–orbit contamination in HfH_2 91
spin–orbit coupling 34
spin–orbit interaction 33
square prismatic structure 535
stability constant 564, 572
stability of actinide dioxides 456
– order Th > Pu > Bk > Am > Cm > Cf 456
stable oxides
– for Cm, Cf, Es 455
– for Fm, Md, Lr 455
standard electrode potential 542
standard enthalpies, free energies of formation and standard entropies of important rare-earth and actinide species 244, 245
standard enthalpies of formation 543
standard-state enthalpies of formation of aqueous ions 254
states of diatomic lanthanide and actinide halides 101
status of actinide elements (1990) 19
stoichiometry considerations 459
strain energy 532
structural properties of actinide oxides 461
structural relationships 301–303, 307
structure of La^+ inside C_{60} 147
structures of lanthanide and actinide trihalides at room temperature and pressure 371
structures of lanthanide oxides 429
structures of $(ONPO^+)_2$ 138
sub-doppler Zeeman spectroscopy of CeO 111
substitution reactions 582
suggested electron configurations for actinide and lanthanide elements 10
suggestion of actinide concept 4
suggestion of "actinide series" (1944) 4
sulfonic acids 202, 211
sulfur and iodine 380
superacids 508, 524
superactinide group 25
supported liquid membrane 229
surface profiles and substructures 439
surface spectroscopies
– inverse photoemission 334
– UV photoemission 329–331
– X-ray photoemission 333, 334
susceptibility of NpO_2 476
synergistic extraction 204
synergistic extraction systems 215
synthesis 368
synthesis of metastable dihalides 397

TALSPEAK (trivalent-actinide/lanthanide separation by phosphorus reagent extraction from aqueous complexes) 228
TCTP structure 534, 535
TETA (1,4,8,11-tetraazacyclotetradecane-1,4,8,11-tetraacetic acid) 579
TRAMEX 210
TTA (thenoyltrifluoroacetone) 202, 211, 215, 217
tarnishing of lanthanide metals 441
Tb 16
TbO_x 428
TbO 442, 443
$TbO_{1.70}$ 442
$TbO_{1.71}$ 445
$TbO_{1.72}$ 442
$TbO_{1.806}$ 442
$TbO_{1.81}$ 442
$TbO_{1.817}$ 442
$TbO_{1.82}$ 445
$TbO_{1.975}$ 442
$TbO_{2.0}$ 442
TbO_2 418, 421, 428, 432, 448, 491
Tb_2O_3 420, 421, 426, 430, 431, 440, 441, 448, 491
$Tb_2O_{3+\delta}$ 445
Tb_4O_7 448
Tb_7O_{12} 421, 426, 435, 437
$Tb_{11}O_{20}$ 421, 435, 437
$Tb_{12}O_{22}$ 421
$Tb_{16}O_{30}$ 435
$Tb_{24}O_{44}$ 435
$Tb_{48}O_{88}$ 435
$Tb_{62}O_{112}$ 421, 423, 432, 435
$Tb_{11}O_{20} \rightarrow Tb_7O_{12}$ 426
temperature-independent paramagnetism 476
temperature-independent paramagnetism in PuO_2 476
temperature–phase diagram for actinide sesquioxides 485
ternary lanthanide oxides 428
1,4,7,10-tetraazacyclododecane-*N*,*N*′,*N*″,*N*‴-tetraacetic acid (DOTA) 229
1,4,7,10-tetraazacyclotetradecane-1,4,7,10-tetraacetic acid (DOTA) 578
1,4,8,11-tetraazacyclotetradecane-1,4,8,11-tetraacetic acid (TETA) 579
tetrad effect 545
tetrahedrally coordinated vacant oxygen site 436
tetrapositive aquo-ions 255
tetravalent actinides 544
tetravalent ions 549, 561
tetravalent states 562
Th 16, 198, 531
Th(c) 473
Th(g) 472
Th metal 511
Th^{4+} 572, 573
Th-232 451
ThO_x 460
ThO 460, 463, 472
ThO(g) 473
ThO_2 452, 455, 459–461, 472, 473, 477, 491
ThO_2(g) 473
thenoyltrifluoroacetone, *see* TTA
theoretical methods for lanthanide and actinide molecules 43
theoretical studies 540
thermal decomposition 419
thermochemical and thermophysical properties 257
thermochemistry 313–321
thermodynamic and high-temperature behavior 489
thermodynamic behavior of protactinium oxides 472
thermodynamic data on actinide halides 260
thermodynamic measurements 585
thermodynamic properties
– of binary oxides 470
– of lanthanide oxides 439
– of lanthanide sesquioxides 441
– of Np oxides 474
– of rare-earth oxides 442
thermodynamic studies 540
thermodynamic values for actinide elements and their gaseous/solid oxides 473
thermodynamics of actinide oxides 472
thermodynamics of hydration 542, 546
thermogravimetric analysis 520
Θp(K) 477
thin films 428
thoride series 3, 4
TiH 85
TiH–ZrH–HfH triad 88
Tm 16
TmH 97
TmO 130, 442, 443
Tm_2O_3 419, 420, 430, 431, 440, 441, 445, 448, 491
tolerance factor 276
tracer chemical observations on neptunium 3
transactinide elements 21, 25
transcalifornium sesquioxides 475
transeinsteinium oxides 470
transferrin 605, 606
transition-intensity analysis 179
transitions of invisible spectrum of uranocene 144
transplutonium actinides 198

transplutonium oxides
– magnetic behavior 476
tribromides 260
tributyl phosphate 205
tricapped trigonal prism (TCTP) 531
trichlorides 260
trihalide hydrates 393
trihalide polytypism 373
triiodides 260
triisooctylamine 223
2, 4, 6-tris(2-pyridyl)-1, 3, 5-triazine (TPTZ) 230
tris(dipicolinato) lanthanate(III) 577
trivalent actinide ions 536, 577
trivalent hydrated actinides 531
trivalent ions 548
trivalent lanthanide and actinide hydrates 393
trivalent lanthanide extraction by tributylphosphate 207
trivalent lanthanide/actinide group separation 233
trivalent oxide–halide systems 392
two-component spinor 46

U 16, 198, 531
U(c) 473
U(g) 472
U metal 510
U-238 451
U(III) 512
U(IV) 538
U–O system 472
U $(C_8H_8)_2$ dipole allowed states 144
UF_ 105
UF 105
UH 96
UH^- 96
UH^+ 96
UO_x 449, 452, 455, 462
UO 462, 463
UO(c) 473
UO(g) 472, 473
UO_2 459–461, 477, 491, 513
UO_2^{2+} 538, 572, 573, 577
$UO_{2.25}$ 462
UO_3 457, 462, 473
U_2O_3 491
U_3O_8 457, 459, 460, 462
U_4O_9 460
UO_2(c) 473
UOF_4
– no adducts formed with AsF_5 518
$UOF_4 \cdot nSbF_5$ 518
UO_2(g) 472, 473
UO_3(g) 473
UO_2^{2+} hydrate 533
u symmetry excited states of $Pu(C_8H_8)_2$ 145
ultrasonic absorption 572
ultrasound 539
ultrasound absorption 582
uranates 277
uranide series 3
uranium oxide tetrafluoride 518
uranium oxides 462
uranium sesquioxide 515, 516
uranium trioxide 515
uranocene 139
uranyl 538
uranyl fluoride 519
uranyl-specific ion electrode 578

valence orbitals of LaH 99
vapor species over sesquioxides 492
vaporization 439
– of Cm_2O_3 475
– of NpO 474
– of NpO_2 474
– of ThO_2 472
– of UO_2 472
vaporization/decomposition of Cf_2O_3 475
vaporization/decomposition of transcalifornium sesquioxides 475
vernier-type halide phases 385
vibronic bands 181
volatility of chlorides and bromides of hahnium 23

water–1, 4-dioxane 538
water–acetone 538, 539
water–acetonitrile 538
water–dioxane 539
Weiss–Matya–Nishimoto formula 52

X-ray absorption fine structure, *see* EXAFS
X-ray diffraction 531, 571
X-ray measurements 538
X-ray scattering 579
X-ray techniques 535
xenon hexafluoride 524
xenotime 198

YCl 105
YF 103
YH 52
YH_2 59
Yb 16
Yb^{2+} 510, 562
Yb(II) 580

YbO 131, 417, 429, 442, 443
Yb_2O_3 419, 420, 430, 431, 440, 441, 448, 491

zero moments 476
zone refining 460
$Zr_{0.858}Ca_{142}O_{1.858}$ 444
ZrH 84
ZrH_2 93